SEISMIC PERFORMANCE OF THE SLOTTED BEAM DETAIL IN REINFORCED CONCRETE MOMENT RESISTING FRAMES

A THESIS
SUBMITTED TO THE UNIVERSITY OF CANTERBURY
IN PARTIAL FULFILMENT OF THE REQUIREMENTS
FOR THE DEGREE OF
DOCTOR OF PHILOSOPHY

By
Craig Alan Muir
2014

Department of Civil and Natural Resources Engineering
College of Engineering
University of Canterbury
Christchurch
New Zealand

For my wife, Rebecca.

Abstract

During recent seismic events, traditional reinforced concrete structures that have been shown to have performed as designed have had to be demolished due to prohibitive rehabilitation costs. The main contributors to rehabilitation costs were residual building inclination and damage to the structural system. In traditional reinforced concrete moment frames, this damage has been shown to be attributable either directly, or indirectly, to the formation of plastic hinge zones and the undesirable behaviour that can result.

This research investigated and developed the reinforced concrete slotted beam as a means to increase the performance and safety of reinforced concrete moment frames during an earthquake. The slotted beam can significantly decrease damage sustained to the frame and floor of a building, while maintaining current build costs. The objective of this research was to develop the reinforced concrete slotted beam detail to a state in which it was ready for use by the New Zealand construction industry. To achieve this objective, many aspects of reinforced concrete slotted beam design, construction and performance were investigated.

Existing design recommendations developed by previous researchers were examined through the design of a realistic large scale superassembly. Based on the results and observations of the experiment, design recommendations were modified and developed. The superassembly was subjected to full biaxial seismic displacements to investigate complex three-dimensional interactions between structural elements within a building typology representative of New Zealand construction. The practicality of the design, manufacture and erection of the reinforced concrete slotted beam detail was examined through the involvement of industry to construct the superassembly. The lessons learnt throughout the design and construction process were used to develop recommendations, which aimed to expedite the specification of the reinforced concrete slotted beam detail.

Well-detailed traditional reinforced concrete structures have had to be demolished following earthquakes due to concerns regarding the residual capacity of the connections. The slotted beam detail increases the plastic strain in the bottom longitudinal reinforcement. Hence, the residual capacity of the slotted beam following a seismic event was examined. Portions of superassembly SA1 were extracted and tested to determine the effect that previous loading had on both performance and reliability. An economically viable method for retrofitting the slotted beam was developed to decrease the life-cycle costs of a slotted beam building by preventing the necessity for demolition after a major earthquake if it were deemed that the residual capacity was not great enough, or not known with sufficient certainty. Recommendations for the design and implementation of a retrofit scheme for the slotted beam

were developed. Preventing the need to retrofit slotted beam connections following an earthquake is preferable. Hence, external dampers that were either easily replaceable or could withstand multiple earthquakes were tested for both retrofit and new-build applications. A structure that exhibits reduced damage during an earthquake, returns to plumb and requires little repair prior to reoccupation is the goal of seismic building design. This can be achieved using the slotted beam detail in conjunction with external energy dissipation devices.

Given the rise in the popularity of numerical models for both research and design, it was important to develop a numerical model that was not only capable of reproducing realistic slotted beam behaviour in three dimensions, but could be quickly set up using only gross section and material properties. The new numerical model was verified against experimental data before being used to compare both connection and structural responses of slotted beam and traditional systems.

Acknowledgements

Research on this scale requires the support of many people and organisations in a variety of different ways. Be it technical, financial or emotional support; know that your support is appreciated and contributed immeasurably to the success of this research project.

Firstly, I would like to thank my supervisor, Professor Des Bull, whose interest in the practical application of knowledge helped shape the direction and focus of this research project. I would like to acknowledge also the contribution that my secondary supervisor, Professor Stefano Pampanin, made to this research project, and the support provided by Professor Athol Carr during the numerical phase of this research project. I am also grateful for the assistance provided by Dr Geoff Rodgers during the design and manufacture of the HF2V dampers.

This research project and I have been fortunate to have benefited from the enthusiasm of many organisations that believed in the value of the research being undertaken, and were generous enough to invest in it. I would like to extend my gratitude to the following organisations and funding schemes:

- University of Canterbury Doctoral Scholarship.
- H.J. Hopkins Postgraduate Scholarship in Civil Engineering.
- SAFER Projects Doctoral Scholarship.
- The Foundation for Science, Research and Technology.
- Todd Foundation Award for Excellence.
- Freemasons University Scholarship.
- New Zealand Concrete Society Concrete Prize.

I would like to thank the technicians who assisted me during the years I spent in the laboratory: Russell McConchie, Gavin Keats, Peter Coursey and John Maley. All of whose practical skills and knowledge proved invaluable.

The enthusiasm and commitment of the construction industry to support the development of this new technology was vital in ensuring the implementation goals of the research were realised. The assistance provided by the following businesses is acknowledged:

- Beca Limited.
- Holmes Consulting Group Limited.
- Bradford Precast Limited.
- BBR Contech Limited.
- Stahlton Engineered Concrete.

I would also like to acknowledge my postgraduate colleagues who supported me throughout my research: Debra Gardiner, Greg Cole, Reuben Costello, Anton Kivell, Andrew Baird and Joseph Byrne. Whether it was in the gym, laboratory or conferences; I have memories that I will treasure for life. Particular thanks are reserved for Peter Grange who, along with much philosophising over coffee, assisted in collecting the DEMEC readings from SA1. I hope you don't suffer any long term back issues.

I wish to express my sincere gratitude to my family. To my mother and father-in-law, Warrick and Julie, thank you for your support and encouragement of Rebecca and me over the years.

To my brother and sister-in-law, Paul and Meg, for all the chats, beverages and barbeques; it was always a welcome escape from reinforced concrete.

To my parents, Wayne and Linda, thank you for your ongoing love, support and encouragement over the years. Without the example you set and the sacrifices that you made I would never have had the opportunity to make this contribution.

Finally, to my wife Rebecca, without your love, support and encouragement none of this would have been possible. You believed in me, you celebrated the successes with me and you carried me through the failures. Thank you, this thesis is dedicated to you.

Craig Muir

28th February 2014

Table of Contents

List of Figures

List of Tables

1. Introduction

1.1 Research Motivation

Extensive experimental and historical earthquake data has shown that well-detailed traditional reinforced concrete structures perform well at the survivability limit state (Priestley et al., 2007). However, during recent seismic events traditional reinforced concrete structures that have been shown to have performed as designed have had to be demolished due to prohibitive rehabilitation costs (Corley, 1996). The main contributors to this cost were residual lateral displacement and structural damage.

Residual drift occurs when the hysteretic response of the structure is not centred about the origin. The structure should be restored to plumb because residual drift can not only impair the seismic performance of the structure during subsequent events, but impose severe serviceability issues.

Structural damage within a traditional reinforced concrete moment resisting frame primarily stems from regions detailed for significant inelastic behaviour, termed ‘plastic hinge zones’. These zones are chosen, and subsequently detailed, to undergo large inelastic deformation that limits the amount of force the structure must be designed for. In a traditional reinforced concrete structure the energy is dissipated through alternative tensile yielding of the top and bottom longitudinal reinforcement over cyclic reversals. This mechanism results in the points of rotation at either beam end not being coincident. In addition to the tensile strain accumulation in the longitudinal reinforcement, this tends to lengthen the beams. Beam elongation has the potential to cause significant damage to the structure through the formation of undesirable inelastic mechanisms, such as column sway and tearing of the floor diaphragm. Floor diaphragm damage has been shown to inhibit lateral force transfer (Bull, 2004) and in extreme cases cause complete loss of the floor gravity carrying capacity, leading to collapse (Matthews, 2004).

The deficiencies with current reinforced concrete design had to be rectified. Efforts to date have primarily focussed on developing low damage connections using dry jointed ductile connections (Priestley, 1996). Whilst these systems have addressed connection damage, they have neglected floor and column damage caused by beam elongation. A new system was

required that addressed both issues, and did so utilising existing technology and construction techniques to ensure the new system was both practically and financially feasible as an alternative to current practices.

In response to the observed shortcomings in the performance of traditional reinforced concrete structures, the reinforced concrete slotted beam was proposed in Japan by Ohkubo and Zhang (1997). The reinforced concrete slotted beam is a detail designed to reduce the damage sustained by the seismic frame and floor diaphragm during an earthquake. A slot is provided in the end of the beam approximately ¾ of the way up the column face, which allows rotation to occur about the top of the section during both positive and negative flexure. As a result, the plasticity in the connection occurs in the bottom longitudinal reinforcement, which is unbonded for a length to limit the strain induced. The slotted beam has been proven capable of addressing many of the undesirable traits displayed by traditional connections. Early experimental observations highlighted the potential of the slotted beam to reduce connection damage and beam elongation (Ohkubo & Hamamoto, 2004). Furthermore, the construction of the slotted beam was similar to the traditional concrete beam, which reduced barriers to implementation by industry compared to more complex details such as post-tensioned rocking connections.

Recent New Zealand research on the slotted beam has built on the work conducted in Japan. Researchers at the University of Canterbury have investigated the slotted beam parametrically, analytically and experimentally (Au, 2010; Leslie, 2010; Byrne, 2012). The aim of these investigations was to improve the performance of the slotted beam and develop design recommendations for use by practitioners. The research conducted by Au (2010) was particularly relevant to the research described in this dissertation as it represented the state-of-the-art for the reinforced concrete slotted beam at the commencement of this research project. Au (2010) developed details to improve the performance and reliability of the reinforced concrete beam through both an experimental programme, which tested cruciform subassemblies in-plane, and spreadsheet based moment-rotation analyses.

The slotted beam presented an attractive proposition to improve the performance of reinforced concrete moment frames during an earthquake without significantly increasing construction costs. However, whilst the slotted beam has shown promise in two-dimensional cruciform experimental tests (Ohkubo & Hamamoto, 2004; Au, 2010; Leslie, 2010; Byrne, 2012) the detail remained unproven in realistic three-dimensional structural systems. The performance of the reinforced concrete slotted beam connection has been vastly improved through the concerted efforts of the above researchers. However, there remained scope to further improve

connection performance through the development of new, and the refinement of existing, details.

There was uncertainty about the residual capacity of the slotted beam following a large earthquake and there existed no means to retrofit a slotted beam if the residual capacity was deemed insufficient. The use of external replaceable energy dissipation devices for retrofit and new-build applications had not been investigated. This type of detailing had the potential to not only improve the connection performance of the slotted beam, but to also reduce building rehabilitation costs should it be subject to a large earthquake.

Existing numerical models for representing the response of the reinforced concrete slotted beam were cumbersome to implement and were restricted to two-dimensional analyses. For a numerical model to be useful to both researchers and practitioners it needed to not only be capable of accurately representing slotted beam response in three dimensions, but also be simple to set up using only basic material and section properties.

1.2 Research Objectives

The principal objective of this research was to develop the reinforced concrete slotted beam detail to a state in which it was ready for implementation into the New Zealand construction industry. It was determined that success would be measured not only by the significance of the technical outcomes of the research, but also by the application of the technology in practice. The construction of the first slotted beam structure in New Zealand, using details and techniques developed during this research programme, would define the achievement of the research objective.

To achieve this objective, it was necessary to investigate many aspects of reinforced concrete slotted beam design, construction and performance.

1. Existing design recommendations developed by previous researchers were tested through the design of a realistic large scale superassembly. Based on results and observations, design recommendations were modified and developed.
2. The practicality of the design, construction and erection of the slotted beam detail was examined through the involvement of industry to construct a large scale three-dimensional slotted beam superassembly. Recommendations to expedite the design and manufacture of the slotted beam were made based on lessons learnt throughout the design and construction process.
3. Whilst slotted beam connection performance had been previously investigated (Au, 2010; Leslie, 2010; Byrne, 2012), the relationship of the connection with other structural elements had not. Complex three-dimensional interactions between elements were

examined by subjecting a large scale slotted beam superassembly to biaxial seismic displacements. Recommendations for the design and detailing of slotted beam systems were developed based on the results and observations of the experiment.

4. The construction and testing of a large scale slotted beam superassembly, which was representative of typical New Zealand construction practice, provided a proof of concept to industry. It was often difficult for industry to relate to small cruciform experiments and the assurance that the detail would work as part of a complete structural system. Constructing the slotted beam detail as part of a complex three-dimensional system removed any uncertainty, and enabled effective dissemination of the research results.
5. Well detailed traditional reinforced concrete structures have had to be demolished following earthquakes due to concerns regarding residual reinforcement capacity (Corley, 1996). Compared to traditional connections, the slotted beam detail increases the plastic strain in the bottom longitudinal reinforcement during flexure (Au, 2010). Hence, the residual capacity of the slotted beam following an earthquake was examined. Following the completion of the superassembly testing, two superassembly connections were extracted and tested to determine the effect that previous loading had on performance and reliability.
6. If the residual capacity of a slotted beam is not great enough following a large earthquake, or not known with sufficient certainty, then the connection would require retrofit to re-establish connection capacity. An economically viable method for the retrofit of slotted beams was developed to decrease the life-cycle costs of a slotted beam structures by preventing the necessity for demolition after a major earthquake. Recommendations for the design and implementation of slotted beam retrofit were developed.
7. Preventing the need to retrofit slotted beam connections following an earthquake is preferable because the building life-cycle costs are minimised. Hence, external dampers, which were installed in lieu of the unbonded bottom longitudinal reinforcement, that were easily replaceable or could withstand multiple earthquakes, were tested for retrofit and new-build applications. Recommendations for the use of external dampers in slotted beam connections were developed based on the experimental results.
8. Given the rise in the popularity of numerical models for both research and design, it was important to develop a numerical model that was not only capable of reproducing realistic slotted beam behaviour in three dimensions, but could be quickly set up without calibration using only gross section and material properties. The new numerical model

was verified against experimental data, before being used to compare both connection and structural response of slotted beam and traditional reinforced concrete systems.

1.3 Thesis Organisation

The research described within this dissertation is divided into three phases; superassembly experimental testing, subassembly experimental testing and numerical modelling. This dissertation is comprised of eight chapters.

Chapter 2 describes the historic events, and technical shortcomings in traditional design, that motivated researchers to develop low damage structural systems. The development of non-tearing floor systems and the reinforced concrete slotted beam is described. Recent investigations into the reinforced concrete slotted beam are critiqued.

Chapters 3 and 4 describe the superassembly experimental phase of this research. Chapter 3 presents the background and design of a two-storey, two-by-one bay, slotted beam superassembly, which is termed SA1 herein. The construction of the precast components and the erection of the structure are detailed and examined. Recommendations to increase the efficiency of the design, manufacture and erection of slotted beam structures are made. Finally, the development of the reaction frame, loading protocol, actuator control program and instrumentation are presented. Chapter 4 presents the issues encountered and the observations made during simulated seismic testing of the superassembly. The collected data is presented and the implications discussed. Recommendations based on observations and measurements are offered.

Chapters 5 and 6 describe the subassembly experimental phase of this research. The background and origin of the two subassemblies, termed SA2 and SA3 herein, is presented. The design and implementation of a retrofit scheme for the slotted beam is detailed, and the experimental setup used to seismically examine the subassemblies is described. Chapter 6 presents the observations and data collected during testing, which are discussed in a wider context and recommendations are made.

Chapter 7 details the numerical modelling phase of this research project. Existing two-dimensional numerical models are extended to three dimensions using several methods. The 'R3D' slotted beam multispring element is developed to reduce the cost and complexity of using numerical models for design and research, whilst maintaining accurate representation of slotted beam behaviour. Validation of the R3D element is undertaken against the experimental data presented in Chapters 3 – 6 and a numerical floor diaphragm model is developed and implemented. Direct comparison of slotted and traditional beam connection behaviour is undertaken to determine differences in mechanics. Finally, a comparison of the

differences in overall structural response is undertaken by subjecting prototype slotted and traditional reinforced concrete model buildings to a suite of recorded earthquake records.

Chapter 8 presents a summary of the research undertaken and the outcomes achieved. The conclusions of the research are presented along with areas of further research recommended to be undertaken.

1.4 References

Au, E. (2010). *The mechanics and design of a non-tearing floor connection using slotted reinforced concrete beams.* Masters Dissertation, University of Canterbury, Christchurch, New Zealand.

Bull, D. K. (2004). Understanding the complexities of designing diaphragms in buildings for earthquakes. *Bulletin of the New Zealand Society for Earthquake Engineering, 37*(2), 70-88

Byrne, J. D. R. (2012). *Bond and shear mechanics within reinforced concrete beam-column joints incorporating the slotted beam detail.* Masters Dissertation, University of Canterbury, Christchurch, New Zealand.

Corley, W. G. (1996). Northridge earthquake of January 17, 1994 reconnaissance report. *Earthquake Spectra, 12*(S1), 1-278.

Leslie, B. J. (2010). *The development and validation of a non-tearing floor precast concrete structural system for seismic regions.* Masters Dissertation, University of Canterbury, Christchurch, New Zealand.

Matthews, J. G. (2004). *Hollow-core floor slab performance following a severe earthquake.* Doctoral Dissertation, University of Canterbury, Christchurch, New Zealand.

Ohkubo, M., & Hamamoto, T. (2004). *Developing reinforced concrete slotted beam structures to reduce earthquake damage and enhance seismic structural performance.* Paper presented at the 13th annual World Conference on Earthquake Engineering. Vancouver, B.C., Canada. Retrieved from http://www.iitk.ac.in/nicee/wcee/article /13_3285.pdf

Ohkubo, M., & Zhang, A. (1997). *Lateral Loading Behaviour of Beam-column Sub-assemblages Designed by Limited Flexural Mechanism of Bottom Rebar Yielding at Beam-end Region*. Proceedings of the Japan Concrete Institue, 19(2), 867-872.

Priestley, M. J. N. (1996). The PRESSS program - Current status and proposed plans for phase III. *PCI Journal, 41*(2), 22-40.

Priestley, M. J. N., Calvi, G. M., & Kowalsky, M. J. (2007). *Displacement-based seismic design of structures*. Pavia, Italy: IUSS Press.

2. Research Background

2.1 New Zealand Reinforced Concrete Design

2.1.1 Historic Reinforced Concrete Design

Prescriptive seismic design requirements were introduced in New Zealand in 1935. Since this time, and through subsequent code revisions, reinforced concrete has remained a popular building material (CAE, 1999). Until the 1960s structural components were primarily constructed from cast insitu reinforced concrete. There has been a steady increase in the use of precast reinforced concrete for structural components since. Precast concrete construction involves the manufacture of concrete components off-site or in advance of building erection; these components are then connected during erection to assemble the building.

Until the 1980s the use of precast elements as part of the seismic resisting system was relatively rare, instead precast concrete elements were used primarily for one-way flooring systems. The rapid increase in the application of precast concrete was driven by advantages of familiar materials, higher erection speeds, higher quality and increased precision. However, time and resources were not available to experimentally verify these new systems and extrapolation of insitu concrete results was generally assumed, which was not always the case (CAE, 1999).

The concrete structures standard at that time, NZS3101:1982 (Standards New Zealand, 1982), was well equipped for the seismic design of insitu reinforced concrete structures; however, it contained little provision for precast design. Despite this, the use of precast concrete continued to increase; driven by precast manufacturer innovation. The increasing use of precast concrete raised awareness in the engineering profession that some design solutions should be more fully researched. As a result, a study group was formed involving the New Zealand Concrete Society, the New Zealand National Society for Earthquake Engineering and the Centre for Advanced Engineering. The goal of the study group was to summarise existing data, indicate recommended practices and identify topics requiring further research (CAE, 1999).

There have been cases of poor performance of precast structural elements during earthquakes around the world. Poor performance was observed in precast concrete parking structures during the 1994 Northridge Earthquake (Corley, 1996). The 1988 Armenian Earthquake highlighted the consequences of poor detailing for continuity in precast concrete moment frames; with the collapse of numerous buildings and corresponding loss of life (Wyllie-Jr & Lew, 1989). Likewise, poor detailing design was observed between precast elements during the reconnaissance following the February 22nd 2011 Christchurch Earthquake (Kam et al., 2012). Failures such as these have generally been attributed to brittle behaviour of connections between precast elements and inadequate detailing. Conversely, cases where well detailed insitu reinforced concrete structures have performed well have been highlighted by past earthquakes and experimental testing (CAE, 1999). Subsequently, the philosophy of precast construction in New Zealand has evolved to involve joining together precast elements to achieve comparable levels of seismic performance to a traditional insitu system. Due to the strength hierarchy of the connection being such that inelasticity will form preferentially elsewhere in the system, whilst the connection remains elastic, this philosophy is sometimes termed a 'strong connection' type. There are many ways of connecting the precast elements together in this manner, three of the most popular in moment frames are presented in Figure 2-1.

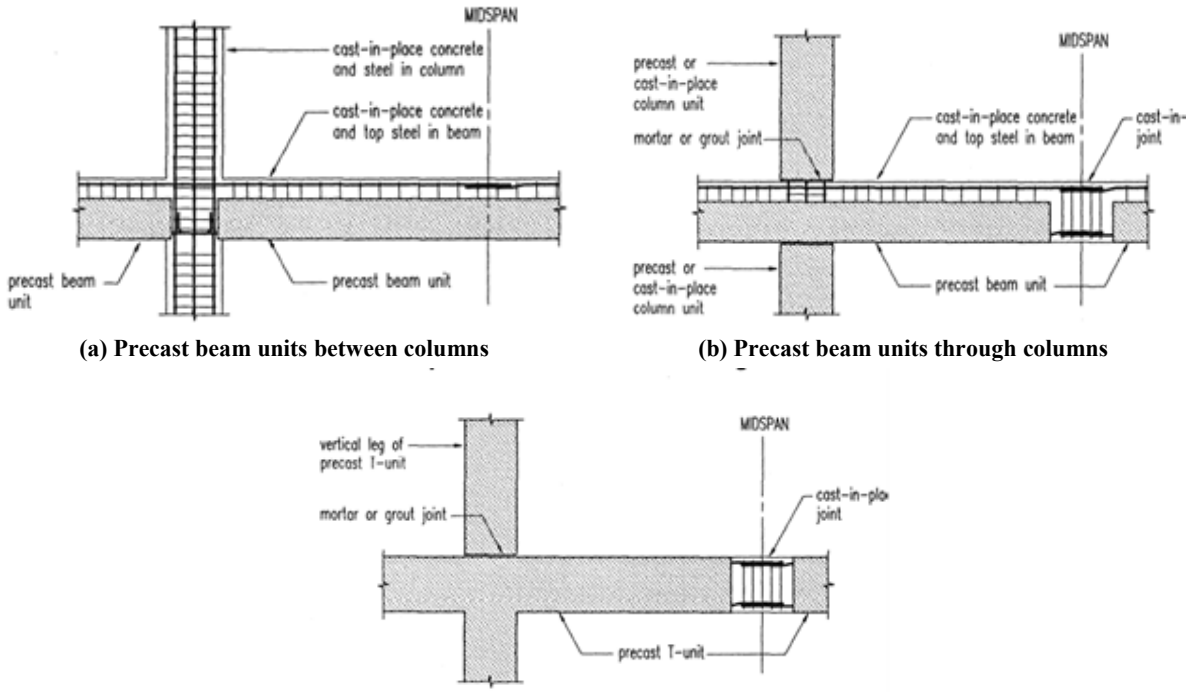

(a) Precast beam units between columns

(b) Precast beam units through columns

(c) Precast T-Units

Figure 2-1: Arrangement of precast elements and insitu concrete to achieve a strong connection type (CAE, 1999).

2.1.2 Capacity Design Philosophy

Regardless of the final construction method, reinforced concrete buildings in New Zealand are typically designed using 'capacity design' principles. Capacity design is a design philosophy where elements in the primary lateral load resisting systems are chosen and suitably detailed for large inelastic deformation under severe loading (Hollings, 1969; Park & Paulay, 1975). The regions designed to undergo plasticity are termed 'plastic hinge zones'. The preferred failure mechanism is achieved in practice by assigning a strength hierarchy to elements in the structure such that some elements will deform plastically preferentially, forcing the building to deform in the manner the designer intended. In reinforced concrete moment frames, the plastic hinge zones are generally located at the beam ends and column bases. In reference to the strength hierarchy of the system, this deformation mode is often termed 'weak-beam strong-column'. It can be seen in Figure 2-2 that for the same structural displacement, Δ, the rotational demand on the plastic hinge zones is significantly less for the weak-beam strong-column mechanism in comparison to the alternative mechanisms. In practice, it is difficult to detail a column to achieve the rotational ductility required to achieve design level structural displacements for a structure greater than approximately three stories when using a 'weak-column strong-beam' deformation mode. Once P-Δ effects are considered, the element can display negative stiffness, in this state the structure is in danger of imminent collapse.

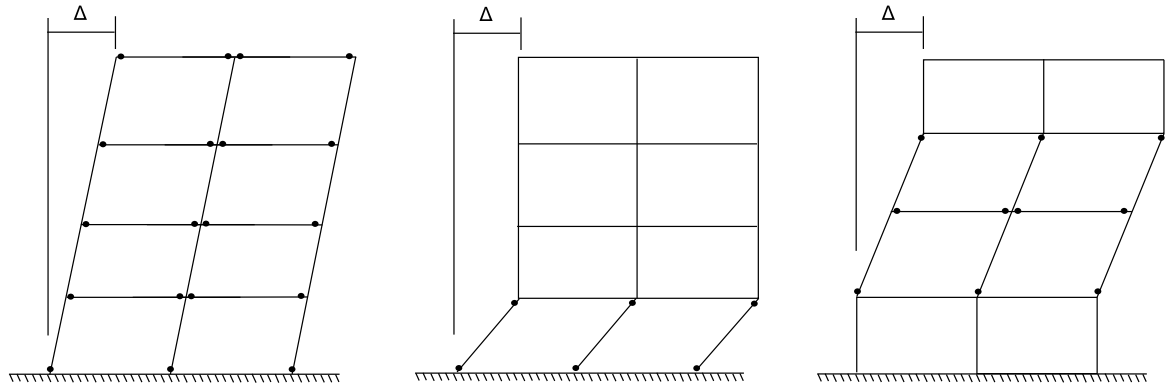

(a) Weak-beam Strong-column **(b) Weak-column Strong-beam** **(c) Mixed**

Figure 2-2: Deformation modes in moment frames.

Elements that are not intended to deform plastically are designed to have sufficient strength to elastically resist the actions imposed by the ductile regions. In this manner, the total force the building must be designed to withstand can be reduced based on the ductility available in the system.

Prior to the development of capacity design, buildings were designed using demands from scaled linear elastic analyses. The calculated structural demands from the analyses were often less than what would be induced during an earthquake. Hence, the post-elastic mechanisms

that formed in buildings during a major seismic event were unpredictable and often undesirable.

2.1.3 Design Deficiencies in Reinforced Concrete

In traditional reinforced concrete structures, plasticity is provided through the formation of plastic hinges. There are two types of plastic hinges that can form in moment resisting reinforced concrete frames; uni-directional and reversing. These plastic hinge types are shown in Figure 2-3. The type of plastic hinge that forms is dependent on the building geometry, loading and detailing. Several unwanted consequences are associated with plastic hinge formation.

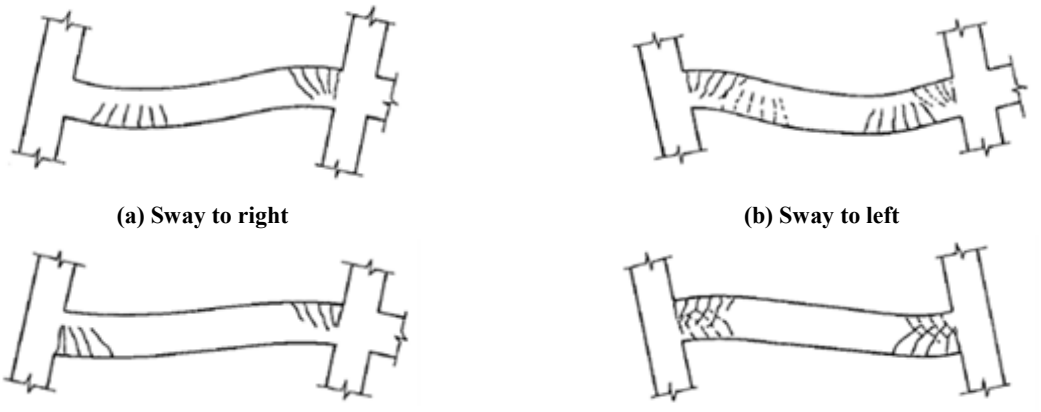

(a) Sway to right **(b) Sway to left**

(c) Sway to right **(d) Sway to left**

Figure 2-3: Uni-directional (a & b) and reversing (c & d) plastic hinges (Fenwick & Megget, 1993).

The first consequence is damage to the structural elements. The cracking of concrete necessitated to provide adequate ductility means that at the end of a significant seismic event the plastic hinge zones are heavily damaged, such as shown in Figure 2-4. Following the 1995 Kobe and 2011 Christchurch earthquakes there were examples of buildings that had formed plastic hinges, as designed, being demolished due to prohibitive rehabilitation costs (Earthquake Engineering Research Institute, 1995; Kam et al., 2012).

Figure 2-4: Damage to plastic hinge zone in traditional reinforced concrete beam (Matthews, 2004).

A further consequence of plastic hinge formation is beam elongation. It has been shown that over the course of a significant seismic event a plastic hinge can lengthen by 2-5% of the beam depth (Fenwick & Fong, 1979; Fenwick & Megget, 1993; Ingham et al., 2002; Walker, 2007). Beam elongation can be attributed to two main contributors; geometric and material.

The geometric contribution stems from the points of rotation at either beam end not being coincident for a traditional reinforced concrete beam. Hence, this contribution is more prevalent in deep beams and structures that are subject to large drift demands. A schematic of the geometric beam elongation mechanism is shown in Figure 2-5.

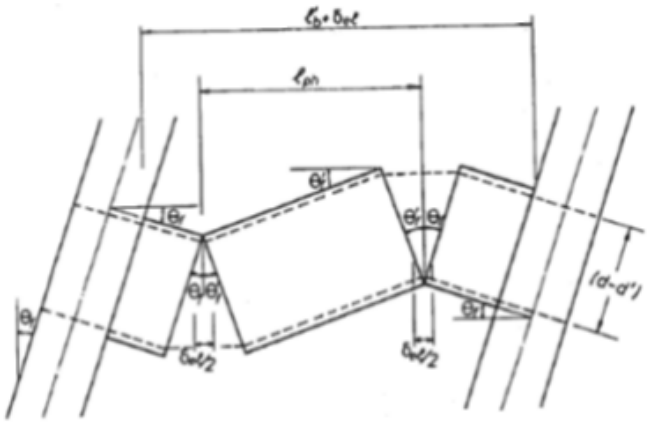

Figure 2-5: Geometric beam elongation (fib, 2003).

The material contribution is a consequence of the shear transfer mechanism that forms across a plastic hinge zone. As cracks form in the plastic hinge zone, the shear force must be transferred by way of truss-like action (Fenwick & Megget, 1993). By considering the forces in Figure 2-6, it can be seen that the tensile force in the longitudinal reinforcement, T, will always be greater than the compressive force, C, due to the horizontal component of the compression strut induced by shear, V. Regardless of the direction of loading, this component is always additive to the tensile reinforcement force induced by flexure.

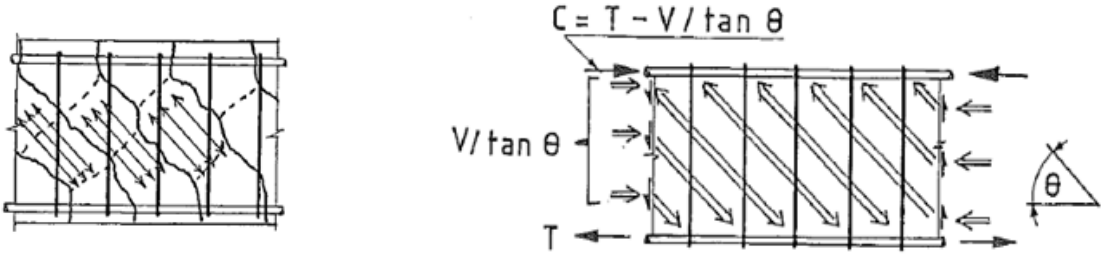

(a) Diagonal compression **(b) Truss action**

Figure 2-6: Shear transfer mechanism in a plastic hinge zone (Fenwick & Megget, 1993).

The difference between uni-directional and reversing type plastic hinges is that the tensile reinforcement yielding occurs at different locations along the beam length for positive and negative flexure. Hence, the tensile strains cannot be recovered upon load reversal.

Spalled aggregate particles prevent cracks from completely closing upon loading reversal. The net effect is that tensile strains govern the response and tend to accumulate over a loading history, which causes the beam to lengthen.

Whilst the emerging PREcast Seismic Structural Systems (PRESSS) addresses the material contribution to beam elongation, the system does not address the geometric contribution to beam elongation. The geometric contribution in some cases can be worsened due to the required armouring of the beam ends, which is provided to confine the concrete and prevent spalling. However, this can have the effect of reducing the neutral axis depth, which maximises the geometric beam elongation.

The elongation of beams can be resisted by the floor diaphragm. As shown in Figure 2-7, portions of the floor diaphragm can act as deep beams to resist the elongation of the perimeter beams (Peng, 2009). Compressive axial forces can be induced in the beams, which can increase the beam overstrength moments. The strength hierarchy in the system can be rearranged as a result. Activation of resistance from the floor diaphragm can result in significant damage to the floor, particularly at the interface between the floor and supporting beams.

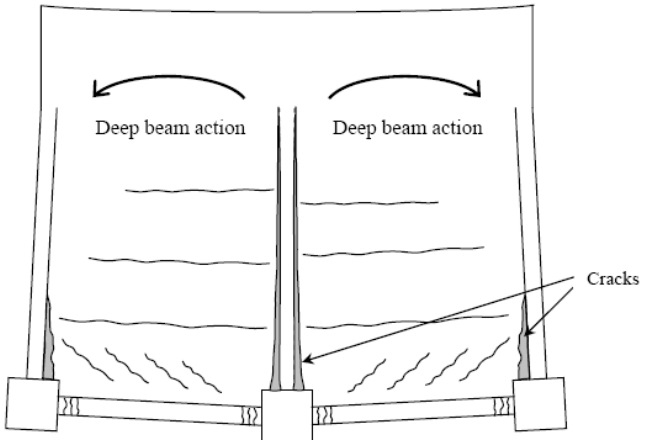

Figure 2-7: Deep beam action restraining beam elongation (Peng, 2009).

Elongation of beams is one cause of displacement incompatibility between the seismic frame and the flooring system. Another cause of displacement incompatibility is the differences between the deformation modes of the precast flooring and the parallel beam, which is discussed in Section 2.3.

The cumulative damage resulting from beam elongation and displacement incompatibility can compromise the structural performance of a building. Figure 2-8 demonstrates the deformation modes that can occur in a structure as a result of beam elongation. Separation of the supporting beams from the floor can occur and result in extensive damage along this interface, which can inhibit the ability of the floor to transmit horizontal forces induced by an

earthquake. The length that this damage extends along the beam is dependent on how the displacement in the supporting beam is distributed. Mode 1 demonstrates the deformation mode if this displacement is distributed over the plastic hinge zone only, whilst in mode 2 it is distributed over the entire beam length.

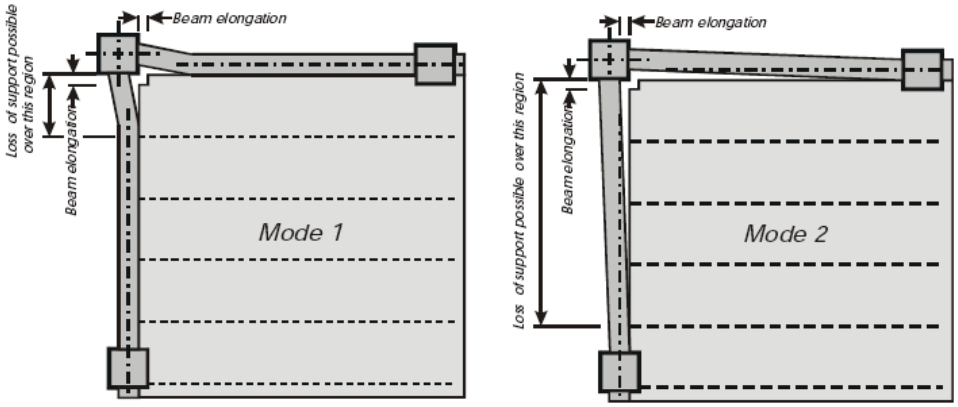

Figure 2-8: Deformation modes with beam elongation (Bull, 2004).

Figure 2-9 demonstrates the superposition of a weak-beam strong-column mechanism and beam elongation. The resulting mechanism can involve unfavourable column hinging immediately below the first storey due to the beam elongation altering the deformation mode of the structure, which changes the distribution of the internal actions throughout the structure. The increased flexure, shear and plasticity demands are not typically taken into account by the designer, and structural instability can occur. Beam elongation is additive along bays; hence, the more bays a structure has, the greater the risk of developing this unfavourable deformation mode.

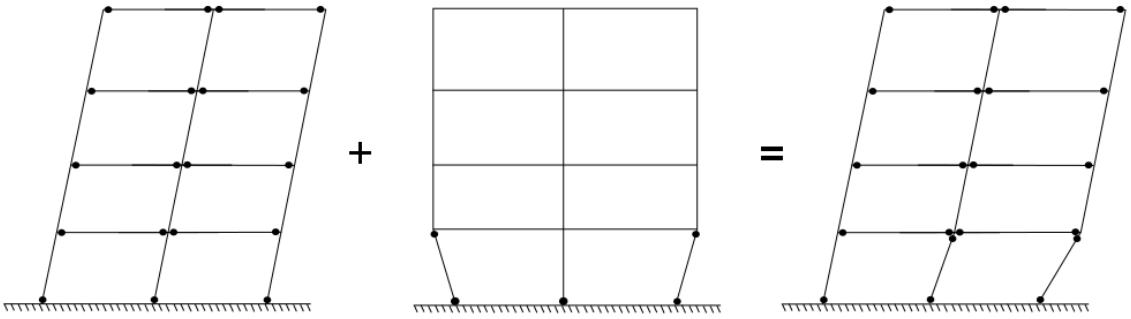

Figure 2-9: Possible failure mechanism as result of beam elongation.

In extreme cases, the beam elongation and damage to the floor diaphragm can be so severe that complete loss of the gravity support system can occur. This has been proven experimentally by Matthews (2004) as shown in Figure 2-10.

Figure 2-10: Loss of floor gravity support due to displacement incompatibilities (Matthews, 2004).

In light of these undesirable failure modes, it was recognised that there was a need for a new generation of design procedures. The SEAOC Vision 2000 Committee (1995) was formed to develop a framework of procedures that would produce structures of predicable performance in response to specified levels of seismic excitation, within definable levels of reliability (SEAOC Vision 2000 Committee, 1995; Pampanin, 2005). The framework is capable of explicitly addressing life safety, damageability and functionality issues. For a given structural importance, the performance level can be related to the earthquake intensity by way of probability through the use of the performance objective matrix shown in Figure 2-11.

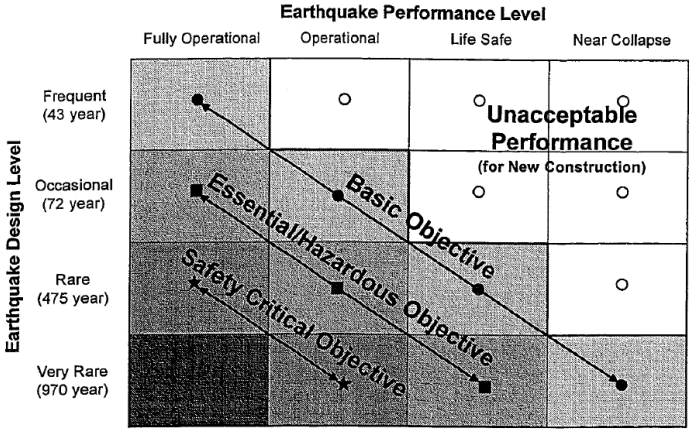

Figure 2-11: Recommended performance objectives matrix (SEAOC Vision 2000 Committee, 1995).

2.2 Development of Ductile Precast Connections

In New Zealand, traditional connections between precast elements have been designed to be sufficiently strong to avoid inelastic deformation, forcing plastic hinges to form elsewhere (CAE, 1999). The use of strong connection types resulted from a lack of experimental data from precast concrete and observed cases of brittle behaviour of precast concrete structures during historic earthquakes (Wyllie-Jr & Lew, 1989; Norton et al., 1994).

An alternative method is to connect precast concrete elements in a ductile manner, whereby the plasticity in the system is accommodated at the connection. These types of connections

typically exhibit rocking behaviour, the mechanics of which was first investigated for structural use by Housner (1963).

The National Institute of Standards and Technology (NIST) research program began in 1987 with the aim of developing guidelines for the design of precast beam-column connections for regions of high seismicity (Cheok & Stone, 1991). The PRESSS research programme began in 1991 and was a joint effort between the United States and Japan. It aimed to develop effective seismic structural systems for precast buildings and prepare design recommendations for inclusion in building codes.

The NIST and PRESSS programmes developed the ductile connection to a point where the seismic response was comparable to, and in some cases better than, an equivalent traditional connection. Furthermore, the ductile connections minimised damage to the main structural frame and provided recentring behaviour. However, both research programmes largely neglected the issues associated with beam elongation and the resulting damage to the floor diaphragm.

2.2.1 National Institute of Standards and Technology Research Programme

Precast concrete construction has been common place in the United States since the 1950s. Similarly to New Zealand, there had been limited experimental studies conducted on precast concrete performance. As a consequence, it was generally assumed that precast concrete was less ductile and had a less stable hysteretic response than equivalent insitu reinforced concrete. In the early 1980s, the need for a more comprehensive guideline for precast concrete design was recognised by both designers and researchers. A workshop was held in 1981 by the Applied Technology Council on the design of prefabricated concrete structures subjected to seismic loading. The purpose of this workshop was to determine current knowledge and identify areas requiring research (Applied Technology Council, 1981). The outcome was a set of 40 recommendations for areas of research, which were all assigned a priority according to need. The second highest priority was the development of recommended practices for joints between precast beam and column elements.

NIST initiated a study of the behaviour of precast beam-column connections subjected to cyclic inelastic loading in response to the recommendations made by the Applied Technology Council. The goal of the programme was to develop guidelines for the design of precast beam-column connections in seismically active regions (Cheok & Stone, 1990). An emphasis was placed on economic and constructible connections. All specimens were internal beam-column joints of cruciform configuration. The experiments were performed at 1/3 geometric

scale due to capacity limitations of the NIST laboratory. The programme was conducted in four phases.

In the first phase, four benchmark traditional beam-column connections and two equivalent post-tensioned precast connections were tested experimentally, shown in Figure 2-12. Two traditional specimens were designed for Universal Building Code (UBC) zone two, A-M-Z2 and B-M-Z2, and two specimens for UBC zone four, A-M-Z4 and B-M-Z4 (International Conference of Building Officials, 1985). Two post-tensioned precast connections, A-P-Z4 and B-P-Z4, were designed to have the equivalent flexural strength of the zone four traditional connections. Threaded post-tensioning bars were used over tendons to reduce the loss of post-tensioning force due to anchorage slip.

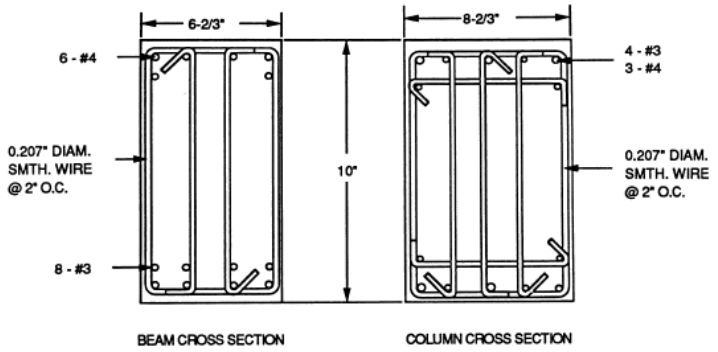

(a) Zone two

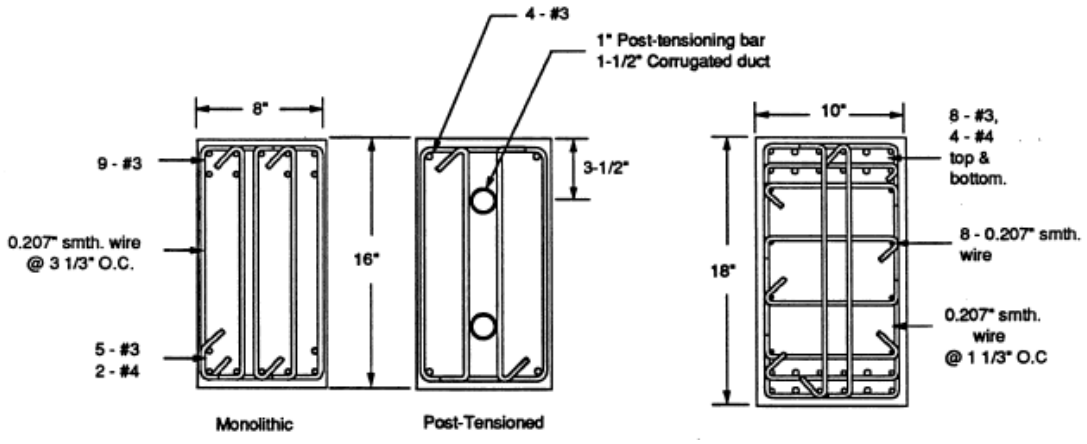

(b) Zone four

Figure 2-12: Details of phase I test specimens (Cheok & Stone, 1990).

Failure of the traditional specimen, designed for zone two, was by way of joint failure due to inadequate confinement. The traditional specimens, designed for zone four, failed by way of beam plastic hinge formation and deterioration. The post-tensioned specimens failed through post-tensioning bar yield and concrete crushing. Due to a greater initial stiffness, the ultimate displacement ductility of the post-tensioned connections was greater than for the traditional connections. Column drifts were comparable between the two systems. However, the post-tensioned connection dissipated 30% of the energy of the traditional connection on a per cycle

basis. The phase I experimentation showed that post-tensioned precast concrete connections had promise as a solution for application in high seismic regions.

The goal of Phase II was to improve the energy dissipation characteristics of the post-tensioned precast connections (Cheok & Stone, 1991). The post-tensioning bars were replaced with tendons, and the post-tensioning ducts were located closer to the beam centroid in an effort to reduce strain in the post-tensioning system. These concepts were tested in four specimens incorporating two connection types designed for zone four; C-P-Z4, D-P-Z4, E-P-Z4 and F-P-Z4. In addition, a zone two post-tensioned connection was designed and tested in two specimens: A-P-Z2 and B-P-Z2. The failures of the specimens tested during phase II were similar to the failures observed in phase I. The zone four post-tensioned specimens were 135% stiffer than the equivalent traditional connection. It was found that replacing the post-tensioning bars with tendons increased the energy dissipation per cycle by 30% and also strengthened the connection. Moving the post-tensioning ducts closer to the beam centroid increased the energy dissipation per cycle by 40%. However, the energy dissipated per cycle was still poor compared to traditional connections. The connection designed for zone two did not perform as well as an equivalent traditional connection in terms of ductility and cumulative energy dissipation.

Experiments conducted during phases I and II had shown the presence of a slip zone between the beam end and the column face that exhibited effectively zero stiffness upon load reversal in the latter stages of testing. It was hypothesised that this was due to yielding of the post-tensioning tendons (Cheok et al., 1993). The use of partially bonded post-tensioning tendons was tested in phase III to determine if strain in the tendons could be reduced. Connections with partially unbonded post-tensioned tendons, introduced by Priestley and Tao (1993), displayed a bilinear hysteretic response with recentring behaviour. Two specimens, G-P-Z4 and H-P-Z4, were tested with a design identical to that tested in phase II, except the post-tensioning tendons were unbonded through the column and for 381mm either side. The unbonded tendons were shown to perform well; however, the energy dissipation of the connections was reduced (Cheok & Lew, 1993).

Phase IV of the NIST research programme was further broken down into two sub-phases, A and B. In phase IV A, three connection designs were investigated over six tests (Cheok et al., 1993). In phase IV B, production testing of the connection details developed during the NIST research programme was undertaken over four experimental tests (Cheok & Stone, 1994).

During phase IV A, post-tensioning for moment resistance and mild steel for enhanced energy dissipation were combined to create a hybrid system. Three different hybrid connections were

tested. The geometry of the connection was changed slightly in this phase to replicate a design by a commercial precast company for a proposed structure. The design used 'dogbones' to accommodate the post-tensioning bars and/or mild steel reinforcement, as shown in Figure 2-13. These were akin to beam haunches and allowed easy installation of the post-tensioning bars and/or mild steel reinforcement. The first design used fully grouted post-tensioned tendons located at the beam centroid and fully grouted mild steel reinforcement in the dogbones. These specimens were named I-P-Z4 and K-P-Z4, and are shown in Figure 2-13. Specimen I-P-Z4 failed prematurely due to bond failure through the dogbone. This was due to heavy strain gauge instrumentation through this region diminishing the available bond area. Specimen K-P-Z4 failed due to fracture in the mild steel reinforcement, which was likely due to large strains caused by an absence of debonding.

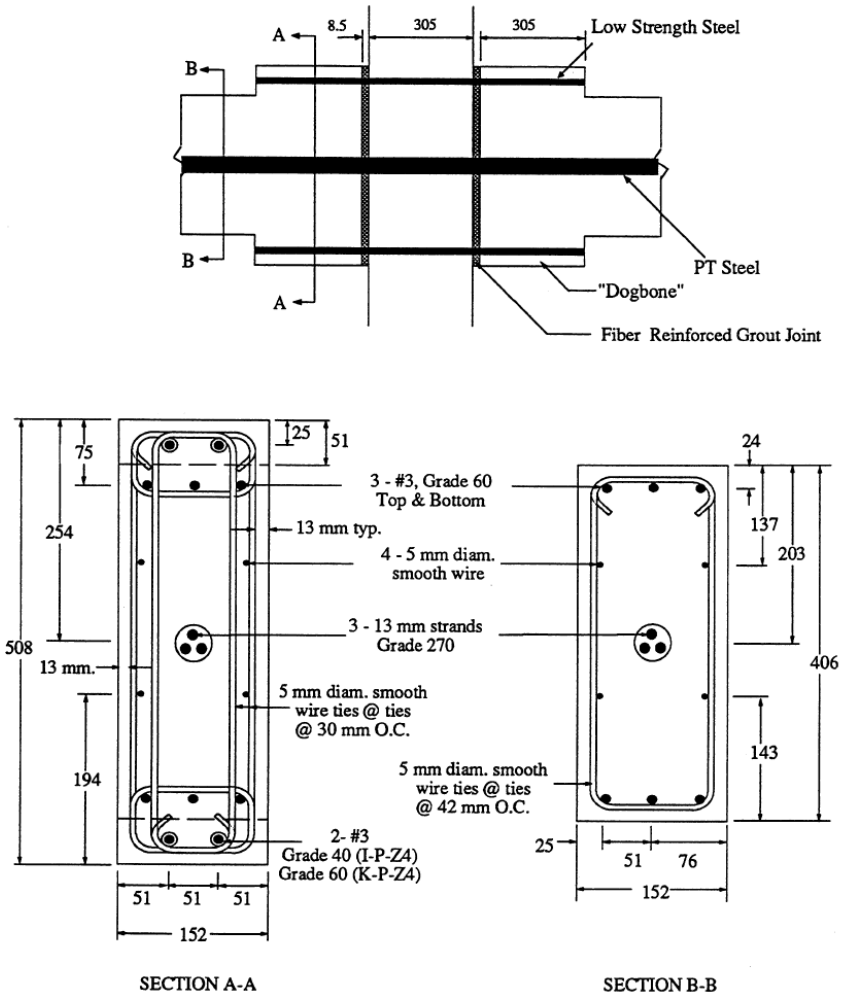

Figure 2-13: Detail for specimens I-P-Z4 and K-P-Z4 (Cheok et al., 1993).

The second design used unbonded post-tensioning bars and fully bonded mild steel reinforcement located in the dogbones. The design, which allowed for construction on a column-by-column basis, was called J-P-Z4 and is shown in Figure 2-14. Specimen J-P-Z4 failed due to fracture of the fully bonded mild steel reinforcement.

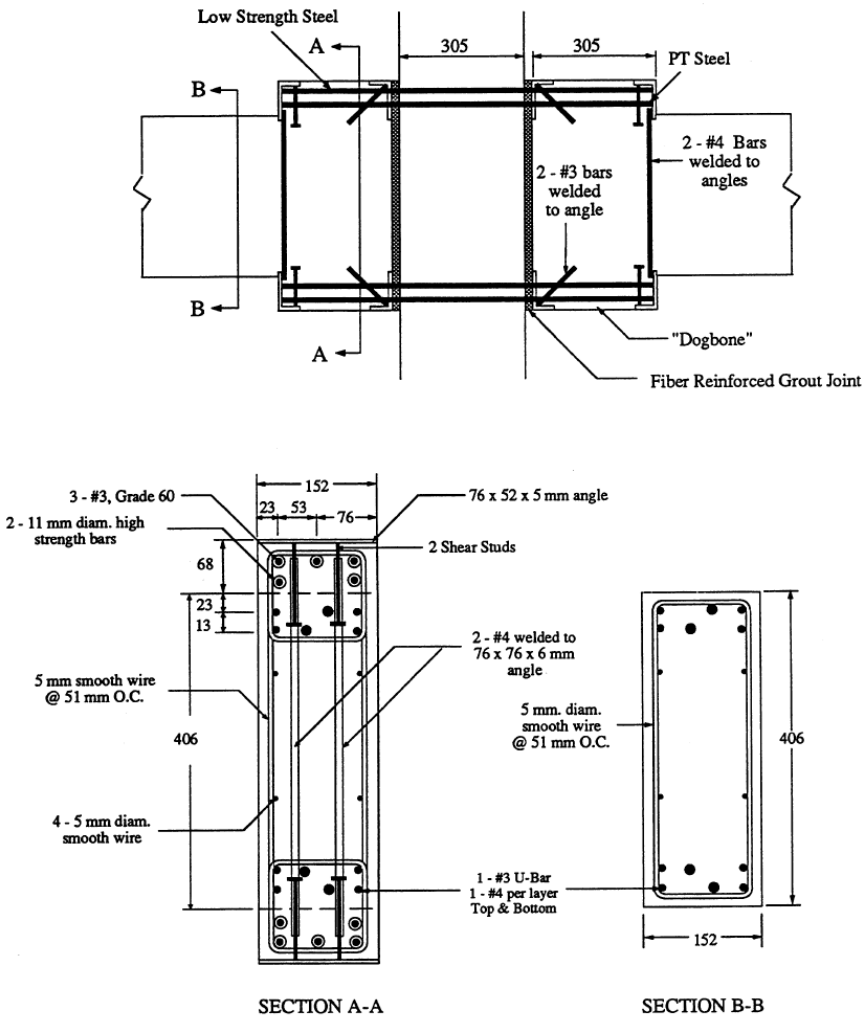

Figure 2-14: Details of specimen J-P-Z4 (Cheok et al., 1993).

The third design used replaceable unbonded post-tensioning bars and mild steel reinforcement located in the dogbones. In this manner, it was similar to specimen J-P-Z4 with the exception that the post-tensioning bars and mild steel reinforcement were replaceable at the end of a test, which enabled the same specimen to be tested three times. The three specimens were called L-P-Z4 A-C and are shown in Figure 2-15. Specimens L-P-Z4 A and B were not tested until failure; instead, these two specimen were used to trial mild steel reinforcement and post-tensioning bar combinations for specimen L-P-Z4 C, which was tested until failure. The failure of specimen L-P-Z4 C was by way of shear along the interface between the dogbones and the beam, which was an unintended failure mechanism.

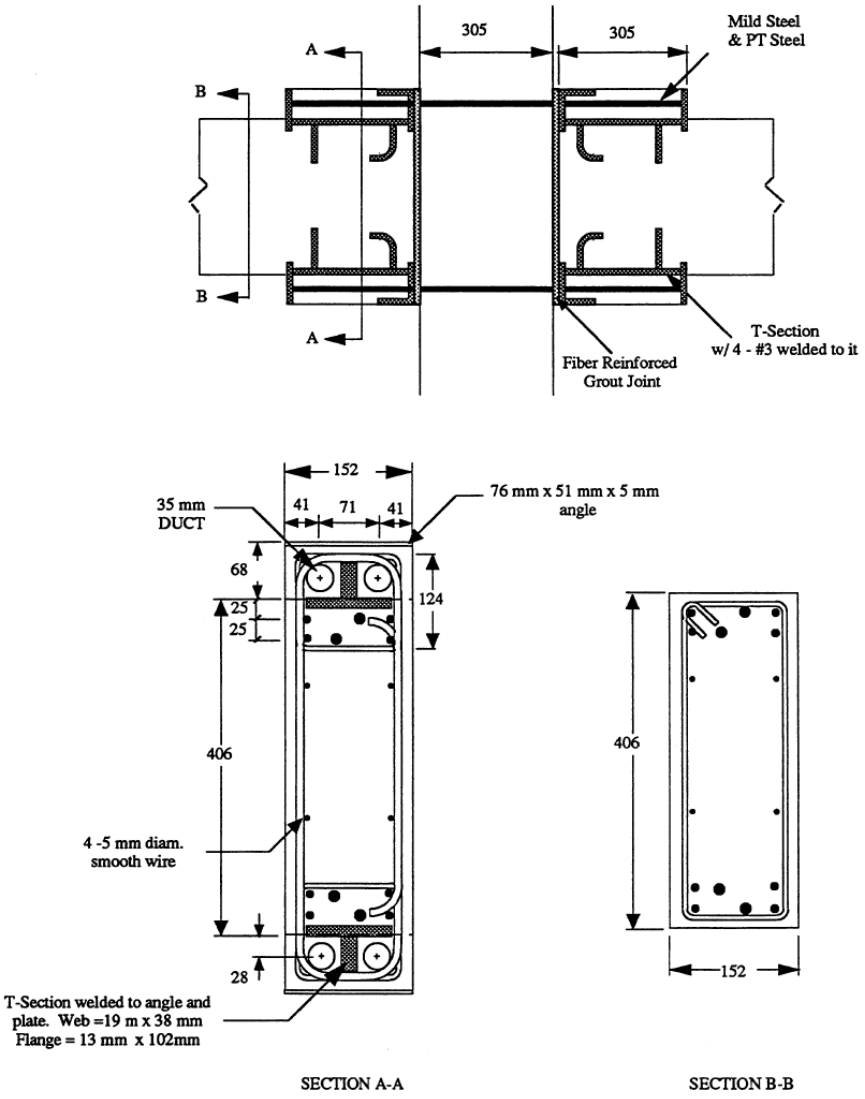

Figure 2-15: Details of specimen L-P-Z4 A-C (Cheok et al., 1993).

It was concluded from the phase IV A research that post-tensioning tendons extending through the entire member was more effective at reducing shear cracking than increased levels of transverse reinforcement. The energy dissipated by the connections tested in this phase was inferior to those tested in phase II.

In Phase IV B, four production type specimens that were manufactured by a commercial precast company and assembled at the NIST laboratory were tested (Cheok & Stone, 1994). The debonded post-tensioning tendons remained at the beam centroid and the amount and type of mild steel reinforcement was varied. Both mild steel and 304 stainless steel reinforcement were tested. The 304 stainless steel reinforcement was tested to determine if the increased ductility compared to mild steel reinforcement could prevent failure due to reinforcement fracture. The details of the four specimens tested in phase IV B are shown in Figure 2-16.

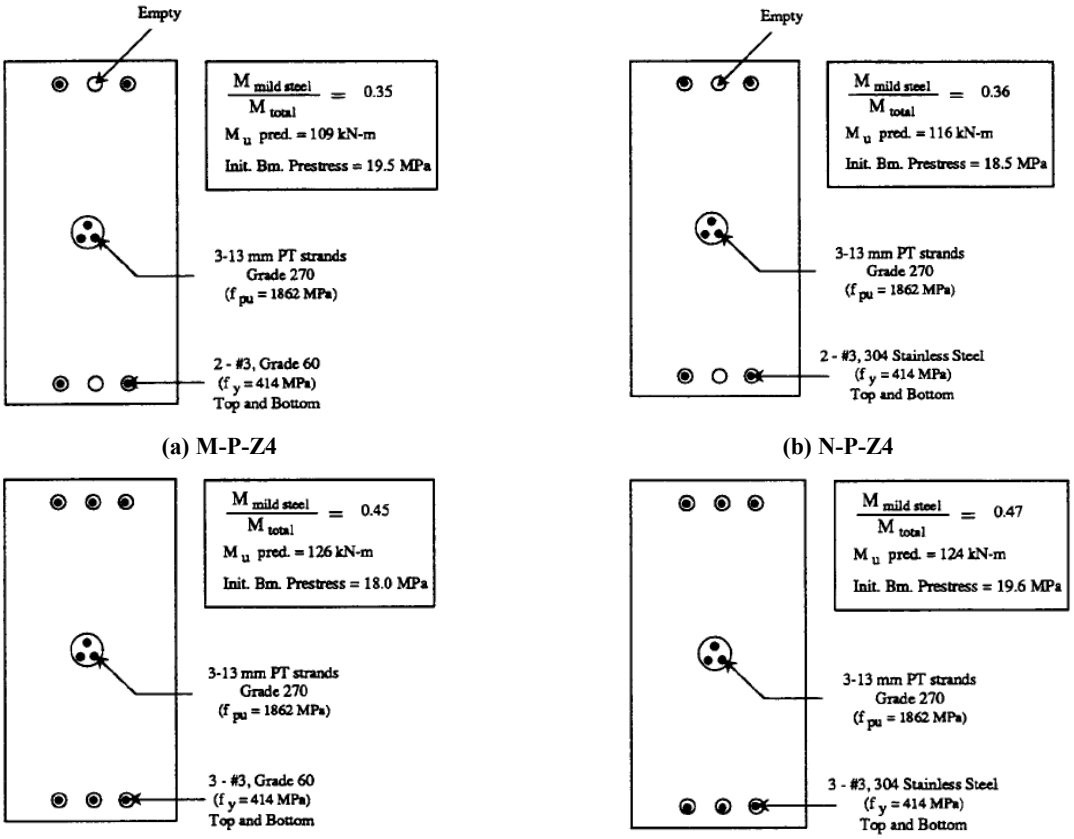

Figure 2-16: Details of specimens tested in Phase IV B (Cheok & Stone, 1994).

Specimen M-P-Z4 failed due to reinforcement fracture at 2.9% drift. Specimen N-P-Z4 failed due to reinforcement bond deterioration at 2.0% drift. O-P-Z4 and P-P-Z4 failed due to reinforcement fracture at 3.5% and 2.0% drifts respectively. The post-tensioning tendons in all specimens remained in the elastic range throughout the testing. Energy dissipation per cycle was greater than a comparable traditional connection for drifts less than approximately 1%, but was significantly less during the advanced stages of testing.

The NIST research program demonstrated that a hybrid connection can be designed to match or exceed the performance of a comparable traditional reinforced concrete connection (Cheok & Stone, 1994).

2.2.2 Precast Seismic Structural Systems Research Programme

The Precast Seismic Structural Systems (PRESSS) research programme was initiated in 1991 and was a coordinated research effort between the United States and Japan. The programme was initiated as part of the United States-Japan protocol on large scale testing for seismic response of precast concrete buildings, under the auspices of the United States-Japan Cooperative Program in Natural Resources (UJNR) Panel on Wind and Seismic Effects (Priestley, 1991).

The PRESSS programme had two fundamental objectives. The first objective was to develop comprehensive and rational design guidelines based on fundamental and basic research data that emphasised the viability of precast construction in various seismic zones. The second objective was to develop new materials, concepts and technologies for precast construction in various seismic zones (Priestley, 1991).

The PRESSS programme was conducted in three phases. The most promising structural concepts for precast concrete building systems in seismically active regions were identified and evaluated in phase I (Priestley, 1991). In phase II, detailed experimental studies of components and subassemblies were undertaken on the most promising connection details identified in phase I. In phase III, a 60% geometric scale five storey specimen, constructed using the connections developed during phase II was tested at the University of California, San Diego.

The connections tested during phase II were divided into four subcategories; tension/compression yielding, energy dissipating, nonlinear elastic and shear yielding (Priestley, 1996). The latter connection type was tested by Popov in steel frames with eccentric bracing, but not developed further in moment resisting frames in the PRESSS programme (Popov & Engelhart, 1988). Schematic examples of the connection types considered during phase II of the PRESSS programme are shown in Figure 2-17.

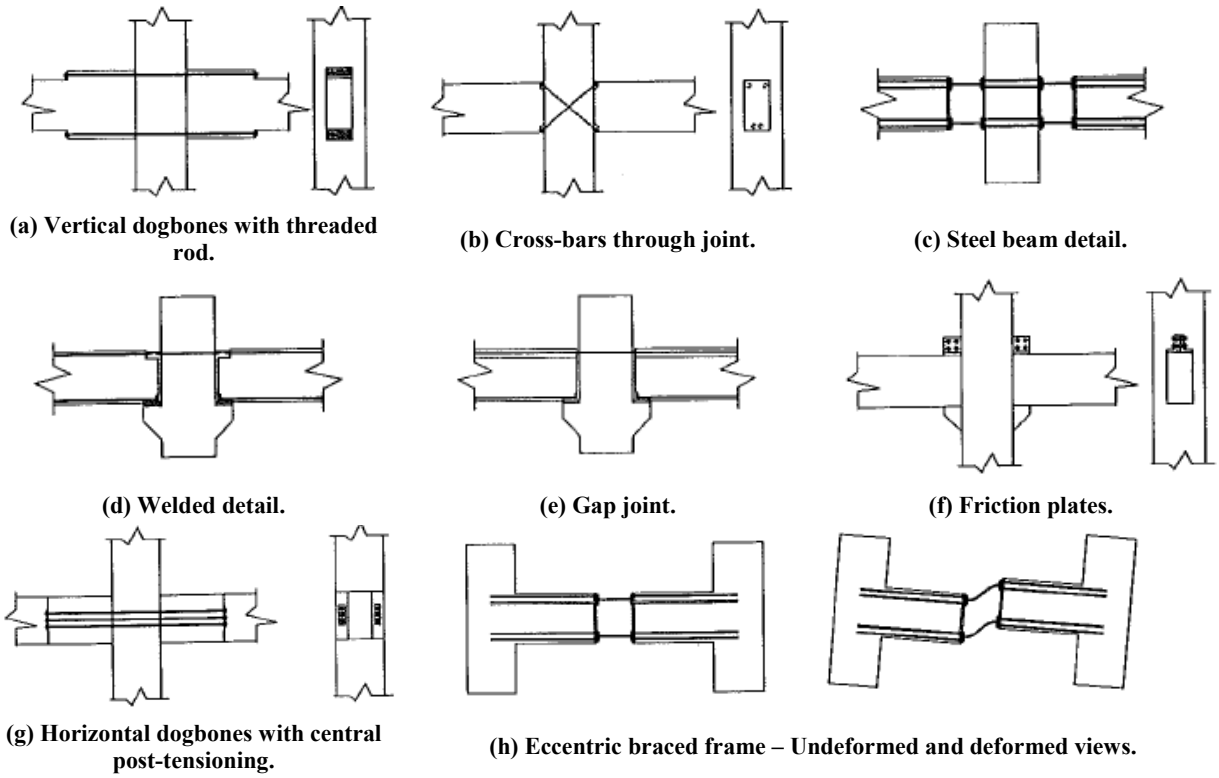

(a) Vertical dogbones with threaded rod.

(b) Cross-bars through joint.

(c) Steel beam detail.

(d) Welded detail.

(e) Gap joint.

(f) Friction plates.

(g) Horizontal dogbones with central post-tensioning.

(h) Eccentric braced frame – Undeformed and deformed views.

Figure 2-17: Connection types considered in phase two of this PRESSS programme (Palmieri et al., 1996).

2.2.2.1 PRESSS Tension-Compression Yielding Connections

Four examples of tension-compression yielding connections were tested; UT-GAP, UT-DB, UMn-Gap and UMn-TCY. UT-GAP was a gap-joint type system that was well received by the precast industry advisory group (Palmieri et al., 1996). The connection, shown in Figure 2-18, allowed rotation to occur about the base of the connection whilst gap opening or closing occurred at the top. The orientation of this connection, with the gap facing upwards, was considered favourable due to the ease of fabrication. Connection UT-GAP is especially relevant to the research described in this dissertation because it marked the first development of a slotted beam. The response of the connection was favourable; however, some pinching of the hysteresis loops was observed due to flexural and shear deformations of the vertical shear dowels (Palmieri et al., 1996). Positive flexural stiffness of the connection was less than the negative due to the beam end contacting the column face, which limited the deformation of the vertical shear dowels.

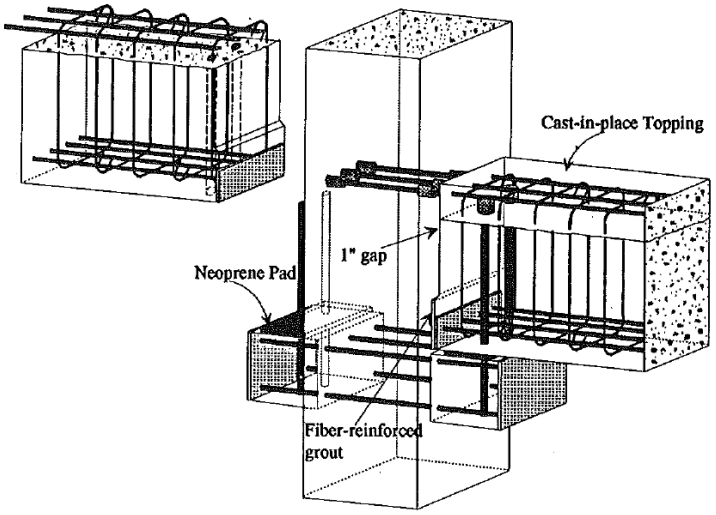

Figure 2-18: UT-GAP connection detail (Palmieri et al., 1996).

The UT-DB specimen used the same dogbone detail tested during the NIST program. As shown in Figure 2-19, connection UT-DB used high strength threaded rods secured between the dogbones and the column to provide moment resistance. During testing the connection performed poorly and failure occurred at approximately 1% drift. Prior to failure of the connection pinching of the hysteresis was observed. The failures of both UT-GAP and UT-DB were attributed to the use of connections that provided an indirect path for force transfer between precast elements.

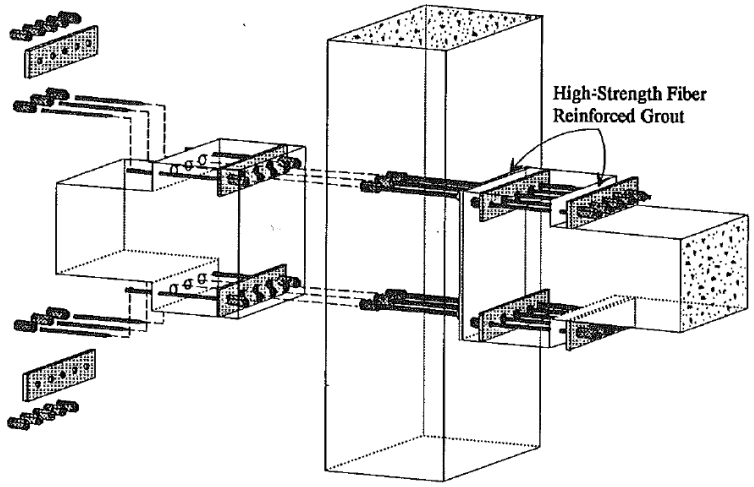

Figure 2-19: UT-DB connection detail (Palmieri et al., 1996).

Specimen UMn-TCY, shown in Figure 2-20, was a simple system that used block-outs in the beam to maintain reinforcement continuity through the column and avoid mechanical couplers. The top and bottom of the beams were cast insitu after the precast beam was installed between the longitudinal reinforcement, which was cast integral with the column. This specimen was similar to a traditional connection, except a discontinuity existed between the column and the beam where rotation could occur preferentially. Connection UMn-TCY performed well up to 4% drift; however, pinching of the response was observed due to bond slip, reinforcement buckling and relative vertical movement between the beam and column face.

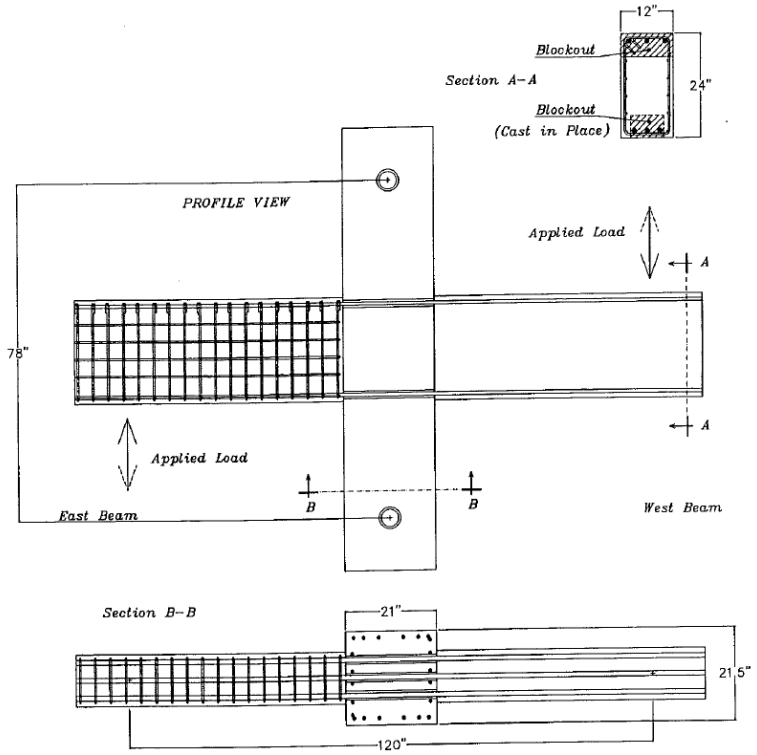

Figure 2-20: UMn-TCY connection detail (Palmieri et al., 1996).

Specimen UMn-GAP, shown in Figure 2-21, was a refined version of the gap-joint system. In the UMn-GAP connection, a gap was provided for ¾ of the beam height between the column face and the beam end to allow rotation to occur about the bottom of the beam. The vertical shear dowels used in connection UT-GAP were replaced by post-tensioning bars, which improved horizontal restraint and shear transfer via friction. The connection performed satisfactorily up to 2% drift, when fracture of the top mild steel reinforcement occurred at the face of the bar couplers. The inelastic demand in the top reinforcement of specimen UMn-GAP was larger than that in UT-GAP due to the stiffer connection between the beam and the column provided by the post-tensioning. It was noted that if the connection was inverted, then the lack of translation at the top surface would prevent large cracks from developing in the flooring system (Palmieri et al., 1996).

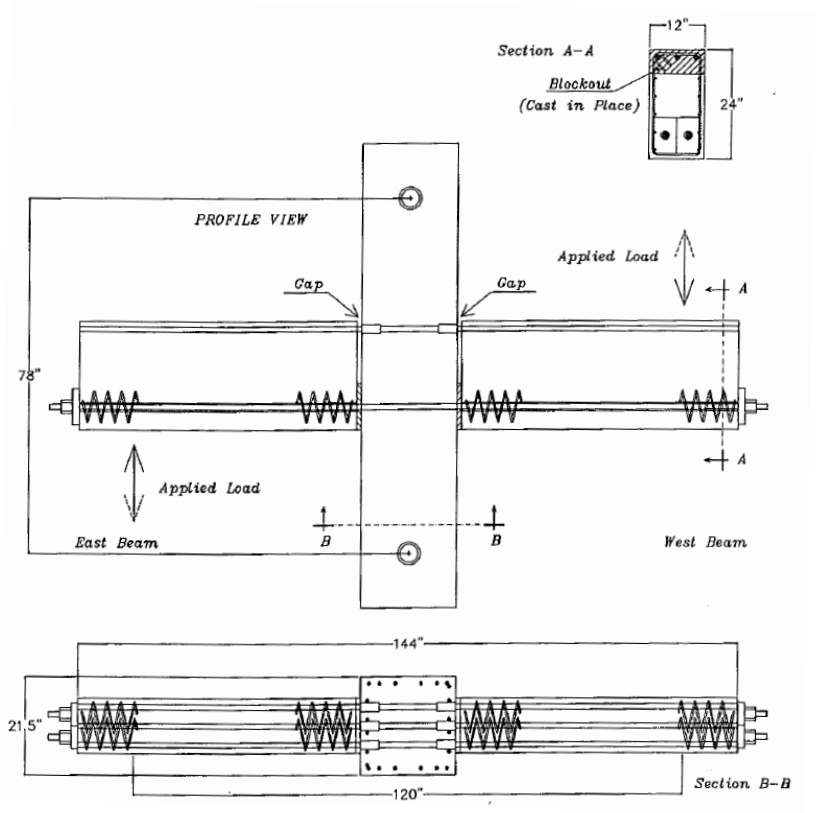

Figure 2-21: UMn-GAP connection detail (Palmieri et al., 1996).

2.2.2.2 PRESSS Energy Dissipating Connections

One specimen, UT-FR was tested incorporating special connection hardware to enhance energy dissipation. This connection, shown in Figure 2-22, was based on the design of specimen UT-GAP, except the corbel was improved to provide a direct load path and in place of top reinforcement an energy dissipation device was fitted. The energy dissipation device was based on research conducted in 1993 on sliding friction between steel plates (Grigorian et al., 1993). The force required to cause slip between the steel surfaces was controlled by the clamping force supplied by the bolts. The connection behaviour was acceptable during the

first two cycles to 3% drift and energy dissipation was higher than any other detail tested in the programme. Connection failure occurred during the third 3% drift cycle due to weld failure in the top plate connection. The weld failure was due to higher than anticipated forces being generated in the connection, which was caused by binding of the connection bolts in the slotted plates. It was concluded that proportions of connections between precast elements can be controlled by stiffness rather than strength (Palmieri et al., 1996).

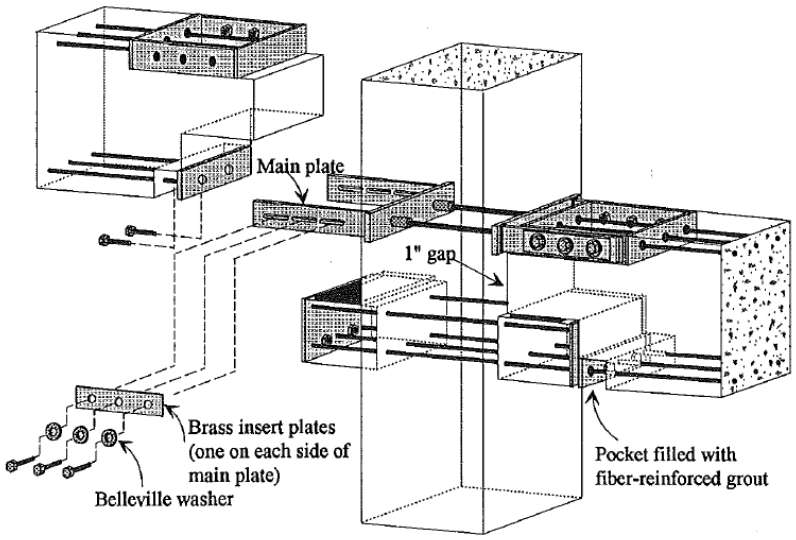

Figure 2-22: UT-FR connection detail (Palmieri et al., 1996).

2.2.2.3 PRESSS Nonlinear Elastic Connections

Three specimens were tested using nonlinear elastic connections; UMn-PTS, UMn-PTB and UT-PTS. UMn-PTS and UMn-PTB were identical apart from the method of post-tensioning and member sizes. UMn-PTS used post-tensioning tendons and UMn-PTB used post-tensioning bars. As shown in Figure 2-23, both specimens used dogbones located at the beam ends to accommodate the post-tensioning systems, which were unbonded through the dogbones and column. Both specimens performed well to the design 3% drift. During subsequent loading, UMn-PTS failed due to fracture of the post-tensioning tendons. UMn-PTB displayed stable hysteretic behaviour up to 5% drift.

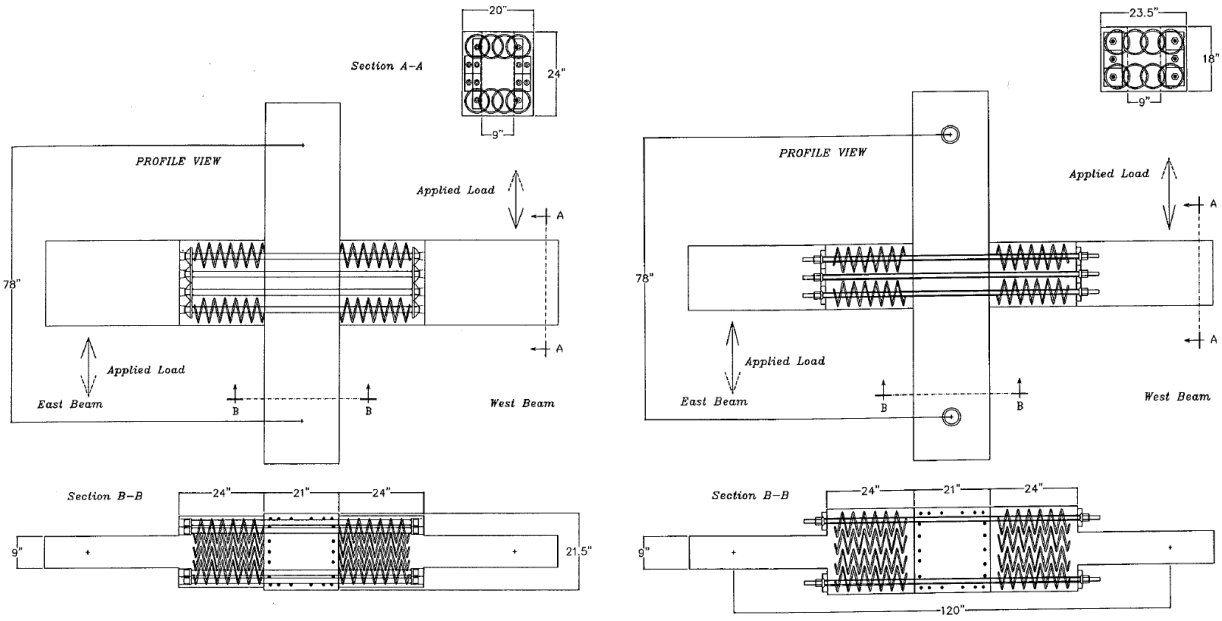

(a) UMn-PTS **(b) UMn-PTB**

Figure 2-23: UMn-PTS and UMn-PTB connection details (Palmieri et al., 1996).

Specimen UT-PTS, shown in Figure 2-24, was designed to display nonlinear elastic behaviour. Prestressed tendons, unbonded at the beam ends and through the column, were used in place of post-tensioned tendons. The construction method had to change from the columns being continuous through the beam-column joint to the beams being continuous, which required splicing of the column longitudinal reinforcement. The response of UT-PTS was similar to UT-PTS up to 2% drift; however, the hysteresis was more pinched due to slip in the column bar splices. Recorded energy dissipation above 2% drift was larger than anticipated due to failure in the joint region. The prestressed tendons remained elastic up to 5% drift, when the joint strength degraded and the test was halted.

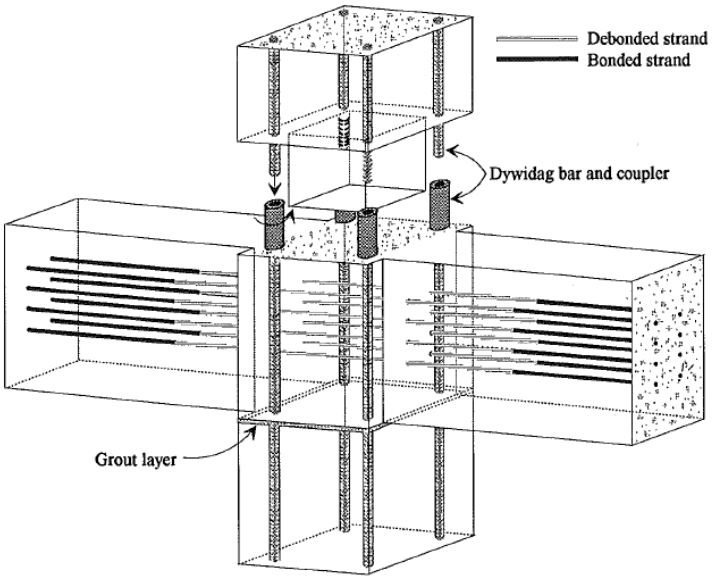

Figure 2-24: UT-PTS connection detail (Palmieri et al., 1996).

During phase III of the PRESSS programme, a 60% geometric scale five-storey specimen was tested at the University of California, San Diego. The completed test specimen is shown in

Figure 2-27. The objectives of this final phase were to; validate a rational design procedure for precast seismic structural systems, provide acceptance of prestressing of precast seismic systems, provide experimental proof of overall building seismic performance and establish a set of design recommendations for precast seismic structural systems (Nakaki et al., 1999).

The test structure was designed using direct displacement based design principles (DDBD), which were developed in response to the shortcomings of traditional force based design when designing for damage limit states. DDBD uses the secant stiffness of the structure to the target ultimate inelastic displacement, along with equivalent viscous damping, to more accurately predict structure response at predefined limit states (Priestley, 1998).

The lateral resistance of the specimen was provided by walls in one direction and moment frames in the other. The flooring system in the first three floors was provided by pre-topped double-tees and the top two floors used hollow-core with an insitu topping, as shown in Figure 2-25.

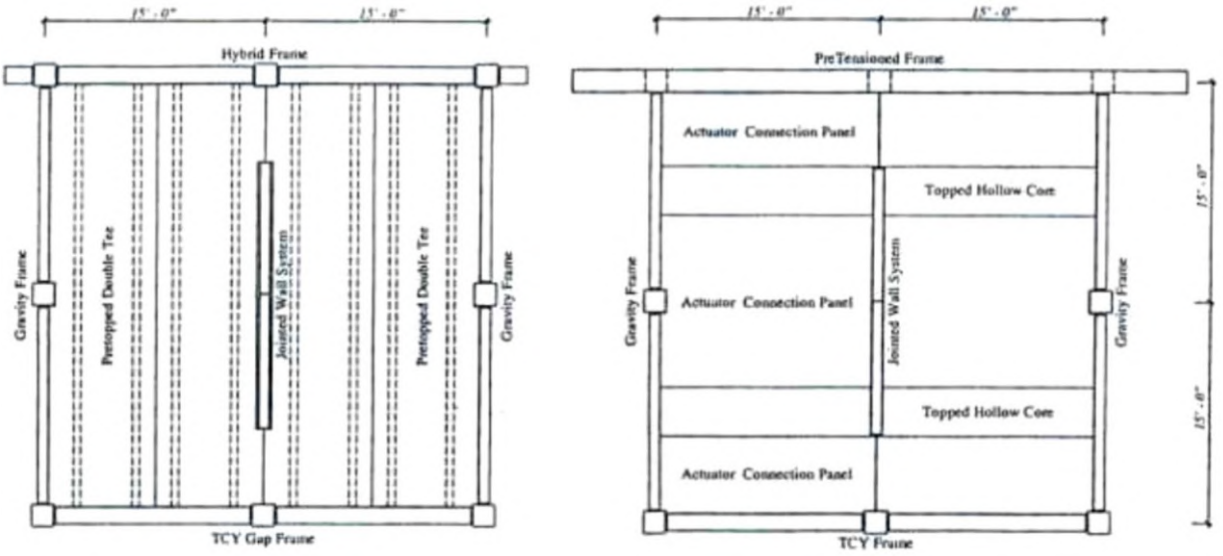

(a) Floors 1 to 3. **(b) Floors 4 and 5.**

Figure 2-25: Floor plans of PRESSS superassembly (Nakaki et al., 1999).

The moment frames were comprised of four connection details developed during phases I and II. As shown in Figure 2-25, the bottom three stories used hybrid and gapping connections, whilst the top two stories used pre-tensioned and tension-compression yielding connections.

Figure 2-26(a) shows the hybrid connection detail tested in the specimen, which was developed during the NIST research program (Cheok & Stone, 1994). The connection combined post-tensioning tendons and mild steel reinforcement to provide a connection with moment resistance, recentring and energy dissipation.

The pre-tensioned connection, shown in Figure 2-26(b), differed from the other connections in the specimen in that it used pre-tensioned tendons rather than post-tensioned. Prestressing required that both beam bays could be precast simultaneously off-site in a traditional stressing

bed, which had some construction advantages. The tendons were unbonded through the beam-column joint to promote an elastic response.

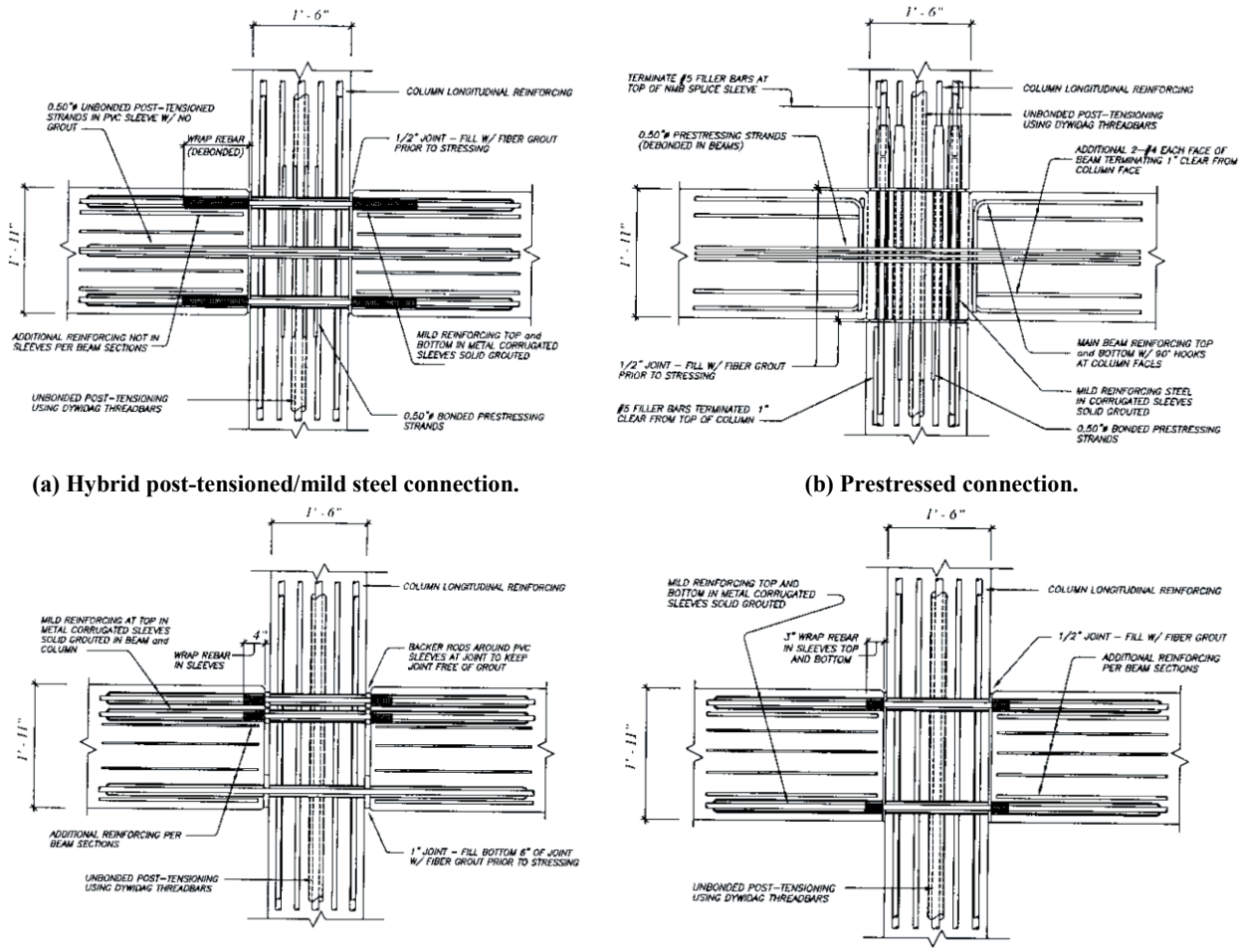

(a) Hybrid post-tensioned/mild steel connection.

(b) Prestressed connection.

(c) Tension-compression yielding gapping connection (TCY-GAP).

(d) Tension-compression yielding connection (TCY).

Figure 2-26: Moment connections tested in the PRESSS five-storey specimen (Nakaki et al., 1999).

The TCY-GAP connection detail, shown in Figure 2-26(c), was a modified version of the connection tested in phase II. Reinforcement fracture in the phase II specimen occurred at the connection between the reinforcement and the mechanical coupler, this detail was replaced with a grout sleeve to prevent this type of failure. Connection rotation occurred about the bottom of the section, which was founded on a fibre reinforced grout pad. Post-tensioning tendons were used to provide a reaction force to the force induced in the debonded top reinforcement, and to create adequate friction for shear resistance between the beam end and the column face.

The TCY connection, shown in Figure 2-26(d), was identical to that tested during phase II. Despite the pinched hysteresis loop obtained during testing, the connection was included because it was conceptually similar to traditional methods of construction (Nakaki et al., 1999).

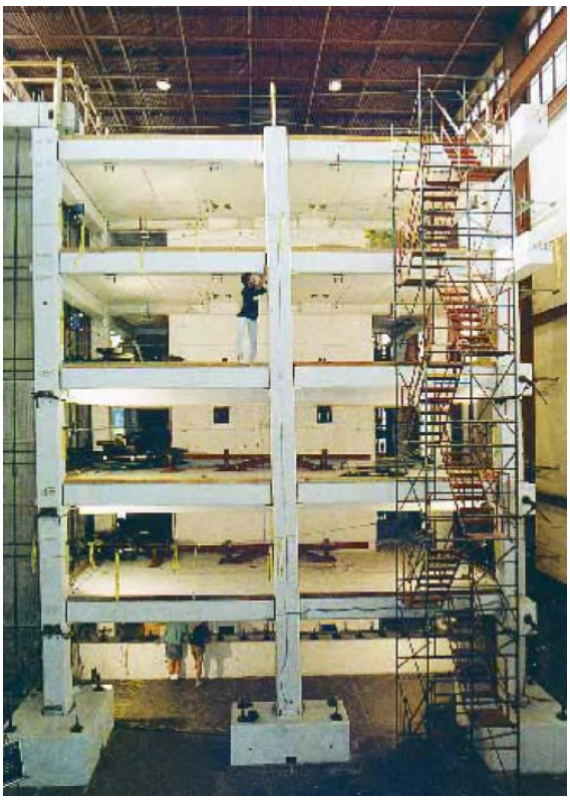

Figure 2-27: PRESSS five-storey test specimen during testing (Priestley et al., 1999).

The structural response of the PRESSS five-storey test specimen under simulated seismic loading was deemed extremely satisfactory (Priestley et al., 1999). Damage to the building in the frame direction was less than would be expected for an equivalent traditional reinforced concrete structure.

The hybrid frames were observed to behave very favourably; however, the beam underwent significant rotation about the longitudinal axis. The beam rotation was attributed to the large gravity load from the double-tee flooring units being applied eccentric to the beam centre of resistance. The torsional strength of the hybrid system primarily stemmed from the compression zone at the beam-column interface, which was shown to be insufficient to resist the demands.

The pre-tensioned connection performed extremely well and no repair would be required to this connection after a design level seismic event. Beam-column joint zone cracking was less in the pre-tensioned connection than the hybrid connection. Inelastic action was concentrated across a single crack that opened up near the reveals formed at the interface between the beam and column.

The TCY-GAP connection experienced significant spalling of the soffit and crushing of the fibre reinforced bearing pad, which was caused by sliding of the beam relative to the column face. Due to larger than expected forces in the mild steel reinforcement during positive flexure, larger reaction forces from the post-tensioning tendons were required, which reduced the post-tensioning force available to provide shear friction across the bottom hinge and

resulted in sliding at the interface. The mild steel reinforcement fractured in the later stages of testing due to the sliding displacement across the interface between the beam and column. Despite the damage observed, the behaviour of this connection was deemed satisfactory.

The behaviour of the TCY connection was similar to that observed during the phase II subassembly testing, where sliding of the beam end relative to the column face occurred and resulted in a pinching response.

The x-plate connections, which were used to connect the pre-topped double-tee flooring system to the supporting beams, performed well. However, the x-plate connections, which are shown in Figure 2-28, experienced large inelastic deformation during testing and as a result were left with significant permanent distortion at end of testing.

Figure 2-28: X-plate connector between pre-topped double-tee and supporting beam (Priestley et al., 1999).

During pseudo-dynamic testing, much larger floor forces were experienced than designed for. The increased forces stemmed from reduction factors for ductility being applied equally across all deformation modes, which led to a critical underestimation of diaphragm forces. The higher diaphragm forces caused column shear forces and moment distributions that were larger than allowed for during typical design using traditional inverted triangle base shear distribution (Priestley et al., 1999).

2.3 Precast Concrete Frame Research at the University of Canterbury

Research into the seismic behaviour of traditional precast reinforced concrete moment frames with prestressed flooring systems was initiated at the University of Canterbury in response to recommendations by the New Zealand study groups responsible for writing *Guidelines for the Use of Structural Precast Concrete in Buildings* (CAE, 1999; Matthews, 2004). Questions had been raised by the construction industry about the integrity of the New Zealand building stock following the poor performance of precast buildings during the 1994 Northridge earthquake (Norton et al., 1994; Corley, 1996). Of particular concern was the detail used to

connect hollow-core flooring systems to the lateral load resisting system. The failure of the Meadows Apartments car park structure during the Northridge earthquake, shown in Figure 2-29, highlighted the discrepancies between assumed and actual behaviour during seismic events. The brittle failure mechanisms observed were cause for concern in New Zealand, where the predominant connection detail used for hollow-core seating since the 1980s was similar to that used in California.

(a) Collapse of hollow-core floor.

(b) Web splitting in hollow-core.

Figure 2-29: Failure of hollow-core flooring at Meadows Apartment car park, Northridge 1994 (Norton et al., 1994).

Matthews (2004) investigated the seismic performance of a superassembly representative of typical New Zealand commercial buildings. The origin of the superassembly was the second storey of a ten storey prototype structure. The second storey was chosen over the first to avoid 'first floor effects'. First floor effects are the result of cumulative beam elongation along several bays of the first floor of a building. The beam elongation is resisted by the ground floor columns, which induces an axial force in the first floor beams. The superassembly was subsequently repaired and retested by Lindsay (2004), and rebuilt and tested by MacPherson (2005). Peng (2009) and Gardiner (2011) carried out numerical investigations on the mechanics of beam elongation within traditional reinforced concrete moment frames and floor diaphragm behaviour respectively. The work conducted by these researchers represented an important era of experimentation at the University of Canterbury.

2.3.1 Beam Elongation

Beam elongation occurs when plastic hinge zones form in traditional beams under cyclic loading. It has been well reported by previous research (Fenwick & Fong, 1979; Fenwick & Megget, 1993; Ingham et al., 2002; Matthews, 2004; Walker, 2007; Peng, 2009) and the underlying mechanics are described in Section 2.1.3.

It has been shown that beam elongation can increase the lateral resistance of a moment resisting frame and cause significant damage to the floor diaphragm (Fenwick et al., 1999; Matthews, 2004; Peng, 2009). The increase in lateral strength stems from two contributions; axial load in beams and activation of floor reinforcement.

Beam elongation is resisted by the floor diaphragm. The mechanism in the floor diaphragm that resists beam elongation is often termed deep beam action or the bowstring effect (Fenwick et al., 1999; Matthews, 2004; Peng, 2009). The resistance to beam elongation provided by the floor induces axial compression in the beams and tension in the floor. Axial compression increases the moment capacity of the beam by providing a force couple that resists both positive and negative flexure. During negative connection flexure, the floor reinforcement, which is resisting beam elongation, contributes to the connection overstrength moment within an effective flange width. The influence of the floor reinforcement on the flexural capacity of the adjacent connection is often termed the 'flange effect' or 'flange activation'. Flange activation is smaller during positive flexure due to the reduced lever arm between the floor reinforcement and the neutral axis. An increase in beam overstrength due to flange activation has been demonstrated experimentally to be as much as 100% of the nominal beam moment (Lindsay, 2004; Matthews, 2004; MacPherson, 2005; Peng, 2009). The large increase in connection flexural capacity is not fully accounted for when using NZS3101:2006 methods to evaluate the floor slab contribution to overstrength (Peng, 2009).

Beam elongation can cause significant damage to the floor diaphragm. The diaphragm damage is caused primarily by two mechanisms. The first is cracking at the interface between the connections and the floor diaphragm due to the diaphragm restraining the elongation of the beams. The second is loss of precast floor seating width due to the beams parallel to the precast floors elongating, which forces the beams supporting the floors apart. The consequence of damage to the floor diaphragm was graphically demonstrated during Matthews' (2004) experiment, which used floor details typical of construction in New Zealand. Beam elongation and damage to the precast floor seating caused such extensive damage to the floor diaphragm that complete loss of gravity support occurred, as shown in Figure 2-30.

(a) North-east perspective. **(b) East elevation.**

Figure 2-30: Complete collapse of precast floor during Matthews (2004) experiment.

Beam elongation is not unique to traditional moment resisting frames. Elongation is also observed in hybrid connections such as those tested during the PRESSS research programme (Priestley, 1991). Due to the low damage characteristics of hybrid connections, the material contribution to beam elongation is not significant. However, the geometric contribution can be significant in beams of reasonable depth when rocking behaviour occurs at the interface between the beam and column.

2.3.2 Displacement Incompatibility between the Seismic Frames and the Floor Diaphragm

Displacement incompatibly is a consequence of the difference in boundary conditions between the frame and the adjacent prestressed floor. The seismic beams are fixed at each end and deform in double curvature, whereas the one-way floors are effectively pinned at each end and deform in a sagging mode, as shown in Figure 2-31. Damage can result between the elements due to the incompatibly of the displacement modes.

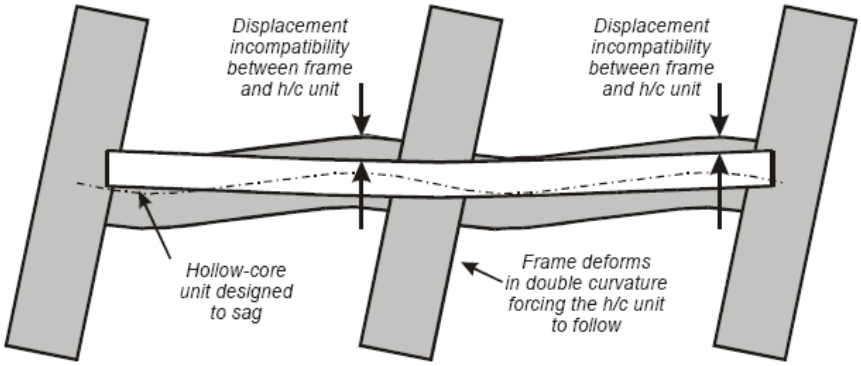

Figure 2-31: Displacement incompatibility between the frame and the first hollow-core unit (Matthews, 2004).

Displacement incompatibility was observed during experimentation by Matthews (2004) on a full scale traditional moment frame superassembly. Matthews placed the first hollow-core unit against the seismic beam, which was a construction detail that was common in New Zealand at the time and is shown in Figure 2-32(a). The hollow-core unit was not designed to deform in the same manner as the seismic beam and failed due to web splitting, causing the bottom of the unit to drop onto the laboratory floor below. Delamination of the topping concrete from the hollow-core units was observed in the experiment also.

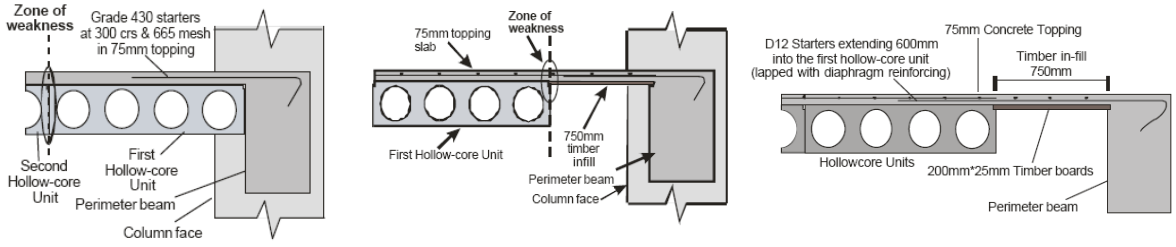

(a) Matthews (2004) detail. **(b) Lindsay (2004) detail.** **(c) MacPherson (2005) detail.**

Figure 2-32: Different connection details between parallel beam and hollow-core tested at University of Canterbury.

A Technical Advisory Group (TAG) was formed following Matthews' (2004) experimental programme to develop details to improve hollow-core performance. A flexible link was proposed by the TAG between the first hollow-core unit and the seismic beam to address displacement incompatibility. The link was designed to accommodate the relative displacements caused by the differences in deformation. The detail, shown in Figure 2-32(b), was tested by Lindsay (2004) and failed by tearing along the interface between the flexible link and the first hollow-core unit. Because the starter reinforcement length was insufficient to bridge the entire link, tensile diaphragm forces were unable to be transferred across the timber infill and diaphragm rupture occurred at the termination of the starter reinforcement. Because the timber infill detail is more flexible than the adjacent floor diaphragm, it is less effective at transferring compressive diaphragm forces. The timber infill should be designed to resist the worst case diaphragm forces induced by an earthquake. MacPherson (2005) tested a similar detail to Lindsay (2004), except the starter reinforcement was not terminated until midway across the first hollow-core unit, as shown in Figure 2-32(c). Performance of the link was satisfactory and the detail was implemented in the New Zealand Concrete Structures Standard (Standards New Zealand, 2006).

2.3.3 Precast Concrete Floor Unit Seating Details

The boundary conditions of hollow-core units have a significant effect on the performance of the floor during a seismic event. Excessive connection strength can rearrange the strength hierarchy and cause an undesirable brittle mechanism to form, whilst simple connections cannot offer structural redundancy.

The seating detail tested by Matthews (2004) was the typical detail used by the New Zealand construction industry at that time. The detail, shown in Figure 2-33, founded the hollow-core unit on a grout bed and plastic dams were placed in the hollow-core ends to allow the topping concrete to penetrate 75mm into the voids.

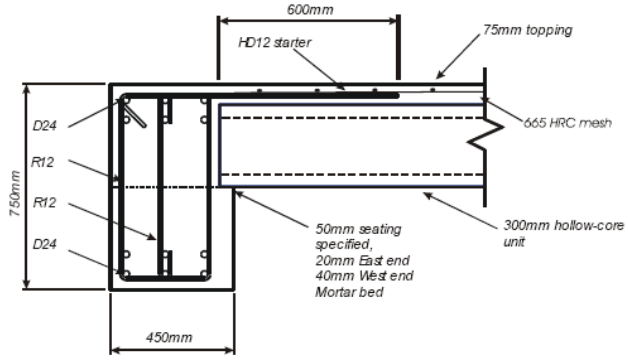

Figure 2-33: Hollow-core connection detail used by Matthews (2004).

The experimental program highlighted discrepancies between assumed deformation modes and actual. In design, the hollow-core end was assumed to be able to rotate and slide on the

grout pad; however, Matthews (2004) experiment showed that fixity was provided by the connection, as shown in Figure 2-34. The moment connection at the hollow-core end, termed a 'continuity moment', resulted in failure by way of brittle snapping of the hollow-core unit, which led to collapse, as shown in Figure 2-30. The TAG recommended two possible connection detailing changes which were tested in subassemblies by Bull and Matthews (2003). The experimentation demonstrated the improved seating details performed well and it was recommended further testing of both details be undertaken using the same three-dimensional superassembly that Matthews (2004) had used.

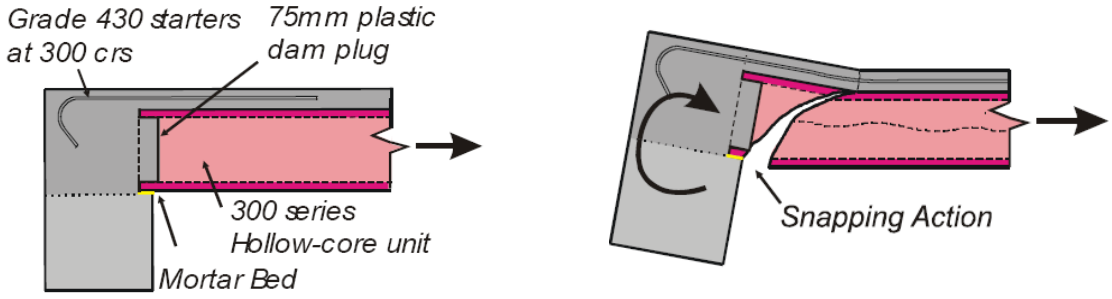

(a) Assumed behaviour. **(b) Observed behaviour.**

Figure 2-34: Assumed and actual deformation behaviour of hollow-core connection tested by Matthews (2004) (Lindsay, 2004).

The first proposed detail to address this issue was tested by Lindsay (2004) and is shown in Figure 2-35. The detail prevents the topping concrete entering the hollow-core voids, provides a slip surface on which the unit is founded and allows space between the unit end and the supporting beam face for both positive and negative relative rotations. The connection performed well during the experiment; however, the low-friction bearing strip was not adequately affixed to the beam and slid with the hollow-core unit. A new bearing strip that had a higher coefficient of friction on the bottom than the top, or was bonded to the beam, was recommended to prevent the movement.

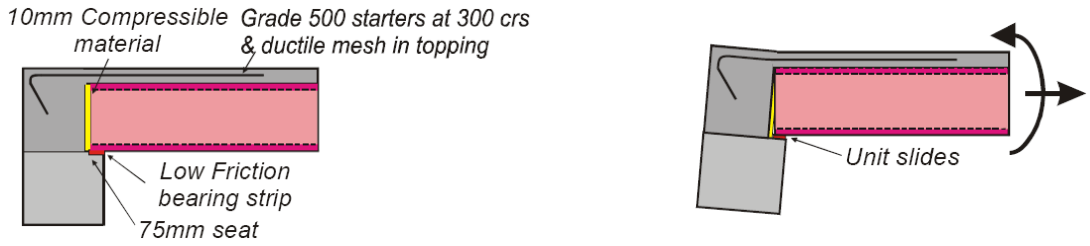

(a) Improved detail. **(b) Observed behaviour.**

Figure 2-35: Improved detail and deformation behaviour of hollow-core connection tested by Lindsay (2004).

The second detail recommended to address the connection issue encountered in the Matthews (2004) experiment was tested by MacPherson (2005). The detail, shown in Figure 2-36, founded the hollow-core unit on a low-friction bearing strip in a similar manner to the detail tested by Lindsay (2004). However, two of the hollow-core unit voids were broken out over a length three times the unit depth, R16 reinforcement was placed in the bottom of the void and the broken out voids were filled with topping concrete. The cores that were not filled had a

bond breaker installed across the entrance to prevent a moment connection between the hollow-core end and the supporting beam being established.

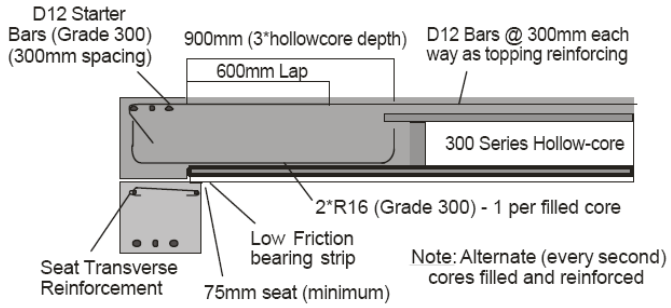

Figure 2-36: Improved hollow-core connection detail tested by MacPherson (2005).

The detail tested by MacPherson (2005) offered a degree of redundancy against loss of seating that was not available in the detail tested by Lindsay (2004), which was particularly important when the effects of beam elongation were considered. If the seating of the hollow-core unit was lost, the reinforcement installed in the voids could act in tension to prevent complete collapse. The connection performed well during experimentation and was subsequently implemented into the New Zealand Concrete Structures Standard (Standards New Zealand, 2006).

2.3.4 Floor Diaphragm Warping

Floor warping occurs in a frame during in-plane lateral drifts when, due to the inclination, one side of the column rises relative to the other, as shown in Figure 2-37(a). The difference in displacement can be significant for large column depths, which are often required when using slotted beams. During drifts out-of-plane, as shown in Figure 2-37(b), the inclination of the beam and column can cause the supporting edge of the beam to rise and move away from the floor. During biaxial displacement, the warping deformation modes combine and have the potential to cause significant damage to the floor diaphragm.

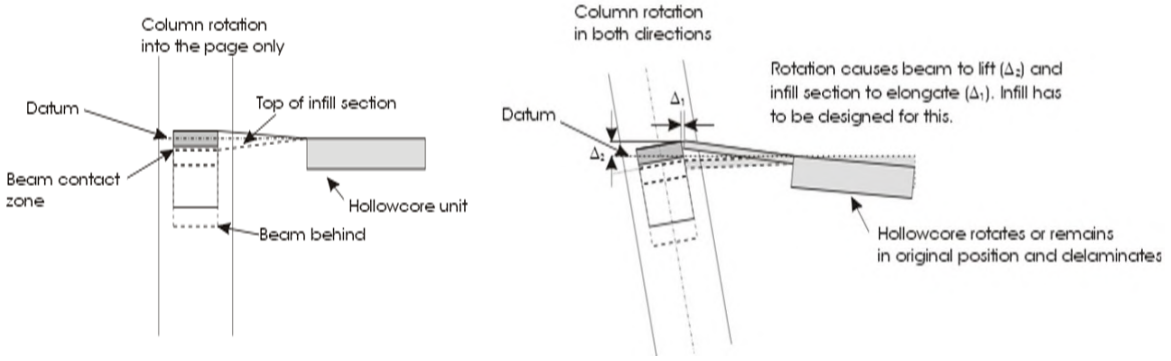

(a) Warping due to in-plane drift. **(b) Warping due to out-of-plane drift.**

Figure 2-37: Floor warping in reinforced concrete structures with timber infill (Bull, 2007).

A flexible infill is used to accommodate the differences in displacement between the elements. The infill is designed to be able to deform adequately under design level displacements, whilst minimising the damage it sustains. The designer must also consider the

possibility of inducing delamination between the topping slab and the prestressed precast flooring due to excessive infill displacements.

2.3.5 Beam Torsion

Beam torsion in structures with a one-way precast flooring system is caused by three mechanisms. The first is rotation of the beams relative to the precast floor. Because the floor is connected to the supporting beam with some rotational fixity, the imposed rotation induces a moment. This mechanism is shown in Figure 2-38. The second mechanism is the application of the floor gravity load eccentric to the supporting beam centre of resistance, which creates a moment. The third is beam elongation which induces tension in the floor, unless this tension force resultant is coincident with the supporting beam centre of resistance a moment is created. The application of moments from the floor seating connection along the length of the supporting beam results in beam torsion.

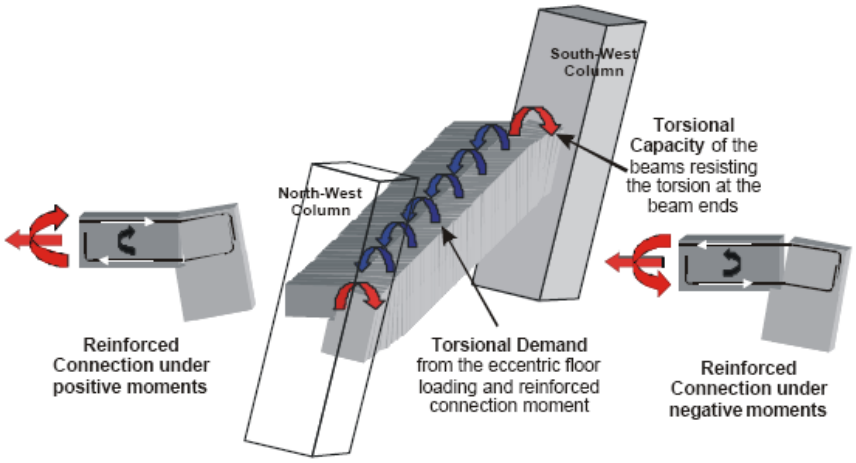

Figure 2-38: Torsional demand and capacity in a traditional reinforced concrete connection (MacPherson, 2005).

During the Matthews (2004) and Lindsay (2004) experiments, the torsion along the transverse beam was observed to increase approximately linearly from the middle of the span to the column face, as shown in Figure 2-39. The beam torsion observed in the experiments was similar despite the continuity moment from the hollow-core connection being substantially reduced in the Lindsay (2004) experiment compared to the Matthews (2004) experiment.

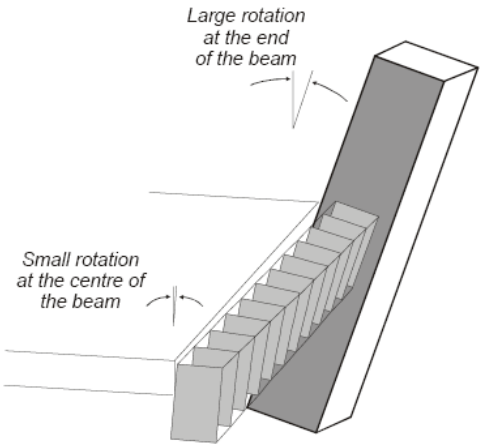

Figure 2-39: Beam torsion behaviour observed in Matthews and Lindsay experiments (Lindsay, 2004).

The torsional behaviour of the supporting beams in the MacPherson (2005) experiment was different than observed in the Matthews (2004) and Lindsay (2004) experiments. Instead of the torsion being evenly distributed over the length, it was concentrated over the plastic hinge zones whilst the remainder of the beams stayed approximately upright, as shown in Figure 2-40. The beams in the MacPherson (2005) experiment used Grade 500 longitudinal reinforcement, whereas Grade 300 was used in the Matthews (2004) and Lindsay (2004) experiments. The beams in all three experiments were designed to have similar moment capacities. Hence, the reduced longitudinal steel content in the beams of the MacPherson (2005) experiment caused a decrease in the torsional strength, which resulted in beam torsion being distributed over the beam plastic hinge zone lengths rather than over the entire beam lengths.

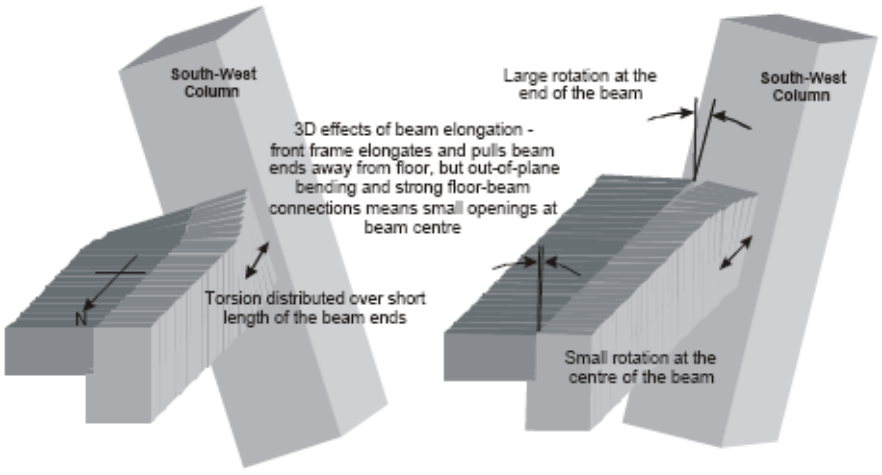

Figure 2-40: Beam torsion behaviour observed in MacPherson experiment (MacPherson, 2005).

Peng (2009) tested a reinforced concrete moment frame similar in geometry to the tests by Matthews (2004), Lindsay (2004) and MacPherson (2005). However, Peng's specimen was scaled at 2/3 geometrically, used a rib and infill flooring system and had a central transverse beam. The differences between the experiments meant that beam torsion was applied in a different manner. The transverse beams being rotationally fixed at one end whilst being

subjected to column rotation at the other induced beam torsion, rather than the continuity moment from the flooring system. Figure 2-41 presents deformation data along the top of transverse beam centrelines due to torsion at 4% column drift. Torsional rotation in the external transverse beams was larger in one direction than the other and torsion decreased more rapidly when it imposed compression in the floor slab (Peng, 2009).

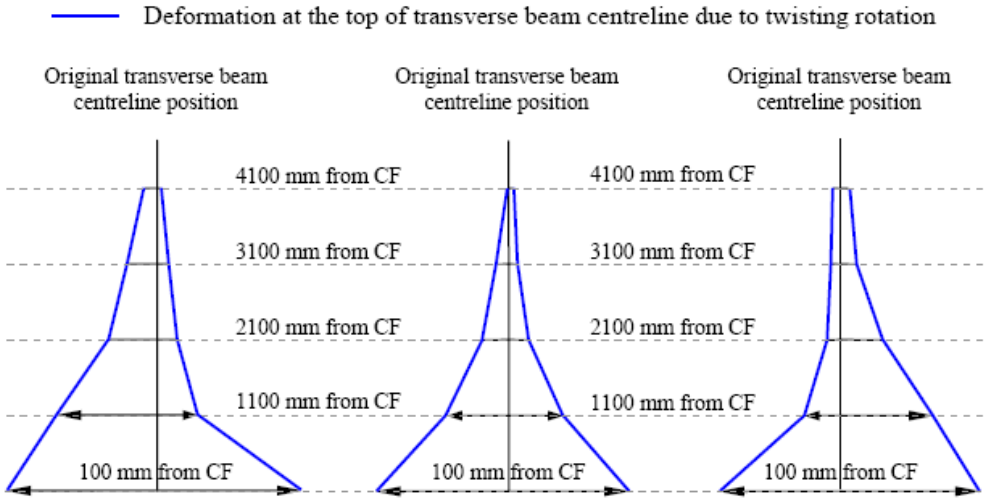

(a) West transverse beam **(b) Centre transverse beam** **(c) East transverse beam**

Figure 2-41: Deformation along the top of transverse beams centreline due to torsion at peak 4% drift cycle (Peng, 2009).

The boundary conditions of the Matthews (2004) and Peng (2009) tests were not truly representative of a real structure. The applied displacements were uniaxial along one bay only; hence, the transverse beams had to be restrained by some means at the unloaded end. In the case of the Matthews (2004) experiment, the unloaded bay had been designed to represent the remainder of the prototype structure and was restrained in the transverse direction only. However, in the experiment by Peng (2009) the transverse beams were restrained in the transverse direction and rotationally. The boundary conditions in these experiments, particularly those in the Peng (2009) experiment, could have induced rotational demands in the beams that are greater than would be expected in a real structure.

Beam torsion is especially relevant to slotted beam structures given the reduced concrete area of the connection between the beam and column, which reduces the shear and torsional capacity of the section compared to a traditional connection. Diagonal hanger reinforcement is required to transfer actions from the beam to the column. Diligent and rational design of the diagonal hangers is required to elastically resist these actions.

2.4 The Development of Non-tearing Floor Solutions

Non-tearing floor solutions are a broad category of details that aim to limit the damage sustained by the floor diaphragm during a seismic event. Non-tearing floor solutions can be further divided into two subcategories; articulated floors and gapping frames. Articulated

floors protect the floors from damage by isolating them from the elongating beams. Gapping frames minimise beam elongation so that a traditional frame to floor connection can be used.

2.4.1 Articulated Floor System

The concept of articulated floors was conceived during phase III of the PRESSS programme, where x-plate connectors were used between the pre-topped double-tee floors and the supporting beams. This system was discussed in Section 2.2.2, and the x-plate connector can be seen in Figure 2-28. The connection underwent large inelastic deformation during testing and had significant plastic deformation at the end of testing (Priestley et al., 1999). How the x-plate connected the floors to the beams resulted in the application of a significant torsional moment to the supporting beams. The torsional moment applied to the beams was a result of the force from the floor gravity load and the tensile force from the connector being applied eccentric to the beam centre of resistance, which is illustrated in Figure 2-42. The resultant torsional moment caused rotation of the beam during testing.

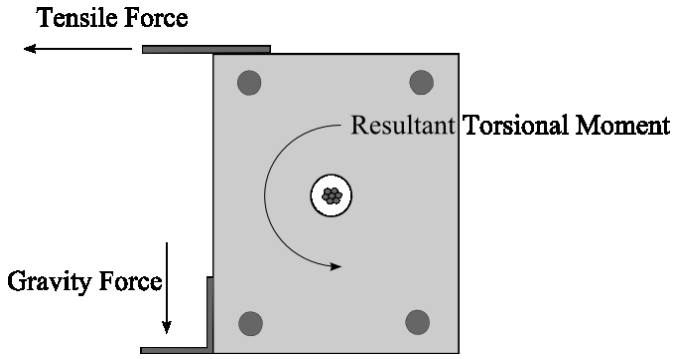

Figure 2-42: Beam torsional moment from x-plate double-tee connectors.

Cyclic in-plane shear loading of connectors such as the x-plate can cause a reduction in shear deformation capacity and ductility (Pincheira et al., 2005). Hence, monotonic capacity values cannot be used for design. It is likely that the connectors would need replacing after a significant seismic event.

The shear key system extended the x-plate connector concept by uncoupling the parallel and orthogonal components of the force transferred between the floor and the frame. This system, shown in Figure 2-43, reduced the torsional moment applied to the supporting beam by not only applying the floor gravity loads near the centre of resistance of the beam, but also providing near zero connection stiffness in the direction orthogonal to the supporting beam (Pampanin et al., 2006).

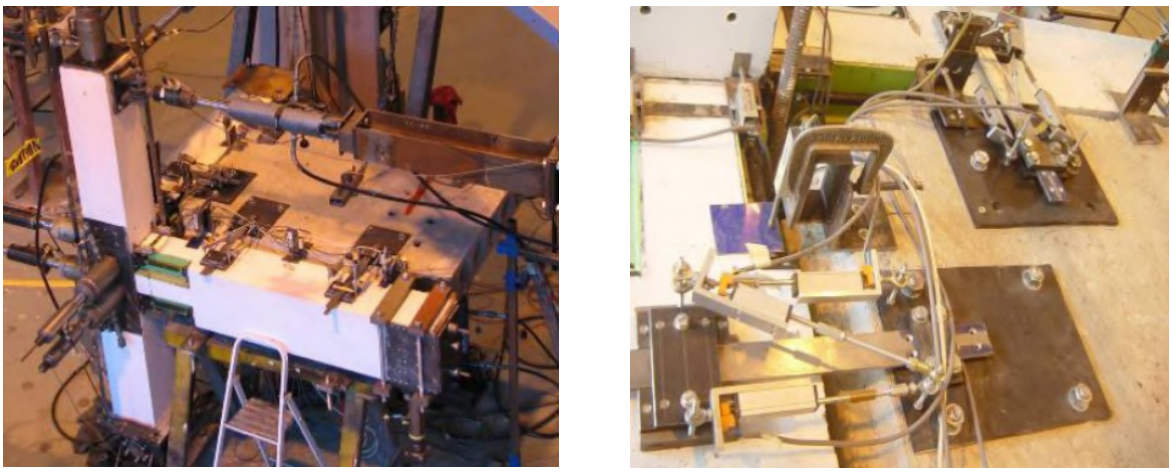

(a) Biaxial specimen setup. (b) Detail of shear key system.

Figure 2-43: Shear key articulated floor system (Amaris et al., 2008).

The system was shown to perform well experimentally, with no perceivable difference in response between the bare subassembly and the subassembly with the floor (Pampanin et al., 2006). However, the system may be impracticable within a structure and is uneconomic to construct compared to traditional details.

2.4.2 Gapping Frame Systems

Articulated floors isolate the floors from the elongation of the frames, whereas gapping frames reduce the elongation so that traditional flooring systems may be used. Because gapping frames reduce beam elongation, other undesirable effects on the frame are reduced also.

2.4.2.1 Post-tensioned Gapping Frames

The first gapping connection was developed during phase I of the PRESSS programme. The UT-GAP connection, shown in Figure 2-18, was well received by the precast industry during workshops (Palmieri et al., 1996). During the PRESSS programme, the UT-GAP connection was developed into the TCY-GAP connection, which was tested during phase III. The connection behaviour was satisfactory despite pinching due to insufficient post-tensioning force. The development of the TCY-GAP connection is presented in more detail in Section 2.2.2.

Post-tensioned gapping connections were subsequently tested at the University of Canterbury by Amaris et al. (2007, 2008). The detail, shown in Figure 2-44, differed from the TCY-GAP connection by having the top hinge constructed from structural steel and located at the top of the beam section. The steel top hinge meant that shear was not transferred through friction, which had proven unreliable during the PRESSS programme.

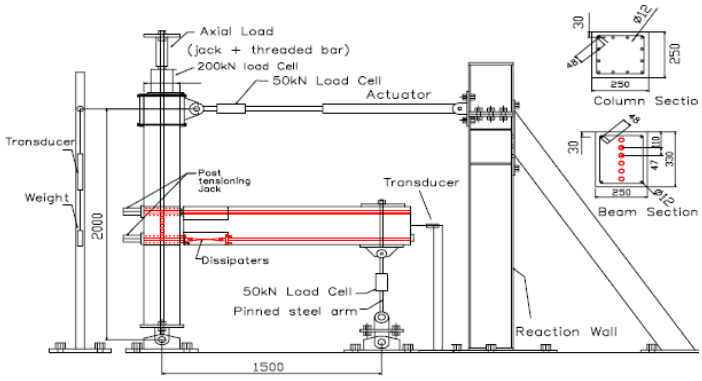

(a) Post-tensioned gapping frame with straight tendons experimental setup.

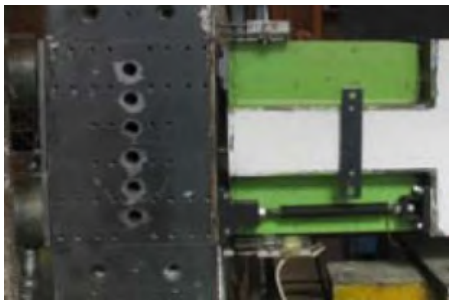

(b) Detail of post-tensioned gapping frame with straight tendons

Figure 2-44: Post-tensioned gapping frame with straight tendons (Amaris et al., 2007).

The connection performed well during testing; however, the absence of recentring behaviour prompted a change in the post-tensioning tendon profile from straight to draped. The recentring post-tensioned gapping frame specimen can be seen in Figure 2-45.

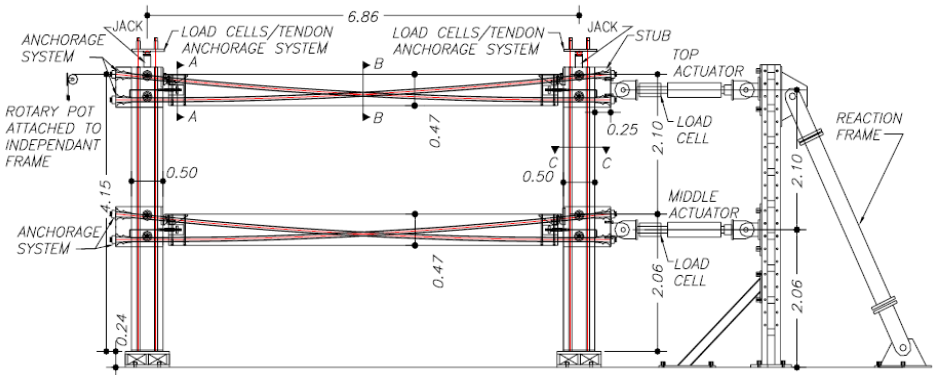

(a) Recentring post-tensioned gapping frame experimental setup.

(b) Specimen prior to testing.

Figure 2-45: Recentring post-tensioned gapping frame with anti-symmetric tendons (Amaris et al., 2008).

The draped post-tensioning tendons provided connection recentring as well as moment capacity. External mild steel dampers were used for energy dissipation. The connection details are shown in Figure 2-46.

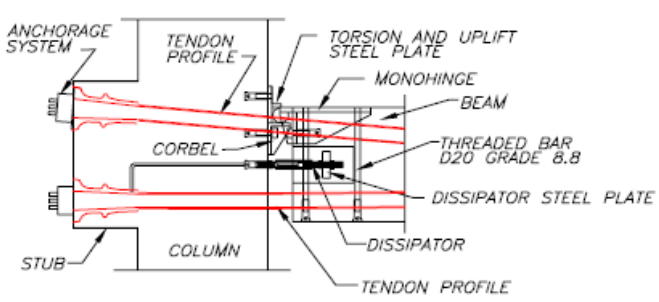

(a) Connection details.

(b) Connection prior to testing.

Figure 2-46: Details of recentring post-tensioned gapping connection (Amaris et al., 2008).

The connection performed well experimentally, with a stable hysteresis and negligible beam elongation. An analytical model was created and compared favourably with experimental results. However, connection construction practicality issues were cited (Amaris et al., 2008).

2.4.2.2 Japanese Gapping Frame Research

The gapping connection, herein referred to as a slotted beam, in reinforced concrete originated in Japan. The slotted beam was developed following the Kobe earthquake of January 17th 1995. This damaging earthquake left many relatively modern traditional reinforced concrete structures with significant repair costs due to cracking caused by flexural inelastic mechanisms, a situation which was experienced also in New Zealand following the 22nd February Christchurch earthquake (Kam et al., 2012). The slotted beam was an effort to reduce damage in reinforced concrete structures caused by the formation of inelastic flexural mechanisms (Ohkubo, 2004). By reducing damage, building downtime and repair costs could be reduced after damaging earthquakes.

The first clear example of a slotted beam was published by Matsuoka and Ohkubo (1996). The connection, shown in Figure 2-47(a), had a slot up the column face extending half of the beam depth. The width of the slot provided was in excess of what was required to satisfy design rotation demands. Five different connection configurations were tested: one traditional connection version and four slotted beam connection versions. It can be seen in Figure 2-47(b) that the slotted beams had a strength ratio between the top and bottom longitudinal reinforcement of two, which was provided to limit the strain in the top reinforcement and reduce cracking. The issue of shear transfer in a slotted beam was recognised, and addressed through the use of a diagonal hanger and an external transverse tie. However, it is likely that the diagonal hanger did little due to the lack of development length. Because 50% of the section depth remained in the connection, it was likely that a traditional equivalent truss mechanism formed to transfer shear between the beam and column.

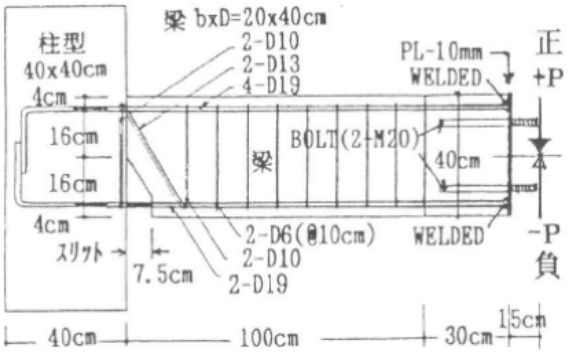

(a) Original slotted beam test specimen.

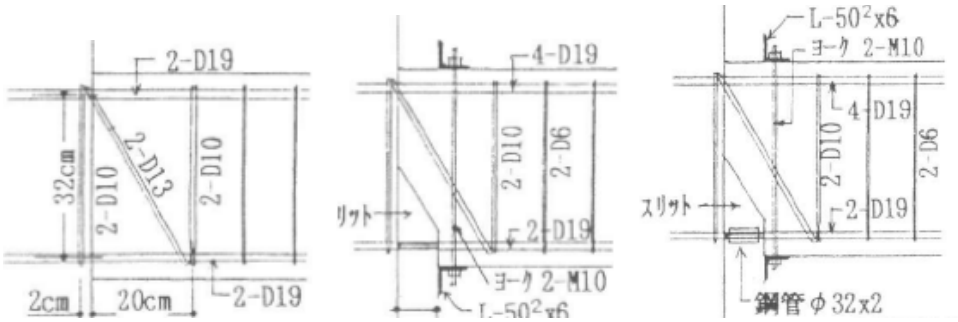

(b) Connection configurations tested, left to right; traditional, slotted and slotted with buckling restraint.

Figure 2-47: Details of original reinforced concrete slotted beam experiments (Matsuoka & Ohkubo, 1996).

The role of the external transverse reinforcement is unclear. The same role could have been achieved using traditional internal stirrups as used in the remainder of the beam. The final specimen tested used a steel sleeve over the longitudinal reinforcement in the slot as a primitive buckling restraint device.

The experimental results were encouraging, with the slotted beam detail showing comparable levels of performance to the traditional connection. A more stable hysteretic response was obtained for the specimen with reinforcement buckling restraint compared to those without it.

The next generation of slotted beam research concentrated on improving the hysteretic response and reducing damage. An important modification was the increase in slot depth and a decrease in the slot width, as shown in Figure 2-48 (Ohkubo & Zhang, 1997). The geometry modification reduced the variation in neutral axis depth for positive and negative flexure, which reduced cracking and beam elongation. During the experimental programme, six specimens were tested: one traditional connection version and five slotted beam connection versions. The slotted specimens had different configurations of diagonal shear reinforcement and of bottom longitudinal reinforcement debonded length.

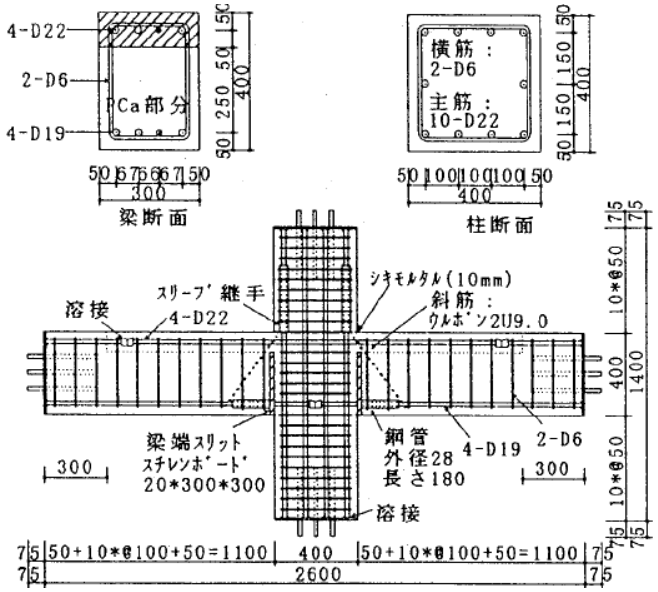

Figure 2-48: Second generation slotted beam (Ohkubo & Zhang, 1997).

In general, the shorter the unbonded length provided, the greater the strength degradation in the later stages on testing. The inclusion of shear hangers had little effect on specimen performance, which was likely due to insufficient development length rendering them ineffective. Damage sustained by the slotted specimens was observed to be less than the traditional specimen. Furthermore, damage was observed to reduce in specimens with increasing bottom longitudinal reinforcement unbonded lengths.

The third generation of research focussed on comparing the behaviour of a slotted connection with an equivalent traditional connection. The specimens required larger column depths to accommodate the discontinuous bottom longitudinal reinforcement. The spacing of the stirrups was reduced over the debonded length in the slotted specimen to restrain reinforcement buckling (Ohkubo et al., 1998). The specimen details can be seen in Figure 2-49. Both specimens had portions of a floor slab cast integral to the frames to investigate the difference in damage to the floor between the connection types. The traditional connection specimen had a slot provided through the beam centroid at the column face as shown in Figure 2-49(b).

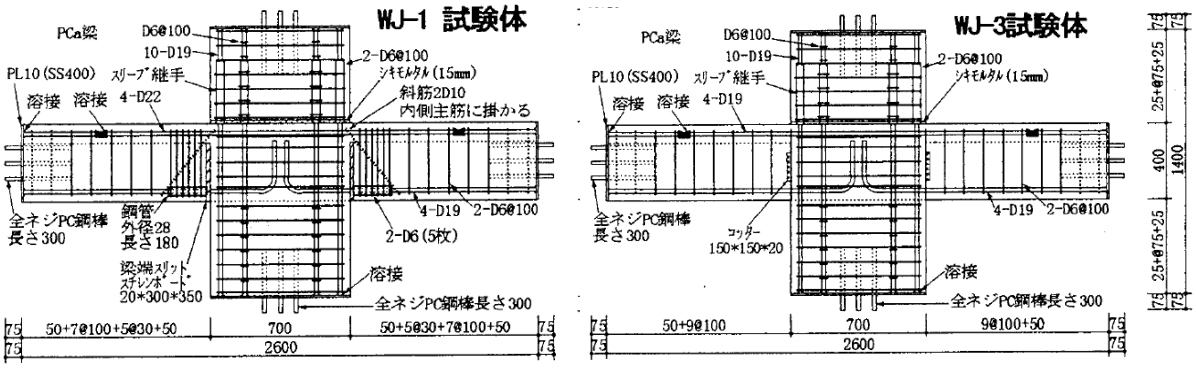

(a) Slotted specimen. **(b) Traditional specimen.**

Figure 2-49: Third generation slotted beam investigation (Ohkubo et al., 1998).

The response of the slotted beam specimen was stable, but heavily pinched. The pinching was likely due to shear deformation at the beam ends. Shear hangers without sufficient development length were used in the slotted specimen. The damage to both the frame and floor of the slotted beam specimen was significantly less than that in the traditional connection specimen, as shown in Figure 2-50.

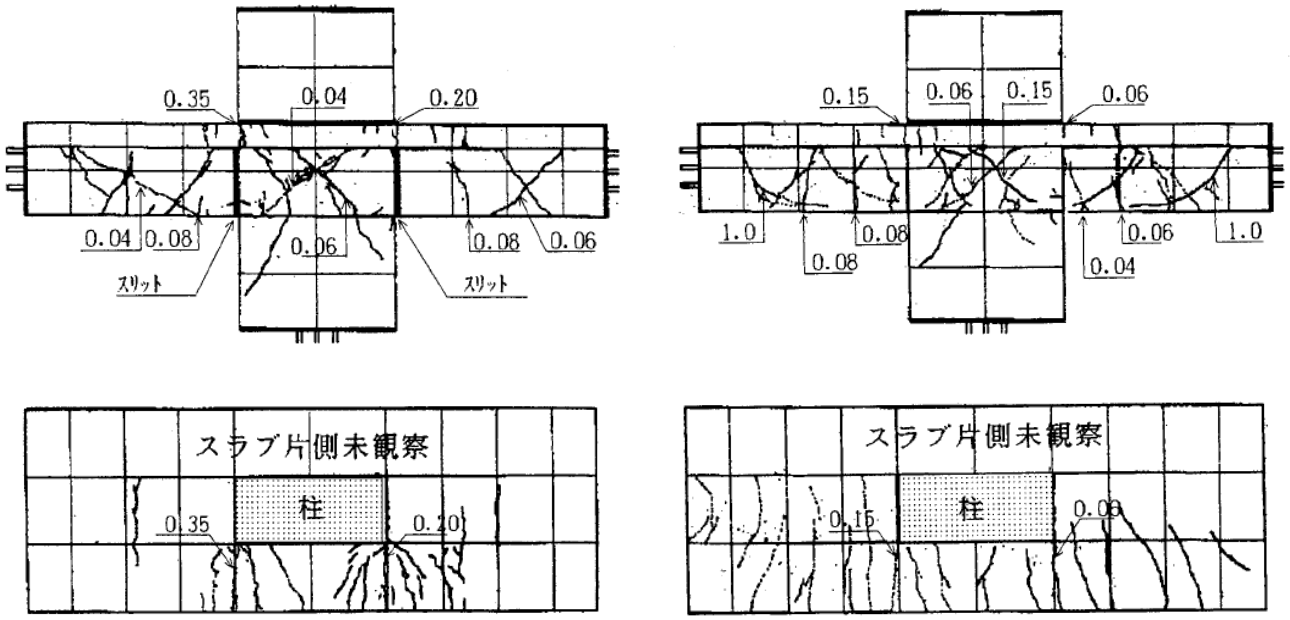

(a) Slotted specimen. **(b) Traditional specimen.**

Figure 2-50: Damage to frame and floor for slotted and traditional connection types (Ohkubo et al., 1998).

Ohkubo et al. (1999) investigated the shear transfer mechanism in slotted beams. Ohkubo et al. (1999) investigated seven specimen over two phases. Six of the specimen had slotted beam connections and one had a traditional connection. The only additional measure to improve shear transfer in the specimens tested in the first phase was the addition of inclined reinforcement in specimen RCSB2, as shown in Figure 2-51.

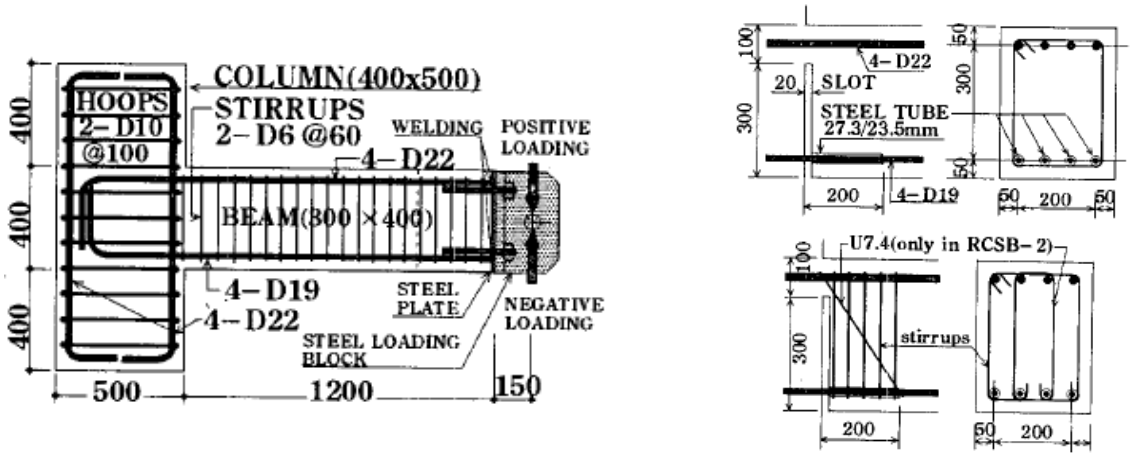

(a) Generic test specimen setup. **(b) Details for slotted specimens**

Figure 2-51: Details of specimens in phase two of shear transfer investigation (Ohkubo et al., 1999).

The response of both slotted specimens was poor. Large shear cracks, termed ‘s-cracks’, opened up in the beams to the right of the unbonded length, as shown in Figure 2-52. The

crack formation was due to a breakdown in the shear transfer mechanism. Tension induced by the diagonal compression strut could not be resisted by the bottom longitudinal reinforcement due to the presence of the unbonding tubes, which resulted in concrete tension being relied upon. Once the concrete tensile capacity was exceeded, a large diagonal crack occurred.

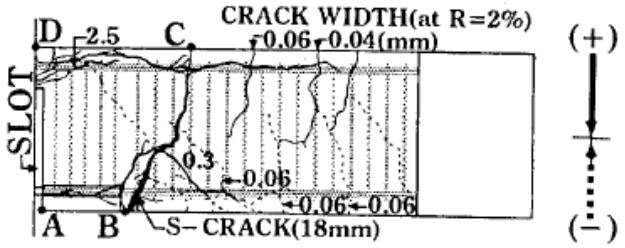

Figure 2-52: S-cracks observed in slotted specimens during phase one of shear transfer investigation (Ohkubo et al., 1999).

The phase two specimens, RCSB3-5, were similar to those tested during phase one except additional shear reinforcement was included. Specimen RCSB3 had inclined reinforcement that was anchored into the column core and extended past the end of the debonded length. Specimen RCSB4 had additional longitudinal reinforcement across the end of the debonded length and an inclined stirrup set. The specimen details are presented in Figure 2-53.

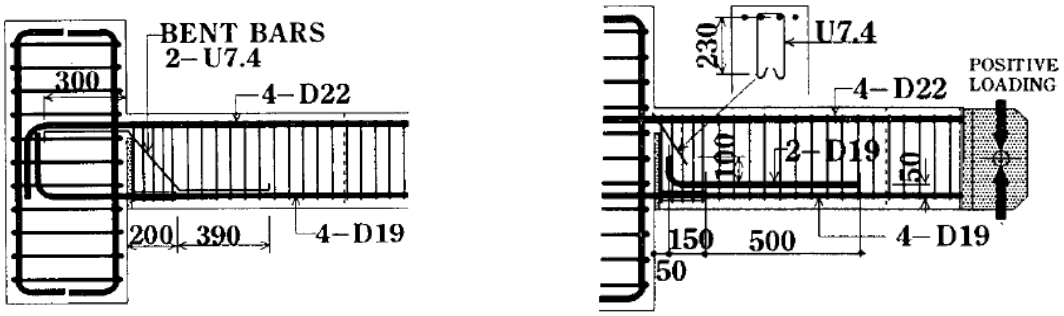

(a) Details of specimen RCSB3. **(b) Details of specimen RCSB4.**

Figure 2-53: Details of specimens in phase two of shear transfer investigation (Ohkubo et al., 1999).

The performance of specimens RCSB3 and RCSB4 was improved compared to RCSB1 and RCSB2, with stable response to design level drifts observed. The investigation showed the importance of an effective and robust shear transfer mechanism in the slotted beam.

In 2000, the slotted beam was tested as part of a larger frame system for the first time (Ohkubo et al., 2000). Two specimens were tested, one with a slotted beam connection and the other with a traditional connection. The two specimens had four interconnected connections each to represent a portion of a moment resisting frame, as shown in Figure 2-54. The specimen used the same shear transfer details as Ohkubo et al. (1999) used in RCSB3. The study was focused on the overall response of the systems in terms of damage, force-displacement response and for the first time explicitly, elongation of the beams.

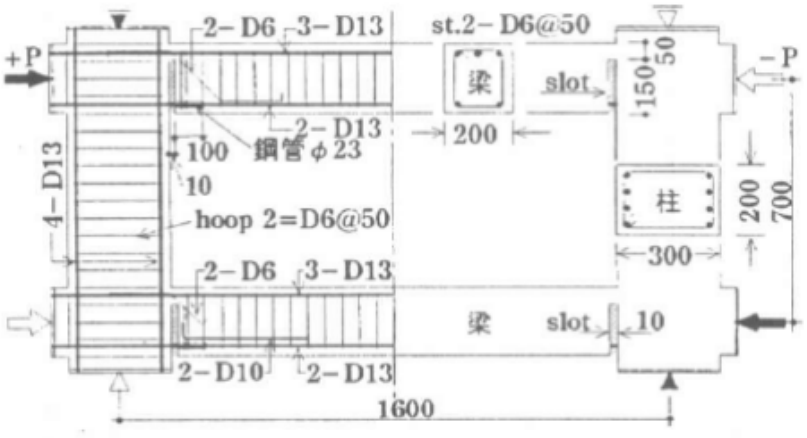

Figure 2-54: Details of slotted frame specimen (Ohkubo et al., 2000).

The force-drift response of the slotted beam frame, shown in Figure 2-55(a), was very satisfactory. The response of the specimen was stable, with high energy dissipation and little pinching observed, however; the yield force was lower than predicted. S-cracks and large cracks along the length of the de-bonded reinforcement were observed in the specimen. Overall, the damage observed was less than the traditional frame. The elongation of the uppermost storey, shown in Figure 2-55(b), of the slotted specimen was significantly less than the traditional specimen. Whilst the experimental results were promising, the boundary conditions of the specimen were not fully representative of a moment frame due to the location of the points of contraflexure in the columns.

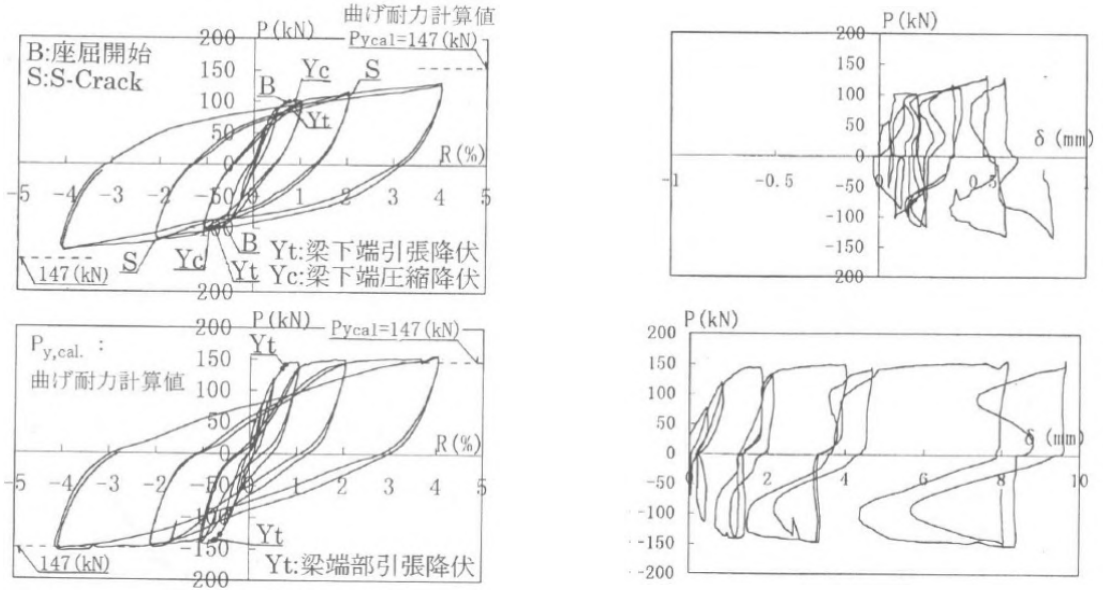

(a) Force-drift response of specimens. **(b) Bay elongation of top storey of specimens.**

Figure 2-55: Results of slotted (top) and traditional (bottom) frame experiments (Ohkubo et al., 2000).

Ohkubo and Hamamoto (2004) tested three cruciform specimens with insitu floor slabs. Two of the specimens had slotted beam detailing and one had traditional detailing. The slotted beam specimens tested three different shear transfer details, as shown in Figure 2-56. Large column widths were required to allow adequate anchorage of the beam bottom longitudinal reinforcement and space for the diagonal hanger 90° return detailing.

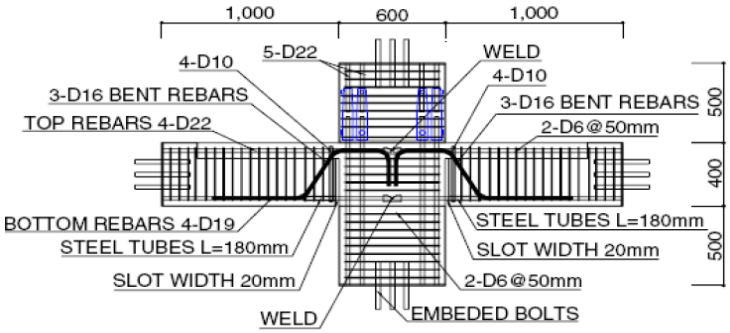

(a) Specimen SB1.

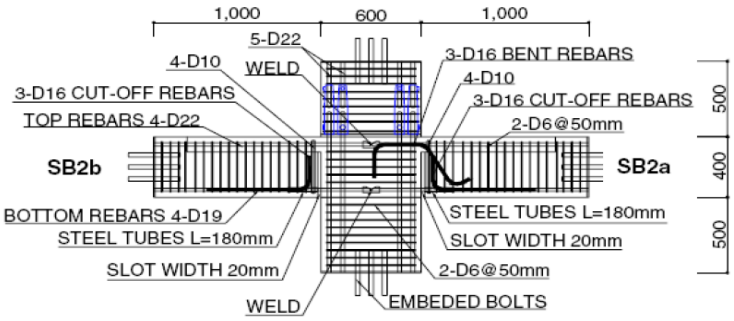

(b) Specimen SB2a and SB2b.

Figure 2-56: Slotted beam specimens tested in damage investigations (Ohkubo & Hamamoto, 2004).

Satisfactory performance of the slotted beam connections was observed during testing. No strength degradation or pinching was observed in the response of the slotted beam specimens, whereas pinching was observed in the response of the specimen with traditional beams. Elongation of the slotted beam specimen was significantly less than the traditional beam (Ohkubo & Hamamoto, 2004). As shown in Figure 2-57, damage to the frame and floor was significantly less in the slotted beam specimen when compared to the traditional beam specimen.

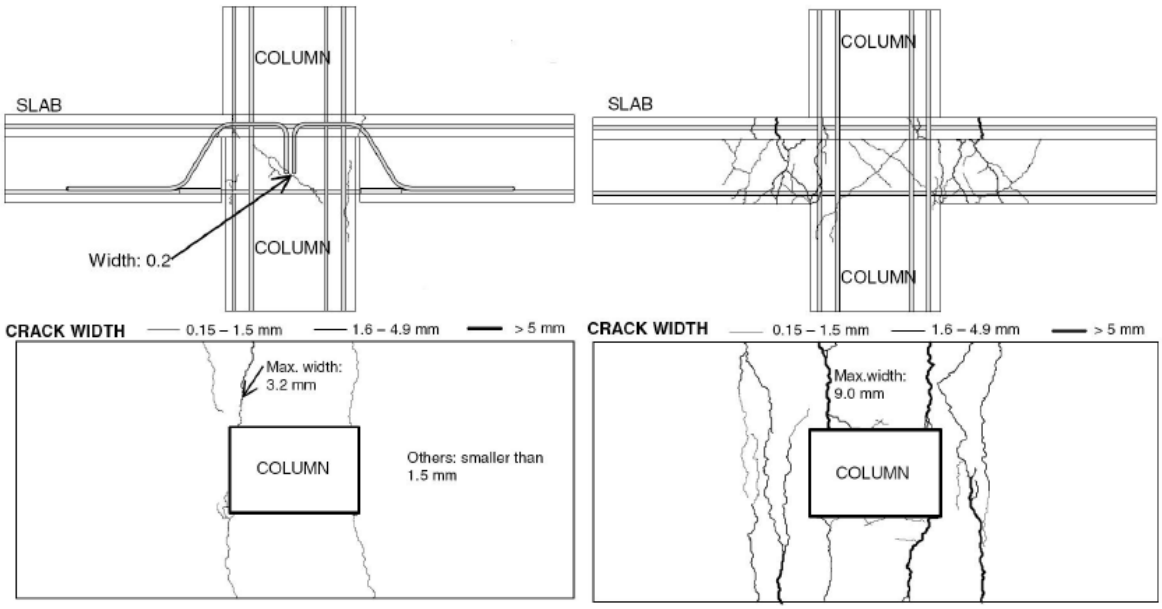

Figure 2-57: Damage to frame and floor for SB1 (left) and RCB (right) (Ohkubo & Hamamoto, 2004).

Whilst the importance of effective shear transfer to achieve stable slotted beam response was recognised in these tests, the effect of combined gravity shear, seismic shear and beam torsion

on diagonal hanger performance was neglected. In New Zealand, where one-way precast floor construction methods can result in significant beam torsion, the effect of combined beam actions on diagonal hanger performance cannot be neglected.

2.4.2.3 New Zealand Gapping Frame Research

Gapping frame connection research began in New Zealand at the University of Canterbury with research conducted by Park (1996) on pinned connections. Subsequent research in New Zealand followed on from the work conducted in Japan on moment resisting slotted beams. Researchers at the University of Canterbury have investigated the slotted beam parametrically, analytically and experimentally (Au, 2010; Leslie, 2010; Byrne, 2012b). The aim of the investigations was to understand the mechanics, improve the performance and develop design recommendations for the slotted beam for general practice.

Park

Park (1996) tested a connection detail for use in the secondary framing system of a structure. The detail was not intended to form part of the primary lateral load resistance system. As shown in Figure 2-58, the connection was conceptually similar to the moment resisting connections tested in Japan (Ohkubo and Hamamoto, 2004). However, the key differences were the absence of bottom longitudinal reinforcement and shear transfer being by way of a corbel rather than internal diagonal reinforcement. A vertical dowel was provided between the corbel and the beam soffit. The connection was intended to behave as a pinned joint; however, friction between the corbel the beam soffit, and shear force from the dowel, resulted in a connection moment being generated. Specimen 1 had no edge armouring and suffered premature failure due to loss of cover concrete in the corbel and beam end. Specimen 2 was armoured and satisfactory behaviour was observed during testing.

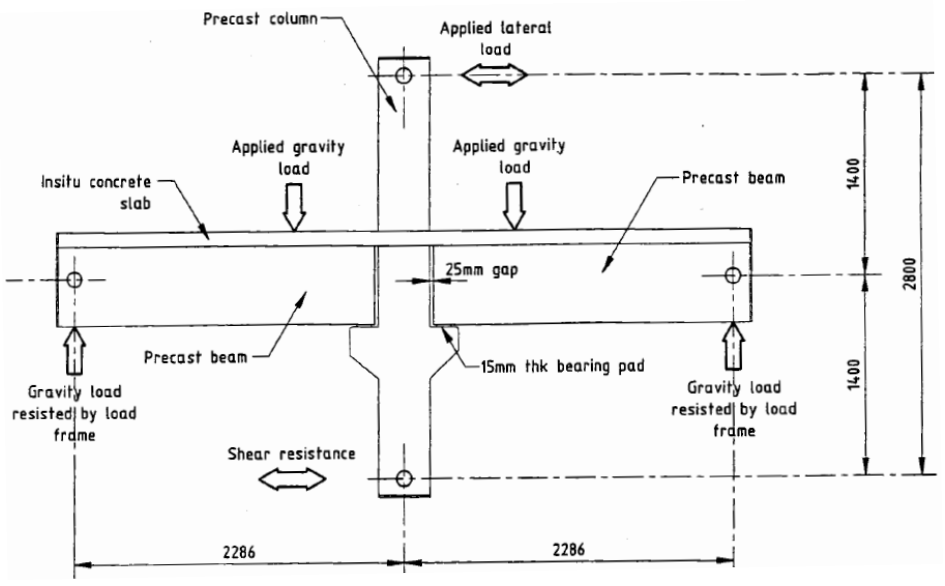

Figure 2-58: Gapping frame connection for secondary frame tested by Park (1996).

Leslie

The objective of the research conducted by Leslie (2010) was to develop and experimentally validate a variety of precast concrete non-tearing connection details for rapid implementation into New Zealand practice. The research was undertaken in three phases.

The theoretical phase involved investigation of the mechanics governing the behaviour of slotted beams. Through consideration of the parameters involved in the response, design recommendations were tentatively made.

The experimental phase involved the uniaxial testing of a 2/3 geometric scale specimen, shown in Figure 2-59(a) – (c). The specimen geometry was designed to be similar to the specimen tested by Peng (2009). A portion of insitu floor slab was included in the specimen design.

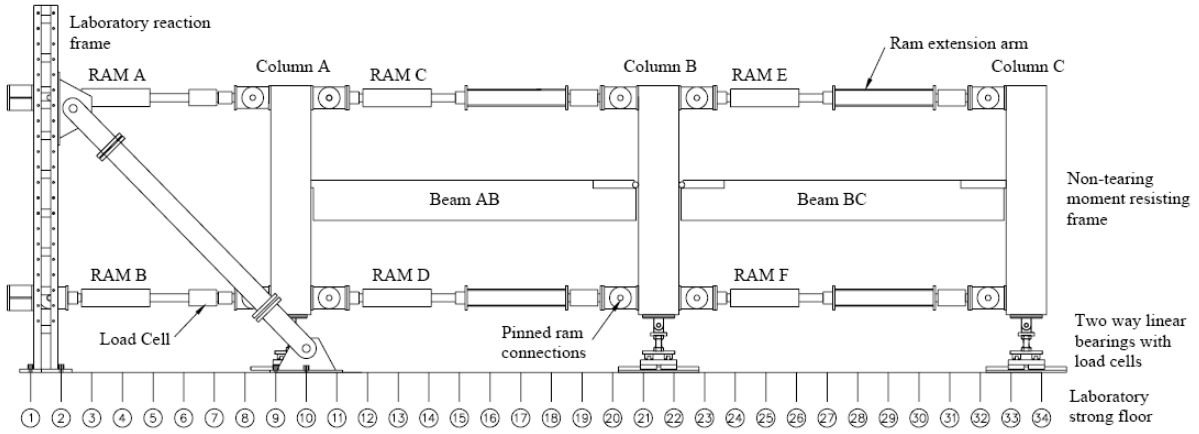

(a) Front elevation.

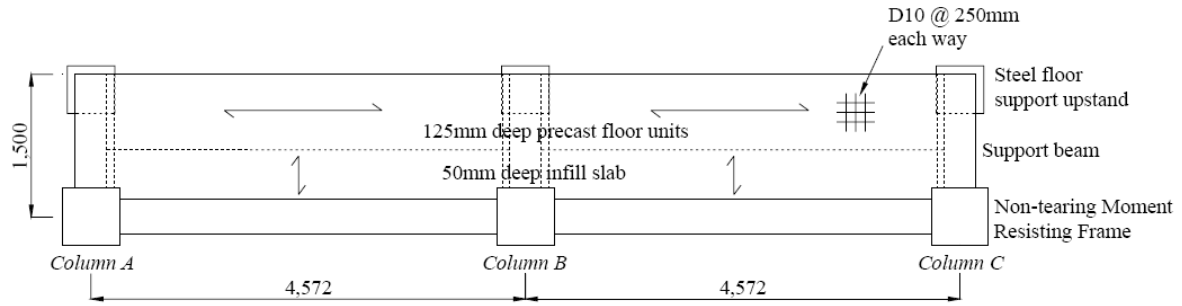

(b) Plan view.

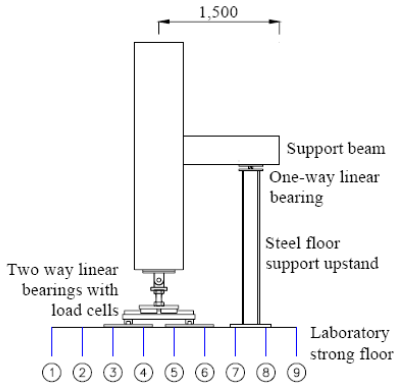

(c) Side elevation.

Figure 2-59: Specimen tested by Leslie (2010).

The specimen incorporated three different connections details, as shown in Figure 2-60(a). A reinforced concrete slotted beam was tested, which represented a familiar 'wet' connection type. A connection was defined as wet if it was completed when pouring the insitu concrete for the floor. Conversely, the circular and open-end top hinge details tested, shown in Figure 2-60(b) and (c), were examples of 'dry' type construction because the connections could be completed prior to the insitu concrete floor being poured. The dry connection types allowed for extensive prefabrication.

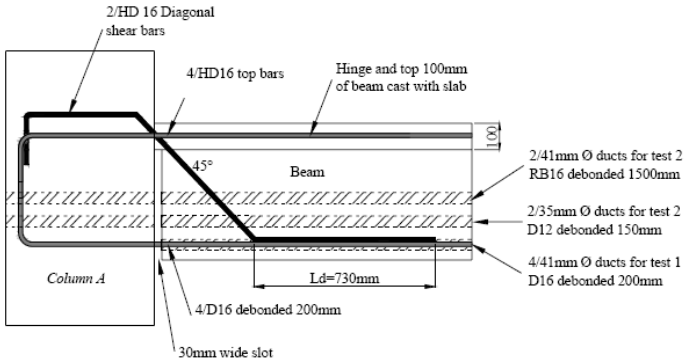

(a) Reinforced concrete hinge detail, which used a reinforced concrete top hinge to connect the beam to the column.

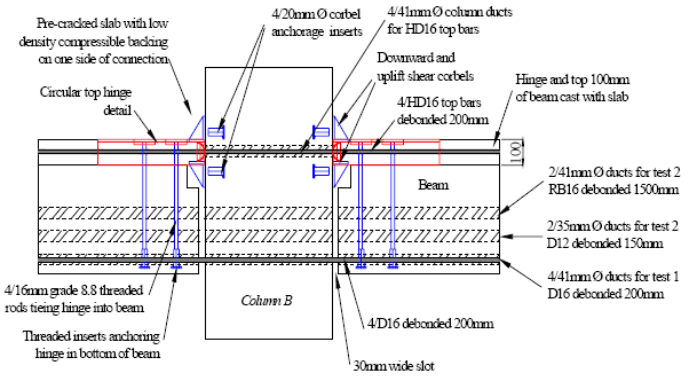

(b) Circular profile top hinge detail, which used a circular fabricated steel top hinge to connect the beam to the column.

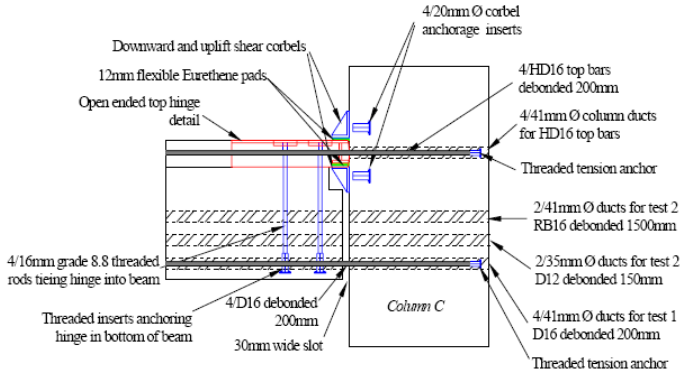

(c) Open end top hinge detail, which used a open-ended fabricated steel top hinge to connect the beam to the column.

Figure 2-60: Connection details tested by Leslie (2010).

The experimental results showed that damage to the frame and floor was minimal, especially if a pre-cracked floor detail was used. The pre-cracked detail built a zone of weakness into the floor where cracking would occur preferentially. It is possible that forcing the cracks to form at a predetermined location could result in larger local strains, increasing the risk of

reinforcement fracture. The pre-cracked detail could potentially inhibit diaphragm force transfer and cannot be recommended until thoroughly tested.

Activation of the floor slab reinforcement was minimal. It was found that the use of high strength reinforcement could reduce the residual drifts experienced by a structure after an earthquake. However, the use of high strength reinforcement encouraged buckling of the bottom longitudinal reinforcement. The fabricated steel top hinge connections were shown to deform excessively in shear, which promoted pinching of the hysteretic response.

The final stage of the investigation developed a two-dimensional compound spring model of the slotted beam. The numerical model was calibrated using experimental data. Satisfactory agreement between the model and the experimental results was demonstrated.

Au

Research conducted by Au (2010) aimed to develop details for the reinforced concrete slotted beam connection that would increase the performance and constructability of the connection in New Zealand. The research was conducted in four phases; theoretical, experimental, parametrical and numerical.

The theoretical phase was similar in concept to that performed by Leslie (2010). However, Au (2010) focused exclusively on the slotted beam in reinforced concrete. Design considerations unique to the slotted beam detail were investigated and recommendations to address the issues were developed from engineering principles. The theoretical phase received input from the experimental, numerical and parametric phases of the research to improve the recommendations as new data was generated. Due to the small pool of experimental data available, some recommendations developed by Au may have been conservative.

In the experimental phase of the research, Au (2010) tested four specimens. Three specimens, SB1-3, were slotted beam connections and the remaining specimen, RCB1, was a traditional reinforced concrete connection. Specimen RCB1 was tested as a performance reference to compare specimens SB1-3 to. The first three specimens were designed not only to allow direct comparison of the performance of the slotted beam detail against an equivalent traditional detail, but also to trial different slotted beam design details. Specimens SB1 and SB2 are shown in Figure 2-61(a) and (b) respectively.

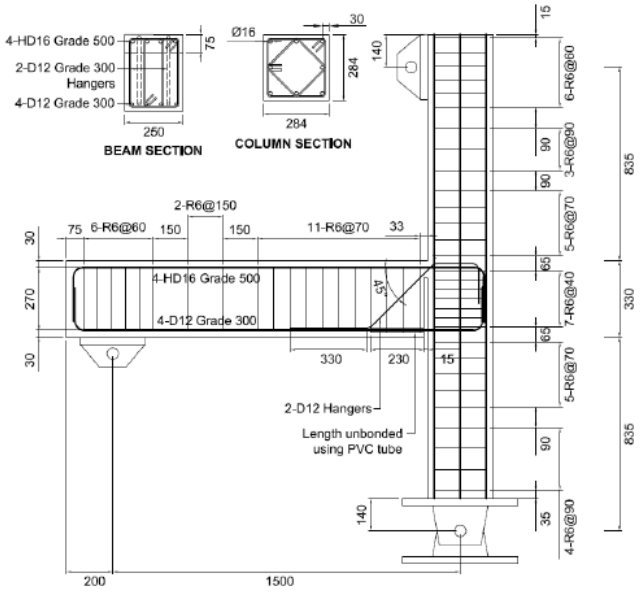

(a) Specimen SB1.

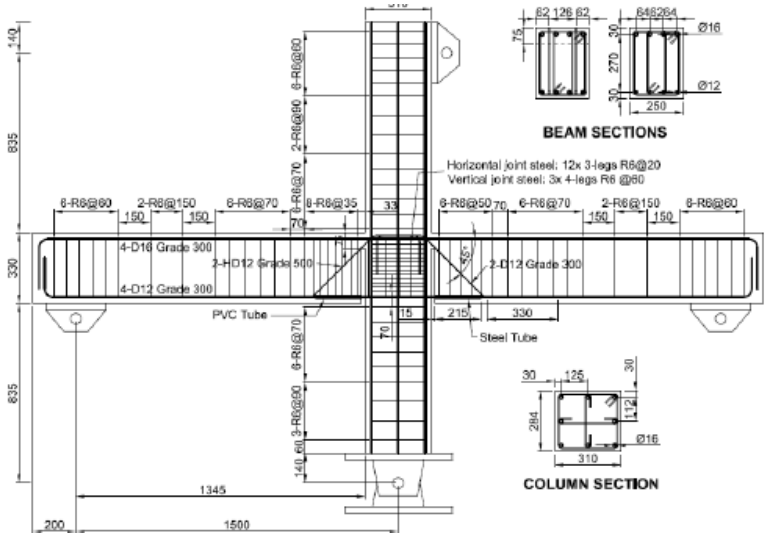

(b) Specimen SB2.

Figure 2-61: Details of specimens SB1 and 2 tested by Au (2010).

Specimen SB1 performed well, and failed by way of bottom longitudinal reinforcement buckling at 3.5% drift. Specimen SB2 failed by bond slip of the bottom longitudinal reinforcement through the column following the 2.5% drift cycle. The grouted debonding sleeves trialled in specimen SB2 were observed to increase the post-elastic stiffness during negative flexure. The stiffening influence of confinement on the compressive response of reinforcement and yielding dampers has also been noted by Amaris et al. (2008) and Marriott (2009). Greater damage was sustained by specimen RCB1 compared to specimens SB1 and SB2. The elastic stiffness and degradation of stiffness was observed to be similar for the slotted beam and traditional connection specimens. The slotted specimens exhibited greater hysteretic energy dissipation than the traditional specimen. Beam elongation of the slotted beam specimens were approximately a tenth of that recorded in the traditional specimen.

Specimen SB3 was geometrically similar to SB2. However, it had a floor slab and used detailing improvements that were developed following the previous two experiments, such as improved buckling restraint of bottom longitudinal reinforcement, increased beam torsion restraint, increased bottom longitudinal reinforcement bond through the column and increased joint shear reinforcement. Specimen SB3, shown in Figure 2-62(a) – (c), was tested with a simulated gravity load on the floor.

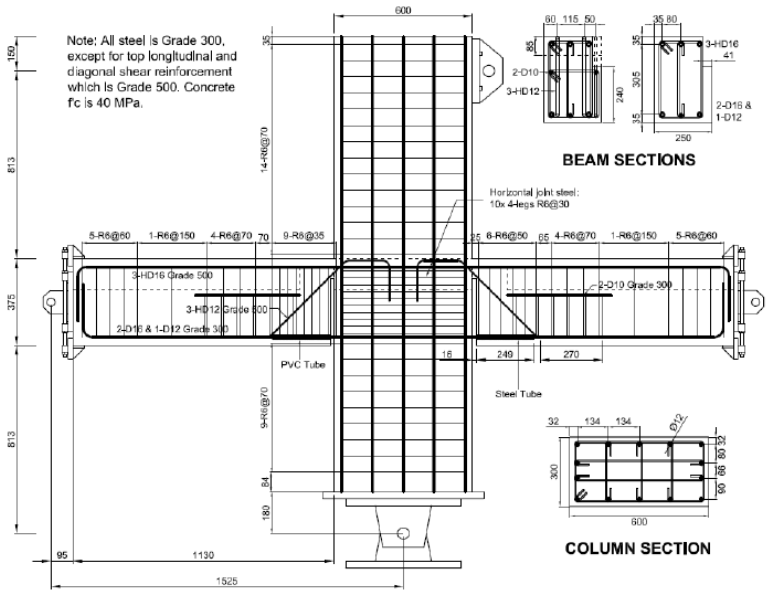

(a) Front elevation.

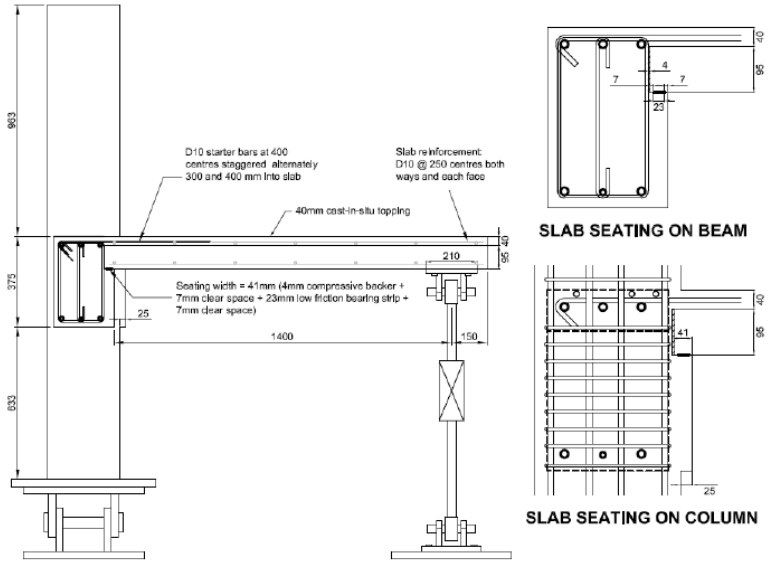

(b) Side elevation.

Figure 2-62: Specimen SB3 tested by Au (2010).

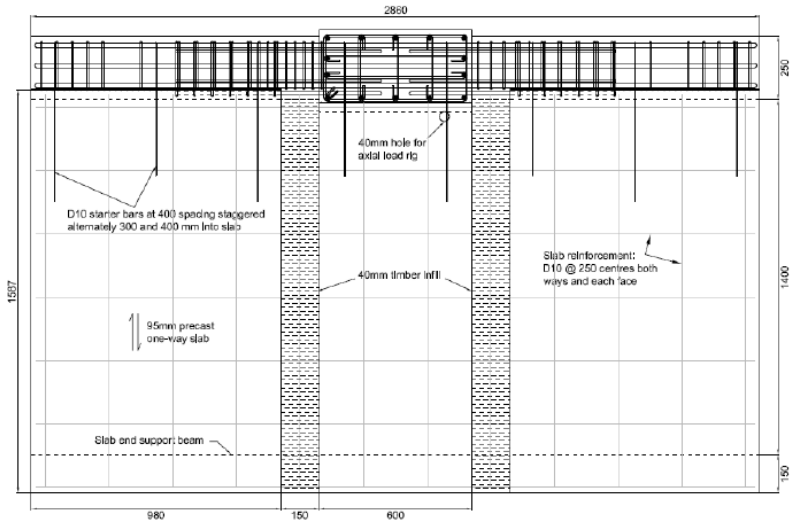

(c) Plan view.

Figure 2-62: Specimen SB3 tested by Au (2010) (Continued).

Specimen SB3 performed well during testing, with stable hysteretic response and high energy dissipation observed. SB3 failed due to fracture of the bottom longitudinal reinforcement, which was likely due to low cycle fatigue. Structural damage and floor slab activation was lower than would be expected in an equivalent traditional connection. However, due to errors in the boundary conditions of the floor, the worst case torsional demands could not be applied to the supporting beams to assess the connection torsion restraint provisions. Due to the large column width required for bond of the bottom longitudinal reinforcement, joint shear was transferred by concrete tension, which meant that evaluation of the additional joint shear reinforcement provisions could not be undertaken.

During the parametric analysis phase, a moment-rotation analysis method was developed. Many analyses were performed to determine the sensitively of response on several key input parameters. The analyses showed that the response of the slotted connection was sensitive to the assumed strain penetration, unbonded length, effective slab contribution and top hinge depth.

In the analytical phase, two-dimensional multispring representations of the slotted beam specimens SB2 and SB3 were created and calibrated using experimental data. The plastic hinge multispring element, developed by Peng (2009), was used to model specimen RCB1. Close agreement between the numerical models and the experimental data from SB3 and RCB1 was achieved. The connection models were used to create slotted beam and traditional connection versions of a five storey moment resisting frame, as shown in Figure 2-63.

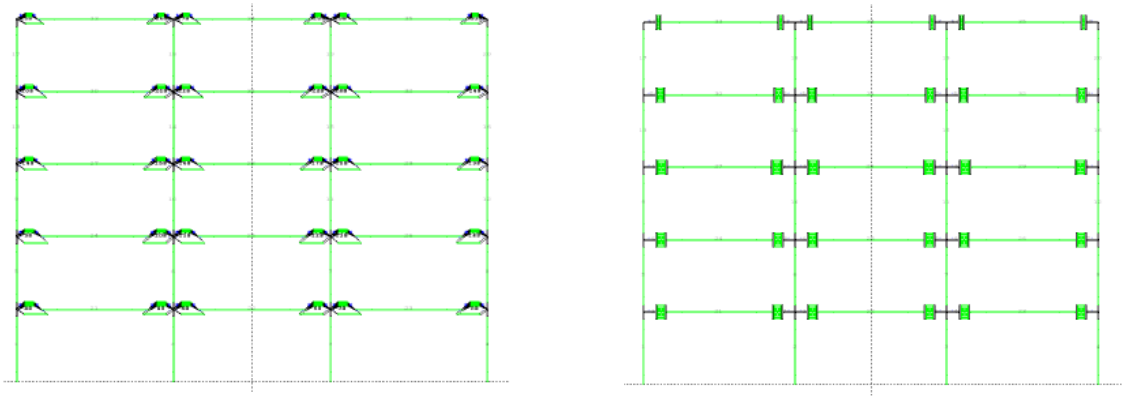

(a) Slotted beam frame. (b) Traditional beam frame.

Figure 2-63: Five storey numerical models created by Au (2010).

The slotted and traditional frames were subjected to a suite of earthquakes to determine the differences in response. It was found that response of the two systems was similar; however, peak floor acceleration was less in the slotted frame due to a slightly lower initial stiffness and lower yield base shear. Peak interstorey drifts were lower in the slotted beam system due to the higher hysteretic damping. The slotted system had lower residual drifts at the end of the analyses due to a combination of higher hysteretic damping and slightly greater post yield stiffness.

Byrne

Byrne (2012b) investigated slotted beam joint shear mechanics and the bond of the bottom longitudinal reinforcement through internal columns. A database study of historical subassembly tests resulted in Byrne (2012b) modifying bond recommendations by Au (2010) to be less conservative. Alternative joint shear reinforcement recommendations were made; however, the recommended detail used a complex vertical reinforcement, as shown in Figure 2-64(b). Two 80% geometric scale subassemblies were tested to examine the design recommendations. The specimen setup is shown in Figure 2-64(a). Specimen A used 40MPa concrete and had 135% of the horizontal joint reinforcement calculated using NZS 3101:2006 (Standards New Zealand, 2006). Specimen B used 30MPa concrete and 120% of the required NZS3101:2006 horizontal joint reinforcement.

Stable response and high energy dissipation was observed in both specimens up to 5.5% drift. Both specimens failed by low-cycle fatigue of the bottom longitudinal reinforcement. Overstrength values of 1.69 and 1.7 were recorded for Specimen A and B respectively.

The performance of the specimens tested by Byrne (2012b) was satisfactory; however, the detail was difficult to construct. Recommendations made by Byrne (2012b) resulted in no reduction to column dimensions or reinforcement quantities. Hence, the detail is unlikely to be used in practice.

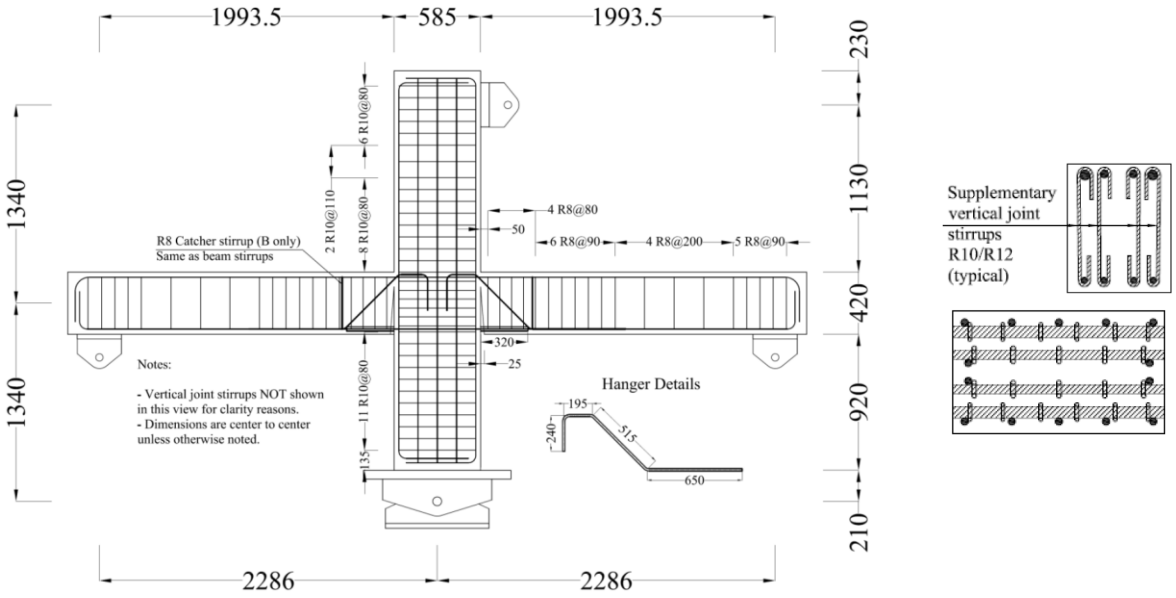

(a) Experimental setup.

(b) Supplementary joint reinforcement detail.

Figure 2-64: Byrne (2012b) subassembly test.

The investigations by Au (2010), Leslie (2010) and Byrne (2012a) were conducted in two dimensions. In-plane experimentation alone cannot adequately assess the effects of the floor diaphragm on response and the effect of beam plasticity on floor damage. Au (2010) and Leslie (2010) recognised the limitations of two-dimensional investigations and recommended an extension to three dimensions in future research.

2.5 Conclusions

This chapter presented an extensive review of relevant research involved in the development of the reinforced concrete slotted beam. The performance of the slotted beam had been significantly improved through the concerted efforts of many researchers; however, it was not in a state where it was ready for full scale implementation into New Zealand construction practice.

Unresolved performance issues remained with the reinforced concrete slotted beam, such as shear transfer, beam torsion, longitudinal reinforcement bond, unbonded reinforcement buckling restraint and reinforcement low-cycle fatigue. Three-dimensional slotted beam specimens had not yet been tested. Similarly, biaxial experimentation had not been conducted on the slotted beam connection. The assessment of the residual capacity, and subsequent rehabilitation, of slotted beams following a design earthquake had not been considered.

Previous research had focussed almost exclusively on connection behaviour, which was well suited to two-dimensional in-plane experimentation. In-plane experimentation ensured that the measured response was that of the connection alone and not coupled with contributions from other elements. It also allowed the test costs to be minimised to permit a greater number

of experiments to be performed. However, the response of real structures depends not only on the connections, but also on the influence that the connections have on other structural elements, and vice versa. There was a need to extend the research on slotted beams into three dimensions to fully evaluate the likely system response, whilst still being able to assess connection behaviour and develop design recommendations.

Analytical models developed to date have been two-dimensional and in-plane. The analytical models have been used in parametric analyses to assess the effect of varying key input parameters quickly and efficiently. However, when the two-dimensional numerical models were used to assemble prototype structures to investigate overall structural response, the results could not be interpreted with the same confidence. Furthermore, two-dimensional analytical models were unable to capture interactions between structural elements.

Whilst slotted beam connections have been constructed, comparatively little effort has been spent investigating the practical aspects of producing and erecting them. Researchers have at times erroneously assumed that a detail produced in a laboratory setting could be accurately reproduced in a commercial setting, which was often not the case. Commercial operators are subject to factors that cannot be replicated in a laboratory, such as schedule pressures, the need to be profitable and a lack of specialised expertise. It was important that production and erection methods for the slotted beam system were considered.

2.6 References

ACI Committee 374. (2005). *Acceptance Criteria for Moment Frames Based on Structural Testing and Commentary (ACI374.1-05)*. Farmington Hills, Michigan: American Concrete Institute.

Amaris, A., Pampanin, S., Bull, D. K., & Carr, A. J. (2007). *Development of a Non-tearing Floor Solution for Jointed Precast Frame Systems*. Paper presented at the New Zealand Society for Earthquake Engineering Conference, Palmerston North, New Zealand. Retrieved from http://www.nzsee.org.nz/db/2007/Paper14.pdf

Amaris, A., Pampanin, S., Bull, D. K., & Carr, A. J. (2008). *Experimental Investigation on a Hybrid Jointed Precast Frame with Non-tearing Floor Connections*. Paper presented at the New Zealand Society for Earthquake Engineering Conference, Wairakei, New Zealand. Retrieved from http://www.nzsee.org.nz/db/2008/Paper26.pdf

Applied Technology Council. (1981). *Design of prefabricated concrete buildings for earthquake loads (Report number ATC-8)*. Berkeley, California: Author.

Au, E. (2010). *The mechanics and design of a non-tearing floor connection using slotted reinforced concrete beams.* Masters Dissertation, University of Canterbury, Christchurch, New Zealand.

Bull, D. K. (2004). Understanding the complexities of designing diaphragms in buildings for earthquakes. *Bulletin of the New Zealand Society for Earthquake Engineering, 37*(2), 70-88.

Bull, D. K. (2007). *Issues of Deformation Incompatibility within Floor Diaphragms - Non-tearing Floor Solution*. Unpublished Manuscipt, University of Canterbury, Christchurch, New Zealand.

Bull, D. K., & Matthews, J. G. (2003). *Proof of Concept Tests for Hollowcore Floor Unit Connections (Report number 2003-1)*. University of Canterbury, Christchurch, New Zealand. Retrieved from http://precastnz.org.nz/wp-content/downloads/Hollowcore .pdf

Byrne, J. D. R. (2012a). *Bond and shear mechanics witihin reinfroced concrete beam-column joints incorporating the slotted beam detail.* Masters Dissertation, University of Canterbury, Christchurch, New Zealand.

Byrne, J. D. R., & Bull., D. K. (2012b). *Design and testing of reinforced concrete frames incorporating the slotted beam detail*. Paper presented at the New Zealand Society for Earthquake Engineering Conference, Christchurch, New Zealand. Retrieved from http://www.nzsee.org.nz/db/2012/Paper065.pdf

Centre for Advanced Engineering. (1999). *Guidelines for the use of structural precast concrete in buildings*. Christchurch, New Zealand: Author.

Cheok, G. S., & Lew, H. S. (1993). Model Precast Concrete Beam-Column Connections Subject to Cyclic Loading. *PCI Journal, 38*(4), 80-92.

Cheok, G. S., & Stone, W. C. (1990). *Performance of 1/3-Scale Model Precast Concrete Beam-Column Connections Subjected to Cyclic Inelastic Loads - Report No. 1 (Report number NISTIR4433)*. Gaithersburg, Maryland: U.S. Department of Commerce.

Cheok, G. S., & Stone, W. C. (1991). *Performance of 1/3-Scale Model Precast Concrete Beam-Column Connections Subjected to Cyclic Inelastic Loads - Report No. 2 (Report number NISTIR4589).* Gaithersburg, Maryland: U.S. Department of Commerce.

Cheok, G. S., & Stone, W. C. (1994). *Performance of 1/3-Scale Model Precast Concrete Beam-Column Connections Sunjected to Cyclic Inelastic Loads - Report No. 4 (Report number NISTIR5436).* Gaithersburg, Maryland: U.S. Department of Commerce.

Cheok, G. S., Stone, W. C., & Lew, H. S. (1993). *Performance of 1/3-Scale Model Precast Concrete Beam-Column Connections Subjected to Cyclic Inelastic Loads - Report No.*

3 (Report number NISTIR5246). Gaithersburg, Maryland: U.S. Department of Commerce.

Corley, W. G. (1996). Northridge earthquake of January 17, 1994 reconnaissance report. *Earthquake Spectra, 12*(S1), 1-278.

Earthquake Engineering Research Institute. (1995). *The Hyogo-Ken Nanbu Earthquake January 17, 1995 Preliminary reconnaissance report*. Oakland, California: Author.

Fenwick, R. C., Davidson, B. J., & Lau, D. (1999). Strength Enhancement of Beams in Ductile Seismic Resistant Frames due to Prestressed Components in Floor Slabs. *Journal of the Structural Engineering Society New Zealand, 12*(1), 35-40.

Fenwick, R. C., & Fong, A. (1979). The behaviour of reinforced concrete beams under cyclic loading. *Bulletin of the New Zealand National Society for Earthquake Engineering, 12*(3), 158-167.

Fenwick, R. C., & Megget, M. (1993). Elongation and load deflection characteristics of reinforced concrete members containing plastic hinges. *Bulletin of the New Zealand National Society for Earthquake Engineering, 26*(1), 28-41.

Gardiner, D. (2011). *Design Recommendations and Methods for Reinforced Concrete Floor Diaphragms Subjected to Seismic Forces.* Doctoral Dissertation, University of Canterbury, Christchurch, New Zealand

Grigorian, C. E., Yang, T. S., & Popov, E. P. (1993). Slotted bolted connection energy dissipators. *Earthquake Spectra, 9*(3), 491-504.

Hollings, J. P. (1969). Reinforced concrete seismic design. *Bulletin of the New Zealand National Society for Earthquake Engineering, 2*(3), 217-250.

Housner, G. W. (1963). Behaviour of inverted pendulum structures during earthquakes. *Bulletin of the Seismological Society of America, 53*(2), 403-417.

Ingham, J. M., Liddell, D., & Davidson, B. J. (2002). Influence of loading history on ultimate displacement of concrete structures. *Bulletin of the New Zealand Society for Earthquake Engineering*. *35*(1), 1-16.

International Conference of Building Officials. (1985). *Uniform Building Code*. Whittier, California: Author.

International Federation for Structural Concrete (2003). *Seismic design of precast concrete building structures (Report number 27)*. Lausanne, France: International Federation for Structural Concrete.

Kam, W. Y., Pampanin, S., & Elwood, K. (2012). Seismic Performance of Reinforced Concrete Buildings in the 22 February Christchurch (Lyttelton) Earthquake. *New Zealand Society for Earthquake Engineering, 44*(4), 239-279.

Leslie, B. J. (2010). *The development and validation of a non-tearing floor precast concrete structural system for seismic regions.* Masters Dissertation, University of Canterbury, Christchurch, New Zealand.

Lindsay, R. (2004). *Experiments on the seismic performance of hollow-core floor system in precast concrete buildings.* Masters Dissertation, University of Canterbury, Christchurch, New Zealand.

MacPherson, C. (2005). *Seismic performance and forensic analysis of a precast concrete hollow-core floor super-assemblage.* Masters Dissertation, University of Canterbury, Christchurch, New Zealand.

Marriott, D. (2009). *The Development of High-Performance Post-Tesioned Rocking Systems for the Seismic Design of Structures.* Doctoral Dissertation, University of Canterbury, Christchurch, New Zealand.

Matsuoka, T., & Ohkubo, M. (1996). *Energy Dissipation Mechanism Controlled Bottom Rebar Yielding at Beam-end*. Proceedings of the Japan Concrete Institue, 18(2), 803-808.

Matthews, J. G. (2004). *Hollow-core floor slab performance following a severe earthquake.* Doctoral Dissertation, University of Canterbury, Christchurch, New Zealand.

Nakaki, S. E., Stanton, J. F., & Sritharan, S. (1999). An overview of the PRESSS five-story precast test building. *PCI, 44*(2), 26-39.

Norton, J. A., King, A. B., Bull, D. K., Chapman, H. E., McVerry, G. H., Larkin, T. J., et al. (1994). Northridge Reconnaissance Report. *Bulletin of the New Zealand National Society for Earthquake Engineering, 27*(4), 235-344.

Ohkubo, M., & Hamamoto, T. (2004). *Developing reinforced concrete slotted beam structures to reduce earthquake damage and enhance seismic structural performance.* Paper presented at the 13th annual World Conference on Earthquake Engineering. Vancouver, B.C., Canada. Retrieved from http://www.iitk.ac.in/nicee/wcee/article /13_3285.pdf

Ohkubo, M., Matsuoka, T., & Yoshioka, T. (2000). Lateral Load Tests of Reinforced Concrete Beam-yield Type Frames with Slots at the Beam-ends. *Proceedings of the Japan Concrete Institue, 22*(3), 1513-1518.

Ohkubo, M., Matsuoka, T., Yoshioka, T., & Anderson, D. L. (1999). Shear transfer mechanism of reinforced concrete beams with a slot at the beam-end. *Proceedings of the Japan Concrete Institute, 21*(3), 301-306.

Ohkubo, M., & Zhang, A. (1997). Lateral Loading Behaviour of Beam-column Sub-assemblages Designed by Limited Flexural Mechanism of Bottom Rebar Yielding at Beam-end Region. *Proceedings of the Japan Concrete Institute, 19*(2), 867-872.

Ohkubo, M., Zhang, A., Matsuoka, T., Hashimoto, A., & Yoshioka, T. (1998). 梁端下端エネルギー消費型RCラーメン構造に関する研究. *AIJ Journal, 37*(3), 281-284.

Palmieri, L., Saqan, C., French, C., & Kreger, M. (1996). Ductile connections for precast concrete frame systems. *ACI, 162*, 313-356.

Pampanin, S. (2005). Emerging Solutions for High Seismic Performance of Precast/Prestressed Concrete Buildings. *Journal of Advanced Concrete Technology, 3*(2), 207-223.

Pampanin, S., Amaris, A., Akguzel, U., & Palermo, A. (2006). *Experimental investigations of high-performance jointed ductile connections for precast frames*. Paper presented at the First European Conference on Earthquake Engineering and Seismology, Geneva, Switzerland. Retrieved from http://ir.canterbury.ac.nz/bitstream/10092/409/1/12605048_Main.pdf

Park, A. R. L. (1996). *Precast Reinforced Concrete Frames with Beams Supported on Column Corbels Subjected to Simulated Seismic Displacements.* Masters Dissertation, University of Canterbury, Christchurch, New Zealand.

Park, R., & Paulay, T. (1975). *Reinforced Concrete Structures*. New York, U.S.A: Wiley

Peng, B. H. H. (2009). *Seismic performance assessment of reinforced concrete buildings with precast concrete floor systems.* Doctoral Dissertation, University of Canterbury, Christchurch, New Zealand.

Pincheira, J. A., Oliva, M. G., & Zheng, W. (2005). Behaviour of Double-Tee Flange Connectors Subjected to In-Plane Monotonic and Reversed Cyclic Loads. *PCI Journal, 50*(6), 32-54.

Popov, E. P., & Engelhart, M. D. (1988). Seismic eccentrically braced frames. *Journal of Constructional Steel Research, 10*, 321-354.

Priestley, M. J. N. (1991). Overview of PRESSS research program. *PCI Journal, 36*(4), 50-57.

Priestley, M. J. N. (1996). The PRESSS program - Current status and proposed plans for phase III. *PCI Journal, 41*(2), 22-40.

Priestley, M. J. N. (1998). *Displacement-based approaches to rational limit states design of new structures.* Keynote Address, Eleventh European World Conference on Earthquake Engineering, Paris, France.

Priestley, M. J. N., Sritharan, S., Conley, J. R., & Pampanin, S. (1999). Preliminary results and conclusions from the PRESSS five-storey precast concrete test building. *PCI Journal, 44*(6), 42-67.

Priestley, M. J. N., & Tao, J. R. (1993). Seismic Response of Precast Prestressed Concrete Frames with Partially Debonded Tendons. *PCI Journal, 38*(1), 58-69.

SEAOC Vision 2000 Committee. (1995). *Performance-based seismic engineering*. Sacramento, California: Structural Engineers Association of California.

Standards New Zealand. (1982). *Code of Practice for Design of Concrete Structures (NZS 3101:1982)*. Wellington, New Zealand: Author.

Standards New Zealand. (2006). *Concrete Structures Standard (NZS3101:2006)*. Wellington, New Zealand: Author.

Walker, A. (2007). *Assessment of material strain limits for defining different forms of plastic hinge region in concrete structures.* Masters Dissertation, University of Canterbury, Christchurch, New Zealand.

Wyllie-Jr, L. A., & Lew, H. S. (1989). Armenian Earthquake of December 7, 1988 reconnaissance report. *Earthquake Spectra, 5*(S1), 1-175.

3. Design, Construction and Experimental Setup of the Superassembly Experiment

3.1 Introduction

Recent research has shown well detailed reinforced concrete slotted beam connections to perform well when subjected to simulated earthquake displacements (Au, 2010; Byrne & Bull, 2012). However, there remained unsolved detailing issues, which are discussed in Section 2.5, and biaxial response had not been assessed. Complex three-dimensional interactions between the slotted beam connection and other structural elements had not been evaluated. A realistic slotted beam structural system had never been constructed; hence, the effectiveness of the system had not been proven to the construction industry.

Biaxial testing of a three-dimensional reinforced concrete slotted beam specimen was undertaken in this phase of the research programme. The specimen was a two-storey, two-by-one bay, superassembly scaled at 2/3 geometrically. The experiment was designed to assess the overall performance of the slotted beam detail in a large three-dimensional specimen representative of New Zealand construction practice. The interactions between structural elements, connection performance, damage levels and overall performance were examined. Importantly, the practicality of the detail was tested through the involvement of industry.

This chapter describes the design, development and construction of the superassembly, described herein as SA1. The merits and deficiencies of previous relevant experimentation are discussed in Section 3.2. The design of the prototype structure that SA1 was extracted from is presented in Section 3.3. The overall layout and detailed design of the specimen is described in Section 3.4, whilst Section 3.5 chronicles construction. The design of the experimental setup is presented in Section 3.6. The loading protocol and specimen instrumentation is detailed in Sections 3.7 and 3.8 respectively.

3.2 Literature Review

Extensive experimentation has been undertaken on components of moment resisting reinforced concrete frames. The majority of these tests involved statically determinate specimens, which reduced costs and simplified interpretation of results. Recently,

experiments have included more complex statically indeterminate specimens. Indeterminate specimens allowed more realistic modelling of structural response, including moment redistribution. However, in some cases the boundary conditions have been unrealistic and affected the applicability of the results.

Megget and Fenwick (1989) tested a reinforced concrete portal frame subject to gravity loads to investigate uni-directional plastic hinges. As shown in Figure 3-1, the portal frame was loaded with two 120kN simulated gravity loads and subjected to a lateral quasi-static cyclic loading protocol. The experiment showed that when uni-directional plastic hinges formed, the inelastic rotation at the plastic hinges was not recovered upon load reversal; hence, the hinge rotation accumulated over the loading record. The accumulated plastic hinge rotation caused the beam to sag by 15% of the beam depth. Maximum beam elongation was 8% of the beam depth.

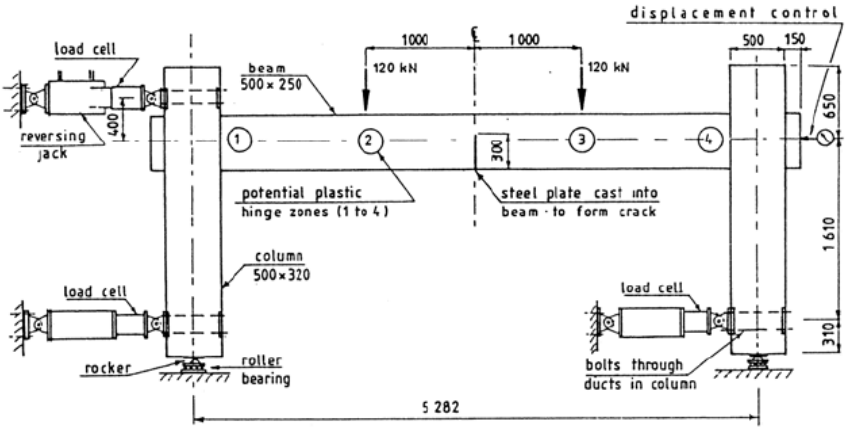

Figure 3-1: Reinforced concrete portal frame specimen tested by Megget and Fenwick (1989).

Zerbe and Durrani (1990) tested a series of two-bay, one-storey, reinforced concrete specimens. Specimens with and without a cast-insitu floor slab and transverse beams were tested. As shown in Figure 3-2, the specimen was attached to the laboratory floor and header beam via pinned supports. The experimental setup forced each column to incline the same amount and restrained beam elongation, which induced axial forces in the beams and increased the flexural capacity of the beams. The specimen boundary conditions did not emulate those of a real structure and as a result the measured beam elongation was not representative. However, the researchers noted the contribution of the floor slab to flexural overstrength and hence lateral resistance (Zerbe & Durrani, 1990).

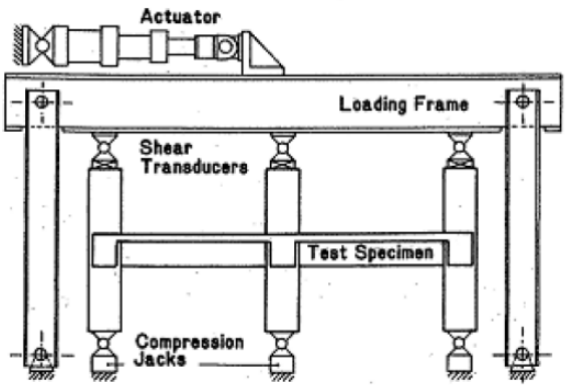

Figure 3-2: Test setup used by Zerbe and Durrani (1990).

Qi and Pantazopoulou (1991) tested a two-bay, single-storey, reinforced concrete specimen with a cast-insitu floor. The specimen was similar to that tested by Zerbe and Durrani (1990); however, the boundary conditions were more realistic. The specimen was intended to represent the first storey of a multi-storey structure so the column bases were fixed, as shown in Figure 3-3(a). The actuators between each bay were adjusted to account for measured beam lengthening during testing, which significantly altered the displaced shape of the specimen at the end of testing, as shown in Figure 3-3(b). The flexural cracks observed in the exterior columns at the underside of the beams highlighted the potential for beam elongation to alter the force distribution and strength hierarchy within a structure. The researchers observed that the presence of the floor diaphragm increased the beam flexural capacity.

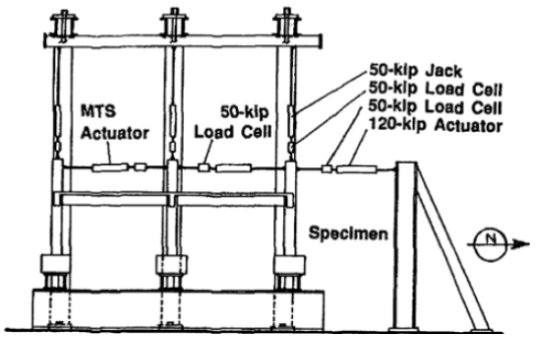

(a) Test setup.

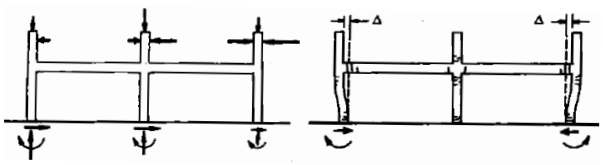

(b) Applied forces (left) and final displacement due to beam elongation (right).

Figure 3-3: Experiment by Qi and Pantazopoulou (1991).

McBride et al. (1996) conducted experiments on a single-storey, three-bay, reinforced concrete moment resisting frame at 1/3 scale. Two versions of the specimen, shown in Figure 3-4(a), were tested; one with a cast-insitu floor slab and the other without. The origin of the subassembly was the fourth storey of a prototype five storey moment resisting frame. However, because the column bases were pinned, to represent the points of contraflexure, the boundary conditions were not representative of the subassembly origin. The boundary conditions were representative of a subassembly extracted from the ground floor. The column tops were loaded at a constant force ratio of 2:1 between the interior and exterior columns.

The final displaced shape, shown in Figure 3-4(b), highlighted how beam elongation could cause failure mechanisms not anticipated by designers.

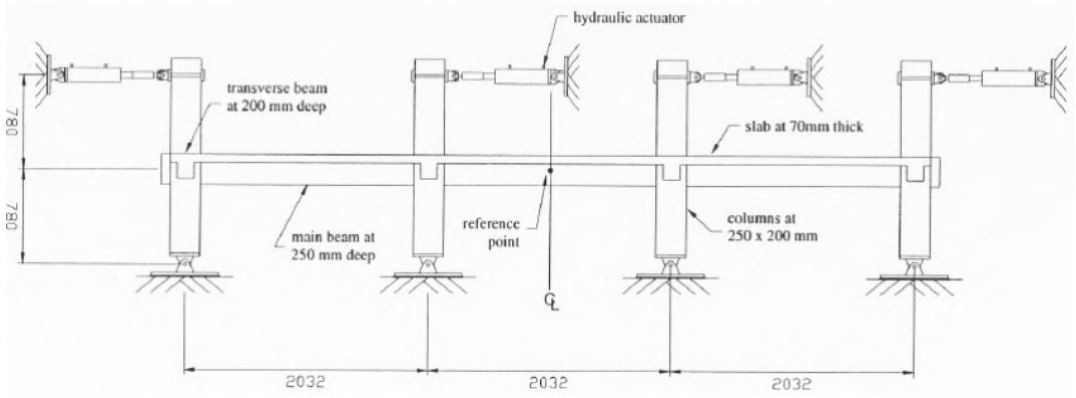

(a) Experimental setup.

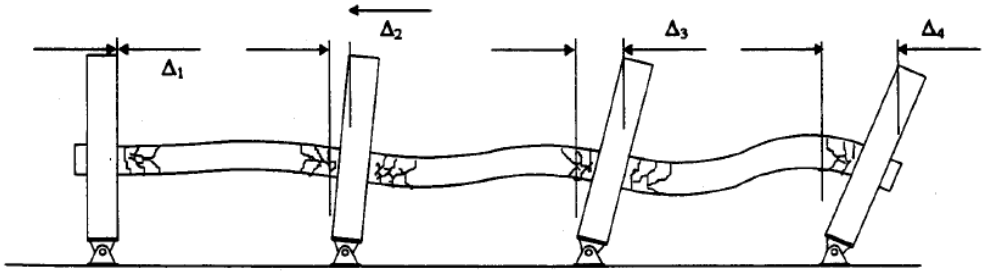

(b) Final displaced shape.

Figure 3-4: Specimen setup and final displaced shape of McBride et al. (1996) experiment.

The results of the experiments conducted by McBride et al. (1996) showed that the presence of a floor slab significantly increased the initial stiffness and overall strength of the system. However, it was observed that the floor did not inhibit beam elongation. The floor reinforcement fractured prematurely, possibly due to the tempering process used to scale the reinforcement steel properties.

The experiment conducted by Wuu (1996) built on the work of McBride et al. (1996). The specimen tested remained three bays long but was extended to two and a half stories, as shown in Figure 3-5. The specimen was scaled at 1/3 and the origin was the lower two and a half stories of a five storey prototype structure. Because the column bases were rigidly fixed to a foundation beam the boundary conditions were more realistic than the experiment by McBride et al. To simplify the specimen, floor slabs were not included. The loading protocol was identical to that used by McBride et al. The results showed that beam elongation affected the frame behaviour. As a consequence of the foundation beam resisting beam elongation, the specimen developed compression in the first storey beams and tension in the second storey beams. The beam elongation and the induced axial forces in the beams changed the distribution of actions in the specimen and caused the formation plastic hinges in the external columns above the first floor beam soffit (Fenwick et al., 1996).

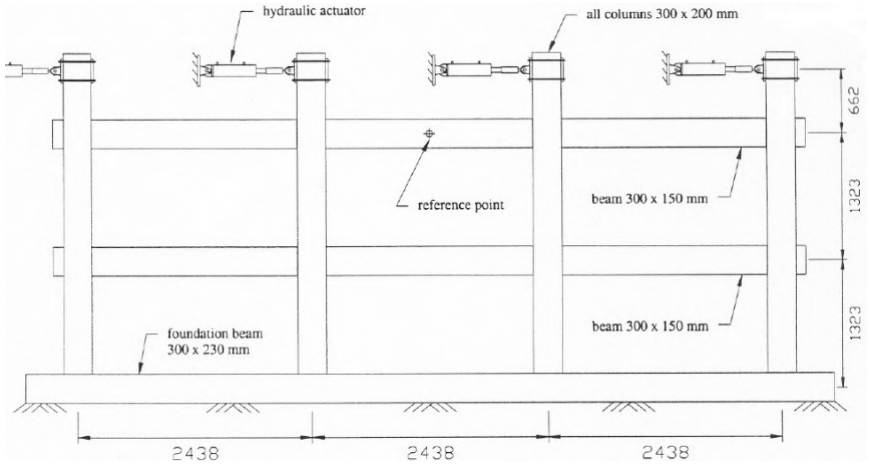

Figure 3-5: Experiment setup by Wuu (1996).

Following the failure of relatively modern reinforced concrete car parking garages during the 1994 Northridge earthquake, which were constructed using details similar to those used in New Zealand at the time, research conducted at the University of Canterbury focussed on determining the likely performance of New Zealand buildings constructed using similar details. Matthews (2004), Lindsay (2004) and MacPherson (2005) conducted a series of experiments to test the adequacy of the current detailing and developed new details where the performance was unsatisfactory. The specimen that formed the basis of the experiments was a one-storey, two-by-one bay, superassembly at full scale. The superassembly, shown in Figure 3-6(c) and (d), was extracted from mid-height of a prototype multi-storey moment resisting structure designed to be representative of New Zealand construction. The specimen was loaded uniaxially in both directions using a self-equilibrating frame. The loading frame, shown in Figure 3-6(a) and (b), was developed by Matthews (2004) and was designed to neither exaggerate nor restrain beam elongation. Equal forces were applied to the top and bottom of the columns using the primary loading frame, whilst the secondary loading frame ensured that the same displacement profile was maintained across all columns.

Matthews (2004) concluded that the observed failure mode of hollow-core connections was different to that assumed in design. A displacement incompatibility was observed between the first hollow-core unit and the adjacent seismic beam, and extensive damage occurred at the interface between the two elements as a consequence. It was shown that current methods for estimating the floor contribution to flexural overstrength, such as NZS3101:1995 and ACI318-02, were unconservative (Standards New Zealand, 1995; American Concrete Institute, 2005). Recommendations were made by Bull and Matthews (2003) to increase the robustness of hollow-core connections in reinforced concrete moment resisting frames. The improved connection details were tested in two subsequent tests by Lindsay (2004) and MacPherson (2005) and shown to perform well.

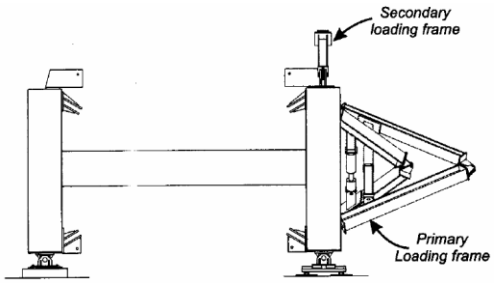

(a) Side elevation of loading frame.

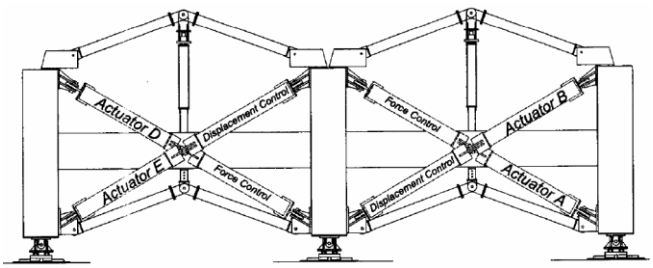

(b) Side elevation of loading frame.

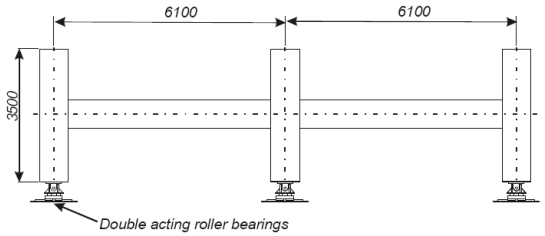

(c) Front elevation of specimen.

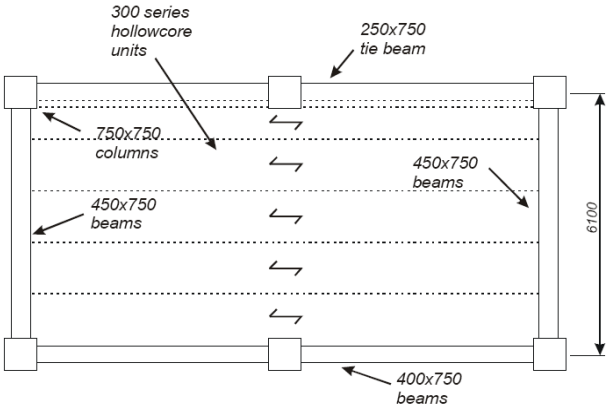

(d) Plan of specimen.

Figure 3-6: Loading frame and specimen developed and tested by Matthews (2004).

Peng (2009) tested a one-storey, two-bay, reinforced concrete subassembly with a precast floor. The purpose of the experiment was to collect data to enable calibration of a numerical plastic hinge model developed by Peng (2009) to be undertaken. As shown in Figure 3-7(a), the specimen was loaded uniaxially by actuators located at the top and bottom of the columns. The column bases were founded on two-way linear bearings to allow elongation to be accommodated, whilst maintaining realistic column displacements. The floor was constructed using a precast concrete rib and infill system supported on transverse beams, which were supported on one-way linear bearings.

The experimental results showed that the behaviour of the interior and exterior plastic hinges was different. Column demands were underestimated by current code methods for predicting floor contributions to beam flexural capacity, such as those described in ACI318-05 and NZS3101:2006 (American Concrete Institute, 2005; Standards New Zealand, 2006).

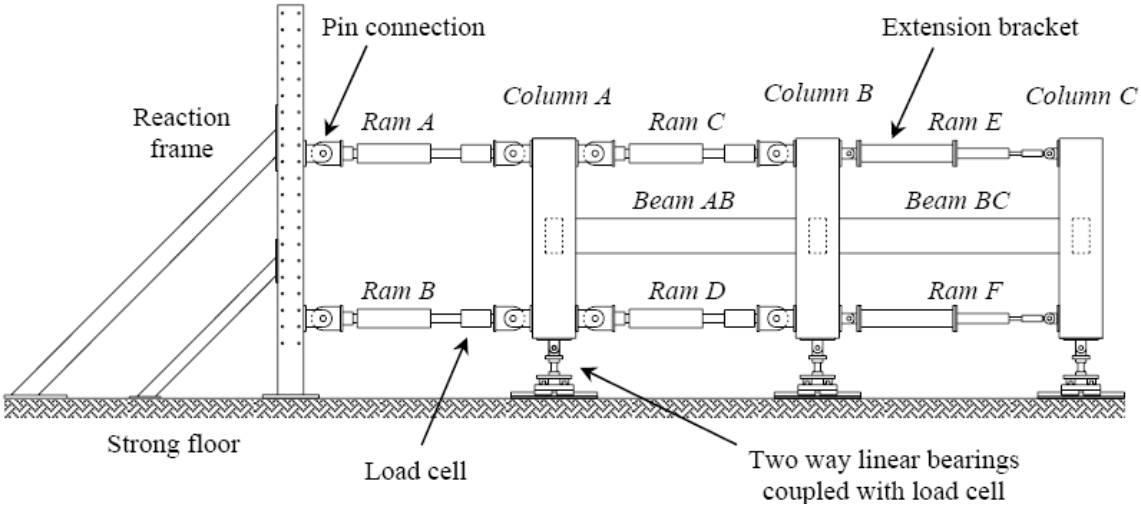

(a) Front elevation.

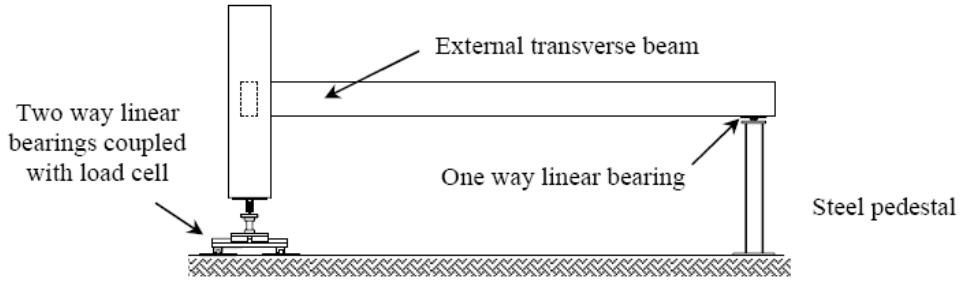

(b) Side elevation.

Figure 3-7: Experimental setup by Peng (2009).

Newcombe (2011) tested a two-storey, two-by-one bay, post-tensioned timber specimen. The performance of the specimen, shown in Figure 3-8, was not relevant to this thesis; however, the experimental setup was. The specimen was subjected to biaxial loading through the column ends. The actuator forces were applied using a splitter beam, which maintained a constant force ratio of 2:1 between the second and first floors respectively. Specimen rotation about the vertical axis was actively restrained to simplify subsequent analysis. The effect of loading the specimen through one end could not be assessed due to local joint deformations effectively cancelling out beam elongation. Because the specimen was designed as a two storey structure, inertial forces could not be considered insignificant compared to column shears from the levels above. Hence, in subsequent tests on the same specimen the actuator forces were applied through the diaphragms instead of the columns.

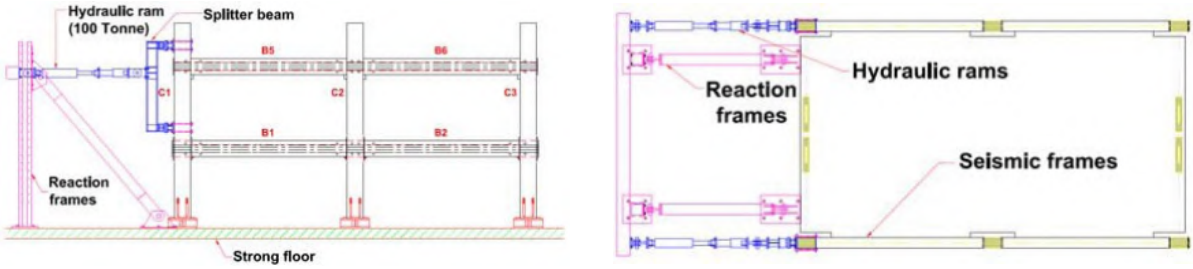

(a) Front elevation. **(b) Plan view.**

Figure 3-8: Experimental setup by Newcombe (2011).

3.3 Seven Storey Prototype Building

The prototype building from which specimen SA1 originated was a seven storey moment resisting frame with a one-way precast flooring system. The prototype structure, shown in Figure 3-9, was designed to be typical of New Zealand construction. The design of the prototype structure was based on a 50 year service life. It was assumed that the building was located in Wellington, subject to near fault effects and on a site with soil class C (Standards New Zealand, 2004). The prototype building was three-by-two bays in plan, and each bay was 7.43m and 6.29m in the long and short directions respectively; the interstorey height was 3.00m. The lengths were a consequence of the maximum size specimen that could be fit into the structures extension laboratory after geometric scaling was applied.

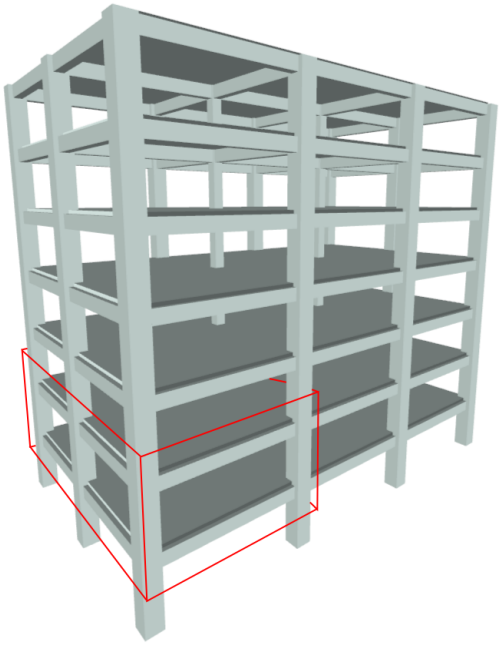

Figure 3-9: Seven storey prototype building with origin of superassembly SA1 highlighted.

The columns dimensions were 900x900mm and the beams were 654x447mm. All frames contributed to seismic resistance. The floors were a one-way precast system with a 90mm insitu topping. To determine design actions, the prototype structure was analysed using both modal response spectrum and numerical integration time history methods in accordance with NZS1170:2004 (Standards New Zealand, 2004).

3.3.1 Specimen Nomenclature

Within this dissertation portions of the specimen are referred to by codes based on plan Grids and physical locality. The beams and columns are referred to by the prefix Bm or Col respectively. Following the prefix is a string of characters in the form of X/Y-Z; where X is the north-south Grid (A, B or C), Y is the east-west Grid (1 or 2) and Z is the level. For beams, Z can be 1 or 2, which refers to the storeys; whereas for columns it can be A, B or C,

which refers to the bottom, middle or top columns respectively. Furthermore, the beam codes may have a suffix to denote the framing direction of the beam that is being identified. The naming convention is presented graphically in Figure 3-10.

By way of example, the beam extending in the northern direction of the central southern span on Level One is instead referred to as Bm B/2-1 north. Similarly, the middle column of the south-east corner is referred to as Col C/2-B.

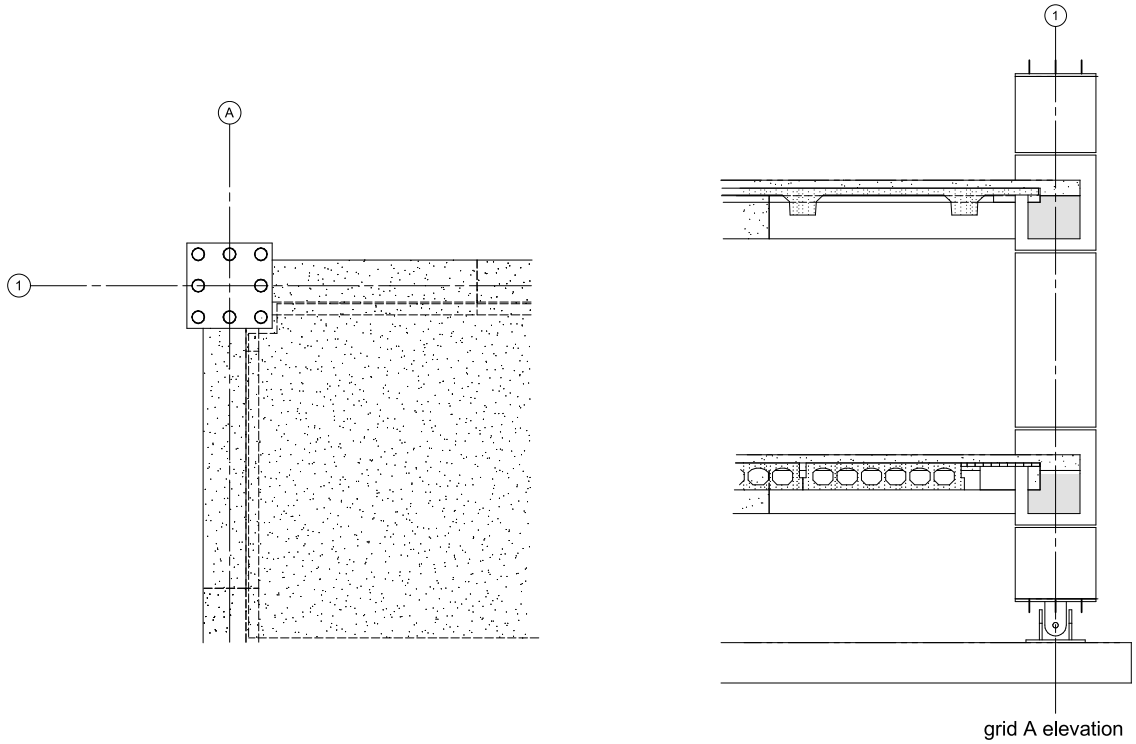

(a) Corner beam unit Bm A/1-2

(b) Column units Col A/1-A, A/1-B and A/1-C with beam units Bm A/1-1 south and Bm A/1-2 south.

Figure 3-10: Specimen SA1 component naming conventions.

When the reinforcement within a beam is being discussed, an additional naming convention is used in conjunction with the component naming convention. The naming convention for the various reinforcement types is presented in Figure 3-11. The diagonal shear hangers along Grid A, C, 1 and 2 are denoted either internal, centre or external. An external hanger describes the hanger closest to the outside perimeter of the specimen. On Grid B, because both sides are internal, cardinal directions are used instead. The same naming convention is used when discussing main longitudinal reinforcement, except the reinforcement being discussed is prefixed by top or bottom denoting the relative position within the beam.

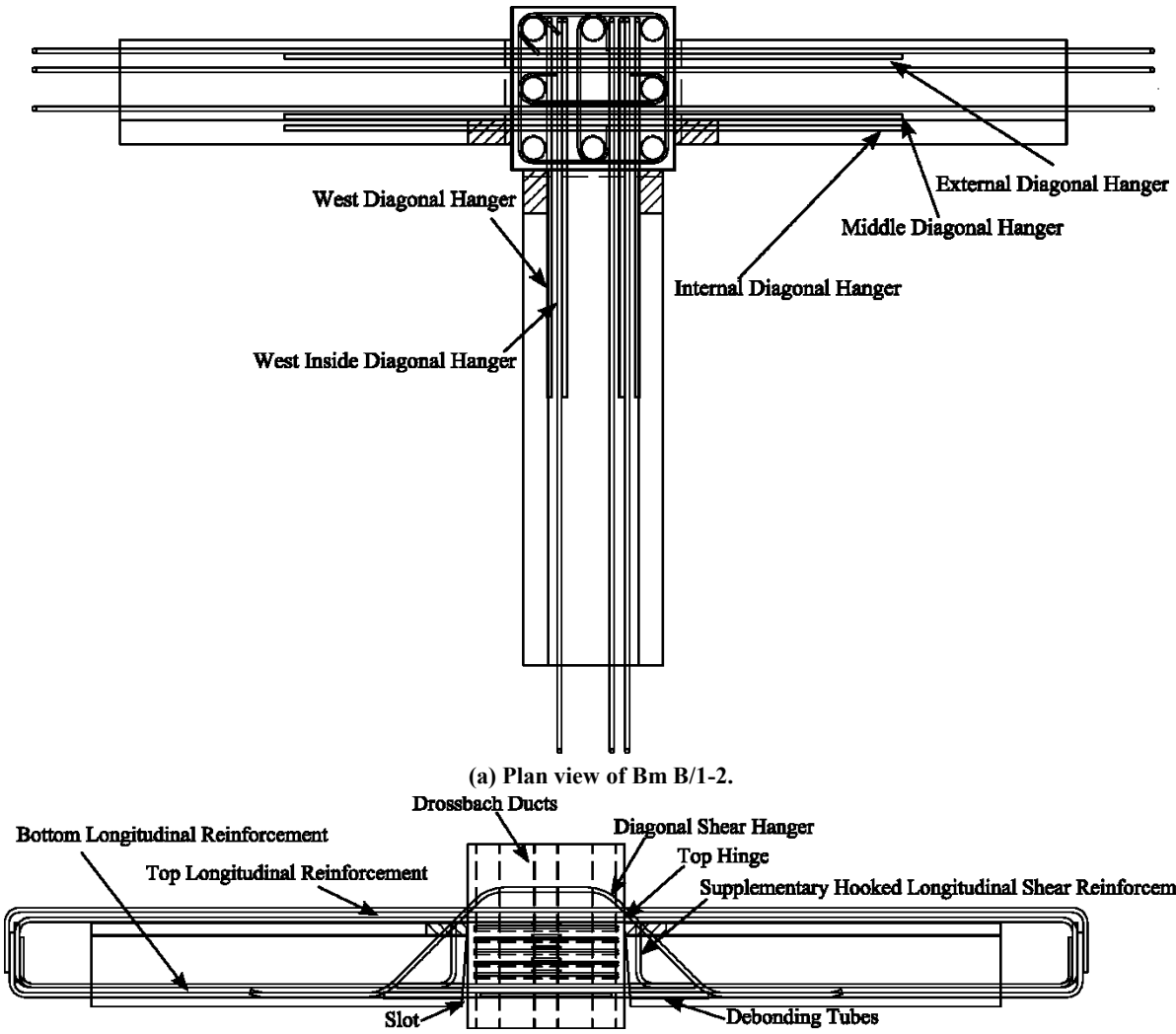

(a) Plan view of Bm B/1-2.

(b) Elevation of Bm B/1-2 east and west beams.

Figure 3-11: Specimen SA1 reinforcement naming conventions.

Precast floor units are described by the location of the units within specimen SA1 because they are not located on Grids. For example, the northern-most hollow-core unit in the eastern bay is referred to as the north-east hollow-core unit.

3.4 Specimen SA1 Design

Specimen SA1 was a two-storey, two-by-one bay, superassembly which represented the first and second stories of a prototype building. Superassembly SA1 was scaled geometrically at two-thirds; similitude details can be found in Section 3.4.6. The origin of SA1 is shown in Figure 3-9 and a three-dimensional perspective of the specimen on the laboratory strong floor is presented in Figure 3-12. The specimen was designed in accordance with the New Zealand Concrete Structures Standard (Standards New Zealand, 2006) and recommendations from recent research (Au, 2010; Leslie, 2010). To provide a favourable weak-beam strong-column failure mechanism, capacity design principles were applied.

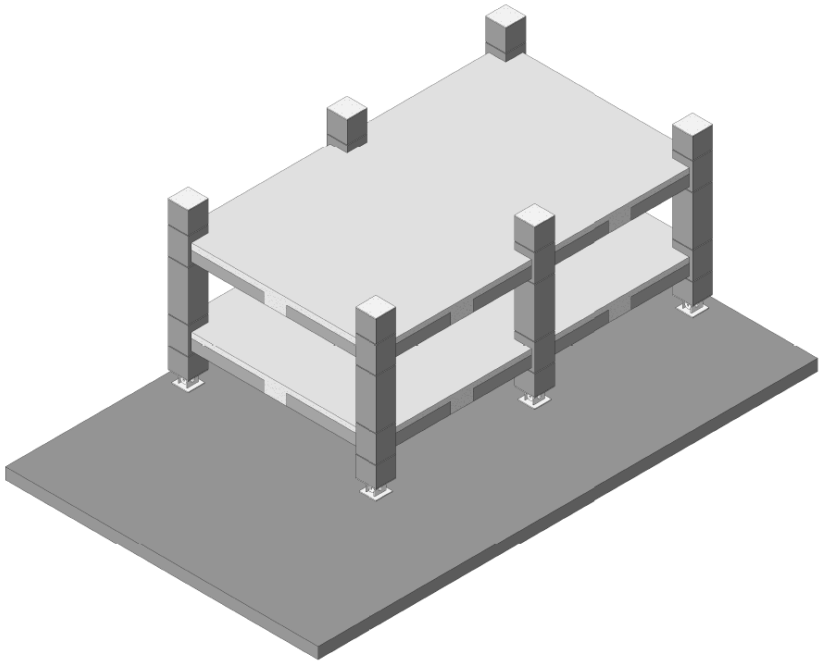

Figure 3-12: SA1 superassembly test specimen.

3.4.1 SA1 General Layout

Construction drawings of SA1 are shown in Figure 3-13(a) – (d). Grids A, B and C ran north-south; Grids 1 and 2 ran east-west. The interstorey height was 2000mm and the bay lengths were 4953mm and 4191mm in the north-south and east-west directions respectively. The column and beam dimensions were 600x600mm and 436x296mm respectively. Full construction and precast drawings can be found in Appendix B at a larger scale.

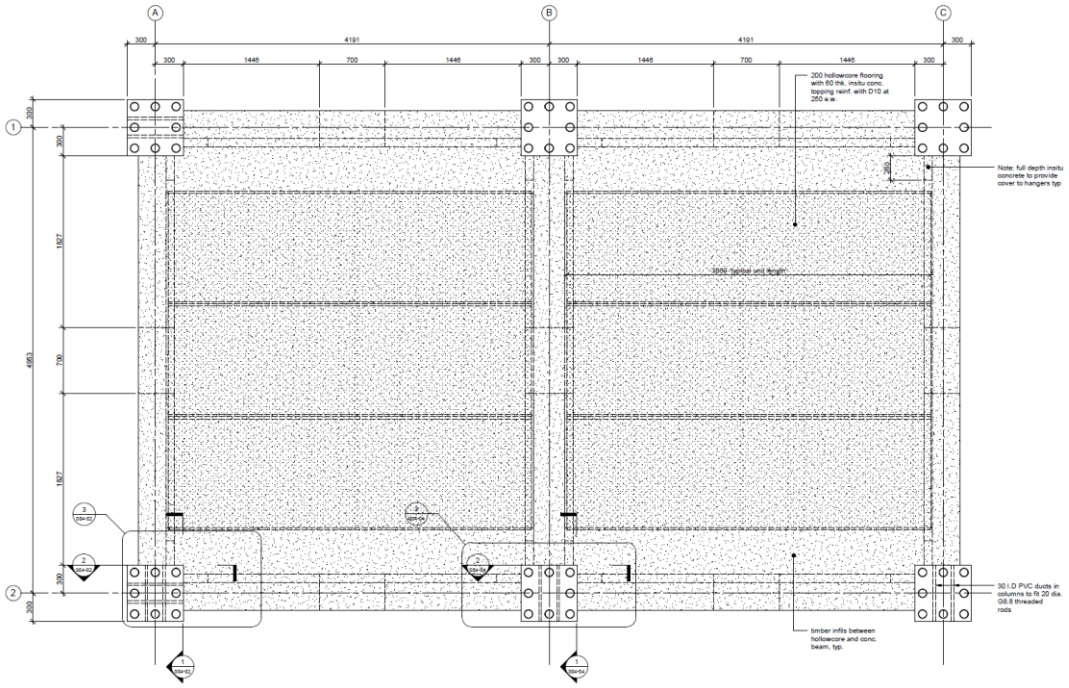

(a) Level One plan.

Figure 3-13: Dimensions and arrangement of specimen SA1.

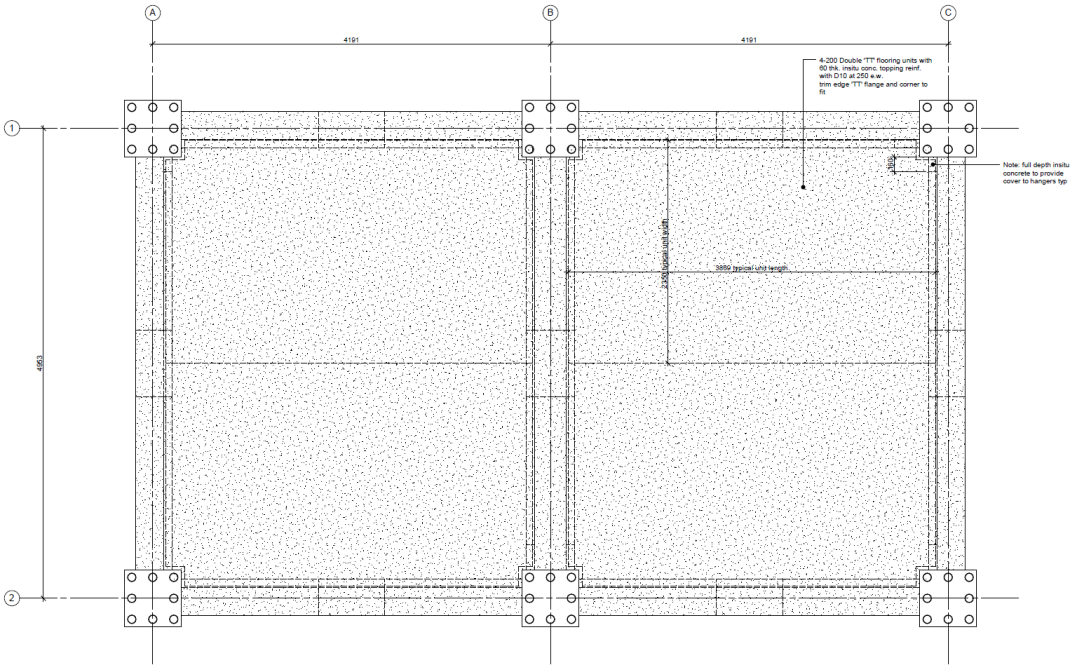

(b) Level Two plan.

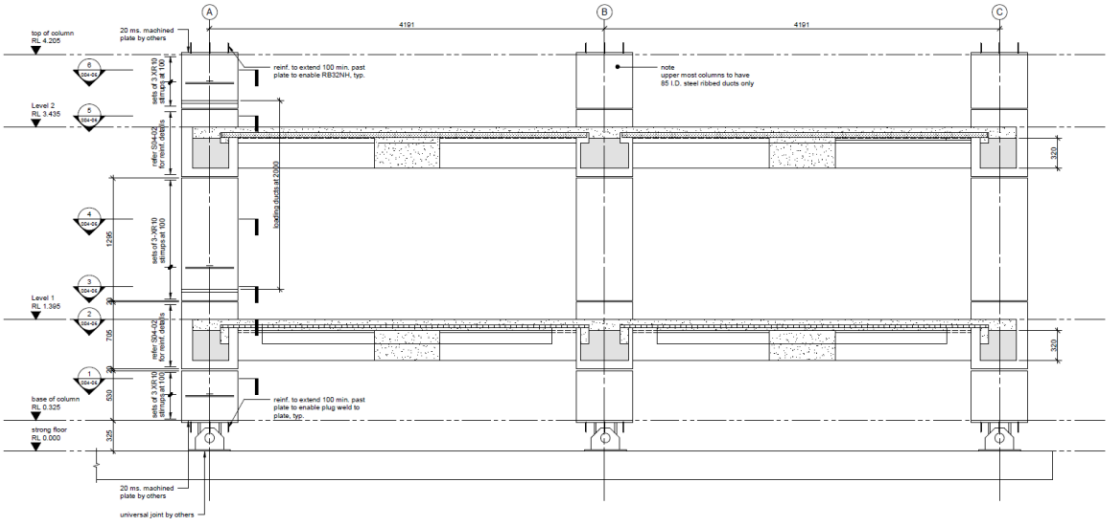

(c) Grid 1 elevation.

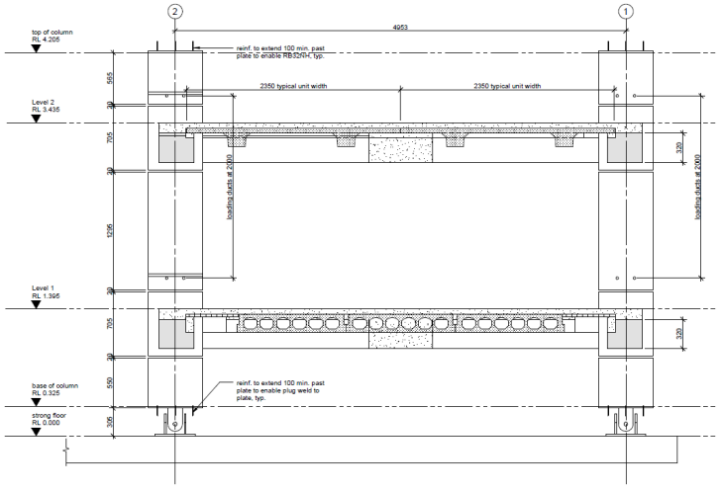

(d) Grid A elevation.

Figure 3-13: Dimensions and arrangement of specimen SA1 (Continued).

The specimen was tested in the structures extension laboratory at the University of Canterbury and was located in the north-east corner of the strong floor.

The specimen was designed to replicate realistic New Zealand building geometry and construction techniques. As such, the precast concrete elements were designed as system two units (CAE, 1999). The beam-column joint zones were cast full height to avoid the construction complexities that the diagonal hangers would have introduced if cast insitu. The beams were cast to partial height and the remainder was cast with the diaphragm once the prestressed floors were installed. The beams were connected together at mid-span using a double hooked lap joint (CAE, 1999). The columns were precast and the column longitudinal reinforcement was continuous through corrugated steel ducts in the beam-column joints. Above the beam-column joints, grouted reinforcement splice sleeves were used to connect the column longitudinal reinforcement.

3.4.2 SA1 Beam Design

The design moment capacities of the beams were extracted from the scaled results of the analyses performed on the prototype structure. However, minimum reinforcement ratios recommended by Au (2010) governed the bottom longitudinal reinforcement design. To reduce the risk of low-cycle fatigue failure, Au's (2010) recommendations suggest a tensile reinforcement ratio of greater than 0.7%. The bottom longitudinal reinforcement was Grade 300 to reduce bond demands through the interior columns. Ohkubo et al. (1999) introduced the use of top longitudinal reinforcement with a greater capacity than the bottom longitudinal reinforcement to reduce the reinforcement strain in the top hinge. Parametric analyses by Au (2010) showed that a strength ratio between the top and bottom longitudinal reinforcement of approximately two was required to minimise top hinge cracking. This relationship is shown in Equation 3-1, where A_s and f_y are the area and yield strength of the bottom longitudinal reinforcement respectively and primes denote the top longitudinal reinforcement. The use of Grade 500 steel for the top longitudinal reinforcement increased the strength by approximately 66% compared to the bottom longitudinal reinforcement. Hence, the required increase in top longitudinal reinforcement area could be minimised to improve the connection constructability.

$$\frac{A'_s f'_y}{A_s f_y} \approx 2 \qquad \textbf{Equation 3-1}$$

The diameter of the longitudinal beam reinforcement was limited by bond requirements through the interior columns. For the top longitudinal reinforcement, bond provisions for elastic reinforcement from NZS3101:2006 were used (Standards New Zealand, 2006). For the

bottom longitudinal reinforcement, bond recommendations developed by Au (2010) were used. These recommendations are based on theory presented by Paulay and Priestley (1992) and take into account the greater bond demand experienced in slotted beams. To protect against premature bond failure through interior columns, specimen SA1 used a detail to improve bond. Additional reinforcement was fillet welded to either side of the main longitudinal reinforcement through the column region, as shown in Figure 3-14. This detail reduced strain penetration and increased the effective bond area.

Figure 3-14: Supplementary welded reinforcement in interior joint.

Supplementary welded reinforcement has been used extensively by researchers at the University of Auckland to concentrate plasticity in beam plastic hinge zones by providing an elastic joint zone (Fenwick & Nguyen, 1981; Fenwick, 1983; Budiono, 1988; Davidson & Fenwick, 1993). Based on the recommendations of these researchers, the additional reinforcement was welded beside the main longitudinal reinforcement, rather than above and below, to reduce flexural strain induced by joint shear deformation. Two lengths of reinforcement were used rather than one to prevent warping during welding. There are other means of decreasing reinforcement bond stresses through internal columns, such as mechanical couplers, grout sleeves and bearing plates; however, the supplementary welded reinforcement design was chosen over others because it was the most practical and economical solution.

It has been shown that correct welding of reinforcement does not affect the strength or ductility of seismic Grades 300E and 500E (HERA, 1998; Scholz & Roberts, 2000). Welding was performed in accordance with the New Zealand Structural Steel Welding Standard AS/NZS 1554.3:2008 (Standards New Zealand, 2008). Additional information on the detail is presented in Section 3.5.1.9.

Top hinge depth was governed by minimum concrete cover depths and the geometry of the two layers of top reinforcement framing in from orthogonal directions. Parametric analyses by

Au (2010) showed that the top hinge depth, expressed as a fraction of the beam depth, d, should be approximately 0.25d to limit strain in the top longitudinal reinforcement. Due to the geometric restraints imposed by the reinforcement, the top hinge depth for specimen SA1 was 0.27d.

From the initial concept of the slotted beam during the PRESSS programme (Nakaki et al., 1999), to the adaptation by Japanese and New Zealand researchers (Ohkubo et al., 1999; Au, 2010; Leslie, 2010), the slot shape has always been rectangular. However, a rectangular geometry is disadvantageous due to shallower diagonal compressive shear struts, smaller clearances with the shear hangers, localised stresses in the corners and unpleasing aesthetics. To address these issues, the geometry was changed from rectangular to triangular for specimen SA1. The difference between the slot shapes can be seen in Figure 3-15.

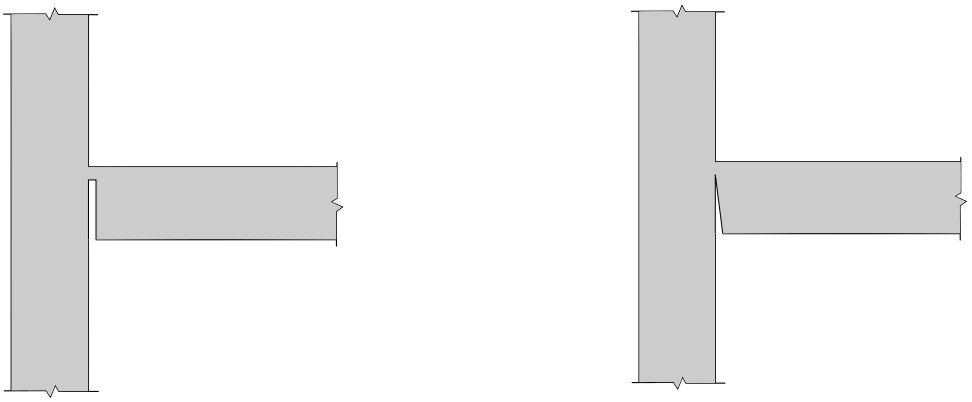

(a) Slot geometry historically used. **(b) New slot geometry.**

Figure 3-15: Connection slot geometries.

The width of the slot was designed to be sufficient to accommodate connection rotations caused by design level interstorey displacements. A wider than necessary slot was undesirable due to the increased risk of bottom unbonded longitudinal reinforcement buckling.

The length and type of debonding tube used over the bottom longitudinal reinforcement was important to prevent reinforcement rupture, reduce the likelihood of low-cycle fatigue failure and restrain reinforcement buckling. The unbonded length was maximised to delay the onset of low-cycle fatigue; however, limits existed to the maximum length that was practically achievable. If the unbonded length was not terminated before the bottom bend of the shear hangers then the shear transfer mechanism could be disrupted. A reaction force could not be generated in the bottom longitudinal reinforcement to maintain equilibrium with the diagonal compressive concrete shear strut and tensile diagonal hanger force. Cracks through the section could result as a consequence of tensile stresses being induced in the concrete; these types of cracks are termed ‘s-cracks’ (Ohkubo et al., 1999). The strut and tie mechanism that can result in s-crack formation is shown in Figure 3-16.

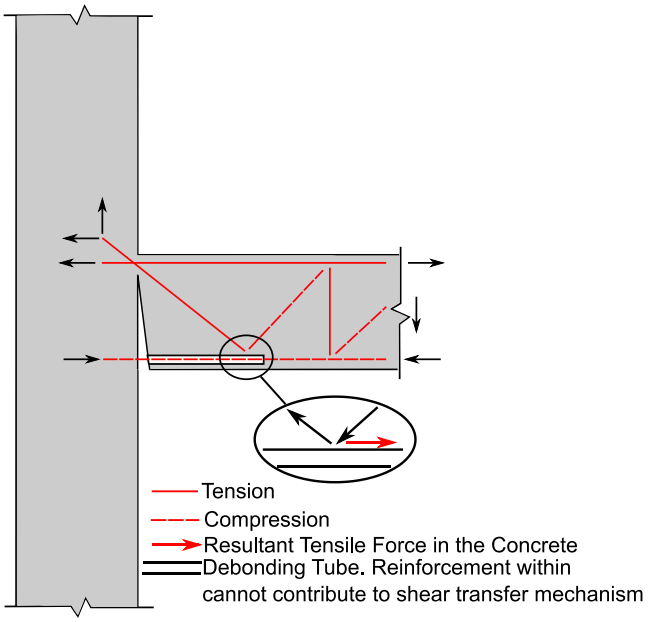

Figure 3-16: Strut and tie mechanism within a slotted beam that results in s-crack formation.

In specimen SA1, shear transfer was made more difficult by two of the three diagonal hangers being located outside of the main beam reinforcement cage, as shown in Figure 3-17. The location of the diagonal hangers had the potential to inhibit their ability to effectively capture the horizontal tensile force induced by the diagonal concrete shear strut, which could have induced tensile strains in the concrete and lead to the formation of s-cracks. Supplemental XD16 reinforcement, terminated with a 90° return, was provided in the beam ends to resist this undesirable failure mechanism. The X prefix denotes Grade 500 reinforcement; the D prefix denotes deformed reinforcement. In SA1, this additional reinforcement was continuous through the remainder of the beam to provide gravity resistance. For the north-south direction, the frames were gravity dominated due to the one-way flooring system.

In SA1, the unbonded length was restricted to a practical limit of approximately 80% of the beam depth. This limit existed because the diagonal hangers were designed to enter the beam on a 45˚ angle. The maximum practical unbonded length could have been increased by using diagonal hangers with a shallower angle; however, the shear and torsional strength of the connection would have been decreased. Au (2010) showed that the most effective debonding method to restrain buckling of the longitudinal reinforcement was mild steel tubing in conjunction with a reduced beam stirrup spacing over the unbonded length. Seamless mild steel tubing with wall thickness of 3.73mm and 3.91mm was used to debond the D12 and D16 reinforcement respectively. Stirrups were located at $4d_b$ centres, where d_b denotes the diameter of the bottom longitudinal reinforcement. The reinforcement was wrapped in insulation tape to reduce the ingress of concrete paste into the unbonding tubes.

The design of the diagonal hangers was based on demand from gravity shear, seismic shear, beam torsion and induced tension from connection flexure. Beam torsion was comprised of

two components, which are presented graphically in Figure 3-17. Because the weight of the floor was applied eccentric to the shear centre of the supporting beam, a moment was generated along its length. Similarly, the continuity moment generated by the floor connection during specimen displacement caused a moment along the beam length. The moments applied to the supporting beam caused beam torsion, which was resisted by the shear hangers.

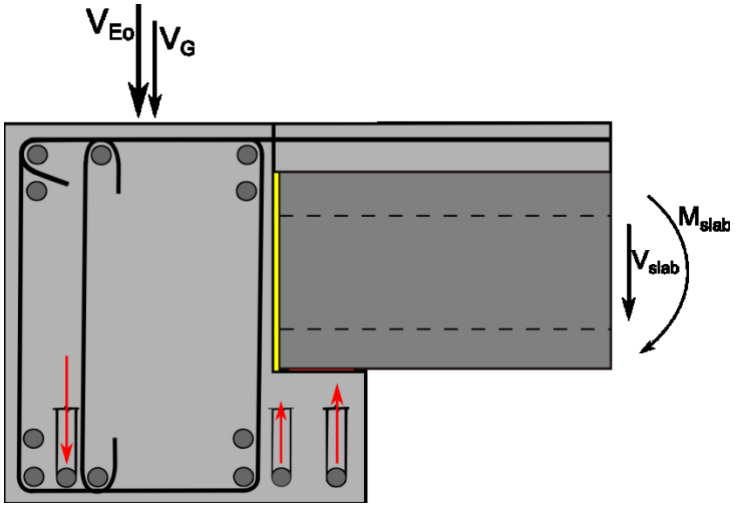

Figure 3-17: External and internal forces acting on shear hangers.

The magnitude and sign of the hanger forces changes with the direction of the earthquake. For design, the combinations that gave the worst case tension and compression in the hangers were used. The worst case hanger loading scenarios occur when positive and negative earthquake shear, V_{Eo}, combine with the negative moment contribution of the slab, M_{slab}. The different load combinations that the hangers can be subject to are shown in Figure 3-18. If the vertical component of earthquake demand is ignored, then beam shear, V_G, and floor slab shear, V_{slab}, do not change direction or magnitude upon reversal of earthquake loading. The induced strain in the hangers due to connection flexure was determined by sectional analysis and considered in the design. The induced strain was minimised by positioning the diagonal hanger through the top hinge so as to minimise its distance from the neutral axis during both positive and negative connection flexure.

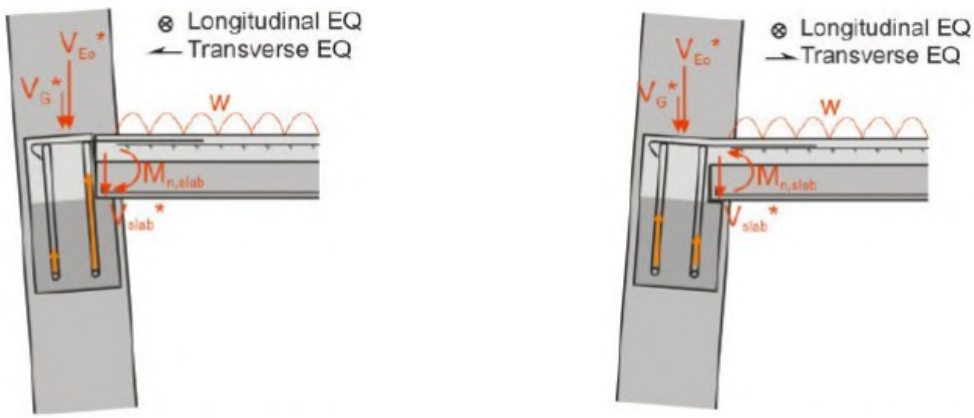

(a) Drifts left and into page. **(b) Drifts right and into page.**

Figure 3-18: External and internal forces resulting from biaxial earthquake loading (Au, 2010).

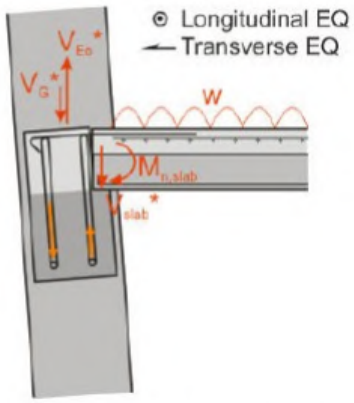

(c) Drifts left and out of page.

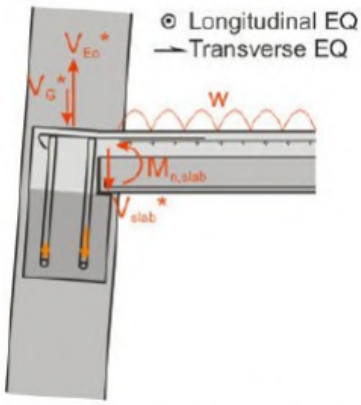

(d) Drifts right and out of page.

Figure 3-18: External and internal forces resulting from biaxial earthquake loading (Au, 2010) (Continued).

Three hangers were used in each perimeter connection to increase the shear and torsional capacity of the connection. The hanger detailing used in specimen SA1 improved the three hanger detail, first tested by Au (2010), by placing two of the three hangers outside the main beam reinforcement. Positioning two hangers in the beam ledge increased the torsional capacity of the connection by increasing the distance between the hangers in tension and compression.

The demand on the interior beams on Grid B differed from the exterior beams on Grids A and C. The seismic shear was the same as the beams on Grids A and B; however, the gravity shear was approximately double. Furthermore, because there were precast floor connections on either side of the beam on Grid B, the reaction forces were equal and opposite. However, the induced continuity moments on either side of the Grid B beam were additive. Design actions were determined for the internal beam in the same matter as for the external beams, expect with different applied actions. Due to the large shear demands on Grid B, a new four hanger design was developed for internal beams.

The 45˚ angle of the hanger was a compromise between ensuring hanger axial force and stiffness was reasonable, and being able to provide sufficient unbonded length to the bottom longitudinal reinforcement. The radius of the top and bottom hanger bends was designed based on concrete splitting as per §8.4.2.1 of NZS3101:2006 (Standards New Zealand, 2006). Anchorage of the hangers in exterior columns was by way of standard 90˚ returns. A continuous hanger detail was developed for the interior columns; therefore, the hanger had to satisfy requirements for maximum reinforcement diameter permissible through an interior joint. The continuous hanger design allowed for a less congested, and more compact, joint than previously tested designs.

To reduce the demand on the shear hangers in the slotted beam, the continuity moment from the floor support was minimised. How this was achieved in specimen SA1 is outlined in Section 3.4.5.

To determine the design forces in the shear hangers an analysis based on a spring model, proposed by Au (2010), was undertaken. A schematic of the spring model is presented in Figure 3-19. The spring model was required due to the statically indeterminate nature of the problem. The springs allowed for deformations in the system, which changed the centre of rotation. The contribution that the concrete in the top hinge made to the torsional strength and stiffness of the slotted beam connection was conservatively ignored. Because cracking through the top hinge occurs at approximately 0.5% beam drift, as shown in Section 4.6, the contribution of the top hinge concrete to torsional strength and stiffness cannot be relied upon during a design level earthquake. Furthermore, it is possible that cracking in the top hinge could have occurred prior to a design earthquake occurring due to serviceability level loading or shrinkage. Hence, it is assumed that the torsional stiffness of a slotted beam connection relies only on the contributions from the diagonal hangers.

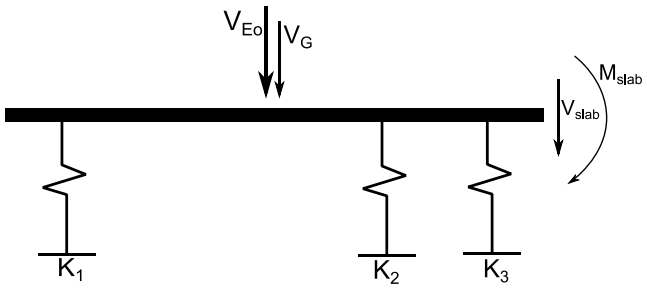

Figure 3-19: Spring model of slotted beam diagonal hangers.

The analysis of the diagonal hangers was undertaken with the worst case loading scenarios for maximum tension and compression in the hangers. The hangers were designed to elastically resist the maximum forces determined from the analyses.

The top bend of the hangers was located inside the column longitudinal reinforcement, which introduced the compressive strut which forms on the inside of the bend into the joint region. This detail ensured that shear forces were transferred through inclined axial force and not dowel-action of the reinforcement. Axial force transfer is a stiffer mechanism than dowel-action, which reduced shear deformation through the connection. Shear deformation was undesirable as it could hasten the onset of bottom longitudinal reinforcement buckling.

To limit strain impose by connection flexure, the hangers were positioned to pass through the top hinge midway between the top two layers of longitudinal reinforcement. Parametric studies by Au (2010) have shown that the hangers should be placed at approximately 0.7 the top hinge depth to minimise strain due to flexure. However, the investigation by Au (2010) was undertaken on singly reinforced beams only. The upper and lower top longitudinal reinforcement were at different elevations in the north-south and east-west direction to avoid them interfering through the joint zones. The different reinforcement layouts had the potential to affect the neutral axis variation in each of the orthogonal directions. Hence, the hangers

were located between the two layers of top reinforcement through the top hinge, which were at different elevations for the east-west and north-south directions.

The design of the slotted beam transverse reinforcement differed slightly from that of a traditional reinforced concrete beam. The $4d_b$ spacing of the stirrups over the unbonded length of the longitudinal reinforcement was governed by anti-buckling restraint recommendations (Au, 2010). NZS3101:2006 (Standards New Zealand, 2006) requirements for transverse reinforcement were applied for the remainder of the beams. Within two beam depths of the column face, the potential plastic hinge zone in traditional connections, the stirrup spacing was the minimum of d/4 or $6d_b$. Outside of the potential plastic hinge zones the stirrup spacing was the minimum of d/2 or 400mm (Standards New Zealand, 2006). Potential plastic hinge stirrup spacing requirements were applied over the length of the mid-beam splice to increase the robustness of the connection.

3.4.3 SA1 Column Design

The specimen columns were designed according to capacity design principles. The design actions were determined by calculating the peak overstrength demands that could be generated in the beams, which included contributions such as material enhancement. In slotted beams, increased plasticity in the bottom longitudinal reinforcement can result in increased cyclic strain hardening. Based on experimental results, an overstrength factor of 1.4 was recommended by Au (2010).

The floor diaphragm can contribute significantly to flexural overstrength of beams. NZS3101:2006 (Standards New Zealand, 2006) has provisions to account for the influence of the floor diaphragm on connection capacity; however, Peng (2009) showed that the method described in the standard can underestimate this contribution by as much as 80%. It has been stated that slotted beam connections activate less floor reinforcement than traditional connections during negative flexure due to the reduced lever arm between the neutral axis and the floor (Au, 2010). Experimentation by Au (2010) suggested a total slotted beam connection overstrength of 1.6 could be expected due to the influence of the floor diaphragm.

Peng (2009) showed that the torsional resistance of transverse beams can contribute to system overstrength. The loading method of Peng's (2009) specimen was such that one end of the transverse beam was fixed, which maximised the beam torsion. Both ends of the transverse beams SA1 rotated by similar amounts; however, the continuity moment provided by the one-way floor connections resulted in beam torsion being generated. The floor connection detail used in SA1 reduced continuity moments compared to connections used by previous researchers (MacPherson, 2005; Peng, 2009).

The possible layout of the column longitudinal reinforcement was restricted by the beam reinforcement and diagonal hangers framing into the columns on both axes. Hence, a typical layout of 12 longitudinal reinforcement bars could not be achieved, and the use of eight was necessitated. This meant that the spacing between adjacent longitudinal column reinforcement was greater than the specified maximum in NZS3101:2006 (Standards New Zealand, 2006). The intent of this clause is to provide the column with limited ductility. The Standard is based around the premise of design using traditional reinforced concrete beams; hence, many clauses within the Standard are a consequence of the undesirable behaviour that traditional reinforced concrete connections can exhibit. Slotted beams exhibit less beam elongation than traditional concrete beams and have a smaller floor contribution to beam overstrength; hence, the likelihood of column hinging and the need for column ductility is reduced. The column longitudinal reinforcement spacing requirements are potentially not as relevant for the design of slotted systems as they are for traditional systems.

The longitudinal column reinforcement layout necessitated large reinforcement diameters to obtain the required reinforcement ratio. As result, the diameter of the bars were in excess of the NZS3101:2006 requirement for maximum reinforcement diameters through a beam-column joint (Standards New Zealand, 2006). Due to the limited reinforcement sizes that were available, a larger than desired diameter reinforcement had to be used, which resulted in the column reinforcement being 31% greater than required. The column longitudinal reinforcement was expected to remain elastic throughout testing. Given the column reinforcement diameters were greater than the limits specified by NZS3101:2006, calculations were undertaken to check bond stress demands (Standards New Zealand, 2006). The maximum calculated bond stress demand was 2.9MPa, which was less than the 5MPa maximum recommended value for unyielding column longitudinal reinforcement (Fenwick & Nguyen, 1981). The bond stress limit recommended by Fenwick and Nguyen (1981) was based on 30MPa concrete, which was conservative for specimen SA1.

The design of the transverse column reinforcement was undertaken according to NZS3101:2006 (Standards New Zealand, 2006). The design for shear could not depend on any concrete shear capacity due to the absence of any column axial load, which was the worst case loading condition. Hence, the transverse reinforcement had to resist the entire column shear force. Confinement and anti-buckling requirements did not govern.

The column longitudinal reinforcement had to be spliced between precast elements. Due to the large diameter of the longitudinal reinforcement, the development length was prohibitively large to use traditional lap splices; hence, proprietary grout sleeve couplers were used instead. The only system available in New Zealand at the time was the Reidbar grout

splice, which required the use of Reidbar for the column longitudinal reinforcement. Reinforcement splicing systems are considered less ductile than well-detailed traditional lap splices due to the localised strain that can result at the connection. However, because the columns had been designed to remain elastic throughout response the use of couplers could be justified.

3.4.4 SA1 Beam-column Joint Design

The beam-column joint was designed according to NZS3101:2006 and recommendations developed by recent research (Standards New Zealand, 2006; Au, 2010). The shear transfer mechanism within the beam-column joint of a slotted beam connection differs from that of a traditional connection. During negative flexure, the slot up the column face prevents the concrete compression force from the bottom of the beam from entering the beam-column joint as it does in a traditional connection. However, the total shear force in a slotted beam joint is the same as for a traditional joint; hence, all force across the joint must be transmitted via a diagonal concrete strut to the bottom longitudinal reinforcement and truss-like action. The proportion of force transferred by each respective mechanism depends on the integrity of the bond of the bottom longitudinal reinforcement. The concrete strut mechanism is the most efficient means of force transfer across the joint. There may be loading scenarios where an efficient concrete strut mechanism cannot be maintained; hence, a truss-like transfer mechanism for shear transfer must exist also. Due to the absence of a concrete compressive force from the bottom of the adjacent beam, in the slotted beam joint there is additional force that must be transferred by the horizontal shear reinforcement. The slotted beam joint mechanics are presented in Figure 3-20. To restrain the additional force, Au (2010) recommended that horizontal joint reinforcement be increased 25-40% over the quantity specified by NZS3101:2006 (Standards New Zealand, 2006). Furthermore, it was recommended that the additional stirrups be located in the lower 50% of the joint. Because SA1 had doubly reinforced beams, the space available for the horizontal shear reinforcement was limited.

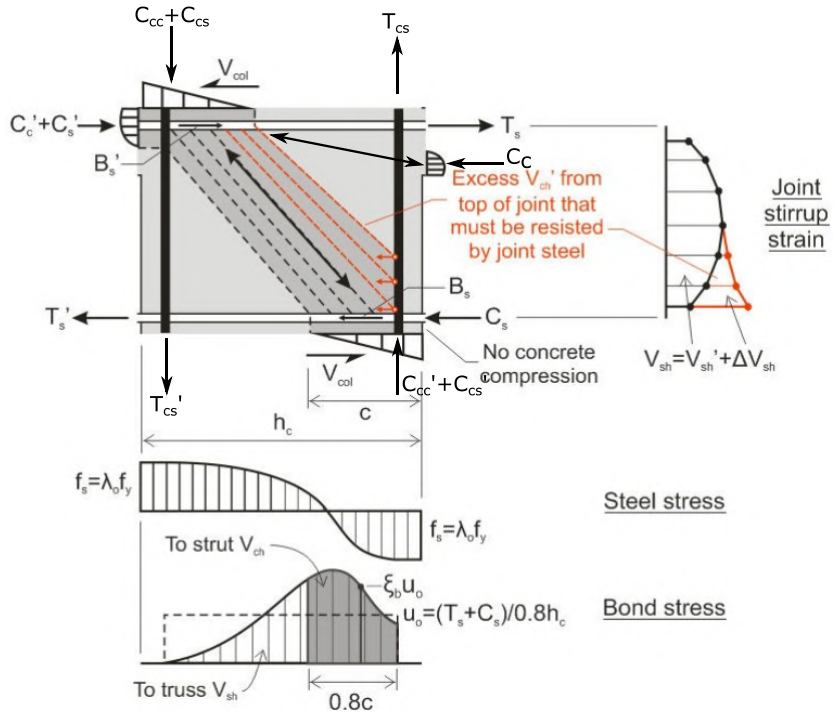

Figure 3-20: Mechanics for slotted beam interior beam-column joint (Modified after Au, 2010).

A three-dimensional rendering of connection Bm B/2-1 is shown in Figure 3-21. Grade 500 reinforcement was used to reduce the number of stirrups required. It was not possible to install the recommended additional stirrups in the lower half of the joint and leave sufficient room for the concrete to be placed correctly. Hence, the additional reinforcement recommended by Au (2010) was distributed over the entire joint region. The stirrup set beside the longitudinal reinforcement is excluded from the provided horizontal reinforcement sum in NZS3101:2006 (Standards New Zealand, 2006). However, the stirrup beside the bottom longitudinal reinforcement was considered to contribute to the additional reinforcement provided due to the steep potential shear failure angle in the beam-column joint zones of slotted beam connections. Hence, NZS3101:2006 and the additional reinforcement recommendation were able to be satisfied in the beam-column joints of SA1 (Standards New Zealand, 2006).

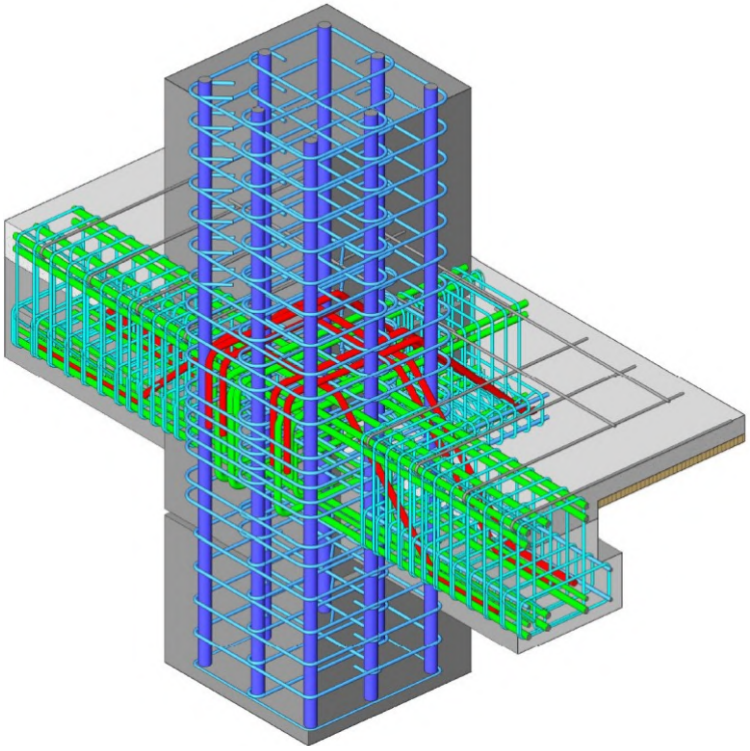

Figure 3-21: Three-dimensional rendering of connection Bm B/2-1.

Vertical joint reinforcement requirements are identical between slotted beam and traditional beam-column joints. These requirements were satisfied by the column longitudinal reinforcement in SA1.

Byrne and Bull (2012) investigated the effectiveness of supplemental vertical reinforcement in the joint region of slotted beams. The thesis was to increase joint stiffness and increase the efficiency of the diagonal strut mechanism of shear transfer. The results were promising; however, the detail was impractical to construct and enabled no reductions in member dimensions or steel content.

3.4.5 SA1 Floor Diaphragm Design

Two precast prestressed flooring systems used in New Zealand were tested in specimen SA1. Six hollow-core units were used in the first floor and four double-tee units in the second. To satisfy similitude requirements, 200mm deep units were used for both types of precast flooring. The manufacture of the prestressed flooring systems is described in greater detail in Sections 3.5.1.12 and 3.5.1.13

NZS3101:2006 prescribes connection requirements for the design of hollow-core flooring systems (Standards New Zealand, 2006). The connections were designed to prevent the initiation of a brittle failure mechanism in the hollow-core as a consequence of displacement incompatibility between the hollow-core unit and the surrounding structure. A conforming design is presented in the Standard and is shown in Figure 3-22 (Standards New Zealand, 2006).

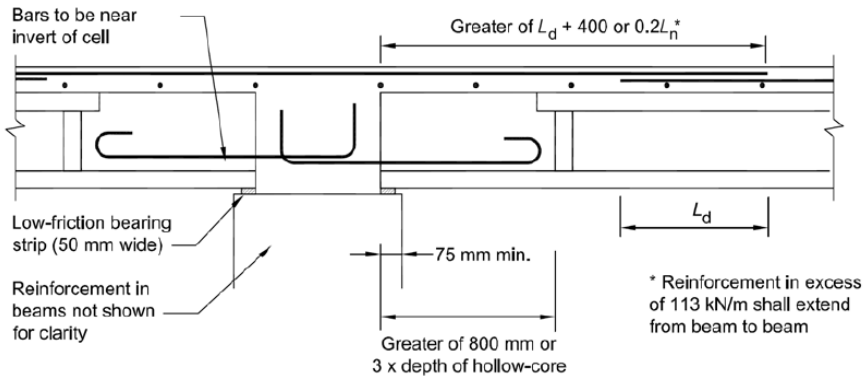

Figure 3-22: Hollow-core seating detail recommended by NZS3101:2006 (Standards New Zealand, 2006).

The detail presented in the Standard was the result of research conducted by Matthews (2004) and MacPherson (2005) at the University of Canterbury (Standards New Zealand, 2006). The original hollow-core connection detail recommended by MacPherson (2005) is shown Figure 3-23.

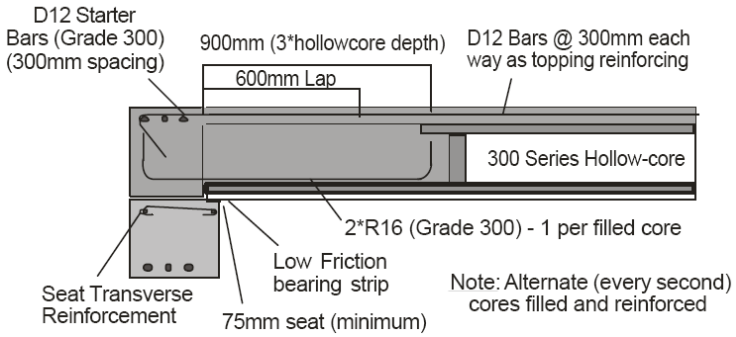

Figure 3-23: Hollow-core seating detail recommended by MacPherson (2005).

The connection detail has been shown to exhibit favourable behaviour when tested in traditional reinforced concrete beam systems; however, the behaviour could be quite different in a slotted beam system (MacPherson, 2005). A significant continuity moment can be generated in the hollow-core connection when subjected to relative rotations caused by earthquake loading. The continuity moment, in conjunction with the eccentric shear loading from the floor, can cause significant torsion in the supporting beam.

Beam torsion was addressed by using the seating detail proposed by Matthews (2004) and tested experimentally by Lindsay (2004). The connection, shown in Figure 3-24, predates that developed by MacPherson (2005) and was developed using the same experimental apparatus designed by Matthews.

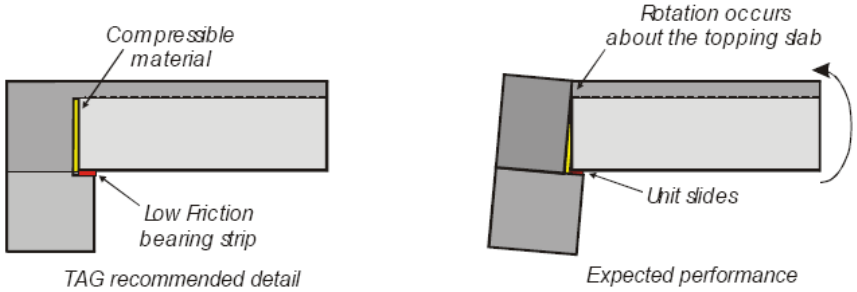

Figure 3-24: Hollow-core seating detail recommended by Matthews (2004).

Because the detail allowed rotation to occur about the topping concrete, the only force couple that could be generated, if contact with beam face is precluded, was due to friction between the hollow-core and the low-friction bearing strip. The connection detail resulted in reduced continuity moment and subsequent supporting beam torsion.

A lack of redundancy was an inherent shortcoming of the connection detail, which had to be addressed when the connection was to be used in a traditional reinforced concrete structure. Because the beam elongation of a slotted beam is significantly less than for a traditional beam, the risk of hollow-core seating length loss is reduced. Hence, there is less importance in having redundancy in the connection, such as catenary bars, to prevent collapse should seating be lost. Hence, the detail suggested by Matthews (2004) was ideally suited to slotted beam applications and was used in SA1.

Displacement incompatibility between structural elements has been shown to cause significant damage in buildings with one-way flooring systems (Matthews, 2004). The difference in deformation modes between the seismic beams and the adjacent floor can result in damage at the interface between the two elements. The damage can be particularly catastrophic in pre-2004 structures, where the hollow-core units have been rigidly connected to the parallel seismic beams. Matthews (2004) suggested a flexible link between the parallel beam and hollow-core unit to address the displacement incompatibility between the elements. This detail is often termed a 'timber infill', in reference to the timber formwork used, and is shown in Figure 3-25.

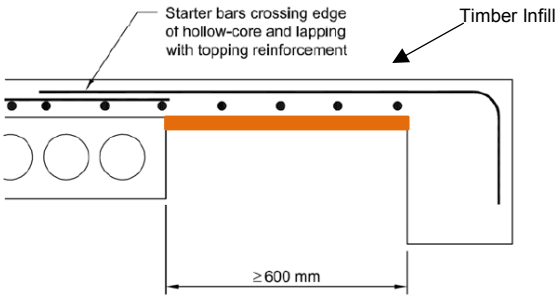

Figure 3-25: Flexible link between hollow-core unit and parallel beam (Standards New Zealand, 2006).

The timber infill provides a gap between the structural units bridged by a thin flexible concrete link. The flexibility of the link allows the two structural units to deform in their natural mode, without generating large forces at the interface. The timber infill detail has been shown to perform well experimentally and was used in specimen SA1 (Lindsay, 2004; MacPherson, 2005).

As shown in Figure 3-26, the double-tee seating detail is similar to that used for the hollow-core. To minimise the continuity moment contribution to supporting beam torsion a dapped double-tee unit was specified. Whilst the seating friction forces in the double-tee connection

were constant for a given span, the reduction in the connection lever arm reduced the continuity moment able to be generated.

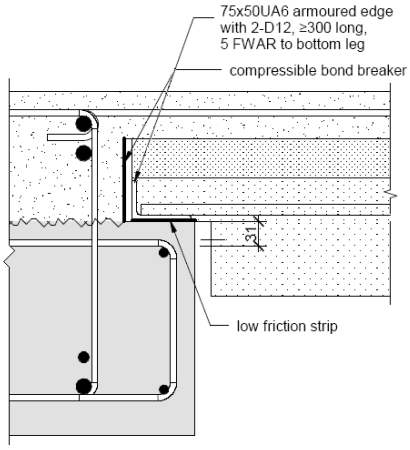

Figure 3-26: Double-tee seating detail.

As shown in Figure 3-26, additional reinforcement was required to transfer shear from the double-tee units to the supporting beam ledge. An unequal angle was welded to the reinforcement to armour the bearing area and prevent concrete spalling. A gap was required between the supporting beam face and the lower half of the double-tee unit to allow for relative rotation between the two. A timber infill was not required on level two of SA1 because the flanges of the double-tee units were sufficiently flexible to accommodate displacement incompatibility.

Precast floor seating width on the supporting beam is an important aspect of floor connection design. The seating width specified in New Zealand has historically has been narrow, with some buildings using 'zero seating' details where the floors are supported by reinforcement placed in the hollow-core cells only. However, research has shown that larger bearing widths are required to provide adequate protection from loss of gravity support during an earthquake (Matthews, 2004). The calculation of the required one-way flooring seating length for SA1 was comprised of many contributions (Hare et al., 2009).

1. Residual seating

   After a major seismic event there must remain sufficient seating to prevent collapse. The seating width estimated to be required to prevent collapse was 20mm.

2. Spalling of the support or unit

   Relative rotations between the precast unit and the seating ledge can cause friction forces, which can lead to a loss of bearing length by spalling the concrete from the supporting beam and the precast unit. Spalling was conservatively assumed to occur outside the ledge reinforcement, as shown in Figure 3-27.

3. Shrinkage and creep

   The concrete in the precast prestressed unit will continue to hydrate and dry out over time, which causes contraction of the precast unit. Furthermore, the constant axial force provided by the tendons can cause axial creep. The axial shortening of the prestressed units was estimated as 1mm per metre.

4. Construction Tolerances

   Tolerances are realistic estimates of attainable construction accuracy. If all likely tolerances are added algebraically the resultant is 36mm. However, it is unlikely that every maximum tolerance will be required simultaneously. Hence, the alternative root-sum-of-squares method was used, which resulted in 17mm of tolerance being calculated (CAE, 1999).

5. Beam Elongation

   Elongation in the beams parallel to the flooring units can reduce the bearing length by forcing the floor supports apart. Whilst beam elongation is significantly reduced in a slotted beam compared to a traditional beam, a conservative upper bound estimate of 0.5% of beam depth was used for design.

6. Geometric displacement of the floor relative to the support

   Rotation of the supporting beam caused by building lateral displacement during an earthquake can reduce bearing width if the seating ledge does not coincide with the beam centre of rotation. Due to the relatively small rotations involved, the displacement was approximated by the rotation multiplied by the distance between the beam ledge and the geometric centre of the beam.

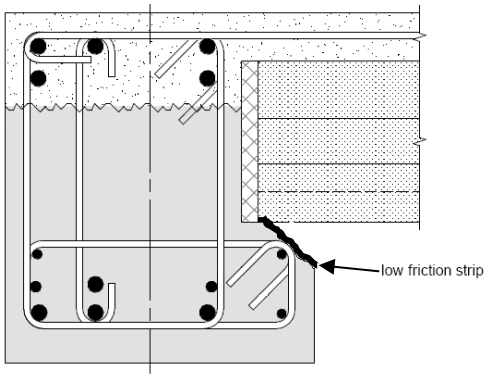

Figure 3-27: Residual seating when cover concrete is lost.

When all contributions were summed, 90mm was the resulting seating width required for specimen SA1. The ledge reinforcement was designed using strut and tie principles.

3.4.6 SA1 Geometric Scaling

It was not possible to test specimen SA1 at full scale due to geometric restraints and capacity limits of the strong floor in the structures extension laboratory at the University of Canterbury. Hence, the superassembly was scaled at 2/3 according to a 'practical true model' philosophy (Harris & Sabnis, 1999). When scaling a test specimen, careful consideration must be paid to similitude for the results to be applicable to a full scale prototype. Similitude relationships are derived from dimensional analysis. Through nondimensionalisation of variables, generic relationships between them can be established. Table 3-1 presents guidelines suggested by Harris and Sabnis (1999) for scaling reinforced concrete models.

Table 3-1: Scale factors for reinforced concrete models.

Category	Quantity	Dimension	True Model	Practical True Model
Material	Stress	FL^{-2}	S_σ	1
	Strain	-	1	1
	Elastic Modulus	FL^{-2}	S_σ	1
	Poisson's Ratio	-	1	1
	Specific Weight	FL^{-3}	S_σ/S_L	$1/S_L$
Geometry	Linear dimension	L	S_L	S_L
	Displacement	L	S_L	S_L
	Angular Displacement	-	1	1
	Area	L^2	S_L^2	S_L^2
Loading	Concentrated Load	F	$S_\sigma S_L^2$	S_L^2
	Line Load	FL^{-1}	$S_\sigma S_L$	S_L
	Pressure	FL^{-2}	S_σ	1
	Moment	FL	$S_\sigma S_L^3$	S_L^3

The parameters S_σ and S_L are stress and length scale factors respectively. To have a 'true model' both stress and length scale factors are required to be applied. However, due to the complex nonlinear properties of the materials being investigated and the difficulties involved in scaling them, a 'practical true model' is applied in the majority of tests. A 'practical true model' is scaled by only the length factor, whilst leaving the stress scale factor as unity. Specimen SA1 was a 'practical true model' and was scaled by S_σ=1.0 and S_L=2/3.

3.5 Construction of Specimen SA1

To enable the practicality of constructing the slotted detail to be assessed, the components of specimen SA1 were manufactured by reputable commercial precast companies. Examining the practicality of the slotted beam system was an important objective of this research. For the slotted beam detail to be a viable alternative to traditional detailing it has to be able to be economically and practically constructed. The use of commercial companies allowed the

slotted beam detail to be tested as it would be built in practice, rather than an idealised version that could be created in a laboratory. The primary frame of specimen SA1 was cast by Bradford Precast Limited in Ashburton, New Zealand. The hollow-core and double-tee flooring units were manufactured by Fulton Hogan Stahlton Limited in Christchurch, New Zealand.

The construction of specimen SA1 is described in this section. Issues that were encountered are described and techniques to mitigate them are developed and proposed. This section is divided into two subsections. Section 3.5.1 describes the manufacture of the precast components. Section 3.5.2 describes the erection of the superassembly.

3.5.1 Manufacture of SA1 Precast Concrete Components

3.5.1.1 Shape of the Slot Form

From the inception of the slotted beam concept the shape of the slot has been rectangular, as shown in Figure 3-28. As presented in Section 3.4.2, triangular slots were designed for SA1. However, during construction issues were encountered in manufacturing the slot form accurately and with the robustness of the form during beam casting.

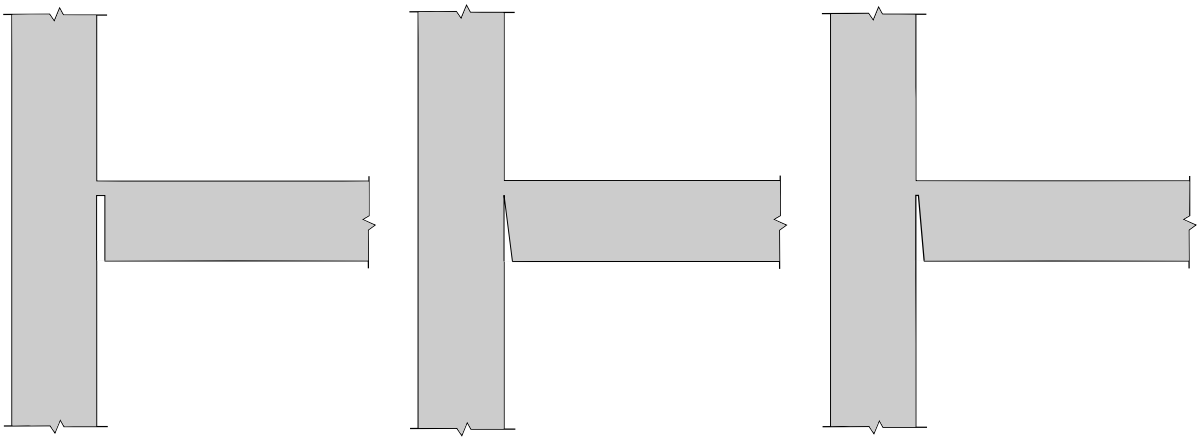

(a) Original square slot shape. **(b) Proposed triangle slot shape.** **(c) Revised trapezoid slot shape.**

Figure 3-28: Slot profiles investigated.

The slot form was manufactured using 'Norski Polyurethane Pour-In foam', a marine grade expanding foam. As shown in Figure 3-29, the mixture was poured into timber formply moulds and left to set before being removed, trimmed and installed. The use of expanding foam for the slot form was suggested by the precaster because it could be formed into any shape and was easy to trim after hardening.

(a) Formply slot mould.

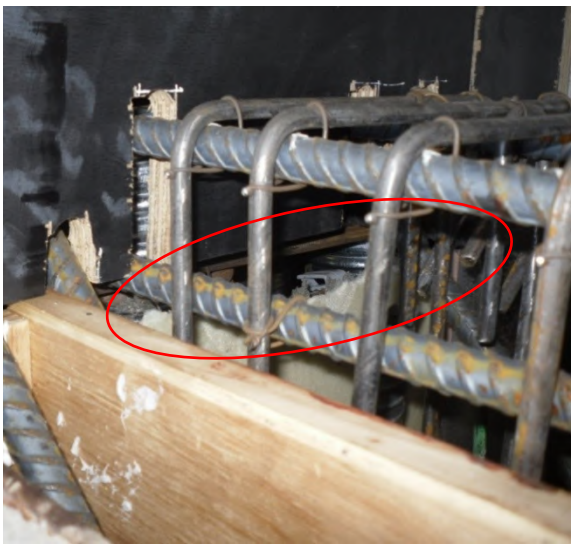

(b) Imprecise dimensions of installed slot form. The top of the foam slot form that should have been flush with the bottom of the formply is highlighted.

Figure 3-29: Manufacture and application of triangular slot form.

It proved difficult to accurately manufacture the triangular slot form. Due to the narrow triangular shape the form became very thin near the top, which made it difficult to get the foam to flow into the end of the forms. As a result, the slot forms often had inaccurate dimensions and a ragged top edge. An example of a ragged slot form top edge is shown in Figure 3-29(b).

The triangular slot form was used in the first beam unit cast, Bm-A1/1. The slot form was installed after the cage had been assembled to avoid damage to the foam. The form had to be installed in 3 pieces, as shown in Figure 3-30, to allow it to be installed after the cage was assembled and to fit around the two layers of reinforcement. Section 1 was installed after cage assembly, whereas sections 2 and 3 were installed after the cage had been placed in the beam formwork and set in the correct position.

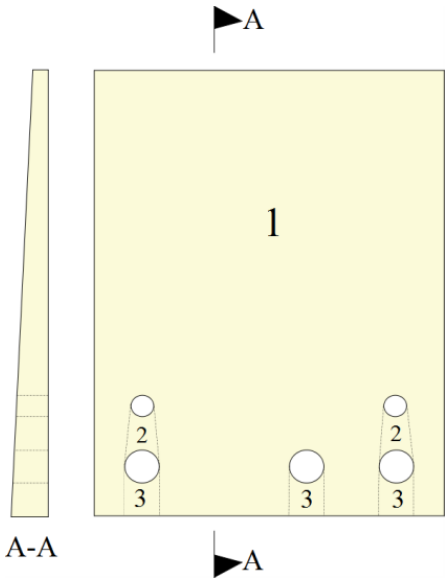

Figure 3-30: Slot form assembly

It proved difficult to achieve a tight seal around the reinforcement and between the slot form sections, and as a result concrete paste seeped into the slot region. As shown in Figure 3-31, in some instances section 2 was damaged, leaving a relatively large void which allowed ingress of concrete into the region between the upper and lower layer of bottom reinforcement. In subsequent testing, it was found that this concrete around the bars would spall and be ejected over loading reversals.

Figure 3-31: Concrete ingress between upper and lower bottom longitudinal reinforcement.

Beam Bm-A1/1 was cast in one pour, as would be conducted in a conventional beam. However, this caused undesirable consequences in a slotted beam. As shown in Figure 3-32, the difference in the height of the wet concrete between the beam-column joint and the beam resulted in an imbalance of hydrostatic pressures occurring on either side of the slot form. The pressure imbalance caused the slot form to be pushed into the beam until it was resting against the diagonal hanger bars. The bottom of the slot form was held in place by the debonding tubes. The final position of the slot form is shown in Figure 3-32(b) and (c). Beam Bm-A/1-1 was not fit for purpose and was rejected.

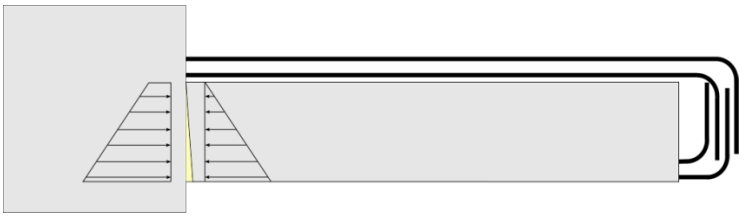

(a) Hydrostatic forces acting on slot form of beam Bm-A/1-1 during casting.

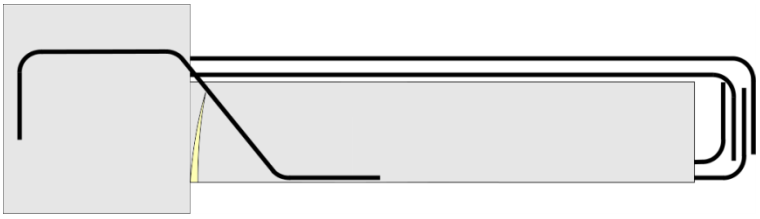

(b) Resulting shape of slot form in beam.

Figure 3-32: Beam Bm-A/1-1 slot form actions and movement, with form work omitted for clarity.

(c) Final position of the slot form in beam Bm-A/1-1.

Figure 3-32: Beam Bm-A/1-1 slot form actions and movement, with form work omitted for clarity (Continued).

To prevent the slot form moving whilst casting the remainder of the beam units, the pressure difference on either side of the slot form and the slot form rigidity were addressed. To increase the rigidity of the slot form the shape was changed from triangular to trapezoid. This shape can be seen in Figure 3-28(c) and Figure 3-30. This subtle change in geometry was small enough not to reinstate the issues that were the reason for using a triangular shape, whilst having a significant increase on slot form rigidity due to the cubic relationship to depth.

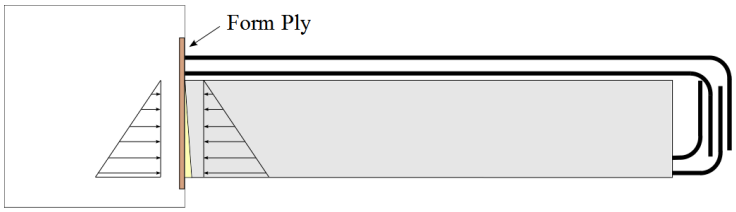

(a) First stage of beam casting

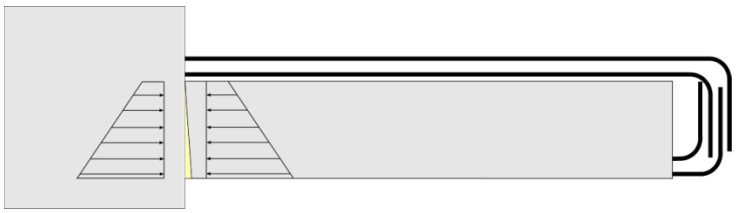

(b) Second stage of beam casting

(c) Final position of slot form in Beam Bm-B/2-1

Figure 3-33: Revised beam casting procedure, with form work omitted for clarity.

To address the difference in hydrostatic pressure on either side of the slot form, a two stage casting procedure was devised. During the first stage, shown in Figure 3-33(a), a formply

backing board was placed flush with the formply and attached to the beam-column formwork. The board supplied equal and opposite reaction to the hydrostatic pressure generated whilst casting the beam. Once the beam has set, the formply backing board was removed and the beam-column joint was cast. Because the beam had hardened, the hydrostatic pressure generated during the beam-column pour could be resisted. The system worked well and the final position of the slot form was as intended, as shown in Figure 3-33(b) and (c).

Whilst this procedure resulted in the accurate positioning of the slot form, it increased the amount of work required. With many beam units being manufactured the increase in work was partly mitigated by using two sets of formwork. In one set of formwork the beam was cast, whilst in the other the beam-column joint was cast, and vice versa once cured. In this manner, smaller and more frequent concrete batches were not required. Similarly, when column units were being cast the same concrete batch could be used to cast the beam or beam-column units. The differential pressures on either side of the slot forms could be avoided if the beam-column joint was only cast to the height of the beam. However, with the diagonal hanger and beam longitudinal reinforcement protruding from the precast beam units, cast insitu columns would be required.

Removing the slot forms after concrete curing was labour and time intensive. The stable nature of the polyurethane foam meant it could not be dissolved to remove it. Regardless, dissolution was an unsatisfactory method due to the environmental issue with disposal of the solution and the possibility of concrete staining. The only viable option for removal of the slot form was mechanical. This method was not ideal in that it provided a barrier to implementation and presented a risk of damaging the longitudinal reinforcement.

To be truly competitive with traditional construction there needs to be as few barriers to implementation as possible. Hence, a slot form that can be left in place after casting should be used. The form would need to have a high compressibility so as not to interfere with connection behaviour, while being sufficiently robust to remain in place during casting. A slot form that can be left in place is desirable from a durability perspective. If the primary structure is outside of the building envelope the longitudinal reinforcement will need to be protected from corrosion. A slot form that is left in place could protect the reinforcement from corrosive agents.

3.5.1.2 Debonding Tube Installation

Debonding tubes are a critical component of a reinforced concrete slotted beam. The tubes are designed to reduce longitudinal reinforcement strains to acceptable levels to prevent fracture, either by way excessive plastic strain or low-cycle fatigue.

It was found during construction that positioning the debonding tubes correctly with the specified details and tolerance was extremely difficult. Due to the returns at either end of the bottom longitudinal reinforcement, the debonding tubes had to be installed after cutting the reinforcement to length, but prior to bending it. This meant that the tubes were in place during cage assembly, which hindered cage assembly. To avoid this issue, a longitudinal reinforcement detail that was not terminated in a 90° return could have been used, or a debonding tube that was split in two. However, each of these options carried further complications.

Polyvinylchloride (PVC) tape was applied to the longitudinal reinforcement over the unbonded length. This served two purposes: to reduce the ingress of cement paste into the unbonding tube and to prevent bond between the reinforcement and any cement paste that did enter. However, because the slot position was not known accurately until the cage was placed in the formwork, excess tape was often applied at either end of the debonding tube to allow for adjustment in either direction. The excess tape was difficult to remove once in the formwork and was often left in place, as shown in Figure 3-34. The excess tape could have inhibited bond between the reinforcement and the concrete in a critical zone, near the bottom bend of the shear hangers. Complete removal of all PVC tape flush with the end of the unbonding tube was unrealistic in a practical setting; however, efforts should be made to minimise the excess tape.

Figure 3-34: Excess PVC tape at end of debonding tube prior to adjustment in beam form.

The debonding tubes were adjusted into position once the assembled cage was placed in the formwork. However, some debonding tubes proved practically impossible to adjust due to a very snug fit over the PVC tape, the debonding tube being tied to the stirrups and access to the tube being very limited. In these cases, the debonding tube could not be adjusted flush against the slot form without removing the entire cage to gain access. An example of this gap is shown in Figure 3-35.

Figure 3-35: Gap between debonding tube end and slot form.

As shown in Figure 3-36, the debonding tubes on Grids A and C were the correct design length of 300mm, while the debonding tubes on Grid B were the incorrect length of 275mm. The error was traced back to the incorrect drawing revision of Grid B beam units being held by the precast company. The error was discovered too late to be rectified.

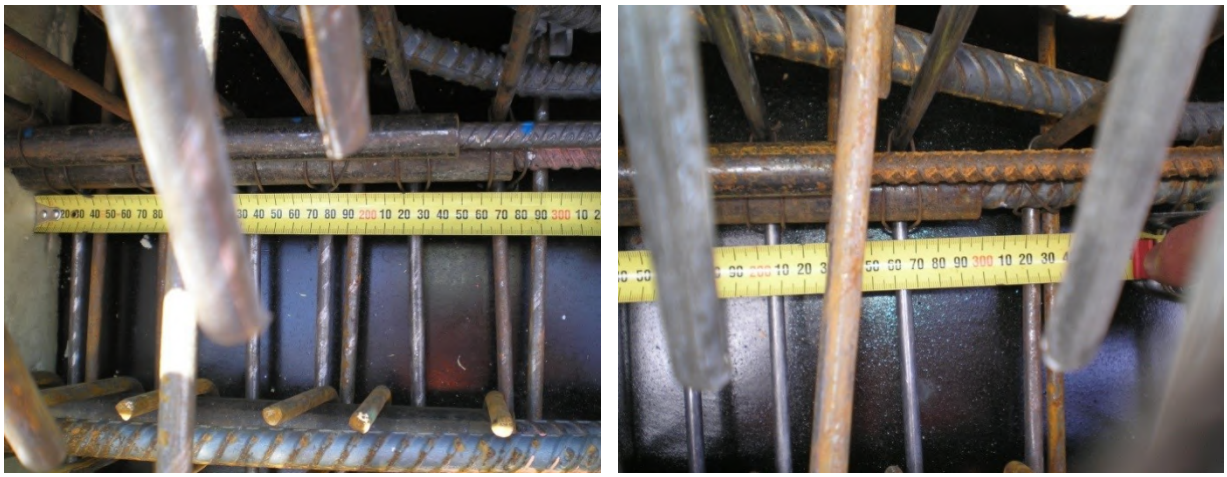

(a) 275mm debonding tube. **(b) 300mm debonding tube.**

Figure 3-36: Debonding tube length discrepancies.

Shorter debonding tubes would result in larger strains being experienced in the bottom longitudinal reinforcement, which would increase the risk of fracture and failure due to low-cycle fatigue. No discernible difference in response was observed between connections with different unbonded lengths during testing. However, this was likely a consequence of there being insufficient strain history to initiate low-cycle fatigue failure.

Errors can be made during construction and in the absence of competent supervision they can go unnoticed. This is not an issue unique to slotted beams, but in construction in general. However, the consequences of seemingly benign details being overlooked in slotted beams can be severe. It is recommended that the reinforcement cages are inspected by the engineer prior to casting.

3.5.1.3 Reinforcement Cage Assembly Tolerances

The assembly tolerances of the beam and column cages were generally accurate. Variance was observed in the spacing between the two layers of both the top and bottom longitudinal reinforcement. At the beam-column joint end this was less of an issue due to the spacing being determined by the intersection of the longitudinal reinforcement from each perpendicular beam. However, at the beam end, inconsistencies in the supplied length of the longitudinal reinforcement 90° returns affected assembly tolerances. As shown in Figure 3-37, the returns from the top longitudinal reinforcement could interfere with the bottom reinforcement, forcing it to sit higher in the beam section than intended, which reduced the spacing between the two layers of longitudinal reinforcement.

(a) Longitudinal reinforcement with design returns.

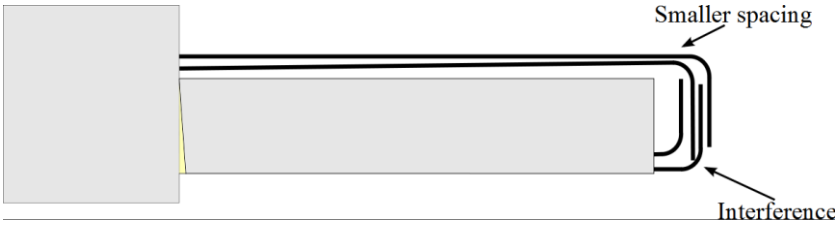

(b) Longitudinal reinforcement with supplied returns.

Figure 3-37: Variances in design and supplied longitudinal reinforcement 90° hook returns.

The beam stirrups were in general installed accurately. In some cases the spacing between them was inconsistent, but within normal tolerances. In an isolated case a stirrup was omitted from the cage Bm A/1-1R. The missing stirrup was installed at the beam end and the rest of the stirrup spacing reset.

All beam stirrups were distorted due to the reinforcement coming off a coil at the reinforcement supplier and being straightened using a rotary straightener. The straightener caused the reinforcement to twist and resulted in stirrup distortion. As shown in Figure 3-38, the distortion was evident in the assembled beam cage and had to be manually removed in the beam formwork by twisting the entire beam cage and tying it in place.

Figure 3-38: Distorted beam cage due to twisted stirrups.

The beam ledge trimmers in some cases were too long and extended into the slot region. During negative flexure this could have resulted in the trimmer contacting the column face, which could have disrupted the expected flexural response. The issue was identified early in Bm A/1-1 and rectified for the remaining beam units.

The most challenging tolerance issue was the geometry of the diagonal hangers. The angle, bend radius and lengths of the hangers delivered from the supplier were inconsistent and on several occasions incorrect. An example of this is shown in Figure 3-39, where the hangers shown are two supplied for beam unit Bm C/1-2 and should have been identical.

Figure 3-39: Supplied diagonal hanger geometrical inconsistencies.

The inaccurate hanger geometries could have had severe implications on hanger performance. The hanger was designed to pass through the top hinge between the two layers of longitudinal reinforcement to minimise strain induced by connection flexure. Variance from the recommended position would have resulted in increased hanger strain from flexure and reduced the capacity of the hanger to resist shear and torsion demands. The second issue was the position of the bend at the bottom of the hanger. The bend needed to occur before the start of the unbonded length of longitudinal reinforcement to prevent a breakdown in the shear transfer mechanism. It can be seen in Figure 3-39 that there was a large variance in the bottom bend location in the supplied hangers. Due to these important issues, where possible the incorrect hangers were rejected and reordered from the reinforcement supplier.

3.5.1.4 Beam-column Joint Reinforcement Assembly

Due to the additional horizontal reinforcement required in slotted beam joints, congestion can become an issue. In SA1 this issue was compounded by the use of two layers of longitudinal beam reinforcement; however, the issue was partly mitigated through the use of Grade 500 stirrups.

In general, the accuracy of the assembled beam-column joints was high. Issues were encountered with ensuring the consistency of the spacing between stirrups; however, the majority of these were within typical tolerances.

The major issue encountered was ensuring the correct distribution of stirrups immediately above and below the beam-column joint. The stirrups above the beam-column joint were installed after the assembled cage was positioned in the formwork. Due to the height of the top of the shear hangers the stirrup links immediately above the beam-column joint had to be installed underneath hangers. As shown in Figure 3-40, it was observed that in some instances the link immediately above the beam-column joint had been installed above the diagonal hangers, instead of below it. Due to the two layers of longitudinal reinforcement and the diagonal hangers in this region, anti-buckling and confinement requirement were challenging to satisfy. Hence, any deviation from the specified layout could have resulted in the beam-column joint becoming code non-compliant. The column demands above the hangers are identical to a traditional connection and code non-compliance could not be justified.

(a) Correct placement in Bm A/1-1.

(b) Incorrect placement in Bm B/1-1.

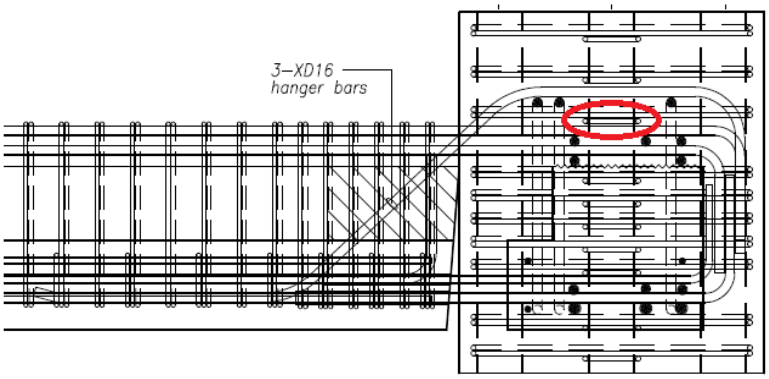

(c) Design stirrup placement, with link highlighted.

Figure 3-40: Beam-column joint stirrup location discrepancies.

3.5.1.5 Reinforcement Grade Segregation

Many different sizes and grades of reinforcement were used in specimen SA1. It was anticipated that issues would be encountered with incorrect grades being installed. However, these concerns proved unfounded. The supplier delivered all reinforcement bundled within shape and grade groups. The reinforcement cage assemblers had no issues interpreting the precast drawings and the bundled reinforcement.

The only issue was that reinforcement steel of Taiwanese origin arrived onsite. This steel was cheaper than locally produced steel; however, it had not been as rigorously tested and therefore compliance with AS/NZS4671:2001 could not be guaranteed with the same certainty (Standards New Zealand, 2001). All reinforcement not from local producers was rejected.

It is recommended that the engineer ensure that different reinforcement grades are clearly specified on drawings and the importance of the different grades emphasised to the cage assemblers.

3.5.1.6 Constructability of the Precast Concrete Slotted Beam Units

Constructability of the slotted beam was a lingering concern amongst academics and practitioners alike. All slotted beam specimens before SA1 had been manufactured in laboratory settings where the experimenters had fine control over tolerances, and in those experiments there was little emphasis on timeliness and cost effectiveness. There was apprehension that the required tolerances would not be able to be achieved by a commercial precaster and that manufacturing the detail would significantly increase costs.

Specimen SA1 was cast by commercial precast firm, Bradford Precast Limited (BCL). The feedback from BCL was invaluable and generally positive. BCL commented that the job was not as challenging as some traditional beam designs they had manufactured in the past. The most common complaints regarded the slot form, beam-column joint congestion and the accuracy of the supplied reinforcement.

Congestion in slotted beams is an issue that cannot be completely alleviated due to the additional reinforcement required compared to traditional connection details. However, congestion can be largely mitigated through thoughtful and attentive design, use of experienced cage assemblers and accurately bent reinforcement. The latter was a major issue with SA1, and BCL was optimistic that greater accuracy could be achieved by using a reinforcement supplier that BCL has a better working relationship with.

Over the course of manufacturing the precast components for SA1, both the speed and accuracy of the precast component manufacture increased dramatically. On a larger

commercial job the increase in manufacturing efficiency would enable the slotted beam detail to be cast with similar speed and ease to a traditional detail.

It is recommended that the designer considers carefully how the cage will be assembled and the effect that tolerances may have. Experienced cage assemblers and reinforcement suppliers should be used where possible.

3.5.1.7 Temporary Lifting Loads

Care must be taken when lifting precast slotted beams. Due to the partial cast height of the beams used in SA1, the top hinge had not been cast when lifting the beams. This meant that the design moment couple with the bottom longitudinal reinforcement had not yet been established. As a consequence, there was much greater flexibility in the connection. Cracks formed in the concrete paste over the sides of the slot form during lifts. The deformations were recovered upon unloading. It is recommended that the stiffness of precast component connections is checked by the designer to ensure that the stiffness is sufficient to withstand the demands generated by lifting.

3.5.1.8 Practical Construction Considerations

Due to commercial pressures in a precast yard, recommended concrete curing practices were seldom followed. Precast components were removed from the formwork and placed in outside storage 24 hours after casting. The final appearance and performance of the precast components would have benefited from improved curing conditions. However, removing the components early was a commercial decision. If the cast components could gain early strength then they could be lifted from the formwork the following morning, which increased casting bed turnover. Concrete cylinder samples taken from SA1 yielded consistently higher compressive strengths than specified. It was suspected that higher strength concrete may have been used to increase early strength gain. There were many shrinkage cracks present in the precast elements of SA1. Preventing shrinkage cracks is important to maintain the aesthetics of the structure and enhance the durability. Shrinkage cracks provide a preferential path for corrosive agents to reach the reinforcement and initiate corrosion. Workers had little appreciation for the impact that deviations from structural specifications could potentially have. There was a general willingness to cut reinforcement returns to expedite cage assembly; an example of which is shown in Figure 3-41.

Figure 3-41: Example of a cut reinforcement return on Bm B/1-1.

The reinforcement cages were assembled prior to being installed in the formwork, which required the slot forms and debonding tubes to be adjusted insitu to obtain the correct geometry. This was time consuming and difficult to achieve in practice due to the close stirrup spacing in the ends of the beams. Reinforcement was invariably damaged due to the force required to adjust the debonding tubes. The slot form and unbonding tubes should be installed correctly during cage assembly, which would require increased accuracy from the cage assemblers. An alternative, if the beams are being cast full height, would be to cast the entire beam upside down to gain easier access to the slot form and unbonding tubes. This technique would also remove the hydrostatic gradients discussed in Section 3.5.1.1 and mean that the entire beam could be cast in one pour.

3.5.1.9 Additional Reinforcement Welded to the Beam Bottom Longitudinal Reinforcement

The design of the additional reinforcement welded to the bottom D16 longitudinal reinforcement passing though interior joints is described in Section 3.4.2.

The welding was performed in accordance with NZS1554.3:2008 by a local engineering company (Standards New Zealand, 2008). The welding was performed in the company shop using metal inert gas welding with a low heat. The resulting welds were very high quality and resulted in little warping of the reinforcement. Two specimens of the supplementary welded reinforcement, shown in Figure 3-42(a), were prepared for axial testing. Both specimens failed away from the welded section and full test results can be found in Appendix A. An example of the supplementary reinforcement in an assembled cage can be seen in Figure 3-42(b).

(a) Specimens for axial testing. **(b) Supplementary welding reinforcement in Bm B/1-1.**

Figure 3-42: Supplementary welded reinforcement.

It is important to the performance of the structure that the welding is performed by a qualified individual to the relevant Standard (Standards New Zealand, 2008). The precast company must plan ahead to allow sufficient time to have the work performed so as not to impede the cage assembly and casting programme.

3.5.1.10 Reinforcement Strain Gauge Installation

Connections Bm B/1-2 and Bm C/1-2 were strain gauged using Tokyo Sokki FLA-5-11-3L electrical resistance wire strain gauges. There were a total of 184 strain gauges applied between the two precast components. The locations where the gauges were installed is presented in Section 3.8.3. Due to the large number of gauges required and the limited data logging equipment available, no redundancy was able to be designed into the instrumentation plan.

Some reinforcement preparation was able to be undertaken in the laboratory; however, the gauges were applied to the assembled reinforcement cages onsite at BPL to prevent damage to the strain gauges. This proved a difficult prospect due to the remote location and poor facilities available.

Once the reinforcement had been filed flat and smoothed with emery paper, the first step in applying the gauges, shown in Figure 3-43(a), was to adhere the gauge to the reinforcement with cyanoacrylate. Once the cyanoacrylate had dried, three coats of waterproofing were applied, as shown in Figure 3-43(b). During the application of subsequent coats of waterproofing, the lead was folded back over the gauge to further protect it. The third stage, shown in Figure 3-43(c) was to cover the entire gauge in rubber mastic to protect the gauge during transport and casting. Lastly, the resistance of the gauges was checked to ensure it functioned correctly, as shown in Figure 3-43(d). If any gauges returned abnormal results they were replaced.

(a) Adhering strain gauge to prepared surface.

(b) Application of waterproofing.

(c) Application of rubber mastic.

(d) Checking circuit resistance.

Figure 3-43: Application of strain gauges.

Once the strain gauging was complete, the cages had to be transported across the site to the casting beds and lowered into the forms. This had to be undertaken with care to protect the gauges or leads. The completed cages ready for casting are shown in Figure 3-44.

Care had to be taken when pouring and compacting the concrete. The concrete was specified with a higher slump than usual to improve flow, and was poured in a section of the beam that had no gauges. Vibration of the casting platform was considered for these beams; however, the forms did not have stiff enough connections to the casting bed to ensure adequate compaction. Instead, traditional pencil vibrators were used and care had to be taken not to hit any gauges. Zones where the vibrators were not to be applied were marked on the formwork.

(a) Cage prior to casting. Plastic bag contains strain gauge leads.

(b) Beam-column joint prior to casting.

Figure 3-44: Bm C/1-2 cage in formwork.

On other precast beam units setting retardant was applied to the top of the concrete and water-blasted off to achieve the target surface roughness of 5mm. However, with leads and gauges exposed on the beam surface water-blasting was not possible. Instead, no retardant was used and a roughened finish was achieved by hand, which was not ideal for bond with insitu concrete. However, no bond failure was observed in the beam cold joints during subsequent testing.

3.5.1.11 Column Longitudinal Reinforcement Grout Sleeve Installation

Grout sleeve couplers were required above Level One to splice the column longitudinal reinforcement. The supplied grout sleeves were poorly finished, and grinding was required to enable the RB32 to be threaded into the coupler.

The standard large diameter grout ports on the coupler were fitted with reducers to allow smaller diameter grout lines to be used. The smaller lines reduced the concrete cross-section lost to grouping of the grout lines, as shown in Figure 3-45(a). There is no rational reason why larger grout sleeves should require larger diameter lines than smaller sleeves because the same grout is used in both. Due to the profile of the grout sleeve varying over the length, it was difficult to install stirrups hard-up against the sleeves in all cases.

(a) Grout port reducer.

(b) Assembled column cage.

(c) Grout line routing.

(d) Grouping of grout feed and bleed lines.

Figure 3-45: Col B/1-B assembly.

To ensure there were no kinks in the grout lines, large radii bends were used to orientate the line to the exit locations. Grout sleeve ports were orientated into the column to maintain cover concrete requirements and avoid the stirrups, as shown in Figure 3-45(c). As shown in Figure 3-45(d), the grout lines exited the column in groups of two over two elevations to minimise the reduction in column cross-section. Exhaust and feed lines were clearly labelled to allow correct identification during grouting.

3.5.1.12 Manufacture of the precast Hollow-core units

The prestressed hollow-core flooring units used in SA1 were manufactured by Fulton Hogan Stahlton Limited in Christchurch, New Zealand. Prestressing tendons were laid out along a steel casting bed and hydraulic actuators were used to apply the desired prestress force, as shown in Figure 3-46(a). Concrete was extruded through a die by screw augers around the tendons on the casting bed, as shown in Figure 3-46(b). Different hollow-core sections can be formed by changing the die. The hollow-core was left overnight to cure on the heated casting bed. It was then cut to the desired length using a concrete saw. It was typical for the concrete saw to not cut the entire hollow-core section depth to avoid striking the casting bed. As shown in Figure 3-46(c), the lip left along the bottom of the hollow-core end caused spalling when the units were lifted from the casting bed.

The hollow-core was cut to length the day after casting, which did not allow sufficient time for the concrete to develop its full stiffness. Due to insufficient bond, the prestressed tendons relaxed and ‘pulled in’ to the unit after they were cut. This could have reduced the flexural and shear capacities at the end of the units. The maximum recorded ‘pull in’ was 2mm, as shown in Figure 3-46(d). The cutting process resulted in the entire unit being covered in concrete slurry from the cutting blade coolant, which dried on the top of the hollow-core unit leaving a film of concrete dust. Concrete dust could inhibit bond with the insitu floor concrete and should be removed prior to casting.

(a) Tendons being stressed over the casting bed.

(b) Hollow-core being extruded on to tendons.

(c) Example of typical hollow-core corner damage.

(d) Measurement of tendon 'pull in'.

Figure 3-46: SA1 hollow-core flooring.

The units received for SA1 varied in length by up to 12mm. The accuracy of an engineered product should have been better. Due to the prestress being applied at the bottom of the hollow-core unit, a slight hogging pre-camber was observed. The precamber was minor for SA1 hollow-core units; however, for long span units with deeper profiles and greater prestress force the pre-camber could be significant.

3.5.1.13 Manufacture of the precast Double-tee units

The prestressed double-tee concrete flooring units used in SA1 were manufactured by the same company as the hollow-core units. As shown in Figure 3-47(a), tendons were placed in the bottom of the steel formwork and hydraulic actuators used to apply the desired prestress force. Stirrups were installed at the end of the units to transfer shear. D10 trimmers and mesh reinforcement was installed to control concrete cracking. Unequal steel angles were installed at the unit ends to prevent spalling of the ends of the units due to relative motion between the unit and the supporting beam. Reinforcement was welded to the angle to complete the shear transfer mechanism as shown in Figure 3-47(b) and (c).

(a) Reinforcement in double-tee casting bed.

(b) Detail of dapped end reinforcement.

(c) Dapped end detail after casting.

(d) Camber due to prestress.

Figure 3-47: SA1 double-tee flooring.

Several issues were encountered during casting the double-tee units. The dimensions of the units were incorrect when first inspected. After the dimensions were rectified, it was observed that both the prestressing tendons and the reinforcement mesh were larger diameter than specified due to no stock being held for the specified sizes. Since the tendon prestress force is controlled by strain, the larger tendon diameter applied a larger prestress force and caused significant hogging camber in the units, as shown in Figure 3-47(d). The larger centres between reinforcement in the mesh resulted in poor crack control.

The amount of concrete required to cast the double-tee units was incorrectly calculated by the precaster and was insufficient to complete the pour. There was insufficient time to batch more concrete due to the hot and dry weather, which caused the concrete to cure quickly. To avoid a cold joint being formed in the unit, concrete that had already been batched for another job was requisitioned. The concrete hardened rapidly, and it was discovered afterwards that the requisitioned concrete batch had in it a setting accelerant. As a result, there were numerous blowholes in the concrete due to inadequate vibration. More seriously, due to the combination of excessive prestress, non-specified mesh and rapidly curing concrete there were numerous

shrinkage cracks in the double-tee units. This situation highlighted the importance of monitoring work for quality assurance.

3.5.2 Erection of SA1

3.5.2.1 Transportation of SA1 Precast Concrete Components

The SA1 precast elements were designed to be able to be transported on a standard truck trailer and fit through the laboratory door. However, when delivery of the Level One beams and columns was received the 'B' columns had been loaded on the highest part of the trailer and were too tall to allow the trailer to enter the laboratory. As shown in Figure 3-48(b), a mobile crane was used to unload the precast elements from the trailer and place them inside the laboratory door.

(a) Level One beams and columns outside laboratory.

(b) Bm A/1-1 being unloaded by mobile crane.

Figure 3-48: Precast components being delivered to structures extension laboratory.

The constraints imposed by the laboratory will not be an issue in practice. However, transporting full scale elements could be problematic if the same construction methodology were used as SA1. To enable efficient transport a different precast methodology could be used or the precast elements could be cast on site.

3.5.2.2 Universal Joint Installation

Universal joints were used to support specimen SA1 and represent the points of contraflexure in the columns. The universal joints were designed to be used in a self-equilibrating superassembly experiment by Matthews (2004). Hence, they were not intended to resist large lateral forces and a full analysis was undertaken to determine the ultimate capacity of the supporting joints.

Due to the age of the strong floor in the structures extension laboratory, there were significant variations in elevation over the plan. Shims were used to raise all the universal joints up to the same elevation as the highest one. The shims were triangulated to allow the universal joint to be levelled. Once the correct number of shims had been determined, the universal joint was

placed on a grout pad. The grout pad, shown in Figure 3-49(a), enabled a stiffer connection with the strong floor.

(a) Grout bed and shims used to level and found the universal joint.

(b) Detail of levelled universal joint.

Figure 3-49: Universal joint set out.

The universal joints were locked by welding small RHS struts between the base and top plate, as shown in Figure 3-49(b). Locking the universal joints allowed the 'A' columns to be subsequently erected without propping.

3.5.2.3 Ground Floor 'A' Column Erection

Erecting the ground floor 'A' columns was simple after the universal joints were locked and levelled. The base of the columns had a 20mm mild steel plate to which the column longitudinal reinforcement was plug welded to fully develop it. Four 24mm diameter Grade 8.8 bolts were installed through the base plate to connect to the universal joint, as shown in Figure 3-49(b). The installed 'A' columns were rotated until square with each other and the connecting nuts tightened. The erected column Col A/1-A is shown in Figure 3-50.

Figure 3-50: Column Col A/1-A erected.

3.5.2.4 Propping and Level One Beam Erection

The erection of SA1 took place following the M_W 7.1 September 4th 2010 Darfield (Canterbury) earthquake. The fault trace and locations of the immediate aftershocks is presented in Figure 3-51(a) and an example of the displacement that occurred across the fault line is shown in Figure 3-51(b). The event was felt strongly in Christchurch and resulted in moderate damage; however, due to the fortunate early morning timing and distance from main population centres, no deaths resulted.

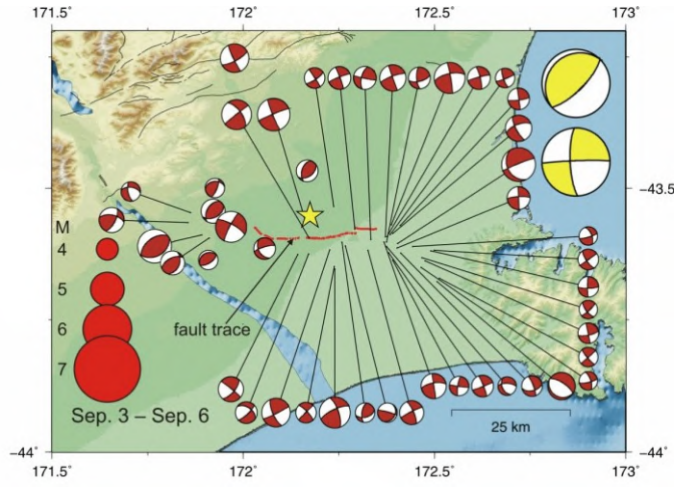

(a) Focal mechanisms for Darfield (Canterbury) earthquake.

(b) Displacement along Clintons Road, Canterbury.

Figure 3-51: Darfield (Canterbury) earthquake (GNS Science, 2011).

Due to the increased probability of a damaging earthquake occurring, the propping used during the erection of SA1 was designed to resist the design seismic forces induced in the specimen. Significant time and expense was expended on the propping design, and as a result the propping used in the erection of SA1 was not typical. There is little difference between the propping required to erect a slotted beam structure and a traditional structure. Propping is a significant cost component during construction and the need for additional propping could render an otherwise comparable system less economic.

Sourcing propping was problematic due to the standard scaffolding sizes not being well suited to the scaling applied to SA1. This issue was compounded by the chronic shortage of propping following the Darfield (Canterbury) earthquake, where much of the supply was being utilised in temporary shoring of damaged structures.

The Level One beam units were lowered through the hollow corrugated steel Drossbach ducts onto the 'A' columns, as shown in Figure 3-52(a). Three 20mm steel spacers were installed between the column and the beam to allow space for grout to be pumped. Each beam unit was supported by steel header beams seated on screw jacks, as shown in Figure 3-52(b). Laser levels were set up and the beam units were adjusted in elevation, rotation and inclination.

Because of the five point support system (seven point on Grid B) it was challenging to adjust the set out in one direction without affecting the perpendicular direction. In this manner obtaining an accurate set out was achieved in an iterative manner. A more traditional propping regime would expedite the process.

(a) Lowering Bm B/2-1 onto Col B/2-A.

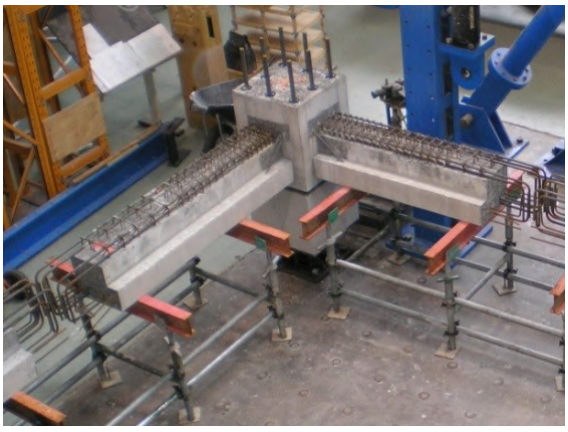

(b) Propped corner on Grid B-3.

(c) Setting out beam units using laser.

(d) Level One beam units set out and propped.

Figure 3-52: Erection of Level One beam units.

Where tolerance issues between elements were encountered the difference was split between the two conflicting elements. The precast components were able to be set out within 1% of the construction plan. The final set out of the Level One beams can be seen in Figure 3-52(d).

3.5.2.5 Mid-beam Splice Assembly

Specimen SA1 was designed with a double hooked lap mid-beam splice. A compact splice was able to be achieved with this type of design, which was important due to the space limitations imposed by geometric scaling. However, the splice also resulted in extreme reinforcement congestion, as can be seen in Figure 3-53(a) and (b). Because of the small tolerances, the splice could only be assembled in one order. Standard stirrups could not be used in the splice because the standard 135° returns made them impossible to pass over the longitudinal reinforcement. Half stirrups were used instead, and the legs of the final portion of the stirrups bent 45° into the cage insitu. It is recommended that, if possible, alternatives to the double hooked lap are used to decrease labour demand.

(a) Assembled Grid B mid-beam splice.

(b) Assembled Grid 2 mid-beam splice.

(c) Poured, compacted and finished mid-beam splice.

Figure 3-53: Mid-beam splice.

Once the formwork, detailed in Section 3.5.2.6, was installed the mid-beam splice was poured. The ledge was trowelled, but the rest was left as rough as possible to aid the subsequent cold joint, as shown in Figure 3-53(c). Minor shrinkage cracking was observed between the precast beam ends and the mid-beam splice when the formwork was removed.

The mid-beam splices were cast separate from the floor. The congestion in the mid-beam splice would have made it difficult to ensure adequate concrete compaction in the bottom of the splice. Completing the mid-beam splice in two pours, instead of one, significantly increased time and labour demand. On a full scale structure the congestion would be less of an issue so the splice could be poured with the rest of the floor.

3.5.2.6 Formwork Installation

Formwork was required around the entire perimeter of SA1 to enable the beams to be finished to full height and the insitu floor topping to poured. The forms were constructed from waxed formply to make them easier to remove after curing. The formwork was assembled longer than required and progressively sanded until a snug fit between the columns was achieved. As shown in Figure 3-54(a), the beam face had to be ground flat with a diamond grinder to allow the formwork to sit flush with the beam face. As shown in Figure 3-54(b), 16mm threaded rods epoxied into the precast beams were used to fasten the formwork against the beams.

Formwork was installed around the inside perimeter of the beams to contain the topping concrete and to support the formwork for the timber infill. Concrete screws were used to attach the formply to the precast beam directly. On Level Two the gap between the beam and the flange of the double-tee unit was small, which allowed polystyrene blocks to be used to contain the poured concrete as shown in Figure 3-54(d).

Because the precast beams were cast the same height as the top of the slot, and the slot forms were removed following casting, it was necessary to seal the top of the slot to prevent the ingress of concrete during the insitu floor pour. Polystyrene rod and room temperature vulcanising sealant (RTV) sealant were used to seal the gap, as shown in Figure 3-54(e). Figure 3-54(c) shows the formwork required for the concrete confinement of the diagonal hangers. The hanger confinement is discussed in more detail in Section 3.5.2.9.

The completed formwork is shown in Figure 3-54(f). It may be possible to avoid to the use of internal formwork by either matching the precast height to the desired timber infill height, or by tolerating some inclination in the infill. However, because the timber infill had to be removed from SA1 prior to testing, additional formwork was required. Similarly, it may be possible to eliminate the need for formwork around the perimeter of the beams by casting the beams full height. This could reduce labour demand onsite and expedite construction time.

(a) Bevelling beam edge with diamond grinder.

(b) Exterior beam formwork on Grid 2.

(c) Interior beam formwork of Grid 2 Level One.

(d) Interior beam formwork of Grid 2 Level Two.

Figure 3-54: Level One formwork.

(e) Sealing top of slot with RTV to prevent ingress on concrete.

(f) Completed beam formwork.

Figure 3-54: Level One formwork (Continued).

It is recommended that the height of the precast beams be designed to minimise the formwork required during erection. Slot forms that can be left in place would prevent the need to seal the slot against ingress of concrete during the insitu topping pour.

3.5.2.7 Level One 'B' Column Erection

Erecting the Level One 'B' columns was made easier due to the accurate tolerances achieved during the manufacture of the precast components, which was important because the large diameter column longitudinal reinforcement was too stiff to be guided into the grout couplers. Figure 3-55(a) shows a column being lowered on to the longitudinal reinforcement. The columns were positioned on three 20mm mild steel spacers placed in a triangular arrangement, and by iteratively adding shims to the appropriate spacers the column was made vertical. Figure 3-55(b) shows the verticality level of the 'B' column being checked. Lasers were used to confirm that the set out of the 'B' columns were within acceptable tolerances.

(a) Lowering 'B' columns on to protruding longitudinal reinforcement.

(b) Levelling Col A/1-B.

Figure 3-55: Level One 'B' columns.

3.5.2.8 Connection Grouting

To connect the precast components, cementitious grout was pumped into the grout couplers and Drossbach tubes. The work was undertaken by a commercial company with extensive experience in grout pumping: Construction Techniques Limited, Christchurch (BBR Contech). A commercial firm was used to ensure that the connections were representative of what could be achieved in practice and to identify any potential issues.

Cementitious dry-pack was first installed between the precast elements. The purpose of the dry-pack was to form a barrier to contain the flowable grout and to install the grout tubes, as shown in Figure 3-56. A water and latex mix was applied to the exterior of the dry-pack to increase cement hydration and create an external seal to reduce water permeation during grouting.

(a) Level One column on Grid A-1 after dry-pack.

(b) Dry-pack and tube detail.

Figure 3-56: Dry-pack procedure.

Plain cementitious grout was used in specimen SA1. A 1:5 ratio of super-plasticiser to water was used to enable an appropriate water to cement ratio to be achieved, whilst maintaining adequate flowability. Figure 3-57(a) shows the grout being mixed. A high strength proprietary grout with micro-aggregates was considered, but was rejected because it was not representative of typical construction practice.

The grout was pumped into the connections through the lowest grout port, as shown in Figure 3-57(b). When grout started flowing out of the remaining grout ports they were closed. Filling the connection in this manner expelled the air inside and ensured that the connection was completely full with grout. A completed connection with all grout ports full and blocked off is shown in Figure 3-57(c). Although the exterior of the dry-pack was sealed, significant water permeation was observed as shown in Figure 3-57(d).

(a) Mixing cementitious grout.

(b) Pumping grout into connection.

(c) Filled and sealed exhaust ports.

(d) Example of water bleeding through dry pack.

Figure 3-57: Grouting procedure.

It was observed during grouting that some grout ports were blocked. The blockages were likely caused by the tubes not being installed completely through the dry-pack. When ducts were blocked it was difficult to confirm that all the air in a connection had been completely expelled. On one occasion it was not identified that a duct was blocked before pumping commenced. When the pressure built up, the connection between the pump and the duct failed explosively.

As shown in Figure 3-56(b), the grout ducts between the precast elements were installed with an upwards slope to ensure that they could be closed off while completely full. The grout ducts in the 'B' columns were angled downwards, which meant that when the grout reached the exhaust port it would run out. The duct was then blocked off and although the grout had

reached that level, the duct would appear empty as shown in Figure 3-58(a). It was then difficult to be certain that the connection had been fully grouted.

Whilst pumping grout into column Col C/2-B, the contractors continued pumping after closing off all exhaust ports in an effort to ensure the connection was completely full. However, because neither air nor grout could be released from the system, the internal pressure built up, which resulted in the column starting to rise. The column displacement caused 1mm cracks to form in the dry-pack, as shown in Figure 3-58(b). It was fortunate that the issue was noticed before the dry-pack failed completely; however, the displacement was not recovered and the column remained slightly out of vertical.

(a) Air in grout exhaust port.

(b) Crack in dry-pack caused by column displacement.

Figure 3-58: Grout issues.

It is recommended that the engineer specifies the routing and orientation of the grout ducts. The exhaust ports in the dry-pack should be inclined upwards, and the ducts for the grout sleeves should exit the column at a higher elevation than the sleeve. These details will make it easier for the engineer to check if connections have been grouted correctly.

3.5.2.9 Internal Hanger Confinement Installation

When the Level One precast elements were delivered it was observed that the internal hangers appeared very slender, as shown in Figure 3-59(a). Despite being cast in concrete during the insitu floor pour, the concrete was unconfined and potentially susceptible to spalling. Analysis showed that the interior hanger would be in tension for the majority of response; however, it was decided that confinement and anti-buckling reinforcement should be added as a precaution.

The most practical method for installing the confinement reinforcement was to use ‘u’ shaped deformed reinforcement stirrup, as shown in Figure 3-59(b). The top of the reinforcement

lapped with the main beam reinforcement cage. The bottom of the reinforcement was drilled and epoxied into the beam. Drilling in the end of the beam was difficult due to the extremely close stirrup spacings in that region. Figure 3-59(c) shows the drilled holes filled with Hilti HIT-RE-500 structural epoxy. The completed confinement retrofit, with formwork in place, is shown in Figure 3-59(d). The internal hangers on Grid B were provided with one confinement stirrup only due to access difficulties. Hanger confinement reinforcement was not required on Level Two due to the deeper ledge necessitated by the dapped ends of the double-tee floors. It is recommended that confinement for diagonal hangers outside of the main beam reinforcement cage be considered at the design stage and installed when the precast components are manufactured.

(a) Level One interior hanger unrestrained length.

(b) D10 hooked stirrup for confinement and anti-buckling.

(c) Drilled holes filled with epoxy ready for stirrup installation.

(d) Installed interior hanger confinement stirrups with formwork.

Figure 3-59: Internal hanger confinement.

The concrete around the interior hanger was not precast in SA1 because it was believed that this would facilitate more simplistic formwork and an integral connection with the floor diaphragm, which was erroneous. As shown in Figure 3-60, additional work had to be completed to reinstall portions of the slot forms, as well as the required timber formwork.

(a) Level One slot form.

(b) Level Two slot forms.

Figure 3-60: Formwork for internal hangers.

It is recommended that the concrete around the diagonal hanger be precast to the same height as the rest of the beam. This will significantly reduce erection time and labour required.

3.5.2.10 Level One Floor Installation

Air pockets were formed along the beam ledge due to the way the beams were cast. Surface irregularities were unfavourable along the beam ledge because they could lead to force concentrations that could cause the low-friction strip under the precast floor elements to bind. To avoid this issue, a thin layer of cementitious mortar was spread over the entire ledge, as shown in Figure 3-61(a). Once the mortar had cured, low-friction strips were adhered to the ledge with a bead of RTV, as shown in Figure 3-61(b).

(a) Casting mortar filler on beam ledge.

(b) Low-friction strip installed.

Figure 3-61: Installing low-friction strip on beam ledge.

The hollow-core units were placed on the beam ledges with an equal spacing to the beam face at either end of the unit, as shown in Figure 3-62(a) – (c). A low density polystyrene compressible backer was installed between the end of the hollow-core unit and the beam face. The backer was adhered to the end of the hollow-core units with RTV sealant to prevent ingress of concrete into the hollow-core voids. The backer allowed the end of the hollow-core unit to rotate relative to the beam face, which reduced continuity moments compared to current code details (Standards New Zealand, 2006).

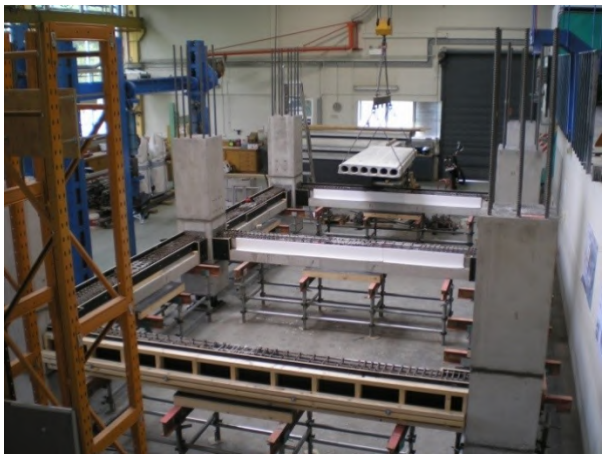

(a) First hollow-core unit being lifted in to position.

(b) Eastern bay complete.

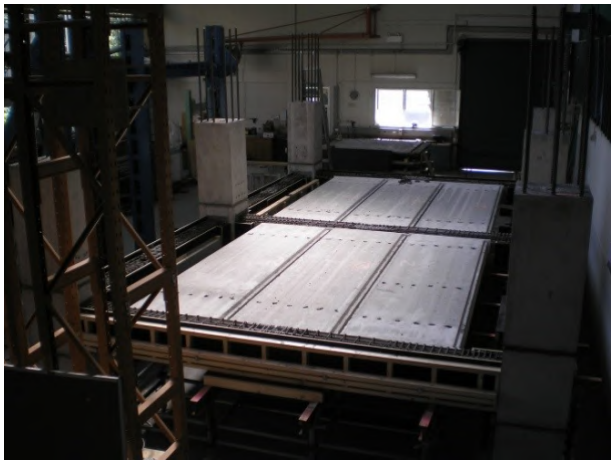

(c) Level One hollow-core in position.

(d) Hollow-core seating detail.

Figure 3-62: Hollow-core unit installation.

Penetrations were cast into the top of the hollow-core units to enable the voids to be broken out if the seating detail described in the Concrete Structures Standard were to be used (Standards New Zealand, 2006). Because the holes were not required for the seating detail used in SA1, the holes were filled with expanding foam and trimmed flush to prevent concrete ingress, as shown in Figure 3-63(a).

In practice, the timber infill would have been formed with rough sawn timber planks that were left in place after curing. In SA1 it was important to monitor the cracking in the infill, so the formwork was designed to be removed after curing. The formwork was constructed in four sections to enable it to be removed in a piecewise fashion. The timber propping required to

support the infill formwork is shown in Figure 3-63(b). As shown in Figure 3-63(c), the edges of the infill formwork were bevelled to allow the edges to rotate away from the concrete without binding. The completed Level One formwork is shown in Figure 3-63(d).

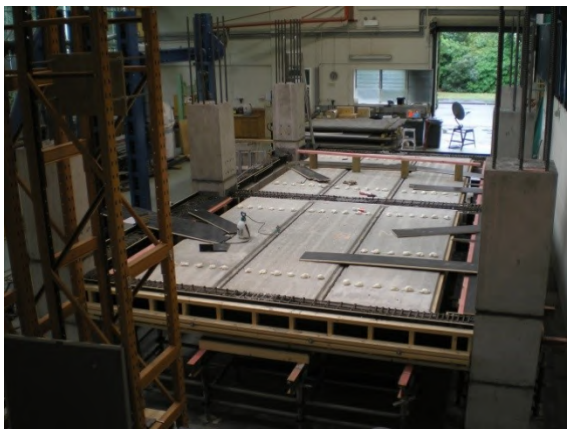

(a) Plugging holes in hollow-core.

(b) Support structure for removable timber infill.

(c) Completed formwork for removable timber infill.

(d) Level One ready for reinforcement.

Figure 3-63: Hollow-core timber infill.

Grade 300 deformed reinforcement was used in both floors. The starter reinforcement around the perimeter of the specimen alternated in length to disrupt any potential failure plane. The starter reinforcement extended beyond the timber infill to prevent tearing at the interface between the hollow-core and the infill, as shown in Figure 3-64(a). The remainder of the floor reinforcement was lapped with the starter reinforcement, tied in place and set up on chairs to control the reinforcement height. The completed floor reinforcement can be seen in Figure 3-64(b).

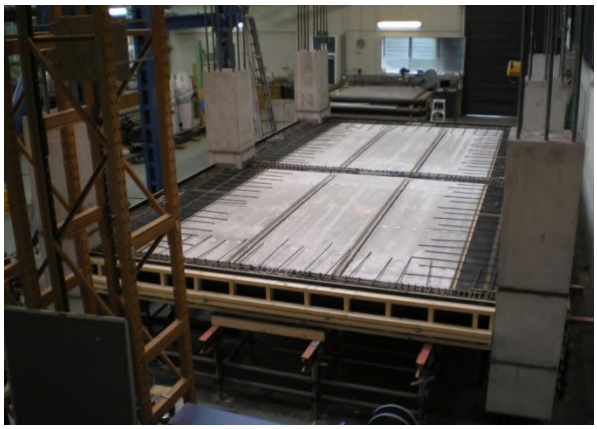

(a) Starter reinforcement installed.

(b) Floor reinforcement complete.

Figure 3-64: Level One floor reinforcement.

To ensure that the floors were representative of what could be achieved in a commercial construction project, Bradford Precast Limited was employed to undertake the concrete placing. The concrete was placed with a hopper, compacted and screeded level, as shown in Figure 3-65(a) and (b). When the concrete had stiffened the floor was power trowelled, as shown in Figure 3-65(c). Power trowelling was repeated a further three times until a U3 surface finish had been achieved (Standards New Zealand, 1987). The floor was covered in wet hessian cloth and tarpaulin for seven days, as shown in Figure 3-65(d). It was important to provide adequate curing conditions to improve the final strength and durability of the floor, whilst minimising shrinkage cracking.

(a) Pouring concrete with hopper.

(b) Screeding concrete.

(c) Power trowelling floor.

(d) Floor completed and covered for curing.

Figure 3-65: Level One floor pour.

3.5.2.11 Propping and Level Two Beam Erection

The Level Two propping followed the same regime used for Level One, as shown in Figure 3-66. The props were founded on the Level One props outside of the specimen, and on the Level One floor inside the specimen. The Level One timber infill did not have sufficient strength to support the weight of the Level Two beams, so the props were positioned over the timber struts supporting the timber infill formwork.

(a) South-east perspective.

(b) North-east perspective.

Figure 3-66: Level Two propping.

Due to the height of specimen SA1, the gantry crane in the laboratory did not have sufficient head room to erect the Level Two beams. Hence, a mobile crane with a telescopic boom had to be used to lift the beams into position, as shown in Figure 3-67(a) and (b). The method described to level and set out the Level One beams was used also for the Level Two beams. However, significant time was spent setting out Bm C/2-2 due to the inclination of column Col C/2-B caused by grouting issues. Bm C/2-2 was installed as far east as possible and Bm B/2-2 moved west 5mm to allow sufficient distance between the Grid B and C beams for the double-tee floor to be installed. The as-built geometries being different from designed was not ideal, but it highlighted the importance of designing with sensible tolerances to allow for such discrepancies. Failure to do so could have expensive and time consuming repercussions for a project.

(a) Installing Bm C/1-2.

(b) Installing Bm C/2-2.

Figure 3-67: Erecting Level Two beams.

(c) Level Two beams installed.

Figure 3-68: Erecting Level Two beams (Continued).

3.5.2.12 February 22nd 2011 Christchurch Aftershock

At 1251 on Tuesday February 22nd 2011 a M_L=6.3 aftershock of the September 4th M_W=7.1 earthquake struck 10km southeast of Christchurch City at a focal depth of 5km. The focal mechanisms of the earthquakes are shown in Figure 3-68(a). The earthquake was felt at intensity up to MM9 (Modified Mercalli) in Christchurch City. Collapsed buildings and falling debris resulted in the deaths of 185 persons. Damage to buildings and infrastructure was extensive and widespread. Examples of the types of building damage sustained are presented in Figure 3-68(b).

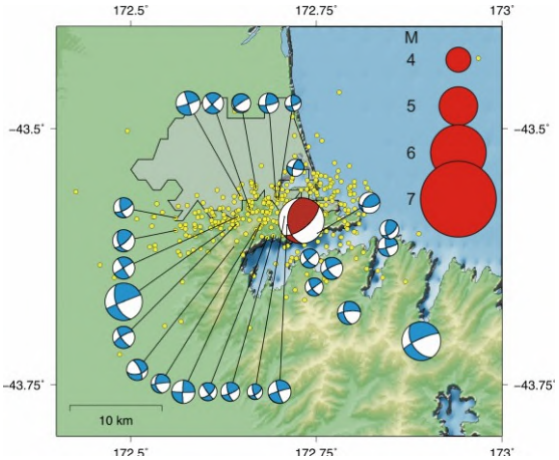

(a) Focal mechanisms for Christchurch earthquake.

(b) Building damage in Christchurch city. Building in background is inclined.

Figure 3-68: February 22nd earthquake (GNS Science, 2011).

The earthquake caused massive disruption to all Christchurch residents and their normal activities; this research project was no exception. The University of Canterbury was shut down for several weeks while structural inspections of university buildings were undertaken. During this time, access to campus was forbidden and the author instead volunteered at the Emergency Operations Centre, undertaking structural inspections within the Central Business

District. Following the reopening of the University of Canterbury, it was discovered that the clerestory of the laboratory had collapsed onto specimen SA1. As shown in Figure 3-69, scaffolding had to be assembled on top of specimen SA1 to access the clerestory for repair, which severely restricted the work that could be undertaken on the specimen.

(a) Perspective from north-west corner. **(b) Perspective from south-east corner.**

Figure 3-69: Scaffolding assembled on top of SA1 to repair the laboratory clerestory damaged during the February 22nd 2011 Christchurch earthquake (Clerestory obscured).

Due to the increased frequency of earthquakes following the September 4th 2010 event, the propping regime used for SA1 was designed to resist the design seismic forces induced in the specimen. The conservative design rationale was validated during the February 22nd 2011 earthquake. As shown in Figure 3-70(a), the propping shifted approximately 40mm during the earthquake, but remained elastic and limited the damage caused to specimen SA1. However, because the Level Two beams had not been grouted, or joined at the mid-beam splice, they displaced significantly.

Figure 3-70(b) shows an example of typical damage to the beam-column joint region of the Level Two beam units. The damage was caused by the beam unit displacing during the earthquake, which caused the inside of the Drossbach tubes to collide with the column longitudinal reinforcement. Figure 3-70(c) shows cracking in the cement paste at the base of the slotted beam connection, while Figure 3-70(d) presents an example of the cracking above the Level One hollow-core connections. It was evident from the cracking observed that specimen SA1 had displaced during the earthquake; however, the width of the cracks suggested the displacement was recovered.

(a) Displacement of second floor propping.

(b) Cracking in column due to collision with longitudinal reinforcement.

(c) Cracking through slotted beam section.

(d) Cracking in Level One floor diaphragm.

Figure 3-70: Specimen SA1 damage due to 22nd February 2011 Christchurch earthquake.

It was concluded that the damage sustained by SA1 would not affect the results gathered during testing significantly. The Level Two beams were levelled and set out again, and the erection of SA1 continued.

3.5.2.13 Level Two 'C' Column Erection

Due to the height of SA1, the 'C' columns could not be erected with the laboratory gantry crane. As shown by Figure 3-71(a), they were lifted into place by a mobile crane with a telescopic boom. The 'C' columns were set out and levelled in the same manner as the 'B' columns. The Level Two connections were grouted in the same manner as described for the Level One connections in Section 3.5.2.8. As shown in Figure 3-71(b), a steel capping plate

was installed on a bed of cementitious mortar at the top of the columns. Washers and nuts were installed to anchor the column longitudinal reinforcement.

(a) Col C/2-C being lifted into place.

(b) Top plate and anchor detail on Col B/2-C.

Figure 3-71: Erecting 'C' columns.

3.5.2.14 Level Two Floor Installation

Low-friction strips were installed on the Level Two beam ledges only where the double-tee units were seated, as shown in Figure 3-72(a). The double-tee units were then lifted into place, as shown in Figure 3-72(b). Due to the tight tolerances between the A, B and C Grids discussed in Section 3.5.2.11, the compressible polystyrene backers were installed with the floor still suspended from the gantry crane to allow the backer to be levered into position. The double-tee connection detail, shown in Figure 3-72(d), was identical to that used in Level One, except it was half as deep.

(a) Low-friction strips installed.

(b) Double-tee unit being installed in west bay.

Figure 3-72: Erecting Level Two floors.

(c) Level Two double-tee floors installed.

(d) Double-tee seating detail.

Figure 3-72: Erecting Level Two floors (Continued).

Gaps between the double-tee flooring and the columns were plugged using compressible foam rod, as shown in Figure 3-73(a). The floor reinforcement for Level Two was identical to Level One, except the starter reinforcement along Grids 1 and 2 did not need to be longer to span the timber infill. The completed floor reinforcement is shown in Figure 3-73(b).

(a) Compressible foam plugging gaps between double-tee flooring and column.

(b) Level Two floor reinforcement installed.

Figure 3-73: Level Two floor formwork and reinforcement.

The concrete for the Level Two floor was placed by the same company that completed Level One. However, because the laboratory gantry crane did not have sufficient head room to operate the concrete hopper, a concrete pump was used instead. When the concrete arrived at the laboratory the slump was not high enough to facilitate pumping and super-plasticiser had to be added to increase the flowability. The rest of the pour followed the same steps undertaken on the Level One floor and are shown in Figure 3-74(b) – (d).

(a) Concrete being pumped on to the second floor.

(b) Screeding concrete.

(c) Power and hand trowelling floor.

(d) Floor covered with hessian and tarpaulin for curing.

Figure 3-74: Level Two floor pour.

3.5.2.15 Specimen De-propping and Painting

Level One remained propped while Level Two was constructed to avoid introducing excessive construction loads onto the Level One floor, and to enable a baseline DEMEC (DEmountable MEChanical gauge) measurement to be taken of Level One. Details of the DEMEC instrumentation applied to SA1 are presented in Section 3.8.2. It was important to take a true baseline measurement of the diaphragms in a zero stress state. If a baseline measurement were not taken, then the diaphragm strain from gravity loading could not be decoupled from the strain induced by lateral loading.

Specimen SA1 was painted so that cracks were easier to observe and record. As shown in Figure 3-75(a), Level Two was painted first and the DEMEC grid was installed. A baseline DEMEC measurement was taken, then Level Two was de-propped and another DEMEC measurement was taken. The rest of the specimen was then painted and the Level One DEMEC grid installed, as shown Figure 3-75(c). As with Level Two, a baseline measurement was taken before Level One was de-propped and another measurement was taken afterwards. Figure 3-75(d) shows the completed specimen SA1.

(a) Painting Level Two floor.

(b) Level Two propping removed.

(c) Painting Level One floor and columns.

(d) Level One propping removed and painting complete.

Figure 3-75: De-propping and painting SA1.

3.6 Reaction Frame Design

3.6.1 Experimental Setup

The reaction frame for SA1 was assembled from modular steel components and the complete setup is shown in Figure 3-76. The reaction frame was extensive and additional modular components had to be fabricated to complete the setup. The frame was designed to have maximum strength and stiffness, given the geometry and materials available.

Displacements were applied to SA1 by 1000kN and 440kN hydraulic actuators in the east-west and north-south direction respectively. Splitter beams attached to the end of the actuators divided the applied force in a ratio of 2:1 between Level Two and Level One. The forces were applied through the columns, which resulted in axial forces being transferred through the beams and floor. In a system with traditional connections, axial compression in the beams will increase the connection flexural capacity regardless of whether the connection is undergoing positive or negative flexure. However, in a slotted beam system a compressive axial force will increase the flexural capacity of a connection undergoing positive flexure, and decrease the flexural capacity of a connection undergoing negative flexure. Hence, over a building bay the

increase in strength due to beam axial force is largely mitigated. Axial forces in the beams can also affect the development of beam elongation. However, because slotted beams elongate approximately 75% less than an equivalent traditional connection the effect is much less pronounced. Connections in both bays were instrumented to allow the influence of axial force in the beams to be quantified.

Spherical bearings at each end of the actuators allowed for displacement out-of-plane during biaxial loading. The hydraulic actuators were mounted on cantilevered header beams of built-up section construction, as shown is Figure 3-76(b) and (c). The header beam was attached to towers, and braces connected the towers to the floor. Both the towers and the braces were anchored to the strong floor.

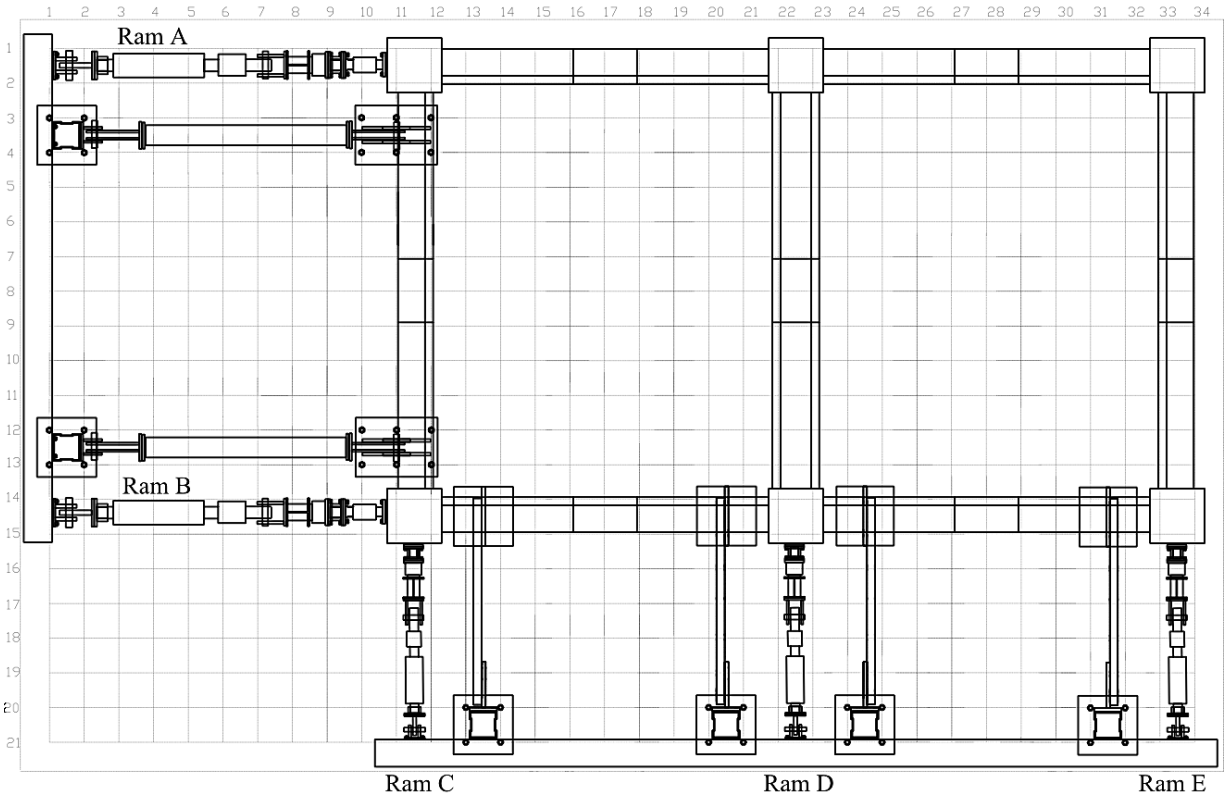

(a) Plan.

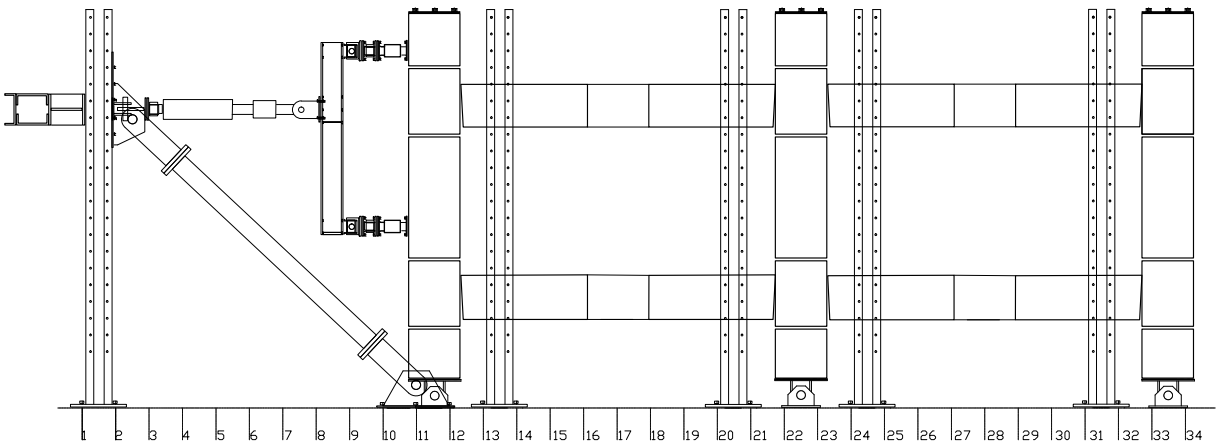

(b) East-west elevation.

Figure 3-76: Reaction frame drawings.

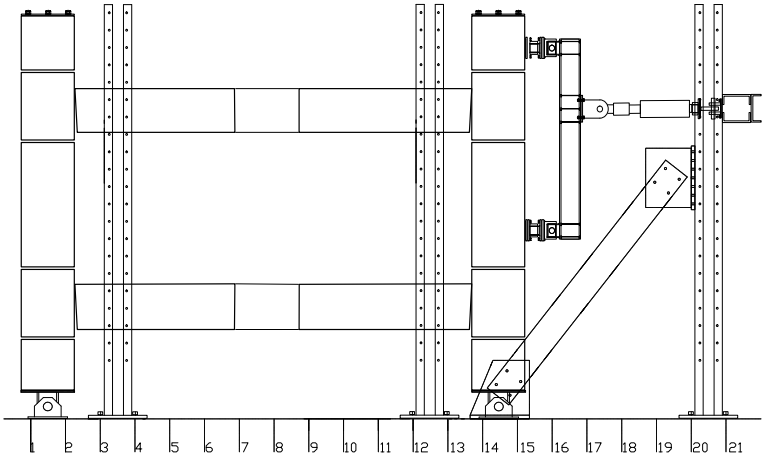

(c) North-south elevation.

Figure 3-76: Reaction frame drawings (Continued).

The five hydraulic actuators were connected in series and driven by a high flow pump, as shown in Figure 3-77. An electronically operated hydraulic bypass was fitted to the pump to allow the system pressure to be purged in an emergency.

(a) South-west perspective.

(b) South-east perspective.

Figure 3-77: Assembled SA1 reaction frame.

3.6.2 Laboratory Strong Floor Capacity Assessment

The superassembly experiment was conducted on the strong floor in the structures extension laboratory at the University of Canterbury. There was uncertainty surrounding the true capacity of the strong floor amongst technical and academic staff. Design had historically been based around a 10 tonne anchorage capacity. Floor actions were seldom checked due to a flawed logic that if the fixing capacities were not exceeded, then the floor capacity was empirically greater than demand.

The forces required to deform specimen SA1 were very large, and the absence of a reaction wall required all forces to be transferred through the floor. Higher demand specimens have been tested in the laboratory; however, complex and expensive self-equilibrating loading frames had to be developed to avoid loading through the floor (Matthews, 2004). The cost involved in developing a self-equilibrating loading frame for biaxial testing of a two storey structure was prohibitive. Hence, safe force and displacement limits for the strong floor were determined and adhered to during testing.

The strong floor was constructed in late 1960s and is 43'-4" by 27'-1" (13208mm by 8255mm) and 12" (305mm) thick. Post-tensioning the east-west direction is provided by 99-12W/.276 tendons staggered at 5" (127mm) centres above and below the 22-12/½" tendons at 14½" (368mm) centres in the north-south direction. The ultimate tensile strength and initial stress of the tendons is unspecified. The cables have a straight profile and are located at, and about, the centre of the floor in the short and long directions respectively. Figure 3-78(a) – (c) shows the plan and details of the strong floor. The floor is underlain by a damp-proof membrane and 2" (51mm) of site concrete. All concrete compressive strengths are unspecified. Located within the strong floor are mild steel anchorages located at 15" (381mm) centres The anchorages and are threaded for 1.5" (38mm) bolts.

To simplify the analysis procedure it was conservatively assumed that the floor acts as a one-way system, which enabled analysis in a strip-wise manner. The compressive strength of the concrete was assumed to be 45MPa. The post-tensioning tendons were assumed to have been stressed to 75% of their 1620MPa ultimate capacity. It was calculated that the factored axial and shear capacity of the anchorages was 205kN and 127kN respectively. It was assumed that the core area is 75% nominal and the ultimate tensile stress of the bolt was 300MPa.

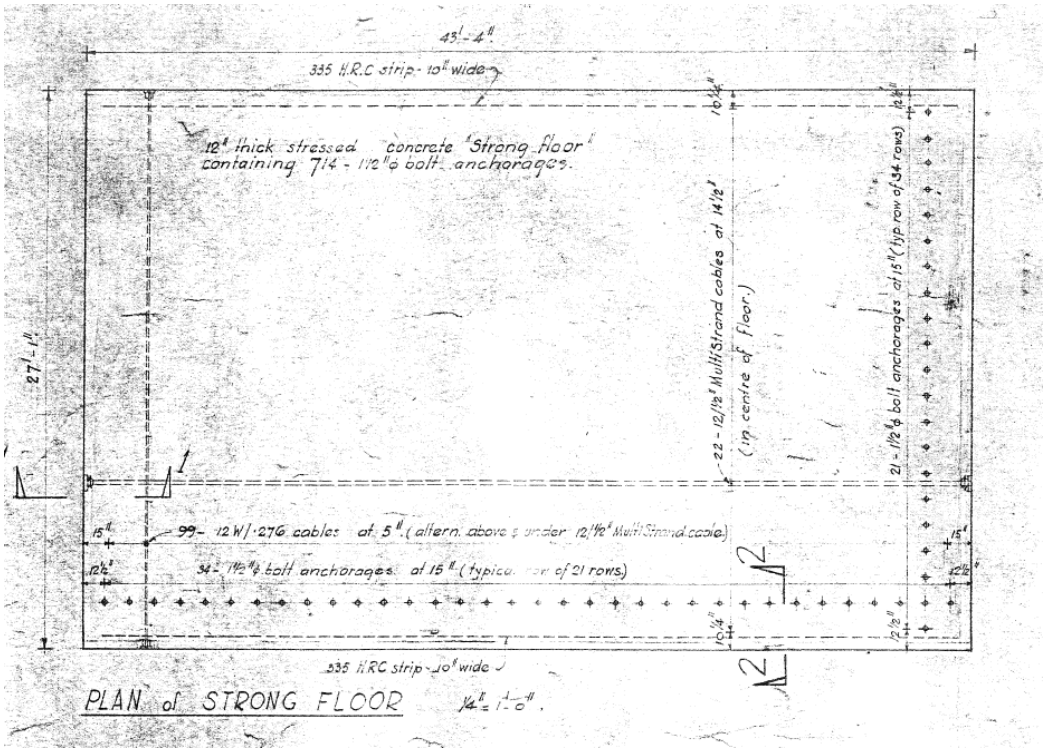

(a) Plan.

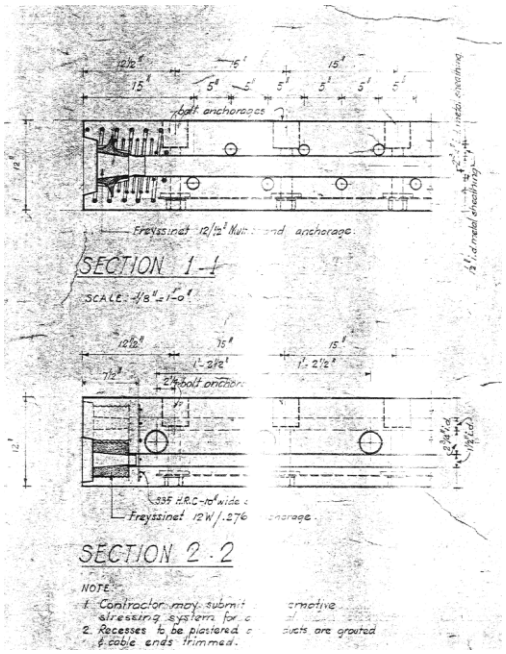

(b) Post-tensioning detail.

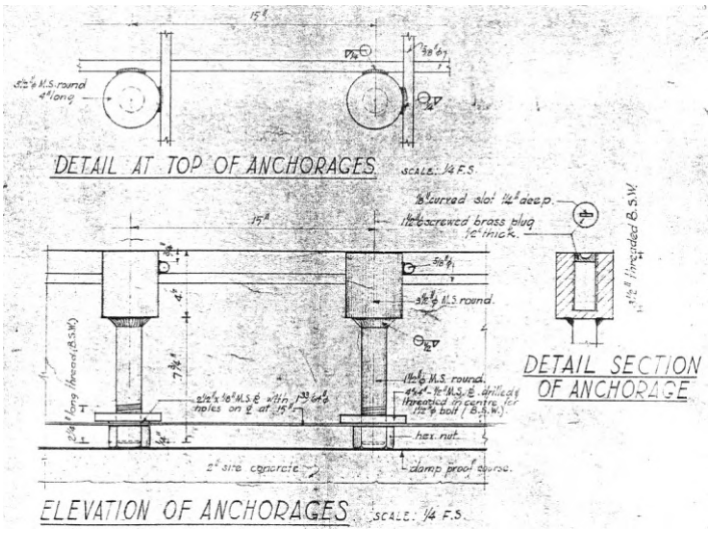

(c) Anchorage detail.

Figure 3-78: Structures extension strong floor drawings.

The analysis of the strong floor was undertaken using the sectional analysis software Response-2000 (Bentz, 2000). The predicted moment-curvature response of the strong floor is shown in Figure 3-79(a). The predicted deformation plots, measured from the reaction frame brace footing, are shown in Figure 3-79(b) and (c) for the east-west and north-south directions respectively.

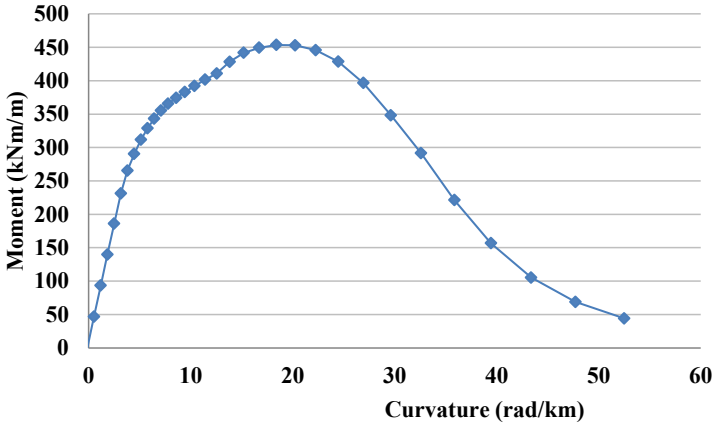

(a) Floor moment-curvature.

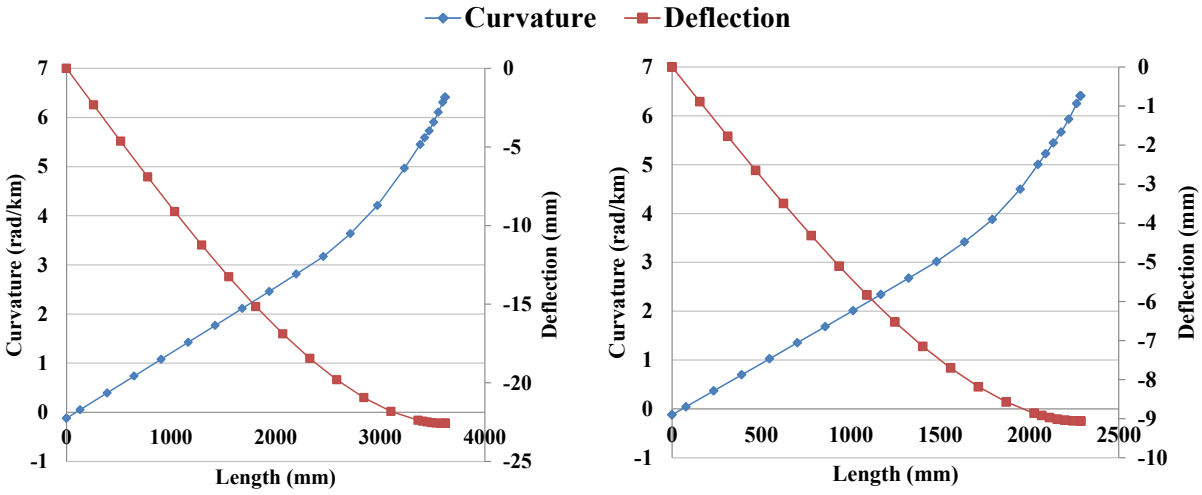

(b) East-west deformation.

(c) North-south deformation.

Figure 3-79: Analysis of strong floor.

Given the geometry of the reaction frame and the capacity of the strong floor, the maximum ram forces attainable were 450kN and 481kN in the east-west and north-south directions respectively. The floor displacements were monitored during testing to ensure the floor was not overloaded. The maximum allowable floor displacements were 16mm and 7mm for the east-west and north-south direction respectively. The capacity of the strong floor limited the maximum force that could be applied to the specimen. The reaction frame was designed for specimen overstrength of 1.75. The design capacity allowed for 25% greater post-yield strength gain than the 1.6 overstrength factor recommended by Au (2010).

3.7 SA1 Experimental Method Development

3.7.1 Seismic Testing Methods

Seismic demands on a specimen can be simulated in many ways; however, they can generally be broken down into four categories. The first is termed quasi-static monotonic and involves the application of an increasing lateral load to the specimen until failure, as shown in Figure 3-80(a). A quasi-static monotonic test is well suited to determining the initial stiffness, yield

point and displacement ductility of a specimen; however, because the loading is not cyclic, it is not representative of seismic loading.

Quasi-static cyclic loading involves the application of an increasing lateral load to achieve a predetermined displacement. The load is then reversed to achieve the same displacement in the reverse direction. The process is repeated for increasing displacements until the specimen fails, as shown schematically in Figure 3-80(b). Because the applied loads are cyclical, this type of loading is representative of the displacements a structure might experience during an earthquake. Quasi-static cyclic loading is most often applied at a rate which is many orders of magnitude less than what would be expected in an actual earthquake. This means that time dependent effects cannot be captured. Quasi-static cyclic loading is widely accepted for the seismic assessment of both new and existing details. The American Concrete Institute (ACI) standard for the assessment of structural details that are not prescribed in Chapter 21 of the American Building Code is based on quasi-static cyclic testing (ACI Committee 374, 2005; American Concrete Institute, 2005).

Pseudo-dynamic testing involves displacing the specimen as if it were subjected to an earthquake; however, the displacements are achieved without moving the foundation. A numerical model of the specimen is created and a nonlinear time history (NLTH) analysis is undertaken using a scaled earthquake record. At the end of each time-step of the NLTH analysis, the resulting displacement vector is applied to the specimen. The forces required to apply these displacements represent the nonlinear stiffness terms and are used as the restoring force for the next time-step (Priestley et al., 1999). A simplified schematic of this method is shown in Figure 3-80(c). Pseudo-dynamic testing is useful in evaluating the realistic response of a structure to a specific earthquake record; however, the cost of pseudo-dynamic testing is considerable.

The final method is using a shake table to induce loads in the specimen by displacing the foundation, as shown in Figure 3-80(d). A ground motion record is applied to the structure by displacing the shake table with high speed hydraulic actuators. Shake table testing is advantageous because it can closely replicate the actual loading conditions experienced during an earthquake. However, shake table testing is extremely expensive, and very few shake tables exist with the capacity to test large scale specimens.

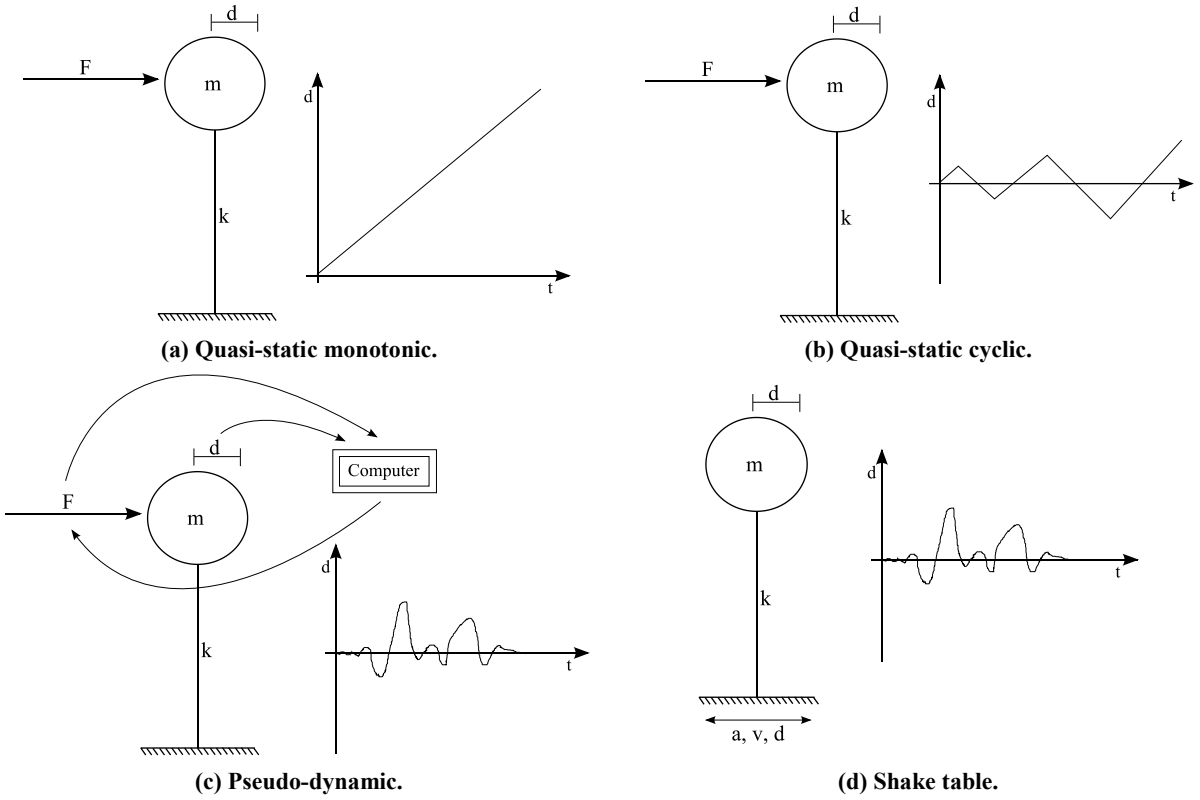

Figure 3-80: Schematics of test loading methods.

Building rotation about the vertical axis during an earthquake is generally caused by an eccentricity between the building centre of resistance and centre of mass, rather than the rotational component of an earthquake. Decoupling the torsional and translational contributions to response is very difficult in nonlinear systems; hence, specimen rotation about the vertical axis was restrained in this investigation. Rotation about the horizontal axes was ignored due to the negligible contribution it makes to building response. Vertical loading had little influence on the parameters of interest in this investigation and was ignored.

The testing of SA1 was required to be demanding and representative, but also applicable to many locations and structural forms. Hence, the quasi-static testing form recommended by ACI Committee 374 (2005) for appraising new details was used to develop the loading protocol applied to SA1.

3.7.2 SA1 Loading Protocol Development

The assessment of existing and newly developed details is often undertaken using different loading protocols. Less demanding loading protocols have sometimes been used to assess existing details because there was less uncertainty about the connection geometry and material properties. The slotted beam detail is a newly developed detail; hence, a more conservative loading protocol was required to determine the dependable performance.

3.7.2.1 Uniaxial Loading Protocols

Some of the earliest modern examples of structural experimentation were performed around 1815 in France on iron bridges and wooden ships (Leon & Deierlein, 1996). As shown in Figure 3-81, quasi-static cyclic tests were performed on riveted connections following the collapse of the first Quebec Bridge in 1907.

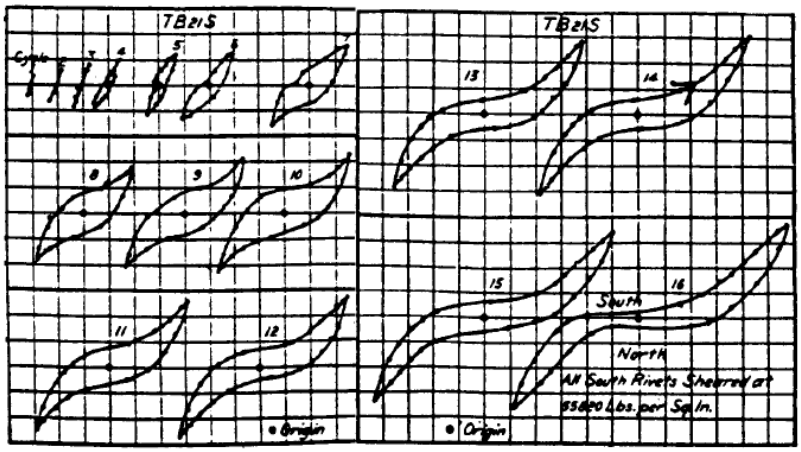

Figure 3-81: Results of early cyclic shear test of riveted connection (Department of Railways and Canals, 1919).

Ductility and stiffness are important parameters when undertaking design in accordance with capacity design principles, and quasi-static loading protocols have been adapted to specifically examine these parameters during structural testing. Two examples of ductility based loadings protocols are presented in Figure 3-82. The two protocols were essentially the same in their purpose; however, because of the path dependence of hysteretic response, the results from experiments where different loadings protocols have been applied may not have been directly comparable. Furthermore, because the two loading protocols were defined in terms of ductility, the specimen yield point had to be determined. Reinforced concrete generally does not have a well-defined yield point and some interpretation had to be made, which could result in ductility not being comparable between two tests.

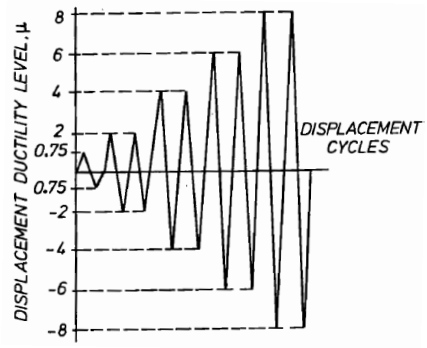

(a) Quasi-static loading protocol used at University of Canterbury.

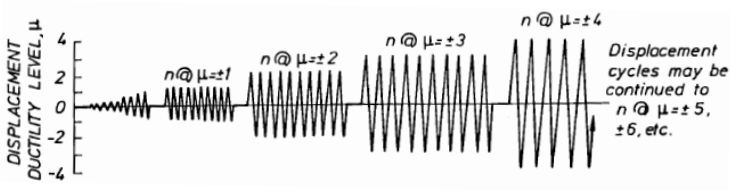

(b) Quasi-static loading protocol used at the Construction Technology Laboratory, Skokie, USA and at the Public Works Research Institute of the Ministry of Construction, Tsukuba, Japan.

Figure 3-82: Quasi-static loading protocols used at different institutions circa 1989 (Park, 1989).

Loading protocols used to evaluate the performance of newly developed connection details are generally more demanding than those used to assess the performance of existing details.

When seismically testing a newly developed detail, the final as-built form of the detail is not known. Factors affecting the response of the connection detail, such as the geometry, material properties and construction tolerances are variable. Hence, for the results of a test to be general the loading protocol applied must be demanding enough to allow for the variations in connection design.

The American Concrete Institute (ACI) has defined a standard quasi-static loading protocol for the verification of details that are not prescribed by Chapter 21 of ACI 318M-05 (American Concrete Institute, 2005). The protocol and criteria for evaluating connection performance are prescribed in ACI 374.1-05 (ACI Committee 374, 2005). The loading protocol is defined in terms of applied column drift, which is a more prescriptive definition of loading protocol than ductility. The loading protocol prescribes three fully reversed loading cycles be applied at each drift increment. The initial drift increment must be within the elastic range of the connection, and the applied columns drifts are increased in increments of 25% to 50% of the previously applied drift.

3.7.2.2 Biaxial Loading Protocols

Historically, there has been wide variety of biaxial loading histories used to test specimens, as shown in Figure 3-83. The displacement traces presented in the figure show that applied biaxial displacements have varied from loading in each orthogonal direction alternately, to combined loading in both directions simultaneously. Some biaxial loading histories are more representative of expected earthquake induced displacements than others.

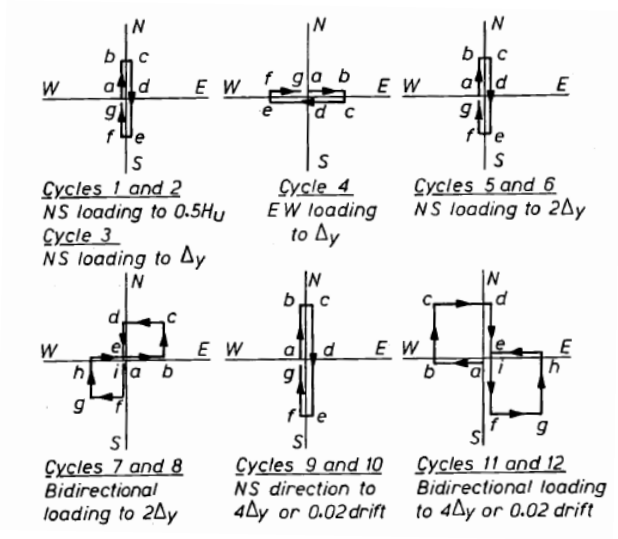

(a) Displacement history used in US-New Zealand-Japan-China collaborative research project on reinforced concrete beam-column joints (Park, 1989).

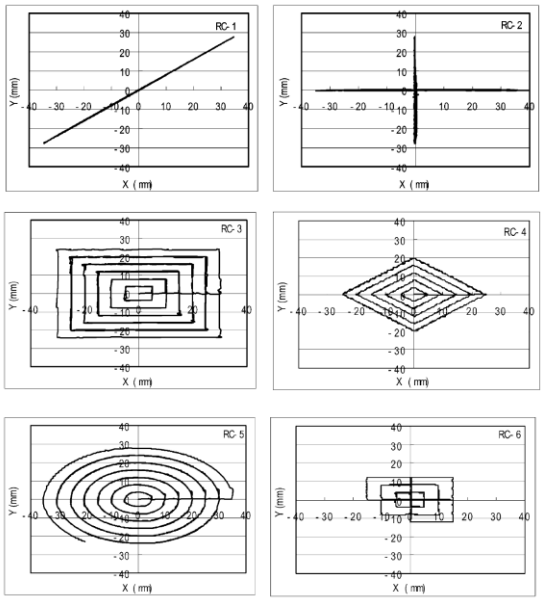

(b) Example of displacement histories used to test reinforced concrete columns in China (Qiu et al., 2002).

Figure 3-83: Displacement traces used to test reinforced concrete specimen biaxially.

A popular biaxial displacement history is the cloverleaf, shown in Figure 3-84. This has been used extensively for biaxial quasi-static experimentation at the University of Canterbury.

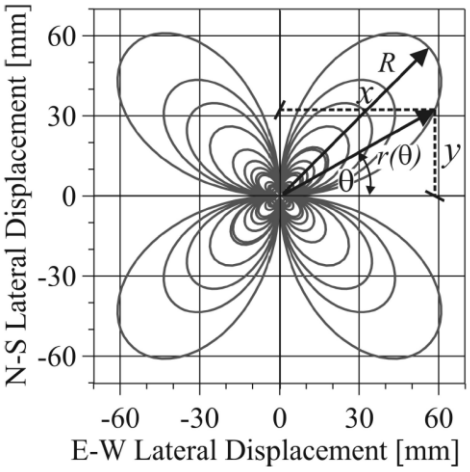

Figure 3-84: Bi-directional cloverleaf displacement trace (Marriott, 2009).

The cloverleaf displacement history can be described mathematically to aid in the development of input for a loading controller programme. The radius, r, at any point is described by Equation 3-2, where R is the maximum radial distance from the origin. The x and y coordinates are given by Equation 3-3 and Equation 3-4 respectively.

$$r(\theta) = R \sin 2\theta$$ **Equation 3-2**

$$x(\theta) = r(\theta) \cos\theta$$ **Equation 3-3**

$$y(\theta) = r(\theta) \sin\theta$$ **Equation 3-4**

The cloverleaf displacement history subjects a specimen to two completely reversed cycles in each orthogonal direction per cycle, which limits the number of cycles that can be applied using this shape to even denominations only. The loading protocol described by ACI 374.1-05 is for uniaxial loading only; hence, interpretation was required to apply the requirements to biaxial loading protocols (ACI Committee 374, 2005). It is not possible to apply three fully reversed cycles in each orthogonal direction if biaxial loading only is applied, only two or four.

Amaris et al. (2006) and Marriott (2009) interpreted ACI 374.1-05 to require three complete biaxial cycles, as shown in Figure 3-85 (ACI Committee 374, 2005). This interpretation resulted in six complete cycles being applied in each orthogonal direction for every imposed drift. This loading protocol was excessively demanding.

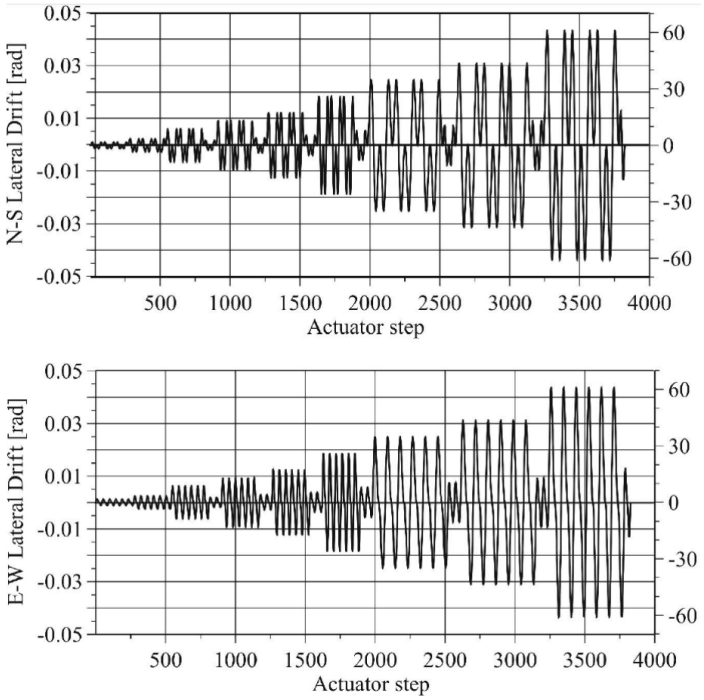

Figure 3-85: Displacement histories of principal axis applied in experiments by Marriott (2009).

A different interpretation of ACI 374.1-05 was made by Boys (2009) in developing the biaxial loading protocol he used to test poorly detailed reinforced concrete columns (ACI Committee 374, 2005). The developed loading protocol combined one complete biaxial cloverleaf displacement trace with a reversed uniaxial cycle along each orthogonal axis at every drift increment. This loading protocol enabled the requirements of ACI 374.1-05 to be met in each direction, and also meant that the difference in response between biaxial and uniaxial loading could be assessed.

The loading protocol applied to specimen SA1 is presented in Figure 3-86. The loading protocol was based on that developed by Boys (2009), and combined uniaxial and biaxial cloverleaf loading. Drift increments of 0.1%, 0.25%, 0.5%, 0.75%, 1.0%, 1.5%, 2.0%, 2.5% and 3.5% were applied. The reversed uniaxial excursions were applied first, followed by the biaxial cloverleaf loading. The loading protocol enabled three fully reversed cycles at every drift increment along each principal axis to be applied, which allowed the requirements of ACI 374.1-05 to be satisfied (ACI Committee 374, 2005).

Due to the shape of the biaxial cloverleaf loading protocol, it was impossible to have every loading cycle occur in the opposite direction to the preceding cycle in both directions. At least one cycle had to be reversed in the same direction as the preceding cycle. In the loading protocol applied to SA1, this occurred in the final full cycle at every drift increment in the north-south loading direction, as shown in Figure 3-86(c). The east-west loading protocol exclusively used reversed cycles in alternating directions, as shown in Figure 3-86(b). The

differences in order that displacements were applied in each direction meant that the measured response in each direction had a slightly different form.

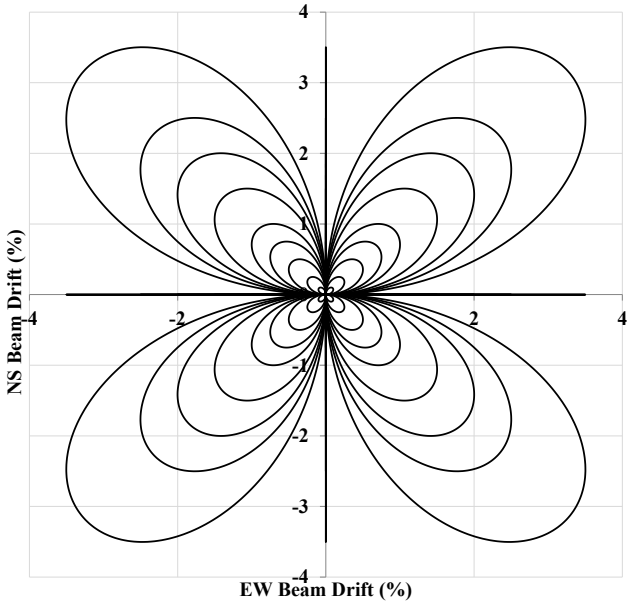

(a) Biaxial displacement trace.

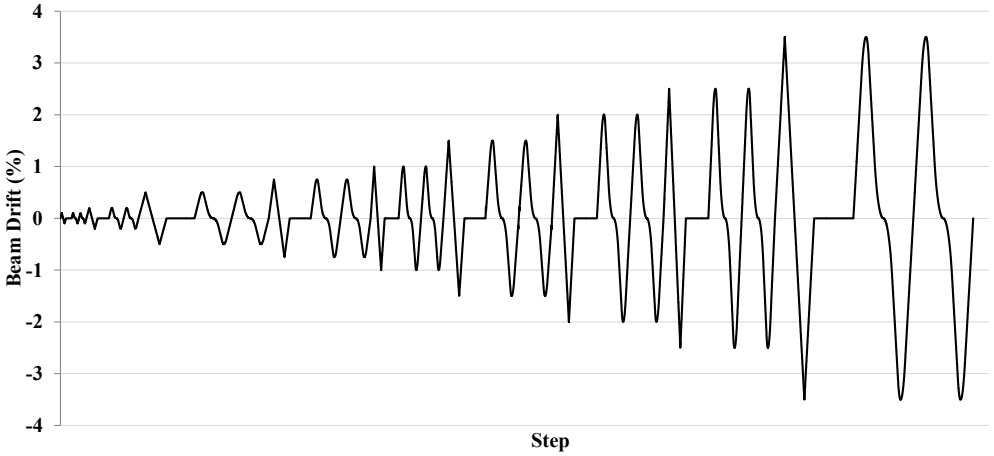

(b) East-west Component.

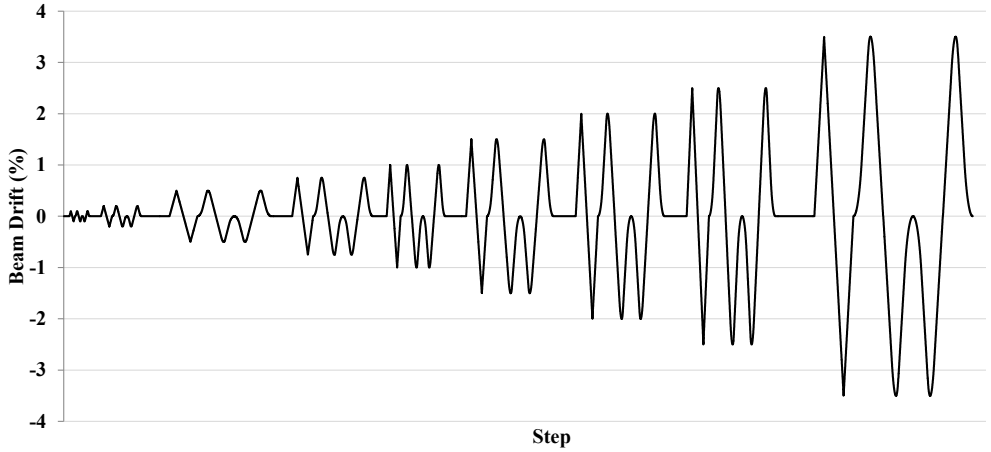

(c) North-south Component.

Figure 3-86: Loading protocol applied to specimen SA1.

Due to the scale of this experiment, testing had to be carried out over a long period of time. When testing was halted overnight, storey shears were left as close to zero as practicable to reduce additional stresses in the system.

3.7.2.3 Geometric Adjustments Applied to SA1

ACI 374.1-05 defines the drift ratio of a specimen as the inclination of the column chord; however, in this research programme the drift ratio was defined by beam drift (ACI Committee 374, 2005). Beam drift is defined as the relative inclination between the column face and the beam chord, and is shown schematically in Figure 3-87. The relationship between column drift and beam drift is expressed in Equation 3-5. Slotted beam connections often require larger column depths than equivalent traditional connections, due to the bottom longitudinal reinforcement bond demands through the column. If the same column drift were applied to a slotted beam superassembly and a traditional beam superassembly, the slotted beam superassembly would experience larger beam drifts. This example highlights a major shortcoming of defining specimen drift in terms of column inclination. When a specimen is tested, in most cases the region of interest is the connection between the beam and column, and it is the relative inclination between the beam end and the column face which dictates specimen response. When the measured response is related back to column drift it makes it difficult to compare the experimental response of different specimens.

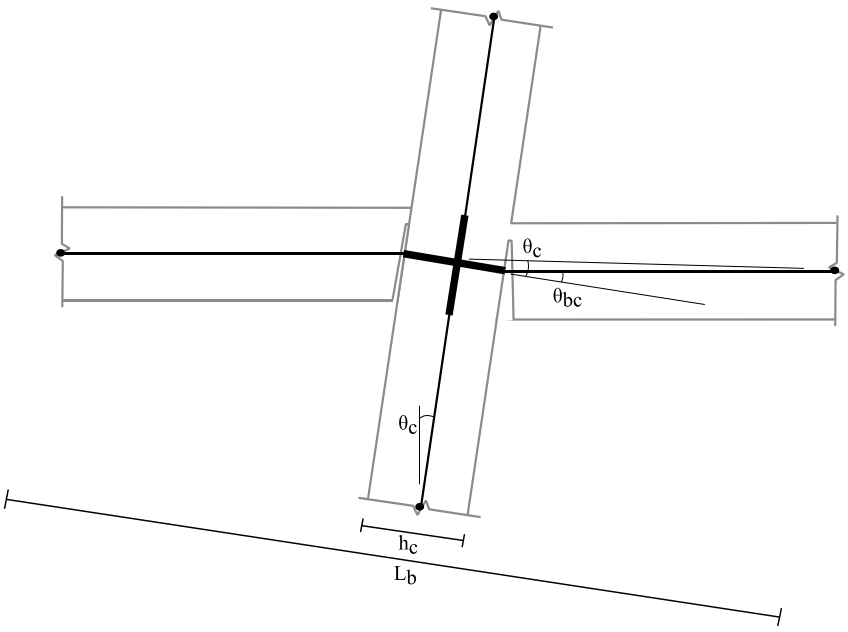

Figure 3-87: Beam drift definition.

$$\theta_{bc} = \frac{\theta_c}{1 - {h_c}/{L_b}}$$ **Equation 3-5**

For the same column inclination, the column depth and beam length both influence the induced beam drift. Beam drift is always constant regardless of specimen geometry. Thus,

because the bay lengths in the east-west and north-south directions of specimen SA1 were different, the induced column inclinations in each direction had to be different to produce the same beam drift in each direction. In the east-west direction the column inclination was 86% of the desired beam drift, and in the north-south direction it was 88%.

During biaxial testing, the specimen was displaced out-of-plane relative to the actuators and control instruments, as shown in Figure 3-88. The displacement out-of-plane resulted in components of force and displacement from the orthogonal axis affecting the measured force and displacement in the principal axis. To correct the measured displacements and forces, a series of geometrical modifications were performed.

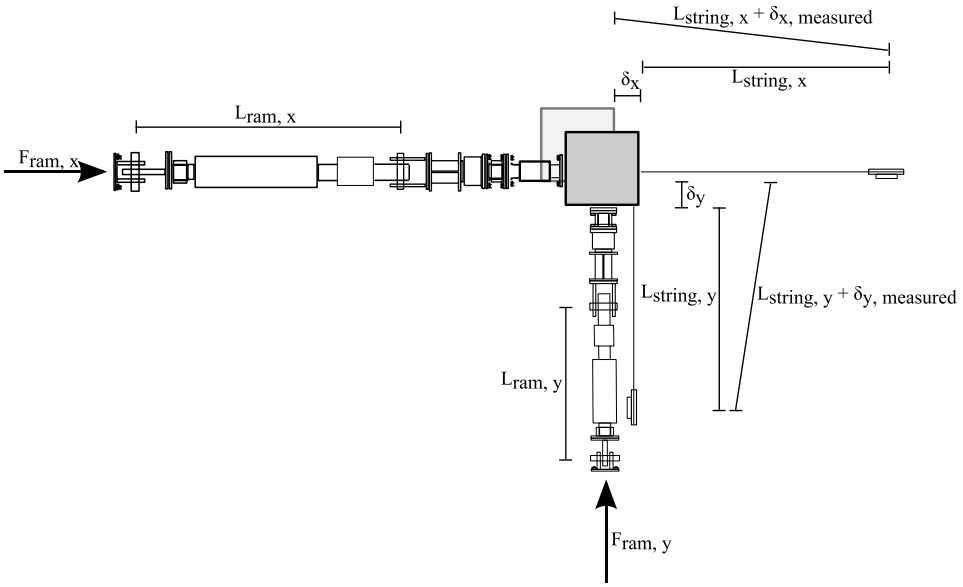

Figure 3-88: Geometric influences on measured forces and displacements.

Equation 3-6 and Equation 3-7 present the geometrical corrections that were applied to the measured specimen displacements. The force components of each actuator were calculated and summed to determine the true force being applied along each axis, as shown in Equation 3-8 – Equation 3-13. The error involved in neglecting iteration in the formulations was insignificant due to the length of the actuators and rotational potentiometer string lines.

$$\delta_x = \sqrt{\left(\left(L_{string,x} + \delta_{x,measured}\right)^2 - {\delta_y}^2\right)} - L_{string,x}$$ **Equation 3-6**

$$\delta_y = \sqrt{\left(\left(L_{string,y} + \delta_{y,measured}\right)^2 - {\delta_x}^2\right)} - L_{string,y}$$ **Equation 3-7**

$$F_{x(ram,x)} = F_{ram,x}\left(\frac{L_{ram,x} + \delta_x}{\sqrt{\left(\left(L_{ram,x} + \delta_x\right)^2 + {\delta_y}^2\right)}}\right)$$ **Equation 3-8**

$$F_{x(ram,y)} = F_{ram,y}\left(\frac{\delta_x}{\sqrt{\left(\left(L_{ram,y} + \delta_y\right)^2 + {\delta_x}^2\right)}}\right)$$ **Equation 3-9**

$$F_{y(ram,x)} = F_{ram,x}\left(\frac{\delta_y}{\sqrt{\left(\left(L_{ram,x}+\delta_x\right)^2+\delta_y{}^2\right)}}\right)$$ **Equation 3-10**

$$F_{y(ram,y)} = F_{ram,y}\left(\frac{L_{ram,y}+\delta_y}{\sqrt{\left(\left(L_{ram,y}+\delta_y\right)^2+\delta_x{}^2\right)}}\right)$$ **Equation 3-11**

$$F_{x(total)} = F_{x(ram,x)} + F_{x(ram,y)}$$ **Equation 3-12**

$$F_{y(total)} = F_{y(ram,x)} + F_{y(ram,y)}$$ **Equation 3-13**

3.7.2.4 Actuator Electronic Valve Controller Design

To apply the intended displacement protocol to SA1, a valve controller program to drive the five hydraulic actuators was developed using LabVIEW software (National Instruments, 2011). The conceptual design and development of the hydraulic actuator valve control program was undertaken by the author; however, the implementation of the underlying code for the program was performed by the Senior Software Technician at the University of Canterbury, Peter Coursey. The software sent displacement targets to controller boxes. Each controller box was connected to an actuator and rotational potentiometer, and extended or retracted the actuator until the displacement target was achieved.

The first version of the software developed was controlled entirely by displacement. Displacement control was the most reliable way to ensure that the intended displacement protocol was applied. All controller boxes were operated simultaneously; however, the actuators in the east-west direction influenced those in the north-south direction. As actuator A extended, it would force actuator E to retract. However, the control box for actuator E would then extend the actuator to maintain its displacement target and push actuator A off target. This process would repeat, and the forces would increase until the force limits were reached. A schematic of this process is shown in Figure 3-89(a). The interaction of the actuators in the east-west and north-south directions was caused by three factors:

1. The controller program was only capable of recognising the displacements it needed to reach and maintain. It was not capable of determining the simplest way to achieve them. Hence, equal and opposite moments applied along each axis was as viable a solution as equal forces applied along each axis, so long as the resulting displacements were the same.
2. The low stiffness of the reaction frame. The absence of a reaction wall in the laboratory necessitated the construction of a triangulated steel reaction frame, which was not stiff in comparison to SA1.

3. The high stiffness of specimen SA1. Along each axis, and in-plane across the floor diaphragms, the stiffness of SA1 was extremely high.

It was not practical to increase the stiffness of the reaction frame. Hence, the actuator interaction issue was addressed through factors 1 and 3. This subsection describes development of an actuator controller program that allowed for the stiffness incompatibility between the specimen and the reaction frame. Section 4.4 details how the high specimen stiffness was addressed.

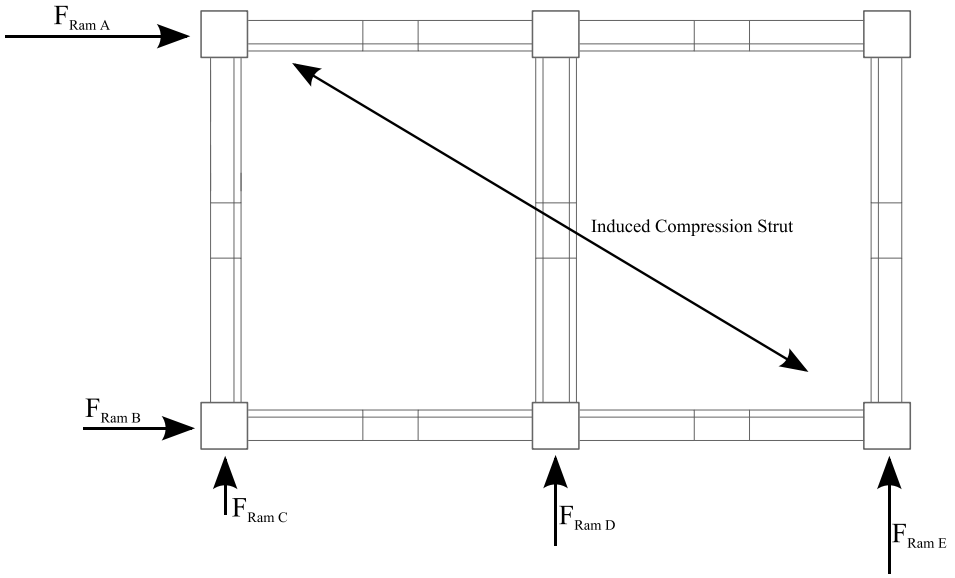

(a) Induced moments along orthogonal axes.

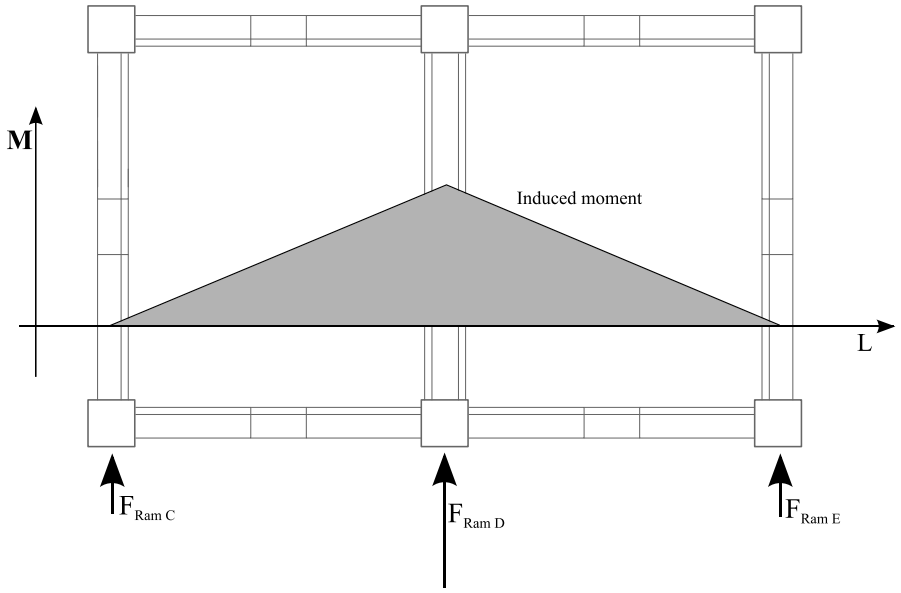

(b) Induced moment in-plane.

Figure 3-89: Unintended force distributions in test setup. Equilibrium is maintained by reaction forces from specimen, but not shown for clarity.

To prevent actuator forces from building up iteratively during testing, a compromise between displacement and force control was trialled. A sub-routine was added to the program to balance the force between actuators A and B in an effort to reduce the moment applied to the specimen. Once actuators A and B reached their displacement targets, the force imbalance

between them was checked. If the force imbalance was outside of a specified tolerance each actuator was retracted or extended to reduce the imbalance until the tolerance was met. This modification improved behaviour; however, because the next drift increment applied after the load balancing had been completed was displacement controlled, the force continued to increase over successive drift increments. The actuator force limits in the program were set at the maximum allowable in an effort to determine if the actuator forces would plateau. The force did not plateau, and testing had to be suspended when actuator A reached the force limit of 450kN. At the suspension of testing, actuator B had a force of 200kN. The moment applied to the specimen by the actuators in the east-west direction was resisted by the actuators in the north-south direction.

Whilst developing the actuator control program, an additional stiffness incompatibly between the reaction frame and the specimen was observed. The force in actuator D was often significantly higher than the force in actuators C and E. This force imbalance was caused by the high in-plane stiffness of SA1 and the comparatively low stiffness of the reaction frame. Actuator D was mounted in the centre of the north-south reaction frame strong-back, where it was supported on both sides by braces. Actuators C and E were mounted on cantilevered portions of the strong-back, and had one brace each. When actuators C, D and E were given a displacement target, actuator D, as the stiffest connection, would attract more load than actuators C and E. As shown in Figure 3-89(b), the floor diaphragms were forced to act as deep beams.

To be able to continue testing and realise the project goals, the decision was made to reduce the specimen stiffness in stages, as described in Section 4.4, and redesign the actuator controller program. Whilst the actuator control program was developed over many stages, only the final version is presented.

The final version of the actuator controller software used both force and displacement inputs to apply the intended loading protocol to SA1. Actuators B, C and E were displacement controlled, which allowed the correct translation to be applied in the east-west and north-south directions respectively. Actuators C and E were used to restrain specimen rotation about the vertical axis. The greater length between actuators C and E, compared to actuators A and B, made this arrangement stiffer and less prone to force increases. The same force that was applied to SA1 by actuator B was applied by actuator A. Similarly, the average force applied to SA1 by actuators C and E was applied by actuator D. Small displacement steps had to be applied when using this methodology to avoid large force differentials within displacement steps. Figure 3-90 presents a flow diagram describing the process that the final actuator control program followed to apply the loading protocol.

Within a displacement increment applied to SA1, the actuators were controlled in a sequence. Previously, all actuators were controlled at the same time and remained active until the force or displacement targets had been met. While there was the capability within LabVIEW to send force or displacement targets to the controller boxes, there was no means to shut the controller boxes down once they had reached their targets (National Instruments, 2011). However, there existed a safety feature within the controller boxes that would shut the controller box down if no dialogue was received from the controller program for a period of time. This safety feature was exploited to enable the controller boxes to be shut down after each target was met, effectively locking the actuator in position. This meant that the actuators could be activated sequentially, which prevented the actuators from interacting with each other and building up force within the application of a displacement increment to SA1. The 'time out' feature of the controller boxes was exploited in the program by a sub-routine that shut down all communication with the controller box for a predetermined period of time, as shown in Figure 3-90. The controller box 'time-out' allowed the intended displacement increments to be applied by actuators C and E first. These actuators controlled both north-south translation and rotation about the vertical axis. Once the controller boxes for actuators C and E had timed out, the average force being applied to SA1 by actuators C and E was applied to the specimen by actuator D. When the controller box for actuator D had timed out, the intended displacement increment was applied by actuator B. This actuator controlled the translation in the east-west direction. Actuator B was selected to apply the specimen displacement in the east-west direction rather than actuator A because it had less influence on actuator E. This was because the line of action of actuator B was in-line with the points where the actuators C, D and E applied their forces. Finally, after actuator B controller box had timed out, actuator A was force matched to actuator B.

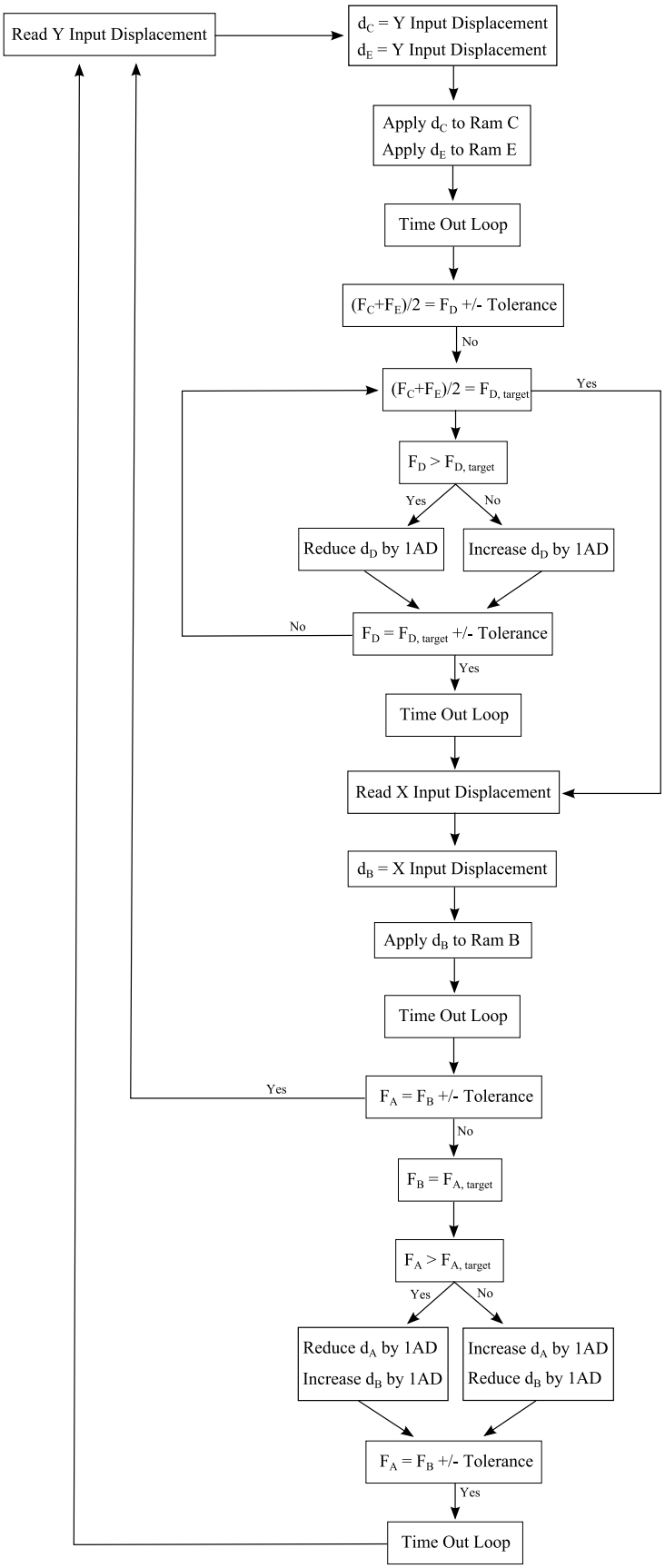

Figure 3-90: Actuator control program logic.

3.8 SA1 Instrumentation Design

Specimen SA1 was extensively instrumented. A Universal Data Logger (UDL) program was used to simultaneously log 521 data channels. The number of data channels that could be logged was limited by the capability of the UDL. In addition, 314 DEMEC points were attached to the Level One and Level Two floor diaphragms. Due to the size of SA1, every connection could not be instrumented. Hence, the instrumentation regime was an optimisation of the available equipment to enable sufficient data to be collected to satisfy the test objectives.

3.8.1 Control Instrumentation

The control instrumentation for the east-west and north-south directions is shown in Figure 3-91(a) and (b). The actuator forces were measured using two 1000kN load cells for actuators A and B, and three 440kN load cells for actuators C, D and E. Specimen displacement at each level was measured along every Grid using rotary potentiometers. To provide a fixed datum from which to measure the specimen displacements, the rotary potentiometers were mounted on instrument towers.

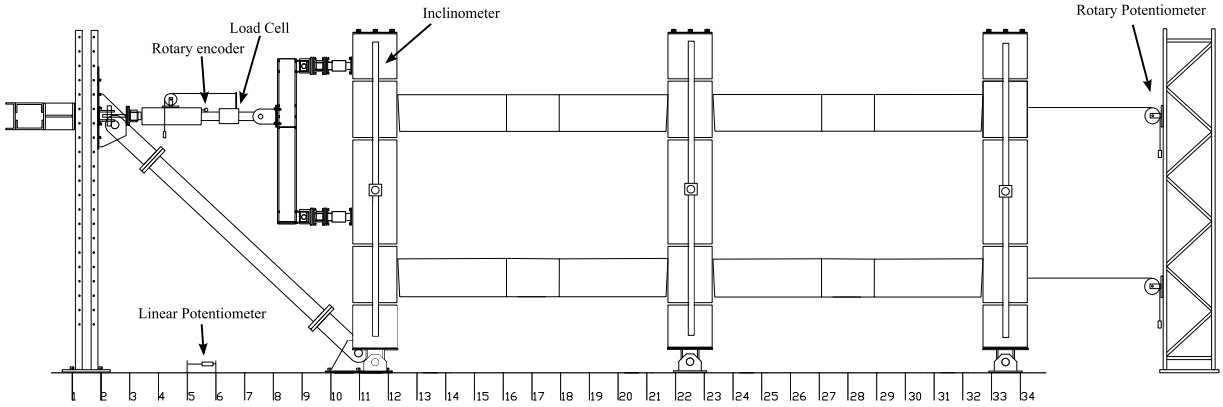

(a) East-west.

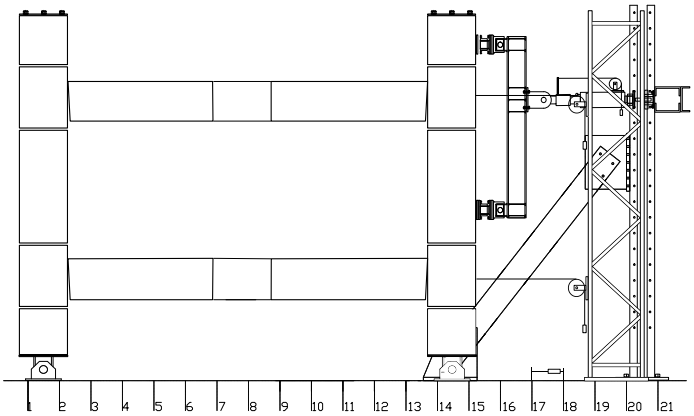

(b) North-south.

Figure 3-91: Control instrumentation.

The actuators forces, Level Two displacements and ram encoders were used as inputs for the actuator controller program, which is described in Section 3.7.2.4. The rotary encoder data

was used as input for a safety feature in the actuator control program, which would terminate testing if the ram extension exceeded pre-set limits. Because the forces that were applied to SA1 were close to the maximum capacity of the laboratory strong floor, the strain induced in the strong floor was recorded throughout testing. Two inclinometers orientated 90° to each other were attached to each column to measure column inclinations in each direction. The inclinometers were attached to a stiff steel section that was attached at the top and bottom of the columns to mitigate the effect of column flexure on measurements.

3.8.2 Floor Diaphragm Instrumentation

The top of the Level One and Two floor diaphragms were instrumented with linear potentiometers and DEMEC points, as shown in Figure 3-92(a) and (b) respectively. The 30mm gauge length linear potentiometers were installed in pairs to enable both linear and shear strains to be measured. The linear potentiometers were installed only on the western portion of the floor diaphragms so that they would not interfere with the collection of DEMEC data.

The DEMEC points were stainless steel buttons with a 1mm diameter target drilled in the centre, as shown in Figure 3-93. The DEMEC points were attached to the floor diaphragm with a two-part epoxy. Both 250mm and 500mm grid spacings were used. The greater resolution 250mm grid was applied in regions where larger strain was expected, such as over the timber infill and precast floor seating. Longitudinal strain in both the east-west and north-south directions was measured between DEMEC points using 250mm and 500mm DEMEC gauges. Shear strain also was measured using a 354mm DEMEC gauge over the 250mm grid. The first floor had 178 DEMEC points and the second floor had 136 DEMEC points.

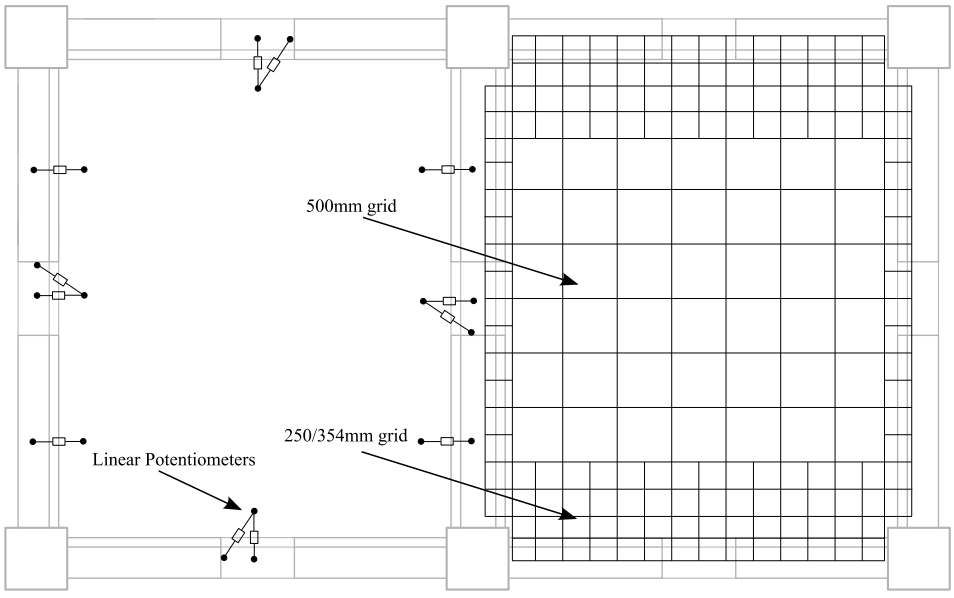

(a) Level One.

Figure 3-92: Instrumentation of top of floor diaphragms.

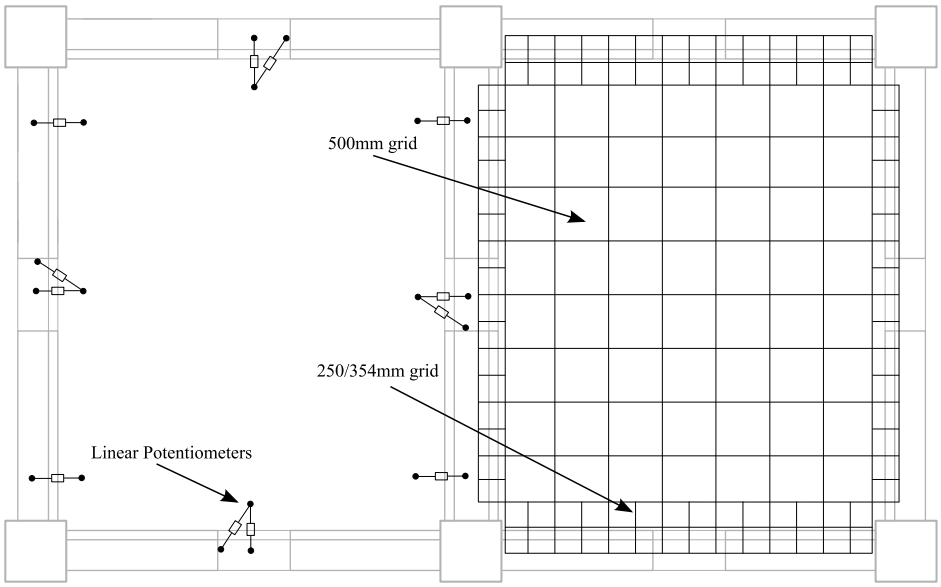

(b) Level Two.

Figure 3-92: Instrumentation of top of floor diaphragms (Continued).

Collecting DEMEC data was a laborious task, as the distance between each point had to be manually measured for each loading scenario that was investigated. To minimise the number of measurements that had to be performed, and prevent duplication, DEMEC grids were only applied in the eastern floor diaphragms of both levels. Baseline measurements were taken before the specimen was de-propped, as described in Section 3.5.2.15. The baseline measurements formed the basis of the subsequent strain calculations.

DEMEC measurements were made after de-propping the specimen and immediately before prior to testing. During testing, DEMEC measurements were made during the 1%, 2.5% and 3.5% beam drift cycles. The measurements were collected at the peak displacements during the uniaxial portion of the loading protocol. During the biaxial portion of the loading protocol, measurements were collected at the 45°, 135°, 225° and 315° points. In total, approximately 40,000 DEMEC readings were collected.

(a) Detail of DEMEC point.

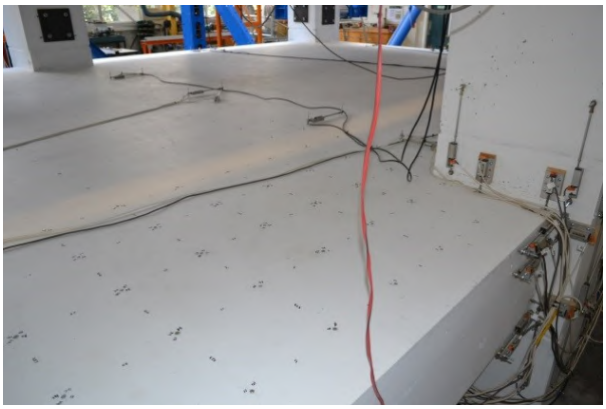

(b) Portion of DEMEC grid with linear potentiometers in background.

Figure 3-93: Level One top of floor diaphragm instrumentation.

Figure 3-94(a) and (b) show the instrumentation installed underneath the Level One and Two floor diaphragms respectively. The 50mm gauge length spring potentiometers, in conjunction with the matching 30mm linear potentiometers on the floor above, allowed the precast floor unseating to be measured. To measure beam torsion over the beam length, five inclinometers were attached to the underside of Grids B and C over both levels.

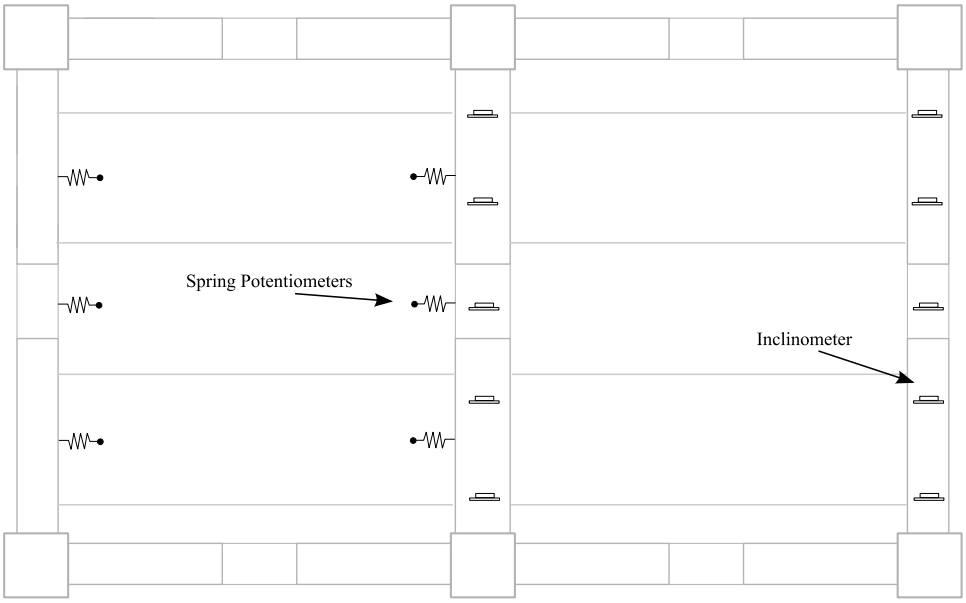

(a) Level One.

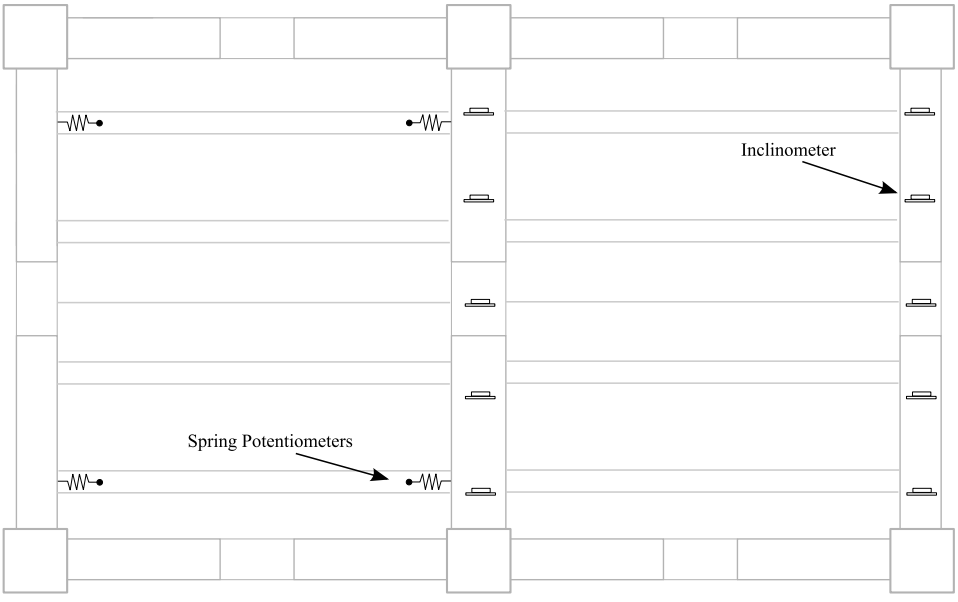

(b) Level Two.

Figure 3-94: Instrumentation of bottom of floor diaphragms.

3.8.3 Frame Instrumentation

The 12 connections that were instrumented over both floors on Grids 1, B and C are shown in Figure 3-95(a) – (c). This arrangement allowed the displacements of all the connections with different boundary conditions or loading states to be measured. There was insufficient equipment available to install instrumentation on all connections.

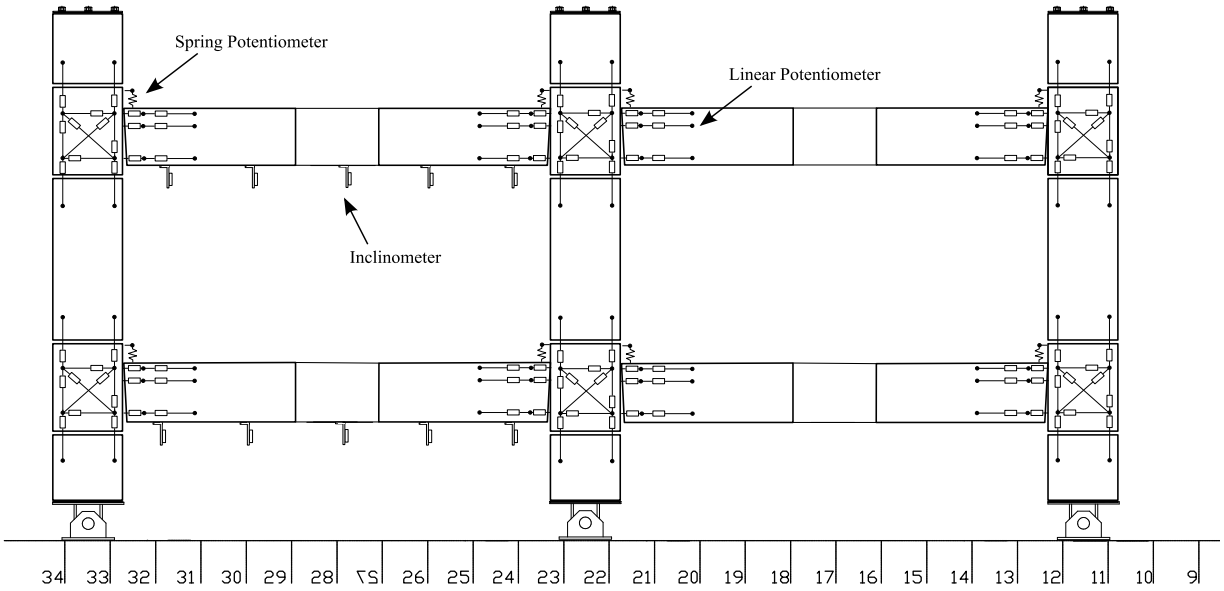

(a) Grid 1.

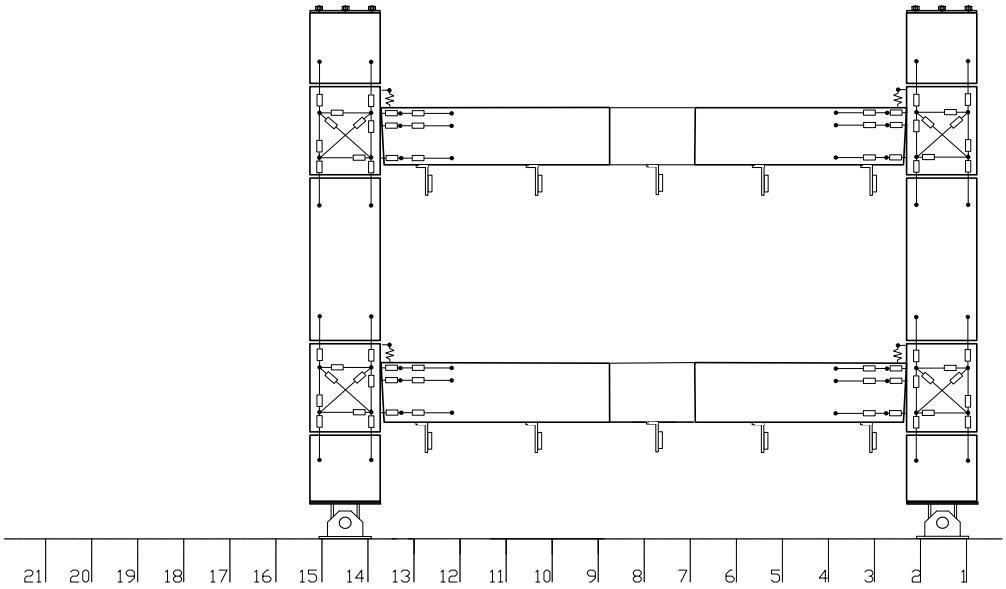

(b) Grid C.

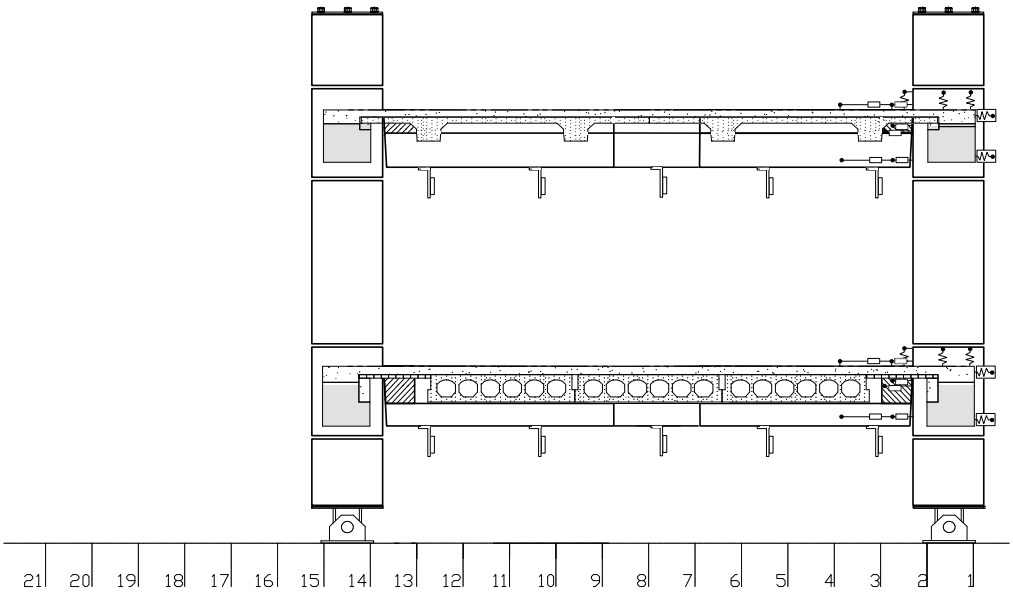

(c) Grid B.

Figure 3-95: Drawings of frame instrumentation.

Each connection had four 30mm gauge length spring potentiometers, located in pairs above and beside the beam, to measure fixed end rotation about the beam longitudinal axis, as shown in Figure 3-95(c) and Figure 3-96(b). Linear potentiometers with a 30mm gauge length were attached to the beam-column joints in a rosette arrangement to measure shear deformations. Above and below the rosettes, pairs of 30mm linear potentiometers were installed to measure column flexure. Six 50mm gauge length linear potentiometers were installed at the beam ends. Three potentiometers were attached to the beam only and measured beam flexure. The remaining three potentiometers were attached between column face and the beam end to measured beam fixed end rotation. All potentiometers were attached to SA1 with 6mm threaded rod epoxied into pre-drilled holes. The instruments were installed as close to the surfaces as practical to reduce error from out-of-plane deformations.

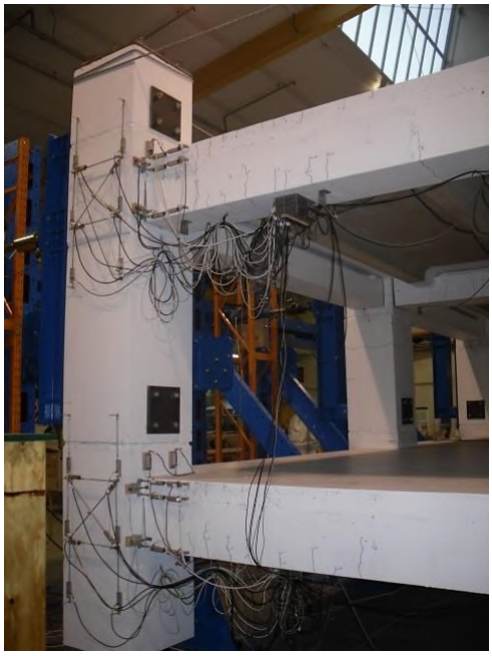

(a) Instrumentation on Bm C/2-1 and 2.

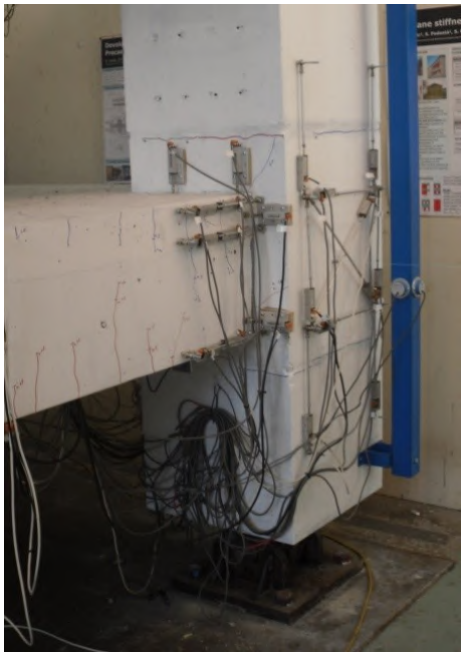

(b) Detail of instrumentation on Bm C/1-1.

Figure 3-96: Frame instrumentation.

As described in Section 3.5.1.10, strain gauges were installed in units Bm B/1-2 and Bm C/1-2 to measure the local strains in the reinforcement. Bm B/1-2 and Bm C/1-2 were selected because they were the least susceptible to any potential influence from boundary conditions and loading conditions. Both the east-west and north-south directions were instrumented in both units. Figure 3-97 and Figure 3-98 show the locations that strain gauges were applied in units Bm B/1-2 and B C/1-2 respectively. Strain gauges were applied to the beam-column stirrups in both loading directions to enable the strain profile over the joint to be measured. Strain gauges were applied along the length of the top and bottom longitudinal reinforcement and the diagonal hangers to measure the strain profile, strain penetration and bond stresses. Both the interior and exterior reinforcement had strain gauges applied to them. In regions that were subject to flexural strains, strain gauges were installed on opposite sides of the

reinforcement to enable a compensated strain to be calculated. To prevent any influence that the strain gauges could have on the initiation of reinforcement buckling, no strain gauges were installed along the unbonded portion of the bottom longitudinal reinforcement.

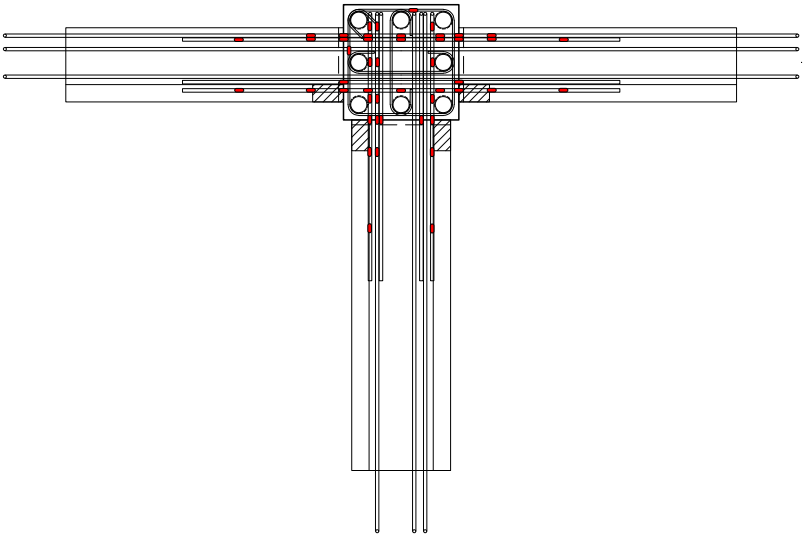

(a) Plan.

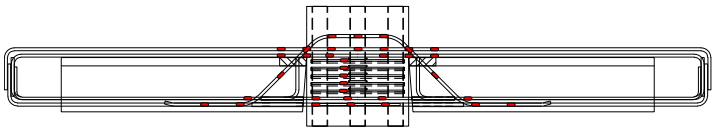

(b) East-west elevation.

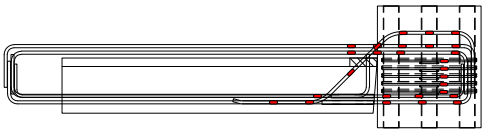

(c) North-south elevation.

Figure 3-97: Strain gauges attached to Bm B/1-2.

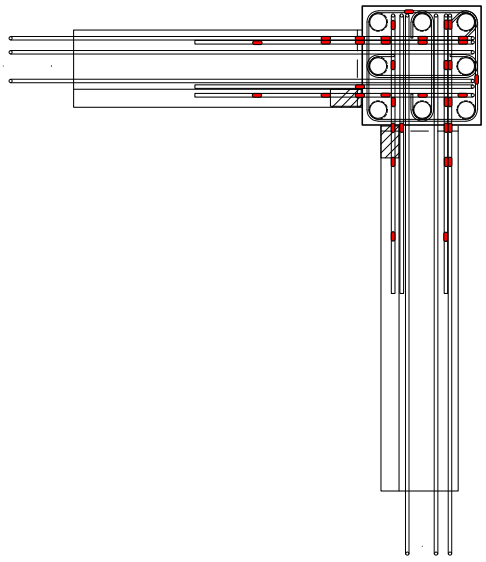

(a) Plan.

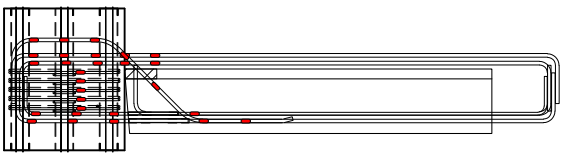

(b) East-west elevation.

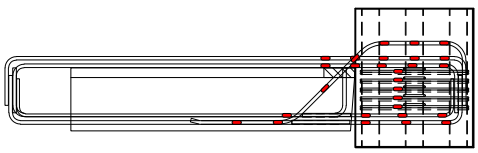

(c) North-south elevation.

Figure 3-98: Strain gauges attached to Bm C/1-2.

3.8.4 Interpolation of Frame Deformations

The four main deformation components that contributed to measured specimen displacement were elastic column flexure, elastic beam flexure, beam fixed end rotation and beam-column joint shear. These components are presented schematically in Figure 3-99(a) – (d) respectively. Beam and column shear deformations were assumed to be insignificant because sufficient shear reinforcement was supplied and these types of failure mechanisms were protected against through capacity design.

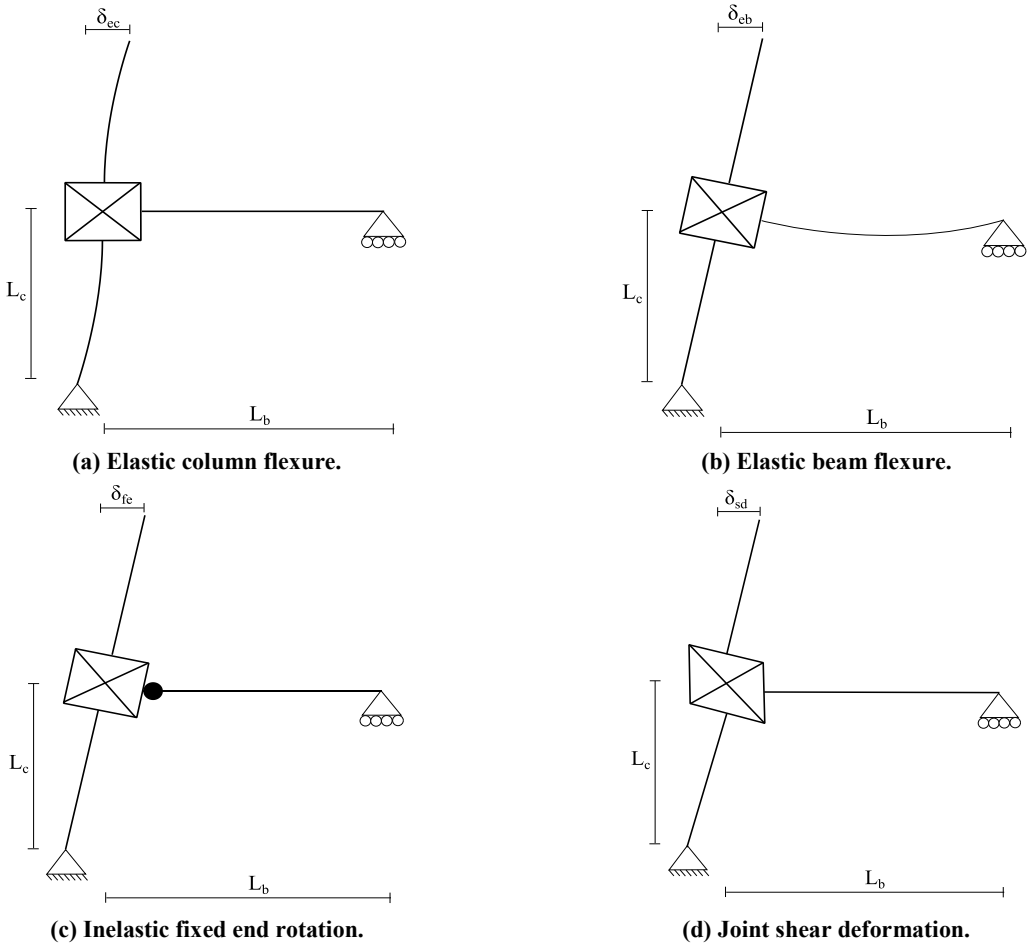

(a) Elastic column flexure. **(b) Elastic beam flexure.**

(c) Inelastic fixed end rotation. **(d) Joint shear deformation.**

Figure 3-99: Main components of specimen deformation.

Peng (2009) described a method to calculate the contribution of shear and flexure contributions to specimen displacement by piecewise measurement along the beam and column lengths. However, this method would have required extensive instrumentation and could not be undertaken in specimen SA1. For specimen SA1 direct measurement of deformations was made and the corresponding displacement contributions estimated through geometrical relationships. The contributions of elastic beam and column flexure to specimen displacement were measured using pairs of linear potentiometers. The member curvatures were calculated from the measurements, and the curvatures were extrapolated over the length of the members to determine their contribution to specimen displacement. Linear potentiometers over the slotted section allowed the fixed end rotation to be determined. The

contribution to measured displacement was then determined using geometrical relationships. The total shear distortion in the beam-column joint zone was calculated using potentiometers arranged in a rosette and geometrical relationships (Cheung, 1991). The specimen geometry was then used to determine the contribution of joint distortion to measured specimen displacement. The percentage that each displacement component contributed to the overall specimen displacement was calculated from the sum of all of the components.

3.9 Conclusions

Historical experimental investigations conducted on indeterminate moment resisting frames were examined and critiqued to guide the design of a slotted beam superassembly. Superassembly SA1 was a two storey, two-by-one bay, reinforced concrete slotted beam superassembly. The specimen represented the lower two stories of a prototype seven storey building designed for Wellington, New Zealand. Specimen SA1 was designed in accordance with NZS3101:2006 and recommendations from recent research (Standards New Zealand, 2006; Au, 2010). The specimen was designed to closely replicate typical New Zealand construction practices in terms of geometry and erection procedures. SA1 was the first complete slotted beam system to be constructed, which allowed complex three-dimensional behaviour and interactions between structural elements to be examined. New details designed to improve the performance of the slotted beam detail were tested. These details included;

1. Two layers of top and bottom longitudinal reinforcement in the beam, which was representative of realistic beam reinforcement layouts.
2. The modified three hanger detail for perimeter beams, which had two of the diagonal hangers located outside of the main beam reinforcement cage to increase the torsional strength of the connection.
3. The four hanger detail for internal beams, which provided greater resistance to the large gravity shear demands that the internal connections of SA1 were subjected to.
4. The supplemental hooked reinforcement detail, which maintained a stable shear transfer mechanism from the main beam reinforcement cage to the base of the shear hangers.
5. The continuous shear hanger detail for internal connections, which simplified and decongested internal beam-column connections.
6. Supplementary reinforcement welded to the bottom longitudinal reinforcement, which increased the bond area and reduced strain penetration through the internal beam-column joints. This detail was developed for use in slotted beam connections based on research undertaken at the University of Auckland (Fenwick & Nguyen, 1981; Fenwick, 1983; Budiono, 1988; Davidson & Fenwick, 1993).

The precast concrete components of specimen SA1 were manufactured by reputable commercial precast companies. Commercial precast companies were used to enable the practicality of specifying the slotted beam detail to be assessed. Recommendations were developed during the manufacture of the precast components:

1. A quadrilateral slot form should be used, in conjunction with staged concrete pours, to ensure the accurate placement of the beam slot when hydrostatic pressures exist.
2. A compressible, yet flexurally rigid, slot form that can be left in place after the precast components have cured is the ideal solution for forming the beam slot. The slot form would protect the longitudinal reinforcement against corrosion.
3. The engineer should inspect the assembled beam reinforcement for accuracy prior to casting. Components such as the diagonal hangers, debonding tubes and confinement stirrups have a significant effect on slotted beam performance; adherence to the design documentation must be ensured.

The erection of specimen SA1 was conducted by the author, University of Canterbury technicians and commercial construction companies. Commercial construction companies were used to enable the practicality of erecting a slotted beam building to be assessed. Several observations and recommendations were made during the erection of SA1:

1. The double hooked mid-beam lap splice used in SA1 was compact and efficient; however, it was congested and difficult to assemble. If space allows, a traditional lap splice should be used.
2. If the beam precast height is well matched to the precast floor height, the speed of erection can be significantly improved by reducing the quantity and complexity of the formwork required.
3. To simplify the quality assurance process during construction monitoring, the grout tube routing should be designed by the engineer to ensure that the ducts can be completely filled with grout, and remain filled after the grout pumping has ceased.
4. To prevent reinforcement buckling, it is recommended that stirrups are provided around diagonal hangers that are installed outside of the main beam reinforcement cage. The confinement reinforcement should be cast integral with the rest of the beam unit.
5. Damage sustained by SA1 during the 22nd February 2011 Christchurch earthquake did not significantly affect the results gathered during testing.

A large reaction frame was designed and assembled using modular structural steel components. The reaction frame was designed to provide maximum strength and stiffness, given the geometry and materials available. An analysis of the laboratory strong floor was

undertaken to determine safe working loads. The laboratory strong floor governed the maximum actuator forces that could be applied to the specimen. Existing actuator control programs caused interference between the actuators, which resulted in the actuator forces building up over successive displacement increments. A new program was developed to control the hydraulic actuators, which reduced the actuator interference and allowed the intended biaxial displacements to be applied to SA1.

Specimen SA1 was extensively instrumented with load cells, strain gauges, DEMEC points, inclinometers and linear, spring and rotational potentiometers. Because of the limitations of the data logging equipment, not every connection in SA1 could be instrumented. The instrumentation regime was an optimisation of the available equipment to collect sufficient data to satisfy the test objectives.

It can be concluded that the reinforced concrete slotted beam can be manufactured by competent New Zealand precast companies. The recommendations developed in this chapter will expedite the slotted beam manufacturing process.

3.10 References

ACI Committee 318. (2005). *Building Code Requirements for Structural Concrete (ACI318-05)*. Farmington Hills, Michigan: American Concrete Institute.

ACI Committee 374. (2005). *Acceptance Criteria for Moment Frames Based on Structural Testing and Commentary (ACI374.1-05).* Farmington Hills, Michigan: American Concrete Institute.

Amaris, A., Pampanin, S., & Palermo, A. (2006). *Uni and Bi-directional Quasi Static Tests on Alternative Hybrid Precast Beam Column Joint Subassemblies*. Paper presented at the New Zealand Society for Earthquake Engineering Conference, Napier, New Zealand. Retrieved from http://www.nzsee.org.nz/db/2006/Paper24.pdf

Au, E. (2010). *The mechanics and design of a non-tearing floor connection using slotted reinforced concrete beams.* Masters Dissertation, University of Canterbury, Christchurch, New Zealand.

Bentz, E. (2000). *Sectional Analysis of Reinforced Concrete Members*. Doctoral Dissertation, University of Toronto, Canada.

Boys, A. (2009). *Assessment of the Seismic Performance of Inadequately Detailed Reinforced Concrete Columns.* Masters Dissertation, University of Canterbury, Christchurch, New Zealand.

Budiono, B.(1988). *The Hysteretic Response of Reinforced Concrete Structures under Seismic Loading*. Masters Dissertation, University of Auckland, Auckland, New Zealand.

Bull, D. K., & Matthews, J. G. (2003). *Proof of Concept Tests for Hollowcore Floor Unit Connections (Report number 2003-1)*. Christchurch, New Zealand: University of Canterbury.

Byrne, J. D. R., & Bull., D. K. (2012). *Design and testing of reinforced concrete frames incorporating the slotted beam detail*. Paper presented at the New Zealand Society for Earthquake Engineering Conference, Christchurch, New Zealand. Retrieved from http://www.nzsee.org.nz/db/2012/Paper065.pdf

Centre for Advanced Engineering. (1999). *Guidelines for the use of structural precast concrete in buildings*. Christchurch, New Zealand: Author.

Cheung, P. C. (1991). *Seismic Design of Reinforced Concrete Beam-Column Joints with Floor Slab.* Doctoral Dissertation, University of Canterbury, Christchurch, New Zealand.

Davidson, B. J., & Fenwick, R. C. (1993). *The Seismic Response of Ductile Reinforced Concrete Frames with Uni-directional Hinges (Report number 527)*. Auckland, New Zealand: University of Auckland.

Fenwick, R. C. (1983). *Strength Degradation of Reinforced Concrete Beams under Cyclic Loading (Report numner 304)*. Auckland, New Zealand: University of Auckland.

Fenwick, R. C., Ingham, J. M., & Wuu, P. J. Y. (1996). *The Performance of Ductile R/C Frames under Seismic Loading*. Proceedings of the New Zealand National Society for Earthquake Engineering Technical Conference, New Plymouth, New Zealand, 20-26.

Fenwick, R. C., & Nguyen, H. T. (1981). *Reinforced concrete beam-column joints for seismic loading (Report number 220)*. Auckland, New Zealand: University of Auckland.

GNS Science. (2011). Retrieved March 8th, 2013, from http://www.geonet.org.nz.

Department of Railways and Canals. (1919). *The Quebec Bridge Over the St. Lawrence River Near the City of Quebec on the Line of the Canadian National Railways: Report of the Government Board of Engineers, Volume 1*. Ottawa, Canada: Author.

Hare, J., Fenwick, R. C., Bull, D. K., & Built, R. (2009). Precast Double Tee Support Systems. *Journal of the Structural Engineering Society New Zealand, 22*(1), 10-44.

Harris, H. G., & Sabnis, G. M. (1999). *Structural modelling and experimental techniques*. Boca Raton, Florida, USA: CRC Press.

HERA. (1998). *Welding Pacific Steel Reinforcement Bars - Phase 1 (Report number TR9807)*. Auckland, New Zealand: Author.

Leon, R. T., & Deierlein, G. G. (1996). Considerations for the Use of Quasi-Static Testing. *Earthquake Spectra, 12*(1), 87-109.

Leslie, B. J. (2010). *The development and validation of a non-tearing floor precast concrete structural system for seismic regions.* Masters Dissertation, University of Canterbury, Christchurch, New Zealand.

Lindsay, R. (2004). *Experiments on the seismic performance of hollow-core floor system in precast concrete buildings.* Masters Dissertation, University of Canterbury, Christchurch, New Zealand.

MacPherson, C. (2005). *Seismic performance and forensic analysis of a precast concrete hollow-core floor super-assemblage.* Masters Dissertation, University of Canterbury, Christchurch, New Zealand.

Marriott, D. (2009). *The Development of High-Performance Post-Tesioned Rocking Systems for the Seismic Design of Structures.* Doctoral Dissertation, University of Canterbury, Christchurch, New Zealand.

Matthews, J. G. (2004). *Hollow-core floor slab performance following a severe earthquake.* Doctoral Dissertation, University of Canterbury, Christchurch, New Zealand.

McBride, A., Fenwick, R. C., & Davidson, B. J. (1996). *The influence of slabs on the lateral cyclic behaviour of ductile concrete frames (Report number 566)*. Auckland, New Zealand: University of Auckland.

Megget, M., & Fenwick, R. C. (1989). Seismic behaviour of a reinforced concrete portal frame sustaining gravity loads. *Bulletin of the New Zealand National Society for Earthquake Engineering, 22*(1), 39-49.

Nakaki, S. E., Stanton, J. F., & Sritharan, S. (1999). An overview of the PRESSS five-story precast test building. *PCI, 44*(2), 26-39.

National Instruments. (2011). LabVIEW. Texas, USA: Author.

Newcombe, M. P. (2011). *Seismic Design of Post-Tensioned Timber Frame and Wall Buildings.* Doctoral Dissertation, University of Canterbury, Christchurch, New Zealand.

Ohkubo, M., Matsuoka, T., Yoshioka, T., & Anderson, D. L. (1999). Shear transfer mechanism of reinforced concrete beams with a slot at the beam-end. *Proceedings of the Japan Concrete Institute, 21*(3), 301-306.

Park, R. (1989). Evaluation of Ductility of Structures and Structural Assemblages from Laboratory Testing. *Bulletin of the New Zealand National Society for Earthquake Engineering, 22*(3), 155-166.

Paulay, T., & Priestley, M. J. N. (1992). *Seismic design of reinforced concrete and masonry buildings*. New York, USA: John Wiley & Sons, Inc.

Peng, B. H. H. (2009). *Seismic performance assessment of reinforced concrete buildings with precast concrete floor systems.* Doctoral Dissertation, University of Canterbury, Christchurch, New Zealand.

Priestley, M. J. N., Sritharan, S., Conley, J. R., & Pampanin, S. (1999). Preliminary results and conclusions from the PRESSS five-storey precast concrete test building. *PCI Journal, 44*(6), 42-67.

Qi, X., & Pantazopoulou, S. J. (1991). Response of RC frame under lateral loads. *Journal of Structural Engineering, 117*(4), 1167-1188.

Qiu, F., LI, W., Pan, P., & Qian, J. (2002). Experimental tests on reinforced concrete column under biaxial quasi-static loading. *Engineering Structures, 24*(4), 419-428.

Scholz, W., & Roberts, B. (2000). *Welding Newly Developed, High Strength, Seismic Grade Reinforcing Bars*. Paper presented at the 12th World Conrference in Earthquake Engineering, Auckland, New Zealand. Retrieved from http://www.iitk.ac.in/nicee/wcee/article/1173.pdf

Standards New Zealand. (1987). *Specification for concrete surface finishes (NZS3114:1987*). Wellington, New Zealand: Author.

Standards New Zealand. (1995). *New Zealand Concrete Structures Standard (NZS3101:1995).* Wellington, New Zealand: Author.

Standards New Zealand. (2004). *Structural Design Actions Part 5: Earthquake Actions - New Zealand (NZS1170.5:2004).* Wellington, New Zealand: Author.

Standards New Zealand. (2006). *Concrete Strucutures Standard (NZS3101:2006)*. Wellington, New Zealand: Author.

Standards New Zealand. (2008). *Structural steel welding Part 3: Welding of reinforcing steel (AS/NZS1554.3:2008).* Wellington, New Zealand: Author.

Standards New Zealand. (2001). *Steel reinforcing materials (AS/NZS4671:2001).* Wellington, New Zealand: Author.

Wuu, P. J. Y. (1996). *Deformations in plastic hinge zone of RC beam in ductile frame structures subjected to inelastic cyclic loading.* Masters Dissertation, University of Auckland, Auckland, New Zealand.

Zerbe, H. E., & Durrani, A. J. (1990). Seismic Response of Connections in Two-Bay Reinforced Concrete Frame Subassemblies with a Floor Slab. *ACI Journal of Structural Engineering, 115*(11), 406-415.

4. Testing and Experimental Results of the Superassembly Experiment

4.1 Introduction

This chapter details the experimental testing undertaken on the three-dimensional superassembly SA1 described in Chapter 3. Section 4.3 describes the unexpected events encountered during the test, and the measures taken to mitigate the effects of the events. Section 4.4 presents the global hysteretic response of SA1. Visual observations and a chronicle of the significant events that occurred during the test are presented in Section 4.5. The performance of separate elements of SA1 is detailed in Sections 4.5-4.18.

4.2 Material Testing

Many different concrete batches were used to construct specimen SA1. A summary of the aggregated compressive strengths is presented in Table 4-1. Four certified concrete plants supplied concrete for the precast components and insitu pours: Ashburton Contracting Limited, Firth Concrete Ashburton, Firth Concrete Christchurch and Allied Concrete Christchurch. Cementitious grout was supplied by Construction Techniques Limited for the grouted connections between the precast components.

Table 4-1: Summary of concrete compressive strengths.

Level	Element	f'c (MPa)	28 Days (MPa)		Test Start (MPa)	
			Mean	Std Dev	Mean	Std Dev
One	Beams	40	51.8	7.1	61.1	3.4
	Columns	40	51.9	7.2	60.3	4.3
	Splices	40	51.2	0.3	56.6	3.1
	Grout	60	56.9	10.3	62.6	16.7
	Insitu topping	40	44.5	4.2	48.8	1.6
Two	Beams	40	50.1	3.2	57.7	3.4
	Columns	40	49.2	7.2	58.5	4.6
	Splices	40	50.4	0.2	53.7	0.7
	Grout	60	28.7	7.8	68.8	9.1
	Insitu topping	40	61.9	2.2	57.1	6.2
	Exceedance		28%		42%	

Standard 100mm diameter concrete cylinders were collected from all batches and cured in a fog room. Due to the smaller volume of material involved, 50mm diameter cylinders were taken for the grout batches. The cylinders were loaded compressively until failure in a 1500kN universal testing machine, as shown in Figure 4-1.

(a) Concrete cylinder failure.

(b) Grout cylinder failure.

Figure 4-1: Concrete and grout compressive testing.

It was difficult to collect quality grout samples because the grout would leak from the cylinder forms due its low viscosity, which resulted in cylinders of varying heights and surface flatness. Surface irregularities can encourage stress concentrations and premature failure; hence, the data collected from grout samples can be considered conservative.

One concrete batch did not meet the specified 28 day compressive strength. A plant breakdown at Ashburton Contracting Limited meant that a concrete batch had to be supplied by Firth Concrete, Ashburton. The specified strength at 28 days was 40.0MPa; however, only 30.8MPa was achieved. The batch had improved to 42.8MPa at commencement of testing.

The average concrete strength was 28% higher than the specified strength after 28 days. At the commencement of testing the average concrete strength was 42% higher than the specified strength. The concrete supplied for the Level Two insitu floor pour had a mean 28 day strength of 61.9MPa, despite being specified as 40.0MPa at 28 days. The higher than specified cement content resulted in higher shrinkage strains in the floor, which is described in Section 4.3. Measured concrete compressive strengths greater than specified are typical in practice; however, the magnitude of the difference between specified and measured concrete strengths may have been exacerbated in SA1 due to the small concrete batches used. Additional concrete testing results are presented in Appendix A.1.1.

Three specimens of each type of reinforcement used in SA1 were tested in tension to determine the average material properties. The results of the tensile tests are presented in

Table 4-2, where f_y and f_u refer to the yield and ultimate stress respectively. The yield, initiation of strain hardening and ultimate strain are represented by ε_y, ε_{sh} and ε_u. An R prefix refers to plain round reinforcement and D refers to deformed reinforcement. Reinforcement with an X or RB prefix was Grade 500 and all other reinforcement was Grade 300. D16 test specimens with additional D10 reinforcement welded to them were also tested in both single weld (SW) and double weld (DW) variations. All reinforcement specimens were ordered with the rest of the reinforcement to ensure that it was from the same steel batch. The yield stress of the R8 and D10 reinforcement samples was approximately 430MPa, yet the reinforcement was specified as Grade 300. This cause of this discrepancy was unknown.

Table 4-2: Summary of reinforcement properties.

Steel	f_y (MPa)		f_u (MPa)		ε_y (Milli-Strain)		ε_{sh} (Milli-Strain)		ε_u (Milli-Strain)	
	Mean	Std Dev	Mean	Std Dev	Mean	Std Dev	Mean	Std Dev	Mean	Std Dev
R8	430.87	13.72	477.63	12.55	1.60	0.07	32.01	5.16	160.18	51.86
D10	425.33	16.98	501.67	16.46	1.68	0.04	3.58	1.35	87.31	28.17
XR10	538.83	6.98	673.43	4.64	5.51	0.96	10.16	1.71	180.50	94.60
D12	369.83	10.81	465.70	7.09	1.23	0.11	8.21	2.70	202.06	34.39
D16	314.70	6.99	448.00	1.56	2.47	0.33	33.66	2.48	223.45	5.36
XD16	521.10	6.41	632.17	1.62	3.30	0.69	22.57	2.74	162.39	57.87
RB32	555.93	0.47	686.77	1.06	3.03	0.01	20.84	0.82	150.74	21.78
SW	305.50	NA	438.70	NA	2.05	NA	32.98	NA	223.12	NA
DW	297.10	NA	435.90	NA	1.93	NA	31.03	NA	215.68	NA

The reinforcement specimens were tested in tension using an Avery universal testing machine and strain was measured with an extensometer, as shown in Figure 4-2(a). All specimens achieved or exceeded the minimum performance criteria specified in AS/NZS4671:2001 (Standards New Zealand, 2001). Figure 4-2(b) shows typical examples of the ductile failure mode observed in the reinforcement. The stress-strain relationships of all tested reinforcement are presented in Appendix A.1.2.

(a) Tensile test apparatus. **(b) Ductile failure mechanisms in XD16 reinforcement.**

Figure 4-2: Tensile testing of reinforcement.

4.3 Initial Specimen Strain

To establish a baseline reading of diaphragm strain, DEMEC readings of both floors were taken prior to depropping. This enabled the strain introduced from gravity support to be decoupled from lateral displacement.

Dial gauges were used to measure beam mid-span sagging displacements due to depropping. The average beam sagging displacement was 0.34mm. The peak beam sagging displacement of 0.86mm was recorded on Grid B Level One.

Following specimen depropping, DEMEC readings were taken to determine the strain induced in the floor due to gravity load. The DEMEC data was used to generate contour plots of the floor strain, as shown in Figure 4-3. In the strain contour plots, positive strain corresponds to compression in the floor diaphragm and the strains are measured at the top surface of the floor diaphragm. The DEMEC data correlated well with the measurements made with the dial gauges.

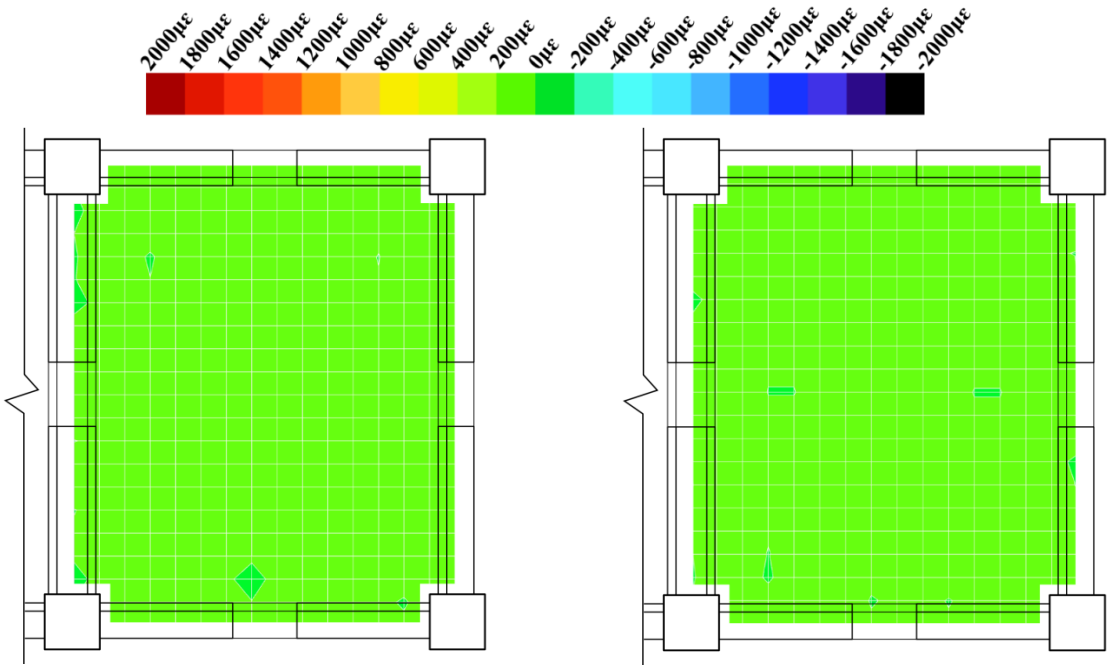

(a) Level One east-west strain. **(b) Level Two east-west strain.**

Figure 4-3: Diaphragm strain contours after de-propping.

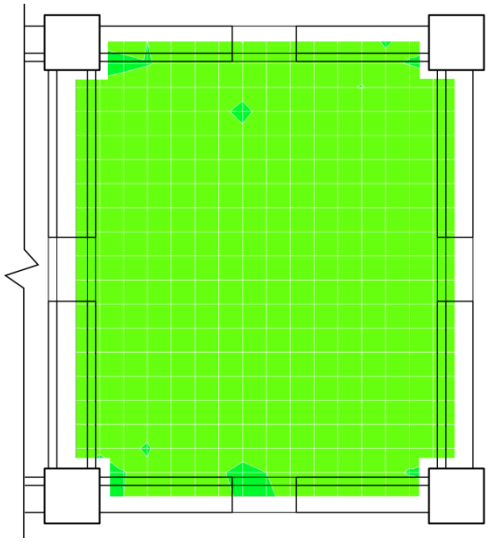

(c) Level One north-south strain.

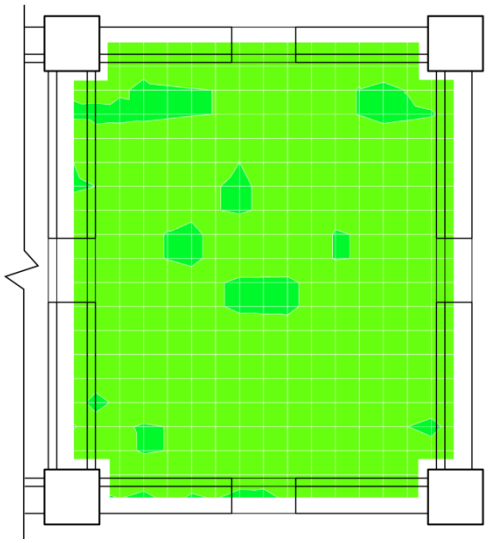

(d) Level Two north-south strain.

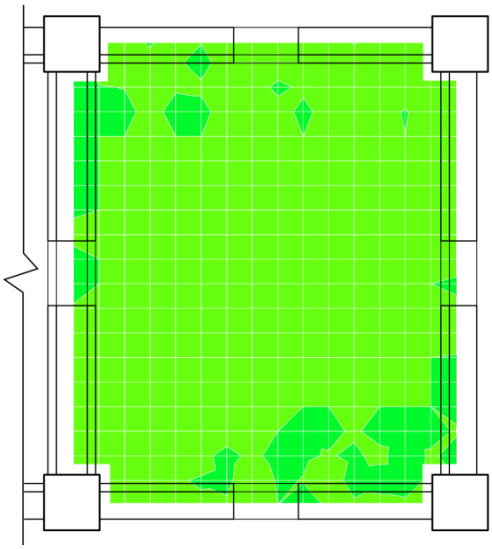

(e) Level One shear strain.

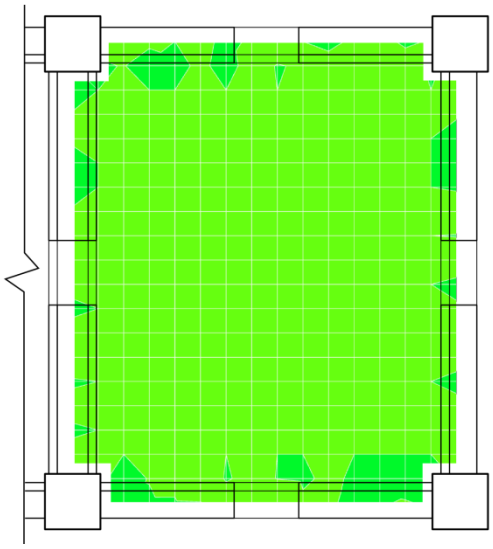

(f) Level Two shear strain.

Figure 4-3: Diaphragm strain contours after de-propping (Continued).

Prior to testing SA1, another DEMEC reading was undertaken to measure the shrinkage strain in the floor diaphragm. The strain contours generated from this data are presented in Figure 4-4. It can be seen that shear strain due to shrinkage was very small on both Level One and Level Two. However, longitudinal strains in the north-south and east-west directions were significant. On Level One, the shrinkage strains were concentrated over the timber infill. Shrinkage strains that occurred in the topping concrete above the hollow-core were restrained by composite action.

The shrinkage strains that occurred on Level Two were extensive. The shrinkage was likely due to the insitu floor concrete being supplied 55% over the specified strength. It can be seen that shrinkage strain was relatively evenly distributed over the floor; however, in Figure 4-4(d) the strain was smaller over the webs of the double-tee units.

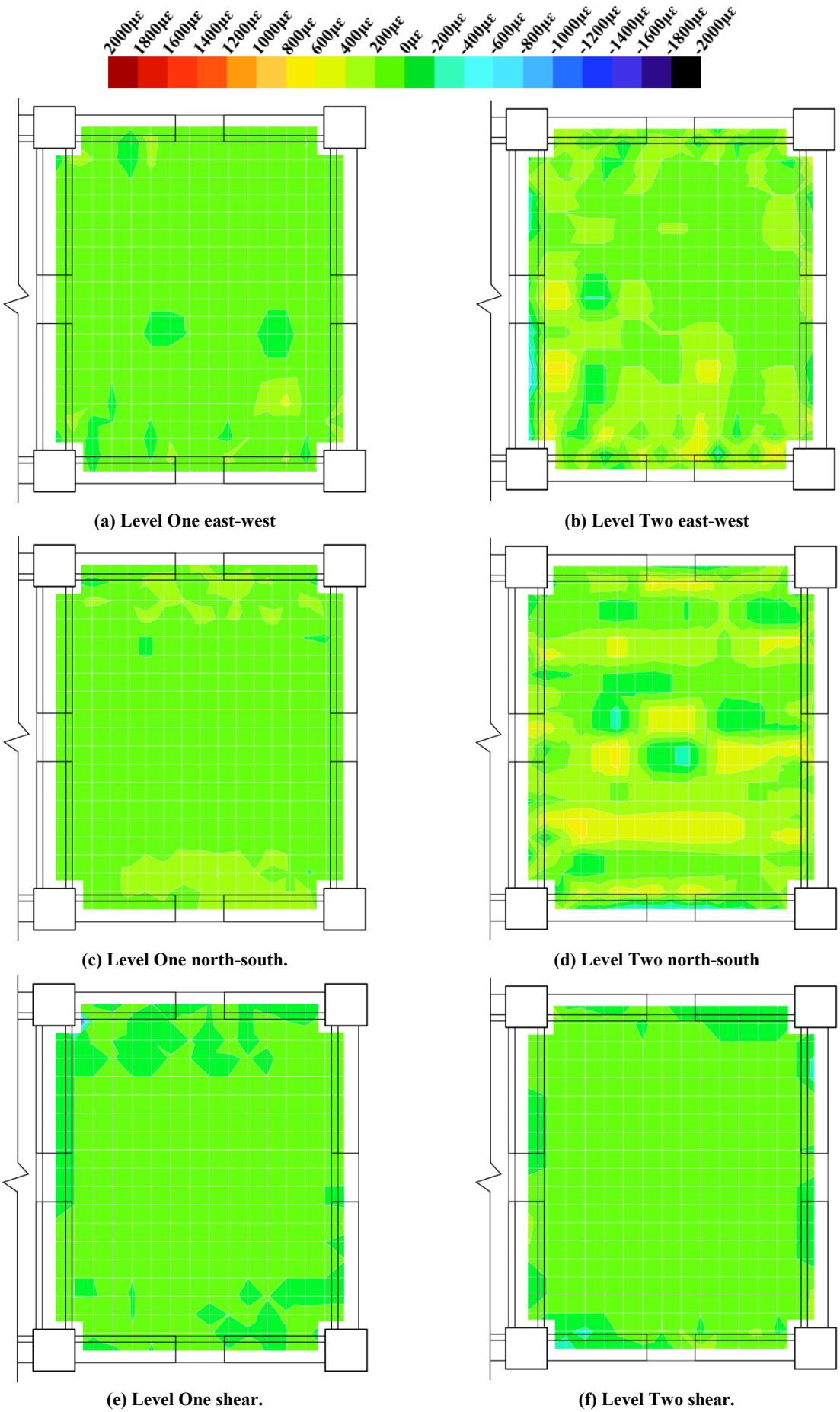

(a) Level One east-west

(b) Level Two east-west

(c) Level One north-south.

(d) Level Two north-south

(e) Level One shear.

(f) Level Two shear.

Figure 4-4: Diaphragm strain contours prior to testing.

As shown in Figure 4-5, floor shrinkage strains in both floors resulted in many cracks forming. However, cracking was particularly extensive on Level Two. The complete crack map of SA1 conducted prior to testing is presented in Appendix C.1. In Level One, the cracking was concentrated over the timber infill and the connections between the hollow-core units and supporting beams. The observed crack patterns correlated well with the measured shrinkage strains. A more uniform distribution of cracks was observed on Level Two when compared to Level One. However, cracking was particularly prevalent between the double-tee units and above the floor seating. As shown in Figure 4-5(c), the cracking above the double-tee seating reached a peak of 0.35mm.

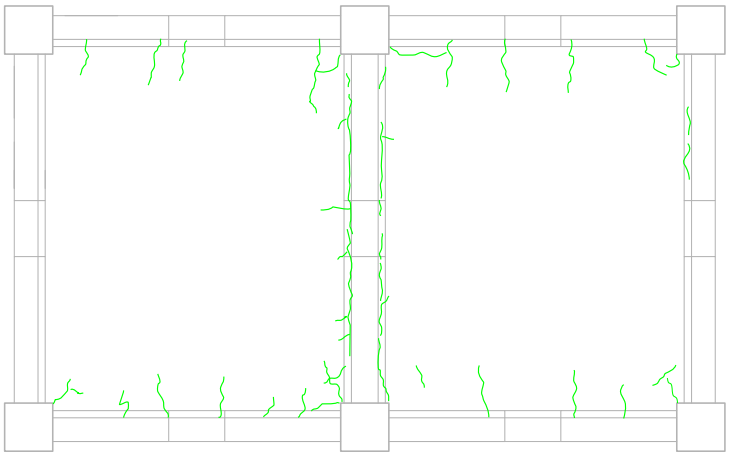

(a) Level One floor diaphragm top.

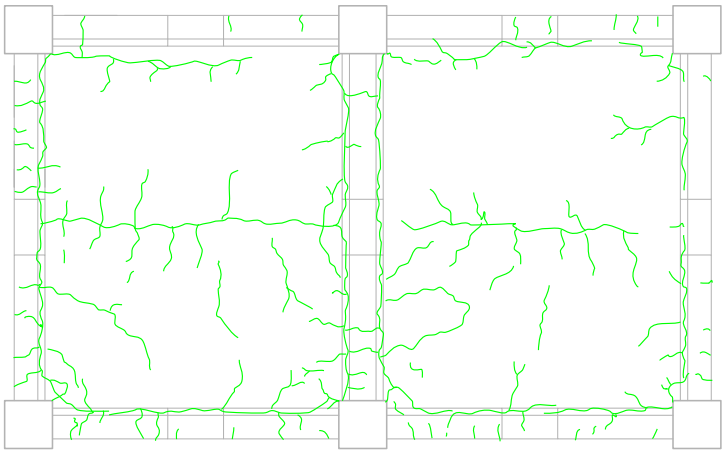

(b) Level Two floor diaphragm top.

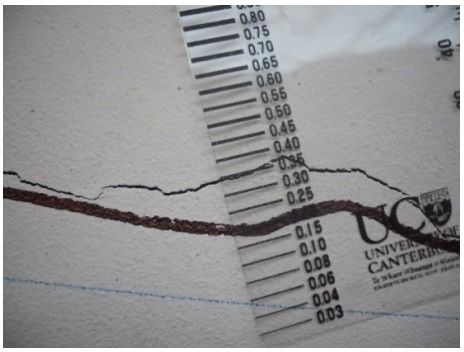

(c) Peak crack width of 0.35mm above central double-tee to beam connection (Black line is marker pen highlighting approximate crack position).

Figure 4-5: Diaphragm cracking prior to testing.

The cracking that had formed in the floor diaphramgs of SA1 was extensive; however, it was with the limits recommended in Table C2-1 of NZS3101:2006 for serviceability limit state loading for a B2 exposure classification (Standards New Zealand, 2006). It is possible that the cracking may have influenced the global response of the superassembly; however, from the data collected there was no inducation of this occurring.

It can be concluded that the induced strain in the floor diaphragm due to depropping was small in relation to shrinkage. Establishing a baseline DEMEC reading after depropping would have had negligible effect on subsequent measurements.

Attention should be paid to the quality of the concrete used for the insitu floor topping. The engineer should consider the use of low shrinkage concrete to prevent cracking. Ductile deformed reinforcement conforming to AS/NZS4671:2001 was used in SA1 and excellent diaphragm performance was observed, as described in Section 4.16 (Standards New Zealand, 2001). It is recommended that ductile deformed reinforcement is used over traditional cold-drawn wire mesh reinforcement.

4.4 Problems Encountered During SA1 Experimental Testing

Excessive actuator forces were an ongoing issue throughout the testing of SA1. The high actuator forces were partly caused by the actuator control program, as discussed in Section 3.7.2.4. However, as discussed in Section 4.5, the higher than expected strength of the specimen also contributed to the high actuator forces. The identification, mitigation and effect of the excessive actuator forces, and other interference issues related to the reaction frame, are discussed in this section.

4.4.1 Reaction Frame Displacement

As discussed in Section 3.6.1, the reaction frame was designed to have the maximum strength and stiffness possible given the materials and geometry available. As shown in Figure 4-6(a) and (b), significant deformation was observed in the reaction frames in both loading directions. The plots compare the recorded specimen displacement to the actuator stroke, which is the sum of the specimen and reaction frame displacements. The displacements have been normalised by the load height and the maximum specimen displacement. As expected, the specimen displacement increased linearly. The actuator extension increased at a greater rate initially, up to approximately 0.75%, before it continued to increase at a rate slightly greater than the specimen displacement. The greater rate of reaction frame displacement initially was due to the tolerances in the reaction frame connections being taken up at low force levels, and the specimen stiffness being higher in the elastic range.

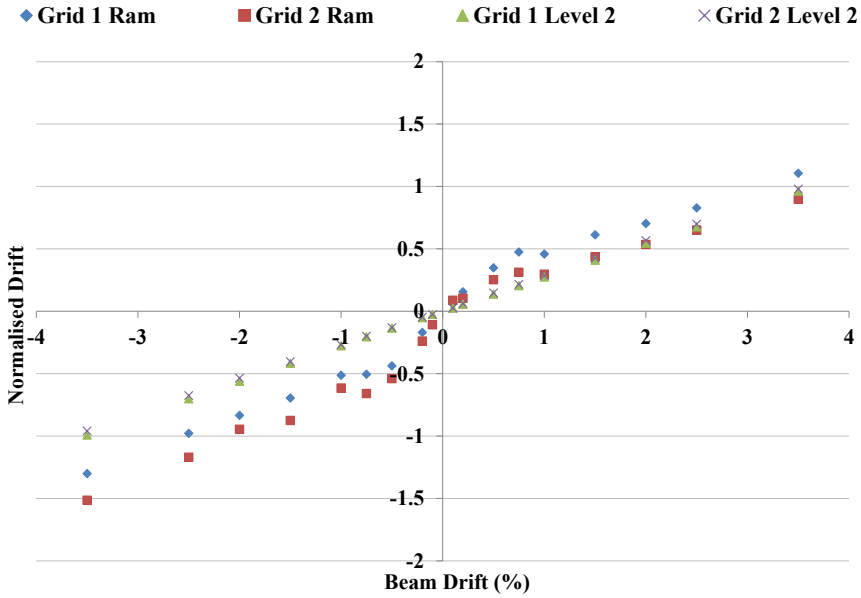

(a) East-west.

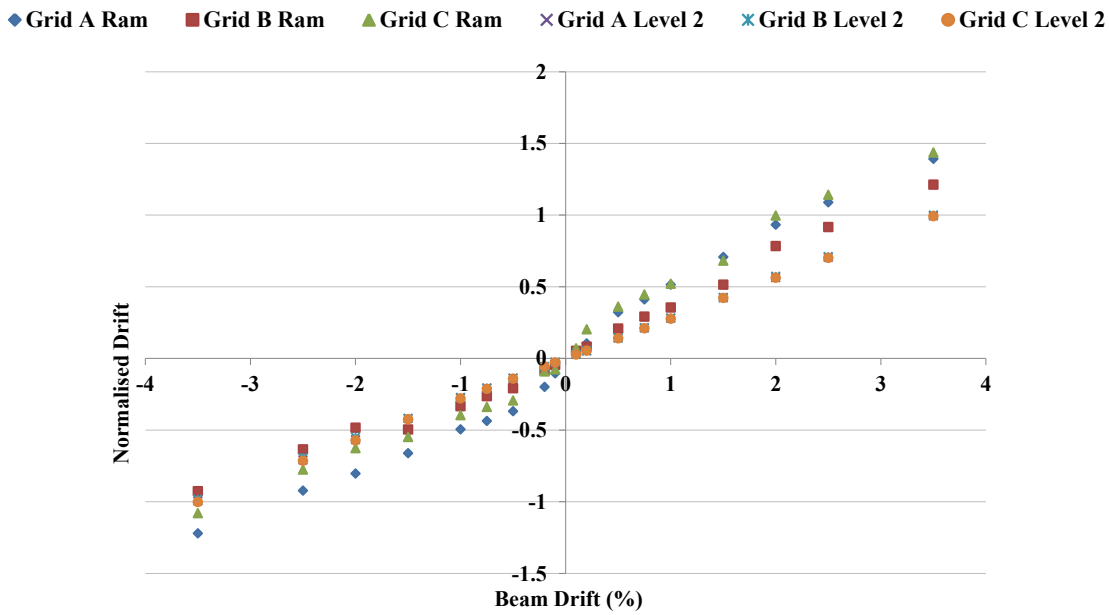

(b) North-south.

Figure 4-6: Normalised specimen displacement and actuator displacement.

The displacement data for the actuator control program was measured from a fixed datum. Hence, as long as the reaction frame deformations were elastic, and the actuators had sufficient stroke, the reaction frame displacement was not an issue. However, when the 450kN actuator force limit was reached in the east-west direction and testing was suspended, it was noted that a bolt pull-out failure mechanism had initiated in the connection between the header beam and the tower. The deformation in the tower web due to the bolt pull-out is shown in Figure 4-7(b). A large mild steel backing plate was installed on the inside of the tower to increase the bolt pull-out capacity.

(a) Header beam displacement in east-west direction. Mezzanine handrail is fixed and white marks line up at zero force.

(b) Initiation of bolt pull-out failure in east-west direction.

Figure 4-7: Examples of reaction frame strain.

As described in Section 3.6.2, the displacement of the strong floor was expected to limit the maximum force that could be applied to the specimen. Hence, the strong floor displacement was monitored throughout testing. The strain induced in the strong floor midway between the north-south brace and tower footings in presented in Figure 4-8. The strain at the top of the strong floor gave an approximation of strong floor curvature. Data from the instrument measuring strong floor strain in the east-west direction was unreliable due to the low resolution potentiometer box used in that location. The shape of the plot presented in Figure 4-8 is similar to that of the overall reaction frame displacement. Because the strong floor remained elastic throughout testing, strain was proportional to actuator force. However, the negative strain was greater than positive due to the support provided by the underlying site concrete during negative strong floor flexure.

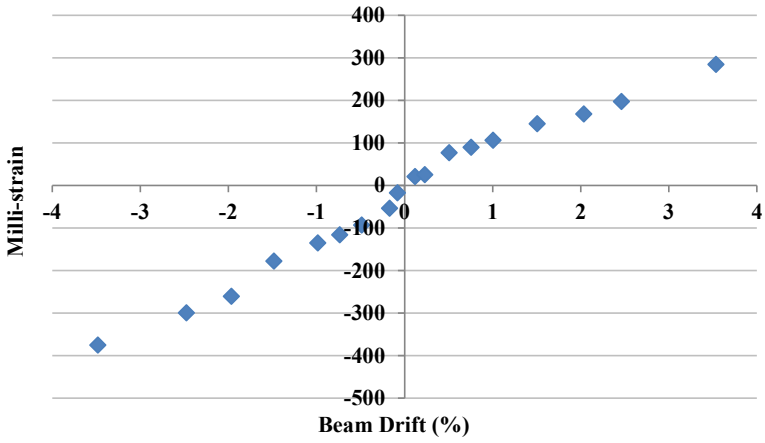

Figure 4-8: North-south strong floor strain at top surface.

Dial gauges were installed between the strong floor and the adjacent laboratory floor, as shown in Figure 4-9. The dial gauges were constantly checked during testing to ensure that

the strong floor edge displacements were within the limits presented in Section 3.6.2. Maximum displacements of 10.6mm and 5.1mm were recorded in the east-west and north-south respectively.

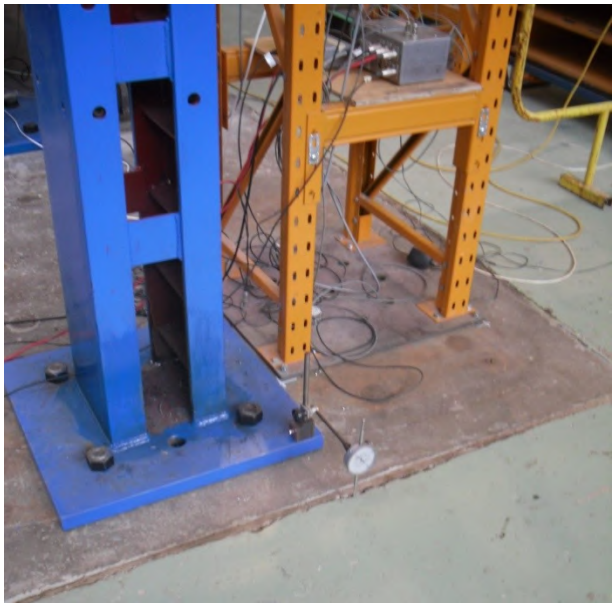

Figure 4-9: Measurement of strong floor edge displacement with dial gauge.

4.4.2 Excessive Actuator Forces

As discussed in Section 3.7.2.4, excessive actuator forces and imbalances between actuator forces were an ongoing issue during testing. Figure 4-10(a) and (b) present the actuator forces recorded during the 0.1% beam drift cycle. The differences between the actuator forces in each loading direction were significant. Figure 4-10 presents an example of the differences in actuator force only; the actual force imbalances were much larger. The maximum force imbalances occurred whilst applying the displacement increments; however, data logging was triggered only once all of the displacements had been applied and the actuator force balancing had been undertaken by the loading controller software. Hence, the largest force spikes were not able to be captured by data logging.

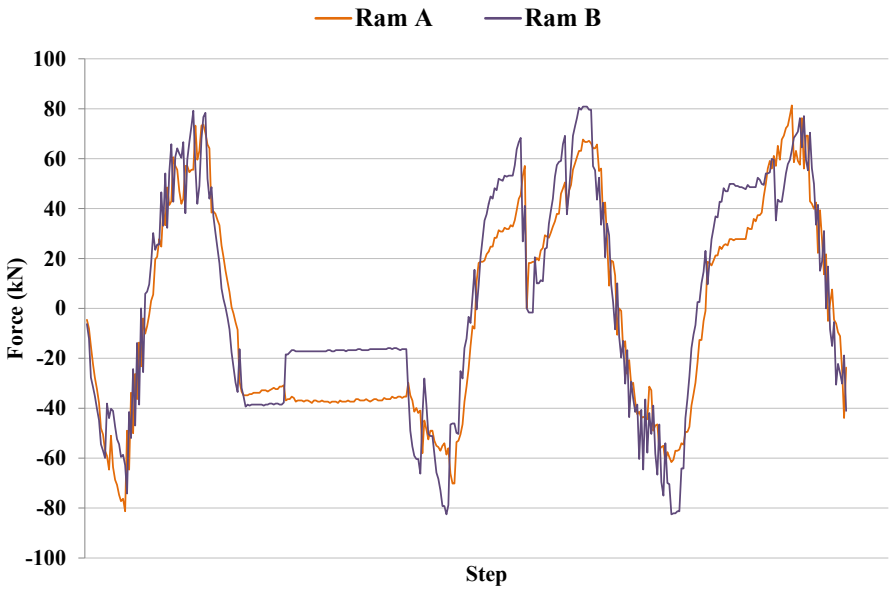

(a) East-west.

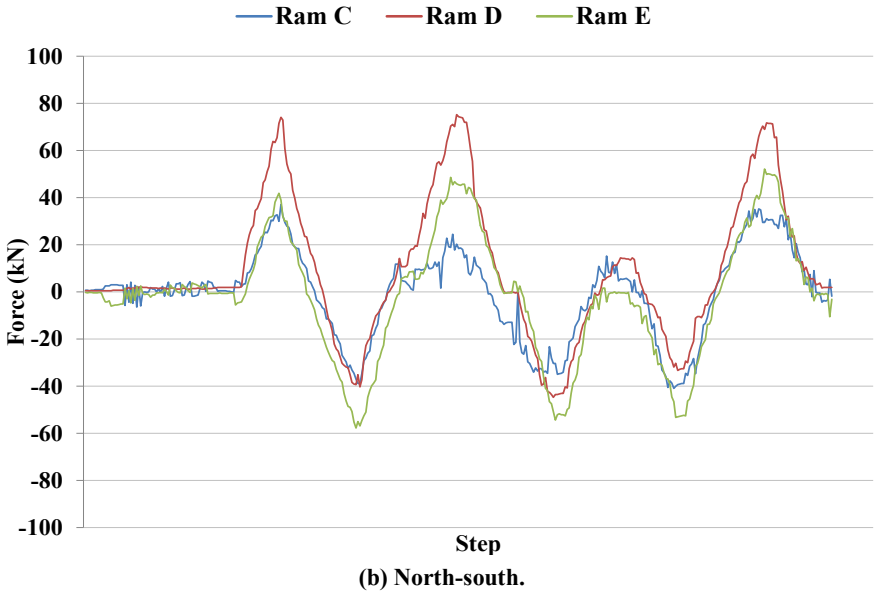

(b) North-south.

Figure 4-10: Force imbalance during 0.1% beam drift cycle.

Actuator force limits were set to protect the laboratory strong floor from damage. When the force limits were reached in the east-west direction during the 0.75% beam drift cycle, testing had to be suspended. There were two main causes of the actuator force limit being exceeded:

1. The interaction between actuators acting in the same direction, and the interaction between actuators acting in perpendicular directions. This component was addressed through the development of the actuator control program and is described in Section 3.7.2.4.
2. The higher than expected specimen strength and stiffness. The cause of the higher specimen strength is described in Section 4.5. The mitigation of this issue so that testing could continue, whilst being able to achieve all of the original objectives, is described below.

Despite the actuator force imbalance being minimised through development of the actuator controller program, a small force imbalance remained after the application of each

displacement increment. A larger actuator force imbalance always occurred during the application of a displacement increment before the actuator controller program could balance the actuator forces. The imbalance of actuator forces during the application of a displacement increment, and the higher than expected specimen strength, meant that the maximum actuator force limits were reached. Hence, there were two options to continue testing; strengthen the reaction frame or weaken the specimen.

The factor limiting the maximum actuator force that could be applied to the specimen was the strong floor flexural capacity. Therefore, increasing the maximum allowable actuator force would require strengthening the flexural capacity of the strong floor. Several methods were investigated to increase the strong floor capacity, such as bolting steel channels to the strong floor, connecting the strong floor to the laboratory floor and adding a back-stay from the reaction frame to the laboratory floor. All investigated options were discounted as being technically, practically or economically unachievable. Hence, the only option available to resume testing and realise the project goals was to selectively weaken the specimen. Because the moment capacity of a slotted beam is controlled by the bottom longitudinal reinforcement, reducing the connection flexural capacity is easier than for a traditional connection. To reduce the slotted beam moment capacity, bottom longitudinal reinforcement was severed until the desired reduction in moment capacity was achieved.

The selective weakening was performed in two stages to prevent an excessive and unnecessary reduction in the lateral load capacity being made. The first stage involved the removal of the centre D16 from the bottom layer of the bottom longitudinal reinforcement in all connections. The reinforcement that was removed is shown schematically in Figure 4-11(a) and (b) for the east-west and north-south directions respectively. Based on simplified design equations by Au (2010), removing the centre D16 reinforcement resulted in a 24% reduction in connection moment capacity.

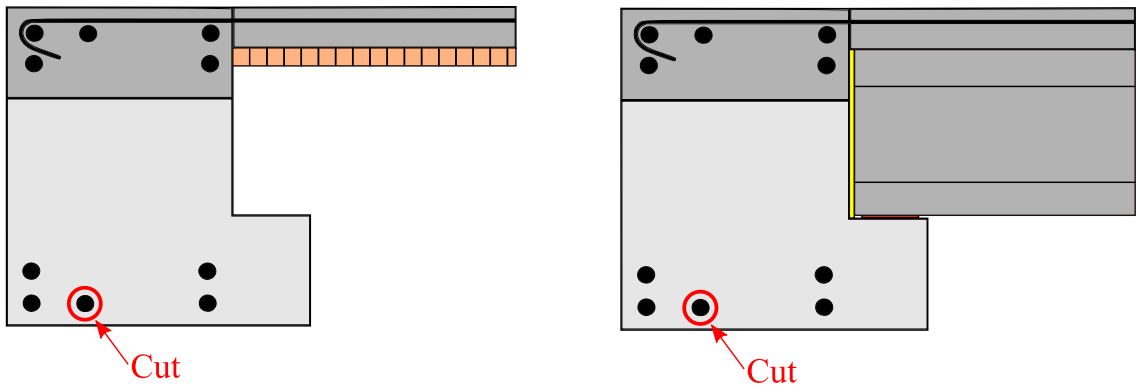

(a) East-west beams. **(b) North-south beams.**

Figure 4-11: Stage one selective weakening.

The stage one selective weakening allowed testing to continue until the 1.5% beam drift cycle. During the 1.5% beam drift loading cycle the force limit in the east-west direction was reached again; however, the north-south direction was within acceptable limits. Hence, further selective weakening of the connections in the east-west direction was required to enable testing to continue.

Because the Grid A connections did not influence the diaphragm strain recorded by the DEMEC grids and there were identical connections on Grid C, the decision was made to remove all bottom longitudinal reinforcement from these connections. This gave the connection zero theoretical moment. Furthermore, the remainder of the connections in the east-west connection had the two D12 in the upper layer of the bottom longitudinal reinforcement removed. The schematic of the stage two selective weakening is presented in Figure 4-12(a) – (c). The stage two selective weakening reduced the total lateral resistance of the specimen to within acceptable limits and allowed testing to continue until completion.

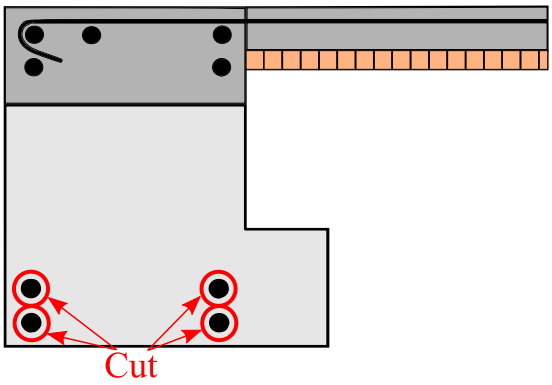

(a) Grid A east-west beams.

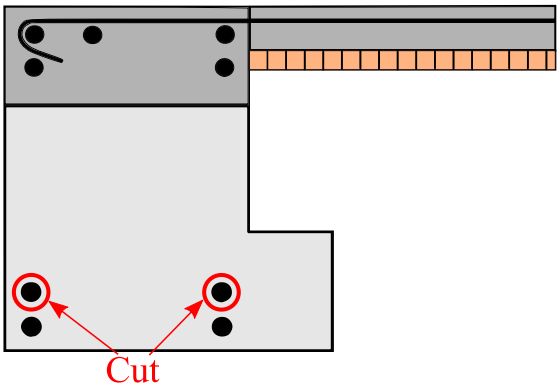

(b) Grid B and C east-west beams.

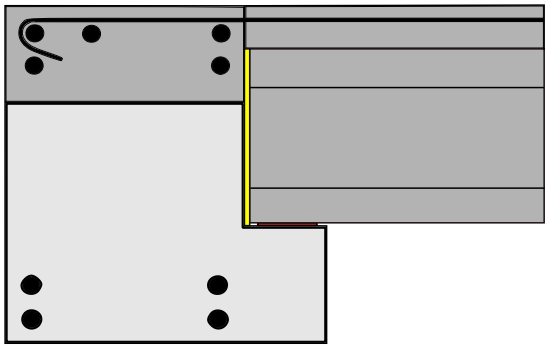

(c) North-south beams.

Figure 4-12: Stage two selective weakening.

The selective weakening was performed using a reciprocating saw, as shown in Figure 4-13(a). The flexibility of the bi-metallic blade meant that it was possible to curve the blade up the column face to perform a cut flush with the concrete. The reinforcement was cut flush with the end of the debonding tube and the column face, which enabled the section of reinforcement spanning the slot to be removed. A length of reinforcement equal to the slot width was removed to ensure that the ends of the severed reinforcement would not contact

during negative flexure and increase the connection moment capacity. Figure 4-13(b) presents a close up of a connection slot after a length of reinforcement has been removed.

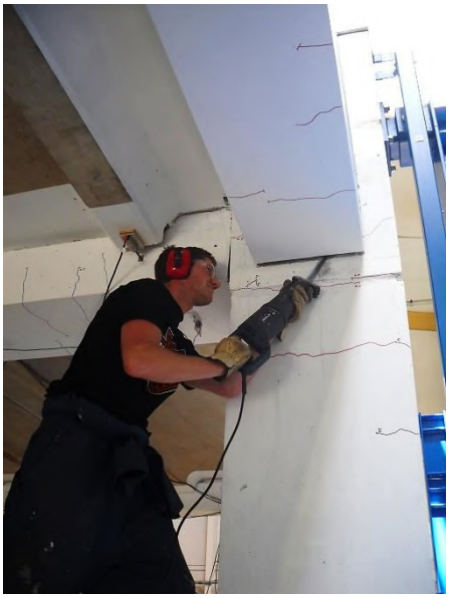

(a) Reinforcement being severed with a reciprocating saw.

(b) Detail of removed section of reinforcement.

Figure 4-13: Selective weakening performed on SA1.

4.4.3 Effect of Experimental Problems on Results

Weakening the specimen during testing was not desirable; however, there was no other viable option to enable testing to continue. It was important that the selective weakening performed on SA1 did not affect the original project objectives. A summary of the effect that the selective weakening had on each performance objective is presented in Table 4-3. Because most of the original project performance objectives were based on displacement rather than force, the effect of selective weakening was minimal.

Table 4-3: Effect of selective weakening on performance objectives.

Performance Objective	Data	Effect
Floor Diaphragm	DEMEC Crack Monitoring Photographic Log Linear Potentiometers	Slightly reduced displacement incompatibility due to reduced beam curvature
Floor Seating	Crack Monitoring DEMEC Photographic Log Spring Potentiometers Force-Displacement	Negligible
Flange Activation	Force-Displacement DEMEC Linear Potentiometers	Negligible
Elongation	Linear Potentiometers Crack Monitoring	Negligible

Table 4-3: Effect of selective weakening on performance objectives (Continued).

Reinforcement Unbonding	Crack Monitoring Reinforcement Straightness Monitoring Photographic Log	Negligible
Bond	Crack Monitoring Force-Displacement Strain Gauges	Negligible
Double Layered Reinforcement	Linear Potentiometers Strain Gauges Force-Displacement	Negligible
Beam Torsion	Spring Potentiometers Inclinometers Crack Monitoring Photographic Log Strain Gauges	Negligible Reduced seismic shear
Joint Shear	Crack Monitoring Linear Potentiometers Strain Gauges	Reduced
Columns	Crack Monitoring Linear Potentiometers	Reduced
Global Response	Force-Displacement	Reduced
Boundary Conditions	Observations Rotary Potentiometers Linear Potentiometers Inclinometers	Negligible
Reaction Frame Deformation	Observations Rotary Potentiometers	Reduced
Constructability	Timelapse Photographic Log Observations	Negligible
Marketing	Timelapse High Standard of Presentation Laboratory Tours Photographic Log Print Media Television Media Conferences Papers	Negligible

Selective weakening reduced the beam fixed end moments. This reduced the elastic curvature in the beams and resulted in less displacement incompatibility between the beams and precast floor units. However, as shown in Section 4.16, the displacement incompatibility that occurred between the precast floors and the parallel beams in SA1 was significant.

The connection selective weakening reduced the joint shear demand, which resulted in the joint zone being over-reinforced. Regardless, the joint zone was unlikely to yield during

testing due to the design being governed by the minimum reinforcement requirements prescribed in NZS3101:2006 (Standards New Zealand, 2006). Furthermore, 50% more horizontal joint reinforcement was included in accordance with recommendations by Au (2010).

It is possible that there was a slight reduction in the recorded beam elongation due to a reduction in the top longitudinal reinforcement strain. During negative connection flexure, the reduced axial capacity of the bottom longitudinal reinforcement resulted in the induced axial tension in the top longitudinal reinforcement being reduced. However, because the top longitudinal reinforcement was twice as strong as the bottom reinforcement, the strain in the top longitudinal reinforcement was relatively insensitive to changes in the axial force capacity of the bottom longitudinal reinforcement.

The critical diagonal hangers in SA1 were in the north-south direction, due to the shear and torsion beam demand from the precast floors. The north-south beam connections were weakened by a smaller amount than the east-west connections. Furthermore, the connection seismic shear demand was comparable to the gravity shear demand on Grids A, B and C. Hence, a modest reduction in seismic shear had an even smaller influence on total positive shear force. Beam torsion demand accounted for approximately 45% of the peak force in the diagonal hangers. The beam torsion demand on the diagonal hangers was not affected by the selective weakening undertaken.

The strength and stiffness of SA1 was reduced by the selective weakening undertaken. However, because the specimen was assessed in accordance with ACI374.1-05, the absolute strength and stiffness were not important (ACI Committee 374, 2005). Instead, the relative strength and stiffness were used to assess the performance of SA1, which were not significantly affected by the selective weakening undertaken.

Due to actuator interaction and larger than expected specimen strength, the maximum actuator force limits were reached. Selective weakening of the specimen was undertaken to enable testing to continue. The selective weakening was able to be undertaken in a manner such that all of the original test performance objectives were able to be achieved.

4.5 Overall Response

The overall performance of specimen SA1 was very promising. Stable specimen response and high energy dissipation was observed to 3.5% beam drift. The specimen was ductile and deformed in the intended weak-beam strong-column mode.

At serviceability limit state level displacements the specimen would not require any repairs. At both design and survival limit state displacements the specimen sustained significantly less damage than would be expected in an equivalent traditional specimen. Recommendations by Priestley et al. (2007) are used to define limit states.

The global force-displacement plots are presented in Figure 4-14 and Figure 4-15 for the east-west and north-south directions respectively. The force-displacement plots have been normalised to account for the selective weakening undertaken. This allowed the true shape of the specimen response to be presented. The specimen yielded at approximately 0.75% beam drift. The nominal specimen capacities marked on the plots refer to the revised nominal forces derived in Table 4-4 are are based on specified 'design' material strengths. There was an approximately 8% difference in calculated flexural capacity if measured material strengths were used in place of specified strengths.

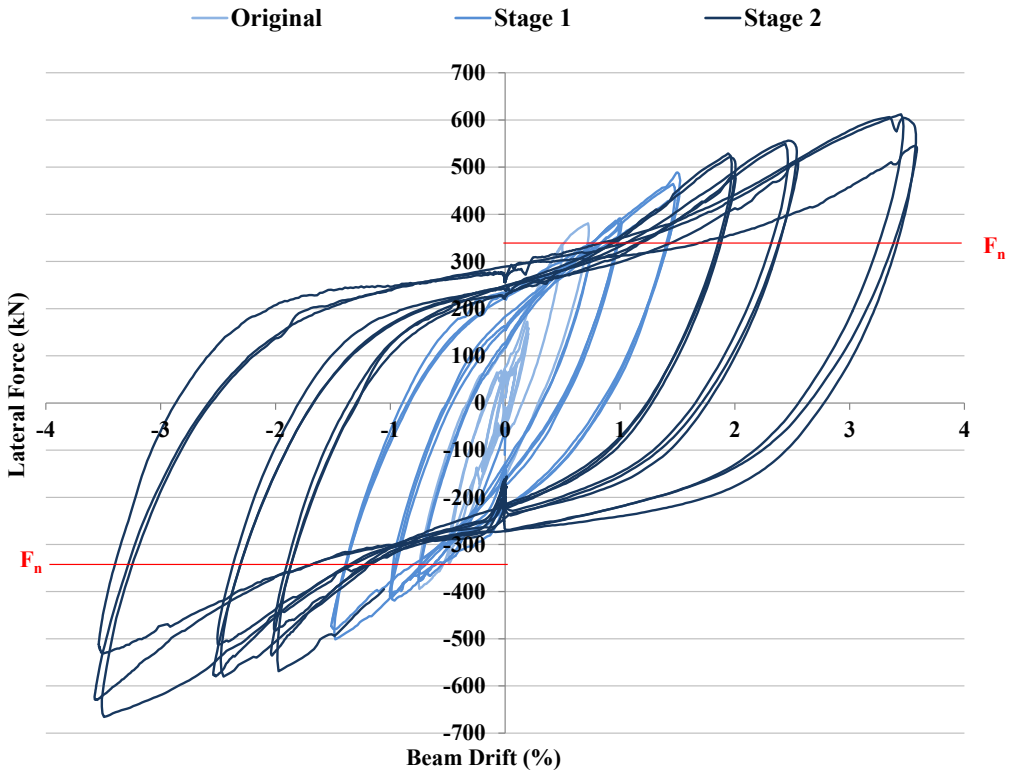

Figure 4-14: Total force-displacement response for east-west direction.

The recorded response along each axis was similar for both uniaxial and biaxial loading. Hence, the axes could be effectively decoupled for lateral design; however, biaxial loading should still be considered on structural elements. The overall force-displacement response was similar in both the east-west and north-south directions. However, the different displacement histories applied in each direction meant that the shape of the responses were slightly different. Furthermore, the east-west direction displayed a slightly more pinched response than the north-south direction. No evidence of slip in the bottom longitudinal reinforcement was observed in either direction. The pinched response in the east-west

direction was emphasised by the high post-yield strength development in that direction. The specimen strength degradation was low in both directions. Further analysis of stiffness and strength degradation is undertaken in Section 4.8.

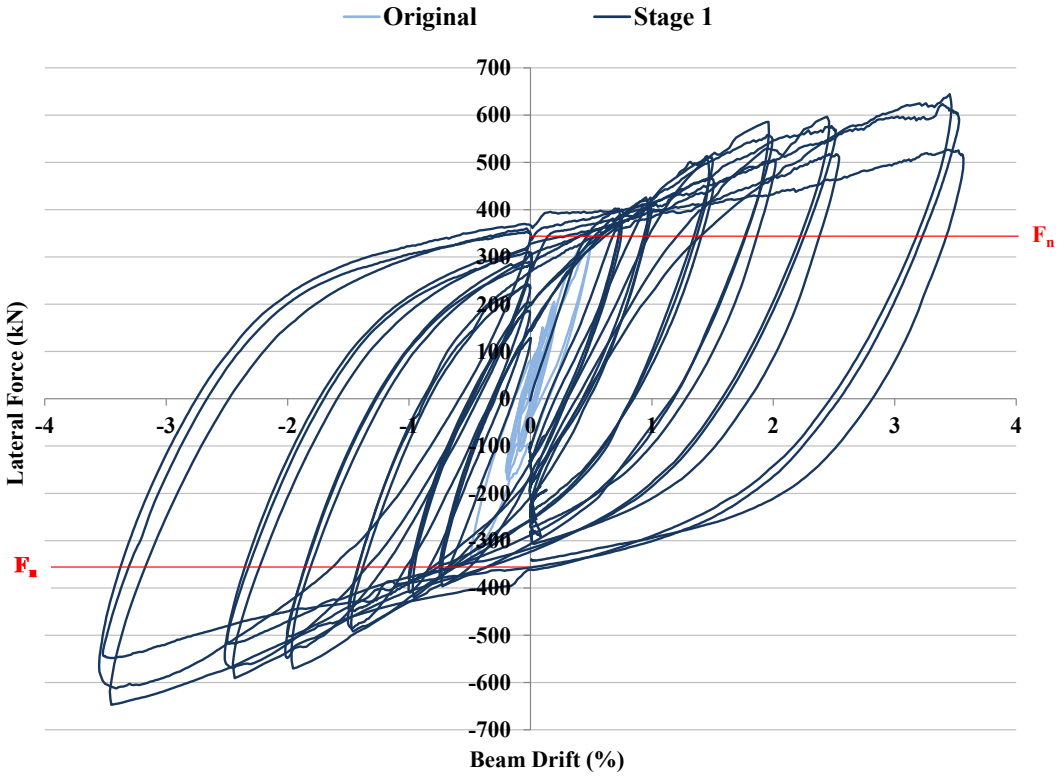

Figure 4-15: Total force-displacement response for north-south direction.

As discussed in Section 4.4.2, the lateral strength of specimen SA1 was significantly higher than expected. The specimen was designed according to recommendations by Au (2010) and NZS3101:2006 (Standards New Zealand, 2006). Au recommended the use of the simplified design equations shown in Equation 4-1 and Equation 4-2 to determine the nominal connection flexural capacity. Au also recommended that effective slab width calculations be omitted from nominal moment capacity calculations. An overstrength factor of 1.6 was recommended by Au to account for both post-yield connection strength gain and the influence of the adjacent floor diaphragm.

$$M_n^+ = A_s f_y \left(d - {}^{a}/_{2}\right) \qquad \textbf{Equation 4-1}$$

$$M_n^- = A_s f_y (d - d') \qquad \textbf{Equation 4-2}$$

As shown in Table 4-4, overstrength factors of 3.5 and 2.5 were calculated for the east-west and north-south directions respectively. These overstrength factors were large and misleading. Au (2010) reasoned that because the neutral axis in a slotted beam remained around the same level as the floor diaphragm for positive and negative flexure, the strain imposed in the floor diaphragm was reduced. Neutral axis data presented in Section 4.11 shows that during negative connection flexure, the neutral axis was located at the bottom of the top hinge. This enabled a significant lever arm to form between the neutral axis and the floor reinforcement,

and also between the neutral axis and the top longitudinal reinforcement. Due to the top longitudinal reinforcement being twice as strong as the bottom longitudinal reinforcement, the top longitudinal reinforcement could contribute significantly to the connection moment. Flange activation and top longitudinal reinforcement should be included in the calculation of slotted beam nominal moment capacities. NZS3101:2006 §9.3.1.4 should be used to determine the effective slab width (Standards New Zealand, 2004). The influence of flange activation on the nominal moment capacity of a slotted beam is significantly less than a traditional concrete beam due to the reduced lever arm between the neutral axis and the floor.

Continuity moments generated by the connections of the one-way precast flooring to the supporting beams contributed to the lateral strength of SA1. To adhere to capacity design principles, continuity moment contributions to lateral resistance should be accounted for during design. NZS3101:2006 §18.6.7 does not provide guidance to calculate continuity moments, or their contribution to lateral resistance (Standards New Zealand, 2004). As shown in Section 2.4.2.3, specimen SB3 tested by Au (2010) included a floor diaphragm in an attempt to assess the effect that the floor had on the connection response. The floors spanned orthogonal to the supporting beams, so the contribution of continuity moments to lateral resistance could not be assessed. The subsequent recommendations made by Au (2010) for total system overstrength, including the influence of the floors, were unconservative. It is recommended that continuity moments from precast floor connections be included in the calculation of the nominal frame strength. Continuity moment contributions should be apportioned by considering the tributary width that contributes to a connection.

If flange activation (FA), top reinforcement (TR) and floor seating continuity moments (CM) were included in the calculation of the nominal system capacity, the total system overstrength calculated for SA1 changed significantly. Table 4-4 compares system overstrength factors if FA, TR and CM are included in the nominal system capacity calculations. When all the components of lateral resistance were included, the calculated overstrength moments reduced to 1.87 and 1.86 in the east-west and north-south direction respectively. Because the one-way precast floor spanned east-west, the continuity moments did not contribute to lateral resistance in the north-south direction. The specimen overstrength factors of 1.86 and 1.87 were higher than those determined by Au (2010). However, an overstrength factor of 1.82 was observed in a recent experimental investigation on reinforced concrete slotted beams by Byrne (2012).

Table 4-4: Comparison of lateral capacity for various design methodologies.

Scenario	East-West		North-South	
	Force (kN)	Overstrength	Force (kN)	Overstrength
Experimental – 3.5%	638	NA	640	NA
Design Nominal Force	182.7	3.5	254.3	2.5
Design Nominal + TR	249.5	2.25	324.2	1.97
Design Nominal + TR + FA	312.2	2.04	343.2	1.86
Design Nominal + TR + FA + CM	340.4	1.87	343.2	1.86

In slotted beams, the plasticity in the connection is concentrated in the bottom unbonded longitudinal reinforcement. Because the bottom longitudinal reinforcement is subjected to both tension and compression yielding, it experiences higher cumulative strain than a comparable traditional connection, which results in increased cyclic strain hardening. It has been shown that in the context of slotted beams, cyclic strain hardening, which occurs due to cyclic applied loading, can result in up to 15% greater moment capacity being generated compared to monotonic loading (Au, 2010). The completely reversed loading protocols applied in laboratory tests maximise the effect of cyclic strain hardening.

It has been shown that overstrength moments are greater for negative flexure than positive flexure (Au, 2010; Byrne, 2012). Because SA1 was statically indeterminate, the difference between positive and negative flexural overstrength was not able to be specifically examined. The greater negative moment capacity was likely caused by the effect that Poisson's ratio had on the restrained bottom longitudinal reinforcement during negative connection flexure. Axial tests on reinforcement are generally performed only in tension, and the compressive behaviour is assumed to be the same as the tensile due to the isotropic nature of steel. Axial tests on reinforcement are generally reported in terms of stress and strain; usually engineering stress and strain are used. These are calculated in terms of an initial cross-sectional area and gauge length respectively. Due to the effect of Poisson's ratio, engineering stress underrepresents axial stress in tension. Poisson's ratio describes the transverse strain of a loaded material as a ratio to the axial strain. The change in material cross section that occurs during an axial test changes also the calculated stress. True stress is calculated using the instantaneous cross-sectional area, and natural strain is the integral of the change in gauge length over the current gauge length. Axial tests reported in terms of true stress and natural strain present a more accurate representation of the steel properties. A comparison of the two methods is shown in Figure 4-16. In practical terms, the difference between the two methods

is rarely significant due to buckling generally governing compressive response. However, in slotted beams the bottom longitudinal reinforcement is effectively restrained against buckling by the steel unbonding tube and stirrups at close centres. During negative flexure, the bottom reinforcement can buckle at a high enough mode that the full compressive strength of the reinforcement is able to be developed. Hence, due to Poisson's ratio the compressive force able to be developed is greater than in tension. It has been shown that this difference can be up to 25% between tension and compression (Restrepo-Posado, 1992). It was postulated that the effect of Poisson's ratio on the restrained bottom longitudinal reinforcement during negative connection flexure increases the slotted beam moment capacity. This effect is more prevalent in slotted beam connections compared to traditional connections because the bottom longitudinal reinforcement is strained further into net compression, which allows the effects to manifest and become more significant.

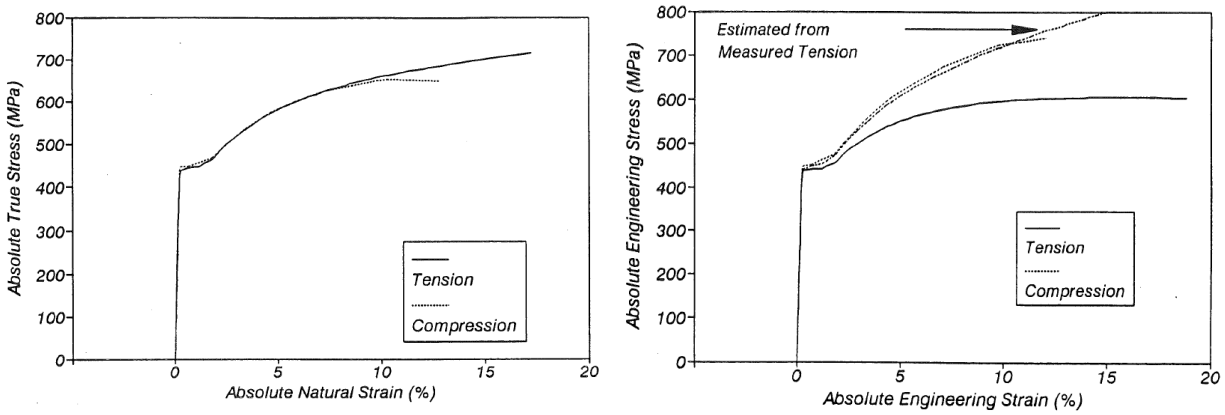

(a) True stress and natural strain. **(b) Engineering stress and strain.**

Figure 4-16: Comparison of steel stress-strain relationships (Restrepo-Posado, 1992).

In tests SA2 and SA3, described in Chapter 6, it was found that the positive and negative flexural overstrength was relatively similar. This was likely due to two mechanisms. The first was the lowering of the neutral axis during negative flexure negating the increase in bottom longitudinal reinforcement force. The second was the initiation of a lower mode of buckling in the bottom longitudinal reinforcement. Because specimen SA2 and SA3 had previously been tested, well developed cone-type pull-out mechanisms had formed at the column faces. This increased the unsupported length that the reinforcement spanned across the slot. Because the unsupported length of the bottom reinforcement had increased, the maximum mode that the reinforcement could buckle at was lower and the reinforcement was prevented from developing its full compressive force. Buckling was observed in the slot of both specimen SA2 and SA3.

It has been stated that the slotted beam system is not susceptible to overstrength caused by compressive force in the beams and it need not be considered in design (Au, 2010). The reasoning behind this assertion was that because connection rotation occurs about the top of

the section for both positive and negative flexure, an axial force in the beam would increase the connection moment at one end and reduce it by an equal amount at the other end (Au, 2010). Whilst this is true, it ignores the influence of neutral axis variation in the top hinge during flexure. Considering the mechanics of moment generation in slotted beams, shown in Figure 4-17, expressions for the nominal moment for positive and negative flexure can be determined, as shown in Equation 4-3 and Equation 4-4.

$$M_n^+ = F_s(d-c) + F'_s(d-c) + F_h(d_h-c) + C_c\left(a/2 - c\right) + N\left(h/2 - c\right) \quad \textbf{Equation 4-3}$$

$$M_n^- = F_s(d-c) + F'_s(d-c) + F_h(d_h-c) + C_c\left(d_c - a/2 - c\right) + N\left(h/2 - c\right) \quad \textbf{Equation 4-4}$$

It can be seen that the axial terms are identical for both positive and negative flexure. The axial force at each end of the beam would be approximately equal, as would the beam height. However, the neutral axis height, about which the connection moment is calculated, differs for positive and negative flexure. The increase in moment at one end of the beam cannot equal the decrease at the other end. The disparity between the two, and hence the increase in bay capacity, is larger as the top hinge depth is increased. Because the actuator forces were applied to SA1 through the columns on Grids A and 2, axial forces would have been induced in the axial beams. However, as discussed in Section 4.10, the beam axial forces were unable to be measured.

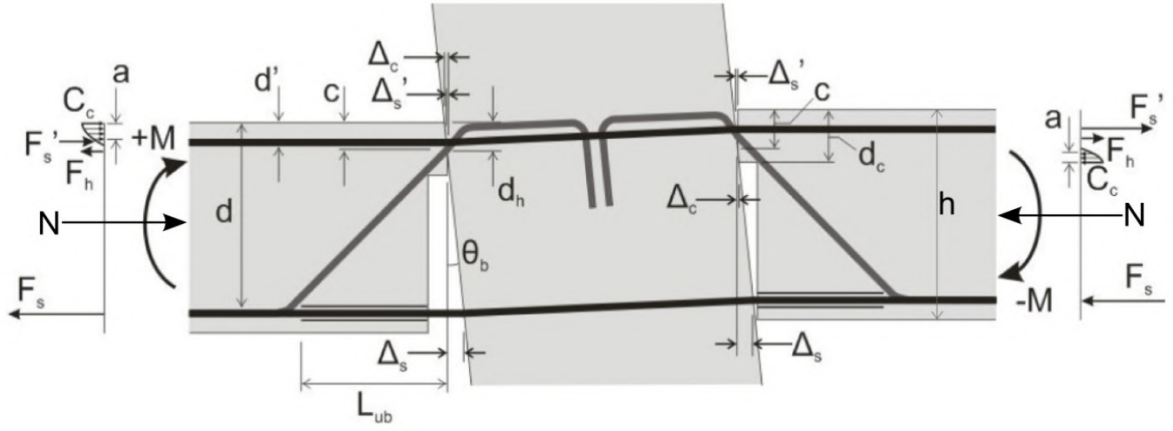

Figure 4-17: Slotted beam moment generation mechanism. Modified after Au (2010).

Once the oversimplification of the recommended design equations and the effect of floor activation were taken into account, the post-yield strength gain of SA1 was comparable to recent subassembly experiments (Au, 2010; Byrne, 2012).

Table 4-5 presents a comparison of the performance of SA1 when assessed against acceptance criteria stipulated in ACI374.1-05 (ACI Committee 374, 2005). All performance levels were achieved, with the exception of the second. The reasons for the large specimen overstrength have been outlined in this section. If the following recommendations are applied the design can be expected to conform to the ACI374.1-05 acceptance standard for moment frames.

Table 4-5: ACI374.1-05 acceptance criteria (ACI Committee 374, 2005).

Acceptance Criteria	Pass/Fail
Reached nominal resistance.	Pass
Maximum resistance not greater than column overstrength.	*Fail*
On final cycle peak resistance greater than 75% of peak resistance	Pass
On final cycle relative energy dissipation greater than 1/8	Pass
On final cycle secant stiffness greater than 5% initial stiffness	Pass

Based on the evidence presented within this section, the following recommendations are offered for the design of slotted beam systems.

1. The contribution of the top longitudinal reinforcement should be included in the calculation of nominal connection flexural moments.
2. Flange activation should be included in the calculation of nominal connection flexural moments. NZS3101:2006 §9.3.1.4 should be used to determine the appropriate effective flange widths (Standards New Zealand, 2004).
3. Continuity moments from the one-way precast flooring connections to the supporting beams should be included in calculation of nominal system strength.
4. An overstrength factor of 1.6 should be applied to the design of slotted beam connections.

4.6 Damage Observed During Testing

There were many cracks in the specimen prior to testing as a result of shrinkage strain and on-going earthquakes in the Christchurch region, as discussed in Section 4.3. The first displacement induced cracks were observed during the 0.2% beam drift cycles. These cracks were between the precast columns and the dry-pack, as shown in Figure 4-18(a). Cracks also formed at the top of the top hinge, as shown Figure 4-18(b). All new cracks were hairline and were recovered upon specimen unloading.

(a) Cracking between precast column and dry-pack. (b) Cracking at top of top hinge.

Figure 4-18: First cracks observed at 0.2% drift.

The first flexural cracks in the beam ends were observed during the 0.5% beam drift cycle. A typical example of this type of cracking is shown in Figure 4-19(a). The flexural cracks were hairline and recovered during specimen unloading. As shown in Figure 4-19(b), material that remained between the reinforcement in the slot region begun to be ejected. The debris was composed mostly of fine dust and small portions of aggregate than would pose no risk to occupant safety.

Cracks formed in the ends of the dapped double-tee floors, as shown in Figure 4-19(c). The tension in the corner of the dapped end was induced by displacement and was accounted for as part of the floor design, described in section 3.4.5. The tension zone in double-tee floor seating is not always accounted for by the suppliers of double-tee floors. Sometimes a 'loop detail' or 'pig-tail' detail is used in flange-hung double-tee designs. This detail is not sufficient to transfer the induced tension force and complete the strut and tie mechanism (Hare et al., 2009). An example of a failed flange-hung double-tee floor is shown in Figure 4-19(d). This floor was installed mid-height in a multi-storey moment frame structure in Christchurch and was subject to strong motion during both the 4th September and 22nd February earthquakes. It is recommended that designers design and specify the reinforcement detail for the ends of the double-tee units.

Cracking in the floor above the precast floor seating was extensive prior to testing. During the first 0.5% east-west beam drift cycle the cracking extended the entire seating width. The first displacement incompatibility cracks formed in the timber infill on Level One, as shown in Figure 4-19(e). As shown in Figure 4-19(f), hairline cracks formed in the columns on Grid B.

(a) Flexural cracking at beam ends.

(b) Debris being cleared from slot region.

Figure 4-19: Damage observed up to 0.5% drift.

(c) Cracking in dapped double-tee seating.

(d) Example failure of flange-hung double-tee floor during February 22nd Christchurch Earthquake. Picture taken looking up beam face.

(e) Displacement incompatibility crack forming between first hollow-core unit and parallel beam in the infill.

(f) Flexural cracks in Grid B columns.

Figure 4-19: Damage observed up to 0.5% drift (Continued).

During the 0.75% beam drift cycle, a crack formed at the end of the south-east hollow-core unit seated along Grid C, as shown in Figure 4-20(a). This type of damage was commonly observed in structures with hollow-core floors following the 22nd February Christchurch earthquakes. The corners of the hollow-core units were unreinforced. It is likely that the relative rotation between the hollow-core unit and the supporting beam during testing induced tensile forces in the end of the unit. The concrete did not have sufficient concrete tension capacity to resist the forces and cracked.

During the 1.0% beam drift cycles, cone-type pull-out mechanisms began forming around the reinforcement at the column face. An example of the initiation of this type of mechanism is presented in Figure 4-20(b). This particular example on column B/2 appeared to behave as a group failure, as opposed to the more commonly observed mechanism around individual reinforcement. The group failure mode likely formed due to the supplemental reinforcement

welded to the longitudinal reinforcement through the joint, which allowed greater force transfer to occur closer to the face of the column.

The cracks in the dapped double-tee seating that initiated during the 0.5% drift cycle widened and spread during testing. At the end of testing the cracks had widened to 0.2mm. The cracks did not present an issue for gravity support of the double-tee floors due to the reinforcement that had been designed to maintain shear transfer in the ends of the units.

Warping deformations were observed around the columns during the 1.0% beam drift cycles, as shown in Figure 4-20(c) and (d). This type of deformation occurs in traditional reinforced concrete structures; however, in slotted beam structures it is exacerbated by the increased column widths necessitated by beam reinforcement bond requirements. Coinciding with the initiation of warping cracking in the floor diaphragm, was the formation of hairline torsional cracks in the east-west beams. This was evidence of a significant continuity moment being generated by the precast flooring connection to the supporting beam.

Cracking in the floor diaphragm around the beam ends was evident on both floors. This type of damage was consistent with flange activation. The observed and measured cracking during the 1.0% beam drift cycles was consistent with the effective flange width of 436mm calculated in Section 4.4.1 using existing provisions in the NZS3101:2006 (Standards New Zealand, 2006).

The serviceability limit state for the prototype structure that SA1 was extracted from was considered to be approximately 1.0% based on recommendations by Priestley et al. (2007). The limit states recommended by Priestley et al. (2007) are an extension of the performance based design principles presented in the Vision 2000 document (SEAOC Vision 2000 Committee, 1995). At the serviceability limit state the structure should require no significant remediation. Yielding of reinforcement is allowed and cracks must be small enough to not require epoxy injection. Likewise, some minor damage to non-structural components is allowed; however, the structure must be in a fully functional condition. Specimen SA1 conformed to these requirements after the 1.0% beam drift loading cycles.

(a) Crack in eastern end of south-east hollow-core unit.

(b) Initiation of cone-type pull-out.

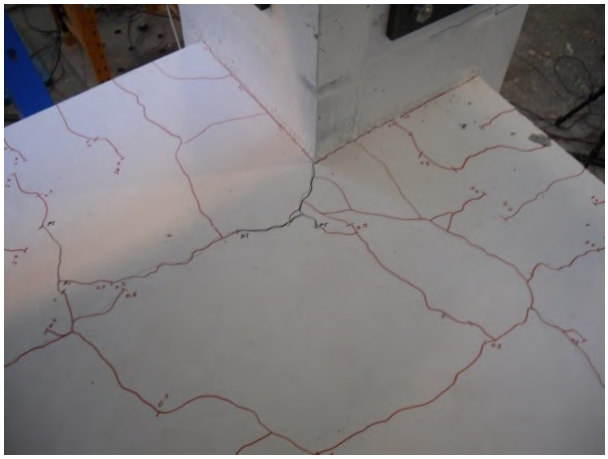

(c) Cracks from warping deformation and flange activation at column A/2.

(d) Close-up of warping deformation.

Figure 4-20: Damage observed up to 1.0% drift.

During testing to 1.5% beam drift, existing cracks lengthened and widened. Figure 4-21(a) shows the maximum crack width of 0.7mm, which was observed in the diaphragm adjacent to column A/2. The cone-type pull-out mechanism, initiated by strain penetration of the bottom longitudinal reinforcement into the column, continued to develop, as shown in Figure 4-21(b).

A crack formed in the eastern end of the north-east hollow-core unit, as shown in Figure 4-21(c). This crack was similar to that observed in the eastern end of the south-east unit. The initiation of delamination between the hollow-core units and the insitu topping was observed, as shown in Figure 4-21(d). The delamination was caused by displacement incompatibility between the unit and the parallel beam, which induced flexural deformation in the timber infill. Delamination was undesirable because it reduced the composite action of sections of the floor and made them less effective at lateral force transfer.

Figure 4-21(e) shows damage to the seating area of a double-tee unit. The main crack is along a cold joint and recommendations made in Chapter 3 will improve performance in this area. The spalled concrete is due to relative motion between the beam and the double-tee. Concrete was allowed to enter this region during the insitu floor pour. It is recommended that a gap is provided in this area to prevent this type of damage occurring.

During the 1.5% beam drift loading, spalling at the top of the slotted beam top hinge initiated, as shown in Figure 4-21(f). This was caused by large compressive forces in the top concrete chord during positive flexure and, to a much lesser extent, shear and rotational deformation across the slotted section. This type of damage has been observed in other reinforced concrete slotted beam tests (Au, 2010; Byrne, 2012). The spalled concrete can lead to a softening in response due to a lowering of the neutral axis; however, it is easily repaired following an earthquake.

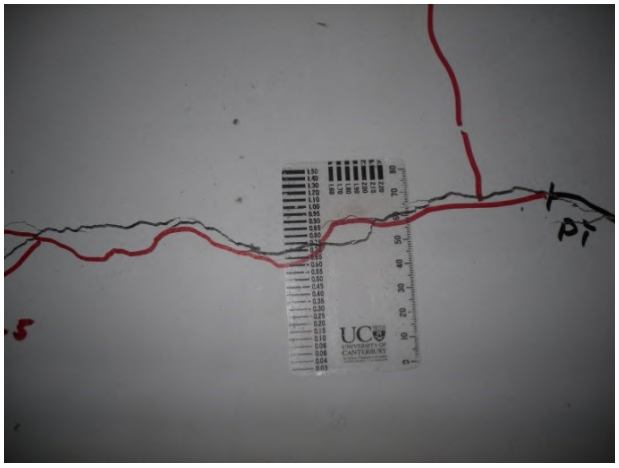

(a) Maximum crack width of 0.7mm in floor diaphragm adjacent to column A/2.

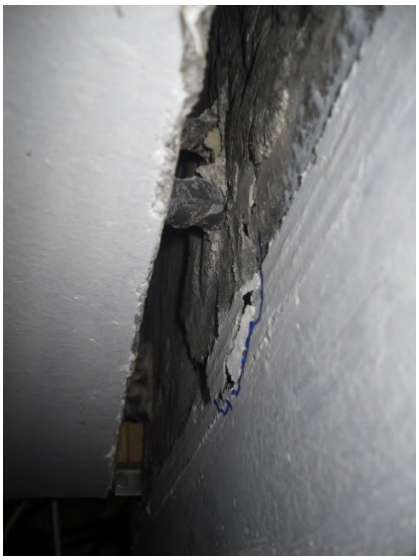

(b) Strain penetration cone pull-out mechanism development.

(c) Crack in eastern end of north-east hollow-core unit.

(d) Delamination between hollow-core unit and insitu topping.

Figure 4-21: Damage observed up to 1.5% drift.

(e) Double-tee seating damage and flange cracking.

(f) Initiation of concrete spalling at the top of the slotted beam top hinge.

Figure 4-21: Damage observed up to 1.5% drift (Continued).

The damage-control limit state is analogous to the design limit state, and for specimen SA1 was approximately 2.5% beam drift (Priestley et al., 2007). This limit state requires that life safety of the building occupants be protected. Damage is permitted; however, the repair cost should be significantly less than the replacement cost of the structure. Reinforcement fracture should not occur and the strength of the structure should not be reduced. Damage to non-structural components should likewise be predominantly repairable. Specimen SA1 conformed to the damage-control limits state requirements at the end of testing to 2.5% beam drift.

As shown in Figure 4-22(a), during the 2.5% beam drift cycle a large portion of the seating for the western end of the south-east hollow-core unit was lost. The spalling was caused by the low-friction strip binding between the hollow-core and the seating during positive flexure. This type of failure highlighted the importance of specifying a pragmatic seating width and using reinforcement in the ledge. Failure to do so could result in complete loss of gravity support. Also evident was the poor performance of the low-friction strips. During the subsequent demolition of SA1, many instances of distorted and torn bearing strips were observed. The assumed low-friction sliding type deformation mode in many cases did not exist. Instead, a higher force, shear deformation mode of the strip itself occurred, which created significantly higher continuity moments. A two-piece genuine low-friction strip would be more effective, and is recommended.

Cracks extending completely around the perimeter of both the timber infill and double-tee flange was observed during the 2.5% cycles. This mechanism is formed to accommodate displacement incompatibility between the precast floor units and the parallel beams and can be seen in Figure 4-22(b) and (c). Because the timber infill depth was uniform across its width, the resulting cracks were numerous and spread relatively evenly over the infill. Conversely, the 50mm flange depth of the double-tee flooring in conjunction with the insitu

topping, meant that the region over which the displacement incompatibility had to be accommodated was significantly stiffer. This caused a primary crack to form in the weakest section between the double-tee flange and the adjacent beam, which was only the thickness of the insitu topping. Hence, the cracks in the double-tee flanges were generally less numerous and larger than found in the Level One timber infill. The crack between the double-tee flange and the parallel beam peaked at 0.9mm during the north-south 2.5% cycle.

(a) Spalled hollow-core seating.

(b) Timber infill cracks.

(c) Double-tee flange cracks.

(d) Level One warping damage.

Figure 4-22: Floor damage observed up to 2.5% drift.

Damage around the columns due to warping displacements was observed to worsen during the 2.5% beam drift cycles, as shown in Figure 4-22(d). Due to forces induced by contact with the corner of the column, the concrete from the Level One infill begun to spall during the 2.5% cycle. Cracks around column A/2 peaked at 1.6mm during the 2.5% cycle.

It was observed during the 2.5% beam drift cycles that torsional type cracks had developed in the beam ends on the north-south beams, as shown in Figure 4-23(a). The north-south beams were the most susceptible to torsion due to the continuity moments applied to the beam by the precast floor connections. Figure 4-23(b) shows a torsion type crack on the inside of the beam end; however, because the cracking runs in line with the diagonal hangers it is possible that the cracks were caused by strain penetration of the diagonal hangers.

Existing cone-type pull-out mechanisms due to strain penetration of the bottom longitudinal reinforcement continued to develop during the 2.5% beam drift loading, as shown in Figure 4-23(c). Figure 4-23(d) shows strain penetration damage to connection Bm B/2-2. In this connection, the stirrups below the beam longitudinal reinforcement had been incorrectly placed and were not adjacent to the reinforcement, which enabled cone-type pull-out failure to develop over a greater area. The cracks extended down to the stirrup set immediately above the dry-pack connection.

(a) Diagonal cracks on outside of beam ends.

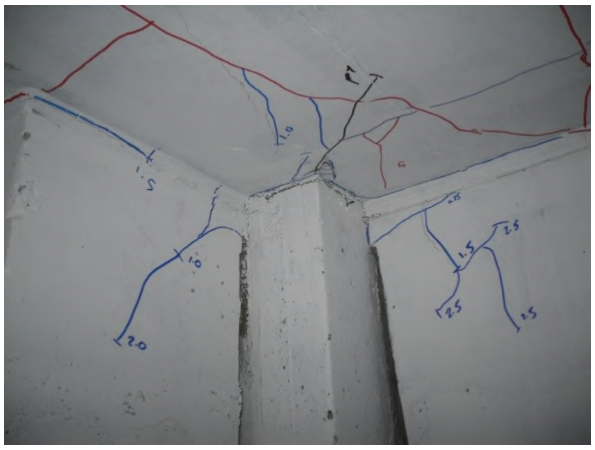

(b) Diagonal cracks on inside of beam ends.

(c) Spalling due to strain penetration.

(d) Column cracking stemming from poorly placed stirrups.

Figure 4-23: Structure damage observed up to 2.5%

The survival limit state exists so that during the strongest feasible ground shaking sufficient reserve capacity exists in the structure to prevent collapse (Priestley et al., 2007). The survival limit state for specimen SA1 corresponded to approximately 3.5% beam drift. At this limit state the life safety of the occupants must be protected but extensive structural damage is permitted, to the extent that it may not be economically feasible to repair the structure. Specimen SA1 not only satisfied the requirements for this limit state, it exceeded them. The specimen could have been economically repaired at the conclusion of testing. The damage observed in specimen SA1 at the survival limit state is similar to what would be expected in a traditional structure at the damage-control limit state.

Figure 4-24(a) shows the final condition of the slotted beam top hinge at the conclusion of testing. There was a small amount of spalling of the top chord of the top hinge; however, this could have been easily repaired. It was likely that the cracks in the column extending from the top and bottom of the top hinge were a result of strain penetration from the top longitudinal reinforcement.

Figure 4-24(b) shows a fully developed cone-type pull-out mechanism due to strain penetration. This image was taken during the demolition of SA1. The spalling was extensive and the column stirrups were clearly identifiable. The maximum measured depth of the spalling was 48mm. Concrete failure planes varied in angle between 30° and 45°. The closer the column stirrups were to the reinforcement, the less effective column depth was lost to strain penetration.

During the third cycle at 3.5%, the outside D12 on the southern connection of unit Bm A/1-1 fractured, as shown in Figure 4-24(c). In the preceding cycles, the D12 reinforcement was observed to buckle between the column face and the end of the debonding tube. The reinforcement buckling caused flexure in the reinforcement, which created stress concentrations that allowed crack roots to form at the base of the reinforcement deformations. Over the subsequent strain reversals the crack propagated until failure. Details to delay this type of failure are discussed in Section 6.4.1.

Following specimen demolition, portions of reinforcement from various locations of the structure were removed to observe damage and to enable hardness testing to be undertaken by Holmes Solutions Limited. Hardness testing allows an estimate of the remaining strain capacity of a sample of reinforcement to be made by comparing the measured hardness to the hardness of a sample of reinforcement with a known strain history. Unfortunately, due to the demands placed on engineering firms following the Christchurch earthquakes, this work was never completed. A portion of reinforcement removed from the unbonded length of the

bottom longitudinal reinforcement is shown in Figure 4-24(d). It can be observed in Figure 4-24(d) that the buckling length of the reinforcement was approximately 90mm or $5d_b$. This demonstrates that the close stirrup spacing of $4d_b$ specified in this region is effective to restrain reinforcement buckling; however, it is recommended the thick walled steel confinement tubes are used as per recommendations by Au (2010).

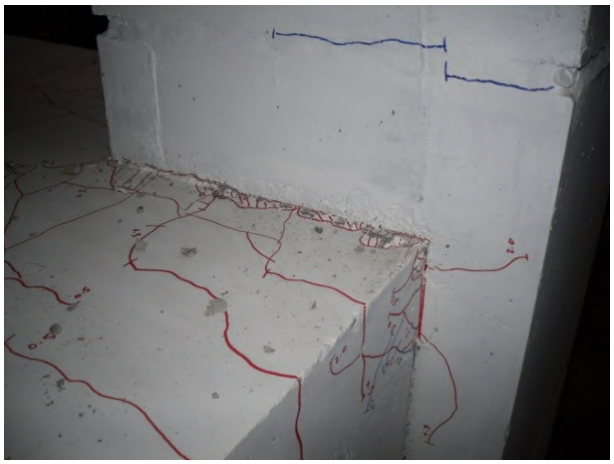

(a) Concrete spalling in top chord of the top hinge.

(b) Fractured D12 in connection Bm A/1-1.

(c) Fully developed cone-type spalling.

(d) Extracted reinforcement from unbonded region showing buckling mode.

Figure 4-24: Damage observed up to 3.5% drift.

During the 3.5% beam drift cycles, damage to the precast floor connections continued to worsen. Figure 4-25(a) presents additional spalling that occurred in the seating on the western end of the south-east hollow-core unit. Whilst there was no risk of the hollow-core unit losing gravity support, this type of spalling is not desirable in a structure that is occupied due to the hazard the falling concrete may pose to occupants. It is difficult to prevent this type of damage occurring when using low-friction seating strips and NZS3101:2006 minimum reinforcement cover requirements (Standards New Zealand, 2006). Armoured ledges can be used; however, there is a significant cost premium to using this detail.

The cracking at the ends of the hollow-core units worsened during the 3.5% beam drift cycles, as shown in Figure 4-25(b) and (c). Another incidence of this type of failure mechanism initiated at the eastern end of the north-west hollow-core unit. The prevalence of this type of damage in SA1, as well as in field surveys following the Christchurch earthquakes, was alarming and possibly unacceptable. Figure 4-25(d) shows an example of a hollow-core unit lifting off the supporting ledge during biaxial specimen displacement. This deformation was due to both the flexure of the supporting beam, and the moment imposed by the timber infill.

(a) Further loss of hollow-core seating.

(b) Crack in eastern end of north-east hollow-core unit.

(c) Crack in eastern end of south-east hollow-core unit.

(e) Eastern end of central hollow-core in the eastern bay lifting off seating

Figure 4-25: Diaphragm damage observed up to 3.5% drift.

Figure 4-26(a) shows the main crack that formed above the double-tee floor seating. The crack width peaked at 2.0mm during the 3.5% cycle, and following the completion of testing maintained 0.75mm residual width. Figure 4-26(b) shows an example of the cracks that formed on the inside of the outermost double-tee webs during the 3.5% cycle. The double-tee flange had a higher stiffness than the timber infill used on Level One. The higher stiffness, in conjunction with the narrow width of the seating, meant that during north-south specimen displacements, flexure in the flange rotated the web and caused a crack to form.

Figure 4-26(c) – (f) shows damage that occurred around the interface between the column and the floor diaphragm during the 3.5% beam drift cycles. The damage was due to warping deformations in the floor and contact between the column and the floor. To prevent this type of damage, it is recommended that a compressible backer is installed between the column face and the floor diaphragm. However, the designer must consider the force path of diaphragm forces into the columns if this detail is used.

(a) Crack above double-tee seating.

(b) Crack on inside of double-tee web.

(c) Spalling damage underneath timber infill due to warping.

(d) Warping damage on column A/2-1.

Figure 4-26: Diaphragm damage observed at 3.5% drift.

(e) Warping displacements on column A/2-2.

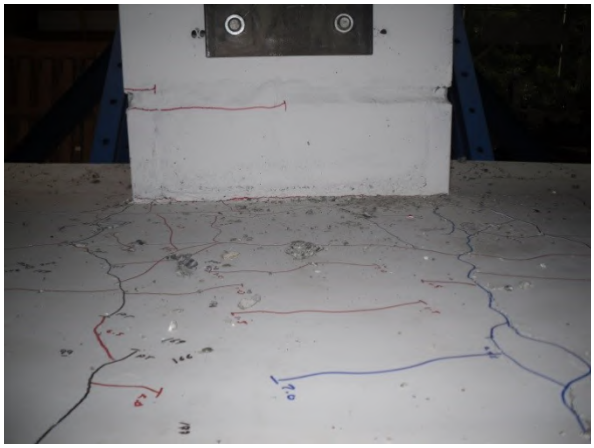

(f) Warping deformation along Grid B.

Figure 4-26: Diaphragm damage observed at 3.5% drift (Continued).

Figure 4-27(a) – (d) shows the floor diaphragm at the completion of experimentation. The cracking over the precast unit seating is clearly defined, as is the development of cracks over the timber infill and double-tee flanges. At the interface between the timber infill and the hollow-core seating cracking due to delamination can be seen. It can be seen in Figure 4-27(a) that there are no diagonal cracks in the infill adjacent to the perimeter beams. The diagonal cracks that have been observed in the infill region in experiments with traditional detailing have been attributed to an induced force transfer mechanism between the floor and the parallel beams, caused by beam elongation (Matthews, 2004; Peng, 2009). The absence of diagonal cracking showed that beam elongation, and hence induced beam axial forces, was reduced in SA1 when compared to similar traditional connection systems. Due to the numerous shrinkage cracks on the second floor, the cracks due to lateral displacement are not as easily distinguishable.

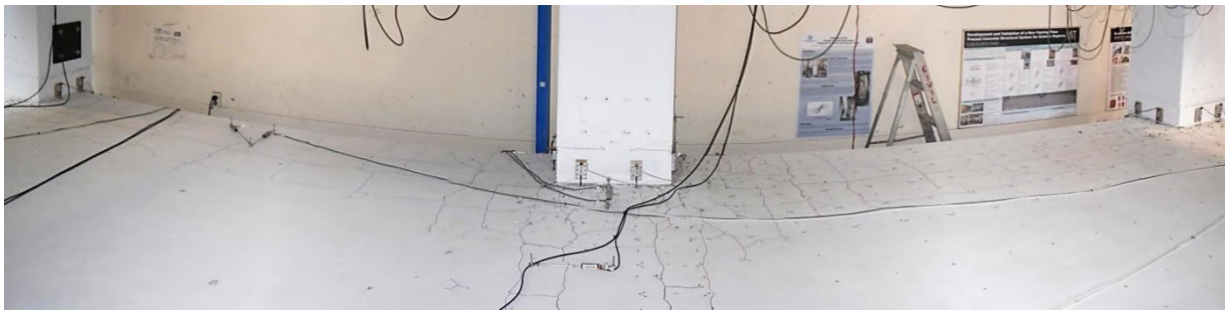

(a) Level One north.

(b) Level One south.

Figure 4-27: Floor diaphragms at the completion of testing.

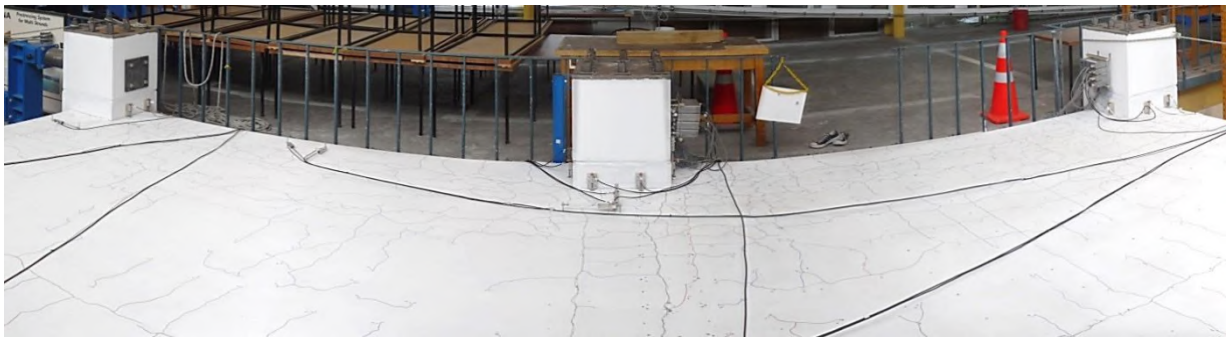

(c) Level Two north.

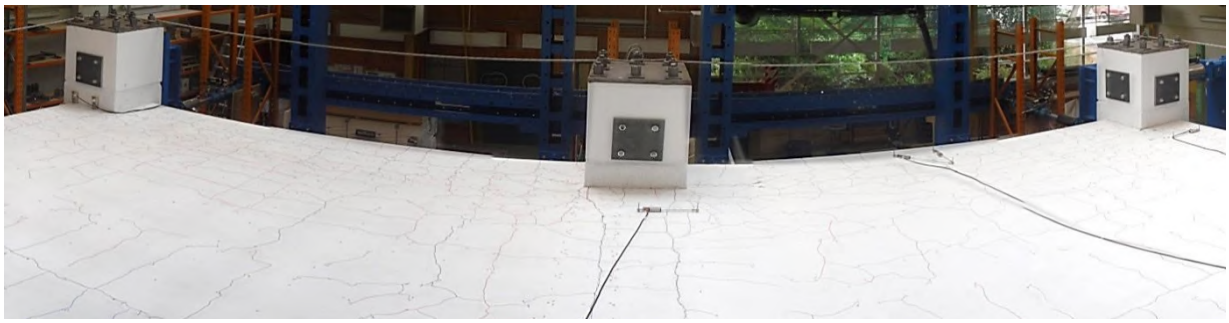

(d) Level Two south.

Figure 4-27: Floor diaphragms at the completion of testing (Continued).

Figure 4-28(a) – (n) shows the crack patterns that had formed in the specimen at the conclusion of testing. These figures show the distinction between the extensive cracking that had formed on the Level Two diaphragm prior to testing, and those formed as a result of lateral loading. Figure 4-28(l) and (n) show the cracks that formed over the precast floor seating on both levels, the activation of the timber infill and the areas of delamination. It can be seen that most cracking due to displacement incompatibility on Level Two occurred in the double-tee flange closest to the parallel beam. At the conclusion of testing, the maximum residual crack width was recorded at 1.0mm around column A/2-1. The same crack had a peak width of 2.2mm during the 3.5% beam drift cycles.

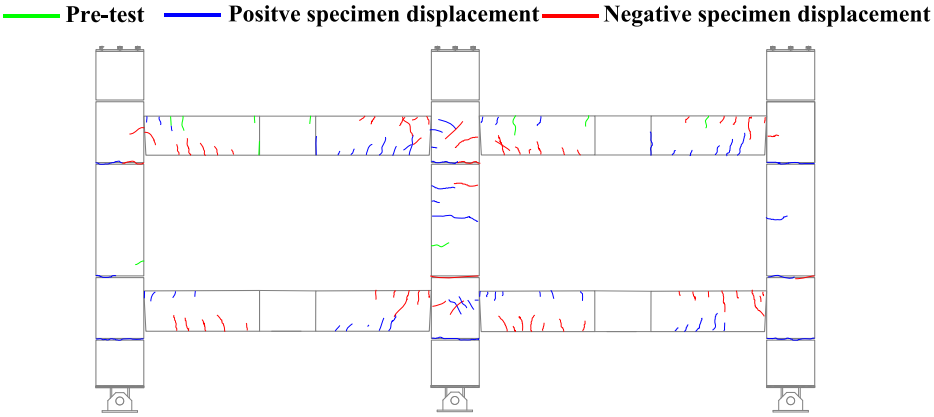

(a) Grid 1 north face.

Figure 4-28: Specimen crack patterns at completion of testing.

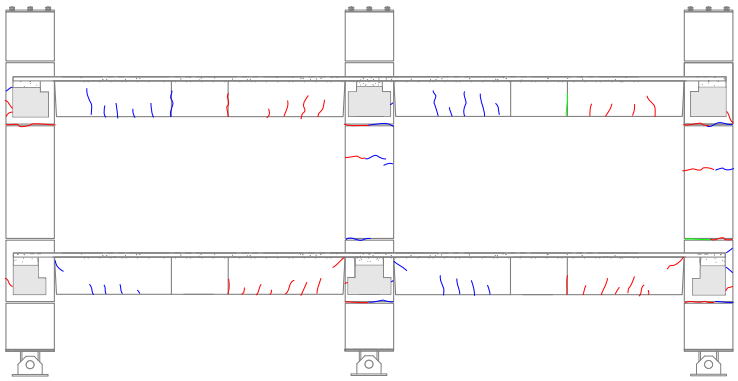

(b) Grid 1 south face.

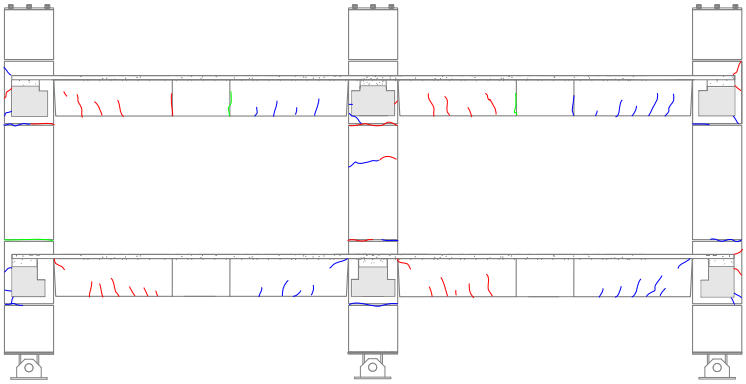

(c) Grid 2 north face.

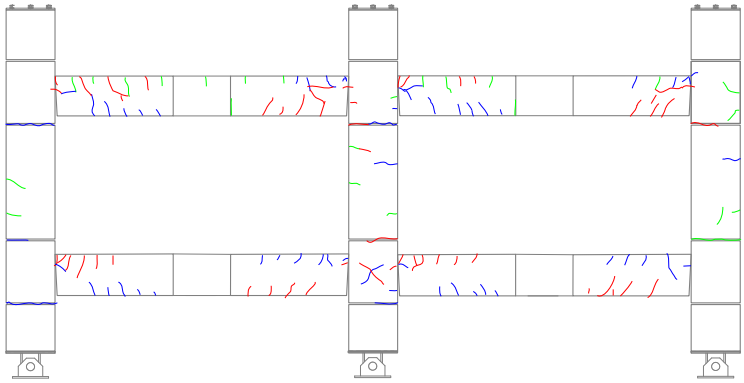

(d) Grid 2 south face.

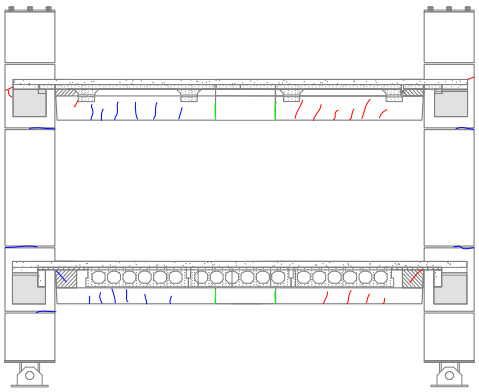

(e) Grid A east face.

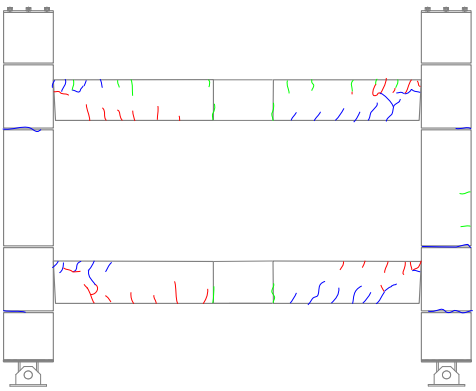

(f) Grid A west face.

Figure 4-28: Specimen crack patterns at completion of testing (Continued).

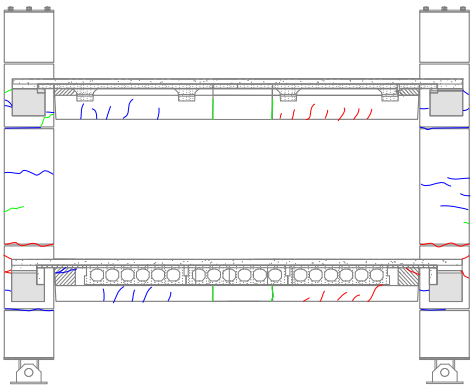

(g) Grid B east face.

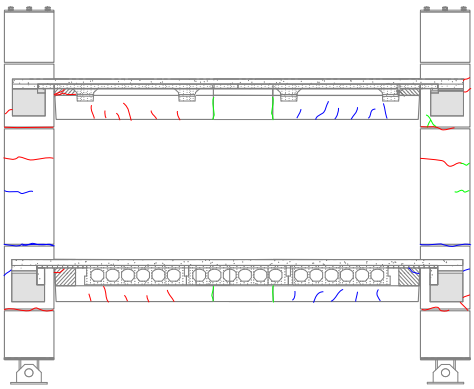

(h) Grid B west face.

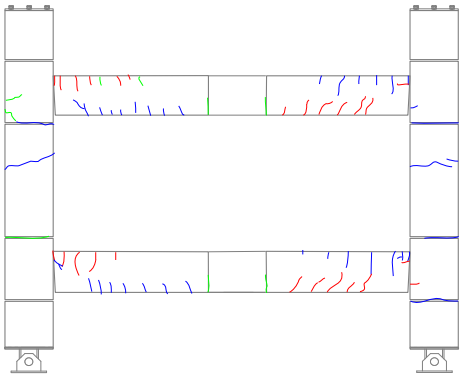

(i) Grid C east face.

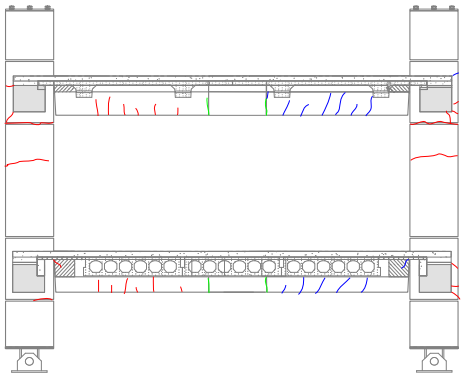

(j) Grid C west face.

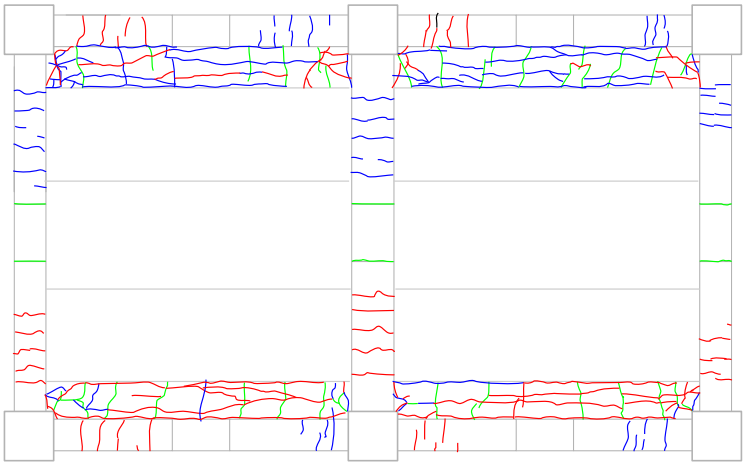

(k) Level One floor diaphragm bottom.

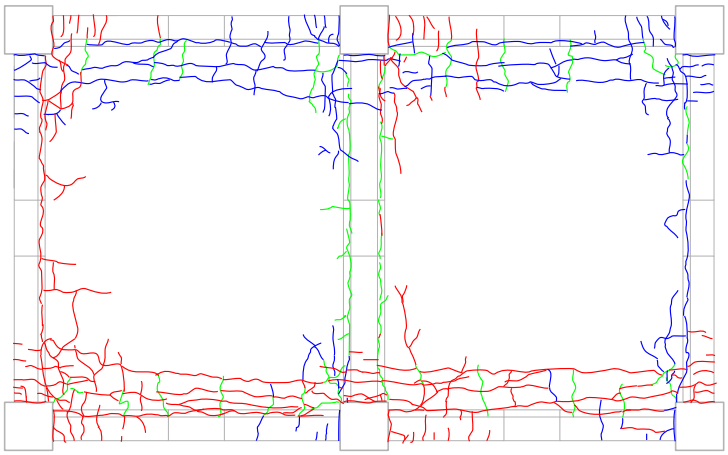

(l) Level One floor diaphragm top.

Figure 4-28: Specimen crack patterns at completion of testing (Continued).

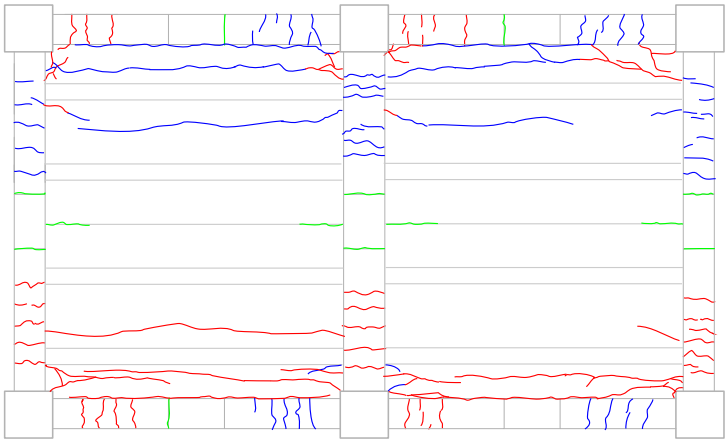

(m) Level Two floor diaphragm bottom.

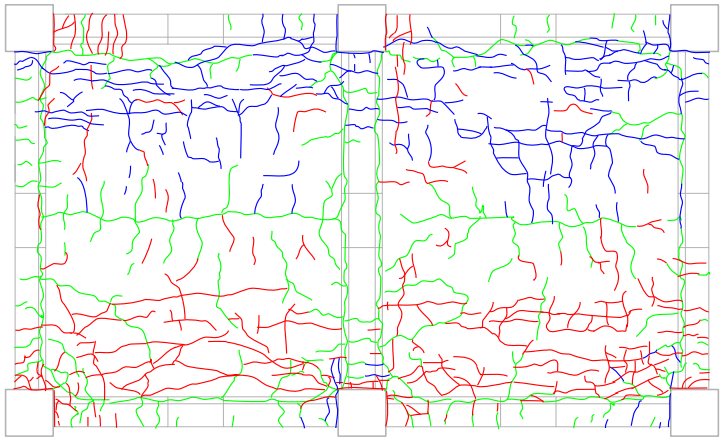

(n) Level Two floor diaphragm top.

Figure 4-28: Specimen crack patterns at completion of testing (Continued).

Overall, the damage that SA1 sustained during testing was low. Furthermore, the damage observed was significantly lower than would be expected in an equivalent structure with traditional connections, as shown in Figure 4-29. At the survival limit state the damage sustained was at a level that was economically feasible to repair. It can be concluded that damage sustained by a slotted beam system during a large earthquake is lower than would be expected in a comparable traditional beam system. Similarly, the damage sustained in a slotted beam system is generally economically viable to repair.

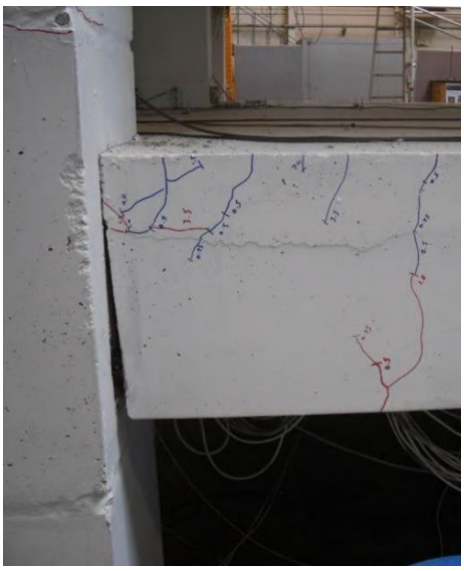

(a) Damage to slotted beam connection Bm A/2-1 east from SA1.

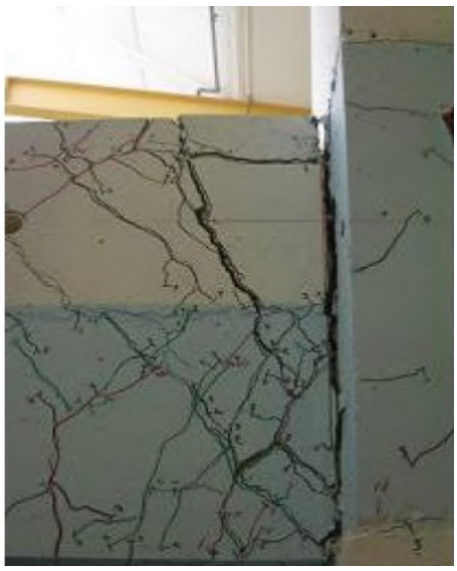

(b) Damage to plastic hinge zone in a traditional reinforced concrete connection (MacPherson, 2005).

(c) Damage to the infill between the seismic frame and the first hollow-core unit in SA1.

(d) Damage to the infill between the seismic frame and the first hollow-core unit in a specimen constructed with traditional reinforced concrete connections (Lindsay, 2004).

Figure 4-29: Structural damage comparison, at survival limit state displacements, between SA1 and a comparable specimen that was constructed using traditional reinforced concrete connections (Priestley et al., 2007).

4.7 Energy Dissipation

Hysteretic damping models can be very complex. To simplify analysis and facilitate direct comparison between systems, energy dissipation is often expressed in terms of equivalent viscous damping. As presented in Equation 4-5, equivalent viscous damping relates the hysteretic energy dissipated, $E_{D,}$ to the amount of energy an elastic system would have absorbed given the same displacement, E_{So} (Chopra, 2001). Equation 4-6 presents the formulation for the E_{So}, where k is the stiffness and Δ_o is the maximum displacement.

$$\xi_{eq} = \frac{E_D}{4\pi E_{So}}$$ **Equation 4-5**

$$E_{So} = \frac{k\Delta_o^{\,2}}{2}$$ Equation 4-6

Figure 4-30(a) and (b) show the energy dissipated by SA1 over successive cycles at each drift magnitude. Both the east-west and north-south directions displayed similar energy dissipation behaviour. The energy dissipated by SA1 increased with increasing specimen displacement. The equivalent viscous damping behaviour exhibited by SA1 was corroborated by the results presented by Byrne (2012). It can be concluded that, for practical structural displacements, slotted beam and traditional connections are capable of dissipating comparable amounts of energy. However, the manner by which energy was dissipated in SA1 resulted in significantly less damage than would be expected in a comparable specimen with traditional connection detailing.

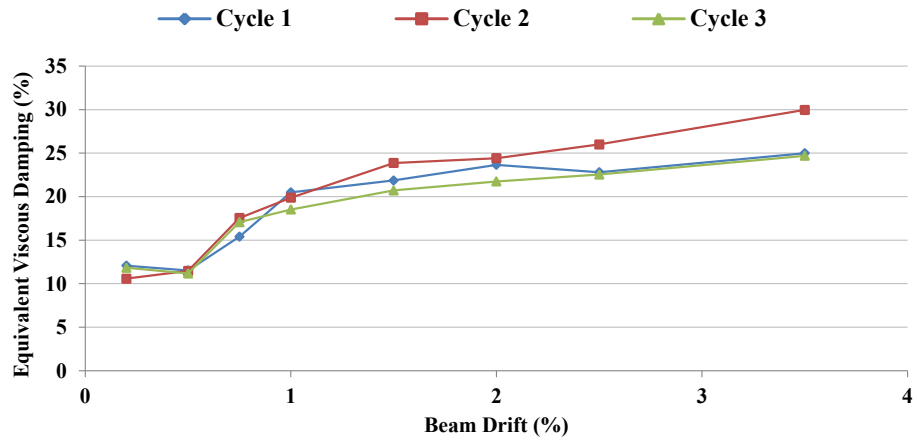

(a) East-west.

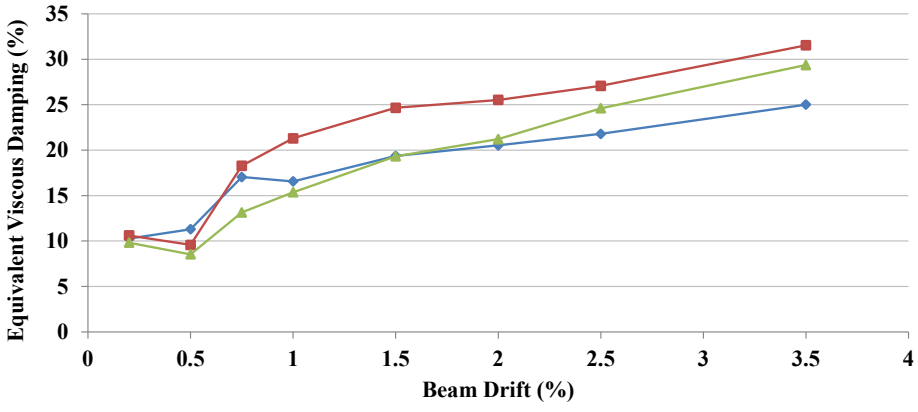

(b) North-south.

Figure 4-30: Equivalent viscous damping.

The equivalent viscous damping in the elastic range of SA1 was calculated at approximately 10%, which was significantly greater than the commonly assumed 3-5%. It is possible that this figure could be misleading due to error introduced by the relatively large influence that inaccuracies in the measurement of small displacements can have on the subsequent calculation of equivalent viscous damping. It is recommended that dynamic testing be

undertaken on a large scale slotted beam specimen to determine the amount of elastic viscous damping that is inherent in a slotted beam system.

4.8 Stiffness Degradation

The secant stiffness, k_p, is a means by which stiffness can be quantified in a nonlinear system. Equation 4-7 presents how k_p is calculated, where F is force and Δ is displacement.

$$k_p = \frac{F_{max+} - F_{max-}}{\Delta_{max+} - \Delta_{max-}} \qquad \text{Equation 4-7}$$

Figure 4-31(a) and (b) present the secant stiffness of the east-west and north-south directions respectively in log-log scale. In both loading directions the secant stiffness reduced over the course of testing, which was typical of a nonlinear system. Figure 4-31(a) and (b) show that the secant stiffness in both loading directions reduced relatively constantly between 1% and 3.5% beam drift. This indicated that the response of SA1 was very stable throughout testing. The reduction in secant stiffness observed in SA1 was comparable to what would be expected in an equivalent specimen with traditional connections.

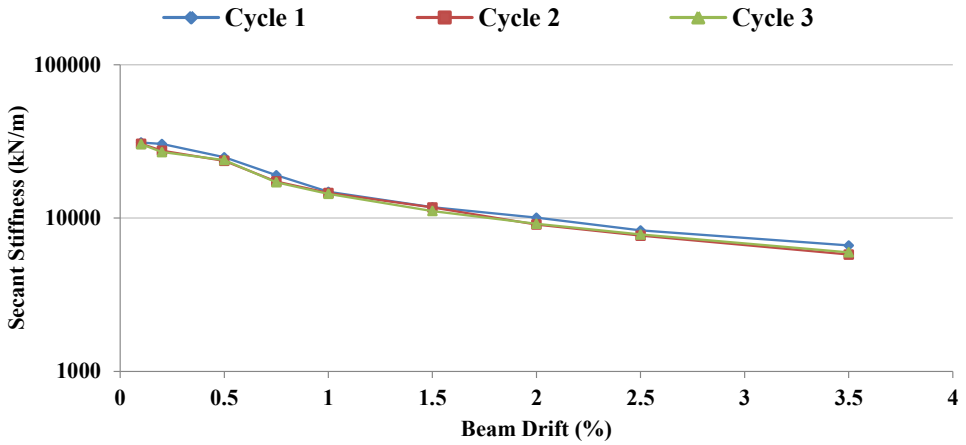

(a) East-west.

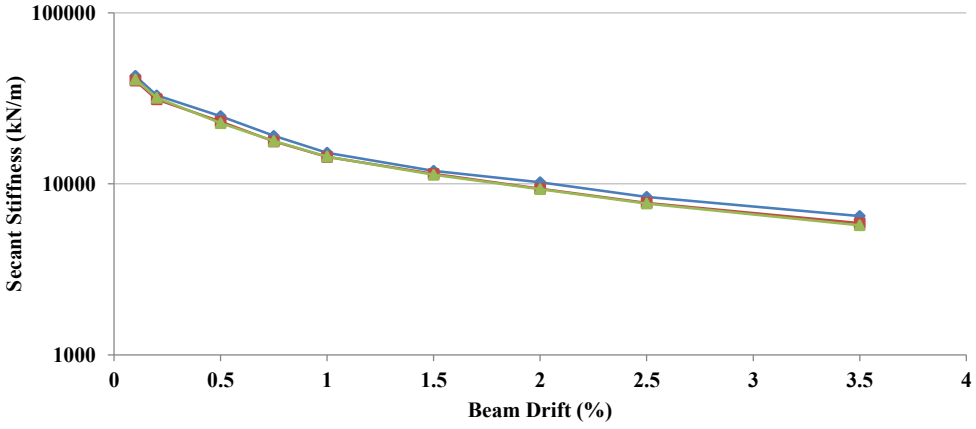

(b) North-south.

Figure 4-31: Peak to peak secant stiffness.

Because of reduced cross sectional area of a slotted beam connection relative to a traditional connection, it is inevitable that a slotted beam will exhibit softer negative elastic flexure. However, it has been shown that the difference in stiffness between traditional and slotted beams in the elastic range is small and inconsequential (Au, 2010). A comparison between the elastic stiffness of comparable slotted beam and traditional beam specimens is presented in Figure 4-32. Given the inherent uncertainty in elastic design, it is reasonable to apply the effective section properties specified in §C6.9.1 of NZS3101:2006 when conducting elastic analyses of slotted beam structures (Standards New Zealand, 2006). Designers should be aware that if NZS3101:2006 effective section properties are used in an analysis, instead of the actual elastic section properties, slightly lower structural displacements will be calculated. Furthermore, because slotted beam connections exhibit greater post-yield strength gain than traditional connections, when the elastic displacements are scaled by the expected system ductility the resulting displacements may be larger than would be expected to occur. These two factors may partially offset each other.

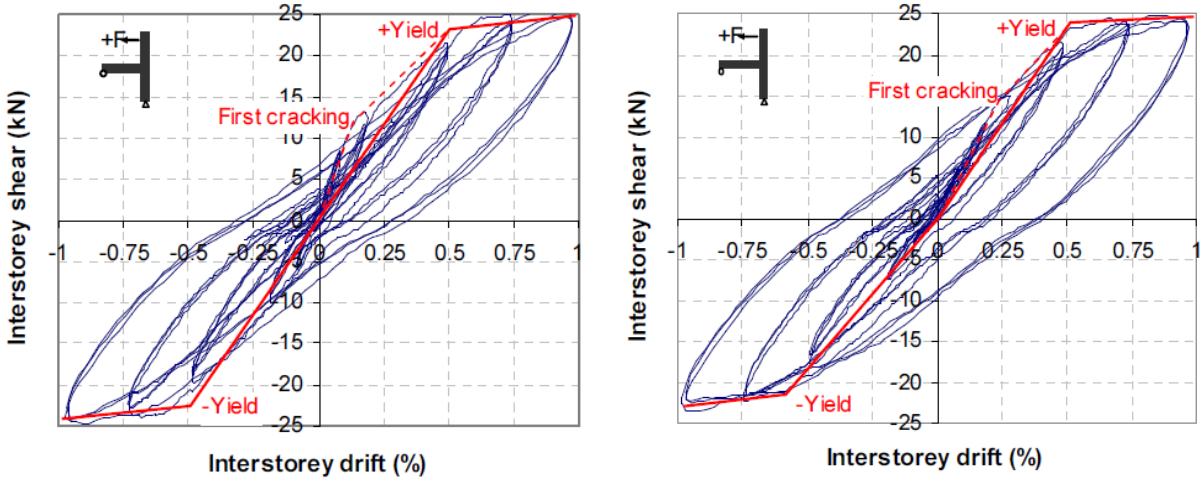

(a) Traditional beam. **(b) Slotted beam.**

Figure 4-32: Comparison of elastic stiffness of traditional and slotted beams (Au, 2010).

When more than one fully reversed cycle is performed at every drift level, as required by the ACI374.1-05 requirements, the normalised peak force (NPF) can be used to evaluate the strength degradation of a system (ACI Committee 374, 2005). As shown in Equation 4-8, the NPF represents the peak force attained in subsequent cycles as a fraction of that attained in the first loading cycle.

$$NPF = \frac{F_{cycle\ 2/3}}{F_{cycle\ 1}} \qquad \text{Equation 4-8}$$

Figure 4-33(a) and (b) present the NPF calculated for SA1 in the east-west and north-south direction respectively. The NPF plots show that there was little strength degradation in SA1 throughout testing.

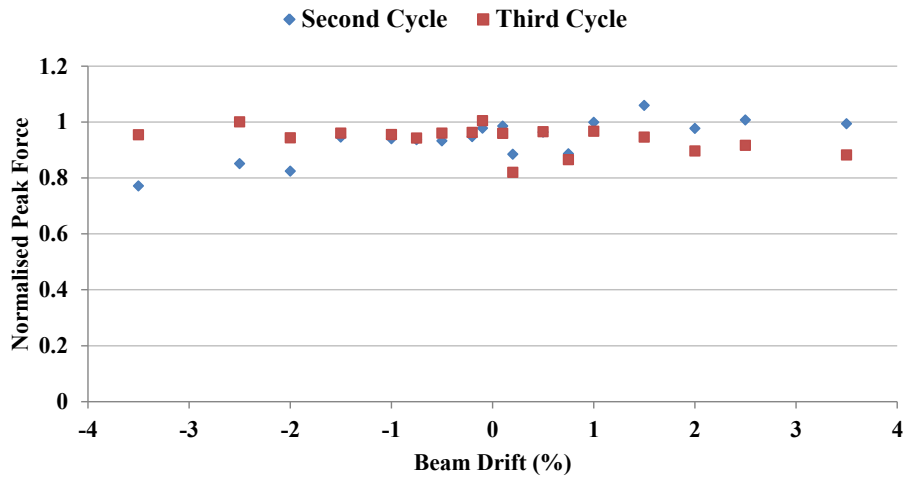

(a) East-west.

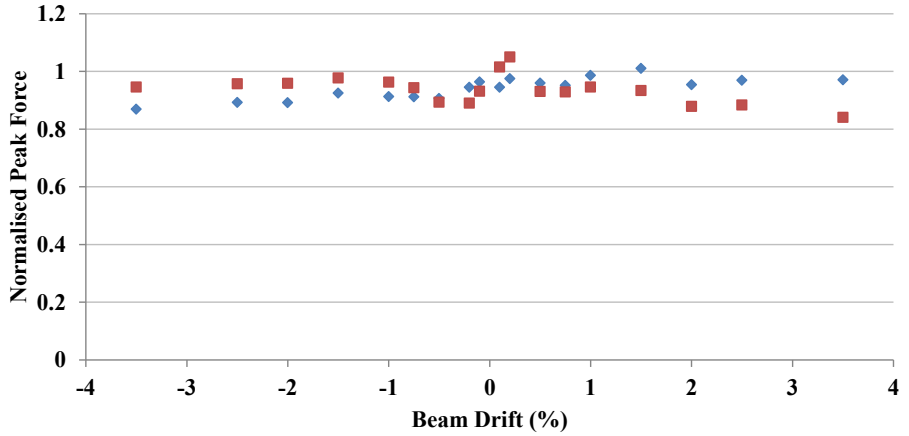

(b) North-south.

Figure 4-33: Strength degradation over testing.

It can be concluded that the strength and stiffness degradation observed in SA1 was low and conformed with acceptance criteria prescribed in ACI374.1-05 (ACI Committee 374, 2005).

4.9 Decomposition of Lateral Displacement

As presented in Section 3.8.4, the main four components of displacement were measured in SA1 to identify their relative contribution to overall displacement. The Level One and Two north-south displacement components are presented in Figure 4-34. The east-west displacement components from Level One and Two can be found in Appendix C.5. Because of the selective weakening performed on SA1, as described in Section 4.4.2, the absolute contributions of the elastic beam, elastic column and joint shear components were reduced. However, because these components were expected to remain elastic they were all reduced by the same proportion. Hence, observations could still be made based on the relative proportions and trends. Due to the small displacements involved in the calculations, the data was very noisy and had to be corrected to reduce the effect of extreme values.

As expected in a ductile moment frame designed to capacity design principles, the contribution to overall displacement by beam fixed end rotation increased over the course of

testing. The beam fixed end rotation is comprised of both elastic and inelastic components. Because the elastic slotted beam connection stiffness was less than the rest of the beam, which had greater reinforcement ratio, elastic deformations occurred preferentially in the slotted connection. This resulted in the relative contribution of the beam fixed end rotation being greater than would be expected in a traditional connection. Due the lower section stiffness, the contribution to overall displacement by beam elastic flexure was large in comparison to column flexure and beam-column joint shear.

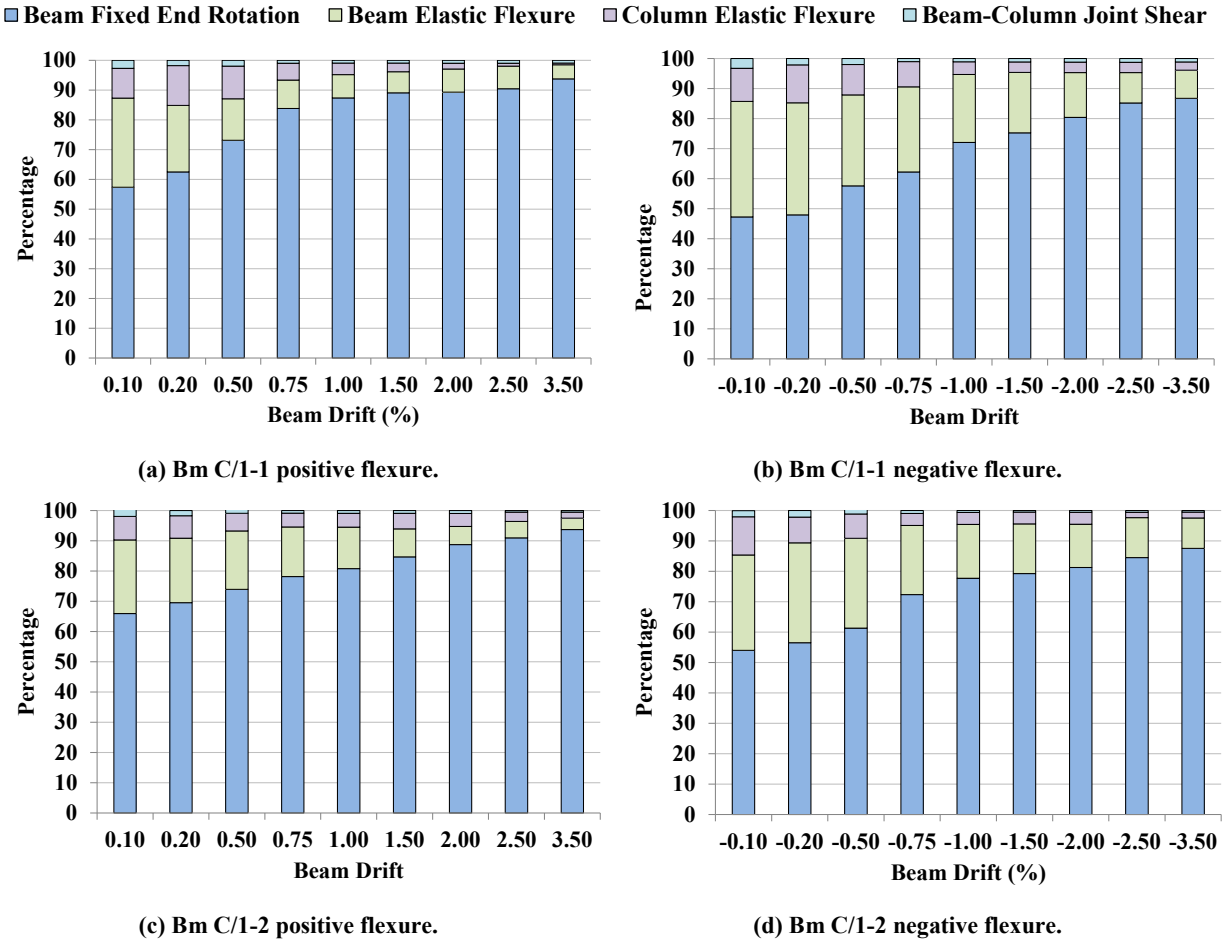

(a) Bm C/1-1 positive flexure.

(b) Bm C/1-1 negative flexure.

(c) Bm C/1-2 positive flexure.

(d) Bm C/1-2 negative flexure.

Figure 4-34: North-south lateral displacement components.

The contribution to overall displacement by column elastic flexure was low. Columns in modern ductile reinforced structures have a high degree of protection against plasticity. This was especially true for in SA1 due to the large column reinforcement ratio that was a result of the limited availably of reinforcement sizes, as described in Section 3.4.3. The contribution to overall displacement by beam-column joint shear was low also. As discussed in Section 3.4.4, the beam-column joints in SA1 were designed with horizontal reinforcement additional to that required by NZS3101:2006 (Standards New Zealand, 2006). Hence, the columns and beam-column joints were stiff compared to the elastic beam flexure and beam fixed end rotation.

The contribution of beam fixed end rotation to lateral displacement was greater for positive flexure than negative. This suggested that the stiffness of the slotted beam connections was

greater for negative flexure than for positive flexure, which corroborates observations made in Section 4.5. However, the opposite observation was made by Au (2010).

4.10 SA1 Displaced Shape

Figure 4-35(a) and (b) present a comparison of the column inclinations in the east-west and north-south directions respectively. The inclinations were calculated from rotary potentiometers which measured the displacement of both levels along each Grid and have been normalised by the instrument height. Despite the forces from the actuators being applied to SA1 in a 2:1 ratio between the second and first floors, in general the displacements of both levels were relatively similar. It is likely that the linear displacement profile was maintained by the stiff columns.

In the east-west direction, negative specimen displacements resulted in the Level Two displacements being larger than Level One displacements, whereas the opposite was observed in the north-south direction. In the east-west direction the rotary potentiometers were mounted on the opposite side of SA1 from the actuators, whereas they were mounted on the same side as the actuators in the north-south direction. The difference between the measured positive and negative specimen displacements could have been caused by the small amount of beam elongation recorded in the slotted beam connections. However, the difference could also have been caused by axial forces induced in the beams. Because the actuator forces in the east-west direction were applied to the specimen through the columns on Grid A, axial forces would have been induced in the beams. The induced axial forces in the beams would have been different during positive and negative specimen displacements, which were caused by negative and positive actuator forces. Because specimen SA1 was statically indeterminate, the induced axial forces in the beams could not be measured directly. Hence, it was planned to observe the induced axial forces in the beams indirectly by comparing the observed responses of connections of Grid A and C. However, due to the selective weakening performed on SA1, which is described in Section 4.4, the response of the connections on Grids A and C were too different for any conclusions to be made regarding the induced axial forces in the beams. Not being able measure the induced axial forces in the beams was a limitation of the research performed on SA1.

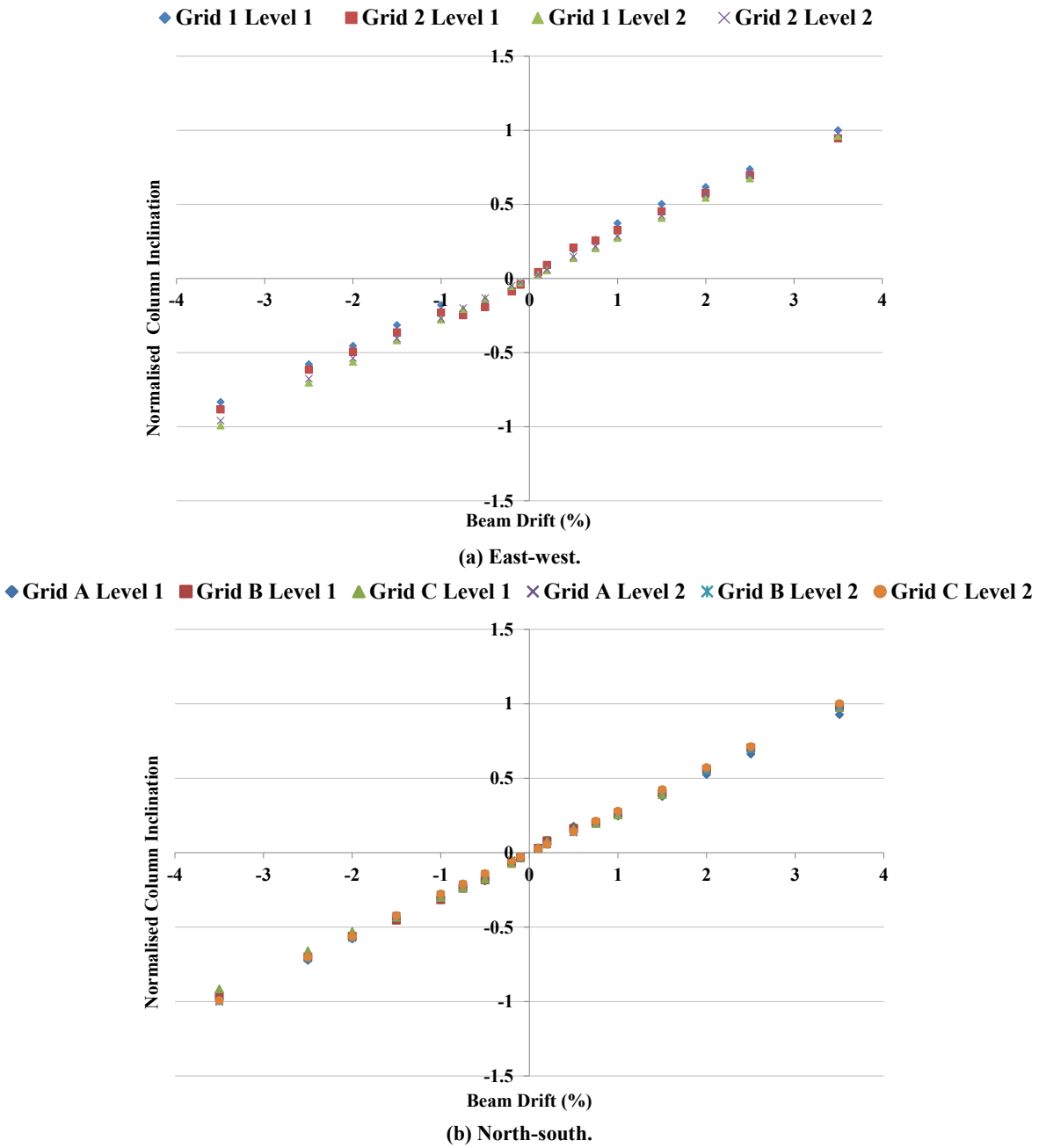

Figure 4-35: Normalised column inclination measured at Levels One and Two in east-west direction.

Figure 4-36 presents the inclinations of all columns in both the east-west and north-south directions. There was little variation between the columns throughout testing. The accuracy of the recorded inclinations in both directions for column C/2 were almost perfect because the column was connected to control rotary potentiometers in both directions. The differences in the recorded inclinations between the columns were caused by a combination of factors, such as actuator load balancing, beam elongation and beam axial strain. The variations between the column inclinations were small and insignificant.

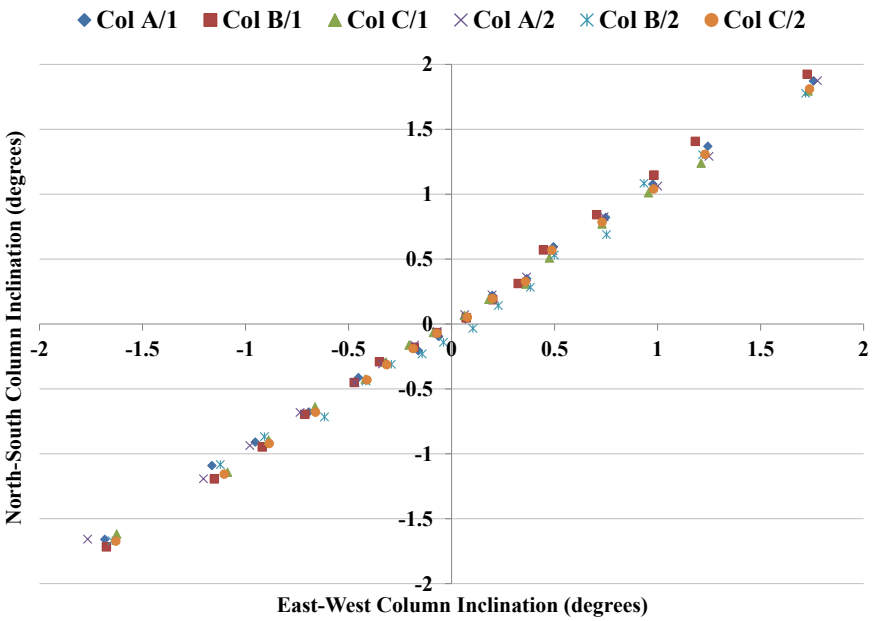

Figure 4-36: Column inclinations.

It can be concluded that although forces were applied to the specimen ends through the columns, the intended specimen displacements were faithfully replicated across the entire specimen.

4.11 Neutral Axis Variation

To allow for two layers of top longitudinal reinforcement, specimen SA1 had a deeper top hinge than previously tested slotted beam specimens (Au, 2012; Byrne, 2012). Figure 4-37 presents the neutral axis variation for interior connections along Grid 1 on Levels One and Two. During positive flexure, the neutral axis depth decreased with increasing beam drift. This was similar to what would be expected to occur in a traditional connection. However, during negative connection flexure, the neutral axis remained relatively stable at the bottom of the top hinge during response.

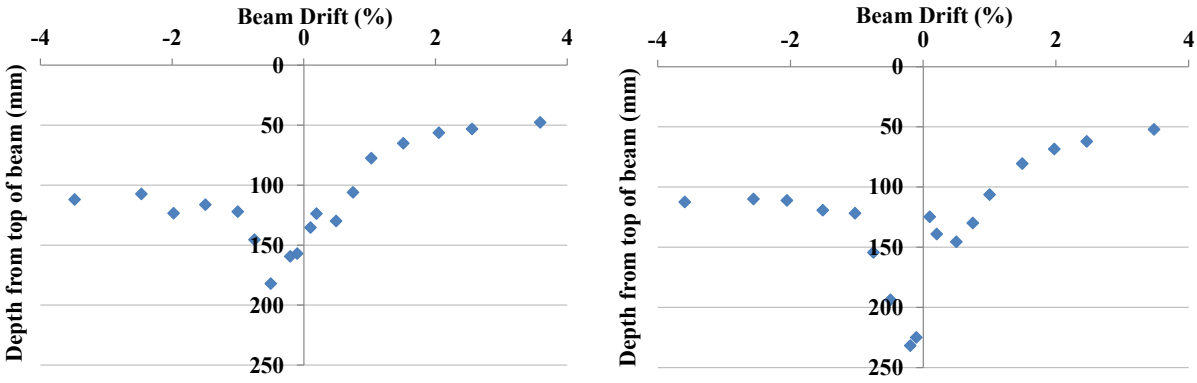

(a) Bm B/1-1, west beam. **(b) Bm B/1-1, east beam.**

Figure 4-37: Neutral axis depth in east-west direction.

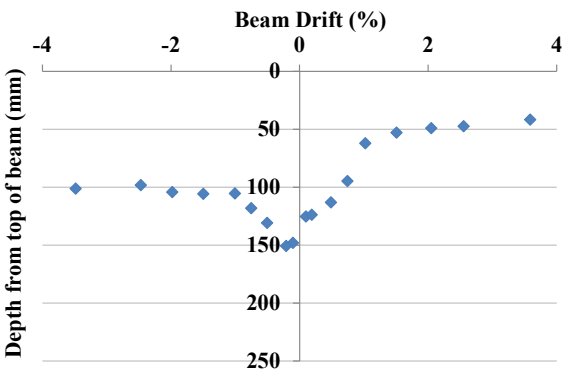

(c) Bm B/1-2, west beam.

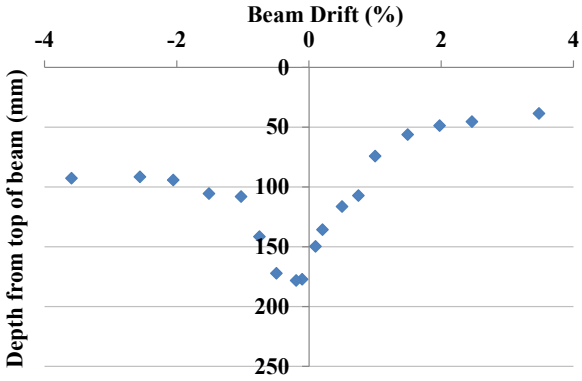

(d) Bm B/1-2, east beam.

Figure 4-37: Neutral axis depth in east-west direction (Continued).

Figure 4-38 presents the neutral axis variation for exterior connections along Grid C on Levels One and Two. Expressed as a fraction of the top hinge depth, the average neutral axis depth during positive flexure was $0.38d_h$ at 3.5% beam drift, which was similar to neutral axis depths observed during recent experimentation on slotted beams with a single top layer of reinforcement (Au, 2010; Byrne, 2012). During negative flexure, the average neutral axis depth was $0.94d_h$ at 3.5% beam drift, which was larger than observed in recent slotted beam experiments by Au (2010) and Byrne (2012). The neutral axis depth was likely lower in SA1 due to the induced negative moments that were not present in the aforementioned experiments.

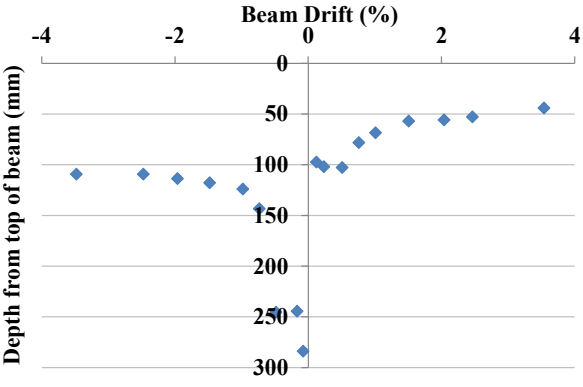

(a) Bm C/1-1.

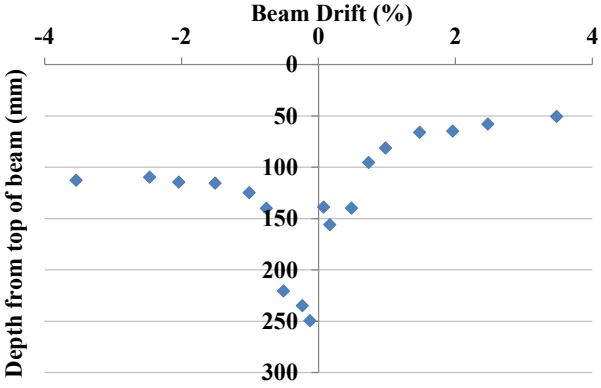

(b) Bm C/2-1.

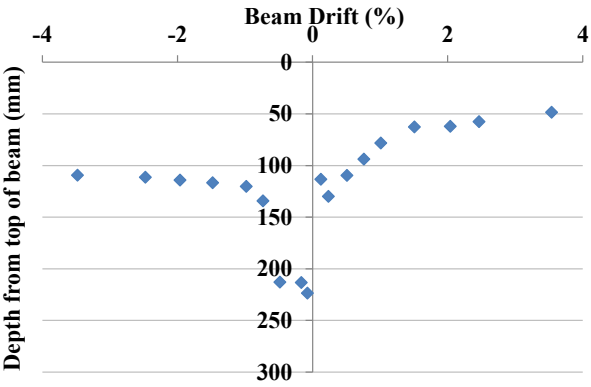

(c) Bm C/1-2.

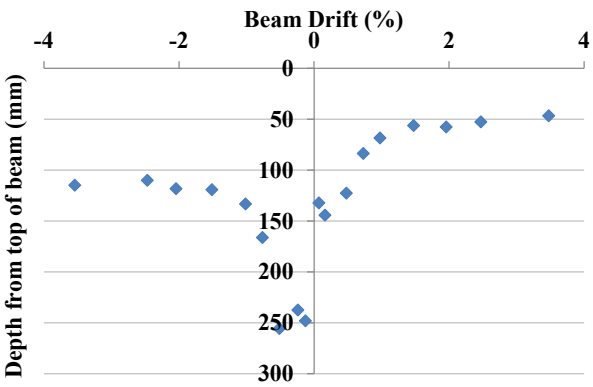

(d) Bm C/2-2.

Figure 4-38: Neutral axis depth in north-south direction.

Increasing the top hinge depth did not significantly alter the neutral axis depth when expressed in terms of the top hinge depth. However, the distance between the neutral axis and the top longitudinal reinforcement was greater during negative flexure than has been observed in recent experiments (Au, 2010; Byrne, 2012). This can increase the nominal and overstrength flexural capacities of the slotted beam connection. As stated in Section 4.5, simplified design equations recommended by Au (2010) are unconservative and a full sectional analysis is recommended to determine the flexural capacity of a slotted beam connection.

4.12 Diagonal Hanger Performance

Ohkubo et al. (1998) conducted the first experiment on a slotted beam specimen with a floor slab. However, the floor slab was included to observe damage caused by the slotted beam connection, rather than as a genuine loading condition. Au (2010) attempted to examine beam torsion by testing a specimen with precast floors. The precast floors were seated on the supporting beam eccentric to the beam centre of resistance, which induced a moment along the length of the beam. However, errors in the boundary condition of Au's (2010) experiment meant that the influence of beam torsion on the slotted beam connection was not able to be examined. Hence, specimen SA1 was the first test conducted that was able to examine the performance of the diagonal hangers under realistic loading conditions.

Figure 4-39 presents the strain profiles from connection Bm B/1-2 in the east-west direction. This connection used the new continuous hanger detail to reduce congestion, as presented in Section 3.4.2. The continuous hanger detail was an alternative to using separate hangers anchored with 90° returns within the joint. Relatively low strain was measured in the hanger through the column. Accurate bond stresses are difficult to calculate from a small number of strain gauges; however, by assuming full overstrength yielding on either side of the column simultaneously, an average bond stress of $1.42\sqrt{f'_c}$ was calculated. This bond stress was below the maximum design bond stress of $2.5\sqrt{f'_c}$ recommended by Paulay and Priestley (1992). The diagonal hangers in the connections on Grids 1 and 2 were subject to the lowest shear and torsion demands. The diagonal hangers remained elastic throughout testing, and the hanger strain increased roughly in proportion to specimen displacement. Since gravity shear was constant, and seismic shear did not increase proportionally to displacement after connection yield, this suggested that a significant portion of the strain in the hangers was induced by flexure in the top hinge. The strain data from the connection Bm C/1-2 south is presented in Appendix C.2.

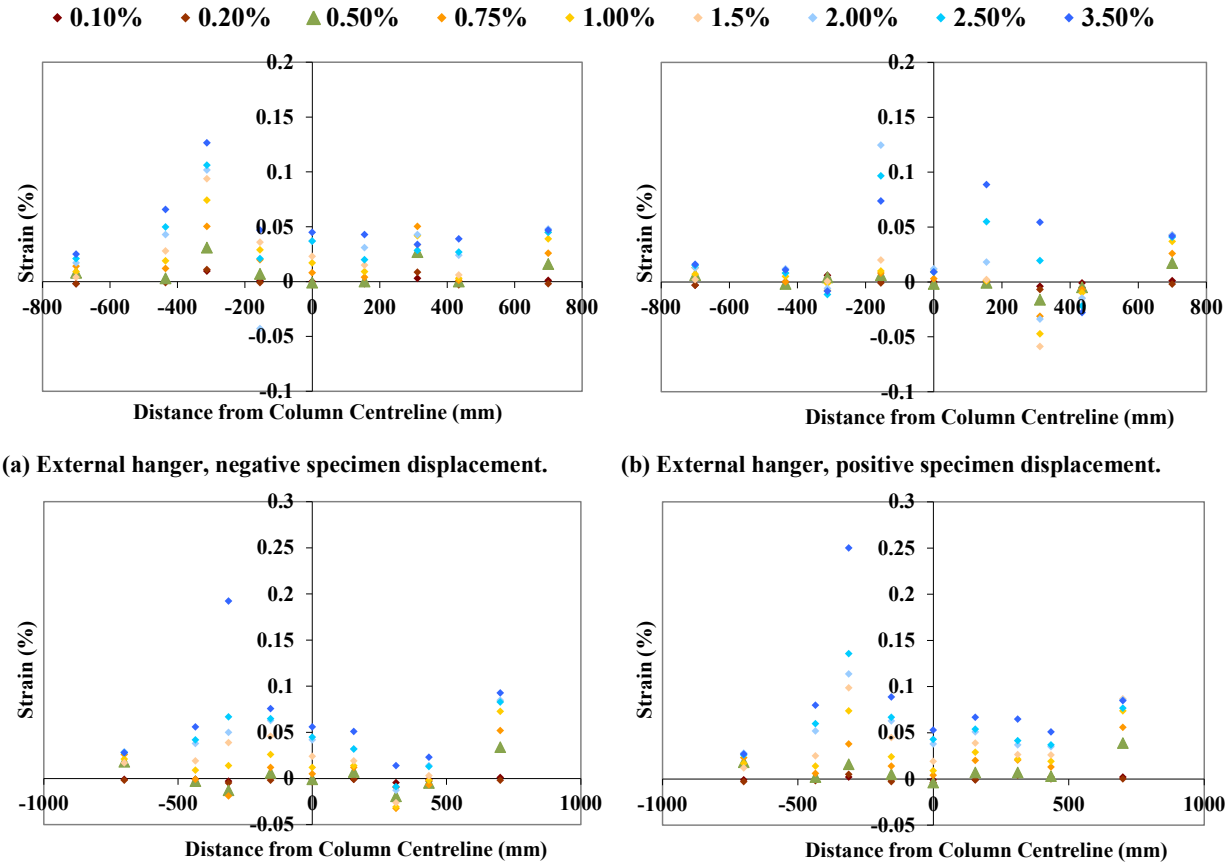

(a) External hanger, negative specimen displacement. **(b) External hanger, positive specimen displacement.**

(c) Internal hanger, negative specimen displacement. **(d) Internal hanger, positive specimen displacement.**

Figure 4-39: Bm B/1-2 east-west diagonal hanger strain profiles.

Strain penetration length can be calculated by equating the integral of the strain over the reinforcement length to the peak reinforcement strain through the top hinge. When expressed in terms of the reinforcement diameter and the characteristic yield strength, the average strain penetration length into the column for the diagonal hangers was $0.047f_yd_b$. The strain penetration length for the diagonal hangers calculated by Au (2010) was $0.044f_yd_b$.

Figure 4-40 presents the strain profiles from the north-south connection of Bm B/1-2. In comparison to Figure 4-39, a clear distinction can be seen between the connections on Grids B and 1, with beam torsion and shear dominating response. Negative specimen displacement induced positive strain in the east hanger, whereas negative specimen displacement induced negative strain in the west hanger.

The relatively high strains observed in the lower end of the hangers was likely due to the hangers contributing to both flexural and shear resistance. Hence, the hangers placed outside of the main beam cage were effective for shear transfer. However, the effectiveness in future applications will depend on the geometry and application. As shown in Figure 4-28, the absence of s-cracks in the beams of SA1 during testing confirmed the effectiveness of the additional hooked bars in the beam end region to maintain an effective shear transfer

mechanism. Recent tests have highlighted the risks of s-crack failure in slotted beams without sufficient detailing in this region (Byrne, 2012).

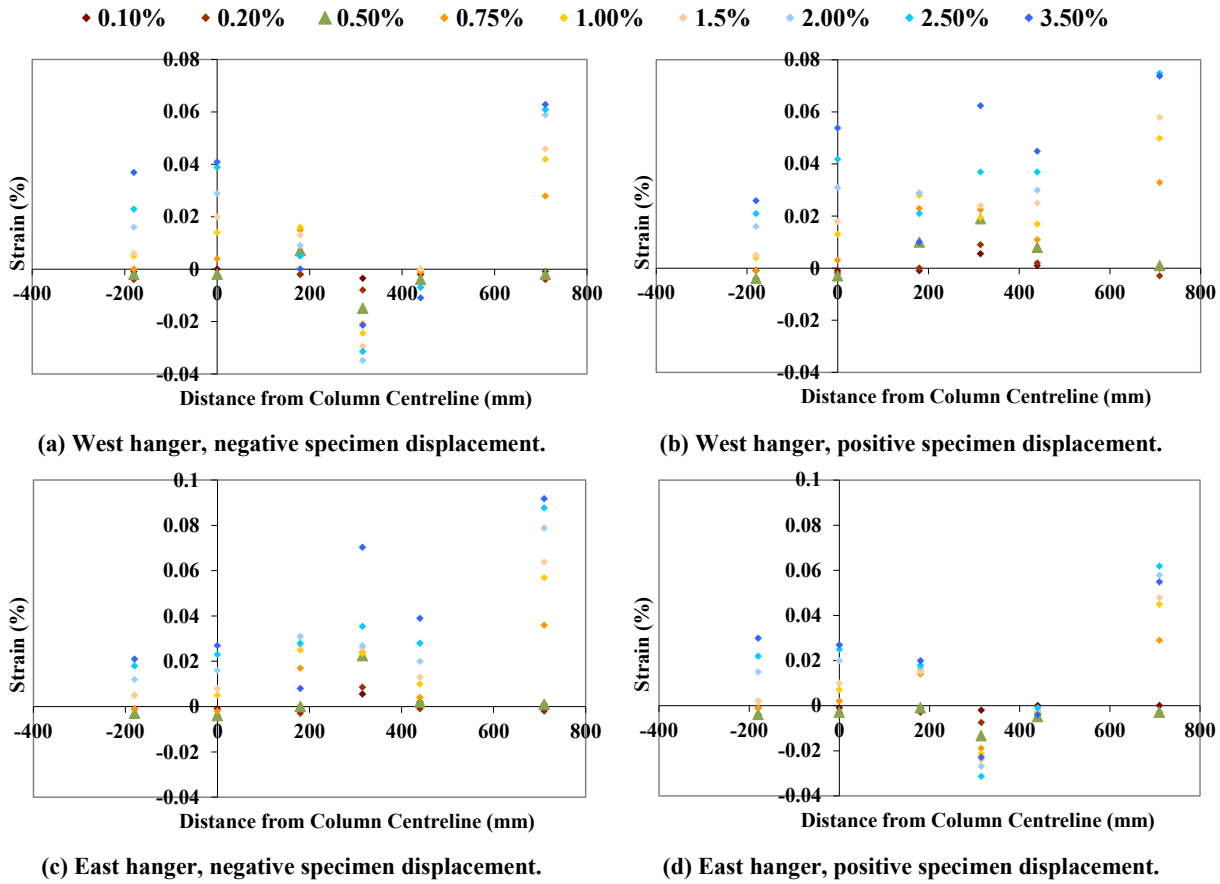

(a) West hanger, negative specimen displacement.

(b) West hanger, positive specimen displacement.

(c) East hanger, negative specimen displacement.

(d) East hanger, positive specimen displacement.

Figure 4-40: Bm B/1-2 south beam diagonal hanger strain profiles.

Figure 4-41 presents the strain profiles recorded in the diagonal hangers of connection Bm C/1-2. The loads applied along Grids A and C were different to Grid B due to the reduced floor tributary area they support, and the gravity load from the precast floors being applied to one side of the beams only. The sign of the continuity moment induced in the precast floor seating connection changes depending on the specimen loading direction. The moment applied to the supporting beams by the floor gravity load on the beam ledge is constant regardless of specimen loading direction. Hence, the moments applied along the lengths of the beams on Grid A and C are additive in one direction and subtractive in the other. This meant that the hanger strains in the connection Bm C/1-2 south did not display the same symmetry as connection Bm B/1-2 south.

The exterior hanger in connection Bm C/1-2 yielded during testing, as shown in Figure 4-41(a) and (b). The hanger yielding occurred through the top hinge section, but also on either side of the top hinge, which indicated that significant strain penetration had occurred. The strain penetration indicated by the strain data correlated well with the observed strain penetration cracking in the top hinge region during testing. To minimise the effect of strain penetration in the hangers, and to maintain the shear and torsional stiffness of the slotted

beam connection, it is recommended that confinement reinforcement is provided for the hangers.

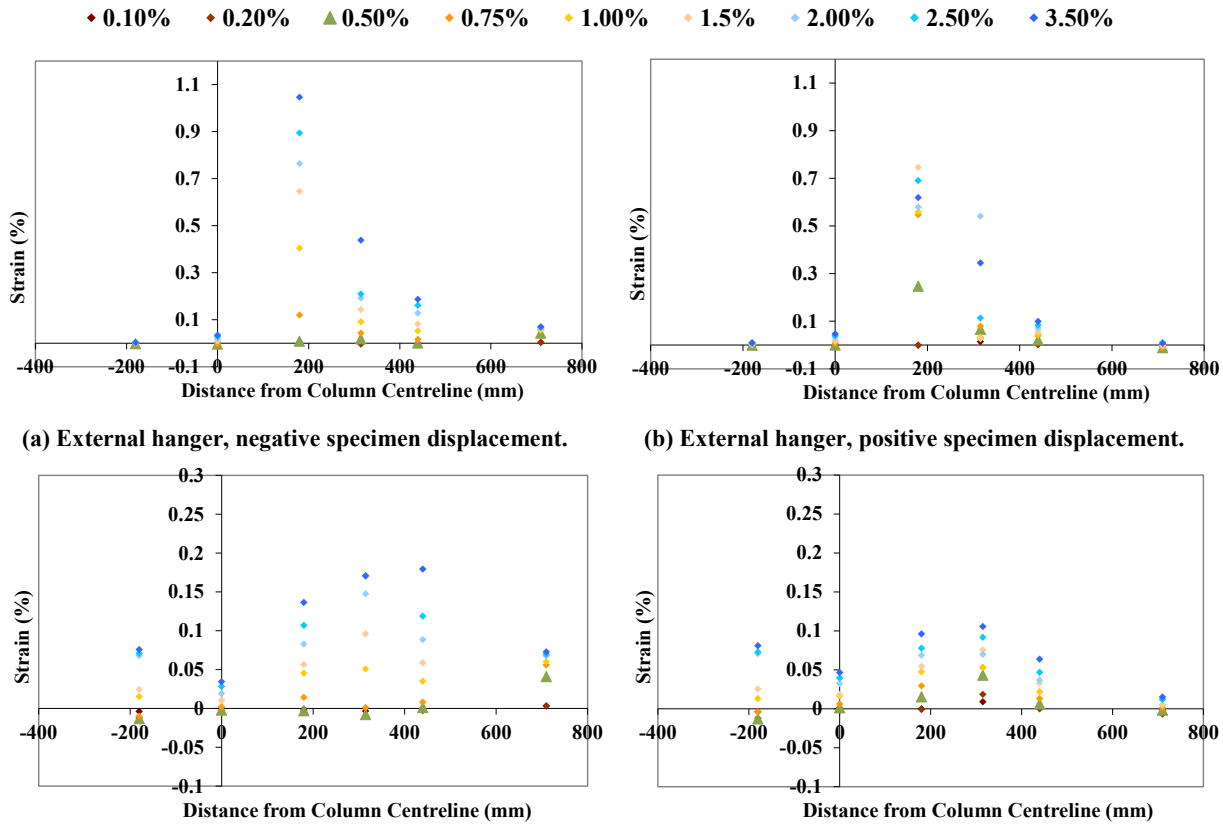

(a) External hanger, negative specimen displacement.

(b) External hanger, positive specimen displacement.

(c) Internal hanger, negative specimen displacement.

(d) Internal hanger, positive specimen displacement.

Figure 4-41: Bm C/1-2 south beam diagonal hanger strain profiles.

Figure 4-42 presents the shear deformation that occurred at the beam ends during testing. The measured shear deformation was consistent with the hanger strain data presented above. The only connections to exhibit a nonlinear response were those on Grid C, where yielding was observed in the hangers. All other connections displayed an essentially linear response.

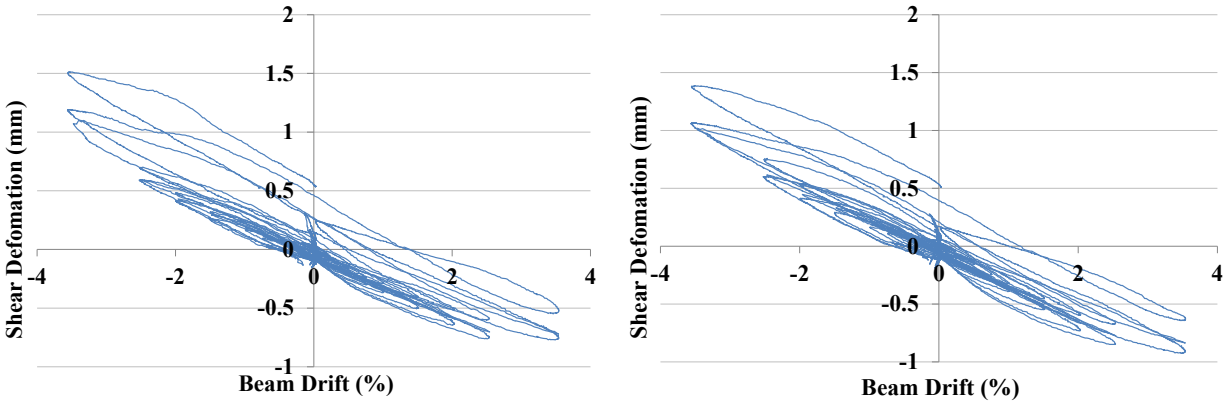

(a) Bm C/2-1 north connection.

(b) Bm C/2-2 north connection.

Figure 4-42: Shear deformation across slotted section.

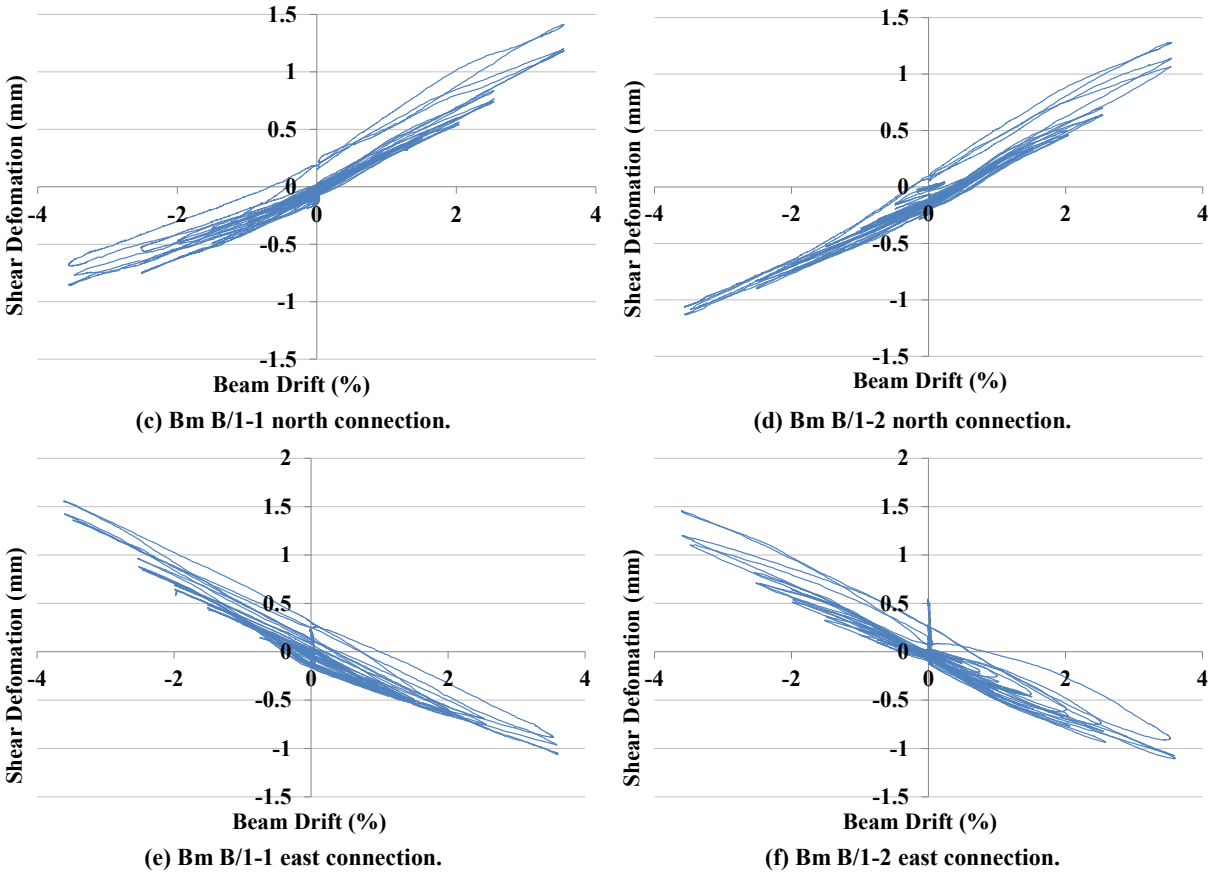

(c) Bm B/1-1 north connection.

(d) Bm B/1-2 north connection.

(e) Bm B/1-1 east connection.

(f) Bm B/1-2 east connection.

Figure 4-42: Shear deformation across slotted section (Continued).

The diagonal hangers proved effective at transferring beam shear and torsion to the column throughout testing. The three hanger detail was superfluous on Grids 1 and 2; a two hanger detail could have been used in these locations. The four hanger detail on Grid B was effective and is recommended for connections that are subjected to high shear demands. The revised three hanger detail used on Grids A and C proved effective up to 2.5% beam drift, after which some softening in shear response was observed. It is recommended that hangers positioned outside of the main beam reinforcement cage should be confined. The continuous shear hanger detail for internal connections proved effective at force transfer and reducing congestion. The supplemental hooked reinforcement provided in the beam ends to maintain the shear transfer mechanism proved effective. This detail should be used in situations where force transfer cannot be facilitated by the diagonal hangers alone, or when there is uncertainty regarding the potential effectiveness of the hangers due to their location.

It is impossible to locate the diagonal hangers to prevent entirely the strain induced by connection flexure. However, to minimise the influence of strain induced by connection flexure it is recommended that the diagonal hangers be located at approximately $0.65d_h$ below the top of the top hinge.

4.13 Beam Torsion

The strains measured in the hangers through the top hinge sections, across the width of the connections, are presented in the plots below. The strain in the hangers across a connection width indicated the force that had been induced in the hangers to resist beam torsion. Figure 4-43 presents the hangers strain from the connections along Grid 1. The connections along Grid 1 were not heavily loaded in either shear or torsion, and this was reflected in the erratic strain data that was recorded. No meaningful moments were generated along the longitudinal axes of the beams. The hanger strains recorded in the connections along Grid 1 were caused by connection flexure. The variations in recorded strain across hangers in the same connection were due to small variations in the height that the hangers were installed at.

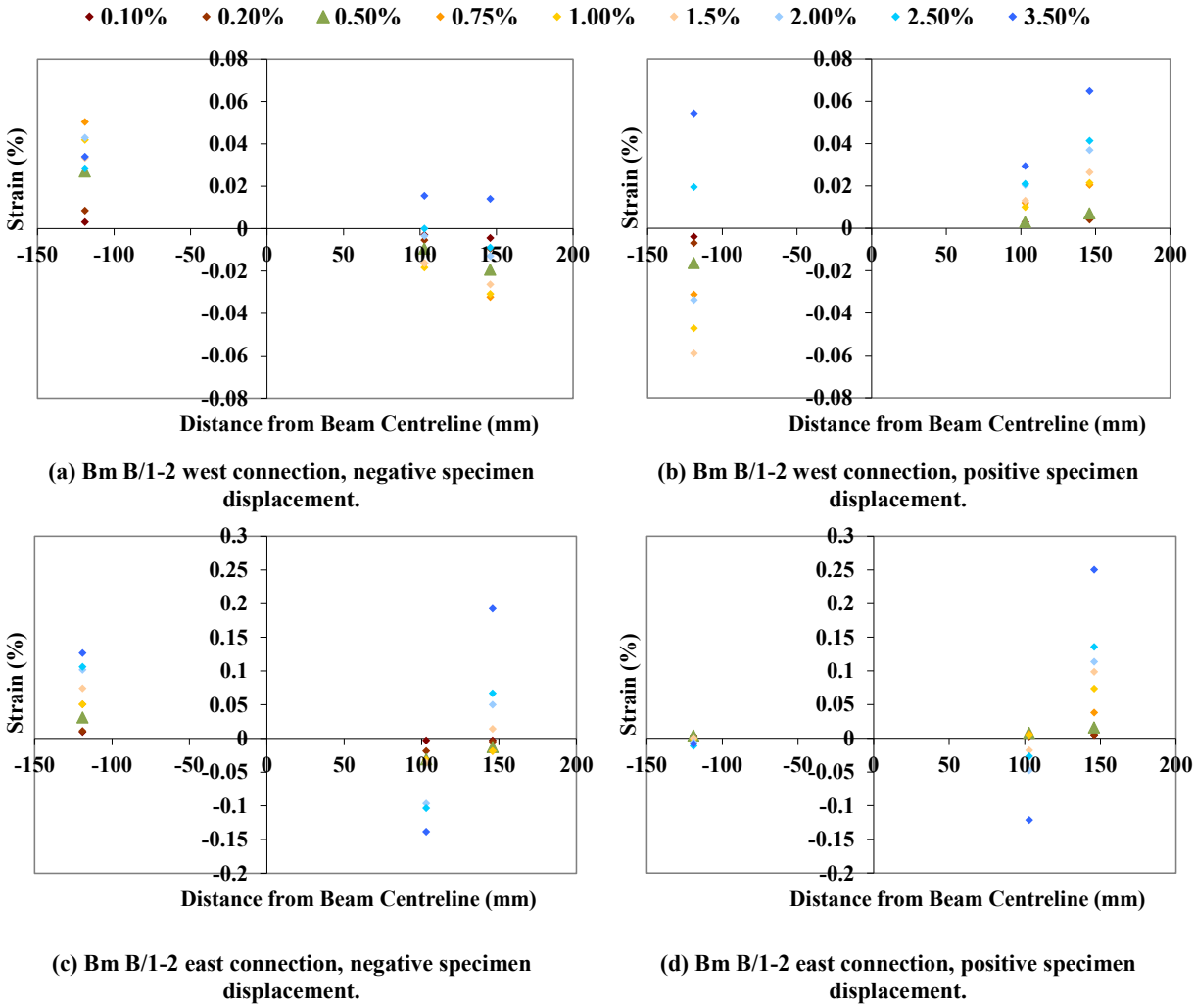

(a) Bm B/1-2 west connection, negative specimen displacement.

(b) Bm B/1-2 west connection, positive specimen displacement.

(c) Bm B/1-2 east connection, negative specimen displacement.

(d) Bm B/1-2 east connection, positive specimen displacement.

Figure 4-43: Hanger strain through slotted section in east-west direction.

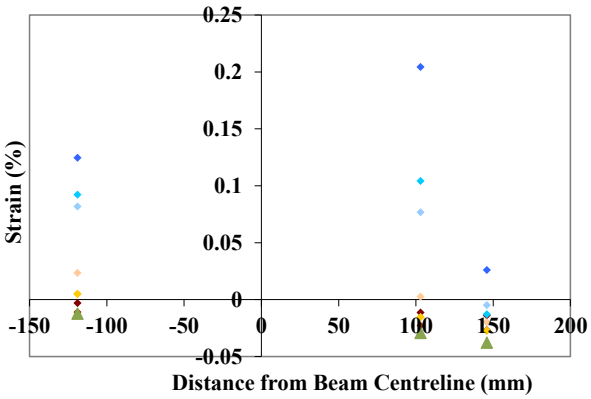

(e) Bm C/1-2 east connection, negative specimen displacement.

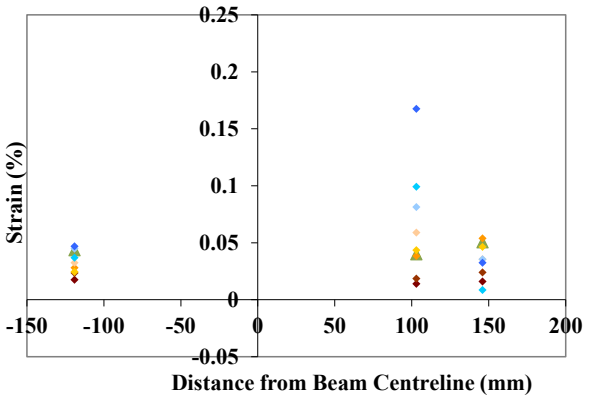

(f) Bm C/1-2 east connection, positive specimen displacement.

Figure 4-43: Hanger strain through slotted section in east-west direction (Continued).

Figure 4-44 presents the hanger strain data from connections Bm B/1-2 south and C/1-2 south. These two connections were loaded heavily in shear and torsion. Directionality can be identified in the data as a moment along the beams axes was generated to resist torsion. The axial forces that formed in the hangers to generate the moments along the beams axes were not as clear as anticipated for two reasons. The first was that strain induced by connection flexure resulted in predominantly tensile strain being recorded. The second was due to a simplification made during the hanger design. It was assumed that the concrete in the top hinge did not contribute to the torsional resistance of the beam; however, this may not have been the case. Tensile forces were transferred through the hangers; however, it is possible that for compressive forces a concrete strut mechanism was established as a reaction to the hanger tensile forces. The net result of these two mechanisms was that over several cycles a bias towards tensile strains in the hangers emerged.

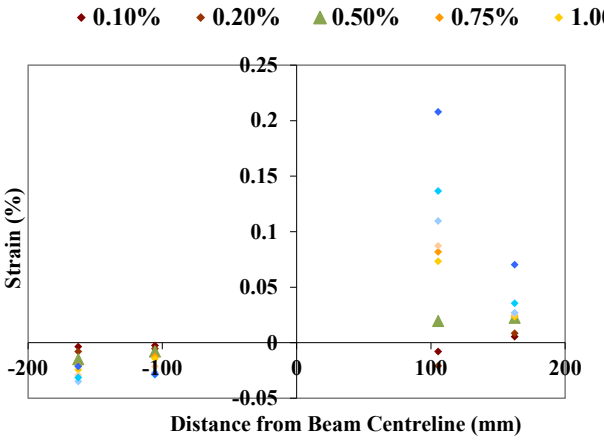

(a) Bm B/1-2 south connection, negative specimen displacement.

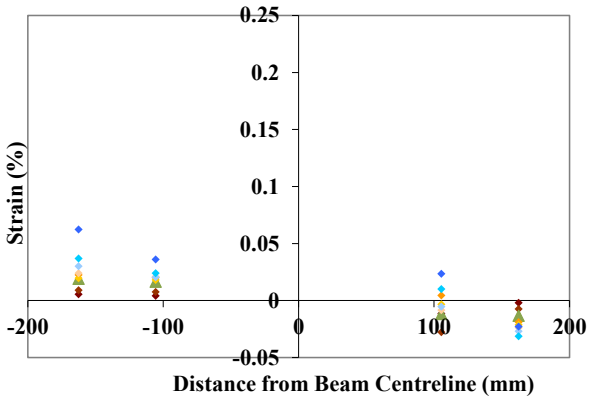

(b) Bm B/1-2 south connection, positive specimen displacement.

Figure 4-44: Hanger strain through slotted section in north-south direction.

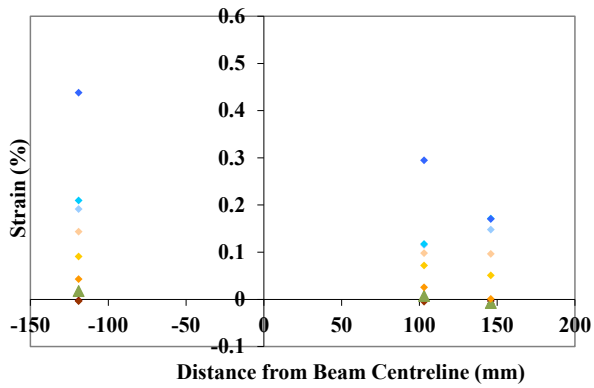

(c) Bm B/1-2 south connection, negative specimen displacement.

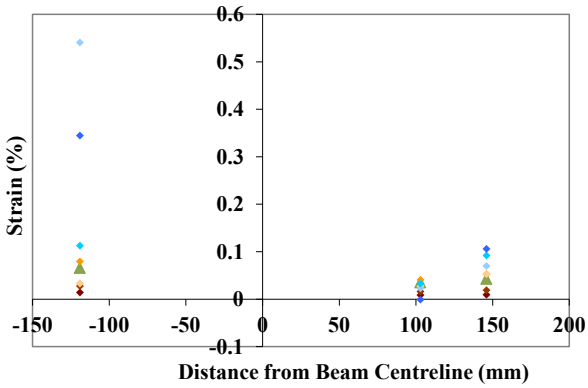

(d) Bm B/1-2 south connection, positive specimen displacement.

Figure 4-44: Hanger strain through slotted section in north-south direction (Continued).

Figure 4-45 demonstrates how tensile strains were accumulated in the hangers over the course of testing. Through the connection region strain gauges were attached in pairs on either side of the reinforcement to be able to correct for flexure in the reinforcement. The difference in the strain readings of the gauges on either side of the reinforcement was caused by reinforcement flexure. However, the strain data could not be corrected for tensile strains induced by top hinge flexure. Hence, tensile strains in the hangers were observed to accumulate during testing.

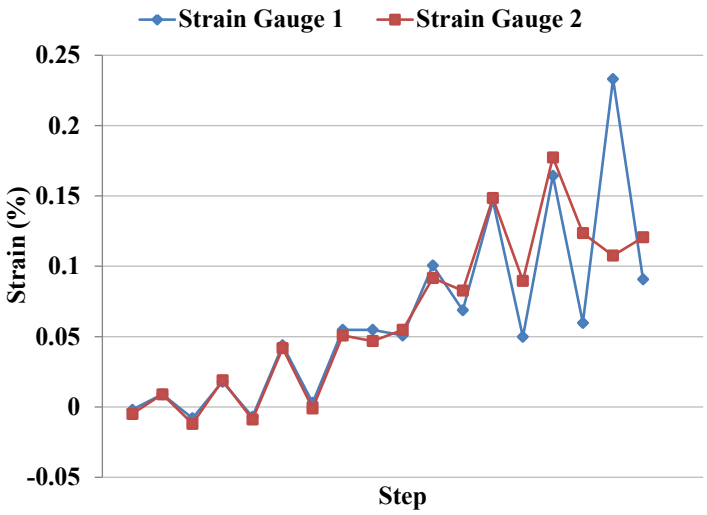

Figure 4-45: Bm C/1-2 interior hanger strain data over testing.

Figure 4-46 presents the inclination profiles along Grids B and C on Level One and Two. Because the beam inclined as the specimen was displaced, torsion is presented in the plots as a difference between recorded inclinations along the beam length. Most beam torsion occurred over the slotted beam connection. This was because the slotted beam connection was subject to the largest demands and had a reduced torsional stiffness in comparison to the remainder of the beam. There was greater inclination along the length of Grid C for positive inclinations compared to negative, whilst Grid B is comparatively even in both loading directions. On Grid C the continuity moments from the precast floor connections and the moment induced by the floor gravity load on the beam ledge were additive in one loading

direction and subtractive in the other; hence, the torsion demands on the beam were uneven and resulted in uneven beam inclination between the loading directions.

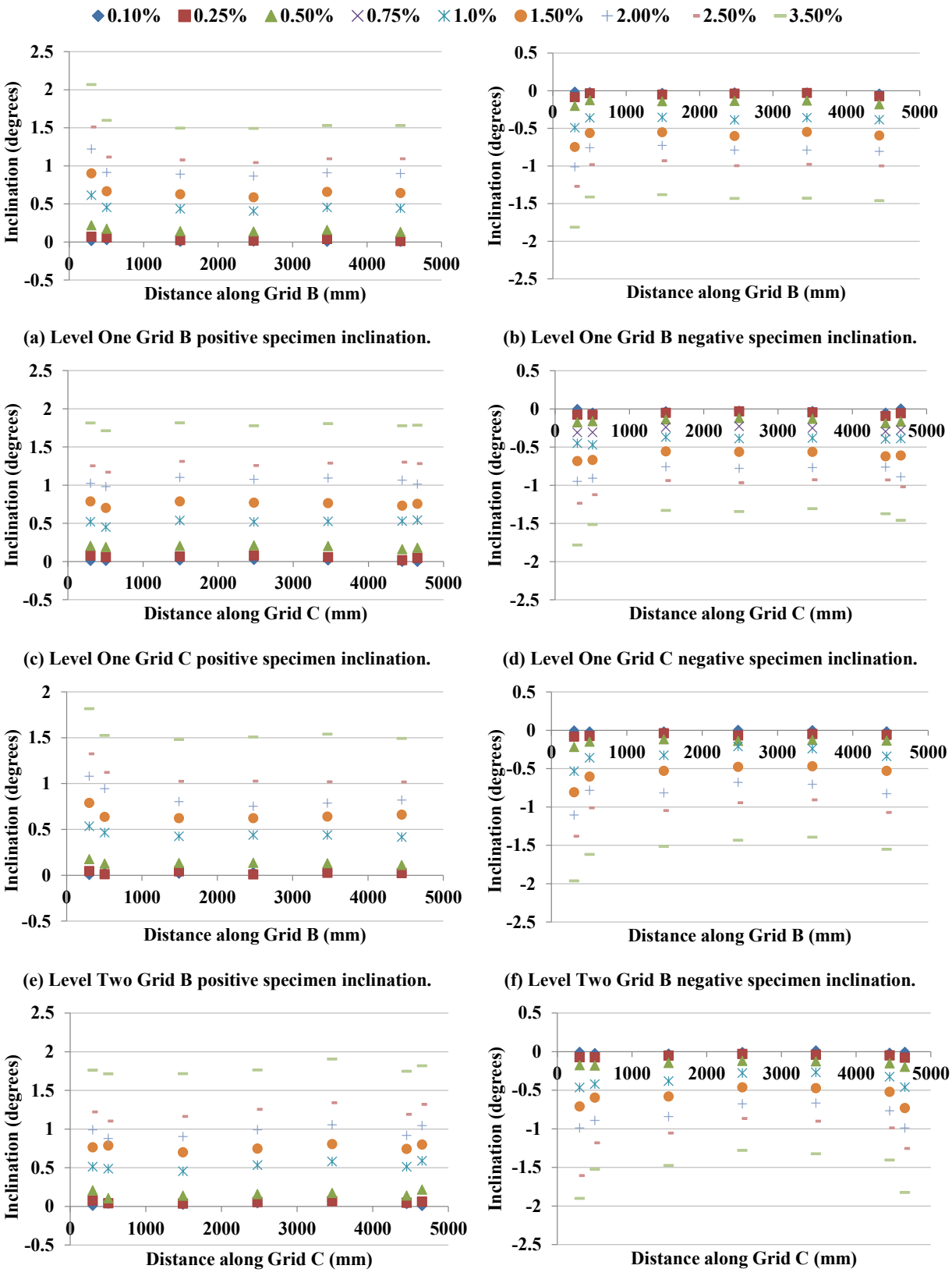

(a) Level One Grid B positive specimen inclination.

(b) Level One Grid B negative specimen inclination.

(c) Level One Grid C positive specimen inclination.

(d) Level One Grid C negative specimen inclination.

(e) Level Two Grid B positive specimen inclination.

(f) Level Two Grid B negative specimen inclination.

(g) Level Two Grid C positive specimen inclination.

(h) Level Two Grid C negative specimen inclination.

Figure 4-46: Beam inclination profiles.

Figure 4-47 presents the rotation of the ends of the beams about the longitudinal axes of the beams. The connections on Grids 1 and 2 remained linear throughout testing, as did the

connections Grids B and C on Level Two. However, the connections on Grids B and C on Level One displayed a nonlinear response during the 2.5% cycle. The nonlinear response was observed on Level One, and not on Level Two, because the continuity moment from the hollow-core connections was larger than that from the double-tee connections. This generated larger torsional demands on the Level One slotted beam connections compared to the Level Two connections.

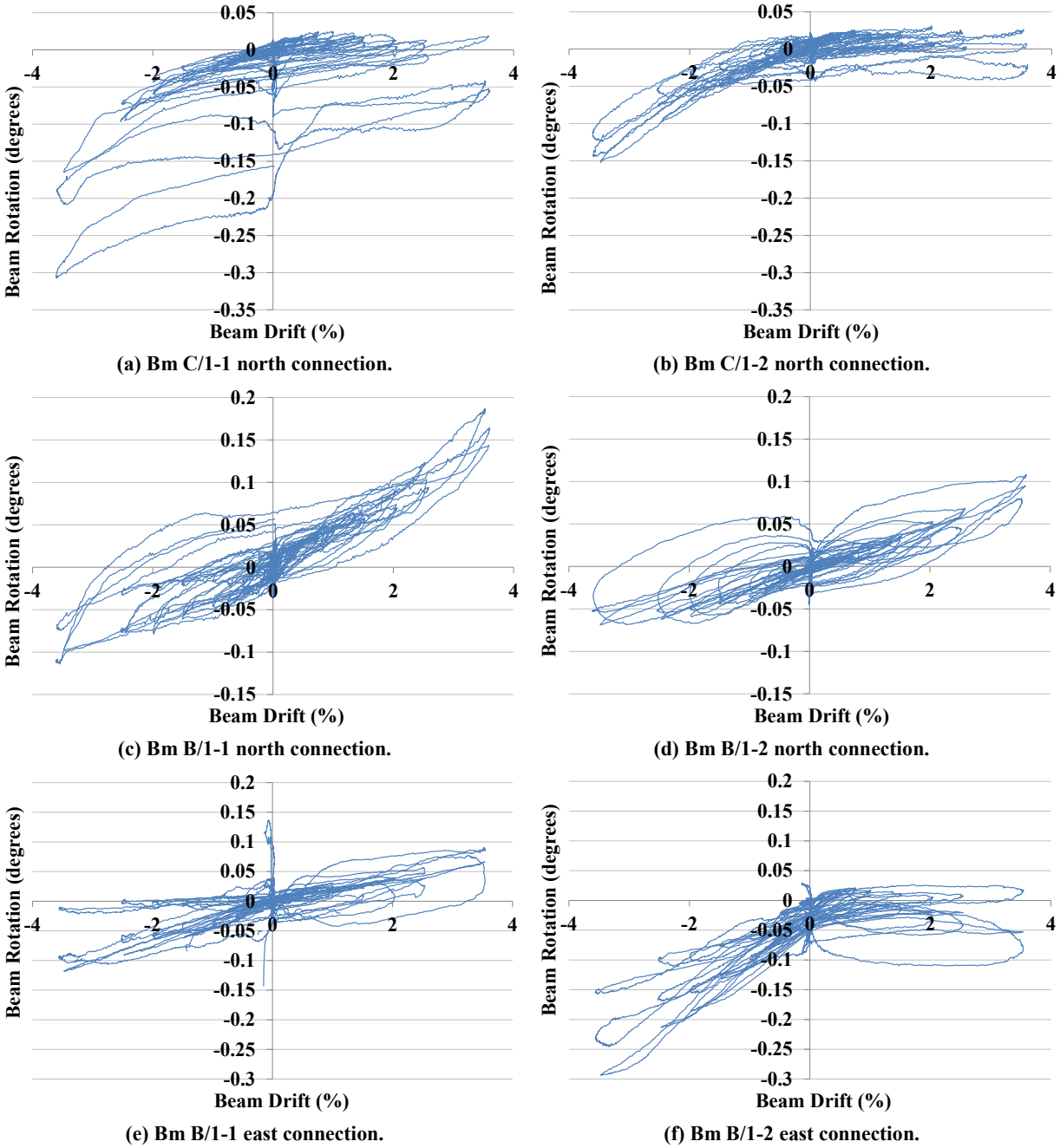

(a) Bm C/1-1 north connection.

(b) Bm C/1-2 north connection.

(c) Bm B/1-1 north connection.

(d) Bm B/1-2 north connection.

(e) Bm B/1-1 east connection.

(f) Bm B/1-2 east connection.

Figure 4-47: Fixed end beam torsional rotation.

The design of diagonal hangers must account for the worst case combination of shear, torsion, axial force and flexure. The worst case shear results from the combination of gravity and seismic actions, which are well defined. Likewise, the worst case beam torsion stems from the combination of full continuity moment and moment induced by the eccentric floor gravity

load on the beam ledge. However, the contribution of connection flexure to hanger strain cannot be reduced without decreasing the design connection rotation, or reducing the top hinge depth. However, these options are often impractical. Despite this, hanger strains induced by connection flexure were observed to contribute significantly to the overall hanger strains. The simplified design of shear hangers does not account for the compressive contribution of concrete to connection torsional resistance; however, because this contribution is difficult to quantify and can be unreliable, it is conservative to ignore it. Despite these issues, the diagonal hangers performed well overall. A linear response was observed up to damage limit state displacements. A nonlinear response was observed only during life safety limit state displacements, and only in hangers that were subject to the largest demands. No hanger failures were observed. The revised three hanger design was effective at resisting beam torsion in exterior beams. The four hanger design was effective at resisting beam torsion in internal beams. The torsional demands on beams along Grids 1 and 2 were low enough that a two hanger design would have sufficed.

Alternative details could be used in slotted beams to resist shear and torsion, such as shear keys or corbels. However, issues such as stiffness, binding and cost would need to be considered and the details thoroughly tested.

4.14 Beam Elongation

A reduction in beam elongation, compared to traditional connections, is one of the most important attributes of the slotted beam. As shown in Figure 4-48, very low beam elongation was observed in the connections of SA1. Beam elongation, expressed as a percentage of the beam height, h, peaked at 0.38%h and 0.44%h for internal and external connections respectively. In comparison, traditional connections elongate approximately 1.20%h and 2.80%h for internal and external connections respectively (Peng, 2009). Due to the increased restraint provided by the floor diaphragm, internal connections elongate less than external connections (Peng, 2009). However, in SA1 little restraint was generated by the floor diaphragm to resist beam elongation because the connections elongated very little. Hence, there was less difference in the recorded beam elongation between internal and external connections in SA1 compared to traditional systems.

It can be seen in Figure 4-48 that there was a small difference in recorded beam elongation between Levels One and Two. Because the ground floor columns are usually fixed in buildings, if beam elongation occurs and the columns are forced apart, an unwanted force distribution can be introduced in the system. This mechanism is termed a ‘first floor effect’. Because SA1 represented the lower two stories of a structure, if first floor effects were present

they would have manifested as an increase in beam axial force in Level One compared to Level Two. This would have resulted in lower beam elongation being observed in Level One compared to Level Two. Despite beam elongation being significantly less than traditional connections, the initiation of first floor effects was observed. However, the influence was very modest and would not have significantly affected the force distributions within the system. The elongation plots in this section have been plotted in terms of the beam drift of east and south connections. This was done to emphasise how gap opening and closing actions at either end of the beams largely cancel each out, resulting in minimal bay elongation.

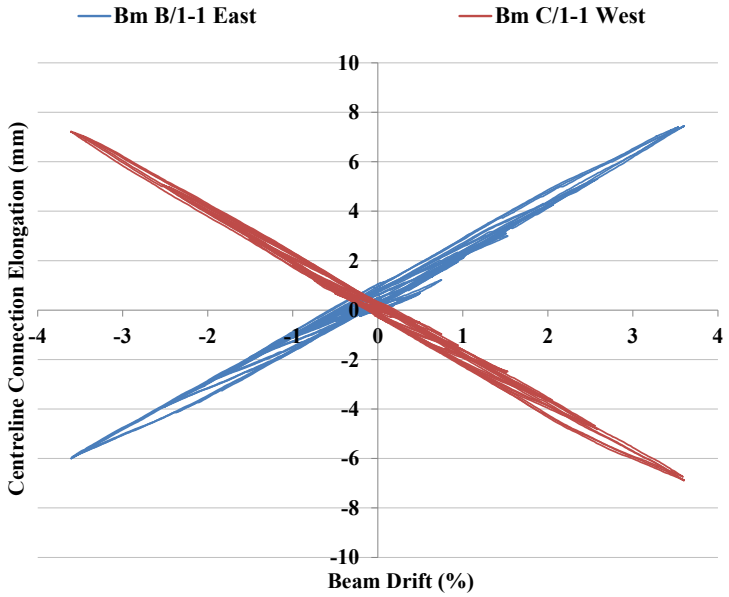

(a) Level One.

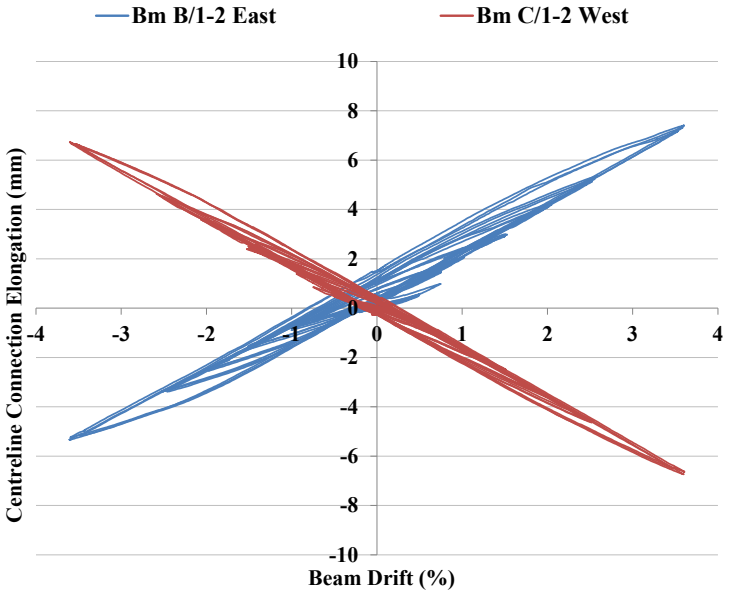

(b) Level Two.

Figure 4-48: Centreline connection elongation for Grid one, east bay.

As shown in Figure 4-49, the beam elongation recorded in the connections along Grid C were similar to that recorded in connection Bm C/1-2 west. The increased shear demands due to the gravity load from the floor did not have a significant effect on recorded beam elongation. To

control strain in the top hinge, the top longitudinal reinforcement was designed to be twice as strong as the bottom longitudinal reinforcement. If beam elongation was sensitive to the force in the bottom longitudinal reinforcement, recorded beam elongation would have increased rapidly during the elastic range and increased at a reduced rate once yield had occurred. However, a relatively steady increase in beam elongation was observed throughout testing. This suggested that it was driven by beam connection flexure. Due to the variation in neutral axis location during positive and negative flexure, strains were induced in the top longitudinal reinforcement. These strains were not completely recovered upon connection unloading and accumulated over the course of testing, resulting in beam elongation.

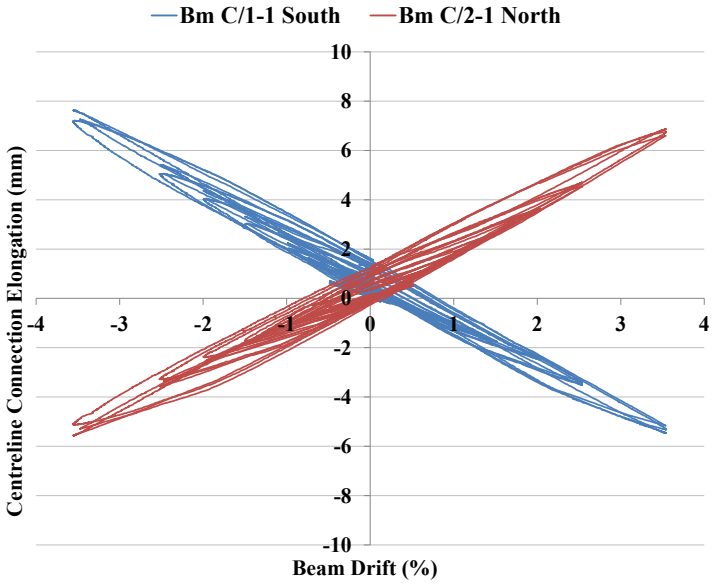

(a) Level One.

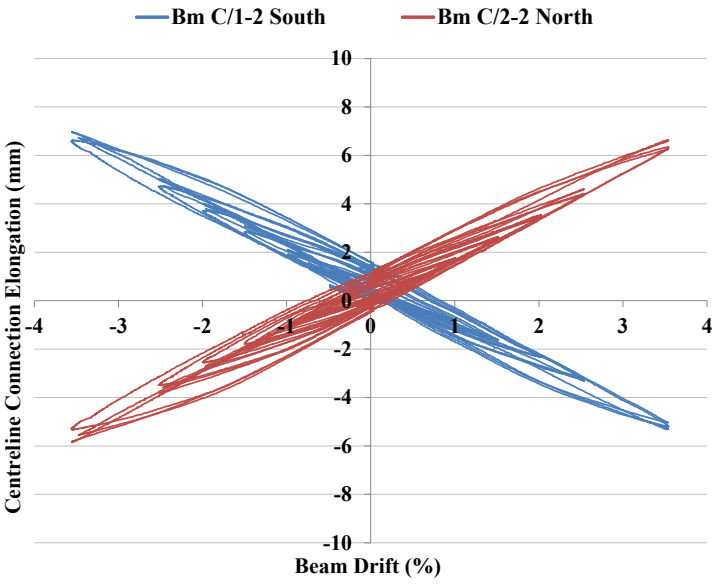

(b) Level Two.

Figure 4-49: Centreline connection elongation for Grid C.

Beam elongation was measured at the beam centreline, so positive and negative flexure, which caused opening and closing of the slot, were recorded as beam elongation. However,

because gap opening and closing occurred at either end of a bay simultaneously, the net beam lengthening effect was reduced. This is demonstrated in Figure 4-50, which presents plots of cumulative beam elongation of two of the bays in SA1. During an earthquake in a system with traditional connections, rotation occurs about the top of the beam section at one end of the beam; whilst at the other end of the beam rotation occurs about the bottom of the section. This results in the geometric contributions to beam elongation at either end of the beam being additive, which results in significantly greater beam elongation over the bay than in a comparable slotted beam system. Because bay elongation is what forces the column apart in the building, it is more important than connection elongation.

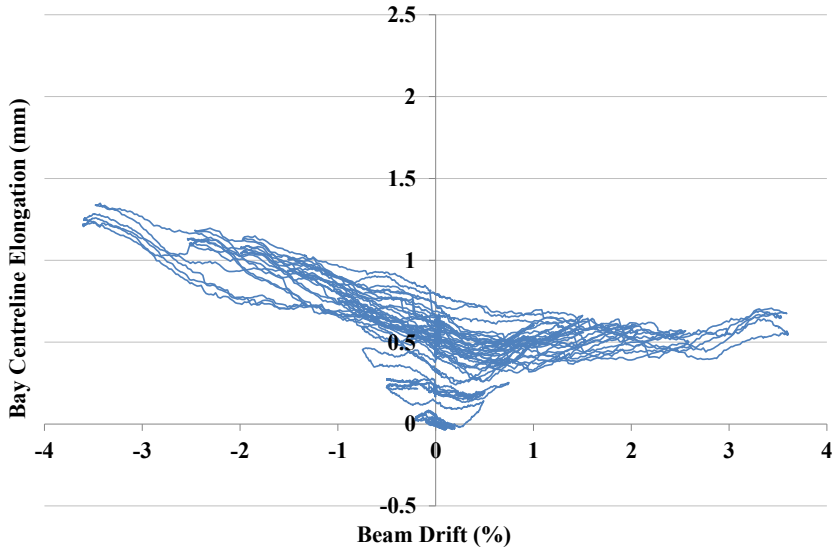

(a) Level One, eastern bay of Grid 1.

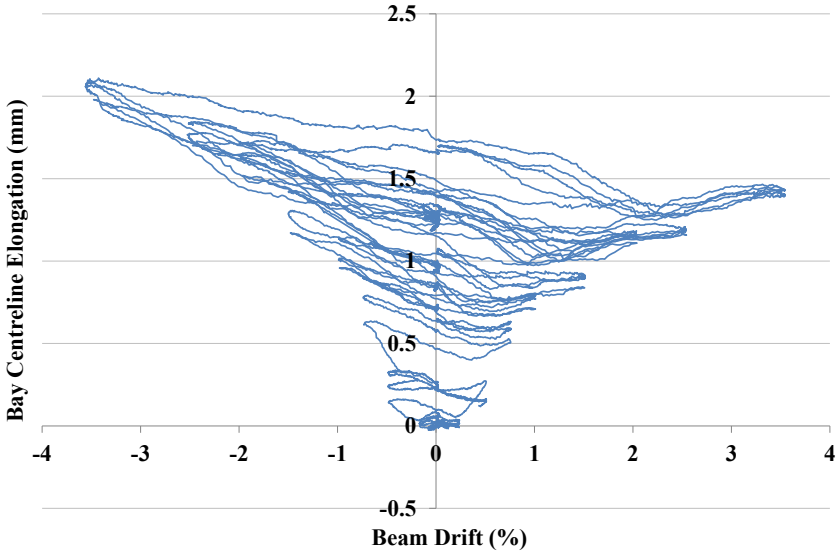

(b) Level One Grid C.

Figure 4-50: Bay cumulative elongation.

The beam elongation observed in SA1 was significantly reduced compared to what would have been expected in a comparable specimen was traditional connections. The maximum recorded beam elongation in SA1, in terms of beam depth, was 0.48%h. This was approximately 12% of the elongation that was recorded by Peng (2009) in a specimen with

traditional connection detailing. Correspondingly, the reduced beam elongation resulted in decreased damage to the adjacent floor diaphragm, maintained the precast floor seating widths and preserved the hierarchy of strength in the system.

4.15 Longitudinal Reinforcement Strain

4.15.1 Top Longitudinal Reinforcement Strain

Figure 4-51 presents the top longitudinal reinforcement strain profiles from loading in the east-west direction. Peak strains occurred through the top hinge for both the upper and lower top reinforcement. Peak strain in the upper top reinforcement occurred during negative flexure, whilst the opposite was true in the lower top reinforcement. This was due to the variation in neutral axis depth between positive and negative flexure. Strain in the top longitudinal reinforcement was related to connection flexure, rather than the force couple between the top and bottom reinforcement that was established during negative flexure. Tensile reinforcement strains were not completely recovered upon load reversal and over successive cycles the tensile strains accumulated, causing beam elongation. Yield initiated in the top reinforcement during the 2.5% cycle.

Figure 4-51(e) – (h) presents the strain data from Bm C/1-2 during loading in the east-west direction. The large spike in strain for the upper top reinforcement for both positive and negative flexure, and the low strain the lower top reinforcement, are not consistent with other readings or observations. This data is not considered reliable.

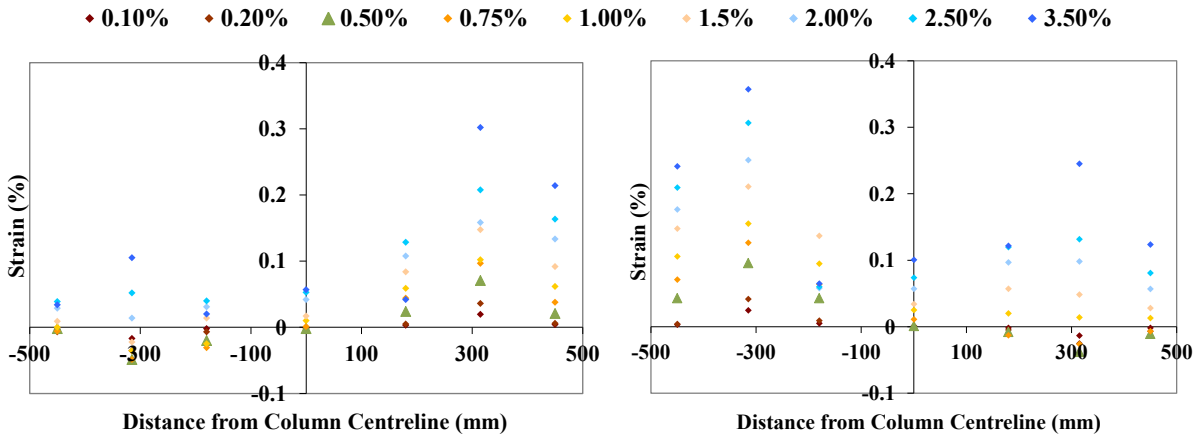

(a) Bm B/1-2 upper top reinforcement negative specimen displacement.

(b) Bm B/1-2 upper top reinforcement positive specimen displacement.

Figure 4-51: Top longitudinal reinforcement strain profiles on Grid 1.

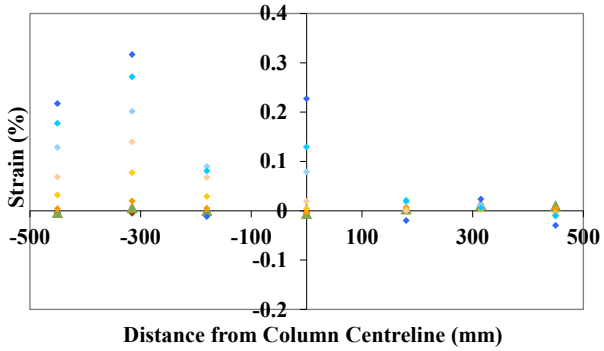

(c) Bm B/1-2 lower top reinforcement negative specimen displacement.

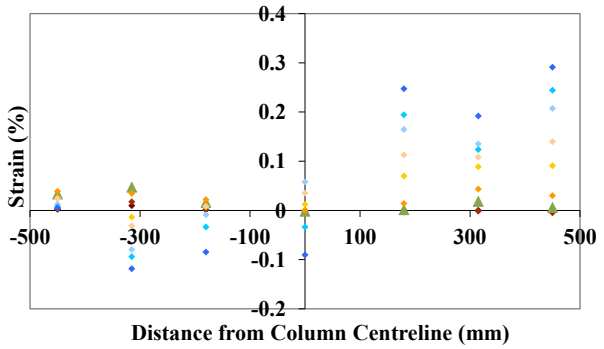

(d) Bm B/1-2 lower top reinforcement positive specimen displacement.

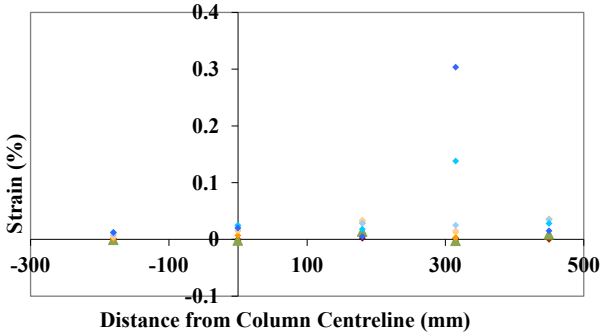

(e) Bm C/1-2 upper top reinforcement negative specimen displacement.

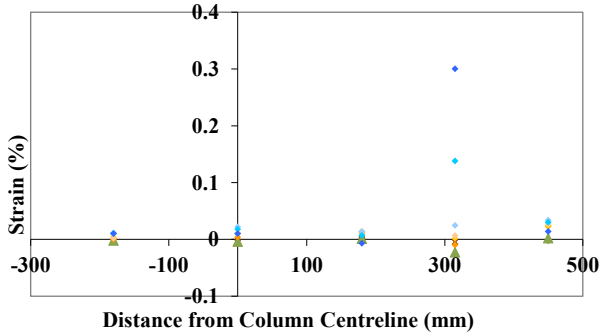

(f) Bm C/1-2 upper top reinforcement positive specimen displacement.

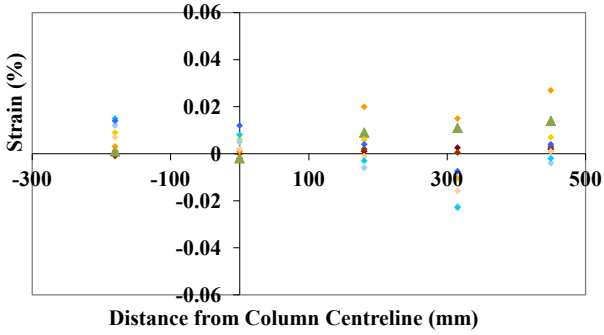

(g) Bm C/1-2 lower top reinforcement negative specimen displacement.

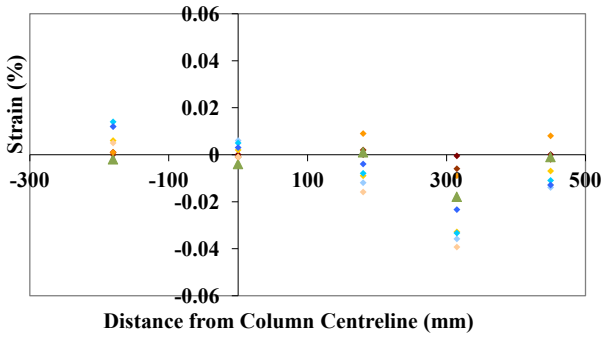

(h) Bm C/1-2 lower top reinforcement positive specimen displacement.

Figure 4-51: Top longitudinal reinforcement strain profiles on Grid 1 (Continued).

Figure 4-52 presents the top longitudinal reinforcement strain data from Grids B and C. The response in the north-south direction was similar to that observed in the east-west direction. The strain penetration either side of the slotted region was relatively even. By integrating the strain over the length of the reinforcement and equating it to the peak strain through the top hinge, a strain penetration length of $0.027f_yd_b$ was determined, which corroborated the values of $0.026f_yd_b$ and $0.027f_yd_b$ determined by Byrne (2012).

The average maximum bond stress over the effective column depth was $2.2\sqrt{f'_c}$. This value assumes full overstrength yield in tension and compression on either side of the joint and full development of strain penetration. It is unlikely that these circumstances would occur simultaneously, as evidenced by the strain data presented in Figure 4-51. The maximum average bond stress was less than the $2.5\sqrt{f'_c}$ maximum recommended by Paulay and Priestley (Paulay & Priestley, 1992).

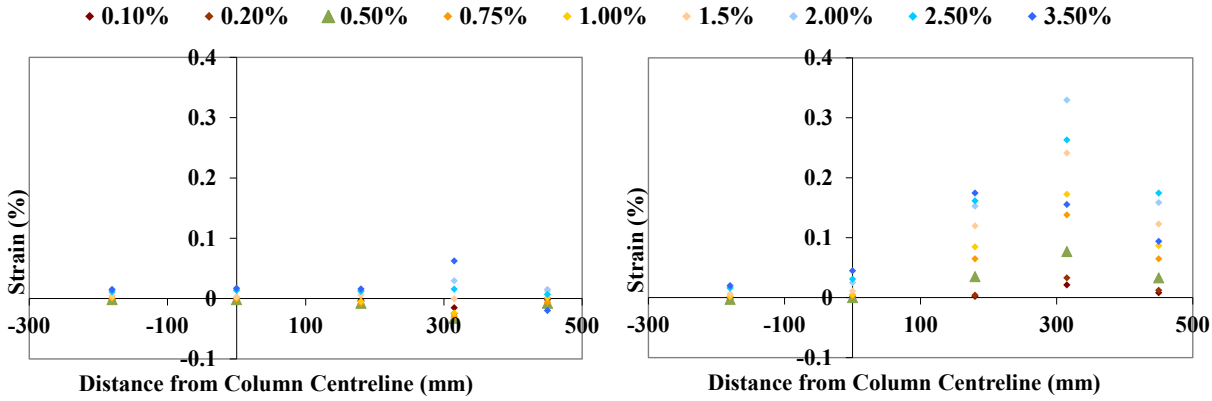

(a) Bm B/1-2 upper top reinforcement negative specimen displacement.

(b) Bm B/1-2 upper top reinforcement positive specimen displacement.

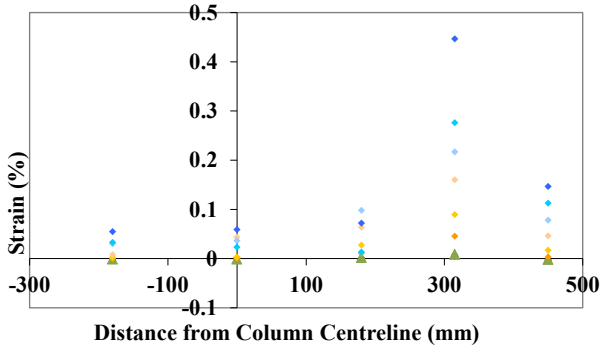

(c) Bm B/1-2 lower top reinforcement negative specimen displacement.

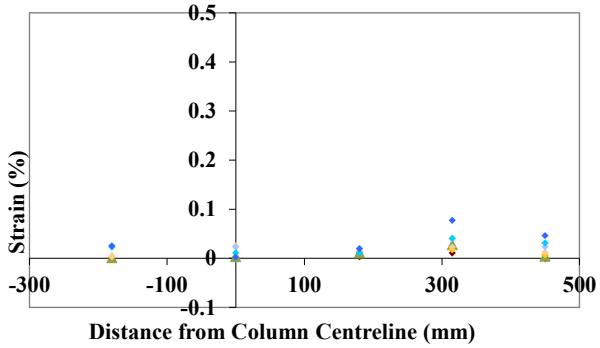

(d) Bm B/1-2 lower top reinforcement positive specimen displacement.

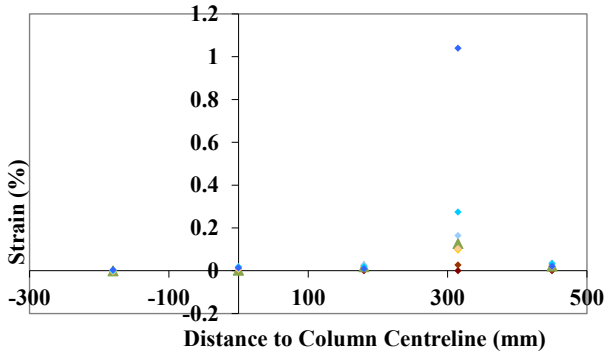

(e) Bm C/1-2 upper top reinforcement negative specimen displacement.

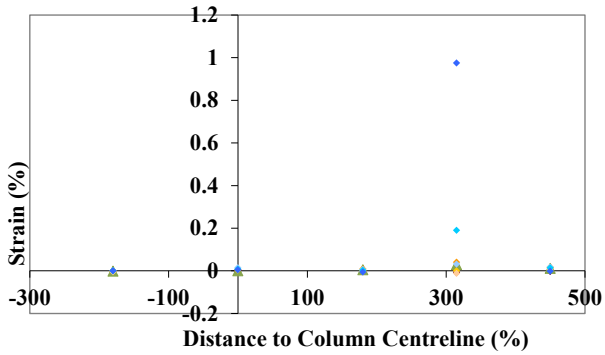

(f) Bm C/1-2 upper top reinforcement positive specimen displacement.

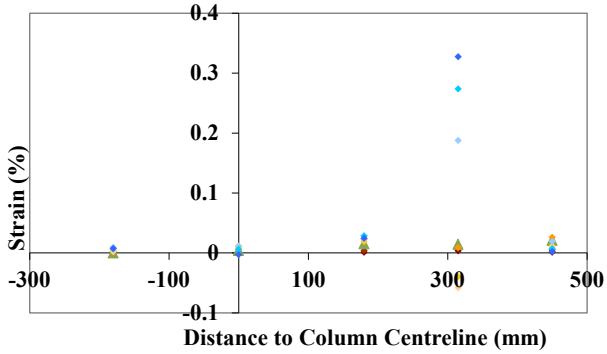

(g) Bm C/1-2 lower top reinforcement negative specimen displacement.

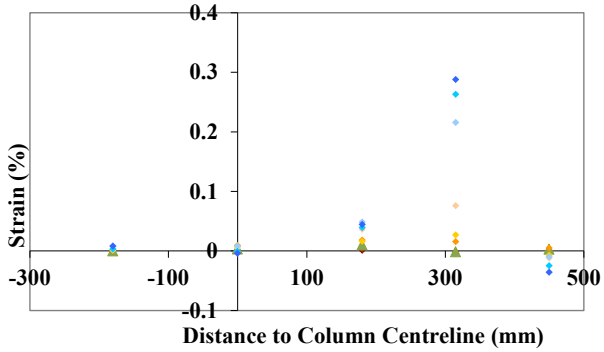

(h) Bm C/1-2 lower top reinforcement positive specimen displacement.

Figure 4-52: Top longitudinal reinforcement strain profiles on Grids B and C.

4.15.2 Bottom Longitudinal Reinforcement Strain

The strain profile for the bottom longitudinal reinforcement of the beam in the east-west direction is presented in Figure 4-53. Because of the selective weakening performed on SA1, the strain data from the upper bottom longitudinal reinforcement was incomplete.

The reinforcement strain profiles through all columns were relatively linear. The bottom reinforcement strain remained in the elastic range in the centre of the joints throughout testing. Furthermore, the integrity of the strain gauges was maintained for the entire experiment, which indicates that there was no reinforcement slip. Hence, it can be concluded that dependable anchorage of the bottom longitudinal reinforcement of the beams was attained in SA1.

The reinforcement strain in the centre of the Bm B/1-2 beam-column joint was very low. Despite connection Bm B1/-2 having to transfer twice as much force through reinforcement bond as the external connections, the reinforcement strain was comparable to that observed in the exterior connections. This was due to the supplementary reinforcement welded to either side of the main longitudinal reinforcement, which created a larger bond area and lowered bond forces and reinforcement strains.

Strain on either side of the unbonded length of reinforcement was comparable. Hence, strain penetration on either side of the unbonded length of reinforcement was similar. This was contrary to what Byrne (2012) observed, but corroborated the findings of Au (2010). It is recommended that a designer assumes that strain penetration affects both ends of the unbonded reinforcement equally.

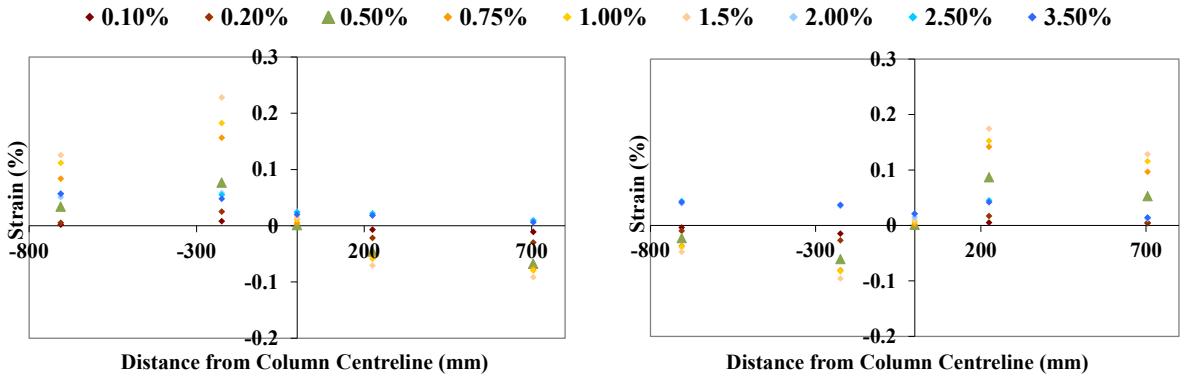

(a) Bm B/1-2 upper bottom reinforcement negative specimen displacement.

(b) Bm B/1-2 upper bottom reinforcement positive specimen displacement.

Figure 4-53: Bottom longitudinal reinforcement strain profiles on Grid 1.

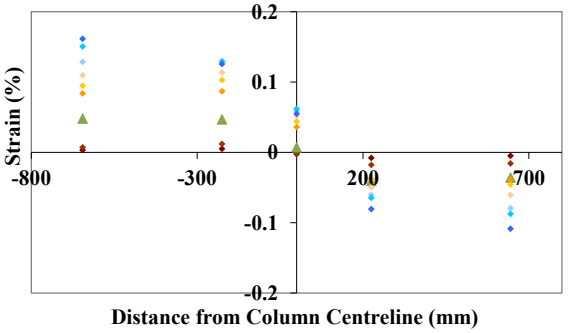

(c) Bm B/1-2 lower bottom reinforcement negative specimen displacement.

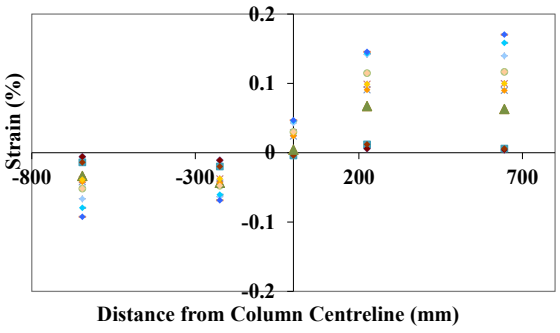

(d) Bm B/1-2 lower bottom reinforcement positive specimen displacement.

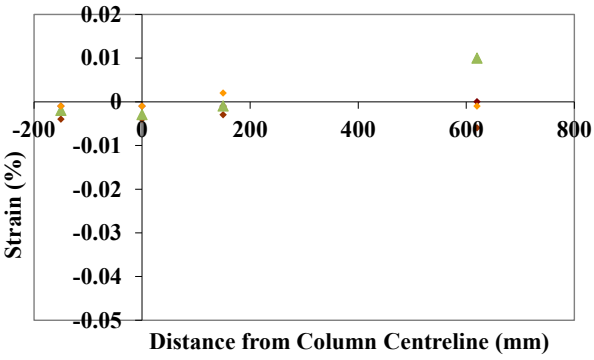

(e) Bm C/1-2 upper bottom reinforcement negative specimen displacement.

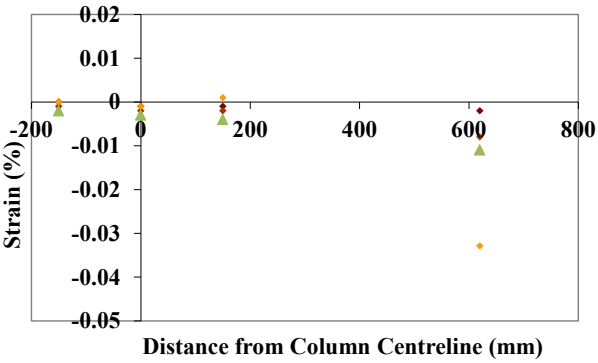

(f) Bm C/1-2 upper bottom reinforcement positive specimen displacement.

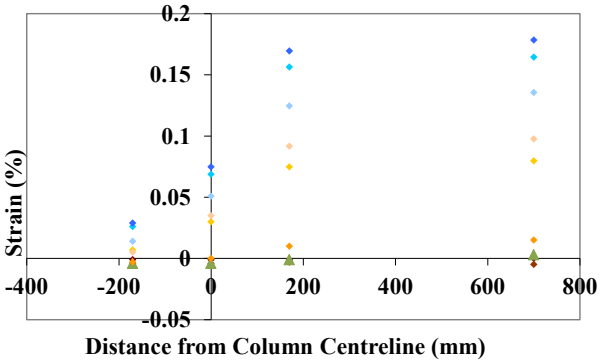

(g) Bm C/1-2 lower bottom reinforcement negative specimen displacement.

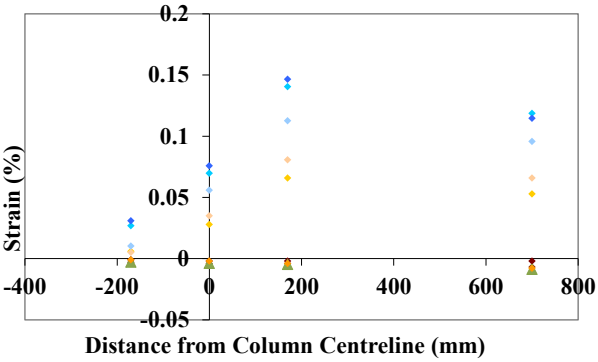

(h) Bm C/1-2 lower bottom reinforcement positive specimen displacement.

Figure 4-53: Bottom longitudinal reinforcement strain profiles on Grid 1 (Continued).

Reinforcement bond stress can be determined by differentiating the strain profile. However, there were not sufficient strain gauges through the beam-column joint for this method to be meaningful. The average bond stress over the beam-column was instead estimated by considering the reinforcement forces on either side of the joint, and the effective column width. Without the supplementary reinforcement welded to the main reinforcement, the maximum average bond force through the interior connections was approximately $1.21\sqrt{f'_c}$. With the addition of the supplemental reinforcement, the maximum average bond dropped to $0.66\sqrt{f'_c}$. In the exterior connections it was assumed that all reinforcement force was transferred through bond prior to the 90° return in the reinforcement, and a maximum average bond stress of $0.82\sqrt{f'_c}$ was calculated. The peak bond stress values calculated for SA1 were within the $2.5\sqrt{f'_c}$ maximum bond stress limit recommended by Paulay and Priestly (1992).

Figure 4-54 presents the strain profiles from the bottom longitudinal reinforcement in the north-south direction. The data from the bottom reinforcement of Bm C/1-2 in the north-south direction was considered erroneous and not reliable for positive specimen displacement.

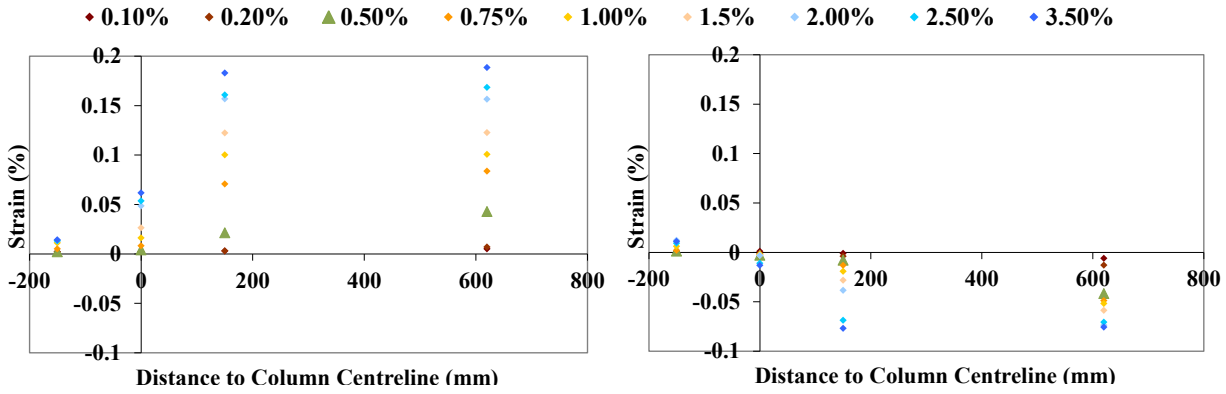

(a) Bm B/1-2 upper bottom reinforcement negative specimen displacement.

(b) Bm B/1-2 upper bottom reinforcement positive specimen displacement.

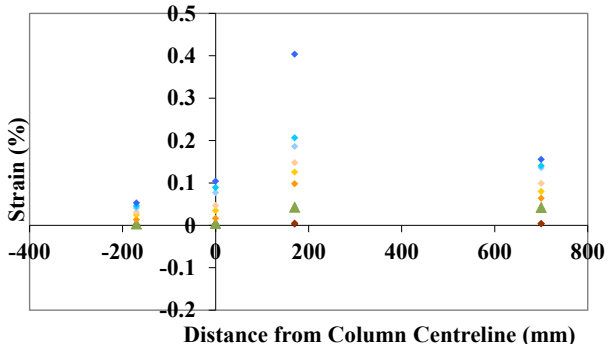

(c) Bm B/1-2 lower bottom reinforcement negative specimen displacement.

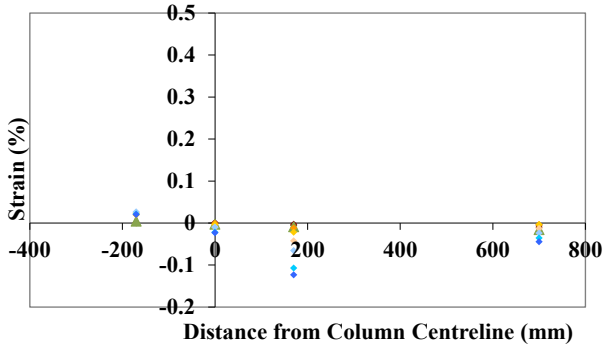

(d) Bm B/1-2 lower bottom reinforcement positive specimen displacement.

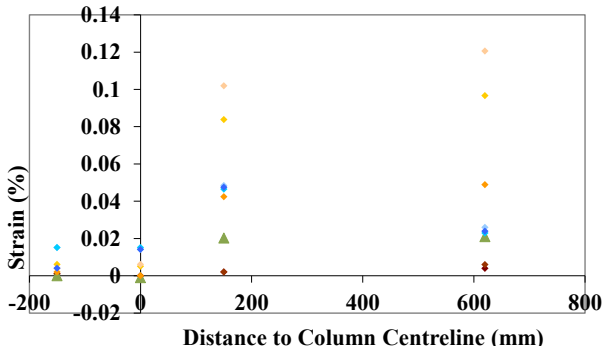

(e) Bm C/1-2 upper bottom reinforcement negative specimen displacement.

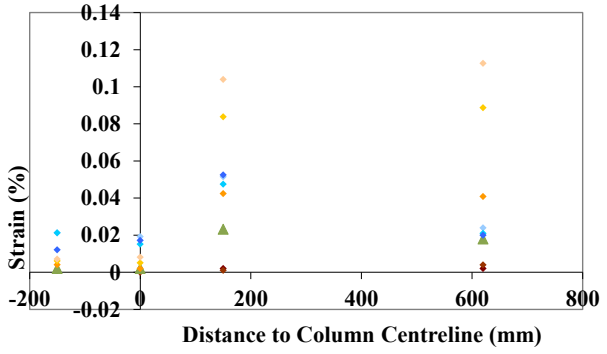

(f) Bm C/1-2 upper bottom reinforcement positive specimen displacement.

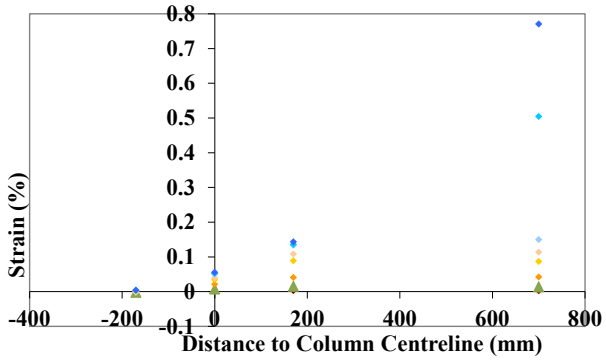

(g) Bm C/1-2 lower bottom reinforcement negative specimen displacement.

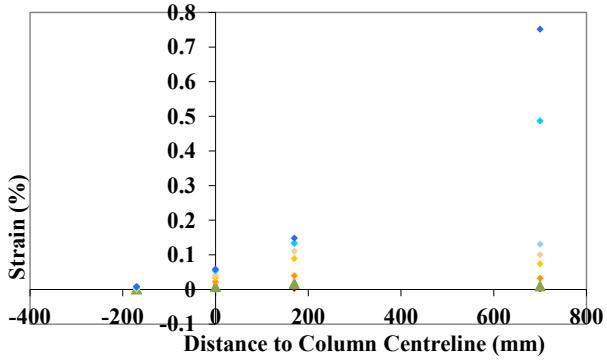

(h) Bm C/1-2 lower bottom reinforcement positive specimen displacement.

Figure 4-54: Bottom longitudinal reinforcement strain profiles on Grids B and C.

Because the strain in the unbonded length of reinforcement was unknown, direct calculation of strain penetrations lengths by the integration of recorded strain data was impossible. Strain gauges were not installed over the unbonded lengths of reinforcement because the reinforcement preparation required to attach the strain gauges could have hastened reinforcement failure. However, direct measurement of the strain penetration length was undertaken. It was found that the maximum strain penetration into the column was approximately 48mm, or $0.01f_yd_b$. This strain penetration value was slightly higher than the value determined by Byrne (2012). Due to the two layers of bottom longitudinal reinforcement SA1 had, the stirrups on either side of the bottom longitudinal reinforcement were further apart than they were in the specimens tested by Byrne. The stirrups either side of the longitudinal reinforcement form a compressive strut, at approximately 45°, to the longitudinal reinforcement and the unconfined concrete is spalled (Viwathanatepa et al., 1979). This mechanism is often termed cone-type pull-out. Hence, the further apart the adjacent stirrups are, the more strain penetration can develop. The supplementary reinforcement welded to the bottom longitudinal reinforcement was effective at reducing the strain penetration length. Figure 4-55 compares the strain penetration cone-type pull-out mechanism observed in external and internal connections. The additional reinforcement prevented the strain from penetrating as far into the interior joint, which resulted in less concrete being spalled and a greater column effective width being maintained.

(a) Exterior joint elevation. **(b) Interior joint elevation.**

Figure 4-55: Strain penetration comparison.

The bottom longitudinal reinforcement in slotted beams is subject to large inelastic strain cycles which hasten low-cycle fatigue failure. A major consideration in the assessment of the residual capacity of a slotted beam following an earthquake is the residual strain capacity of the bottom longitudinal reinforcement. As described in Section 4.6, one reinforcement

fracture was observed during the 3.5% cycle. In Chapter 7 an investigation into the low-cycle fatigue life of reinforcement in slotted beams is presented.

Given the low strain observed in the centre of the column, the low maximum average bond stresses and the absence of any observed bond slip, it can be concluded that adequate anchorage for the bottom longitudinal reinforcement was provided in all connections. Given the effectiveness of the 90° returns in exterior connections and supplementary welded reinforcement in interior connections, it is possible that the dimensions of columns in slotted beam systems could be reduced. However, further research is required on a variety of bond lengths before this recommendation can be made. Any benefits from a reduction in column dimensions should be weighed up against the increased reinforcement congestion that could result.

4.16 Floor Diaphragm Performance

4.16.1 Precast Floor Unit Seating Loss

The loss of seating width during an earthquake is of critical importance in a structure built using precast flooring systems. The hollow-core seating detail used in SA1 differs from that specified by NZS3101:2006 (Standards New Zealand, 2006). The seating detail was designed to minimise the continuity moment generated and was based on research conducted by Lindsay (2004). However, the seating detail used also had reduced restraint against seating loss, and reduced redundancy in the gravity support system if the entire seating width were lost.

Figure 4-56(a) and (b) present the change in seating width recorded in Level One and Two respectively. Unseating on both levels was very low; a maximum loss of approximately 1mm was recorded at each end of the precast floor units. The precast floor depth at the connection to the supporting beam on Level Two is half that of Level One. Hence, similar seating loss over both levels indicates that seating loss was not related to relative rotations between the flooring unit and the supporting beam. Rather, seating loss was related to bay elongation, which was approximately an eighth of that recorded in structures with traditional connections.

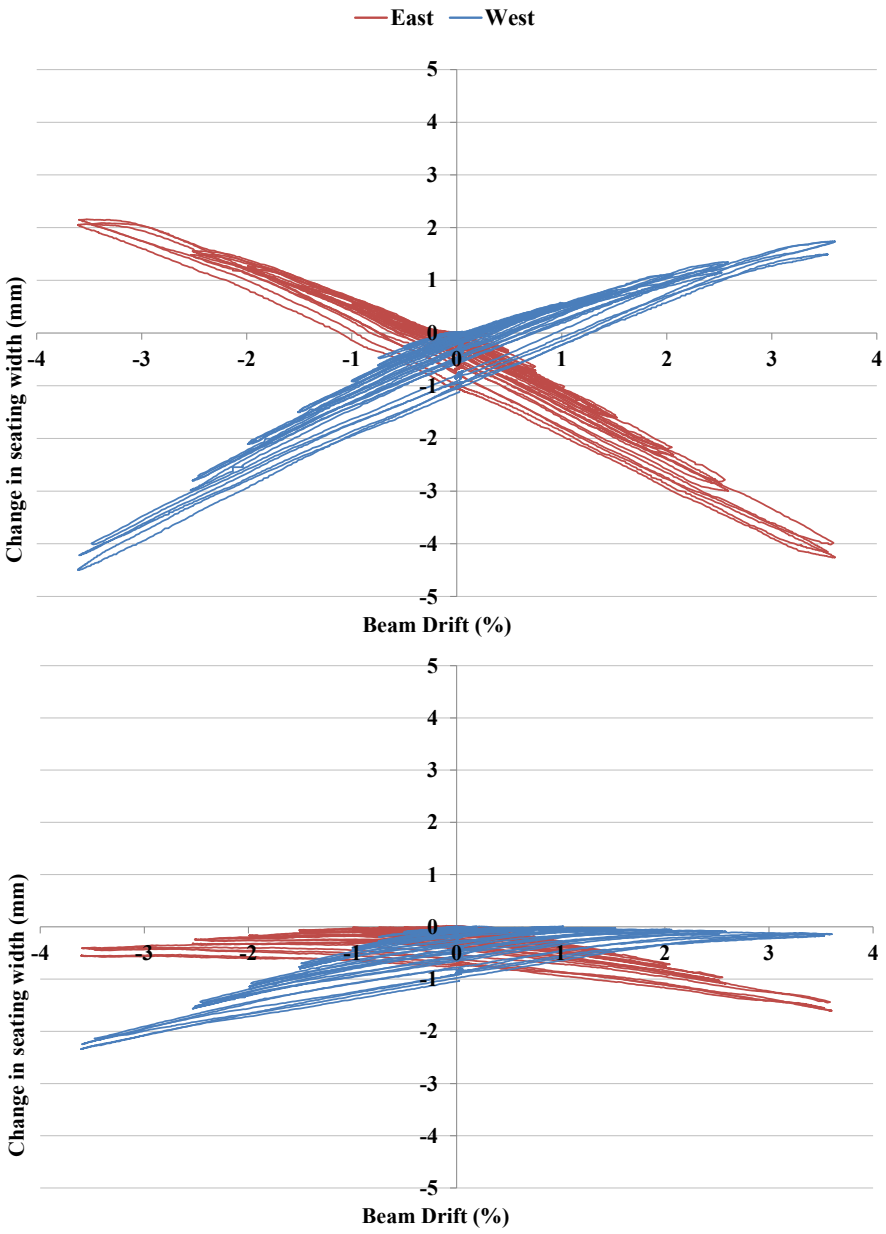

(b) Level Two northern double-tee unit.

Figure 4-56: Change in precast flooring unit seating width.

In a system built using traditional connection detailing, significant beam elongation can occur during an earthquake. Hence, there is a need for redundancy in the precast floor seating detailing to provide an alternative gravity support mechanism if the seating width is completely lost. However, because beam elongation is significantly reduced in a slotted beam system, there is a reduced need to provide redundancy is the precast floor connection detailing. Furthermore, the large continuity moment that the precast floor seating detail specified in NZS3101:2006 can produce could increase the beam torsion demand and complicate the design of the diagonal hangers (Standards New Zealand, 2006).

Figure 4-57(a) presents the compressible backing board that was placed behind the hollow-core units on Level One. The impression of the end of the hollow-core unit left in the backing board showed that the intended relative rotation between the end of the hollow-core unit and

the supporting beam took place during testing. However, as shown in Figure 4-57(b), binding between the base of the precast flooring unit and the supporting ledge was observed. The precast floor connection binding resulted in several undesirable effects, such as damage to the bearing strips, larger continuity moments, wider cracks above the seating and ledge concrete spalling. These undesirable effects could be avoided by using a bearing strip with a lower coefficient of friction. Using two low-friction strips placed on top of each other would present an acceptable solution. However, a two-piece bearing strip with a low friction contact surface would be preferable.

(a) Crushed backing board showing that the intended seating displacements had occurred.

(b) Damaged low-friction strip due to binding between the hollow-core soffit and supporting ledge.

Figure 4-57: Hollow-core seating displacements observed during demolition.

The seating detail used in SA1 is recommended for slotted beam structures. However, a lower friction bearing strip is recommended to reduce continuity moments. The compressible backing board should be sized to allow for the maximum expected hollow-core rotation and should be as compressible as practical.

4.16.2 Longitudinal Floor Diaphragm Strain

The strain in the eastern portion of the concrete floors on both levels of SA1 were measured during testing using the DEMEC grid described in Section 3.8.2. Measurements were taken during both the uniaxial and biaxial portions of the loading protocol at 1%, 2.5% and 3.5% beam drift. Strain was calculated based on an original baseline reading, as described in Section 4.3. Additional DEMEC results are presented in Appendix C.3.

4.16.2.1 East-west Longitudinal Floor Diaphragm Strain

The east-west longitudinal strain contours for Level One at 3.5% beam drift are presented in Figure 4-58. Significant strain occurred over the top of the precast floor connections. During eastern specimen displacement cracks opened up above the eastern end of the precast floor units, which are visible as regions of negative strain in Figure 4-58(a). The crack widths

above all precast floor connections were in excess of what was required to induce yield in the starter reinforcement. This was evidence of significant continuity moment having been generated in the precast floor connections. Tensile strains from negative flexure were induced over a wider area than compressive strains from positive flexure. It can be seen in Figure 4-58(c) and (d) that the cracks above the precast floor connections were not fully recovered when the specimen was unloaded in the east-west direction.

Little strain was observed in the east-west direction when the specimen was loaded in the north-south direction. The strain that was observed in the east-west direction during specimen displacement in the north-south direction was concentrated around the columns due to warping. During biaxial loading, the same strain patterns discussed above are present. However, increased strain around the columns due to warping was observed. In general, the recorded strains during biaxial testing were well represented by the superposition of the strain recorded in the orthogonal loading directions.

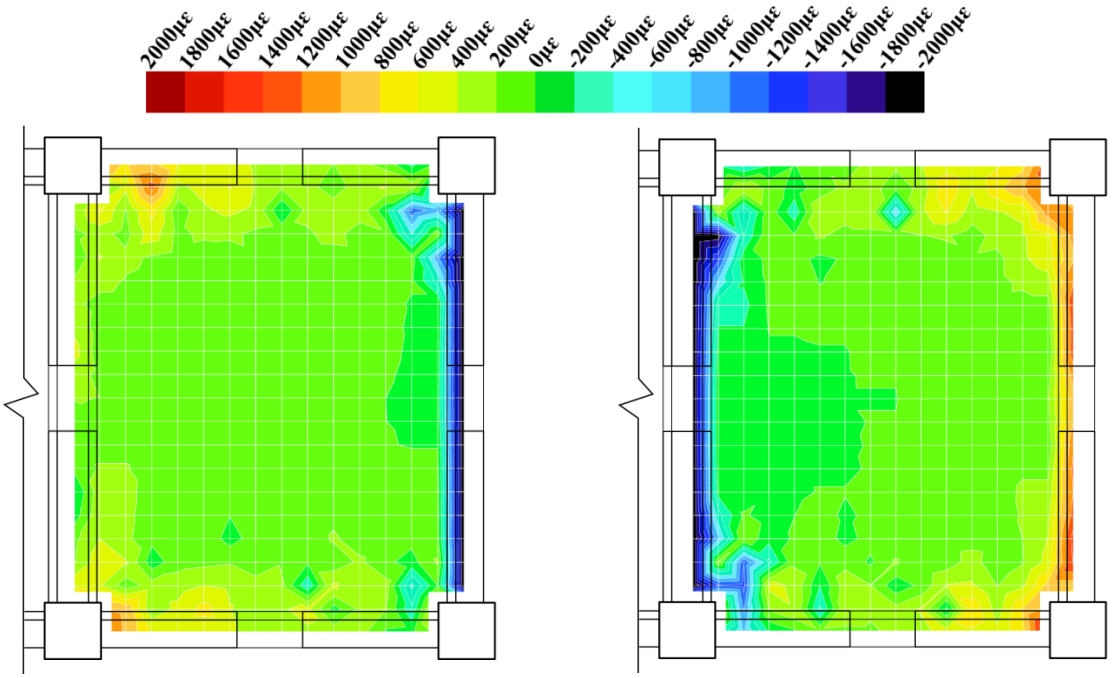

(a) Specimen displacement east. **(b) Specimen displacement west.**

Figure 4-58: Level One floor strain contours from east-west DEMEC measurements at 3.5% beam drift.

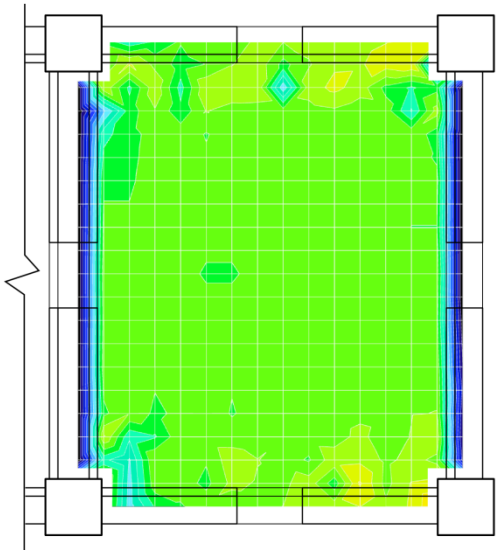

(c) Specimen displacement north.

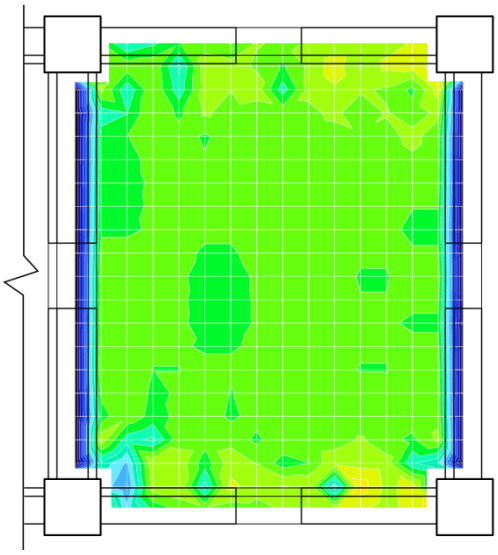

(d) Specimen displacement south.

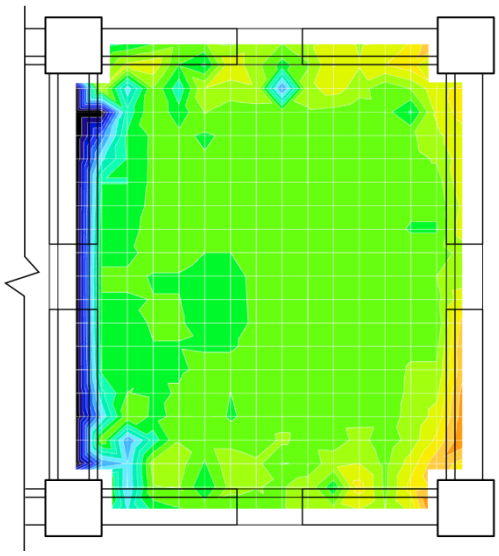

(e) Specimen displacement north-west.

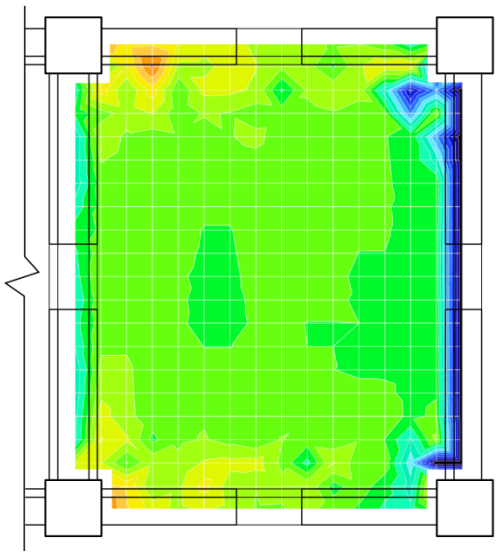

(f) Specimen displacement north-east.

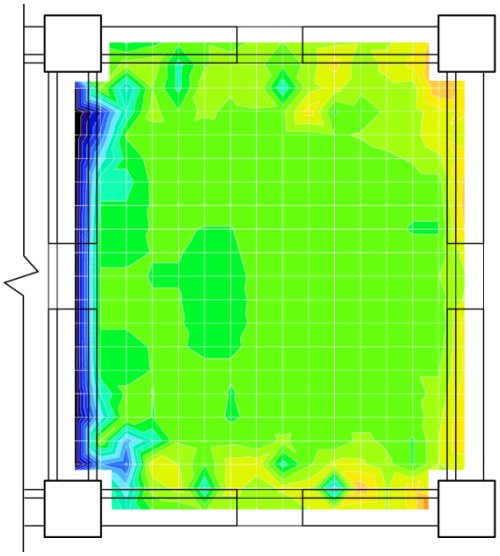

(g) Specimen displacement south-west.

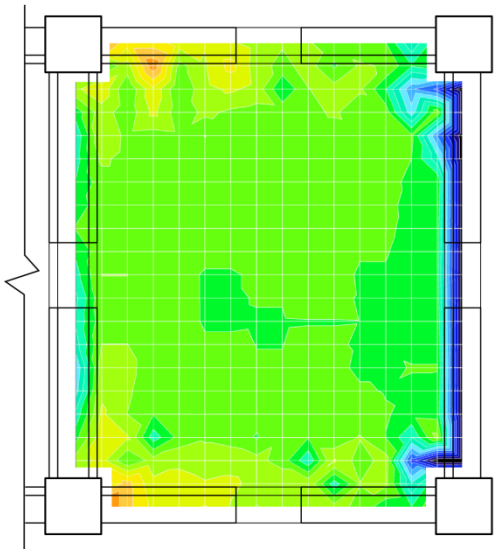

(h) Specimen displacement south-east.

Figure 4-58: Level One floor strain contours from east-west DEMEC measurements at 3.5% beam drift (Continued).

The east-west longitudinal strain contours for Level Two are presented in Figure 4-59. It can be seen that there was little observable difference in diaphragm strain patterns between the

two levels. Considerably larger shrinkage strains were experienced on Level Two and hence the absolute strains are larger than Level One, but the change in strain was similar.

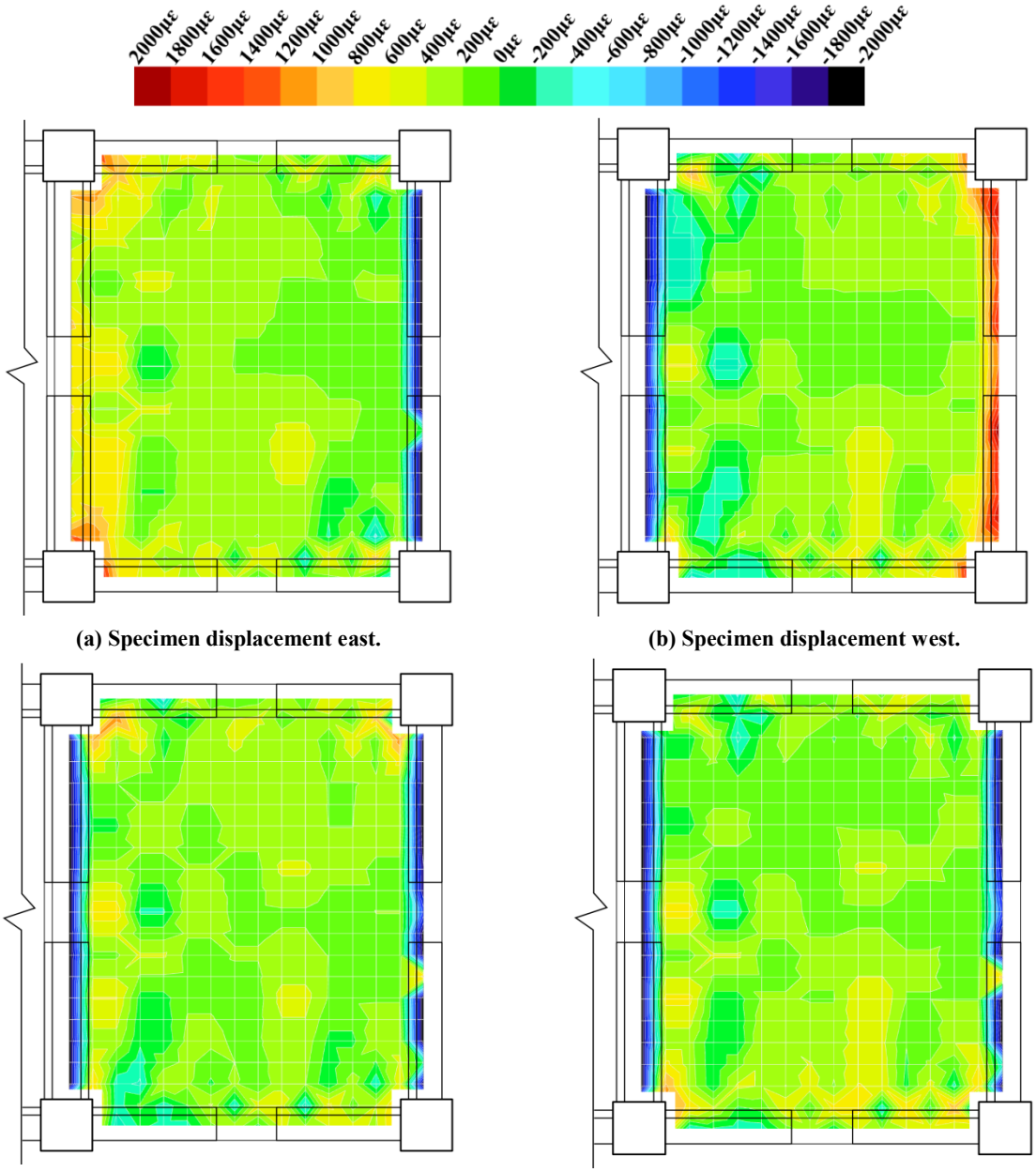

(a) Specimen displacement east. **(b) Specimen displacement west.**

(c) Specimen displacement north. **(d) Specimen displacement south.**

Figure 4-59: Level Two floor strain contours from east-west DEMEC measurements at 3.5% beam drift.

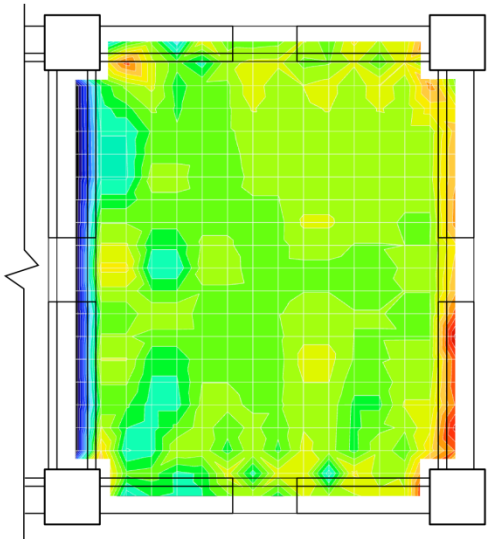

(e) Specimen displacement north-west.

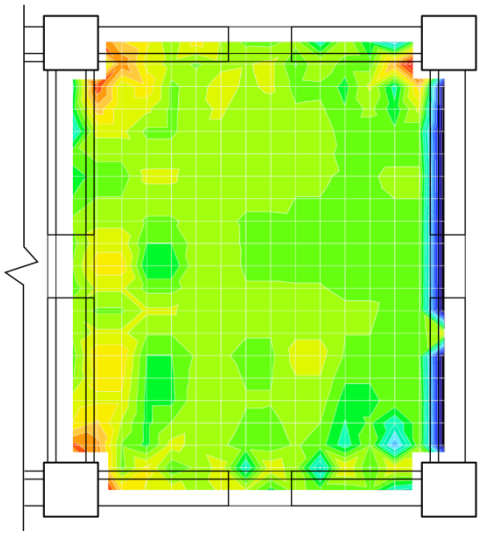

(f) Specimen displacement north-east.

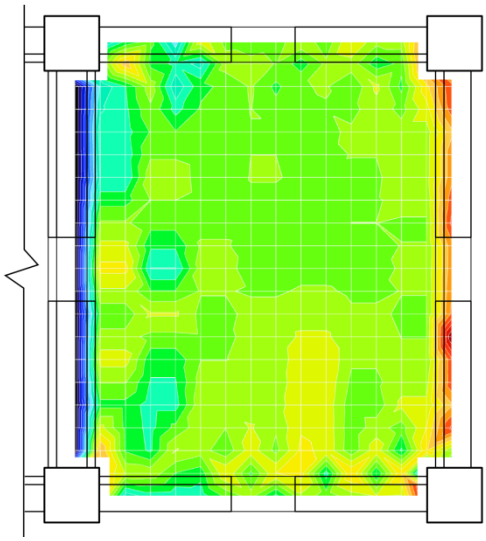

(g) Specimen displacement south-west.

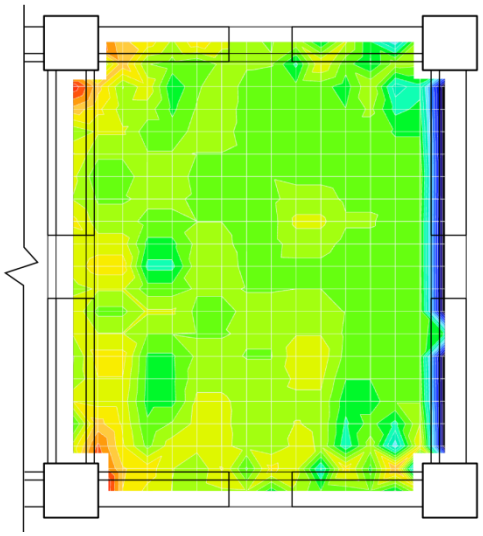

(h) Specimen displacement south-east.

Figure 4-59: Level Two floor strain contours from east-west DEMEC measurements at 3.5% beam drift (Continued).

4.16.2.2 North-south Longitudinal Floor Diaphragm Strain

The north-south longitudinal floor strain contours for Level One are presented in Figure 4-60. Significant strain was recorded during specimen displacement in the east-west direction. The floor strains were caused by both warping deformations around the columns, and displacement incompatibility between the straight profile of the precast floor and the adjacent beam, which deformed in double curvature. During north-south specimen displacement, significant strain was observed in the infill region. For specimen displacement in the north direction, the strain in the northern infill was tensile and in the southern infill the strain was compressive. The strain in the infills was caused by a difference in inclination between the hollow-core and the parallel beam, which induced flexure in the infill. Due to the large tensile strain caused by infill flexure, it was difficult to observe tensile strains that were a result of flange activation by the slotted connections. To determine the extent of flange activation the gradient of the strains was examined, as discussed in Section 4.16.2.3. As observed for floor

strains in the east-west direction, the recorded strains during biaxial testing were well represented by the superposition of the strain recorded in the orthogonal loading directions. However, warping strains became more significant during biaxial specimen displacements.

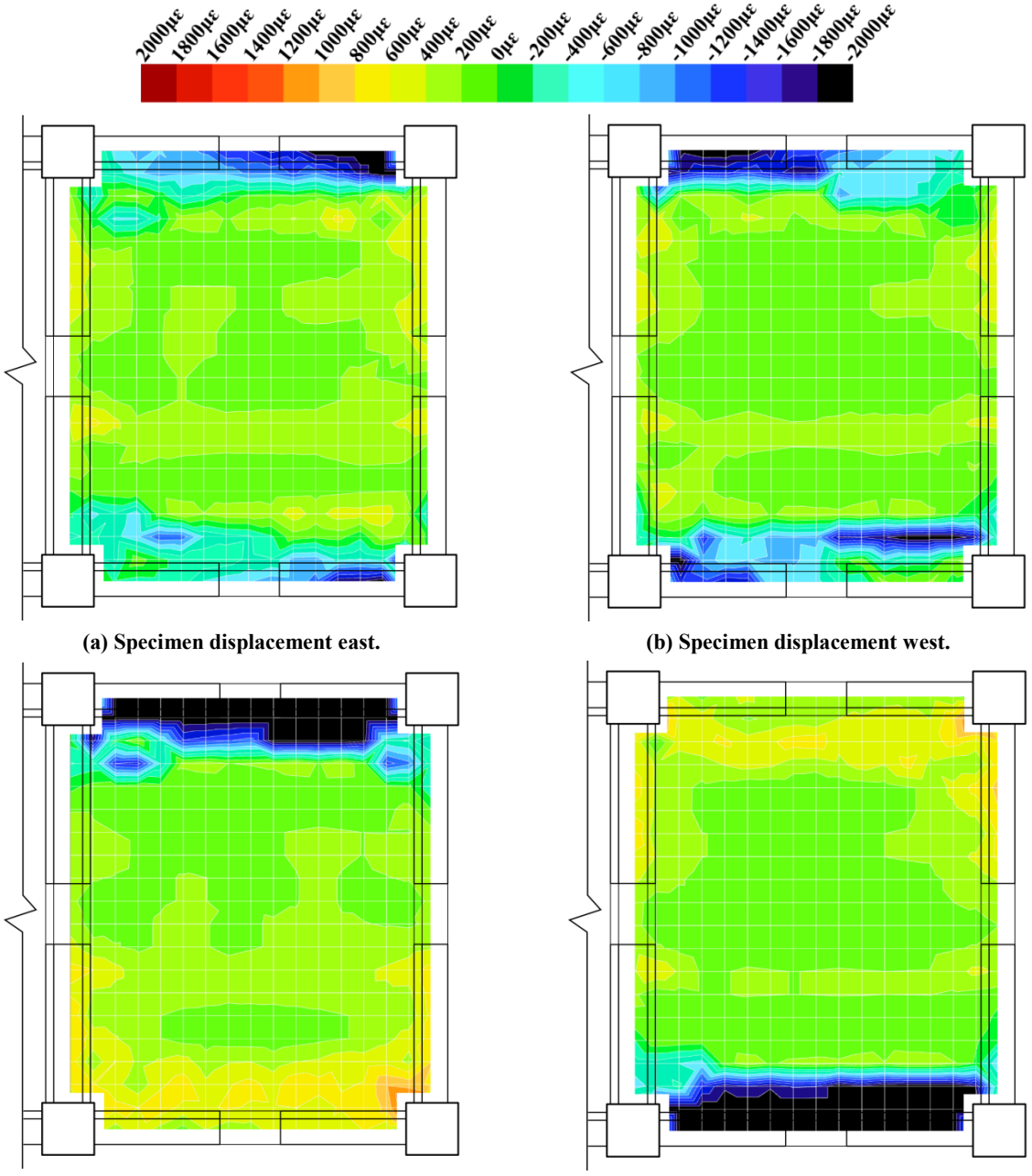

(a) Specimen displacement east.

(b) Specimen displacement west.

(c) Specimen displacement north.

(d) Specimen displacement south.

Figure 4-60: Level One floor strain contours from north-south DEMEC measurements at 3.5% beam drift.

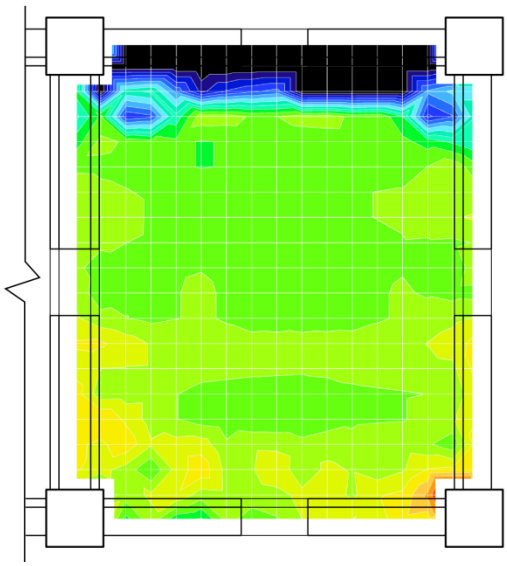

(e) Specimen displacement north-west.

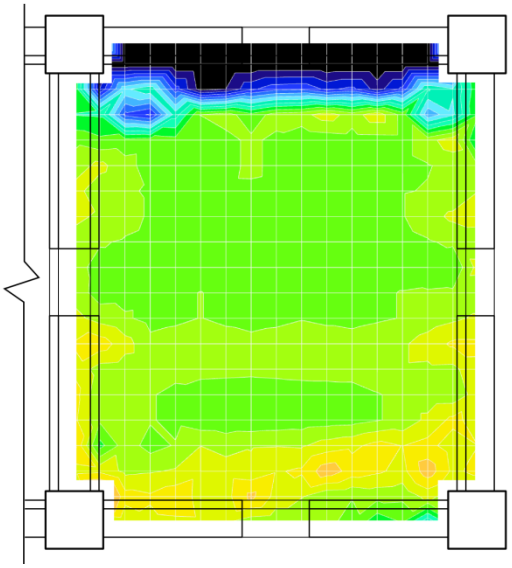

(f) Specimen displacement north-east.

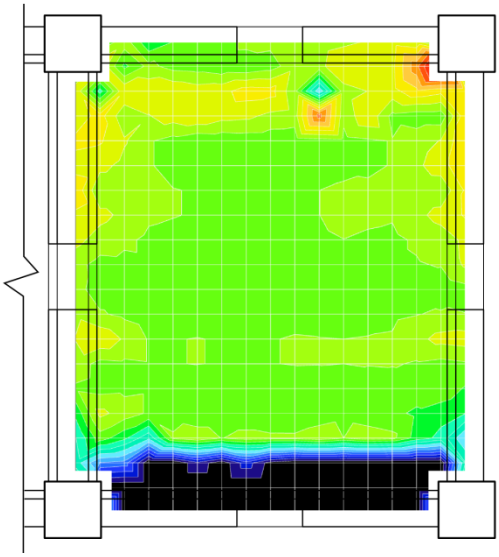

(g) Specimen displacement south-west.

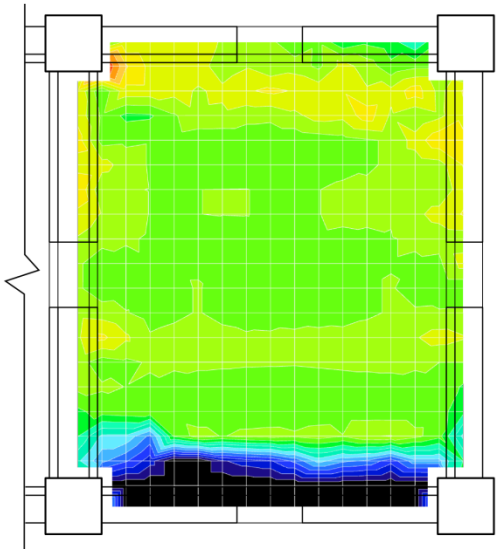

(h) Specimen displacement south-east.

Figure 4-60: Level One floor strain contours from north-south DEMEC measurements at 3.5% beam drift (Continued).

The north-south longitudinal strain contours for Level Two are presented in Figure 4-61. Overall, there was little observable difference in strain distributions between Levels One and Two. The difference in inclination between the double-tee web and the parallel beam was accommodated by flexure in the double-tee flange, as observed in the timber infill on Level One. However, it can be seen that in addition to the strain on the beam side of the double-tee flange, there was also strain in the middle flange between the webs. Physically, this corresponded to one of the webs of the double-tee inclining relative to the other. Cracking was observed in the underside of the double-tee units along the inside of the webs during the 3.5% cycle.

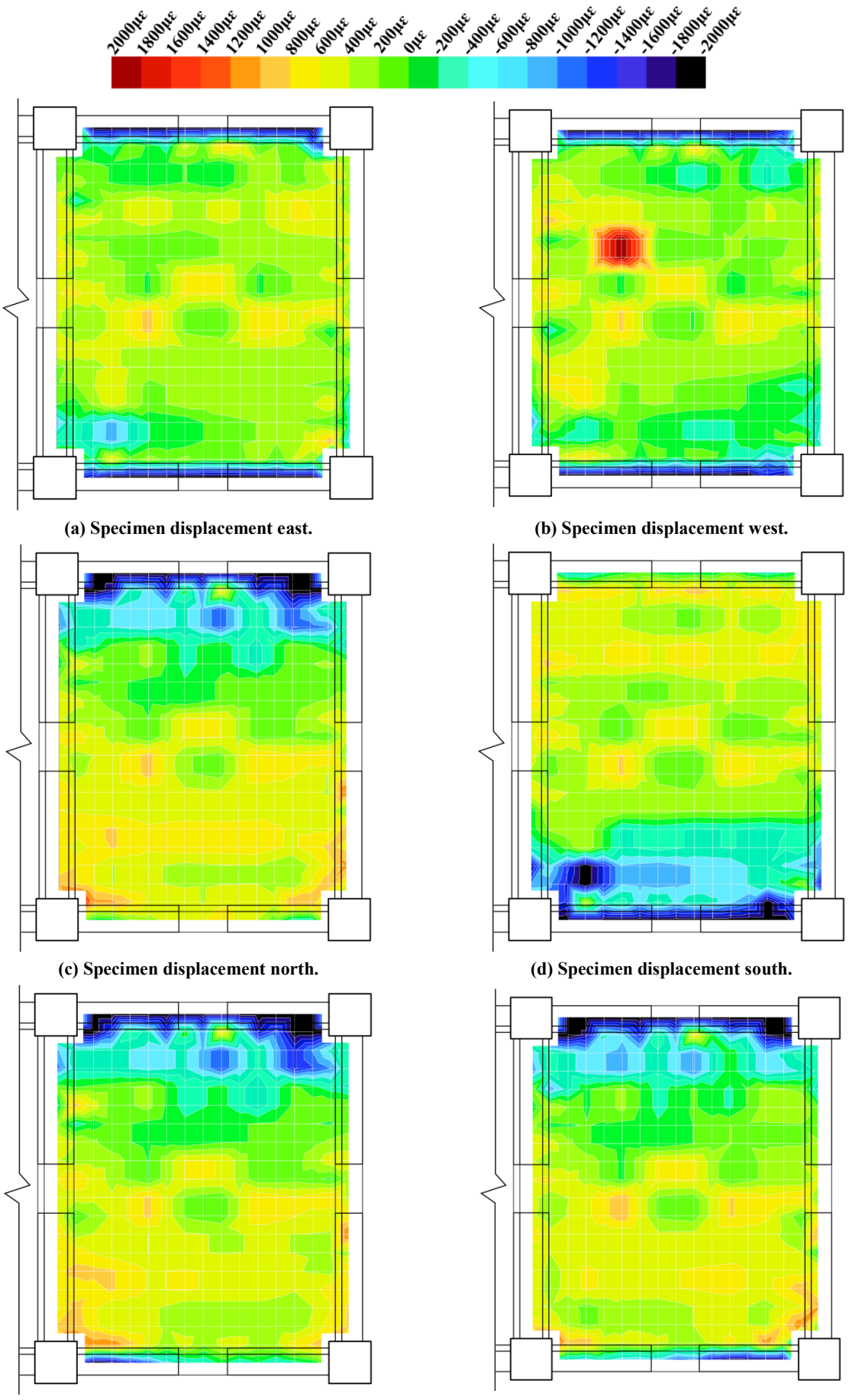

(a) Specimen displacement east.

(b) Specimen displacement west.

(c) Specimen displacement north.

(d) Specimen displacement south.

(e) Specimen displacement north-west.

(f) Specimen displacement north-east.

Figure 4-61: Level Two floor strain contours from north-south DEMEC measurements at 3.5% beam drift.

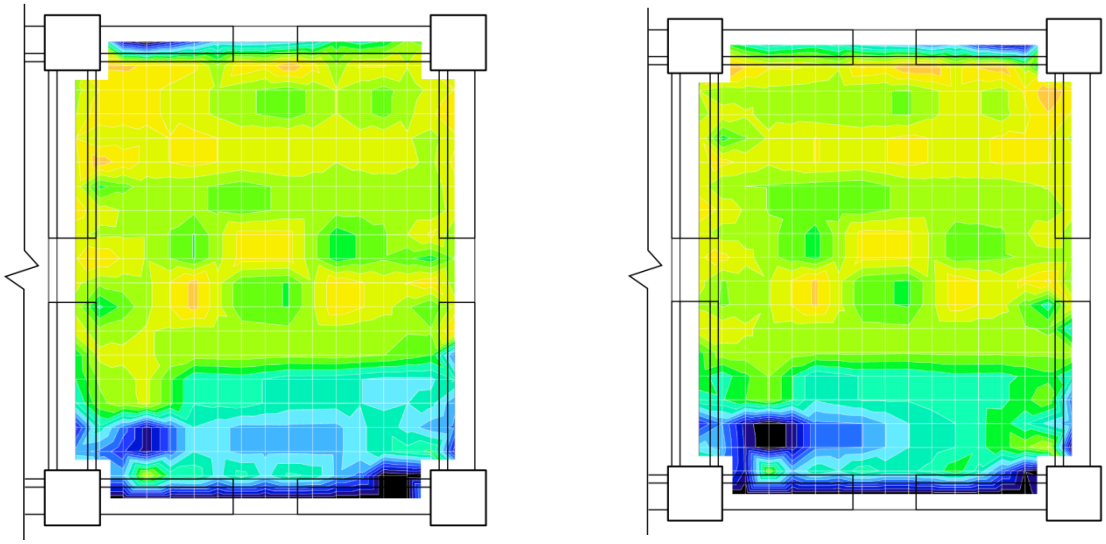

(g) Specimen displacement south-west. (h) Specimen displacement south-east.

Figure 4-61: Level Two floor strain contours from north-south DEMEC measurements at 3.5% beam drift (Continued).

4.16.2.3 Flange Activation Width

One of the claimed benefits of the slotted beam connection is that it produces less flange activation than a traditional connection (Ohkubo & Hamamoto, 2004; Au, 2010). However, this claim has not been properly assessed due to historic slotted beam experiments being either two-dimensional tests without floors, or the boundary conditions have been unsatisfactory if floors were included.

In Section 4.5 it was recommended that flange activation be included when determining the nominal and overstrength capacity of a system constructed with slotted beams. It is important to make a clear distinction between flange activation and continuity moments. Continuity moments are caused by a relative rotation between the precast floor end and the supporting beam. This rotation induces strain in the floor reinforcement, which generates moments that contribute to the overall lateral resistance of a structure. Flange activation is caused by the transfer of connection strain, from neutral axis variation or elongation, via shear lag to the adjacent floor diaphragm. The transferred strain decreases in magnitude with distance perpendicular to the connection. The resulting strain in the floor reinforcement contributes to the flexural moment capacity of the connection, and hence the overall lateral resistance of the system.

To determine the extent to which flange activation contributed to the overall lateral resistance of SA1, firstly a strain distribution in the floor reinforcement was postulated. A generic representation of the strain profile along the exterior starter reinforcement is shown in Figure 4-62(a). In this figure, x is the distance from the fully developed end of the starter reinforcement to the crack where yield has occurred. This distance differed for interior and exterior connections due to the difference in the width of the perpendicular beam. Due to the

different concrete compressive strengths in the floor toppings of the first and second levels, the development length was different for Level One and Level Two. Once the rate of development was known, the proportions of yield strain could be attributed. By integrating the strain profile, the crack width corresponding to reinforcement yield was determined.

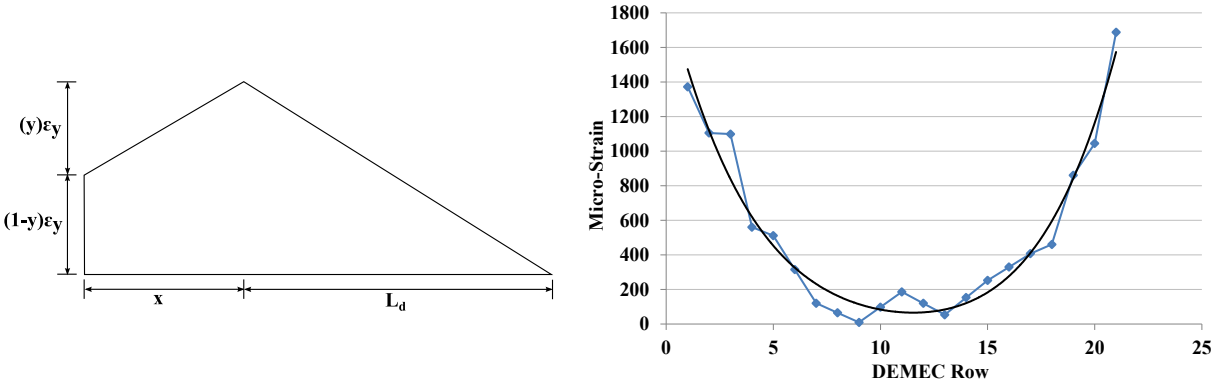

(a) Generic starter reinforcement strain profile.

(b) Example of strain profile across the diaphragm from DEMEC readings.

Figure 4-62: Method for determining extent of flange activation.

This method was used by Peng (2009) to estimate the flange activation width that occurred in a specimen constructed using traditional connections. However, the boundary conditions in that experiment meant that the beam supporting the floor system was restrained against rotation at one end, which meant that cracking along the floor seating was minimised. This meant that Peng (2009) could use the raw displacement measurements across the floor to calculate the flange activation width. Peng's (2009) method makes no distinction between continuity moments and flange activation. For this reason, the displacement values used for the determination of the flange activation width in the east-west direction in SA1 have been offset to minimise the influence of the continuity moments. An example of the strain profile across the floor, perpendicular to the supporting beam, is presented in Figure 4-62 (b). Figure 4-62 (b) shows that strain was greatest near the connections and reduced to a baseline strain near the centre of the span, away from the influence of the connections. The strain gradient across the floor was caused by flange activation. This method differs from the method undertaken by Au (2010), which equated the deformation measured at the top surface of the beam to the integration of the strain profile across the floor. This method could not be undertaken in SA1 because the strain data from the floor reinforcement was not known.

Combining the results from all connections, it was found the average width of flange activation was approximately 90% of that required by §9.4.1.6.1 of NZS3101:2006 (Standards New Zealand, 2006). Upon initial consideration this value seems large; however, the §9.4.1.6.1 requirements have been shown to be unconservative (Matthews, 2004; Peng, 2009). Similarly, because the lever arm between the floor reinforcement and the neutral axis is greatly reduced in a slotted beam system compared to a system with traditional

connections, the contribution of the flange activation to flexural strength of a connection is reduced. Peng (2009) found the flange activation width of interior connections to be greater than exterior; however, the flange activation widths in the slotted system were similar between the interior and exterior connections. This observation corroborates the relatively similar recorded beam elongation between interior and exterior connections observed in SA1, as discussed in Section 4.14.

When expressed in the same manner as §9.3.1.2 and §9.4.1.6.1 of NZS3101:2006 (Standards New Zealand), the effective flange widths tentatively suggested for design of slotted beam structures are shown in Figure 4-63(a) and (b) for nominal and overstrength actions respectively.

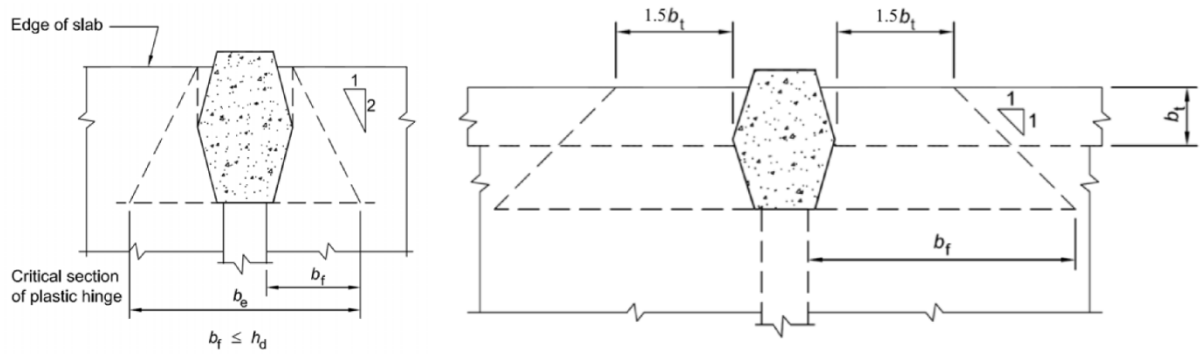

(a) Nominal. **(b) Overstrength.**

Figure 4-63: Proposed effective flange widths for slotted beams. Modified after Standards New Zealand (2006).

It can be concluded that compared to using traditional connection detailing in a system, using the slotted beam detail can result in a modest reduction in flange activation. However, a more significant reduction in flexural overstrength and overall system lateral resistance is achieved during negative flexure due to a significant reduction in the lever arm between the neutral axis in the connection and the floor reinforcement.

4.16.4 Diaphragm Shear Strain

In the western bays of Level One and Two the shear deformation between the floor diaphragm and the beams was measured using triangulated linear potentiometers, as described in Section 3.8.2. Figure 4-64 and Figure 4-65 present the shear displacement from Level One and Level Two respectively. Relative to the beam, floor displacement east and south is defined as positive in the plots. If the floor diaphragm had restrained beam elongation, it would be shown in Figure 4-64 and Figure 4-65 as an accumulation of negative displacement along Grids 1 and 2. Similarly, little accumulation of strain would be expected on Grids A and B because the potentiometers were located on the axis of symmetry of the floor. Neither of these features are apparent in Figure 4-64 or Figure 4-65. Beam elongation was not large

enough for a significant strut and tie restraint system by the floor diaphragm to become established.

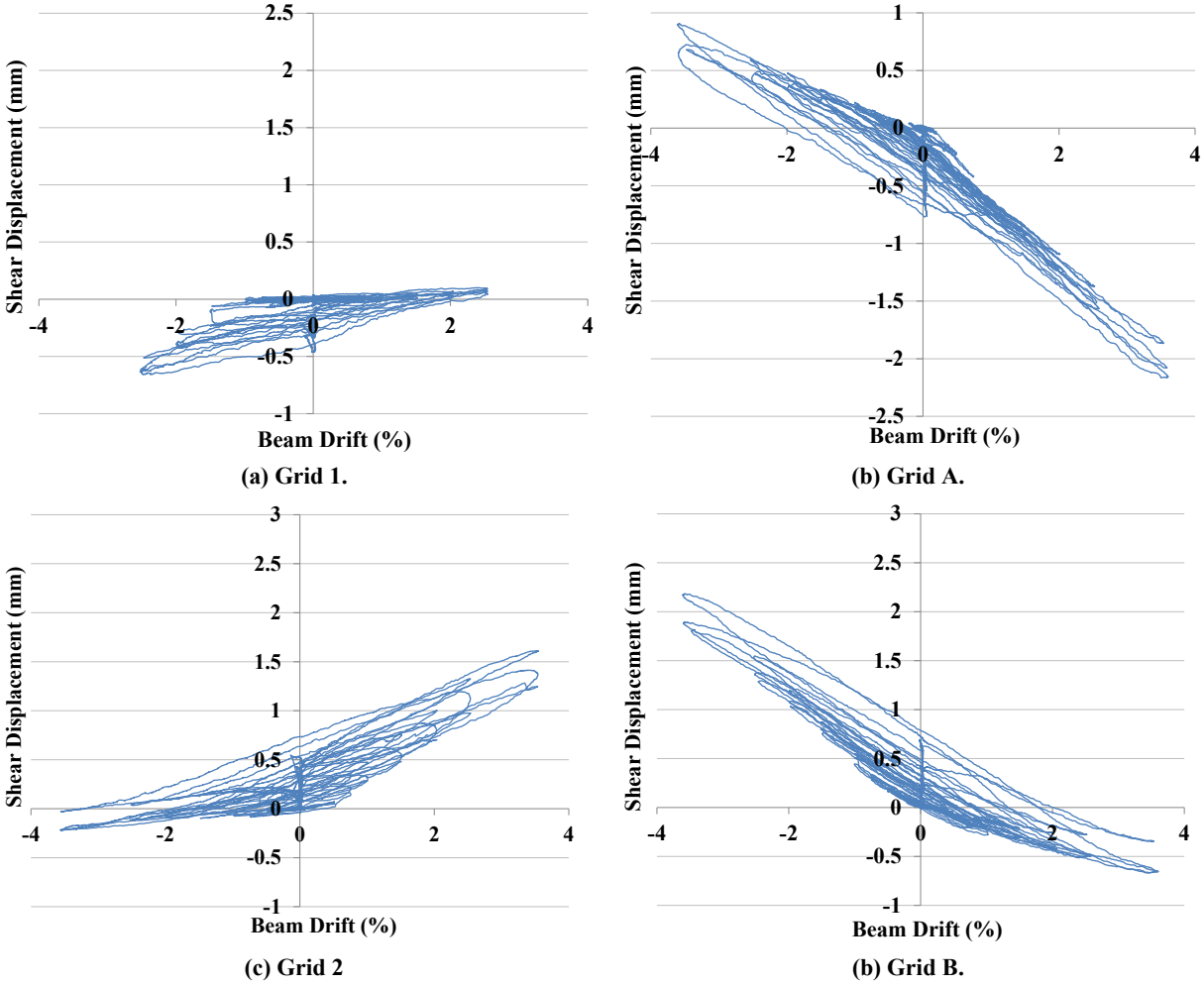

Figure 4-64: Level One shear displacement between beam and floor diaphragm.

It is clear from Figure 4-64 and Figure 4-65 that shear deformation occurred in the floor diaphragms of SA1. Furthermore, the direction and magnitude of the shear deformation was similar over both levels. When looking at the displacements in isolation they appeared not to be in equilibrium, until the unbalanced actuator forces are considered. The cause of the dominant shear across the floor diaphragm was the interaction between actuators. The interaction between actuator A and E caused diaphragm shear along Grids 1 and 2. Similarly, the interaction between actuator D and actuators C and E caused diaphragm shear along Grids A, B and C. Section 3.7.2.4 describes the actuator interaction issue in greater detail.

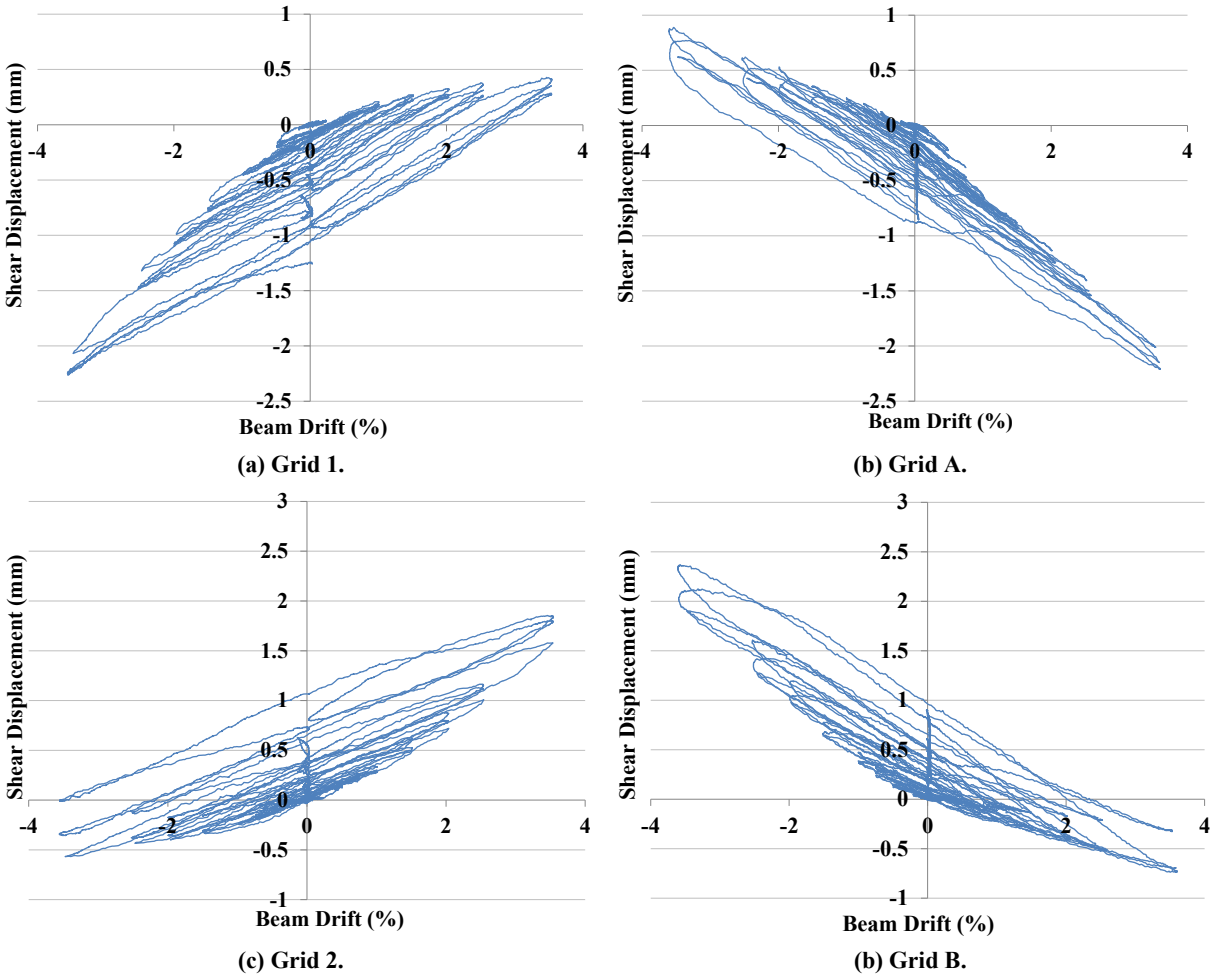

Figure 4-65: Level Two shear displacement between beam and floor diaphragm.

Figure 4-66 presents the shear strain contours from the eastern bay of Level One at 3.5% beam drift. In addition to the longitudinal DEMEC measurements collected and presented above, diagonal readings were recorded to enable shear deformations to be calculated. No measurements were taken over the 500mm grid. The DEMEC grid is described in more detail in Section 3.8.2. These plots confirm the observations from the linear potentiometers presented above. During eastern specimen displacement, the shear along Grids 1 and 2 opposed each other. During western specimen displacement, the signs of the shears reversed because the interaction between the actuators switched from compression to tension. Similarly, actuator D generally had a greater force than actuators C and E regardless of loading direction. Hence, the sign of the recorded shears switch upon load reversal.

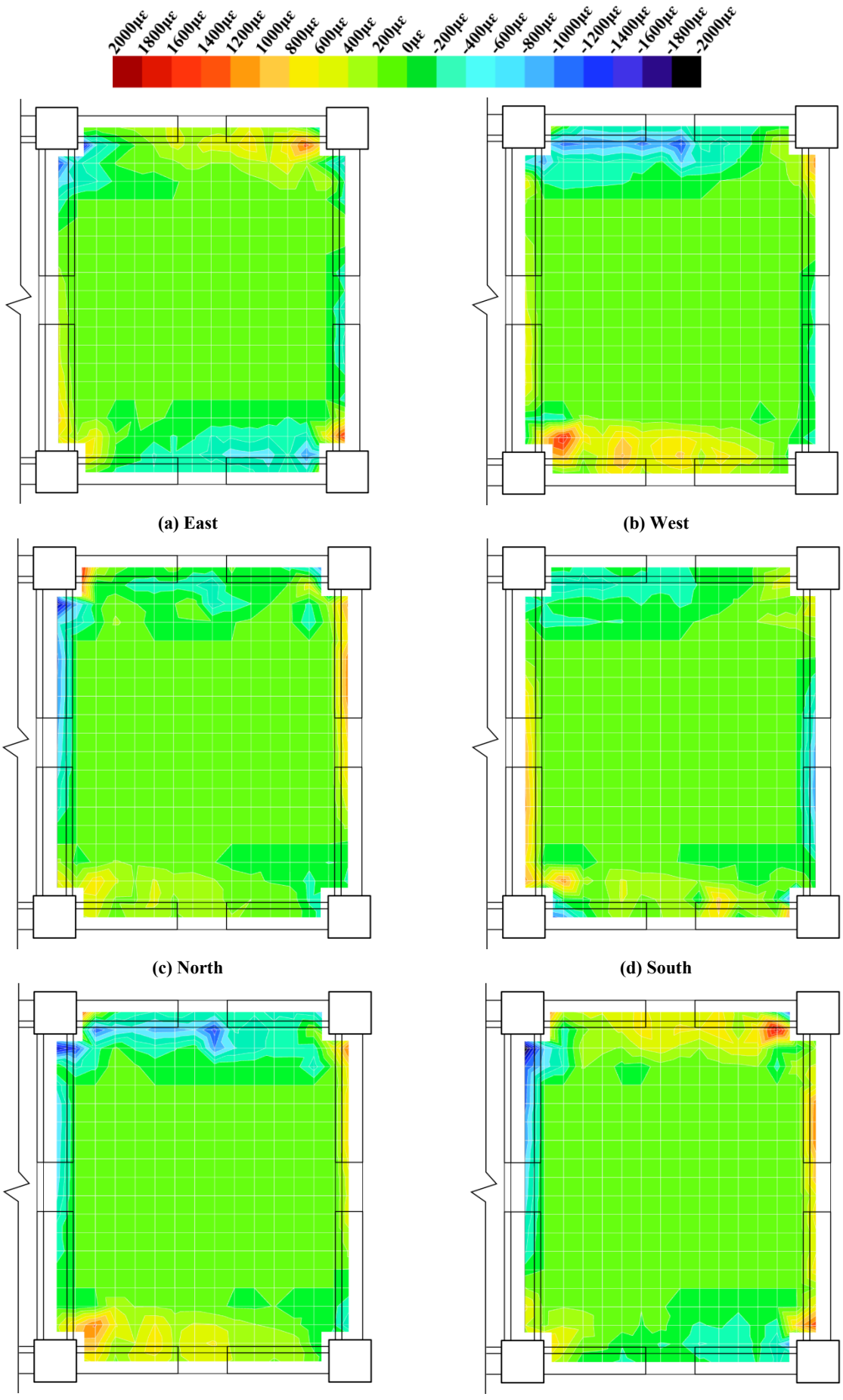

Figure 4-66: Level One floor strain contours from shear DEMEC measurements during 3.5% beam drift cycle.

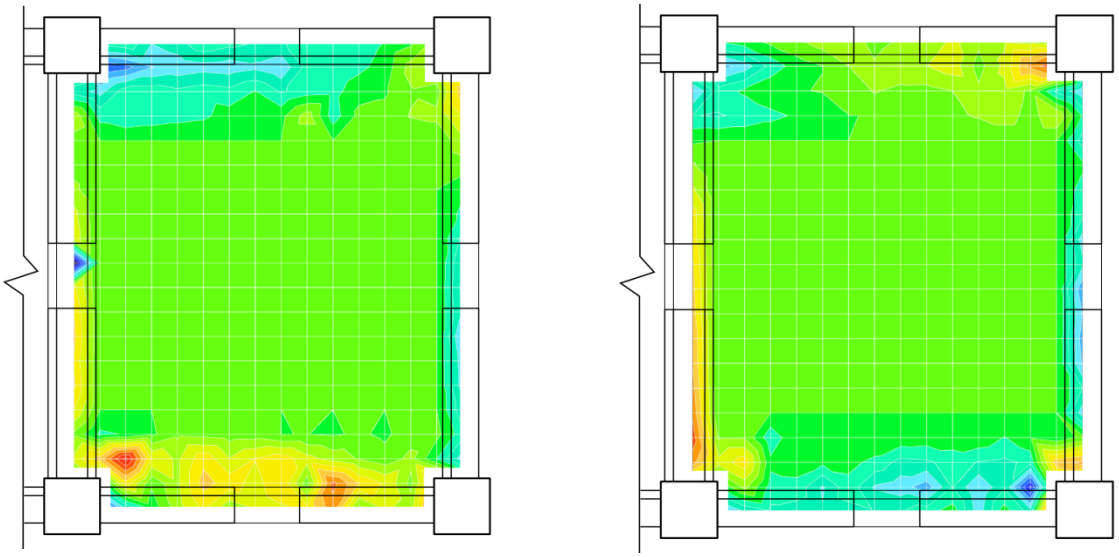

(g) South-west **(h) South-east**

Figure 4-66: Level One floor strain contours from shear DEMEC measurements during 3.5% beam drift cycle (Continued).

Figure 4-67 presents the shear strain contours from the eastern bay of Level Two at 3.5% beam drift. The data presents the same general trends observed for Level One. The recorded shear strains during biaxial testing were well represented by the superposition of the shear strains recorded in the orthogonal loading directions.

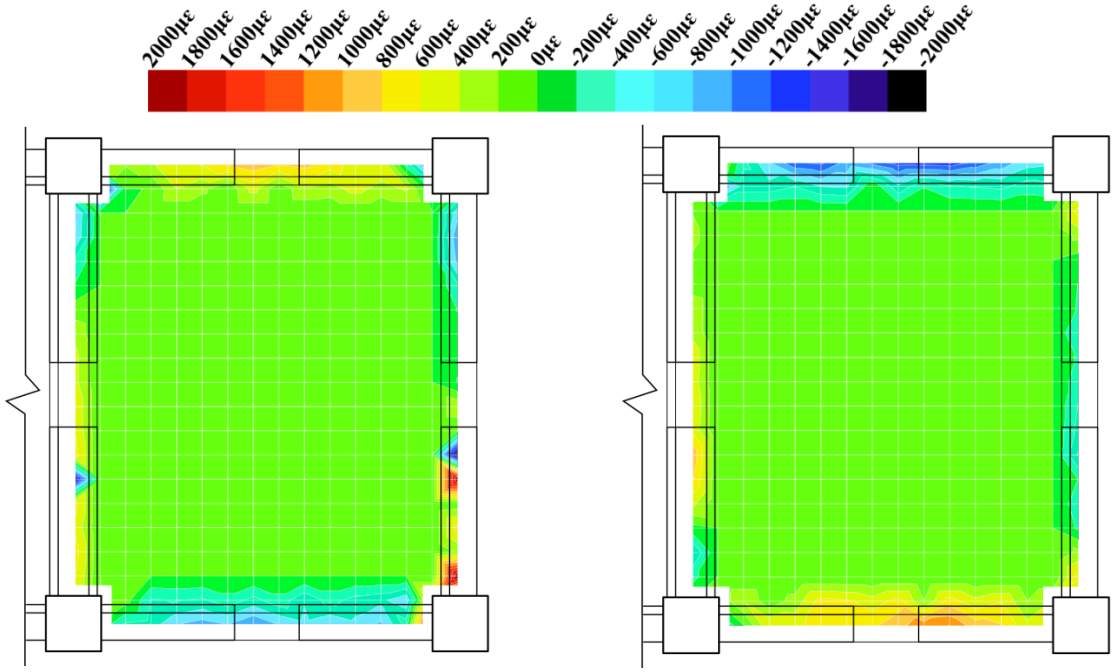

(a) East **(b) West**

Figure 4-67: Level Two floor strain contours from shear DEMEC measurements during 3.5% beam drift cycle.

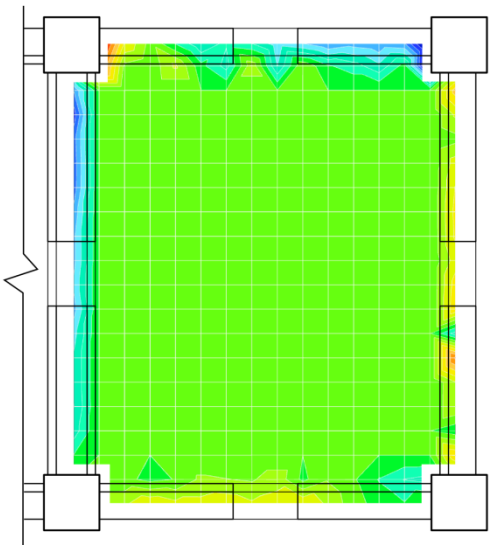

(c) North

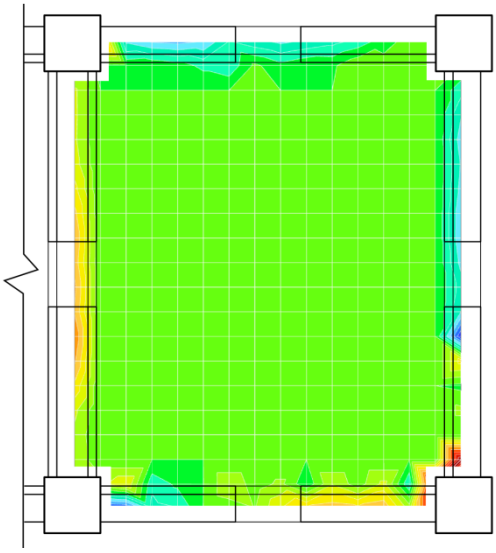

(d) South

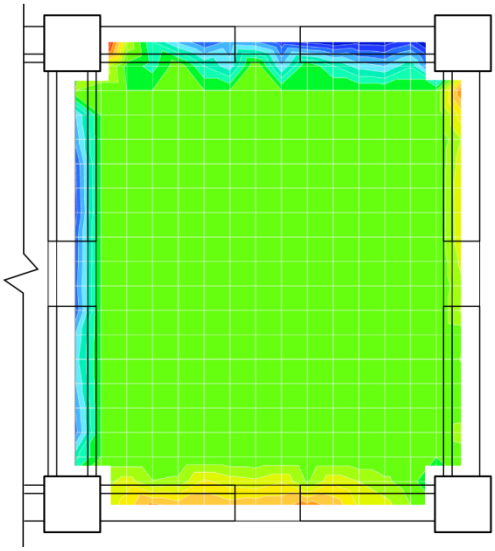

(e) North-west

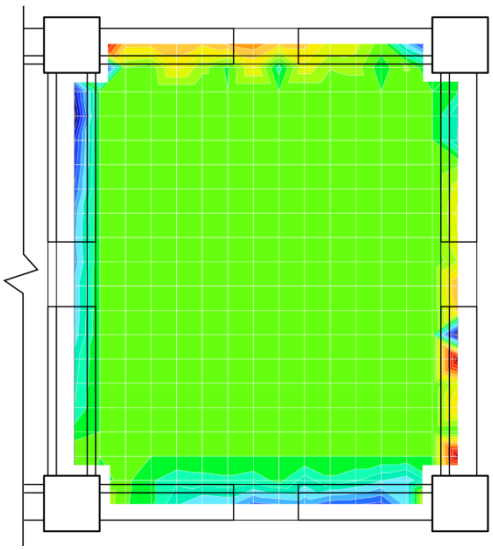

(f) North-east

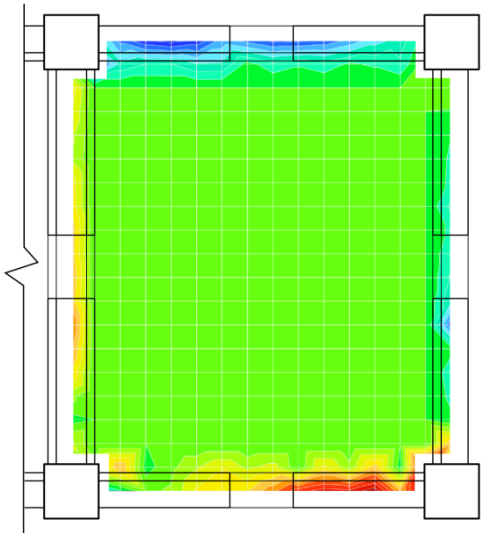

(g) South-west

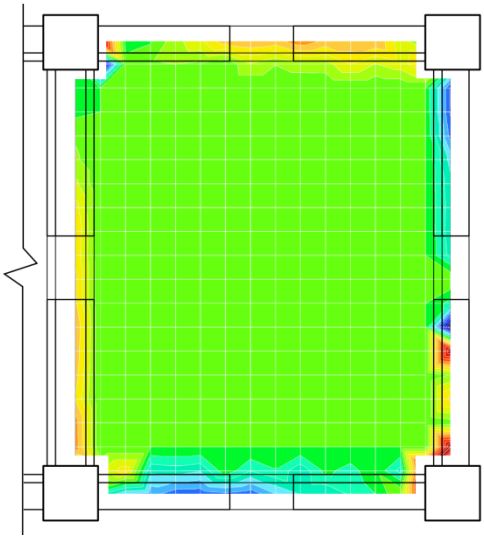

(h) South-east

Figure 4-67: Level Two floor strain contours from shear DEMEC measurements during 3.5% beam drift cycle (Continued).

It was unfortunate that reaction frame interference and actuator imbalances governed the shear strain recorded in the floor diaphragms. It is possible that other internal force transfer

mechanisms existed across the floor diaphragm; however, the dominance of the external forces was such that they could not be decoupled.

4.17 Beam-column Joint Distortion

The beam-column joint distortion for Bm B/1-1 is presented in Figure 4-68. This joint was subject to the worst case joint shear loading in specimen SA1, and the overall joint distortion was very low. The joint reinforcement strain was expected to remain under half of the yield strain. However, the recorded strain was less than this due to the joint zone being over reinforced. The horizontal joint reinforcement provided was 31% greater than required, as explained in Section 3.4.4. Because the beam-column joint was expected to remain in the elastic range, observations could be made independent of the magnitude of the recorded strain.

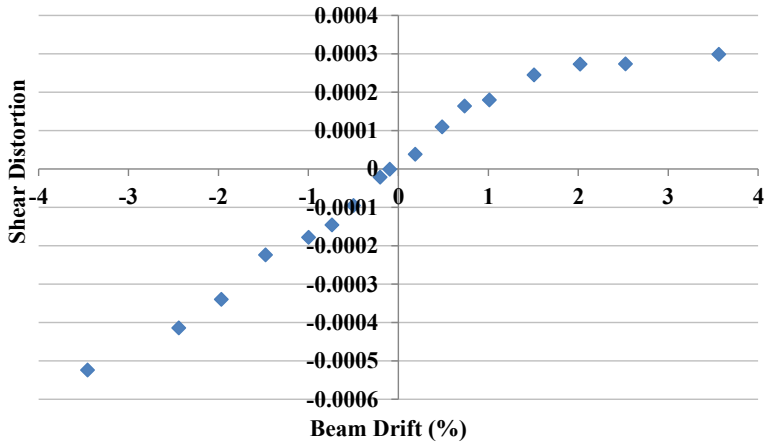

Figure 4-68: Bm B/1-1 east-west joint shear distortion.

Byrne (2012) suggested that the additional horizontal reinforcement in the bottom half of the joint zone, which was recommended by Au (2010), is overly conservative and not necessary. Byrne's (2012) experimental specimen included supplementary vertical stirrups in the beam-column joint. The vertical stirrups were designed to encourage a stiff joint to promote shear transfer via a concrete strut mechanism, rather than an equivalent truss mechanism. In this effort the detailing was successful; however, the detail would be difficult to assemble in a commercial setting. Furthermore, it is likely that the material and labour cost of installing the additional vertical reinforcement would exceed that of providing the additional horizontal joint reinforcement.

The strain profiles from horizontal joint stirrups in Bm B/1-2 and Bm C/1-2 in the east-west and north-south directions respectively are presented in Figure 4-69 and Figure 4-70. This data is contradictory to that presented by Byrne (2012), but corroborates data from specimen SB2 (Au, 2012). Figure 4-69(a) and (b) have a slightly different form to the other plots. This is because Bm B/1-2 was an internal joint, and included supplementary reinforcement welded

to the bottom longitudinal reinforcement through the joint. The supplementary welded reinforcement decreased bond stresses and strain penetration. Hence, there was less strain transferred from the longitudinal reinforcement to the adjacent stirrup. Similarly, due to the top longitudinal reinforcement being strained on both sides of the joint simultaneously, there was greater potential for strain to be transferred to the adjacent stirrup set.

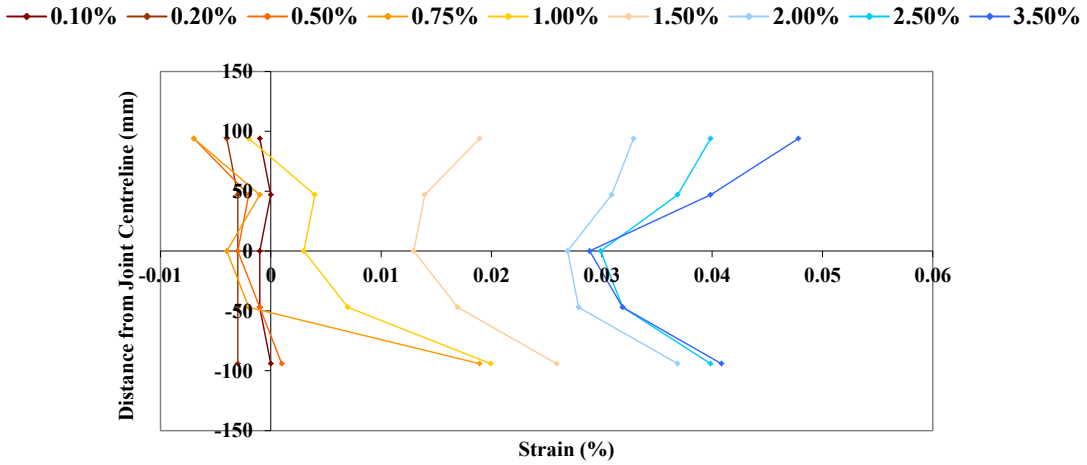

(a) Bm B/1-2 negative displacement

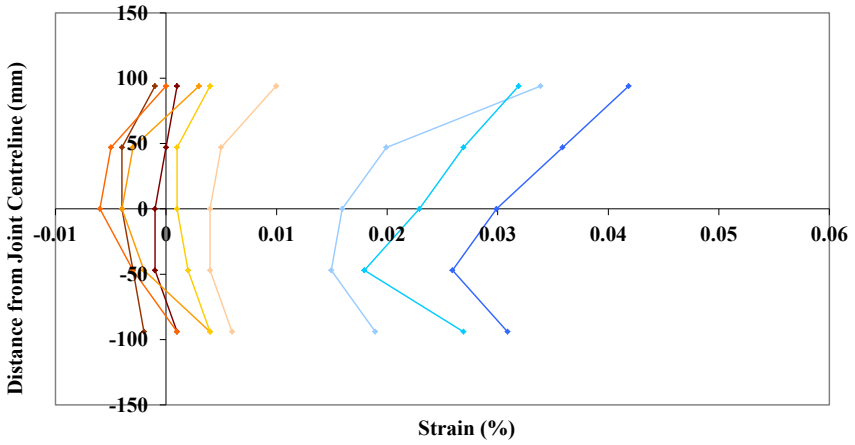

(b) Bm B/1-2 positive specimen displacement.

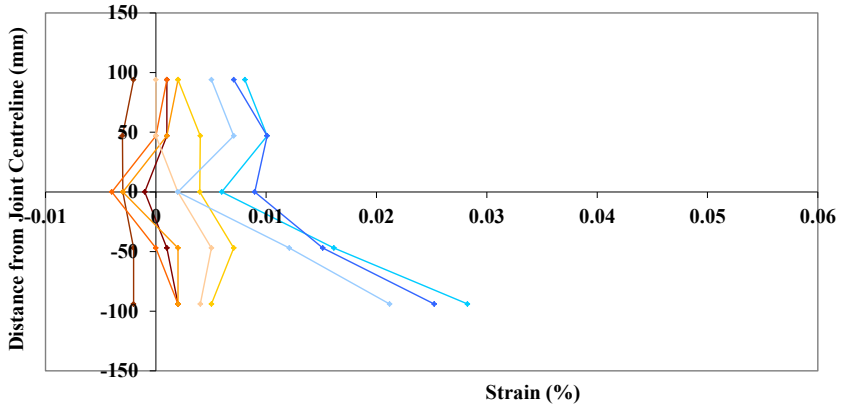

(c) Bm C/1-2 negative specimen displacement.

Figure 4-69: East-west horizontal joint reinforcement strains.

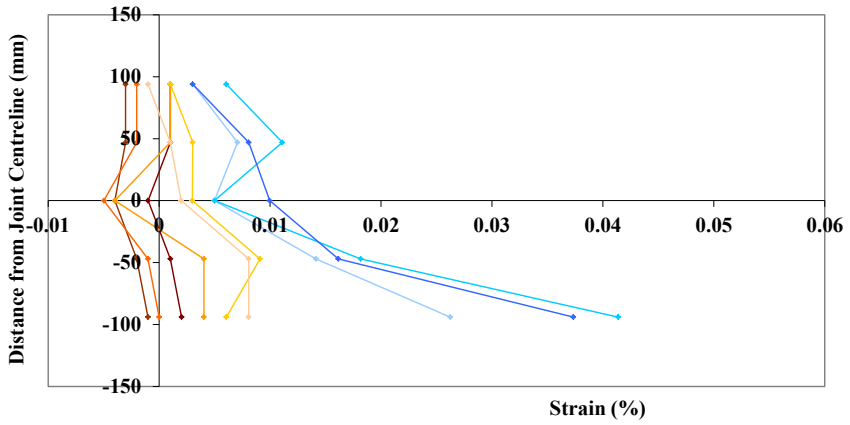

(d) Bm C/1-2 positive specimen displacement.

Figure 4-69: East-west horizontal joint reinforcement strains (Continued).

As shown in Figure 4-70, in the exterior connections of SA1 there was a strain bias towards the horizontal stirrups in the bottom of the joint. There was more force resisted by the horizontal reinforcement in the lower half of the joint than in the top half, which was consistent with the joint mechanics outlined in Section 3.4.4. However, some of the observed strain may have been transferred from the adjacent longitudinal reinforcement.

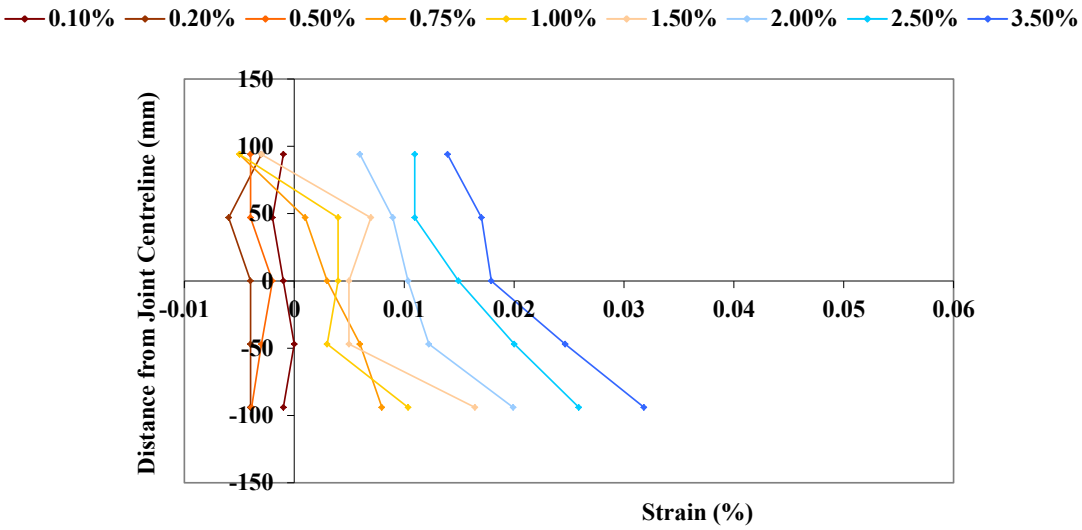

(a) Bm B/1-2 negative displacement

Figure 4-70: North-south horizontal joint reinforcement strains.

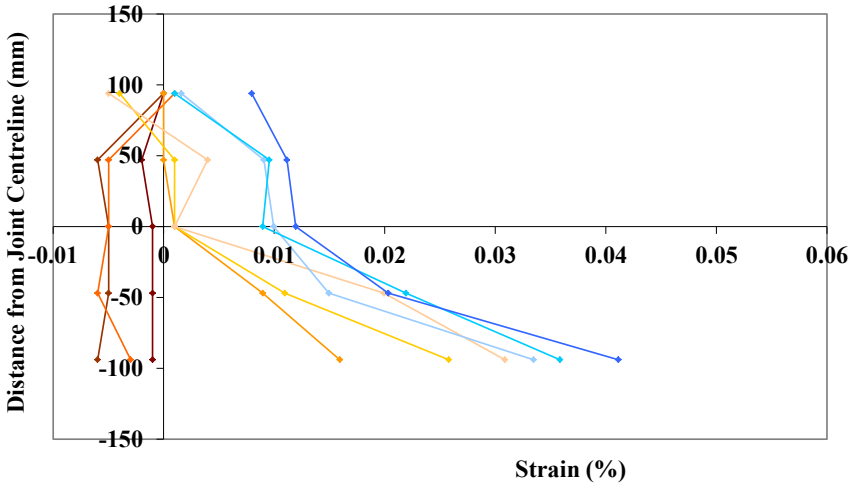

(b) Bm B/1-2 positive specimen displacement.

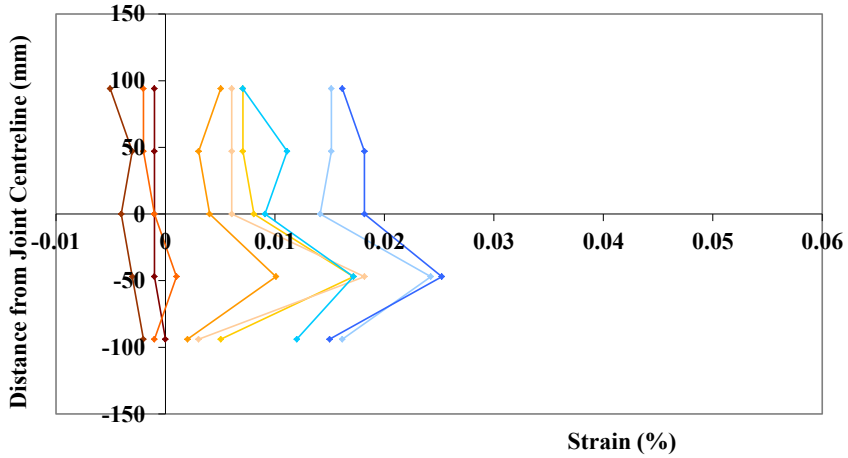

(c) Bm C/1-2 negative specimen displacement.

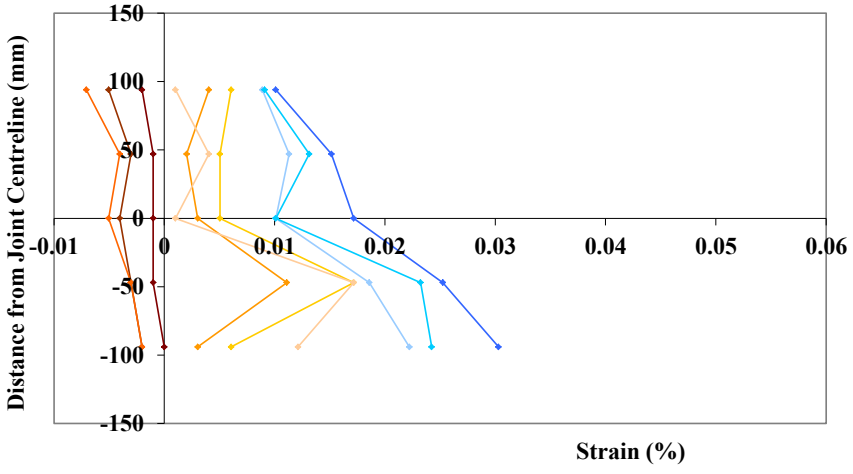

(d) Bm C/1-2 positive specimen displacement.

Figure 4-70: North-south horizontal joint reinforcement strains (Continued).

Byrne's (2012) recommendations may be appropriate for beam-column joints constructed with supplemental vertical reinforcement; however, they are not generally appropriate for the design of slotted beam systems. Additional research is required in this area to be able to broadly recommend reducing beam-column joint reinforcement. It is recommended that the NZS3101:2006 (Standards New Zealand, 2006) provisions for beam-column reinforcement

are applied to the design of slotted beam systems. Furthermore, 25% more joint reinforcement, on top of that calculated using NZS3101:2006 (Standards New Zealand) methods, should be included in the bottom half of the joint as per Au's (2010) recommendations.

4.18 Column Performance

The columns used in specimen SA1 had a very high reinforcement ratio. They were designed according to capacity design principles for a ductile moment frame and had a high degree of protection against plasticity. Furthermore, because of limitations with the supply of mechanical couplers in New Zealand at the time, larger diameter column longitudinal reinforcement than necessary was used. Hence, the columns were not expected to sustain any meaningful damage during testing.

Minor cracking, peaking at 0.1mm, was observed in the columns. Figure 4-71 presents that curvature of column B/1-B in the east-west direction. This column was subject to the worst case flexural loading. Curvature increased relatively linearly up to specimen yield before plateauing. The response of the column was approximately symmetric.

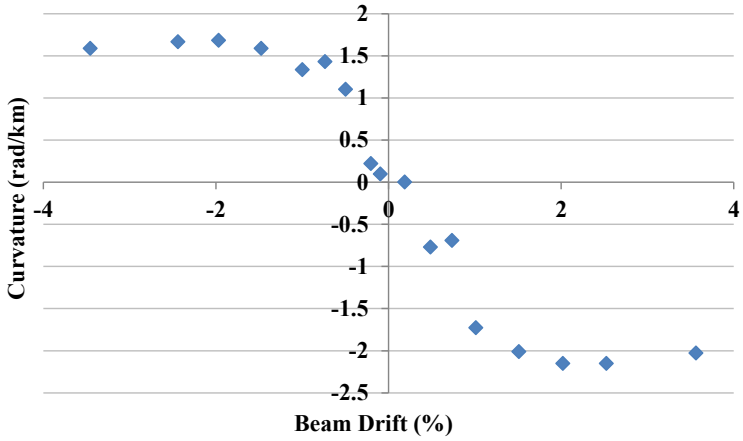

Figure 4-71: Col B/1-B east-west column curvature.

The grouted connections between precast elements performed well. Cracking between the precast components and the dry-pack was observed in all connections, as shown in Figure 4-72(a). These cracks were recovered upon specimen unloading. Reid RB32GS grout sleeve couplers, shown in Figure 4-72(b), were used to splice the column longitudinal reinforcement at the base of 'B' columns. No sign of distress, or any loss of capacity, was observed at the base of the 'B' columns during testing. Hence, it can be concluded that these couplers provide an effective means of developing longitudinal reinforcement and are suitable for seismic applications where reinforcement ductility has been excluded. However, care must be taken during grouting operations to ensure that the grout completely encompasses the embedded reinforcement.

(a) Cracking between dry-pack and precast components.

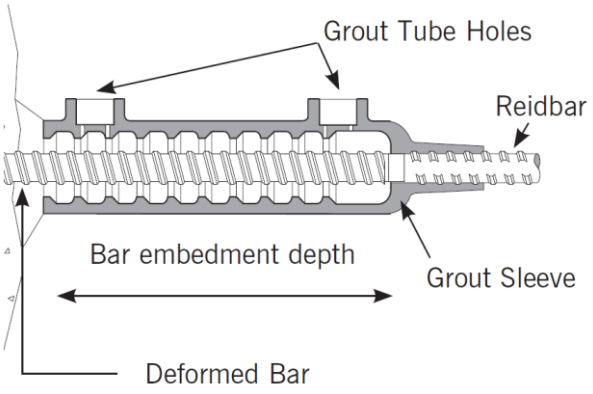

(b) Cross-section of Reid grout sleeve RB32GS (Reid Construction Systems, 2007).

Figure 4-72: Precast component grouted connections.

4.19 Conclusions

The process of testing a two storey, two-by-one bay, reinforced concrete slotted beam superassembly has been described in this chapter. The mitigation of issues that were encountered during the testing process was described. Observations made during the experiment were chronicled. Results from the experiment were presented and their relevance discussed. Based on the results of this experiment, the following conclusions were made:

1. Overall, specimen SA1 performed well during testing. Stable response and high levels of energy dissipation were observed throughout testing. The specimen conformed to serviceability, damage and life safety limit states as defined by Priestley et al. (2007). All criteria were satisfied to conform to the ACI374.1-05 acceptance criteria for moment frames based on structural testing, with the exception of the predicted overstrength (ACI Committee 374, 2005).
2. The damage sustained by SA1 was very low. It can be concluded that the damage sustained by a slotted beam system during a large earthquake is lower than would be expected in a comparable system with traditional connections. The nature of the damage sustained in a slotted beam system is generally economically and practically viable to repair.
3. Many unanticipated issues were encountered during the testing of SA1. The causes of these issues were described, and the measures used to mitigate them were presented.
4. Specimen SA1 was designed using simplified design equations recommended by Au (2010). These were found to be unconservative when used to determine the ultimate flexural capacity of a slotted beam connection. Overstrength factors of 3.5 and 2.5 were recorded in the east-west and north-south directions respectively. The contribution of the top longitudinal reinforcement to the flexural capacity of the connection can be

significant, and should be included in flexural capacity calculations. The effective flange widths specified in §9.3.1.2 of NZS3101:2006 should be used to calculate the nominal flexural moment capacity of slotted beam systems (Standards New Zealand, 2006).

5. Continuity moments from the precast floor connections contributed significantly to beam torsion, and hence the overall lateral strength of the specimen. Continuity moments should be considered separately from flange activation, and should be included in overall lateral strength calculations.
6. When all the contributions to the lateral strength of SA1 were taken into account, the recorded overstrengths were 1.87 and 1.86 for the east-west and north-south directions respectively. The relatively high overstrengths were the result of a combination of factors; however, effective stress in the bottom longitudinal reinforcement of the connections was likely the main factor. Effective stress enabled a larger force to be generated in the bottom unbonded reinforcement in compression than in tension, and is caused by the influence of Poisson's ratio, as discussed in Section 4.5. An overstrength factor of 1.6 is recommended for the design of slotted beam connections when Grade 300 bottom longitudinal reinforcement is used.
7. For practical displacements, slotted beam systems dissipate comparable levels of energy to traditional systems. However, a slotted beam system is able to dissipate energy with reduced damage to both the connection and the adjacent floor diaphragm compared to a system constructed using traditional connection details.
8. The elastic properties are relatively similar between comparable slotted and traditional beam connections. Given the inherent uncertainty in elastic design, it is reasonable to apply the effective section properties specified in §C6.9.1 of NZS3101:2006 to conduct an elastic analysis of a slotted beam structure (Standards New Zealand, 2006). This recommendation applies only if the second moment of area has been determined from gross beam dimensions.
9. Using two layers of top and bottom longitudinal reinforcement is a practical solution in slotted beams. However, the increased top hinge depth necessitated when using two layers of longitudinal reinforcement leads to increased strain in both the diagonal hangers and the top longitudinal reinforcement. Peak reinforcement strain occurred through the slotted section. The average strain penetration in the top longitudinal bars was $0.027 f_y d_b$. For design, it is recommended that top hinge depths be minimised to reduce strain in the longitudinal reinforcement and diagonal hangers.
10. Despite nonlinear shear response being recorded during the 3.5% beam drift loading cycle, the overall performance of the diagonal hangers was acceptable. To minimise the

strain induced in the hangers by connection flexure, the hangers should pass through the top hinge at a depth of $0.65d_h$ from the top of the top hinge. The strain penetration length measured in the hangers across the top hinge was $0.047f_yd_b$. The revised three hanger detail proved effective at resisting shear and torsion in exterior beams supporting the one-way flooring system. The new four hanger detail proved effective at resisting large gravity shear, seismic shear and torsion in internal beams supporting the one-way flooring system. A two hanger detail may be appropriate for beams that are not heavily loaded in shear and torsion. The design of the hangers should be undertaken considering the worst case shear, torsion and flexurally induced tension demands. All hangers located external to the main beam reinforcement cage should be adequately confined by reinforcement. The continuous hanger detail for internal beam-column connections, where the hangers on either side of an internal column are formed from a continuous length of reinforcement, proved effective at reducing connection congestion whilst facilitating effective force transfer.

11. The additional hooked reinforcement detail, which facilitated shear transfer between the equivalent truss mechanism in the beam and the diagonal hangers, was effective at maintaining the shear transfer mechanism throughout testing, as presented in Section 4.12. The additional hooked reinforcement detail should be used in situations where the effectiveness of hangers in this region may be uncertain, or when the unbonding tubes extend beyond the bottom hanger bend. Ensuring a dependable shear transfer mechanism in slotted beam connections is important to preclude a brittle shear failure during an earthquake.
12. Strain penetration in the bottom longitudinal reinforcement of SA1 was $0.010f_yd_b$ and was observed at both ends of the unbonded length of reinforcement. The extent of the strain penetration was exacerbated by using two layers of longitudinal reinforcement, due to the increased distance between the horizontal stirrups adjacent the longitudinal reinforcement. Supplementary reinforcement welded to the beam longitudinal reinforcement through internal beam-column connections proved effective at reducing strain penetration and bond stresses within the joint. It is possible that overall column depths in a slotted beam system may be able to be reduced by using the supplementary welded reinforcement detail, which could increase the cost-effectiveness of the system.
13. The top longitudinal, bottom longitudinal and diagonal hanger reinforcement performed well in bond in all connections of SA1. Low reinforcement strain was observed in the centre of all columns and no reinforcement slip was observed. Through the internal connections, the maximum average bond stresses in the top and bottom longitudinal

reinforcement were $2.20\sqrt{f'_c}$, $1.42\sqrt{f'_c}$ respectively. The maximum average bond stress of the bottom longitudinal reinforcement in the internal connections was $0.66\sqrt{f'c}$, which would have been $1.21\sqrt{f'_c}$ if supplemental welded reinforcement was not used.

14. The average beam elongation recorded in SA1 was an eighth of what would be expected in an equivalent traditional connection. The difference in total elongation between exterior and interior connections was not as significant in SA1 as it has been shown to be in traditional systems (Peng, 2009). Peak elongation in SA1, in terms of beam height, was 0.38%h and 0.44%h for internal and external connections respectively. The large gravity loads on Grid B of SA1 did not affect recorded beam elongation because beam elongation in slotted beam is predominately driven by flexure in the top hinge. Compared to traditional connections, the lower beam elongation exhibited by slotted beams will result in less damage in the floor diaphragm, less loss of precast floor seating and the hierarchy of strength intended by the designer being preserved. However, despite the reduced beam elongation that the slotted beam exhibits, first floor effects were able to be identified in the specimen, as discussed in Section 4.14.
15. All columns remained elastic throughout response. Grout couplers provided an effective means of developing the longitudinal column reinforcement and are suitable for seismic application when ductility has been excluded. The horizontal joint reinforcement remained elastic throughout testing and the observed strain distribution was similar to that observed by Au (2010). It is recommended that the NZS3101:2006 (Standards New Zealand, 2006) provisions for beam-column reinforcement are applied to the design of slotted beam systems. Furthermore, 25% more joint reinforcement, on top of that calculated using NZS3101:2006 (Standards New Zealand) methods, should be included in the bottom half of the joint as per Au's (2010) recommendations.
16. The precast floor unit seating width loss in SA1 was dependent on beam elongation, which was an eighth of what would be expected in an equivalent system with traditional connections. If a pragmatic approach is taken to designing seating widths then the need for redundancy in the floor seating connections is reduced. For this reason, the precast floor seating detail used in SA1 is recommended. This floor connection detail reduces the continuity moments that can be generated, which reduces the demands on the slotted beam diagonal hangers due to beam torsion. To further reduce continuity moments, and prevent spalling of the beam ledge that the floors are seated on, a dual layer low-friction bearing strip is recommended.
17. The reinforcement above the precast floor seating yielded during testing, which indicated that large continuity moments were generated by the precast floor connections. Large

warping deformations were observed in the floors around the columns; however, these were able to be accommodated by the timber infill and double-tee flange portions of the first and second floors. Displacement incompatibility between the precast flooring and the parallel seismic beams was able to be accommodated also by the timber infills and double-tee flanges. Recommendations were made to further reduce the damage to the floor diaphragm around the columns. Strain in the floor diaphragm during biaxial specimen displacements was well predicted by the superposition of strain from the uniaxial displacement components.

18. Designers must make a clear distinction between continuity moments and flange activation, and consider the contribution of both to lateral strength separately. The flange activation in SA1 at the survival limit state was approximately 90% of that observed in traditional systems (Priestley et al., 2007; Peng, 2009). During negative connection flexure the lever arm between the neutral axis and the floor reinforcement was reduced compared to a traditional system; hence, the contribution of flange activation to overall system lateral resistance was reduced also. Relatively even flange activation was observed between internal and external connections. Nominal and overstrength design flange activation widths for slotted beam systems were tentatively recommended in Section 4.16.2.

4.20 References

ACI Committee 318. (2005). *Building Code Requirements for Structural Concrete (ACI318-05)*. Farmington Hills, Michigan: American Concrete Institute.

ACI Committee 374. (2005). *Acceptance Criteria for Moment Frames Based on Structural Testing and Commentary (ACI374.1-05).* Farmington Hills, Michigan: American Concrete Institute.

Au, E. (2010). *The mechanics and design of a non-tearing floor connection using slotted reinforced concrete beams.* Masters Dissertation, University of Canterbury, Christchurch, New Zealand.

Byrne, J. D. R. (2012). *Bond and shear mechanics within reinforced concrete beam-column joints incorporating the slotted beam detail.* Masters Dissertation, University of Canterbury, Christchurch, New Zealand.

Chopra, A. K. (2001). *Dynamics of structures: Theory and application to earthquake engineering*. New Jersey, USA: Prentice Hall

Hare, J., Fenwick, R. C., Bull, D. K., & Built, R. (2009). Precast Double Tee Support Systems. *Journal of the Structural Engineering Society New Zealand, 22*(1), 10-44.

Lindsay, R. (2004). *Experiments on the seismic performance of hollow-core floor system in precast concrete buildings.* Masters Dissertation, University of Canterbury, Christchurch, New Zealand.

MacPherson, C. (2005). *Seismic performance and forensic analysis of a precast concrete hollow-core floor super-assemblage.* Masters Dissertation, University of Canterbury, Christchurch, New Zealand.

Matthews, J. G. (2004). *Hollow-core floor slab performance following a severe earthquake.* Doctoral Dissertation, University of Canterbury, Christchurch, New Zealand.

Ohkubo, M., & Hamamoto, T. (2004). *Developing reinforced concrete slotted beam structures to reduce earthquake damage and enhance seismic structural performance.* Paper presented at the 13th annual World Conference on Earthquake Engineering. Vancouver, B.C., Canada. Retrieved from http://www.iitk.ac.in/nicee/wcee/article /13_3285.pdf

Ohkubo, M., Zhang, A., Matsuoka, T., Hashimoto, A., & Yoshioka, T. (1998). 梁端下端エネルギー消費型RCラーメン構造に関する研究. *AIJ Journal, 37*(3), 281-284.

Paulay, T., & Priestley, M. J. N. (1992). *Seismic design of reinforced concrete and masonry buildings*. New York, USA: John Wiley & Sons, Inc.

Peng, B. H. H. (2009). *Seismic performance assessment of reinforced concrete buildings with precast concrete floor systems.* Doctoral Dissertation, University of Canterbury, Christchurch, New Zealand.

Priestley, M. J. N., Calvi, G. M., & Kowalsky, M. J. (2007). *Displacement-based seismic design of structures*. Pavia, Italy: IUSS Press.

Reid Construction Systems. (2007). *Reinforcement Product Catalogue.* Auckland, New Zealand: Author.

Restrepo-Posado, J. I. (1992). *Seismic behaviour of connections between precast concrete elements.* Doctoral Dissertation, University of Canterbury, Christchurch, New Zealand.

SEAOC Vision 2000 Committee. (1995). *Performance-based seismic engineering*. Sacramento, California: Structural Engineers Association of California.

Standards New Zealand. (2004). *Structural Design Actions Part 5: Earthquake Actions - New Zealand (NZS1170.5:2004).* Wellington, New Zealand: Author.

Standards New Zealand. (2006). *Concrete Strucutures Standard (NZS3101:2006)*. Wellington, New Zealand: Author.

Standards New Zealand. (2001). *Steel reinforcing materials (AS/NZS4671:2001).* Wellington, New Zealand: Author.

Viwathanatepa, S., Popov, E. P., & Bertero, V. V. (1979). *Effects of generalized loadings on bond of reinforcing bars embedded in confined concrete blocks (Report number UCB/EERC-79/22)*. University of California, Berkeley, USA: Earthquake Engineering Reseach Centre.

5. Design, Construction and Experimental Setup of the Subassembly Experiments

5.1 Introduction

As detailed in Chapters 3 and 4, specimen SA1 performed well when subjected to simulated earthquake displacements. Specimen SA1 exhibited high energy dissipation, stable response and low damage throughout testing. However, although the damage sustained by SA1 would have been economically viable to repair, uncertainty remained regarding the residual capacity of the slotted connection. Low-cycle fatigue is an important consideration in slotted beam connections due to the plasticity that the bottom unbonded reinforcement undergoes. Although damage is vastly reduced in slotted beam structures compared to structures with traditional detailing, if the slotted beam connections are not capable of reuse or economical retrofit, then the benefits of using a slotted beam system are diminished.

Five distinct subassembly specimens were tested during the second phase of this research project. Two subassemblies, SA2 and SA3, were extracted from superassembly SA1. The subassemblies were tested to determine the residual capacity of the slotted beam connections following the previous loading that they had been subjected to. The testing was biaxial and the subassemblies included portions of floor diaphragm. Following the testing of specimens SA2 and SA3 until failure, a retrofit technique to restore the moment capacity of the connections was developed. Using this retrofit technique three different external dampers were developed, implemented in specimen SA2 and tested to assess their viability for both retrofit and new-build applications.

A summary and critique of previous experiments is presented in Section 5.2. The origin and extraction of subassemblies SA2 and SA3 is described in Section 5.3. Section 5.4 describes the design of the retrofit regime and external dampers, whilst Section 5.5 chronicles the implementation of the retrofit regime. The design of the experimental setup, loading protocol and instrumentation is presented in Sections 3.6, 3.7 and 3.8.

5.2 Literature Review

Statically determinate experiments on smaller portions of larger structures are a popular form of testing undertaken in structural engineering. Subassembly testing allows the behaviour of details to be assessed in an economical and timely manner. It also simplifies subsequent analysis by avoiding the coupled response between different structural elements that can occur in a larger superassembly. However, subassembly tests can produce over-simplified results that may not be representative of the actual system response. Subassembly tests are well suited to developing details and testing new ideas, rather than as a final proof-of-concept prior to industry implementation. However, the relevance and applicability of the results can be improved if the specimen boundary conditions, loading protocol and specimen geometry are carefully designed.

The simplest subassembly specimen is a two-dimensional exterior beam-column connection with no floor. This type of experiment was undertaken by Au (2010) on a traditional reinforced concrete connection as a baseline for comparison against subsequent slotted beam experiments. The experimental setup used by Au (2010) is shown Figure 5-1. The subassembly was loaded through the points of contraflexure in the beams and column. Uniaxial displacements were applied at the top of the column, whilst the column base and beam end were held static by pinned connections. Because loading was along one axis only, a universal joint at the base of the column was not required and a one-way pivot was used instead. The one-way pivot allowed not only for inclination of the column in-plane, but also provided restrain against specimen inclination out-of-plane and rotation about the vertical axis.

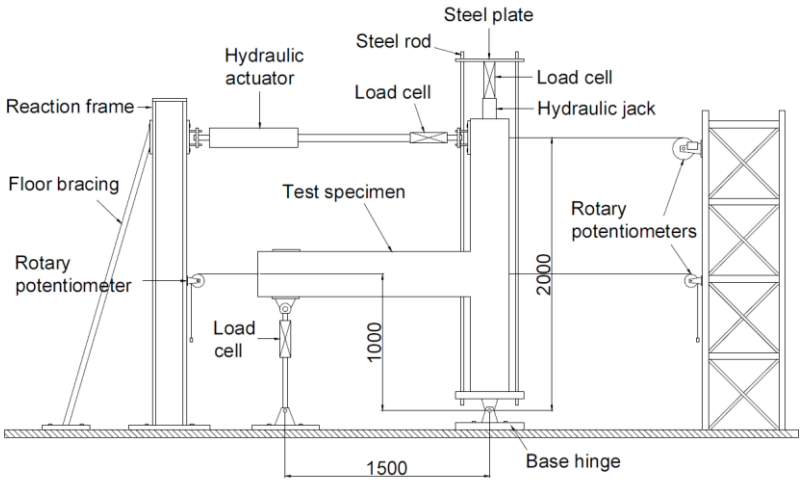

Figure 5-1: Two-dimensional beam-column connection subassembly test (Au, 2010).

A two-dimensional subassembly test on a beam-column connection that includes a portion of floor is sometimes termed a 'two-dimensional plus' specimen. An example of this type of test

was the experiment conducted on specimen SB3 by Au (2010), as shown in Figure 5-2. This experiment aimed to induce beam torsion by applying a simulated gravity load to a portion of floor connected to the beam. The specimen was supported at its points of contraflexure and the displacements were applied to the top of the column. Specimen rotation about the vertical axis was restrained by the floor pivot. Restraint was provided to the top of the column to prevent any specimen displacement out-of-plane, which could have influenced the strain in the floor.

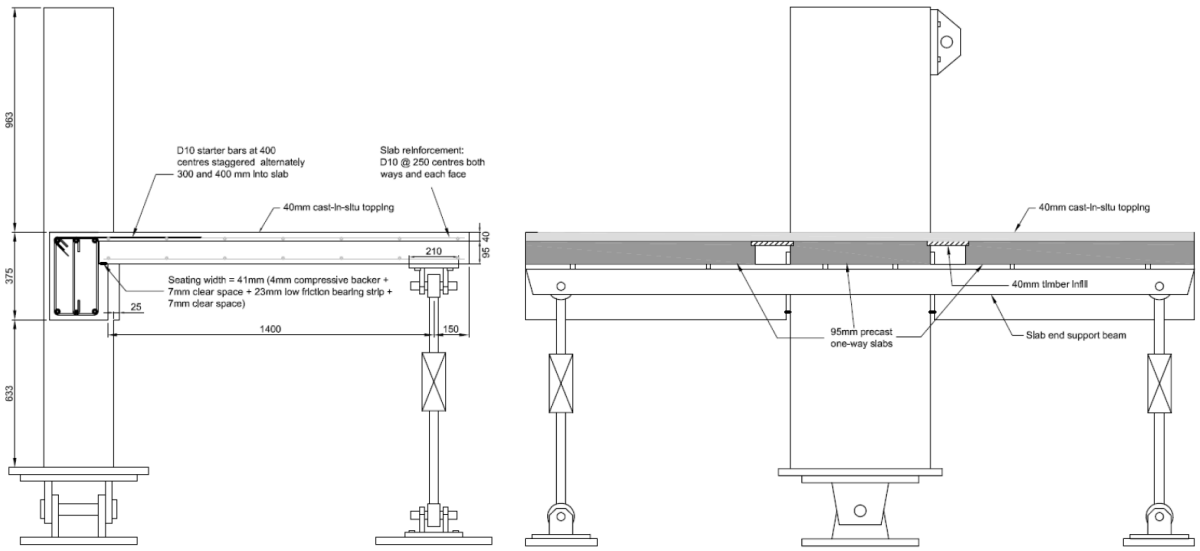

(a) End elevation. **(b) Side elevation.**

Figure 5-2: Two-dimensional beam-column connection with floor subassembly test (Au, 2010).

Three-dimensional subassemblies that are displaced biaxially are more representative of actual building components subjected to earthquake loading. An experiment of this type was conducted by Akguzel (2011) and the setup from that test is shown in Figure 5-3. In each orthogonal loading direction, the setup was similar to that of a two-dimensional test. However, a dual acting universal joint was required at the column base to allow column inclination in both directions. The universal joint was also used to retrain the specimen against rotation about the vertical axis. Because Akguzel's (2011) specimen had no floors, inclination of the beam about its longitudinal axis was restrained by structural steel brackets. The specimen was loaded vertically also, due to the sensitivity of the non-ductile specimen to column axial load.

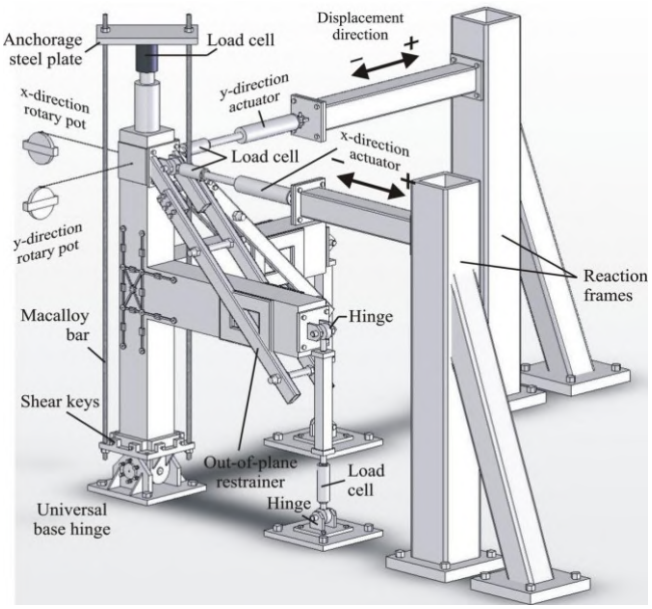

Figure 5-3: Three-dimensional beam-column connection subassembly test (Akguzel, 2011).

Amaris (2010) used the same reaction frame as Akguzel (2011) to undertake biaxial tests on post-tensioned precast subassemblies, as shown in Figure 5-4(b). However, the specimen that was tested incorporated portions of a floor diaphragm. The one-way precast floor was simply supported at its end. As shown in Figure 5-4(a), because rotational restraint of the beams was supplied by the floor there was no need for structural steel brackets to perform this task.

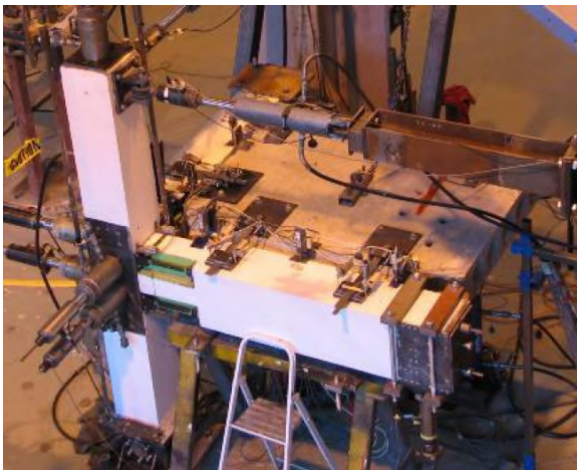

(a) Perspective of test setup.

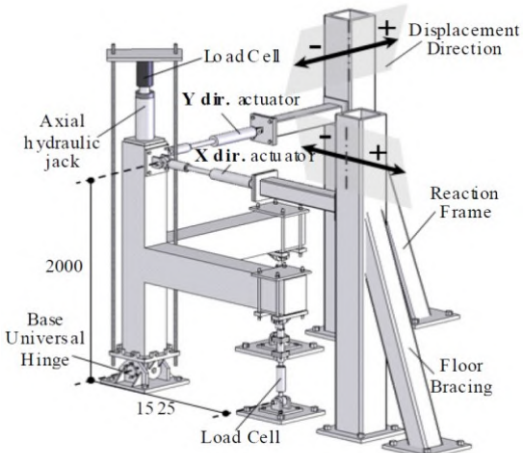

(b) Schematic of test setup, based on work by Akguzel (2011).

Figure 5-4: Three-dimensional beam-column connection with floor subassembly test (Amaris, 2010).

Rodgers (2009) recognised that in large scale subassemblies, that require large actuator forces, the rotational restraint about the vertical axis provided by the universal joint supporting the column would be insufficient. Because of the small forces involved, the three-dimensional experiments of Amaris (2010) and Akguzel (2011) avoided failure by way of specimen rotation about the vertical axis. As shown in Figure 5-5, Rodgers' (2009) experiment investigated the performance of a three-dimensional post-tensioned concrete frame subjected to biaxial displacements. An actuator mounted to the end of one of the beams was used to restrain specimen rotation about the vertical axis. To ensure that specimen

rotation about the vertical axis was not imposed, the displacement applied by actuator C was a fixed ratio of that applied by actuator A. Rodgers' (2009) experimental setup was effective; however, introducing forces to the end of the beam had the potential to induce weak axis bending in the beam. This issue would not occur in a specimen that included a floor diaphragm because the forces would be transferred axially across the floor.

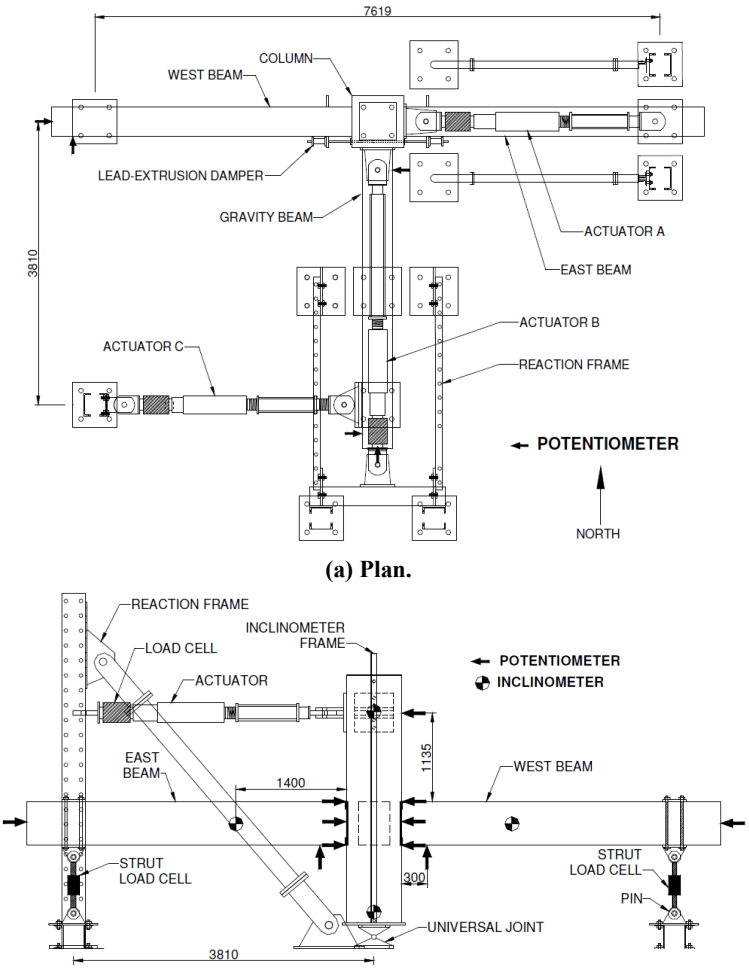

(a) Plan.

(b) Side elevation.

Figure 5-5: Three-dimensional beam-column test with rotational restraint (Rodgers, 2009).

The geometry of the subassemblies extracted from SA1, and the experimental setup designed to test them, was based on the strengths of the historical experiments described above.

5.3 Subassembly Extraction

The beam units Bm C/1-1 and Bm C/2-1 were extracted from specimen SA1 and they subsequently formed the basis of specimens SA2 and SA3 respectively. Specimen SA1 was demolished in stages, both to preserve the integrity of subassemblies SA2 and SA3 and to prevent damage to the strong floor, improve worksite safety and conform to the load limit of the gantry crane.

The first task in the demolition of SA1 was to remove all the instrumentation from SA1 and disassemble the reaction frames. As shown in Figure 5-6(b), the Level Two floors were then

cut around the perimeters of the precast units with a ground saw. While it would have been possible to undertake the concrete cutting without propping the precast floor units, given the displacements that SA1 had been subjected to, propping was installed as a safety measure. A concrete core drill was used to create an opening to pass lifting strops through, and then the units were removed with the gantry crane. Removing the slotted beams from SA1 was a simple process compared to removing traditional beams from a structure. In the slotted beam, only the top hinge needed to be broken out with a concrete breaker, and then the reinforcement was severed. The beam unit, which was propped during the extraction process, was then lifted clear with the gantry crane, as shown in Figure 5-6(c). As shown in Figure 5-6(d), the Level One floor was then removed. The process for removing the Level One components was identical to that undertaken for Level Two. When subassemblies SA2 and SA3 were extracted from SA1, the beam along Grids C was cut in the centre. The beams along Grids 1 and 2 were then cut to match the length of the orthogonal beam. The length of both beams in the subassemblies was made the same so that subassemblies SA2 and SA3 were mirror images of each other, which simplified comparison between the specimens. Because the loading protocol applied to the specimen was based on beam drift, a change in specimen geometry did not change the demands that the slotted connection was subjected to.

(a) End of testing.

(b) Removing Level Two floors.

(c) Removing Level Two beams.

(d) Level One floors removed.

Figure 5-6: SA1 Superassembly demolition and extraction of subassemblies.

(e) Removing Level One beams and lowering columns.

(f) Demolition complete and SA2 and SA3 remaining.

Figure 5-6: SA1 Superassembly demolition and extraction of subassemblies (Continued).

The Level One precast components were removed in a different order to those from Level Two. The column being extracted was first supported with the gantry crane to prevent it from toppling. The ends of the beams framing into the column being extracted were then propped and the top hinge reinforcement broken out and severed. The column could then be safely lowered and the operation repeated on the remaining columns, as shown in Figure 5-6(e).

The demolition of specimen SA1 was undertaken safety and efficiently. Figure 5-6(f) shows the two extracted subassemblies SA2 and SA3 at the end of demolition; SA3 is in the foreground of the figure. Due to the on-going seismicity in the Christchurch region, it was important to secure the specimens. To prevent the specimens from toppling during an aftershock, a propping regime was designed to support the beams and precast floors. Specimen SA3 had to be moved from the strong floor to free up space for other experiments to be conducted. The beams and floor of SA3 had to be supported during lifting to prevent connection deformations due to gravity loading. However, it was just as important to ensure that the beams and floor were not used as lifting points. Chain blocks were attached between the column and the beams and floor, and tensioned to support only the self-weight. The gantry crane was then attached to the top of the column to lift the specimen, as shown in Figure 5-7(a). Lifting in this manner resulted in the specimen being lifted on an angle; however, it presented the best option to protect the integrity of the specimen. Figure 5-7(b) shows SA2 in position on the strong floor, and SA3 in the background in the correct orientation to be moved across into position on the strong floor after SA2 was demolished.

(a) Lifting SA3.

(b) SA2 and SA3 in final position.

Figure 5-7: Extracted subassemblies SA2 and SA3.

5.4 Subassembly Design

Five distinct subassembly specimens were tested during the second phase of this research project. Specimens SA2 and SA3 were the as-built subassemblies extracted from the superassembly, as described in Section 5.3. Aside from the reaction frame and instrumentation setup described in Section 5.6-5.8, there was no further design or modification undertaken. The remaining three specimens were retrofitted variants of SA2. The specimens were named SA2-TCY, SA2-SFD and SA2-HF2V, where the suffix refers to the type of damper used. The dampers, along with the retrofit technique, are described below.

5.4.1 Slotted Beam Retrofit Design

The retrofit regime was designed to replace the role of the bottom unbonded reinforcement in the slotted beam connection. Following a large earthquake, the bottom reinforcement may not have sufficient residual strength or strain capacity remaining for the structure to be safely reoccupied. Potentially more likely in New Zealand is the scenario where, following a damaging earthquake, an insurer must repair a structure to its pre-earthquake state. Connection retrofit regime presents one means of addressing these issues.

The existing top longitudinal reinforcement and diagonal hangers in the connections were retained in this design because these elements are extremely difficult to rehabilitate. However, shear corbels or external dampers could be used to retrofit the top longitudinal reinforcement or diagonal hangers if required. The strains experienced in the top longitudinal reinforcement and diagonal hangers of a slotted beam during a design earthquake are predominately elastic,

as shown in Section 7.5.3. Hence, it was likely there would be sufficient residual capacity in the top longitudinal reinforcement and diagonal hangers of the connections to withstand the demands of a future earthquake.

The first step to retrofitting SA2 was to cut the remaining bottom longitudinal reinforcement out of the slot region. It was important to cut the reinforcement flush with the face of the columns and ends of the beams. This ensured that the ends of the severed reinforcement did not contact during negative flexure. As shown in Figure 5-8, cleats were installed on the column face and the beam soffit to enable dampers to be attached between them. To enable the cleats to be bolted to the column face and beam soffit, threaded rods were epoxied into holes drilled into the concrete. Because the threaded rods installed in the column face were loaded primarily in tension, they required a long embedment length to fully develop their capacity. However, because the threaded rods in the beam soffit were loaded primarily in shear, they did not need to be fully developed in tension and a shorter embedment length was able to be used.

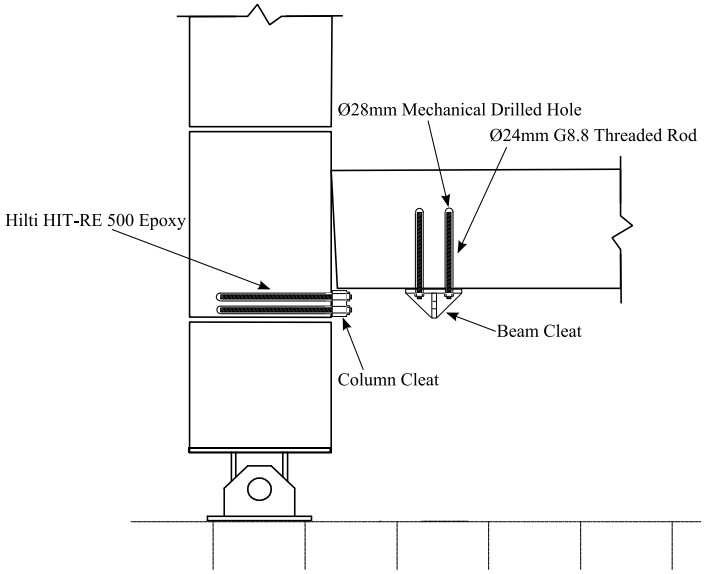

(a) Retrofit schematic.

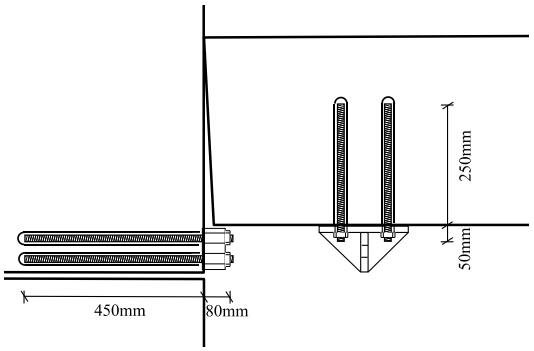

(b) Close up of cleats and connection.

Figure 5-8: Slotted beam retrofit regime.

The location where the threaded bars were installed were congested with reinforcement. The location that the threaded bars were installed had to be carefully considered to avoid severing

critical reinforcement. However, some reinforcement became superfluous after the connection retrofit was completed and could be safely cut to enable practical placement of the threaded rods. For example, the close stirrup spacing over the unbonded region of the bottom longitudinal reinforcement was no longer required for buckling restraint.

The column and beam cleats are shown in Figure 5-9(a) and (b) respectively. The cleats were designed to be compatible with a number of different dampers. Had this not been the case a more elegant design could have been produced. The column cleat was machined from 50mm thick mild steel. This was required to provide sufficient thread depth and bending strength to resist the worst case demands, which were induced by the high force to volume (HF2V) damper. The cleat width was governed by the width of the sliding friction damper (SFD). The threaded rods installed in the columns, and hence the corresponding holes in the cleats, were staggered to ensure that the threaded rods installed in each of the orthogonal column faces were able to pass over each other inside the column. The centre M24 thread was for attachment of the HF2V device; the outside two M24 threads were to attach the tension-compression yielding (TCY) dampers.

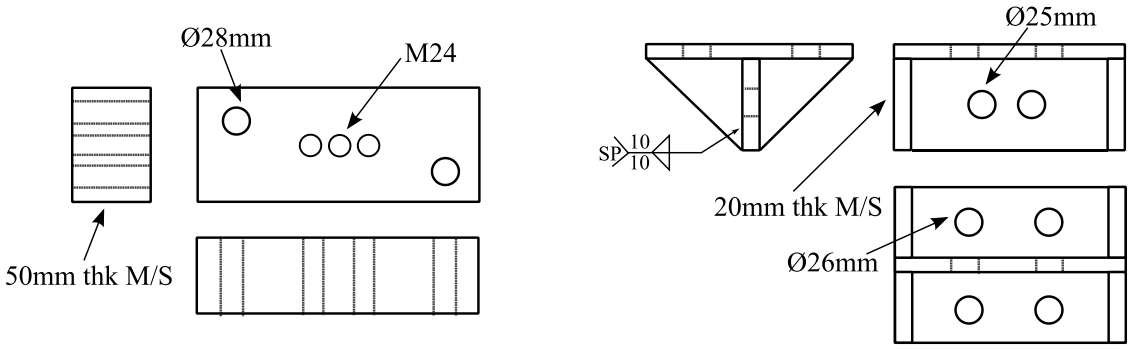

(a) Column Cleat. **(b) Beam Cleat.**

Figure 5-9: Retrofit cleats.

The design of the beam soffit cleat was governed by friction between the cleat and the beam soffit, rather than the shear or axial capacity of the threaded rods. The beam soffit cleat was designed to be compatible for both the SFD and TCY dampers.

The external dampers designed for the slotted beam are described below. These dampers were designed to produce a peak resistance of 120kN and be suitable for both retrofit and new build applications.

5.4.2 TCY Damper Design

The tension-compression yielding (TCY) damper is similar in concept to a buckling restrained brace, and has recently been developed at the University of Canterbury for use in timber and concrete PRESSS type systems (Palermo et al., 2006; Smith et al., 2008; Marriott, 2009). The damper is typically manufactured from plain round mild steel bar, threaded rod or

reinforcement. For the TCY dampers used in SA2-TCY, 24mm diameter plain round mild steel bar was used because a closer fit was able to be achieved between the bar and the buckling restraint tube. The deformed lugs on the surface of reinforcement prevent a close fit between the reinforcement and the buckling restraint tube.

Threads were cut into both ends of the sections of plain round bar. A portion of the plain round bars was lathed down to a 16mm diameter to encourage preferential yielding over this region. Due to the high slenderness of the machined section of the bar, buckling restraint was required to enable compressive yielding to occur. Compressive yielding is more predicable than buckling and dissipates significantly more energy. To restrain buckling, a steel tube was fitted over the turned down section of the bar and the gap between the two components was filled with high strength structural epoxy. This restrained buckling within the machined section of the bar, and increased the buckling capacity of the entire damper. However, as shown in Figure 5-10, filling the interior of the steel confinement tubes with epoxy introduced problems when the damper was loaded in net compression. During tensile loading the turned down section was free to yield in tension. However, during net compressive loading the larger diameter of the threaded portion of the bar could contact the confined epoxy, which would significantly increase the damper axial strength and lead to damper buckling.

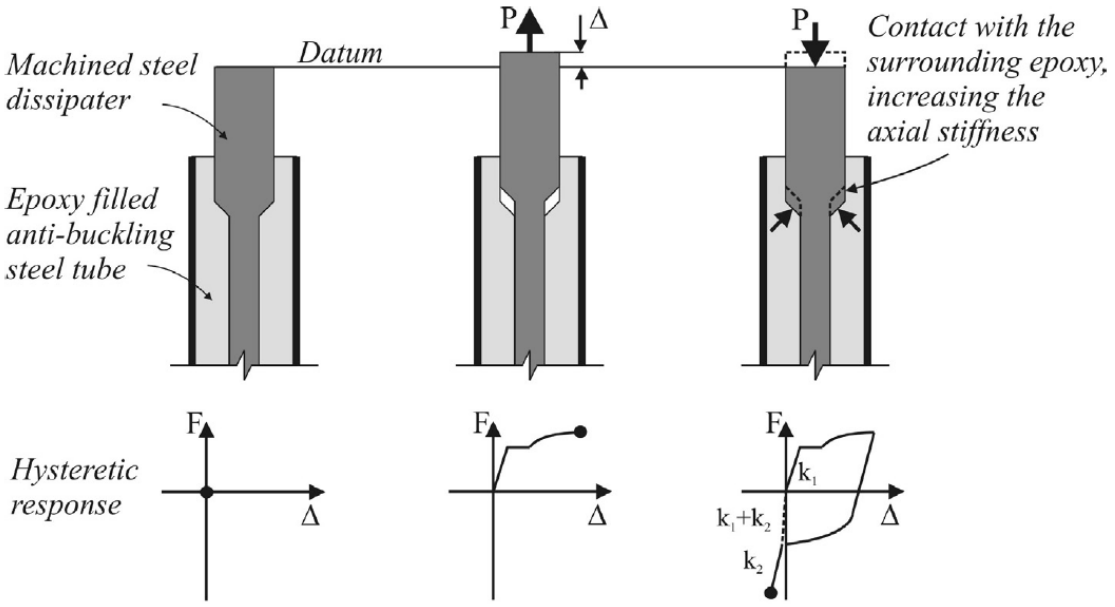

(a) At rest. **(b) Positive displacement.** **(c) Negative displacement.**

Figure 5-10: Effect of restraining epoxy on TCY damper compressive strength (Marriott, 2009).

Historically, TCY dampers have primarily been used in PRESSS type structures, where the damper loading remains predominately in net tension. This has meant that the large increase in TCY damper capacity during net compression had not been an issue. However, in a slotted beam, the compression and tension strain excursions in the TCY dampers were relatively similar. The large increase in TCY damper capacity during net compression was undesirable

as it could cause the damper to buckle, which would lead to unsatisfactory connection response. A detail to mitigate this issue was developed, and is shown in the schematic of the TCY dampers used in SA2-TCY presented in Figure 5-11. Room temperature vulcanising (RTV) silicone plugs were installed at either end of the machined length of the TCY damper. This plug was designed to prevent contact between the epoxy and the threaded portion of the damper during the maximum expected compression displacement. RTV was chosen due to its low stiffness, low cost and workability.

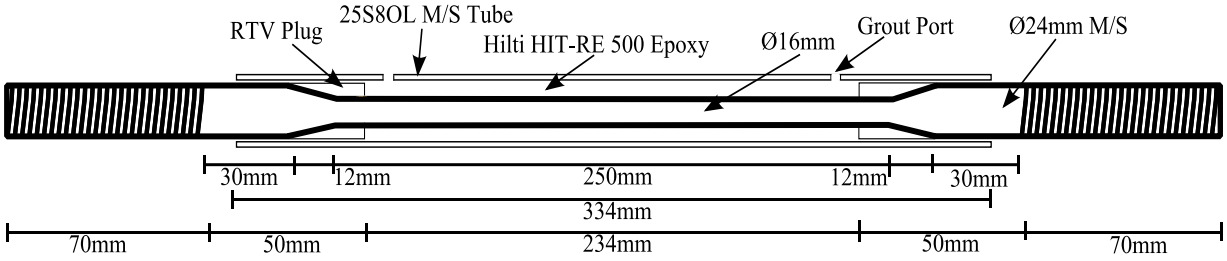

Figure 5-11: Tension-compression yielding damper.

Testing by Sarti et al. (2013) has shown that during cyclic loading the onset of TCY damper buckling occurs at 9% and 6% strain for slendernesses of 75 and 90 respectively. Slenderness is defined as four times the length of the machined section of the damper divided by the diameter. The dampers used in SA2-TCY were designed for a peak strain of 5% and had a slenderness of 63. As discussed above, the design focus for TCY dampers has primarily been for PRESSS type connections, and the testing performed by Sarti et al. (2013) used a loading protocol designed to replicate the displacements that the damper would be subject to in this application. The loading protocol used by Sarti et al. (2013) is shown in Figure 5-12. TCY dampers installed in slotted beams are subject to both positive and negative net displacements, which results in greater total strain and an increased risk of low-cycle fatigue failure. If the strain history applied to the damper is known, there are formulations for predicting the likelihood of low-cycle fatigue failure occurring. This is discussed in more detail in Section 7.5.3. However, in practice the strain history the TCY damper will be subjected to is typically unknown. Hence, although the dampers for SA2-TCY were designed with a comparatively low slenderness, a lower maximum strain value was used to reduce the risk of low-cycle fatigue failure occurring.

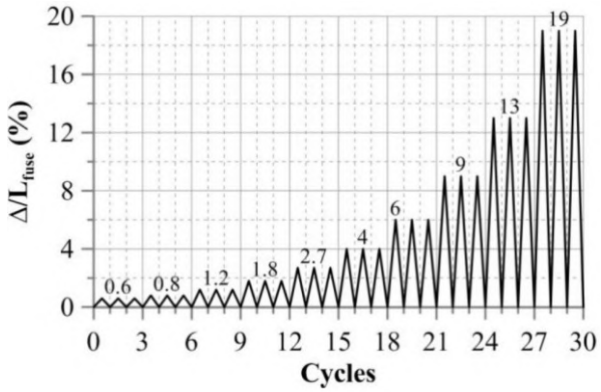

Figure 5-12: Loading protocol used by Sarti et al. (2013) for TCY damper testing.

The TCY damper dissipates energy in the same manner as the unbonded bottom longitudinal reinforcement in a slotted beam. Hence, when used in a slotted beam the resulting connection response is relatively similar to the as-built response. The TCY damper is relatively cheap to manufacture; however, after use it cannot be reused.

5.4.3 SFD Damper Design

The Sliding Friction Damper (SFD) was originally conceived by Grigorian et al. (1993) for use in diagonally braced steel frames. Since then it has been developed for use in structural steel moment frames by Clifton (2005), MacRae et al. (2010) and Chanchi Golondrino et al. (2012). The SFD dissipates energy through friction, as steel plates that have been clamped together slide over one another. Shims can be installed between the steel plates to modify the friction coefficient. The steel plates and shims are clamped together using high strength bolts. Historically, the SFD has been used in structural steel buildings; however, the dampers can be used in reinforced concrete slotted beam connections also. For SA2-SFD, an asymmetrical friction connection was used because it was the simplest configuration. This connection had one plate with holes for the bolts to bear against, and another plate with slots which allowed sliding to occur. A cap on the top of the device provided an additional friction surface. The details of the SFD devices used in SA2-SFD are shown in Figure 5-13.

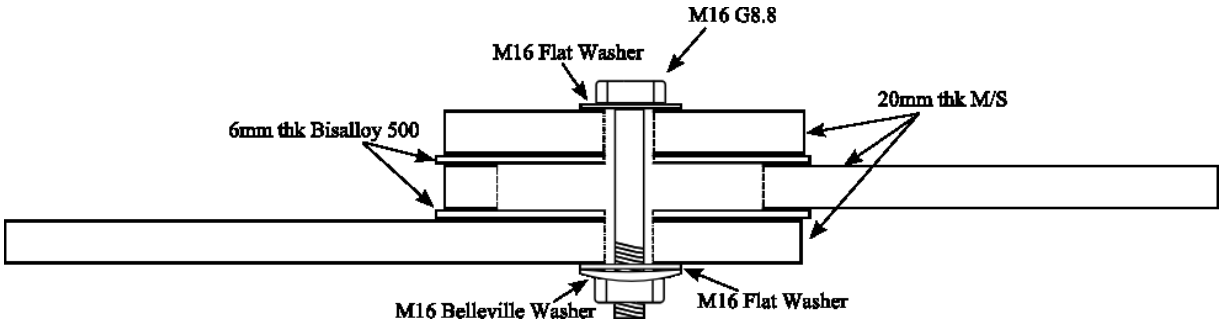

(a) SFD assembly.

Figure 5-13: Sliding friction damper.

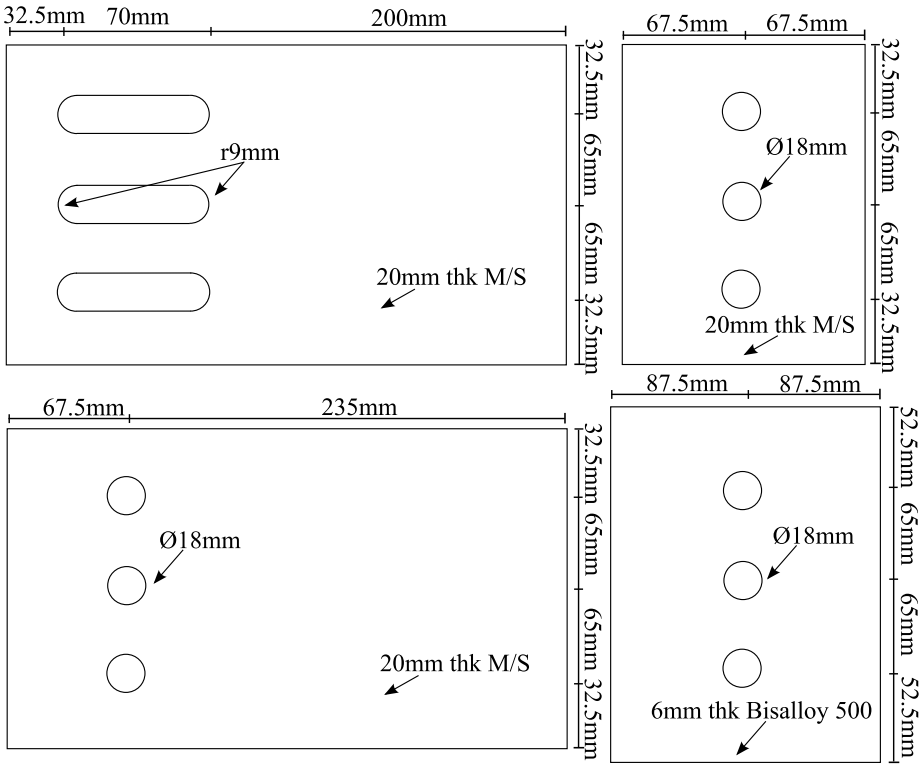

(b) SFD components.

Figure 5-13: Sliding friction damper (Continued).

Recent research by Chanchi Golondrino et al. (2012) focussed on investigating the effect of clamping forces, shim material and loading rates on the capacity of the SFD. Preliminary results from this research, and the geometrical limitations of the slotted beam, guided the design of the SFD used in specimen SA2-SFD. Three M16 G8.8 bolts were used to supply the clamping force, as they were the only bolt type with reliable testing results. These bolts were installed with a belleville washer at the nut end to maintain the clamping force during testing. It had been found that using a shim material with a significantly higher hardness than the steel plates encouraged a more stable hysteretic response; hence, Bisalloy 500 steel was used for the shims (Chanchi Golondrino et al., 2012). Bisalloy 500 has a Brinell hardness of 500HB; mild steel typically has a Brinell hardness of 120HB. It is important to design the SFD with sufficient stroke to avoid the bolts from binding against the mild steel plate. If this occurs, a large and rapid increase in the SFD capacity will result.

The SFD damper can be reused after an earthquake by replacing the bolts that provide the clamping force in the device. The SFD is also relatively cheap to manufacture.

5.4.4 HF2V Damper Design

The high force-to-volume (HF2V) damper is a type of lead extrusion damper developed at the University of Canterbury (Rodgers, 2009). Lead extrusion dampers dissipate energy by forcing confined lead to flow through an annular constriction. The HF2V damper is capable of dissipating large amounts of energy and generating large damper forces. Furthermore, due

to the low re-crystallisation temperature of lead, the damper's properties do not change after loading and are not subject to low-cycle fatigue effects.

Lead extrusion dampers were first proposed by Robinson and Greenbank (1975, 1976). As shown in Figure 5-14(a), these early devices forced a plug of lead through a constraining cylinder with an extrusion orifice machined into it. These devices were effective; however, due to the amount of material and machining required the devices were very expensive. Cousins and Porrit (1993) improved the damper design by changing from a constricted tube which lead is displaced through, to a bulged shaft that is displaced through stationary lead. The improved design reduced fabrication costs compared to the original. However, the size of the damper remained considerable, as shown in Figure 5-14(b). These dampers were designed for base isolation application, so the large size provided no barrier to implementation.

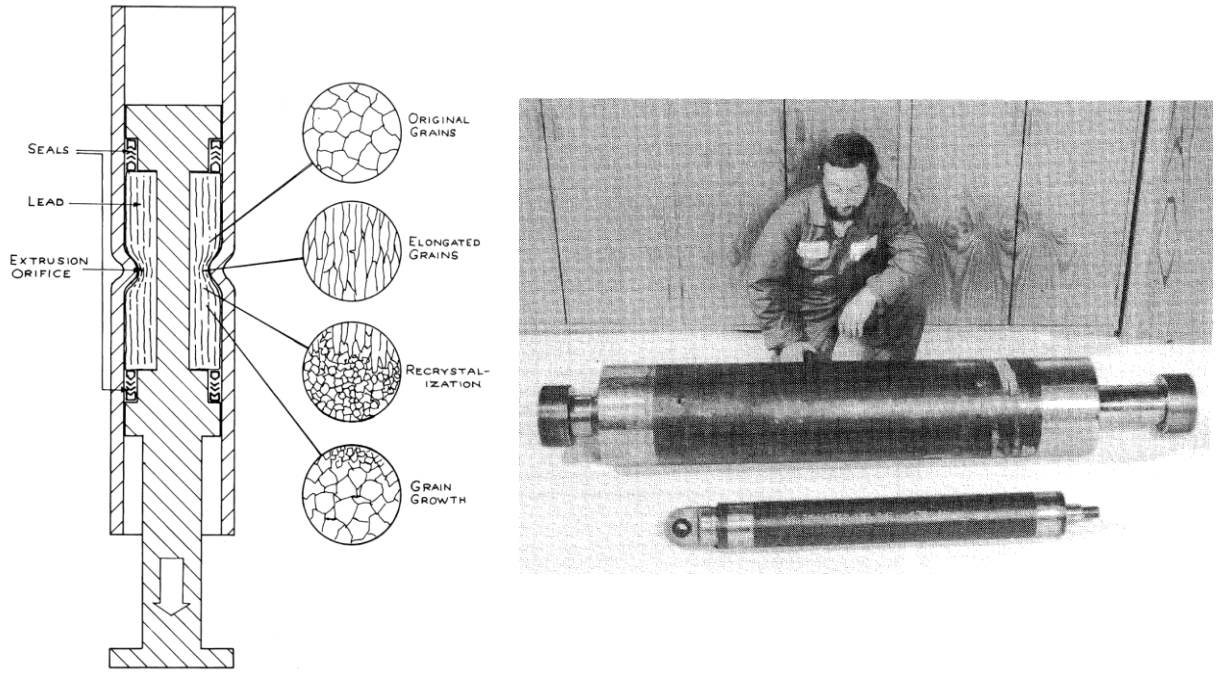

(a) Original lead extrusion device (Robinson & Greenbank, 1975).

(b) Improved lead extrusion devices (Cousins & Porritt, 1993).

Figure 5-14: Early lead extrusion devices.

Rodgers (2009) identified the potential of the lead extrusion damper if it could be drastically reduced in size and cost, yet maintain a high reaction force and stiffness. The lead damper would then be able to be implemented within a frame system to provide lateral resistance, instead of damping rigid body translation. Hence, the HF2V damper was developed. The HF2V damper that was used in specimen SA2-HF2V is presented in Figure 5-15. This device was designed to specified force and stroke requirements by Rodgers (2012). The force is determined by the size of the bulge on the shaft, which creates the annular constriction within the cylinder. It is important to consider the stroke of the device because, as with the SFD device, when the end of the device stroke is reached the force and stiffness rapidly increase.

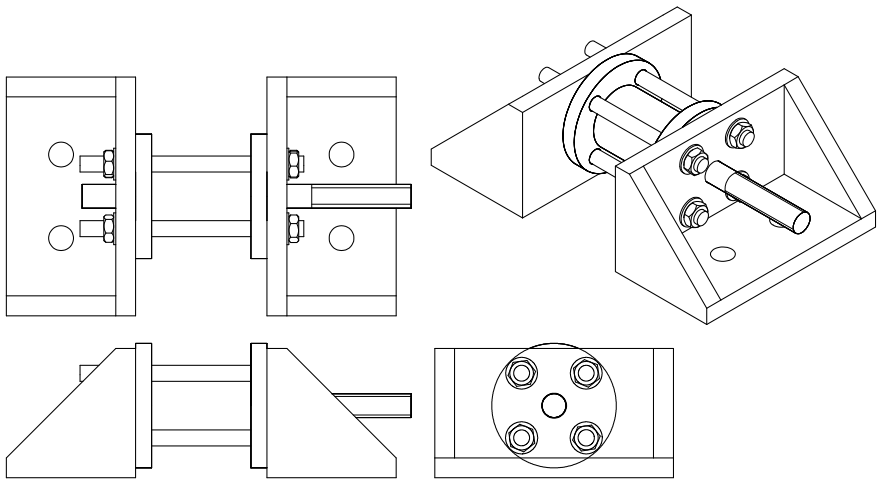

(a) Overall assembly.

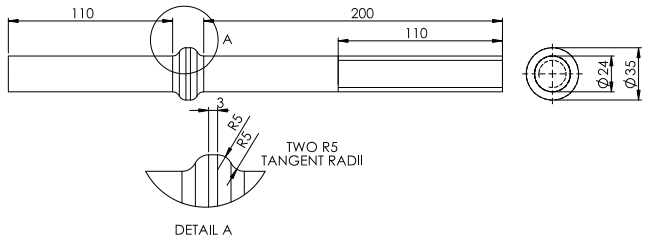

(b) Shaft detail.

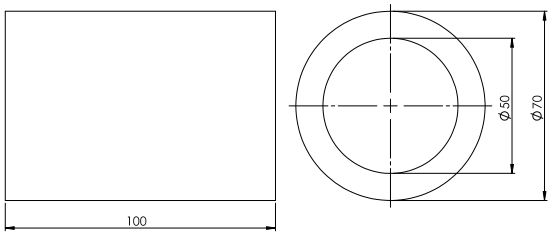

(c) Cylinder detail.

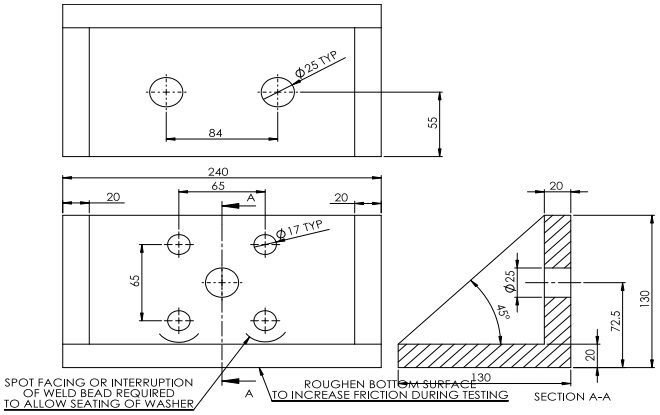

(d) Mount bracket detail.

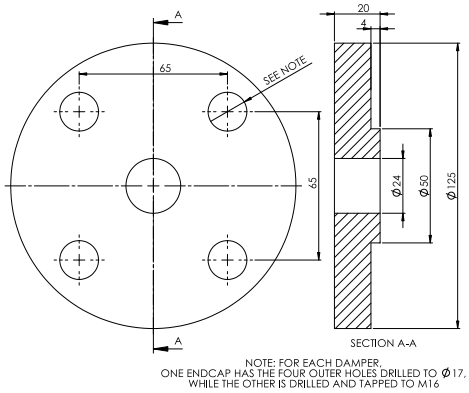

(e) End cap detail.

Figure 5-15: High force-to-volume damper (Rodgers, 2012).

The beam soffit cleat used for the TCY and SFD dampers was not compatible with the HF2V device. Hence, new beam soffit cleats were manufactured. To attach the HF2V beam soffit cleats, new threaded rods were drilled and epoxied into the beam soffit. However, the column cleats were designed to be compatible with the HF2V device.

The cost to manufacture the HF2V device has been significantly reduced over its development; however, it remains expensive compared to other dampers. The device is able to dissipate large amounts of energy, and following a large earthquake the device potentially does not require any maintenance before the building it is installed in is reoccupied. Hence, a designer may determine that the benefits of the HF2V device justify the increased cost, especially if the devices are used strategically over a structure to maximise benefit and amortise the higher cost.

5.4.5 HF2V-FS Damper Design

A combined HF2V damper and friction spring (FS) device was investigated for use in the proposed specimen SA2-HF2V-FS. The HF2V device has many favourable properties, as described in Section 5.4.4. However, due to the shape of the hysteretic response, recentring behaviour is unlikely if HF2V dampers are used as the only dissipating devices in a system. Ensuring that a structure returns to the original plumb position following a large earthquake is an important design consideration and significantly affects the building repair costs. It is possible to provide an overall recentring force on a structural level. However, a recentring force can be provided also through connection response, such as in PRESSS type connections (Priestley, 1996). The HF2V-FS device was designed to provide stable response, high energy dissipation and recentring behaviour when used in a slotted beam connection.

The recentring force for the damper was provided by the use of a friction spring. As shown in Figure 5-16(a), a friction spring stores axial energy through radial strain in stacked rings. This enables friction springs to generate a high force and stiffness compared to traditional torsion springs of comparable dimensions. Depending on the slope of the contact surfaces between the rings and the friction coefficient of the assembly lubricant, energy dissipation of between 0% and 66% of the input energy can be specified. However, greater damping comes at the expense of a reduced unloading stiffness. A FS with a low unloading stiffness, when used in parallel with another energy dissipation device, may not be desirable because full recentring behaviour may not be achieved. This can be seen graphically by considering the conceptual response of a combined HF2V and FS device shown in Figure 5-16(b) – (d). Lead is able to flow at low temperatures; therefore, even if a low recentring force is applied the device can creep back to the original position over time. It may be possible to design a system that does not immediately return to its original plumb position at the end of an earthquake, but returns slowly to that position in the days following the earthquake.

The total force capacity of a HF2V-FS device, as well the proportion of the total force to recentring force, can be tailored to the application. Hence, a HF2V-FS device could be designed to supply large amounts of energy dissipation with full recentring ability. Because the device is not subject to degrading stiffness or low-cycle fatigue, if it were used in a slotted beam connection immediate reoccupation of a building following a design earthquake could be achieved.

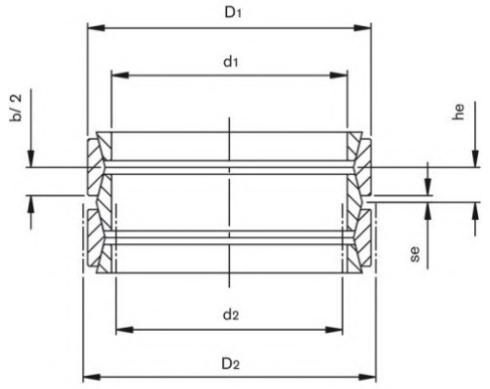

(a) Friction spring cross-section (Ringfeder, 2010).

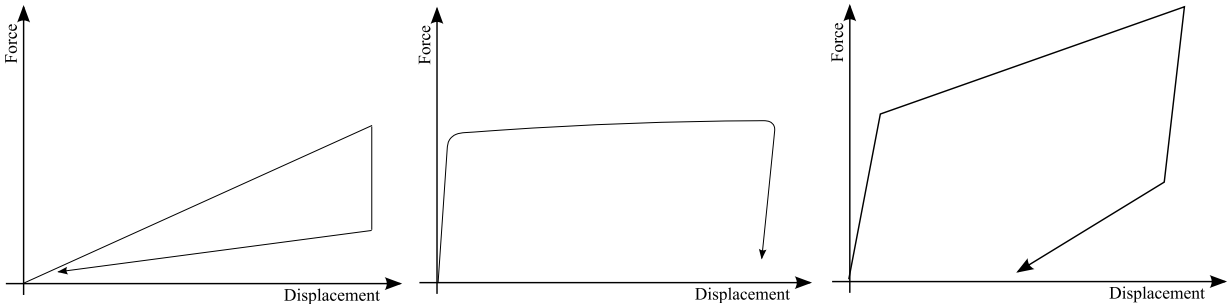

(b) Friction spring. **(c) HF2V.** **(d) HF2V-FS.**

Figure 5-16: HF2V-FS conceptual response.

A schematic of the HF2V-FS device designed to be tested in specimen SA2-HF2V-FS is shown in Figure 5-17. This device was not designed to be fully recentring. Due the reuse of the 120kN HF2V damper used in SA-HF2V, the total recentring force had to be limited to 40kN to remain within force limits of the beam and column attachment cleats.

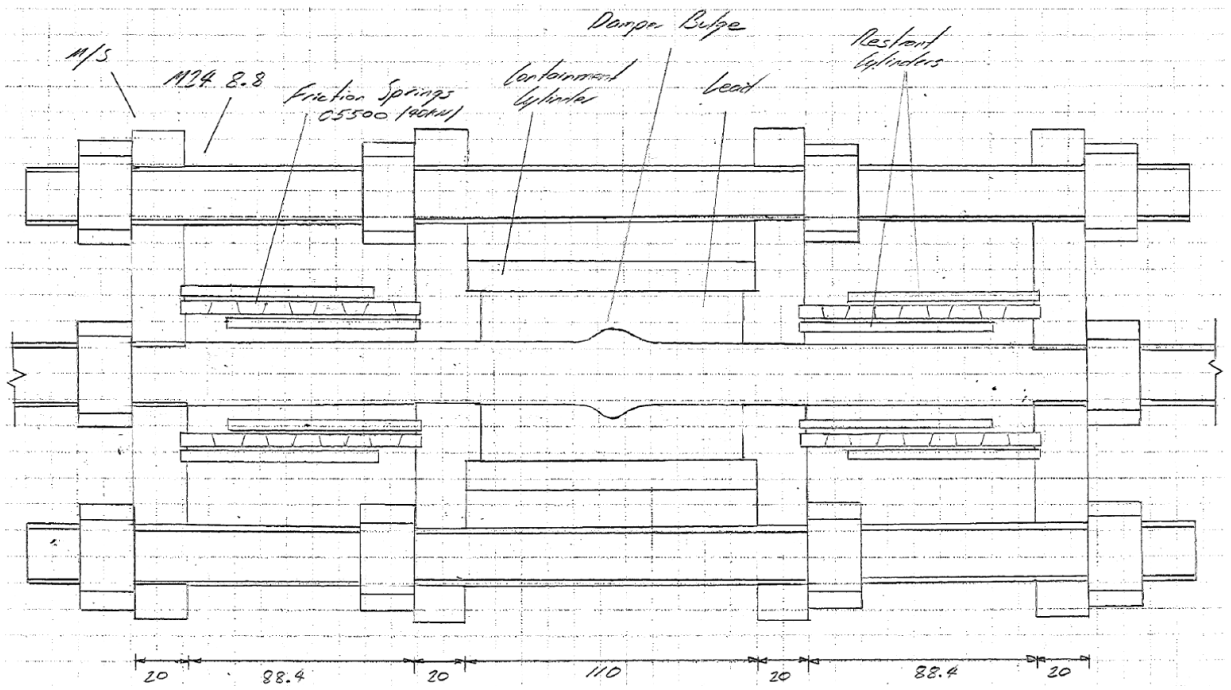

Figure 5-17: Schematic of proposed HF2V-FS device.

Friction springs work only in compression; hence, for the device to work effectively in both compression and tension either two stacks of springs are required, or a double acting design

must be used. A double acting design is more compact and cost efficient; however, because an existing HF2V was being used, two stacks of friction springs presented the most viable option.

The use of the HF2V-FS damper in a slotted beam could provide near-ideal structural response during an earthquake. However, the high cost of friction springs and the long lead times to supply them are barriers to implementation. These barriers would diminish with increased use of this technology. Regardless, due to the inability of the supplier to provide the required friction springs within the testing timeframe, this damper configuration was unable to be tested.

5.5 Subassembly Construction

The retrofit of specimen SA2 was undertaken in the structures extension laboratory at the University of Canterbury by the author. It can be concluded that the slotted beam connection can be effectively retrofitted by suitably trained persons.

5.5.1 Slotted Beam Retrofit Construction

To implement the retrofit regime, holes were first drilled into the column face and beam soffit, as shown in Figure 5-18(a) and (b). The holes were drilled using a Hilti TE 70-ATC combi-hammer with a Ø28mm carbide tipped bit. Reinforcement was encountered in some holes, which made the drilling difficult to undertake accurately. After the holes had been drilled to the required depth they were thoroughly cleaned of dust and debris using a vacuum and compressed air. Hilti HIT-RE 500 structural epoxy was injected into the holes and the M24 G8.8 threaded rod, which had been cut to length, was installed into the holes. The threaded rods were spun into position to distribute the epoxy evenly between the bar and walls of the hole. As shown in Figure 5-18(c), plywood templates of the cleats were used to position the threaded rods correctly while the epoxy cured. Duct tape was used to prevent the threaded rods from falling out of the beam soffits. To encourage a stiff shear connection between the beam soffit and the steel cleat, the beam soffits were scabbled, the cleats were roughened and a structural epoxy was applied between them, as shown in Figure 5-18(d)-(f).

(a) Ø28mm holes drilled in column face.

(b) Ø28mm holes drilled in beam soffit.

(c) Ø24mm G8.8 threaded rod epoxied in position.

(d) Scabbled beam soffit.

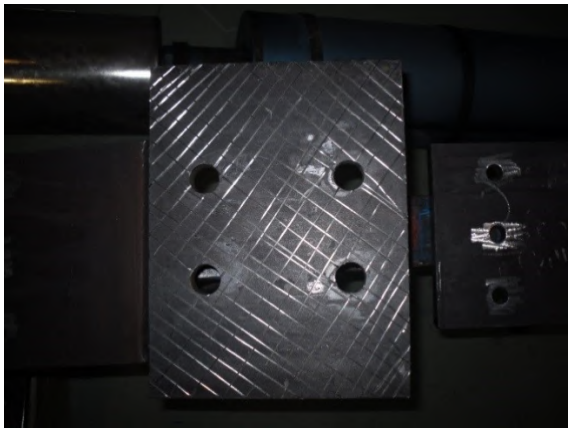

(e) Roughened base of beam cleat.

(f) Beam cleat installed.

Figure 5-18: Slotted beam retrofit.

The column cleats did not require roughening and epoxy pads because the forces were transferred axially. All bolts were hand tightened during installation.

5.5.2 TCY Damper Installation

The TCY dampers were manufactured at the University of Canterbury. The Ø24mm mild steel round bars were first cut to length and then threads were cut in each end. Once the threads were cut, the centre section was lathed to reduce the diameter. A sloped transition was machined between the two different diameters. The transition served two purposes. The first was to reduce the likelihood of stress concentrations occurring in the steel. The second was to

provide a gradual increase in damper stiffness should the threaded portion of the damper make contact with the confinement epoxy during net damper compression. The machined portion of the damper was linished smooth to both remove imperfections that could initiate crack formation, and also to reduce bond forces between the steel and the epoxy. The confining tube was cut to length, and ingress and egress ports were drilled into it to allow the epoxy to be installed. It was important that the confining tube had thick walls and a close fit between the inside of the tube and the threaded portion of the damper. This not only provided confinement to the epoxy, which restrained the buckling of the fused section, but also increased the buckling load of the TCY damper as a whole.

The RTV plugs, described in Section 5.4.2, were simple and cheap to install. RTV was first injected into forms around the fused section, and then once the RTV had cured it was trimmed to length. The completed TCY damper components are shown in Figure 5-19(a). The confinement tube was installed and fixed in place with PVC tape at the top and bottom. While the damper was vertical, Hilti HIT-RE 500 structural epoxy was injected through the bottom port until it flowed out of the top port without any air pockets. The ports were then sealed with PVC tape and the epoxy was left to cure, as shown in Figure 5-19(b). The TCY dampers were installed in the beam and column cleats with lock nuts to prevent slop in the connection. Figure 5-19(c) and (d) shows the completed retrofit.

(a) TCY damper components.

(b) TCY dampers following grout injection.

(c) Dampers installed in beam and column cleats.

(d) Completed connection retrofit.

Figure 5-19: SA2-TCY construction.

The TCY damper was cheap to manufacture and basic workshop tools could be used. Installation of the TCY damper was simple and quick. After a design earthquake the dampers cannot be reused; however, replacing them would be relatively quick and inexpensive.

5.5.3 SFD Damper Installation

The components for the SFD device were supplied by a profile cutting company. Due to the high hardness of the Bisalloy 500 shims, it was not possible to machine the steel at the University of Canterbury. The shims had to be robotically plasma cut to achieve acceptable tolerances.

Upon receipt of the SFD components, measurements were taken and the mild steel plates were trimmed to ensure that the device would be in the centre of its travel once installed. The plate with the slotted holes was welded to the column cleat. The plate with the Ø18mm holes in it was welded to the beam soffit cleat. All welds had a 10mm throat thickness and were structural grade. The heat generated during welding had to be carefully controlled to minimise warping, which would complicate the installation of the dampers. Figure 5-20(a) and (b) demonstrate the order in which the SFD devices were installed. The M16 G8.8 bolts were installed in the slotted SFD plate first, and then the cleat was attached to the beam soffit. The first shim was then installed and the column cleat, with the slotted SFD plate attached, was installed. The second shim and cap plate were then installed and secured in place with the flat washers, belleville washers and nuts.

The capacity of the SFD is sensitive to the clamping force applied by the bolts. Hence, it was important to ontrol the clamping force applied, which was achieved by monitoring the torque applied to the nuts. The torque was monitored in two ways; by using a torque wrench and by recording the nut rotation from snug tight. The markings on the nut for recording rotation can be seen in Figure 5-20(c). The torque was applied to the nuts in three even increments, up to the maximum value of 390Nm. Because the bolt tension was so high, it was important to measure nut rotation in addition to torque to ensure the bolts had not yielded. The completed retrofit can be seen in Figure 5-20(d).

(a) Profile of assembled damper showing layers.

(b) Close up of assembled connection showing welds to the column and beam cleats.

Figure 5-20: SA2-SFD construction.

(c) Close up of damper bolts showing torque markings.

(d) Completed connection retrofit.

Figure 5-20: SA2-SFD construction (Continued).

The SFD device was relatively cheap to manufacture; however, the high hardness of the shims requires specialised cutting. Furthermore, the force that the device can generate is sensitive to the clamping force supplied by the bolts, which is difficult to accurately control in practice. Installation was challenging due to the need to weld and the tight tolerances required. After an earthquake the connection can be reused by replacing and retightening the bolts.

5.5.4 HF2V Damper Installation

The manufacture of HF2V dampers requires precision machining and design by an engineer familiar with the device. For this reason, the device was designed by Dr Geoff Rodgers and fabricated by C&M Technologies Limited, Christchurch (Rodgers, 2012). The components were machined from 4340 steel and arrived as shown in Figure 5-21(a). The lead had been cast around the shaft bulge and lathed to the correct diameter. Sensible precautions must be taken when handling lead to protect worker safety. Once the HF2V damper was assembled, it had to be prestressed to remove any voids in the lead. Voids in the lead can cause incomplete lead flow around the shaft bulge, which results in lower peak forces and softer response. The lead was cast the same length as the confining cylinder, so when the end cap spigots were seated the lead was compressed. The peak force that an HF2V device can generate is related to the initial prestress that is applied. Hence, it is important to follow designer recommendations. As shown in Figure 5-21(b), a 100kN prestress was applied to the HF2V devices in an Avery universal testing machine and the external threaded rods were snug tightened to maintain the force. The HF2V devices were then mounted to the beam soffit cleats. As with the other devices, the beam soffit was scabbled, the cleat roughened and bed of structural epoxy injected between the interfaces. The installed device is shown in Figure 5-21(c); the strop in the figure was used to raise the device into position. Prior to installation, a short section of threaded rod was wound into the centre M24 thread of the column cleats

and a coupler wound completely on to the HF2V shaft. Once the device was in position, the coupler was wound out to join the two sections of threaded rod and complete the retrofit, as shown in Figure 5-21(d).

(a) HF2V damper components.

(b) Applying prestress to damper.

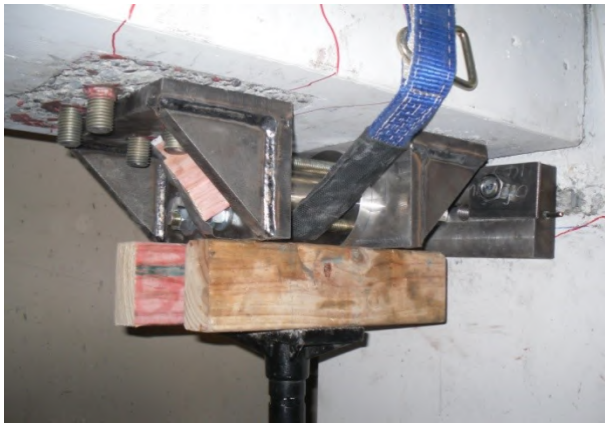

(c) Installing damper on beam soffit.

(d) Completed connection retrofit.

Figure 5-21: SA2-HF2V construction.

The HF2V device was expensive to manufacture; however, the device was able to generate a high reaction force and dissipate a large amount of energy. The ability to reuse the device many times, with minimal maintenance, means that a structure can potentially be reoccupied immediately following a large earthquake. The potential of the HF2V device means that despite the high cost, it remains an attractive option to designers.

5.6 Reaction Frame Design

The reaction frame for the subassembly tests was assembled from modular steel components and the completed setup is shown in Figure 5-22. The reaction frame setup was designed to maximise stiffness. Displacements were applied in both loading directions to the specimen columns by 300kN actuators. The ends of the actuators were bolted to M24 Grade 8.8 threaded rods that were drilled and epoxied into the columns. The subassembly columns were left full height to minimise demolition costs. The actuators were located as high as possible, whilst still being able to achieve the target 3.5% beam drift with maximum actuator stroke.

Maximising the height of the actuators meant that the actuators were installed above the point of contraflexure in the column; however, it enabled the loading protocol to be applied to the specimen more smoothly. The actuators were controlled by displacement, as discussed in Section 5.7, and the rotary potentiometers that recorded the specimen displacement had a fixed resolution. Hence, the greater the height the intended specimen displacements were applied and measured at, the greater the number of displacement increments that the peak specimen displacement could be divided into. Provided the correct column inclination was applied, the beam drift and hence connection mechanics were unaffected by the height the displacements were applied. It is acknowledged that the column shear demand is reduced by the increased loading height; however, this was considered of little consequence because the column and beam-column joint were expected to remain elastic and were not being specifically examined.

The subassemblies were founded on the same dual acting pinned universal joints used in the superassembly test, as described in Section 3.5.2.2. The beam and floor ends were supported by pin ended steel struts attached to the specimen and strong floor. A 150kN load cell was installed between the pinned ends of each of the struts. Actuator C, designed to control the specimen torsion about the vertical axis, was installed between the end of the beam supporting the floor and a cantilevered reaction tower, as shown in Figure 5-22(a). Because the force in Actuator C was expected to be very low, it was determined that the flexural stiffness of the tower would be sufficient. All actuators were connected to a high pressure pump in series. Axial load was not applied to the subassembly column to maintain consistency with the loading conditions of SA1.

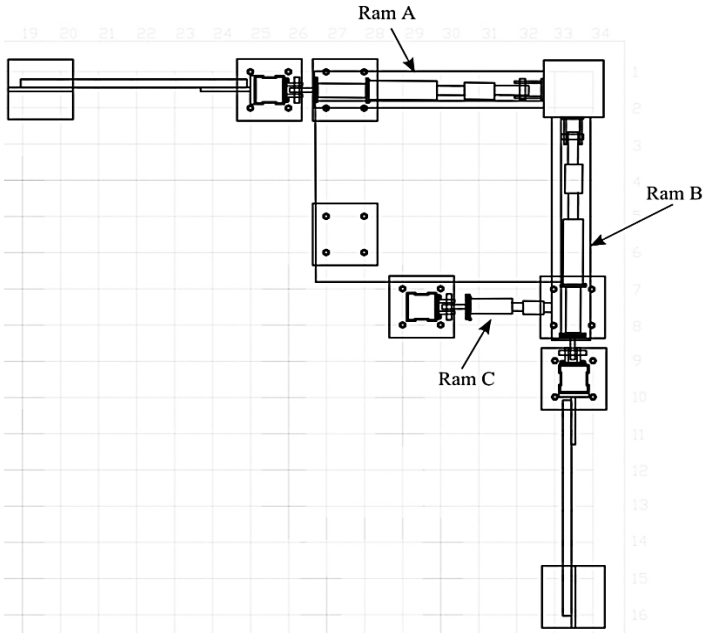

(a) Plan.

Figure 5-22: Reaction frame drawings.

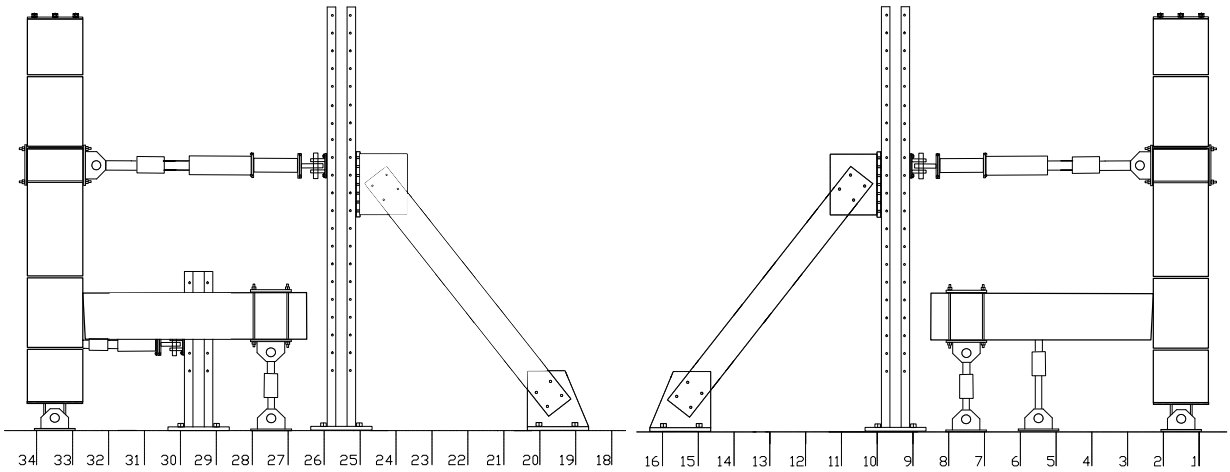

(b) Northern elevation. **(c) Eastern elevation.**

Figure 5-22: Reaction frame drawings (Continued)

Figure 5-23 shows the assembled reaction frame prior to conducting the experiments. For clarity, the smaller out-of-plane braces attached to the towers are not shown in Figure 5-22. These braces stiffened the reaction frames out-of-plane. When a specimen is displaced in the orthogonal direction whilst force is also applied along the primary axis, a force component is generated in the orthogonal direction. In the reaction frame designed for the subassembly tests, this force component, although smaller than the primary, was resisted by the out-of-plane braces. The magnitude of the induced orthogonal force component was minimised by maximising the length between the pinned ends of the actuators. For a given specimen displacement out-of plane, the longer the length between the pinned ends of the actuators, the smaller the angle of the actuator and the resulting force component generated out-of-plane.

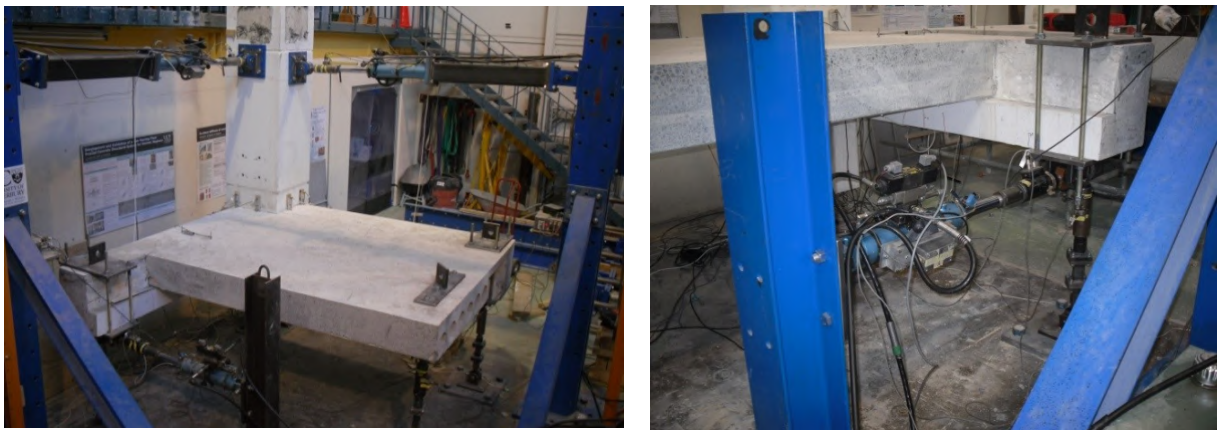

(a) Perspective. **(b) Torsion restraint.**

Figure 5-23: Assembled reaction frame.

5.7 Experimental Method

The displacements were applied to the subassemblies in a quasi-static manner, as defined in Section 3.7.1. The applied displacement protocol was the same cloverleaf shaped biaxial trace based on ACI-374.1-05 that was applied to SA1, and is shown in Figure 5-24 (ACI Committee 374, 2005). As outlined in Section 3.7.2.2, this loading protocol provided

demanding displacement increments, whilst not being unduly severe. In addition, the cloverleaf shape allowed a wide range of loading combinations between the two axes to be assessed. It also facilitated simple comparison between the response of the subassemblies and the superassembly.

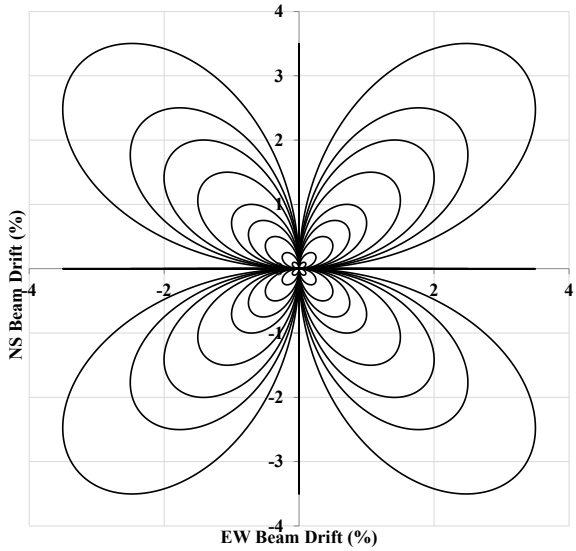

Figure 5-24: Applied loading protocol.

The geometric adjustments that were applied to SA1 were applied to the subassemblies also. Displacement and force corrections were applied to both the controller program input files and collected specimen data to account for error that occurred due to specimen displacement out-of-plane, as described in Section 3.7.2.3. The loading protocol for the subassemblies was defined in terms of beam drift, as it was for the superassembly test. However, because the beam lengths of SA2 and SA3 were made the same length in both directions when they were extracted from SA1, the actuator input displacements were identical along each axis. The beams of the specimens were made the same length along each axis to provide symmetry in the reaction frame design, which allowed SA3 to be quickly set up following the demolition of SA2. Due to SA2 and SA3 being mirror images of each other, the displacements applied along each axis of SA3 were reversed compared to SA2. This meant that, relative to the one-way flooring, the displacements applied to both subassemblies were the same. For the same reason, the response of the specimens, and individual components, was presented relative to the direction that the one-way flooring spanned, rather than relative to cardinal directions. For example, the force-displacement response of specimen SA2 in the direction parallel to the floor refers to the east-west direction, whereas in specimen SA3 it refers to the north-south direction. This convention is used extensively in Chapter 6 to enable the subassemblies to be directly compared.

As discussed in Section 5.6, three actuators were used to apply displacements to the subassemblies. Two actuators applied the intended displacements along each axis to the

column of the specimen, whilst the third actuator restrained the specimen rotation about the vertical axis. A program to control the actuators, which enabled the intended displacements to be applied to the subassemblies, was developed using LabVIEW software (National Instruments, 2011). A schematic of the logic that the actuator controller program followed is presented in Figure 5-25. Lessons learned during the development of the controller program for SA1, as described in Section 3.7.2.4, were applied to develop the controller program for the subassemblies. Time out loops were used to switch off actuator controller boxes, and actuator displacement targets were applied in sequence rather than simultaneously. However, actuators A and B were able to be applied simultaneously because they acted through a comon point, which meant that they could not interfere with each other. The displacement applied by actuator C was the displacement target of actuator A, multiplied by a scaling factor based on the heights of actuators A and C.

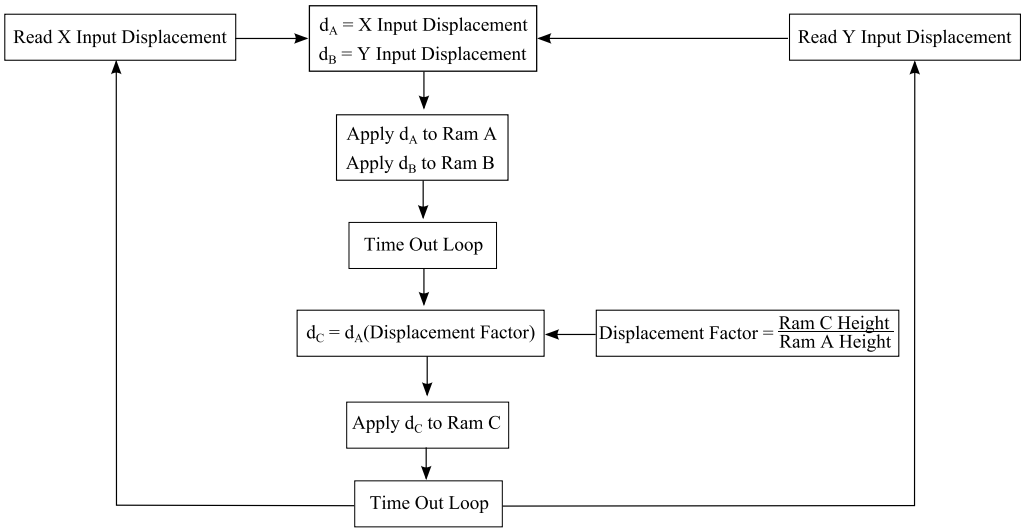

Figure 5-25: Loading controller logic.

Due to the reduced complexity of the actuator controller program compared to that used for SA1, the rate that the subassemblies were loaded at was significantly greater than that for the superassembly experiment. However, the loading rates were still defined as quasi-static. The original program developed performed well throughout testing and no subsequent versions were required.

5.8 Instrumentation Design

The instrumentation used on every subassembly was identical. This simplified the design of the Universal Data Logger (UDL) program and reduced the time spent calibrating instruments. In total, 55 data channels were logged during each subassembly test, which included load cells, inclinometers and rotational, linear and spring potentiometers.

The instrumentation regime used for every subassembly test is presented in Figure 5-26(a)-(d). The displacement and force inputs for the actuator controller program were supplied by the rotary potentiometers mounted to the instrument towers and the load cells at the end of the actuators. These instruments were dual channel, and had output to the data acquisition system as well. The rotary encoders, which were mounted directly on the actuator piston, recorded the extension of the actuators. This data was used by the actuator controller program to determine safe upper and lower displacement limits within each displacement increment. The displacement limits meant that if there was an error in the system which meant that the displacement targets were missed, the controller would shut down before damage was caused.

The frame instrumentation regime for the subassemblies was similar to that used for SA1 and is shown in Figure 5-26(a) and (b). The connections parallel and perpendicular to the one-way flooring span were instrumented identically. Each connection had two pairs of 30mm gauge length spring potentiometers, located above and beside the slotted connection, to measure fixed end rotation about the beam longitudinal axis. A rosette of 30mm gauge length linear potentiometers was installed over the beam-column joints to measure shear deformation. Because the subassemblies were statically determinate and the reactions were known, deformation components such as beam and column flexure could be determined by elastic relationships. Hence, the linear potentiometers that were installed above and below the beam-column joints in SA1 were not required in SA2 and SA3. Six 50mm gauge length linear potentiometers were installed at the beam ends. Three potentiometers were attached to the beam only and measured beam flexure. The remaining three potentiometers were attached between the column face and the beam end to measured beam fixed end rotation. For subassemblies SA2-TCY, SA2-SFD and SA2-HF2V an additional 50mm gauge length linear potentiometer was installed between the damper attachment cleats in each direction. The instrumentation applied to the floors of the subassemblies is shown in Figure 5-26(c) and (d). A 30mm gauge length linear potentiometer was installed on the top of the floor, between the centre of the hollow-core unit and the supporting beam. A 50mm gauge length spring potentiometer was installed in the centre of the bottom of the hollow-core unit.

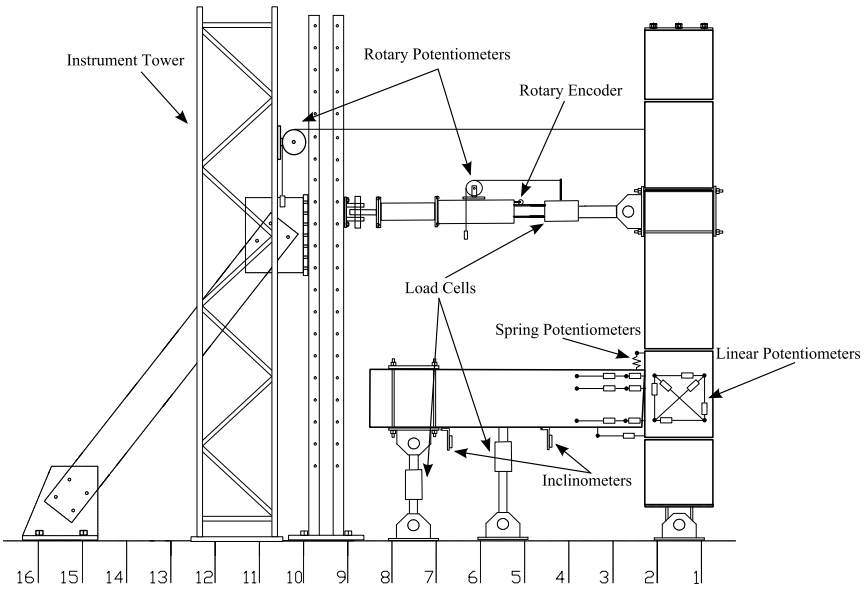

(a) East elevation.

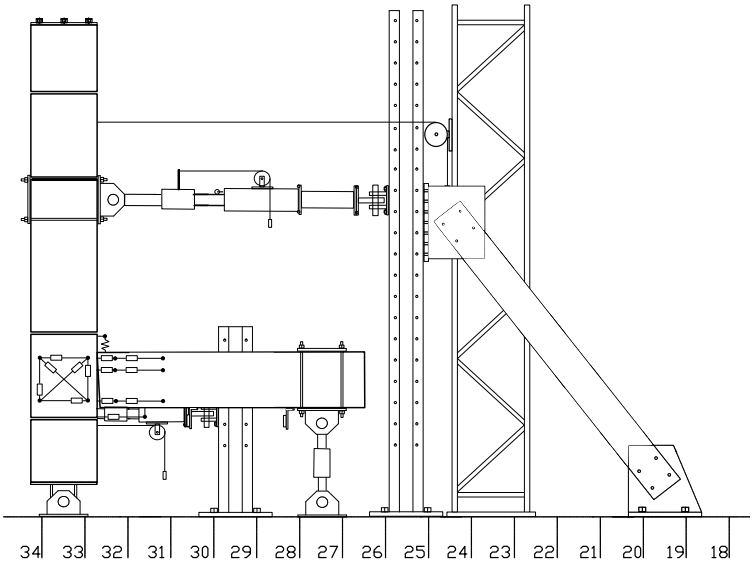

(b) North elevation.

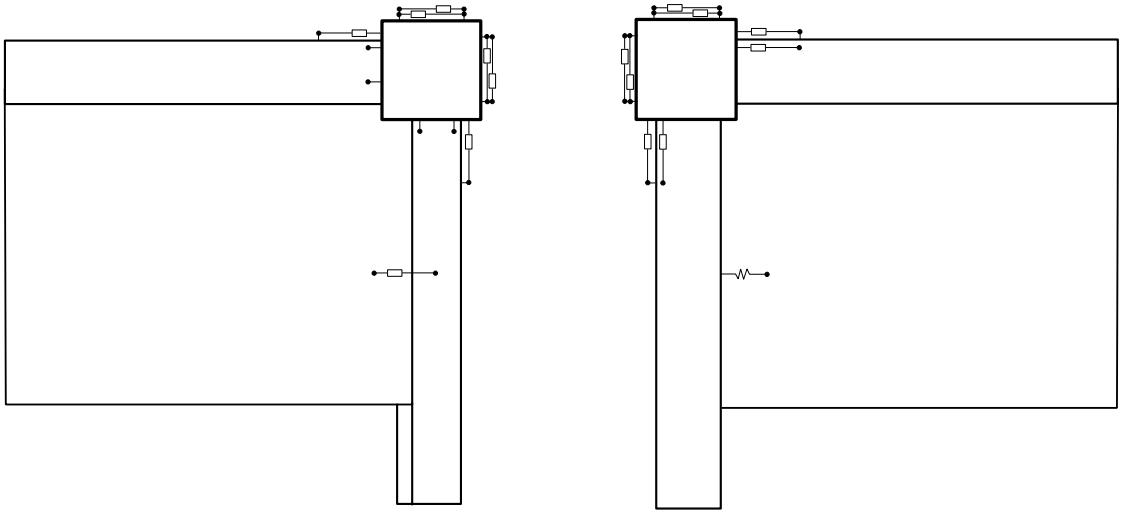

(c) Plan. **(d) Ceiling plan.**

Figure 5-26: Subassembly instrumentation.

As described in Section 3.8.4, the four main deformation components that contribute to measured specimen displacement are elastic column flexure, elastic beam flexure, beam fixed

end rotation and beam-column joint shear. The contributions of beam fixed end rotation and beam-column joint shear to the displacements of the subassemblies were determined in the same manner as they were for SA1. However, because the subassemblies were statically determinate, the reaction forces at each of the points of contraflexure were known. Furthermore, it was shown in SA1 that the columns and beams remained elastic throughout response. Hence, elastic stiffness relationships could be used to determine the contributions of elastic beam and column flexure to the overall displacements of the subassemblies. The stiffness reduction factors from §C6.9.1 of NZS3101:2006 were used in the relationships (Standards New Zealand, 2006). The four components of the specimen displacement were summed and the respective percentages of each contribution calculated from the total, as described in Section 3.8.4.

5.9 Conclusions

Compared to a structural system constructed with traditional connections, a system with slotted beams sustains less damage during an earthquake. However, if slotted beam connections are not capable of reuse or economical retrofit after a large earthquake, the benefits of using the slotted system are greatly reduced. The subassembly test phase of this research programme was undertaken to investigate the residual capacity of slotted connections following a large earthquake. Following the assessment of residual capacity, the connections were rehabilitated with external dampers to assess performance for both retrofit and new-build scenarios.

A methodology to undertake the controlled demolition of slotted beam structures was developed and implemented on superassembly SA1. Using this methodology, two three-dimensional portions of SA1 were extracted safely and without damage. A viable retrofit regime to rehabilitate the moment capacity of slotted beams following a damaging earthquake was developed and implemented. It can be concluded that slotted beam systems, if required, can be economically retrofitted following a large earthquake.

Four energy dissipation devices were developed for use in a slotted beam connection. These devices are suitable for both retrofit and new-build applications. Three of the devices were manufactured, installed and tested in the retrofitted subassemblies. This series of tests was the first time that replaceable dampers had been tested in a reinforced concrete slotted beam. There were many outcomes from the design, manufacture and installation of the replaceable dampers.

1. The tension-compression yielding (TCY) damper presents an attractive alternative to as-built slotted beam construction because it dissipates energy in the same manner as the

unbonded bottom longitudinal reinforcement in a slotted beam. The TCY damper is relatively cheap to manufacture; however, after an earthquake it cannot be reused. A new design to mitigate rapid strength gain during net negative damper displacement was developed.

2. The sliding friction damper (SFD) can be reused after an earthquake by replacing the bolts that provide the clamping force in the device. The SFD is also relatively cheap to manufacture. However, the torque applied to the clamping bolts during installation must be closely monitored due to the sensitivity of the damper force to the applied clamping force.
3. The high force-to-volume (HF2V) lead extrusion damper is able to generate large reaction forces. The device is able to dissipate large amounts of energy, and following a large earthquake the device potentially does not require any maintenance before the building it is installed in is reoccupied. However, the devices are expensive to manufacture and require an experienced engineer to undertake the device design. Despite this, the high energy dissipation and stabile response makes the HF2V damper attractive to designers.
4. The use of the high force-to-volume damper combined with friction springs (HF2V-FS) in a slotted beam could provide near-ideal structural response during an earthquake. However, the high cost of friction springs and the long lead times to supply them are barriers to implementation. These barriers would diminish with increased use of this technology. Due to the inability of the supplier to provide the required friction springs within the testing timeframe, this damper configuration was unable to be tested.

Historical subassembly experiments were examined and critiqued to determine the most appropriate experimental setup to biaxially test subassemblies with integral floor diaphragms. Based on the shortcomings identified in historical subassembly tests, a stiff and strong reaction frame system was developed. The distance between actuator pivots was maximised to reduce the forces induced orthogonal to the primary actuator axes during biaxial loading. In addition to the two actuators required to displace the specimens biaxially, a third actuator was utilised to control specimen rotation about the vertical axis during testing. An actuator controller program was developed to drive the three actuator setup.

The loading protocol applied to all specimens was the same as that applied to SA1, which was based on ACI374.1-05 (ACI Committee 374, 2005). However, because the beam lengths of SA2 and SA3 were made the same length in both directions when they were extracted from SA1, the actuator input displacements were identical along each axis. Because SA2 and SA3 were mirror images of each other, to ensure that their responses were able to be directly

compared the displacements applied along each axis of SA3 were reversed compared to SA2. An instrumentation regime based on that used during the SA1 test was developed, utilising load cells, inclinometers and linear, rotary and spring potentiometers.

5.10 References

ACI Committee 374. (2005). *Acceptance Criteria for Moment Frames Based on Structural Testing and Commentary (ACI374.1-05).* Farmington Hills, Michigan: American Concrete Institute.

Akguzel, U. (2011). *Seismic Performance of FRP Retrofitted Exterior RC Beam-Column Joints under Varying Axial and Bidirection Loading.* Doctoral Dissertation, University of Canterbury, Christchurch, New Zealand.

Amaris, A. D. A. (2010). *Developments of Advanced Solutions for Seismic Resisting Precast Concrete Frames.* Doctoral Dissertation, University of Canterbury, Christchurch, New Zealand.

Au, E. (2010). *The mechanics and design of a non-tearing floor connection using slotted reinforced concrete beams.* Masters Dissertation, University of Canterbury, Christchurch, New Zealand.

Chanchi Golondrino, J., MacRae, G. A., Chase, J. G., Rodgers, G. W., & Clifton, C. G. (2012). *Clamping Force Effects on the Behaviour of Asymmetrical Friction Connections (AFC)*. Paper presented at the 15th World Conference on Earthquake Engineering, Lisbon, Portugal. Retrieved from http://www.iitk.ac.in/nicee/wcee/article/WCEE2012_1911.pdf

Clifton, C. G. (2005). *Semi-Rigid Joints for Moment Resisting Steel Framed Seismic Resisting Systems.* Doctoral Dissertation, University of Auckland, Auckland, New Zealand.

Cousins, W. J., & Porritt, T. E. (1993). Improvements to lead-extrusion damper technology. *Bulletin of the New Zealand National Society for Earthquake Engineering, 26*(3), 342-348.

Grigorian, C. E., Yang, T. S., & Popov, E. P. (1993). Slotted bolted connection energy dissipators. *Earthquake Spectra, 9*(3), 491-504.

MacRae, G. A., Clifton, C. G., MacKinven, H., Mago, N., Butterworth, J., & Pampanin, S. (2010). The Sliding Hinge Joint Moment Connection. *Bulletin of the New Zealand National Society for Earthquake Engineering*. 43(3), 202-212

Marriott, D. (2009). *The Development of High-Performance Post-Tesioned Rocking Systems for the Seismic Design of Structures.* Doctoral Dissertation, University of Canterbury, Christchurch, New Zealand.

National Instruments. (2011). LabVIEW. Texas, USA: Author.

Palermo, A., Pampanin, S., & Buchanan, A. H. (2006). *Experimental Investigations on LVL Seismic Restraint Wall and Frame Subassemblies*. Paper presented at the First European Conference of Earthquake Engineering and Seismology, Geneva, Switzerland. Retreived from http://ir.canterbury.ac.nz/bitstream/10092/186/1/12605046_Main.pdf

Priestley, M. J. N. (1996). The PRESSS program - Current status and proposed plans for phase III. *PCI Journal, 41*(2), 22-40.

Ringfeder. (2010). *Friction Spring Product Brochure.* Krefeld, Germany: Author.

Robinson, W. H., & Greenbank, L. R. (1975). Properties of An Extrusion Energy Absorber. *Bulletin of the New Zealand National Society for Earthquake Engineering, 8*(1), 187-191.

Robinson, W. H., & Greenbank, L. R. (1976). Extrusion Energy Absorber Suitable For The Protection Of Structures During An Earthquake. *Earthquake Engineering & Structural Dynamics, 4*(3), 251-259.

Rodgers, G. W. (2009). *Next Generation Structural Technologies: Implementing High Force-To-Volume Energy Absorbers.* Doctoral Dissertation, University of Canterbury, Christchurch, New Zealand.

Sarti, F., Smith, T., Palermo, A., Pampanin, S., Bonardi, D., & Carradine, D. M. (2013). *Experimental and analytical study of replacable Buckling-Restrained Fused-type (BRF) mild steel dissipaters*. Paper presented at the New Zealand Society for Earthquake Engineering Conference, Wellington, New Zealand. Retrieved from http://www.nzsee.org.nz/db/2013/Paper_29.pdf

Smith, T., Pampanin, S., Buchanan, A. H., & Fragiacomo, M. (2008). *Feasibility and Detailing of Post-tensioned Timber Buildings for Seismic Areas*. Paper presented at the New Zealand Society of Earthquake Engineering Conference, Wairakei, New Zealand. Retrieved from http://ir.canterbury.ac.nz/bitstream/10092/2660/1/12608785_Pampanin.pdf

Standards New Zealand. (2006). *Concrete Strucutures Standard (NZS3101:2006)*. Wellington, New Zealand: Author.

6. Testing and Results of the Subassembly Experiments

6.1 Introduction

This chapter details the experimental testing undertaken on the three-dimensional subassemblies SA2, SA3, SA2-TCY, SA2-SFD and SA2-HF2V. Section 6.3 presents the global hysteretic response of the subassemblies. Visual observations and a chronicle of the significant events that occurred during the tests are presented in Section 6.4. Sections 6.5 – 6.11 detail the performance of separate elements of the subassemblies.

6.2 Material Testing

Because specimens SA2 and SA3 were extracted from specimen SA1, the concrete and steel properties of the subassemblies were as presented in Section 4.2. However, due to the strain that the subassemblies were subjected to during the superassembly testing, the material properties had likely changed. The properties of the dampers used in SA2-TCY, SA2-SFD and SA2-HF2V are presented in Table 6-1. The dampers were tested axially in the Dartec 10MN universal testing machine, as shown in Figure 6-1(a). The displacement protocol applied to the dampers was designed to simulate the displacement that the dampers were subjected to when installed in the slotted beam subassemblies and tested.

Table 6-1: Damper force properties.

	Mean (kN)		Std Dev (kN)		Design Force (kN)		Overstrength	
	Positive	**Negative**	**Positive**	**Negative**	**Positive**	**Negative**	**Positive**	**Negative**
TCY	174.0	-108.1	27.1	2.9	60	60	2.89	1.79
SFD	121.9	-115.3	14.6	10.1	120	120	1.02	0.96
HF2V	221.5	-199.4	5.2	14.1	120	120	1.85	1.66

The agreement between the damper design force and measured force was not close, as shown in Table 6-1. The response of the SFD damper was the closest to the design force, despite the sensitivity of the SFD damper to the clamping force supplied by the bolts. Furthermore, the SFD had the most even response between the positive and negative loading directions.

Large variance was observed between the design and measured capacities of the TCY dampers. It was suspected that the main reason for this was cyclic strain hardening of the steel. The completely reversed positive and negative strain excursions that the TCY dampers

were subjected to resulted in a greater amount of work hardening occurring than would have been expected in a tensile test, which is often used to quantify the overstrength factor for steel.

As described in Section 5.4.2, the TCY dampers were designed to mitigate the large force increase during net compression that can occur when the threaded portion of the damper contacts the confinement epoxy. However, a large disparity between the positive and negative peak forces was observed. The variance was likely due to the effect of Poisson's ratio on the restrained steel, which allowed the effective cross-section of the steel to increase. This increased the effective stress and enabled a higher force to be generated. This mechanism is explained in more detail in Section 4.5.

The measured force of the HF2V dampers was significantly greater than the design value. However, the variance between the measured compression and tension forces was small. The HF2V damper is sensitive to the initial prestress applied. The prestress was applied in accordance with the specifications of the designer; however, due to the difficulty of measuring the actual prestress while securing the top caps it is possible that a greater prestress was applied. The greater prestress applied to the HF2V dampers could have increased their capacity.

(a) TCY damper buckling in DARTEC universal testing machine.

(b) TCY dampers following failure.

(c) Lead expelled from HF2V device at the conclusion of testing.

Figure 6-1: Damper testing.

The loading protocols were applied to all dampers at quasi-static loading rates; however, the loading rates were many times greater than those applied to the subassemblies. An increased loading rate was able to be achieved due to the reduced complexity of the experimental setup

and the large capacity of the Dartec 10MN universal testing machine. Strain rate is important when considering the performance of the SFD and HF2V, which are velocity dependent. The effect of loading rates on these dampers has not yet been quantified; however, research is on this topic is on-going (Chanchi Golondrino et al., 2012).

Figure 6-2(a) presents the response of the TCY dampers. Tensile forces are negative in the plots. It can be seen that, as described above, the response was asymmetric due to the stiffened compressive behaviour. However, the dampers displayed stable response until global buckling of the dampers occurred during the last cycle, which was the equivalent of 3.5% beam drift. Global buckling of a TCY damper is shown in Figure 6-1(a). Figure 6-1(b) shows the tensile failure that occurred in the TCY dampers during the subsequent tensile loading. Failure occurred at the midpoint of the damper due to stress concentrations introduced by flexure induced by damper buckling.

It can be seen in Figure 6-2(b) that the response of the SFD damper was very stable. Also noticeable was that the peak force occurred immediately prior to the damper beginning to slide. Due to the quasi-static loading rate that the dampers were tested at, the devices alternated between static and dynamic friction states, which resulted in a jumpy response.

The response of the HF2V devices was symmetric and stable, as shown in Figure 6-2(c). Furthermore, a large amount of energy was dissipated. However, the peak force generated by the devices reduced with increasing displacements, which resulted in negative stiffness. The negative device stiffness was due in part to friction between the lead and the shaft of the HF2V device. Friction forces were higher when in a static state; hence, when the shaft moved relative to the lead the friction force decreased, which reduced the overall force that the device was able to generate. A further contributing factor to the negative device stiffness could have been the expulsion of lead observed during testing, as shown in Figure 6-1(c).

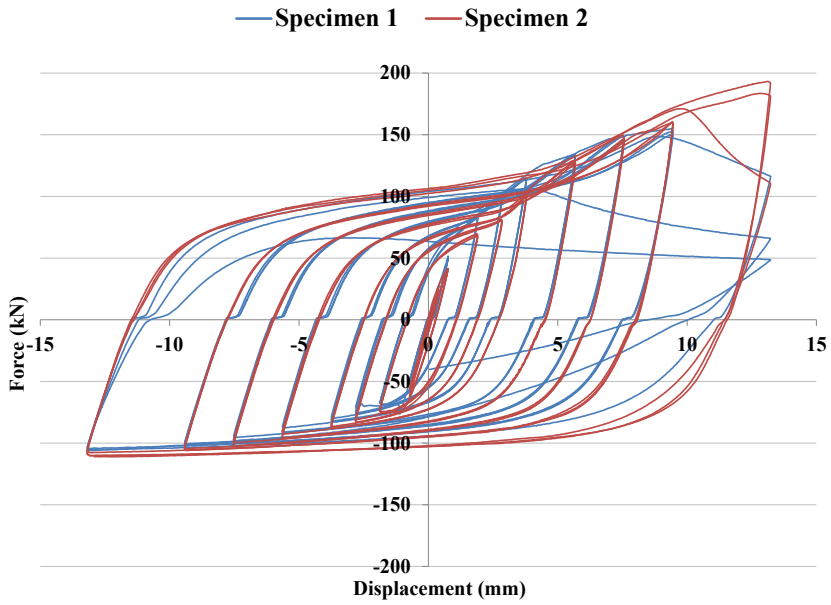

(a) TCY.

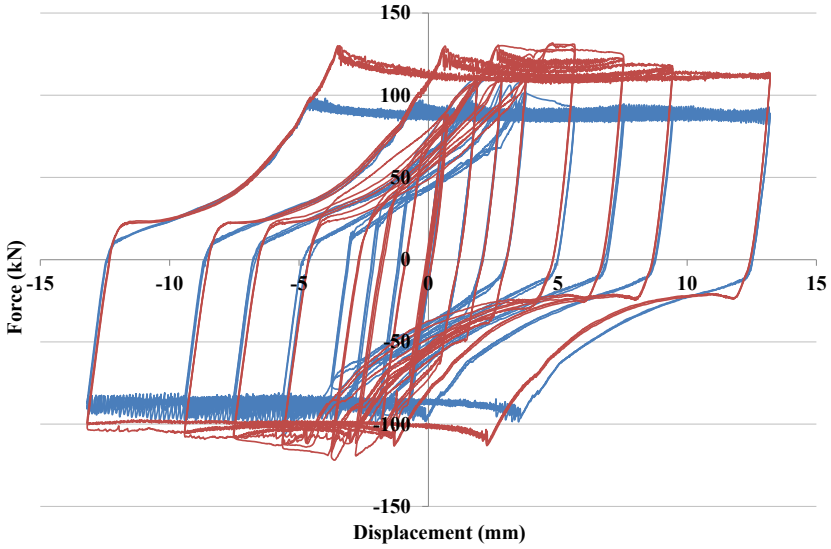

(b) SFD.

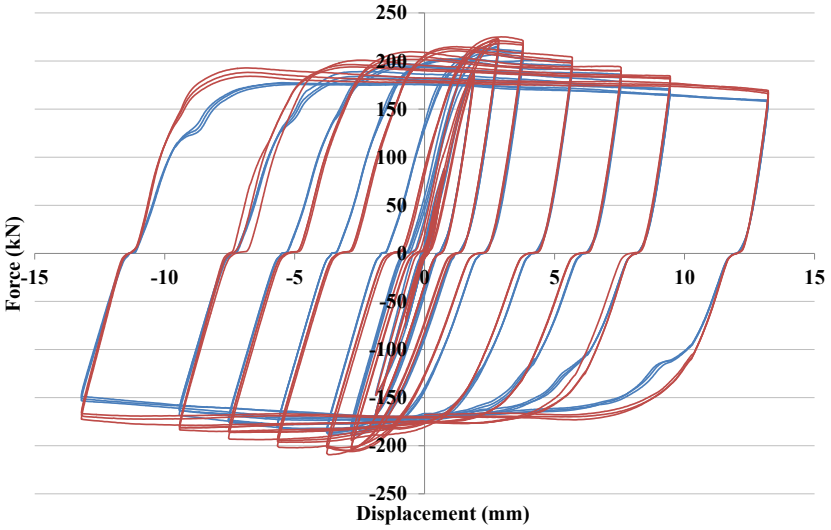

(c) HF2V.

Figure 6-2: Damper hysteretic response.

The variances between the design and measured damper forces were significant. If the dampers were used in a slotted beam structure, and similar discrepancy between the design and actual damper capacities existed, the overall structural response would be significantly affected. Hence, it is recommended that if dampers are to be used in a structure, experimental testing should be conducted to validate the actual damper response against the assumptions made during the design phase. The damper testing should be undertaken at a loading rate representative of the expected damper velocity in the structure.

6.3 Overall Response

All of the subassemblies tested during this phase of the research programme demonstrated extremely promising performance. All specimens exhibited stable response and dissipated large amounts of energy up to 3.5% beam drift. The previously tested specimens SA2 and SA3 displayed impressive resilience and did not fail until the 3.5% beam drift loading cycles. Failure in both specimen SA2 and SA3 was by way of low-cycle fatigue of the bottom longitudinal reinforcement. The retrofitted specimens SA2-TCY, SA2-SFD and SA2-HF2V performed well throughout testing. None of the retrofitted specimens failed during testing.

The overall performance of the specimens, as assessed using the acceptance criteria for moment frames prescribed by ACI374.1-05, is presented in Table 6-2 (ACI Committee 374, 2005). All retrofitted subassemblies met the acceptance criteria; however, because SA2 and SA3 suffered low-cycle fatigue failure of the bottom longitudinal reinforcement during the final loading cycle, they failed.

Table 6-2: Subassembly performance according to ACI374.1-05 acceptance criteria (ACI Committee 374, 2005)

Acceptance Criteria	SA2	SA3	SA2-TCY	SA2-SFD	SA2-HF2V
Reached nominal resistance.	Pass	Pass	Pass	Pass	Pass
Maximum resistance not greater than column overstrength.	Pass	Pass	Pass	Pass	Pass
On final cycle peak resistance greater than 75% of peak resistance.	*Fail*	*Fail*	Pass	Pass	Pass
On final cycle relative energy dissipation greater than 1/8.	Pass	Pass	Pass	Pass	Pass
On final cycle secant stiffness greater than 5% initial stiffness.	Pass	Pass	Pass	Pass	Pass

6.3.1 SA2 and SA3 Overall Response

The overall force-displacement plots for SA2 are presented in Figure 6-3(a) and (b) for the directions parallel and perpendicular to the floor respectively. In these plots positive beam drift causes positive flexure and corresponds to a positive actuator force. Stable response and high energy dissipation was observed up to 3.5% beam drift. Specimen yield occurred at approximately 0.75% beam drift. The overall shape to the hysteretic response of SA2 was

similar to that of SA1; however, there was significantly less pinching, particularly in the direction parallel to the floor. Given that the connection was unchanged, this observation confirmed that the pinching observed in SA1 during testing in the east-west direction was due to displacement in the experimental setup. The incidences of bottom longitudinal reinforcement fractures can be seen in Figure 6-3 as the abrupt reductions in recorded force. These fractures are discussed in greater detail in Section 6.4.1. If the reinforcement fractures are set aside, there was no stiffness degradation of SA2 over the course of testing.

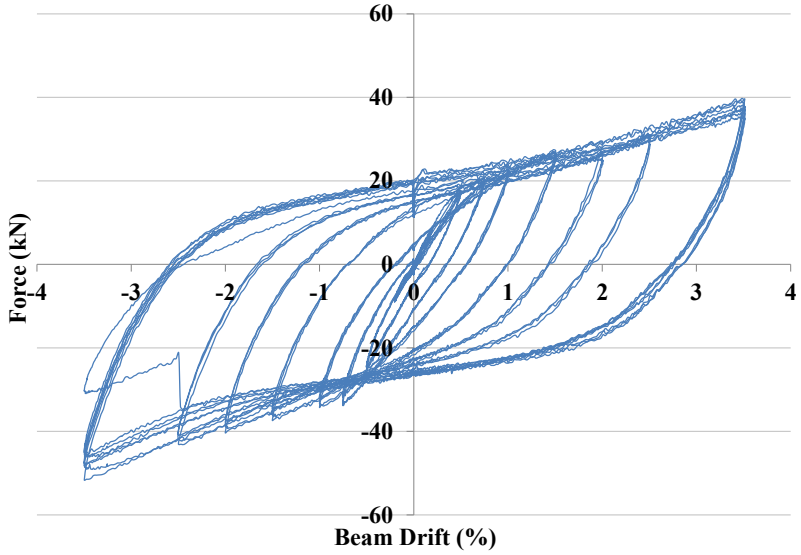

(a) Parallel to floor.

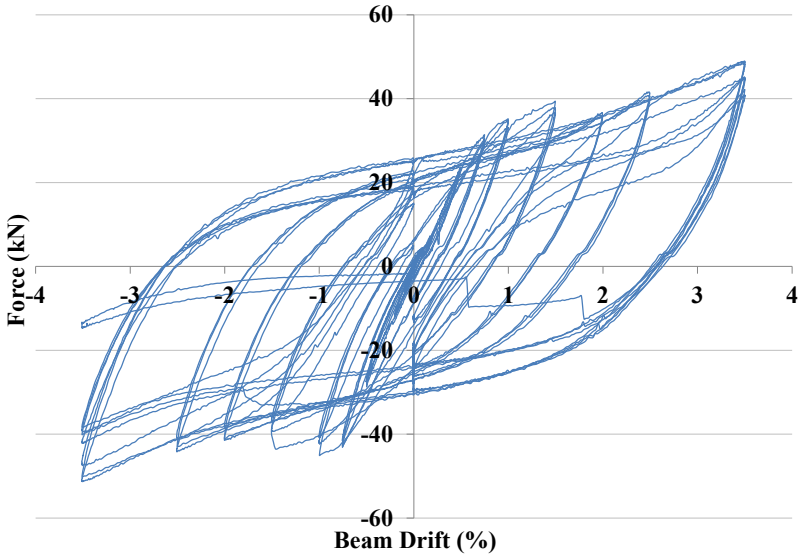

(b) Perpendicular to floor.

Figure 6-3: SA2 global response.

The overall force-displacement plots for SA3 are presented in Figure 6-4(a) and (b). The response of SA3 was similar to SA2, with high energy dissipation and stable response observed throughout testing. The fracture of the bottom longitudinal reinforcement is more apparent in Figure 6-4(b) than in Figure 6-3(b) because the reinforcement in SA3 fractured earlier in the testing than it did in SA2.

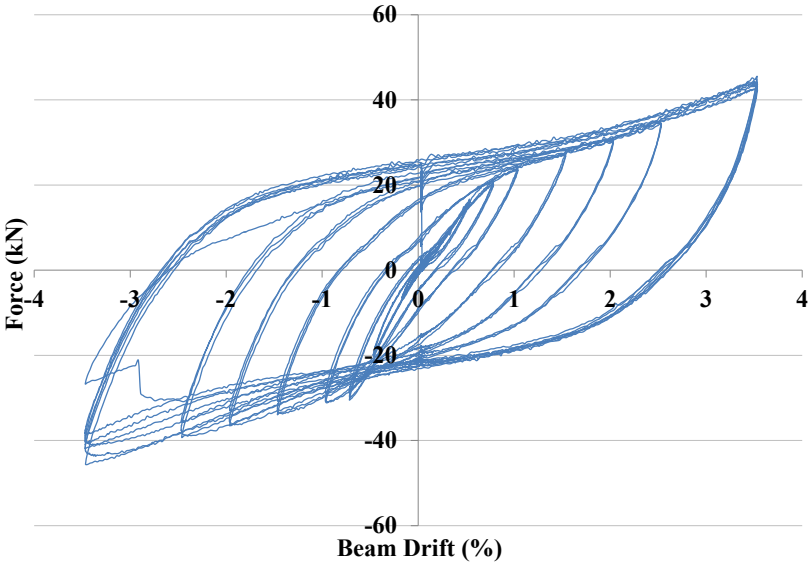

(a) Parallel to floor.

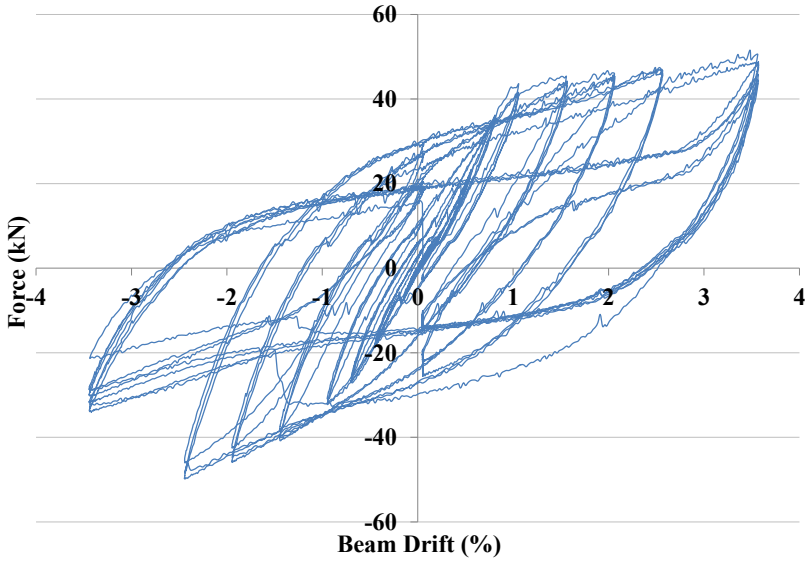

(b) Perpendicular to floor.

Figure 6-4: SA3 global response.

Figure 6-5 presents the force-displacement response of actuator C during the SA2 test. Actuator C restrained specimen rotation about the vertical axis during testing. The response from SA2 was representative of that observed in all subassemblies. It can be seen that little rotational restraint was required during testing. The greatest rotational restraint was required during biaxial specimen displacements. The force required to prevent specimen rotation about the vertical axis was low because the actuator prevented specimen rotation from manifesting, which would have resulted in large restraint forces being required. It is recommended that rotational restraint is used in subassembly tests to prevent specimen rotation about the vertical axis.

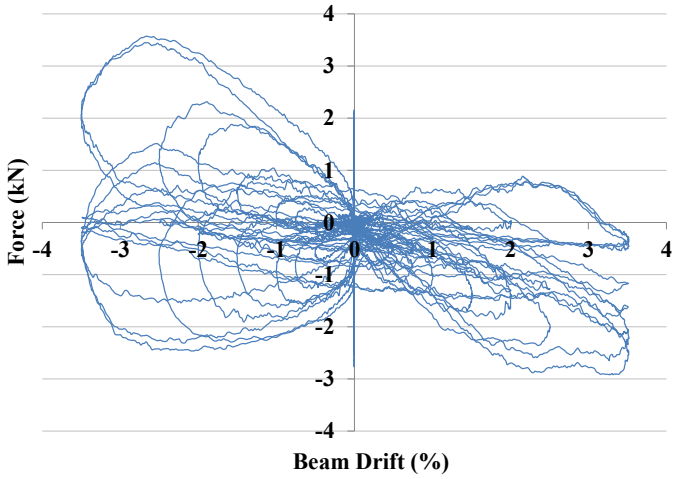

Figure 6-5: SA2 rotation restraint force.

It can be concluded that significant capacity remains in a reinforced concrete slotted connection after it is subjected to a large earthquake. Hence, the potential to reuse a slotted beam structure after a significant seismic event is promising. However, the connections tested were not capable of withstanding two loading protocols that were representative of survival limit state events (Priestley et al., 2007). The likelihood of a structure experiencing two survival limit state events is extremely low. The approximate return period of a survival limit state earthquake is 2500 years. It is possible that the reinforced concrete slotted beam is capable of withstanding two damage limit state earthquake, or even a damage limit state and survival limit state earthquake. However, further research is required before a recommendation can be made. In a practical application, the estimation of residual connection capacity is complicated by the strain history being unknown. Furthermore, in New Zealand most insurance policies stipulate that a building be repaired to the condition it was in prior to the earthquake, which further complicates the reoccupation a structure post-earthquake.

6.3.2 SA2-TCY Overall Response

The force-displacement response of SA2-TCY is shown in Figure 6-6. The specimen response in both directions was extremely stable throughout the entire loading protocol. Because the energy dissipation mechanism was the same in specimens SA2, SA3 and SA2-TCY, the shape of the observed response was similar during the unloading and loading phases. However, during the yielding phase of the response a defined bulge in the response was observed. It is shown in Section 7.3.3.4 that this bulge in response was caused by the contribution of the top longitudinal reinforcement to connection flexural capacity. The peak negative moment attained during testing was greater than the peak positive moment attained. This was due to the asymmetric behaviour of the TCY damper as discussed in Section 6.2.

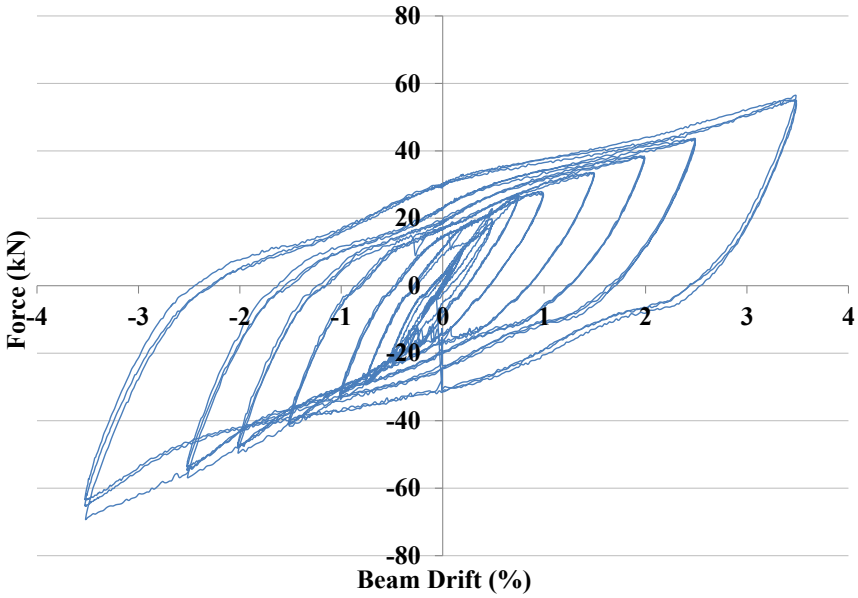

(a) Parallel to floor.

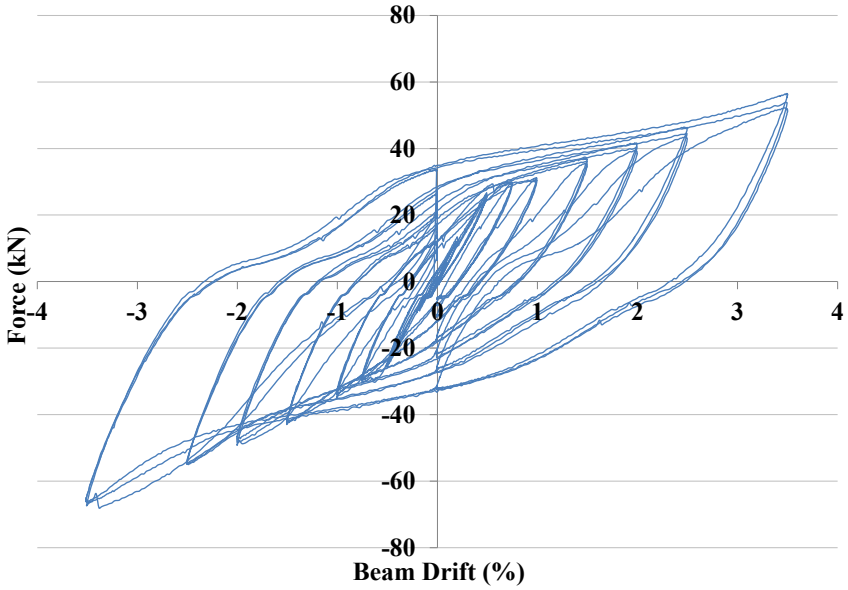

(b) Perpendicular to floor.

Figure 6-6: SA2-TCY global response.

Because the reaction force at the point of contraflexure in the beams was known, and the neutral axis depth was able to be derived from linear potentiometer data, it was possible to estimate the force generated by the dampers during testing. The calculated damper force was an estimate only. Because the total connection moment was used to estimate the damper force, the contributions from the top longitudinal reinforcement, floor diaphragm and diagonal hangers were included also. Without strain data from the reinforcement it was impossible to accurately separate the force components that contributed to the flexural capacity of the connection; however, it was known that the damper was the dominant contributor. The peak force generated by the dampers at every drift increment is presented in Figure 6-7, where compression is negative. It can be seen that the damper forces were greater in compression than in tension in the direction perpendicular to the floor.

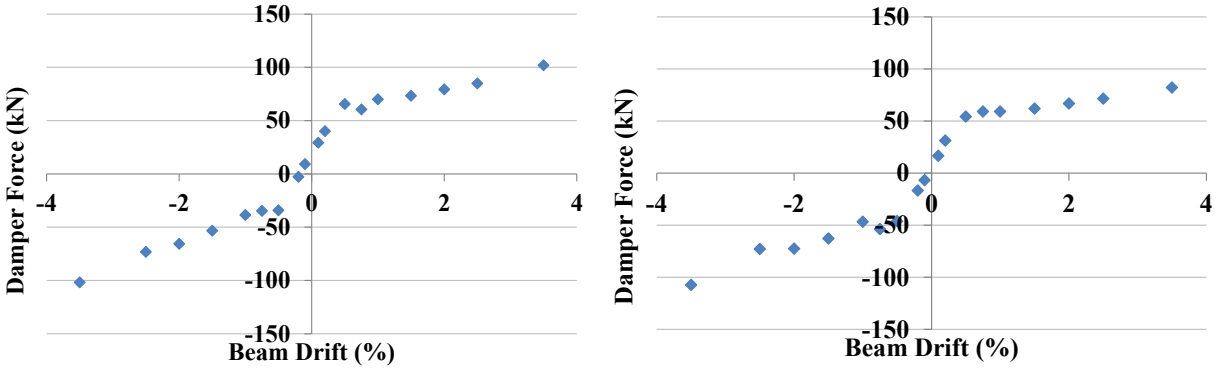

(a) Parallel to floor. **(b) Perpendicular to floor.**

Figure 6-7: SA2-TCY damper force.

6.3.3 SA2-SFD Overall Response

The force-displacement response of SA2-SFD is shown in Figure 6-8; the specimen response was very stable and symmetric. Because of the Coulomb type damping exhibited by the SFD damper, the subassembly was able to dissipate a large amount of energy. As observed in the damper tests presented in Section 6.2, the response of SA2-TCY was very jumpy. This was due to the test being conducted at a quasi-static loading rate, which allowed the SFD damper to constantly switch between static and dynamic friction states.

It can be seen in Figure 6-8 that there was a spike in force between 0.5-1.5% drift in both loading directions, though the spike was more pronounced in the direction perpendicular to the floor. A reduction in peak SFD damper force with increasing displacement was observed also during the damper tests presented in Section 6.2. It was postulated that the decrease in force as testing progressed was due to the wearing down of surface irregularities between the friction surfaces. This decreased the coefficient of friction and reduced the total force required to initiate sliding between the surfaces. The peak damper force decreasing with increasing displacement can result in a negative post-yield stiffness. As discussed in Section 6.3.4, negative post-yield connection stiffness can have undesirable consequences when implemented in a structural system.

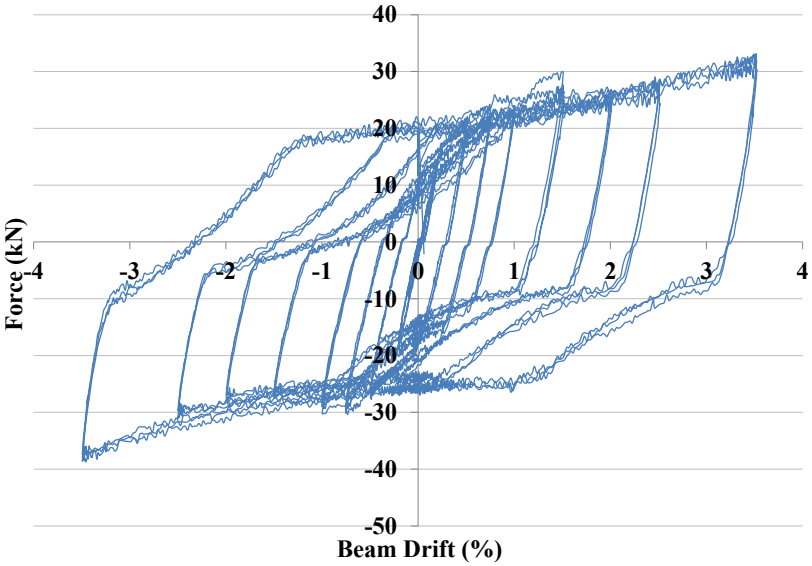

(a) Parallel to floor.

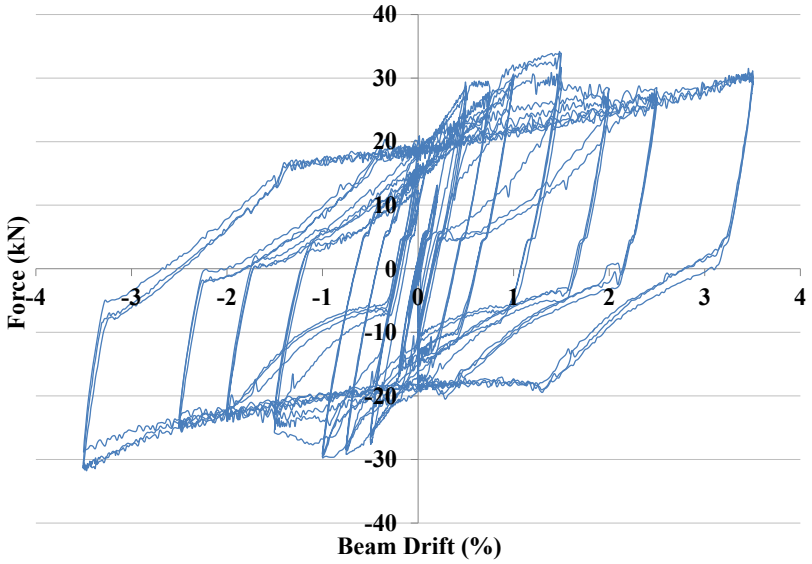

(b) Perpendicular to floor.

Figure 6-8: SA2-SFD global response.

As discussed in Section 5.5.3, the capacity of SFD dampers is sensitive to the clamping force supplied by the bolts. The clamping force applied to the SFD dampers was controlled by the torque applied to the bolts, which was monitored by both a torque wrench and nut rotation. However, as shown in Figure 6-9(a) and (b), there was a difference in peak SFD damper capacity in the direction perpendicular and parallel to the floor. The difference between the SFD damper capacities was likely due to different clamping forces being applied. One of the main issues with using a SFD damper is that the properties of the damper are subject to change depending on the accuracy of installation. Hence, when designing a connection using an SFD device a large overstrength factor would need to be used to preclude inelastic behaviour elsewhere in the structure. Further research is required to quantify an appropriate overstrength factor.

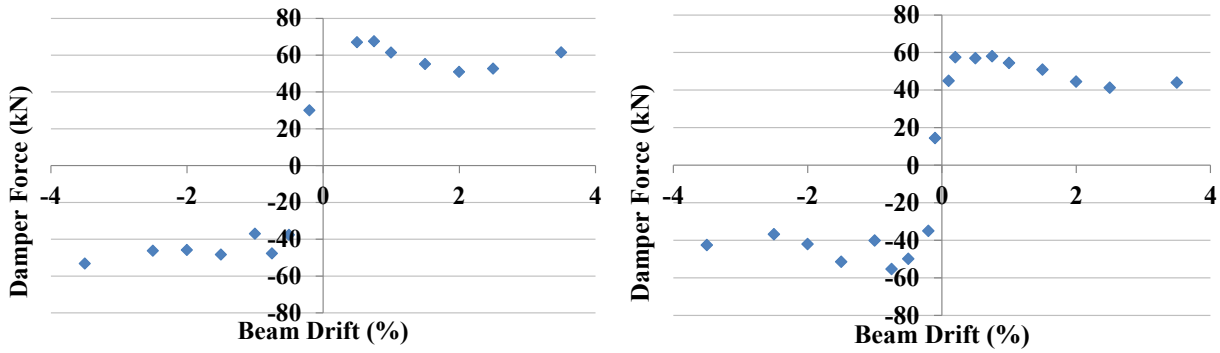

(a) Parallel to floor.

(b) Perpendicular to floor.

Figure 6-9: SA2-SFD damper force.

6.3.4 SA2-HF2V Overall Response

The force-displacement response of SA2-HF2V is shown in Figure 6-10. Both directions displayed a stable response throughout testing with extremely high energy dissipation. However, by comparing Figure 6-10(a) and (b) it can be seen that there was a difference in response between the loading directions. The difference was caused by slip between the beam cleat and the beam soffit in the direction parallel to the floor, which reduced the reloading stiffness significantly. Whilst the peak forces attained in both directions were relatively similar due to the flat post-yield response of the HF2V damper, the amount of energy dissipated in the direction parallel to the floor was significantly less than that dissipated in the direction perpendicular to the floor. This issue highlights the importance of a robust connection between energy dissipation devices and the frame. Stiffness, rather than strength, should dictate the design of the connection between the dampers and the frame.

It can be seen in Figure 6-10(b) that exemplary connection response was observed in the direction perpendicular to the floor. As discussed in Section 5.4.5, the HF2V damper creeps over time to return to a near zero force state. Whilst this effect does not occur rapidly enough to affect device performance during an earthquake, the effect was observed during portions of the biaxial quasi-static testing. During biaxial loading, peak displacements, and hence forces, were sustained for longer periods of time than during uniaxial loading due to displacements being applied to the specimen simultaneously in both loading directions. Hence, the HF2V device has sufficient time to begin to creep. This is shown in Figure 6-10 as a softer response at the peak displacements during the 2nd and 3rd loading cycles. The effect can also be observed as a drop in force around zero displacement during the 2nd and 3rd loading cycles.

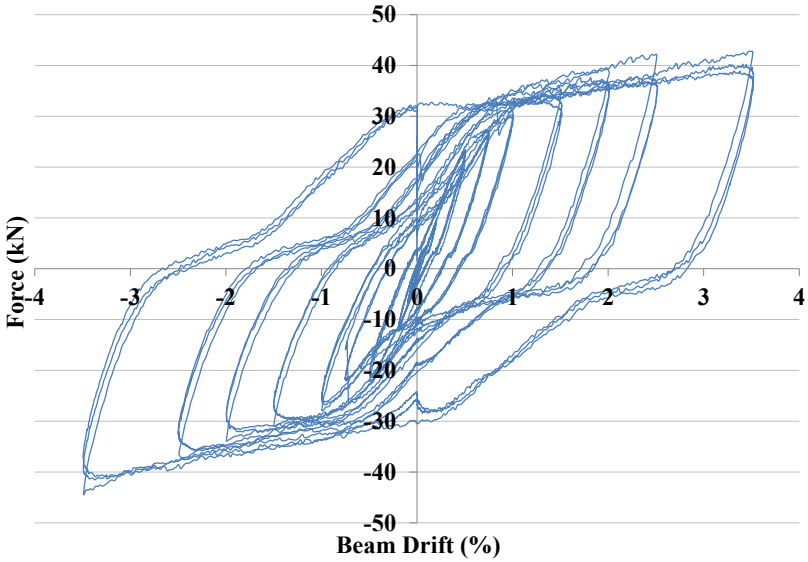

(a) Parallel to floor.

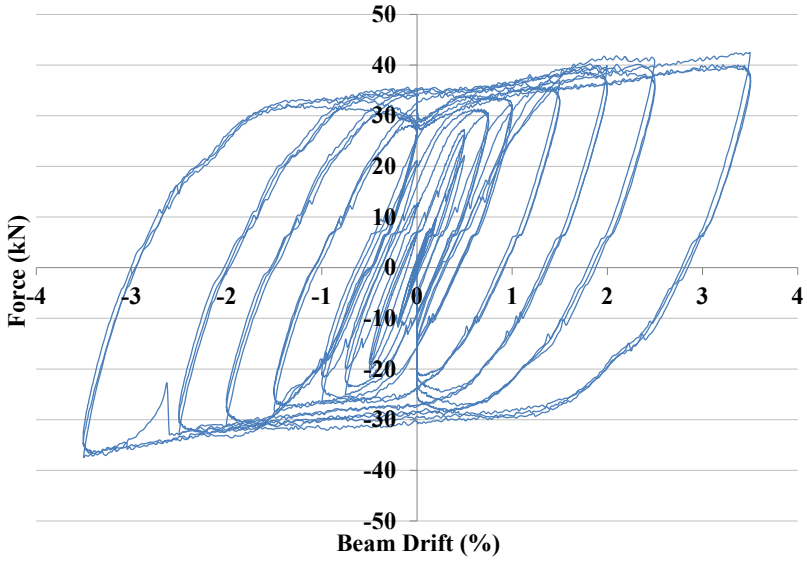

(b) Perpendicular to floor.

Figure 6-10: SA2-HF2V global response.

The HF2V device was shown in Section 6.2 to exhibit negative post-yield stiffness. As a result, specimen SA2-HF2V had the lowest post-yield stiffness of all the subassemblies tested. Due to the contribution of other elements to the connection flexural capacity, the post-yield stiffness of SA2-HF2V remained positive throughout testing. However, a low post-yield stiffness can result in poor control of structural displacements during an earthquake. Furthermore, when large displacements are experienced in a structure P-delta effects can cause the overall system stiffness to become negative, which can jeopardise the overall stability of the structure. The relatively flat post-yield response of the HF2V dampers is illustrated in Figure 6-11. The plots appear relatively similar because the figures represent the force only at peak displacements, so the effect of the slip between the beam cleat and the beam soffit was not captured.

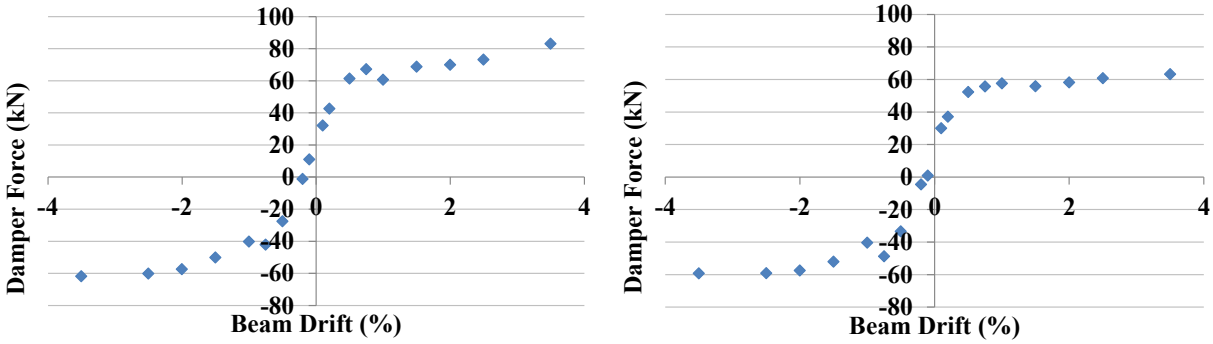

(a) Parallel to floor.

(b) Perpendicular to floor.

Figure 6-11: SA2-HF2V damper force.

The retrofit regime implemented on subassembly SA2 is a viable and economical solution to rehabilitate a reinforced concrete slotted beam following a damaging earthquake. If the bottom longitudinal reinforcement in a slotted beam connection is damaged, or there is uncertainty surrounding its remaining strain life, then the retrofit scheme developed provides a means to rehabilitate the connection.

Building insurance policies in New Zealand generally require an insurer to repair an earthquake damaged building to the condition that it was in prior to the earthquake occurring. Hence, it is possible that a slotted beam connection in an otherwise acceptable condition after an earthquake could be written off on the basis that the bottom longitudinal reinforcement had a lower low-cycle fatigue life then it did prior to the earthquake. The retrofit scheme developed presents a means to rehabilitate a slotted beam connection to pre-earthquake levels of resistance and robustness. This would enable an earthquake affected building to be reused, which reduces the cost to the building owner.

The dampers tested showed extremely promising performance. All dampers exhibited stable response and high energy dissipation during testing. The dampers are able to be used in both retrofit and new-build applications. However, a designer must ensure that the design capacity of the damper that they specify matches the capacity of the manufactured device. Failure to do so may result in unpredictable building response.

The HF2V damper exhibited the best performance of the three dampers tested; however, the high cost to manufacture the device may deter designers. The SFD device was economical to manufacture and exhibited stable response; however, the capacity of the device is sensitive to the torque applied to the clamping bolts. Of the three different damper typologies tested, the TCY damper was the most economical and practical device to implement in a reinforced concrete slotted beam.

6.4 Damage Observed During Testing

Because the subassemblies were extracted from SA1, they had already been tested and as a result they had many pre-existing cracks. During the subassembly testing few new cracks developed. The applied displacements were accommodated by the opening and closing of exiting cracks. Hence, crack monitoring was not explicitly undertaken during subassembly testing.

6.4.1 SA2 and SA3 Observed Damage

A cone-type pull-out mechanism had already formed in the column face of SA2 due to the strain penetration that had occurred in the bottom longitudinal reinforcement when the connection was tested as part of SA1. The cone-type pull-out mechanism worsened over the course of testing SA2. The cone shaped failure plane did not widen because it was restrained by the column stirrups adjacent to the longitudinal reinforcement. However, the already cracked concrete at the column face was spalled completely due to the strain reversals in the bottom longitudinal reinforcement, as shown in Figure 6-12(a).

The first reinforcement fracture in SA2 occurred in the inside D12 in the connection perpendicular to the floor during the first cycle at 1.5%. An example of fractured bottom longitudinal reinforcement in SA2 is shown Figure 6-12(b). Fracture of the bottom longitudinal reinforcement was preceded by reinforcement buckling between the end of the unbonding tube and the column face during negative flexure. Over the course of testing, the unsupported length of the reinforcement between the end of the unbonding tube and the column face increased. This increase in buckling length was caused by reinforcement strain penetration into the column face and the subsequent spalling of concrete that occurred when a cone-type pull-out mechanism was formed. When the buckling length of the reinforcement spanning the slot was sufficiently long, and the compressive force generated in the reinforcement was sufficiently large, the reinforcement buckled. When the bottom longitudinal reinforcement buckled the negative moment capacity of the connection reduced. It was likely that the reinforcement buckling caused stress concentrations in the reinforcement, which created crack roots. The crack root then propagated over the subsequent load reversals until the reinforcement fracture occurred during positive connection flexure. This series of events was observed to precede every incidence of reinforcement fracture. Hence, if bottom longitudinal reinforcement buckling was able to be delayed, reinforcement fracture would be delayed also. It is recommended that designers take practical steps to prevent reinforcement buckling in the connection slot, such as using large diameter reinforcement, minimising strain penetration and minimising the slot width. These factors are

intrinsically related and a compromise must be sought by the designer to maximise connection performance.

The loading protocol was completed without further reinforcement fracture. However, because one of the goals of the experiment was to determine the cumulative strain capacity of the bottom longitudinal reinforcement, additional loading cycles at 3.5% beam drift were undertaken until additional reinforcement fracture occurred. The outside D12 reinforcement in the connection perpendicular to the floor fractured during the first cycle of the second application of the 3.5% loading protocol. The inside and outside D16 reinforcement in the direction perpendicular to the floor fractured during the second cycle of the third application of the 3.5% loading protocol. This was followed by the fracture of the inside D16 reinforcement in the direction parallel to the floor during the same load cycle. The testing of SA2 was then terminated due to the very low lateral strength remaining.

(a) Fully developed cone-type pull-out mechanism.

(b) Fractured D10 and D16 reinforcement.

(c) Cracking at 3.5% beam drift.

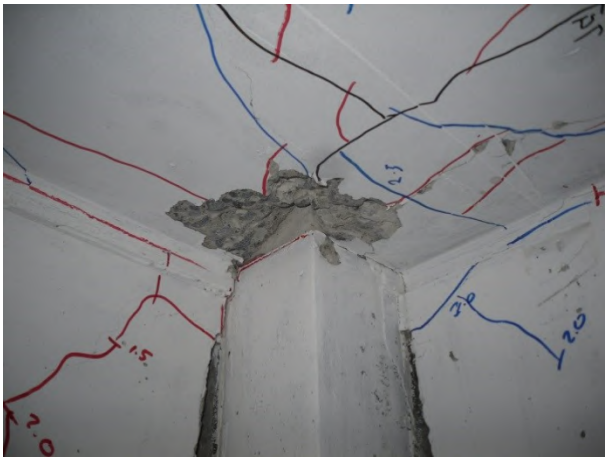

(d) Spalled concrete from infill due to contact with column.

Figure 6-12: SA2 damage.

Bottom longitudinal reinforcement that fractured during the testing of SA3 is shown in Figure 6-13(b). The mode of failure of the reinforcement in SA3 was that same as that described above for SA2. The inner D12 and D16 reinforcement in the direction parallel to the floor fractured during the first cycle of the first application of the 3.5% loading protocol. The outside D16 reinforcement in the direction perpendicular to the floor, and the outside D12 reinforcement in the direction parallel to the floor, fractured during the first cycle of the third application of the 3.5% loading protocol. The testing of SA3 was then terminated due to the very low lateral strength remaining.

(a) Widening of crack in hollow-core unit.

(b) Fractured D10 in foreground, with fractured D10 and D16 in background.

Figure 6-13: SA3 damage.

With the exception of some spalling underneath the infill region caused by contact between the column and the infill, there was little additional damage to the floor diaphragm. The diaphragm damage is shown in Figure 6-12(c) and (d). As shown in Figure 6-13(a), the crack that had formed in the end of the hollow-core during the SA1 test widened during the testing of SA3. In general, little additional damage to the frame and floor diaphragm was observed during the tests performed on SA2 and SA3.

6.4.2 SA2-TCY Observed Damage

Slip was observed during the testing of SA2-TCY between the beam cleat and the beam soffit in the direction perpendicular to the floor. The peak displacement that occurred between the cleat and the beam soffit is shown graphically in Figure 6-14(a). Cracking noises caused by the failure of the epoxy bed between the cleat and the beam soffit could be heard during

testing. The total displacement was small enough that the overall connection response was not significantly affected.

When the displacements applied to SA2-TCY were relatively small, the response was very stable. However, as the applied displacements were increased the relative rotation between the beam soffit and the column face increased also. This caused the TCY dampers to deform in flexure due to the ends of the dampers being rigidly affixed to the beam soffit and column face, as shown in Figure 6-14(c). Flexural yielding was observed in the threaded portions of the TCY dampers, which manifested in a loosening of the lock nuts over several load reversals. At the conclusion of testing, the threaded portions of the TCY dampers were permanently deformed, as shown in Figure 6-14(d).

(a) Slip between beam cleat and beam soffit. Black mark shows original position.

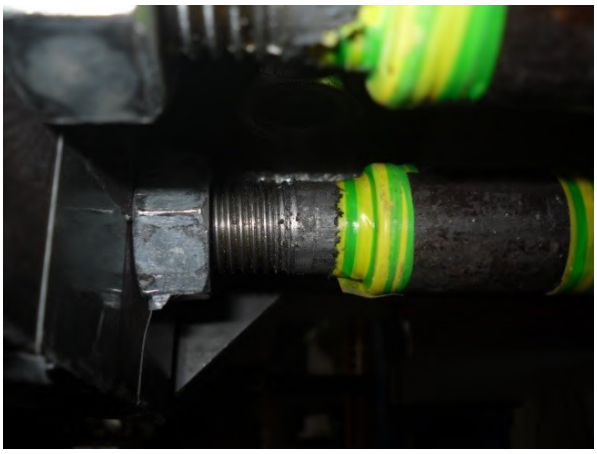

(b) Steel slag spalling from TCY device during tensile strain.

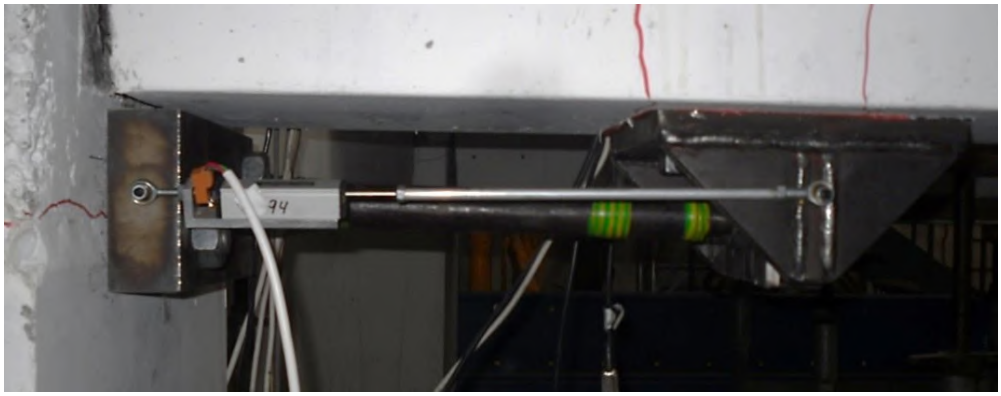

(c) Flexure imposed in TCY dampers during negative connection flexure at 3.5% beam drift.

(d) Permanently deformed TCY damper after extraction from subassembly.

Figure 6-14: SA2-TCY damage.

To avoid inducing flexure in dampers mounted in a slotted beam, the dampers could be affixed to the beam soffit and column face with pinned connections. However, this type of

detail would increase the cost to design and manufacture the dampers and cleats. Furthermore, releasing the end fixities of the dampers significantly decreases the overall damper buckling capacity due to the increase in effective length. This would be particularly problematic when using TCY dampers because yielding occurs in the centre of the device, which reduces the flexural strength through that section and reduces further the overall buckling capacity of the damper. In these situations, the confining tubes of the TCY damper must be relied upon to prevent damper buckling.

For small connection rotations it has been shown that the TCY damper can accommodate flexure whilst maintaining axial performance. However, if large rotations are expected it is recommended that the damper end fixities are released. The designer should be aware of the implications of doing such on damper performance.

6.4.3 SA2-SFD Observed Damage

There was no observed slip between the beam cleat and beam soffit during the testing of SA2-SFD. Damper displacement, induced by connection flexure, was accommodated entirely by sliding between the friction surfaces of the device, as shown in Figure 6-15(a). The cleat to soffit connections were identical between specimens SA2-TCY and SA2-SFD, yet the connections performed better in specimen SA2-SFD. The difference in cleat to soffit connection performance was likely due to the difference in height that the dampers were connected to the beam cleat between the specimens. In SA2-SFD the damper was connected 20mm from the beam soffit, whereas in SA2-TCY the damper was connected approximately 70mm from the beam soffit. The reduced lever from the damper to the beam soffit reduced the moment induced in the beam cleat connection. The decreased moment applied to the cleat meant that less of the connection contact area was in the tension; therefore, a greater area was available to transfer shear. Hence, it is recommended that the moment applied to damper connection cleats be minimised.

The SFD damper was subjected to the same rotation induced flexure that was observed in TCY dampers. Furthermore, because of the asymmetry in the SFD dampers along the horizontal axis, the axial forces at each end of the devices were eccentric and generated flexure in the device. An example of the observed flexure in the SFD dampers during testing is presented in Figure 6-15(b). The SFD dampers had a greater flexural capacity than the TCY dampers; however, the demands on the SFD dampers were sufficient to induce flexural yielding in the dampers ends. Figure 6-15(c) presents the resulting yield lines in the device at the conclusion of testing. Also visible in Figure 6-15(c) are the wear patterns that were formed as a result of the mild steel plates sliding over the Bisalloy 500 shims. This type of

wear pattern is consistent with observations made in Section 6.3.3 regarding the reduction in the peak force of the SFD damper with increasing damper displacement due to the friction surface roughness being worn down.

(a) Displacement between friction elements shown by marker offset during 2.5% beam drift.

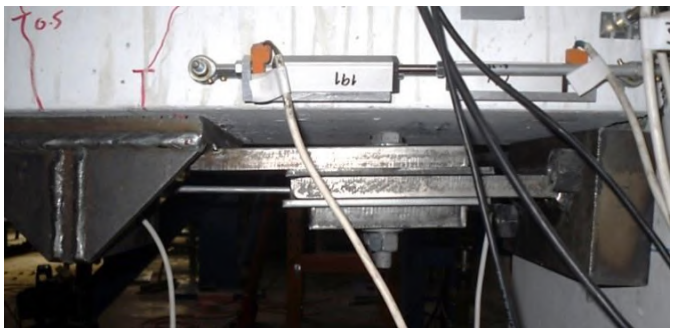

(b) Flexure in the SFD device.

(c) Yield lines and wear patterns in SFD at the conclusion of testing.

(d) Distorted clamping bolts at the conclusion of testing.

Figure 6-15: SA2-SFD damage.

The clamping bolts were subjected to axial, shear and flexural demands during testing. These combined actions resulted in the clamping bolt becoming distorted, as shown in Figure 6-15(d). Plasticity in the clamping bolts can lead to a reduction in clamping force, which would decrease the peak capacity of the SFD damper. The yielding observed in the clamping bolts is potentially a further contributor to the decrease in peak force attained in SA2-SFD over the course of testing.

6.4.4 SA2-HF2V Observed Damage

Although the relative rotation between the column face and the beam soffit was identical in all tests, the geometry of the HF2V damper resulted in greater distortion. As described in Section 5.5.4, the HF2V damper used two beam soffit cleats to affix it to the beam. This decreased the distance between the points of fixity in the HF2V shaft, which increased the imposed flexure. As shown in Figure 6-16(b), significant flexure was induced in the shaft of the HF2V dampers, which resulted in the shaft yielding during testing.

The HF2V damper and the beam soffit cleats were manufactured with very low tolerances. Hence, the flexure induced in the damper shaft caused the shaft to bind where it passed

through the front beam cleat, which induced a moment in that cleat. Because each beam cleat had only two bolts, the flexural stiffness of the beam cleat was reduced compared to that used for the dampers tested in SA2-TCY and SA2-SFD. The rotation induced in the front beam cleat prevented shear forces from being transferred via the epoxy bed between the beam cleat and the beam soffit. The shear force instead had to be transferred via the beam cleat bearing against the threaded rods epoxied into the beam. Due to the tolerances required to install the cleats, this force transfer mechanism required significant relative displacement between the beam cleat and the beam soffit to activate. Slip between the beam cleat and the beam soffit occurred only in the direction parallel to the floor. An example of the total slip that occurred in SA2-HF2V is shown in Figure 6-16(c). Also visible in Figure 6-16(c) is a crack that developed in the beam soffit extending from the threaded rod that was epoxied into the beam. This crack remained stable throughout testing because it was restrained by the close stirrup spacing in the end region of the beam. Figure 6-16(d) shows the HF2V dampers, with the beam cleats still attached, after being removed from specimen SA2-HF2V. The HF2V device cleats in the top of Figure 6-16(d), which were attached to the beam in the direction parallel to the floor, had completed degraded shear surfaces. Conversely, the cleats in the bottom of Figure 6-16(d), which were attached to the beam in the direction perpendicular to the floor, were still adhered to the beam at the conclusion of testing. These observations highlight the different shear transfer mechanisms that were established between the beam cleat and the beam soffits in each loading direction. The slip between the beam cleat and the beam soffit in the direction parallel to the floor significantly influenced the overall slotted beam connection response, as presented in Section 6.3.4. The slip that occurred between the beam cleats and the beam soffits in SA2-HF2V was approximately three times that observed in SA2-TCY.

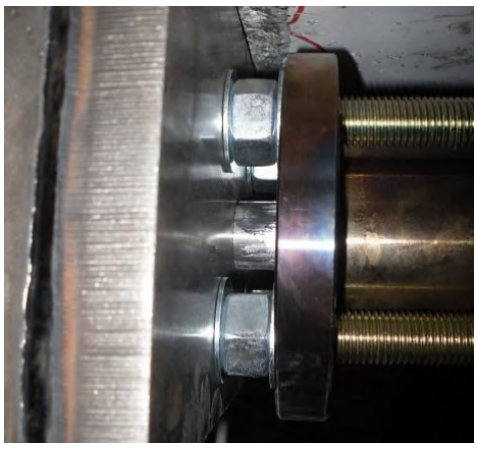

(a) Lead streaking on the shaft during connection negative flexure.

(b) Flexure in the shaft during negative beam drift.

Figure 6-16: SA2-HF2V damage.

(c) Beam cleat displacement relative to black mark and cracking in beam soffit.

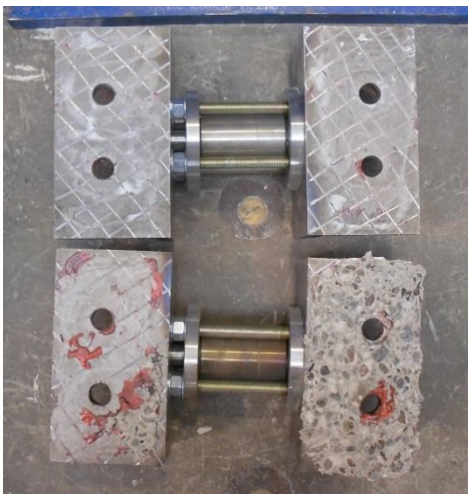

(d) Comparison of HF2V devices at the conclusion of testing highlighting the difference in shear force transfer.

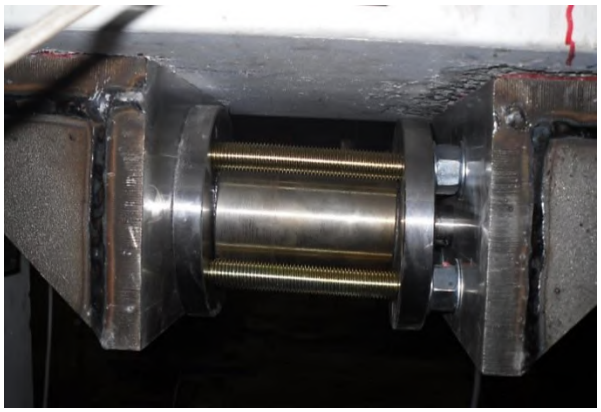

(e) Distortion in the HF2V device.

(f) Lead being expelled between the top cap and cylinder.

Figure 6-16: SA2-HF2V damage (Continued).

A further consequence of the rotation of the front beam cleat, and the flexure of the HF2V shaft, was distortion of the HF2V device. An example of the distortion that occurred in the HF2V device during testing is shown in Figure 6-16(e). The distortion caused the end caps of the dampers to rotate relative to the confining cylinder, which enabled lead to be expelled from the device as shown in Figure 6-16(f). Lead being expelled from HF2V devices can result in a reduction in the capacity of the devices and a reduction in unloading stiffness. These issues highlight the importance of maintaining a stiff connection between the damper and the frame to ensure that the intended system performance is able to be achieved.

6.5 Energy Dissipation

High energy dissipation in a structural system is a desirable attribute. All things being equal, if a system can dissipate greater amounts of energy during an earthquake, then smaller structural displacements will result. Reduced displacements can result in reduced structural and non-structural damage.

As explained in Section 4.7, energy dissipation in structural systems is generally expressed in terms of equivalent viscous damping. Figure 6-17 presents the equivalent viscous damping of the as-built subassemblies. It can be seen that the energy dissipated by SA2 and SA3 was comparable to that dissipated in SA1. Hence, it can be concluded that being previously subjected to seismic actions does not significantly affect the amount of energy that a reinforced concrete slotted beam can dissipate. As explained in Section 4.7, the amount of energy dissipated in a slotted beam is comparable to that dissipated by a traditional connection. However, the manner by which energy is dissipated in slotted beam systems results in significantly less damage than would be expected in comparable systems built with traditional connection detailing.

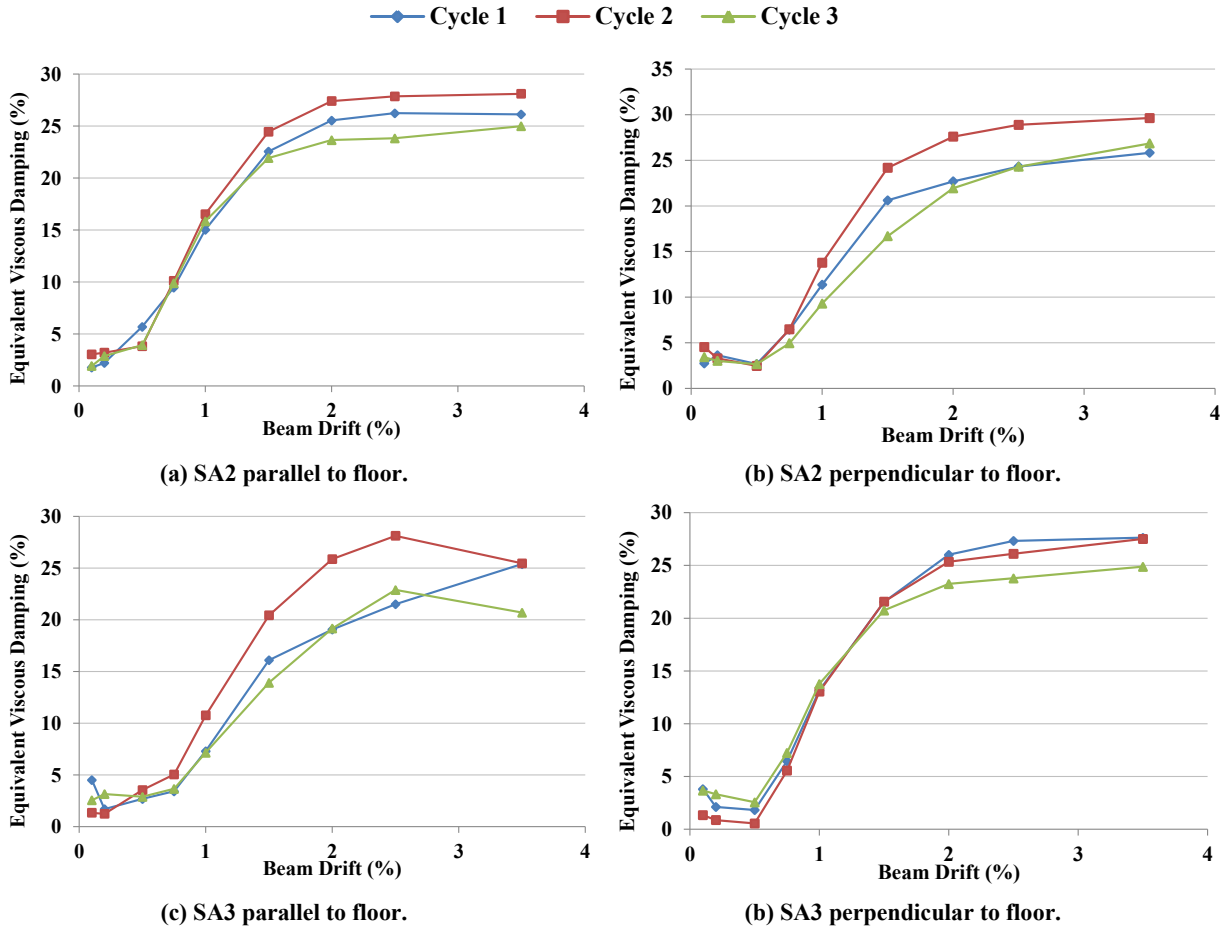

Figure 6-17: Equivalent viscous damping of the as-built subassemblies.

Figure 6-18(a) and (b) present the equivalent viscous damping of SA2-TCY. The energy dissipated by SA2-TCY was slightly lower than that observed in the as-built subassemblies. The way energy was dissipated in specimens SA2, SA3 and SA2-TCY was identical. Hence, the equivalent viscous damping of each specimen would be expected to be similar. However, the equivalent viscous damping recorded in SA2-TCY was lower than that recorded in SA2 and SA3. The likely cause of the discrepancy was the slip observed between the beam cleat and the beam soffit. The equivalent viscous damping recorded in SA2-SFD is shown in

Figure 6-18(c) and (d). Specimen SA2-SFD dissipated more energy than specimen SA2-TCY and the as-built subassemblies. Specimen SA2-SFD was able to dissipate large amounts of energy due to the Coulomb type damping exhibited by the SFD dampers, which resulted in a flat force response and high unloading stiffness.

The energy dissipated by SA2-HF2V was extremely high, as shown in Figure 6-18(e) and (f). The HF2V device was able to dissipate a large amount of energy because it exhibited a flat force response, a high unloading stiffness and a high reloading stiffness. The high reloading stiffness exhibited by the HF2V device largely accounts for the difference in energy dissipation observed between SA2-HF2V and SA2-SFD. Comparing the energy dissipated by SA2-HF2V in each loading direction it can be seen that approximately 15% less energy was dissipated by the connection parallel to the floor when compared to the connection perpendicular to the floor. This difference was due to the slip that occurred between the beam cleat and the beam soffit in the connection parallel to the floor, as described in Section 6.4.4.

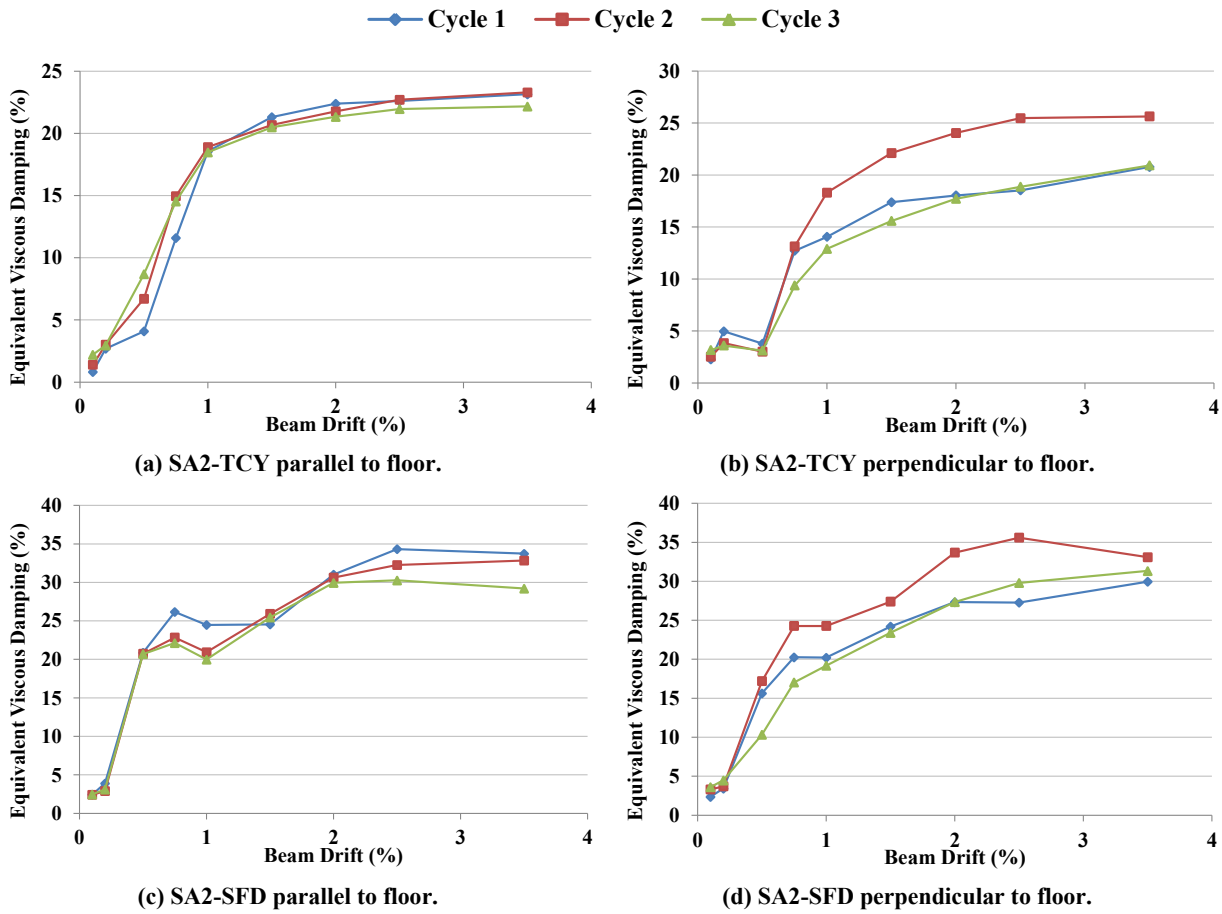

(a) SA2-TCY parallel to floor.

(b) SA2-TCY perpendicular to floor.

(c) SA2-SFD parallel to floor.

(d) SA2-SFD perpendicular to floor.

Figure 6-18: Equivalent viscous damping of the retrofitted subassemblies.

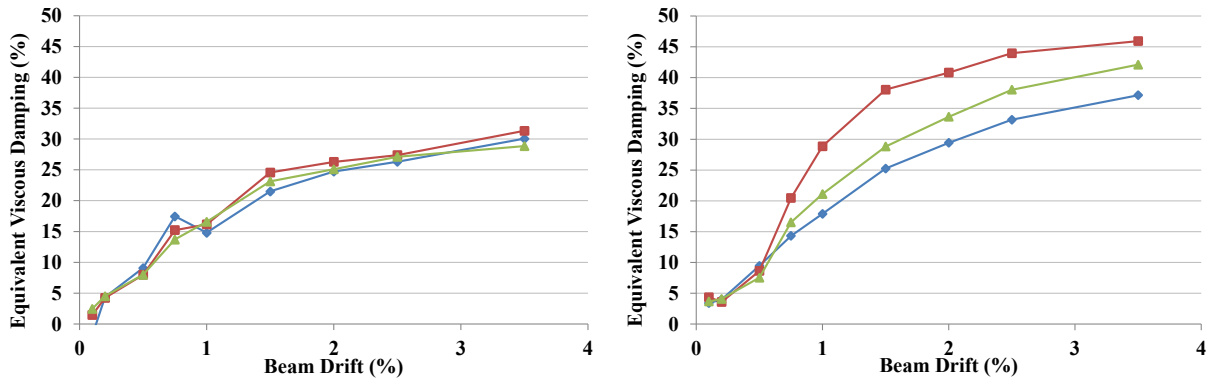

(e) SA2-HF2V parallel to floor.

(f) SA2-HF2V perpendicular to floor.

Figure 6-18: Equivalent viscous damping of the retrofitted subassemblies (Continued).

The use of dampers, in place of conventional reinforcement, in a reinforced concrete slotted beam connection can significantly increase the amount of energy able to be dissipated. Increased energy dissipation in a system will result in lower peak and residual displacements, which can result in lower damage and repair costs. Furthermore, these benefits are able to achieved for both retrofit and new-build applications. However, care must be taken by the designer to ensure that a stiff connection is provided between the dampers and the structure to ensure that the intended response is achieved.

6.6 Stiffness Degradation

The rate at which the stiffness of a structure degrades during loading can indicate how quickly the performance of the structure is diminishing. It is undesirable for the stiffness of a structure to degrade rapidly with increasing lateral displacement, as the increasing P-delta effect can cause global instability. As described in Section 4.8, secant stiffness is a means by which to define stiffness in a nonlinear system and allow for comparison between different types of systems. The secant stiffness of the as-built subassemblies is presented in Figure 6-19. It can be seen that the secant stiffness degrades progressively over the course of testing. The shape of the stiffness degradation response was similar to that observed for SA1.

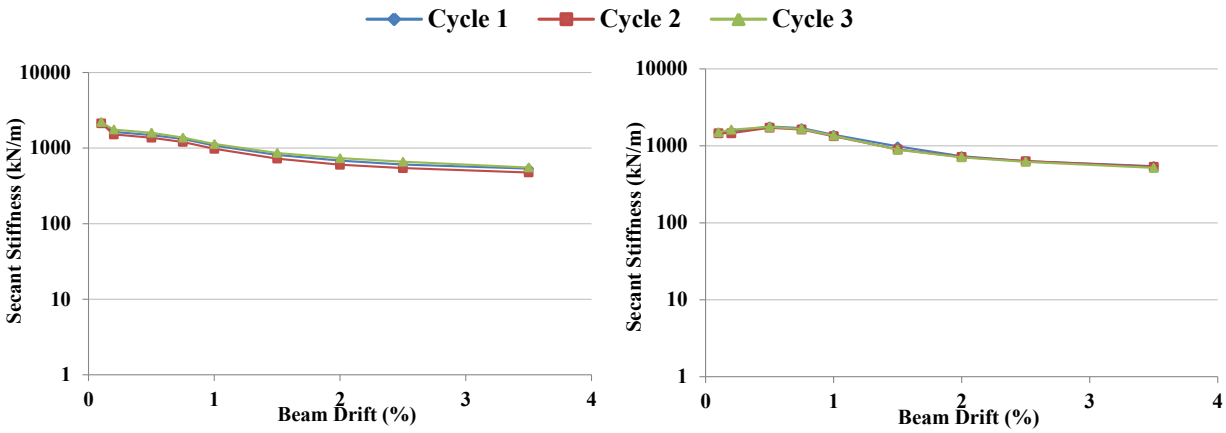

(a) SA2 parallel to floor.

(b) SA2 perpendicular to floor.

Figure 6-19: Secant stiffness of the as-built subassemblies.

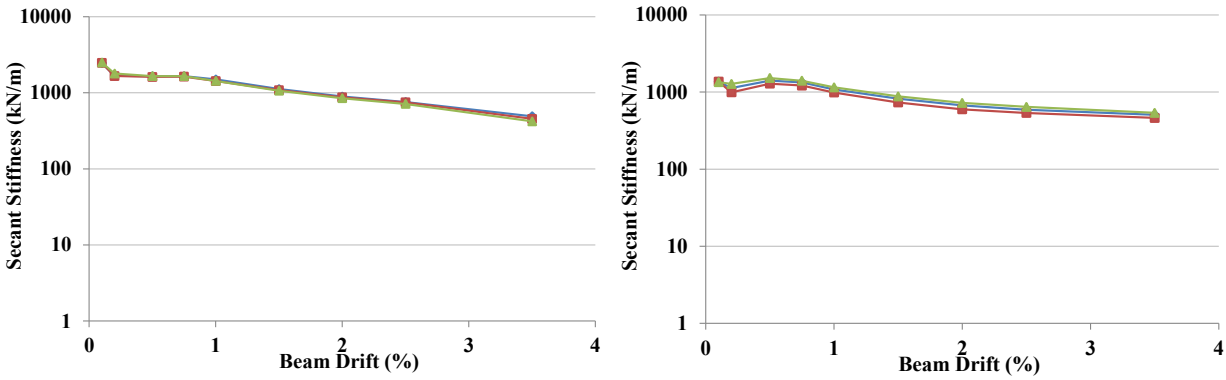

(c) SA3 parallel to floor.

(d) SA3 perpendicular to floor.

Figure 6-19: Secant stiffness of the as-built subassemblies (Continued).

The secant stiffness of the retrofitted subassemblies during testing is presented in Figure 6-20. The stiffness degradation of SA2-TCY is slightly less than that observed in the as-built subassemblies due to the stiffening observed in the TCY dampers during net negative displacement, as described in Section 6.2. The secant stiffness degraded more quickly over the course of testing in SA2-SFD and SA2-HF2V compared to SA2 and SA3. This was due to the flat peak force response that the SFD and HF2V dampers exhibit. However, the effect was somewhat exaggerated by the greater initial stiffness exhibited by both specimen.

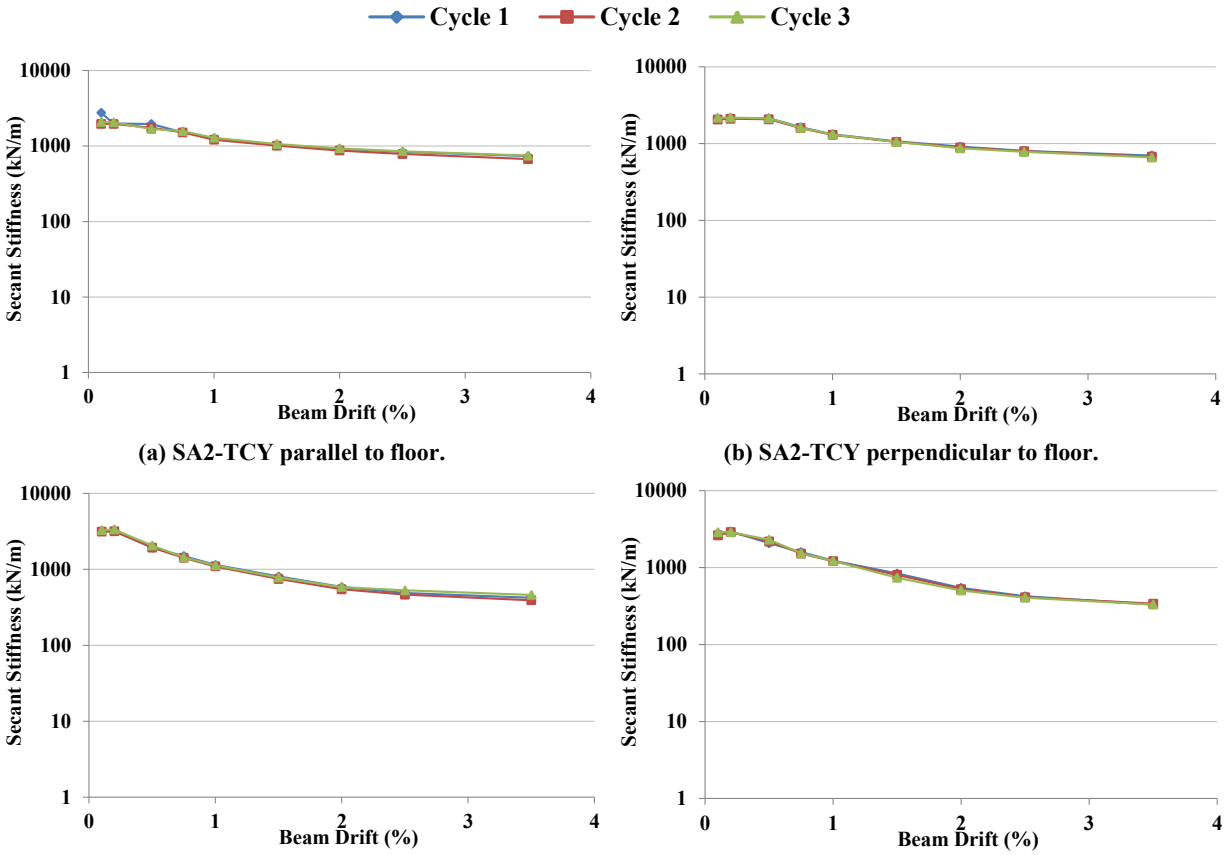

(a) SA2-TCY parallel to floor.

(b) SA2-TCY perpendicular to floor.

(c) SA2-SFD parallel to floor.

(d) SA2-SFD perpendicular to floor.

Figure 6-20: Secant stiffness of the retrofitted subassemblies.

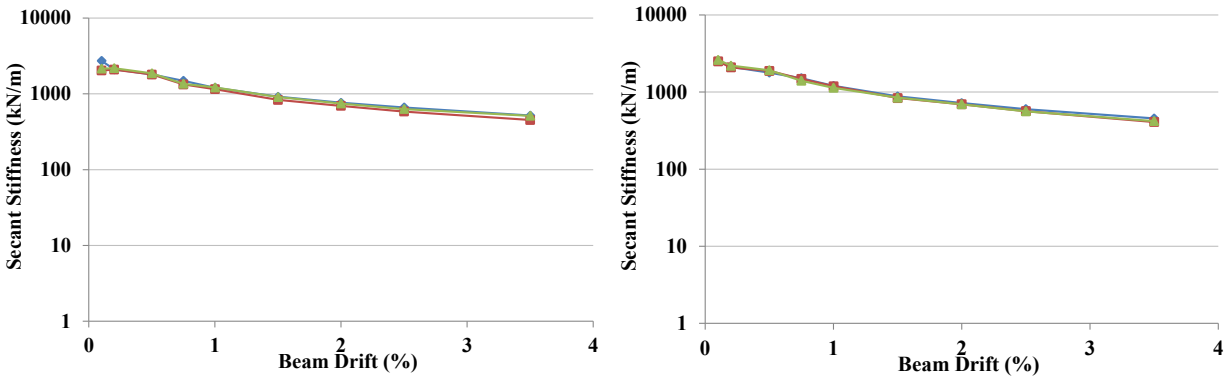

(e) SA2-HF2V parallel to floor. **(f) SA2-HF2V perpendicular to floor.**

Figure 6-20: Secant stiffness of the retrofitted subassemblies (Continued).

It can be concluded that being previously subjected to seismic actions does not significantly affect the rate of stiffness degradation in a slotted beam. The rate of stiffness degradation observed in all retrofitted subassemblies during testing was acceptable. Positive stiffness was maintained by all subassemblies throughout testing. However, when designing connections using devices with a flat peak force response, care must be taken to ensure that positive system stiffness is maintained at all times.

6.7 Decomposition of Lateral Displacement

The four main deformation components that contribute to measured specimen displacement are elastic column flexure, elastic beam flexure, beam fixed end rotation and beam-column joint shear. Figure 6-21 presents the drift components of the as-built specimens SA2 and SA3 for the loading direction parallel to the floor. The drift components of all the subassembly specimens for the loading direction perpendicular to the floor is presented in Appendix D. The dominant contribution to specimen displacement over the entire drift range was beam fixed end rotation. Because yielding occurred in the slotted beam connection, the contribution of beam fixed end rotation to lateral displacement increased as the displacement applied to the specimen increased. After the slotted beam connection had yielded, the connection stiffness was much less than the elastic stiffness of the other displacement components. Hence, the contribution of beam fixed end rotation to specimen displacement increased whilst the other contributions remained relatively constant. The flexural stiffness of the beams was lower than the column and beam-column joints; therefore, beam elastic flexure was the next greatest contribution to specimen displacement.

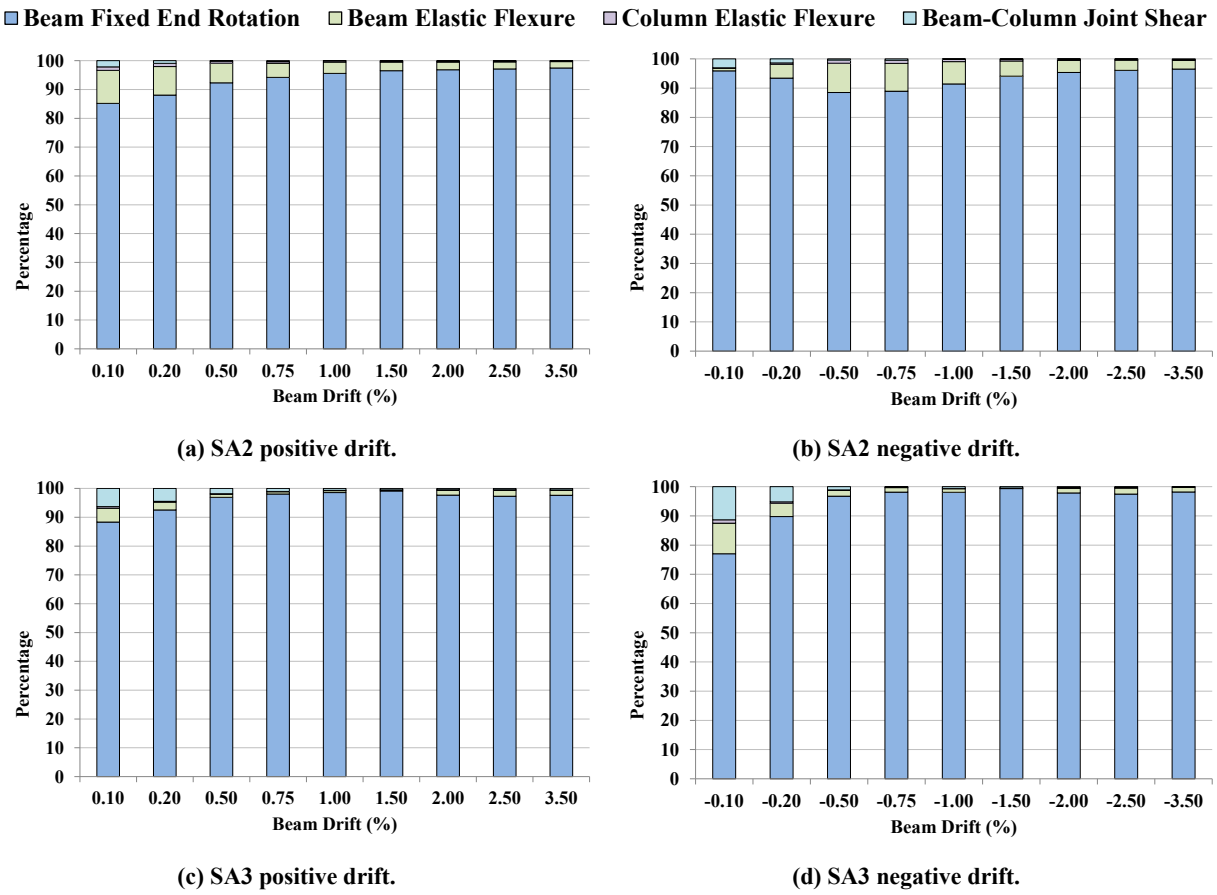

(a) SA2 positive drift. **(b) SA2 negative drift.**

(c) SA3 positive drift. **(d) SA3 negative drift.**

Figure 6-21: As-built subassembly displacement components parallel to floor.

Figure 6-22(e) – (f) shows that for low displacements, the contribution of beam-column joint shear to overall specimen displacement was comparatively large, whilst the contribution from column flexure was low. This was due to the way the contributions were calculated. The contribution to lateral displacement from column elastic flexure was calculated using force based elastic relationships, which are linear. The contribution to lateral displacement from beam-column joint shear was calculated from measured displacements. When the subassemblies were subjected to low lateral displacements, the recorded displacements in the potentiometers that measured the joint shear were so small that they were comparable to the resolution of the instruments. Hence, when the recorded displacements were extrapolated using the specimen geometry, the inaccuracies in the measured displacements were magnified.

Due to the different ways that the contributions to measured specimen displacement have been calculated between the subassembly tests and the superassembly test, the resulting lateral drift component plots are not comparable. The inaccuracies that result from the extrapolation of very small displacements in specimen SA1 meant that the beam and column

flexure and beam-column joint shear data was very noisy, and required correction. The data presented in Figure 6-21 and Figure 6-22 for the subassemblies was not corrected.

The contributions to measured lateral displacement calculated for the retrofitted subassemblies are shown in Figure 6-22. The general observations made above regarding the as-built specimens apply equally to the retrofitted specimens. Furthermore, it can be seen in Figure 6-21 and Figure 6-22 that the contributions of fixed end rotation to measured specimen displacement were larger during positive connection flexure that they were during negative connection flexure. This observation is consistent with the behaviour observed in specimen SA1.

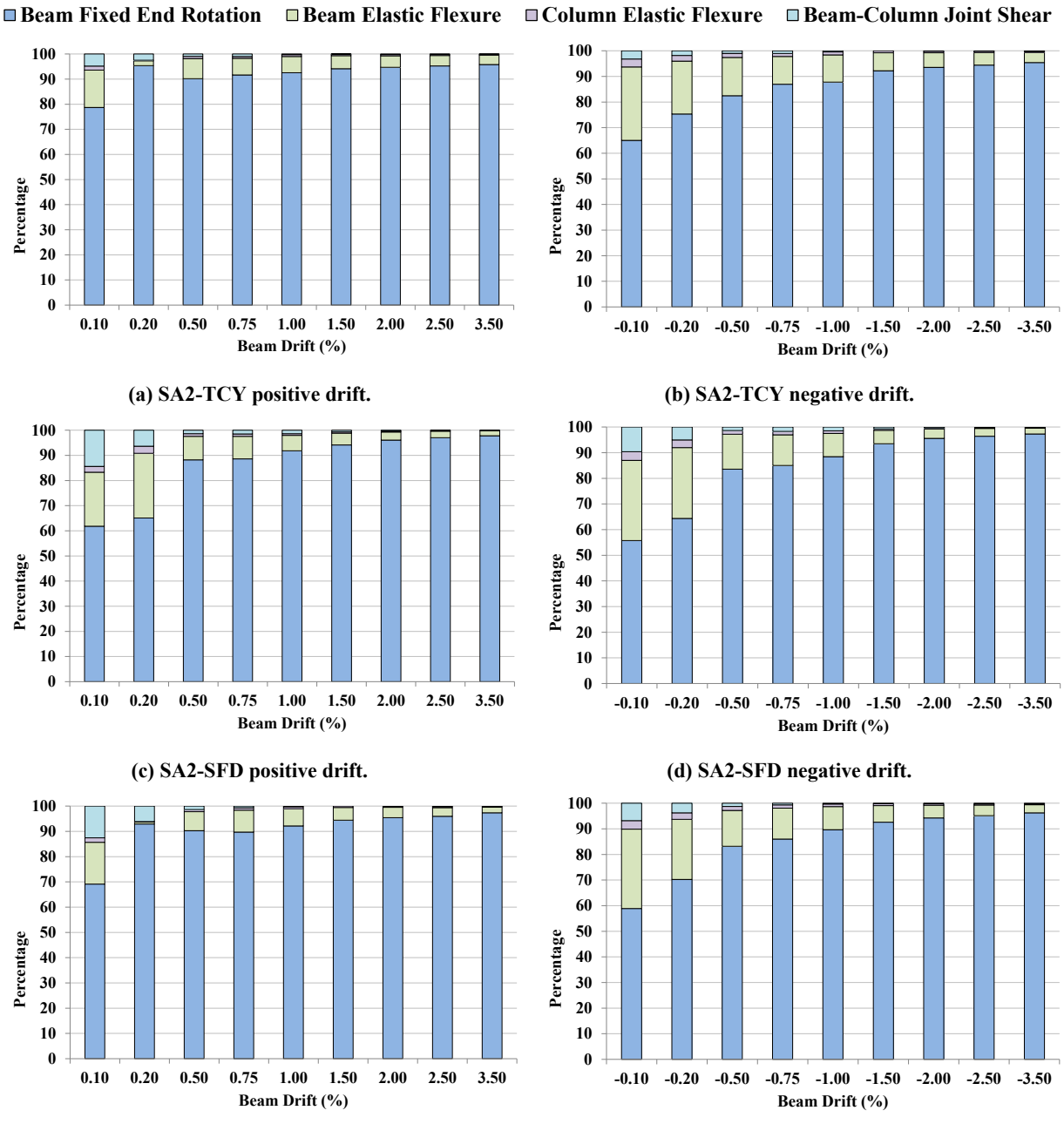

(a) SA2-TCY positive drift. **(b) SA2-TCY negative drift.**

(c) SA2-SFD positive drift. **(d) SA2-SFD negative drift.**

(e) SA2-HF2V positive drift. **(f) SA2-HF2V negative drift.**

Figure 6-22: Retrofitted subassembly displacement components parallel to floor.

6.8 Neutral Axis Variation

Figure 6-23 presents the variation in the connection neutral axis depth during testing for subassemblies SA2 and SA3, where positive beam drift corresponds to positive flexure. Due to a linear potentiometer failure, the neutral axis depth for the SA3 connection in the direction perpendicular to the floor was not able to be determined. For beam drifts in the elastic range of the subassemblies the neutral varies little between positive and negative flexure. As beam drift increases, the variance in the neutral axis depth between positive and negative flexure increases. The peak neutral axis depths observed in the as-built subassemblies for positive and negative flexure were approximately $0.48d_h$ and $0.90d_h$ respectively.

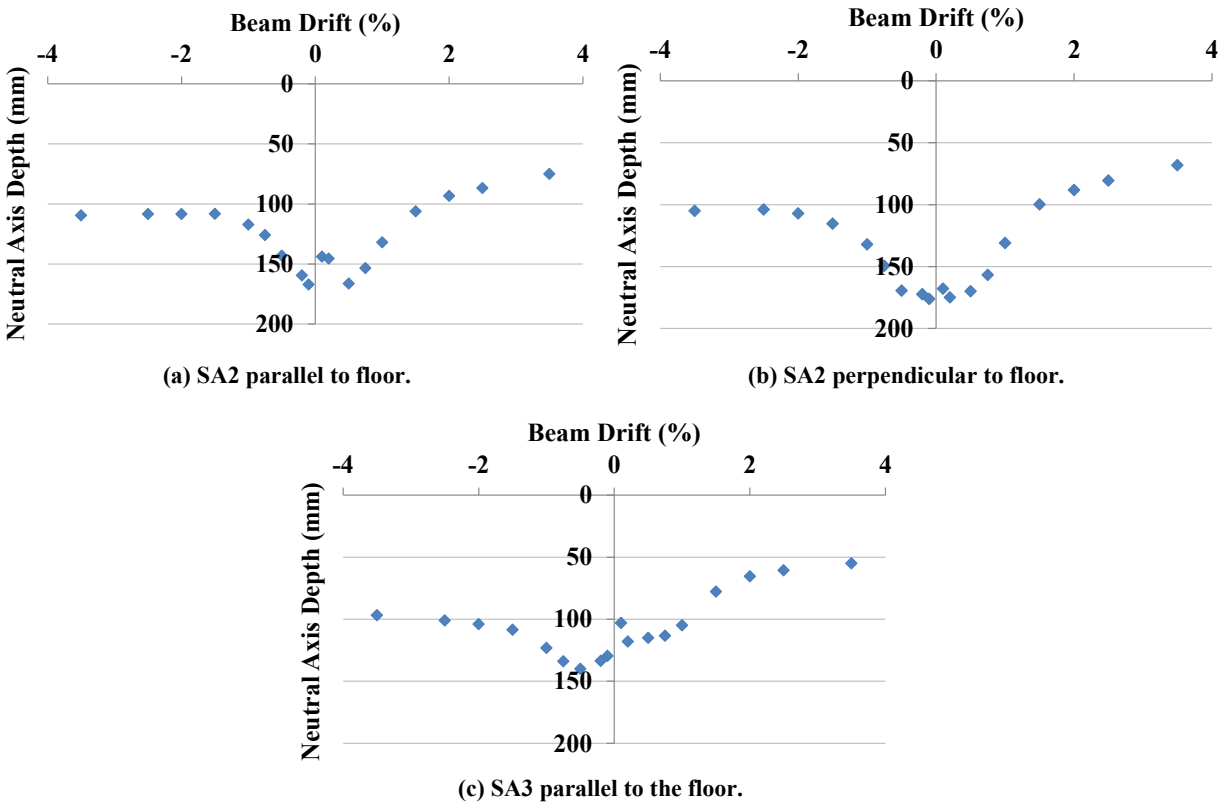

(a) SA2 parallel to floor.

(b) SA2 perpendicular to floor.

(c) SA3 parallel to the floor.

Figure 6-23: Neutral axis depths of as-built subassemblies.

Figure 6-24 presents the neutral axis depths in the retrofitted subassemblies throughout testing. The response was very similar to that observed in the as-built subassemblies. The data presented in Figure 6-23 and Figure 6-24 shows that neutral axis variation in the slotted beam connections was independent of the type of device used in the bottom of the beam to create a connection moment. In reinforced concrete slotted beams the neutral axis depth is dependent on the section geometry, connection capacity and beam drift.

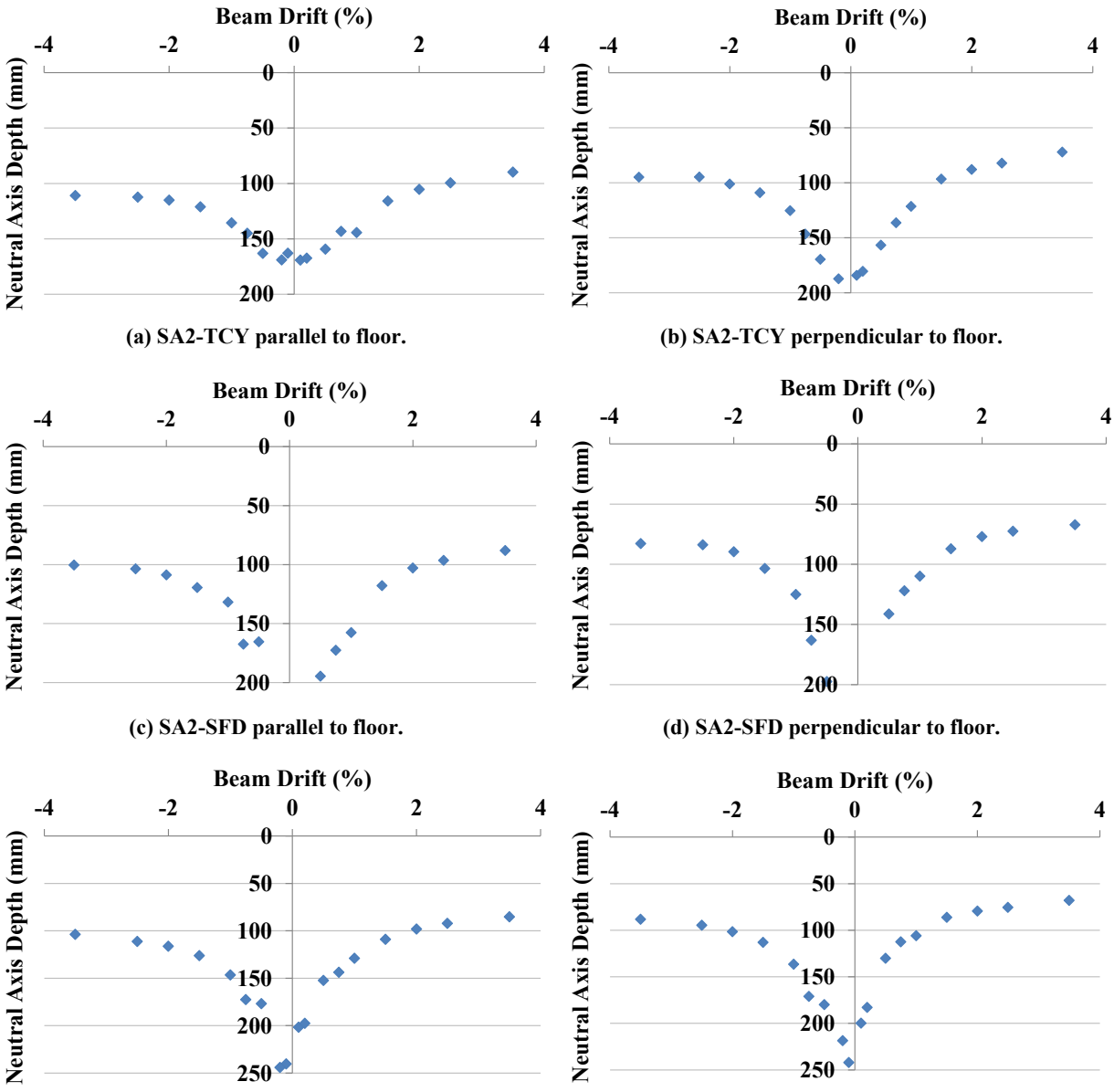

(a) SA2-TCY parallel to floor.

(b) SA2-TCY perpendicular to floor.

(c) SA2-SFD parallel to floor.

(d) SA2-SFD perpendicular to floor.

(e) SA2-HF2V parallel to floor.

(f) SA2-HF2V perpendicular to floor.

Figure 6-24: Neutral axis depths of retrofitted subassemblies.

6.9 Diagonal Hanger Performance

The subassemblies that were extracted from SA1 did not have strain gauges installed on the reinforcement. Hence, the strain in the diagonal hangers could not be directly measured. However, hanger strain was able to be inferred from the shear displacement measured across the slotted beam connections.

Figure 6-25 presents the shear displacement that occurred over the slotted beam connections in the as-built subassemblies SA2 and SA3. In general, the shear displacement that occurred in all connections was small. Slightly greater shear displacement was observed in the connection perpendicular to the flooring direction due to the increased gravity shear demands from the one-way flooring.

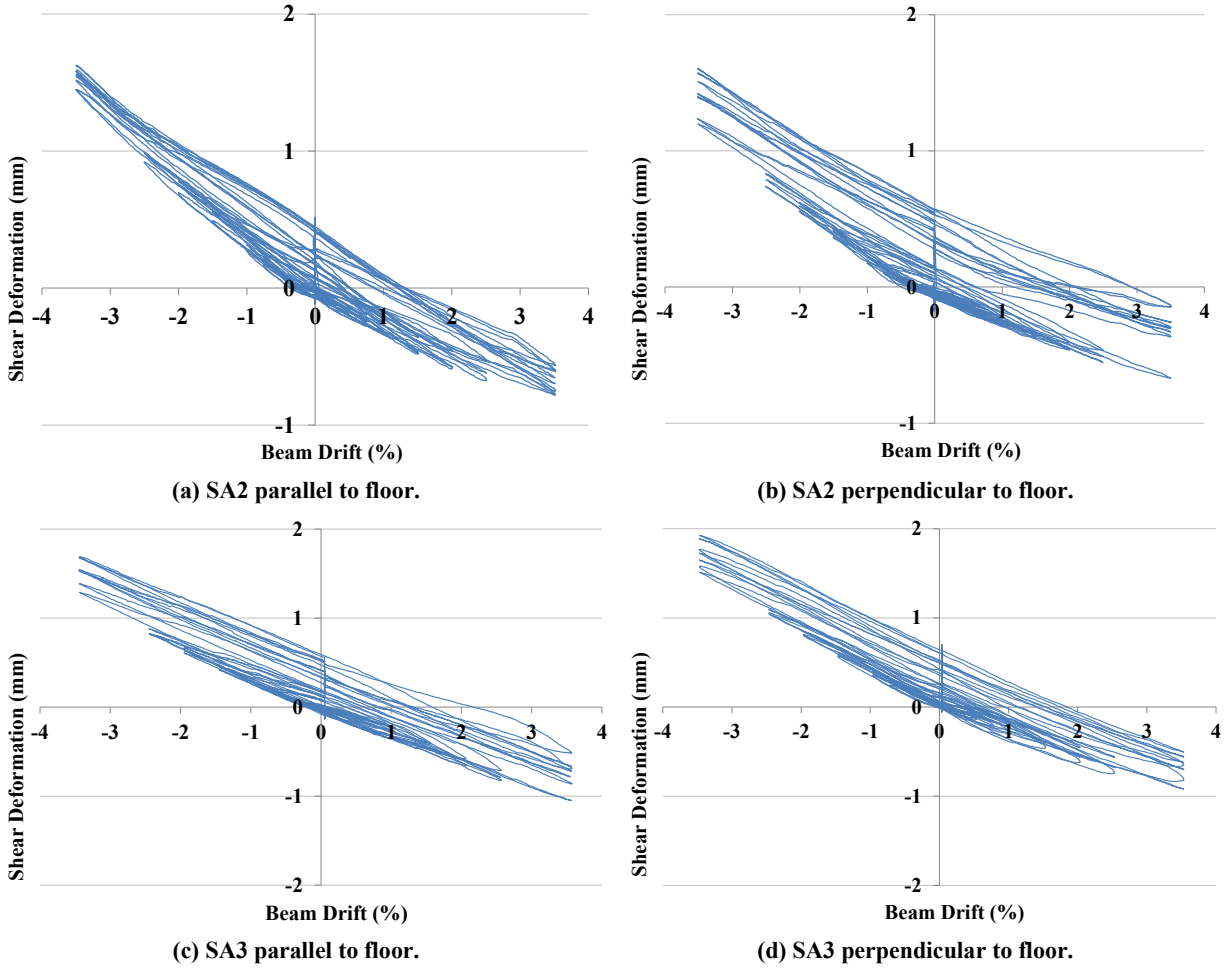

Figure 6-25: Shear deformation of as-built subassemblies.

As shown in Figure 6-26, the shear displacement response recorded in the retrofitted subassemblies was similar to that observed in the as-built subassemblies. The retrofitted subassemblies were tested in the order that they are presented, SA2-TCY first, SA2-SFD next and SA2-HF2V last. Comparing Figure 6-26(b), (d) and (f), it can be seen that the shear displacement in the connection perpendicular to the floor increased over successive subassembly tests. SA2 formed the basis of all three retrofitted subassembly experiments. Hence, portions of the slotted beam connections that were not retrofitted, such as the top longitudinal reinforcement and diagonal hangers, were subjected to a large number of loading cycles. It was shown in SA1 that the top longitudinal reinforcement and diagonal hangers experienced limited yielding during testing. At the conclusion of testing SA2-HF2V, the diagonal hangers and top longitudinal reinforcement had been subjected to five complete loading protocols. Hence, it was postulated that the increasing nonlinearity over successive subassembly tests was due to strain penetration either side of the slotted section and the resulting loss of bond.

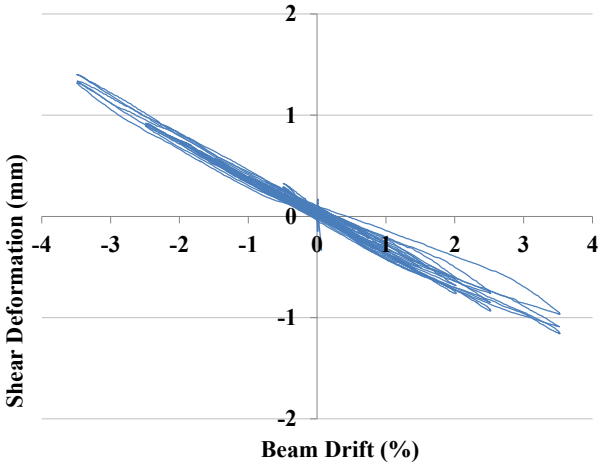

(a) SA2-TCY parallel to floor.

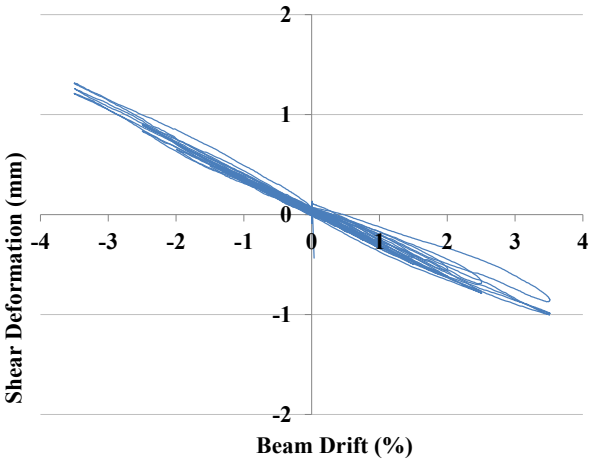

(b) SA2-TCY perpendicular to floor.

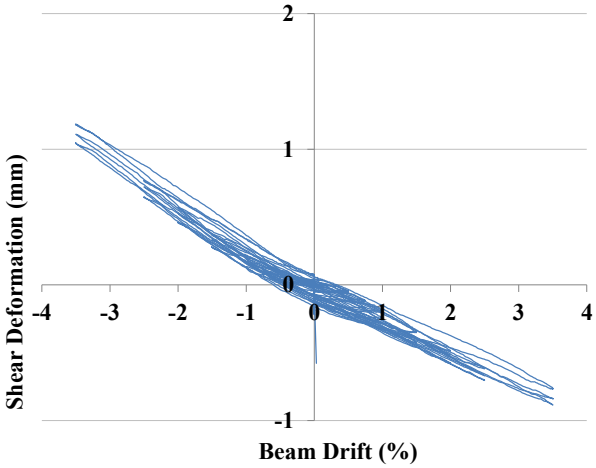

(c) SA2-SFD parallel to floor.

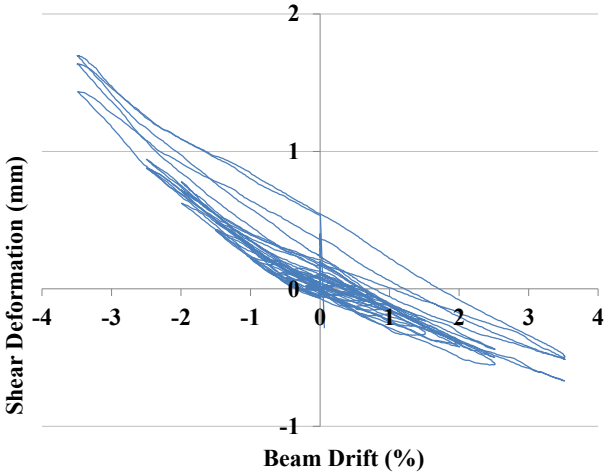

(d) SA2-SFD perpendicular to floor.

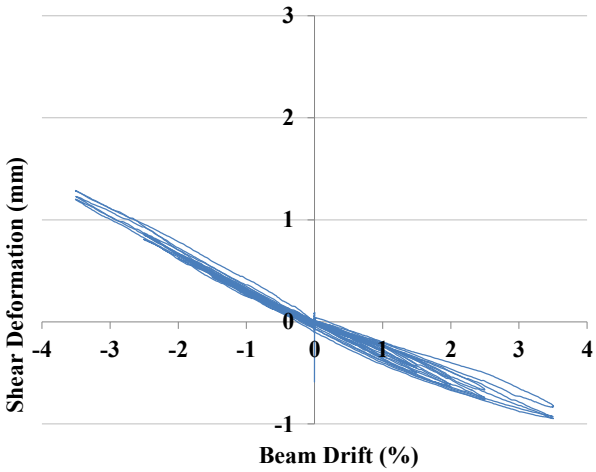

(e) SA2-HF2V parallel to floor.

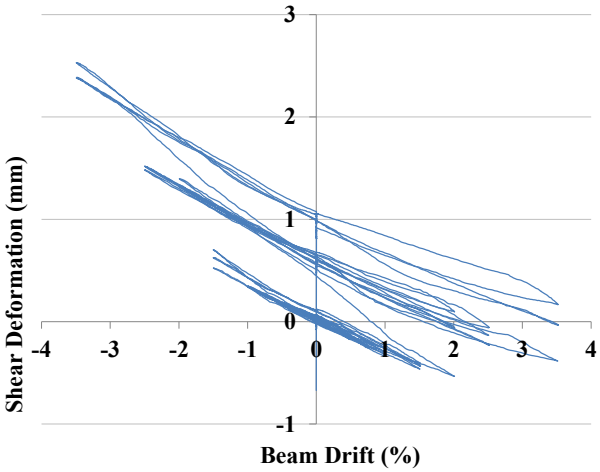

(f) SA2-HF2V perpendicular to floor.

Figure 6-26: Shear deformation of retrofitted subassemblies.

6.10 Beam Torsion

Figure 6-27 presents the beam inclination that occurred over the slotted section of the as-built subassemblies. Greater inclination was observed over the slotted section of the beam perpendicular to the floor, which was consistent with the behaviour observed in SA1. The beam perpendicular to the floor was subjected to greater torsional demands due to the influence of the one-way flooring. When the subassemblies were displaced, the relative

rotation between the end of the hollow-core unit and the supporting beam face induced a moment along the length of the beam. The continuity moment, in conjunction with the gravity load from the one-way flooring being applied eccentric to the beam shear centre, resulted in the connection perpendicular to the floor having to resist larger torsional demands than the connection parallel to the floor.

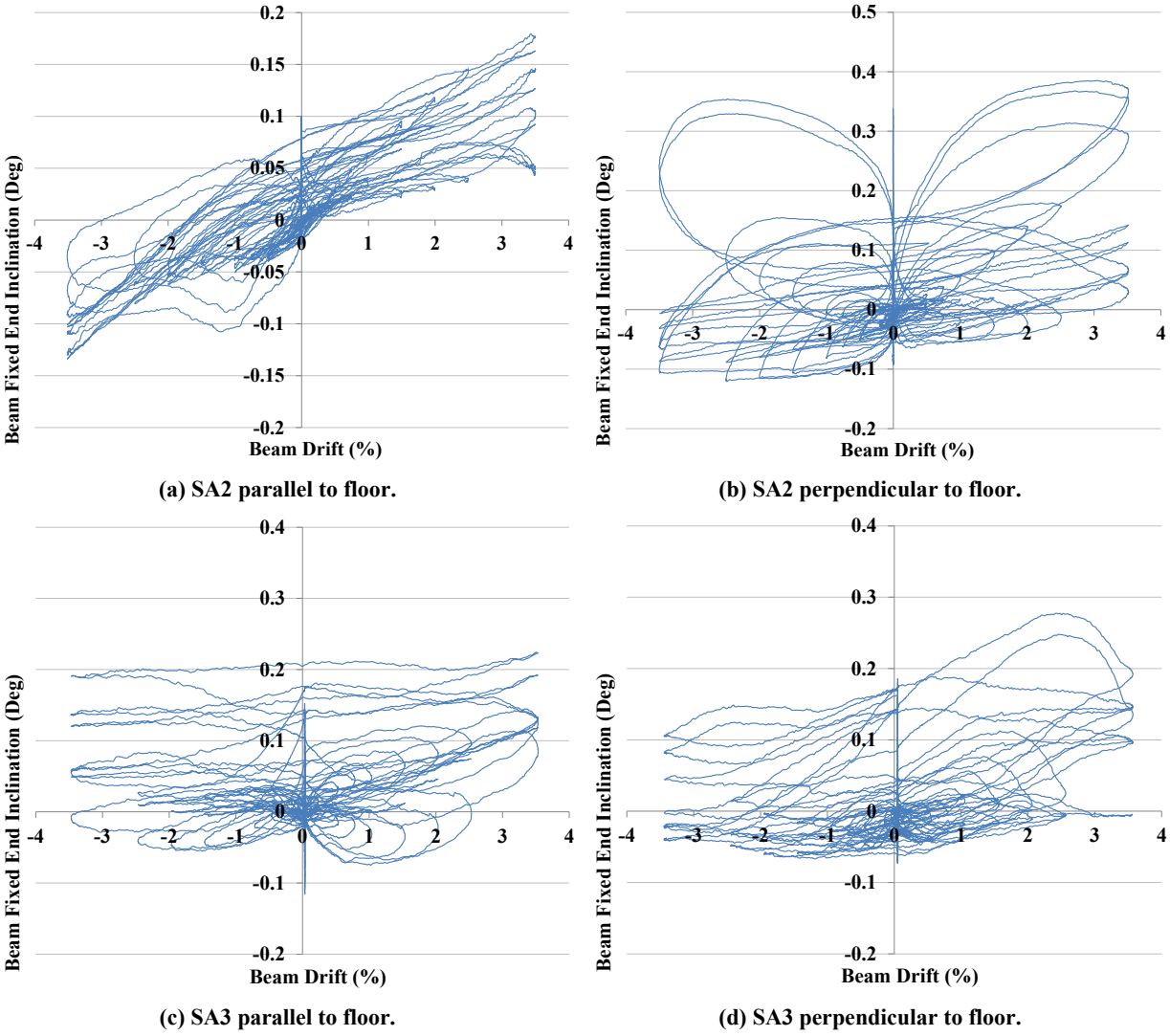

(a) SA2 parallel to floor.

(b) SA2 perpendicular to floor.

(c) SA3 parallel to floor.

(d) SA3 perpendicular to floor.

Figure 6-27: Fixed end rotation of as as-built subassemblies.

The retrofit regime implemented on specimen SA2 had minimal effect of the torsional strength of the slotted beam connections. Because the torsional strength of the retrofitted subassemblies was similar to that of the as-built subassemblies, the torsional response was similar also, as shown in Figure 6-28. Figure 6-28(b), (d) and (f) show that recorded beam end inclination increased over successive subassembly tests. A similar trend was observed for shear displacement in the retrofitted subassemblies, as presented in Section 6.9. It was postulated that the increasing shear displacement over successive subassembly tests was due to strain penetration either side of the slotted section and the resulting loss of bond. It was likely that the same mechanism caused the increasing beam end inclination over successive

retrofitted subassembly tests. This observation highlights the importance of taking a prudent and pragmatic approach to designing the diagonal hangers in a slotted beam connection.

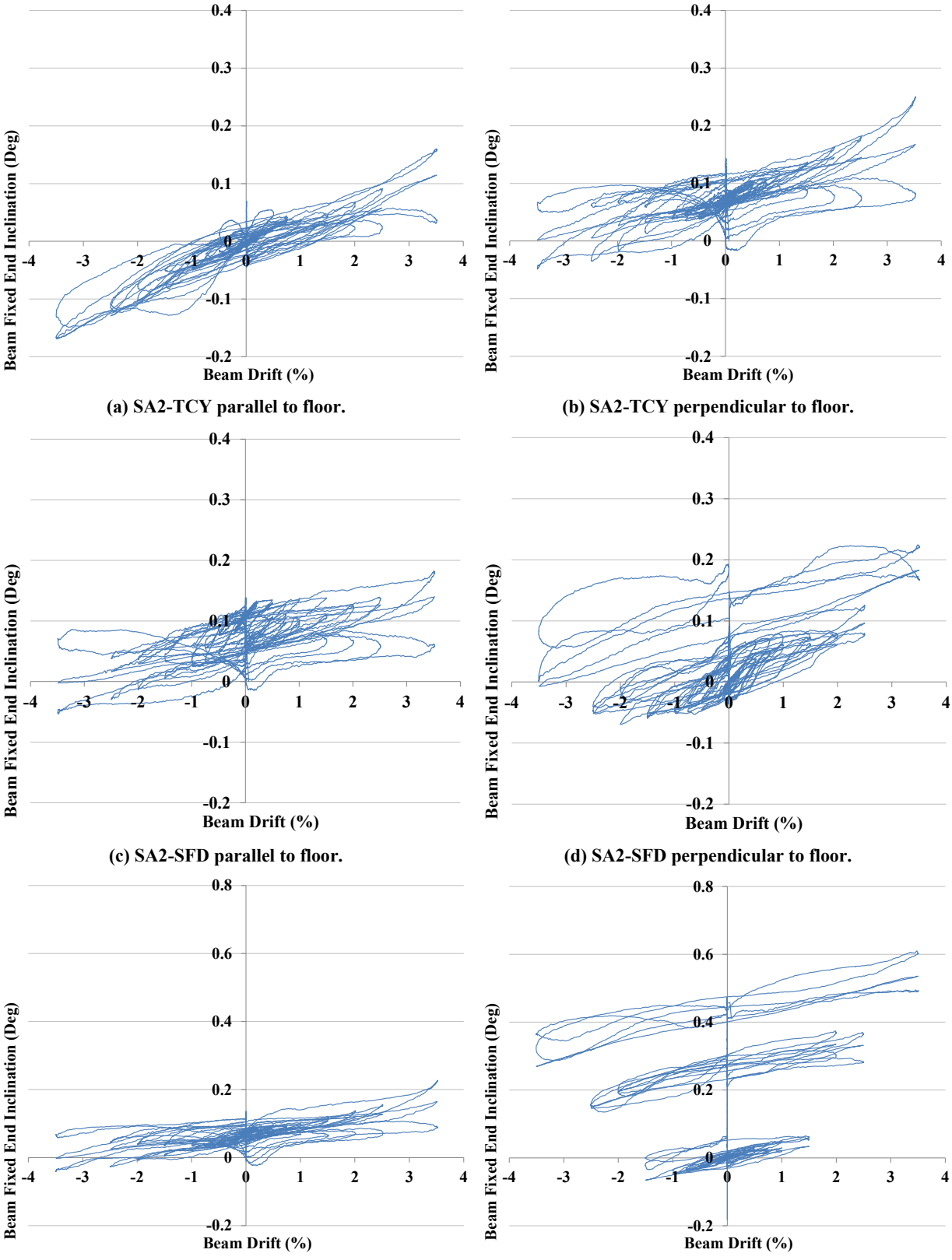

(a) SA2-TCY parallel to floor.

(b) SA2-TCY perpendicular to floor.

(c) SA2-SFD parallel to floor.

(d) SA2-SFD perpendicular to floor.

(e) SA2-HF2V parallel to floor.

(f) SA2-HF2V perpendicular to floor.

Figure 6-28: Fixed end rotation of retrofitted subassemblies.

Beam inclination data was collected along the lengths of both beams of the subassemblies using inclinometers. Beam inclination in all subassemblies occurred predominately over the

slotted section and positive beam inclinations were greater than negative due to the influence of the floor diaphragm. These observations corroborate the observations made in Section 4.13 for specimen SA1.

6.11 Beam Elongation

Beam elongation in the subassemblies was measured at the beam centreline. Hence, opening and closing rotations were recorded as elongation. Figure 6-29 and Figure 6-30 present the beam elongation of the slotted beam connections during testing of the as-built and retrofitted subassemblies respectively. In these plots, beam growth is represented by positive elongation. The beam elongation data for the connection perpendicular to the floor in specimen SA3 could not be calculated due to linear potentiometer failure.

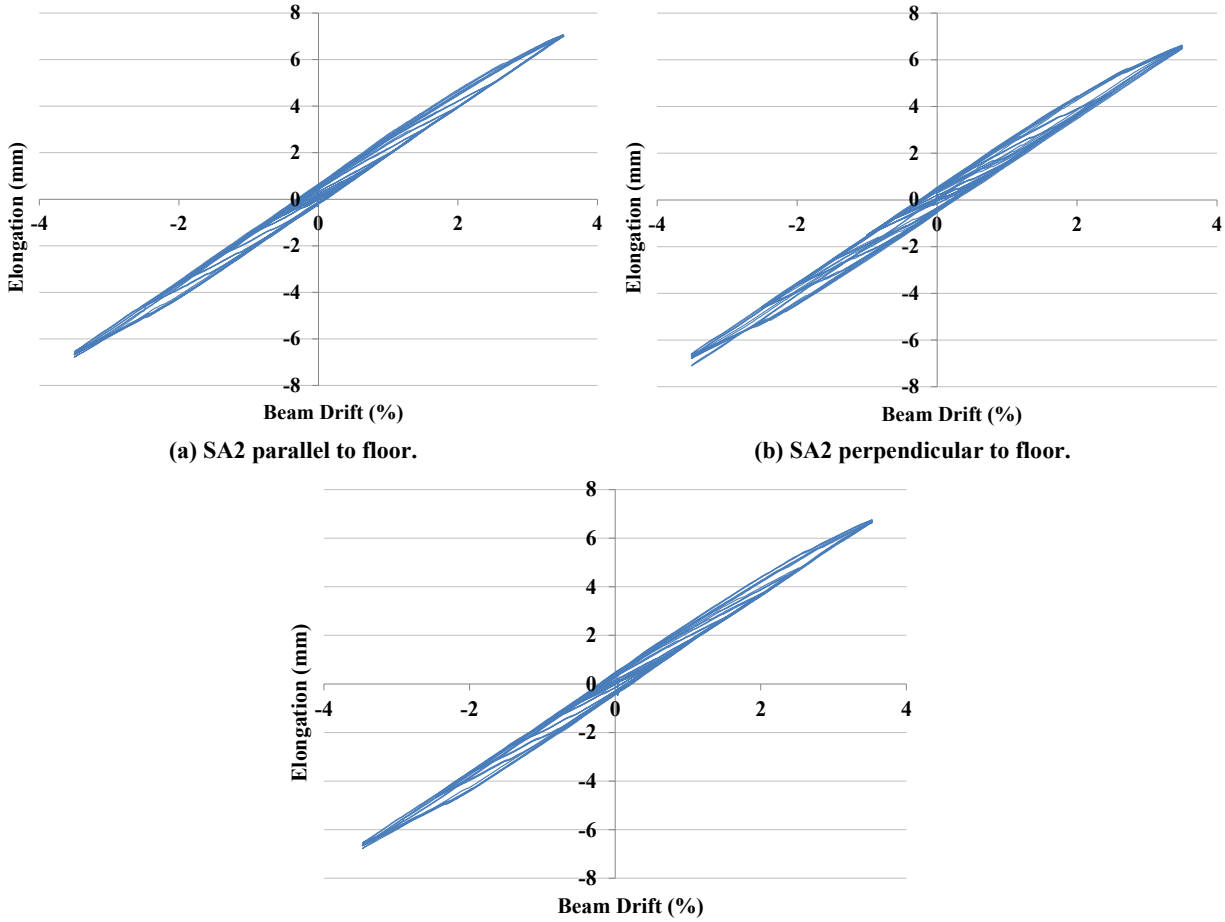

(a) SA2 parallel to floor.

(b) SA2 perpendicular to floor.

(c) SA3 parallel to floor.

Figure 6-29: Centreline beam elongation of as-built subassemblies.

In general, the beam elongation observed in all specimens was very low. The peak cumulative elongation in the subassemblies was 0.28% of the beam depth. Compared to the peak cumulative elongation recorded in SA1, which was 0.38% of beam drift, the subassemblies exhibited less elongation. Because the connections had already elongated when they were tested as components of SA1, the elongated state of the connections became the new baseline from which additional beam elongation was calculated. It was shown in Section 4.14 that

beam elongation is primarily driven by connection flexure. When tested in the subassemblies, the connections were subjected to the same rotations that they had been subjected to in the SA1 test. Hence, because the connections had already elongated prior to testing, subsequent elongation during the subassembly tests was reduced.

Figure 6-30(f) shows that the increasing deformation over successive subassembly tests observed for shear displacement and beam inclination was not observed for beam elongation. The top longitudinal reinforcement in the connections was designed to be twice as strong as the bottom longitudinal reinforcement. Hence, the strain in the top longitudinal reinforcement was lower than the strain in the diagonal hangers. The nonlinear behaviour observed in the top longitudinal reinforcement and the diagonal hangers meant that both types of reinforcement were potentially susceptible to low-cycle fatigue. Low cycle fatigue is examined in more detail in Section 7.5.3.

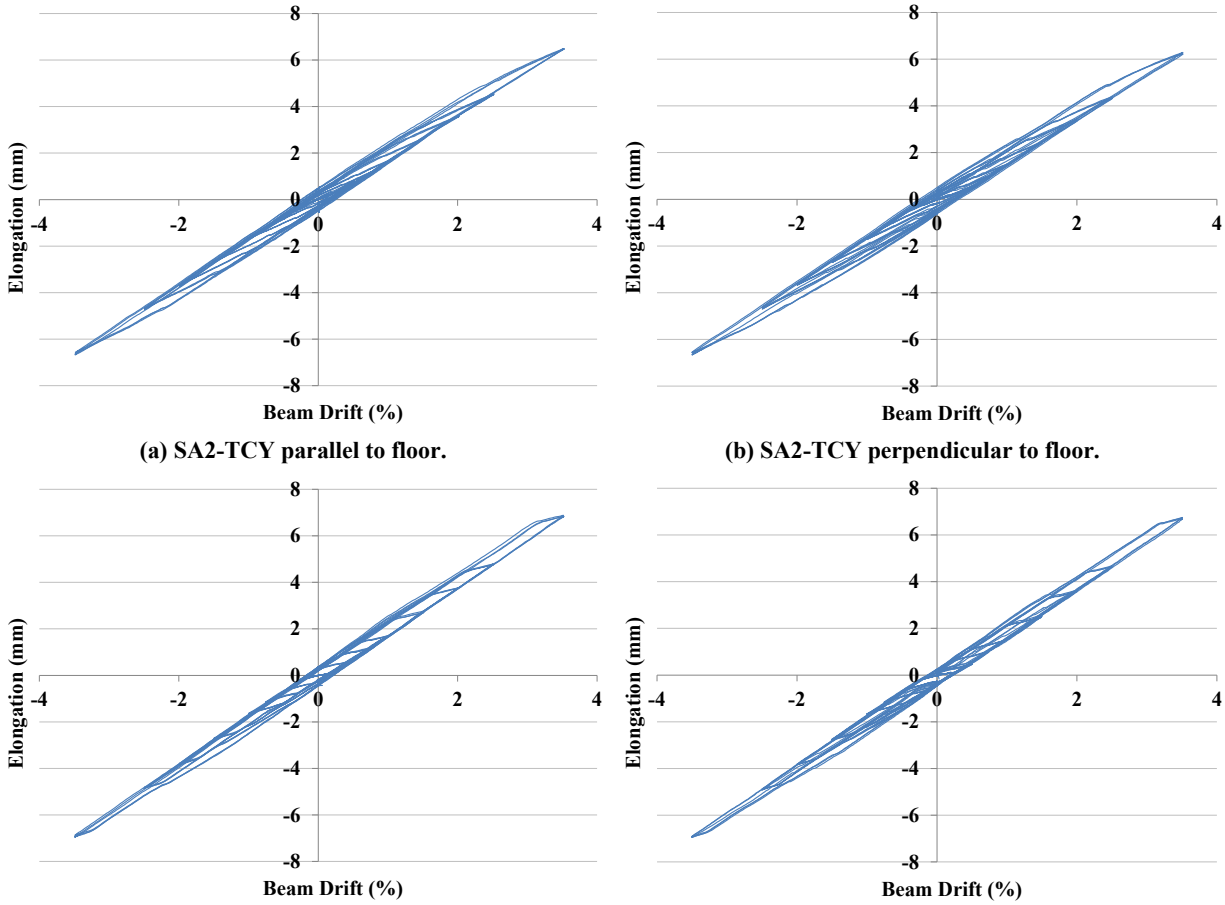

(a) SA2-TCY parallel to floor.

(b) SA2-TCY perpendicular to floor.

(c) SA2-SFD parallel to floor.

(d) SA2-SFD perpendicular to floor.

Figure 6-30: Centreline beam elongation of retrofitted subassemblies.

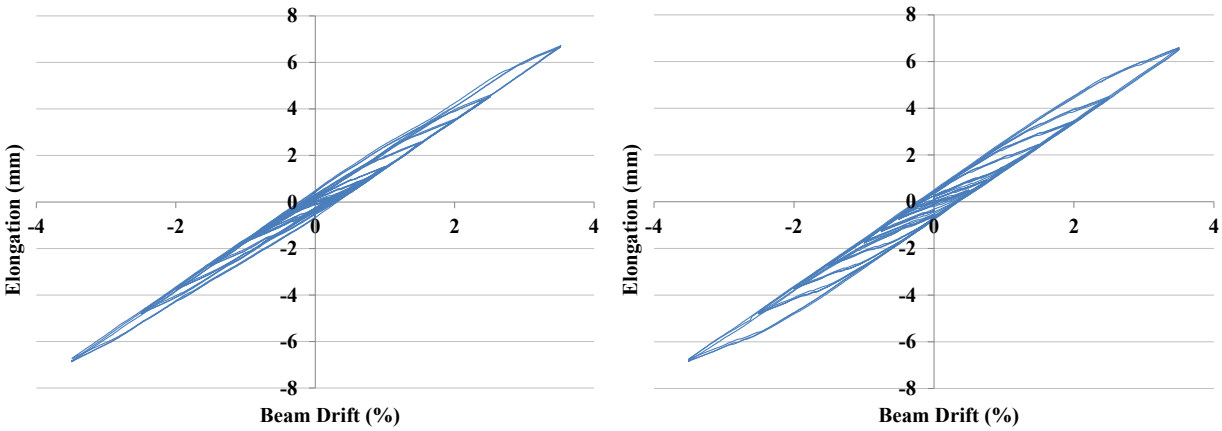

(e) SA2-HF2V parallel to floor.

(f) SA2-HF2V perpendicular to floor.

Figure 6-30: Centreline beam elongation of retrofitted subassemblies (Continued).

It can be concluded that beam elongation in the slotted beam connections was not sensitive to the type of device used in the bottom of the beam to create a connection moment. Furthermore, due to the top longitudinal reinforcement being designed to be twice as strong as the bottom longitudinal reinforcement, the force capacity of the dampers installed to replace the bottom longitudinal reinforcement did not significantly affect the recorded beam elongation. Beam elongation in slotted beams is largely dictated by the top hinge depth, top longitudinal reinforcement location and connection rotation.

6.12 Floor Diaphragm Performance

Because the boundary conditions of the floor diaphragm were less realistic than they were in SA1, any floor strain measurements or crack mapping could potentially be erroneous or misleading. Instead, parameters that could not be measured in SA1 were measured in the subassembly tests.

As described in Section 4.5, continuity moments that were induced in the precast floor seating connections contributed to the overall observed response of specimen SA1. Continuity moments are defined in Section 2.3.3. The magnitude of the continuity moments generated was calculated using engineering principles, since direct measurement of the continuity moments could not be undertaken in SA1. However, in the subassembly tests the continuity moment generated by the hollow-core connection could be measured using the load cell supporting the free end of the floor. The continuity moment generated during the subassembly tests is presented in Figure 6-31(b) and (d), and Figure 6-32(b), (d) and (f). The continuity moment calculated using fundamental connection mechanics was approximately 4.8kNm/m. As shown in Figure 6-31(b) and (d), once the 1.2m width of the hollow-core unit was taken into account the calculated continuity moment was similar to the measured negative continuity moments. The positive continuity moments were significantly less than the negative continuity moments because there was no contact between the end of the hollow-

core unit and the compressible backer. Because of the boundary conditions that the subassemblies had, the axial force that would have been induced in the floor by beam elongation was not able to be captured. Compressive axial force could have significantly increased the measured continuity moments. Hence, the presented continuity moments are considered lower bound.

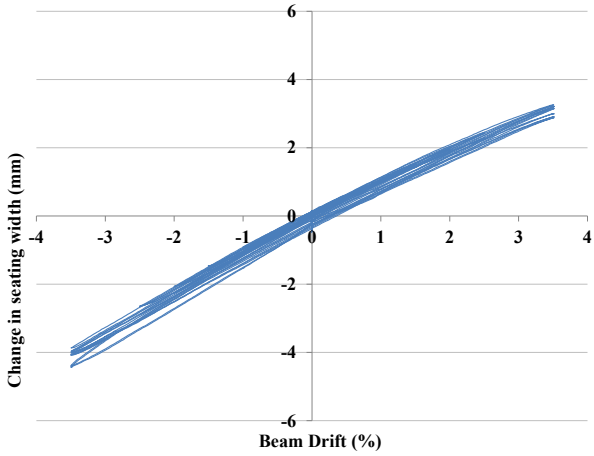

(a) SA2 hollow-core unit change in seating.

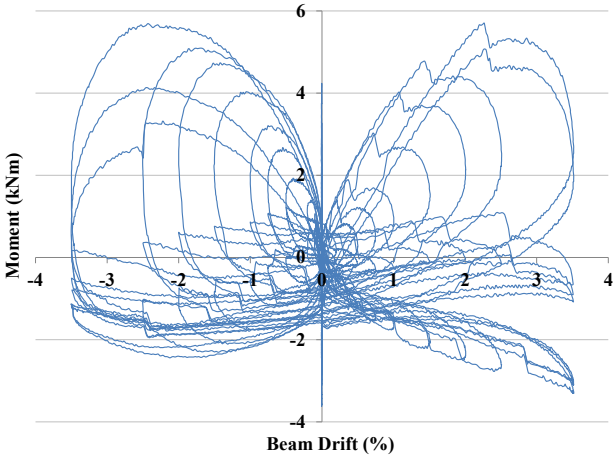

(b) SA2 continuity moment.

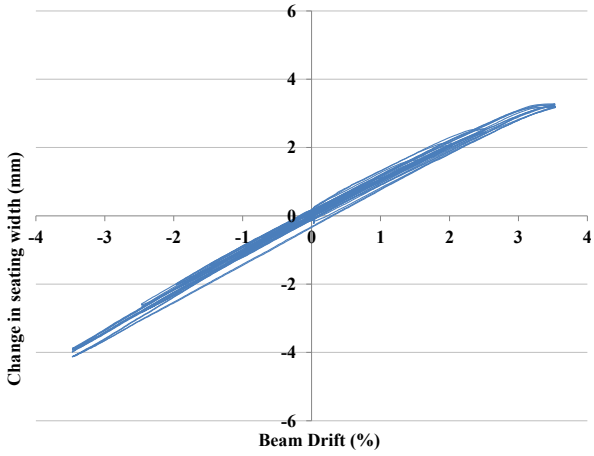

(c) SA3 hollow-core unit change in seating.

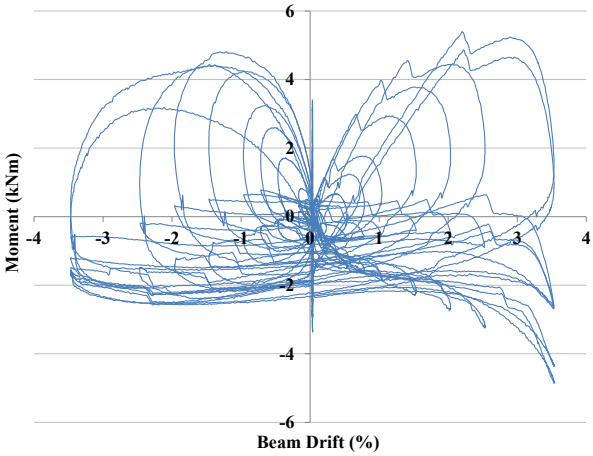

(d) SA3 continuity moment.

Figure 6-31: Floor diaphragm response of as-built subassemblies.

Hollow-core seating loss during testing was very low in all subassemblies, as shown in Figure 6-31(a) and (c); and Figure 6-32(a), (c) and (e). The precast floor seating loss measured in the subassemblies was significantly lower than that measured in SA1, which demonstrated the relationship between beam elongation and precast floor seating loss. In moment frame systems, beam elongation forces apart the columns, and hence the beams that support the one-way floors also. As the beams supporting the one-way floors are forced apart, the seating width is reduced. This effect could not be captured in the subassembly tests. Compared to a system built with traditional connections, a system built with slotted beams will experience less floor seating loss during an earthquake; therefore, increasing the safety of the building by maintaining floor gravity support.

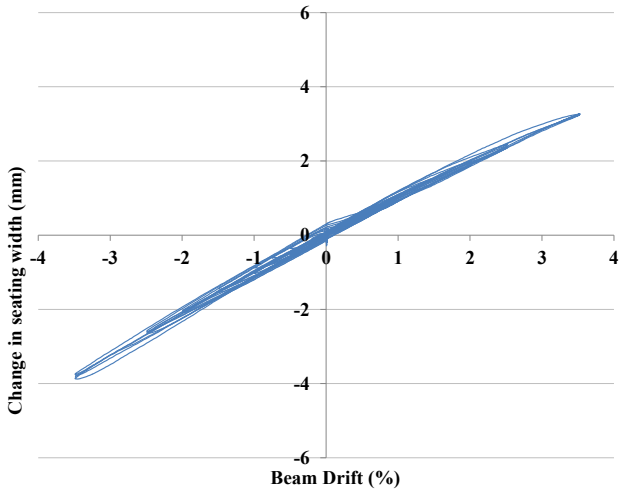

(a) SA2-TCY hollow-core unit change in seating.

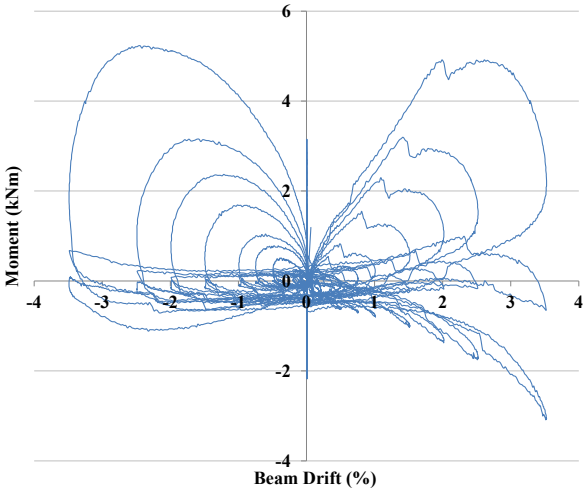

(b) SA2-TCY continuity moment.

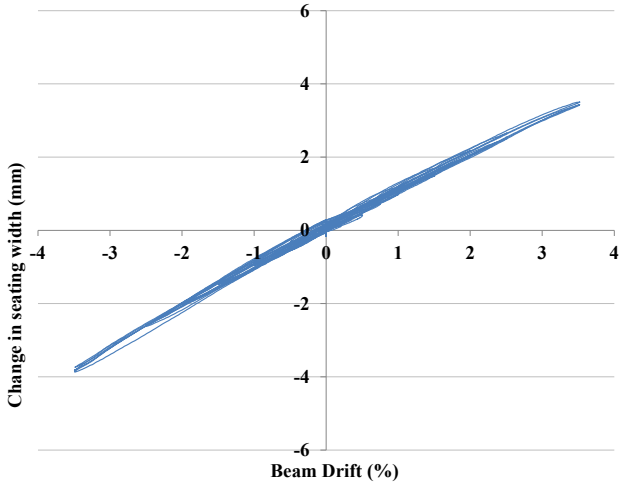

(c) SA2-SFD hollow-core unit change in seating.

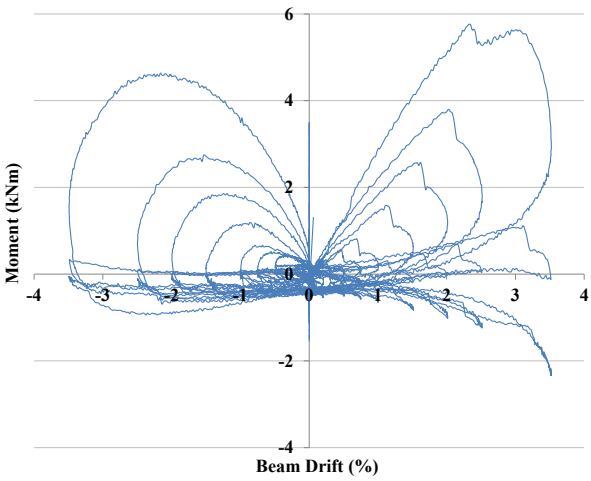

(d) SA2-SFD continuity moment.

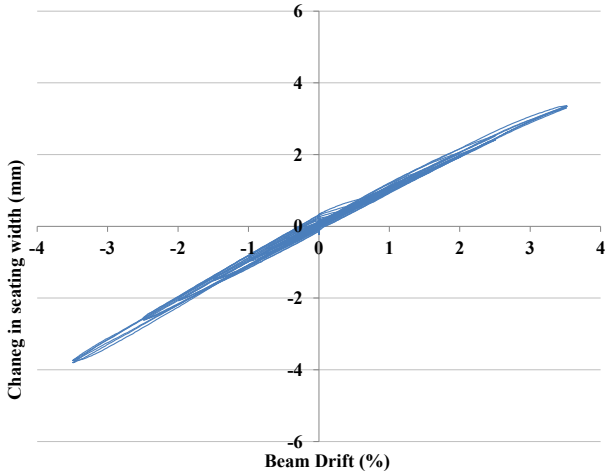

(e) SA2-HF2V hollow-core unit change in seating.

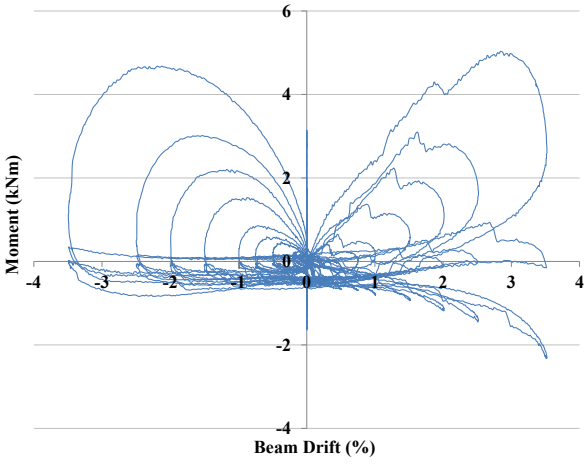

(f) SA2-HF2V continuity moment.

Figure 6-32: Floor diaphragm response of retrofitted subassemblies.

6.13 Conclusions

This chapter described the experimentation performed on five reinforced concrete slotted beam subassemblies. The experimental results obtained from the tests were presented and

their relevance described. Based on the results of these experiments, the following conclusions were made:

1. Significant capacity remains in a reinforced concrete slotted connection after it is subjected to a large earthquake. Hence, the potential to reuse a slotted beam structure after a significant seismic event is promising. In a practical application, the estimation of residual connection capacity is complicated by the strain history being unknown.
2. In all incidences, low-cycle fatigue failure of the bottom longitudinal reinforcement was preceded by buckling in the slot region. It is recommended that designers take practical steps to prevent reinforcement buckling in the connection slot, such as using large diameter reinforcement, minimising strain penetration and minimising the slot width.
3. Less pinching was observed in the force-displacement response of SA2 and SA3 compared to SA1. Therefore, it may be concluded that the pinching observed in SA1 was due to displacements occurring in the universal joints of the experimental setup.
4. For small relative rotations between the column face and the beam soffit, it was shown that the TCY dampers could accommodate induced flexure whilst maintaining axial performance. However, if large rotations are expected it is recommended that the damper end fixities are released. The designer should be aware of the implications of doing such on damper performance.
5. Care must be taken by the designer to provide a stiff connection between the dampers and the structure. Deformation in the connection between the dampers and the structural frame can significantly alter connection response. It is recommended that stiffness, as well as strength, is considered when designing damper connections.
6. The TCY dampers exhibited a stiffer response in compression than they did in tension, despite the design of new provisions to prevent contact between the threaded portion of the dampers and the confinement epoxy. This variance was likely due to the effect of Poisson's ratio on the restrained steel. Because of Poisson's ratio, the effective cross-section of the steel increased, which increased the effective stress and enabled a higher force to be generated. This mechanism is explained in more detail in Section 4.5.
7. The peak force attained in SA2-SFD was observed to decrease over the course of testing. The same drop in peak force with increasing displacement was observed also during the device testing. It was postulated that the decrease in force as testing progressed was due to the wearing down of surface irregularities between the friction surfaces. This decreased the coefficient of friction and reduced the total force required to initiate sliding between the surfaces.

8. Specimen SA2-HF2V was observed to creep during testing due to the ability of the lead in the HF2V dampers to flow at low temperatures. By using a modest recentring force, it may be possible to design a system that does not immediately return to its original plumb position at the end of an earthquake, but returns slowly to that position in the days following the earthquake.
9. Negative stiffness was observed whilst testing the SFD and HF2V devices. However, due to the contribution of other elements, such as the top longitudinal reinforcement, the overall connection stiffness of specimens SA2-SFD and SA2-HF2V remained positive throughout testing. However, low post-yield stiffness can result in poor control of structural displacements during an earthquake. Furthermore, when large displacements are experienced in a structure, P-delta effects can cause the overall system stiffness to become negative, which can jeopardise the overall stability of the structure.
10. The variances observed between the design and measured damper forces were significant. If the dampers were used in a slotted beam structure, and similar discrepancy between the design and actual damper capacities existed, the overall structural response would be significantly affected. Hence, it is recommended that if dampers are to be used in a structure, experimental testing should be conducted to validate the actual damper response against assumptions made during the design phase.
11. Beam elongation in the slotted beam subassemblies was not sensitive to the type of device used in the bottom of the beam to create a connection moment. Furthermore, due the top longitudinal reinforcement being designed to be twice as strong as the bottom longitudinal reinforcement, the force capacity of the dampers installed to replace the bottom longitudinal reinforcement did not significantly affect recorded beam elongation. It follows that neutral axis variation in the subassembly connections was independent of the type of device used in the bottom of the beam to create a connection moment also.
12. The precast floor seating loss measured in the subassemblies was significantly lower than that measured in SA1. This observation demonstrated the relationship between beam elongation and precast floor seating loss. In moment frame systems, beam elongation forces apart the columns, and hence the beams that support the one-way floors also. As the beams supporting the one-way floors are forced apart, the seating width is reduced. This effect could not be captured in the subassembly tests.
13. A reinforced concrete slotted beam being previously subjected to seismic actions does not significantly affect the amount of energy that it can dissipate. Similarly, the stiffness degradation of a reinforced concrete slotted beam is not affected by having been previously subjected to seismic demands.

14. The use of dampers, in place of conventional reinforcement, in a reinforced concrete slotted beam connection can significantly increase the amount of energy able to be dissipated. Increased energy dissipation in a system will result in lower peak and residual displacements, which can result in lower damage, lower repair costs and quicker reoccupation. Furthermore, these benefits are able to be achieved in both retrofit and new-build applications.
15. The retrofitted subassemblies were tested in the order that they were presented, SA2-TCY first, SA2-SFD next and SA2-HF2V last. Shear and torsional displacements in the connection perpendicular to the floor were observed to increase over successive retrofitted subassembly tests. SA2 formed the basis of all three retrofitted subassembly experiments. At the conclusion of testing SA2-HF2V, the diagonal hangers and top longitudinal reinforcement had been subjected to five complete loading protocols. Hence, it was postulated that the increasing nonlinearity over successive subassembly tests was due to strain penetration either side of the slotted section and the resulting loss of bond.

6.14 References

ACI Committee 374. (2005). *Acceptance Criteria for Moment Frames Based on Structural Testing and Commentary (ACI374.1-05)*. Farmington Hills, Michigan: American Concrete Institute.

Chanchi Golondrino, J., Chase, J. G., Rodgers, G. W., MacRae, G. A., & Clifton, C. G. (2012). *Velocity dependence of HF2V devices using different shaft configurations*. Paper presented at the New Zealand Society for Earthquake Engineering Annual Conference, Christchurch, New Zealand. Retrieved from http://ir.canterbury.ac.nz /bitstream/10092/7417/1/12640801_HF2V_Velocity_Paper_Draft.pdf

Priestley, M. J. N., Calvi, G. M., & Kowalsky, M. J. (2007). *Displacement-based seismic design of structures*. Pavia, Italy: IUSS Press.

7. Three-Dimensional Numerical Analyses

7.1 Introduction

The popularity of numerical models to model structural systems in both research and design applications has rapidly increased over the past 50 years. This increase in popularity has been driven by a reduction in the cost of computing, an increase in the complexity of structures and the availability of user-friendly analysis suites. Increasingly, numerical analyses are being undertaken in commercial settings by engineers who perhaps lack knowledge about the processes being undertaken by the tool that they are using. Hence, it is important to develop numerical models that are quick and simple to set up, yet yield accurate results.

This chapter describes the third phase of this research project, the goal of which was to develop a numerical model that was not only capable of reproducing realistic slotted beam behaviour in three dimensions, but could be quickly set up without calibration by using only gross section and material properties. The developed multispring model, described herein as the R3D element, was implemented as an in-built element within the nonlinear time history program Ruaumoko3D (Carr, 2013). Historical research undertaken to develop numerical models of both slotted beam and traditional connections was examined. The response of the R3D element was compared to two-dimensional numerical models developed by Au (2010). Numerical models of the superassembly and subassemblies described in Chapters 3 – 6 were assembled and subjected to the same loading protocol that was applied to the experimental specimens. The response of the numerical models was compared to the response of the experimental specimens. A numerical floor diaphragm model was developed to capture the effect that the floor diaphragm has on overall system lateral resistance. Two numerical models of specimen SA1 were assembled using the R3D element for the slotted beam version, and the plastic hinge element (Peng, 2009) for the traditional beam version. The differences in the observed responses of the numerical models was compared and discussed. Slotted beam and traditional connection versions of the prototype structure described in Section 3.3 were modelled numerically. The models were subject to a suite of earthquake records to enable overall structural performance of the different structural systems to be investigated.

7.2 Literature Review

Conducting research using numerical models is a cost and time effective alternative to experimental testing. Many numerical analyses may be run in a short time period. Parameters can be systematically altered in order to examine the influence that they have on overall behaviour. However, for the results of these types of investigations to be useful the numerical models must accurately replicate experimental response.

Advances in technology have made powerful computing cheaper and more available. This has enabled increasingly complex programs to be developed, which allow increasingly intricate numerical models to be assembled. However, many complex numerical models still require calibration with experimental data, and all require verification to the undertaken.

The limitations of using numerical models are outweighed by the potential for large amounts of data to be collected in a short period of time, and for comparatively little cost. Provided the numerical models are carefully set up, calibrated and verified, the data generated can provide insight into issues that cannot be practically broached experimentally.

7.2.1 Traditional Reinforced Concrete Connection Modelling

Douglas et al. (1996) developed the first numerical model to realistically replicate the behaviour of reinforced concrete plastic hinge zones. As shown in Figure 7-1, the model used four axial elements and a shear element. The two steel elements were assigned a hysteretic rule defined by Tjokrpdimuljo (1985). The concrete elements were assigned a simple hysteretic rule that took into account stiffness degradation, tensile cracking and wedging action. A force, F_d, was applied to either side of the element to represent the horizontal component of the diagonal compressive shear strut that forms in plastic hinge zones. To achieve acceptable response, the element required calibration to experimental data.

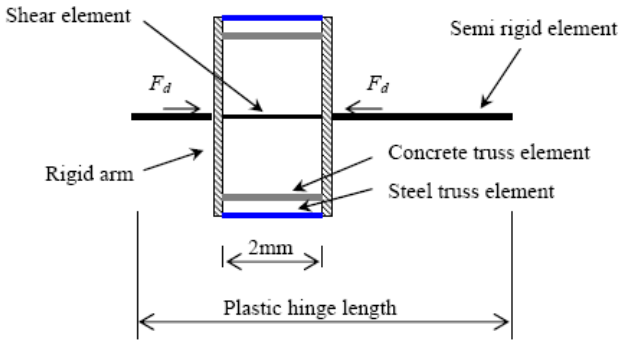

Figure 7-1: Numerical reinforced concrete plastic hinge element developed by Douglas et al. (1996).

Kim et al. (2004) developed a numerical model of a reinforced concrete plastic hinge zone based on earlier research undertaken to numerically model hybrid frame behaviour (Kim, 2002). A schematic of the traditional reinforced concrete plastic hinge numerical model is

shown in Figure 7-2. Kim et al. (2004) developed the model using the nonlinear time history software DRAIN-2DX (Prakash et al., 1993). The model used axial elements at the top and bottom of the interface to resist tension and compression; the axial elements represented reinforcement. Nine gapping elements were distributed over the interface to model crack opening. The gapping elements could resist compression but not tension, and hence their behaviour was analogous to cracked concrete. Shear forces were transferred by a rigid link, which did not enable shear deformation to be modelled. Because the point of rotation of the connection was not coincident with the section centroid, the model was able to replicate geometric beam elongation. However, the elongation was fully recovered when the connection was unloaded, which does not occur in real traditional reinforced concrete connections.

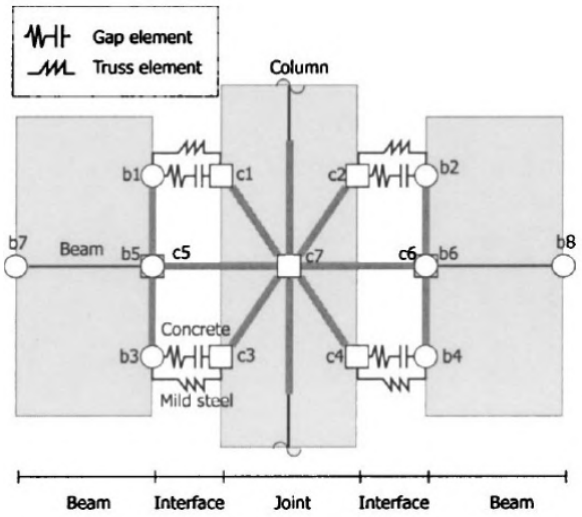

Figure 7-2: Numerical plastic hinge element developed by Kim et al. (2004).

Lau et al. (2007) developed a numerical model of a reinforced concrete plastic hinge based on the work conducted by Douglas et al. (1996). A schematic of the numerical model is shown in Figure 7-3. The element used ten axial elements. Member A represented the longitudinal reinforcement and was assigned a bi-linear hysteresis. Member B represented the longitudinal concrete and was assigned linear elastic compressive behaviour with zero tensile strength. Member C was a concrete compressive strut which represented diagonal shear transfer; Member C had the same properties as Member B. Member D was a diagonal strut required for numerical stability and it was assigned a bi-linear hysteresis. Member E was used to model elongation in the element. Calibration had to be undertaken using experimental data for the element to produce representative response.

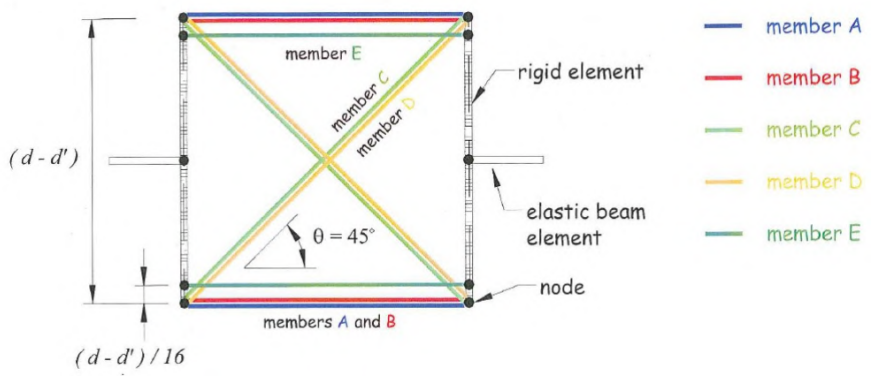

Figure 7-3: Numerical plastic hinge model developed by Lau et al. (2007).

Peng (2009) extended the work of Lau et al. (2007) by developing a numerical plastic hinge model based on fundamental mechanics. The model could be set up without using empirical parameters derived from experiments. The model was developed using the nonlinear time history software Ruaumoko2D (Carr, 2005). A schematic of the plastic hinge element is shown in Figure 7-4. At the top and bottom at the element were axial springs that were assigned a steel hysteresis rule. These axial springs represented the longitudinal reinforcement in the plastic hinge. Outside of the axial steel springs were two axial springs to represent unconfined concrete. Between the axial steel springs were eight axial springs to represent confined concrete. Two diagonal axial springs were used to model shear transfer across the plastic hinge zone. All concrete springs were assigned a cracked concrete hysteresis rule developed by Maekawa et al. (2003).

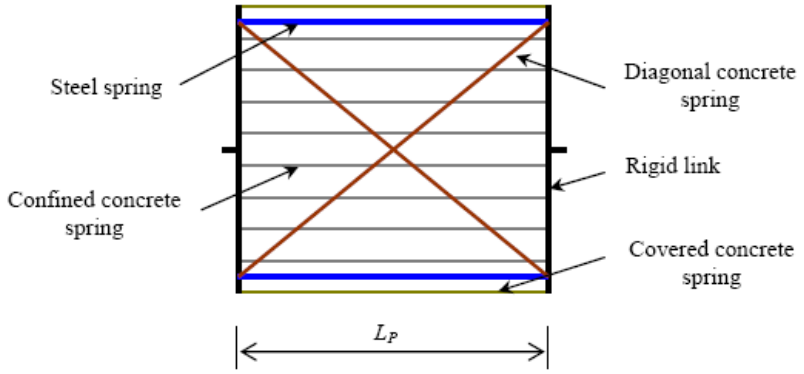

Figure 7-4: Two-dimensional numerical plastic hinge element developed by Peng (2009).

Peng (2009) extended the two-dimensional element into three dimensions using Ruaumoko3D (Carr, 2013). As shown in Figure 7-5, the element used 28 axial springs to represent unconfined concrete around the perimeter of the element. The confined concrete was modelled using 36 axial springs, which were located inside of the eight axial springs used to represent longitudinal reinforcement. Eight diagonal axial springs, two on each face, modelled shear transfer across the plastic hinge element. The plastic hinge element was used to assemble a numerical model of a two bay subassembly that was tested experimentally. The

response of the numerical model showed close agreement with the experimentally observed response.

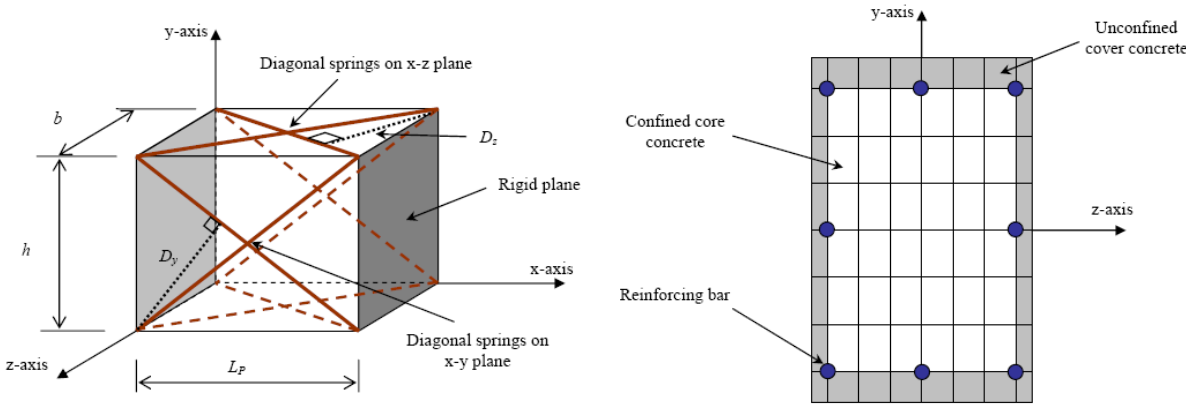

(a) Oblique view of three-dimension element. **(b) Cross-section of three-dimensional element.**

Figure 7-5: Three-dimensional numerical plastic hinge element developed by Peng (2009).

7.2.2 Slotted Beam Connection Modelling

The first numerical model of a reinforced concrete slotted beam was developed in Japan. Ohkubo et al. (1999) used a finite element model of the slotted beam to investigate shear transfer in slotted beams. The numerical investigation was prompted by the premature shear failure of several reinforced concrete slotted beam specimens. Specifically, the directions of principal stress within the slotted beam during negative flexure were examined. A vectorial plot from the analysis is shown in Figure 7-6. It can be seen that concrete tension existed at point B during negative flexure. In experimental reinforced concrete slotted beam specimens, the concrete tension observed in the numerical investigation caused the formation of 's-cracks', which are discussed in more detail in Section 3.4.2.

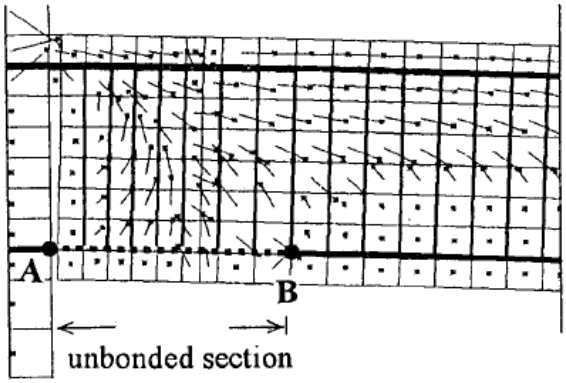

Figure 7-6: Finite element model of reinforced concrete slotted beam by Ohkubo et al. (1999).

Leslie (2010) developed a numerical model of the slotted beam using a compound spring element, as shown in Figure 7-7. The compound spring element can be set up with a number of spring elements between two rigid planes, and is part of an extensive element library in Ruaumoko2D (Carr, 2005). The geometry, material properties and hysteretic rule of each spring within the compound element could be set up individually, which enabled different components of the slotted beam connection to be modelled. The agreement between

experimentally observed slotted beam response and the response of the numerical model was reasonable.

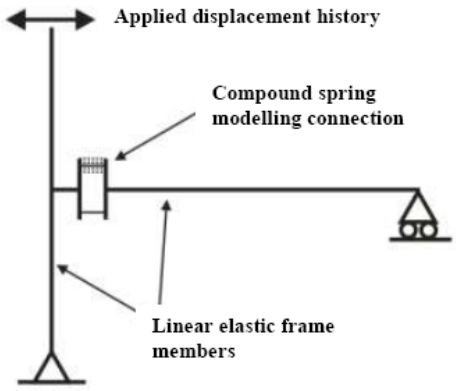

Figure 7-7: Two-dimensional compound spring element developed by Leslie (2010).

Au (2010) modelled the behaviour of reinforced concrete slotted beam connections using lumped plasticity and multispring models. A lumped plasticity model uses a rotational spring, which is assigned an appropriate hysteretic rule, to represent the moment rotation response of a slotted beam connection. A schematic of the lumped plasticity model is shown in Figure 7-8. This type of model is computationally efficient; however, it cannot take into account the subtleties of connection rotation such as shear deformation and variation in neutral axis depth. When a Bounded Ramberg-Osgood (1943) steel hysteresis was used in the lumped plasticity model, reasonable agreement was observed between the numerical model output and experimental results. However, the Bounded Ramberg-Osgood (1943) hysteresis rule requires direct calibration against experimental data.

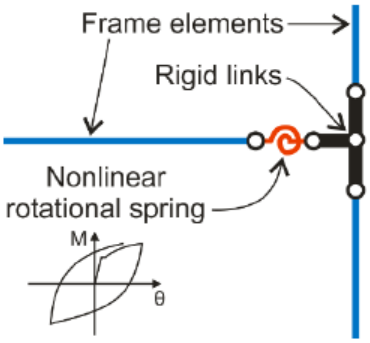

Figure 7-8: Two-dimensional lumped plasticity numerical model of slotted connection (Au, 2010).

A multispring model is similar to a compound element model; however, the length of the springs can be varied. Varying the length of the constituent springs of the element is particularly advantageous when modelling slotted beam connections due to the unbonded length of the bottom longitudinal reinforcement. The two-dimensional multispring model of the reinforced concrete slotted beam developed by Au (2010) is shown in Figure 7-9. This model used six axial springs, which were assigned a cracked concrete hysteresis by Maekawa et al. (2003), to represent the top hinge of the connection. Two axial springs, which were

assigned a steel hysteresis rule developed by Dodd and Restrepo-Posada (1995), were used to represent the longitudinal reinforcement. Shear force was transferred across the connection by an elastic shear spring. The length of each spring was based on experimental observations and theory developed by Au (2010). The multispring numerical model was capable of replicating the response of the slotted beam connections tested experimentally with reasonable accuracy. However, Au's (2010) multispring numerical model overrepresented hysteretic energy dissipation, but not by as much as Leslie's (2010) compound element model.

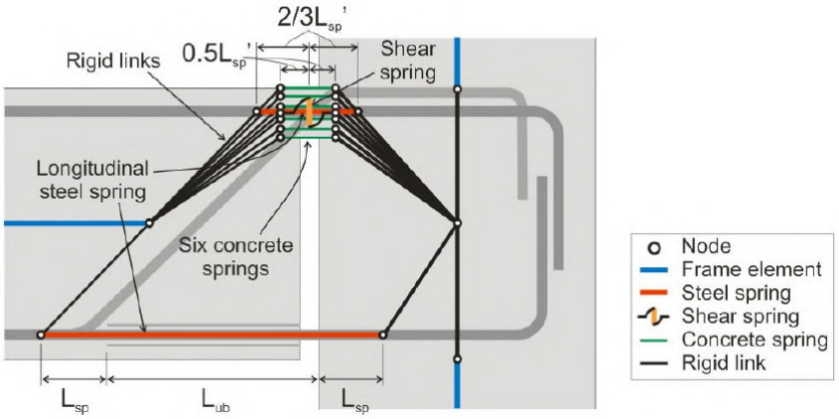

Figure 7-9: Two-dimensional multispring numerical model of slotted beam connection developed by Au (2010).

7.2.3 Floor Diaphragm Modelling

An analytical model designed to capture the effect of the floor diaphragm on the flexural response of adjacent beams was proposed by Shahrooz et al. (1992). The model, shown in Figure 7-10, used kinematic relationships between deformations and strain, which was an improvement upon earlier rigid link models. The interface between the longitudinal beams and floor diaphragm was represented by a network of rigid links and flexible springs. The model was capable of accounting for reinforcement slip, bond deterioration, beam rotation and elongation. The response of the model was compared to experimental data from monotonic tests performed on cruciform subassemblies with floors and reasonable agreement was observed.

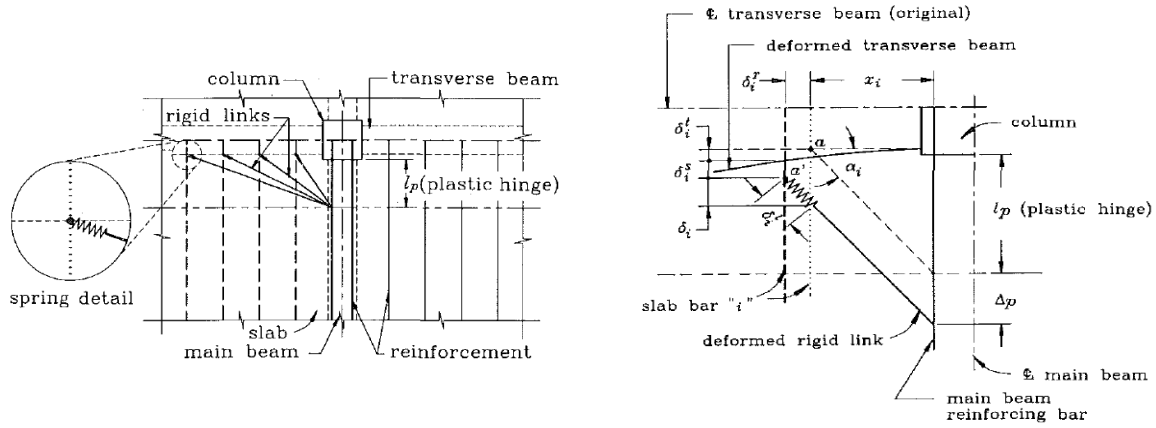

(a) Geometry of slab continuity links. **(b) Kinematics.**

Figure 7-10: Early floor diaphragm model proposed by Shahrooz et al. (1992).

A simple two-dimensional multispring model was proposed by MacRae and Gunasekaran (2006) to capture the contribution of the floor to connection flexural capacity. The model, shown in Figure 7-11, was a modified version of the multispring model for reinforced concrete plastic hinge zones proposed by Kim (2002). The floor slab was represented by a strut between the multispring elements on either side of the column, which provided restraint to beam elongation. The model required calibration to experimental results to yield representative results.

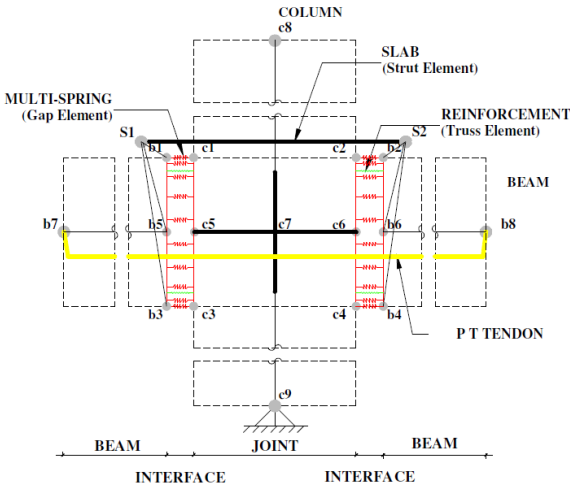

Figure 7-11: Multispring model of post-tensioned connection with slab effect (MacRae & Gunasekaran, 2006).

A complex three-dimensional model of a floor diaphragm and moment frame with traditional reinforced concrete connections was developed by Lau et al. (2007). The floor model, shown in Figure 7-12, was able to represent in-plane horizontal shear transfer and out-of-plane flexure. The floor diaphragm was modelled using springs assembled in a grillage. The numerical model was set up to replicate the behaviour observed in a superassembly experiment undertaken by Lau et al. (2007). There were discrepancies between the response of the numerical model and the experimental response. It was suggested by Peng (2007) that the discrepancies could have been due to errors in how beam elongation was represented in the plastic hinge models used by Lau et al. (2007). The floor model had provisions to model continuity moments from the one-way flooring system. Although the model was three-dimensional, it was not capable of modelling biaxial displacements or capturing three-dimensional actions such as beam torsion.

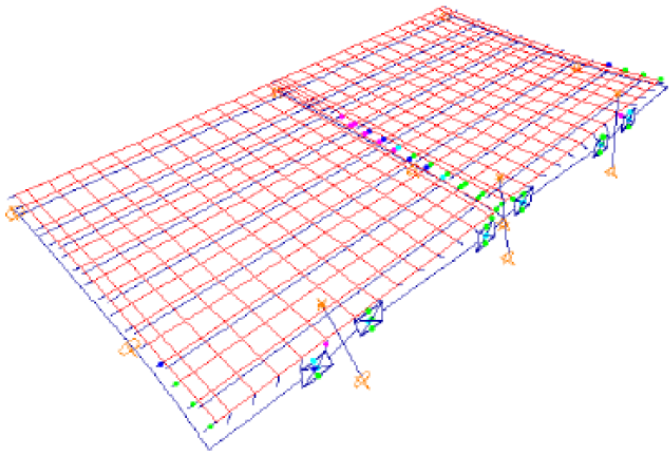

Figure 7-12: Diaphragm model developed by Lau et al. (2003).

Peng (2009) developed a floor diaphragm model, shown in Figure 7-13, using nonlinear axial springs and linear finite elements to model a rib and infill flooring system. The numerical model used the three-dimensional plastic hinge elements described in Section 7.2.1 to replicate the behaviour of the plastic hinge zones. The assembled numerical model was designed to replicate the behaviour observed during a superassembly experiment undertaken by Peng (2009). Close agreement was observed between the response of the numerical model and that observed during the experimental investigation. As with the numerical floor model developed by Lau (2007), biaxial displacements were not investigated. Furthermore, out-of-plane bending in the link slab and floor continuity moments were not modelled.

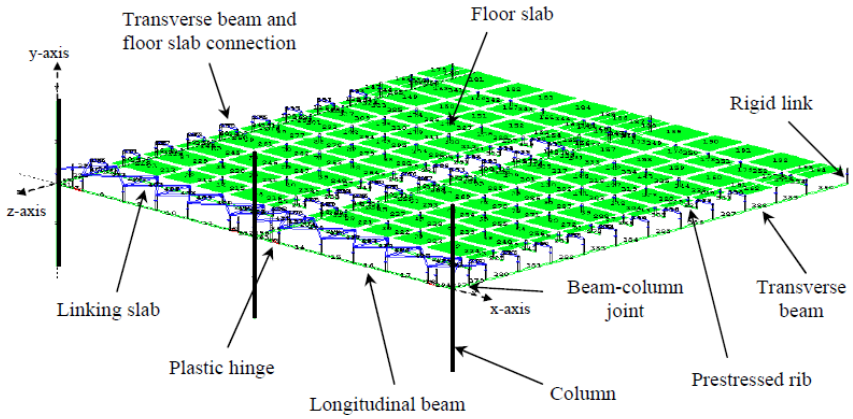

Figure 7-13: Diaphragm model developed by Peng (2009).

7.3 Numerical Element Development

7.3.1 Traditional Reinforced Concrete Connection Numerical Model

Traditional reinforced concrete connections were modelled using the reinforced concrete plastic hinge element within the Ruaumoko3D library (Carr, 2013). The plastic hinge element is a three-dimensional multispring element and was developed by Peng (2009) to capture plastic hinge behaviour such as; strength degradation, shear deformation and beam

elongation. A schematic of the element is shown in Figure 7-14. The development of the element is described in Section 7.2.1.

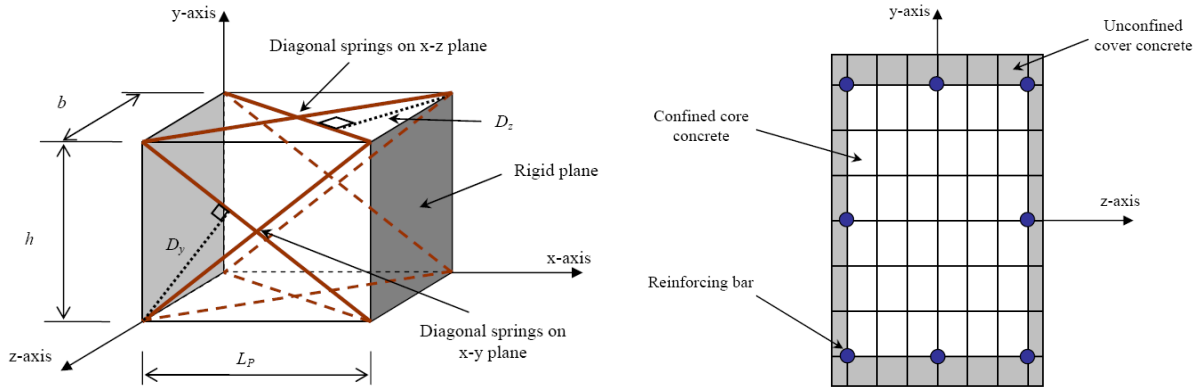

(a) Perspective of three-dimensional plastic hinge element.

(b) Cross-section through plastic hinge element showing longitudinal springs.

Figure 7-14: Traditional reinforced concrete plastic hinge element developed by Peng (2009).

The plastic hinge element was developed with the aim of being able to be set up using fundamental material properties, which meant that the model could be set up without calibration against experimental data. A comparison of the response recorded in a superassembly test and that generated by a numerical model using the plastic hinge element is presented in Figure 7-15. It can be seen that the numerical model was able to replicate the response of the superassembly with reasonable accuracy. However, the plastic hinge element was not able capture the pinching behaviour observed during the superassembly test, which resulted in the numerical model over representing hysteretic energy dissipation. Furthermore, Peng (2009) noted that the plastic hinge element was not able to replicate the torsional response of reinforced concrete plastic hinges.

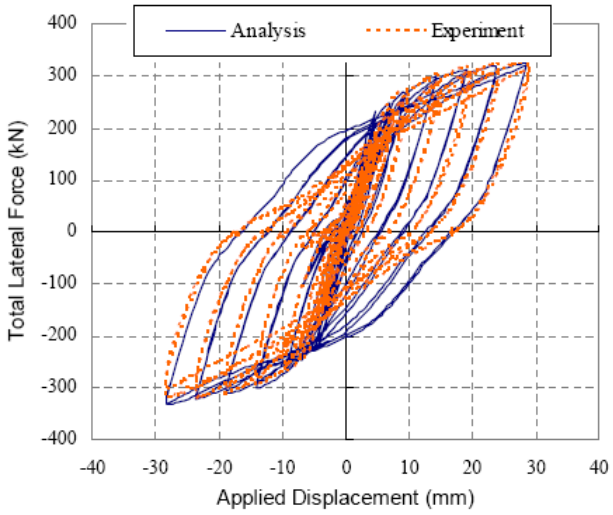

Figure 7-15: Force-displacement comparison between three-dimensional model and experimental observations (Peng, 2009).

7.3.2 Slotted Beam Connection Modelling

The development of a three-dimensional reinforced concrete slotted beam model is described in this section. The model is akin to that described above for traditional reinforced concrete

connections. It was designed to be able to be set up using fundamental material properties, so that calibration against experimental data was not required. Comparison between the newly developed three-dimensional models and existing two-dimensional models was undertaken to validate the response of the element. A sensitivity study was undertaken using the newly developed slotted beam element to determine the relationship between input properties and observed response.

7.3.3.1 Compound Spring Element Numerical Model

The simplest element within the Ruaumoko3D (2013) element library to use to extend existing two-dimensional models to three dimensions was the compound spring element. As shown in Figure 7-16(a), the compound spring element is comprised of two rigid planes, between which up to 20 individual springs may be positioned. Each spring can be assigned individual hysteretic properties. The rigid planes are connected to nodes via rigid links.

To model a slotted beam using compound spring elements, three elements had to be used in parallel to provide a sufficient number of springs. Figure 7-16(b) presents a cross-section demonstrating the total number of springs used to model the connection over the three compound spring elements. The distance between the rigid planes was defined as the unbonded length of the bottom longitudinal reinforcement plus two times the theoretical strain penetration length. This distance was larger than the effective length of the top hinge, top longitudinal reinforcement and shear hangers. The stiffness of the springs was calculated using the effective lengths calculated in Chapter 4.

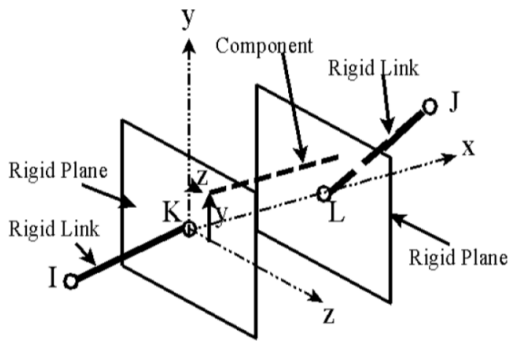

(a) Generic compound spring element defining local coordinates (Carr, 2013).

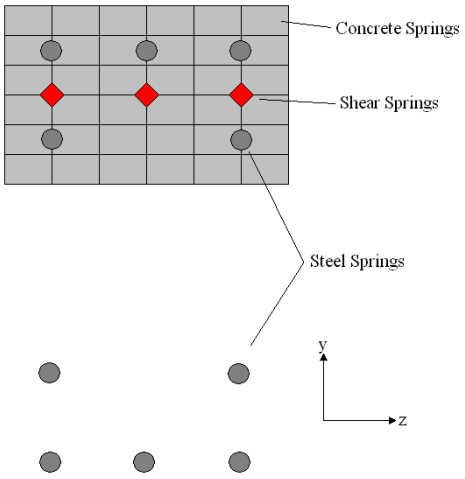

(b) Cross-section of slotted beam compound springs in parallel.

Figure 7-16: Compound spring element.

Two compound spring elements were used to model the top hinge, whilst the remaining compound spring element was used to model the reinforcement. The top hinge was modelled using 36 axial springs. Each axial spring was assigned a cracked concrete hysteresis rule (Maekawa et al., 2003). The geometrical distribution of the springs over the top hinge area

and the assignment of material properties was based on a Lobatto integration (Spieth et al., 2004), as shown in Table 7-1. Spieth et al. (2004) showed that the Lobatto integration could be used to model the effect of concrete confinement. Numerical models that did not take into account concrete confinement were shown to overestimate the neutral axis depth.

Table 7-1: Spring position and weighting for Lobatto integration (Spieth et al., 2004).

Abscissas, $\pm x_i$	Weights, w
±1	±0.0667
±0.7650	±0.3785
±0.2852	±0.5549

The axial springs that represented the top and bottom longitudinal reinforcement were arranged according to the geometry of the connection being modelled. The axial springs that represented reinforcement were assigned a Dodd-Restrepo hysteresis rule (Dodd & Restrepo-Posado, 1995). The properties determined in Section 4.2 were used to set up the properties of the axial springs. The shear hangers were modelled with shear springs. The shear strength and stiffness was calculated based on the vertical component of the diagonal reinforcement.

A comparison of the in-plane response of the three-dimensional compound spring element model and the existing two-dimensional multispring model is presented in Figure 7-17. The in-plane response of the two-dimensional multispring model has been validated against experimental data (Au, 2010). Whilst the overall response of the three-dimensional compound spring element was similar to that of the two-dimensional multispring, the three-dimensional compound spring element overrepresented hysteretic energy dissipation.

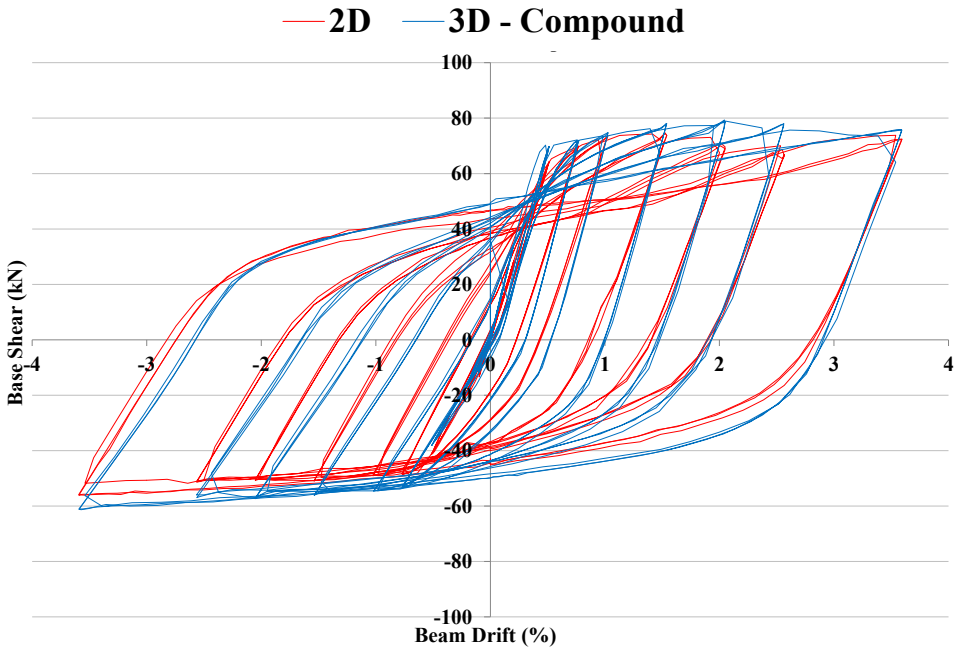

Figure 7-17: Comparison of in-plane response of slotted beam connection subassembly using Au (2010) two-dimensional and multispring three-dimensional numerical models.

The force exhibited by the three-dimensional compound spring element was greater than that of the two-dimensional multispring element, particularly for negative beam drift. The bulge in

response, due to the influence of the longitudinal reinforcement in the top hinge, between 0.5% and 2.0% beam drift was more pronounced in the three-dimensional compound spring element. For positive beam drift, the elastic stiffness of the three-dimensional compound spring element was larger than that of the two-dimensional multispring element; however, the opposite was true for negative beam drift. The discrepancies in response between the two numerical models highlighted the limitations of the compound spring element. The true geometry of the slotted beam could not be accurately replicated because every spring had to have the same length. The longer compound spring element length resulted in an overrepresentation of the connection rotation, which caused a greater variation in the neutral axis depth and increased the moment capacity generated.

7.3.3.2 Multispring Element Numerical Model

To address the shortcomings of the three-dimensional compound spring element model, a three-dimensional multispring model was developed. This model was conceptually similar to the two-dimensional model developed by Au (2010). A multispring model differs from a compound spring element in that each member can be positioned according to position and length, rather than just position. This is important when modelling slotted beam connections because the effective lengths of the reinforcement vary significantly.

The assembled slotted beam multispring model is shown in Figure 7-16, where the blue elements represent reinforcement, the red element represents the top hinge and the green elements represent the beams and columns. The cross section of the element was similar to that presented in Figure 7-16(b); however, individual spring lengths could be set to the effective reinforcement lengths calculated in Chapter 4. The axial springs that represented the reinforcement were assigned the Dodd-Restrepo hysteresis rule (Dodd & Restrepo-Posado, 1995). The shear hangers were represented by shear springs, which were assigned the Dodd-Restrepo hysteresis rule also (Dodd & Restrepo-Posado, 1995).

To represent the slotted beam top hinge, the plastic hinge multispring element was used with all steel spring areas set to zero. This enabled 64 axial springs to be used to represent the top hinge. The location and properties of the axial springs were distributed using a Lobatto integration (Spieth et al., 2004), and the springs were assigned a cracked concrete hysteresis rule (Maekawa et al., 2003).

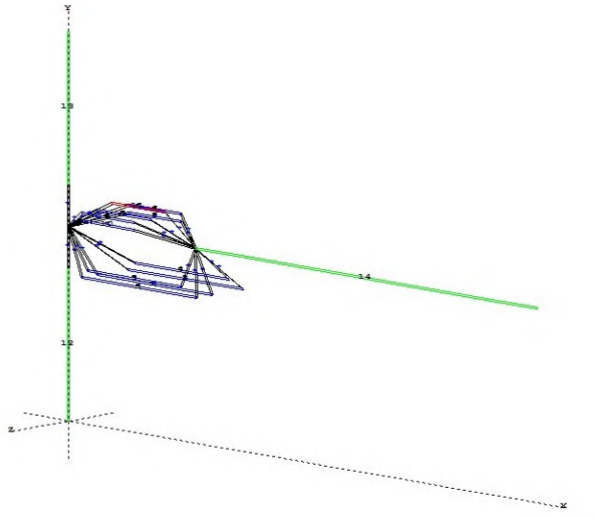

Figure 7-18: Multispring model of slotted beam subassembly.

A comparison of the in-plane response of the three-dimensional multispring model and the existing two-dimensional multispring model is presented in Figure 7-19. Overall, the two numerical models displayed similar response; however, the three-dimensional multispring model dissipated less energy per cycle than the two-dimensional multispring model. The elastic stiffness produced by both numerical models was similar for both positive and negative flexure. A pronounced bulge between 0.5% and 2.0% was evident in the response of both the three-dimensional multispring model and the two-dimensional multispring model.

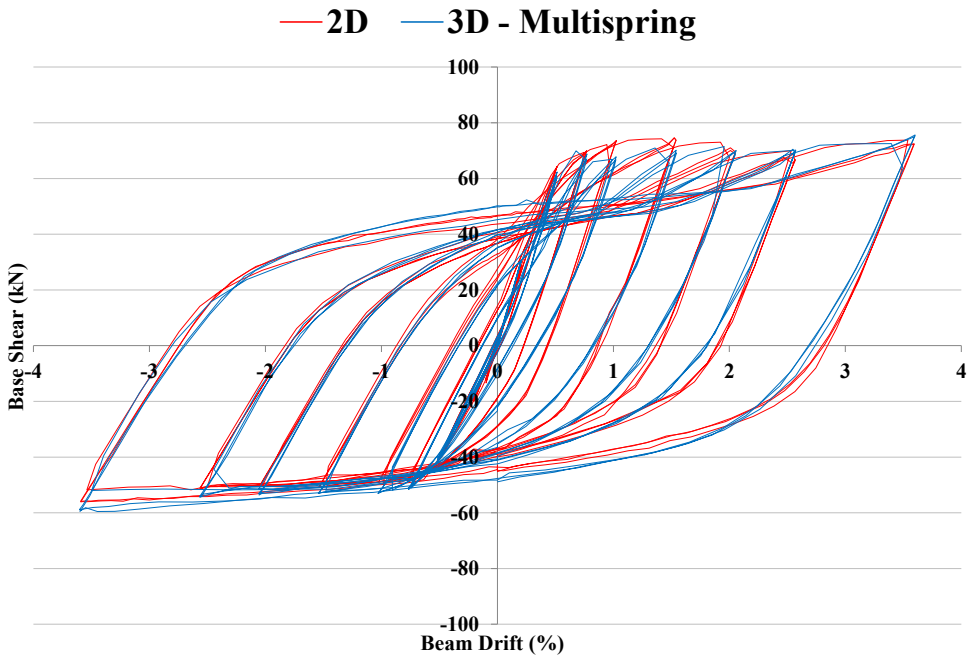

Figure 7-19: Comparison of in-plane response of slotted beam connection subassembly using Au (2010) two-dimensional and three-dimensional spring three-dimensional numerical models.

7.3.3.3 R3D Element Numerical Model

The three-dimensional multispring model provided the most accurate representation of reinforced concrete slotted beam response. However, because the multispring numerical model was so complex, it required considerable expertise to set up the geometry and

properties. The complexity of the multispring numerical model presented a barrier to the implementation of the model by industry to design reinforced concrete slotted beam structures. Hence, a numerical model of the reinforced concrete slotted beam that retained the accuracy of the three-dimensional multispring model, yet was simple to set up, had to be developed.

A new reinforced concrete slotted beam element was developed within the nonlinear analysis program Ruaumoko3D (Carr, 2013). The reinforced concrete slotted beam multispring element is described herein as the R3D element. The conceptual design and development of the R3D element was undertaken by the author; however, the implementation of the underlying code for the R3D element within the Ruaumoko3D was performed by the designer of the software package, Professor Athol Carr, University of Canterbury (Carr, 2013). The R3D element is a genuine three-dimensional multispring model and is conceptually similar to that described in the preceding subsection. However, most of the onerous geometry and property set up is undertaken within the element. Hence, to set up the R3D element the operator only has to know the overall geometry and the basic material properties of the reinforced concrete slotted beam being analysed.

Figure 7-20(a) presents a schematic of the axial springs in the R3D element that represent the reinforcement in the slotted beam. In the R3D element, up to four axial springs can be specified for each of the upper top, lower top, upper bottom, lower bottom and diagonal hanger reinforcement layer. The location and effective length of each axial spring can be specified independently. The bottom and top layers of axial springs can be assigned different hysteretic rules. The diagonal hanger springs resist both y shear and x torsion. The angle of the diagonal hanger springs can be specified. Figure 7-20(b) presents a schematic of the axial springs in the R3D element that represent the concrete in the top hinge. The top hinge in the R3D element is represented by 36 axial springs which can be distributed according to simple summation, Gaussian integration or Lobatto integration. The axial springs are assigned a cracked concrete hysteresis (Maekawa et al., 2003) and an effective length of the top hinge can be specified. Two additional diagonal axial springs are included in the R3D element to resist z shear. These springs are assigned a SINA tri-linear hysteresis (Saiidi & Sozen, 1979).

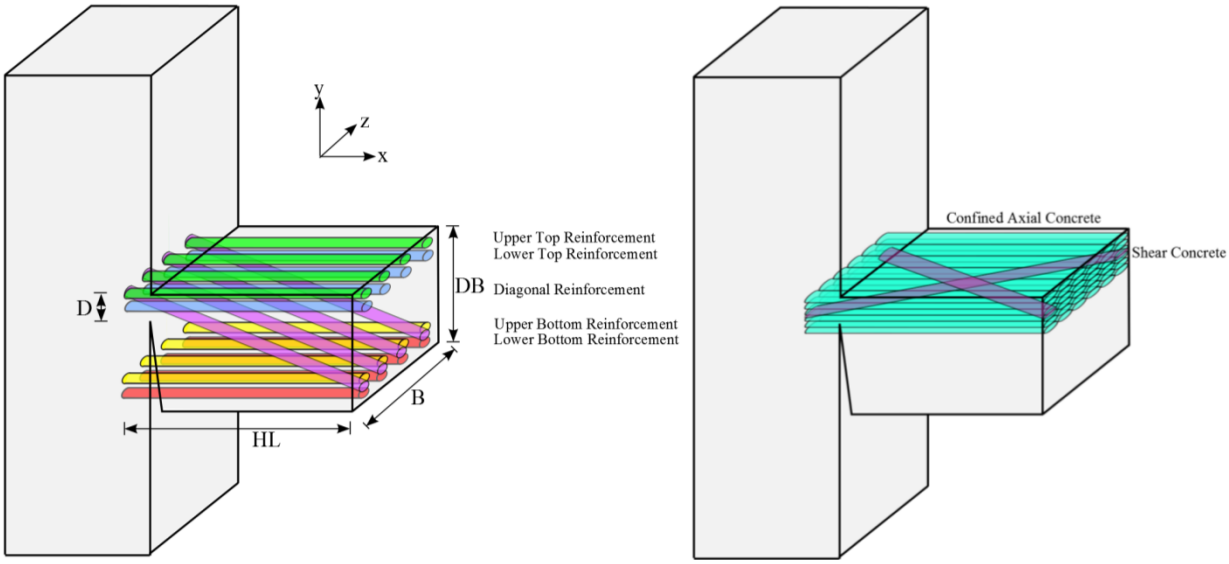

(a) Steel reinforcement springs. **(b) Concrete springs.**

Figure 7-20: Schematic of R3D element.

Figure 7-21 presents a comparison of the response between the three-dimensional multispring model and the R3D element. The overall response of both numerical models was similar. The three-dimensional multispring model displayed slightly higher peak forces for positive beam drift than the R3D element; however, the opposite was true for negative beam drifts. The elastic stiffness produced by both numerical models was similar for both positive and negative flexure. The R3D element had a less pronounced bulge in response between 0.5% and 2.0% beam drift than the three-dimensional multispring model.

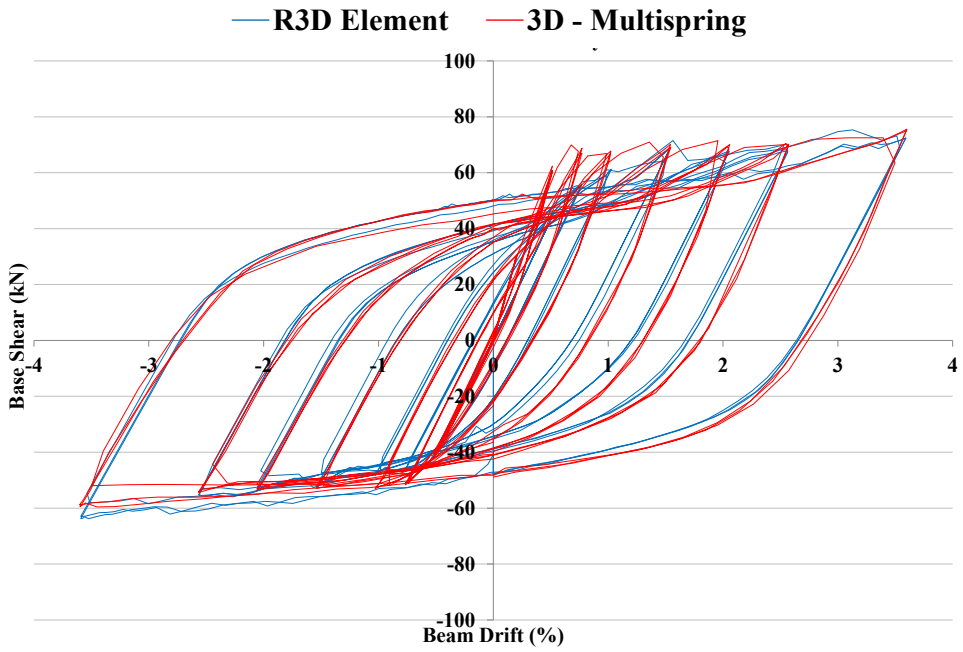

Figure 7-21: Comparison of in-plane response of R3D element and three-dimensional hybrid multispring elements.

The newly developed R3D element is capable of accurately representing reinforced concrete slotted beam behaviour. The R3D element can be set up using only fundamental material and geometric properties. The R3D element does not require calibration to experimental data.

Furthermore, the time and expertise required to set up an accurate numerical model of a reinforced concrete slotted beam has been significantly reduced.

7.3.3.4 R3D Element Sensitivity Study

It was important to understand the influence that changes to input variables for the R3D element had on observed response, not only as a guide to attribute accuracy to the input variables, but also to improve the understanding of slotted beam connection mechanics. This subsection describes an investigation into the sensitivity of the response of the R3D element to changes to the input variables.

Integration Time-Step Size

The stability of nonlinear time history integration analyses is related to the change in displacement that occurs between integration time-steps. Because the integration occurs over time and the applied loading record is constant, the integration time-step is usually reduced to reduce the change displacement that occurs between integration time-steps. The computational efficiency to solve a nonlinear time history analysis decreases as the integration time-steps decrease. Hence, the ideal integration time-step to use in an analysis can be defined as that which, if halved, does not affect the observed response. The control time-step in this comparison is that which yielded a maximum displacement loading step of 0.4mm. Figure 7-22 presents a comparison of the effect of a halved integration time-step on the observed force-displacement and elongation response. Figure 7-22 shows that the change in integration time-step caused no observable difference in response.

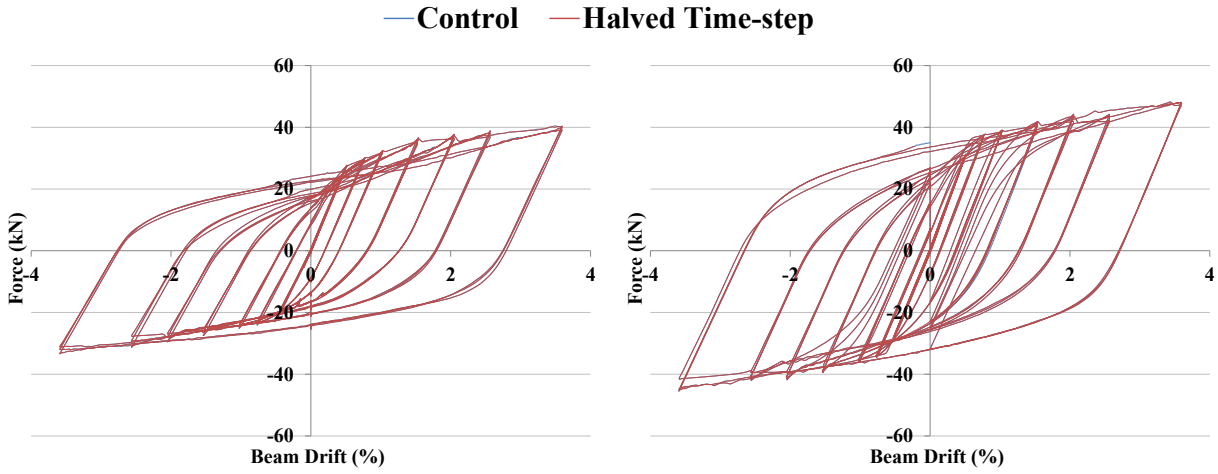

(a) Force-displacement response parallel to floor. **(b) Force-displacement response perpendicular to floor.**

Figure 7-22: Effect of halved integration time-step.

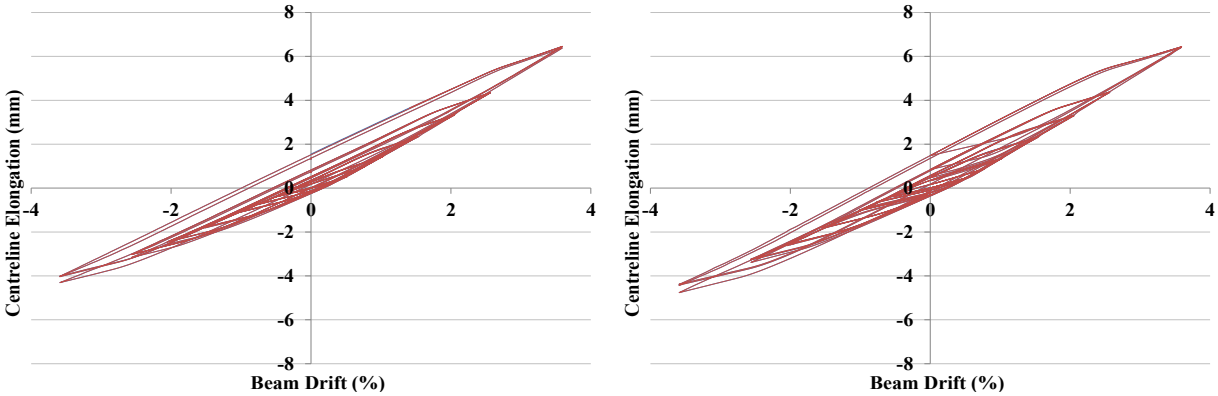

(c) Centreline beam elongation parallel to floor. **(d) Centreline beam elongation perpendicular to floor.**

Figure 7-22: Effect of halved integration time-step (Continued).

If an integration time-step appropriate for the loading rate being applied to the R3D model is used, then further reductions in integration time-step will have little influence on response. The integration time-step should not be reduced unnecessarily because computational effort will be increased significantly. It is suggested that an appropriate integration time-step to apply when using the R3D element is that which yields a change in displacement of less than 0.4mm between the integration time-steps.

R3D Element Length

The effective length of each layer of longitudinal reinforcement springs in the R3D element can be set independently to account for the effect of unbonded length and strain penetration. Hence, a change in the length of the R3D element does not affect the axial stiffness of the springs. However, as shown in Figure 7-23, when the length of the R3D element was doubled there was a slight reduction in flexural capacity. The reduction in flexural capacity was most noticeable during positive beam drifts. Because the geometry of the numerical model was constant, an increase in the length of the R3D element decreased the curvature of the element, which slightly decreased observed stiffness. The decreased flexural stiffness was more noticeable for positive flexure because the high position of the neutral axis maximised the decrease in connection curvature.

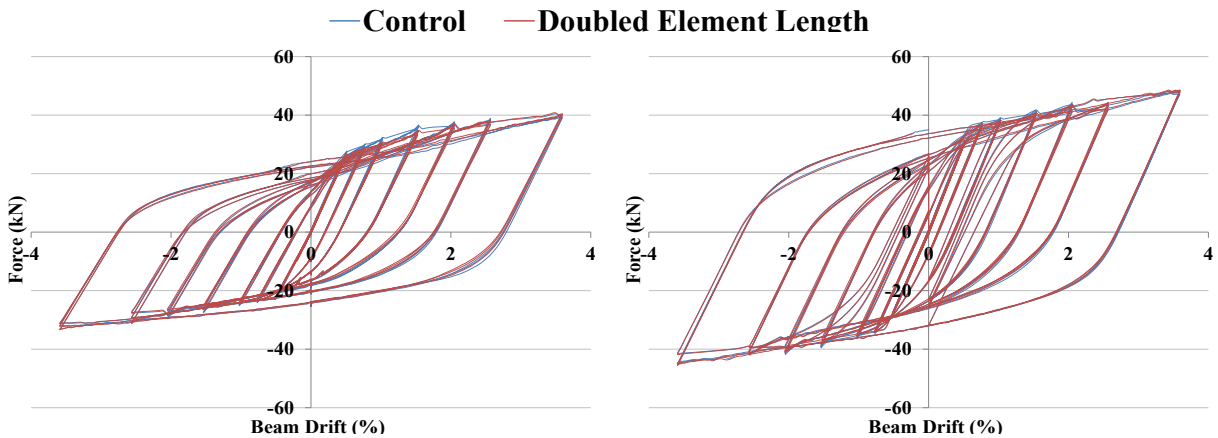

(a) Force-displacement response parallel to floor. **(b) Force-displacement response perpendicular to floor.**

Figure 7-23: Effect of doubled element length.

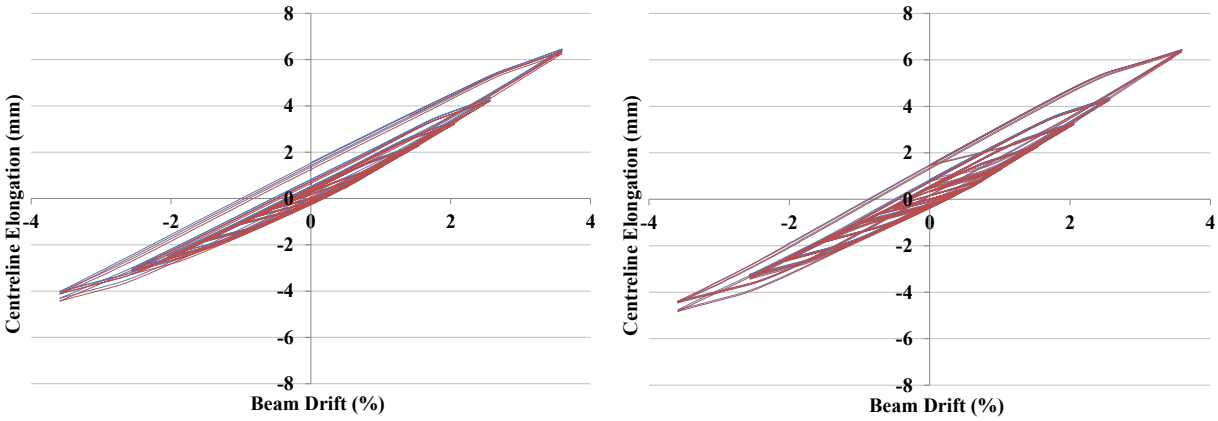

(c) Centreline beam elongation parallel to floor. **(d) Centreline beam elongation perpendicular to floor.**

Figure 7-23: Effect of doubled element length (Continued).

For a given numerical model geometry, where effective lengths are specified, an increase in the length of a R3D element will slightly decrease the observed flexural stiffness. If effective lengths are not specified in the R3D element, a change in the length of the R3D element will have a profound effect on the observed response because the effective lengths of the longitudinal reinforcement springs will default to the overall length of the R3D element.

R3D Element Slot Height

The height of the slot is a fundamental geometric property of a slotted beam connection. Hence, changing the slot height of the R3D element significantly changed the observed response, as shown in Figure 7-24. Decreasing the slot height of the R3D element caused the observed response to become more akin to that of a traditional reinforced concrete connection. This was because the neutral axis was able to drop significantly lower in the section during negative flexure, which induced greater tensile forces in the top longitudinal reinforcement springs and increased the overall negative flexural capacity of the R3D element. It was shown in Chapters 4 and 6 that beam elongation in slotted beam connections is primarily driven by flexure, which induces strain in the top longitudinal reinforcement. The induced strain in the top longitudinal reinforcement is not fully recovered upon connection unloading. Over several loading cycles the unrecovered strain in the top longitudinal reinforcement accumulates and causes the connection to lengthen. This was observed also in the sensitivity study, as shown in Figure 7-24(c) and (d). A decrease in the slot height caused greater strain to be induced in the top longitudinal reinforcement springs, which, over several loading cycles, accumulated and resulted in increased beam elongation in the R3D element.

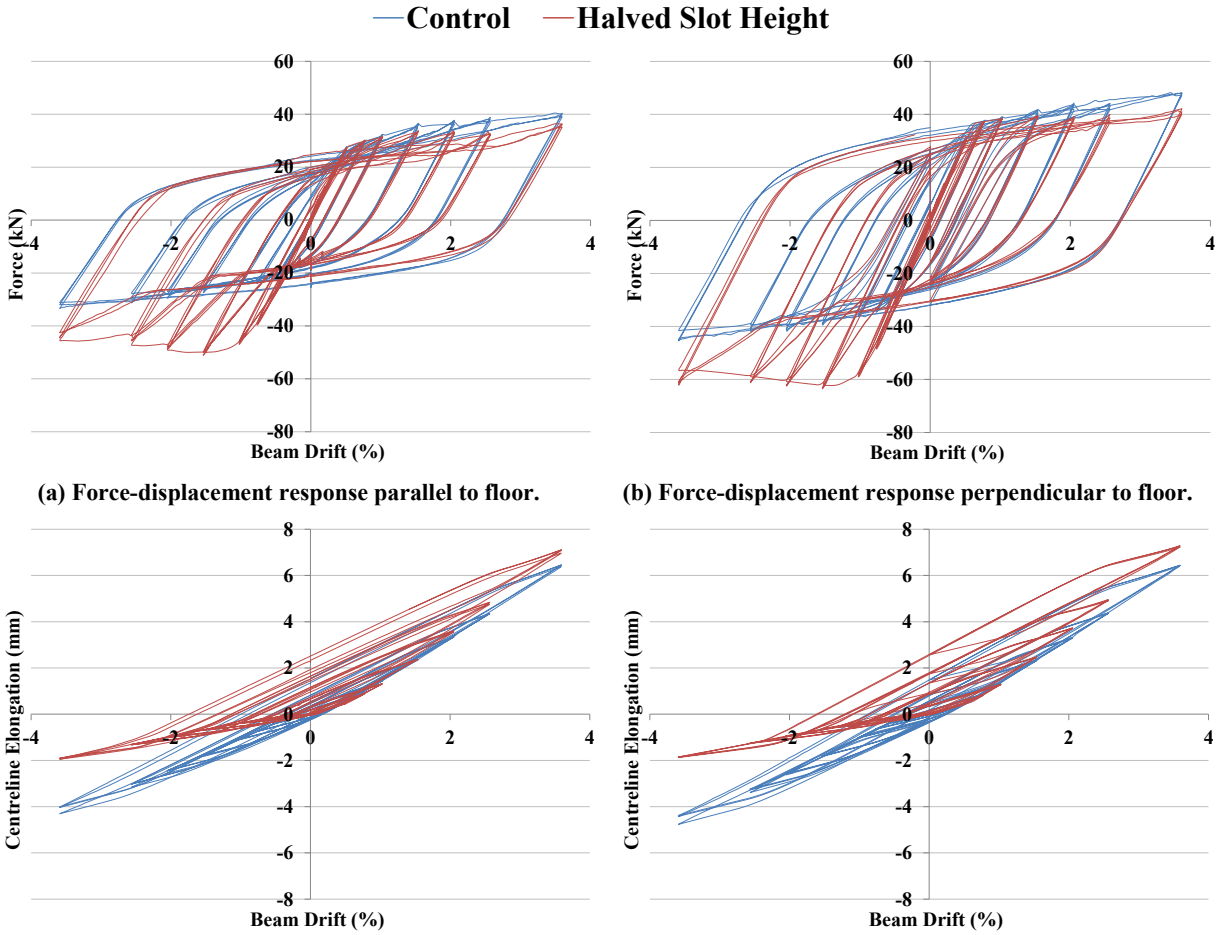

(a) Force-displacement response parallel to floor.

(b) Force-displacement response perpendicular to floor.

(c) Centreline beam elongation parallel to floor.

(d) Centreline beam elongation perpendicular to floor.

Figure 7-24: Effect of halved slot height.

The response of the R3D element is sensitive to a change in the slot height. For the R3D element to be able to generate representative response of a slotted beam connection, the height of the slot must be accurately specified.

Top Longitudinal Reinforcement Spring Position

Au (2010) concluded that the top longitudinal reinforcement in reinforced concrete slotted beam connections had minimal effect the moment capacity. However, it was observed in Chapter 4 that the top longitudinal reinforcement had a significant effect on the moment capacity of slotted beam connections, particularly when deep top hinges were used to accommodate two layers of top longitudinal reinforcement. Figure 7-25 presents a comparison of the effect of raising and lowering the top longitudinal reinforcement springs in the R3D element. Raising the top longitudinal reinforcement springs within the top hinge increased the lever arm between the springs and the neutral axis during negative flexure, which increased the negative flexural capacity of the R3D element. Similarly, when the top longitudinal reinforcement springs were lowered within the top hinge the lever arm between the springs and the neutral axis was increased, which resulted in an increased positive flexural

moment being generated by the R3D element. This is observed in Figure 7-25(a) and (b) as a characteristic bulge in response, which is discussed in Section 6.3.

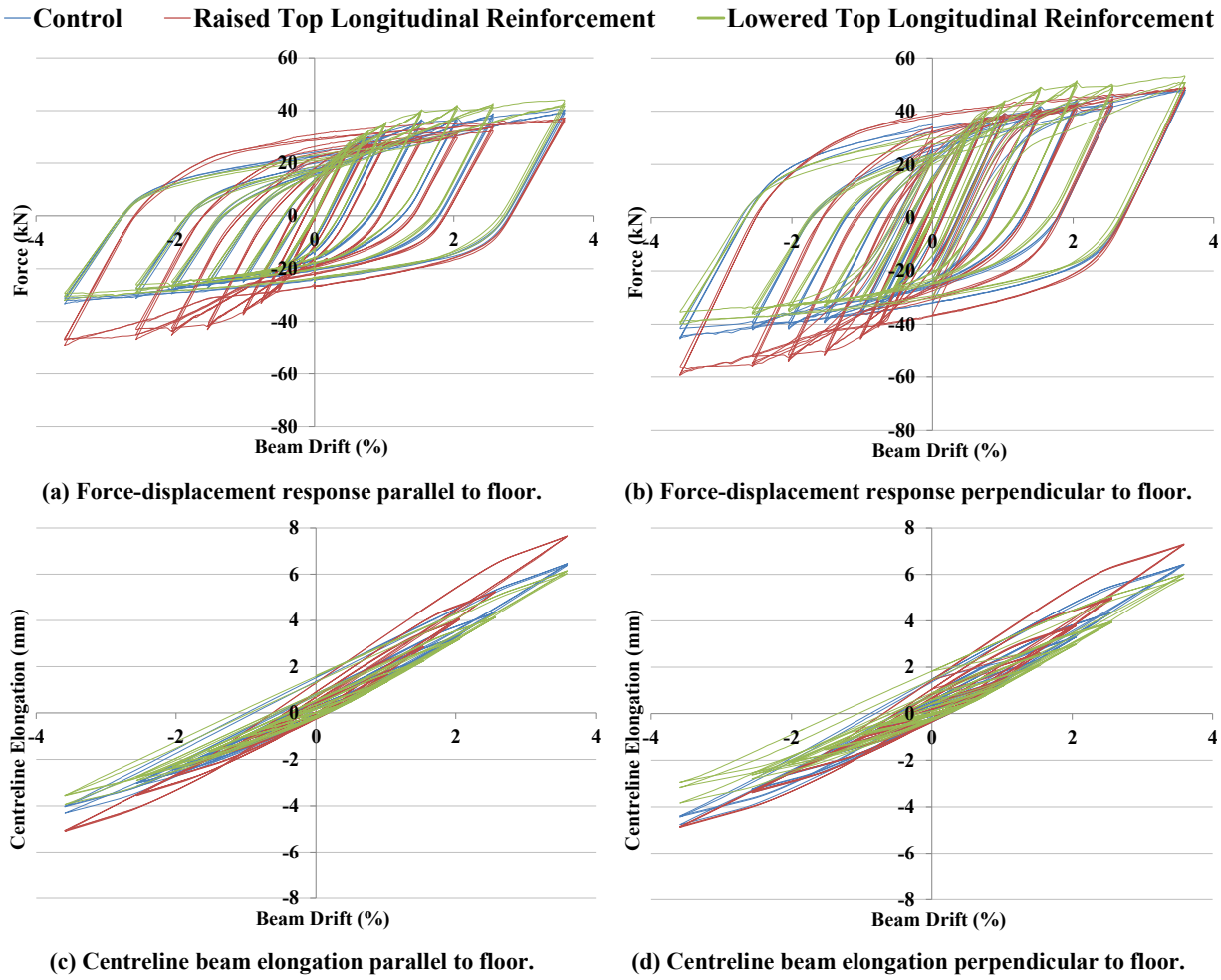

(a) Force-displacement response parallel to floor.

(b) Force-displacement response perpendicular to floor.

(c) Centreline beam elongation parallel to floor.

(d) Centreline beam elongation perpendicular to floor.

Figure 7-25: Effect of top longitudinal reinforcement positioning.

Number of Layers of Reinforcement Springs

If possible, a designer should use a single layer of top longitudinal reinforcement in a reinforced concrete slotted beam. This allows a larger slot height to be used, which improves connection performance. However, it is not always practical to use a single layer of reinforcement. In this investigation, a single layer of top longitudinal reinforcement springs were placed at the force centroid of the two layers of top springs in the R3D element. This enabled the effect that the number of layers of top longitudinal reinforcement in a slotted beam connection has on connection response to be examined. As shown in Figure 7-26(a) and (b), there was little difference between the observed force-displacement responses of the R3D elements with one layer of top longitudinal reinforcement springs and two layers of top longitudinal reinforcement springs. However, the difference between having one layer and two layers of top longitudinal reinforcement in a real slotted beam connection would be more significant. This is because, compared to using two layers of top longitudinal reinforcement,

when a single layer of top longitudinal is used the top hinge depth can be reduced, which improves connection performance. The slot height was constant in this investigation.

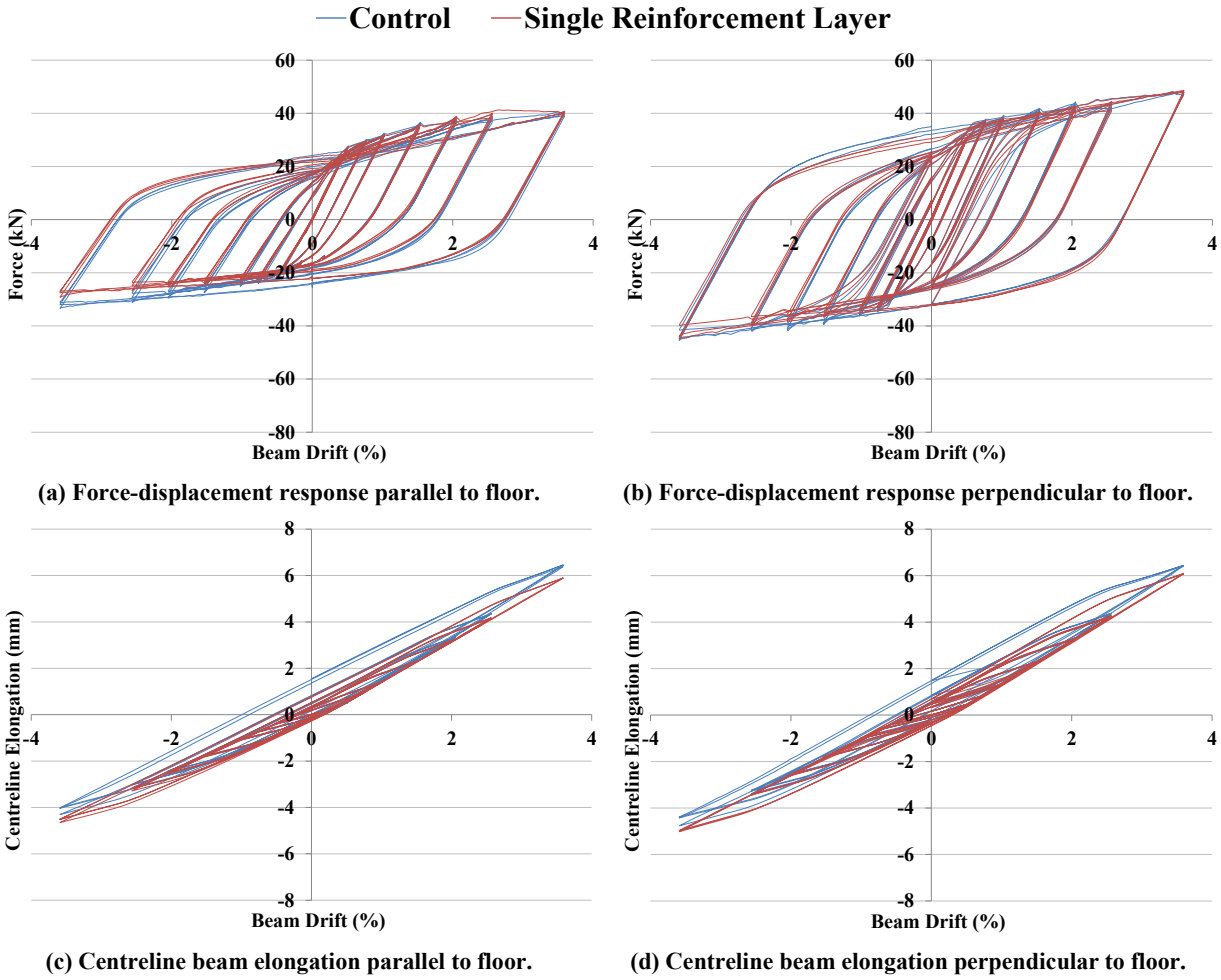

(a) Force-displacement response parallel to floor. **(b) Force-displacement response perpendicular to floor.**

(c) Centreline beam elongation parallel to floor. **(d) Centreline beam elongation perpendicular to floor.**

Figure 7-26: Effect of number of layers of longitudinal reinforcement.

As shown in Figure 7-26(c) and (d), the R3D element with a single layer of top longitudinal reinforcement springs exhibited lower residual beam elongation compared to the R3D element with two layers of springs. This was because the lever arm between the neutral axis and the springs was relatively similar during positive and negative flexure in the R3D element with a single layer of top longitudinal reinforcement springs. Whereas in the R3D element with two layers of top longitudinal reinforcement springs, the lever arm between one layer of the springs and the neutral axis was always greater than it was in the R3D element with a single layer of springs, which increased the strain induced in the upper and lower layers of top longitudinal reinforcement springs during negative and positive flexure respectively. The strain in the top longitudinal reinforcement springs were not fully recovered during loading reversal. Hence, over the course of the loading protocol, the R3D element with two layers of top longitudinal reinforcement springs exhibited greater beam elongation than the R3D element with a single layer of springs.

It can be concluded that the moment capacity of singly and doubly reinforced slotted beams with the same steel content is similar. However, a doubly reinforced slotted beam exhibits increased beam elongation compared to a singly reinforced slotted beam. A designer should, if possible, use a singly reinforced slotted beam design.

Unbonded Length of Bottom Longitudinal Reinforcement Springs

In a reinforced concrete slotted beam, the length that the bottom longitudinal reinforcement is debonded over affects the strain that is induced in the lower longitudinal reinforcement during connection flexure. Hence, a change in the unbonded length of the bottom longitudinal reinforcement springs changed the stiffness of the connection, as shown in Figure 7-27(a) and (b). Similarly, the decreased unbonded length in the R3D element resulted in strain hardening occurring in the bottom longitudinal reinforcement springs earlier than it did in the control R3D element. The increased strain in the bottom longitudinal reinforcement springs resulted in the R3D element with the reduced unbonded length exhibiting greater flexural capacity throughout its response. Increased strain in the bottom longitudinal reinforcement springs would hasten the outset of low-cycle fatigue failure; however, the hysteretic rule specified in the springs of the R3D element was incapable of modelling low-cycle fatigue. It has been shown in Chapter 4 and 6 that beam elongation in reinforced concrete slotted beams is primarily related to connection flexure. Hence, altering the unbonded length of the bottom longitudinal reinforcement springs in the R3D element had negligible effect on the recorded beam elongation, as shown in Figure 7-27(c) and (d).

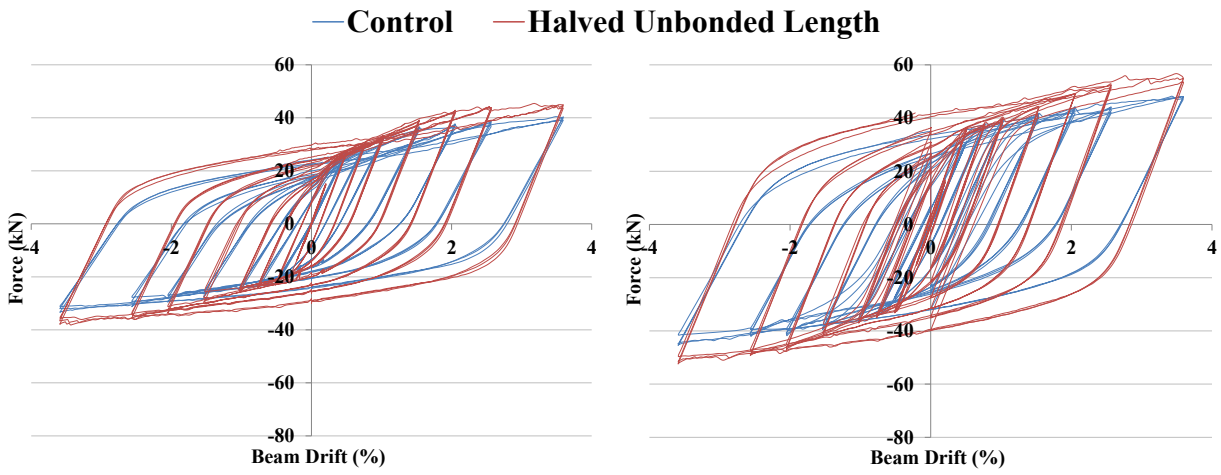

(a) Force-displacement response parallel to floor. **(b) Force-displacement response perpendicular to floor.**

Figure 7-27: Effect of unbonded length.

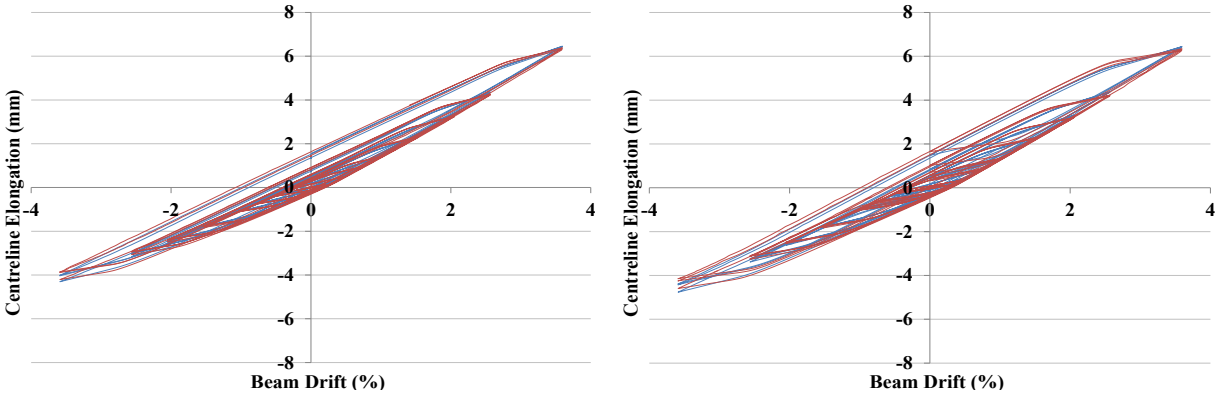

(c) Centreline beam elongation parallel to floor. (d) Centreline beam elongation perpendicular to floor.

Figure 7-27: Effect of unbonded length (Continued).

Concrete Spring Distribution Model

There are three different methods to distribute concrete springs over the top hinge in the R3D element: simple summation, Gaussian and Lobatto (Spieth et al., 2004). Figure 7-28 presents a comparison between R3D elements which used Lobatto integration and simple summation to distribute the geometries and properties of the springs representing the top hinge. It can be seen that the difference in the observed force-displacement response between the R3D elements was negligible. However, as shown in Figure 7-28(c) and (d), there was a small increase in the recorded beam elongation for the R3D element that used a simple summation distribution compared to the R3D element that used a Lobatto distribution. The Lobatto distribution allows for the strength and stiffness of the springs to reduce near the extreme chords of the top hinge to model the effect of unconfined cover concrete. The simple summation distribution assigns the same strength and stiffness to all springs representing the top hinge. Hence, the simple summation distribution allowed the neutral axis to move closer to the extreme chord during connection flexure compared to the Lobatto distribution. This resulted in greater strain being induced in the top longitudinal reinforcement springs of the R3D element that used simple summation distribution compared to the R3D element that used Lobatto distribution, which led to slightly increased beam elongation.

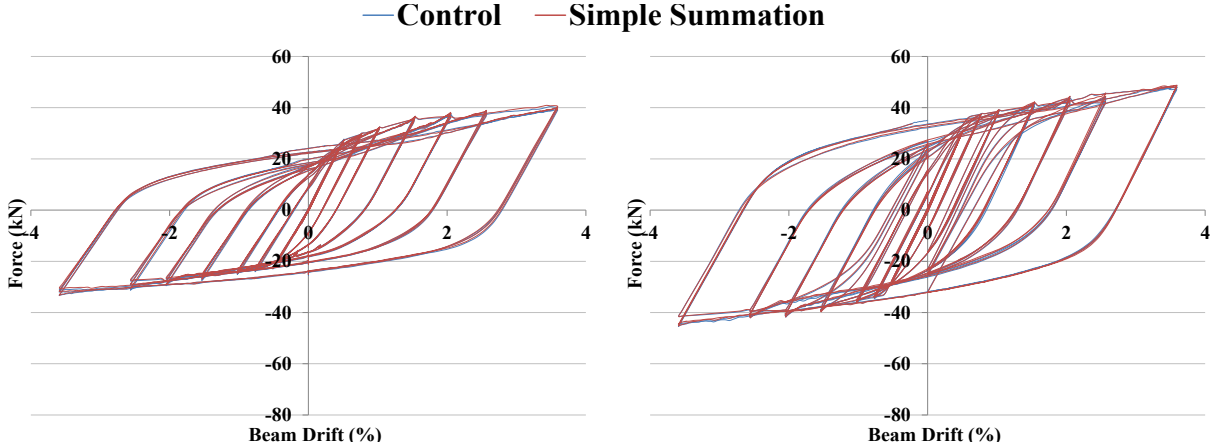

(a) Force-displacement response parallel to floor. (b) Force-displacement response perpendicular to floor.

Figure 7-28: Effect of concrete spring distribution.

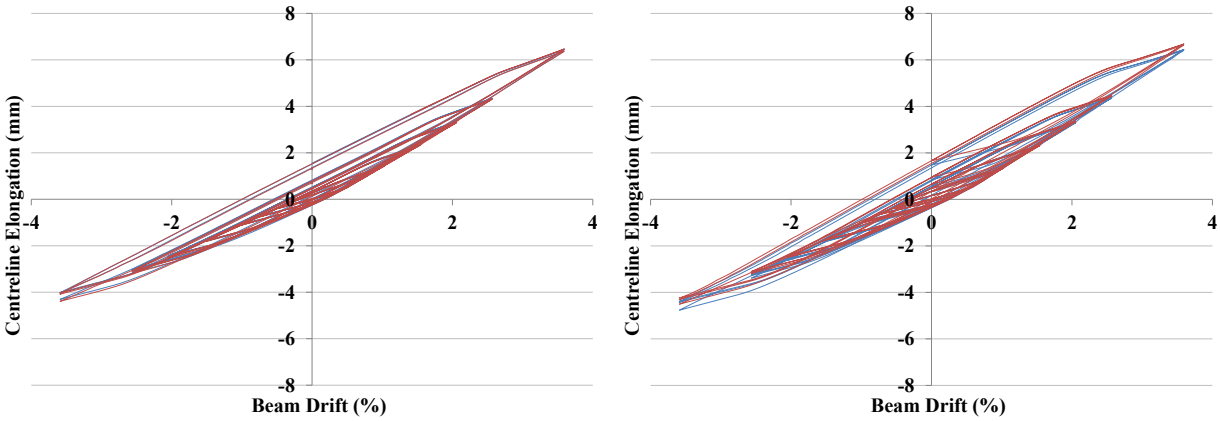

(c) Centreline beam elongation parallel to floor. **(d) Centreline beam elongation perpendicular to floor.**

Figure 7-28: Effect of concrete spring distribution (Continued)

Diagonal Hanger Spring Angle

Diagonal hangers are required to transfer shear and torsion across reinforced concrete slotted beam connections. Due to the location of the diagonal hangers within the top hinge it is inevitable that they contribute to the flexural capacity of the slotted beam connection. The angle that the diagonal hangers are installed at dictates the extent to which they contribute to connection flexural capacity, because the horizontal force component of the diagonal hangers reduces as the angle steepens. Figure 7-29 presents a comparison between a R3D element with diagonal hanger springs at 45° to the horizontal and a R3D element with steeper diagonal hangers. The R3D element with steeper diagonal hanger springs exhibited a slightly lower force-displacement response compared to the control R3D element.

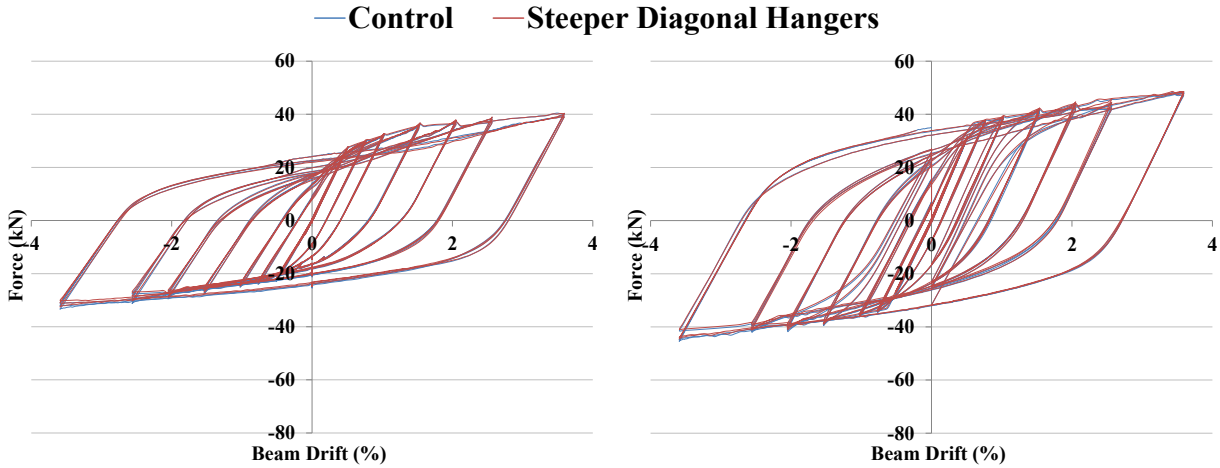

(a) Force-displacement response parallel to floor. **(b) Force-displacement response perpendicular to floor.**

Figure 7-29: Effect of diagonal hanger angle.

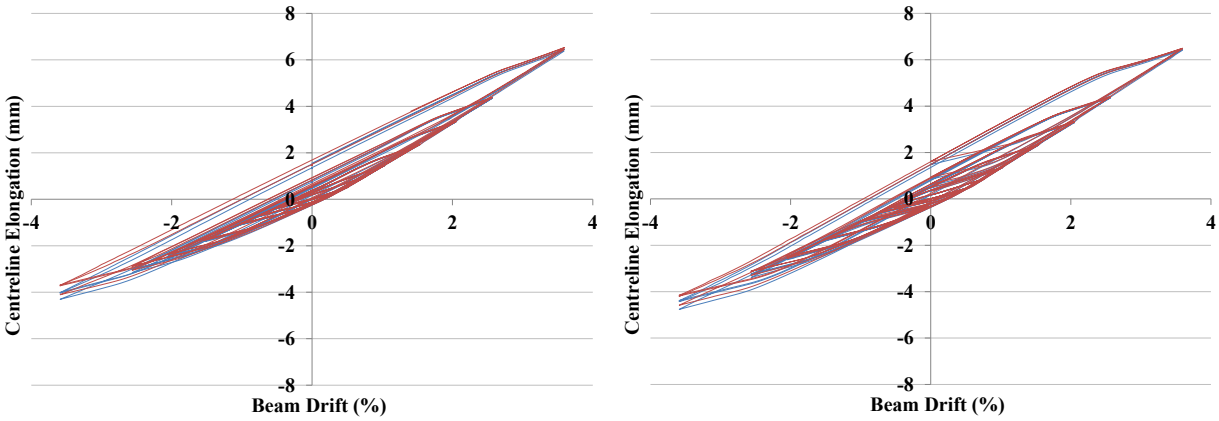

(c) Centreline beam elongation parallel to floor. (d) Centreline beam elongation perpendicular to floor.

Figure 7-29: Effect of diagonal hanger angle (Continued)

Concrete Shear Spring Strength

In the R3D element, the concrete shear springs provide resistance across the element in the local z direction. The concrete shear springs are not subjected to significant forces during typical loading scenarios. Figure 7-30 shows the effect on observed response of doubling the strength of the concrete shear springs in the R3D element. It can be seen that there is negligible variance between the force-displacement responses of two elements. It can be concluded the response of the R3D element is not sensitive to the strength of the concrete shear springs.

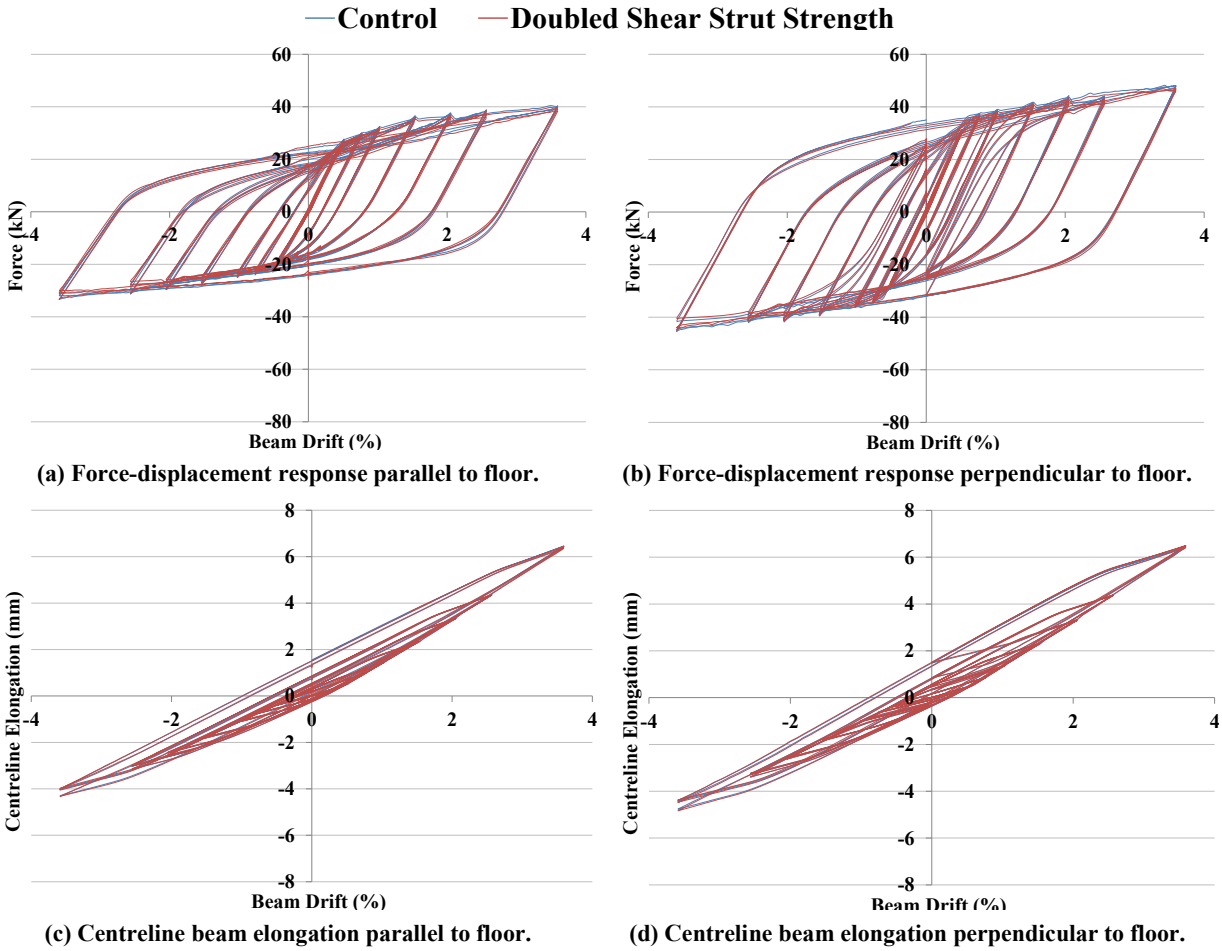

(a) Force-displacement response parallel to floor. (b) Force-displacement response perpendicular to floor.

(c) Centreline beam elongation parallel to floor. (d) Centreline beam elongation perpendicular to floor.

Figure 7-30: Effect of concrete shear spring stiffness.

7.4 R3D Element Verification

Regardless of how complex a numerical model is, it must be capable of faithfully replicating the response of the system it was designed to represent. Furthermore, for a numerical model to be truly useful to designers it must be able to be set up using only fundamental material and geometric properties, and without calibration. In this section the recorded response of the specimens described in Chapter 3 – 6 were compared to the response of numerical models of the specimens assembled using the R3D element. The R3D element was not calibrated. Based on the disparity observed between the recorded response of SA1 and the response of the numerical model of SA1, a numerical model was developed to model the influence of the floor diaphragm on the R3D element.

7.4.1 R3D Element Verification against Subassembly Experimental Data

7.4.1.1 As-built Subassembly Numerical Models

The origin of the subassemblies was specimen SA1; hence, SA2 and SA3 had been subjected to a full loading cycle prior to testing. Due to the path dependence of hysteretic response, the strain history of the subassemblies would have affected their subsequent response. Comparing the response of a previously tested subassembly to a numerical model in an untested condition would have been unrepresentative. The Dodd-Restrepo steel hysteresis rule (Dodd & Restrepo-Posado, 1995) and the Maekawa cracked concrete hysteresis rule (Maekawa et al., 2003) used in the R3D element are path dependent. Hence, the effect of previous loading being applied to the subassemblies was able to be captured. The numerical models of the subassemblies were first subjected to the displacement history that the subassemblies experienced whilst they were a part of superassembly SA1, then the loading protocol used in the subassembly tests was applied to the numerical models of the subassemblies. The effect that previous loading had on the response of the numerical models can be seen by comparing Figure 7-31 and Figure 7-32. The peak force attained during the first and second applications of the loading protocol are similar. However, the significance of Bauschinger effects over successive loading excursions was diminished, as was the influence of the top springs in the R3D element. This was due to the top springs having been subjected to larger strains during the first loading event, which were not fully recovered. Hence, when the R3D element was subjected to a given rotation during the second loading event, the change in top spring strain was less than during the first loading event.

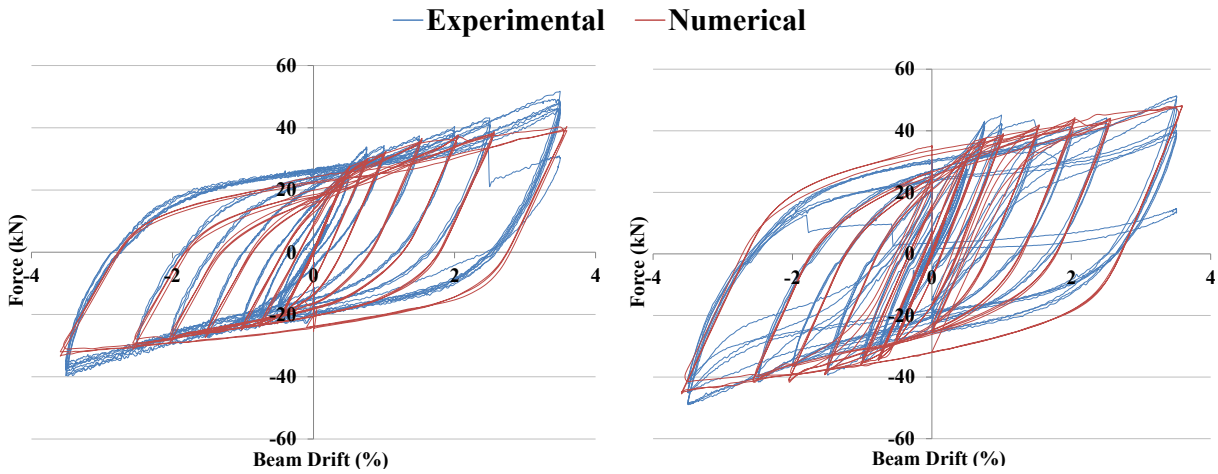

(a) Parallel to floor.

(b) Perpendicular to floor.

Figure 7-31: Comparison of numerical model to SA2 first complete loading protocol.

Figure 7-32 presents a comparison between the recorded response of specimen SA2 and the response of the SA2 numerical model. In general, the SA2 numerical model was able to closely replicate the experimental response of specimen SA2. However, there was discrepancy between the peak lateral force generated by the numerical model and that recorded during the testing of SA2. It was postulated in Section 4.5 that effective stress, due to the influence of Poisson's ratio on the bottom unbonded reinforcement during compression, caused an increase in the observed negative flexural capacity of the slotted beams in SA1. Because the hysteretic rule used to model the behaviour of reinforcement in the R3D element could not replicate the influence of effective stress, discrepancy between the recorded response of the subassemblies and the response of the numerical models was inevitable. The difference in positive flexural moment observed during the SA2 test and generated by the numerical model, particularly in the direction parallel to the floor, was due to the contribution of the top longitudinal reinforcement to connection flexural capacity. As shown in Figure 7-31, during the first loading cycle the contribution of the top springs in the R3D element to the generated connection moment was more effectively captured. This indicated that the strength and stiffness of the springs representing the top hinge in the slotted beam connection were potentially degrading too quickly.

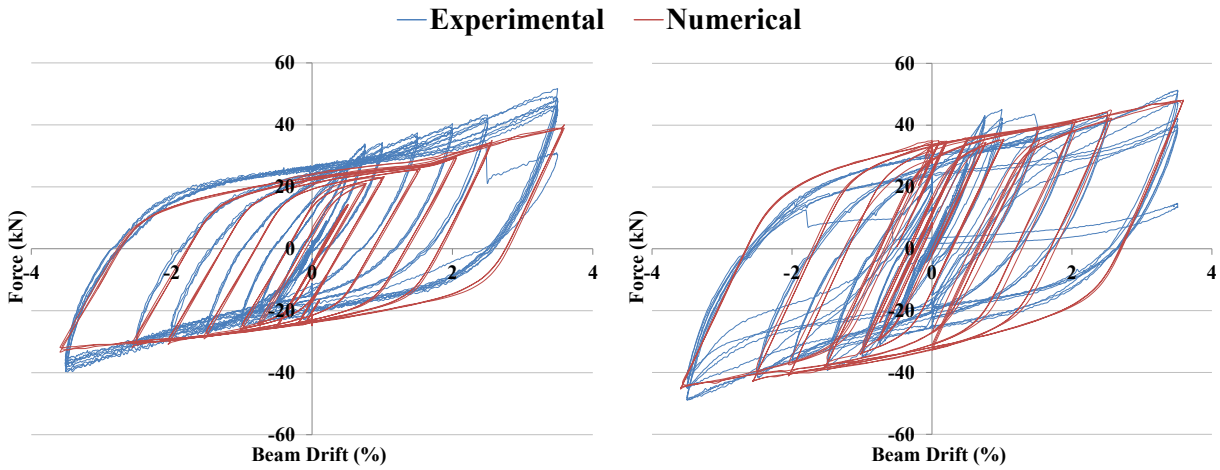

(a) Parallel to floor. **(b) Perpendicular to floor.**

Figure 7-32: Comparison of numerical model to SA2 second complete loading protocol.

Figure 7-33 presents a comparison between the response of the numerical model of SA3 and the experimental response of SA3. In general, the comparison between the experimental and numerical model responses for SA3 was similar to that observed for SA2. However, it can be seen in Figure 7-33(b) that bottom longitudinal reinforcement buckling and fracture had a significant impact on response during the 3.5% beam drift cycle in both loading directions. The Dodd-Restrepo hysteresis rule is unable to capture either reinforcement buckling or fracture due to low-cycle fatigue (Dodd & Restrepo-Posado, 1995).

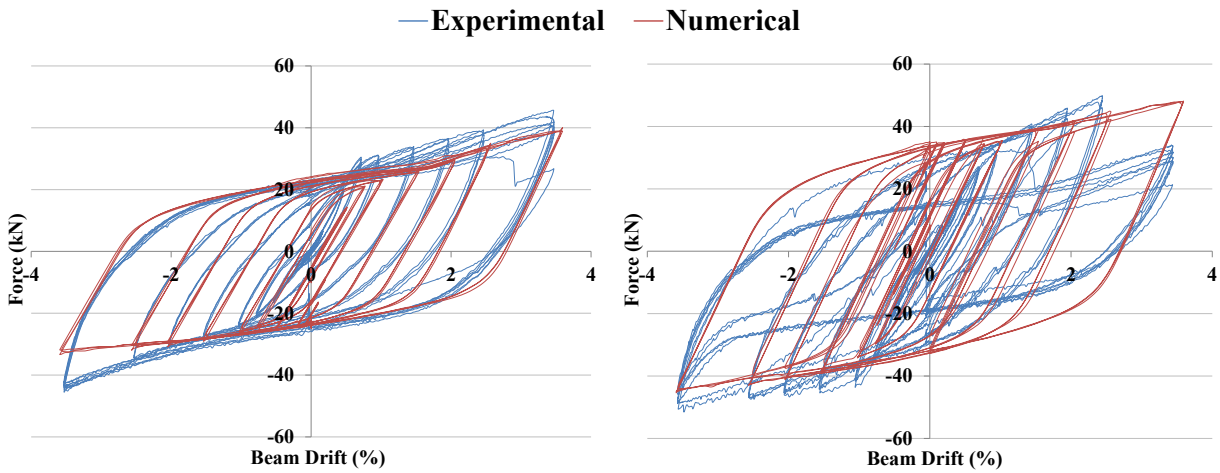

(a) Parallel to floor. **(b) Perpendicular to floor.**

Figure 7-33: Comparison of numerical model to SA3.

The R3D element was capable of accurately representing the response of the as-built subassemblies SA2 and SA3. The discrepancies between the recorded response of the subassemblies and the response of the numerical models were largely due to the limitations of the hysteretic rule used to model the behaviour of reinforcement.

7.4.1.2 Retrofitted Subassembly Numerical Models

TCY dampers dissipate energy through tension and compression yielding of mild steel, which is the same mechanism by which energy is dissipated in the unbonded bottom longitudinal

reinforcement in slotted beams. Hence, the Dodd-Restrepo hysteresis rule was used in the R3D element to model the response of the TCY dampers in the numerical model of SA2-TCY (Dodd & Restrepo-Posado, 1995). In Section 6.2, it was stated that the asymmetric behaviour observed in the TCY dampers during testing was due to the effect of Poisson's ratio on the restrained steel. This allowed the effective cross-section of the steel to increase, which increased the effective stress and enabled higher forces to be generated. Hence, it was expected that during negative flexure the moment capacity generated by the numerical model of SA2-TCY would be less than that recorded during the SA2-TCY experiment. As shown in Figure 7-34, this proved to be the case. The slight reduction in stiffness that was observed in the response of SA2-TCY as the recorded force changed sign was likely due to buckling occurring at a high mode in the machined portion of the TCY dampers. The Dodd-Restrepo hysteresis rule is incapable of modelling buckling, so this behaviour could not be replicated in the numerical model of SA2-TCY (Dodd & Restrepo-Posado, 1995).

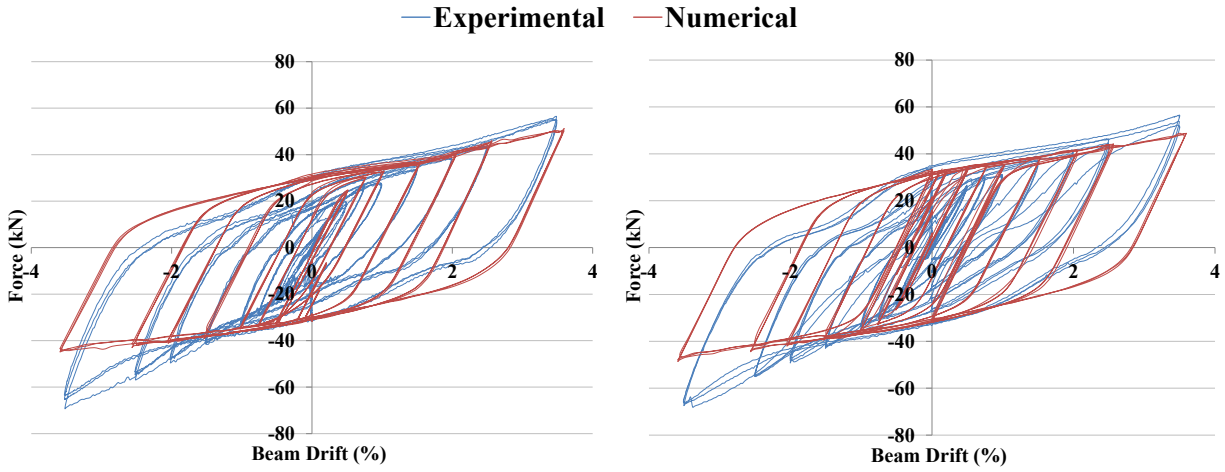

(a) Parallel to floor. **(b) Perpendicular to floor.**

Figure 7-34: Comparison of numerical model to SA2-TCY.

The response of the TCY and HF2V dampers was shown in Section 6.2 to be similar to Coulomb damping. Hence, the most appropriate hysteretic rule available within Ruaumoko3D to model the behaviour of the TCY and HF2V dampers was the bi-linear rule, with a very soft post-yield stiffness specified (Carr, 2013). The use of the bi-linear hysteresis rule to model the response of the SFD dampers in the numerical model of SA2-SFD meant that many of the subtleties of SFD damper behaviour, such as the transition between static and dynamic friction states, could not be replicated. However, as shown in Figure 7-35, the response of the numerical model of SA2-TCY matched the experimental response of SA2-TCY relatively closely. In Figure 7-35(b), it can be seen that the force as which SFD damper sliding initiated was well predicted by the numerical model. However, the asymmetric response observed in the direction parallel to the floor in SA2-TCY was unable to be captured by the numerical model without undertaking calibration.

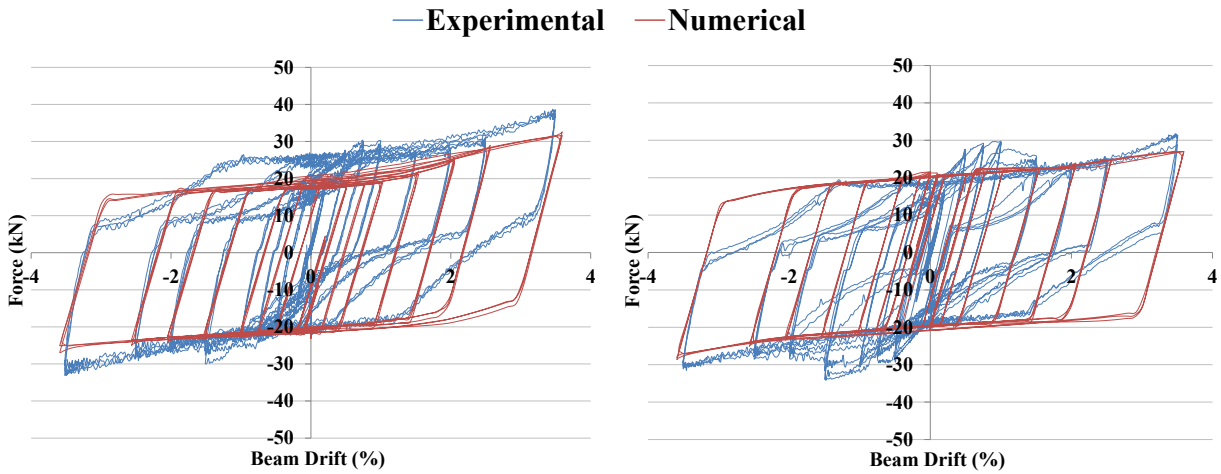

(a) Parallel to floor.

(b) Perpendicular to floor.

Figure 7-35: Comparison of numerical model to SA2-SFD.

As shown in Figure 7-36, the peak force generated by the numerical model of SA2-HF2V matched the experimentally observed peak force of SA2-HF2V relatively well. However, the transition of the lead in the HF2V damper between static and dynamic states was not able to be well represented by the numerical model of SA2-HF2V, as can be seen in Figure 7-36(b). The slip that occurred between the beam cleat and the beam soffit in the direction parallel to the floor in SA2-HF2V could not be replicated by the numerical model. Hence, the significant discrepancy between the responses presented in Figure 7-36(a) is exaggerated. The increase in post-yield stiffness with increasing displacement observed during the testing of SA2-HF2V was able to be captured by the numerical model. This was important because systems with low post-yield stiffness are susceptible to P-delta effects, which can jeopardise the stability of the system.

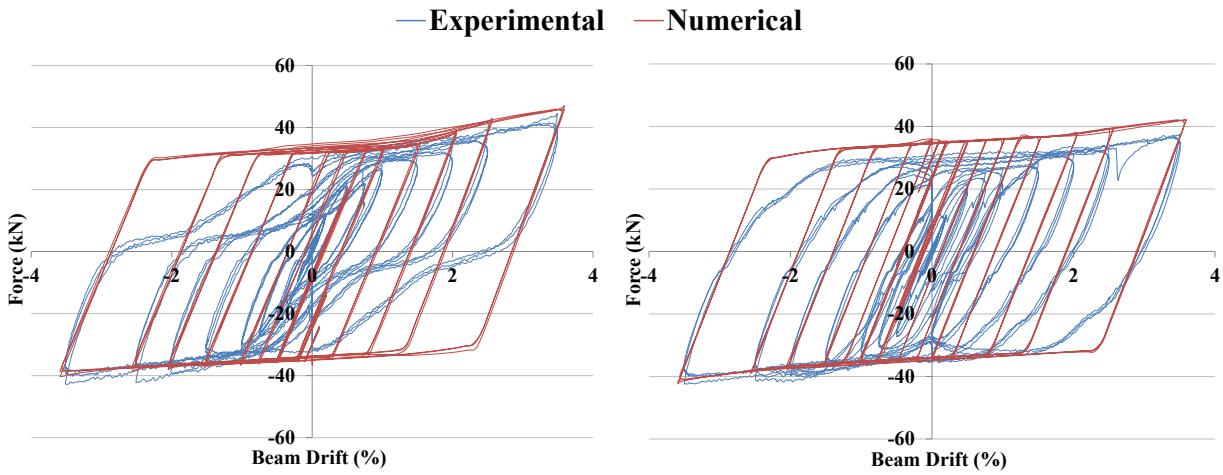

(a) Parallel to floor.

(b) Perpendicular to floor.

Figure 7-36: Comparison of numerical model to SA2-HF2V.

In general, the numerical models assembled using the R3D element were able to replicate the response of the retrofitted subassemblies reasonably well. If more appropriate hysteretic rules for dampers are developed and deployed within Ruaumoko3D (Carr, 2013), the ability of the

R3D element to replicate the response of slotted beam connections that use dampers will be significantly improved.

7.4.2 R3D Element Verification against Superassembly Experimental Data

7.4.2.1 Numerical Model of SA1 – Frame Only

A numerical model of superassembly SA1 was assembled to compare the response of the numerical model to the experimentally observed response of specimen SA1. The numerical model, shown in Figure 7-37, used R3D elements to model the behaviour of the reinforced concrete connections. Due to the selective weakening performed on specimen SA1, four different variants of the R3D element were required in the numerical model to account for the different connection configurations. The beams and columns were modelled using Giberson two component beams. The beams were elastic, whilst the columns were assigned a modified Takeda hysteresis rule (Otani, 1974). Rigid end blocks were used at the end of the beams and columns to model the increased stiffness of the beam-column joint zones.

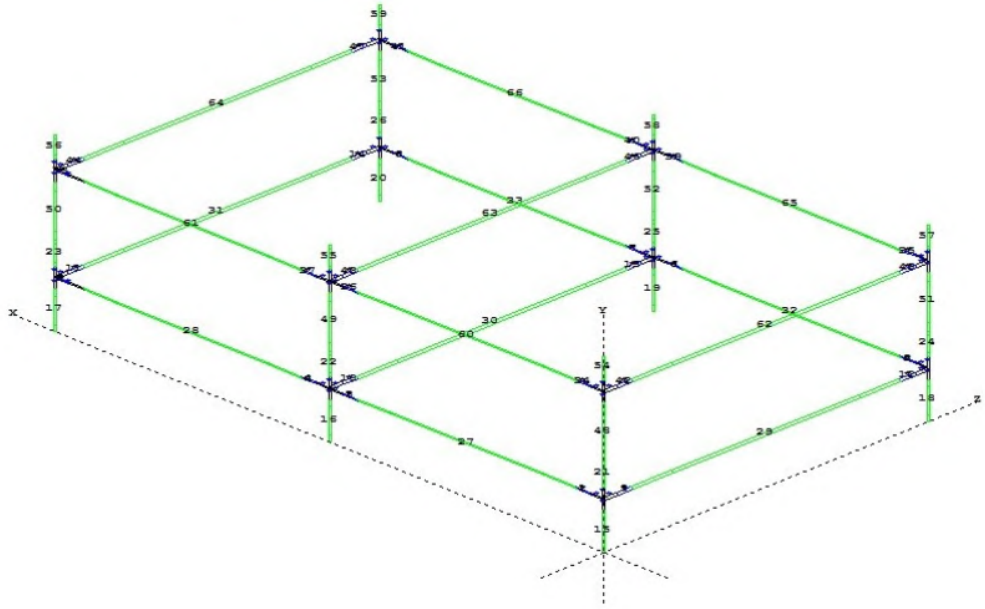

Figure 7-37: Isometric view of SA1 numerical model without floor diaphragm.

The same displacements that were applied to SA1 were applied to the numerical model of SA1. In the numerical model, the displacements were applied to columns A/1, A/2, B/2 and C/2 as they were during the testing of SA1. However, because the numerical model of SA1 had no floor diaphragm, the force transfer mechanism across the model was significantly less stiff than it was in SA1. The intended displacements were not able to be achieved in columns B/1 and C/1 using this method. Hence, a rigid diaphragm assumption was applied to the numerical model of SA1. On each floor, the node at the centre of each beam-column joint was slaved to the node at the centre of the beam-column joint on Grid A/2. The rigid diaphragm

assumption had the potential to stiffen and strengthen the observed response of the numerical model.

Figure 7-38 presents a comparison between the experimentally observed response of SA1 and the response of the numerical model of SA1. In general, the experimental response of SA1 was well represented by the numerical model. The pinched response of SA1 that can be seen in Figure 7-38(a) was not able to be replicated by the numerical model. In the east-west direction the discrepancy between the recorded response of SA1 and the response of the numerical model was larger than it was in the north-south direction. The east-west direction was the direction that the one-way flooring spanned in SA1. Hence, the recorded lateral resistance of SA1 in the east-west direction included the contribution of the continuity moments generated in the one-way flooring connections. The contribution that the floor diaphragm made to the lateral resistance of SA1 was not able to be captured in the simplified numerical model of SA1. It was possible that the discrepancy between the recorded response of SA1 and the response of the numerical model would be greater if node slaving was not used.

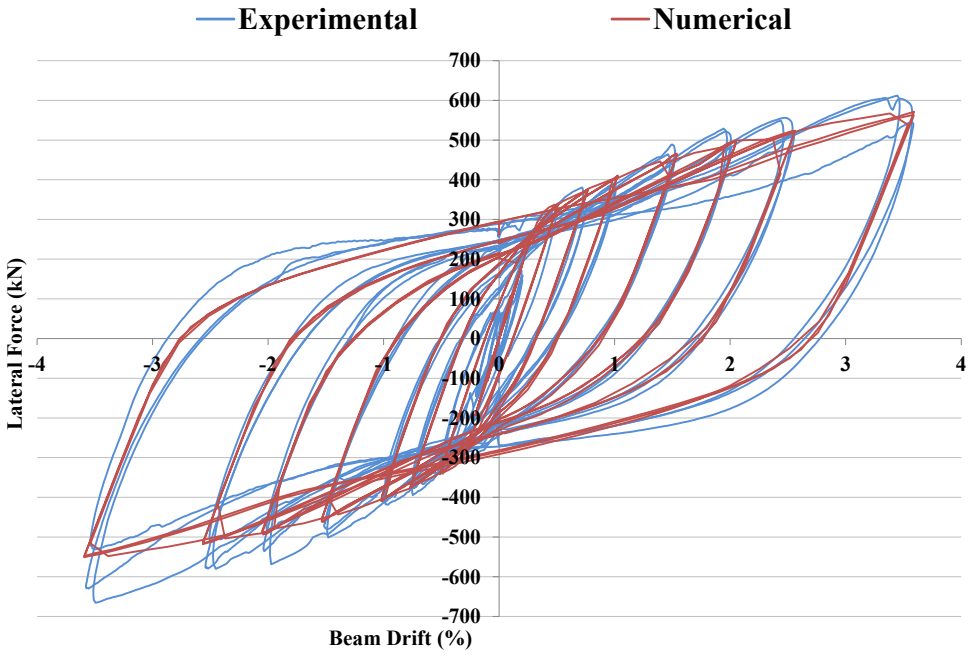

(a) East-west.

Figure 7-38: Comparison of SA1 numerical frame model against experimental response.

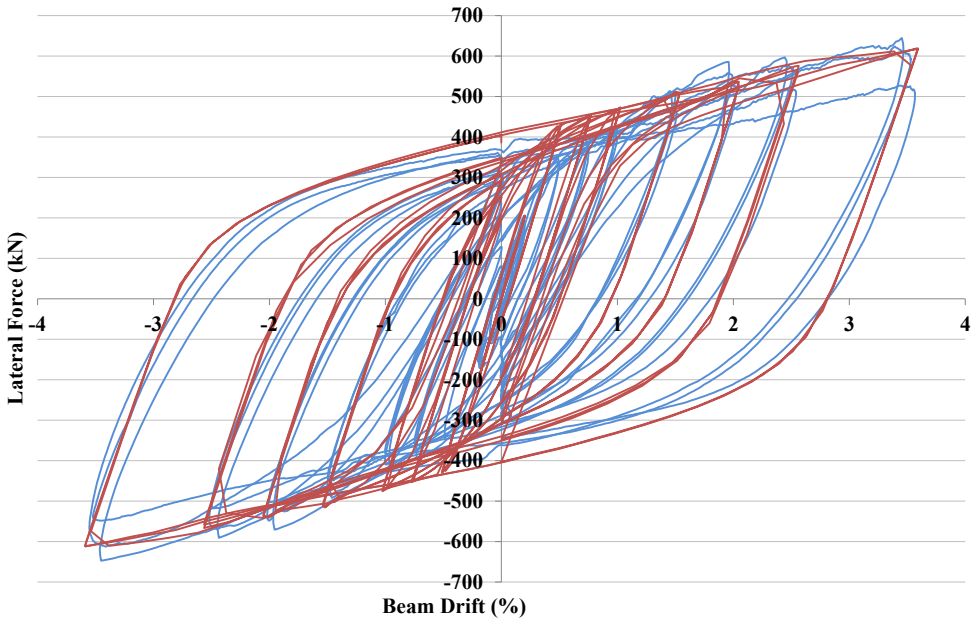

(b) North-south.

Figure 7-38: Comparison of SA1 numerical frame model against experimental response (Continued).

The numerical model of SA1 was able to satisfactorily replicate the experimental response of superassembly SA1. However, it was shown in Chapter 4 that the floor diaphragm of SA1 contributed significantly to the observed response. Hence, it was important to extend the numerical model of SA1 to include the influence that the floor diaphragm had on response.

7.4.2.2 Numerical Model of SA1 – Frame and Floor Diaphragm

To improve the accuracy of the numerical model of SA1, a numerical model of the one-way floor diaphragm system installed in SA1 was developed and implemented in the numerical model of SA1. The goals of the numerical floor diaphragm model were to:

1. Provide realistic restraint to the beam elongation of the R3D elements.
2. Model the contribution of continuity moments to overall lateral resistance in the east-west direction.
3. Model the contribution of infill flexure to overall lateral resistance in the north-south direction.
4. Improve force transfer across the numerical model of SA1.

The numerical model developed to model the floors of specimen SA1 was based on research undertaken by Peng (2009). However, Peng's (2009) numerical floor diaphragm model was extended to enable the influence of continuity moments and infill flexure to be modelled. A schematic of the numerical floor diaphragm model developed is shown in Figure 7-39. The edges of the one-way precast floors were modelled using elastic Giberson two component beams. Elastic finite elements were used between the Giberson two component beams to model the precast floor units. To model continuity moments, rotational springs were used at the ends of the Giberson two component beams to connect to the main seismic frame. The

properties assigned to the rotational springs were based on first principal calculations. The interaction between the numerical model of the precast floor units and the parallel seismic beams was based on a strut and tie analogy. Axial springs assigned a cracked concrete hysteresis rule were installed diagonally between the edge of the precast floor unit and the parallel seismic beam (Maekawa et al., 2003). The concrete springs model shear transfer between the precast floor units and the seismic beams. The properties assigned to the concrete axial springs were based on the thickness of the infill, the concrete strength and the effective strut width. The effective width of the concrete strut was based on recommendations by Peng (2009).

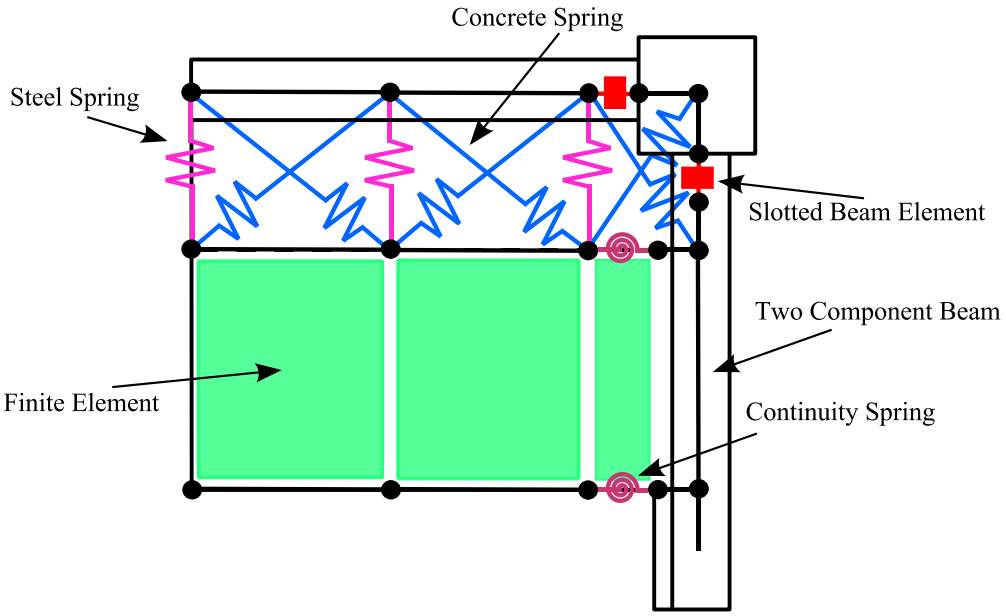

Figure 7-39: Schematic of a portion of the floor diaphragm model.

Axial springs assigned a Dodd-Restrepo hysteresis rule were installed at right angles between the edge of the precast floor unit and the parallel seismic beam (Dodd & Restrepo-Posado, 1995). The steel springs model the tensile capacity of the floor reinforcement and complete the strut and tie model. The properties assigned to the steel axial springs were based on the material properties of the reinforcement and the quantity of reinforcement contained within the tributary area of the spring.

Peng (2009) developed the numerical floor diaphragm model to replicate the response of a two-dimensional reinforced concrete specimen with a floor diaphragm, which was tested uniaxially. To enable the numerical floor diaphragm model to be used in a numerical model that was subjected to biaxial loading, the induced flexure in the infill region had to be modelled. Hence, the steel springs were assigned flexural properties as well as axial properties. The flexural properties assigned to the steel springs were based on first principal calculations.

The completed numerical model of SA1, including the numerical floor diaphragm model, is shown in Figure 7-40. The Ruaumoko3D input file for the numerical model of SA1, including the floor diaphragm model, is presented in Appendix E. Assembling a numerical model such as that shown in Figure 7-40 is complex and time intensive. Hence, it is unlikely that such a numerical model would be assembled by a design engineer to facilitate the analysis of a new structure.

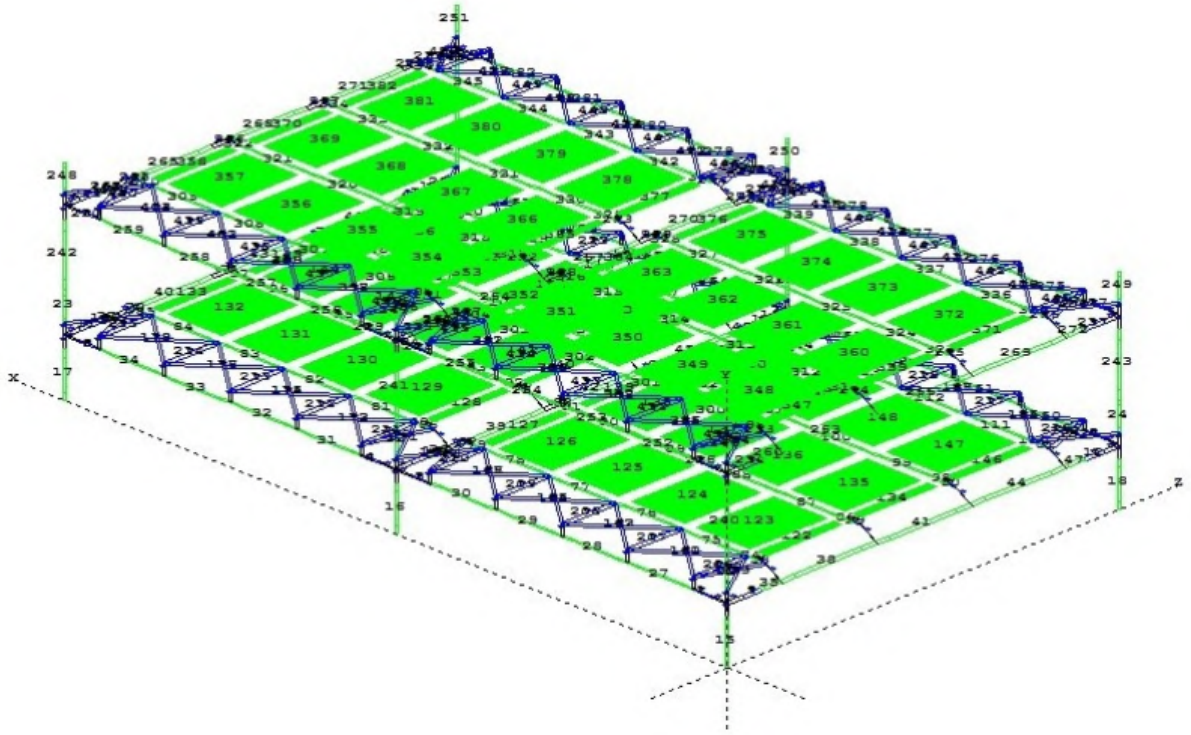

(a) Isometric view of SA1 numerical model.

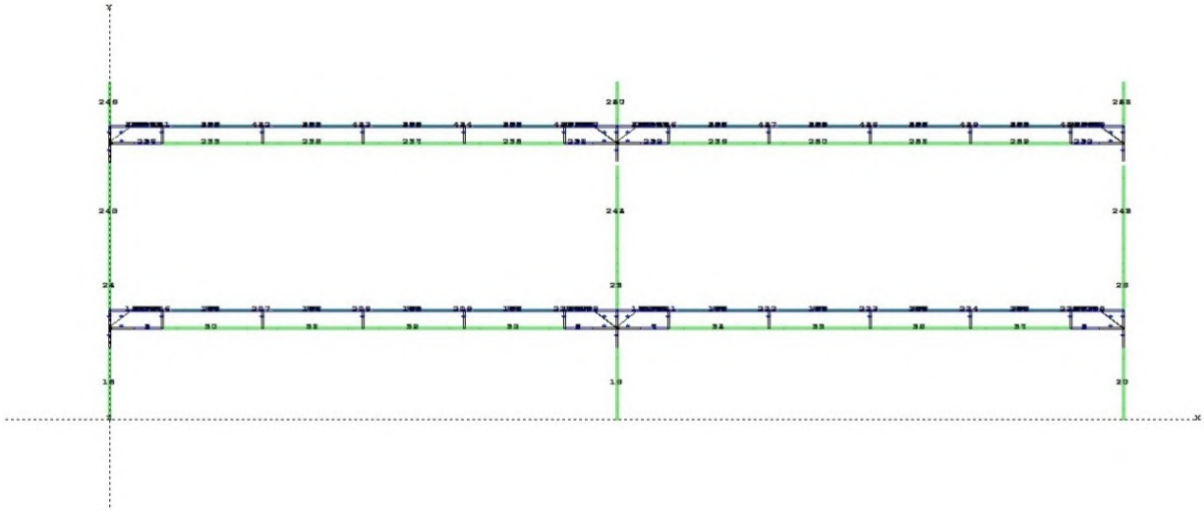

(b) Elevation of SA1 numerical model.

Figure 7-40: Floor diaphragm numerical model.

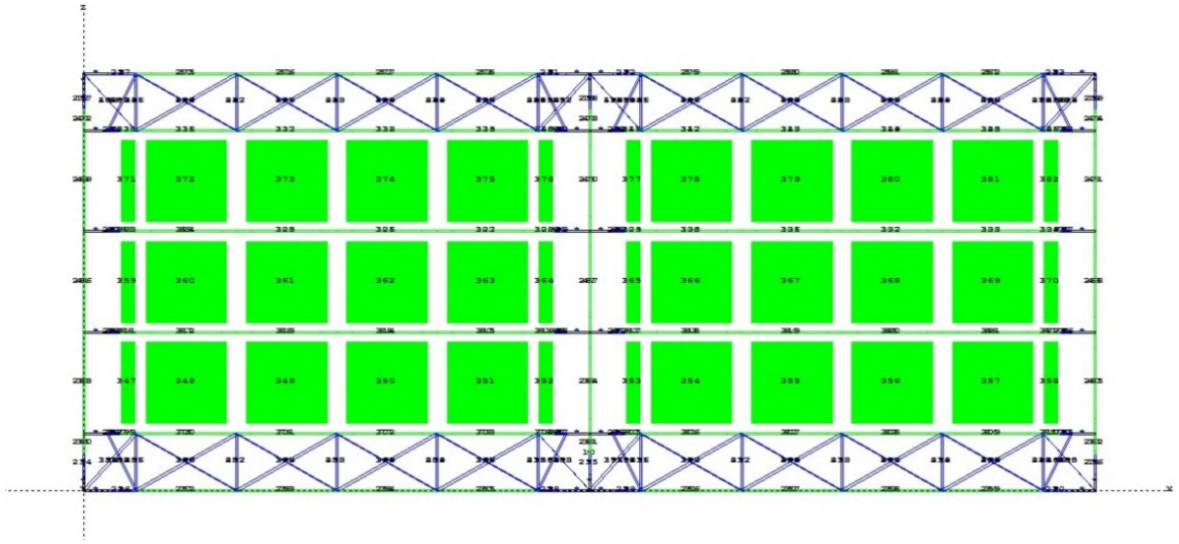

(c) Plan of SA1 numerical model.

Figure 7-40: Floor diaphragm numerical model (Continued).

Figure 7-41 presents a comparison between the experimentally observed response of SA1 and the response of the numerical model of SA1. The experimental response of SA1 was well represented by the numerical model. The stiffness and peak lateral forces observed during the testing of SA1 were replicated accurately by the numerical model of SA1. However, as was observed in Section 7.4.2.1, the pinched response of SA1 in the east-west direction was not able to be replicated by the numerical model. It was shown in Section 6.3.1 that the pinched response of SA1 in the east-west direction was due to displacement in the experimental setup of specimen SA1, which was not modelled numerically. The numerical model of SA1 produced slightly larger yield forces than was observed in SA1; however, it is possible that this discrepancy could have been caused by the normalisation of the experimental data necessitated by the selective weakening described in Section 4.4.

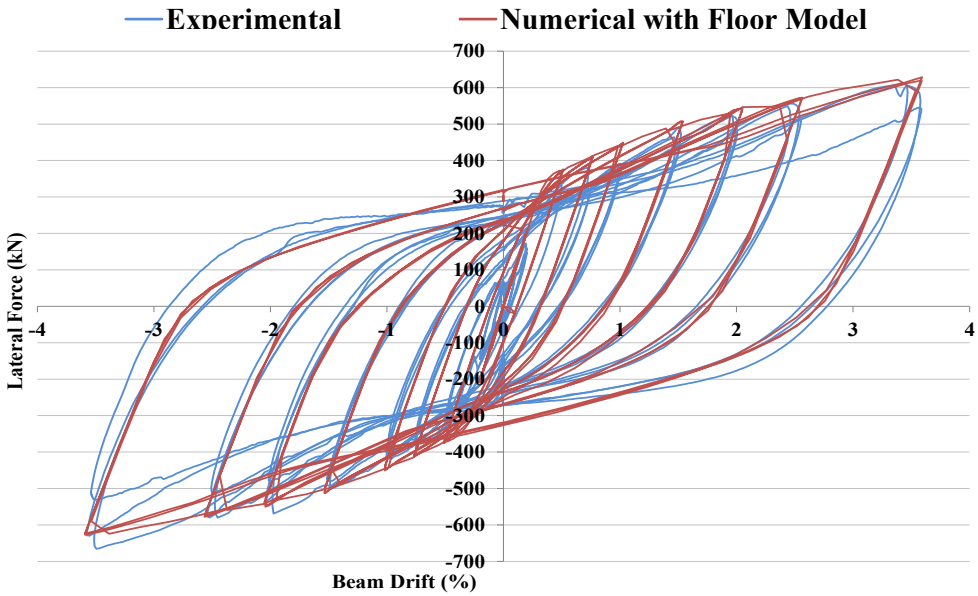

(a) East-west.

Figure 7-41: Comparison of SA1 numerical frame and diaphragm model against experimental response.

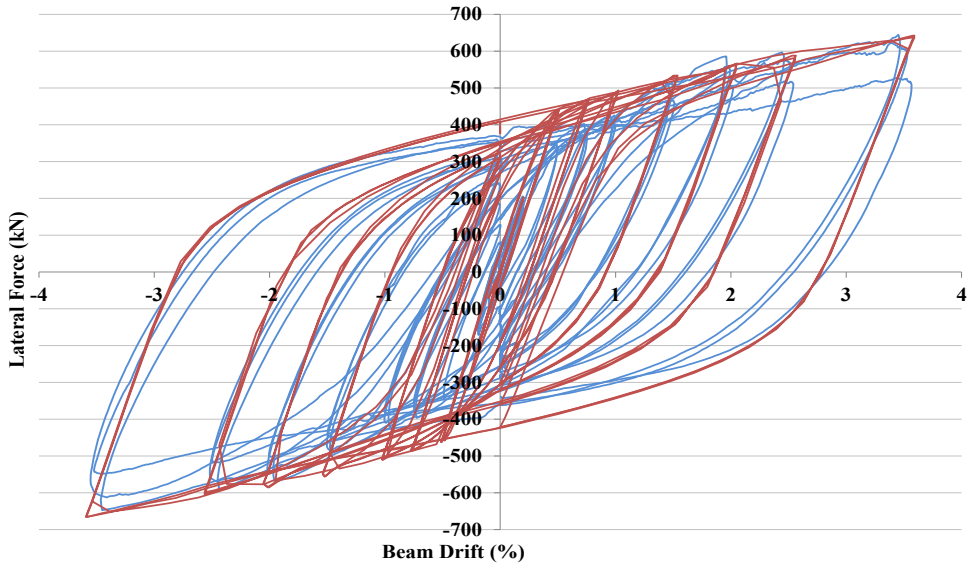

(b) North-south.

Figure 7-41: Comparison of SA1 numerical frame and diaphragm model against experimental response (Continued).

As shown in Figure 7-38 and Figure 7-41, there was an 11% difference in the peak lateral force obtained from the numerical models of SA1 with and without the numerical floor diaphragm model. The relatively modest difference between the two models was likely due to the high stiffness of the floor in SA1. Hence, the difference between the observed response when using a rigid floor diaphragm assumption and the relatively stiff numerical floor diaphragm model was modest. It is possible that the difference could be greater for structural systems with more flexible floor diaphrams.

The numerical floor diaphragm model, used in conjunction with the R3D element, showed excellent agreement with the experimental response of SA1. However, the numerical floor diaphragm model may not be as effective when used to model structures with different geometries or properties. Investigating the general applicability of the numerical floor diaphragm model was beyond the scope of this research project. However, there are limitations that should be considered when using the numerical floor diaphragm model. The finite elements used in the model were linear because at the time of writing there was not a nonlinear finite element available in Ruaumoko3D (Carr, 2013). The use of a linear finite element could have increased the stiffness of the floor diaphragm model compared to a nonlinear finite element. The numerical floor diaphragm model was inadequate for modelling warping deformations in the floor diaphragms induced around columns. This inadequacy could potentially be addressed by using Giberson two component elements in place of the flexural springs that were used to model flexure in the infill region. The Giberson two component elements would allow a more realistic double curvature deformation mode to be modelled. The development of a nonlinear finite element that is capable of modelling both plane and bending stresses would address the aforementioned issues.

7.4.2.3 Numerical Floor Diaphragm Model Sensitivity Study

It was important to understand the influence that changes to input variables for the numerical floor diaphragm model had on the overall observed response of the numerical model of SA1. Examining the relative importance of the input variables provided insight about the relationship between the floor diaphragm and the seismic frame. A sensitivity study was undertaken by Peng (2009) on his formulation of the numerical floor diaphragm model. The sensitivity of the input variables identified by Peng (2009) generally agreed with the findings of the sensitivity study undertaken on the numerical floor diaphragm model developed in Section 7.4.2.2.

Steel Reinforcement Spring Axial Stiffness

The steel reinforcement springs in the numerical floor diaphragm model did not provide a direct load path between the precast floor units and the seismic frame. The steel reinforcement springs instead provided a reactive force to the diagonal concrete springs to complete the strut and tie mechanism. Hence, increasing the stiffness of the steel reinforcement springs did not significantly influence the response of the numerical model of SA1, as shown in Figure 7-42.

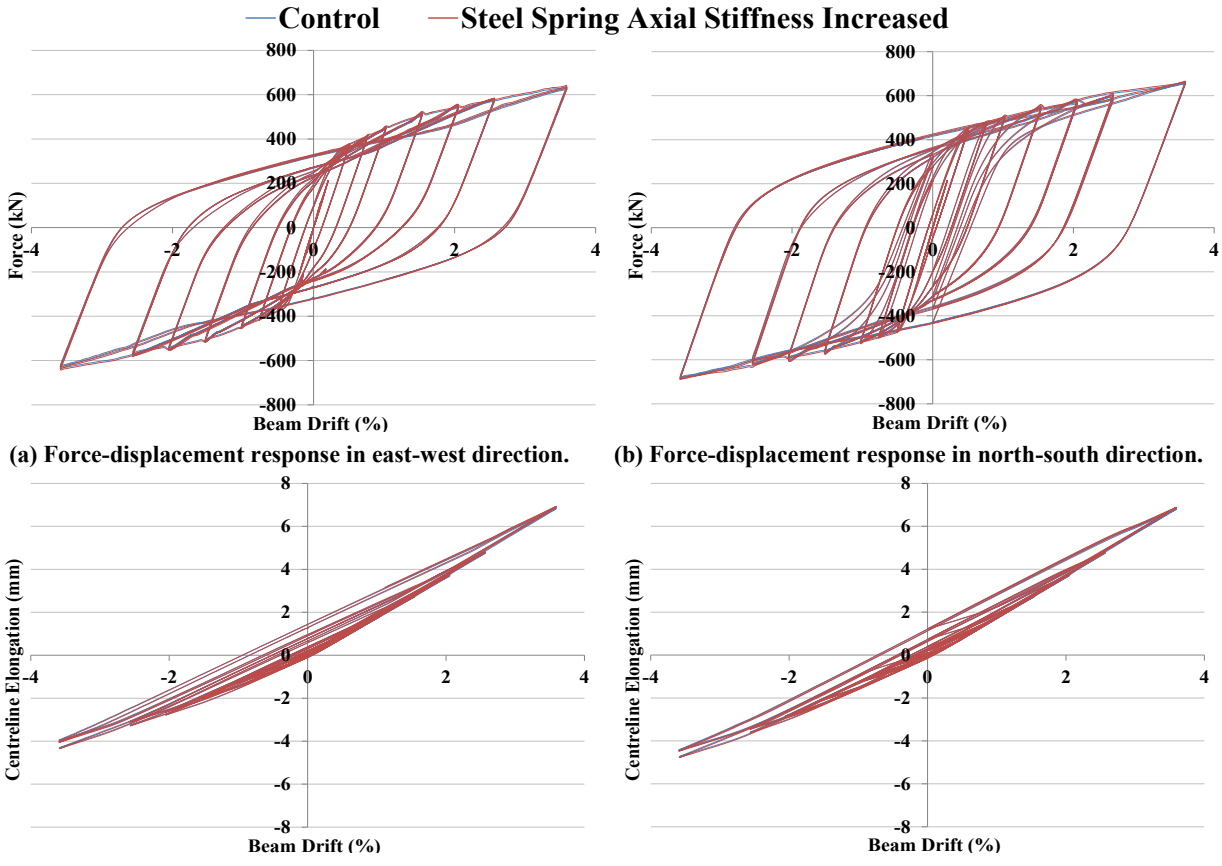

(a) Force-displacement response in east-west direction.

(b) Force-displacement response in north-south direction.

(c) Centreline beam elongation of Bm A/2-1 east.

(d) Centreline beam elongation of Bm A/2-1 north.

Figure 7-42: Effect of increased steel spring axial stiffness.

Concrete Spring Axial Stiffness

The diagonal concrete springs in the numerical floor diaphragm model provided a direct load path between the precast floor units and the seismic frame. Hence, increasing the axial

stiffness of the concrete springs increased the reactive forces that were induced in the concrete springs to restrain beam elongation in the R3D elements. As shown in Figure 7-43, a slight increase in overall lateral resistance and a slight decrease in beam connection elongation were observed in the numerical model with doubled diagonal concrete spring stiffness compared to the control model. Beam elongation in reinforced concrete slotted beam connections is relatively low compared to traditional reinforced concrete connections. Hence, the effect of increasing the stiffness of the diagonal concrete springs on observed response would be more apparent in a numerical model which incorporated traditional reinforced concrete connections compared to a model which incorporated slotted beam connections

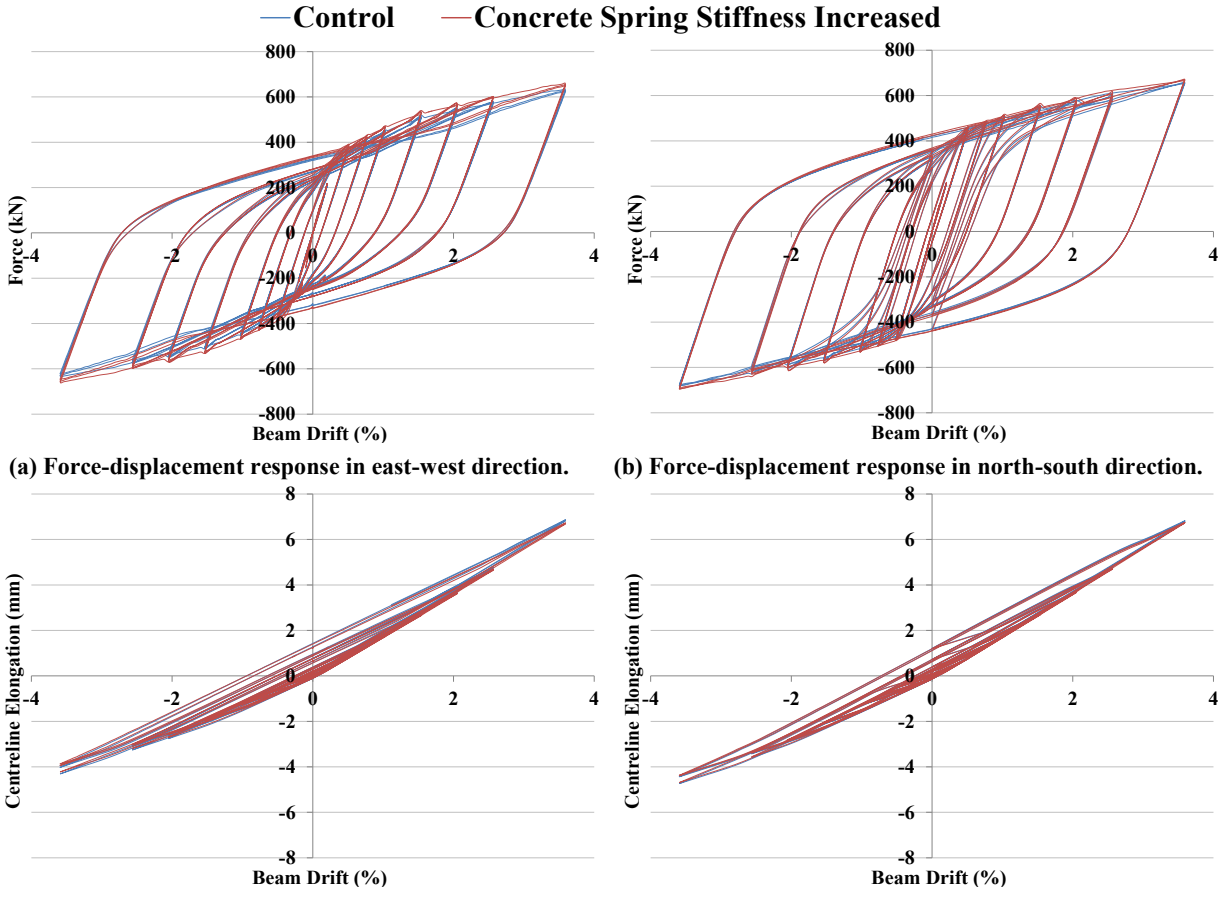

(a) Force-displacement response in east-west direction.

(b) Force-displacement response in north-south direction.

(c) Centreline beam elongation of Bm A/2-1 east.

(d) Centreline beam elongation of Bm A/2-1 north.

Figure 7-43: Effect of increased concrete spring axial stiffness.

The recorded beam elongation has not been presented in the investigation into the sensitivity of response of the following three parameters because zero difference was observed.

Steel Reinforcement Spring Flexural Stiffness

The influence of flexure in the infill regions on observed response was represented in the numerical model by steel reinforcement springs with flexural properties, which connected the precast floor units to the seismic frame. As the numerical model was displaced in the north-south direction, the parallel seismic beam was forced to rotate relative to the precast floor unit, which induced flexure in the steel reinforcement springs. Hence, increasing the flexural

stiffness of the steel reinforcement springs increased the overall lateral resistance of the numerical model in the north-south direction, as shown in Figure 7-44. The increase in steel reinforcement spring flexural stiffness had no effect on the observed response in the east-west direction.

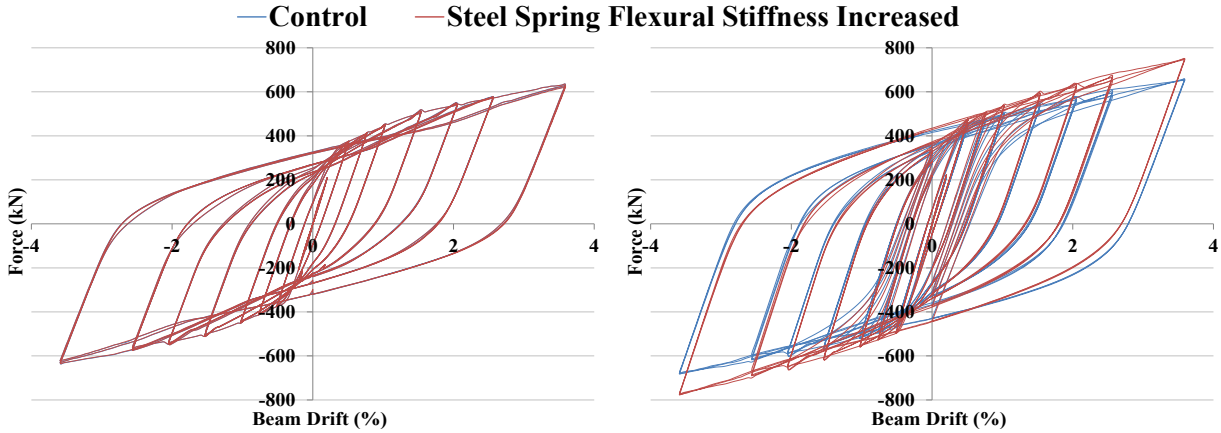

(a) Force-displacement response in east-west direction. **(b) Force-displacement response in north-south direction.**

Figure 7-44: Effect of increased steel spring flexural stiffness.

Continuity Moment Spring Flexural Stiffness

The influence of continuity moments in the precast floor connections was represented in the numerical model by a rotational spring, which connected the ends of the precast floor units to the supporting beam. As the numerical model was displaced in the east-west direction a relative rotation was induced between the end of the precast floor element and the supporting beam, which induced flexure in the continuity moment rotational spring that spanned between the elements. As shown in Figure 7-45, increasing the stiffness of the continuity moment rotational springs increased the overall lateral resistance of the numerical model in the east-west direction. The increase in continuity moment rotational spring stiffness had no effect on the observed response in the north-south direction.

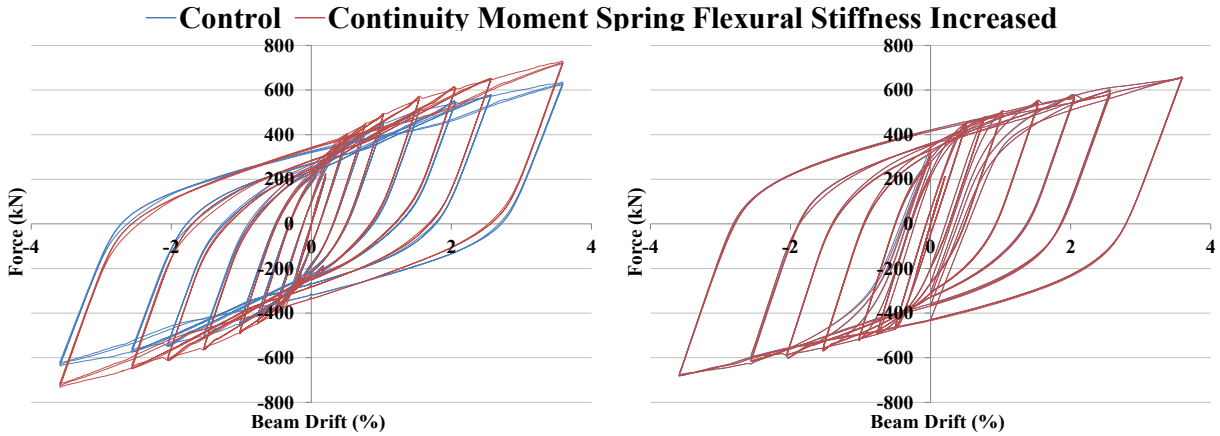

(a) Force-displacement response in east-west direction. **(b) Force-displacement response in north-south direction.**

Figure 7-45: Effect of increased continuity moment spring flexural stiffness.

Floor Diaphragm Finite Element Stiffness

Increasing the stiffness of the finite elements, which represented the precast floor units, had no perceivable influence on the observed response of the numerical model, as shown in Figure 7-46. The stiffness of the floor diaphragm finite elements was far greater than that of the steel reinforcement and concrete springs that connected the precast floor units to the parallel seismic beams, which meant that deformation occurred in the steel reinforcement and concrete springs preferentially to the floor diaphragm finite elements. Hence, the stiffness of the floor diaphragm finite elements had little influence on the observed numerical model response.

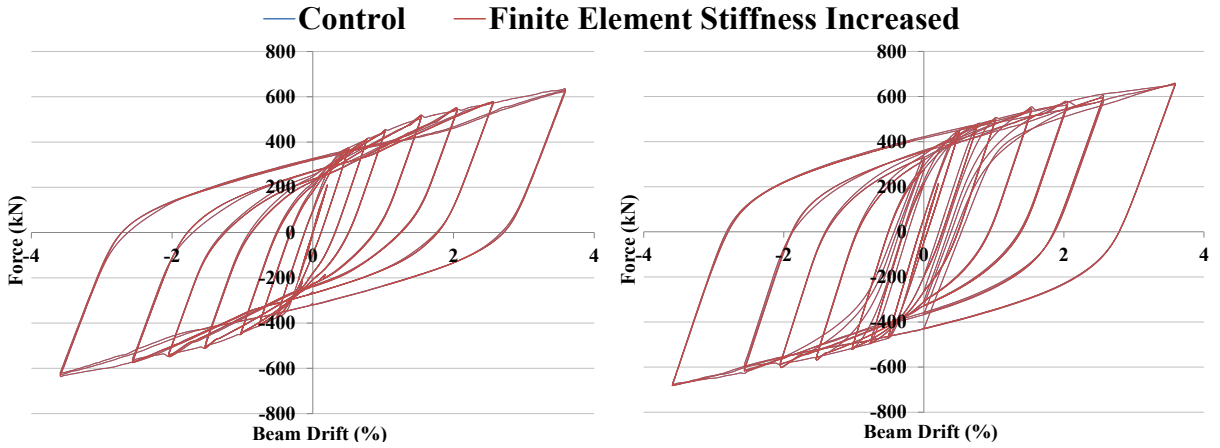

(a) Force-displacement response in east-west direction. **(b) Force-displacement response in north-south direction.**

Figure 7-46: Effect of increased finite element stiffness.

7.5 Comparison between the Responses of Slotted Beam and Traditional Connections

This section describes a comparison between the connection mechanics of a reinforced concrete slotted beam connection and a traditional reinforced concrete connection. The numerical model of SA1, with floor diaphragm model included, was used as the basis of the comparison. Two versions of the numerical model of SA1 were assembled. The slotted beam version of the numerical model used the R3D element developed in Section 7.3 to model the connection behaviour. The traditional reinforced concrete connection version of the numerical used the plastic hinge element described in Section 7.2.1 to model the connection behaviour. The loading protocol applied to both numerical models was the same that applied to SA1, which is described in Section 3.7.2.2.

The R3D element and the plastic hinge element were designed to have similar yield moments; however, this could not be achieved by having the same longitudinal reinforcement layout. Instead, both the top and bottom longitudinal reinforcement of the plastic hinge element were

made the same as the bottom longitudinal reinforcement of the R3D element, which gave the plastic hinge element equal positive and negative moment capacities.

A direct comparison between the torsional responses of each numerical model was not able to be undertaken because the plastic hinge element is not able to model torsion well (Peng, 2009). The response of the plastic hinge element is affected by the plastic hinge length assigned. Even if an appropriate plastic hinge length is assigned to the plastic hinge element the computed strains may not be accurate. In the plastic hinge element, the strain in the longitudinal reinforcement is the same over the length of the element and is calculated based on the total curvature applied to the element. In a real reinforced concrete plastic hinge the strain in the longitudinal reinforcement peaks across the cracks. Because this effect could not be modelled with the plastic hinge element the computed strains were considered lower bound.

7.5.1 Overall Connection Responses

A comparison of the overall hysteretic response of the slotted beam and traditional connection numerical models is shown in Figure 7-47 and Figure 7-48 for the east-west and north-south loading directions respectively. The cardinal directions used in this investigation are the same as those used for SA1. The yield force of both numerical models was similar, which validated the design approach described above. Furthermore, both numerical models exhibited stable response throughout the test.

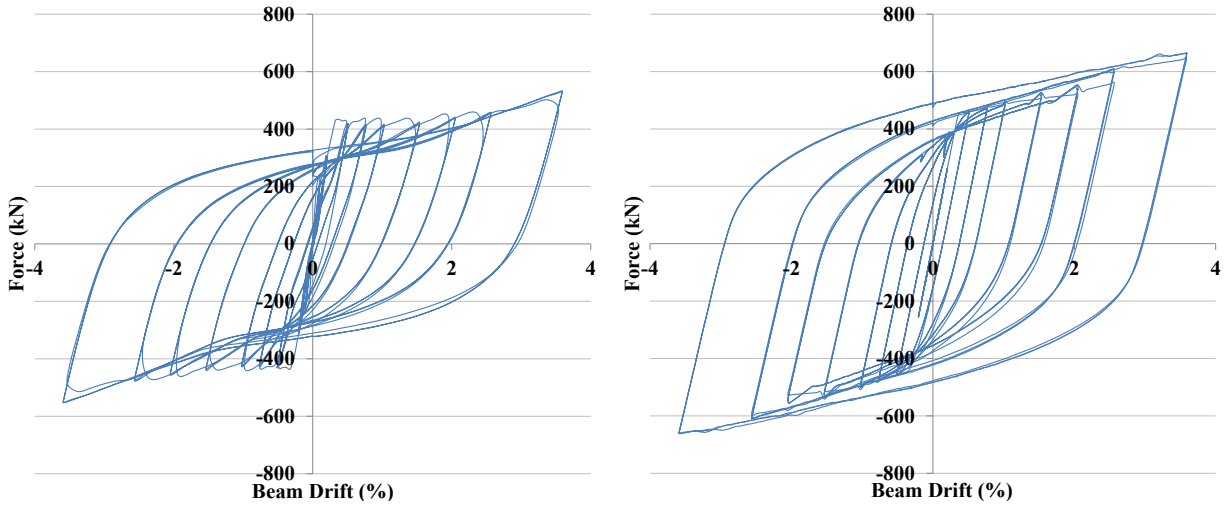

(a) Traditional connections. **(b) Slotted beam connections.**

Figure 7-47: Comparison of force-displacement response in east-west direction.

The shape of the hysteretic response differed significantly between the two numerical models. The slotted beam numerical model exhibited greater post-yield strength gain and less pinching than the traditional connection numerical model. Because the slotted beam numerical model exhibited less pinching, it dissipated a greater amount of energy than did the traditional connection model. A portion of the increased lateral resistance exhibited by the slotted beam

numerical model was attributable to the increased cyclic strain hardening that occurred in the bottom longitudinal reinforcement. However, the difference in the lateral resistance observed between the two numerical models was attributable also to the internal actions generated in the slotted beam. During positive flexure in a reinforced concrete slotted beam the neutral axis will be near the top of the top hinge and during negative flexure it will be near the bottom of the top hinge. Hence, a significant lever arm can exist between the neutral axis and the top longitudinal reinforcement for both positive and negative flexure. The longitudinal reinforcement closest to the neutral axis contributes to the moment capacity of a traditional reinforced concrete connection also; however, in a reinforced concrete slotted beam the contribution of the top longitudinal reinforcement is more significant because the top longitudinal reinforcement is twice as strong as the bottom longitudinal reinforcement. Due to the contribution of the top longitudinal reinforcement to the overall moment of a reinforced concrete slotted beam connection, it is difficult to compare slotted beam and traditional connections. Hence, any claim that the reinforced concrete slotted beam connection exhibits greater energy dissipation, post-yield stiffness or ultimate capacity than a comparable traditional reinforced concrete connection must be tempered by the influence of the top longitudinal reinforcement to slotted beam flexural response. These attributes of reinforced concrete slotted beam response, which have been claimed by researchers (Au, 2010; Leslie, 2010; Byrne, 2012), are not fallacies. However, the observed differences in response between reinforced concrete slotted beams and traditional connections cannot be solely attributed to the increased plasticity in the bottom unbonded longitudinal reinforcement alone.

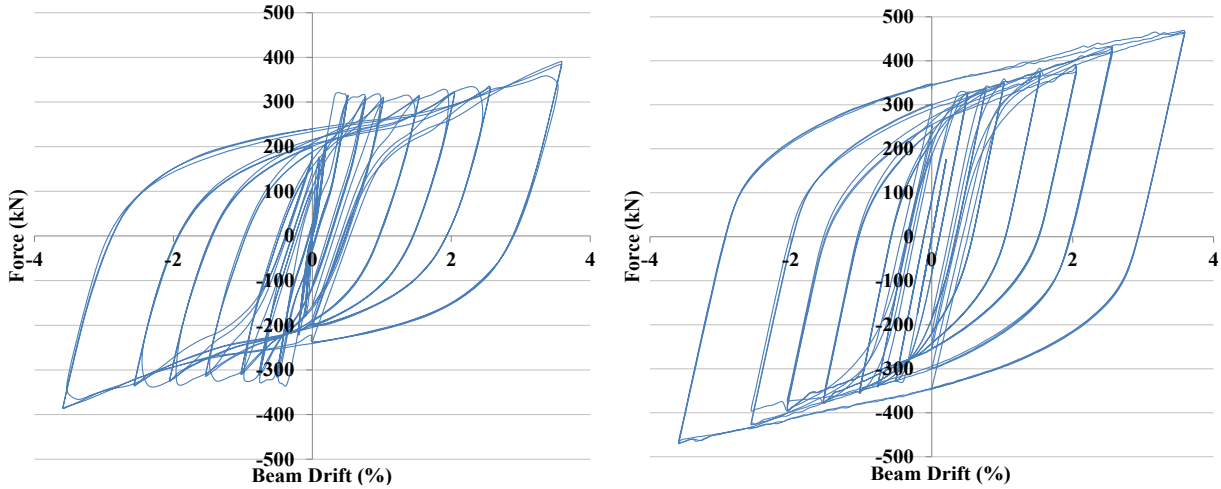

(a) Traditional connections. (b) Slotted beam connections.

Figure 7-48: Comparison of force-displacement response in north-south direction.

7.5.2 Connection Elongation and Induced Beam Axial Force

It was shown in Chapters 4 and 6 that beam elongation is significantly lower in reinforced concrete slotted beams compared to traditional reinforced concrete connections. Figure 7-49

and Figure 7-50 present a comparison between the recorded beam elongation in the plastic hinge element and the R3D element in the east-west and north-south directions respectively. The elongation response recorded in the slotted beam numerical model was similar to that observed for SA1 in both shape and magnitude. Residual beam elongation in the slotted beam numerical model was approximately an eighth of that in the traditional connection numerical model.

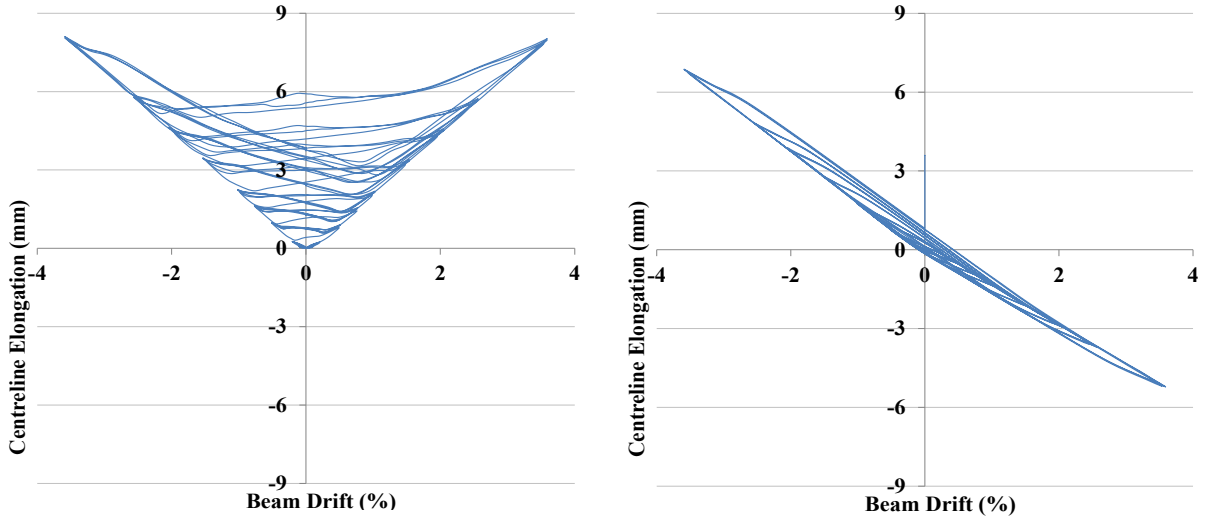

(a) Traditional connections. (b) Slotted beam connections.

Figure 7-49: Comparison of elongation response in east-west direction.

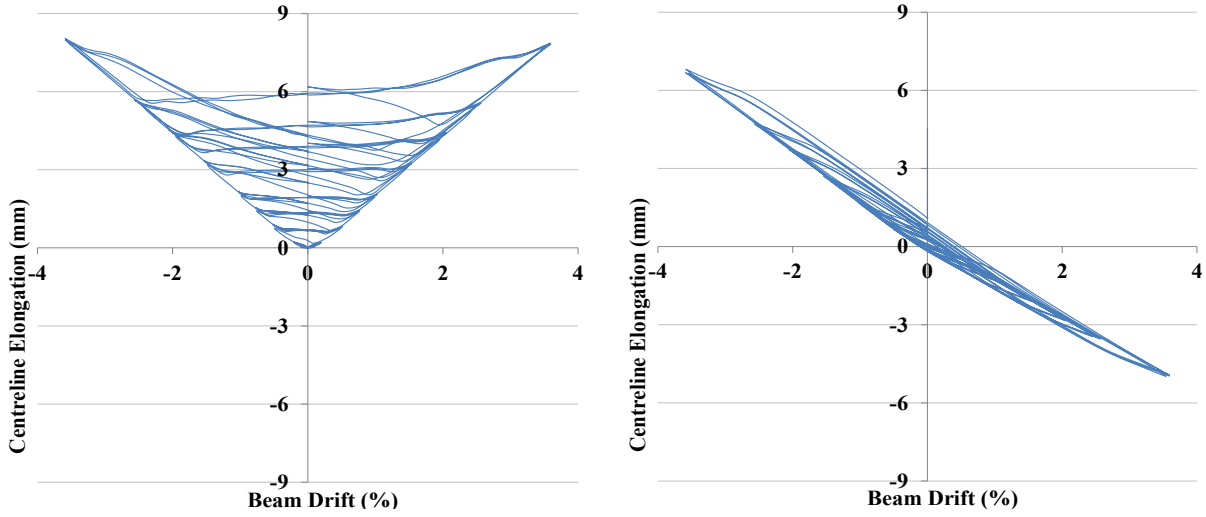

(a) Traditional connections. (b) Slotted beam connections.

Figure 7-50: Comparison of elongation response in north-south direction.

A consequence of beam elongation is the generation of compressive axial forces in the perimeter beams. The lengthening of building bays, which is caused by beam elongation occurring in the connections at both ends of the bays, is restrained by the floor diaphragm, which induces compressive forces in the beams. Because the lengthening of a building bay causes a reduction in the seating length of the precast floors which span between them, beam elongation of a building bay is more important than connection elongation. A slotted beam rotates about the top of the section during both positive and negative flexure. Hence, when elongation is measured along the centreline of the beam, positive flexure is recorded as a

positive elongation and negative flexure is recorded as a negative elongation. However, over a building bay, with positive and negative flexure occurring at each end simultaneously, the apparent elongation of the connections effectively cancels out. Conversely, in a traditional reinforced concrete connection positive flexure occurs about the top of the section and negative flexure occurs about the bottom of the section. Hence, the measured centreline elongation is positive in a traditional reinforced concrete connection for both positive and negative flexure, which is additive over a building bay. The reduced building bay elongation in a reinforced concrete slotted beam system results in significantly reduced induced beam axial forces compared to a system with traditional reinforced concrete connections. This was observed in the response of the slotted beam and traditional connection numerical models, as shown in Figure 7-51 and Figure 7-52 for the eastern beam of Grid 1 and Grid C respectively. In both loading directions, the axial forces generated in the beams of the traditional connection numerical model were significantly greater than those generated in the slotted beam numerical model. This was true of both the residual beam axial forces at the end of loading, and the peaks in beam axial forces that occurred during loading.

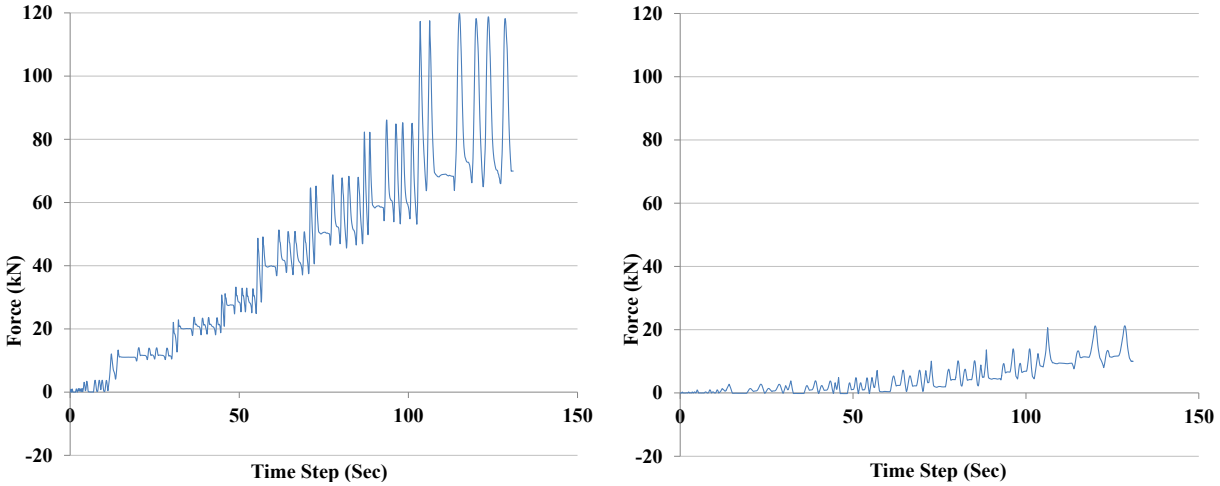

(a) Traditional connections.

(b) Slotted beam connections.

Figure 7-51: Comparison of induced axial force in east-west direction.

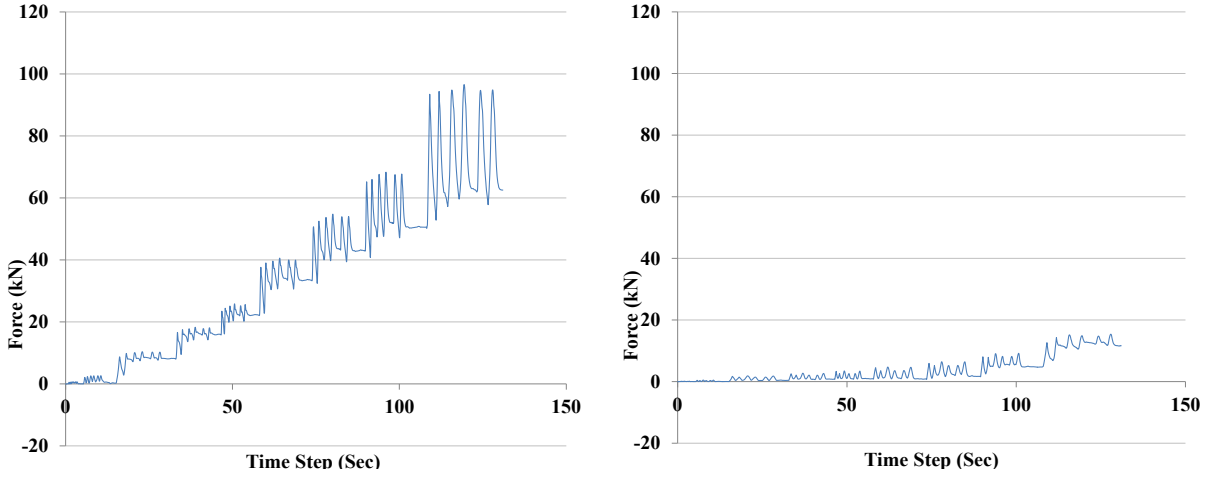

(a) Traditional connections.

(b) Slotted beam connections.

Figure 7-52: Comparison of induced axial force in north-south direction.

7.5.3 Connection Reinforcement Strain and Low-cycle Fatigue

Due to the plasticity in a reinforced concrete slotted beam connection being concentrated in the bottom unbonded reinforcement, low-cycle fatigue failure is an important design consideration. Low-cycle fatigue failure in a reinforced concrete slotted beam can cause a rapid and significant reduction in moment capacity. Low-cycle fatigue failure is difficult to quantify and predict. The most commonly used method to predict low-cycle fatigue failure is based on formulations developed in the 1950s to assess the effect of cyclic thermal stress in aeronautical applications (Manson, 1953; Coffin, 1954). The formulation, which is shown in Equation 7-1, relates the plastic strain from constant amplitude loading, $\varepsilon_{ap,}$ to the number of cycles until failure, N_f. ε'_f and c are empirical constants.

$$\varepsilon_{ap} = \frac{\Delta\varepsilon_p}{2} = \varepsilon'_f(2N_f)^c \qquad \textbf{Equation 7-1}$$

The formulation shown in Equation 7-1 was adapted by Mander et al. (1994) and Brown and Kunnath (2004) for use in structural engineering. These researchers performed experiments on deformed reinforcement of various sizes to determine appropriate values for the empirical constants. The low-cycle fatigue experiments were performed on reinforcement that was prevented from buckling and was loaded using an equi-amplitude cyclic loading protocol. Failure of the reinforcement was defined as the initiation of a low-cycle fatigue crack. The calibrated formulation for 16mm diameter reinforcement is presented in Equation 7-2.

$$\varepsilon_{ap} = 0.08(2N_f)^{-0.5} \qquad \textbf{Equation 7-2}$$

In the context of earthquake engineering, equi-amplitude loading is an unlikely loading scenario. However, by using Miner's rule a summation of the damage accrued, in terms of a damage index, D_i, at different strain amplitudes can be undertaken to determine the amount of strain life that has been used (Miner, 1945). A damage index of unity represents failure due to low-cycle fatigue. Hence, if the strain history of the reinforcement is known, Equation 7-3 can be used to estimate the remaining low-cycle fatigue life.

$$D_{Total} = \sum_{i=1}^{n} D_i = \sum_{i=1}^{n} \frac{1}{N_{f,i}} = \sum_{i=1}^{n} 2\left(\frac{\varepsilon'_f}{\varepsilon_{ap}}\right)^{1/c} \qquad \textbf{Equation 7-3}$$

This subsection presents a comparison between the reinforcement strains, and the resulting damage indices, recorded in the slotted beam and traditional connection numerical models. Only data from connection Bm C/1-1 south has been presented for brevity; however, the data from the other connections was similar.

A comparison between the strain, and the resulting damage indices, from the top longitudinal reinforcement of the slotted beam and traditional connection numerical models is presented in

Figure 7-53 and Figure 7-54. A traditional reinforced concrete connection uses the top longitudinal reinforcement as the main tensile force component to create a negative moment. Whereas a reinforced concrete slotted beam connection uses the bottom longitudinal reinforcement in compression as the main force component to create a negative moment. Furthermore, because the top longitudinal reinforcement in a reinforced concrete slotted beam connection is twice as strong as the bottom longitudinal reinforcement, a greater force is required to cause strain in the top longitudinal reinforcement compared to that required in a traditional reinforced concrete connection. Hence, greater strain was observed in the top longitudinal reinforcement of the traditional connection. It can be seen that over course of testing the top longitudinal reinforcement in the traditional reinforced concrete connection reached approximately $0.9D_i$, whereas approximately $0.09\ D_i$ was recorded in the top longitudinal reinforcement of the reinforced concrete slotted beam connection.

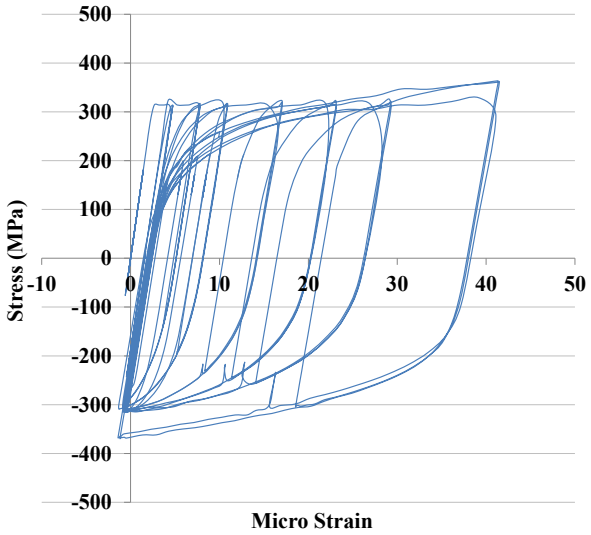

(a) Traditional connection stress-strain response.

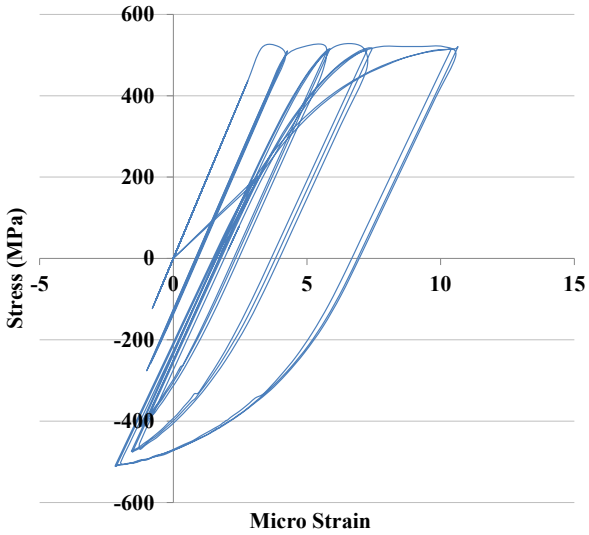

(b) Slotted beam connection stress-strain response.

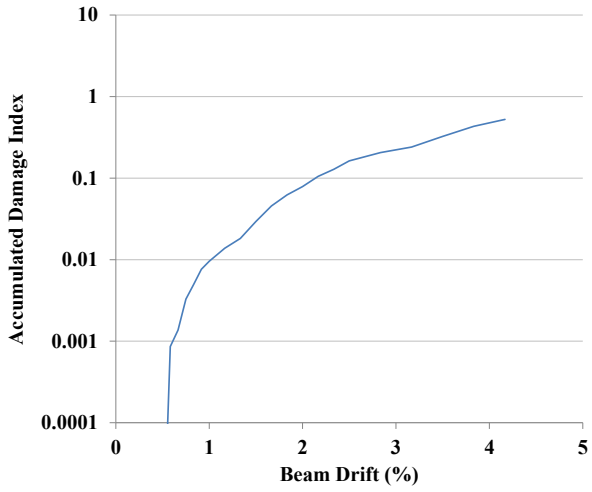

(c) Traditional connection damage index.

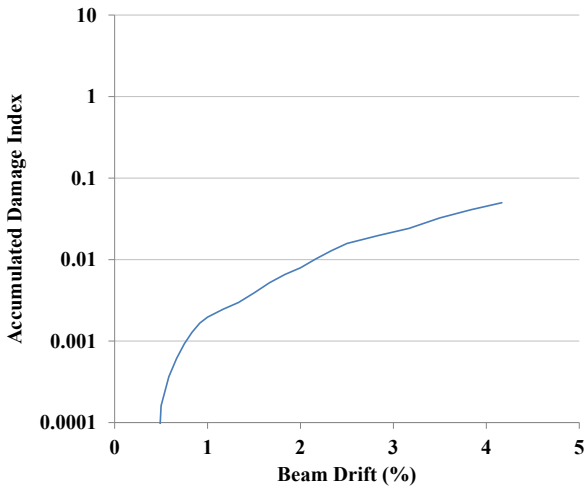

(d) Slotted beam connection damage index.

Figure 7-53: Comparison of upper top longitudinal reinforcement strain in north-south direction.

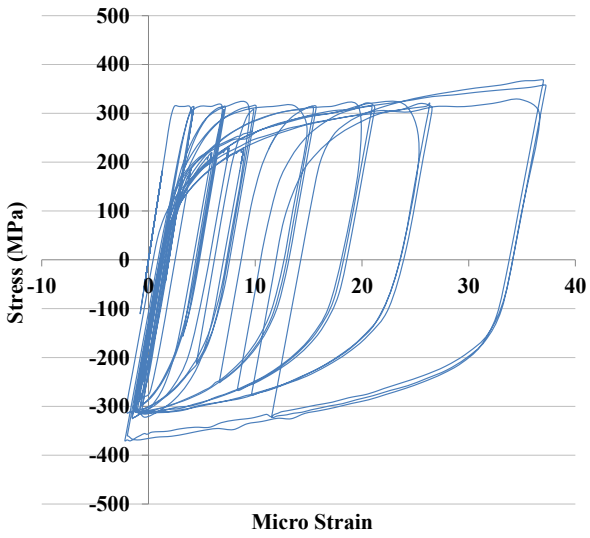

(a) Traditional connection stress-strain response.

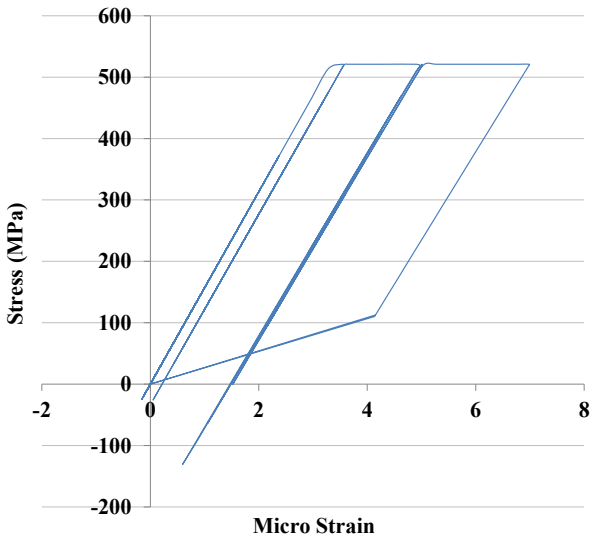

(b) Slotted beam connection stress-strain response.

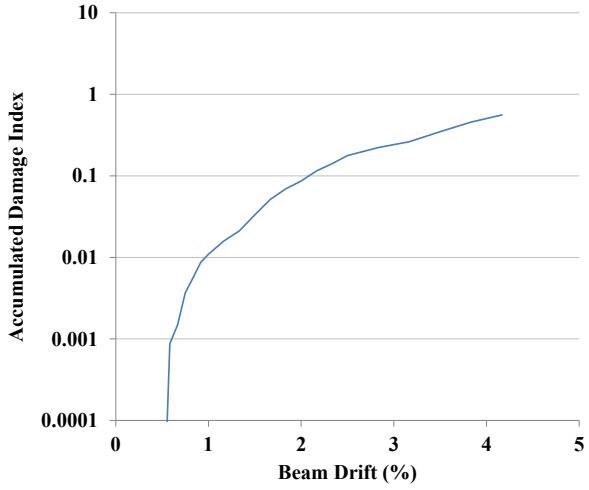

(c) Traditional connection damage index.

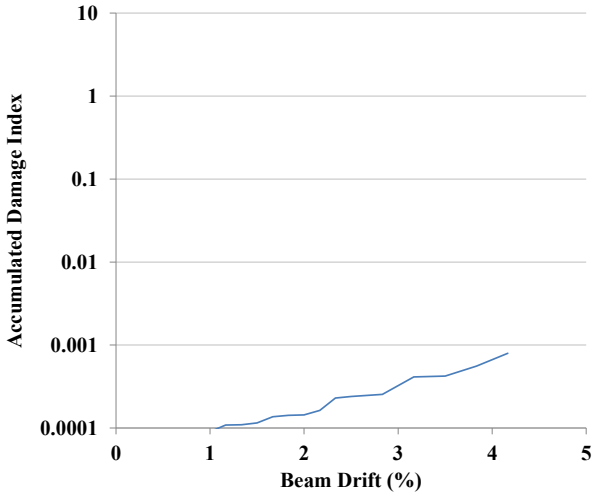

(d) Slotted beam connection damage index.

Figure 7-54: Comparison of lower top longitudinal reinforcement strain in north-south direction.

A comparison between the strain, and the resulting damage indices, from the bottom longitudinal reinforcement of the slotted beam and traditional connection numerical models, is presented in Figure 7-55 and Figure 7-56. The strain in the bottom longitudinal reinforcement of the traditional connection was similar to that observed in the top longitudinal reinforcement. Because the concrete surrounding the longitudinal reinforcement provided a preferential force path for compressive forces in the traditional connection, the bottom longitudinal reinforcement was not subjected to significant net compressive strain. Furthermore, due to the larger beam elongation exhibited by the traditional connection compared to the slotted beam connection, the peak tensile strains in the bottom longitudinal reinforcement were larger in the traditional beam connection also.

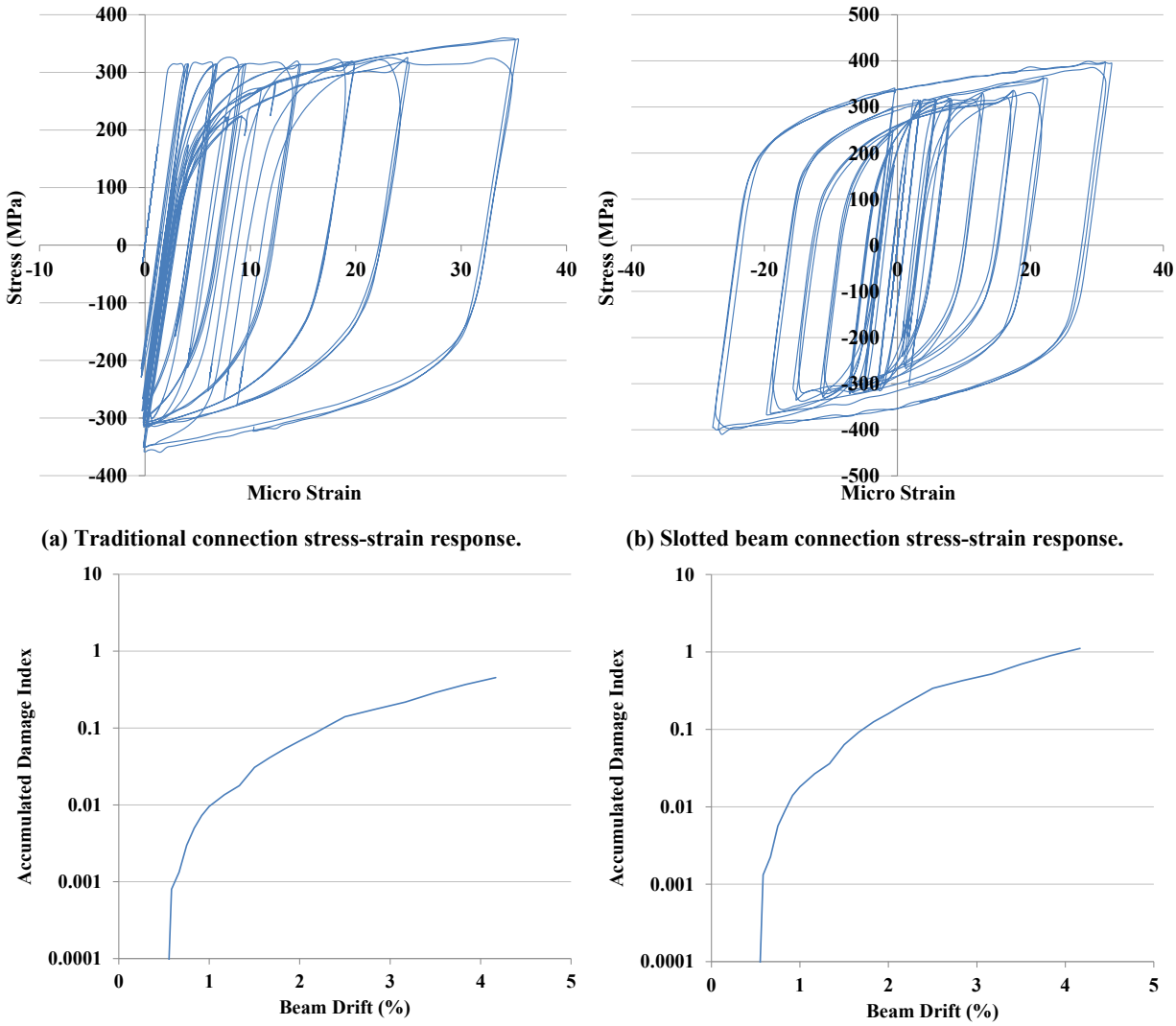

(a) Traditional connection stress-strain response.

(b) Slotted beam connection stress-strain response.

(c) Traditional connection damage index.

(d) Slotted beam connection damage index.

Figure 7-55: Comparison of upper bottom longitudinal reinforcement strain in north-south direction.

The bottom longitudinal reinforcement in the slotted beam connection was subjected to greater plastic strain compared to the traditional connection. This was because the bottom longitudinal reinforcement in a slotted beam connection is used in both tension and compression for positive and negative flexure respectively. Because the lever arm between the neutral axis and the bottom longitudinal reinforcement was larger in the slotted beam connection during positive flexure than it was during negative flexure, the maximum tensile strain recorded in the bottom longitudinal reinforcement was greater than the maximum compressive strain recorded. The accumulated damage index was larger for the slotted beam connection than it was for the traditional connection; however, the difference between the calculated indices for both connection types was relatively small. At the end of the test, the bottom longitudinal reinforcement of the slotted beam connection had reached an accumulated damage index of approximately $1.0D_i$, which indicated that low-cycle fatigue failure was imminent. The lower longitudinal reinforcement of the traditional reinforced

concrete connection reached an accumulated damage index of approximately $0.9D_i$ at the conclusion of the test, which was 10% less than that recorded in the slotted beam connection.

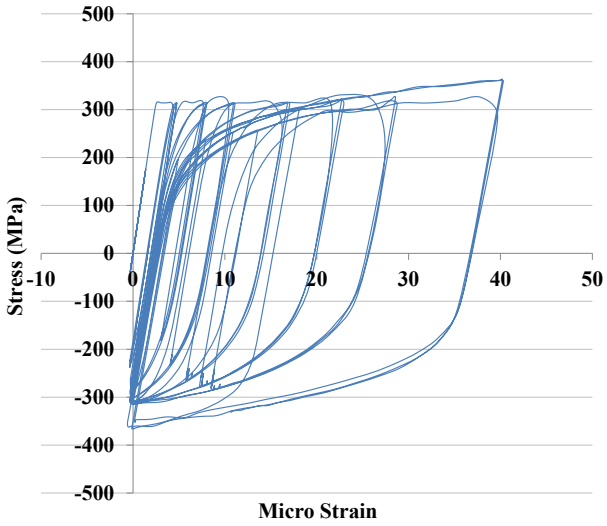

(a) Traditional connection stress-strain response.

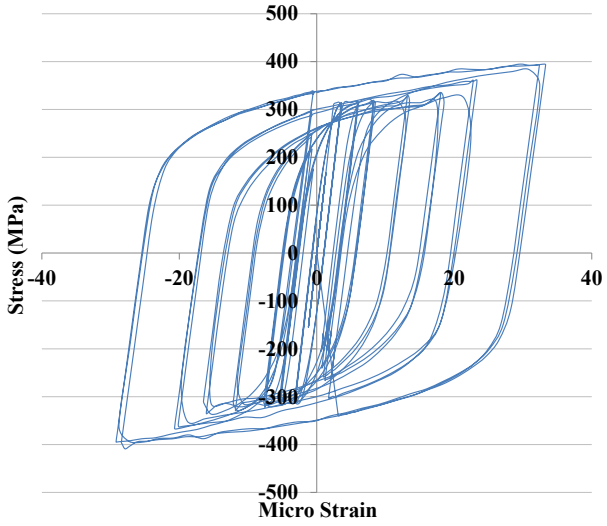

(b) Slotted beam connection stress-strain response.

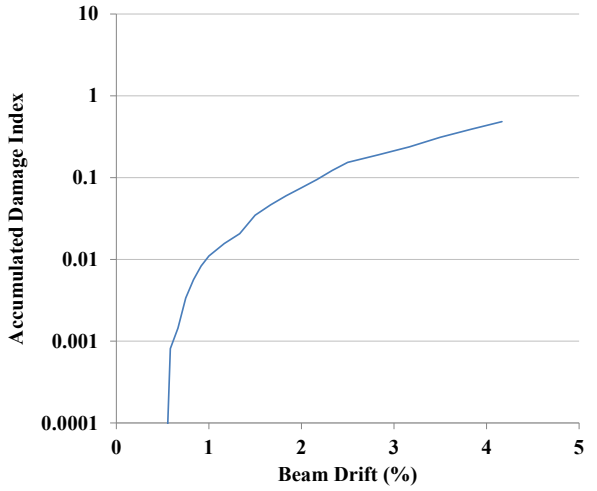

(c) Traditional connection damage index.

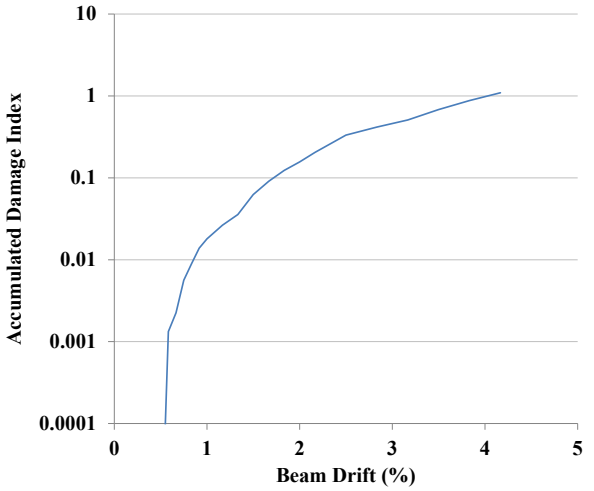

(d) Slotted beam connection damage index.

Figure 7-56: Comparison of lower bottom longitudinal reinforcement strain in north-south direction.

The top and bottom longitudinal reinforcement in the plastic hinge element were close to failure by way of low-cycle fatigue at the end of testing, whereas only the bottom longitudinal reinforcement in the R3D element was close to failure by way of low-cycle fatigue at the end of testing. The consequences of low-cycle fatigue occurring in either a slotted beam or traditional connection are undesirable; however, the consequences are worse in the traditional reinforced concrete connection. Fracture of the longitudinal reinforcement in a traditional connection would cause not only a dramatic reduction in moment capacity, but also a reduction in the shear and torsional capacity of the connection. Furthermore, rehabilitating a traditional connection following fracture of the longitudinal reinforcement would be challenging. If the bottom unbonded longitudinal reinforcement in a slotted beam were to fail then the moment capacity of the connection would be dramatically reduced, however, the shear and torsional capacity of the connection would remain unchanged. Furthermore, it was

shown in Chapter 5 that a slotted beam that had sustained low-cycle fatigue failure of the bottom longitudinal reinforcement could be effectively and economically retrofitted.

As previously stated, a direct comparison between the torsional responses of each numerical model was not able to be undertaken because the plastic hinge element is not able to model torsion well (Peng, 2009). Figure 7-57 presents the strain data recorded in the diagonal hangers of the R3D element during testing. Plasticity initiated in the outside diagonal hanger of the connection between 2.5% and 3.5% beam drift. The strain data from the R3D element was comparable to that measured in the diagonal hangers of SA1, which gave confidence not only to the ability of the R3D element to model slotted beam torsion, but also to the floor diaphragm model to represent floor continuity moments. Despite the onset of plasticity in the diagonal hangers, the accumulated damage indices were relatively low. The peak accumulated damage index calculated for the diagonal hangers was approximately $0.2D_i$.

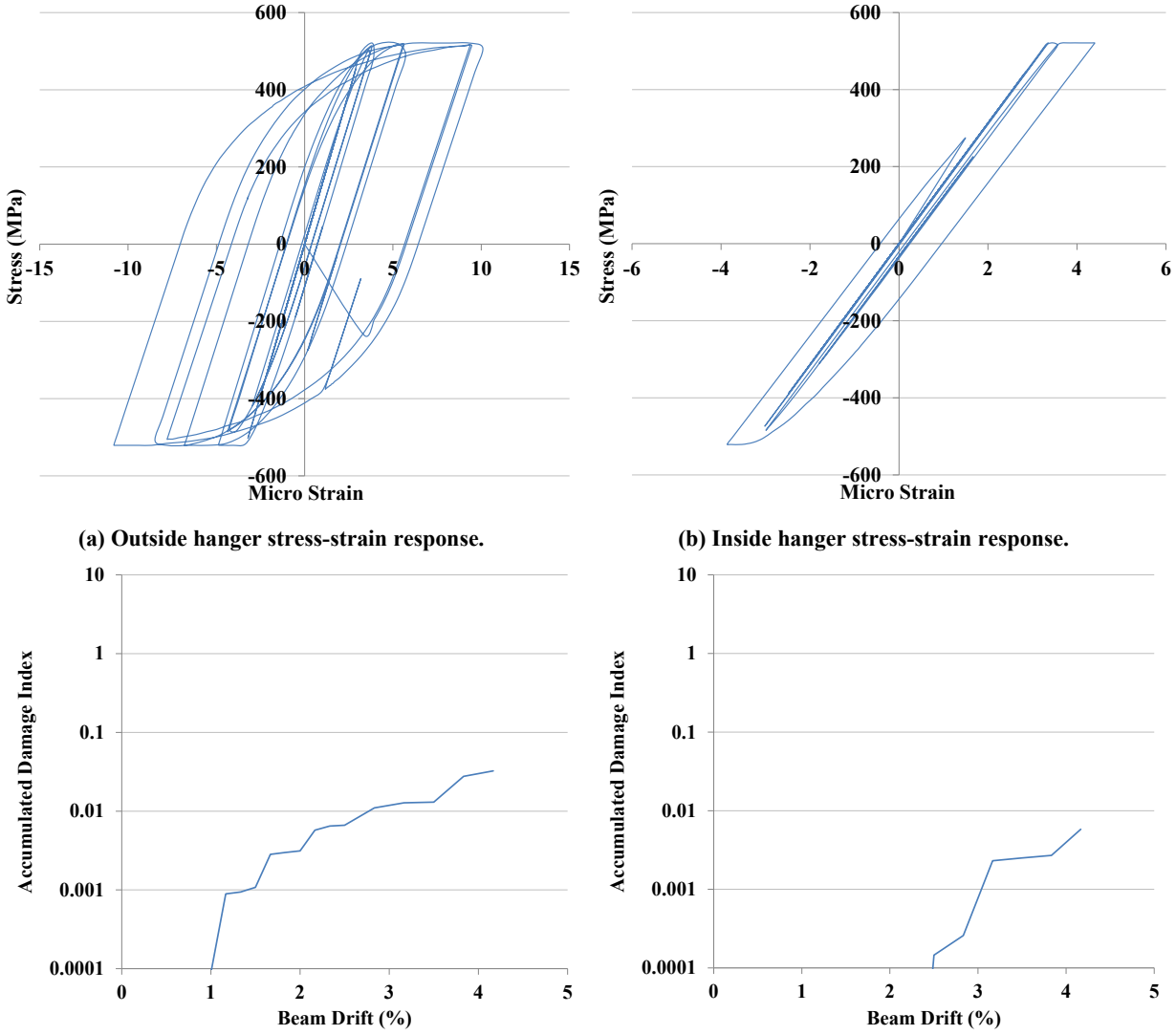

(a) Outside hanger stress-strain response.

(b) Inside hanger stress-strain response.

(c) Outside hanger damage index.

(d) Inside hanger damage index.

Figure 7-57: Comparison of diagonal hanger reinforcement strain in north-south direction.

If the diagonal hangers and top longitudinal reinforcement in a reinforced concrete slotted beam connection are pragmatically designed, they are likely to be capable of withstanding several survivability limit state earthquakes before succumbing to low-cycle fatigue failure. However, the damage indices computed from the numerical model show that the bottom longitudinal reinforcement of a slotted beam is not capable of withstanding two survivability limit state earthquakes without low-cycle fatigue failure occurring. It is possible that the bottom longitudinal reinforcement of a reinforced concrete slotted beam connection has sufficient strain capacity to withstand a damage limit state earthquake and a survivability limit state earthquake.

Current methods for investigating low-cycle fatigue in reinforcement are not ideal because the strain history of the reinforcement must be known. Generally, the displacement that occurs in a structure during an earthquake is unknown, which introduces significant uncertainty into the appraisal of the remaining strain capacity of the reinforcement. However, if the strain history of the reinforcement which is being investigated is known, as is the case in experimental investigations, then a reasonable estimate of the remaining strain capacity is able to be determined using the methods described in this subsection.

7.6 Comparison between the Overall Structural Response of Slotted Beam and Traditional Connection Systems

Section 7.5 describes an investigation that compared the behaviour of slotted beam and traditional reinforced concrete connections, which provided valuable insight about the behaviour of the respective connections. However, perhaps more important than connection behaviour is the effect that the connection behaviour has on the overall structural response of a building during an earthquake.

This section describes a comparison between the overall structural response of a reinforced concrete slotted beam building and a traditional reinforced concrete building. Two numerical models of a prototype building were assembled using R3D elements and plastic hinge elements. The numerical models were subjected to a suite of recorded earthquake records.

7.6.1 Selection and Scaling of Earthquake Records

The nonlinear time history (NLTH) analyses described in this section were performed in accordance with NZS1170.5:2004 (Standards New Zealand, 2004). The earthquake records selected were from stations that had similar soil conditions to the prototype building. Because the prototype building was designed to be subject to near field earthquake effects, three earthquake records that featured directionality were included in the suite of six earthquake

records that were applied to the numerical models. Because the NLTH analyses were conducted in three dimensions, both principal components of each earthquake record were required. Each component of every earthquake record was applied to both horizontal axes of the numerical models, as well as at 45° to the horizontal axes. The vertical acceleration component of the earthquake records was omitted from the analyses because the prototype structure was not considered vertically sensitive.

The earthquake records were scaled to a damage avoidance level earthquake event in accordance with NZS1170.5 (Standards New Zealand, 2004; Priestley et al., 2007). NZS1170.5 requires a scale factor k_1 to be determined, which minimises the error in a root mean square sense of the log of the ratio of the scaled spectral acceleration ($SA_{component}$) and the target spectral acceleration (SA_{target}) over the period range of interest (T_1) (Standards New Zealand, 2004). This relationship is expressed more concisely is Equation 7-4. A family scale factor k_2 is required to ensure that at least one earthquake record in the suite exceeds the target spectrum. As shown in Equation 7-5, the k_2 factor is defined as the maximum value of a ratio of the target spectral acceleration to the maximum principal component of every earthquake record in the suite ($\max(SA_{principal})$) over the period range of interest.

$$error = \sqrt{\sum_{1.3T_1}^{i=0.4T_1} \log\left(\frac{k_1 SA_{component,i}}{SA_{target,i}}\right)} \qquad \text{Equation 7-4}$$

$$k_2 = \max_{0.4 \le T_1 \le 1.3} \frac{SA_{target}}{max(SA_{principal})} \qquad \text{Equation 7-5}$$

It is impossible to compare the response of two building that have been subjected to different input excitations. This is because the differences in building response attributable to connection performance and input energy cannot be decoupled. Hence, the fundamental translational periods along each axis, which were used to scale the suite of earthquake records, were an average of the fundamental periods of the slotted beam and traditional reinforced concrete connection versions of the numerical model of the prototype building. The averaged fundamental translational periods were 0.48sec and 0.45sec in the north-south and east-west directions respectively. A summary of the earthquake records used, and the scale factors applied to the earthquake records, is presented in Table 7-2. The prototype structure presented in Section 3.3 was relatively stiff due to the relatively small interstorey heights and bay lengths, which were a consequence of the maximum specimen size that could be fit into the laboratory.

Table 7-2: Earthquake records used and scale factors applied.

Location	Date	M_w	Duration	Distance	Depth	NF	Component	Scale Factor	
								EW	NS
El Centro, USA	19/5/1940	7.0	63.48s	6km	10km	N	Primary	1.08	1.03
							Secondary	1.58	1.50
La Union, Mexico	19/9/1985	8.1	72.94s	16km	15km	N	Primary	1.89	1.86
							Secondary	2.00	1.99
Hokkaido, Japan	26/9/2003	8.3	78.00s	46km	33km	N	Primary	1.21	1.14
							Secondary	1.39	1.35
Duzce, Turkey	12/11/1999	7.2	25.90s	1km	10km	Y	Primary	0.74	0.72
							Secondary	0.79	0.76
Tabas, Iran	16/9/1978	7.4	73.44s	2km	5km	Y	Primary	0.40	0.40
							Secondary	0.49	0.50
Lucerne, USA	28/6/1992	7.3	48.13s	44km	5km	Y	Primary	1.06	1.05
							Secondary	1.26	1.30

It was concluded in Chapter 4 that because the elastic stiffness of a slotted beam is comparable to that of an equivalent traditional reinforced concrete connection, the effective stiffness factors specified in §C6.9.1 of NZS3101:2006 can be applied to the design and analysis of slotted beams (Standards New Zealand, 2006). However, effective stiffness factors need only be applied when the connection stiffness is determined based on gross section dimensions. When more advanced methods of modelling the behaviour of a reinforced concrete slotted beam are used, such as the R3D element, the effective second moment of area of the connection is calculated based on the area and position of each constituent spring; therefore, effective stiffness factors should not be applied to the beams in an analysis.

The scaled and unscaled spectral acceleration plots of the earthquake records used in Section 7.6.2 are presented in Figure 7-58. The scaled earthquake records do not exactly match the target spectral acceleration at the fundamental translational periods of the prototype building. Instead, the earthquake records were scaled to be as close to the target spectral acceleration as possible over a range between 40% and 130% of the fundamental periods.

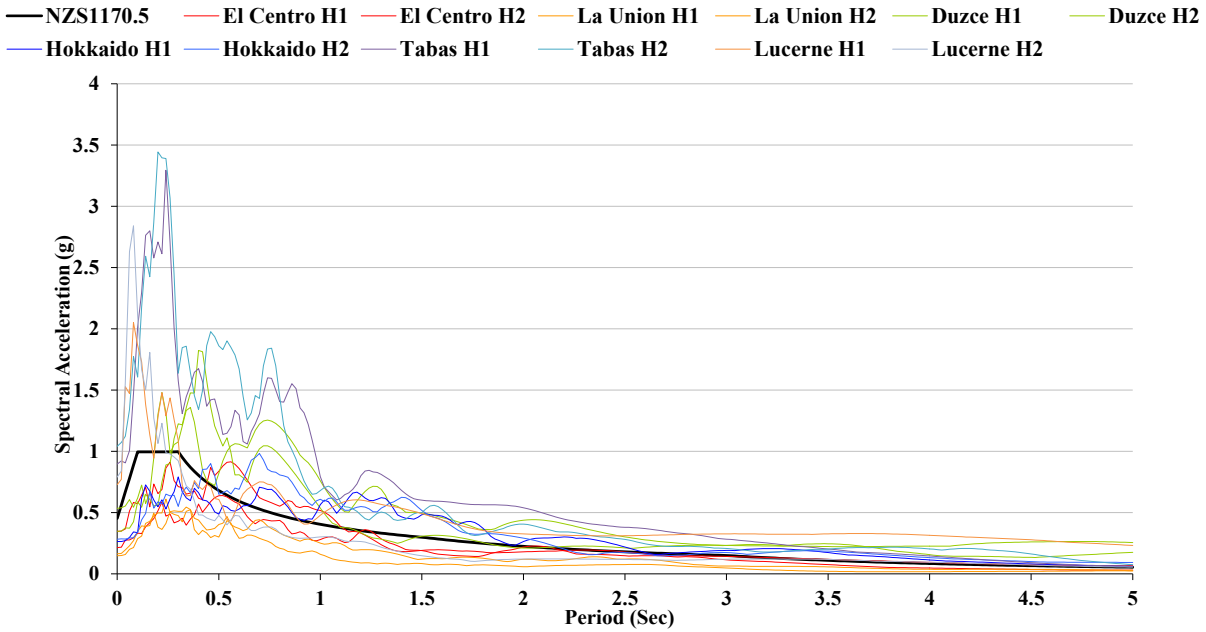

(a) Unscaled records.

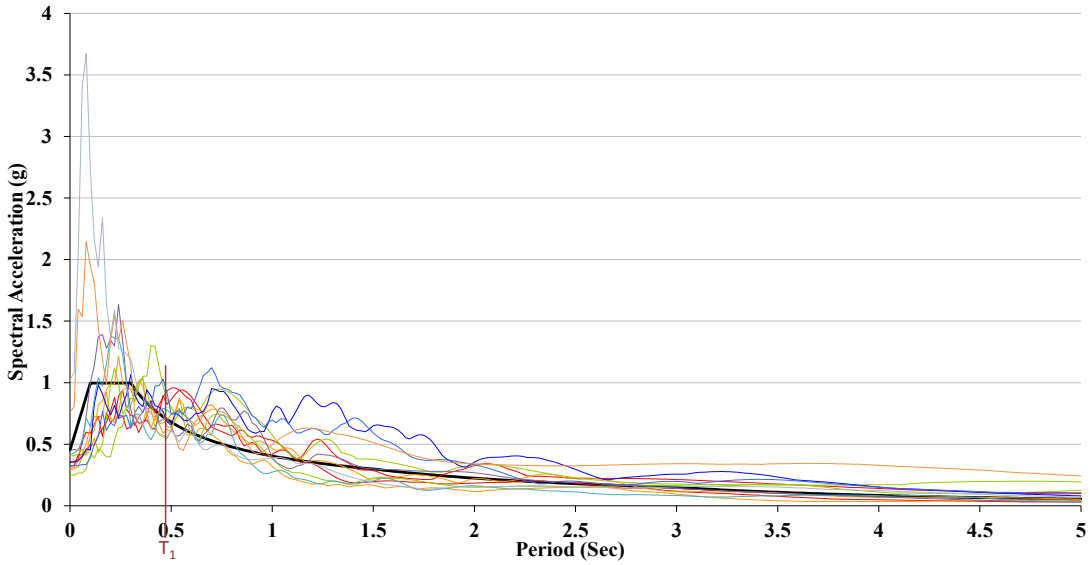

(b) Scaled for x direction fundamental period.

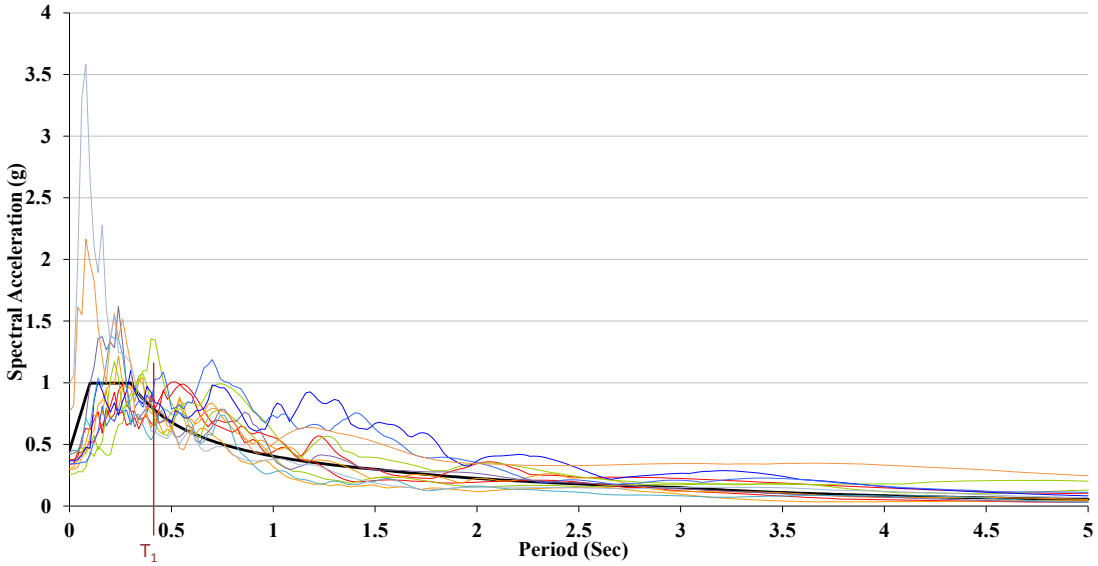

(c) Scaled for z direction fundamental period.

Figure 7-58: Spectral acceleration of earthquake records.

7.6.2 Prototype Building Numerical Models

To investigate the differences in overall structural response during an earthquake between buildings with reinforced concrete slotted beam connections and traditional reinforced concrete connections, two numerical models were assembled. The building used as the basis of the investigation was the seven storey prototype building described in Section 3.3. The numerical models developed in this chapter were used to model the entire structure at full scale. R3D elements were used to model the reinforced concrete slotted beam connections in the slotted beam version of the numerical prototype building model. Plastic hinge elements were used to model the traditional reinforced concrete connections in the traditional beam version of the numerical prototype building model (Peng, 2009). The R3D and plastic hinge numerical elements were designed to have the same yield moments, as described in Section 7.5 (Peng, 2009). The numerical floor diaphragm model used in both versions of the numerical prototype building model was a full scale version of that developed in Section 7.4.2.2. The assembled numerical prototype building model and rendering of the prototype building are presented in Figure 7-59(a) and (b) respectively. The suite of earthquakes described in Section 7.6.1 was applied to both numerical prototype building models, and several performance parameters were extracted from the output.

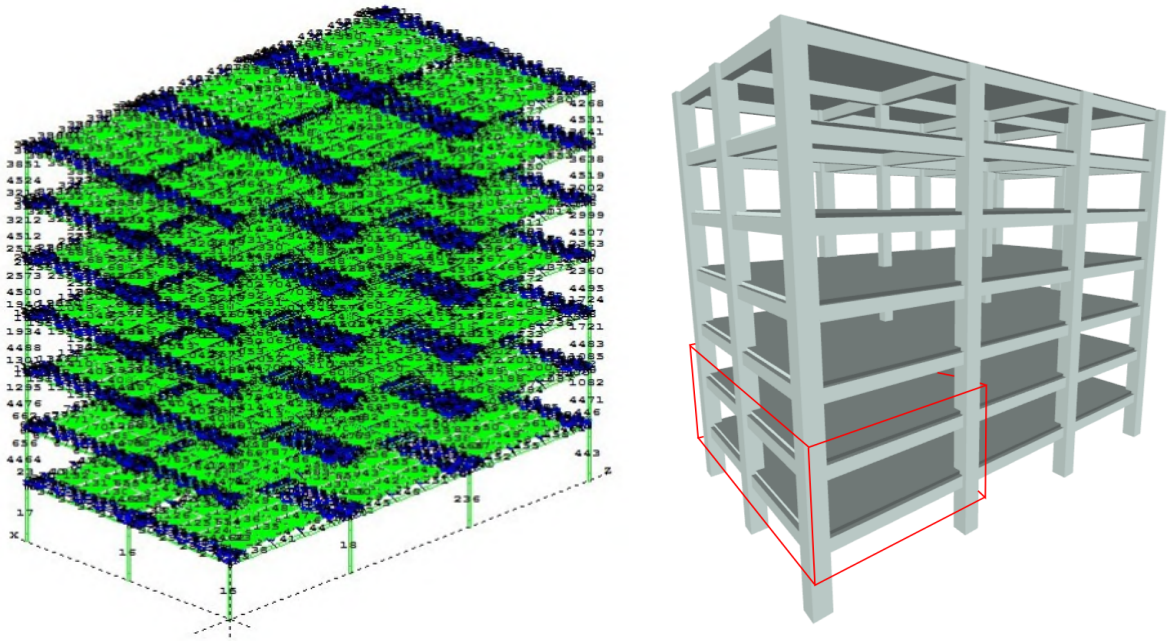

(a) Isometric of view Ruaumoko3D model of prototype structure.

(b) Isometric view rendering of prototype structure, with location of superassembly SA1 highlighted.

Figure 7-59: Numerical model of prototype structure.

7.6.3 Prototype Building Seismic Response

This section presents a comparison between the structural response of the slotted beam and traditional connection numerical models of the prototype building presented in Section 3.3. The numerical models were subjected to the El Centro earthquake record applied at 45° to the

principal horizontal axes of the models. Meaningful conclusions are difficult to draw from one earthquake record; hence, this section was intended only as an example of observed performance of the two structural systems. The aggregated results from the entire suite of earthquake records are presented in Section 7.6.4.

Figure 7-60 presents a comparison between the displacements of the top storey of the slotted beam and traditional connection numerical models. In general, the displacement traces were relatively similar; however, the slotted beam numerical model displays greater displacement in the north-south (x) direction, whilst the traditional connection numerical model displays greater displacement in the east-west direction (z). The differences between the displacement traces of the two versions of the numerical prototype building model highlighted how sensitive the response of nonlinear systems is to earthquake records.

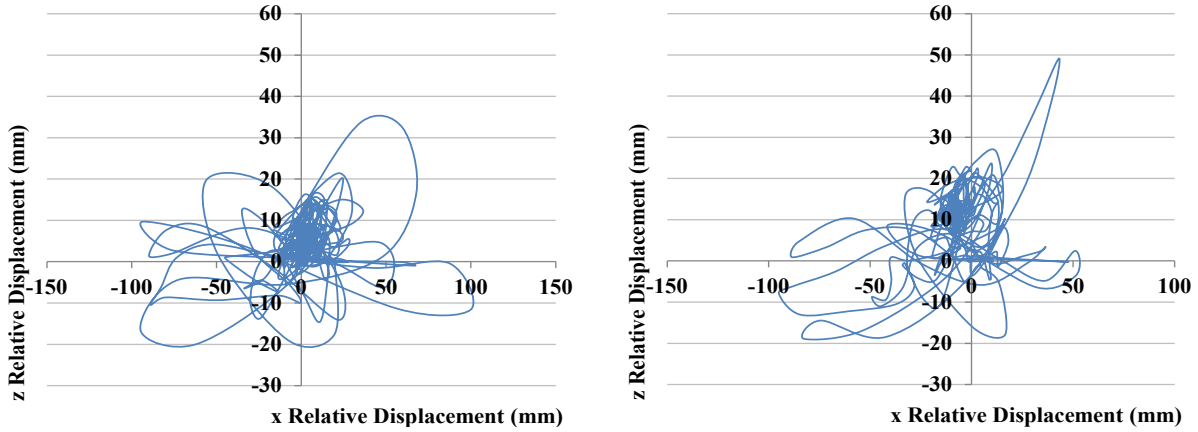

(a) Slotted beam connection structure. (b) Traditional connection structure.

Figure 7-60: Building top displacement during biaxial 45° El Centro earthquake record.

Figure 7-61 presents a comparison of the total force-displacement response of the slotted beam and traditional connection numerical models. The peak base shear generated by both numerical models was relatively similar; however, the response of the slotted beam connection numerical model was more symmetric than the traditional connection numerical model.

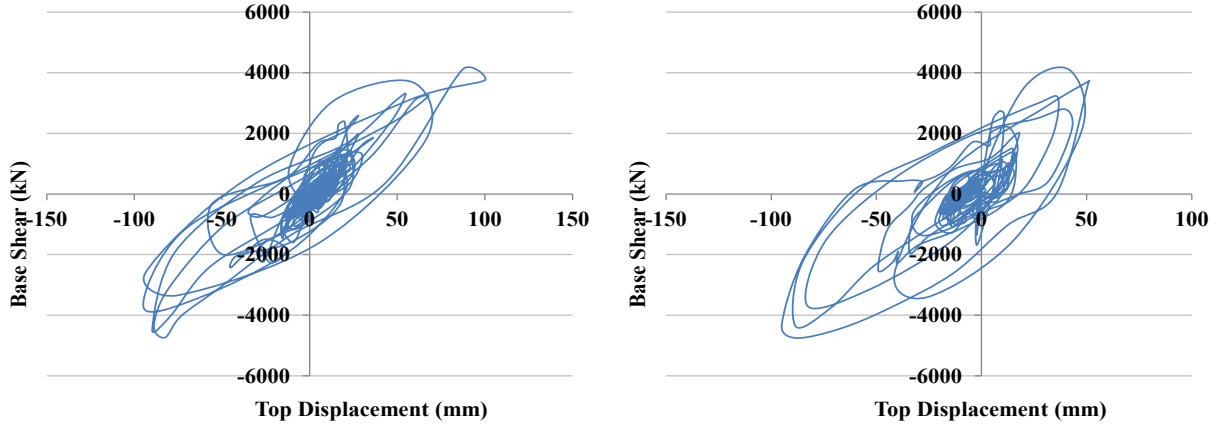

(a) Slotted beam connection structure. (b) Traditional connection structure.

Figure 7-61: Base shear vs structure top displacement in north-south direction during biaxial 45° El Centro earthquake record.

Figure 7-62 presents a comparison of the moments generated in a Level One exterior connection of the slotted beam and traditional connection numerical models. The moment generated in the Level One exterior connection of the slotted beam connection numerical model was greater than that generated in the traditional connection numerical model. This observation highlighted the difficulty in comparing the response of complex nonlinear structures. As shown in Figure 7-61, the total lateral resistance of the two versions of the numerical prototype building model were relatively similar. For this to occur, greater moment resistance must have been generated in other connections in the traditional connection numerical model compared to the slotted beam connection numerical model. Hence, the displacement profiles over the height of the two numerical models during response to the earthquake record must have been different.

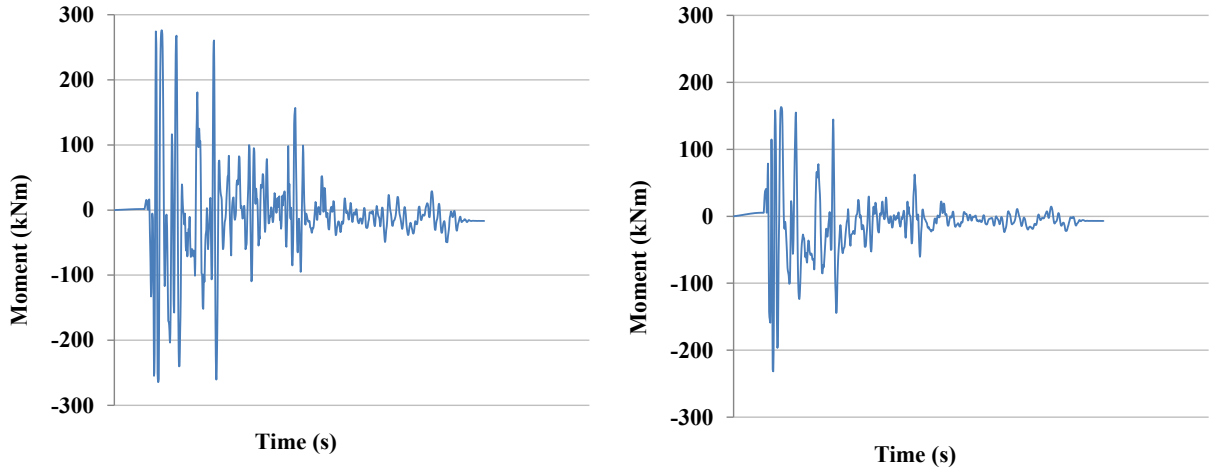

(a) Slotted beam connection structure. **(b) Traditional connection structure.**

Figure 7-62: Moment response of first floor exterior beam-column connection during biaxial 45° El Centro earthquake record.

Figure 7-63 presents a comparison of the axial force generated in the Level One east-west beam of the slotted beam and traditional connection numerical models. Significantly greater axial force was recorded in the beam of the traditional connection model compared to the slotted beam model. Axial forces were induced in the beams of the numerical model because the elongation of the beams was restrained by the floor diaphragm. The beam elongation in the traditional connection model was larger than that in the slotted beam model; hence, greater axial force was generated in the beams of the traditional connection model. First floor effects could have also contributed to the axial forces in the beams of the numerical models. First floor effects are discussed in Section 7.6.4.

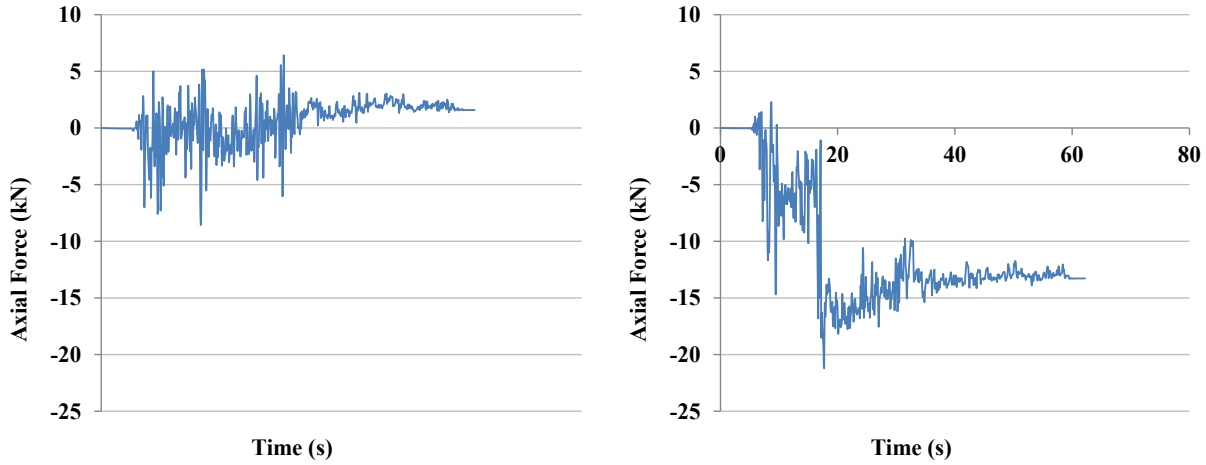

(a) Slotted beam connection structure. **(b) Traditional connection structure.**

Figure 7-63: Level One east-west beam axial force during biaxial 45° El Centro earthquake record.

Comparing the response of two or more different nonlinear systems is extremely difficult due to the path dependence of the response of the systems. Furthermore, due to the random nature of earthquakes, predicting the performance of a system in a future earthquake based on the observed response during an historical earthquake record is unreliable. Hence, to be able to make meaningful observations regarding the response of nonlinear systems during an earthquake, many analyses must be undertaken using a variety of historical earthquake records, and then statistical methods employed to identify common trends across the collected data.

7.6.4 Overall Structural Seismic Response

This section presents the aggregated results from the 36 NLTH analyses undertaken on the slotted beam and traditional connection numerical prototype building models. The results were enveloped using the average (mean) method, rather than the sum of the root mean squared (RMS) method that is more typical when enveloping of NLTH results. The RMS method yields conservative response envelopes that are appropriate for design. However, because the actual response of the numerical prototype building models was of interest, the average (mean) method was a more appropriate method to use to envelope the results.

The total computational time required to analyse the 36 unique numerical models was five weeks. This level of computational efficiency was tolerable for research purposes; however, it may not be appropriate for design. The time required to analyse the numerical models could have been reduced by altering how damping was modelled, reducing the number of degrees of freedom in the models or by using a 64 bit version of the analysis software. At the time of writing, the latter was currently under development by Professor Athol Carr, University of Canterbury.

Figure 7-64 presents a comparison between the peak floor displacements recorded over the height of the slotted beam and traditional connection numerical prototype building models. It can be seen that the displacement profiles of the two numerical models was different along each of the principal horizontal axes. The peak floor displacements in the east-west direction were concentrated over the first three levels, whilst in the north-south direction the peak floor displacements were more evenly distributed over the height of the models. The numerical prototype building model used in the NLTH analyses was asymmetrical in plan; hence, an asymmetric peak floor displacement profile was recorded between the principal horizontal axes.

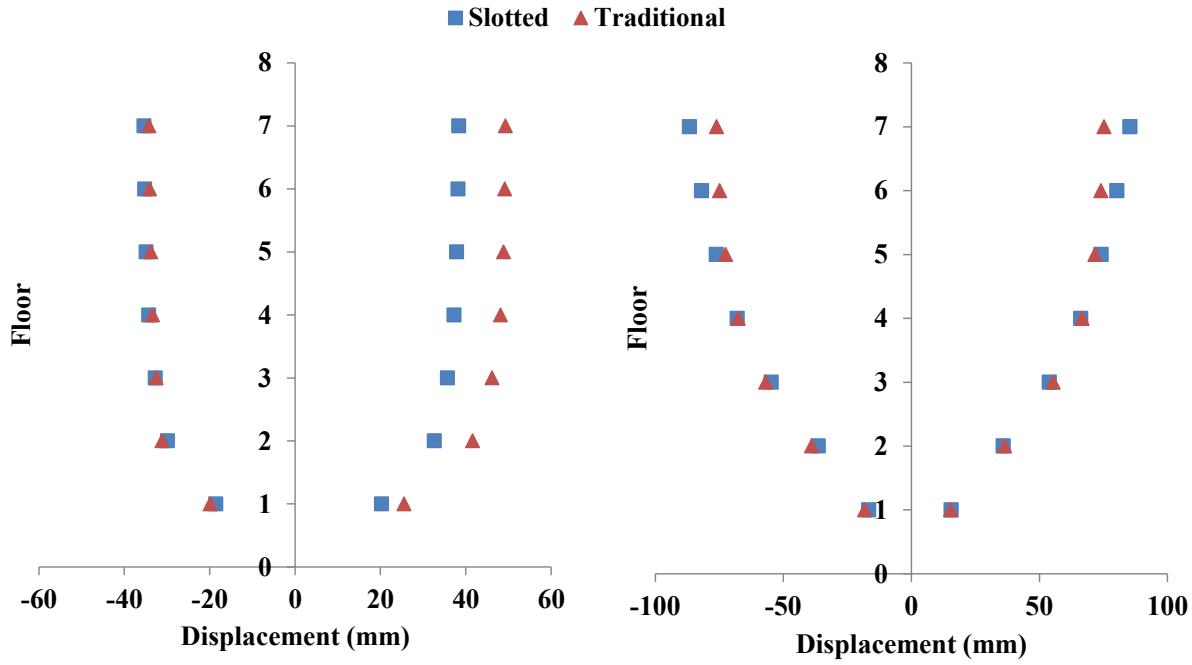

(a) East-west direction. (b) North-south direction.

Figure 7-64: Building relative displacement over height.

In general, the peak displacements recorded in the slotted beam and traditional connection numerical prototype building models was relatively similar; however, in the east-west direction the traditional connection numerical model exhibited larger maximum peak displacements than the slotted beam connection numerical model. As shown in Section 7.5.1, when reinforced concrete slotted beam and traditional connections were designed to have the same yield moment capacity, the slotted beam connection exhibited greater hysteretic energy dissipation than the traditional connection. The additional hysteretic energy dissipation in the slotted beam connection compared to the traditional connection was due to the contribution of the top longitudinal reinforcement to connection flexure. Increased energy dissipation in a structural system results in reduced structural displacements during an earthquake. Over the lower halves of the numerical prototype building models, the maximum peak displacements in the traditional connection model were greater than those in the slotted beam connection

model. This was caused by the increased beam elongation that was recorded in the traditional connection model compared to the slotted beam connection model. The interstorey drifts recorded in both versions of the numerical prototype building models were relatively low. NZS1170.5 allows for peak interstorey drifts of up to 2.5% in a design level earthquake (Standards New Zealand, 2004). The peak interstorey drifts recorded in both versions of the numerical model were within this limit.

As shown in Figure 7-65, the slotted beam connection numerical model exhibited greater peak floor accelerations over the height of the model compared to the traditional connection numerical model. The increased floor accelerations recorded in the slotted beam connection numerical model were due to the flexural stiffness of the slotted beam connection being greater than that of the traditional connection. The slotted beam connections had a greater flexural stiffness than the traditional connections due to the contribution of the top longitudinal reinforcement to slotted beam connection flexure. Large floor accelerations are undesirable in buildings during an earthquake due to the harm that can occur to occupants and the damage that non-structural components can sustain.

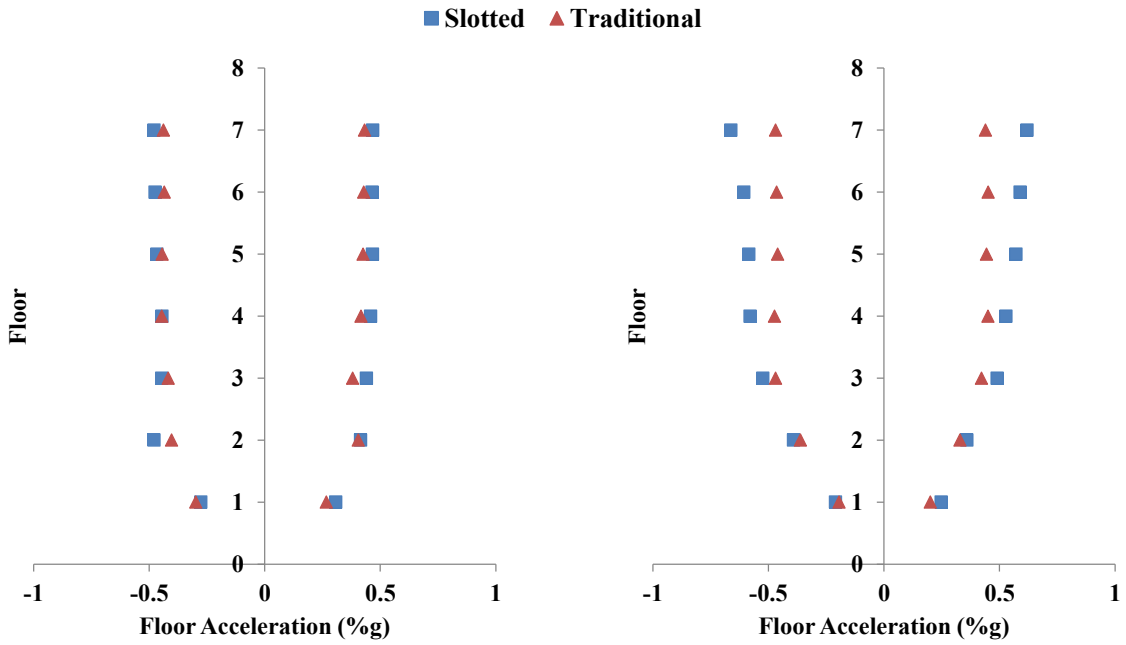

(a) East-west direction. **(b) North-south direction.**

Figure 7-65: Peak floor acceleration over height.

Figure 7-66 presents a comparison between the residual axial beam force recorded over the height of the slotted beam and traditional connection numerical prototype building models. Less beam elongation was exhibited by the slotted beam connections compared to the traditional connections; hence, the residual beam axial forces in the slotted beam numerical model were less than those in the traditional connection numerical model. Furthermore, the spike in residual axial force in the first floor beams that occurred in the traditional connection

model did not occur in the slotted beam model. The spike in residual axial force in the first floor beams was caused by first floor effects. First floor effects are caused when beam elongation in the first floor beams is resisted not only by the floor diaphragm, but also by the ground floor columns. First floor effects have two main influences on structural behaviour. The first effect is that beam axial forces increase the flexural capacity of traditional reinforced concrete connections, which increases the overstrength demands on other structural components. This effect is less significant in systems that use the slotted beam detail because the flexural capacity of slotted beam connections is less sensitive to axial force. The second effect is that that the increased flexural demands in the ground floor columns can cause plastic hinges to form below the first floor beams, as well as at ground level. Hence, first floor effects can cause the force distribution in a structural system to be significantly different to what the designer intended.

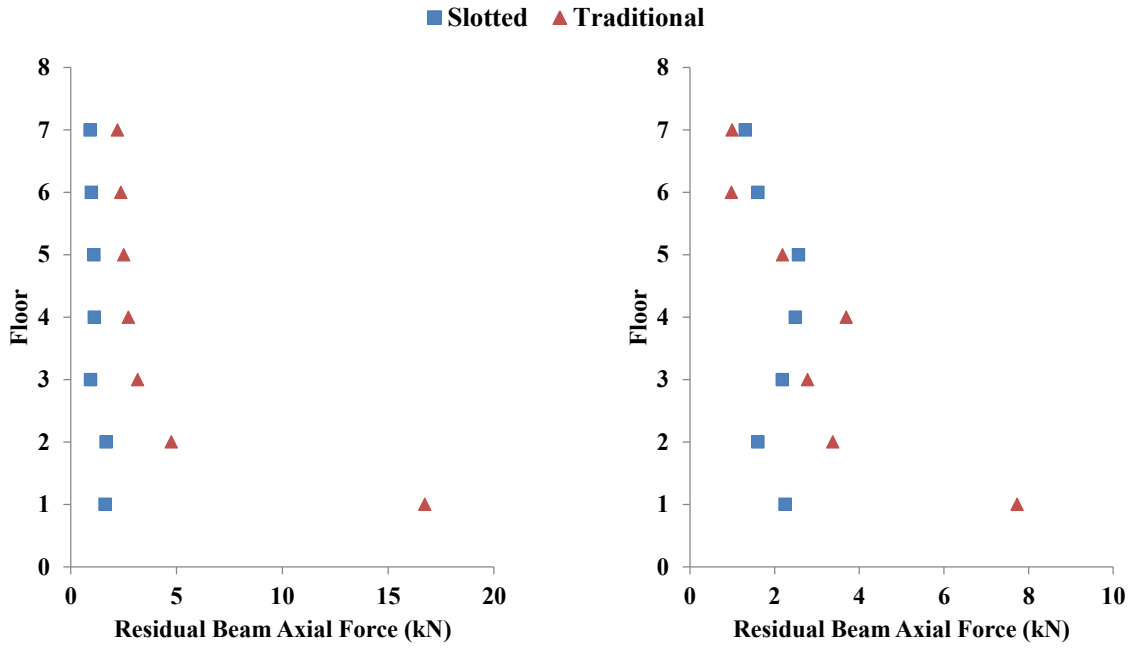

(a) East-west direction. (b) North-south direction.

Figure 7-66: Residual beam axial force over height.

Residual displacements in a structure following an earthquake are undesirable because they can not only decrease the capacity of the structure to withstand future seismic events, but they can also impose severe serviceability issues for the occupants. Figure 7-67 presents the residual interstorey drifts that were recorded in both versions of the numerical prototype building models. The slotted beam connection numerical model exhibited less residual displacement after an earthquake than did the traditional connection numerical model. This was likely due to the ability of slotted beam connections to maintain relatively constant post-yield and unloading stiffness during flexural response.

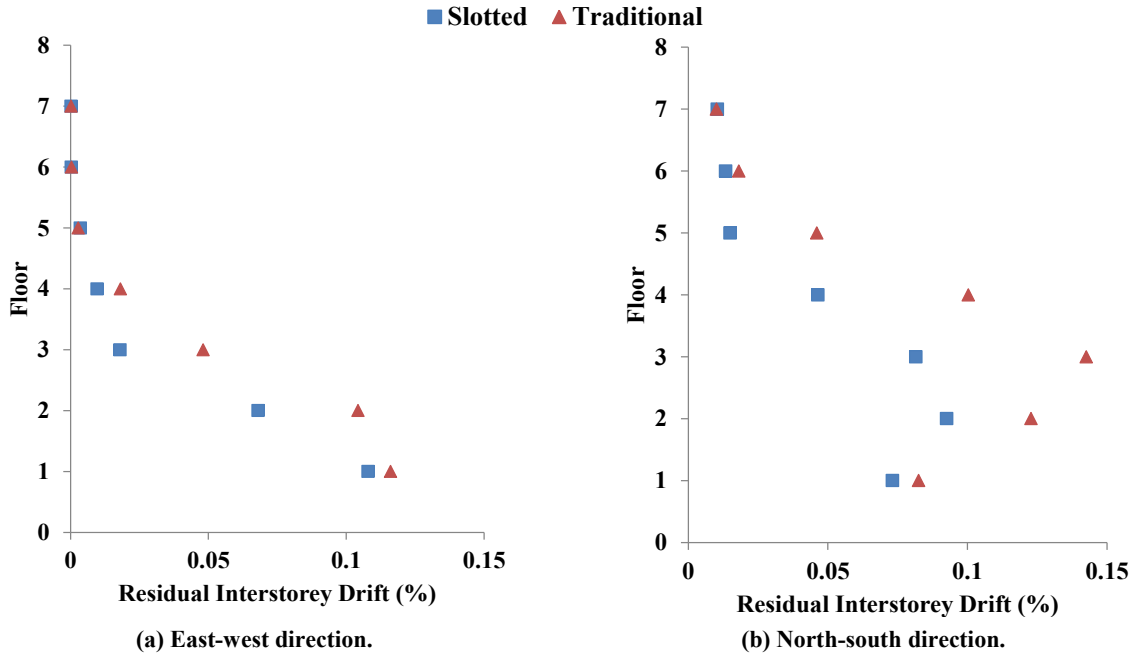

(a) East-west direction. (b) North-south direction.

Figure 7-67: Residual interstorey drift over height.

Figure 7-68 presents residual displacement of the floors over the height of the numerical models. Figure 7-68 and Figure 7-67 are based on the same data; however, Figure 7-68 highlights how residual displacements in a structure following an earthquake can decrease the ability of the structure to withstand future earthquakes by increasing P-delta effects. P-delta effects are induced in a structure when the centre of mass of the building is eccentric to the vertical centre of resistance, which creates a global overturning moment. The distance between the centre of mass and the vertical centre of resistance in the numerical models is presented in Figure 7-68 as the distance that the floors are from the origin. If a portion of the lateral resistance of a structure is used to resist P-delta effects, then there is a reduced capacity available to resist loads imposed by lateral loading.

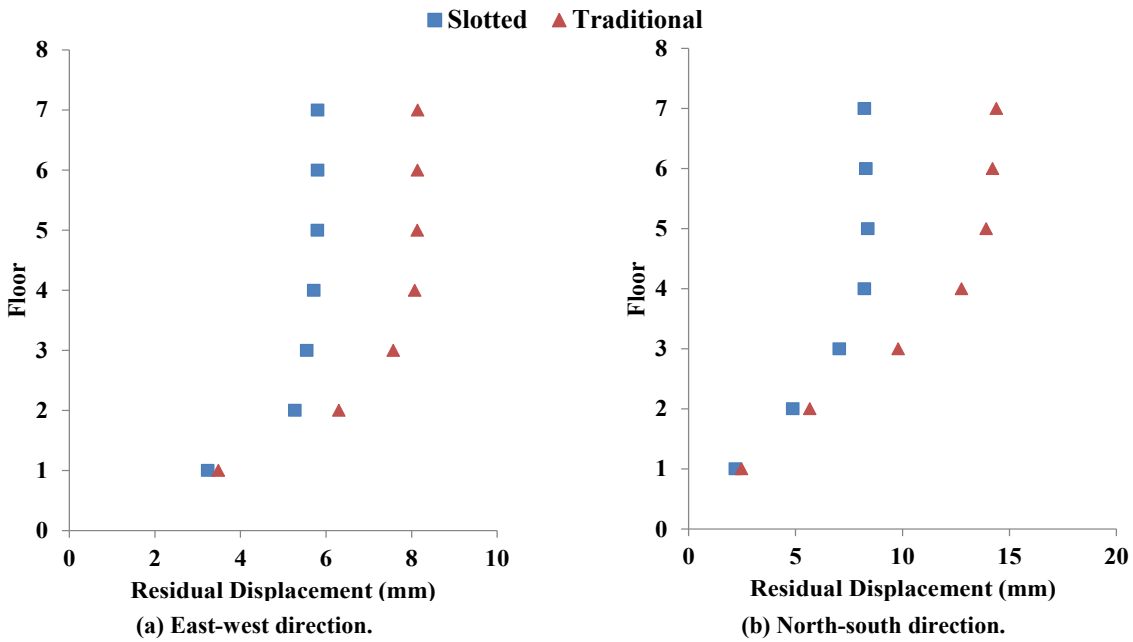

(a) East-west direction. (b) North-south direction.

Figure 7-68: Residual floor displacement over height.

The results of NLTH analyses undertaken on slotted beam and traditional connection versions of a numerical model of a prototype building have shown that the responses of the comparable slotted beam and traditional connection structures during earthquakes are relatively similar. However, compared to the traditional connection version of the numerical model, the slotted beam numerical model exhibited smaller peak and residual structural displacements, smaller induced axial beam forces and larger floor accelerations.

7.7 Conclusions

Existing two-dimensional numerical models of the slotted beam were expanded into three dimensions using various modelling techniques. The newly developed three-dimensional numerical models represented slotted beam behaviour well; however, the knowledge and time required to set the model up would have presented a barrier to implementation. Hence, a three-dimensional slotted beam multispring element (R3D) was developed to accurately represent slotted beam response, whilst being able to be set up with only gross section dimensions and material properties. A sensitivity study on the effect that varying the input parameters of the R3D element had on response was undertaken, and the following observations were made.

1. Provided an appropriate integration time-step is used originally, reducing the time-step had little effect on the recorded response of the R3D element. It is suggested that an appropriate time-step to use is that which yields a change in displacement of less than 0.4mm between the integration time-steps.
2. The response of the R3D element was sensitive to the height of the beam slot, the position of the top longitudinal reinforcement within the top hinge and the unbonded length applied to the bottom longitudinal reinforcement.
3. The response of the R3D element was not sensitive to the distribution of the concrete springs within the top hinge, the strength of the concrete diagonal shear springs or the overall element length.

The response of the R3D element was validated against the experimentally observed results from the superassembly and subassembly experiments described in Chapter 3 – 6. The R3D element was able to accurately replicate the response of the as-built subassemblies SA2 and SA3. The R3D element was able to replicate the response of the retrofitted subassemblies SA2-TCY, SA2-SFD and SA2-HF2V with acceptable accuracy, despite no hysteretic rules being available to model the response of the dampers.

When assembled as part of a frame system to numerically model the response of superassembly SA1, the R3D element was capable of producing close agreement with the

experimental results. However, the interaction between the seismic frame and the floor diaphragm was unable to be modelled. Hence, a numerical floor diaphragm model was developed based on work undertaken by Peng (2009). The numerical floor diaphragm model was able to capture in-plane continuity moments from the precast floor seating as well as out-of-plane flexure in the infill region. A numerical model of SA1 was assembled using the R3D element and the numerical floor diaphragm model. The numerical model of SA1 that included the numerical floor model was capable of closely replicating the observed response of SA1. A sensitivity study on the effect that varying the input parameters of the numerical floor diaphragm model had on response was undertaken, and the following observations were made.

1. The response of the numerical model of SA1 was not sensitive to the infill steel spring axial stiffness or the in-plane stiffness of the floor finite elements.
2. The response of the numerical model of SA1 was moderately sensitive to the axial stiffness of the diagonal concrete infill springs.
3. The response of the numerical model of SA1 was sensitive to the flexural stiffness of both the continuity moment rotational springs and the infill steel springs.

A comparison between slotted beam and traditional connection versions of a numerical model of SA1 was undertaken to investigate the differences in response. It was found that, despite the slotted beam and traditional versions of the numerical models having similar yield forces, the slotted beam connection version exhibited greater post-yield strength gain and dissipated a greater amount of energy than did the traditional connection version. A portion of the increased lateral resistance exhibited by the slotted beam numerical model was attributable to the increased cyclic strain hardening that occurred in the bottom longitudinal reinforcement. However, the difference in the lateral resistance observed between the two numerical models was attributable also to the contribution that the top longitudinal reinforcement made to the flexural moment generated in the R3D elements. Hence, any claim that the reinforced concrete slotted beam connection exhibits greater energy dissipation, post-yield stiffness or ultimate capacity than a comparable traditional reinforced concrete connection must be tempered by the influence of the top longitudinal reinforcement to slotted beam flexural response. Larger beam elongation, and hence beam axial forces induced by the beam elongation, was observed in the traditional connection version of the SA1 numerical model compared to the slotted beam version. It was shown that the bottom longitudinal reinforcement in a slotted beam connection is more susceptible to low-cycle fatigue than that in a traditional reinforced concrete connection; however, is possible that the bottom longitudinal reinforcement in a slotted beam connection has sufficient strain capacity to

withstand a damage limit state earthquake and a survivability limit state earthquake. The top longitudinal reinforcement and diagonal hangers in a slotted beam connection are less susceptible to low-cycle fatigue than is the bottom longitudinal reinforcement.

Slotted beam and traditional connection versions of a numerical model of a seven storey prototype building were subjected to a suite of earthquake records to enable the overall structural responses of the two systems to be compared. It was shown that the response of the comparable slotted beam and traditional connection structures during earthquakes was relatively similar. The slotted beam numerical model exhibited smaller induced axial beam forces, smaller residual structural displacements and larger floor accelerations than did the traditional connection version of the numerical model.

7.8 References

Au, E. (2010). *The mechanics and design of a non-tearing floor connection using slotted reinforced concrete beams.* Masters Dissertation, University of Canterbury, Christchurch, New Zealand.

Brown, J., & Kunnath, S. K. (2004). Low-cycle fatigue failure of reinforcing steel bars. *ACI Materials Journal, 101*(6), 457-466.

Byrne, J. D. R. (2012). *Bond and shear mechanics within reinforced concrete beam-column joints incorporating the slotted beam detail.* Masters Dissertation, University of Canterbury, Christchurch, New Zealand.

Carr, A. J. (2005). *Ruaumoko Manual Volume 2: User Manual for the 2:Dimensional Version Ruaumoko2D*. Christchurch, New Zealand: University of Canterbury.

Carr, A. J. (2013). *Ruaumoko Manual Volume 3: User Manual for the 3:Dimensional Version Ruaumoko3D*. Christchurch, New Zealand: University of Canterbury.

Coffin, J. L. F. (1954). Study of effects of cyclic thermal stresses on ductile metal. *American Society of Mechanical Engineers - Transactions, 76*(6), 931-949.

Dodd, L. L., & Restrepo-Posado, J. I. (1995). Model for Predicting Cyclic Behaviour of Reinforcing Steel. *ASCE Journal of Structural Engineering, 121*(3), 433-445.

Douglas, K. T., Davidson, B. J., & Fenwick, R. C. (1996). *Modelling reinforced concrete plastic hinges*. Paper presented at the 11th World Conference on Earthquake Engineering, Acapulco, Mexico. Retrieved from http://www.iitk.ac.in/nicee/wcee/article/11_468.PDF

Kim, J. (2002). *Behaviour of hybrid frames under seismic loading.* Doctoral Dissertation, University of Washington, Washington, USA.

Kim, J., Stanton, J. F., & MacRae, G. A. (2004). Effect of beam growth on reinforced concrete frames. *ASCE Journal of Structural Engineering, 130*(9), 1333-1342.

Lau, D. B. N., Davidson, B. J., & Fenwick, R. C. (2003). *Seismic performance of r/c perimeter frames with slabs containing prestressed units*. Paper presented at the Pacific Conference on Earthquake Engineering, Christchurch, New Zealand. Retrieved from http://www.nzsee.org.nz/db/2003/Print/Paper109p.pdf

Lau, D. B. N., Fenwick, R. C., & Davidson, B. J. (2007). *The Influence of Precast-Prestressed Flooring on the Seismic Performance of Reinforced Concrete Perimeter Frame Buildings (Report number 653)*. Auckland, New Zealand: University of Auckland.

Leslie, B. J. (2010). *The development and validation of a non-tearing floor precast concrete structural system for seismic regions.* Masters Dissertaton, University of Canterbury, Christchurch, New Zealand.

MacRae, G. A., & Gunasekaran, U. (2006). *A concept for consideration of slab effects on building seismic performance*. Paper presented at the New Zealand Society for Earthquake Engineering Conference, Napier, New Zealand. Retrieved from http://www.nzsee.org.nz/db/2006/Paper22.pdf

Maekawa, K., Pimanmas, A., & Okamura, H. (2003). *Nonlinear mechanics of reinforced concrete*. London, England: Spon Press.

Mander, J. B., Panthaki, F. D., & Kasalanati, A. (1994). Low-cycle fatigue behaviour of reinforcing steel. *Journal of Materials in Civil Engineering, 6*(4), 453-468.

Manson, S. S. (1953). *Behaviour of materials under conditions of thermal stress (Technical note 2933)* Cleveland, Ohio, USA: National Advisory Committee for Aeronautics.

Miner, M. A. (1945). Cumulative Damage in Fatigue. *Journal of Applied Mechanics.*12. A159-A164.

Ohkubo, M., Matsuoka, T., Yoshioka, T., & Anderson, D. L. (1999). Shear transfer mechanism of reinforced concrete beams with a slot at the beam-end. *Proceedings of the Japan Concrete Institute, 21*(3), 301-306.

Otani, S. (1974). Inelastic analysis of R/C frame structures. *ASCE Journal of the Structural Division, 100*(7), 1433-1449.

Peng, B. H. H. (2009). *Seismic performance assessment of reinforced concrete buildings with precast concrete floor systems.* Doctoral Dissertation, University of Canterbury, Christchurch, New Zealand.

Prakash, V., Powell, G. H., & Campbell, S. (1993). *DRAIN-2DX base program description and user guide: Version 1.10 (Report number UCB/SEMM-93/17&18)*. Berkeley, California, USA: Department of Civil Engineering, University of California, Berkeley.

Priestley, M. J. N., Calvi, G. M., & Kowalsky, M. J. (2007). *Displacement-based seismic design of structures*. Pavia, Italy: IUSS Press.

Ramberg, W., & Osgood, W. R. (1943). *Description of stress-strain curves by three parameters (Technical Note 902)*. Washington, USA: National Advisory Committee for Aeronautics.

Saiidi, M., & Sozen, M. A. (1979). *Simple and complex models for nonlinear seismic response of reinforced concrete structures (Report number 465)*. Urbana, Illinois, USA: University of Illinois.

Shahrooz, B. M., Pantazopoulou, S. J., & Chern, S. P. (1992). Modeling slab contribution in frame connections. *ASCE Journal of Structural Engineering, 118*(9), 2475-2494.

Spieth, H. A., Carr, A. J., Pampanin, S., Murahidy, A. G., & Mander, J. B. (2004). *Modelling of Precast Prestressed Concrete Frame Structures with Rocking Beam-Column Connections (Report number 2004-1)*. Christchurch, New Zealand: University of Canterbury.

Standards New Zealand. (2004). *Structural Design Actions Part 5: Earthquake Actions - New Zealand (NZS1170.5:2004).* Wellington, New Zealand: Author.

Standards New Zealand. (2006). *Concrete Structures Standard (NZS3101:2006)*. Wellington, New Zealand: Author.

Tjokrodimuljo, K. (1985). *Behaviour of reinforced concrete under cyclic loading (Report number 374)*. Auckland, New Zealand: University of Auckland.

8. Conclusions and Recommendations for Future Research

8.1 Introduction

In this dissertation, the design, construction and performance of the reinforced concrete slotted beam detail was extensively investigated. The reinforced concrete slotted beam is a detail designed to reduce the damage sustained by the seismic frame and floor diaphragm during an earthquake. A slot is provided in the end of the beam approximately ¾ of the way up the column face, which allows rotation to occur about the top of the section during both positive and negative flexure. As a result, the plasticity in the connection occurs in the bottom longitudinal reinforcement, which is unbonded for a length to limit the strain induced. The slotted beam has been proven capable of addressing many of the undesirable traits displayed by traditional connections. The research was conducted in three main phases: superassembly experimental testing, subassembly experimental testing and numerical modelling. The main conclusions and limitations from this study, along with recommendations for future research, are presented in this chapter.

8.2 Conclusions

A comprehensive investigation into the design, construction, performance, retrofit and numerical modelling of the reinforced concrete slotted beam has been undertaken as part of this research project. The investigation involved the participation of the construction industry, large scale experimental testing and numerical modelling. Numerous observations, refinements, recommendations and developments were made throughout this investigation; the main findings only of each phase are summarised below.

8.2.1 Superassembly Experiment

1. A two storey, two-by-one bay, reinforced concrete slotted beam superassembly was designed based on recent research (Au, 2010) and constructed in the structural extension laboratory at the University of Canterbury. Specimen SA1 was the first complete slotted beam system to be constructed, which allowed complex three-dimensional behaviour and interactions between structural elements to be examined. New details designed to

improve the performance of the reinforced concrete slotted beam detail were developed and tested.

2. The precast concrete components of specimen SA1 were manufactured by reputable commercial precast companies. Commercial precast companies were used to enable the practicality of specifying the slotted beam detail to be assessed. Several recommendations were developed to expedite the manufacture of the reinforced concrete slotted beam.
3. The erection of specimen SA1 was undertaken by the author, University of Canterbury technicians and commercial companies. Construction firms were involved during the erection of SA1 to test the practicality of construction using the reinforced concrete slotted beam detail. Recommendations were made which aim to increase the efficiency of erecting a reinforced concrete slotted beam structure. It can be concluded that the reinforced concrete slotted beam can be manufactured by competent New Zealand precast companies. Damage sustained by SA1 during the 22nd February 2011 Christchurch earthquake did not significantly affect the results gathered during testing.
4. A large reaction frame was designed and assembled using modular steel components. An analysis of the laboratory strong floor was undertaken to determine load and displacement limits that could not be exceeded during testing. The laboratory strong floor governed the maximum actuator forces that could be applied to the specimen. Existing actuator control programs caused interference between the actuators, which resulted in the actuator forces building up over successive displacement increments. A new program was developed to control the hydraulic actuators, which reduced the interference between the actuators and allowed the intended biaxial displacements to be applied to SA1.
5. Overall, specimen SA1 performed well during testing. Stable response and high levels of energy dissipation were observed throughout testing. The specimen conformed to serviceability, damage and life safety limit states as defined by Priestley et al. (2007). All criteria were satisfied to conform to the ACI374.1-05 acceptance criteria for moment frames based on structural testing, with the exception of the predicted overstrength (ACI Committee 374, 2005).
6. The damage sustained by SA1 during testing was very low. It was concluded that a reinforced concrete slotted beam system would sustain less damage during a design level earthquake than a comparable system with traditional connections. The nature of the damage sustained in a slotted beam system is generally economically and practically viable to repair.
7. Specimen SA1 was designed using simplified design equations recommended by Au (2010), which were found to be unconservative when used to determine the ultimate

flexural capacity of a slotted beam connection. Specimen overstrength factors of 3.5 and 2.5 were recorded in the east-west and north-south directions respectively. The contribution of the top longitudinal reinforcement to the flexural capacity of the connection can be significant, and should be included in flexural capacity calculations. The effective flange widths specified in §9.3.1.2 of NZS3101:2006 should be used to calculate the nominal flexural moment capacity of slotted beam systems (Standards New Zealand, 2006). Continuity moments from the precast floor connections contributed significantly to beam torsion, and hence the overall lateral strength of the specimen. Continuity moments should be considered separately from flange activation, and should be included in overall lateral strength calculations.

8. When all the contributions to the lateral strength of SA1 were taken into account, the recorded overstrength was 1.87 and 1.86 for the east-west and north-south directions respectively. The relatively high overstrength was the result of a combination of factors; however, effective stress in the bottom longitudinal reinforcement of the connections was likely the main factor and is discussed in Section 4.5. An overstrength factor of 1.6 is recommended for the design of slotted beam connections when Grade 300 bottom reinforcement is used.
9. Using two layers of top and bottom longitudinal reinforcement is a practical solution in reinforced concrete slotted beams. However, the increased hinge depth that is necessary when using two layers of longitudinal reinforcement leads to increased strain in both the diagonal hangers and the top longitudinal reinforcement. The average strain penetration in the top longitudinal reinforcement was $0.027f_y d_b$. Top hinge depths should be minimised to reduce strain in the longitudinal reinforcement and diagonal hangers.
10. The overall performance of the diagonal hangers was acceptable. To minimise the strain induced in the hangers by connection flexure, the hangers should pass through the top hinge at a depth of $0.65d_h$ from the top of the top hinge, where d_h is the depth of the top hinge. The strain penetration length measured in the hangers across the top hinge was $0.047f_y d_b$. The revised three hanger detail proved effective at resisting shear and torsion in exterior beams supporting the one-way flooring system. The new four hanger detail proved effective at resisting large gravity shear, seismic shear and torsion in internal beams supporting the one-way flooring system. A two hanger detail may be appropriate for beams that are not heavily loaded in shear and torsion. The continuous hanger detail for internal beam-column connections, where the hangers on either side of an internal column are formed from a continuous length of reinforcement, proved effective at reducing connection congestion, whilst facilitating effective force transfer.

11. Strain penetration in the bottom longitudinal reinforcement of SA1 was $0.010f_yd_b$ and was observed at both ends of the unbonded length of reinforcement. The extent of the strain penetration was exacerbated by using two layers of longitudinal reinforcement, due to the increased distance between the horizontal stirrups adjacent to the longitudinal reinforcement. Supplementary reinforcement welded to the beam longitudinal reinforcement through internal beam-column connections proved effective at reducing strain penetration and bond stresses within the joint.
12. The average centreline connection beam elongation recorded in SA1 was an eighth of what would be expected in an equivalent traditional connection. The difference in total elongation between exterior and interior connections was not as significant in SA1 as it has been shown to be in traditional systems (Peng, 2009). Peak elongation in SA1, in terms of beam height, h, was 0.38%h and 0.44%h for internal and external connections respectively. The large gravity loads on Grid B of SA1 did not affect recorded beam elongation. Beam elongation in the slotted beam is predominately generated by flexure in the top hinge.
13. The flange activation in SA1 at the survival limit state was approximately 90% of that observed in traditional systems (Priestley et al., 2007; Peng, 2009). During negative connection flexure the lever arm between the neutral axis and the floor reinforcement was reduced compared to a traditional system; hence, the contribution of flange activation to overall system lateral resistance was reduced also. Relatively even flange activation was observed between internal and external connections. Nominal and overstrength design flange activation widths for slotted beam systems were tentatively recommended in Section 4.16.2.

8.2.2 Subassembly Experiments

1. The subassembly test phase of this research programme was undertaken to investigate the residual capacity of reinforced concrete slotted beam connections following a large earthquake. Following the assessment of residual capacity, the connections were rehabilitated with external dampers to assess the performance for both retrofit and new-build scenarios. A methodology to undertake the controlled demolition of slotted beam structures was developed and implemented on superassembly SA1. Using this methodology, two three-dimensional portions of SA1 were extracted safely and without damage.

2. A retrofit system to rehabilitate the moment capacity of slotted beams following a damaging earthquake was developed and implemented. It can be concluded that slotted beam systems, if required, can be economically retrofitted following large earthquakes.
3. Four energy dissipation devices were developed for use in a slotted beam connection. These devices are suitable for both retrofit and new-build applications. Three of the devices were manufactured, installed and tested in the retrofitted subassemblies. This series of tests was the first time that replaceable dampers had been tested in a reinforced concrete slotted beam. A number of observations and recommendations were made during the process of designing, manufacturing and installing the replaceable dampers.
4. Historical subassembly experiments were examined and critiqued to develop the most appropriate experimental setup to biaxially test subassemblies with integral floor diaphragms. In addition to the two actuators required to displace the specimens biaxially, a third actuator was utilised to control specimen rotation about the vertical axis during testing. An actuator controller program was developed to drive the three actuator setup.
5. Significant capacity remains in a reinforced concrete slotted connection after it has been subjected to a large earthquake. Hence, the potential to reuse a slotted beam structure after a significant seismic event is promising. The eventual failure of SA2 and SA3 was by way of low-cycle fatigue failure of the bottom longitudinal reinforcement in the slot region. In all incidences, low-cycle fatigue failure of the bottom longitudinal reinforcement was preceded by buckling in the slot region. It is recommended that designers take practical steps to prevent reinforcement buckling in the connection slot, such as using large diameter reinforcement, minimising strain penetration and minimising the slot width.
6. The TCY dampers tested in SA2-TCY were capable of accommodating flexure induced by relative rotation between the column face and the beam soffit, whilst maintaining axial performance. However, if large relative rotations are expected it is recommended that the damper end fixities are released. The designer should be aware of the implications of doing such on damper performance.
7. Negative stiffness was observed whilst testing the SFD and HF2V devices. However, due to the contribution of other elements, such as the top longitudinal reinforcement, the overall connection stiffness of specimens SA2-SFD and SA2-HF2V remained positive throughout testing. Low post-yield stiffness can result in poor control of structural displacements during an earthquake.
8. The variances observed between the design and measured damper forces were significant. It is recommended that if dampers are to be used in a structure, experimental testing

should be conducted to validate the actual damper response against the assumptions made during the design phase.

9. Beam elongation in the slotted beam subassemblies was not sensitive to the type of device used in the bottom of the beam to create a connection moment. Furthermore, due to the top longitudinal reinforcement being designed to be twice as strong as the bottom longitudinal reinforcement, the force capacity of the dampers installed to replace the bottom longitudinal reinforcement did not significantly affect recorded beam elongation.
10. A reinforced concrete slotted beam being previously subjected to seismic actions does not significantly affect the amount of energy that it can dissipate. Furthermore, the use of dampers, in place of conventional reinforcement, in a reinforced concrete slotted beam connection can significantly increase the amount of energy able to be dissipated. Increased energy dissipation in a system will result in lower peak and residual displacements, which can result in lower damage, lower repair costs and quicker reoccupation. Furthermore, these benefits are able to be achieved in both retrofit and new-build applications.
11. Specimen SA2 formed the basis of all three retrofitted subassembly experiments. Shear and torsional displacements in the connection perpendicular to the floor were observed to increase over successive retrofitted subassembly tests. It was postulated that the increasing nonlinearity in response observed over successive subassembly tests was due to strain penetration in the hanger reinforcement either side of the slotted section and the resulting loss of bond.

8.2.3 Numerical Investigations

1. Existing two-dimensional numerical models of the slotted beam were expanded into three dimensions using various modelling techniques. The newly developed three-dimensional numerical models represented slotted beam behaviour well; however, the knowledge and time required to set the model up would have presented a barrier to implementation. Hence, a three-dimensional slotted beam multispring element (R3D) was developed to accurately represent slotted beam response, whilst being able to be set up with only gross section dimensions and material properties. A sensitivity study on the effect that varying the input parameters of the R3D element had on response was undertaken.
2. The response of the R3D element was validated against the experimentally observed results from the superassembly and subassembly experiments described in Chapter 3 – 6. The R3D element was able to accurately replicate the response of the as-built

subassemblies SA2 and SA3. The R3D element was able replicate the response of the retrofitted subassemblies SA2-TCY, SA2-SFD and SA2-HF2V with acceptable accuracy.

3. When assembled as part of a frame system to numerically model the response of superassembly SA1, the R3D element was capable of producing close agreement with the experimental results. However, the interaction between the seismic frame and the floor diaphragm was unable to be modelled. A numerical floor diaphragm model, which was capable of modelling in-plane continuity moments from the precast floor seating as well as out-of-plane flexure in the infill, was developed based on work undertaken by Peng (2009). A numerical model of SA1 that was assembled using the R3D element and the numerical floor diaphragm model was capable of closely replicating the observed response of SA1. A sensitivity study on the effect that varying the input parameters of the numerical floor diaphragm model had on response was undertaken.
4. A comparison between slotted beam and traditional connection versions of a numerical model of SA1 was undertaken to investigate the differences in response. The slotted beam connection version exhibited greater post-yield strength gain and dissipated a greater amount of energy than the traditional connection version. A portion of the increased lateral resistance exhibited by the slotted beam numerical model was attributable to the increased cyclic strain hardening that occurred in the bottom longitudinal reinforcement. However, the differences in the lateral resistance observed between the two numerical models was attributable also to the contribution that the top longitudinal reinforcement made to the flexural moment generated in the R3D elements. Larger beam elongation, and hence beam axial forces induced by the beam elongation restraint provided by the adjacent floor, was observed in the traditional connection version of the SA1 numerical model compared to the slotted beam version. The bottom longitudinal reinforcement in a slotted beam connection is more susceptible to low-cycle fatigue than that in a traditional reinforced concrete connection; however, is possible that the bottom longitudinal reinforcement in a slotted beam connection has sufficient strain capacity to withstand a damage limit state earthquake and a survivability limit state earthquake. The top longitudinal reinforcement and diagonal hangers in a slotted beam connection are less susceptible to low-cycle fatigue than is the bottom longitudinal reinforcement.
5. Slotted beam and traditional connection versions of a numerical model of a seven storey prototype building were subjected to a suite of earthquake records to enable the overall structural responses of the two systems to be compared. It was shown that the response of the comparable slotted beam and traditional connection structures during earthquakes was

relatively similar. The slotted beam numerical model exhibited smaller induced axial beam forces, smaller residual structural displacements and larger floor accelerations than did the traditional connection version of the numerical model.

8.2.4 Industry Application

The original objective of this research project was to develop the reinforced concrete slotted beam detail to a state in which it was ready for implementation into New Zealand construction industry. Achievement of this research objective was defined as the construction of the first slotted beam structure in the New Zealand, using details and techniques developed during this research program.

Figure 8-1 presents the details for a reinforced concrete slotted beam building, which was under construction in Christchurch, New Zealand at the time of writing. Following the 4th September 2010 and 22nd February 2011 Christchurch earthquakes, the engineering firm responsible for the design recognised that current construction techniques had resulted in unsatisfactory outcomes for clients during and after those major seismic events. Furthermore, the intended use of the building required a high level of seismic performance during, and rapid reoccupation following, a large earthquake. Hence, the reinforced concrete slotted beam was identified as a detail that could economically achieve these performance objectives.

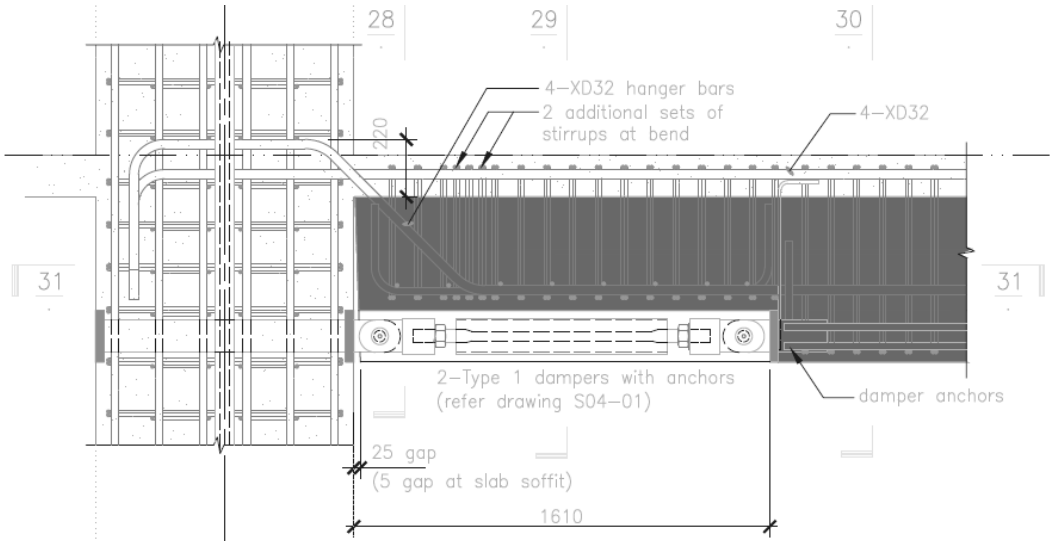

(a) Elevation.

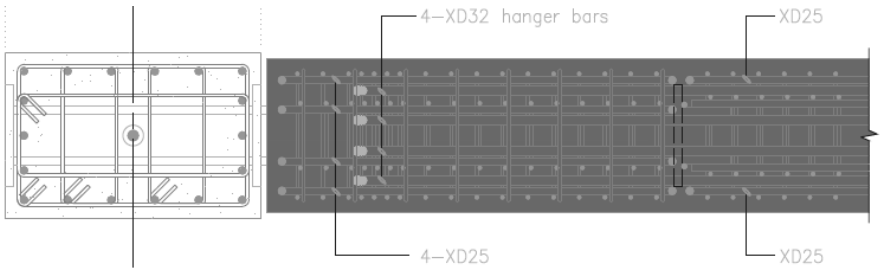

(b) Plan.

Figure 8-1: Details of slotted beam structure under construction.

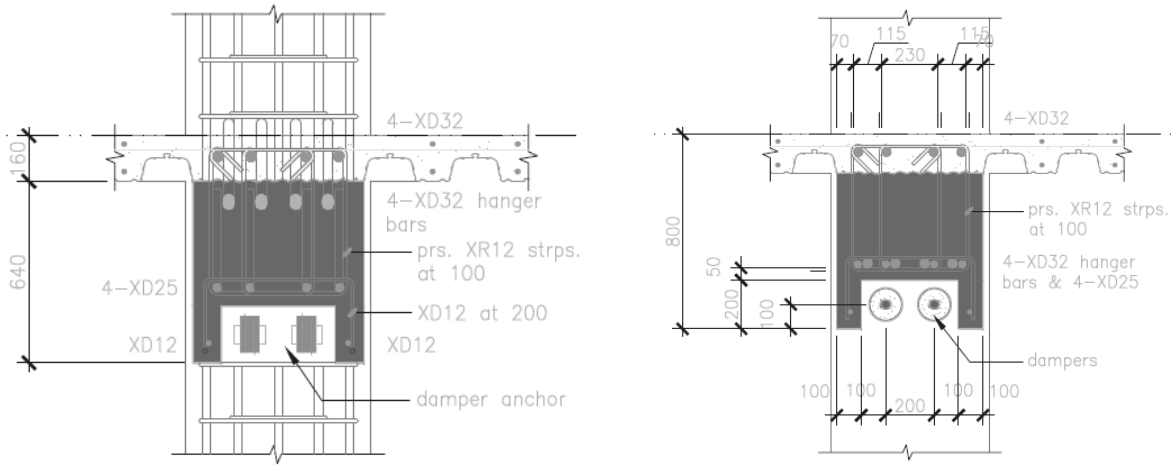

(c) Cross-section one. **(d) Cross-section two.**

Figure 8-1: Details of slotted beam structure under construction (Continued).

The design presented in Figure 8-1 makes use of the advancements made, and design recommendations developed, during this research project. The four diagonal hanger detail was used to provide strong resistance to shear, torsion and flexural demands. The additional longitudinal hooked reinforcement detail was used to maintain a dependable shear transfer mechanism between the main beam and the diagonal hangers. Significantly, the design used replaceable external dampers in place of reinforcement to provide connection moment resistance. The dampers were based on the TCY design implemented in specimen SA2-TCY. The dampers have pinned connections to the structure to isolate the dampers from flexure induced by connection rotation. The design makes use also of practicality and constructability recommendations made during this research project, such as the trapezoidal shape of the slot and the partial precast height of the beams.

8.3 Recommendations for Future Research

Significant advances have been made to the design, application and modelling of the reinforced concrete slotted beam during this research project. However, there remain areas that require further research to address limitations and refine recommendations.

1. The superassembly and subassembly experiments were conducted without axial loads applied to the columns. Recent experiments on slotted beams by Byrne (2012) have included column axial load, but the effect was not specifically investigated. It is recommended that research be conducted on slotted beam connections to investigate the influence of column axial load on the shear transfer mechanism within the beam-column joint and bottom longitudinal reinforcement bond through the joint.
2. Because of the conservative design rationale applied to design the beam-column joint reinforcement in SA1 and the selective weakening necessitated by the large system overstrength exhibited by SA1, the horizontal beam-column joint reinforcement remained

elastic throughout testing. It is possible that the quantity of horizontal reinforcement recommended for the beam-column joints of reinforced concrete slotted beam systems may be reduced. However, a systematic experimental investigation to examine the effect of reduced beam-column joint reinforcement in slotted beam systems is recommended prior to any reductions being made to current recommendations.

3. Due to the limitations of the laboratory facilities at the University of Canterbury, it was necessary to conduct experimentation at quasi-static loading rates. The loading rates were several orders of magnitude less than what would be expected during an earthquake. Hence, strain rate dependent effects could not be considered. It is recommended that high speed testing be undertaken on reinforced concrete slotted beam specimens to determine the sensitivity of response to strain rate.
4. Current methods to predict low-cycle fatigue are based on empirical formulations developed in the 1950s (Coffin, 1954). Whilst these formulations have been adapted for application to reinforcement (Mander et al., 1994), and they are useful to undertake comparative investigations, it has been shown that they cannot accurately predict low-cycle fatigue failure in the bottom longitudinal reinforcement of a reinforced concrete slotted beam. It is recommended that an extensive investigation be performed on low-cycle fatigue failure in reinforced concrete slotted beam connections. The investigation should aim to develop more accurate tools to predict low-cycle fatigue failure of reinforcement in slotted beam connections.
5. It has been shown that the influence of effective stress in the bottom longitudinal reinforcement of slotted beam connections can cause a significant increase in negative flexural capacity. This effect is discussed in Section 4.5. It is recommended that an investigation be undertaken to understand and quantify the influence of effective stress in the bottom longitudinal reinforcement of slotted beam connections. Design recommendations should be developed to mitigate the influence of effective stress on connection performance.
6. It was shown that reinforced concrete slotted beam connections that use replaceable external dampers in place of the bottom unbonded reinforcement exhibit promising performance. It is recommended that a full scale experimental test of a slotted beam specimen specifically designed to use external dampers be conducted to develop attachment details and determine the likely response.
7. Post-tensioned rocking columns should be investigated for use in reinforced concrete slotted beam buildings to provide overall system recentring behaviour. There is the potential for this type of structural system to not only minimise the damage sustained to

the structure during an earthquake, but also reduce the residual structural displacements that remain following an earthquake.

8. The hysteretic rules used to model the response of the external dampers in the numerical models of the retrofitted subassemblies were simplistic. It is recommended that accurate numerical expressions to describe the response of external dampers be developed and implemented into Ruaumoko3D for use in the R3D element (Carr, 2013).
9. The numerical floor diaphragm model developed and tested in Chapter 7 showed promise for modelling the complex interactions between structural elements in structures. However, whilst the performance of the numerical floor diaphragm model was satisfactory for the geometries tested in Chapter 7, its performance in other applications may not be satisfactory. It is recommended that the numerical floor diaphragm model is examined and developed to ensure satisfactory performance over a wide variety of geometries and structural systems.
10. In Section 7.6 a comparison between the overall structural response of a reinforced concrete slotted beam building and a traditional reinforced concrete building was presented. It is recommended that a similar investigation be undertaken to compare the overall structural responses of a reinforced concrete slotted beam building and a PRESSS building (Priestley, 1991).

8.4 References

ACI Committee 374. (2005). *Acceptance Criteria for Moment Frames Based on Structural Testing and Commentary (ACI374.1-05).* Farmington Hills, Michigan: American Concrete Institute.

Au, E. (2010). *The mechanics and design of a non-tearing floor connection using slotted reinforced concrete beams.* Masters Dissertation, University of Canterbury, Christchurch, New Zealand.

Byrne, J. D. R. (2012). *Bond and shear mechanics within reinforced concrete beam-column joints incorporating the slotted beam detail.* Masters Dissertation, University of Canterbury, Christchurch, New Zealand.

Carr, A. J. (2013). *Ruaumoko Manual Volume 3: User Manual for the 3:Dimensional Version Ruaumoko3D*. Christchurch, New Zealand: University of Canterbury.

Coffin, J. L. F. (1954). Study of effects of cyclic thermal stresses on ductile metal. *American Society of Mechanical Engineers - Transactions, 76*(6), 931-949.

Mander, J. B., Panthaki, F. D., & Kasalanati, A. (1994). Low-cycle fatigue behaviour of reinforcing steel. *Journal of Materials in Civil Engineering, 6*(4), 453-468.

Peng, B. H. H. (2009). *Seismic performance assessment of reinforced concrete buildings with precast concrete floor systems.* Doctoral Dissertation, University of Canterbury, Christchurch, New Zealand.

Priestley, M. J. N. (1991). Overview of PRESSS research program. *PCI Journal, 36*(4), 50-57.

Priestley, M. J. N., Calvi, G. M., & Kowalsky, M. J. (2007). *Displacement-based seismic design of structures*. Pavia, Italy: IUSS Press.

Seuss Geisel, T. (Dr Seuss) (1971). *The Lorax*. New York, USA: Randon House.

Standards New Zealand. (2006). *Concrete Structures Standard (NZS3101:2006)*. Wellington, New Zealand: Author.

"Unless someone like you cares a whole awful lot,

Nothing is going to get better. It's not."

Seuss (1971)

Appendix A: Material Properties

A.1 Concrete Properties

Table A-1 presents the results of compressive testing performed on samples of concrete and grout batches used in the construction of superassembly SA1, and subsequently SA2 and SA3. All concrete cylinders were standard 100mm diameter, whereas grout samples were 50mm diameter.

Table A-1: Concrete compressive strengths.

Unit	Batch date	f'c	28 Days		Test Start	
			Mean	Std Dev	Mean	Std Dev
Bm A/1-1	24/09/2010	40	58.0	1.59	62.0	6.08
Col B/1-B	28/09/2010	40	44.0	NA	51.9	6.84
Bm A/1-2 (Bm)	29/09/2010	40	52.2	NA	60.9	0.72
Bm A/1-2 (B-C) Col B/1-C	30/09/2010	40	64.4	NA	62.4	NA
Col C/1-B Col C/1-C	04/10/2010		49.1	NA	66.3	3.06
Bm B/1-1 (Bm) Col A/1-B Col A/1-C	06/10/2010	40	60.8	NA	65.6	4.50
Bm B/1-1 (B-C)	07/10/2010	40	49.4	NA	65.8	0.54
Bm B/2-1 (Bm) Col C/2-B Col C/2-C	11/10/2010	40	57.4	NA	66.65	1.26
Bm B/2-1 (B-C) Bm C/2-1 (Bm) Col A/1-A	12/10/2010	40	56.2	2.47	56.9	2.17
Bm C/2-1 (B-C) Col B/2-B Col A/2-A Col B/2-C	13/10/2010	40	43.8	9.16	51.4	5.22
Col A/2-C Col A/2-B Col B/1-A	14/10/2010	40	48.2	2.91	57.8	1.55
Bm B/2-2 (Bm) Col B/2-A	15/10/2010	40	47.2	4.27	55.7	7.24
Col C/1-A Bm B/2-2 (B-C)	18/10/2010	40	50.9	1.15	64.1	4.94

Table A-1: Concrete compressive strengths (Continued).

Bm A/1-1R (Bm) Col C/2-A	20/10/2010	40	49.0	23.25	65.1	6.25
Bm A/1-1R (B-C)	21/10/2010	40	30.8	4.09	42.8	NA
Bm C/1-1 (Bm) Bm A/2-1 (Bm)	27/10/2010	40	60.4	2.12	70.5	0.39
Bm C/1-1 (B-C) Bm A/2-1 (B-C)	28/10/2010	40	51.8	7.33	64.3	4.12
Bm C/2-2 (Bm) Bm A/2-2 (Bm)	04/11/2010	40	50.5	1.76	53.0	2.43
Bm C/2-2 (B-C) Bm A/2-2 (B-C)	05/11/2010	40	50.1	3.41	58.2	3.58
Bm B/1-2 (Bm) Bm C/1-2 (Bm)	25/11/2010	40	47.7	6.09	61.8	1.73
Bm B/1-2 (B-C) Bm C/1-2 (B-C)	29/11/2010	40	38.1	2.82	45.6	3.42
Grout A1-L1	22/12/2010	60	47.1	NA	39.7	NA
Grout A2-L1		60	66.1	NA	58.1	NA
Grout B1-L1		60	47.1	NA	52.7	NA
Grout B2-L1		60	49.9	NA	63.2	NA
Grout C1-L1		60	60.6	NA	74.7	NA
Grout C2-L1		60	70.8	NA	87.1	NA
Level One Splice	10/01/2011	40	51.2	0.25	56.6	3.07
Level One Floor	26/01/2011	40	44.5	4.15	48.8	1.56
Grout A1-L2	12/05/2011	60	38.2	NA	83.5	NA
Grout A2-L2		60	25.2	NA	66.7	NA
Grout B1-L2		60	25.5	NA	68.4	NA
Grout B2-L2		60	22.6	NA	59.1	NA
Grout C1-L2		60	39.1	NA	74.4	NA
Grout C2-L2		60	21.7	NA	60.6	NA
Level Two Splice	19/05/2011	40	50.37	0.19	53.7	0.67
Level Two Floor	31/05/2011	40	61.94	2.20	57.1	6.16

A.2 Reinforcement Steel Properties

Figure A-1 through Figure A-9 present the results of tensile tests performed on reinforcement steel used in the construction of superassembly SA1, and subsequently SA2 and SA3.

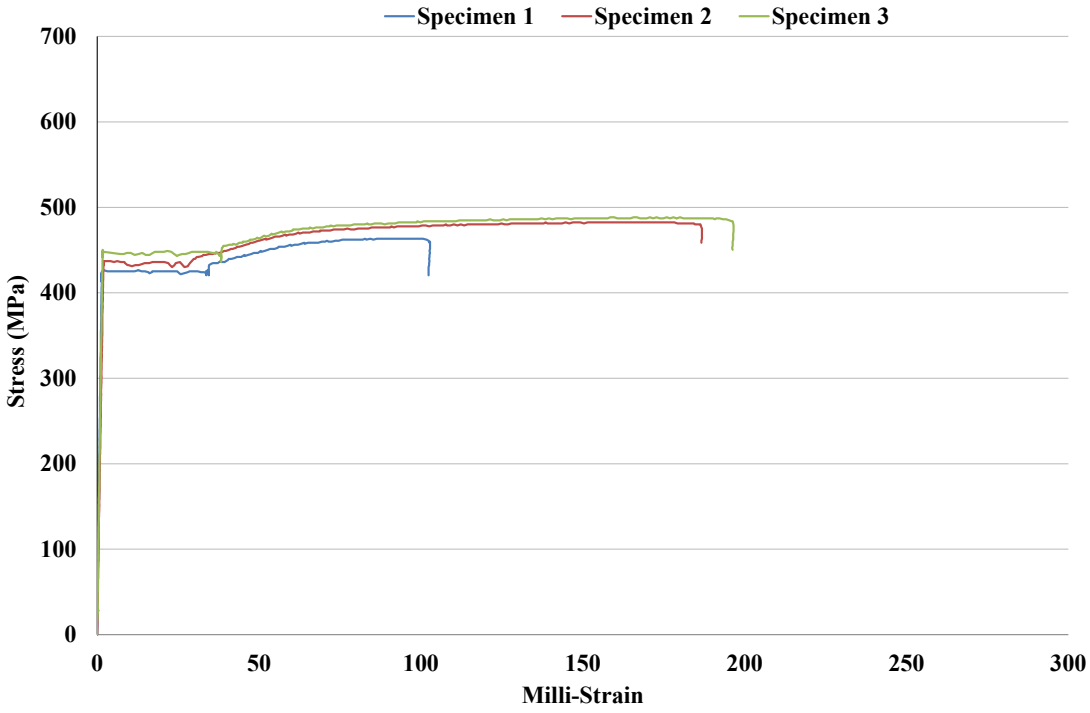

Figure A-1: R8 reinforcement.

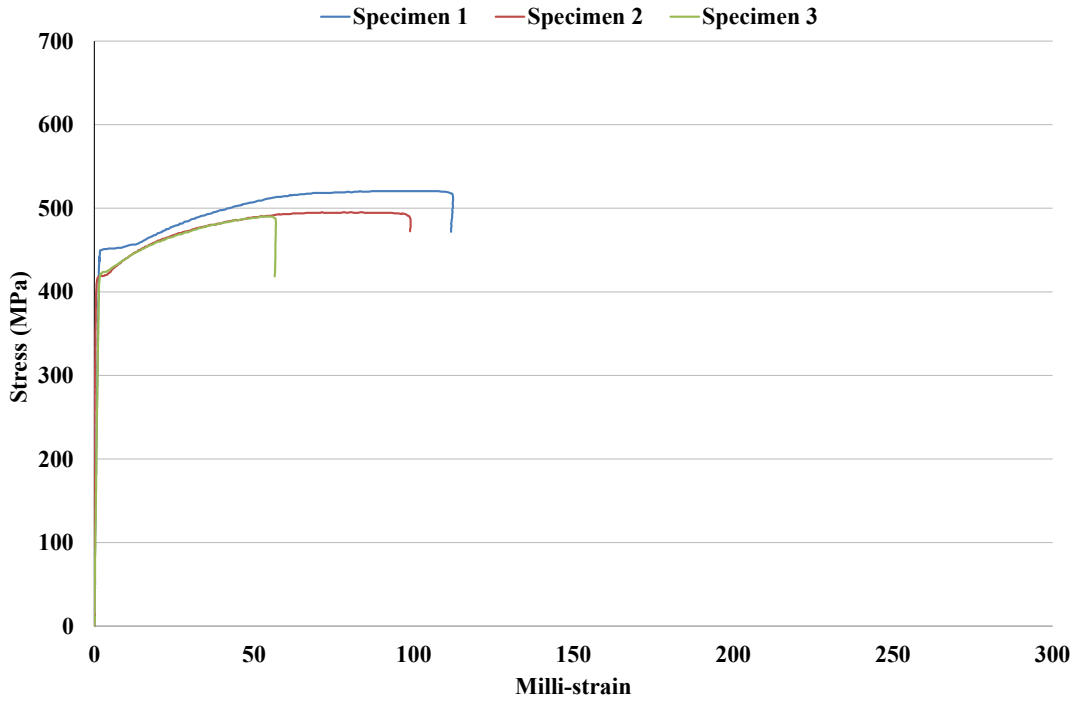

Figure A-2: D10 reinforcement.

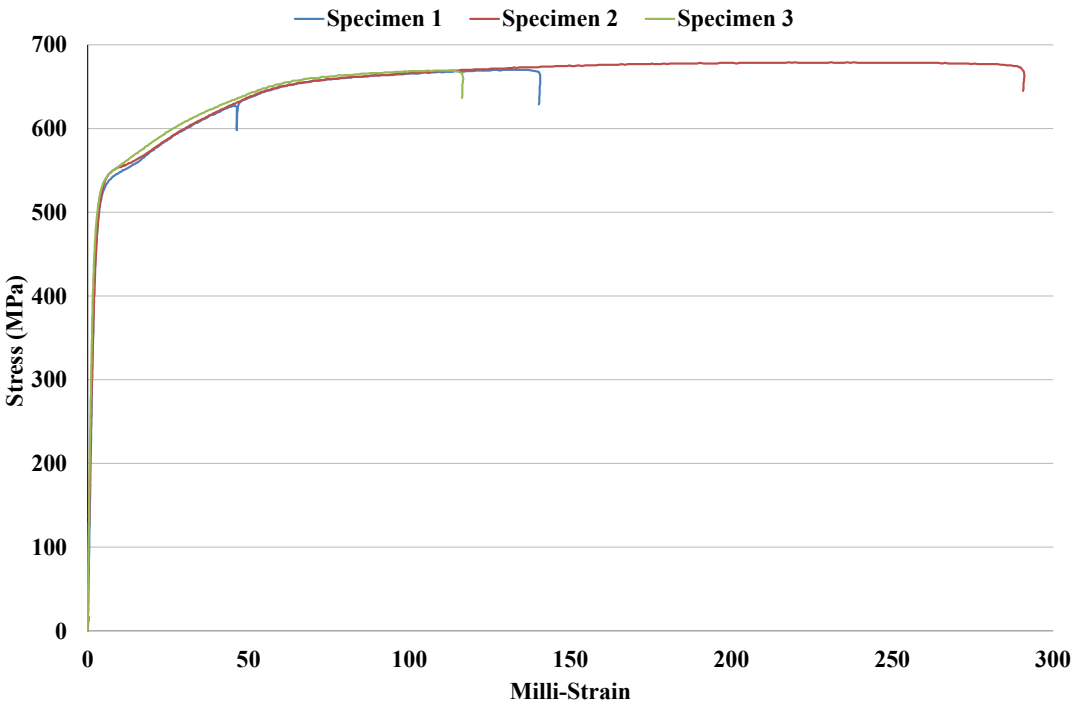

Figure A-3: XR10 reinforcement.

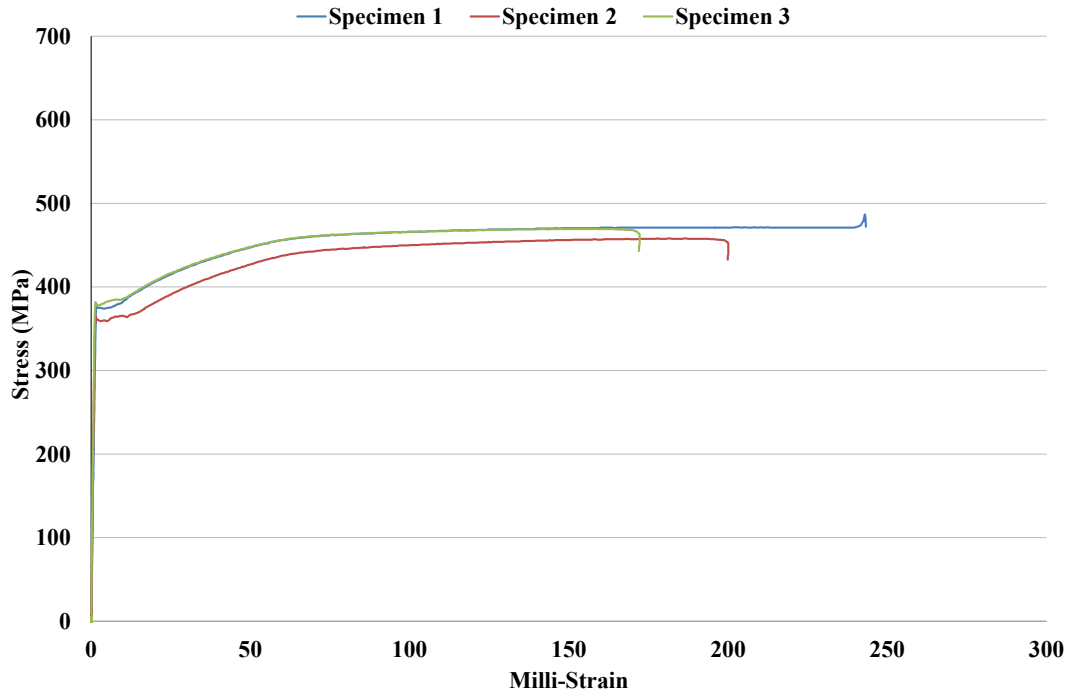

Figure A-4: D12 reinforcement.

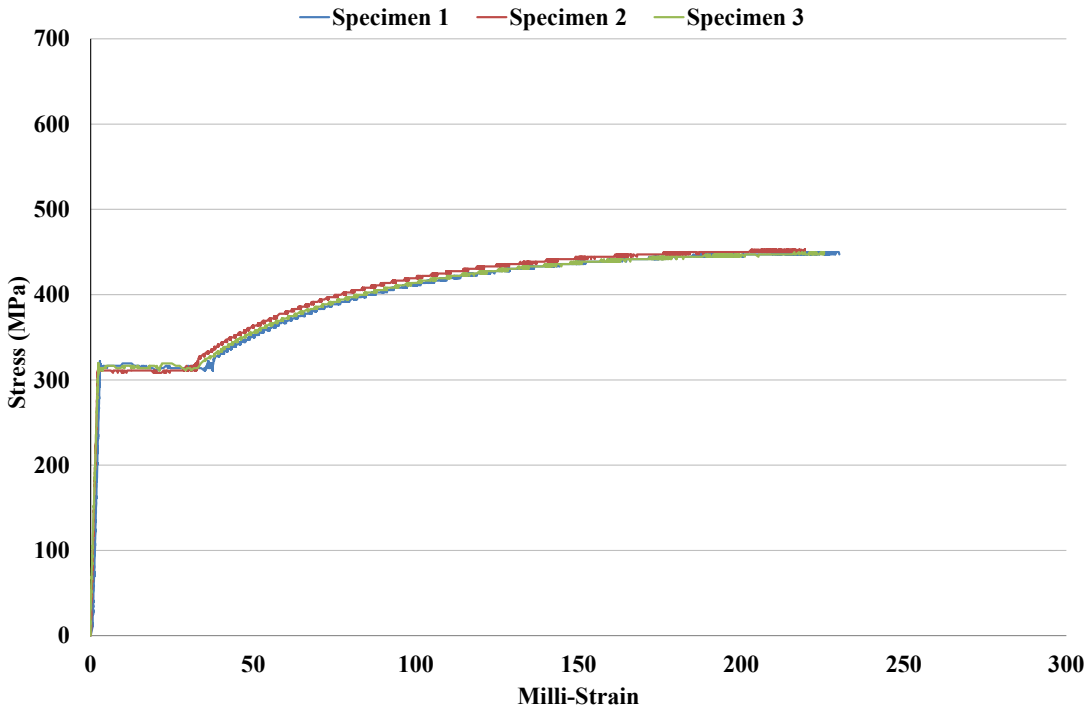

Figure A-5: D16 reinforcement.

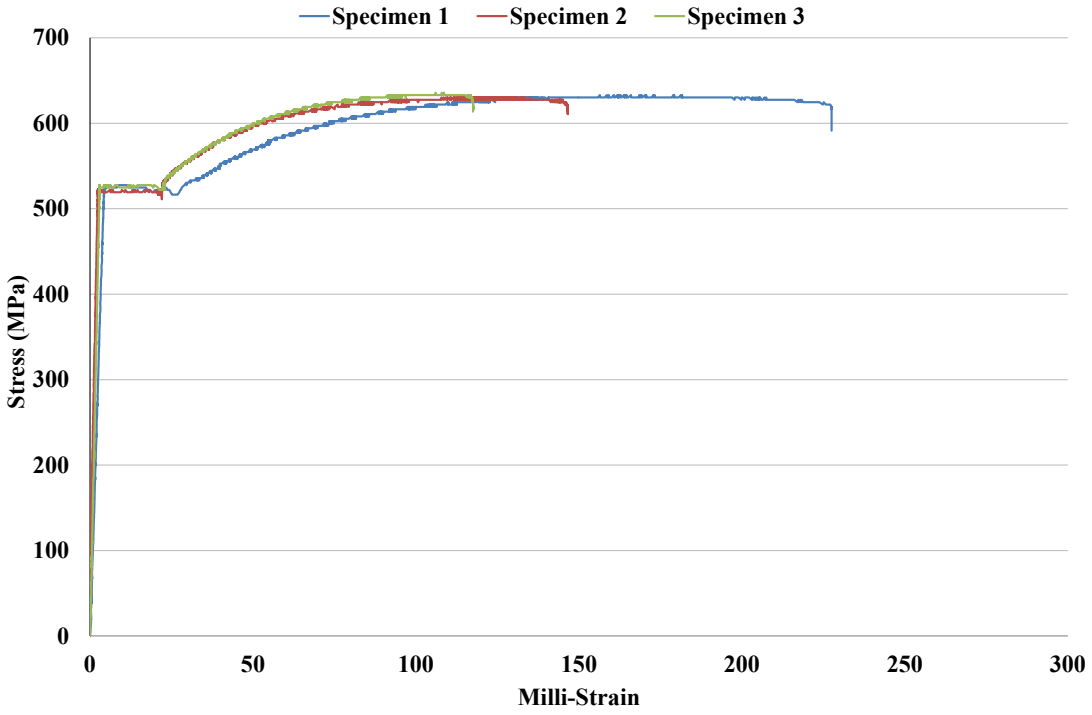

Figure A-6: XD16 reinforcement.

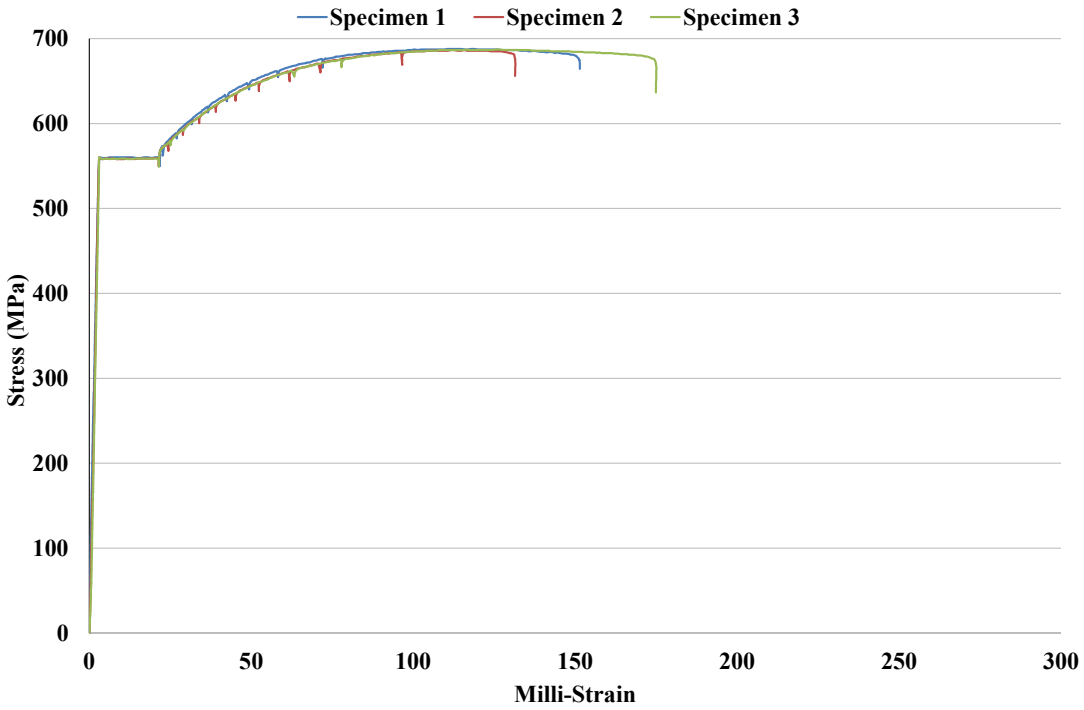

Figure A-7: RB32 reinforcement.

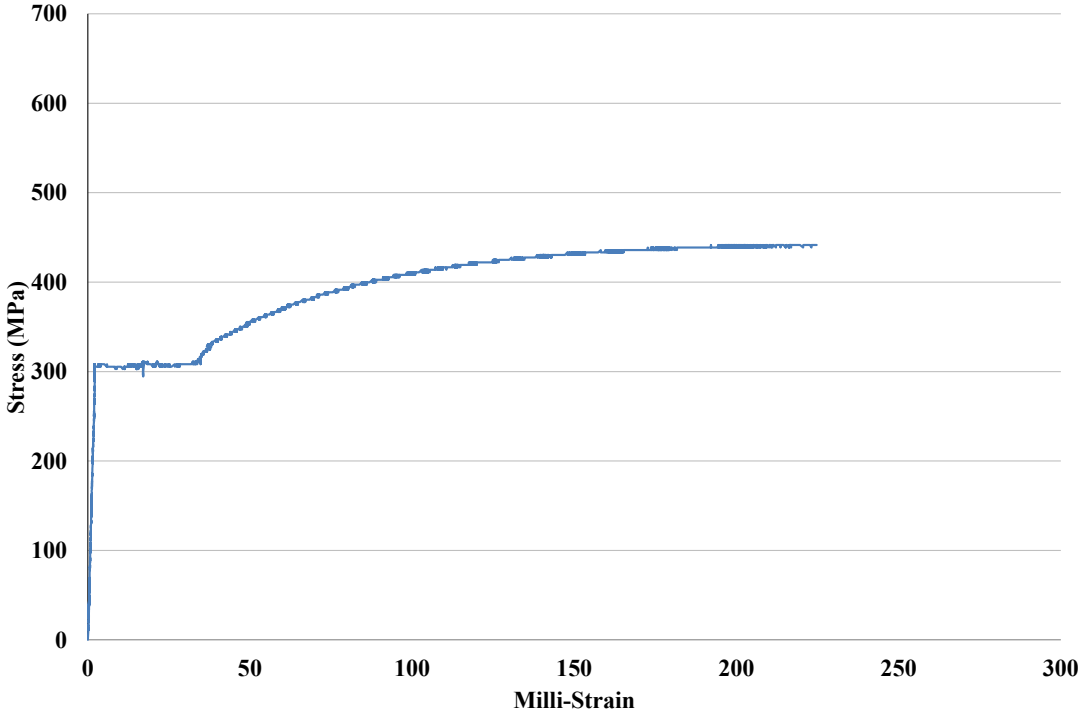

Figure A-8: 2D10 single fillet welded to D16.

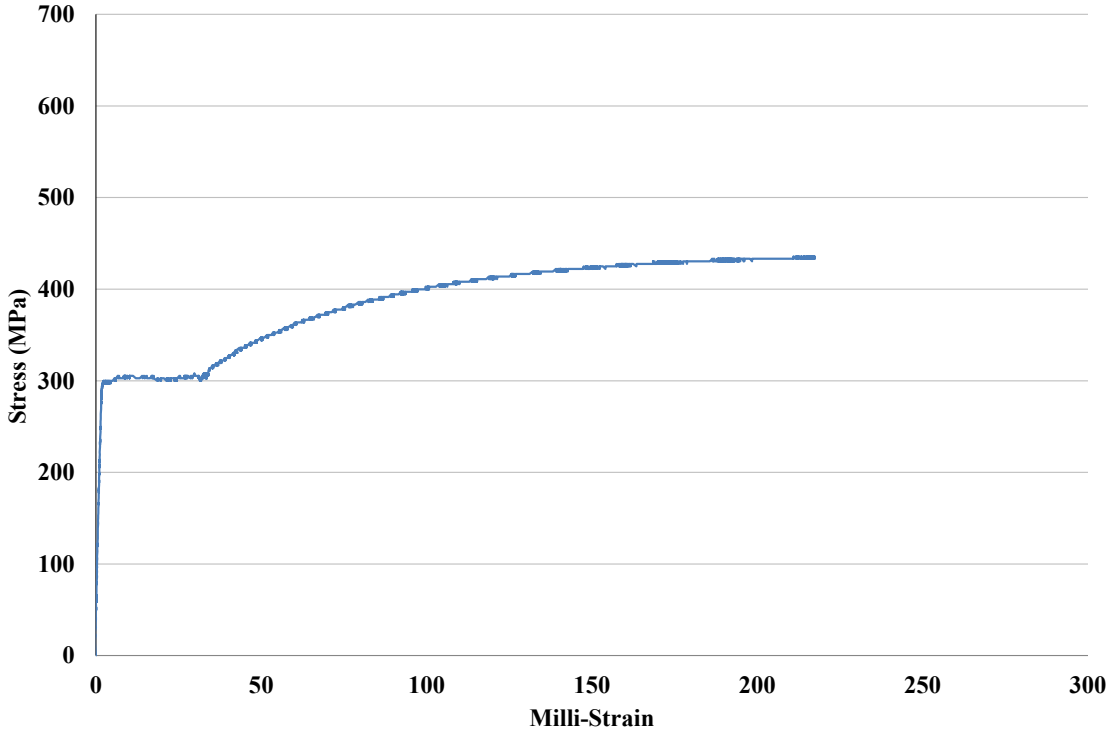

Figure A-9: 2D10 double fillet welded to D16.

Appendix B: Structural Drawings

This appendix presents the construction drawings and precast drawings for specimen SA1. The drawings are no longer to scale as they have been reduced to fit within this document.

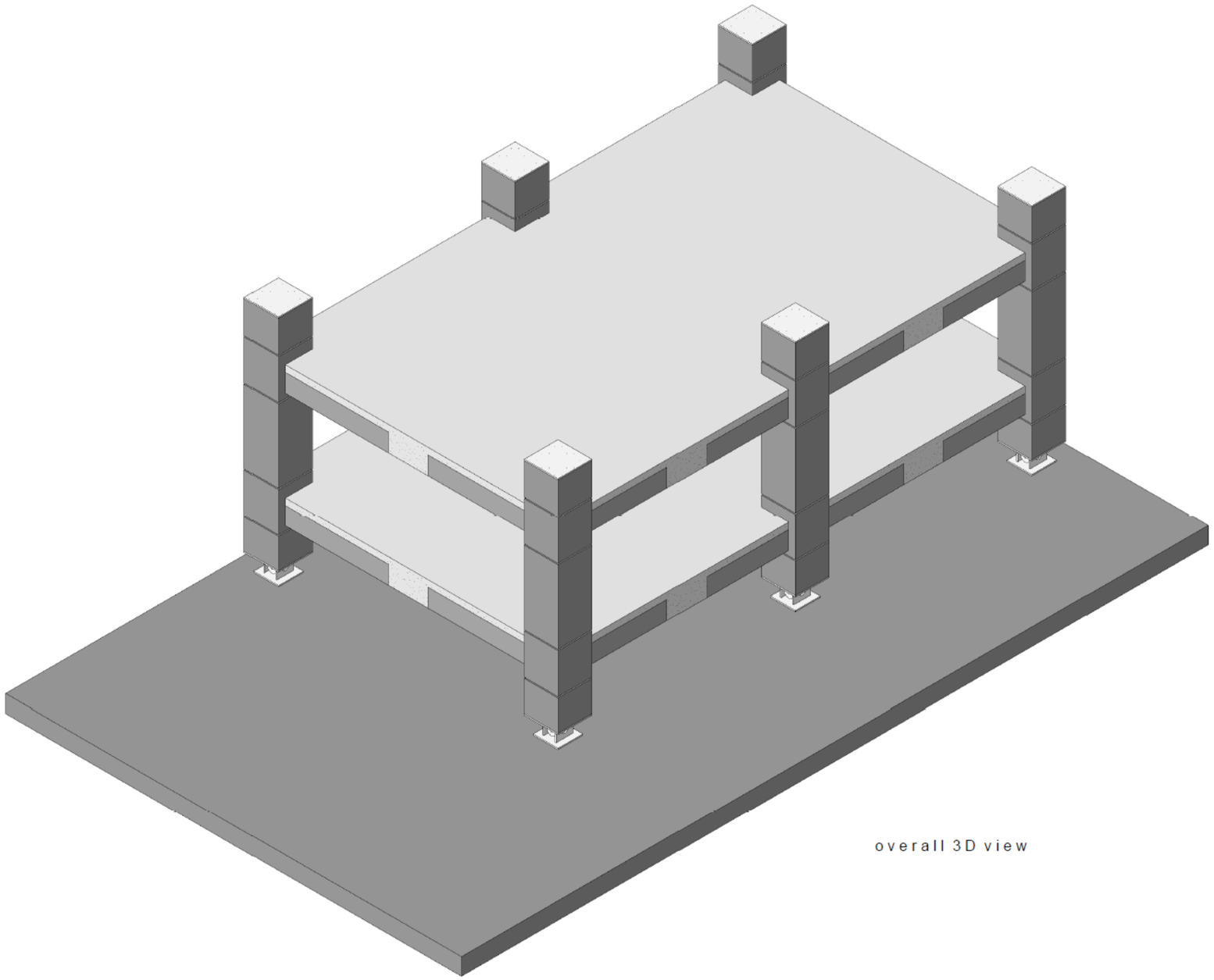

overall 3D view

All dimensions to be verified on site before making any shop drawings or commencing any work.

notes

1. All concrete to have a 28 day strength of 40MPa.
2. Tolerance = ±5mm.
3. Minimum Cover = 23mm.
4. Grout to be general purpose with a 65MPa/28 day compressive strength used in a flowable consistency

Rev	Date	By	Reason
2	18/06/10	EWL	Pricing
1	19/05/10	JEA	Pricing

Consultants

UNIVERSITY OF CANTERBURY
Te Whare Wānanga o Waitaha
CHRISTCHURCH NEW ZEALAND

HolmesConsultingGroup
STRUCTURAL AND CIVIL ENGINEERS
Level 5
123 Victoria Street
PO Box 25355
Christchurch
New Zealand
Telephone
+64 3 366 3366
Facsimile
+64 3 379 2169
www.holmesgroup.com

FRST Future Building Systems

Drawn EWL Scale at A1
Filename

Sheet Title
overall 3D view

Job No	Sheet No	Rev
TD0003.02	S00-01	2

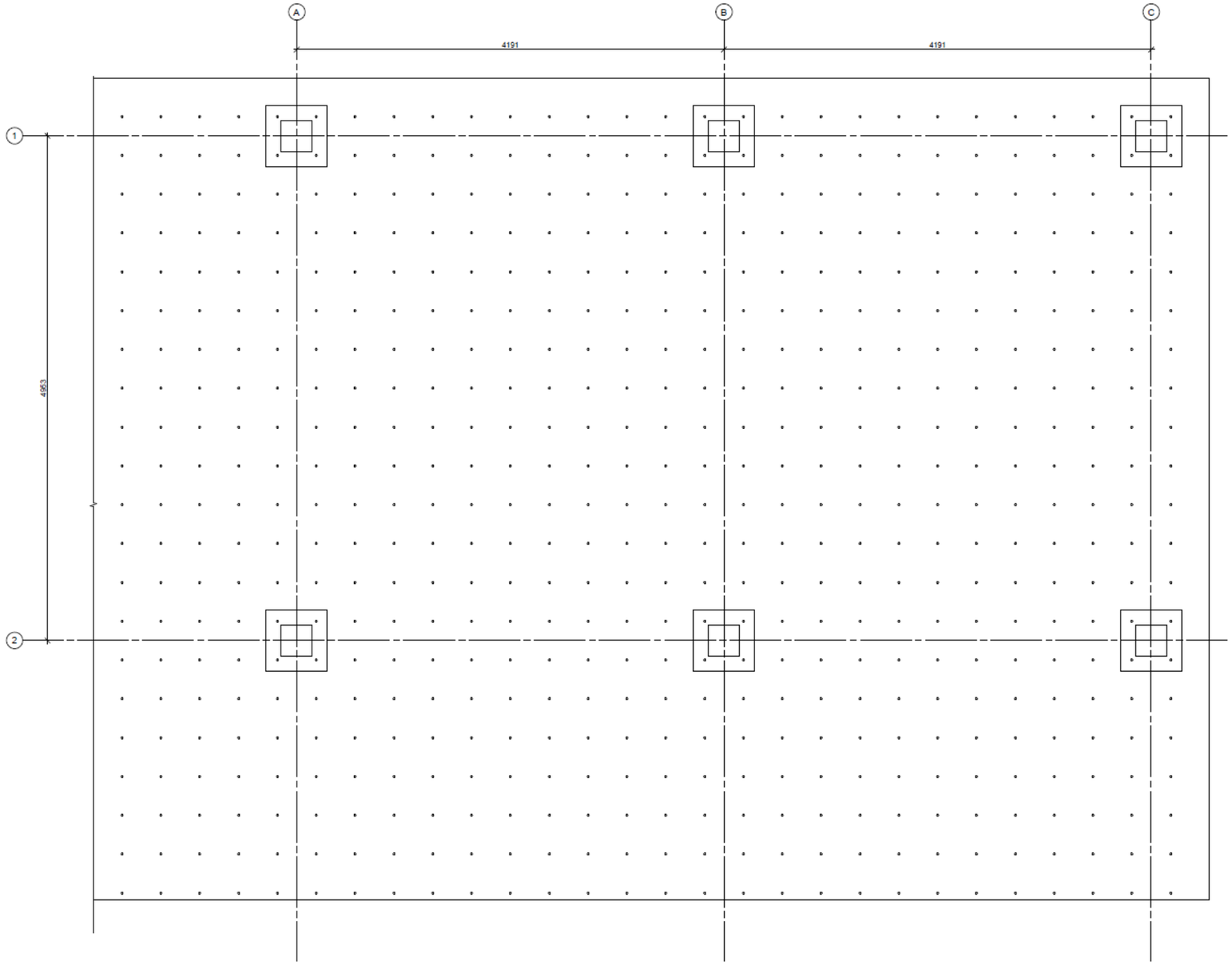

strong floor plan

notes

1. All concrete to have a 28 day strength of 40MPa.
2. Tolerance = ±5mm.
3. Minimum Cover = 23mm.
4. Grout to be general purpose with a 65MPa/28 day compressive strength used in a flowable consistency

Rev	Date	By	Reason
2	18/05/10	EWL	Pricing
1	19/05/10	JEA	Pricing

Consultants

UC UNIVERSITY OF CANTERBURY
Te Whare Wānanga o Waitaha
CHRISTCHURCH NEW ZEALAND

HolmesConsultingGroup
Level 5
123 Victoria Street
PO Box 25355
Christchurch
New Zealand
Telephone
+64 3 366 3366
Facsimile
+64 3 379 2169
www.holmesgroup.com
STRUCTURAL AND CIVIL ENGINEERS

FRST Future Building Systems

Drawn EWL Scale 1 : 20 at A1
Filename

Sheet Title
strong floor plan

Job No	Sheet No	Rev
TD0003.02	S01-01	2

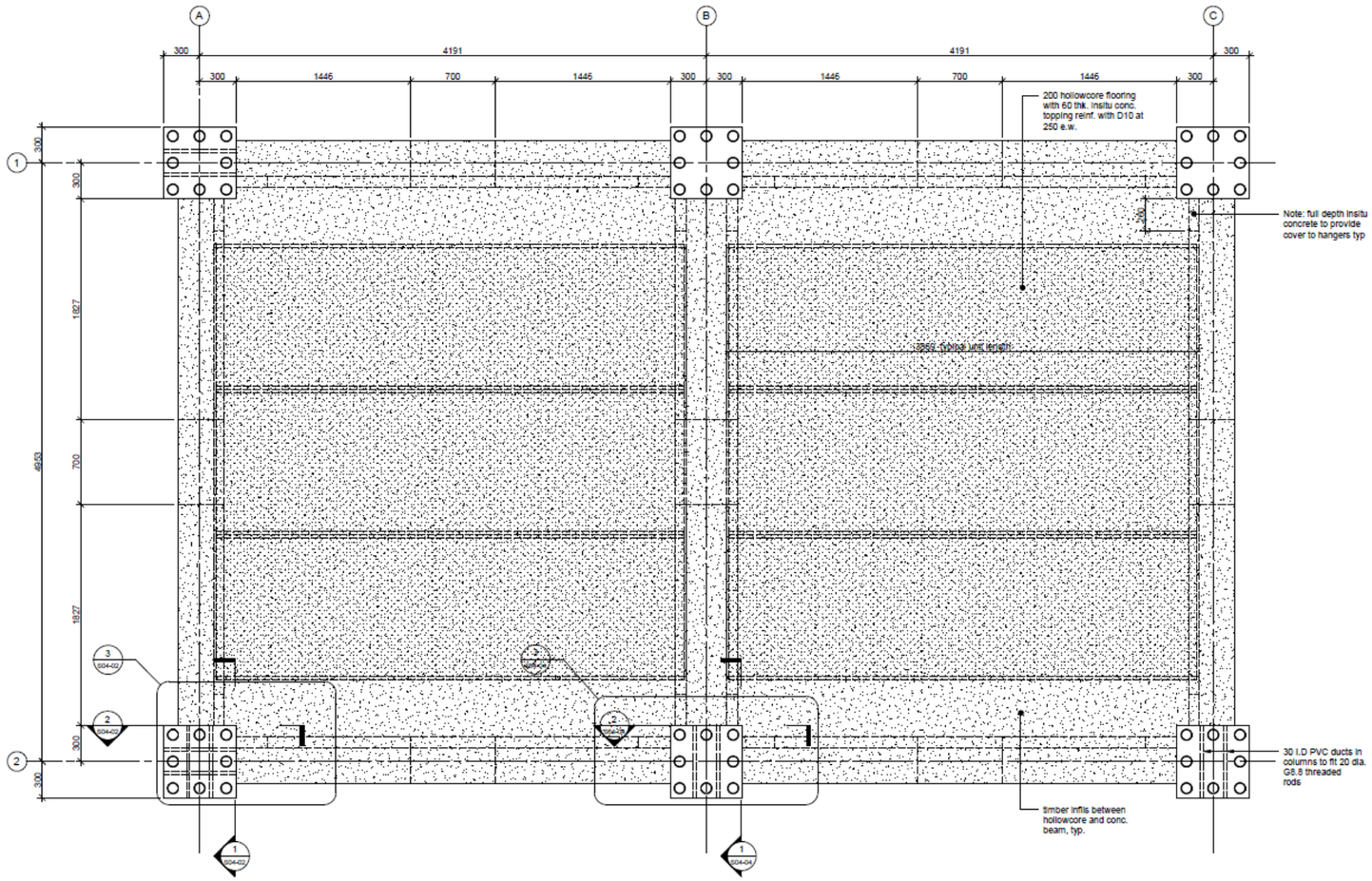

level 1 plan

All dimensions to be verified on site before making any shop drawings or commencing any work.
The copyright of this drawing remains with Holmes Consulting Group

notes

1. All concrete to have a 28 day strength of 40MPa.
2. Tolerance = ±5mm.
3. Minimum Cover = 23mm.
4. Grout to be general purpose with a 65MPa/28 day compressive strength used in a flowable consistency

Rev	Date	By	Reason
2	18/05/10	EWL	Pricing
1	19/05/10	JEA	Pricing

Consultants

UC UNIVERSITY OF CANTERBURY
Te Whare Wānanga o Waitaha
CHRISTCHURCH NEW ZEALAND

HolmesConsultingGroup
Level 5
123 Victoria Street
PO Box 25355
Christchurch
New Zealand
Telephone +64 3 366 3366
Facsimile +64 3 379 2169
www.holmesgroup.com
STRUCTURAL AND CIVIL ENGINEERS

FRST Future Building Systems

Drawn EWL Scale 1 : 20 at A1
Filename

Sheet Title
level 1 floor plan

Job No	Sheet No	Rev
TD0003.02	S01-02	2

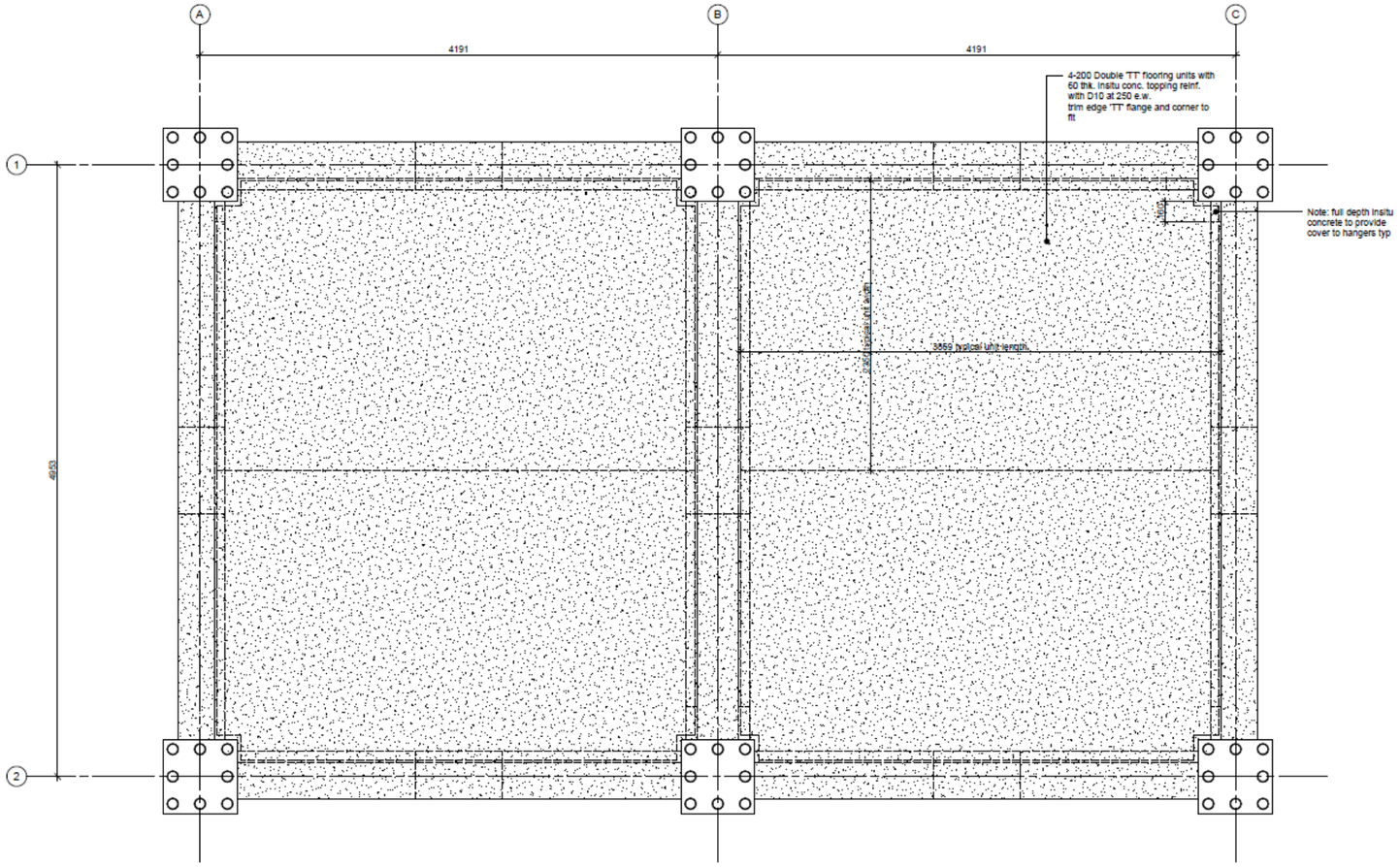

level 2 plan

All dimensions to be verified on site before making any shop drawings or commencing any work.
The copyright of this drawing remains with Holmes Consulting Group

notes

1. All concrete to have a 28 day strength of 40MPa.
2. Tolerance = ±5mm.
3. Minimum Cover = 23mm.
4. Grout to be general purpose with a 65MPa/28 day compressive strength used in a flowable consistency

Rev	Date	By	Reason
2	18/05/10	EWL	Pricing
1	19/05/10	JEA	Pricing

Consultants

UC UNIVERSITY OF CANTERBURY
Te Whare Wānanga o Waitaha
CHRISTCHURCH NEW ZEALAND

HolmesConsultingGroup
Level 5
123 Victoria Street
PO Box 25356
Christchurch
New Zealand
Telephone
+64 3 366 3366
Facsimile
+64 3 379 2169
www.holmesgroup.com
STRUCTURAL AND CIVIL ENGINEERS

FRST Future Building Systems

Drawn EWL Scale 1 : 20 at A1

Filename

Sheet Title

level 2 floor plan

Job No	Sheet No	Rev
TD0003.02	S01-03	2

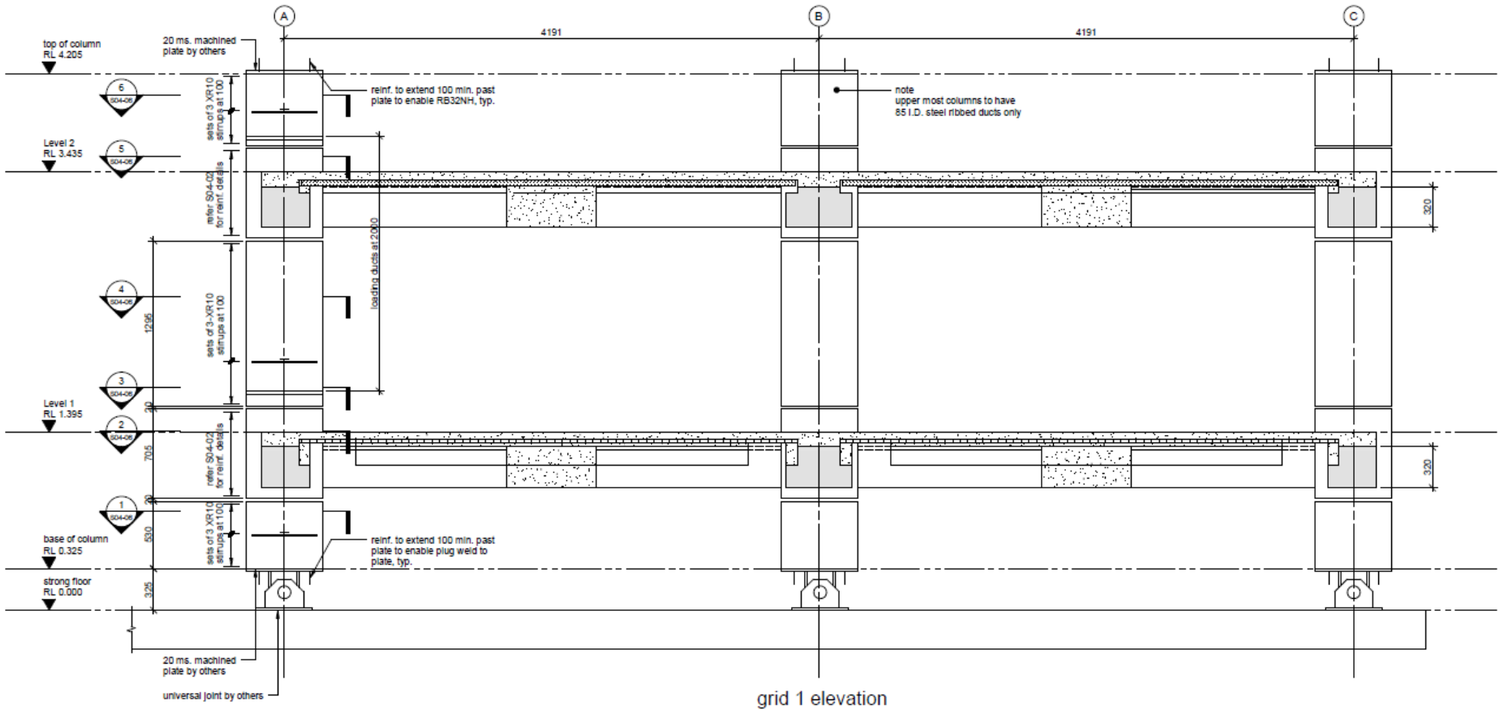

grid 1 elevation

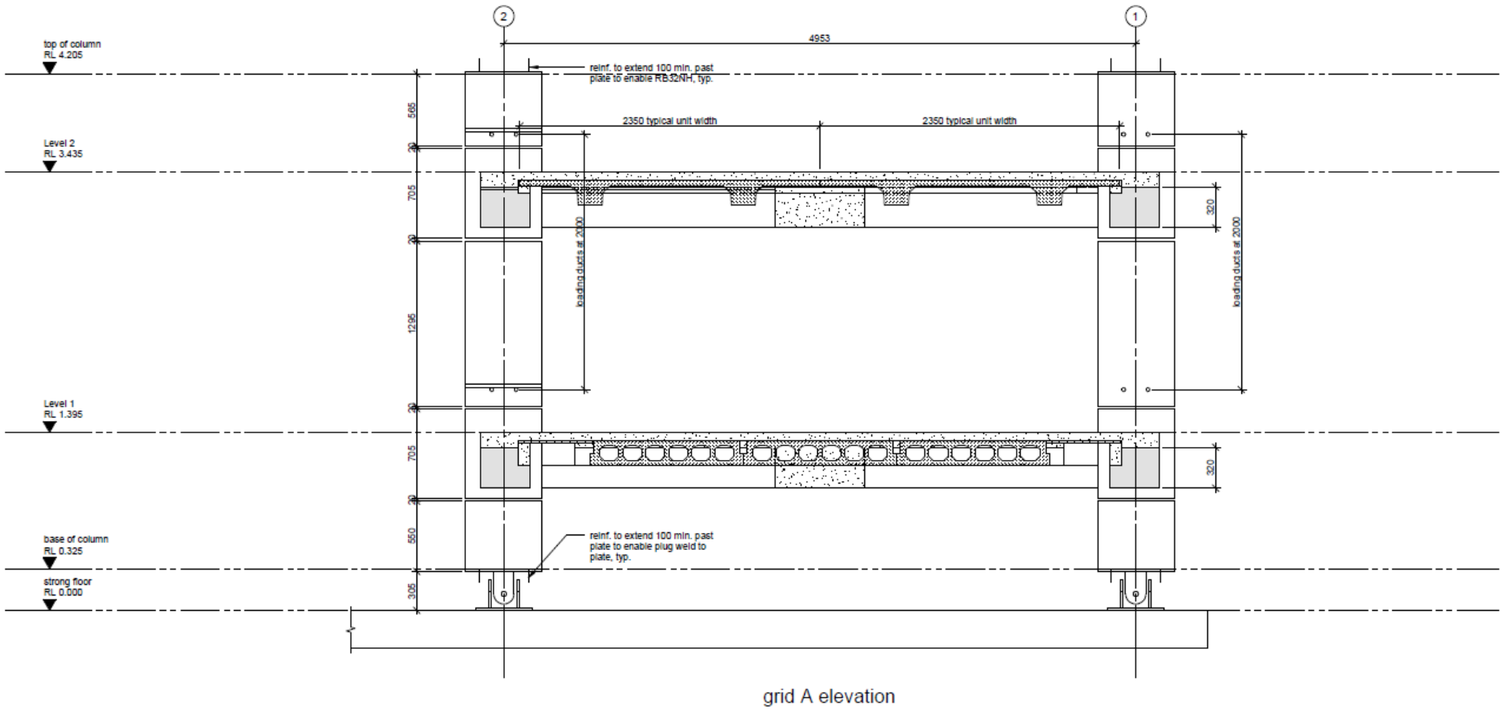

grid A elevation

All dimensions to be verified on site before making any shop drawings or commencing any work.

notes

1. All concrete to have a 28 day strength of 40MPa.
2. Tolerance = ±5mm.
3. Minimum Cover = 23mm.
4. Grout to be general purpose with a 65MPa/28 day compressive strength used in a flowable consistency

Rev	Date	By	Reason
2	18/05/10	EWL	Pricing
1	19/05/10	JEA	Pricing

Consultants

UC UNIVERSITY OF CANTERBURY
Te Whare Wānanga o Waitaha
CHRISTCHURCH NEW ZEALAND

HolmesConsultingGroup
Level 5
123 Victoria Street
PO Box 25365
Christchurch
New Zealand
Telephone
+64 3 366 3366
Facsimile
+64 3 379 2169
www.holmesgroup.com
STRUCTURAL AND CIVIL ENGINEERS

FRST Future Building Systems

Drawn EWL Scale 1 : 20 at A1
Filename

Sheet Title
grid 1 elevation
grid A elevation

Job No	Sheet No	Rev
TD0003.02	S02-01	2

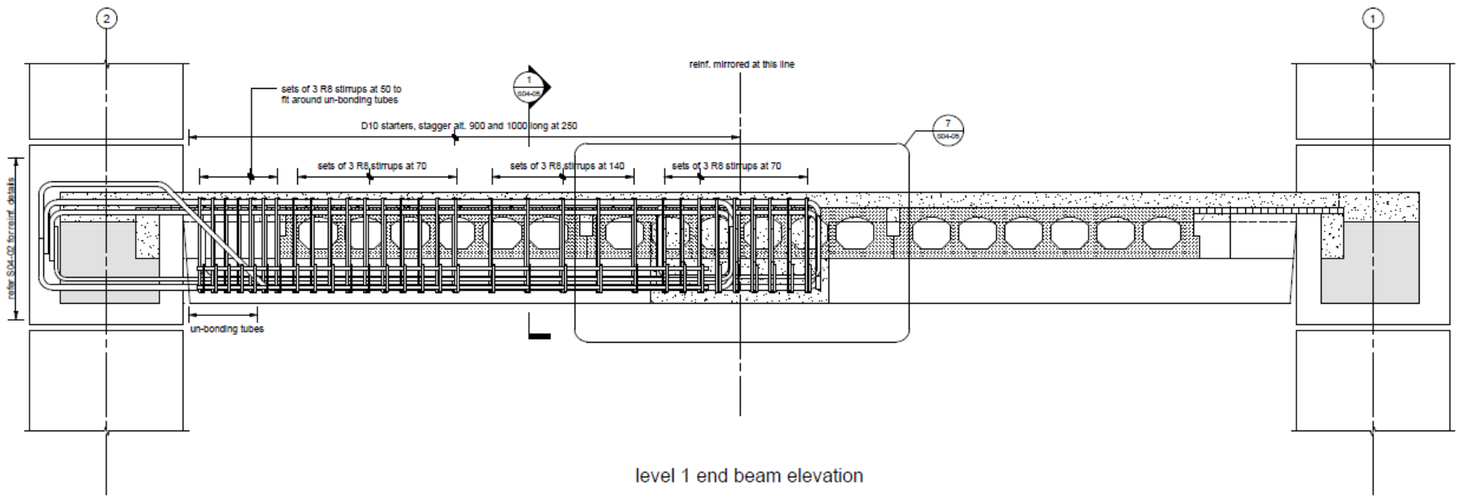

level 1 end beam elevation

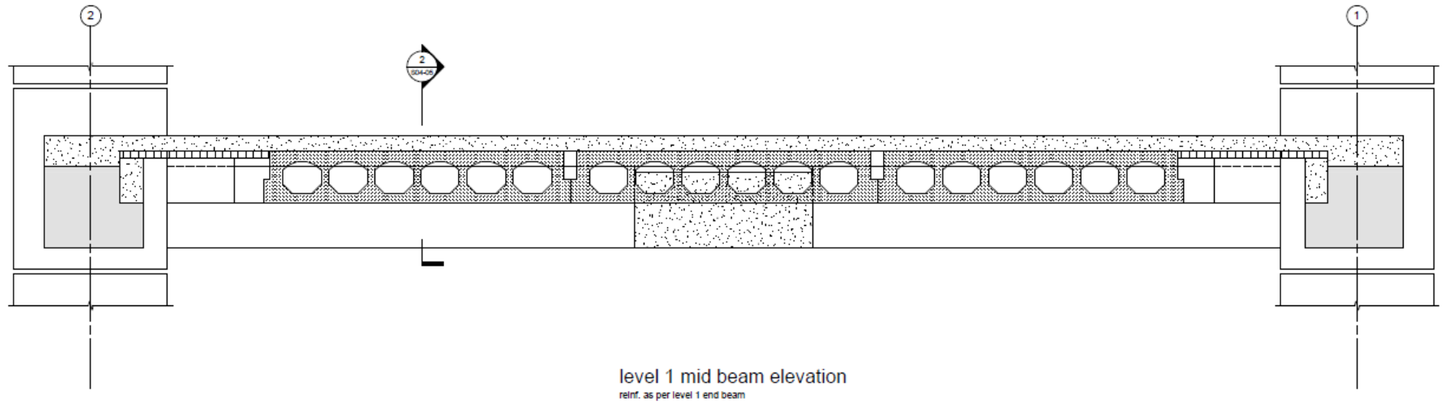

level 1 mid beam elevation

reinf. as per level 1 end beam

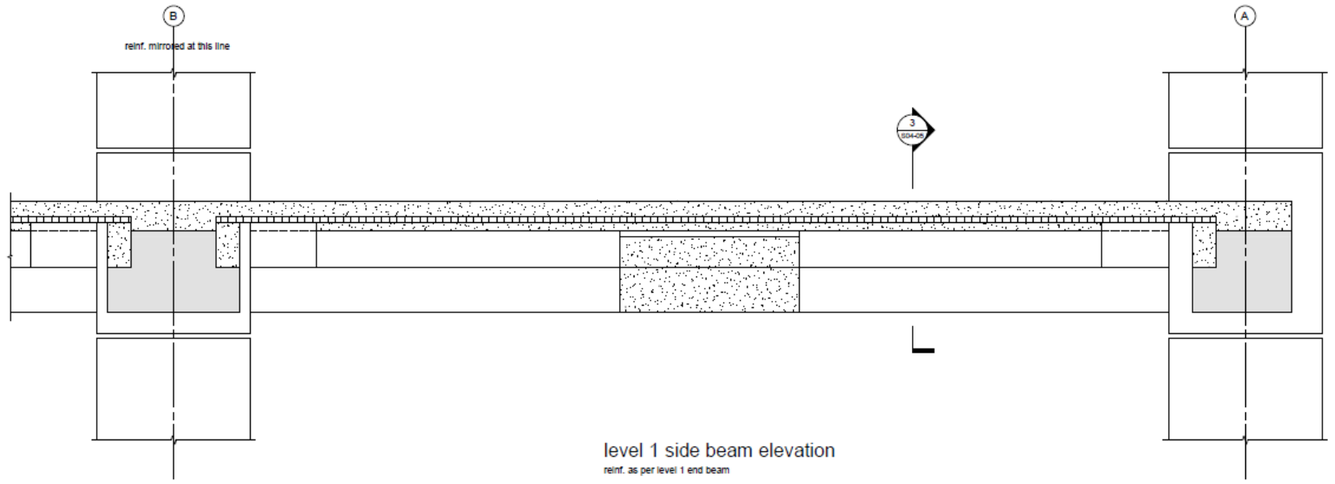

level 1 side beam elevation

reinf. as per level 1 end beam

notes

1. All concrete to have a 28 day strength of 40MPa.
2. Tolerance = ±5mm.
3. Minimum Cover = 23mm.
4. Grout to be general purpose with a 65MPa/28 day compressive strength used in a flowable consistency

Rev	Date	By	Reason
2	18/05/10	EWL	Pricing
1	19/05/10	JEA	Pricing

Consultants

UC UNIVERSITY OF CANTERBURY
Te Whare Wānanga o Waitaha
CHRISTCHURCH NEW ZEALAND

HolmesConsultingGroup
Level 5
123 Victoria Street
PO Box 25355
Christchurch
New Zealand
Telephone
+64 3 366 3366
Facsimile
+64 3 379 2169
www.holmesgroup.com
STRUCTURAL AND CIVIL ENGINEERS

FRST Future Building Systems

Drawn EWL Scale 1 : 10 at A1

Filename

Sheet Title

level 1 beam reinforcing

Job No	Sheet No	Rev
TD0003.02	S03-01	2

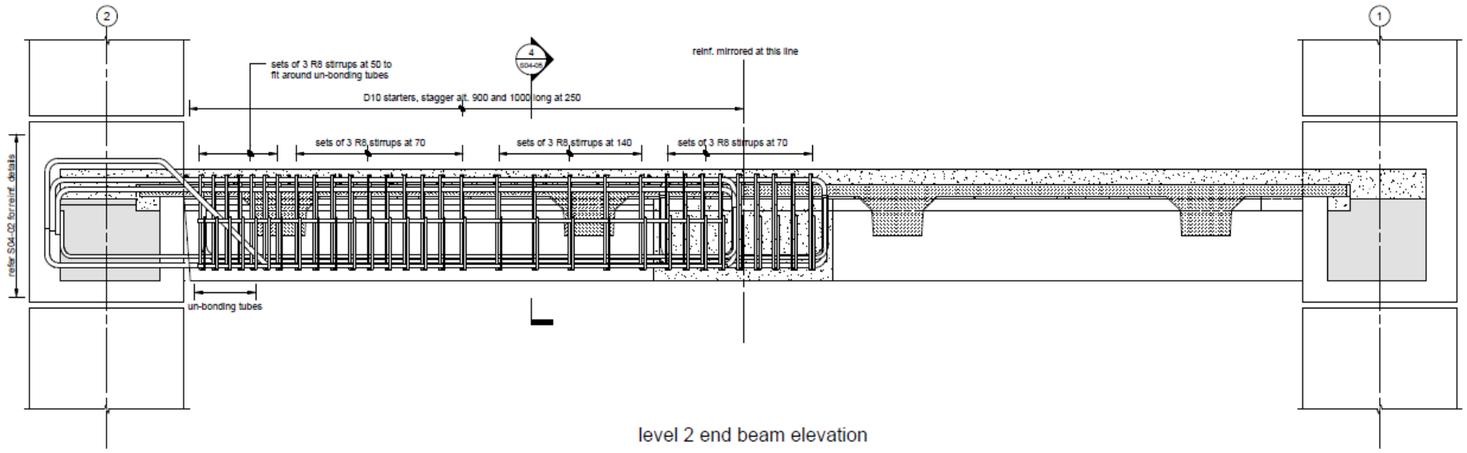

level 2 end beam elevation

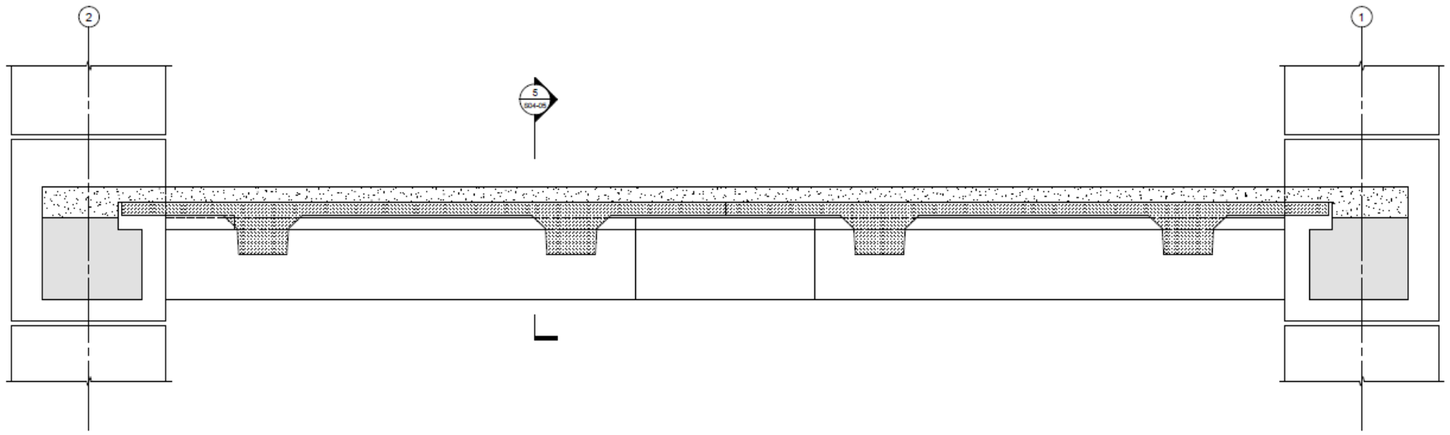

level 2 mid beam elevation
reinf. as per level 2 end beam

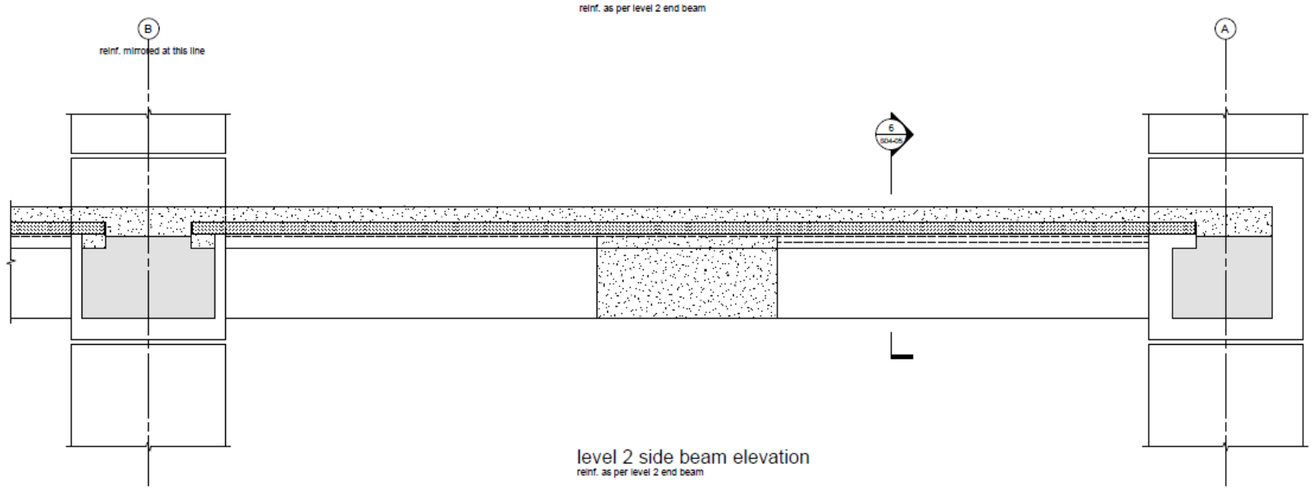

level 2 side beam elevation
reinf. as per level 2 end beam

notes

1. All concrete to have a 28 day strength of 40MPa.
2. Tolerance = ±5mm.
3. Minimum Cover = 23mm.
4. Grout to be general purpose with a 65MPa/28 day compressive strength used in a flowable consistency

Rev	Date	By	Reason
2	18/06/10	EWL	Pricing
1	19/05/10	JEA	Pricing

Consultants

UNIVERSITY OF CANTERBURY
Te Whare Wānanga o Waitaha
CHRISTCHURCH NEW ZEALAND

HolmesConsultingGroup
STRUCTURAL AND CIVIL ENGINEERS
Level 5
123 Victoria Street
PO Box 25355
Christchurch
New Zealand
Telephone
+64 3 366 3366
Facsimile
+64 3 379 2169
www.holmesgroup.com

FRST Future Building Systems

Drawn EWL Scale 1 : 10 at A1
Filename

Sheet Title
level 2 beam reinforcing

Job No	Sheet No	Rev
TD0003.02	S03-02	2

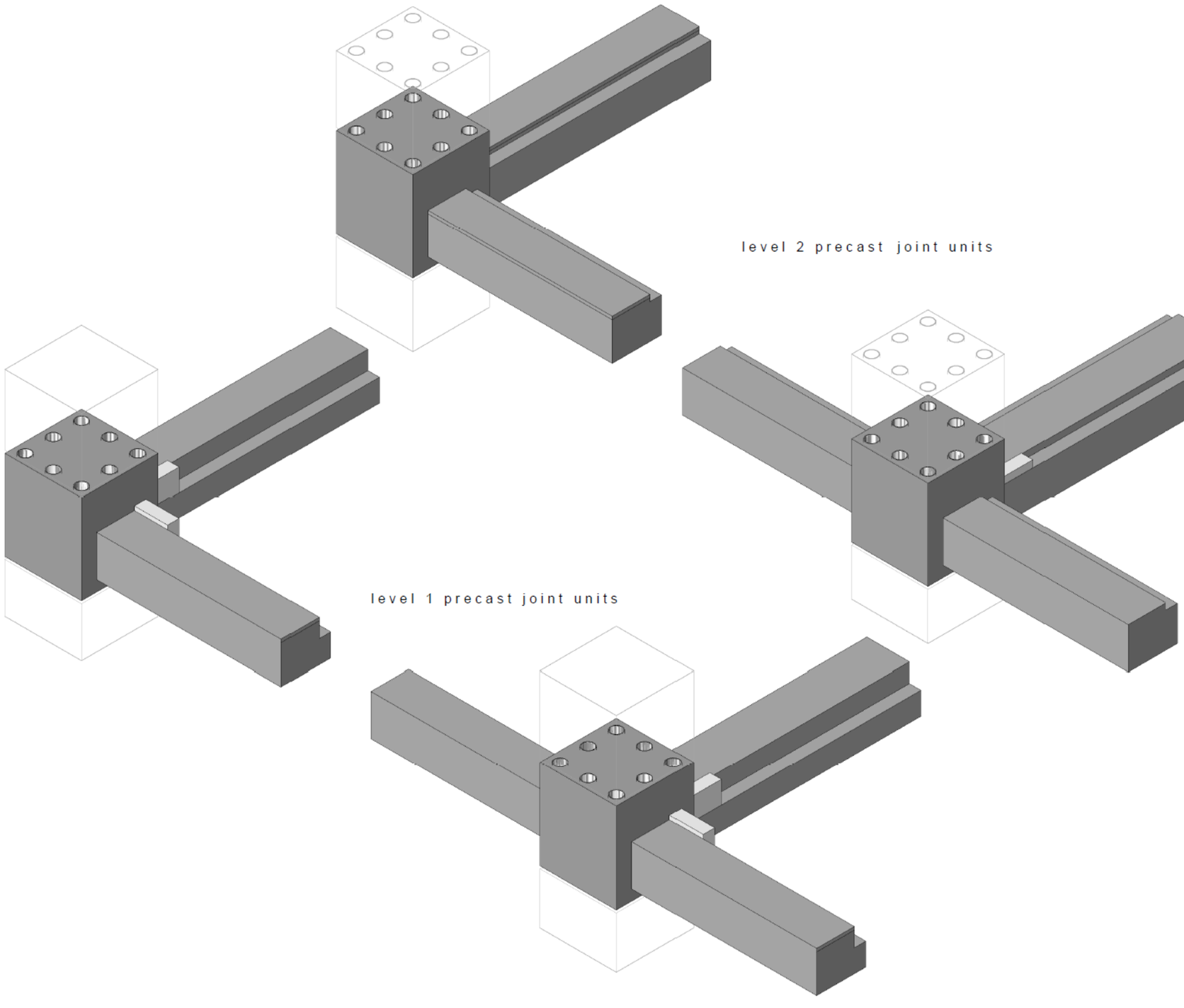

notes

1. All concrete to have a 28 day strength of 40MPa.
2. Tolerance = ±5mm.
3. Minimum Cover = 23mm.
4. Grout to be general purpose with a 65MPa/28 day compressive strength used in a flowable consistency

Rev	Date	By	Reason
2	19/05/10	EWL	Pricing
1	19/05/10	JEA	Pricing

Consultants

UNIVERSITY OF CANTERBURY
Te Whare Wānanga o Waitaha
CHRISTCHURCH NEW ZEALAND

HolmesConsultingGroup
Level 5
123 Victoria Street
PO Box 25355
Christchurch
New Zealand
Telephone
+64 3 366 3366
Facsimile
+64 3 379 2169
www.holmesgroup.com
STRUCTURAL AND CIVIL ENGINEERS

FRST Future Building Systems

Drawn EWL Scale at A1
Filename

Sheet Title
precast unit 3D views

Job No	Sheet No	Rev
TD0003.02	S03-03	2

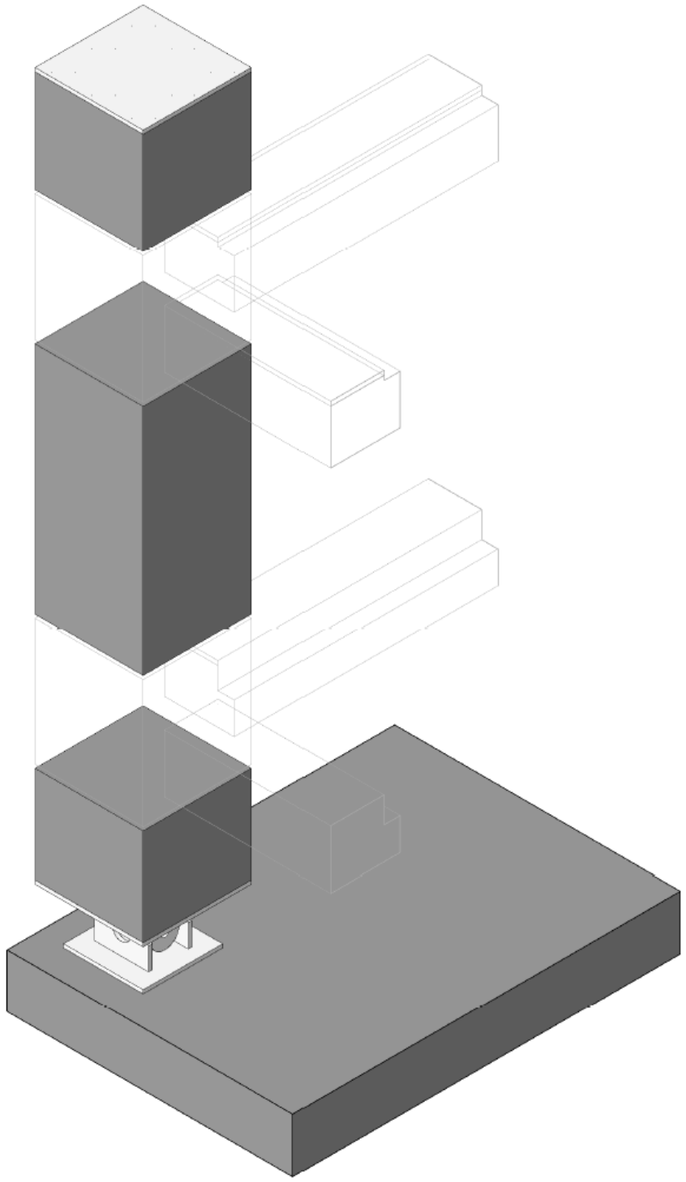

precast column - corner

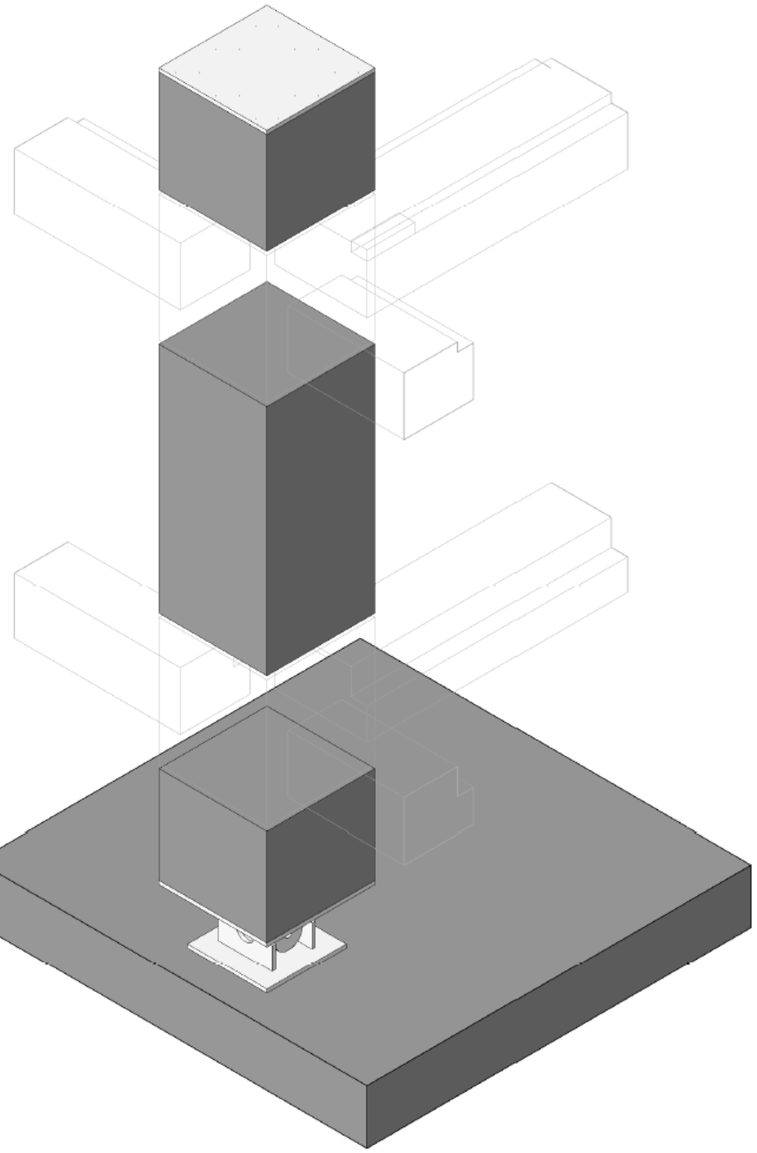

precast column - mid

notes

1. All concrete to have a 28 day strength of 40MPa.
2. Tolerance = ±5mm.
3. Minimum Cover = 23mm.
4. Grout to be general purpose with a 65MPa/28 day compressive strength used in a flowable consistency

Rev	Date	By	Reason
2	18/06/10	EWL	Pricing
1	19/05/10	JEA	Pricing

Consultants

UNIVERSITY OF CANTERBURY
Te Whare Wānanga o Waitaha
CHRISTCHURCH NEW ZEALAND

HolmesConsultingGroup
Level 5
123 Victoria Street
PO Box 25355
Christchurch
New Zealand
Telephone
+64 3 366 3366
Facsimile
+64 3 379 2169
www.holmesgroup.com
STRUCTURAL AND CIVIL ENGINEERS

FRST Future Building Systems

Drawn JEA Scale at A1
Filename

Sheet Title

precast columns 3D views

Job No	Sheet No	Rev
TD0003.02	S03-04	2

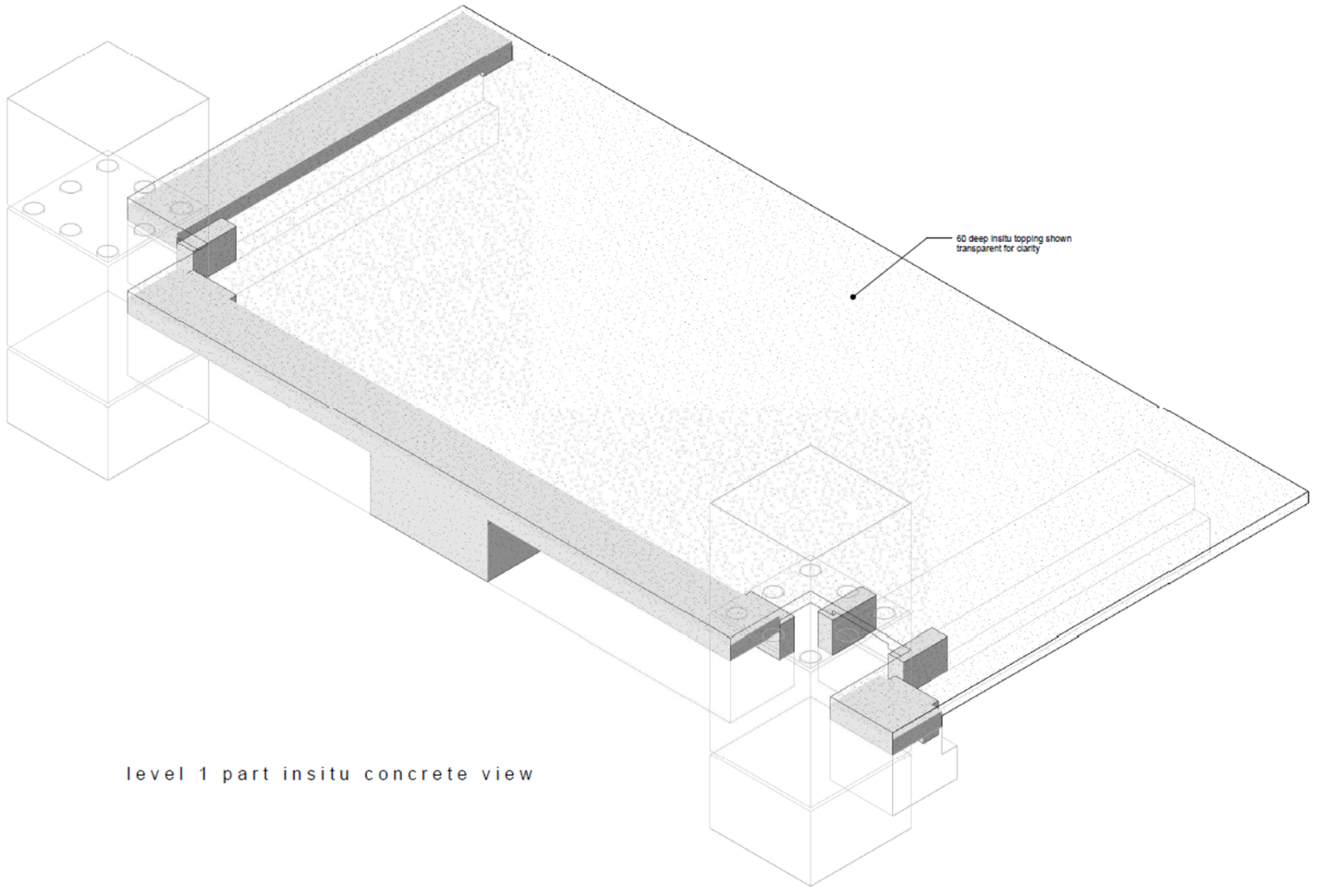

level 1 part insitu concrete view

notes

1. All concrete to have a 28 day strength of 40MPa.
2. Tolerance = ±5mm.
3. Minimum Cover = 23mm.
4. Grout to be general purpose with a 65MPa/28 day compressive strength used in a flowable consistency

Rev	Date	By	Reason
2	18/06/10	EWL	Pricing
1	10/05/10	JEA	Pricing

Consultants

UC UNIVERSITY OF CANTERBURY
Te Whare Wānanga o Waitaha
CHRISTCHURCH NEW ZEALAND

Holmes Consulting Group
STRUCTURAL AND CIVIL ENGINEERS
Level 6
123 Victoria Street
PO Box 25355
Christchurch
New Zealand
Telephone
+64 3 366 3366
Facsimile
+64 3 379 2169
www.holmesgroup.com

FRST Future Building Systems

Drawn Author Scale at A1
Filename

Sheet Title
insitu concrete 3D view

Job No	Sheet No	Rev
TD0003.02	S03-05	2

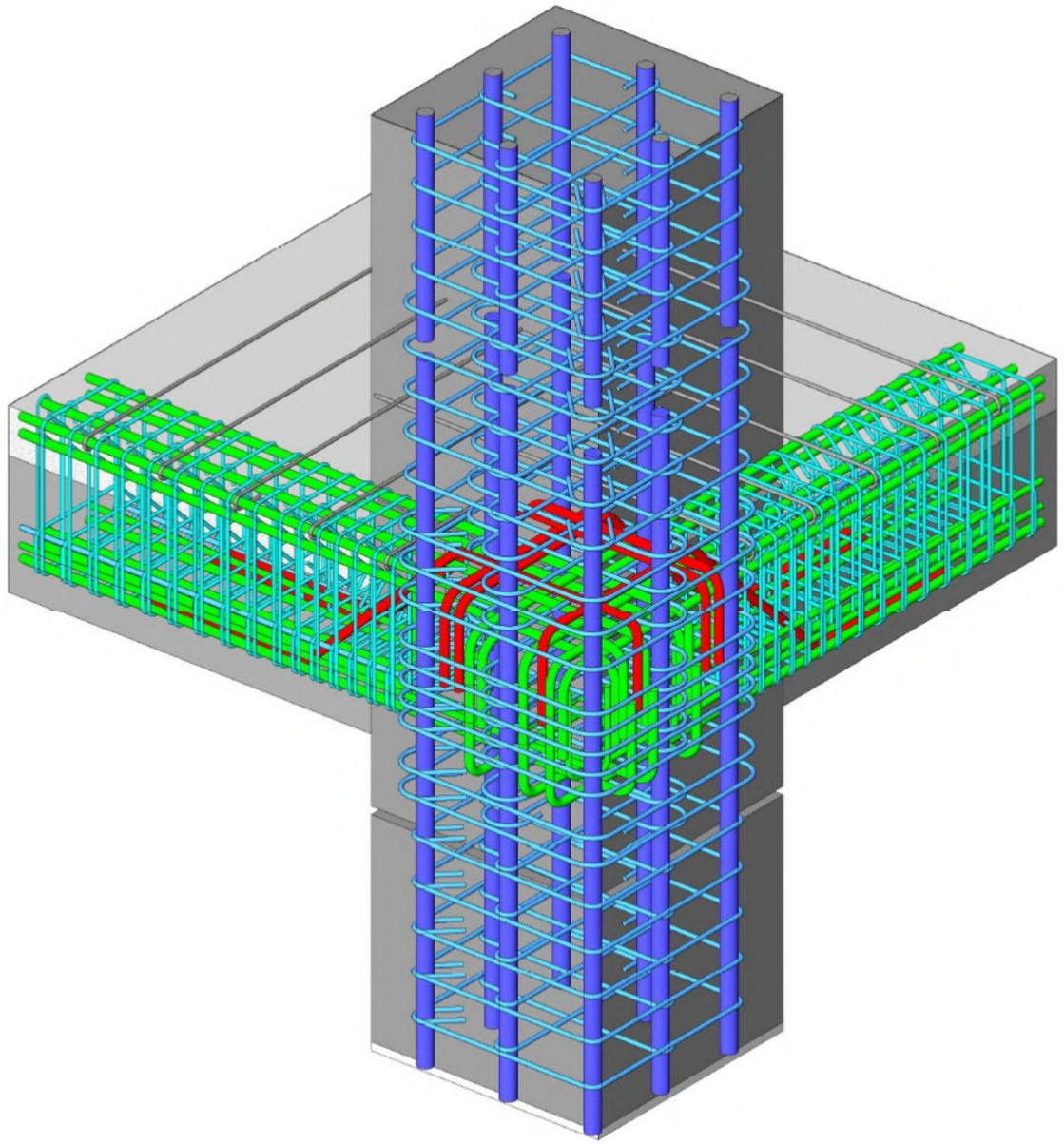

All dimensions to be verified on site before making any shop drawings or commencing any work.

notes

1. All concrete to have a 28 day strength of 40MPa.
2. Tolerance = ±5mm.
3. Minimum Cover = 23mm.
4. Grout to be general purpose with a 65MPa/28 day compressive strength used in a flowable consistency

Rev	Date	By	Reason
2	18/05/10	EWL	Pricing
1	18/05/10	JEA	Pricing

Consultants

UNIVERSITY OF CANTERBURY
Te Whare Wānanga o Waitaha
CHRISTCHURCH NEW ZEALAND

HolmesConsultingGroup
STRUCTURAL AND CIVIL ENGINEERS
Level 5
123 Victoria Street
PO Box 25388
Christchurch
New Zealand
Telephone
+64 3 366 3366
Facsimile
+64 3 379 2169
www.holmesgroup.com

FRST Future Building Systems

Drawn EWL Scale at A1
Filename

Sheet Title

corner beam-column joint 3D view

Job No	Sheet No	Rev
TD0003.02	S04-01	2

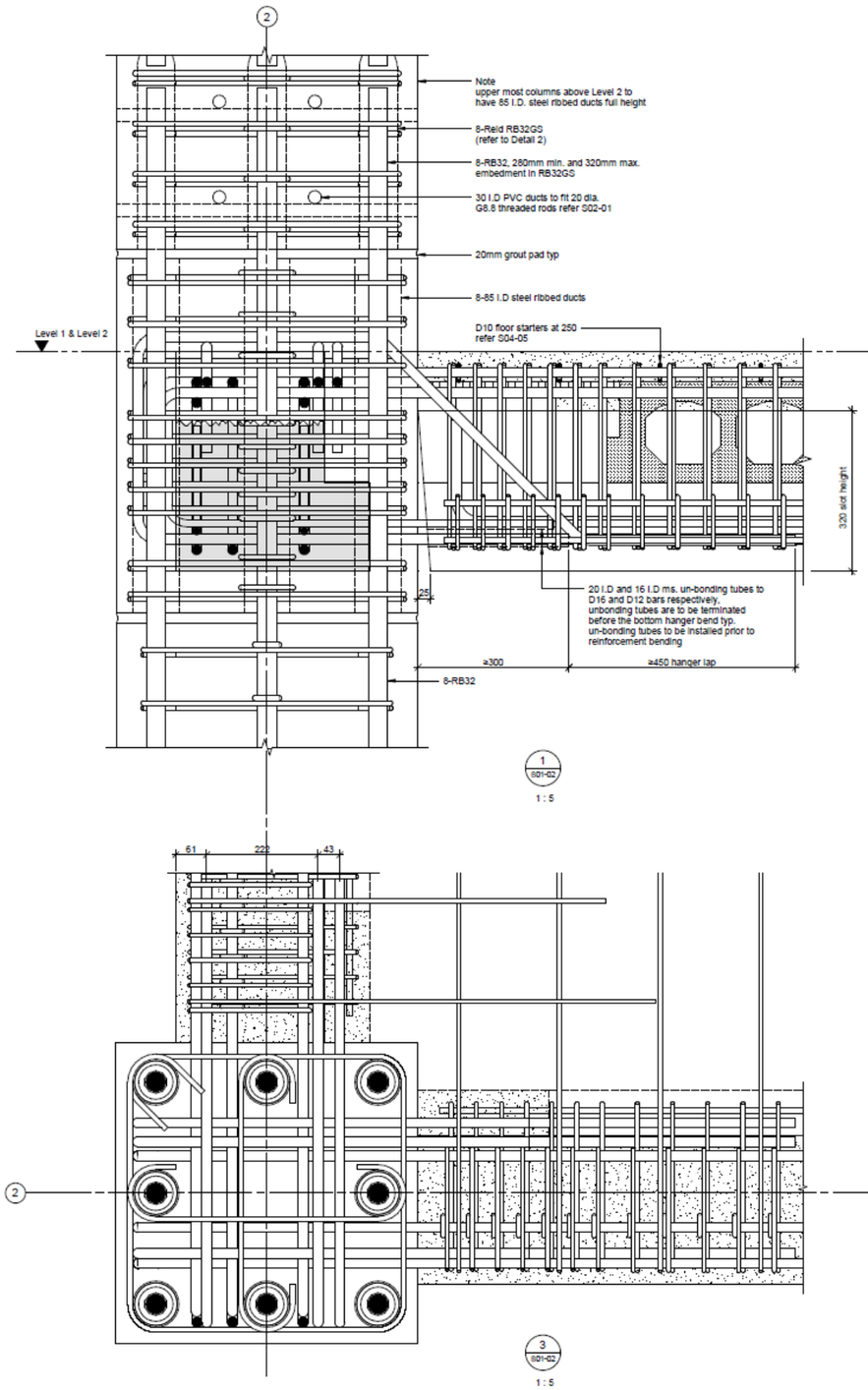

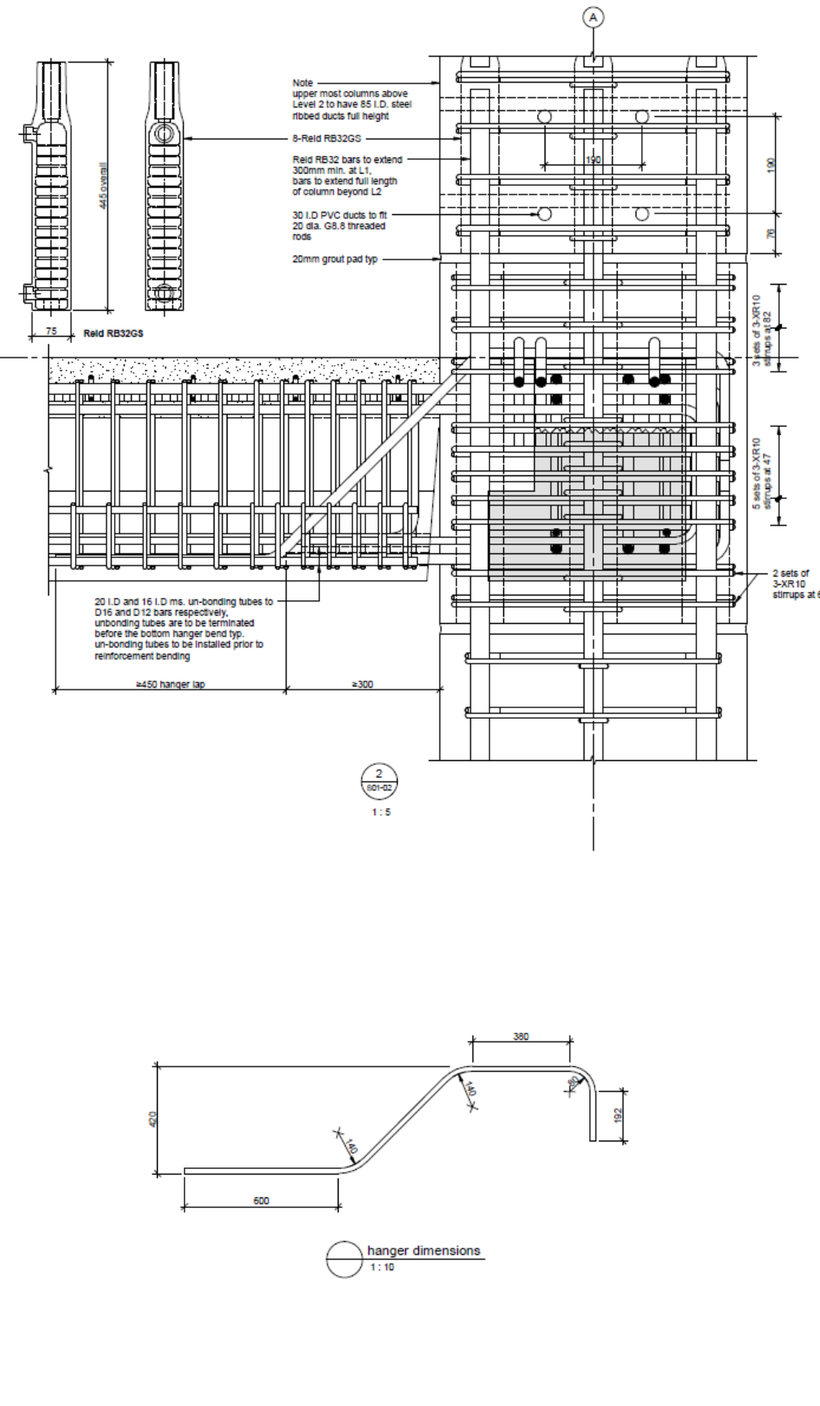

All dimensions to be verified on site before making any shop drawings or commencing any work.

notes

1. All concrete to have a 28 day strength of 40MPa.
2. Tolerance = ±5mm.
3. Minimum Cover = 23mm.
4. Grout to be general purpose with a 65MPa/28 day compressive strength used in a flowable consistency
5. Beam stirrups to fit around un-bonding tubes

Rev	Date	By	Reason
2	18/06/10	EWL	Pricing
1	19/05/10	JEA	Pricing

Consultants

UNIVERSITY OF CANTERBURY
Te Whare Wānanga o Waitaha
CHRISTCHURCH NEW ZEALAND

HolmesConsultingGroup
STRUCTURAL AND CIVIL ENGINEERS
Level 5
123 Victoria Street
PO Box 25355
Christchurch
New Zealand
Telephone
+64 3 366 3366
Facsimile
+64 3 379 2169
www.holmesgroup.com

FRST Future Building Systems

Drawn EWL Scale As indicated
Filename

Sheet Title

corner beam - column joint details

Job No	Sheet No	Rev
TD0003.02	S04-02	2

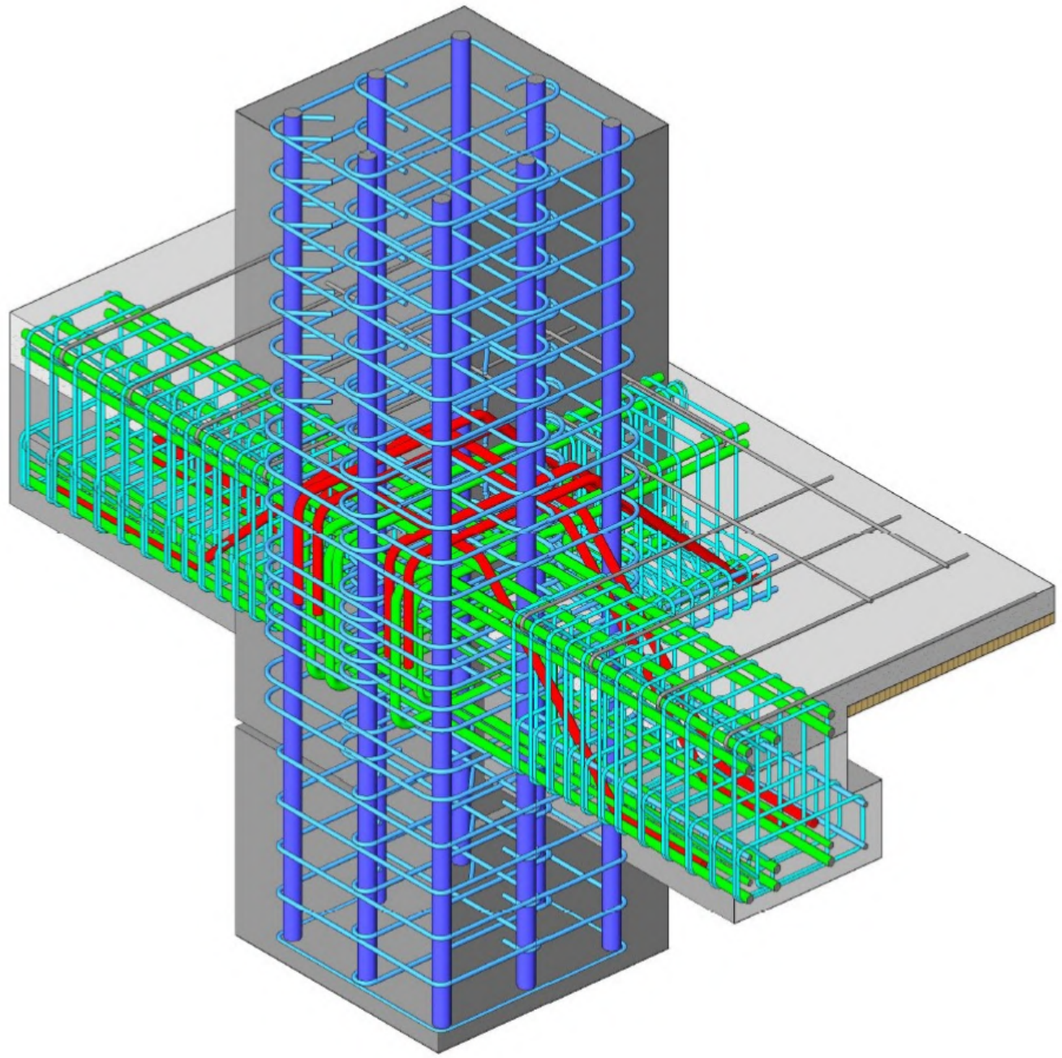

All dimensions to be verified on site before making any shop drawings or commencing any work.

notes

1. All concrete to have a 28 day strength of 40MPa.
2. Tolerance = ±5mm.
3. Minimum Cover = 23mm.
4. Grout to be general purpose with a 65MPa/28 day compressive strength used in a flowable consistency

Rev	Date	By	Reason
2	18/06/10	EWL	Pricing
1	19/05/10	JEA	Pricing

Consultants

UNIVERSITY OF CANTERBURY
Te Whare Wānanga o Waitaha
CHRISTCHURCH NEW ZEALAND

HolmesConsultingGroup
Level 5
123 Victoria Street
PO Box 25366
Christchurch
New Zealand
Telephone
+64 3 366 3366
Facsimile
+64 3 379 2169
www.holmesgroup.com
STRUCTURAL AND CIVIL ENGINEERS

FRST Future Building Systems

Drawn EWL Scale at A1
Filename

Sheet Title

side beam - column joint
3D view

Job No	Sheet No	Rev
TD0003.02	S04-03	2

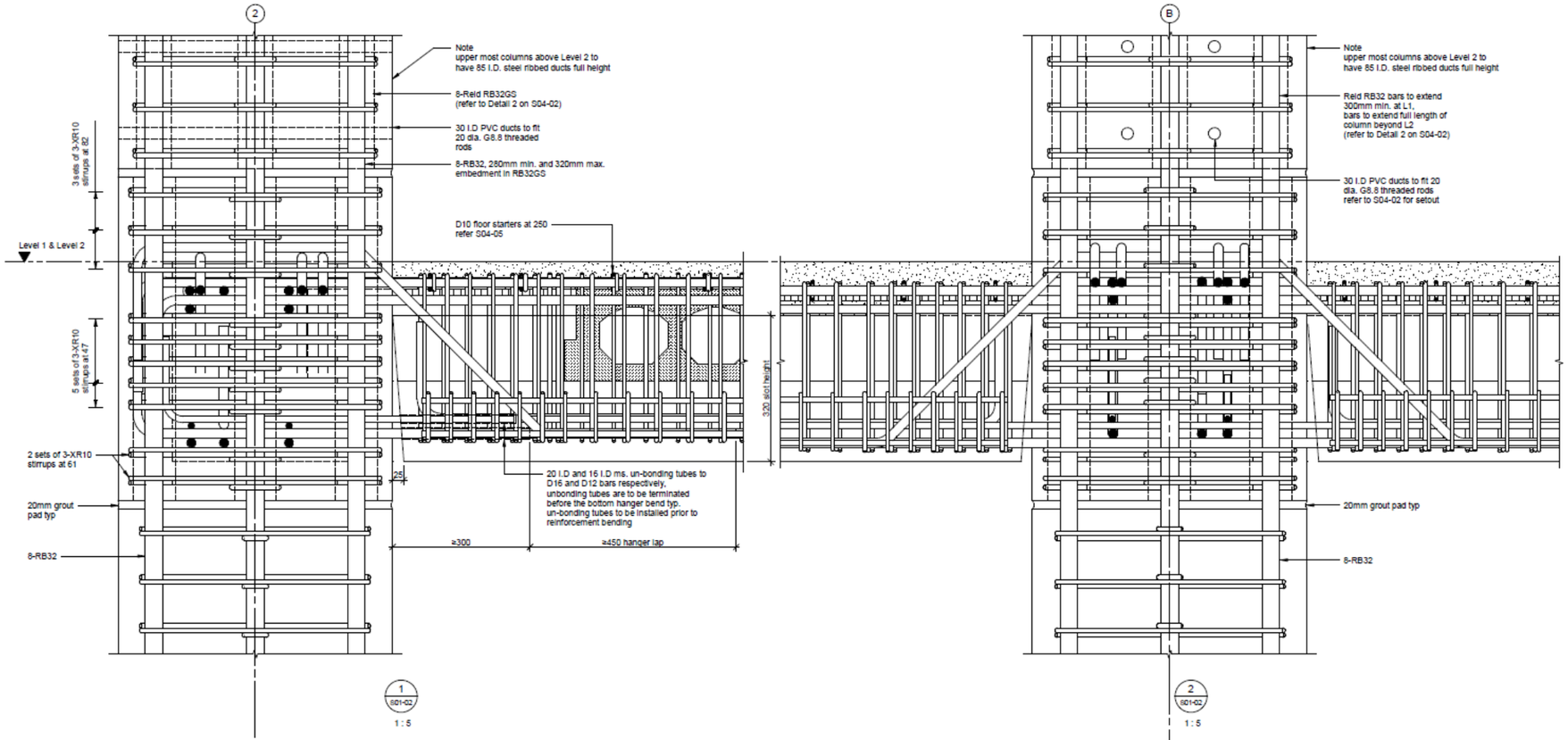

All dimensions to be verified on site before making any shop drawings or commencing any work.
The copyright of this drawing remains with Holmes Consulting Group

notes

1. All concrete to have a 28 day strength of 40MPa.
2. Tolerance = ±5mm.
3. Minimum Cover = 23mm.
4. Grout to be general purpose with a 65MPa/28 day compressive strength used in a flowable consistency
5. Beam stirrups to fit around un-bonding tubes

Rev	Date	By	Reason
2	18/05/10	EWL	Pricing
1	19/05/10	JEA	Pricing

Consultants

UNIVERSITY OF CANTERBURY
Te Whare Wānanga o Waitaha
CHRISTCHURCH NEW ZEALAND

HolmesConsultingGroup
STRUCTURAL AND CIVIL ENGINEERS
Level 5
123 Victoria Street
PO Box 25388
Christchurch
New Zealand
Telephone
+64 3 366 3366
Facsimile
+64 3 379 2169
www.holmesgroup.com

FRST Future Building Systems

Drawn EWL Scale As indicated
Filename

Sheet Title
side beam - column joint

Job No	Sheet No	Rev
TD0003.02	S04-04	2

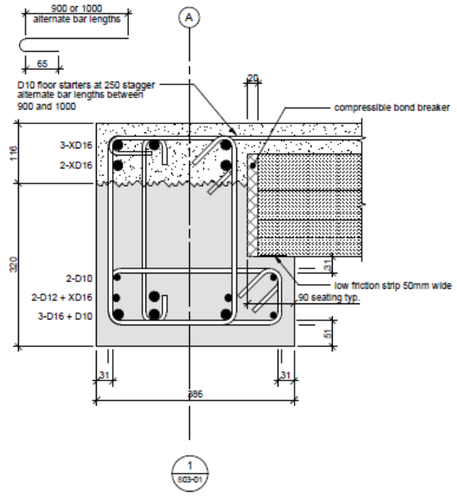

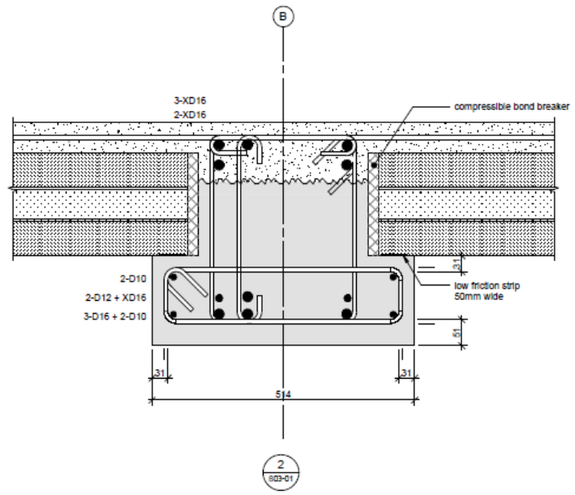

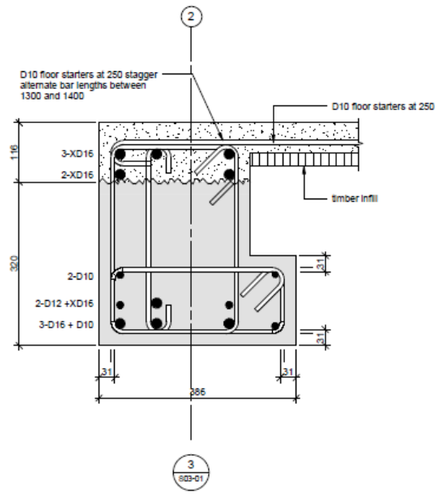

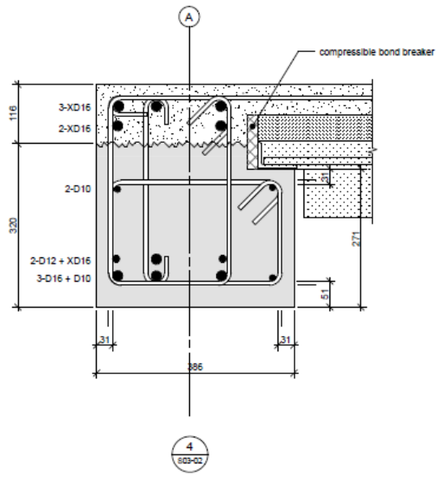

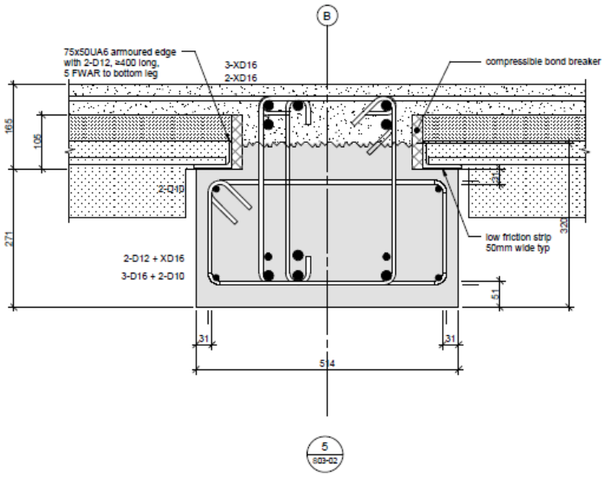

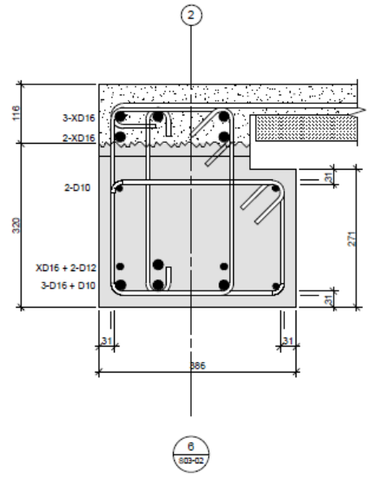

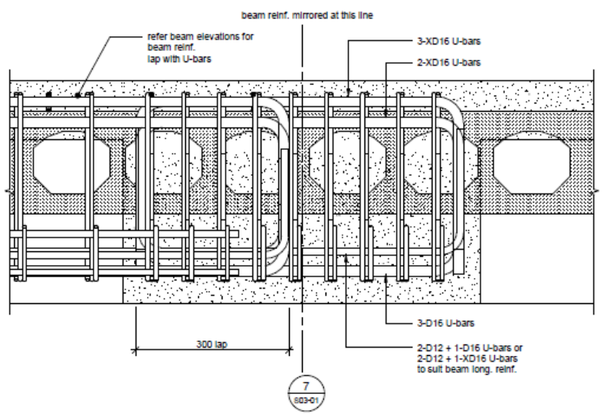

notes

1. All concrete to have a 28 day strength of 40MPa.
2. Tolerance = ±5mm.
3. Minimum Cover = 23mm.
4. Grout to be general purpose with a 65MPa/28 day compressive strength used in a flowable consistency

Rev	Date	By	Reason
2	18/05/10	EWL	Pricing
1	19/05/10	JEA	Pricing

Consultants

UNIVERSITY OF CANTERBURY
Te Whare Wānanga o Waitaha
CHRISTCHURCH NEW ZEALAND

HolmesConsultingGroup
Level 5
123 Victoria Street
PO Box 25355
Christchurch
New Zealand
Telephone
+64 3 366 3366
Facsimile
+64 3 379 2169
www.holmesgroup.com
STRUCTURAL AND CIVIL ENGINEERS

FRST Future Building Systems

Drawn EWL Scale 1 : 5 at A1
Filename

Sheet Title

beam details

Job No	Sheet No	Rev
TD0003.02	S04-05	2

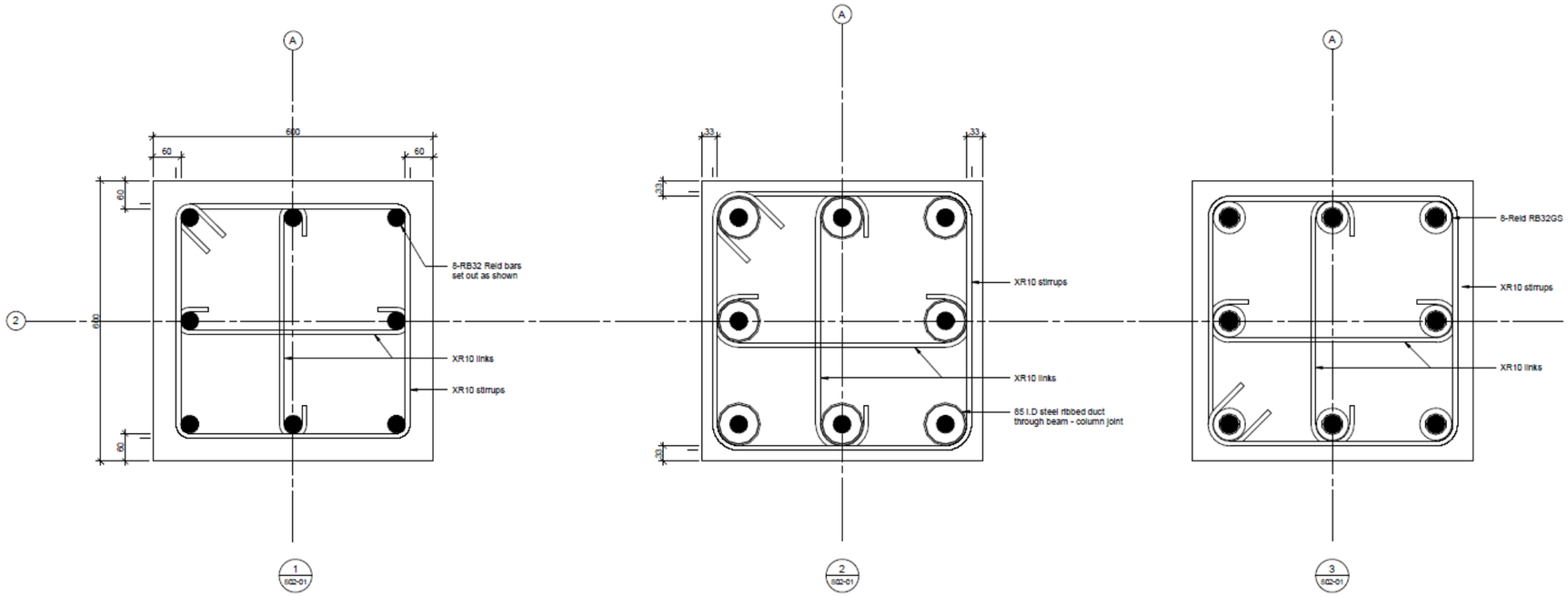

All dimensions to be verified on site before making any shop drawings or commencing any work.
The copyright of this drawing remains with Holmes Consulting Group

notes

1. All concrete to have a 28 day strength of 40MPa.
2. Tolerance = ±5mm.
3. Minimum Cover = 23mm.
4. Grout to be general purpose with a 65MPa/28 day compressive strength used in a flowable consistency

Rev	Date	By	Reason
2	18/06/10	EWL	Pricing
1	19/05/10	JEA	Pricing

Consultants

UC UNIVERSITY OF CANTERBURY
Te Whare Wānanga o Waitaha
CHRISTCHURCH NEW ZEALAND

HolmesConsultingGroup
Level 5
123 Victoria Street
PO Box 25355
Christchurch
New Zealand
STRUCTURAL AND CIVIL ENGINEERS
Telephone
+64 3 366 3366
Facsimile
+64 3 379 2169
www.holmesgroup.com

FRST Future Building Systems

Drawn EWL Scale 1 : 5 at A1

Filename

Sheet Title

column details

Job No	Sheet No	Rev
TD0003.02	S04-06	2

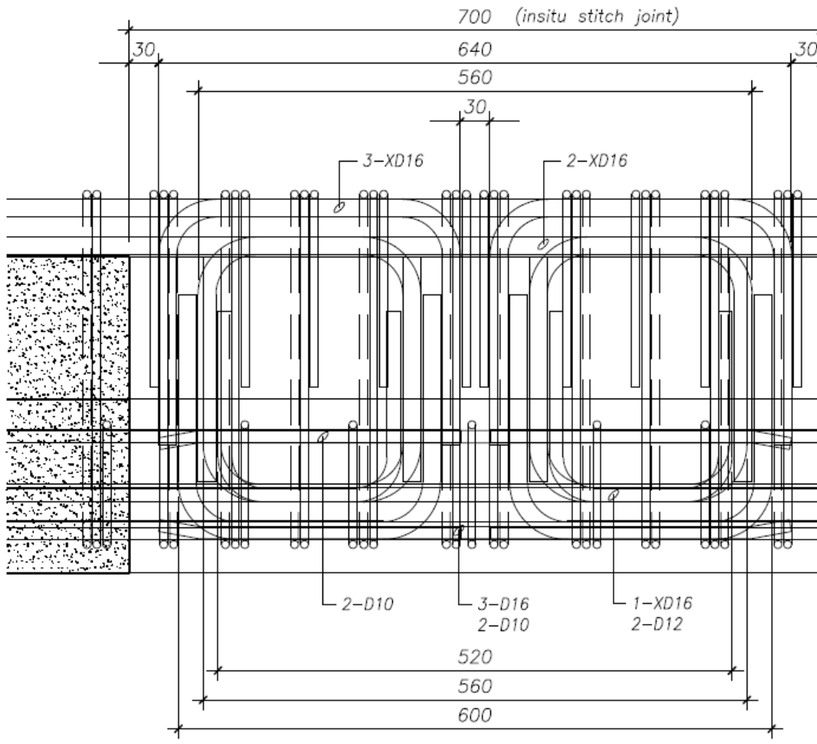

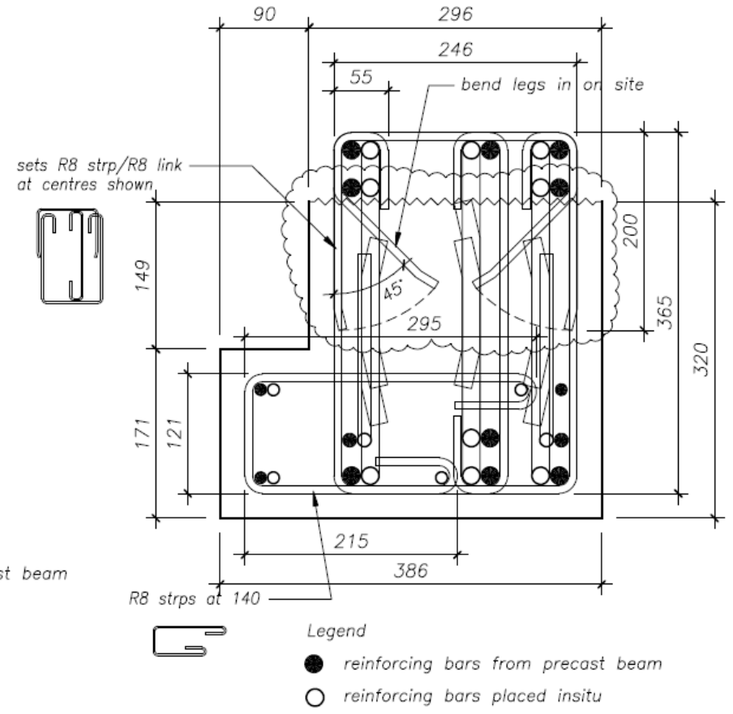

precast shop drawing

RM DRAUGHTING	BRADFORD PRECAST LTD	REV	DATE	REVISION DETAILS	University of Canterbury – FRST Future Building Systems	DRAWN RMM	JOB NO 2278	
P.O.BOX 53	P.O.BOX 214 ASHBURTON	1	02.09.10	Construction				
KIRWEE PH 03 318 1605	Telephone (03) 308-9039	C	24.08.10	Approval update				
CANTERBURY FAX 03 318 1625	Facsimile (03) 308 6300	B	23.08.10	Approval update				
		A	16.08.10	Approval	SUB TITLE beam insitu stitch joint A–1	SCALE 1:5 original size – A3	DRAWING No SJ.A–1	REV 1

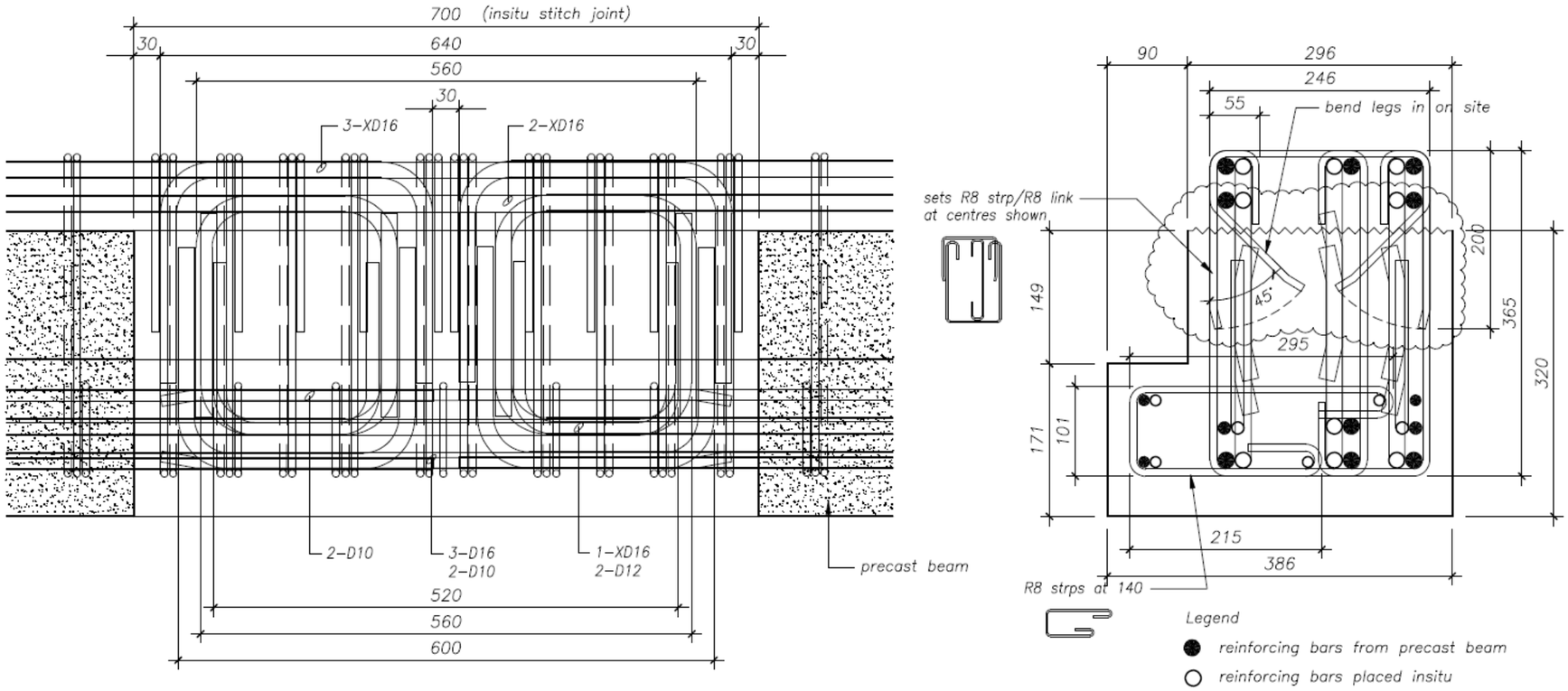

RM DRAUGHTING P.O.BOX 53 KIRWEE PH 03 318 1605 CANTERBURY FAX 03 318 1625	BRADFORD PRECAST LTD P.O.BOX 214 ASHBURTON Telephone (03) 308–9039 Facsimile (03) 308 6300	precast shop drawing

REV	DATE	REVISION DETAILS
1	02.09.10	Construction
B	24.08.10	Approval update
A	16.08.10	Approval

University of Canterbury – FRST Future Building Systems	DRAWN RMM	JOB NO 2278	
SUB TITLE beam insitu stitch joint B–1	SCALE 1:5 original size – A3	DRAWING No SJ.B–1	REV 1

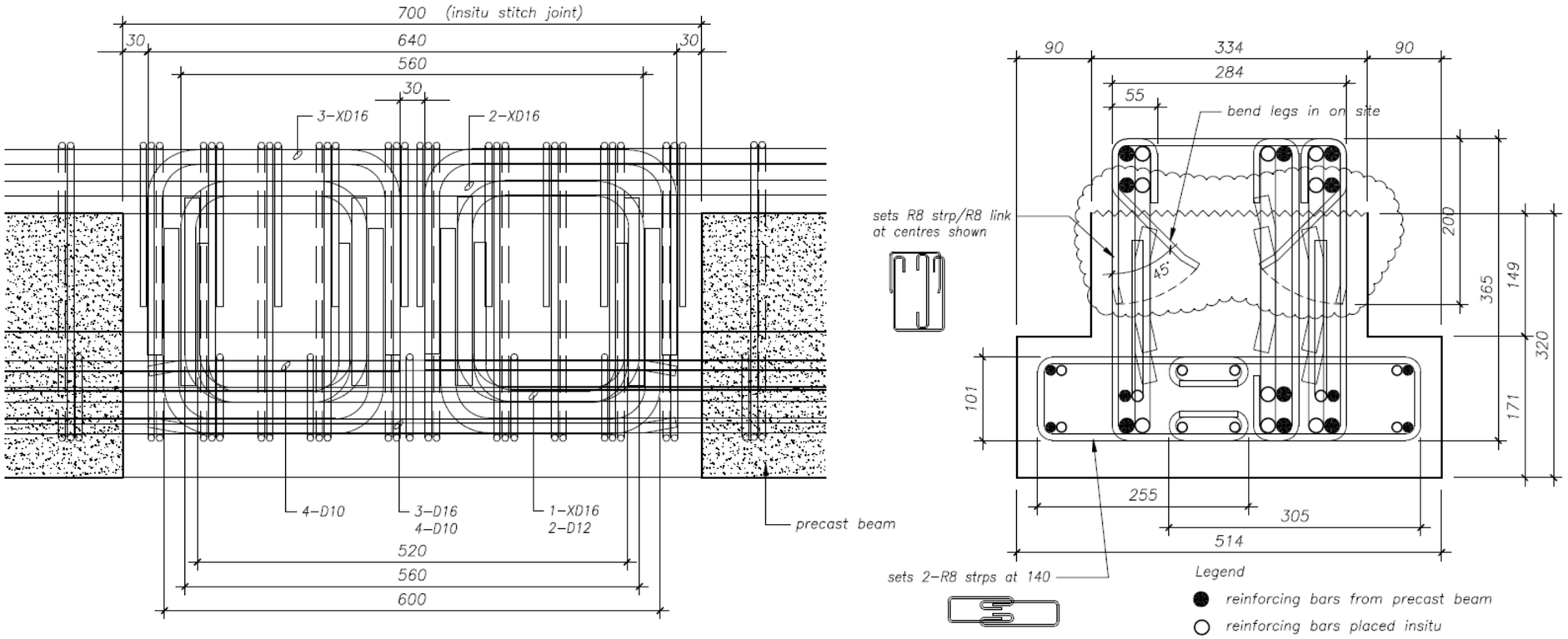

RM DRAUGHTING	BRADFORD PRECAST LTD
P.O.BOX 53	P.O.BOX 214 ASHBURTON
KIRWEE PH 03 318 1605	Telephone (03) 308-9039
CANTERBURY FAX 03 318 1625	Facsimile (03) 308 6300

REV	DATE	REVISION DETAILS
1	02.09.10	Construction
C	24.08.10	Approval update
B	23.08.10	Approval update
A	16.08.10	Approval

precast shop drawing

University of Canterbury – FRST Future Building Systems

SUB TITLE beam insitu stitch joint C-1

DRAWN RMM

SCALE 1:5 original size - A3

JOB NO 2278

DRAWING No SJ.C-1

REV 1

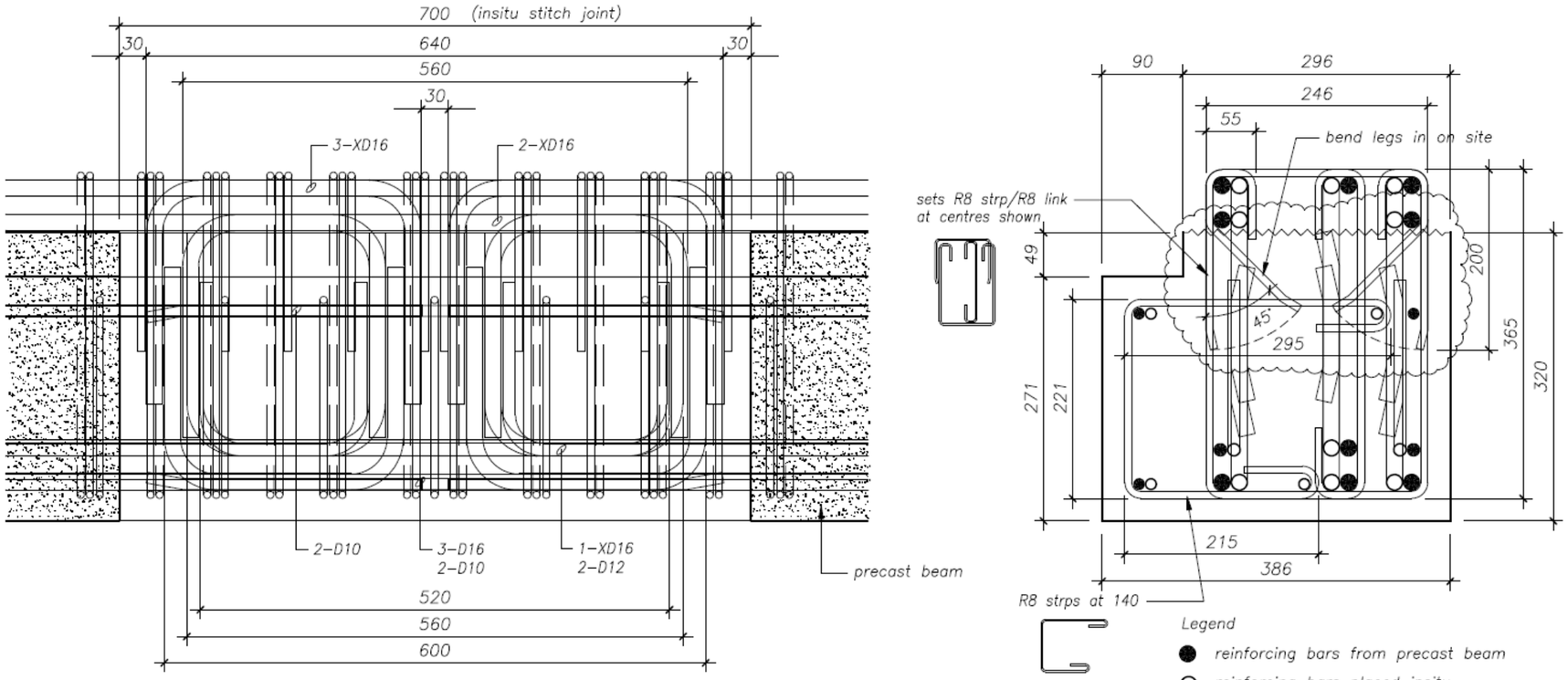

precast shop drawing

RM DRAUGHTING P.O.BOX 53 KIRWEE PH 03 318 1605 CANTERBURY FAX 03 318 1625	BRADFORD PRECAST LTD P.O.BOX 214 ASHBURTON Telephone (03) 308-9039 Facsimile (03) 308 6300	University of Canterbury – FRST Future Building Systems
		SUB TITLE beam insitu stitch joint A–2

REV	DATE	REVISION DETAILS
1	02.09.10	Construction
A	24.08.10	Approval

DRAWN RMM
SCALE 1:5 original size – A3
JOB NO 2278
DRAWING No SJ.A–2
REV 1

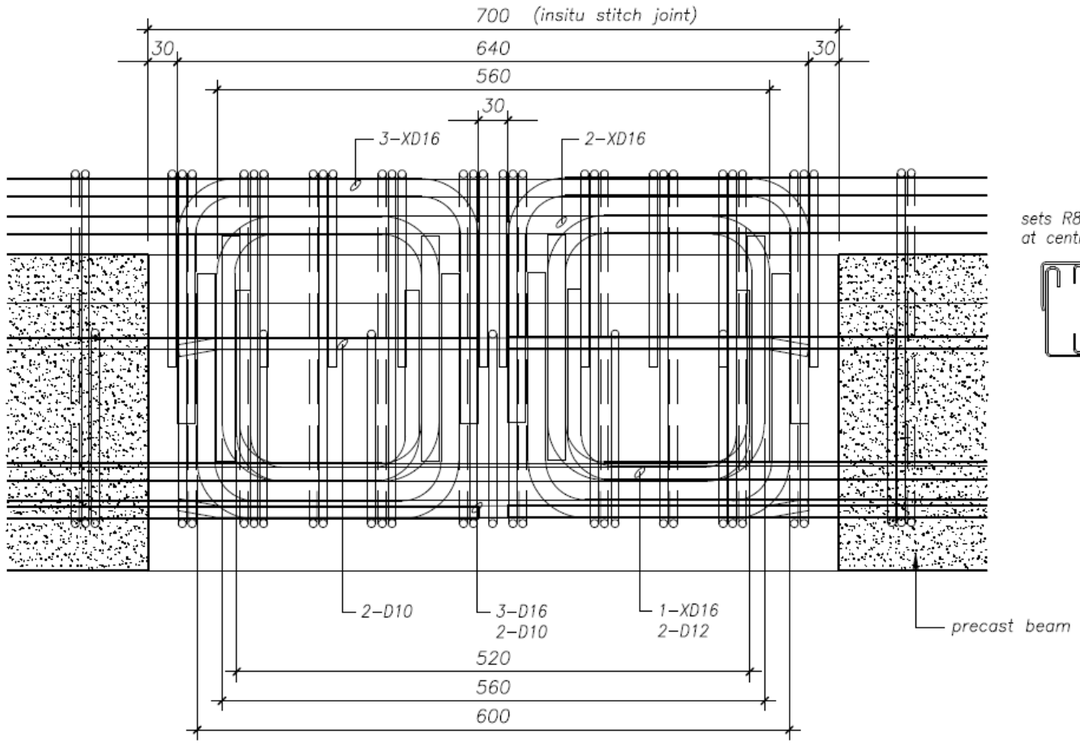

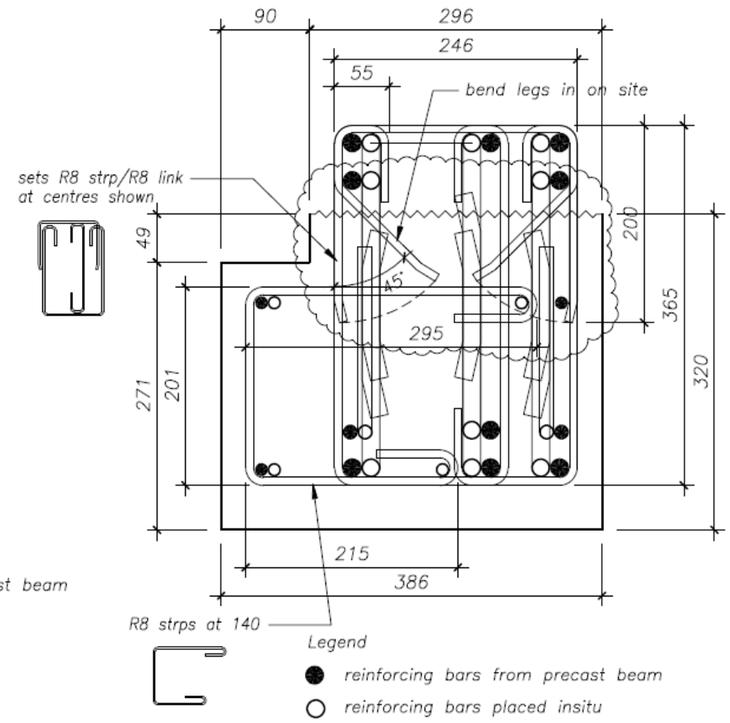

RM DRAUGHTING P.O.BOX 53 KIRWEE PH 03 318 1605 CANTERBURY FAX 03 318 1625	BRADFORD PRECAST LTD P.O.BOX 214 ASHBURTON Telephone (03) 308–9039 Facsimile (03) 308 6300	precast shop drawing
	1 02.09.10 Construction A 24.08.10 Approval REV DATE REVISION DETAILS	University of Canterbury – FRST Future Building Systems SUB TITLE beam insitu stitch joint B–2 DRAWN RMM SCALE 1:5 original size – A3 JOB NO 2278 DRAWING No SJ.B–2 REV 1

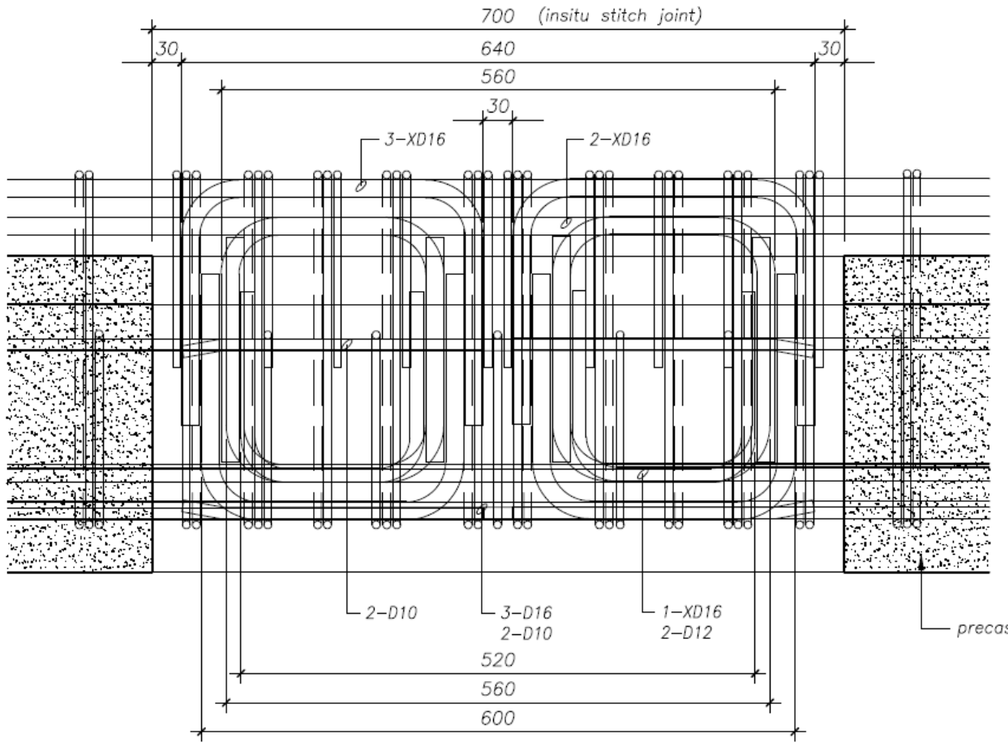

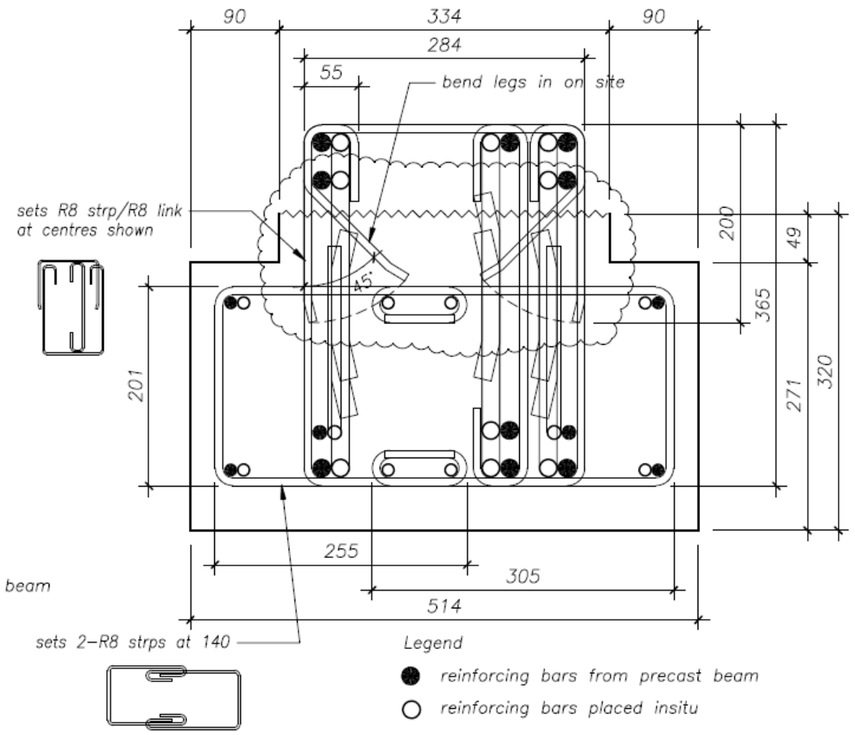

RM DRAUGHTING P.O.BOX 53 KIRWEE PH 03 318 1605 CANTERBURY FAX 03 318 1625	BRADFORD PRECAST LTD P.O.BOX 214 ASHBURTON Telephone (03) 308-9039 Facsimile (03) 308 6300			precast shop drawing
		1	02.09.10	Construction
		A	24.08.10	Approval
		REV	DATE	REVISION DETAILS
University of Canterbury – FRST Future Building Systems		DRAWN RMM	JOB NO 2278	
SUB TITLE beam insitu stitch joint C–2		SCALE 1:5 original size – A3	DRAWING No SJ.C–2	REV 1

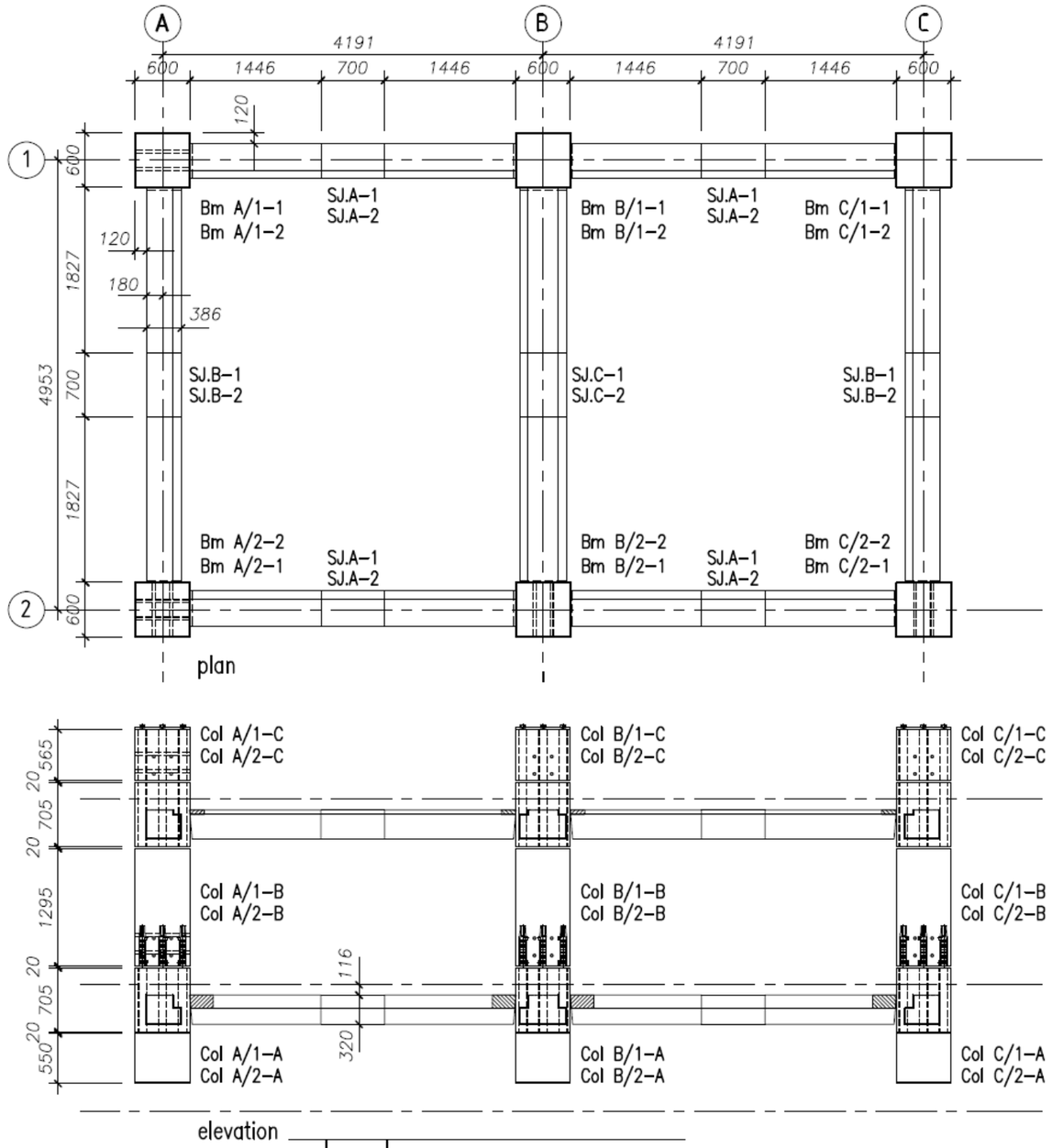

RM DRAUGHTING P.O.BOX 53 KIRWEE PH 03 318 1605 CANTERBURY FAX 03 318 1625	BRADFORD PRECAST LTD P.O.BOX 214 ASHBURTON Telephone (03) 308-9039 Facsimile (03) 308 6300	1	19.08.10	Construction	precast shop drawing
		B	16.08.10	Approval update	University of Canterbury – FRST Future Building Systems
		A	06.08.10	Approval	DRAWN RMM / JOB NO 2278
		REV	DATE	REVISION DETAILS	SUB TITLE mark up plan, elevation / SCALE 1:50 original size – A3 / DRAWING No 01 / REV 1

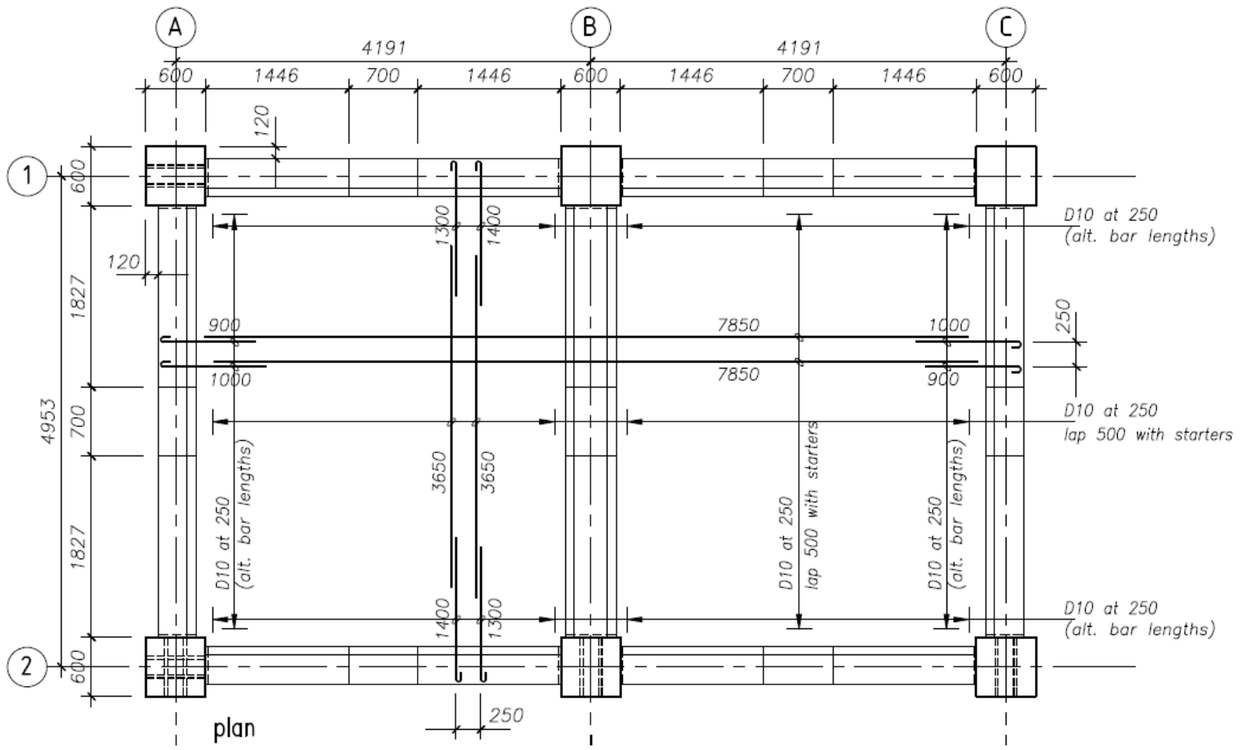

plan

RM DRAUGHTING P.O.BOX 53 KIRWEE PH 03 318 1605 CANTERBURY FAX 03 318 1625	BRADFORD PRECAST LTD P.O.BOX 214 ASHBURTON Telephone (03) 308-9039 Facsimile (03) 308 6300			precast shop drawing
		1	02.09.10	Construction
		A	24.08.10	Approval
		REV	DATE	REVISION DETAILS

University of Canterbury – FRST Future Building Systems

SUB TITLE floor slab reinforcing level 1

DRAWN RMM

SCALE 1:50 original size - A3

JOB NO 2278

DRAWING No 02

REV 1

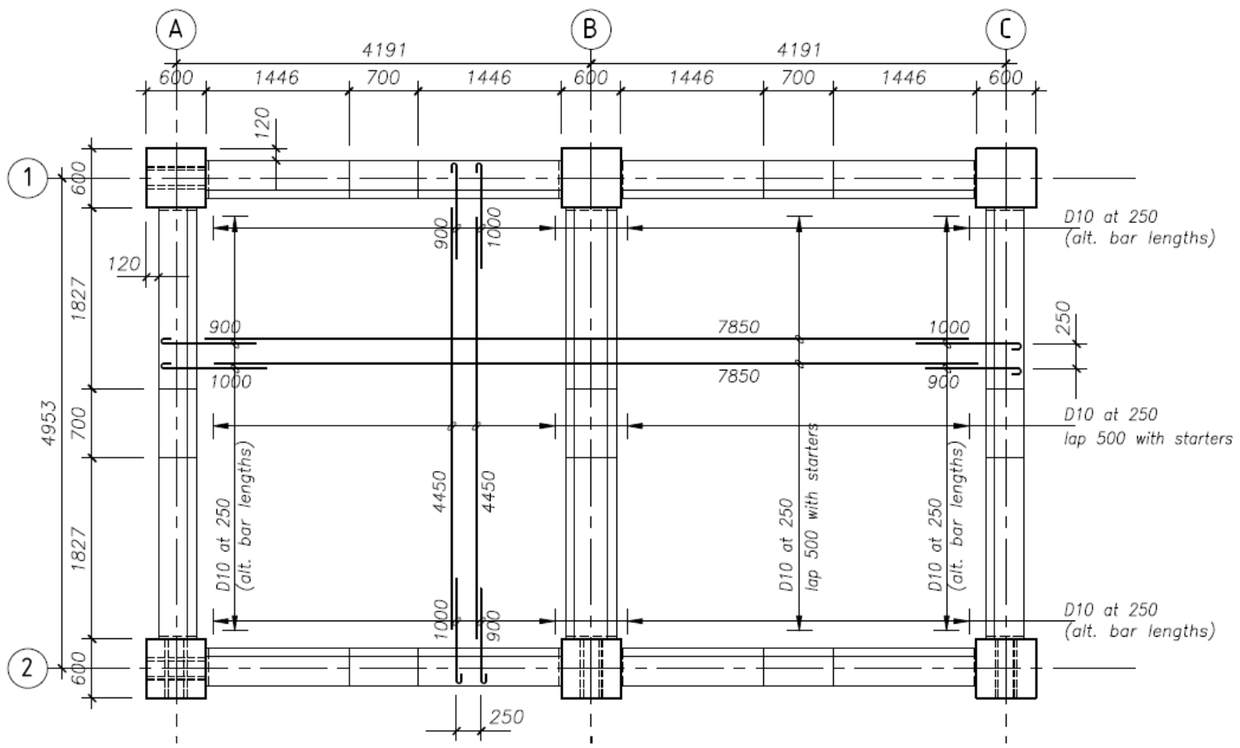

plan

RM DRAUGHTING P.O.BOX 53 KIRWEE PH 03 318 1605 CANTERBURY FAX 03 318 1625	BRADFORD PRECAST LTD P.O.BOX 214 ASHBURTON Telephone (03) 308-9039 Facsimile (03) 308 6300				precast shop drawing
		1	02.09.10	Construction	University of Canterbury – FRST Future Building Systems
		A	24.08.10	Approval	SUB TITLE floor slab reinforcing level 2
		REV	DATE	REVISION DETAILS	

DRAWN RMM | JOB NO 2278 | SCALE 1:50 original size - A3 | DRAWING No 03 | REV 1

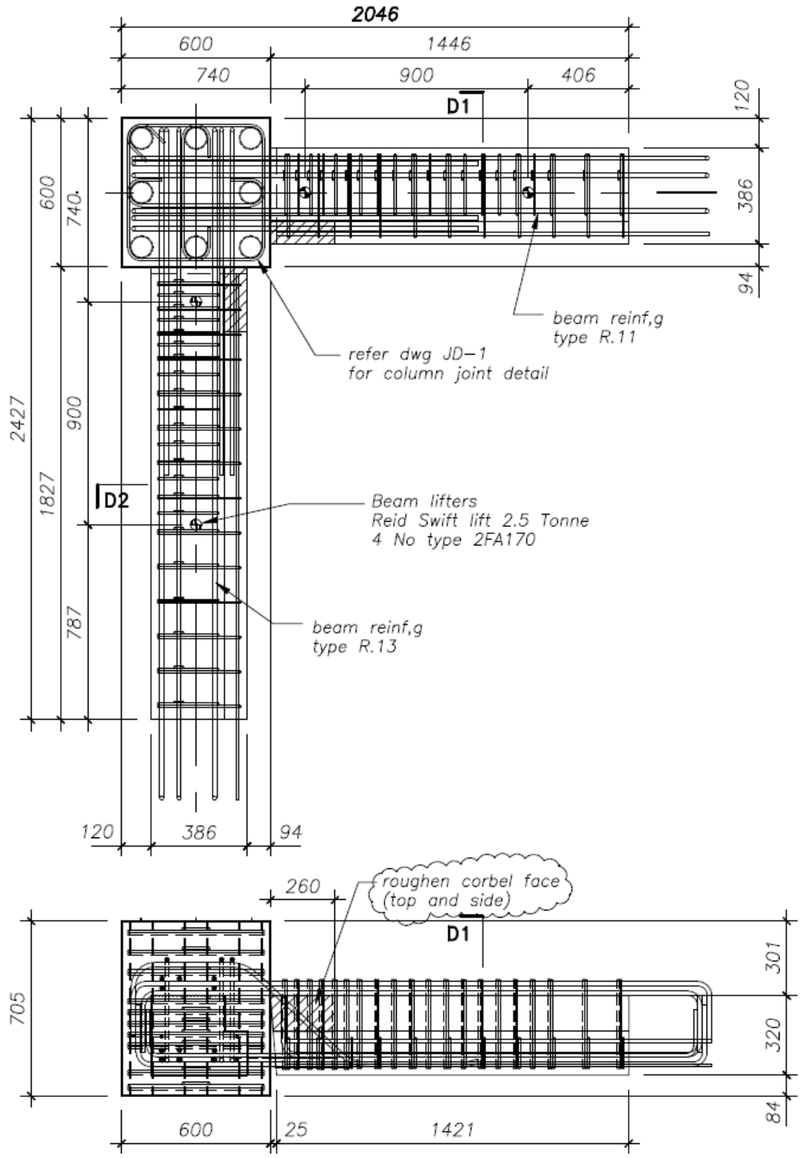

Note:

Conc strength – 40 MPa

Conc. Volume (m^3) = 0.575

Panel mass (tonne) = 1.495

PANEL LIFTERS
"REID" lifters (type as shown on elevation)
Installed and used as per manufactures Spec.

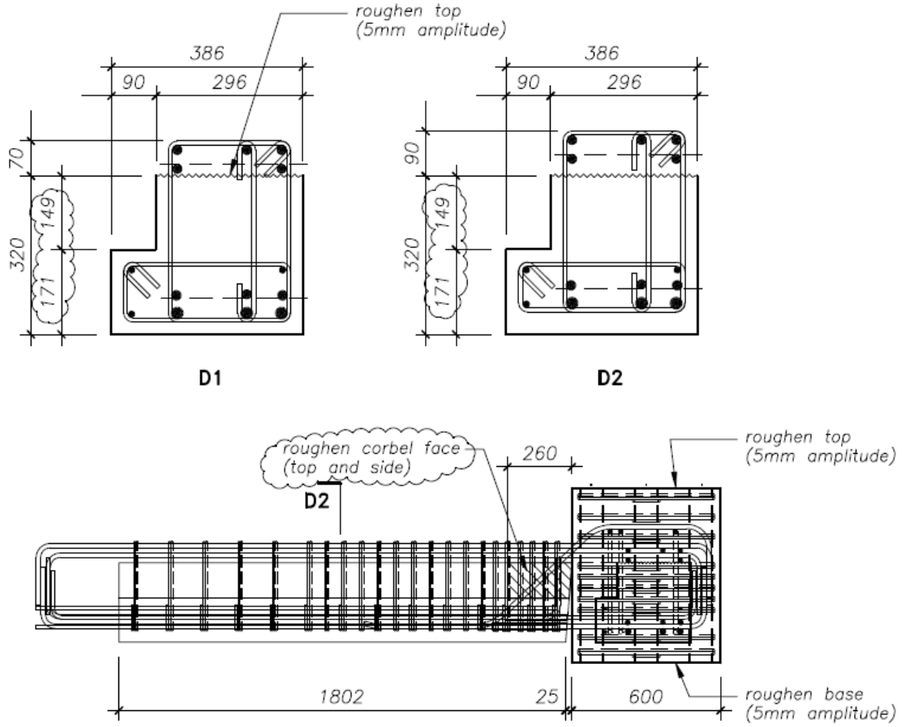

RM DRAUGHTING P.O.BOX 53 KIRWEE PH 03 318 1605 CANTERBURY FAX 03 318 1625	BRADFORD PRECAST LTD P.O.BOX 214 ASHBURTON Telephone (03) 308-9039 Facsimile (03) 308 6300	precast shop drawing

REV	DATE	REVISION DETAILS
1	19.08.10	Construction
A	06.08.10	Approval

University of Canterbury – FRST Future Building Systems

SUB TITLE: beam unit A/1–1

DRAWN RMM | SCALE 1:20, 1:10 original size – A3 | JOB NO 2278 | DRAWING No Bm A/1–1 | REV 1

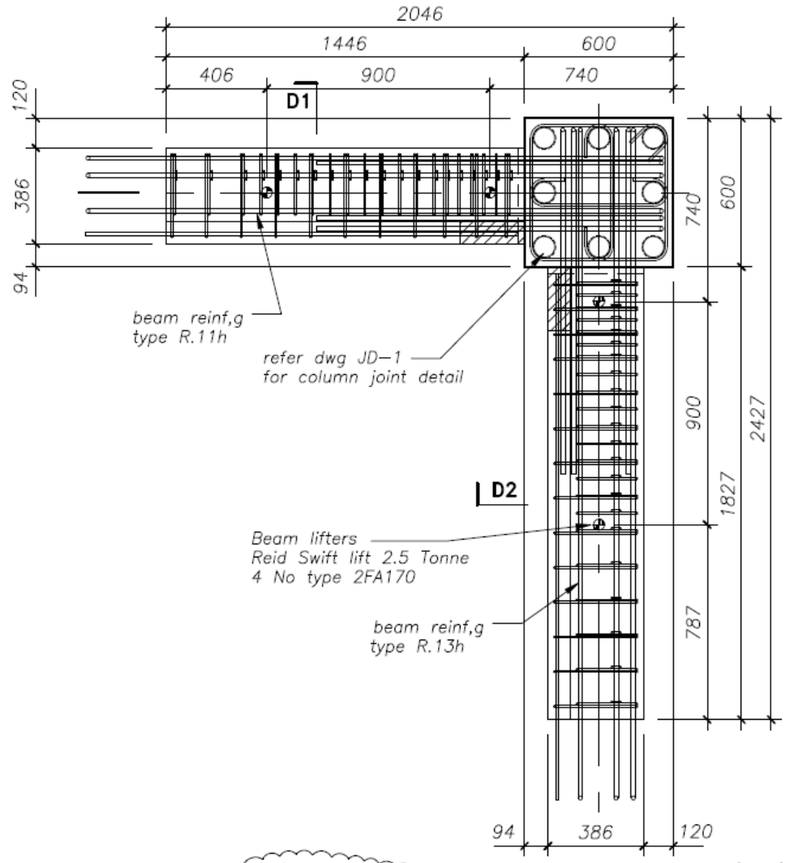

Note:

Conc strength – 40 MPa

Conc. Volume (m^3) = 0.575

Panel mass (tonne) = 1.495

PANEL LIFTERS
"REID" lifters (type as shown on elevation)
Installed and used as per manufactures Spec.

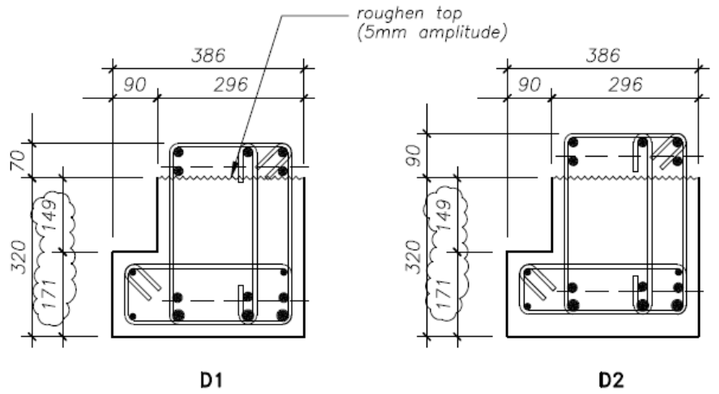

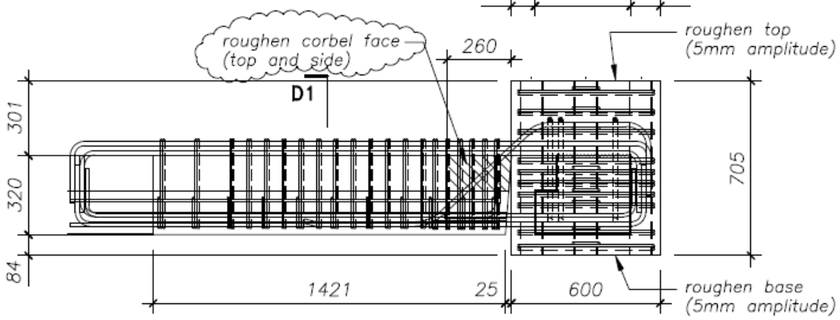

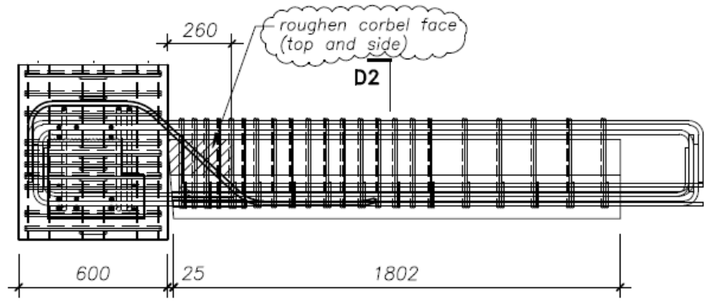

precast shop drawing

RM DRAUGHTING	BRADFORD PRECAST LTD				University of Canterbury – FRST Future Building Systems	DRAWN RMM	JOB NO 2278	
P.O.BOX 53	P.O.BOX 214 ASHBURTON				SUB TITLE beam unit A/2–1	SCALE 1:20, 1:10 original size – A3	DRAWING No Bm A/2–1	REV 1
KIRWEE PH 03 318 1605	Telephone (03) 308–9039	1	19.08.10	Construction				
CANTERBURY FAX 03 318 1625	Facsimile (03) 308 6300	A	06.08.10	Approval				
		REV	DATE	REVISION DETAILS				

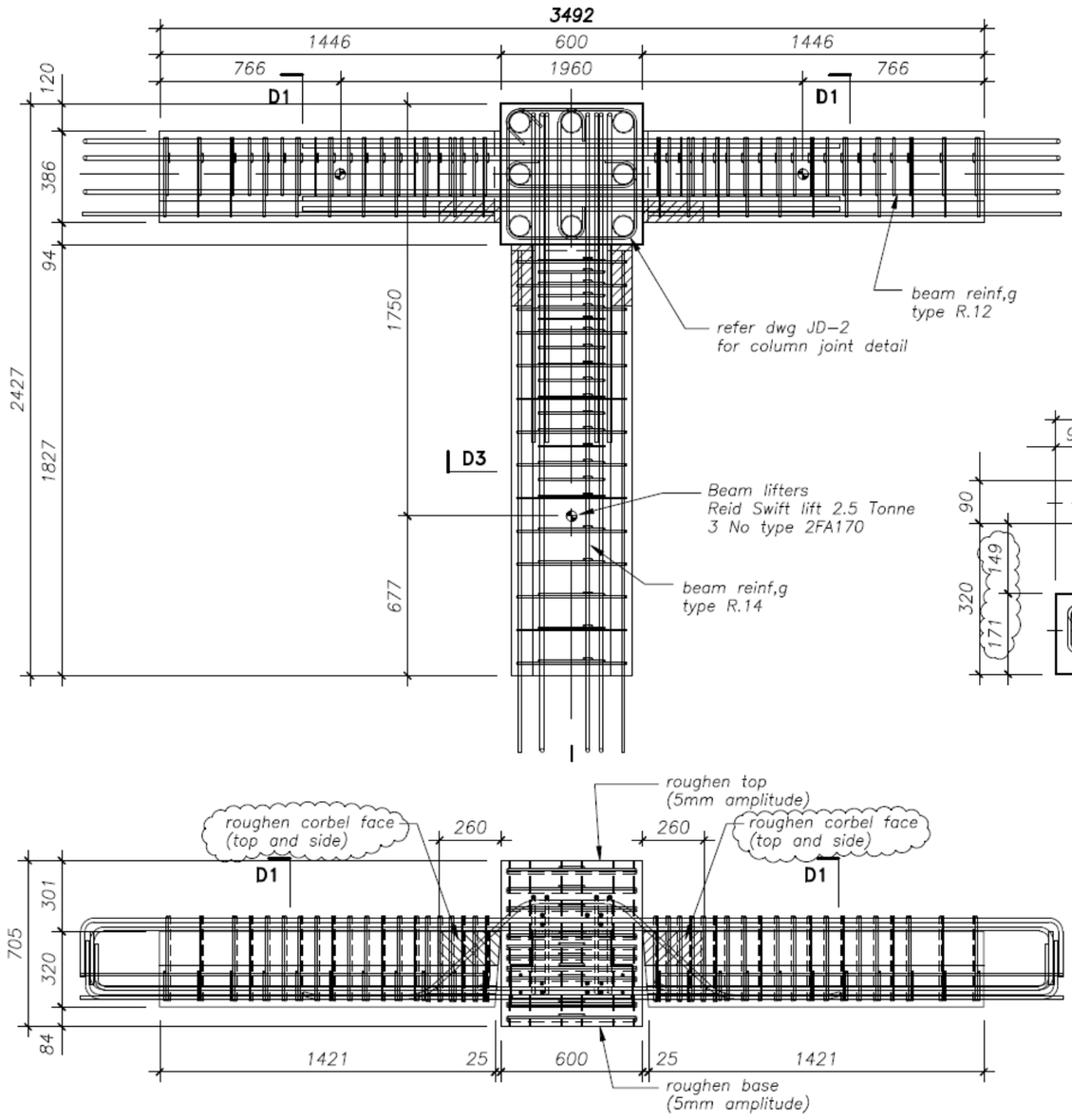

Note:

Conc strength – 40 MPa

Conc. Volume (m^3) = 0.784

Panel mass (tonne) = 2.038

PANEL LIFTERS
"REID" lifters (type as shown on elevation)
Installed and used as per manufactures Spec.

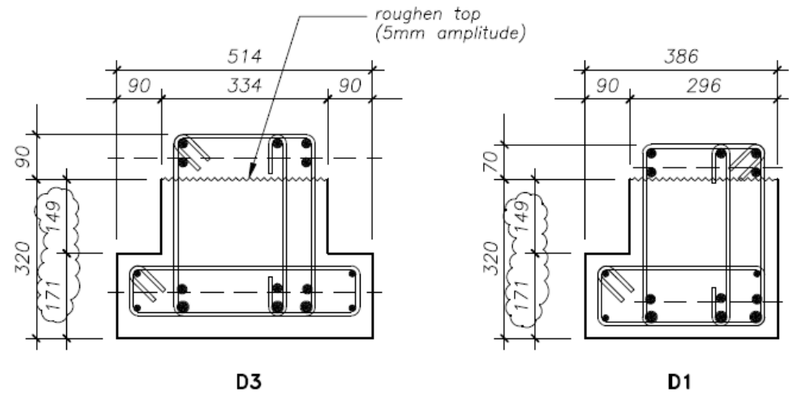

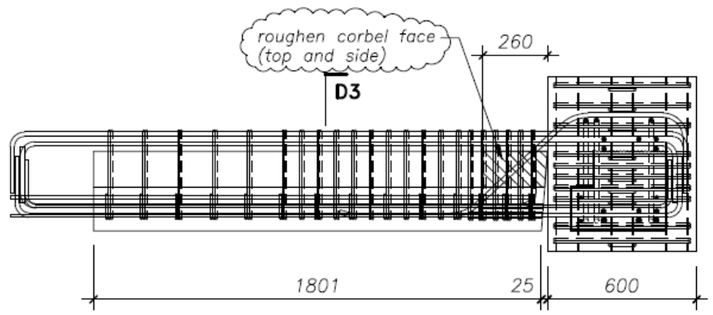

RM DRAUGHTING	BRADFORD PRECAST LTD				precast shop drawing	
P.O.BOX 53 KIRWEE PH 03 318 1605 CANTERBURY FAX 03 318 1625	P.O.BOX 214 ASHBURTON Telephone (03) 308-9039 Facsimile (03) 308 6300				University of Canterbury – FRST Future Building Systems	DRAWN RMM / JOB NO 2278
		1	19.08.10	Construction	SUB TITLE beam unit B/1–1	SCALE 1:20, 1:10 original size – A3 / DRAWING No Bm B/1–1 / REV 1
		A	06.08.10	Approval		
		REV	DATE	REVISION DETAILS		

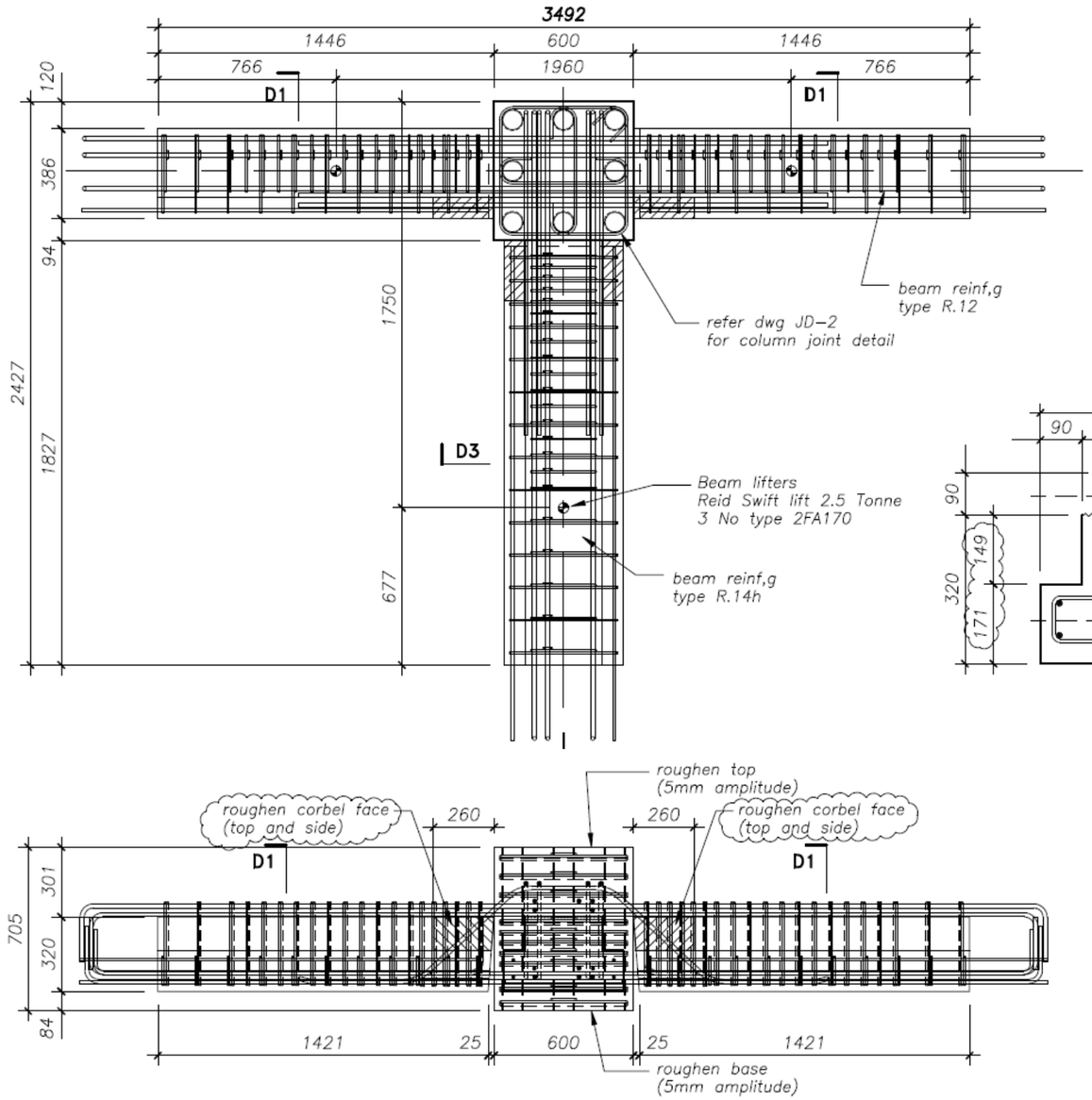

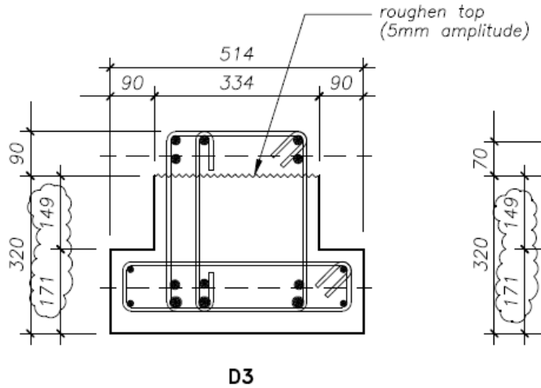

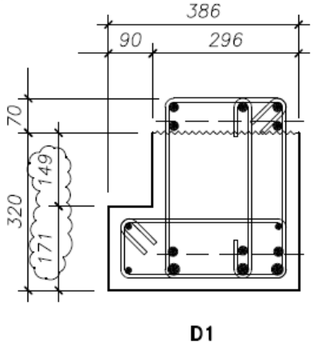

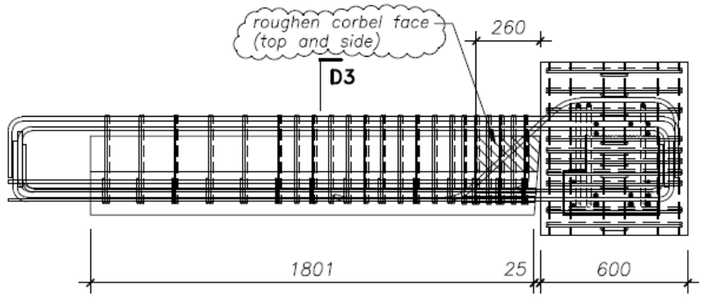

Note:

Conc strength – 40 MPa

Conc. Volume (m^3) = 0.784

Panel mass (tonne) = 2.038

PANEL LIFTERS
"REID" lifters (type as shown on elevation)
Installed and used as per manufactures Spec.

precast shop drawing

RM DRAUGHTING P.O.BOX 53 KIRWEE PH 03 318 1605 CANTERBURY FAX 03 318 1625	BRADFORD PRECAST LTD P.O.BOX 214 ASHBURTON Telephone (03) 308–9039 Facsimile (03) 308 6300	University of Canterbury – FRST Future Building Systems
SUB TITLE	beam unit B/2–1	

REV	DATE	REVISION DETAILS
1	19.08.10	Construction
A	06.08.10	Approval

DRAWN RMM
SCALE 1:20, 1:10
original size – A3
JOB NO 2278
DRAWING No Bm B/2–1
REV 1

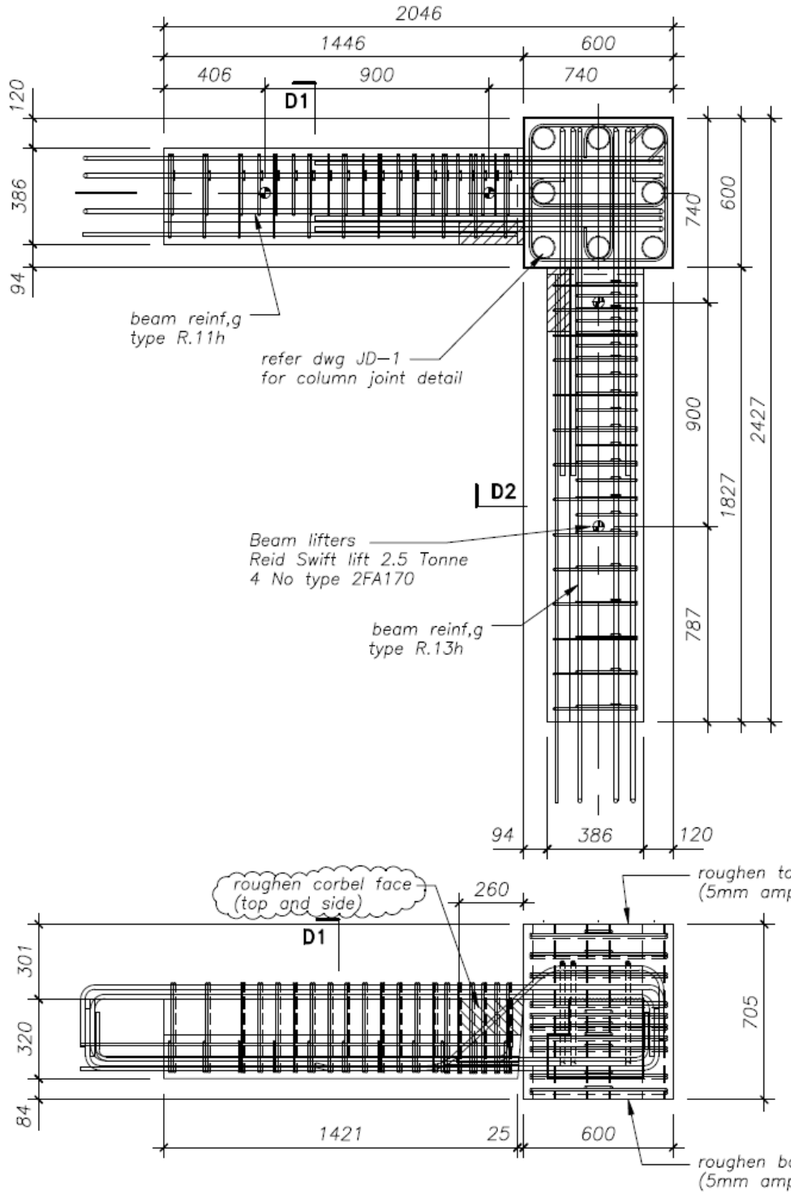

Note:

Conc strength – 40 MPa

Conc. Volume (m^3) = 0.575

Panel mass (tonne) = 1.495

PANEL LIFTERS
"REID" lifters (type as shown on elevation)
Installed and used as per manufactures Spec.

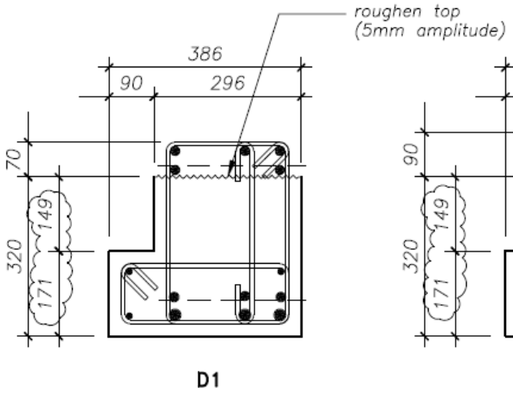

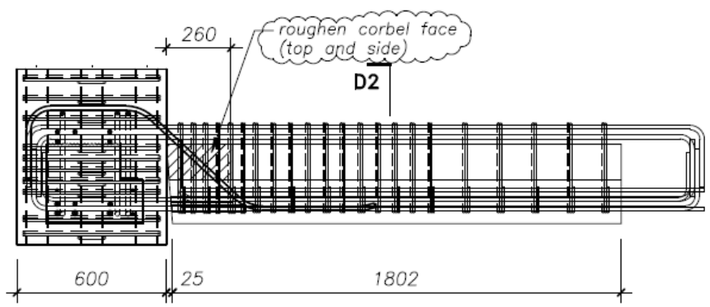

precast shop drawing

RM DRAUGHTING P.O.BOX 53 KIRWEE PH 03 318 1605 CANTERBURY FAX 03 318 1625	BRADFORD PRECAST LTD P.O.BOX 214 ASHBURTON Telephone (03) 308-9039 Facsimile (03) 308 6300	University of Canterbury – FRST Future Building Systems
REV	DATE	REVISION DETAILS
1	19.08.10	Construction
A	06.08.10	Approval
SUB TITLE	beam unit C/1–1	
DRAWN RMM	JOB NO 2278	
SCALE 1:20, 1:10 original size – A3	DRAWING No Bm C/1–1	REV 1

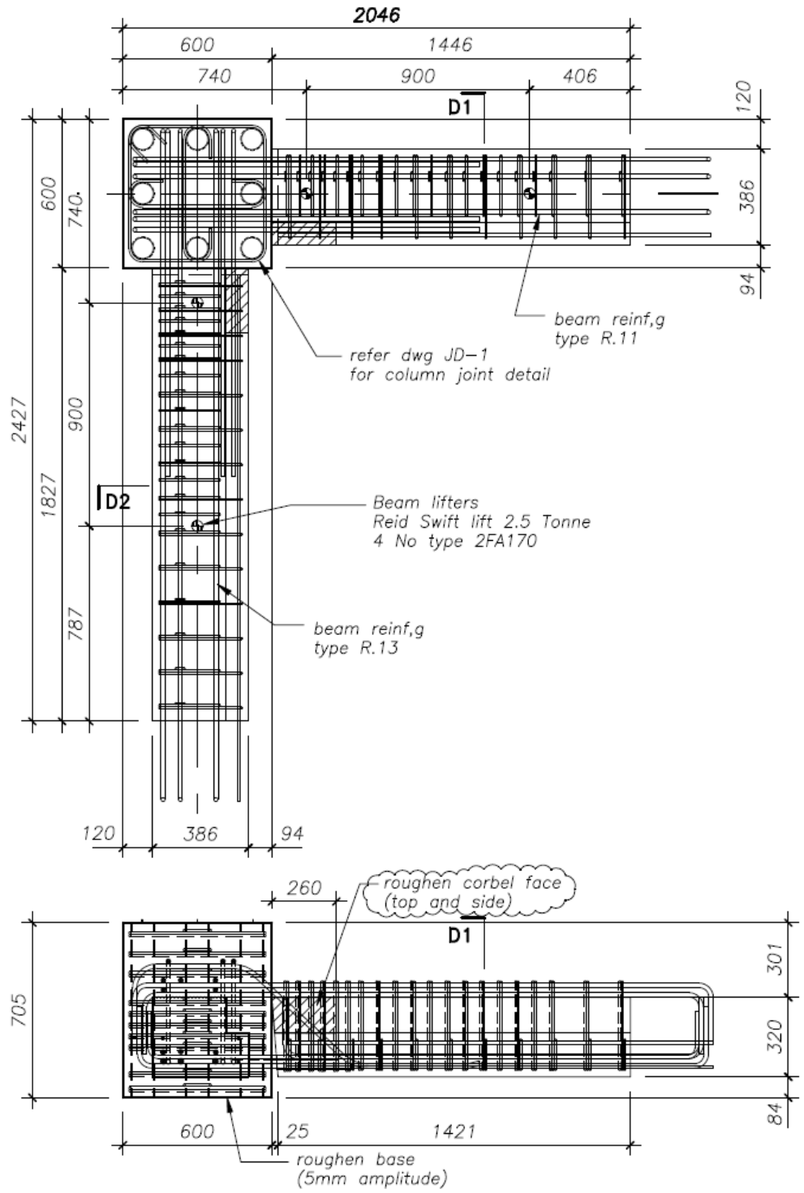

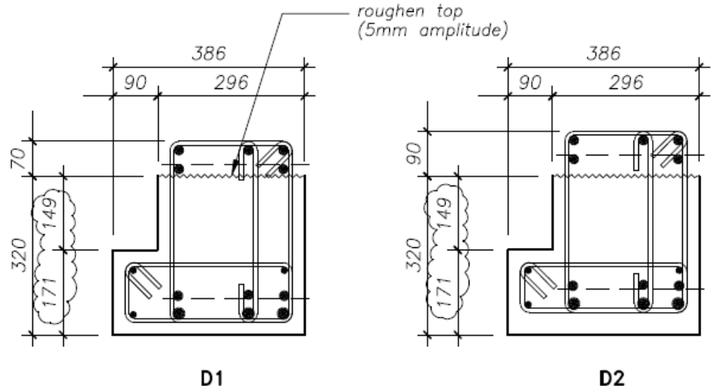

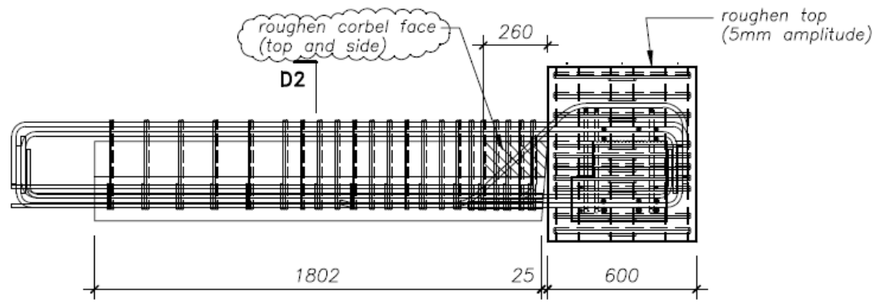

Note:

Conc strength – 40 MPa

Conc. Volume (m^3) = 0.575

Panel mass (tonne) = 1.495

PANEL LIFTERS
"REID" lifters (type as shown on elevation)
Installed and used as per manufactures Spec.

RM DRAUGHTING P.O.BOX 53 KIRWEE PH 03 318 1605 CANTERBURY FAX 03 318 1625	BRADFORD PRECAST LTD P.O.BOX 214 ASHBURTON Telephone (03) 308-9039 Facsimile (03) 308 6300	precast shop drawing

REV	DATE	REVISION DETAILS
1	19.08.10	Construction
A	06.08.10	Approval

University of Canterbury – FRST Future Building Systems

SUB TITLE: beam unit C/2-1

DRAWN RMM | SCALE 1:20, 1:10 original size – A3 | JOB NO 2278 | DRAWING No Bm C/2-1 | REV 1

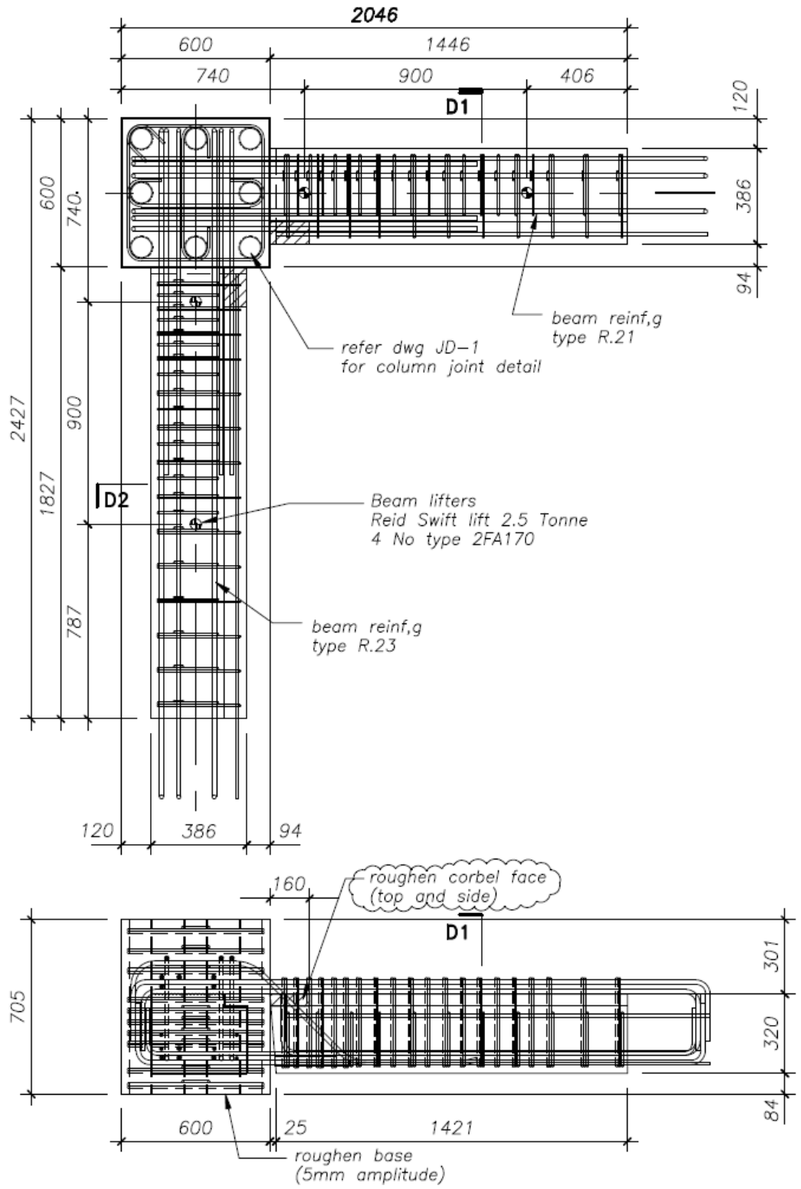

Note:

Conc strength – 40 MPa

Conc. Volume (m^3) = 0.603

Panel mass (tonne) = 1.567

PANEL LIFTERS
"REID" lifters (type as shown on elevation)
Installed and used as per manufactures Spec.

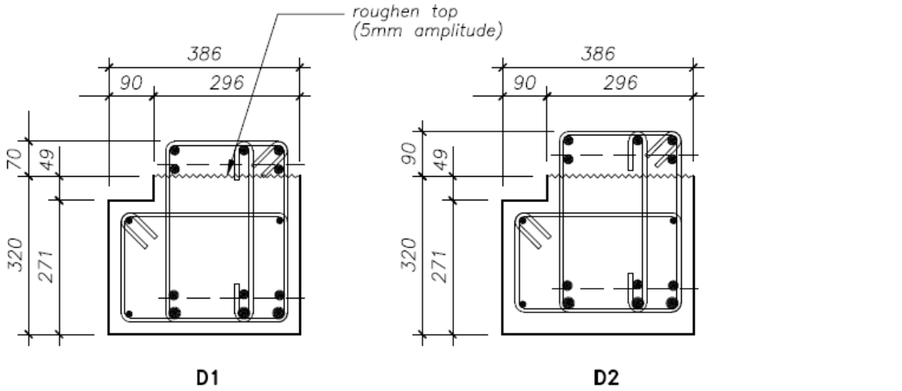

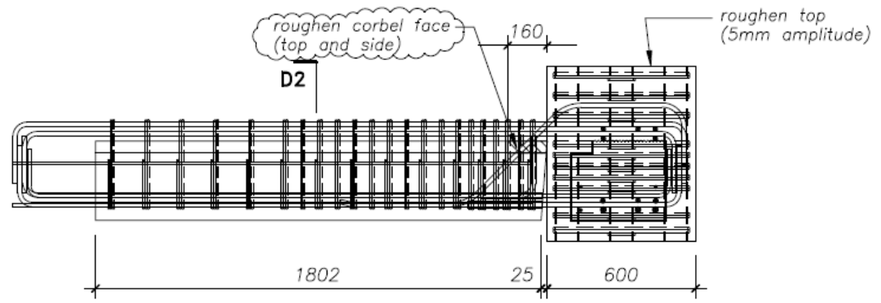

RM DRAUGHTING P.O.BOX 53 KIRWEE PH 03 318 1605 CANTERBURY FAX 03 318 1625	BRADFORD PRECAST LTD P.O.BOX 214 ASHBURTON Telephone (03) 308-9039 Facsimile (03) 308 6300				precast shop drawing
		1	19.08.10	Construction	University of Canterbury – FRST Future Building Systems
		A	06.08.10	Approval	SUB TITLE beam unit A/1–2
		REV	DATE	REVISION DETAILS	DRAWN RMM; SCALE 1:20, 1:10 original size – A3; JOB NO 2278; DRAWING No Bm A/1–2; REV 1

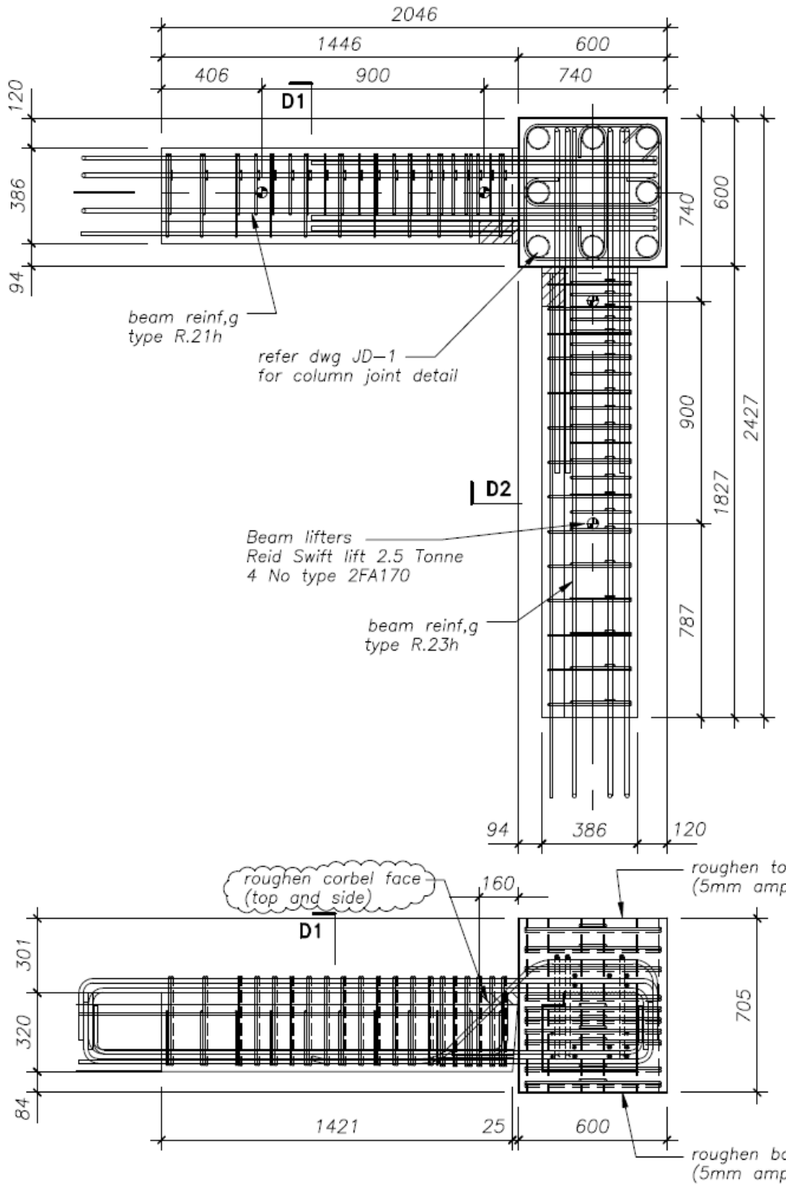

Note:

Conc strength – 40 MPa

Conc. Volume (m^3) = 0.603

Panel mass (tonne) = 1.567

PANEL LIFTERS
"REID" lifters (type as shown on elevation)
Installed and used as per manufactures Spec.

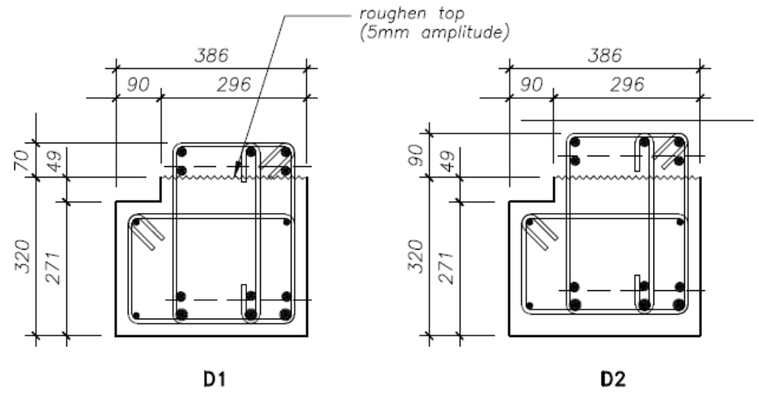

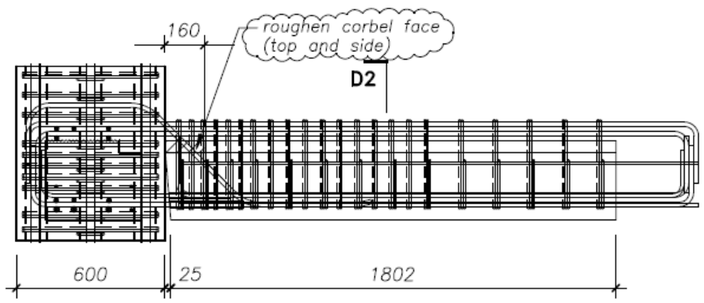

precast shop drawing

RM DRAUGHTING P.O.BOX 53 KIRWEE PH 03 318 1605 CANTERBURY FAX 03 318 1625	BRADFORD PRECAST LTD P.O.BOX 214 ASHBURTON Telephone (03) 308-9039 Facsimile (03) 308 6300	
		1 19.08.10 Construction
		A 06.08.10 Approval
		REV DATE REVISION DETAILS
University of Canterbury – FRST Future Building Systems	DRAWN RMM	JOB NO 2278
SUB TITLE beam unit A/2–2	SCALE 1:20, 1:10 original size – A3	DRAWING No Bm A/2–2 REV 1

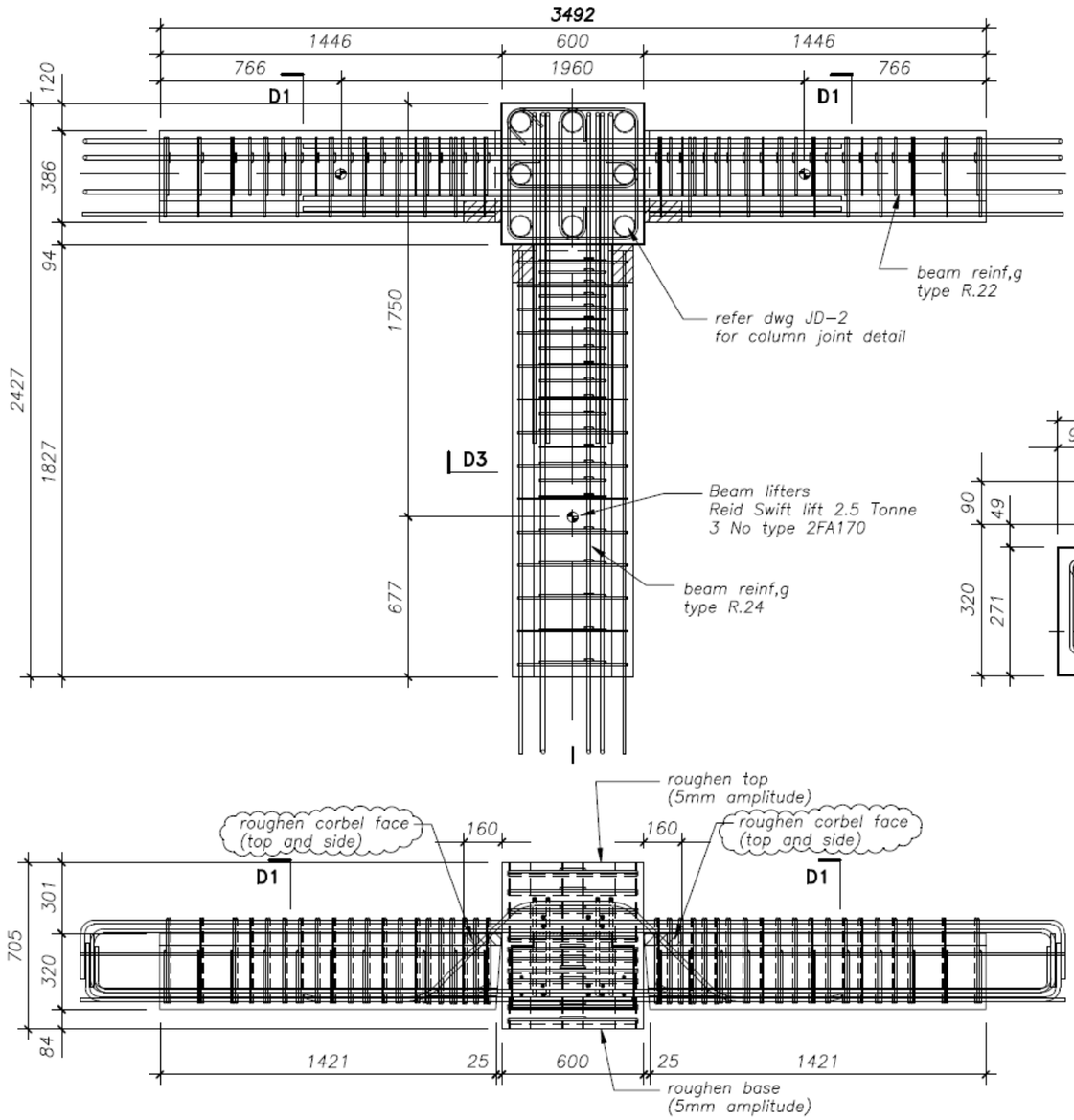

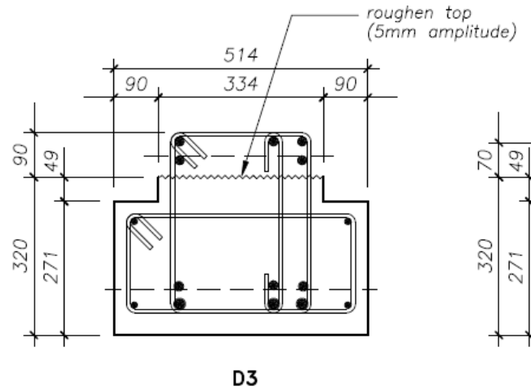

D3

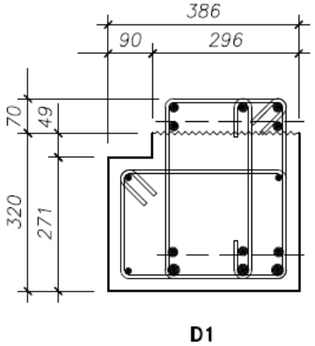

D1

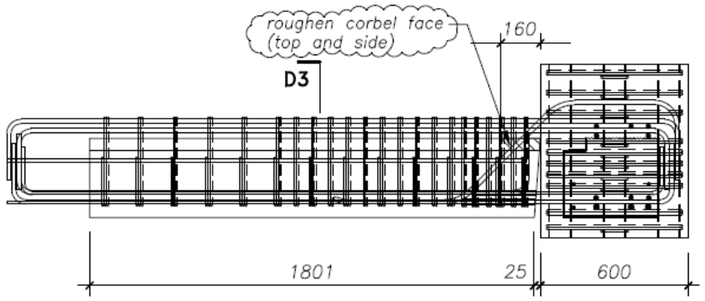

Note:

Conc strength – 40 MPa

Conc. Volume (m^3) = 0.840

Panel mass (tonne) = 2.184

PANEL LIFTERS
"REID" lifters (type as shown on elevation)
Installed and used as per manufactures Spec.

precast shop drawing

RM DRAUGHTING P.O.BOX 53 KIRWEE PH 03 318 1605 CANTERBURY FAX 03 318 1625	BRADFORD PRECAST LTD P.O.BOX 214 ASHBURTON Telephone (03) 308-9039 Facsimile (03) 308 6300	University of Canterbury – FRST Future Building Systems SUB TITLE beam unit B/1–2
DRAWN RMM SCALE 1:20, 1:10 original size – A3	JOB NO 2278 DRAWING No Bm B/1–2 REV 1	

REV	DATE	REVISION DETAILS
1	19.08.10	Construction
A	06.08.10	Approval

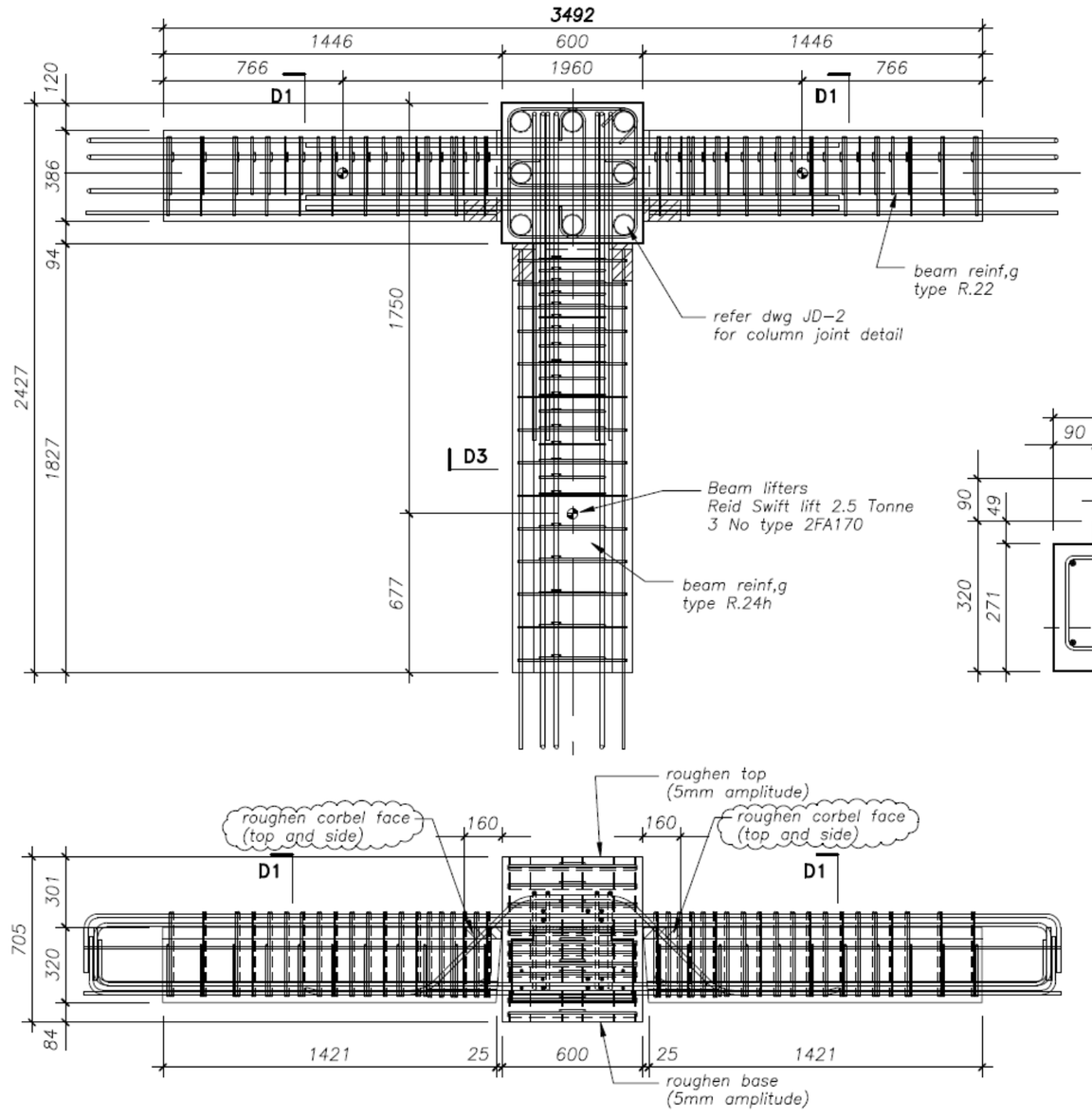

Note:

Conc strength – 40 MPa

Conc. Volume (m^3) = 0.840

Panel mass (tonne) = 2.184

PANEL LIFTERS
"REID" lifters (type as shown on elevation)
Installed and used as per manufactures Spec.

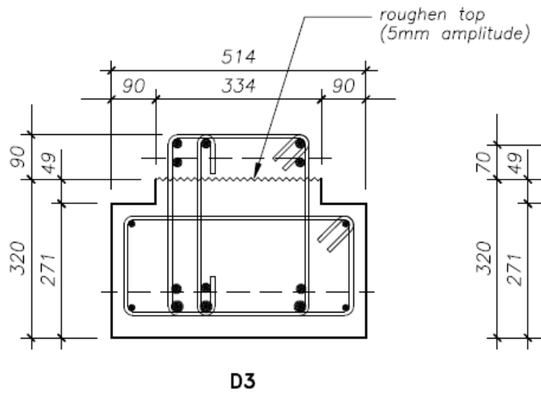

D3

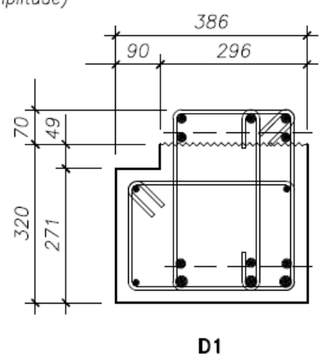

D1

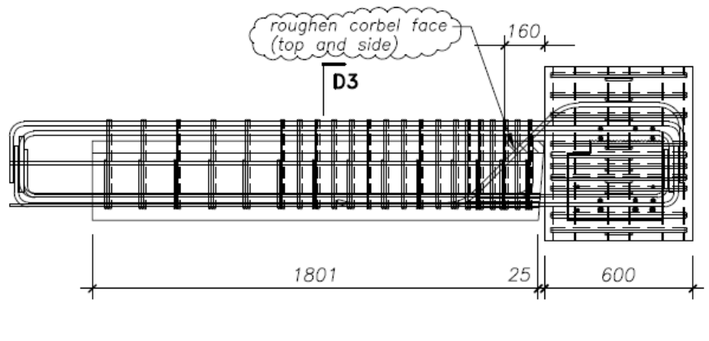

RM DRAUGHTING P.O.BOX 53 KIRWEE PH 03 318 1605 CANTERBURY FAX 03 318 1625	BRADFORD PRECAST LTD P.O.BOX 214 ASHBURTON Telephone (03) 308-9039 Facsimile (03) 308 6300			precast shop drawing
		1	19.08.10	Construction
		A	06.08.10	Approval
		REV	DATE	REVISION DETAILS
University of Canterbury – FRST Future Building Systems		DRAWN RMM	JOB NO 2278	
SUB TITLE beam unit B/2–2		SCALE 1:20, 1:10 original size – A3	DRAWING No Bm B/2–2	REV 1

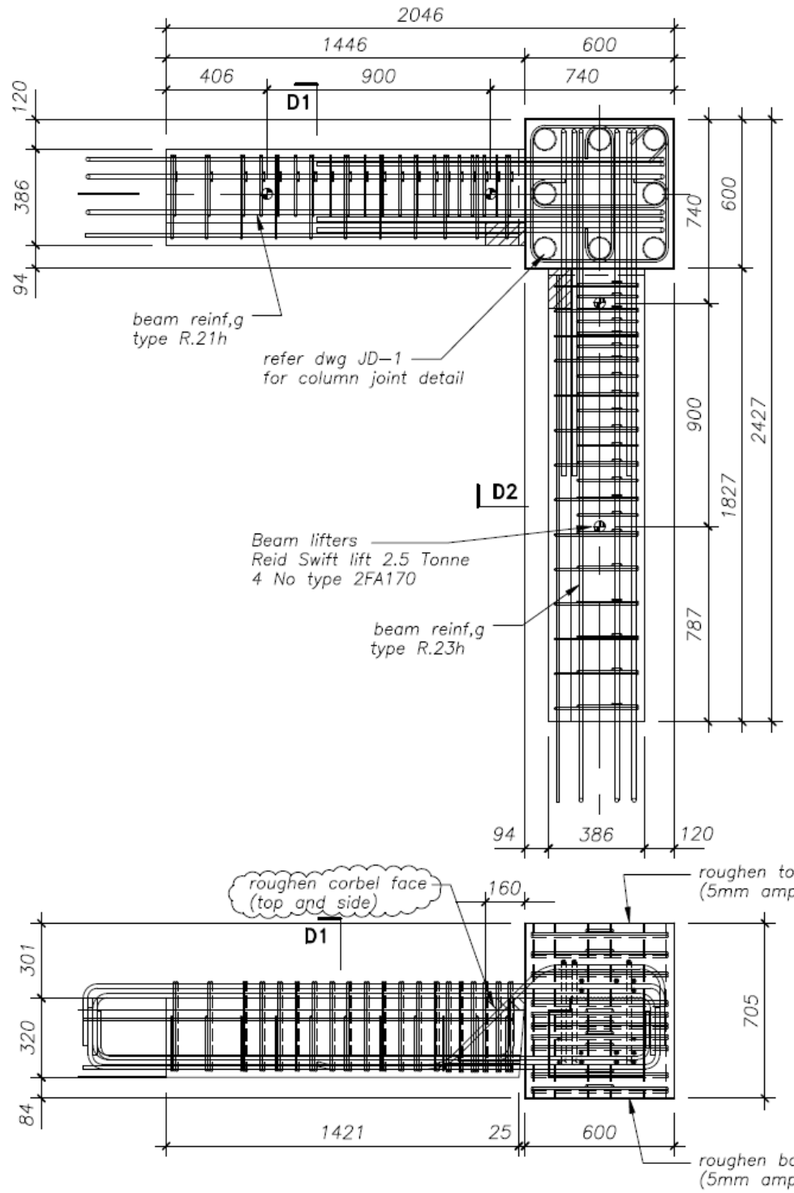

Note:

Conc strength – 40 MPa

Conc. Volume (m^3) = 0.603

Panel mass (tonne) = 1.567

PANEL LIFTERS
"REID" lifters (type as shown on elevation)
Installed and used as per manufactures Spec.

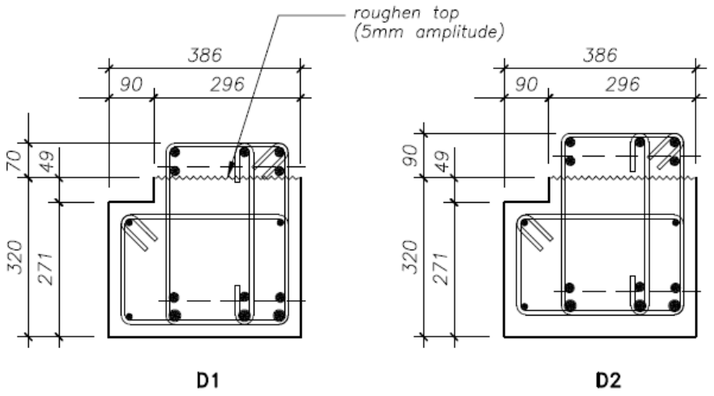

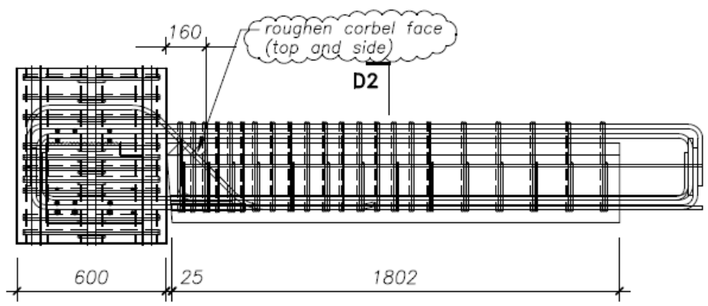

precast shop drawing

RM DRAUGHTING P.O.BOX 53 KIRWEE PH 03 318 1605 CANTERBURY FAX 03 318 1625	BRADFORD PRECAST LTD P.O.BOX 214 ASHBURTON Telephone (03) 308-9039 Facsimile (03) 308 6300	University of Canterbury – FRST Future Building Systems
REV	DATE	REVISION DETAILS
1	19.08.10	Construction
A	06.08.10	Approval
SUB TITLE	beam unit C/1–2	
DRAWN RMM	JOB NO 2278	
SCALE 1:20, 1:10 original size – A3	DRAWING No Bm C/1–2	REV 1

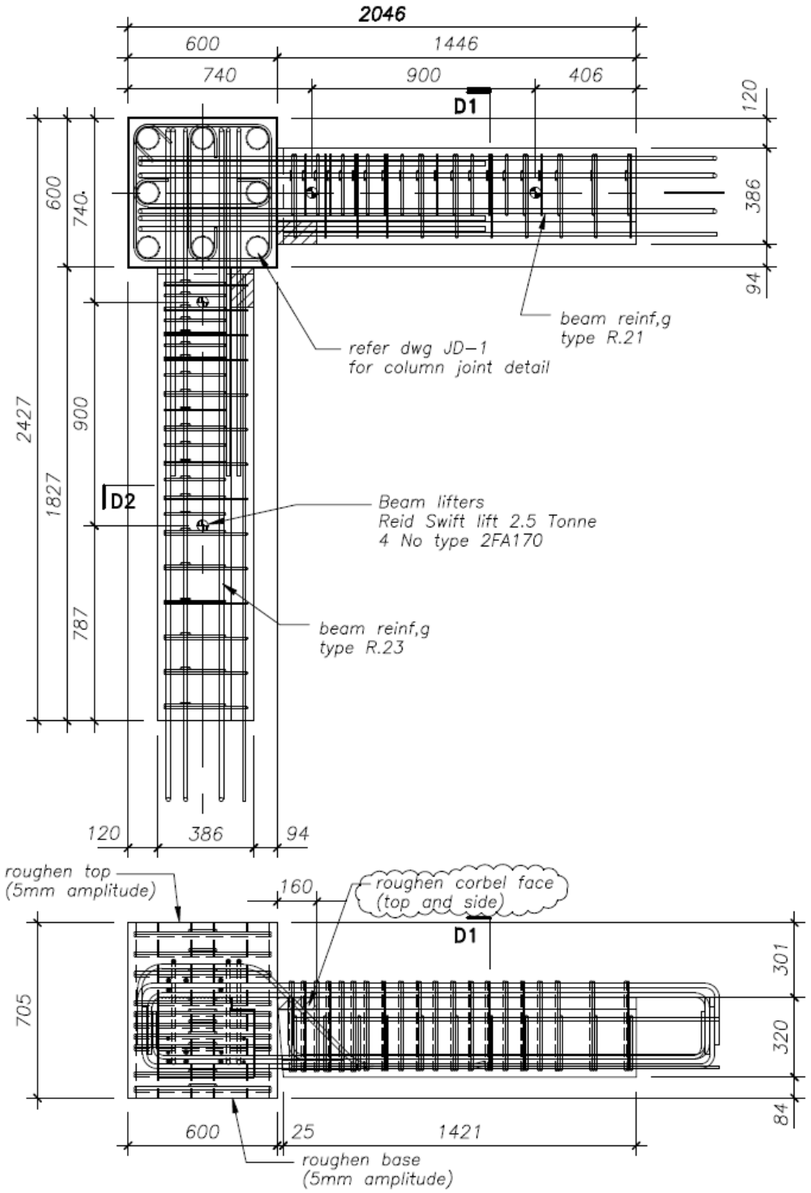

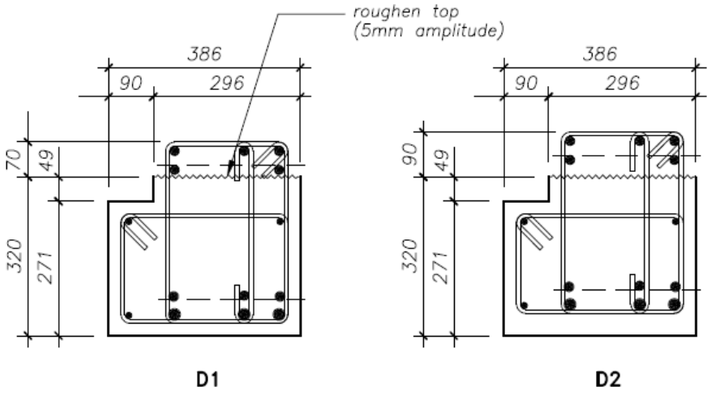

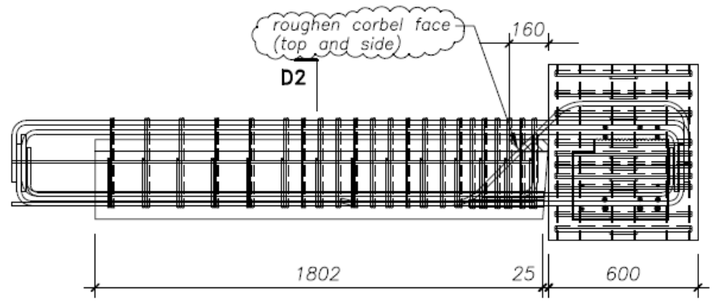

Note:

Conc strength – 40 MPa

Conc. Volume (m^3) = 0.603

Panel mass (tonne) = 1.567

PANEL LIFTERS
"REID" lifters (type as shown on elevation)
Installed and used as per manufactures Spec.

RM DRAUGHTING P.O.BOX 53 KIRWEE PH 03 318 1605 CANTERBURY FAX 03 318 1625	BRADFORD PRECAST LTD P.O.BOX 214 ASHBURTON Telephone (03) 308-9039 Facsimile (03) 308 6300	precast shop drawing

REV	DATE	REVISION DETAILS
1	19.08.10	Construction
A	06.08.10	Approval

University of Canterbury – FRST Future Building Systems

SUB TITLE: beam unit C/2–2

DRAWN: RMM

SCALE: 1:20, 1:10 original size – A3

JOB NO: 2278

DRAWING No: Bm C/2–2

REV: 1

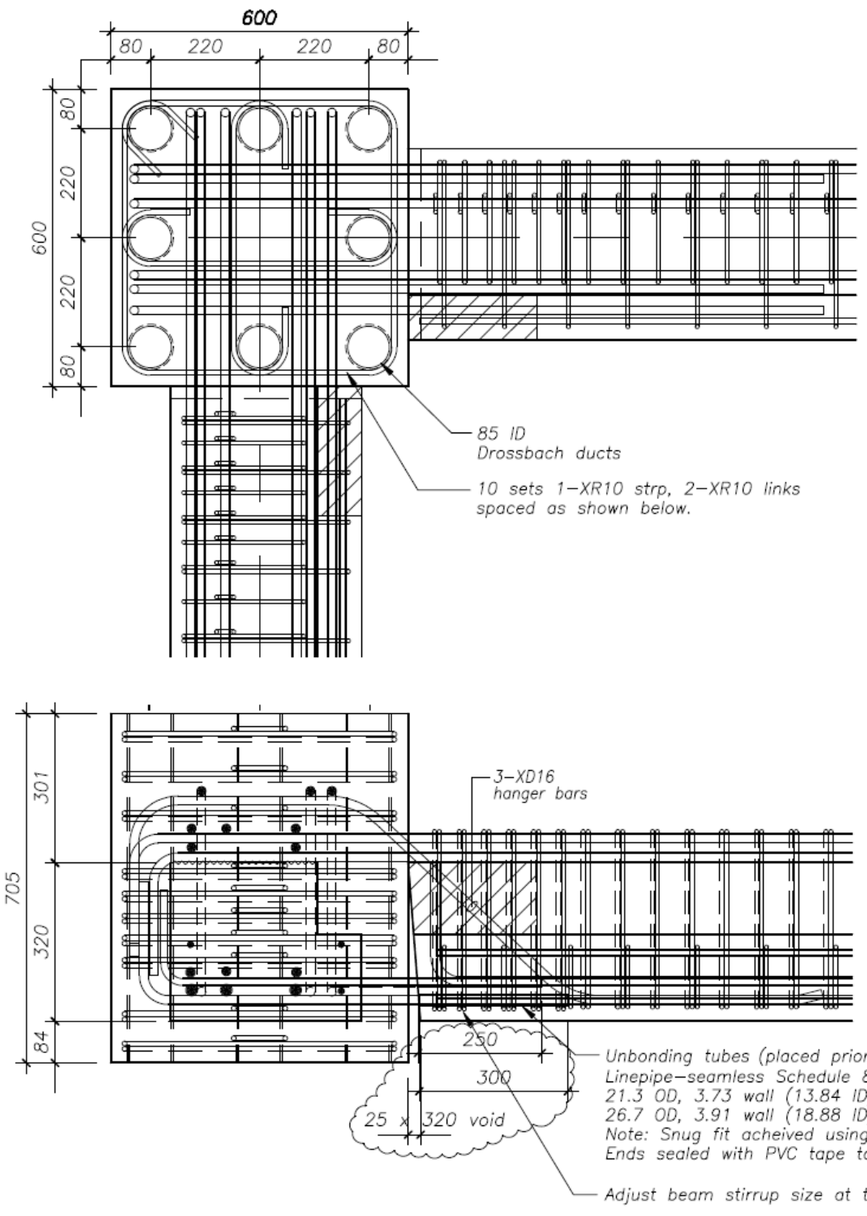

precast shop drawing

RM DRAUGHTING P.O.BOX 53 KIRWEE PH 03 318 1605 CANTERBURY FAX 03 318 1625	BRADFORD PRECAST LTD P.O.BOX 214 ASHBURTON Telephone (03) 308–9039 Facsimile (03) 308 6300

REV	DATE	REVISION DETAILS
2	02.09.10	Construction update
1	19.08.10	Construction
A	06.08.10	Approval

University of Canterbury – FRST Future Building Systems

SUB TITLE: beam corner unit joint detail

DRAWN RMM

SCALE 1:10 original size – A3

JOB NO 2278

DRAWING No JD–1

REV 2

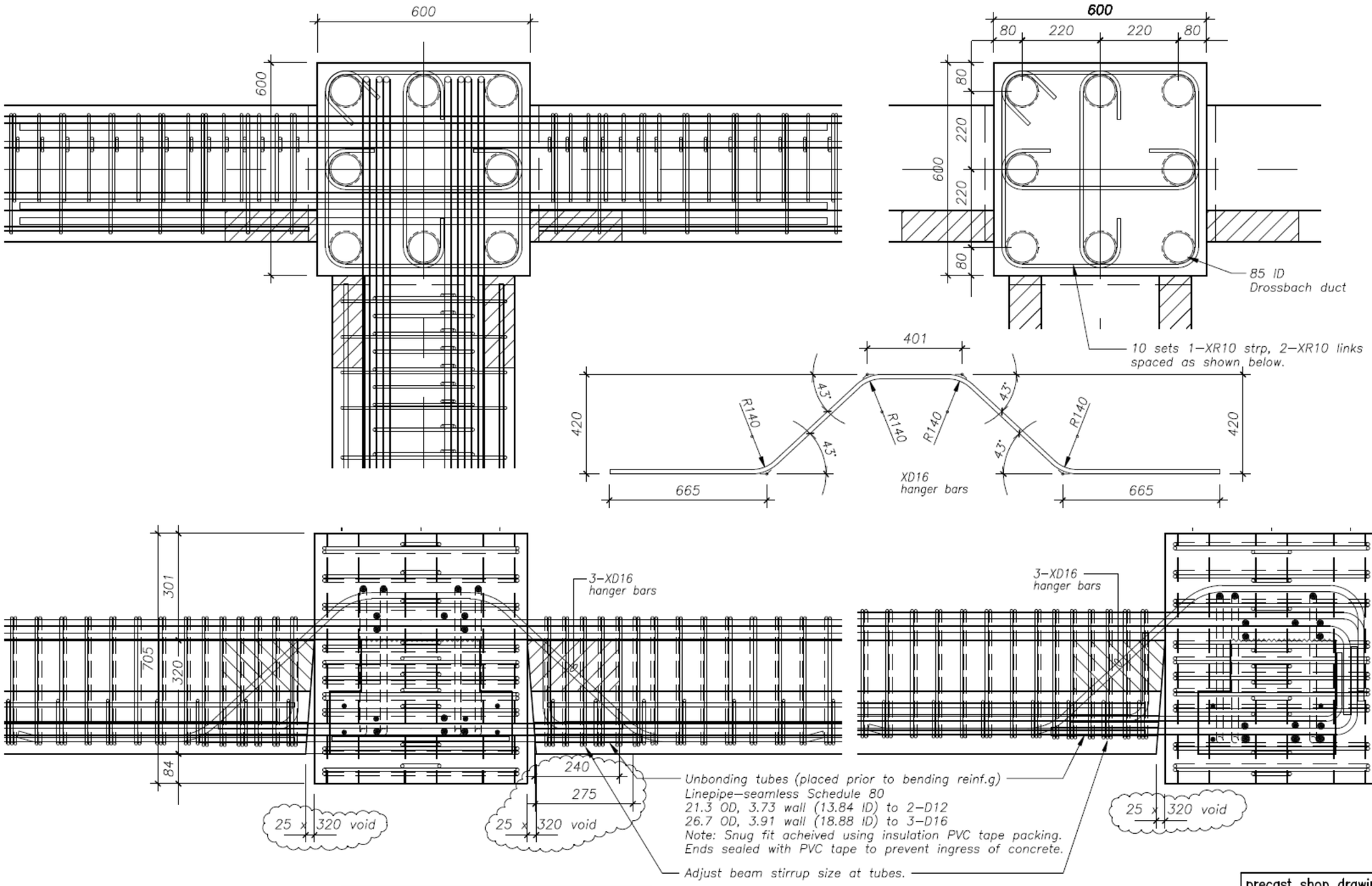

precast shop drawing

RM DRAUGHTING P.O.BOX 53 KIRWEE PH 03 318 1605 CANTERBURY FAX 03 318 1625	BRADFORD PRECAST LTD P.O.BOX 214 ASHBURTON Telephone (03) 308-9039 Facsimile (03) 308 6300

REV	DATE	REVISION DETAILS
2	02.09.10	Construction update
1	19.08.10	Construction
A	06.08.10	Approval

University of Canterbury – FRST Future Building Systems

SUB TITLE: beam "T" unit joint detail

DRAWN RMM | SCALE 1:10 original size - A3 | JOB NO 2278 | DRAWING No JD–2 | REV 2

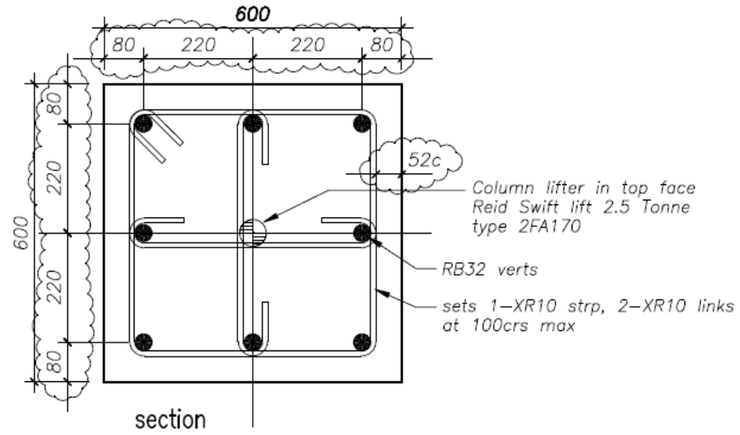

section

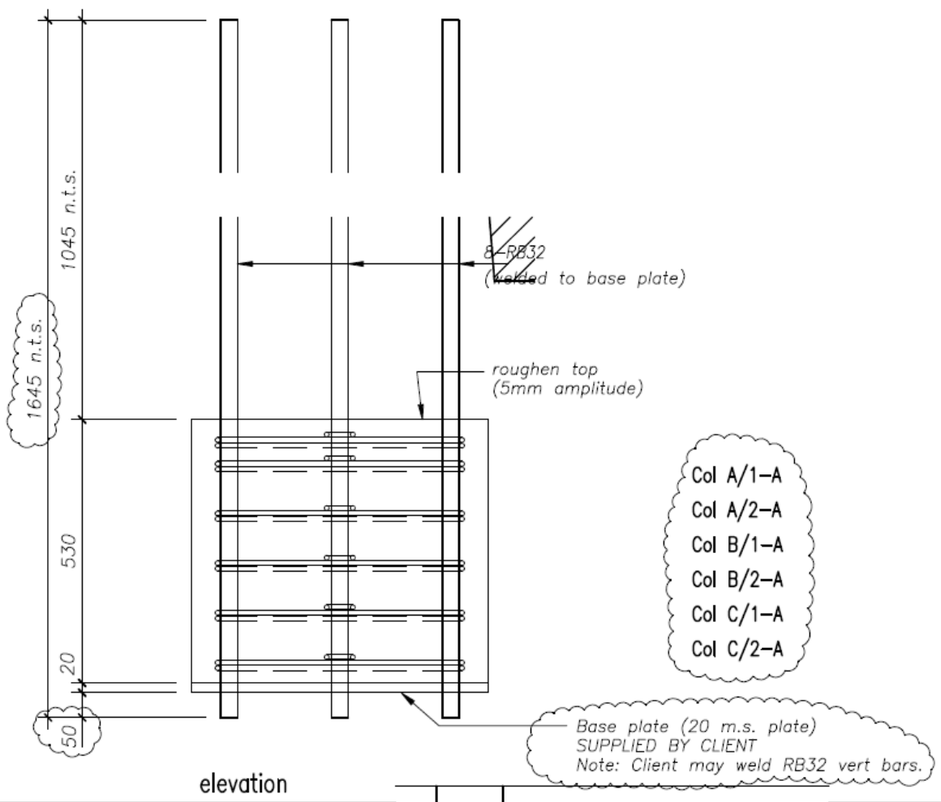

elevation

Note:

Conc strength – 40 MPa

Conc. Volume (m^3) = 0.198

Panel mass (tonne) = 0.496

PANEL LIFTERS
"REID" lifters (type as shown on elevation)
Installed and used as per manufactures Spec.

precast shop drawing

RM DRAUGHTING P.O.BOX 53 KIRWEE PH 03 318 1605 CANTERBURY FAX 03 318 1625	BRADFORD PRECAST LTD P.O.BOX 214 ASHBURTON Telephone (03) 308-9039 Facsimile (03) 308 6300	University of Canterbury – FRST Future Building Systems
SUB TITLE column type A	DRAWN RMM SCALE 1:10 original size – A3	JOB NO 2278 DRAWING No Col A REV 1

REV	DATE	REVISION DETAILS
1	19.08.10	Construction
A	06.08.10	Approval

Note:

Conc strength – 40 MPa

Conc. Volume (m^3) = 0.466

Panel mass (tonne) = 1,212

PANEL LIFTERS
"REID" lifters (type as shown on elevation)
Installed and used as per manufactures Spec.

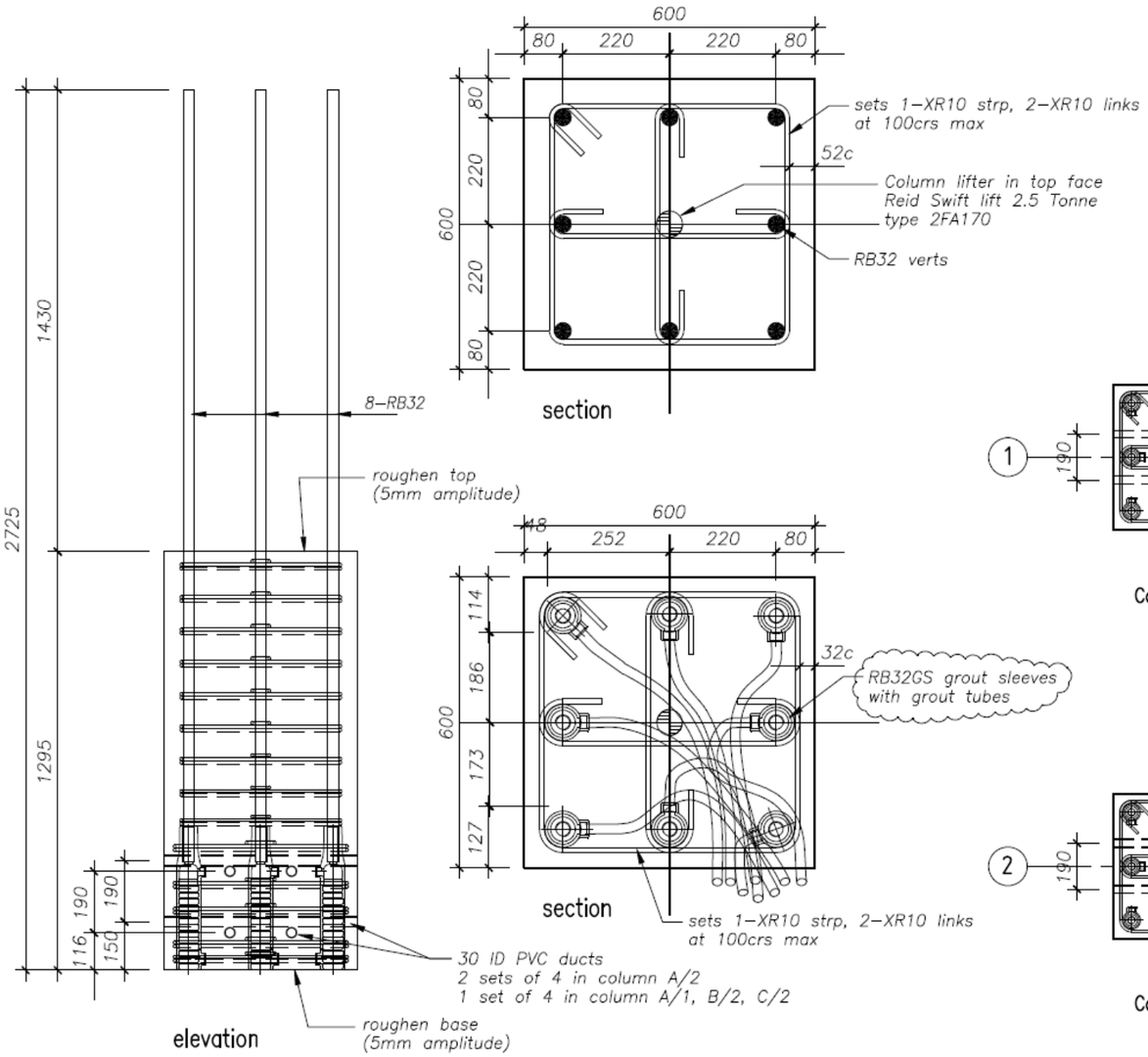

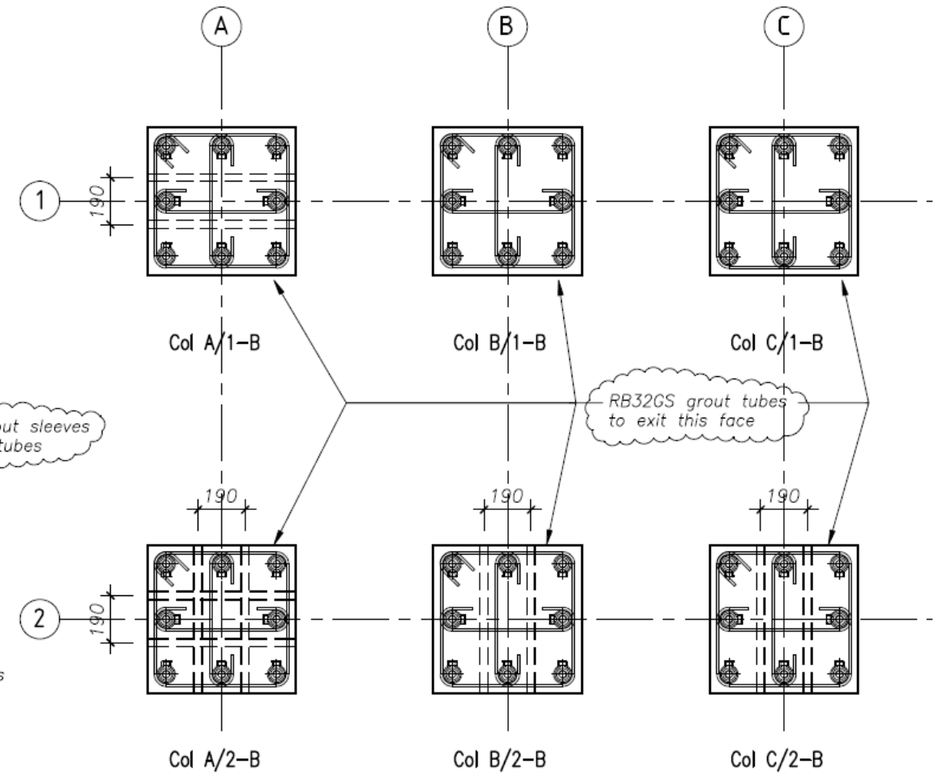

30 ID PVC duct location plan

RM DRAUGHTING P.O.BOX 53 KIRWEE PH 03 318 1605 CANTERBURY FAX 03 318 1625	BRADFORD PRECAST LTD P.O.BOX 214 ASHBURTON Telephone (03) 308-9039 Facsimile (03) 308 6300	2	02.09.10	RB32GS grout tubes shown	University of Canterbury – FRST Future Building Systems	DRAWN RMM
		1	19.08.10	Construction		
		A	06.08.10	Approval	SUB TITLE column type B	SCALE 1:15, 1:10 original size – A3
		REV	DATE	REVISION DETAILS		

precast shop drawing

JOB NO 2278

DRAWING No Col B

REV 2

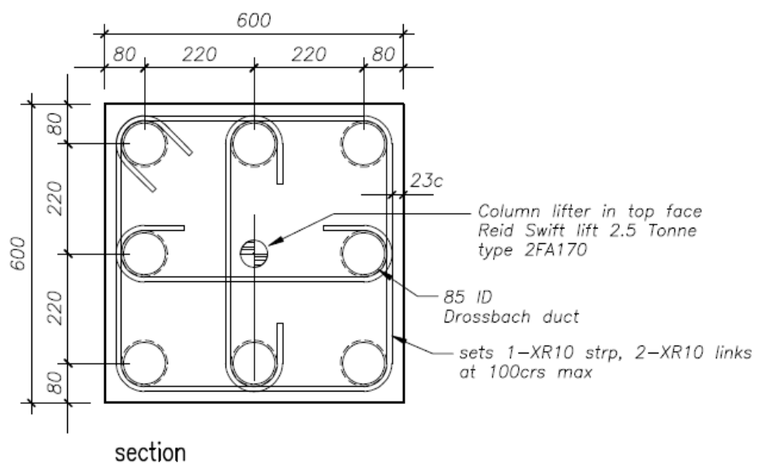

section

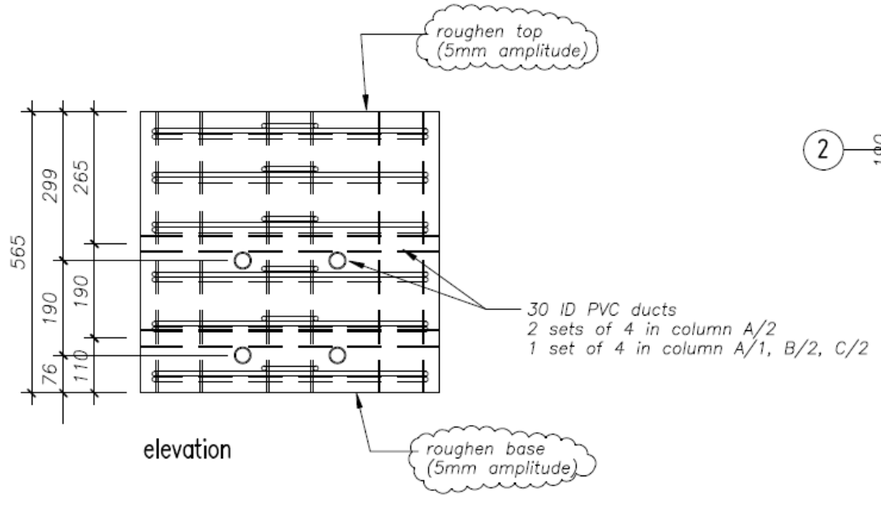

elevation

Note:

Conc strength – 40 MPa

Conc. Volume (m^3) = 0.177

Panel mass (tonne) = 0.443

PANEL LIFTERS
"REID" lifters (type as shown on elevation)
Installed and used as per manufactures Spec.

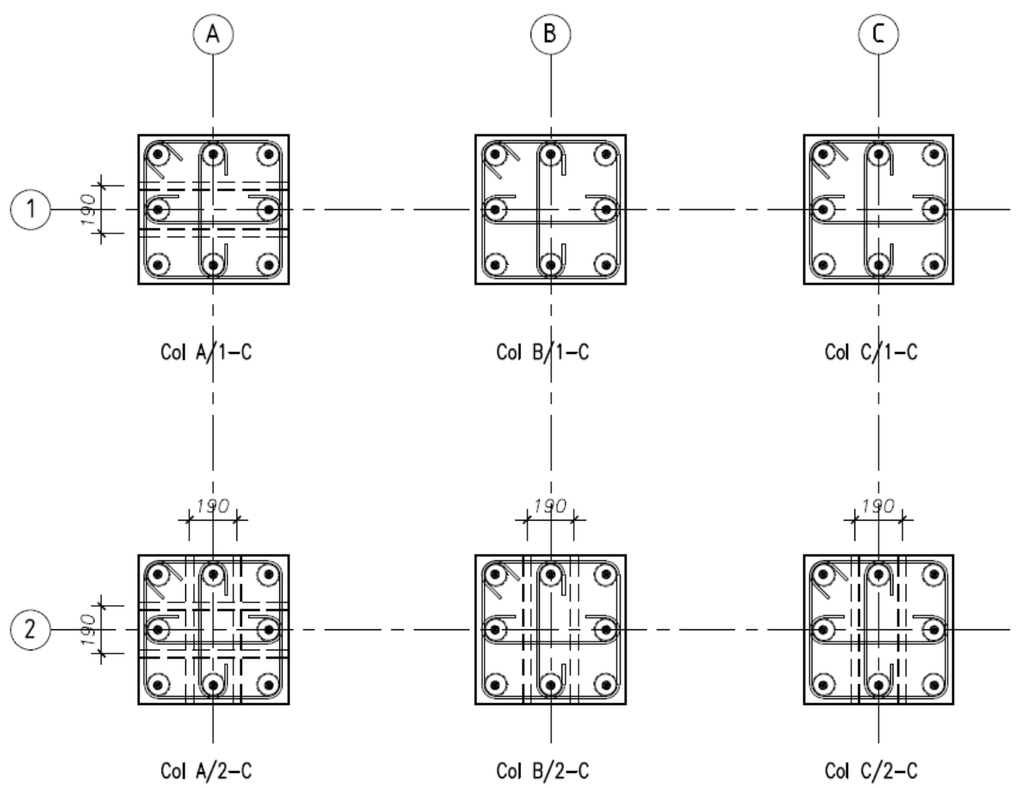

30 ID PVC duct location plan

RM DRAUGHTING P.O.BOX 53 KIRWEE PH 03 318 1605 CANTERBURY FAX 03 318 1625	BRADFORD PRECAST LTD P.O.BOX 214 ASHBURTON Telephone (03) 308–9039 Facsimile (03) 308 6300	precast shop drawing

REV	DATE	REVISION DETAILS
1	19.08.10	Construction
A	06.08.10	Approval

University of Canterbury – FRST Future Building Systems

SUB TITLE: column type C

DRAWN: RMM

SCALE: 1:10 original size – A3

JOB NO: 2278

DRAWING No: Col C

REV: 1

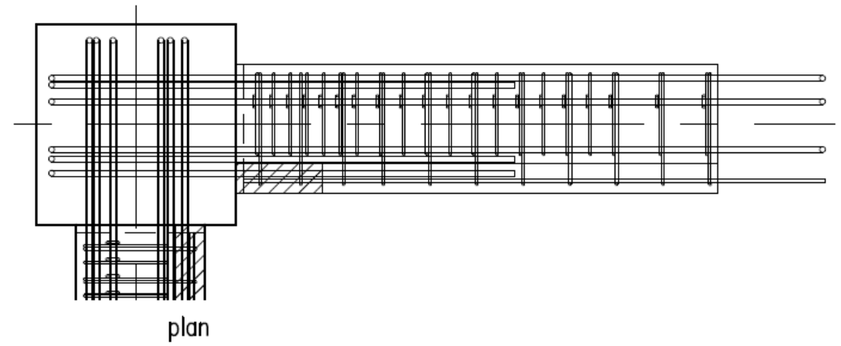

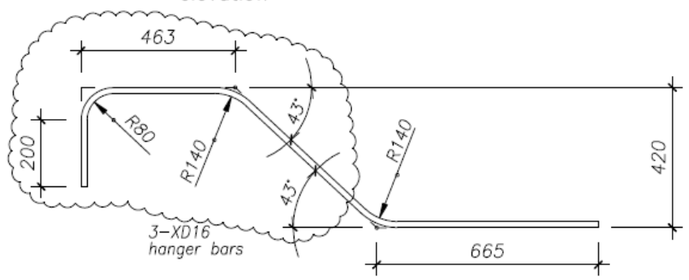

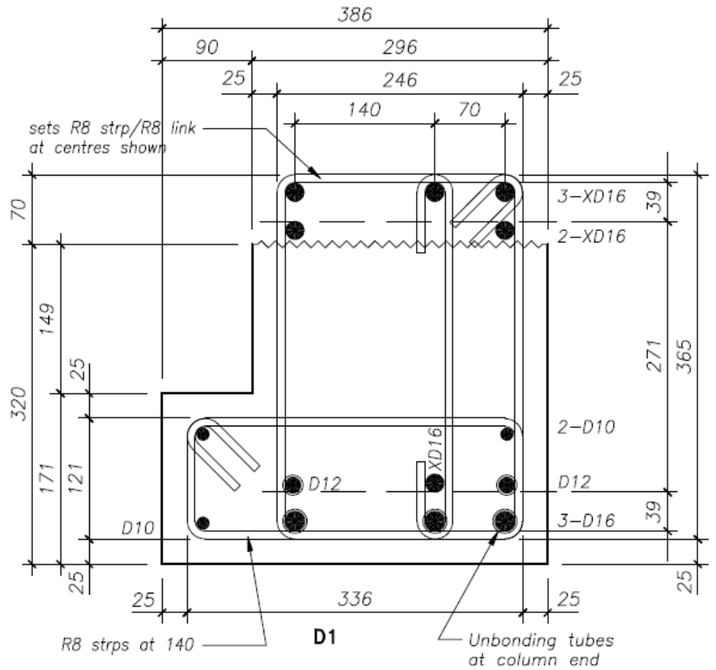

beam reinforcing type R.11 as drawn
beam reinforcing type R.11h handed

Note:
XD16 and D16 grade reinforcing specified
Ensure correct supply and placement of these bars.

REV	DATE	REVISION DETAILS
3	02.09.10	XD16 hanger bars revised
2	23.08.10	Construction update
1	19.08.10	Construction
A	06.08.10	Approval

RM DRAUGHTING
P.O.BOX 53
KIRWEE PH 03 318 1605
CANTERBURY FAX 03 318 1625

BRADFORD PRECAST LTD
P.O.BOX 214 ASHBURTON
Telephone (03) 308–9039
Facsimile (03) 308 6300

precast shop drawing

University of Canterbury – FRST Future Building Systems

SUB TITLE beam reinforcing type R.11

DRAWN RMM

SCALE 1:15, 1:5 original size – A3

JOB NO 2278

DRAWING No R11

REV 3

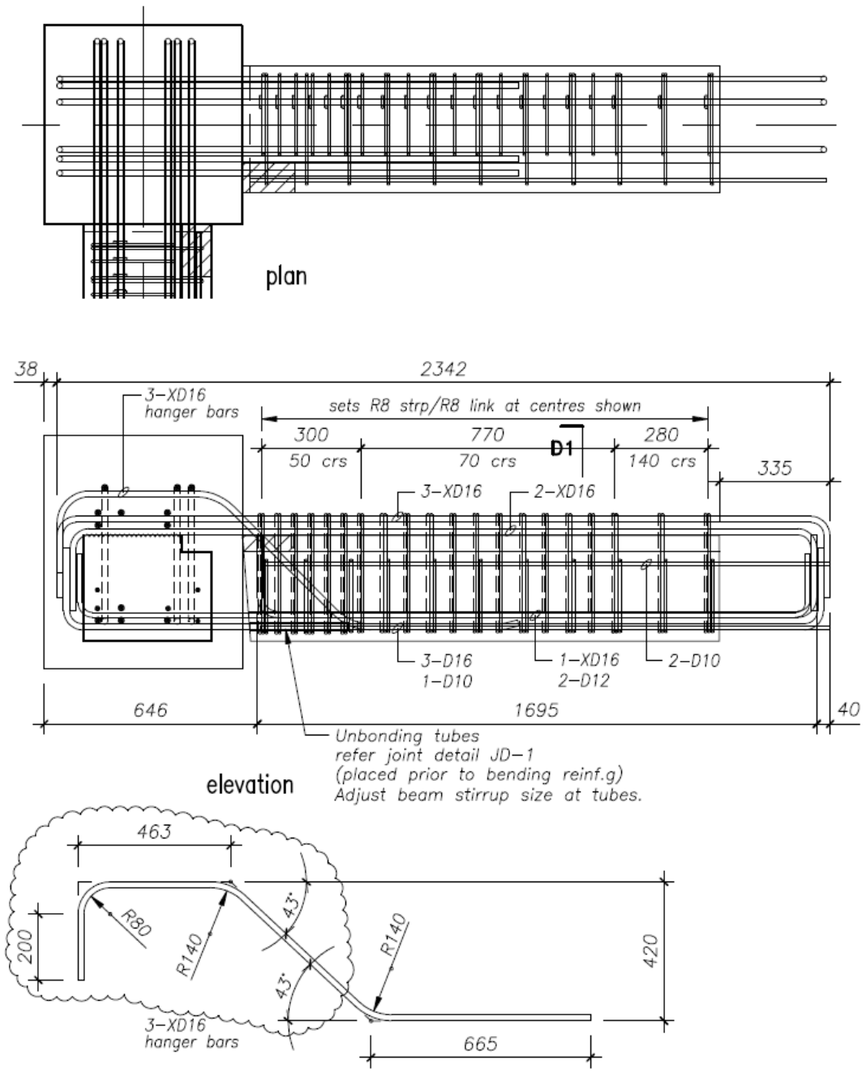

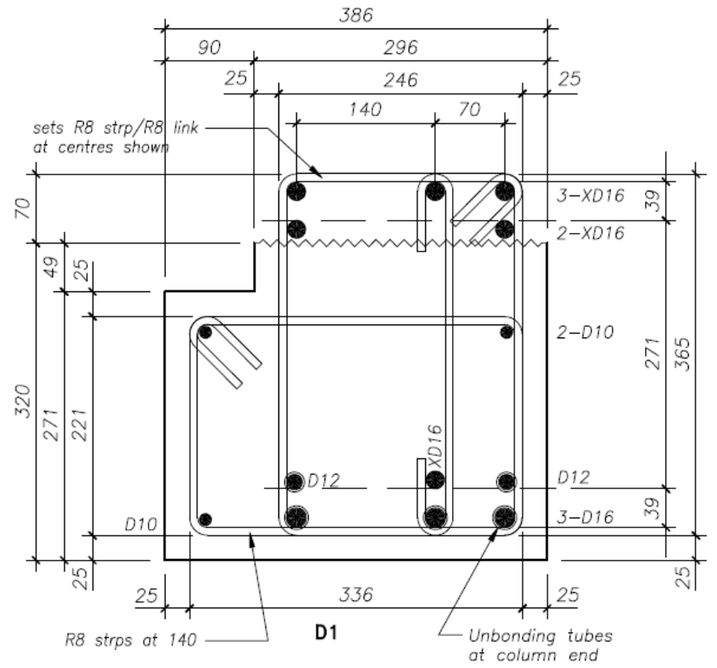

beam reinforcing type R.21 as drawn
beam reinforcing type R.21h handed

Note:
XD16 and D16 grade reinforcing specified
Ensure correct supply and placement of these bars.

precast shop drawing

RM DRAUGHTING P.O.BOX 53 KIRWEE PH 03 318 1605 CANTERBURY FAX 03 318 1625	BRADFORD PRECAST LTD P.O.BOX 214 ASHBURTON Telephone (03) 308-9039 Facsimile (03) 308 6300	

REV	DATE	REVISION DETAILS
2	02.09.10	XD16 hanger bars revised
1	19.08.10	Construction
A	06.08.10	Approval

University of Canterbury – FRST Future Building Systems

SUB TITLE: beam reinforcing type R.21

DRAWN RMM | SCALE 1:15, 1:5 original size - A3 | JOB NO 2278 | DRAWING No R21 | REV 2

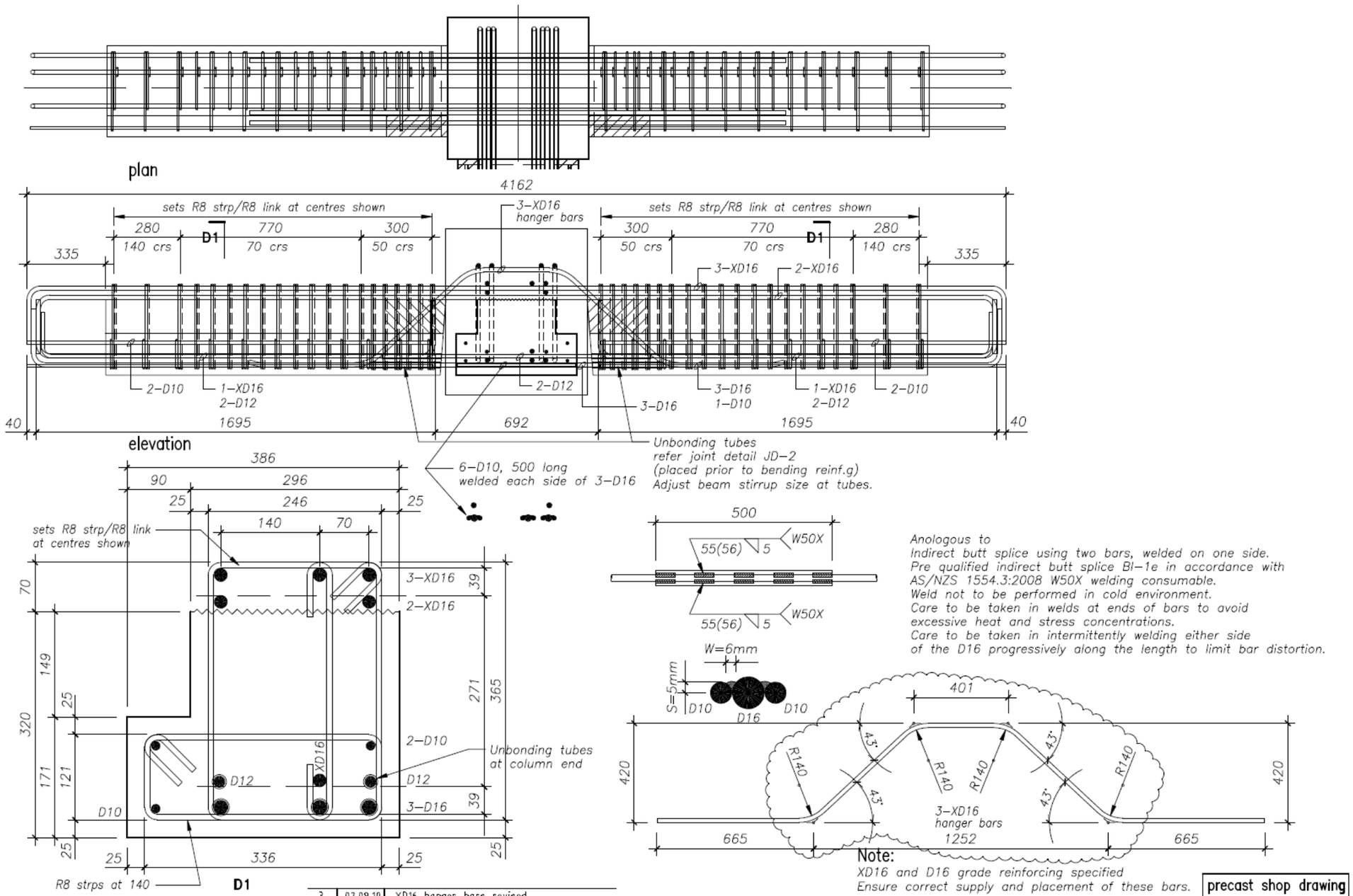

RM DRAUGHTING P.O.BOX 53 KIRWEE PH 03 318 1605 CANTERBURY FAX 03 318 1625	BRADFORD PRECAST LTD P.O.BOX 214 ASHBURTON Telephone (03) 308–9039 Facsimile (03) 308 6300	precast shop drawing

REV	DATE	REVISION DETAILS
3	02.09.10	XD16 hanger bars revised
2	23.08.10	Construction update
1	19.08.10	Construction
A	06.08.10	Approval

University of Canterbury – FRST Future Building Systems

SUB TITLE: beam reinforcing type R.12

DRAWN: RMM

SCALE: 1:15, 1:5 original size – A3

JOB NO: 2278

DRAWING No: R12

REV: 3

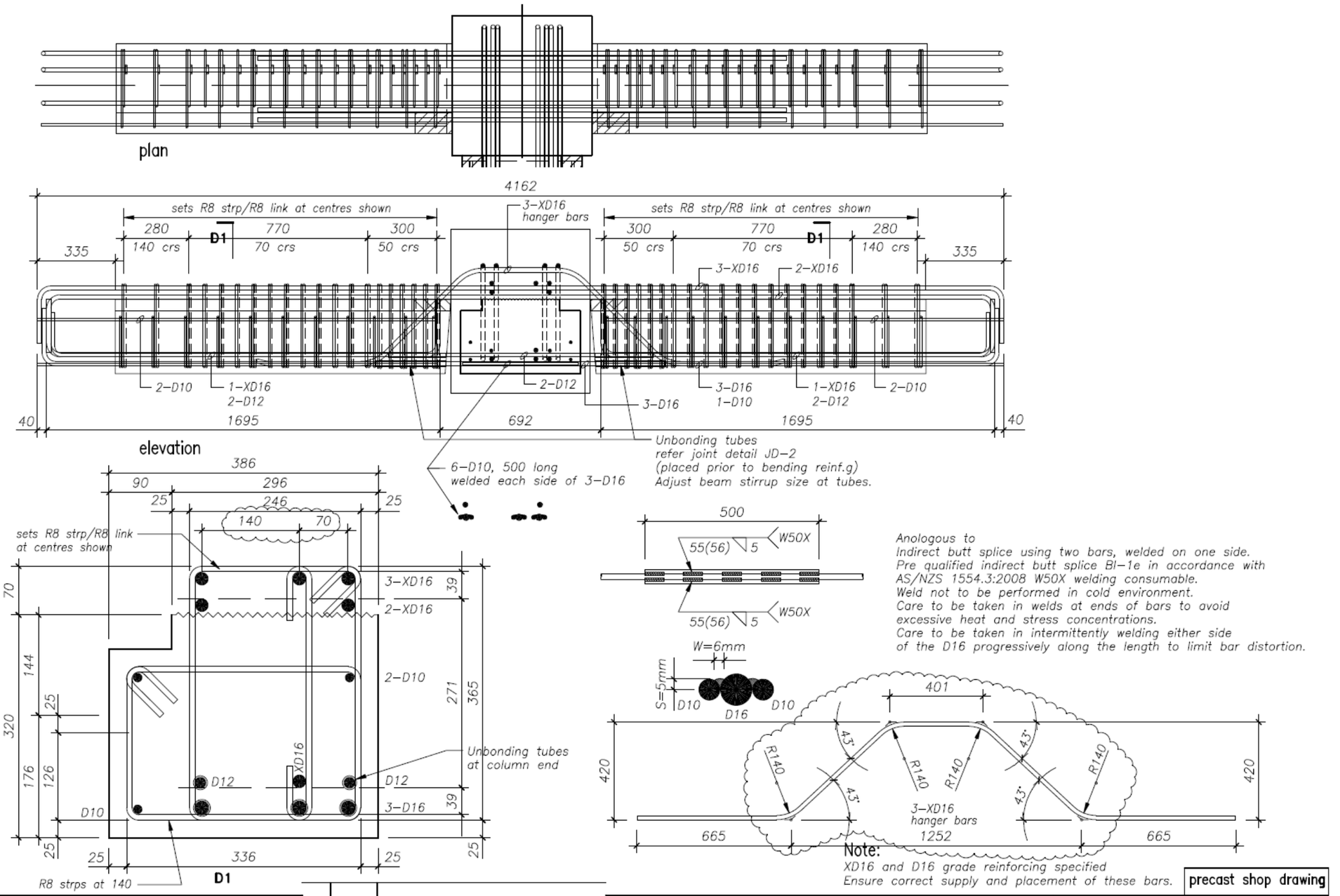

precast shop drawing

RM DRAUGHTING P.O.BOX 53 KIRWEE PH 03 318 1605 CANTERBURY FAX 03 318 1625	BRADFORD PRECAST LTD P.O.BOX 214 ASHBURTON Telephone (03) 308–9039 Facsimile (03) 308 6300	University of Canterbury – FRST Future Building Systems
SUB TITLE	beam reinforcing type R.22	

REV	DATE	REVISION DETAILS
2	02.09.10	XD16 hanger bars revised
1	19.08.10	Construction
A	06.08.10	Approval

DRAWN RMM	JOB NO 2278		
SCALE 1:15, 1:5 original size – A3	DRAWING No R22	REV 2	

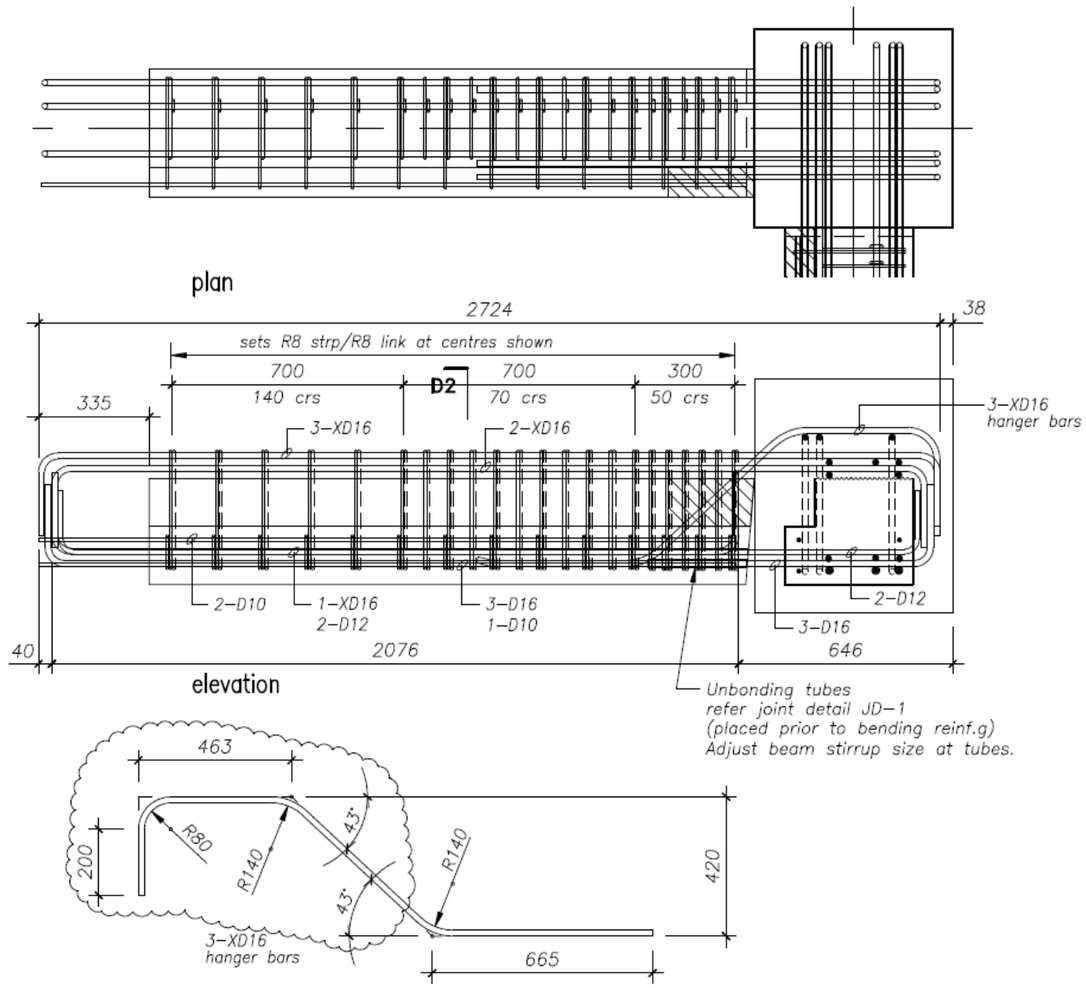

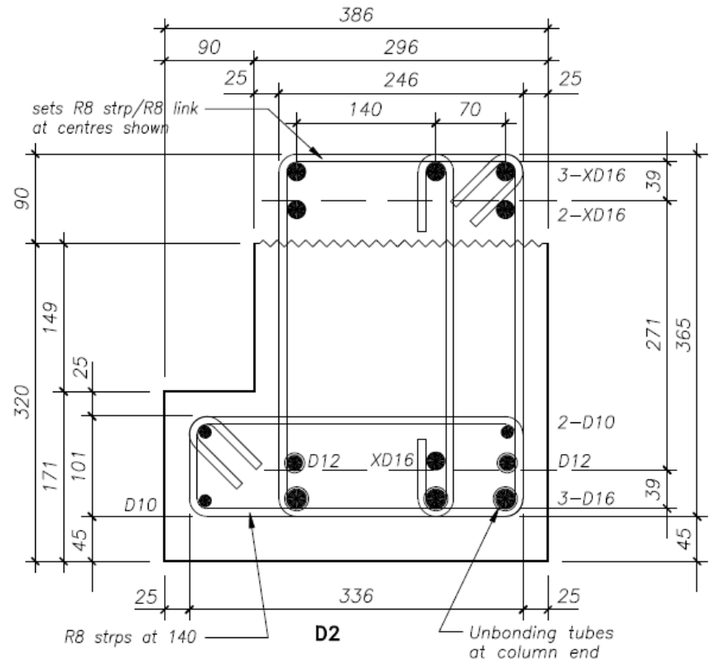

beam reinforcing type R.13 as drawn
beam reinforcing type R.13h handed

Note:
XD16 and D16 grade reinforcing specified
Ensure correct supply and placement of these bars.

precast shop drawing

RM DRAUGHTING P.O.BOX 53 KIRWEE PH 03 318 1605 CANTERBURY FAX 03 318 1625	BRADFORD PRECAST LTD P.O.BOX 214 ASHBURTON Telephone (03) 308-9039 Facsimile (03) 308 6300	

REV	DATE	REVISION DETAILS
3	02.09.10	XD16 hanger bars revised
2	23.08.10	Construction update
1	19.08.10	Construction
A	06.08.10	Approval

University of Canterbury – FRST Future Building Systems

SUB TITLE beam reinforcing type R.13

DRAWN RMM

SCALE 1:15, 1:5 original size - A3

JOB NO 2278

DRAWING No R13

REV 3

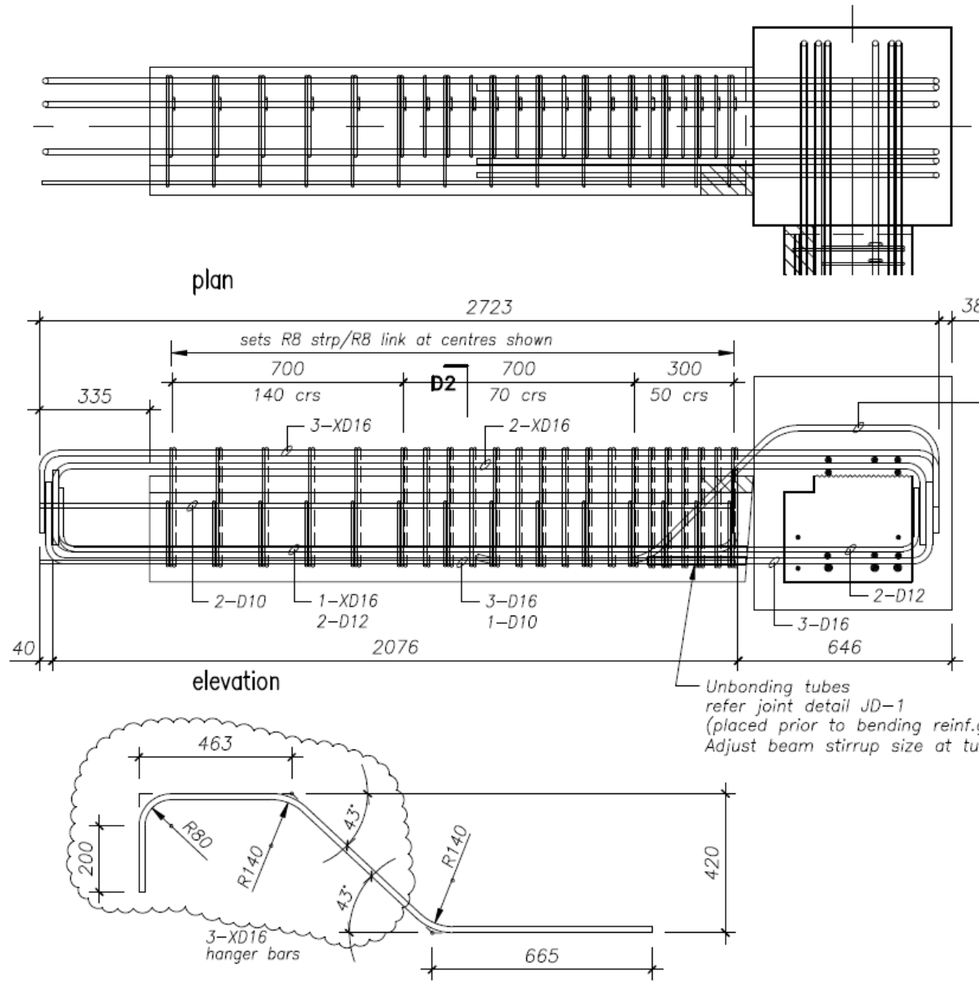

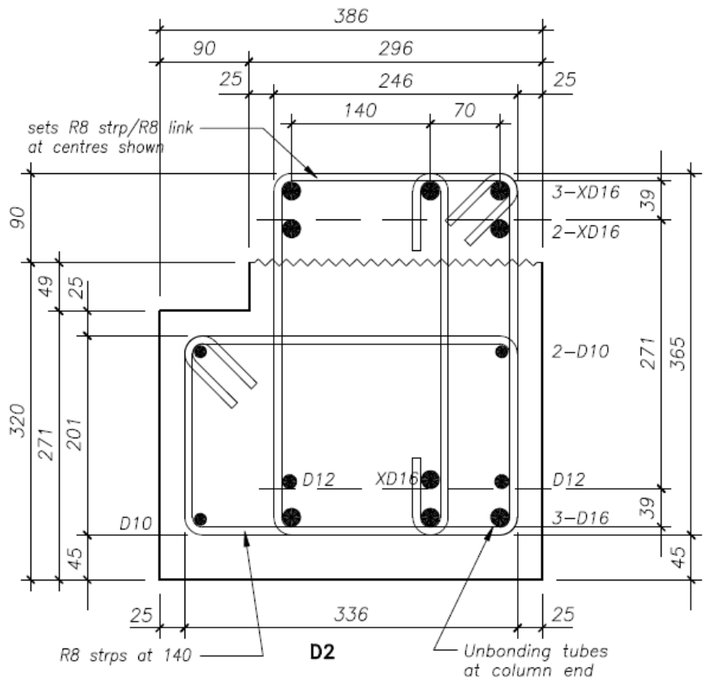

beam reinforcing type R.23 as drawn
beam reinforcing type R.23h handed

Note:
XD16 and D16 grade reinforcing specified
Ensure correct supply and placement of these bars.

precast shop drawing

RM DRAUGHTING P.O.BOX 53 KIRWEE PH 03 318 1605 CANTERBURY FAX 03 318 1625	BRADFORD PRECAST LTD P.O.BOX 214 ASHBURTON Telephone (03) 308-9039 Facsimile (03) 308 6300	

REV	DATE	REVISION DETAILS
2	02.09.10	XD16 hanger bars revised
1	19.08.10	Construction
A	06.08.10	Approval

University of Canterbury – FRST Future Building Systems

SUB TITLE: beam reinforcing type R.23

DRAWN RMM | SCALE 1:15, 1:5 original size – A3 | JOB NO 2278 | DRAWING No R23 | REV 2

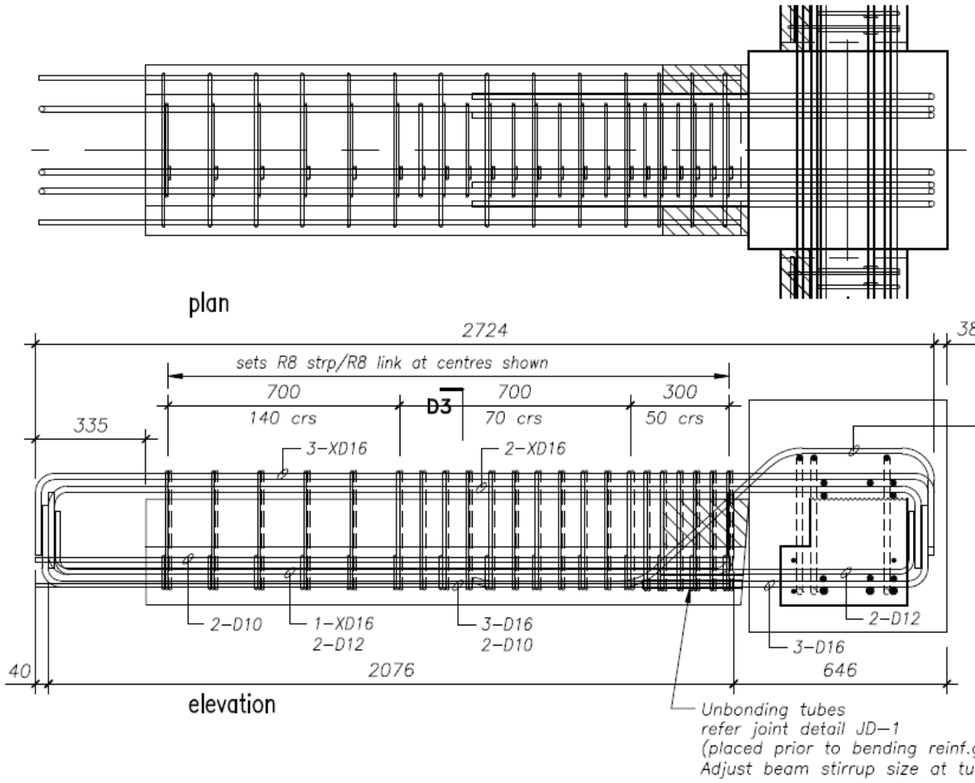

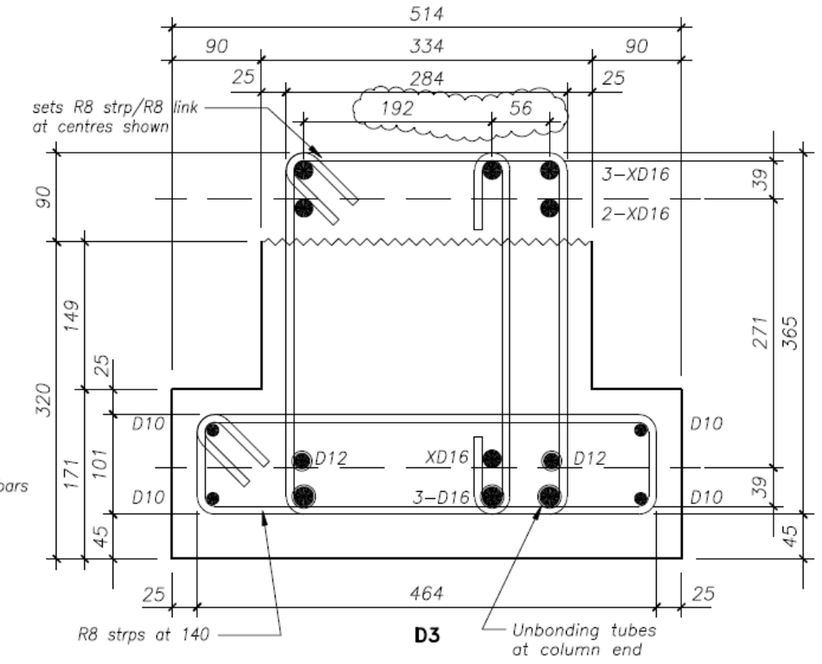

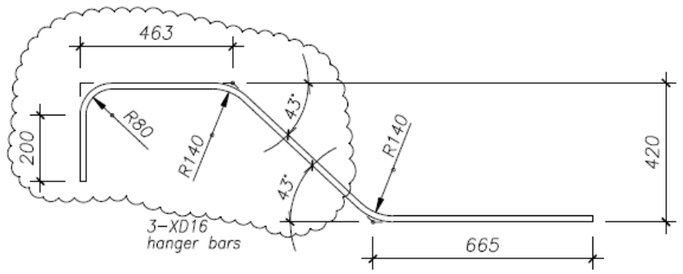

beam reinforcing type R.14 as drawn
beam reinforcing type R.14h handed

Note:
XD16 and D16 grade reinforcing specified
Ensure correct supply and placement of these bars.

precast shop drawing

RM DRAUGHTING P.O.BOX 53 KIRWEE PH 03 318 1605 CANTERBURY FAX 03 318 1625	BRADFORD PRECAST LTD P.O.BOX 214 ASHBURTON Telephone (03) 308–9039 Facsimile (03) 308 6300	

REV	DATE	REVISION DETAILS
3	02.09.10	XD16 hanger bars revised
2	23.08.10	Construction update
1	19.08.10	Construction
A	06.08.10	Approval

University of Canterbury – FRST Future Building Systems	DRAWN RMM	JOB NO 2278	
SUB TITLE beam reinforcing type R.14	SCALE 1:15, 1:5 original size – A3	DRAWING No R14	REV 3

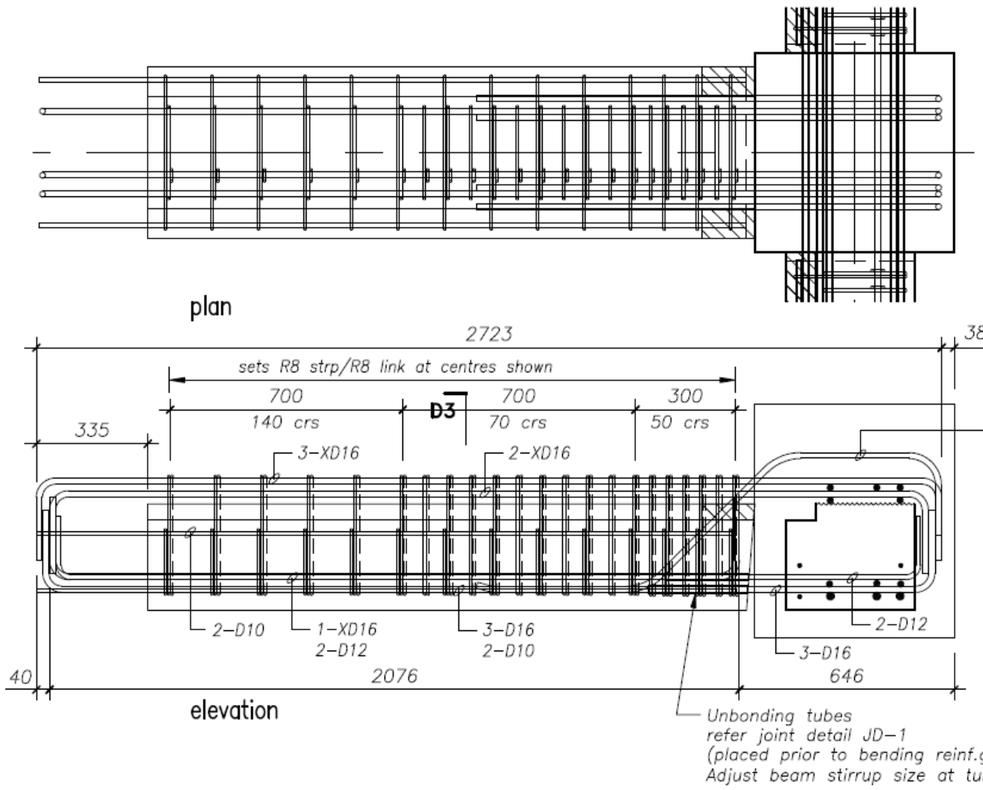

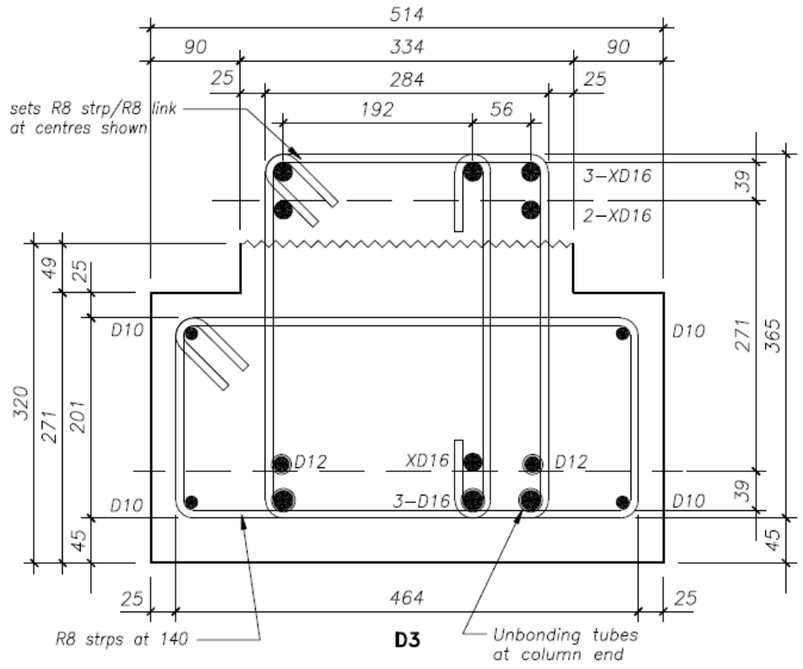

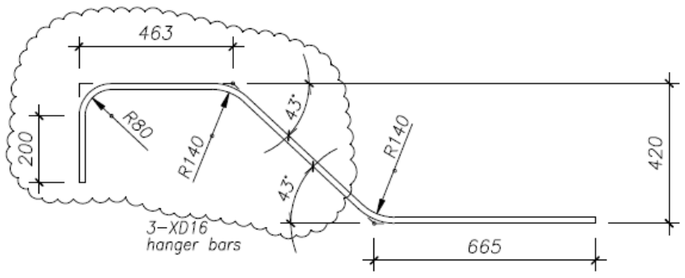

beam reinforcing type R.24 as drawn
beam reinforcing type R.24h handed

Note:
XD16 and D16 grade reinforcing specified
Ensure correct supply and placement of these bars.

precast shop drawing

RM DRAUGHTING P.O.BOX 53 KIRWEE PH 03 318 1605 CANTERBURY FAX 03 318 1625	BRADFORD PRECAST LTD P.O.BOX 214 ASHBURTON Telephone (03) 308–9039 Facsimile (03) 308 6300	

REV	DATE	REVISION DETAILS
3	02.09.10	XD16 hanger bars revised
2	23.08.10	Construction update
1	19.08.10	Construction
A	06.08.10	Approval

University of Canterbury – FRST Future Building Systems	DRAWN RMM	JOB NO 2278	
SUB TITLE beam reinforcing type R.24	SCALE 1:15, 1:5 original size – A3	DRAWING No R24	REV 3

Appendix C: Superassembly Experiment Additional Results

C.1 SA1 Crack Maps

Figure C-1, Figure C-2 and Figure C-3 present crack maps for SA1 from pre-test, 1% beam drift and 2% beam drift respectively.

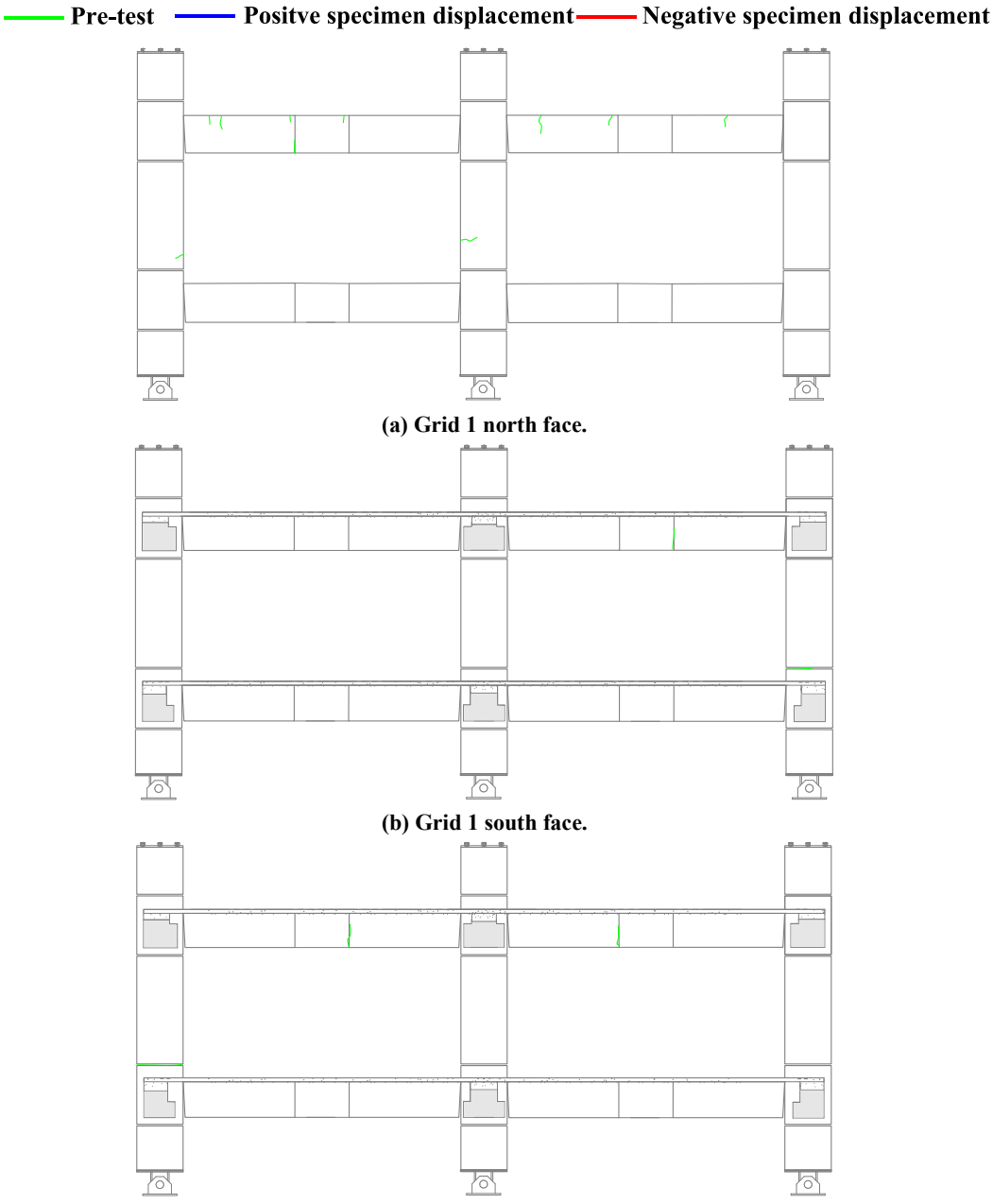

(a) Grid 1 north face.

(b) Grid 1 south face.

(c) Grid 2 north face.

Figure C-1: Specimen crack patterns prior to testing.

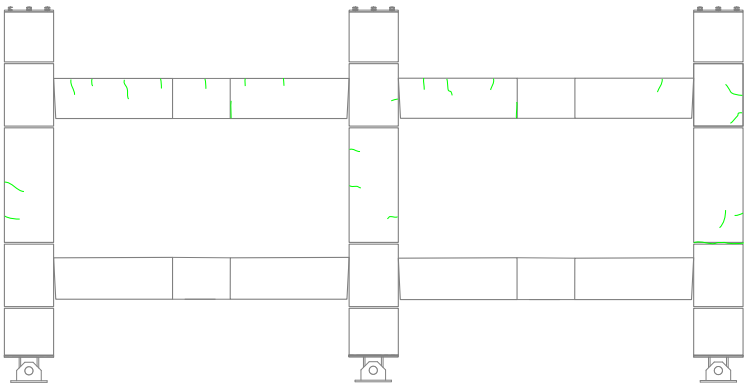

(d) Grid 2 south face.

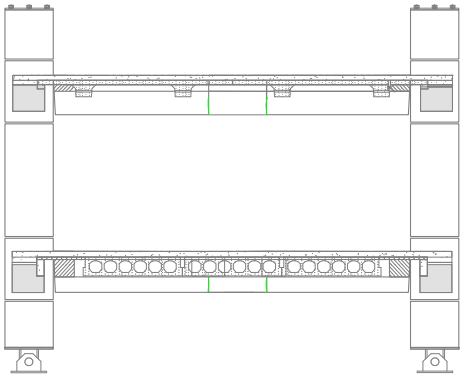

(e) Grid A east face.

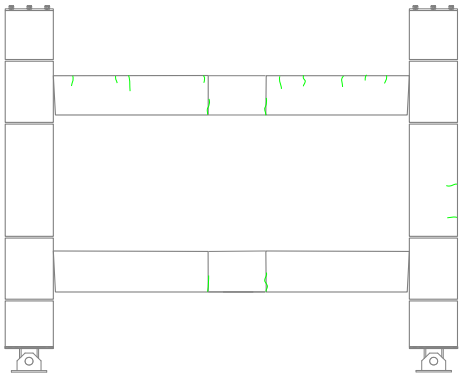

(f) Grid A west face.

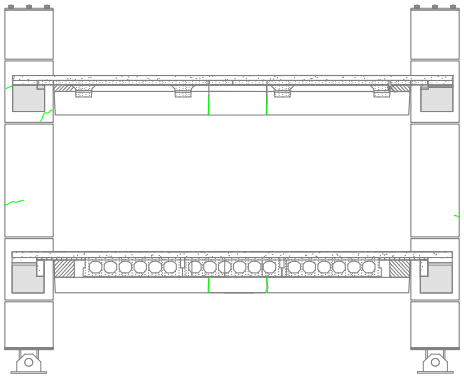

(g) Grid B east face.

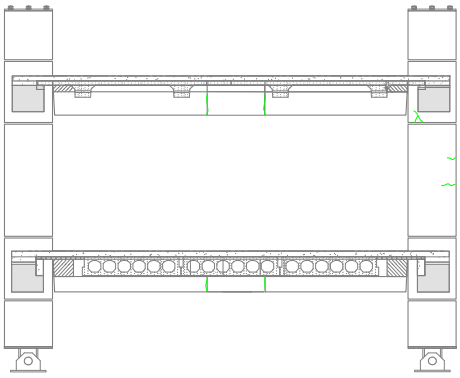

(h) Grid B west face.

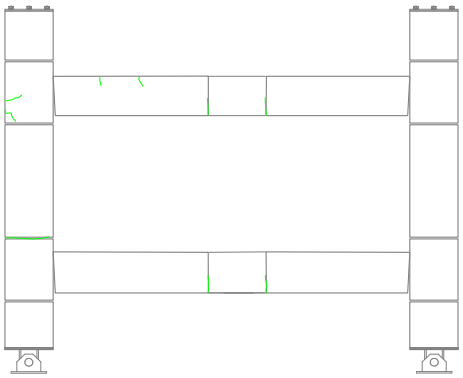

(i) Grid C east face.

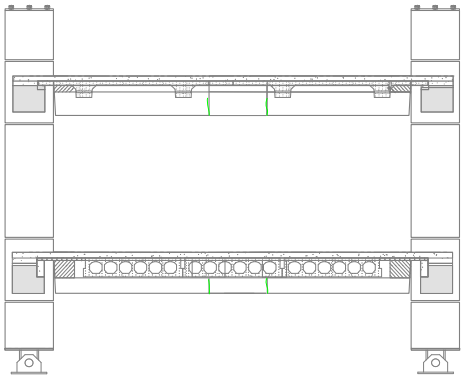

(j) Grid C west face.

Figure C-1: Specimen crack patterns prior to testing (Continued).

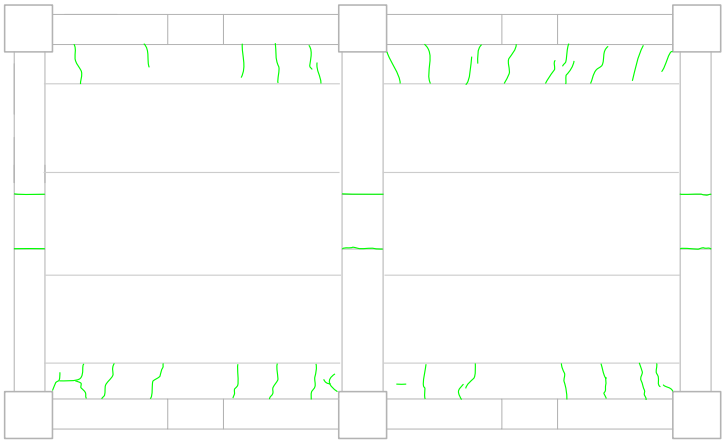

(k) Level One floor diaphragm bottom.

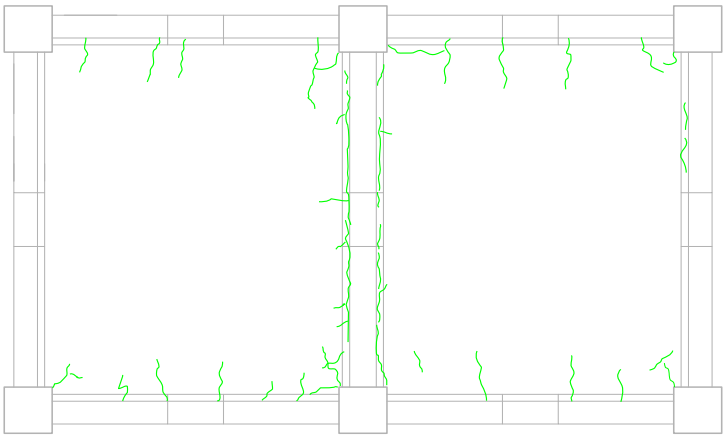

(l) Level One floor diaphragm top.

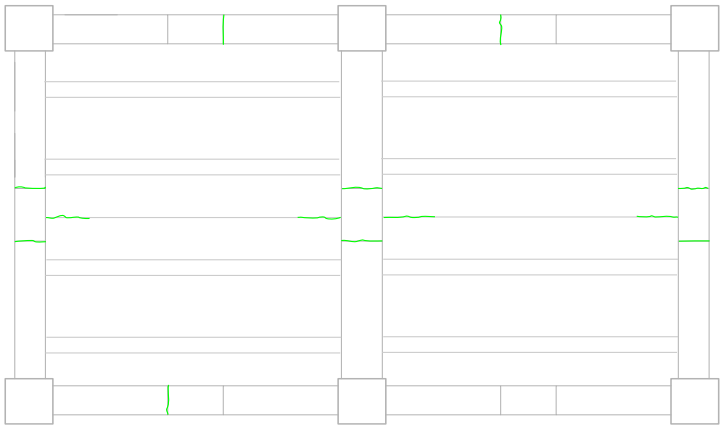

(m) Level Two floor diaphragm bottom.

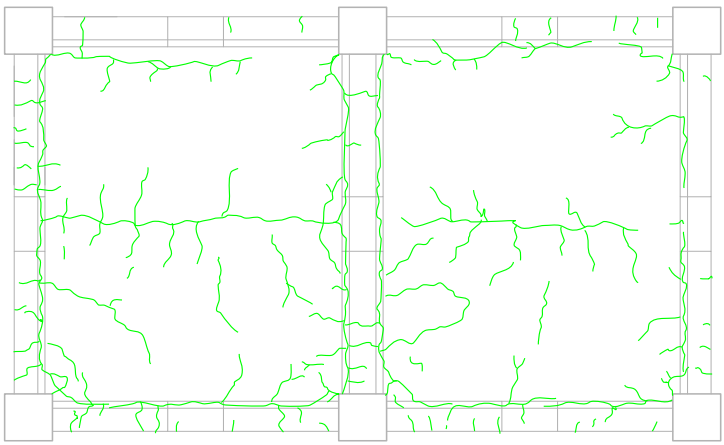

(n) Level Two floor diaphragm top.

Figure C-1: Specimen crack patterns prior to testing (Continued).

Pre-test Positve specimen displacement Negative specimen displacement

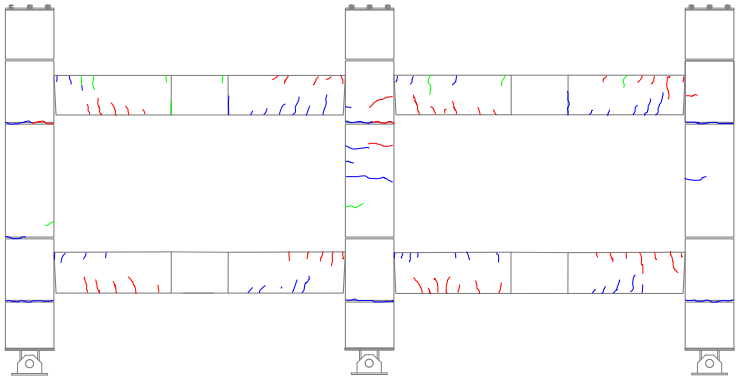

(a) Grid 1 north face.

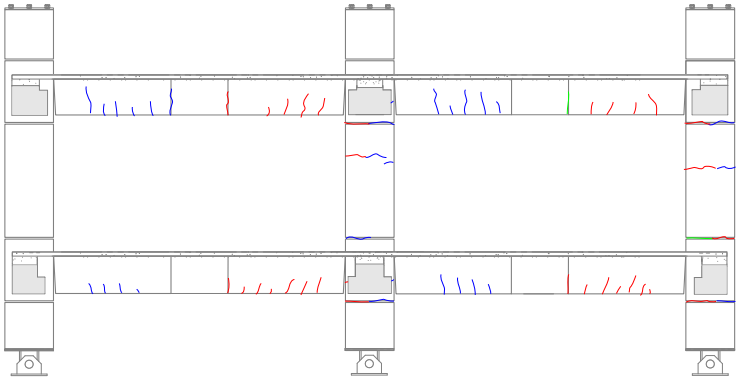

(b) Grid 1 south face.

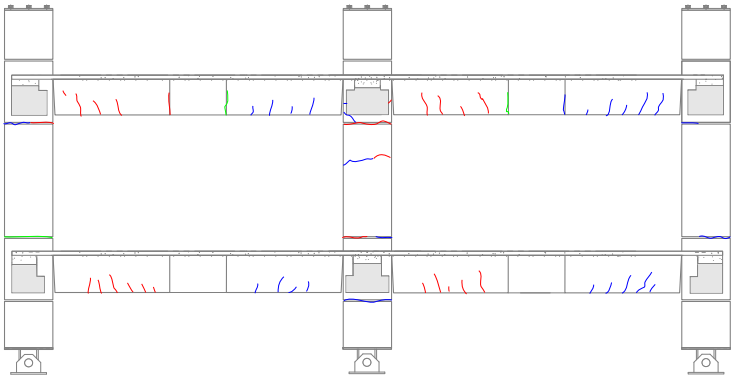

(c) Grid 2 north face.

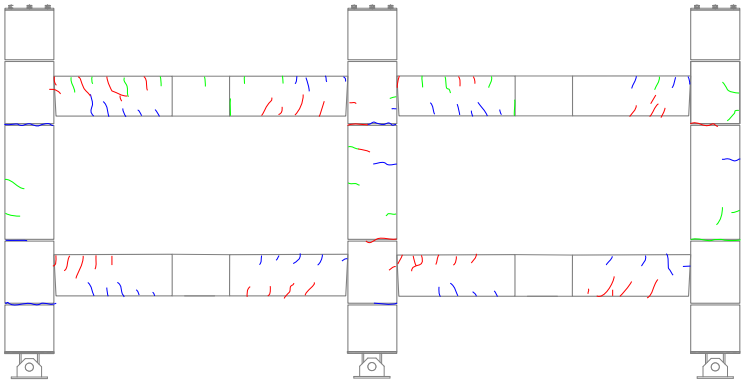

(d) Grid 2 south face.

Figure C-2: Specimen crack patterns at completion of 1.0% beam drift cycles.

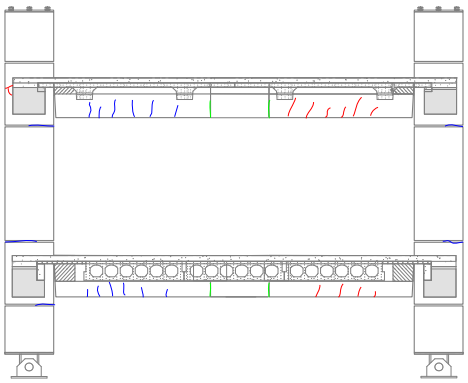

(e) Grid A east face.

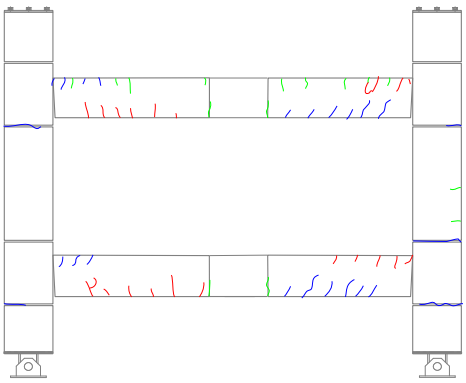

(f) Grid A west face.

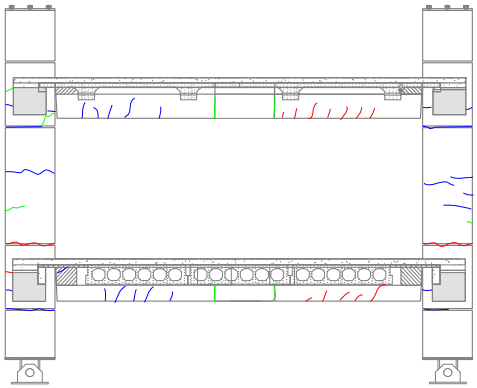

(g) Grid B east face.

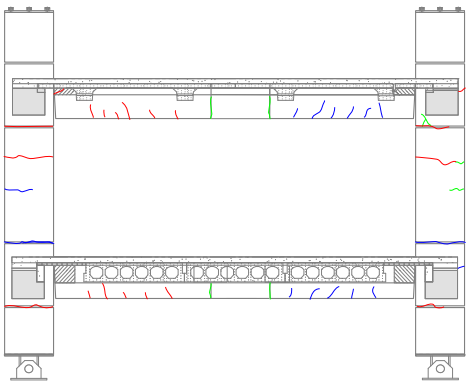

(h) Grid B west face.

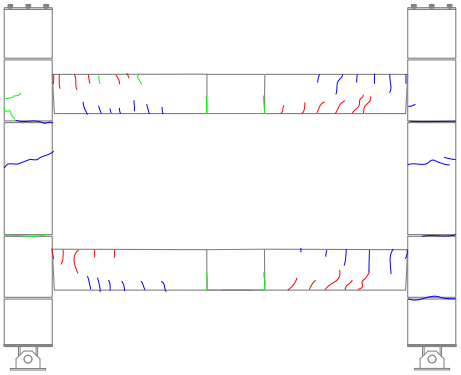

(i) Grid C east face.

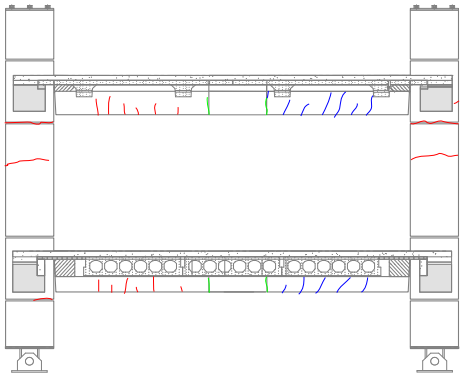

(j) Grid C west face.

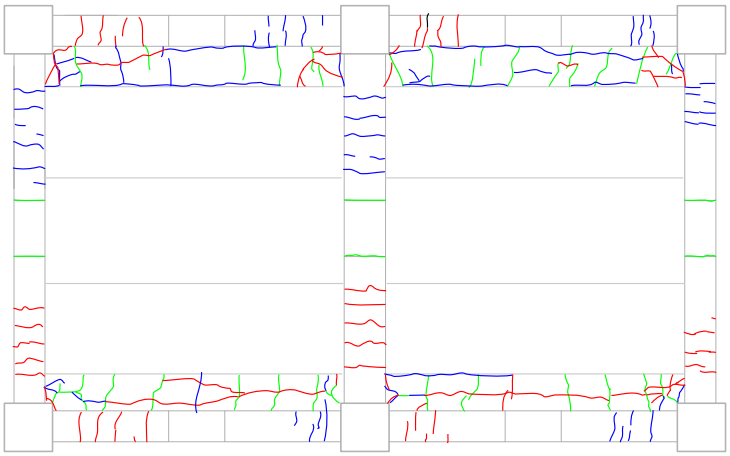

(k) Level One floor diaphragm bottom.

Figure C-2: Specimen crack patterns at completion of 1.0% beam drift cycles (Continued).

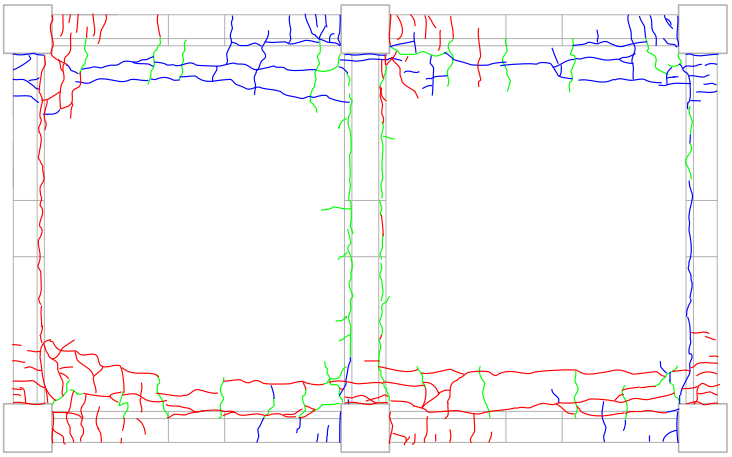

(l) Level One floor diaphragm top.

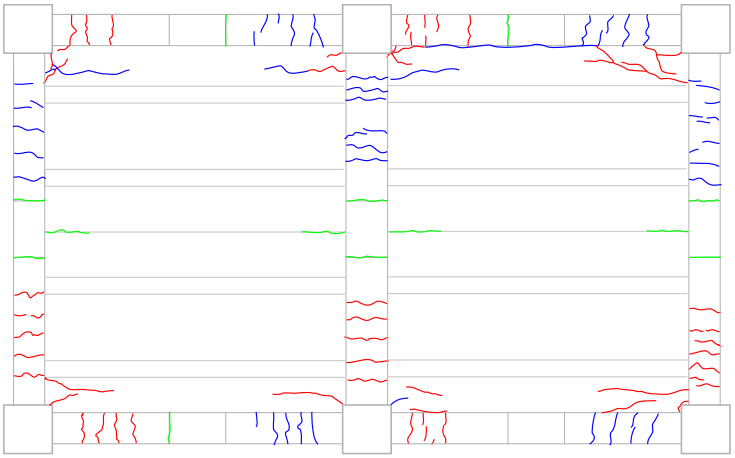

(m) Level Two floor diaphragm bottom.

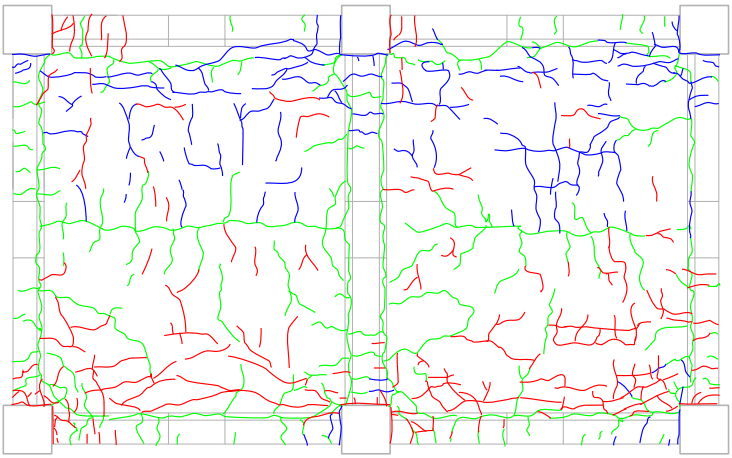

(n) Level Two floor diaphragm top.

Figure C-2: Specimen crack patterns at completion of 1.0% beam drift cycles (Continued).

Pre-test Positve specimen displacement Negative specimen displacement

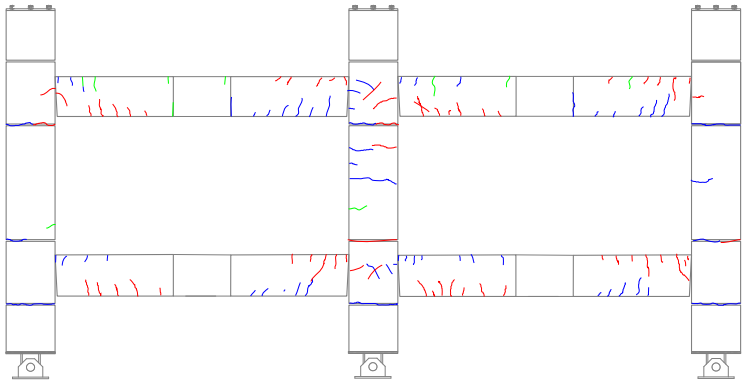

(a) Grid 1 north face.

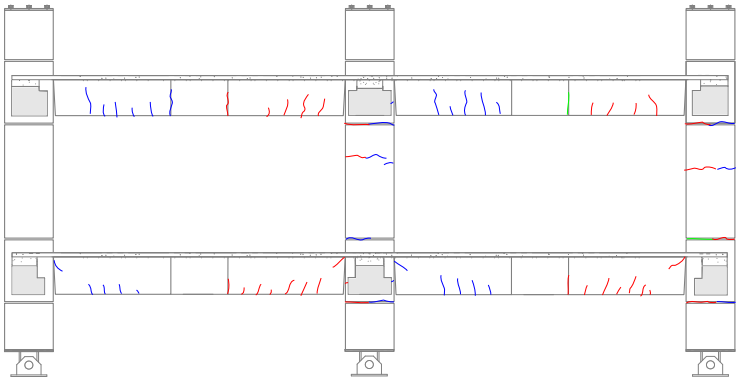

(b) Grid 1 south face.

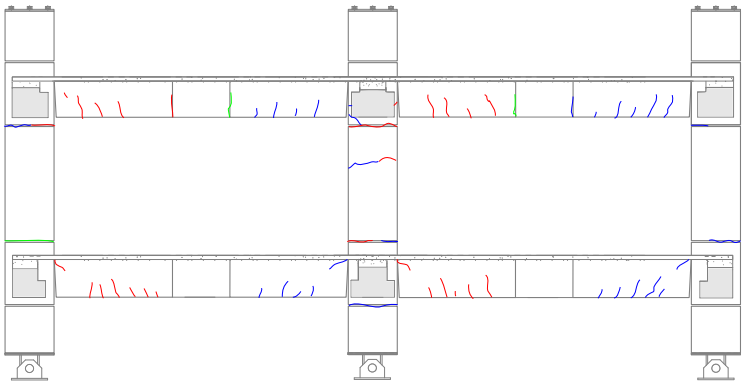

(c) Grid 2 north face.

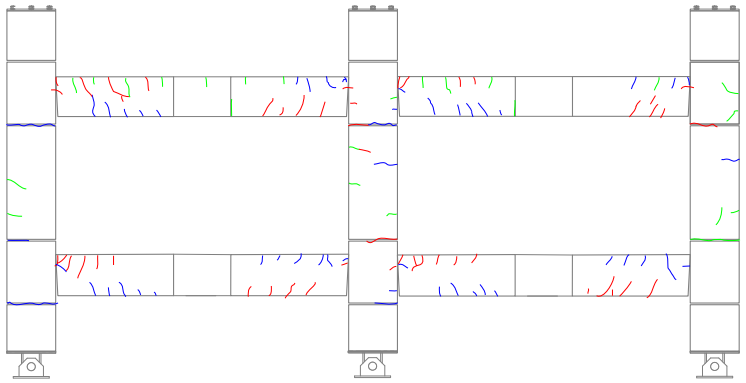

(d) Grid 2 south face.

Figure C-3: Specimen crack patterns at completion of 2.5% beam drift cycles.

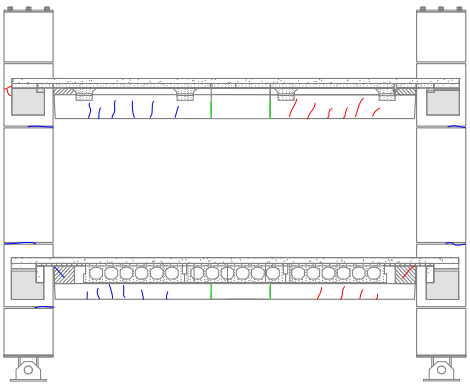

(e) Grid A east face.

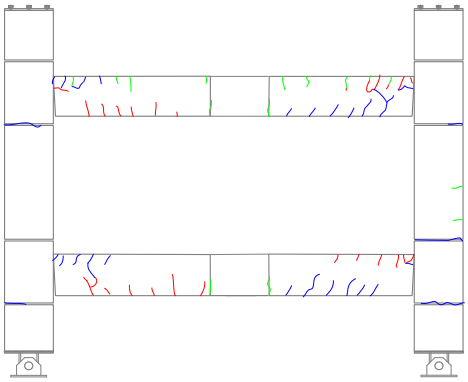

(f) Grid A west face.

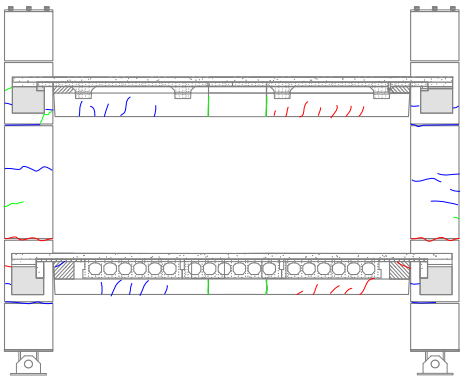

(g) Grid B east face.

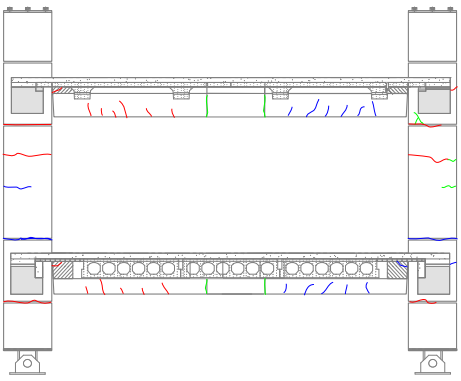

(h) Grid B west face.

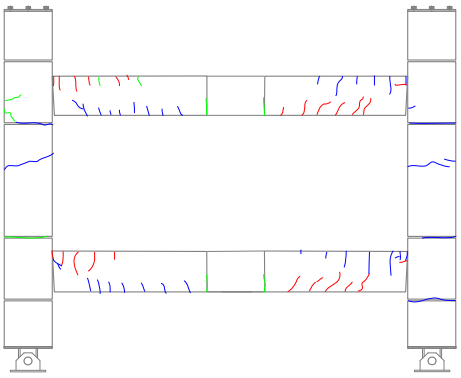

(i) Grid C east face.

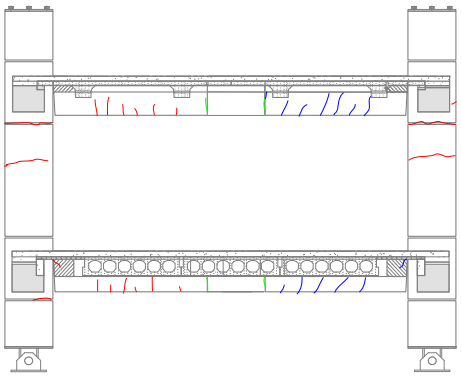

(j) Grid C west face.

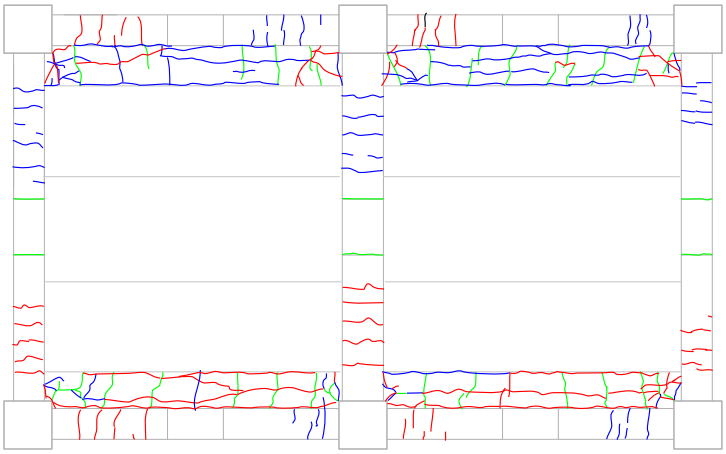

(k) Level One floor diaphragm bottom.

Figure C-3: Specimen crack patterns at completion of 2.5% beam drift cycles (Continued).

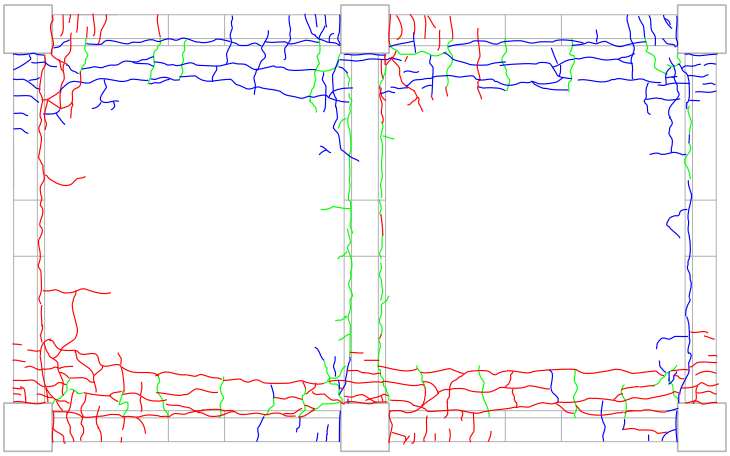

(l) Level One floor diaphragm top.

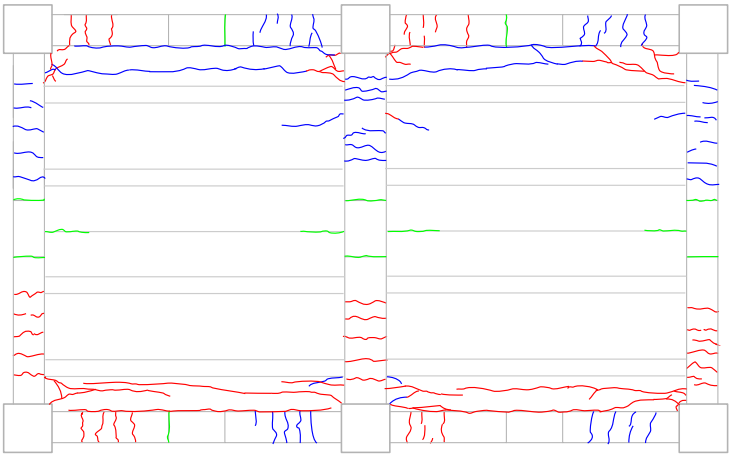

(m) Level Two floor diaphragm bottom.

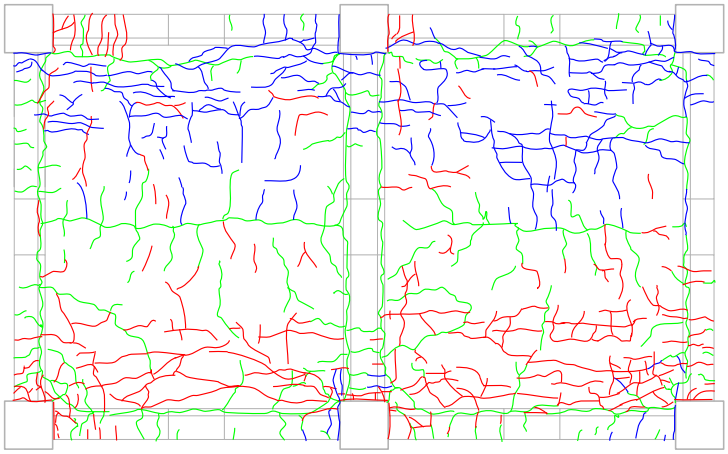

(n) Level Two floor diaphragm top.

Figure C-3: Specimen crack patterns at completion of 2.5% beam drift cycles (Continued).

C.2 Diagonal Hanger Performance

Figure C-4 presents additional strain data from diagonal hangers in SA1.

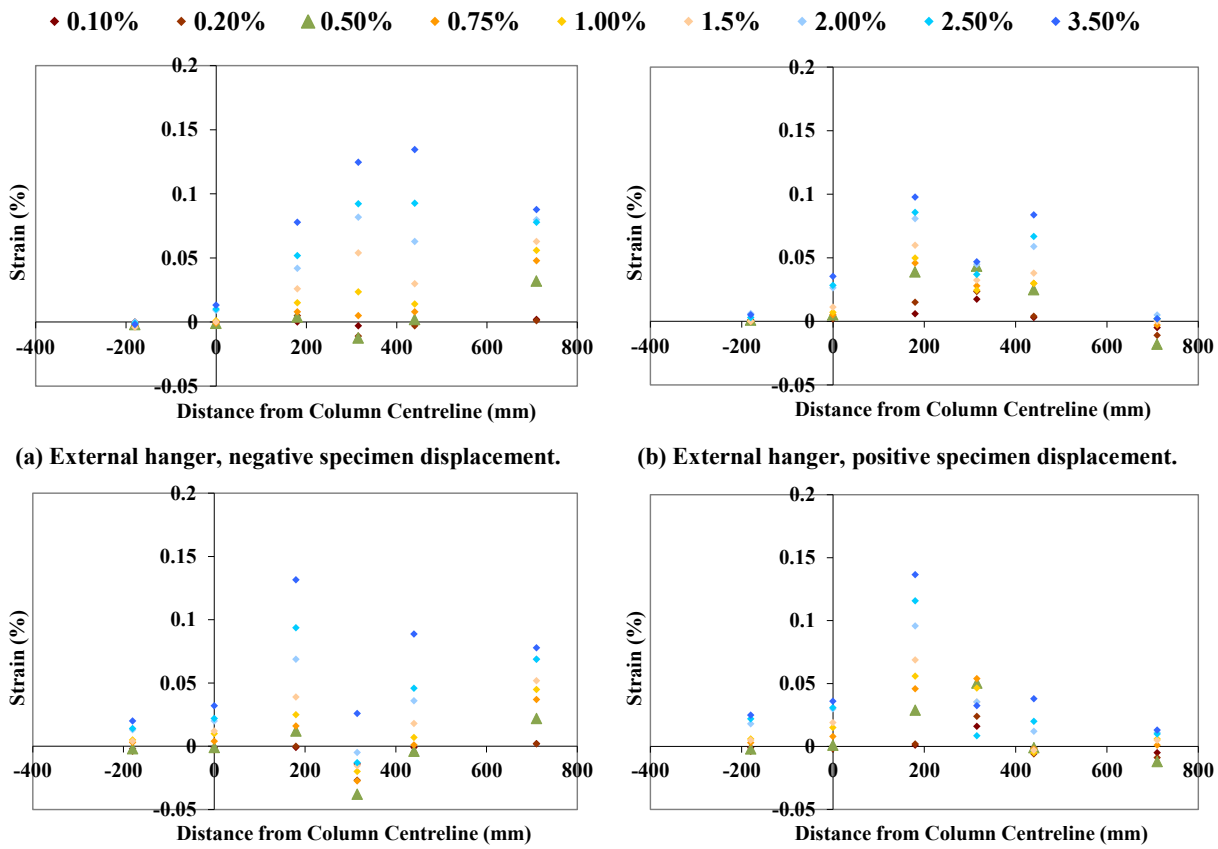

(a) External hanger, negative specimen displacement.

(b) External hanger, positive specimen displacement.

(c) Internal hanger, negative specimen displacement.

(d) Internal hanger, positive specimen displacement.

Figure C-4: Bm C/1-2 east-west diagonal hanger strain profiles.

C.3 Floor Diaphragm Performance

Figure C-5 presents additional unseating data from the precast floors in SA1.

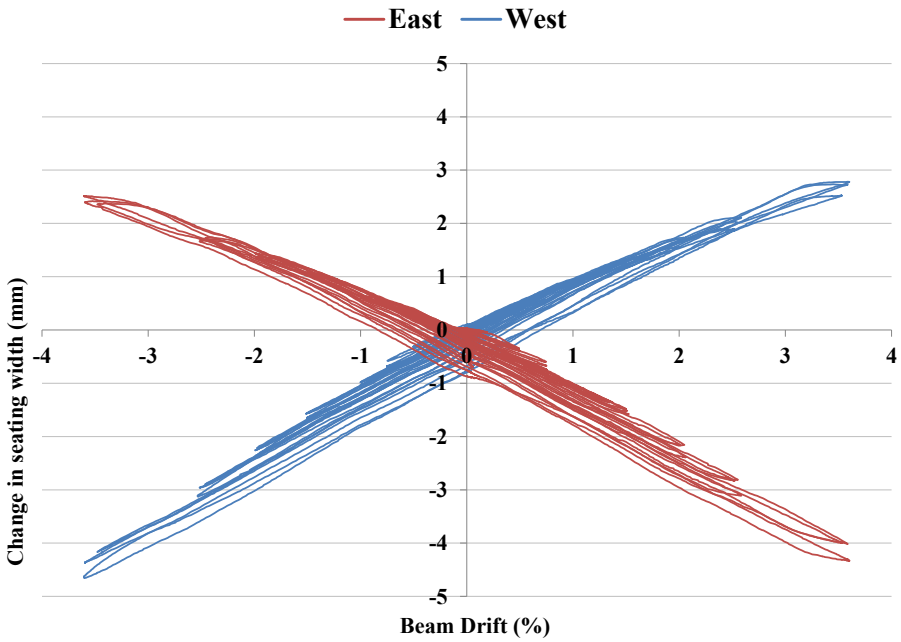

(a) Level One central hollow-core unit.

Figure C-5: Precast floor seating loss.

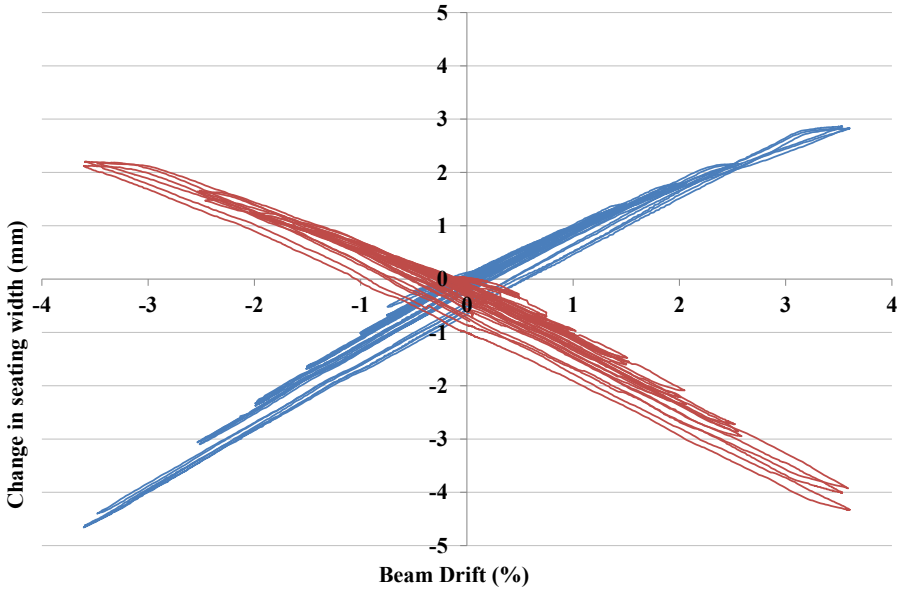

(b) Level One southern hollow-core unit.

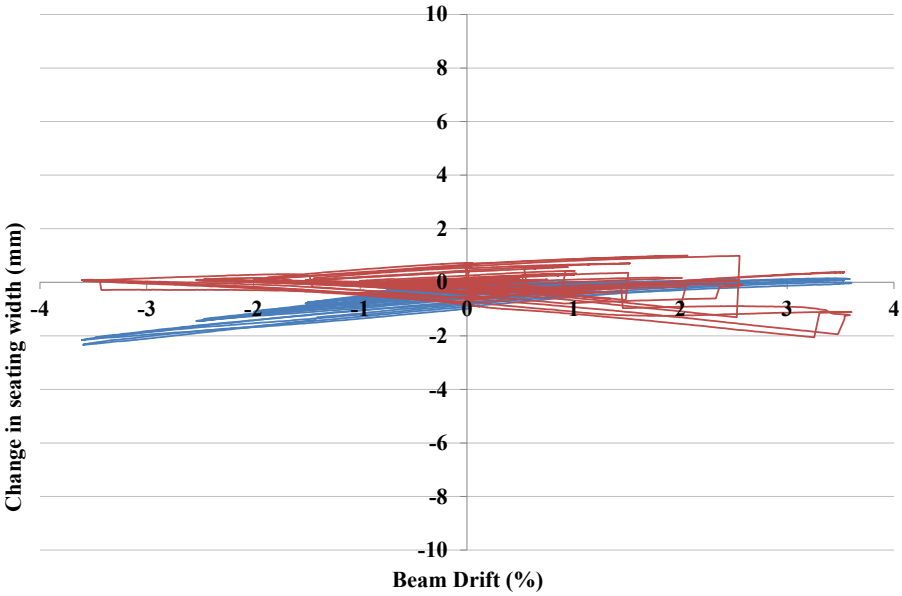

(c) Level Two southern double-tee unit.

Figure C-5: Precast floor seating loss (Continued).

Figure C-6 through Figure C-11 present additional strain contours generated from DEMEC readings undertaken during the 1% beam drift cycle.

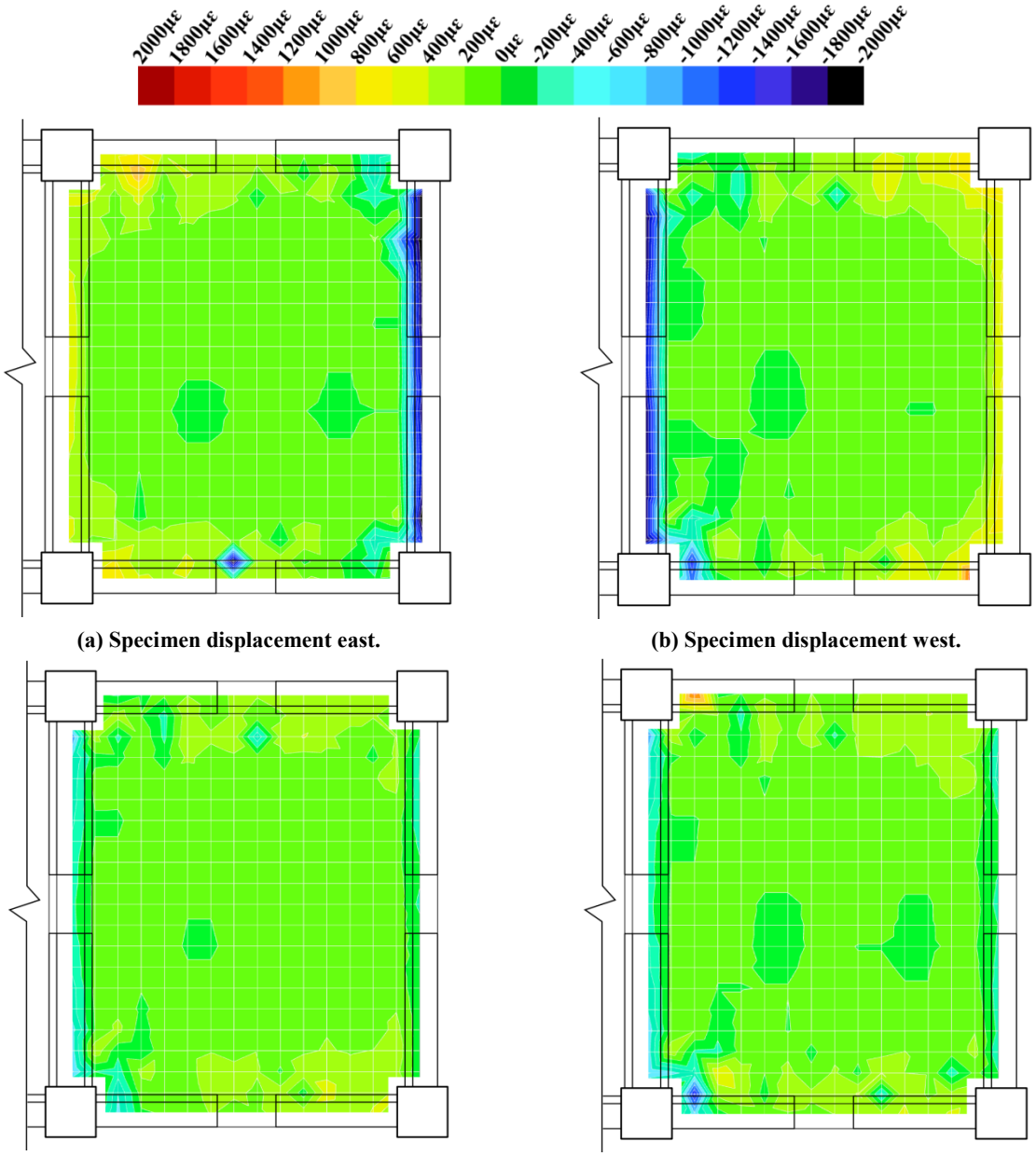

(a) Specimen displacement east.

(b) Specimen displacement west.

(c) Specimen displacement north.

(d) Specimen displacement south.

Figure C-6: Level One floor strain contours from east-west DEMEC measurements at 1.0% beam drift.

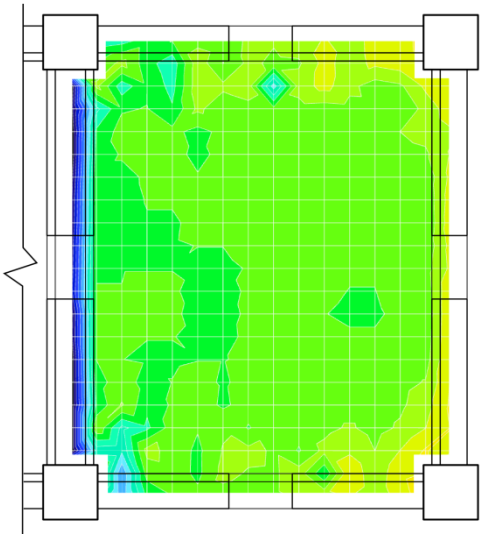

(e) Specimen displacement north-west.

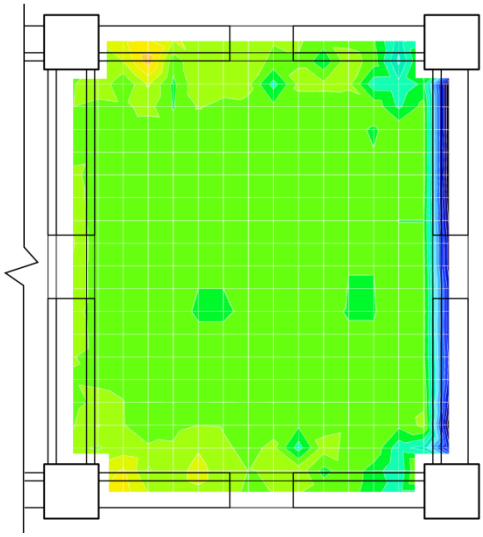

(f) Specimen displacement north-east.

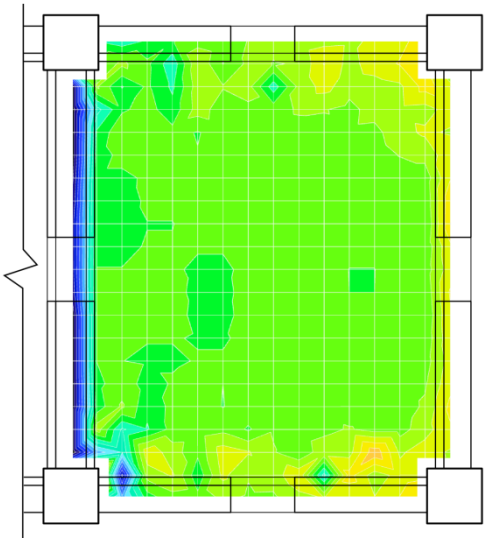

(g) Specimen displacement south-west.

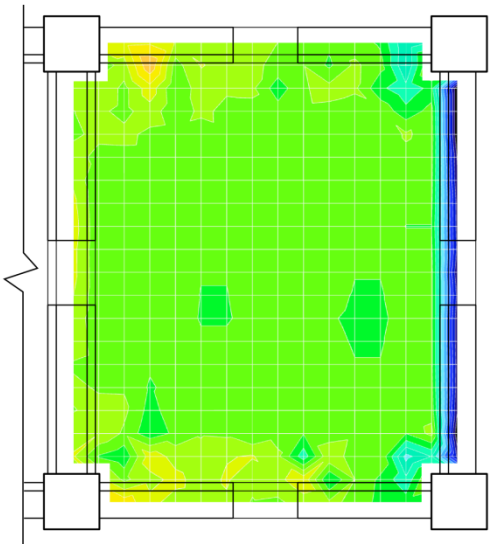

(h) Specimen displacement south-east.

Figure C-6: Level One floor strain contours from east-west DEMEC measurements at 1.0% beam drift (Continued).

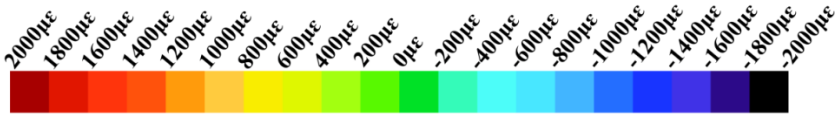

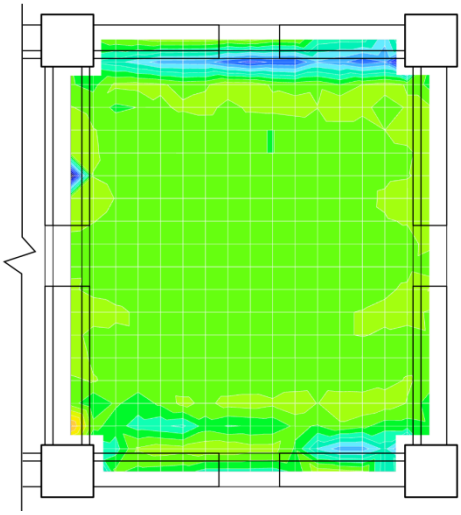

(a) Specimen displacement east.

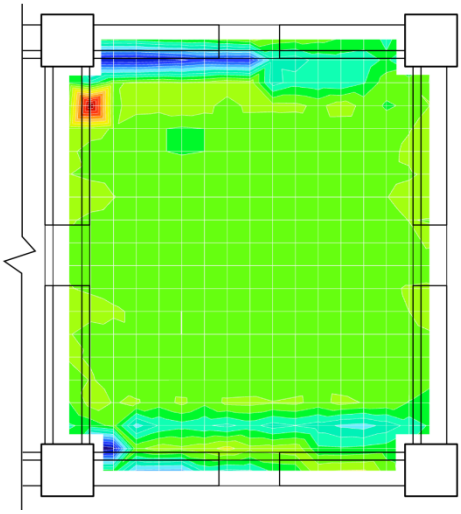

(b) Specimen displacement west.

Figure C-7: Level One floor strain contours from north-south DEMEC measurements at 1.0% beam drift.

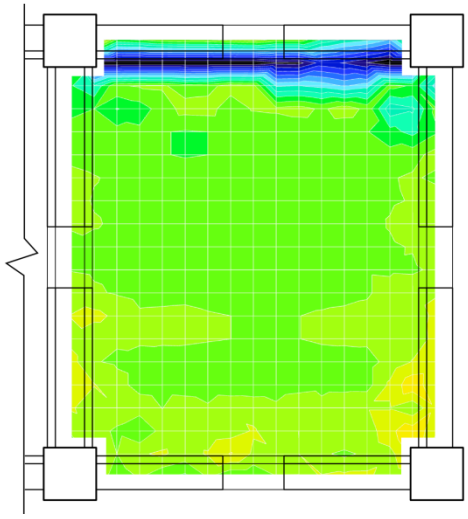

(c) Specimen displacement north.

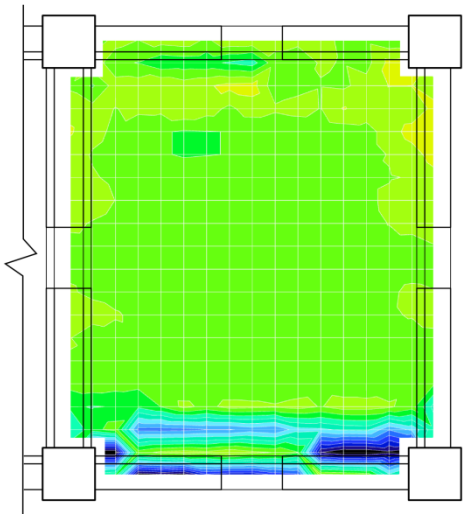

(d) Specimen displacement south.

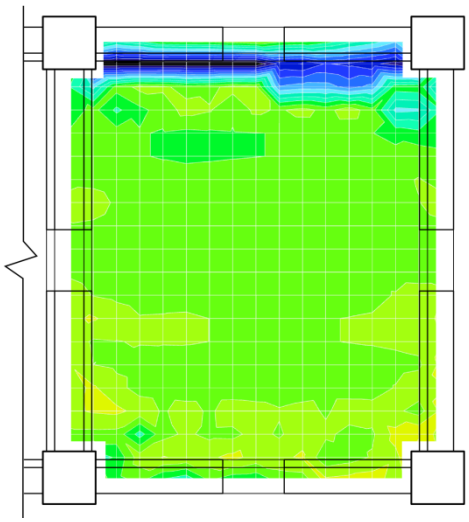

(e) Specimen displacement north-west.

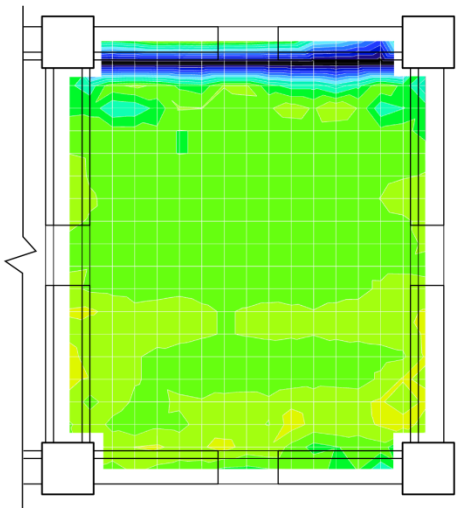

(f) Specimen displacement north-east.

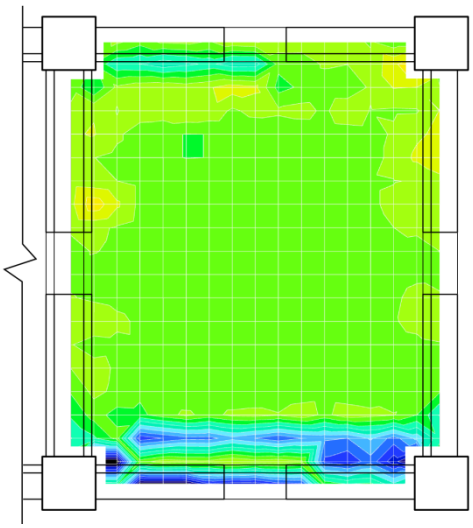

(g) Specimen displacement south-west.

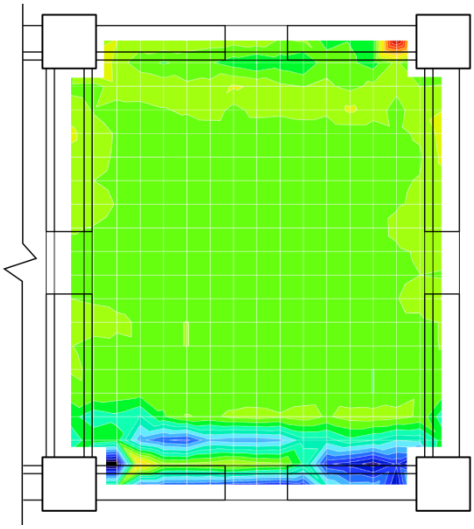

(h) Specimen displacement south-east.

Figure C-7: Level One floor strain contours from north-south DEMEC measurements at 1.0% beam drift (Continued).

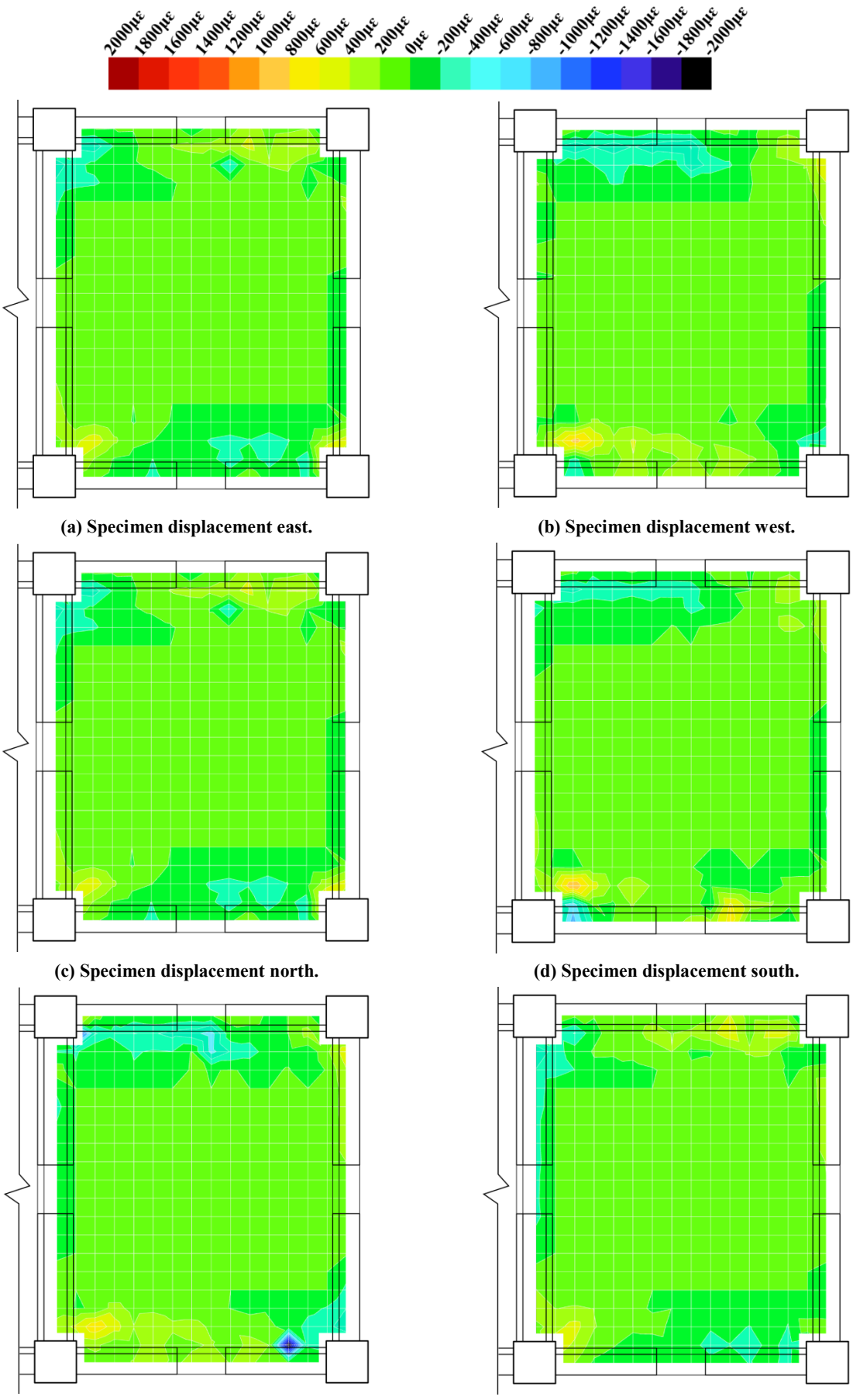

(a) Specimen displacement east.

(b) Specimen displacement west.

(c) Specimen displacement north.

(d) Specimen displacement south.

(e) Specimen displacement north-west.

(f) Specimen displacement north-east.

Figure C-8: Level One floor strain contours from shear DEMEC measurements at 1.0% beam drift.

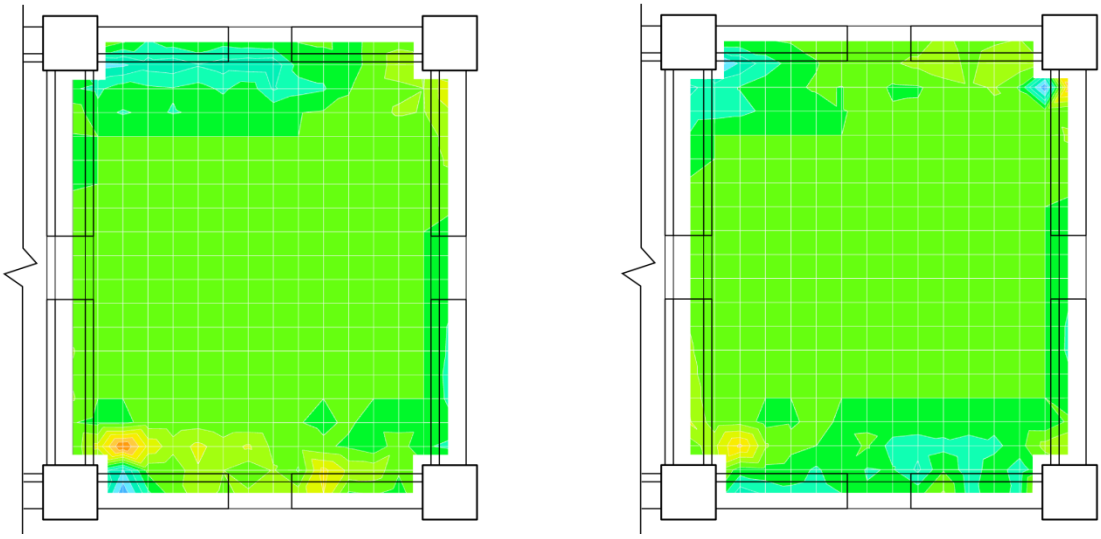

(g) Specimen displacement south-west.

(h) Specimen displacement south-east.

Figure C-8: Level One floor strain contours from shear DEMEC measurements at 1.0% beam drift (Continued).

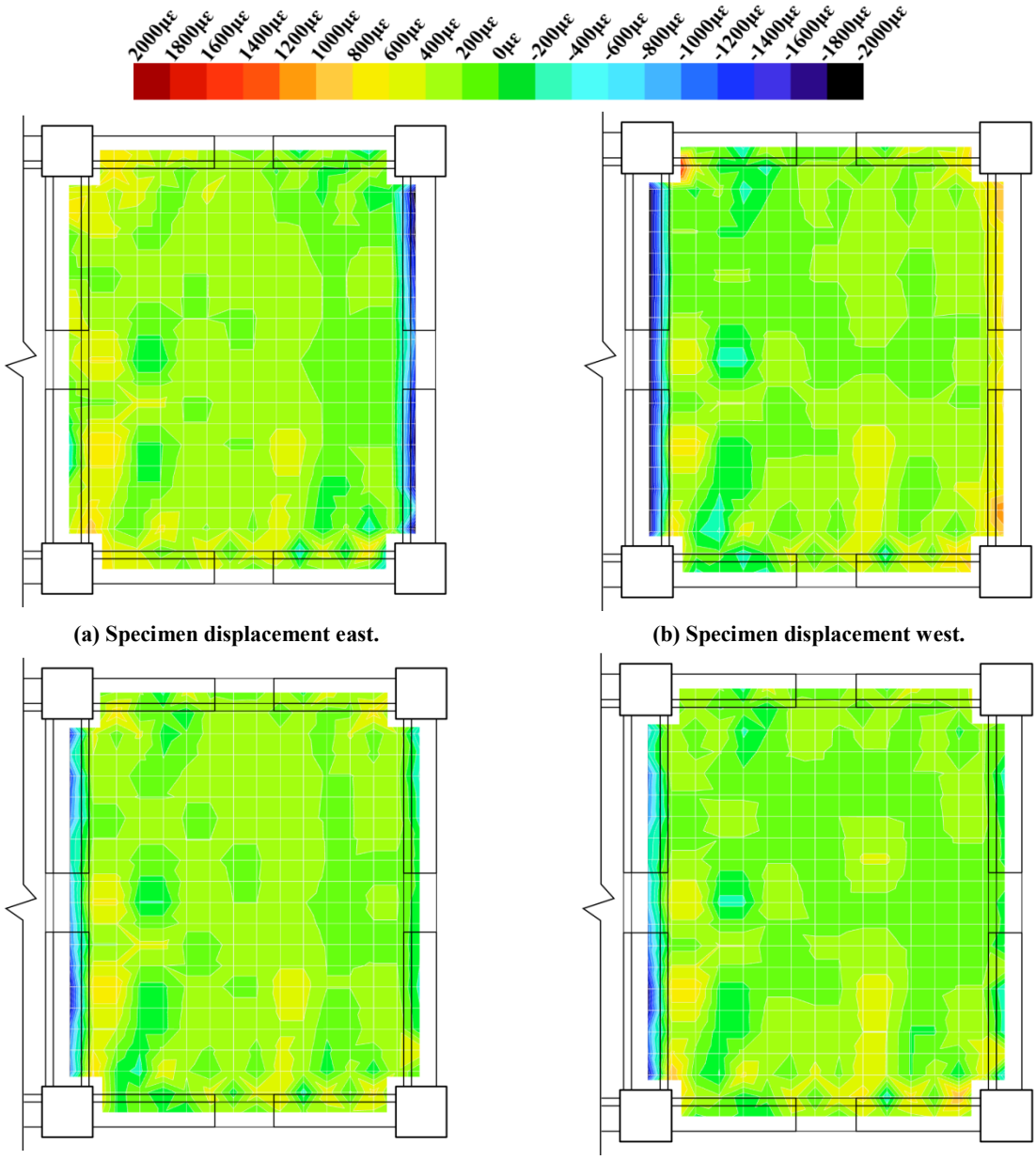

(a) Specimen displacement east.

(b) Specimen displacement west.

(c) Specimen displacement north.

(d) Specimen displacement south.

Figure C-9: Level Two floor strain contours from east-west DEMEC measurements at 1.0% beam drift.

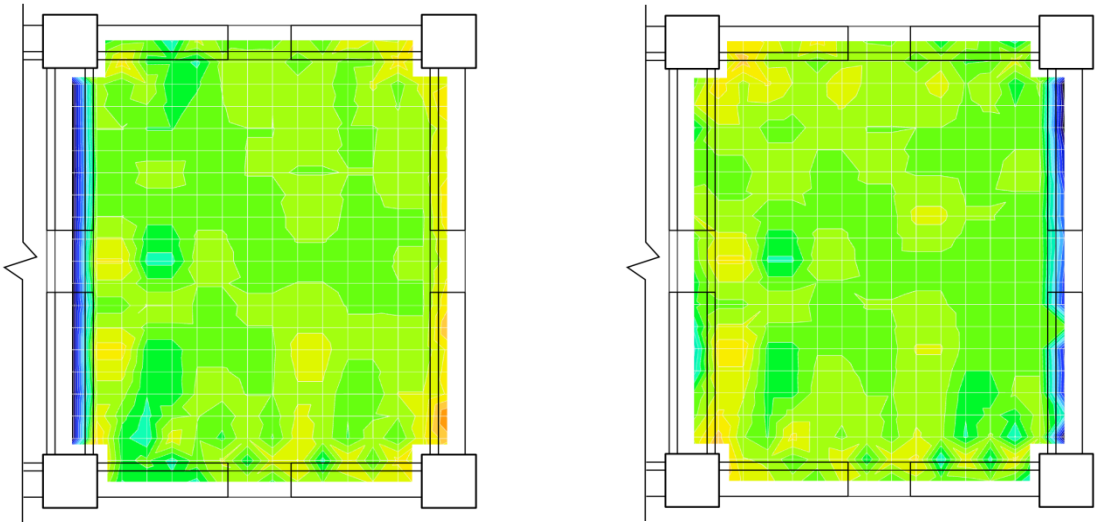

(e) Specimen displacement north-west. (f) Specimen displacement north-east.

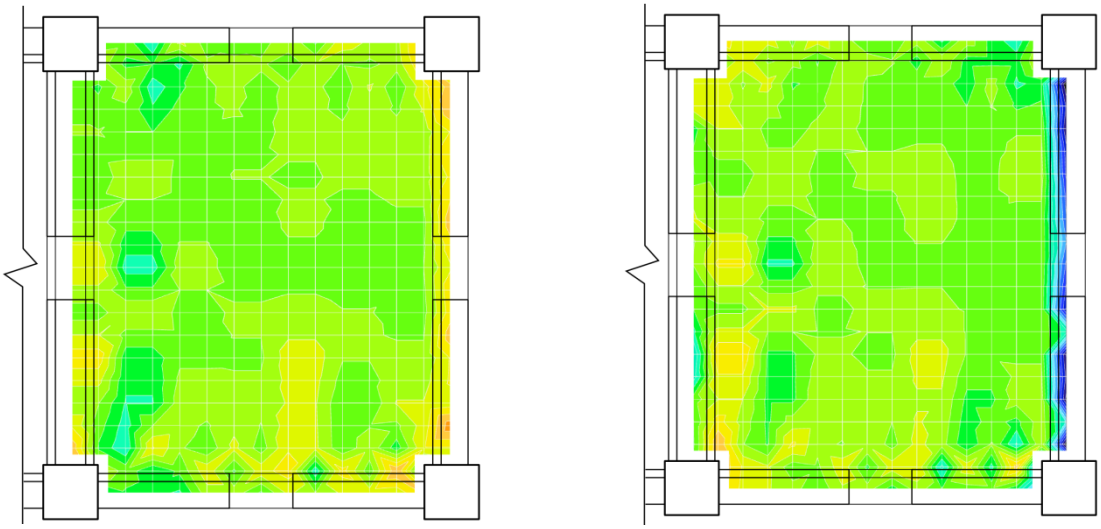

(g) Specimen displacement south-west. (h) Specimen displacement south-east.

Figure C-9: Level Two floor strain contours from east-west DEMEC measurements at 1.0% beam drift (Continued).

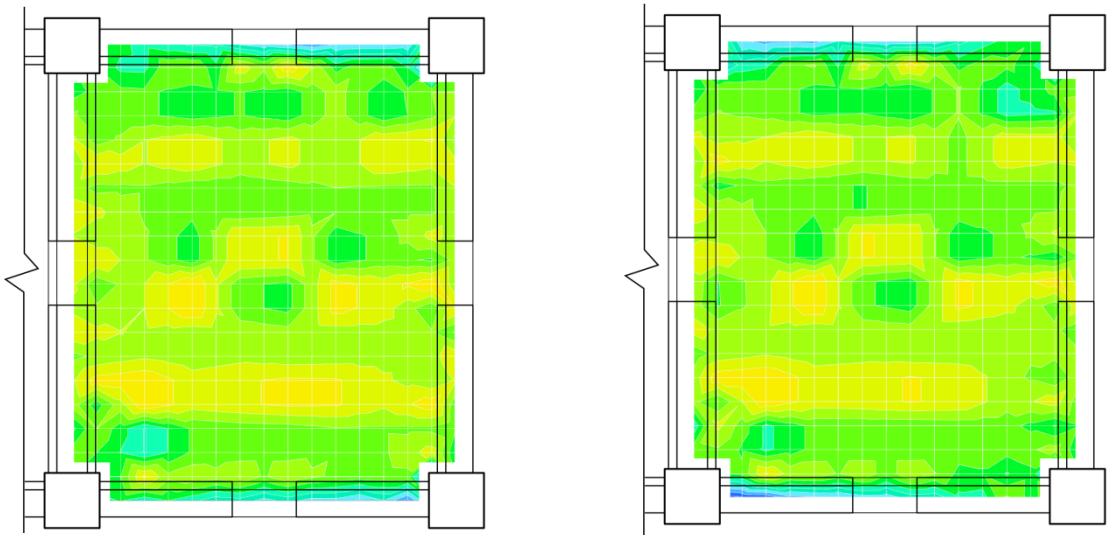

(a) Specimen displacement east. (b) Specimen displacement west.

Figure C-10: Level Two floor strain contours from north-south DEMEC measurements at 1.0% beam drift.

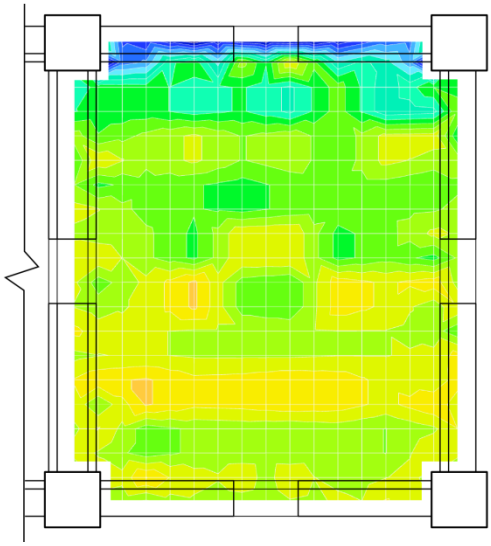

(c) Specimen displacement north.

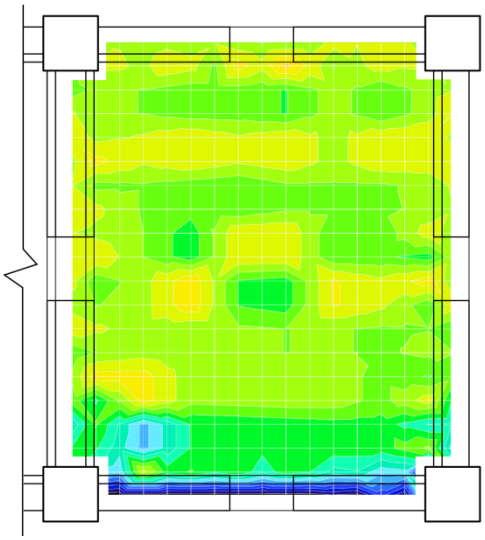

(d) Specimen displacement south.

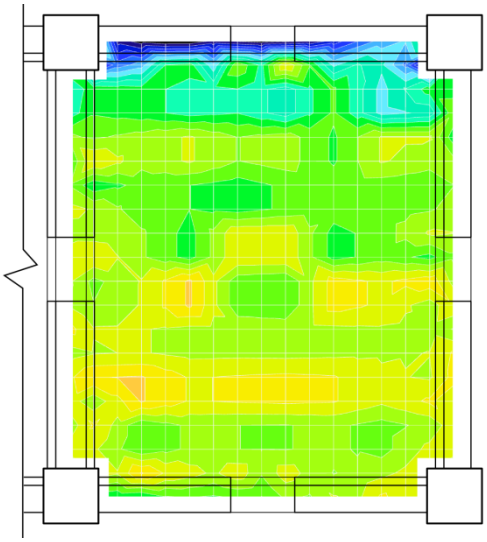

(e) Specimen displacement north-west.

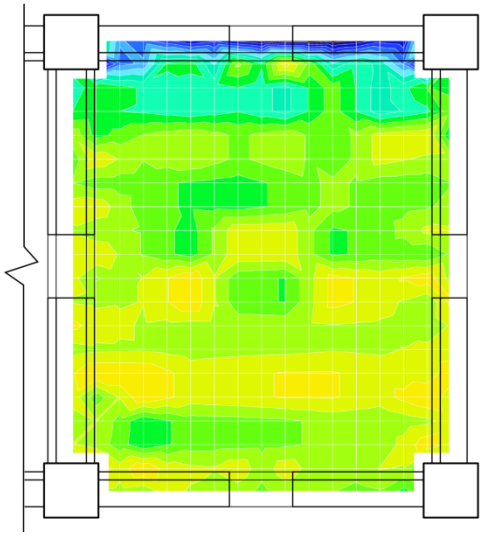

(f) Specimen displacement north-east.

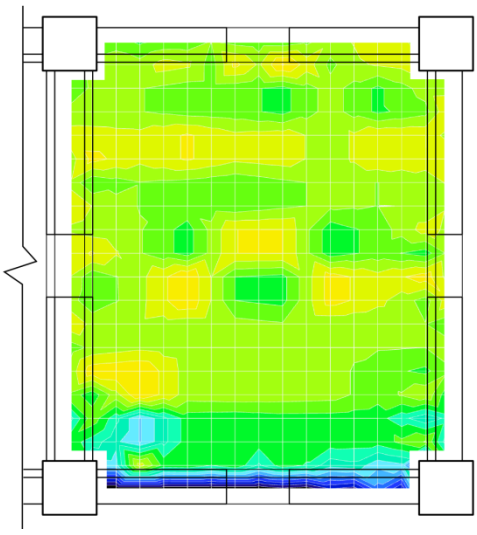

(g) Specimen displacement south-west.

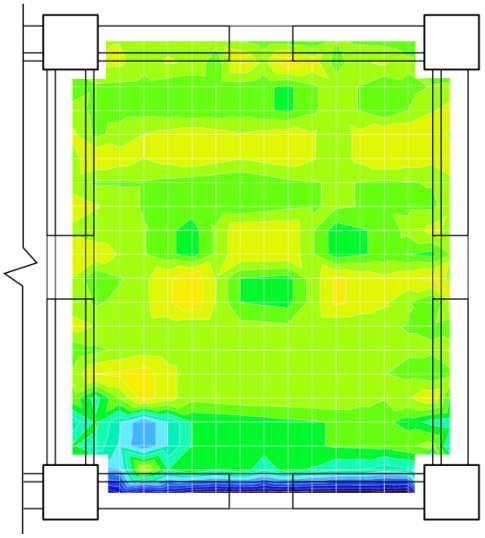

(h) Specimen displacement south-east.

Figure C-10: Level Two floor strain contours from north-south DEMEC measurements at 1.0% beam drift (Continued).

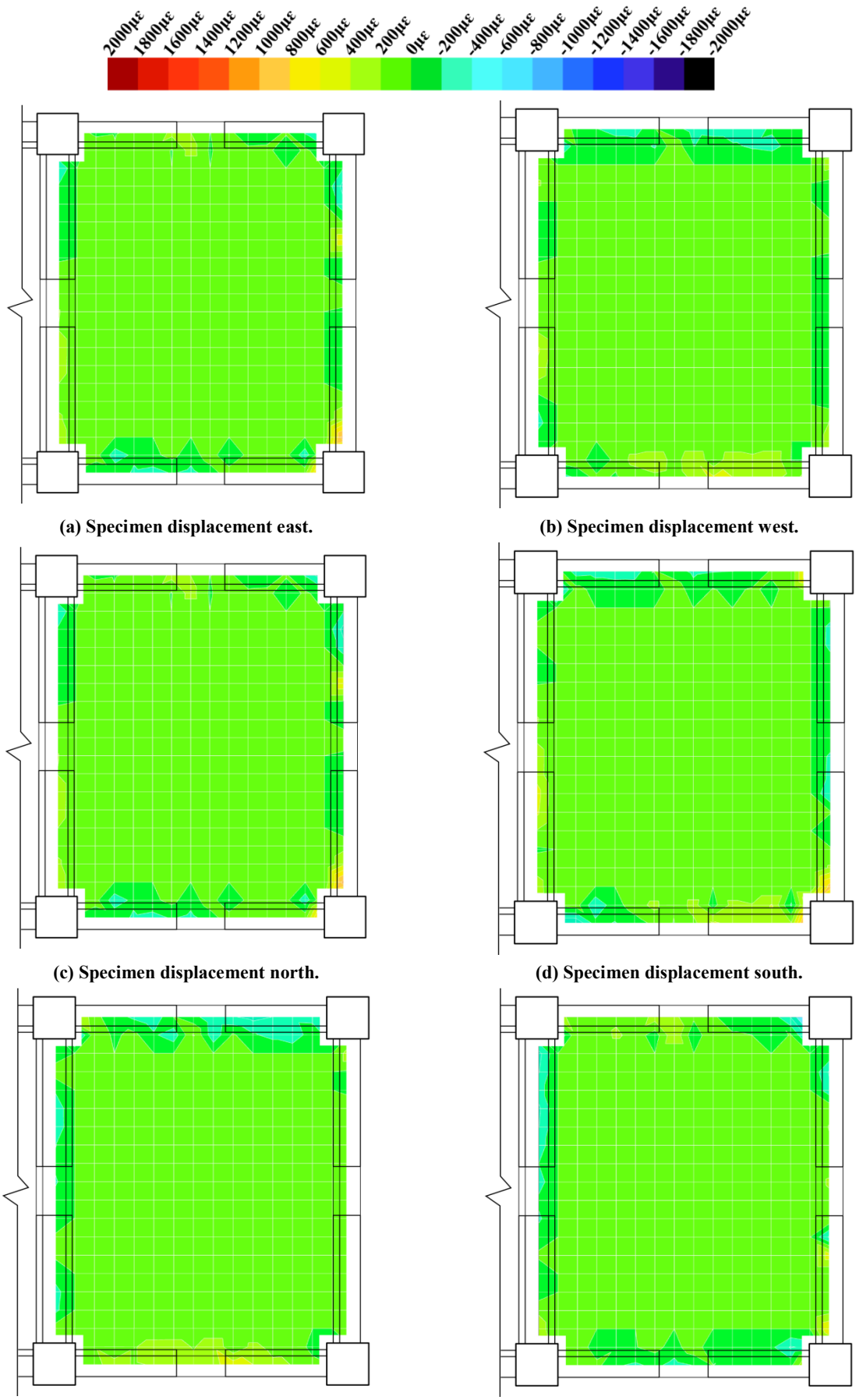

(a) Specimen displacement east.

(b) Specimen displacement west.

(c) Specimen displacement north.

(d) Specimen displacement south.

(e) Specimen displacement north-west.

(f) Specimen displacement north-east.

Figure C-11: Level Two floor strain contours from shear DEMEC measurements at 1.0% beam drift.

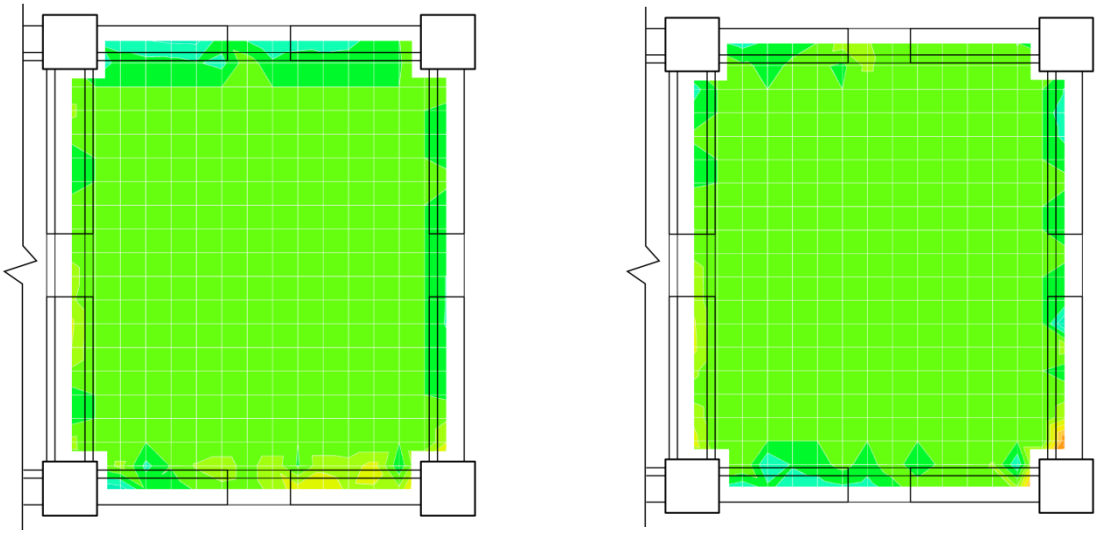

(g) Specimen displacement south-west.

(h) Specimen displacement south-east.

Figure C-11: Level Two floor strain contours from shear DEMEC measurements at 1.0% beam drift (Continued).

Figure C-12 through Figure C-17 presents additional strain contours generated from DEMEC readings undertaken during the 2.5% beam drift cycle.

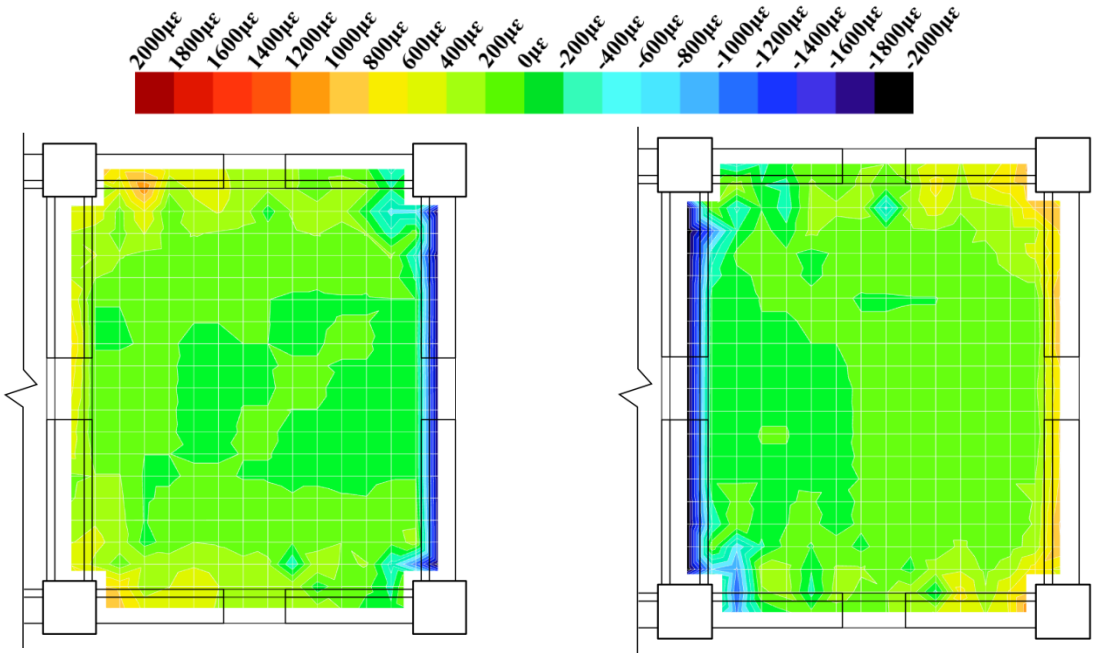

(a) Specimen displacement east.

(b) Specimen displacement west.

Figure C-12: Level One floor strain contours from east-west DEMEC measurements at 2.5% beam drift.

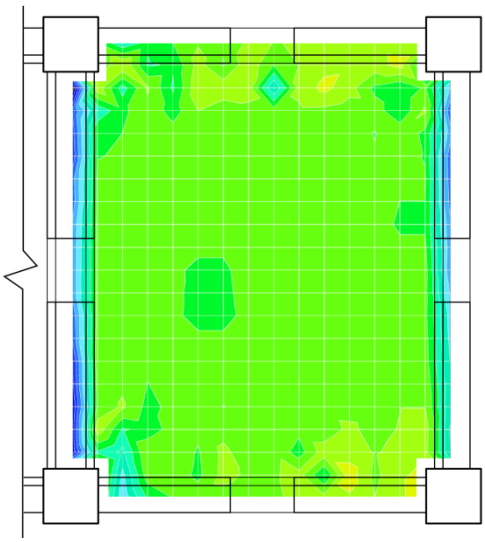

(c) Specimen displacement north.

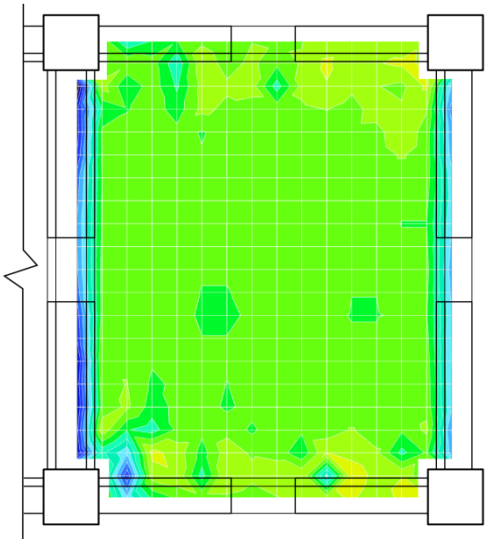

(d) Specimen displacement south.

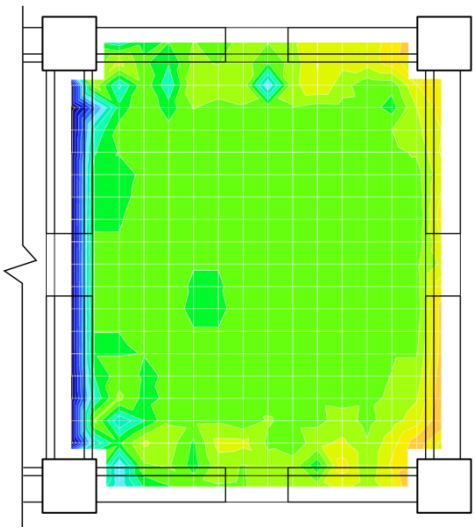

(e) Specimen displacement north-west.

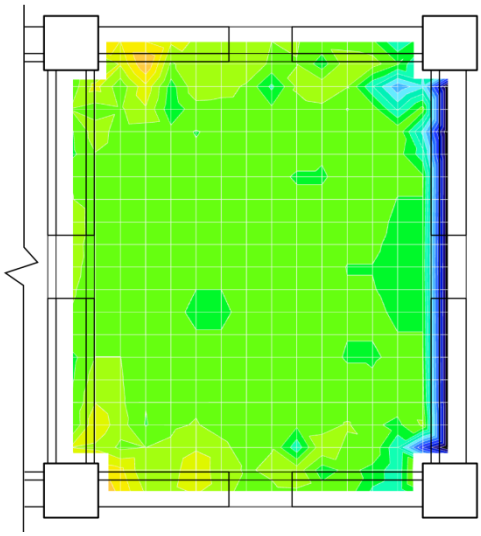

(f) Specimen displacement north-east.

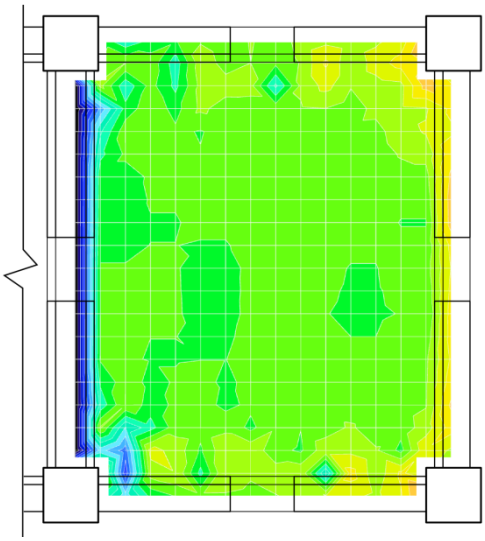

(g) Specimen displacement south-west.

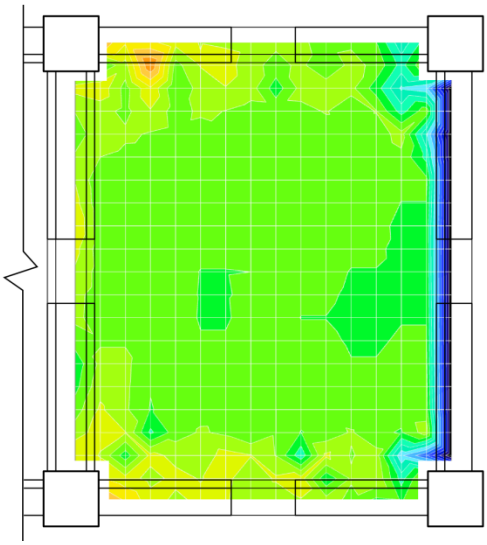

(h) Specimen displacement south-east.

Figure C-12: Level One floor strain contours from east-west DEMEC measurements at 2.5% beam drift (Continued).

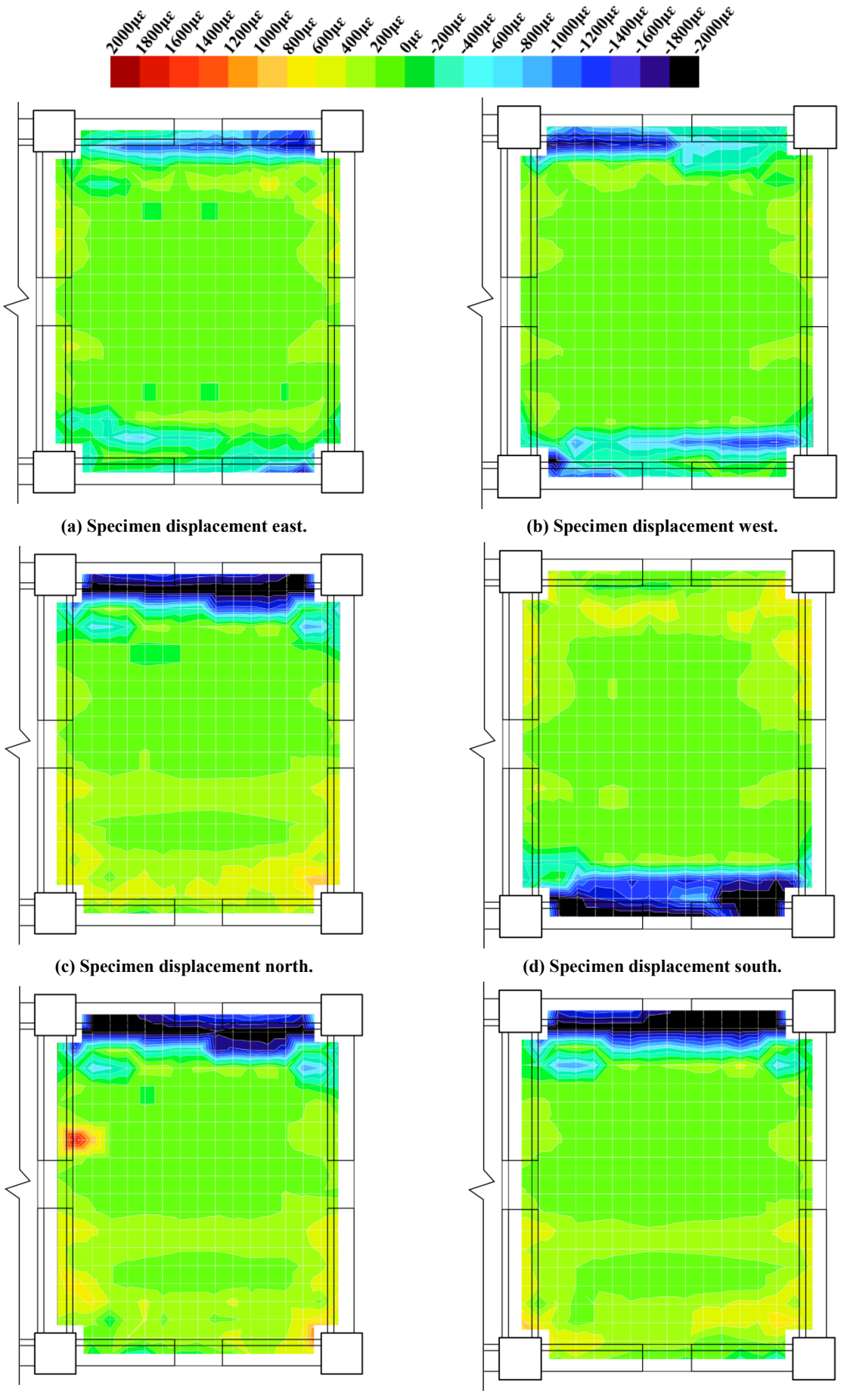

(a) Specimen displacement east.

(b) Specimen displacement west.

(c) Specimen displacement north.

(d) Specimen displacement south.

(e) Specimen displacement north-west.

(f) Specimen displacement north-east.

Figure C-13: Level One floor strain contours from north-south DEMEC measurements at 2.5% beam drift.

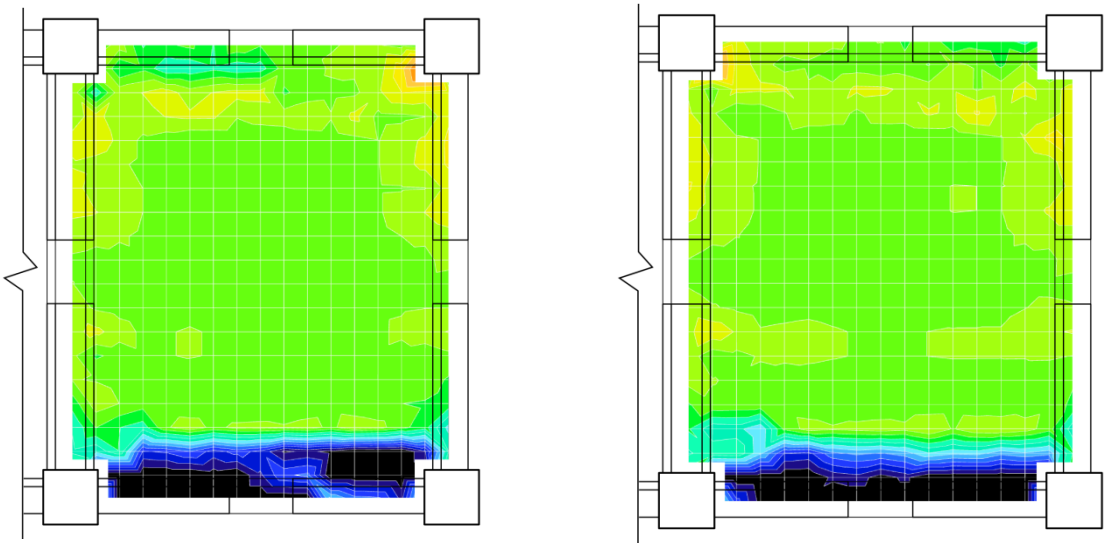

(g) Specimen displacement south-west. (h) Specimen displacement south-east.

Figure C-13: Level One floor strain contours from north-south DEMEC measurements at 2.5% beam drift (Continued).

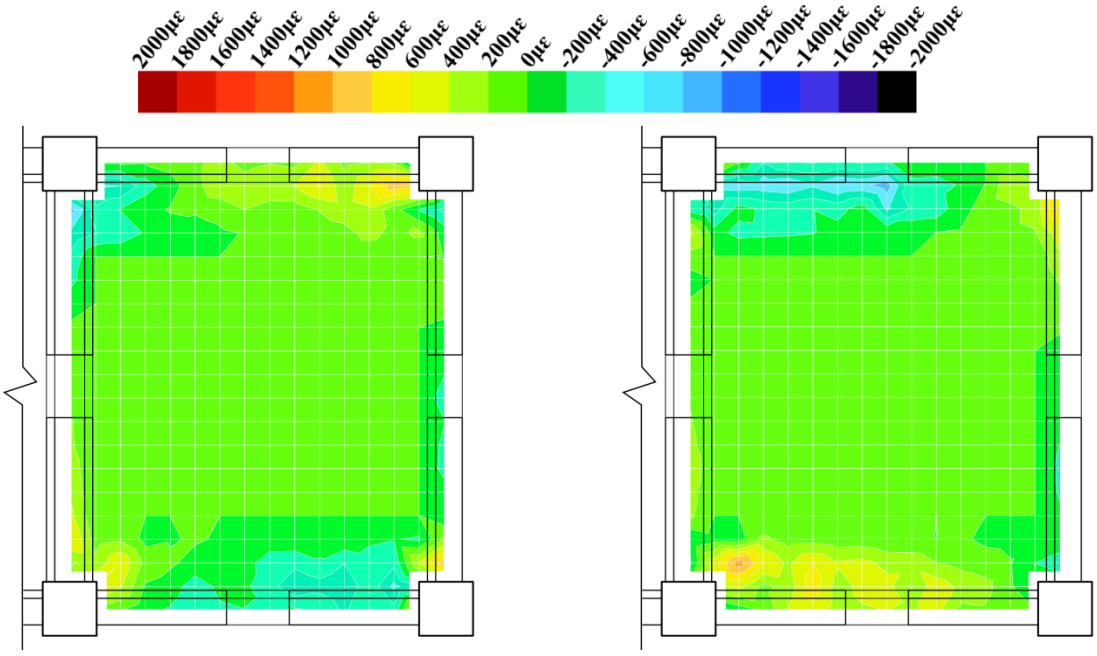

(a) Specimen displacement east. (b) Specimen displacement west.

Figure C-14: Level One floor strain contours from shear DEMEC measurements at 2.5% beam drift.

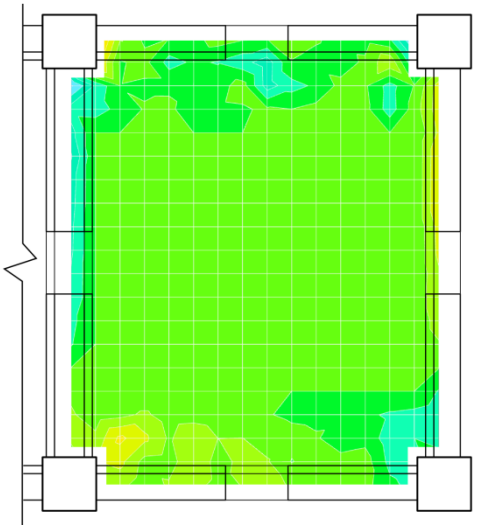

(c) Specimen displacement north.

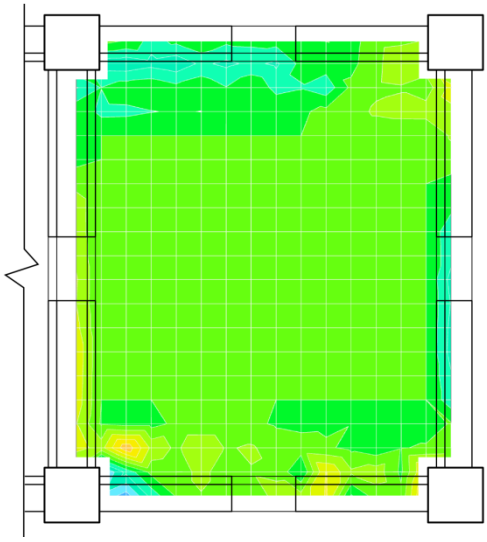

(d) Specimen displacement south.

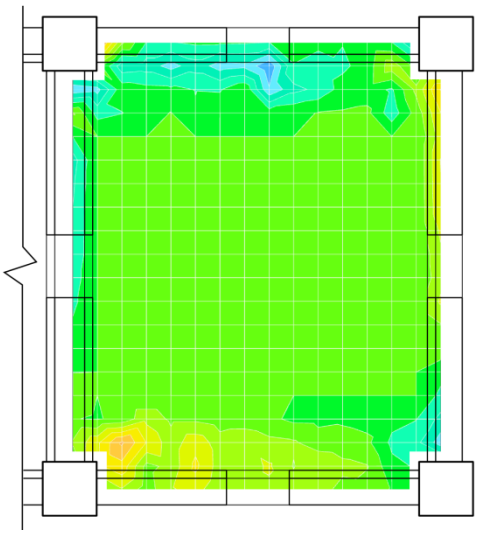

(e) Specimen displacement north-west.

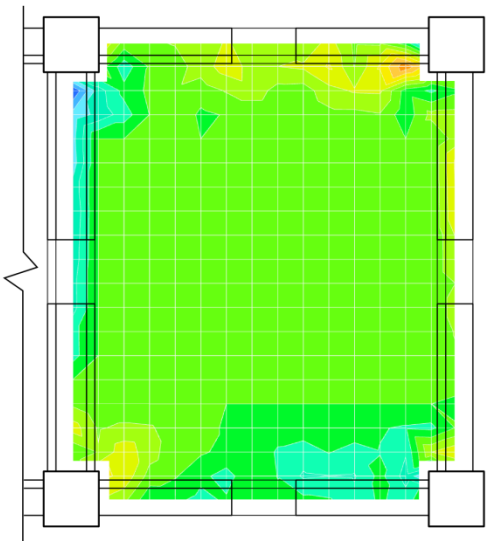

(f) Specimen displacement north-east.

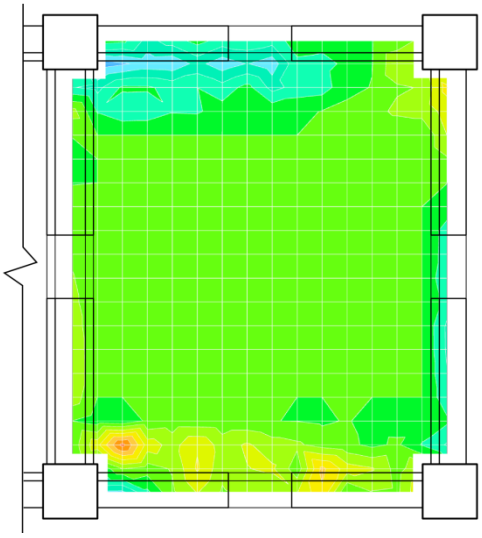

(g) Specimen displacement south-west.

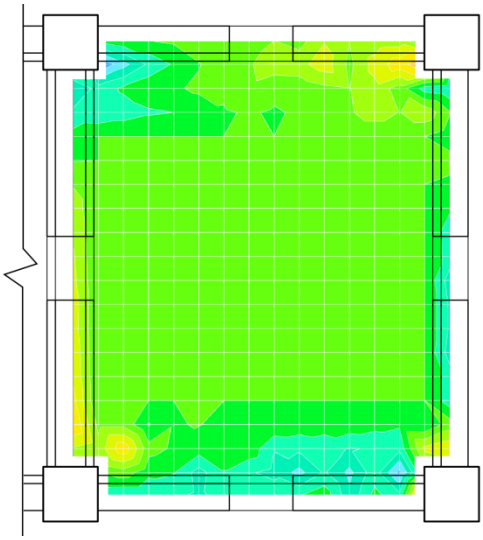

(h) Specimen displacement south-east.

Figure C-14: Level One floor strain contours from shear DEMEC measurements at 2.5% beam drift (Continued).

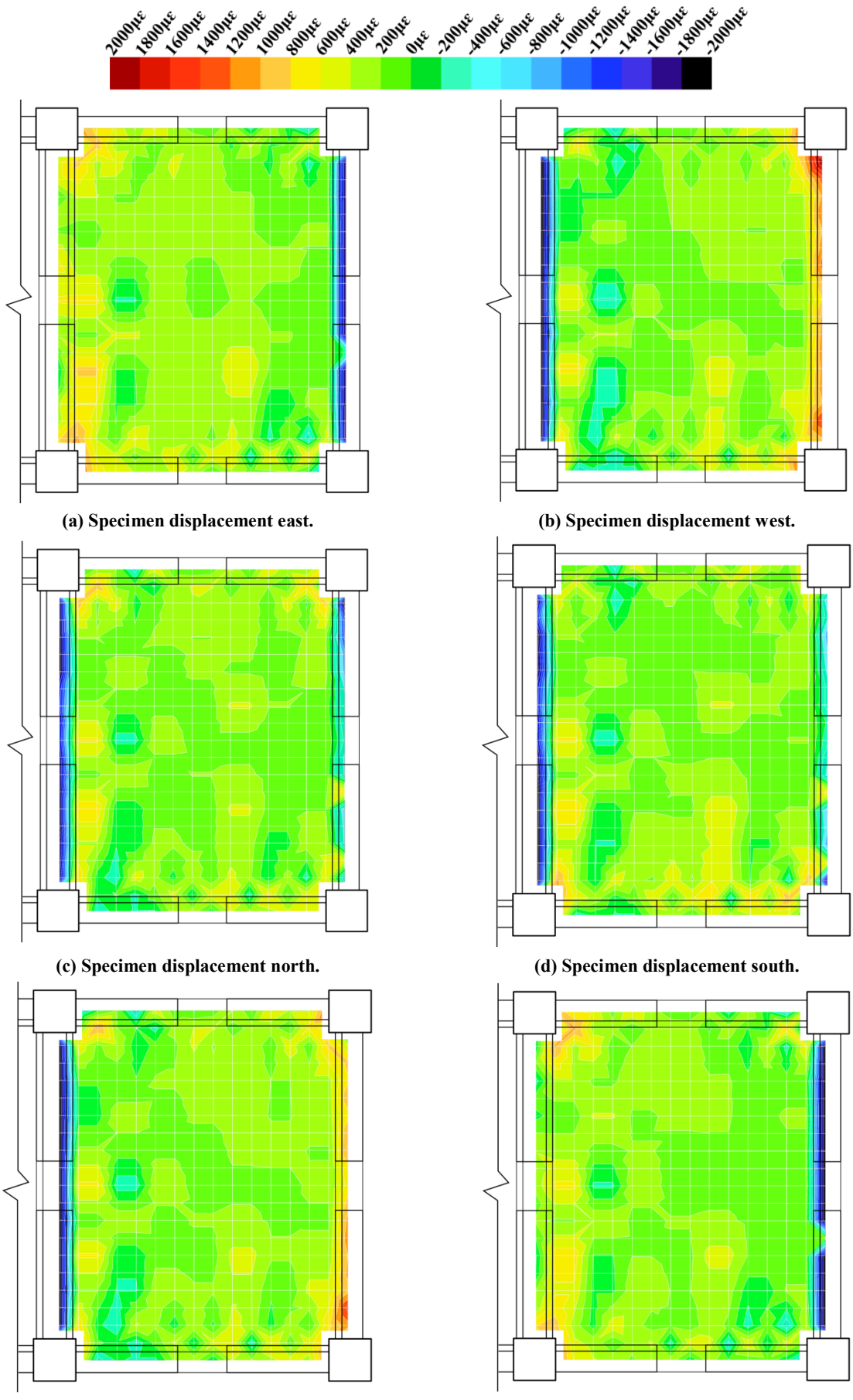

(a) Specimen displacement east.

(b) Specimen displacement west.

(c) Specimen displacement north.

(d) Specimen displacement south.

(e) Specimen displacement north-west.

(f) Specimen displacement north-east.

Figure C-15: Level Two floor strain contours from east-west DEMEC measurements at 2.5% beam drift.

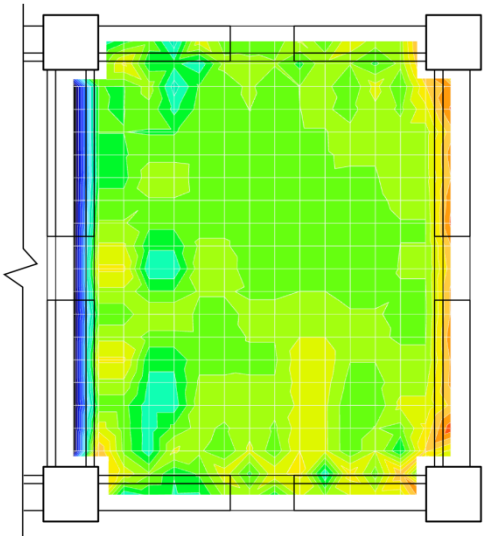

(g) Specimen displacement south-west.

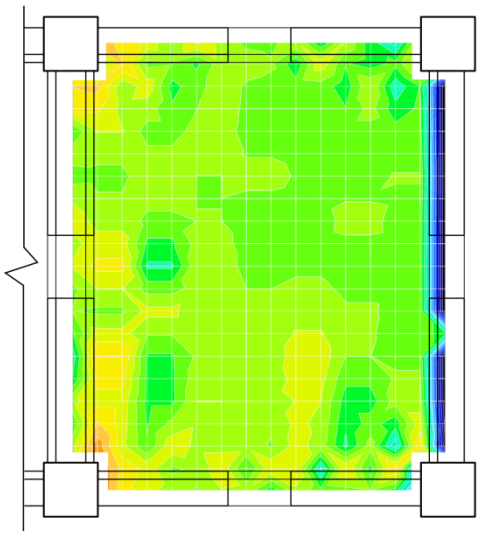

(h) Specimen displacement south-east.

Figure C-15: Level Two floor strain contours from east-west DEMEC measurements at 2.5% beam drift (Continued).

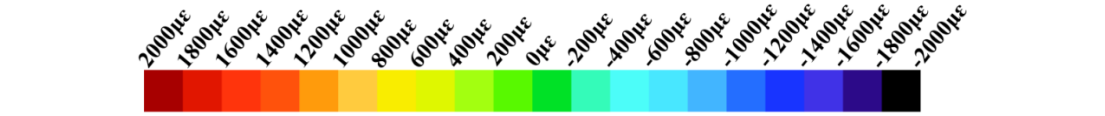

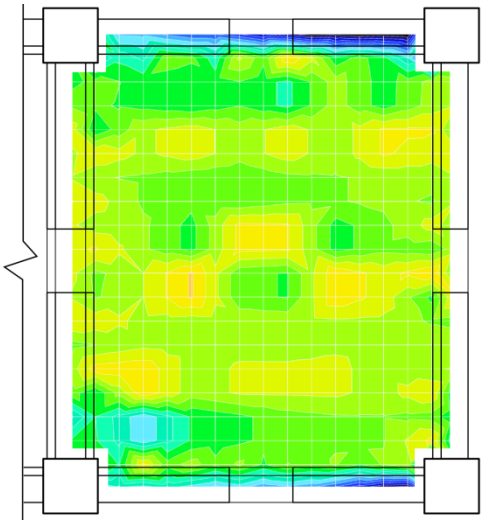

(a) Specimen displacement east.

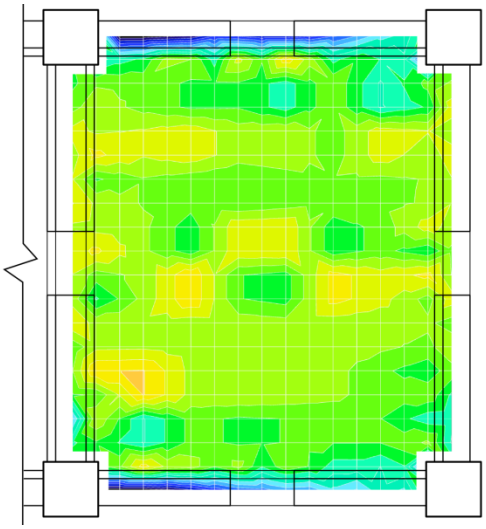

(b) Specimen displacement west.

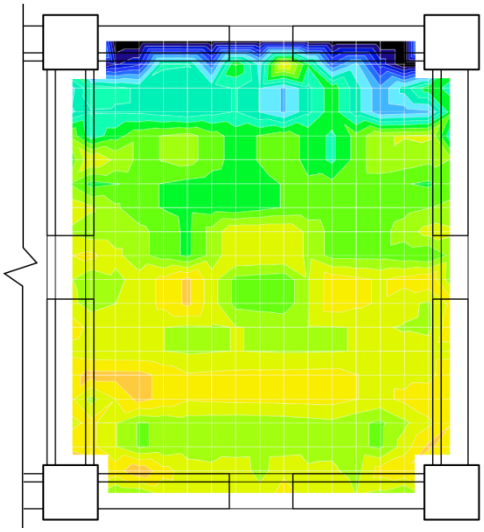

(c) Specimen displacement north.

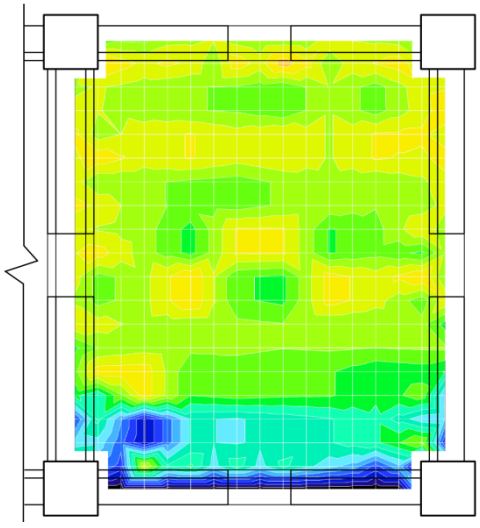

(d) Specimen displacement south.

Figure C-16: Level Two floor strain contours from north-south DEMEC measurements at 2.5% beam drift.

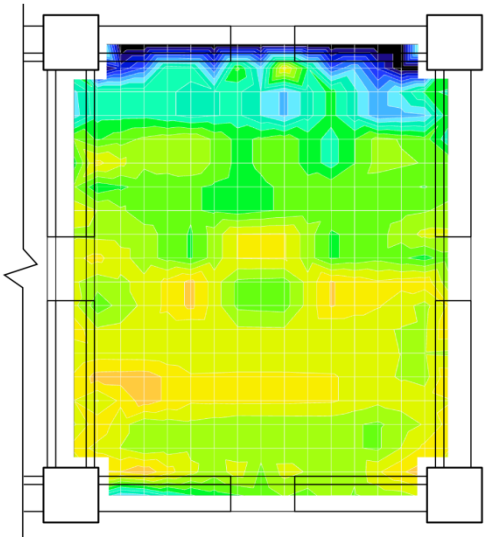

(e) Specimen displacement north-west.

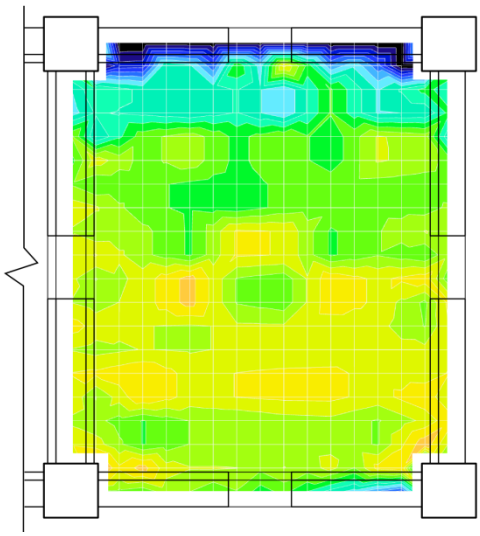

(f) Specimen displacement north-east.

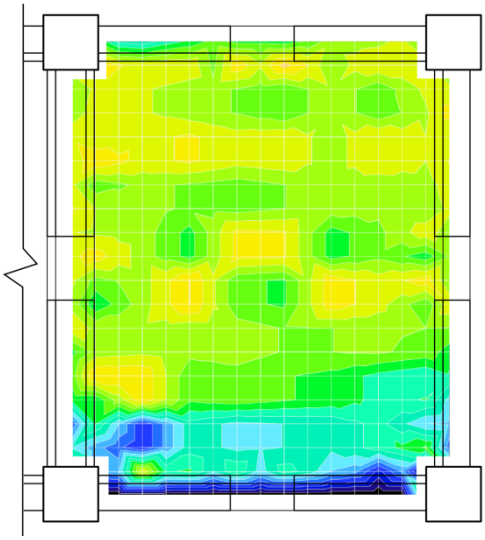

(g) Specimen displacement south-west.

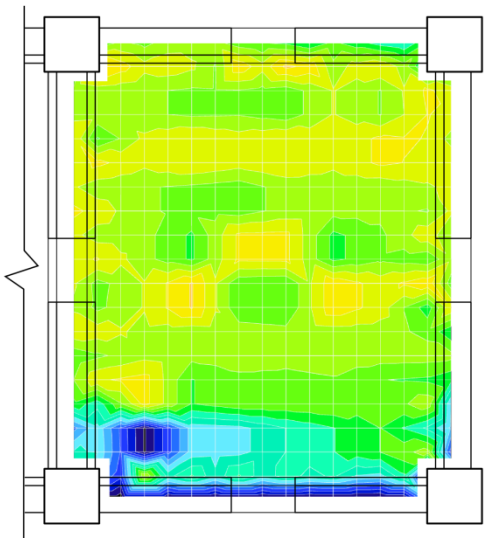

(h) Specimen displacement south-east.

Figure C-16: Level Two floor strain contours from north-south DEMEC measurements at 2.5% beam drift (Continued).

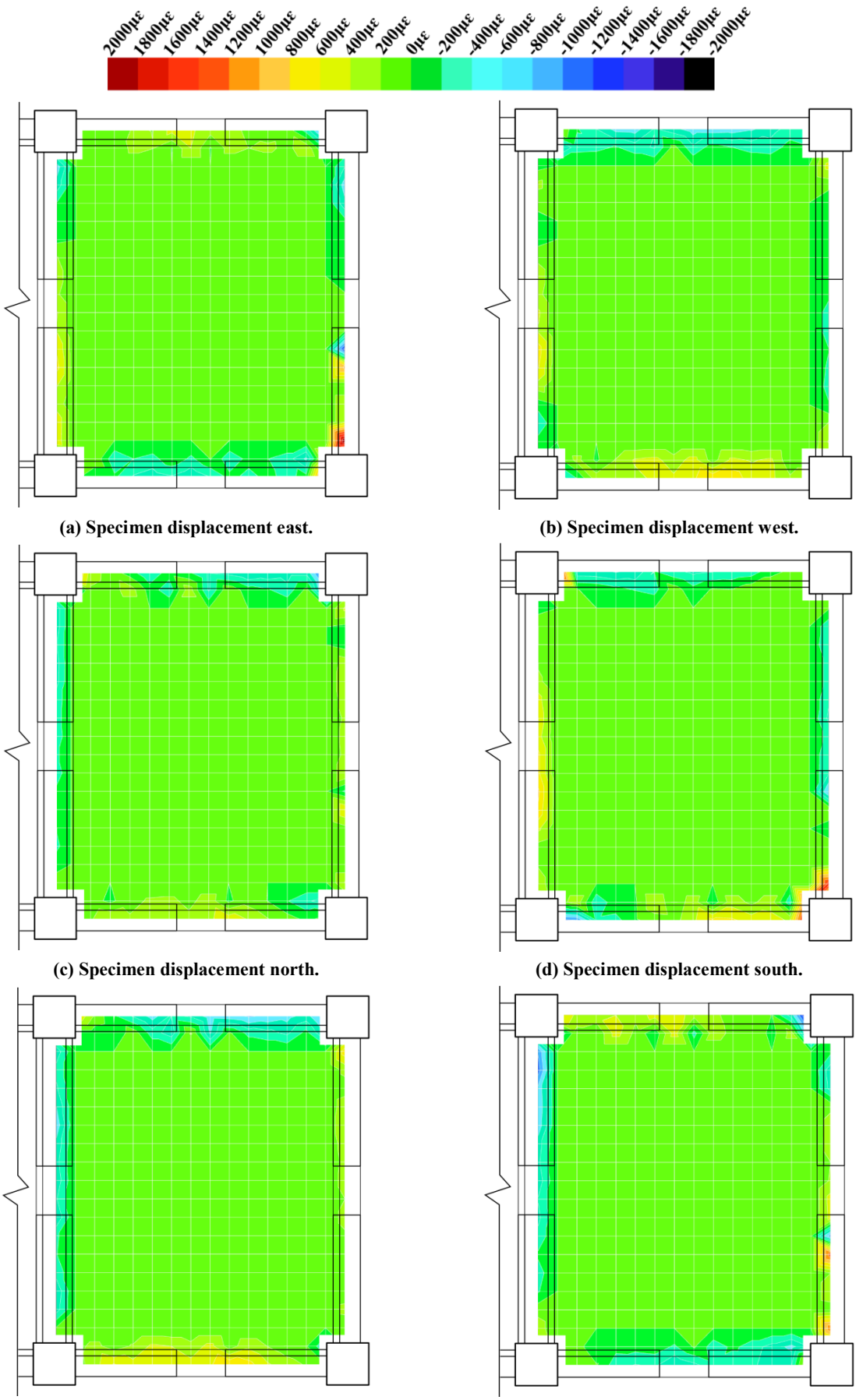

(a) Specimen displacement east.

(b) Specimen displacement west.

(c) Specimen displacement north.

(d) Specimen displacement south.

(e) Specimen displacement north-west.

(f) Specimen displacement north-east.

Figure C-17: Level Two floor strain contours from shear DEMEC measurements at 2.5% beam drift.

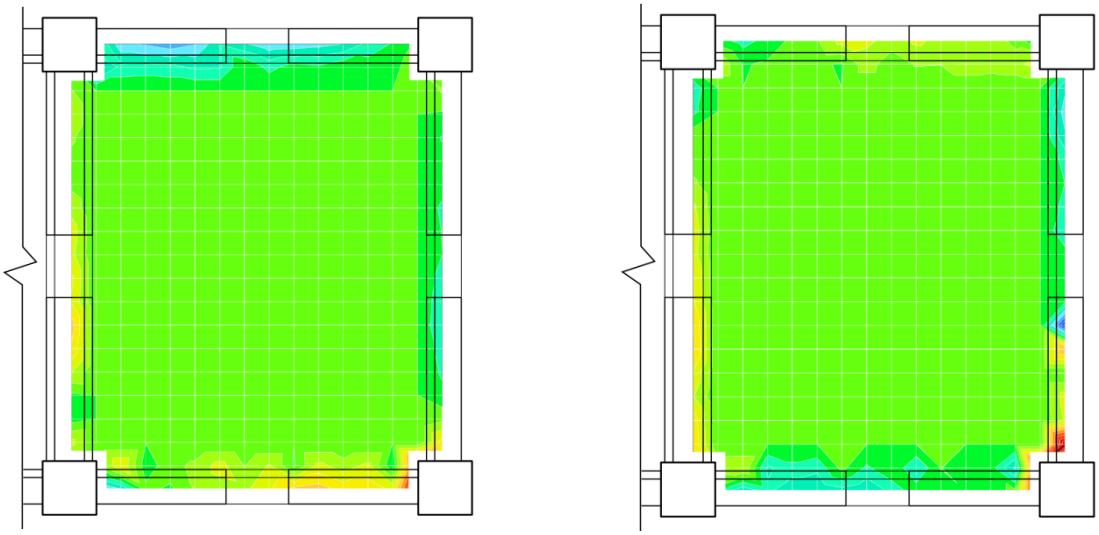

(g) Specimen displacement south-west.

(h) Specimen displacement south-east.

Figure C-17: Level Two floor strain contours from shear DEMEC measurements at 2.5% beam drift (Continued).

C.4 Beam Elongation

Figure C-18 and Figure C-19 present additional elongation data from SA1.

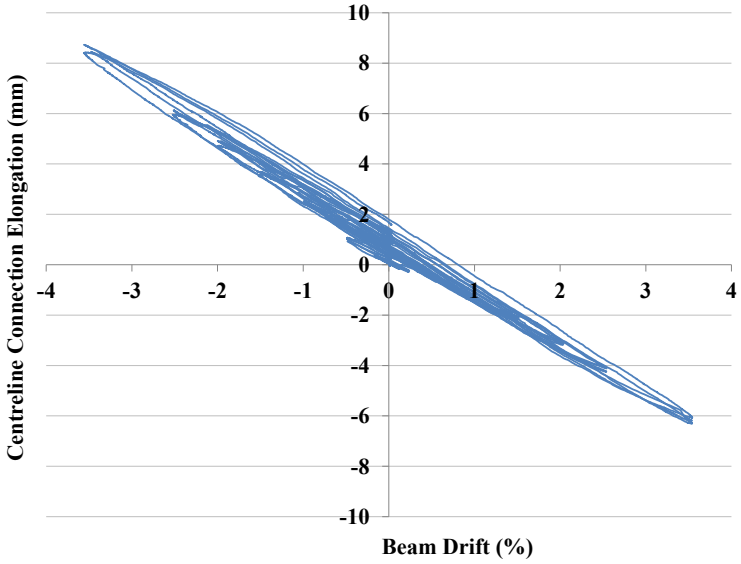

(a) Level One.

Figure C-18: Centreline connection elongation for Grid B.

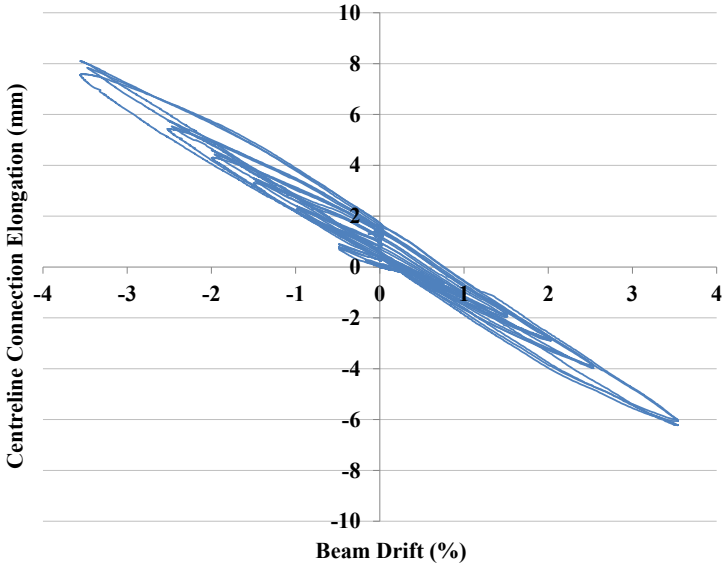

(b) Level Two.

Figure C-18: Centreline connection elongation for Grid B (Continued).

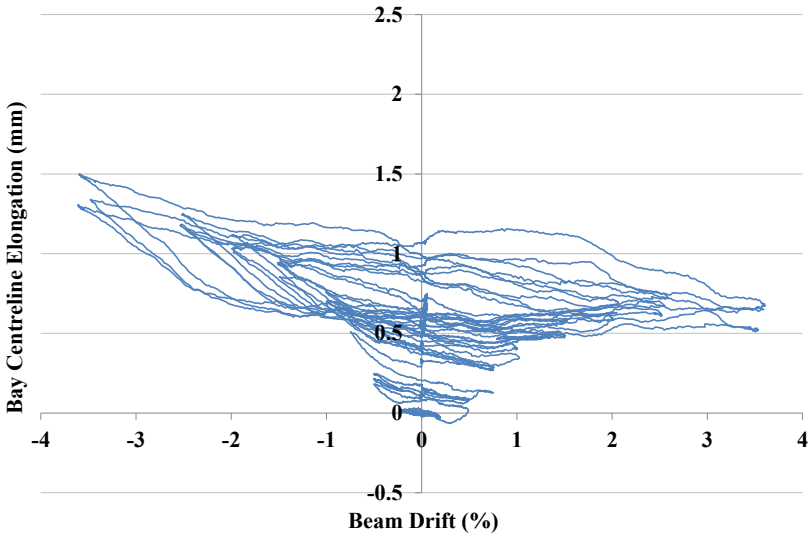

(a) East bay of Grid one, Level Two.

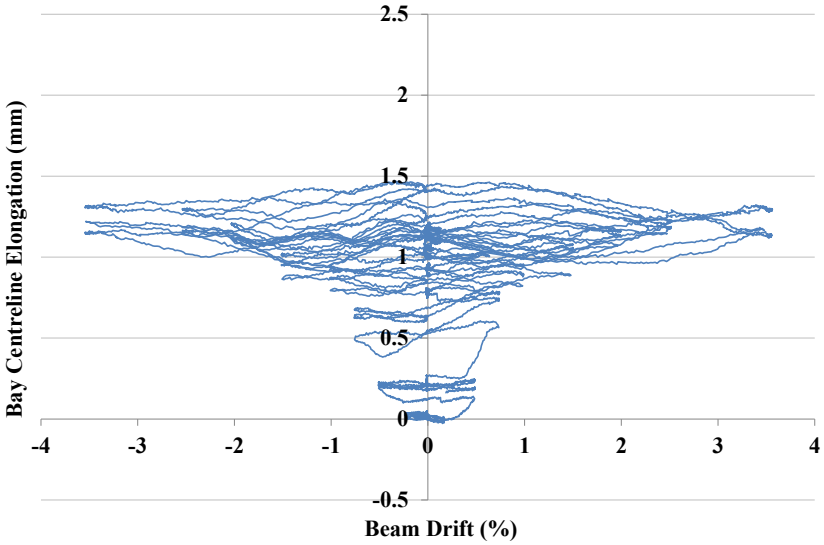

(b) Grid C Level Two.

Figure C-19: Bay cumulative elongation.

C.5 Decomposition of Lateral Displacement

Figure C-20 and Figure C-21 present additional plots of the relationship between different components of displacement for individual connections in SA1.

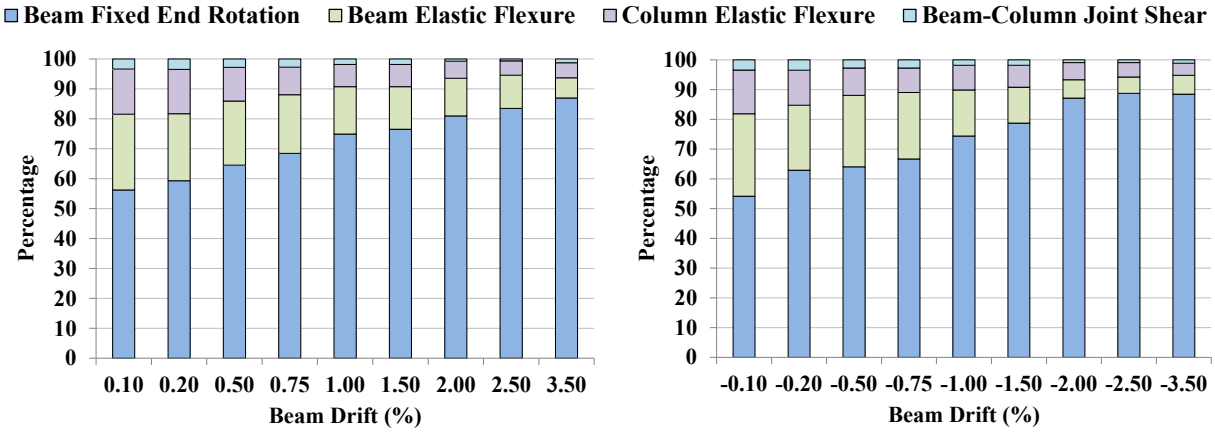

(a) Bm B/1-1 positive flexure.

(b) Bm B/1-1 negative flexure.

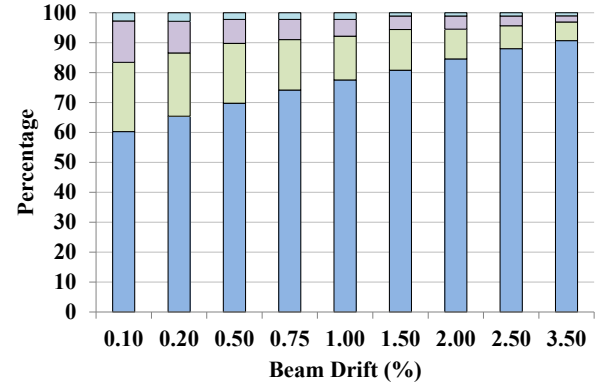

(c) Bm C/1-1 positive flexure.

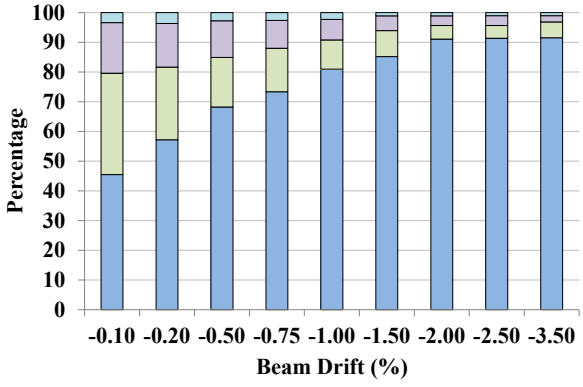

(d) Bm C/1-1 negative flexure.

Figure C-20: Level One east-west lateral displacement components.

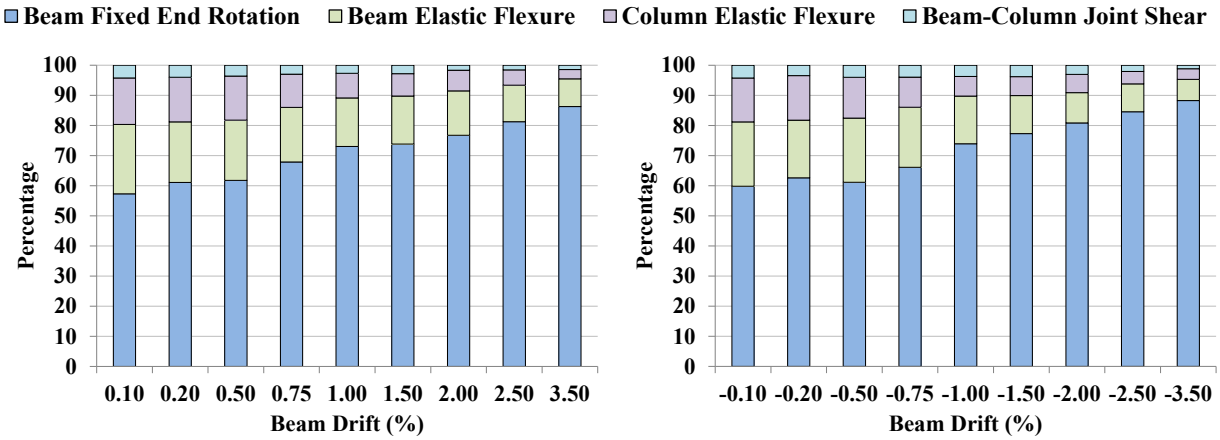

(a) Bm B/1-2 positive flexure.

(b) Bm B/1-2 negative flexure.

Figure C-21: Level Two east-west lateral displacement components.

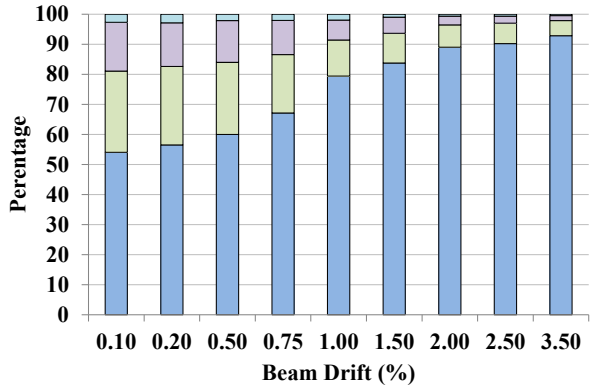

(c) Bm C/1-2 positive flexure.

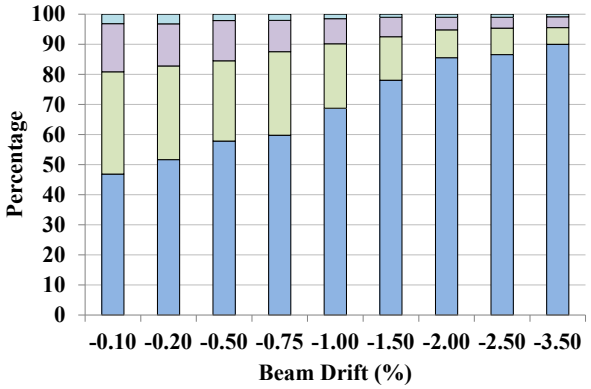

(d) Bm C/1-2 negative flexure.

Figure C-21: Level Two east-west lateral displacement components (Continued).

Appendix D: Subassembly Experiment Additional Results

D.1 Decomposition of Displacement Components

Figure D-1 presents the decomposition of lateral displacement components for specimen SA2 and SA3.

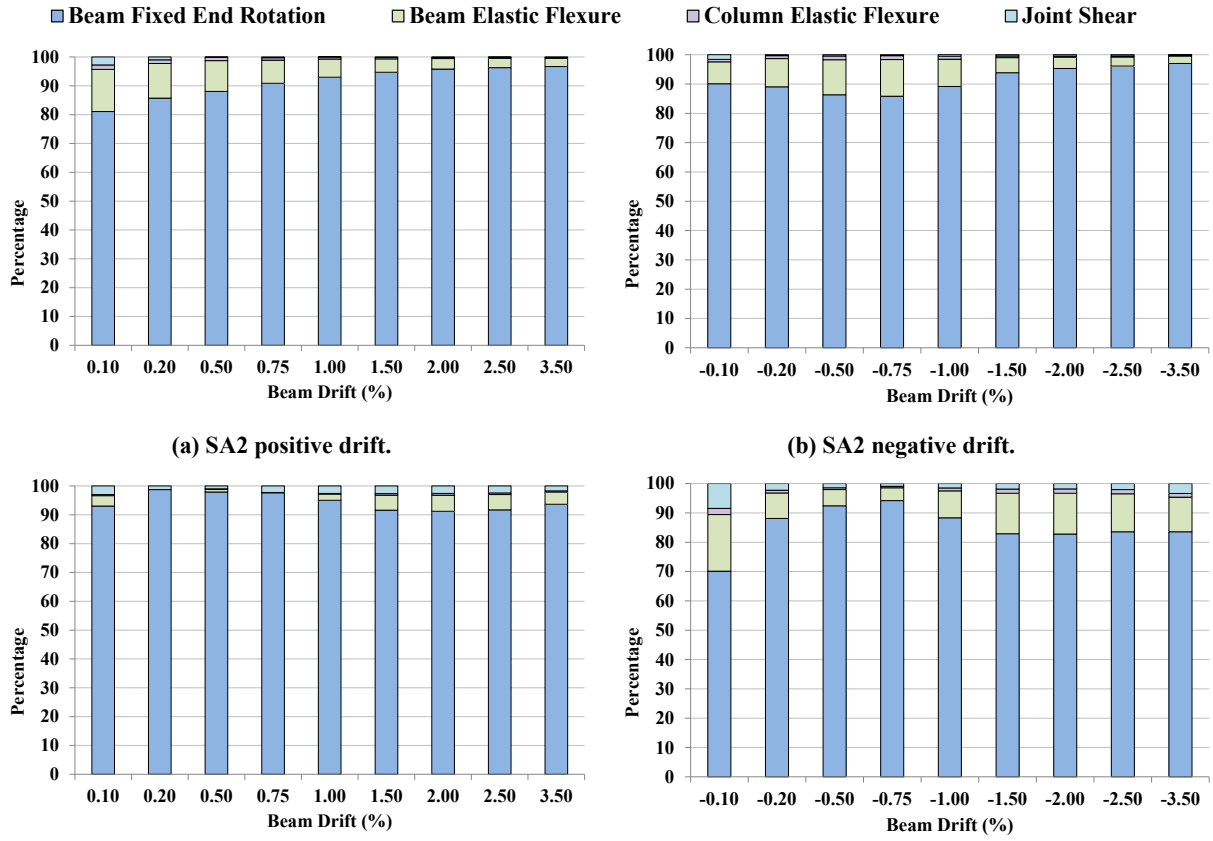

(a) SA2 positive drift. **(b) SA2 negative drift.**

(c) SA3 positive drift. **(d) SA3 negative drift.**

Figure D-1: As-built subassembly displacement components perpendicular to floor.

Figure D-2 presents the decomposition of lateral displacement components for specimen SA2-TCY, SA2-SFD and SA2-HF2V.

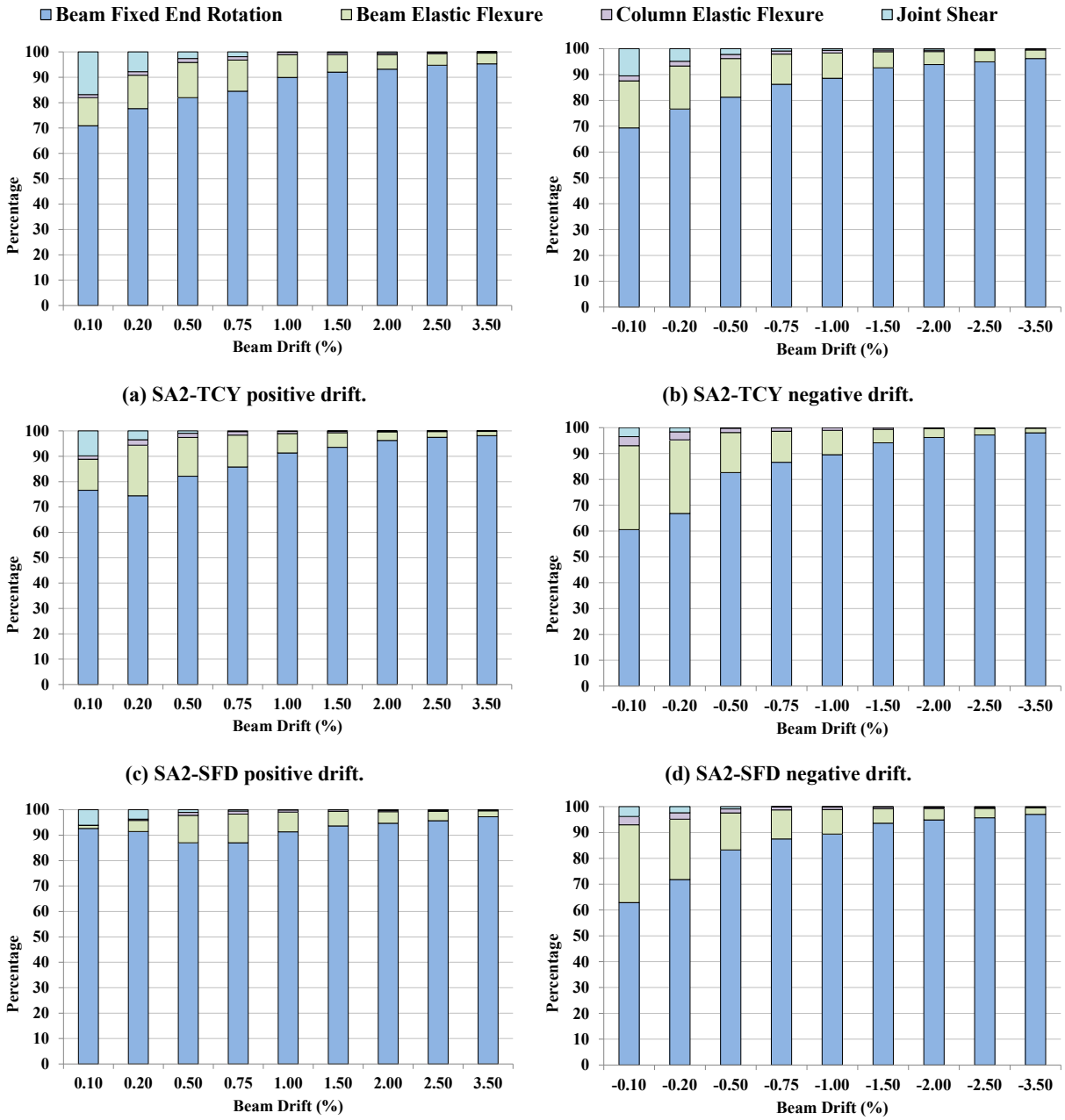

(a) SA2-TCY positive drift.

(b) SA2-TCY negative drift.

(c) SA2-SFD positive drift.

(d) SA2-SFD negative drift.

(e) SA2-HF2V positive drift.

(f) SA2-HF2V negative drift.

Figure D-2: Retrofitted subassembly displacement components perpendicular to floor.

Appendix E: Numerical Model Data

E.1 Superassembly SA1 Numerical Model

Table E-1 presents the Ruaumoko3D input file for the numerical model of SA1. The model includes the R3D slotted beam elements and the floor diaphragm model. Other numerical models used in this research have not been appended for brevity.

Table E-1: Input data for numerical model of SA1.

```
SUPERASSEMBLY SA1
*
*         NOTES
*         =====
*         SA1 Superassembly w/ R3D elements and floor diaphragm - 10/09/13 - Craig Muir
*         Units: N, m, S
*         R3D slotted beam element, Takeda columns, elastic beams, floor diaphragm

!         IPANL     IPLAS     IPCONM    ICTYPE    IPVERT    INLGEO    IPNF      IZERO     ORTHO     IMODE
          8         1         0         2         4         0         0         0         1         0
!         NNP       NMEM      NTYPE     NMODE     MODE1     MODE2     GRAV      C1        C2        DT        T         F
          342       450       30        5         1         5         9.81      5         5         5e-3      131       1
!         KPRINT    KPOST     KPLOT     DFACT     XMAX      YMAX      ZMAX      IFMT      NLEVEL    NUP       IRESID    KDUMP
          0         20        0         2         0.5       0.5       0.5       0         1         3         1         0
!         Txx       Txy       Txz       Tyx       Tyy       Tyz
          -0.866    0         0.866     0.5       1         0.5
!         MAXIT     MAXCIT    FTEST     WAVEX     WAVEY     WAVEZ     DXMAX     DYMAX     DZMAX     D         OMEGA     F
          0         0         0.0001    0         0         0         1         1         1         0         0         0

NODES
!         N         X         Y         Z         N1        N2        N3        N4        N5        N6        KUP       IOUT
          1         0.000     0.000     0.000     1         1         1         0         0         0         0
          2         4.191     0.000     0.000     1         1         1         0         0         0         0
          3         8.382     0.000     0.000     1         1         1         0         0         0         0
          4         0.000     0.000     4.953     1         1         1         0         0         0         0
          5         4.191     0.000     4.953     1         1         1         0         0         0         0
          6         8.382     0.000     4.953     1         1         1         0         0         0         0
          7         0.000     0.797     0.000     1         1         1         1         1         1         0
          8         4.191     0.797     0.000     1         1         1         1         1         1         0
          9         8.382     0.797     0.000     1         1         1         1         1         1         0
          10        0.000     0.797     4.953     1         1         1         1         1         1         0
          11        4.191     0.797     4.953     1         1         1         1         1         1         0
          12        8.382     0.797     4.953     1         1         1         1         1         1         0
          13        0.000     1.015     0.000     0         0         0         0         0         0         0
          14        0.195     1.015     0.000     1         1         1         1         1         1         0
          15        0.430     1.015     0.000     0         0         0         0         0         0         0
          16        1.263     1.015     0.000     0         0         0         0         0         0         0
          17        2.096     1.015     0.000     0         0         0         0         0         0         0
          18        2.928     1.015     0.000     0         0         0         0         0         0         0
          19        3.761     1.015     0.000     0         0         0         0         0         0         0
          20        3.996     1.015     0.000     1         1         1         1         1         1         0
          21        4.191     1.015     0.000     0         0         0         0         0         0         0
          22        4.386     1.015     0.000     1         1         1         1         1         1         0
          23        4.621     1.015     0.000     0         0         0         0         0         0         0
          24        5.454     1.015     0.000     0         0         0         0         0         0         0
          25        6.287     1.015     0.000     0         0         0         0         0         0         0
          26        7.119     1.015     0.000     0         0         0         0         0         0         0
          27        7.952     1.015     0.000     0         0         0         0         0         0         0
          28        8.187     1.015     0.000     1         1         1         1         1         1         0
          29        8.382     1.015     0.000     0         0         0         0         0         0         0
          30        0.000     1.015     0.195     1         1         1         1         1         1         0
          31        4.191     1.015     0.195     1         1         1         1         1         1         0
          32        8.382     1.015     0.195     1         1         1         1         1         1         0
          33        0.000     1.015     0.430     0         0         0         0         0         0         0
          34        4.191     1.015     0.430     0         0         0         0         0         0         0
          35        8.382     1.015     0.430     0         0         0         0         0         0         0
          36        0.000     1.015     0.677     0         0         0         0         0         0         0
          37        4.191     1.015     0.677     0         0         0         0         0         0         0
          38        8.382     1.015     0.677     0         0         0         0         0         0         0
          39        0.000     1.015     1.877     0         0         0         0         0         0         0
          40        4.191     1.015     1.877     0         0         0         0         0         0         0
          41        8.382     1.015     1.877     0         0         0         0         0         0         0
          42        0.000     1.015     3.077     0         0         0         0         0         0         0
          43        4.191     1.015     3.077     0         0         0         0         0         0         0
          44        8.382     1.015     3.077     0         0         0         0         0         0         0
          45        0.000     1.015     4.277     0         0         0         0         0         0         0
          46        4.191     1.015     4.277     0         0         0         0         0         0         0
          47        8.382     1.015     4.277     0         0         0         0         0         0         0
          48        0.000     1.015     4.523     0         0         0         0         0         0         0
          49        4.191     1.015     4.523     0         0         0         0         0         0         0
          50        8.382     1.015     4.523     0         0         0         0         0         0         0
          51        0.000     1.015     4.758     1         1         1         1         1         1         0
```

Table E-1: Input data for numerical model of SA1 (Continued).

52	4.191	1.015	4.758	1	1	1	1	1	1	0
53	8.382	1.015	4.758	1	1	1	1	1	1	0
54	0.000	1.015	4.953	0	0	0	0	0	0	0
55	0.195	1.015	4.953	1	1	1	1	1	1	0
56	0.430	1.015	4.953	0	0	0	0	0	0	0
57	1.263	1.015	4.953	0	0	0	0	0	0	0
58	2.096	1.015	4.953	0	0	0	0	0	0	0
59	2.928	1.015	4.953	0	0	0	0	0	0	0
60	3.761	1.015	4.953	0	0	0	0	0	0	0
61	3.996	1.015	4.953	1	1	1	1	1	1	0
62	4.191	1.015	4.953	0	0	0	0	0	0	0
63	4.386	1.015	4.953	1	1	1	1	1	1	0
64	4.621	1.015	4.953	0	0	0	0	0	0	0
65	5.454	1.015	4.953	0	0	0	0	0	0	0
66	6.287	1.015	4.953	0	0	0	0	0	0	0
67	7.119	1.015	4.953	0	0	0	0	0	0	0
68	7.952	1.015	4.953	0	0	0	0	0	0	0
69	8.187	1.015	4.953	1	1	1	1	1	1	0
70	8.382	1.015	4.953	0	0	0	0	0	0	0
71	0.000	1.203	0.000	0	0	0	0	0	0	0
72	0.430	1.203	0.000	1	1	1	1	1	1	0
73	1.263	1.203	0.000	1	1	1	1	1	1	0
74	2.096	1.203	0.000	1	1	1	1	1	1	0
75	2.928	1.203	0.000	1	1	1	1	1	1	0
76	3.761	1.203	0.000	1	1	1	1	1	1	0
77	4.191	1.203	0.000	0	0	0	0	0	0	0
78	4.621	1.203	0.000	1	1	1	1	1	1	0
79	5.454	1.203	0.000	1	1	1	1	1	1	0
80	6.287	1.203	0.000	1	1	1	1	1	1	0
81	7.119	1.203	0.000	1	1	1	1	1	1	0
82	7.952	1.203	0.000	1	1	1	1	1	1	0
83	8.382	1.203	0.000	0	0	0	0	0	0	0
84	0.193	1.203	0.677	1	1	1	1	1	1	0
85	0.298	1.203	0.677	2	2	2	0	0	0	84
86	0.430	1.203	0.677	0	0	0	0	0	0	0
87	1.263	1.203	0.677	0	0	0	0	0	0	0
88	2.096	1.203	0.677	0	0	0	0	0	0	0
89	2.928	1.203	0.677	0	0	0	0	0	0	0
90	3.761	1.203	0.677	0	0	0	0	0	0	0
91	3.893	1.203	0.677	2	2	2	0	0	0	92
92	3.998	1.203	0.677	1	1	1	1	1	1	0
93	4.384	1.203	0.677	1	1	1	1	1	1	0
94	4.489	1.203	0.677	2	2	2	0	0	0	93
95	4.621	1.203	0.677	0	0	0	0	0	0	0
96	5.454	1.203	0.677	0	0	0	0	0	0	0
97	6.287	1.203	0.677	0	0	0	0	0	0	0
98	7.119	1.203	0.677	0	0	0	0	0	0	0
99	7.952	1.203	0.677	0	0	0	0	0	0	0
100	8.084	1.203	0.677	2	2	2	0	0	0	101
101	8.189	1.203	0.677	1	1	1	1	1	1	0
102	0.193	1.203	1.877	1	1	1	1	1	1	0
103	0.298	1.203	1.877	2	2	2	0	0	0	102
104	0.430	1.203	1.877	0	0	0	0	0	0	0
105	1.263	1.203	1.877	0	0	0	0	0	0	0
106	2.096	1.203	1.877	0	0	0	0	0	0	0
107	2.928	1.203	1.877	0	0	0	0	0	0	0
108	3.761	1.203	1.877	0	0	0	0	0	0	0
109	3.893	1.203	1.877	2	2	2	0	0	0	110
110	3.998	1.203	1.877	1	1	1	1	1	1	0
111	4.384	1.203	1.877	1	1	1	1	1	1	0
112	4.489	1.203	1.877	2	2	2	0	0	0	111
113	4.621	1.203	1.877	0	0	0	0	0	0	0
114	5.454	1.203	1.877	0	0	0	0	0	0	0
115	6.287	1.203	1.877	0	0	0	0	0	0	0
116	7.119	1.203	1.877	0	0	0	0	0	0	0
117	7.952	1.203	1.877	0	0	0	0	0	0	0
118	8.084	1.203	1.877	2	2	2	0	0	0	119
119	8.189	1.203	1.877	1	1	1	1	1	1	0
120	0.193	1.203	3.077	1	1	1	1	1	1	0
121	0.298	1.203	3.077	2	2	2	0	0	0	120
122	0.430	1.203	3.077	0	0	0	0	0	0	0
123	1.263	1.203	3.077	0	0	0	0	0	0	0
124	2.096	1.203	3.077	0	0	0	0	0	0	0
125	2.928	1.203	3.077	0	0	0	0	0	0	0
126	3.761	1.203	3.077	0	0	0	0	0	0	0
127	3.893	1.203	3.077	2	2	2	0	0	0	128
128	3.998	1.203	3.077	1	1	1	1	1	1	0
129	4.384	1.203	3.077	1	1	1	1	1	1	0
130	4.489	1.203	3.077	2	2	2	0	0	0	129
131	4.621	1.203	3.077	0	0	0	0	0	0	0
132	5.454	1.203	3.077	0	0	0	0	0	0	0
133	6.287	1.203	3.077	0	0	0	0	0	0	0
134	7.119	1.203	3.077	0	0	0	0	0	0	0
135	7.952	1.203	3.077	0	0	0	0	0	0	0
136	8.084	1.203	3.077	2	2	2	0	0	0	137
137	8.189	1.203	3.077	1	1	1	1	1	1	0
138	0.193	1.203	4.277	1	1	1	1	1	1	0
139	0.298	1.203	4.277	2	2	2	0	0	0	138
140	0.430	1.203	4.277	0	0	0	0	0	0	0
141	1.263	1.203	4.277	0	0	0	0	0	0	0
142	2.096	1.203	4.277	0	0	0	0	0	0	0
143	2.928	1.203	4.277	0	0	0	0	0	0	0
144	3.761	1.203	4.277	0	0	0	0	0	0	0
145	3.893	1.203	4.277	2	2	2	0	0	0	146
146	3.998	1.203	4.277	1	1	1	1	1	1	0
147	4.384	1.203	4.277	1	1	1	1	1	1	0
148	4.489	1.203	4.277	2	2	2	0	0	0	147
149	4.621	1.203	4.277	0	0	0	0	0	0	0
150	5.454	1.203	4.277	0	0	0	0	0	0	0
151	6.287	1.203	4.277	0	0	0	0	0	0	0
152	7.119	1.203	4.277	0	0	0	0	0	0	0
153	7.952	1.203	4.277	0	0	0	0	0	0	0
154	8.084	1.203	4.277	2	2	2	0	0	0	155

Table E-1: Input data for numerical model of SA1 (Continued).

155	8.189	1.203	4.277	1	1	1	1	1	1	0
156	0.000	1.203	4.953	0	0	0	0	0	0	0
157	0.430	1.203	4.953	1	1	1	1	1	1	0
158	1.263	1.203	4.953	1	1	1	1	1	1	0
159	2.096	1.203	4.953	1	1	1	1	1	1	0
160	2.928	1.203	4.953	1	1	1	1	1	1	0
161	3.761	1.203	4.953	1	1	1	1	1	1	0
162	4.191	1.203	4.953	0	0	0	0	0	0	0
163	4.621	1.203	4.953	1	1	1	1	1	1	0
164	5.454	1.203	4.953	1	1	1	1	1	1	0
165	6.287	1.203	4.953	1	1	1	1	1	1	0
166	7.119	1.203	4.953	1	1	1	1	1	1	0
167	7.952	1.203	4.953	1	1	1	1	1	1	0
168	8.382	1.203	4.953	0	0	0	0	0	0	0
169	0.000	1.726	0.000	-1	0	-2	0	0	0	0
170	4.191	1.726	0.000	-1	0	-2	0	0	0	0
171	8.382	1.726	0.000	-1	0	-2	0	0	0	0
172	0.000	1.726	4.953	-1	0	-2	0	0	0	0
173	4.191	1.726	4.953	-1	0	-2	0	0	0	0
174	8.382	1.726	4.953	-1	0	-2	0	0	0	0
175	0.000	2.837	0.000	0	0	0	0	0	0	0
176	4.191	2.837	0.000	0	0	0	0	0	0	0
177	8.382	2.837	0.000	0	0	0	0	0	0	0
178	0.000	2.837	4.953	0	0	0	0	0	0	0
179	4.191	2.837	4.953	0	0	0	0	0	0	0
180	8.382	2.837	4.953	0	0	0	0	0	0	0
181	0.000	3.055	0.000	0	0	0	0	0	0	0
182	0.195	3.055	0.000	1	1	1	1	1	1	0
183	0.430	3.055	0.000	0	0	0	0	0	0	0
184	1.263	3.055	0.000	0	0	0	0	0	0	0
185	2.096	3.055	0.000	0	0	0	0	0	0	0
186	2.928	3.055	0.000	0	0	0	0	0	0	0
187	3.761	3.055	0.000	0	0	0	0	0	0	0
188	3.996	3.055	0.000	1	1	1	1	1	1	0
189	4.191	3.055	0.000	0	0	0	0	0	0	0
190	4.386	3.055	0.000	1	1	1	1	1	1	0
191	4.621	3.055	0.000	0	0	0	0	0	0	0
192	5.454	3.055	0.000	0	0	0	0	0	0	0
193	6.287	3.055	0.000	0	0	0	0	0	0	0
194	7.119	3.055	0.000	0	0	0	0	0	0	0
195	7.952	3.055	0.000	0	0	0	0	0	0	0
196	8.187	3.055	0.000	1	1	1	1	1	1	0
197	8.382	3.055	0.000	0	0	0	0	0	0	0
198	0.000	3.055	0.195	1	1	1	1	1	1	0
199	4.191	3.055	0.195	1	1	1	1	1	1	0
200	8.382	3.055	0.195	1	1	1	1	1	1	0
201	0.000	3.055	0.430	0	0	0	0	0	0	0
202	4.191	3.055	0.430	0	0	0	0	0	0	0
203	8.382	3.055	0.430	0	0	0	0	0	0	0
204	0.000	3.055	0.677	0	0	0	0	0	0	0
205	4.191	3.055	0.677	0	0	0	0	0	0	0
206	8.382	3.055	0.677	0	0	0	0	0	0	0
207	0.000	3.055	1.877	0	0	0	0	0	0	0
208	4.191	3.055	1.877	0	0	0	0	0	0	0
209	8.382	3.055	1.877	0	0	0	0	0	0	0
210	0.000	3.055	3.077	0	0	0	0	0	0	0
211	4.191	3.055	3.077	0	0	0	0	0	0	0
212	8.382	3.055	3.077	0	0	0	0	0	0	0
213	0.000	3.055	4.277	0	0	0	0	0	0	0
214	4.191	3.055	4.277	0	0	0	0	0	0	0
215	8.382	3.055	4.277	0	0	0	0	0	0	0
216	0.000	3.055	4.523	0	0	0	0	0	0	0
217	4.191	3.055	4.523	0	0	0	0	0	0	0
218	8.382	3.055	4.523	0	0	0	0	0	0	0
219	0.000	3.055	4.758	1	1	1	1	1	1	0
220	4.191	3.055	4.758	1	1	1	1	1	1	0
221	8.382	3.055	4.758	1	1	1	1	1	1	0
222	0.000	3.055	4.953	0	0	0	0	0	0	0
223	0.195	3.055	4.953	1	1	1	1	1	1	0
224	0.430	3.055	4.953	0	0	0	0	0	0	0
225	1.263	3.055	4.953	0	0	0	0	0	0	0
226	2.096	3.055	4.953	0	0	0	0	0	0	0
227	2.928	3.055	4.953	0	0	0	0	0	0	0
228	3.761	3.055	4.953	0	0	0	0	0	0	0
229	3.996	3.055	4.953	1	1	1	1	1	1	0
230	4.191	3.055	4.953	0	0	0	0	0	0	0
231	4.386	3.055	4.953	1	1	1	1	1	1	0
232	4.621	3.055	4.953	0	0	0	0	0	0	0
233	5.454	3.055	4.953	0	0	0	0	0	0	0
234	6.287	3.055	4.953	0	0	0	0	0	0	0
235	7.119	3.055	4.953	0	0	0	0	0	0	0
236	7.952	3.055	4.953	0	0	0	0	0	0	0
237	8.187	3.055	4.953	1	1	1	1	1	1	0
238	8.382	3.055	4.953	0	0	0	0	0	0	0
239	0.000	3.243	0.000	0	0	0	0	0	0	0
240	0.430	3.243	0.000	1	1	1	1	1	1	0
241	1.263	3.243	0.000	1	1	1	1	1	1	0
242	2.096	3.243	0.000	1	1	1	1	1	1	0
243	2.928	3.243	0.000	1	1	1	1	1	1	0
244	3.761	3.243	0.000	1	1	1	1	1	1	0
245	4.191	3.243	0.000	0	0	0	0	0	0	0
246	4.621	3.243	0.000	1	1	1	1	1	1	0
247	5.454	3.243	0.000	1	1	1	1	1	1	0
248	6.287	3.243	0.000	1	1	1	1	1	1	0
249	7.119	3.243	0.000	1	1	1	1	1	1	0
250	7.952	3.243	0.000	1	1	1	1	1	1	0
251	8.382	3.243	0.000	0	0	0	0	0	0	0
252	0.193	3.243	0.677	1	1	1	1	1	1	0
253	0.298	3.243	0.677	2	2	2	0	0	0	252
254	0.430	3.243	0.677	0	0	0	0	0	0	0
255	1.263	3.243	0.677	0	0	0	0	0	0	0
256	2.096	3.243	0.677	0	0	0	0	0	0	0
257	2.928	3.243	0.677	0	0	0	0	0	0	0

Table E-1: Input data for numerical model of SA1 (Continued).

```
          258       3.761     3.243     0.677     0         0         0         0         0         0         0
          259       3.893     3.243     0.677     2         2         2         0         0         0         260
          260       3.998     3.243     0.677     1         1         1         1         1         1         0
          261       4.384     3.243     0.677     1         1         1         1         1         1         0
          262       4.489     3.243     0.677     2         2         2         0         0         0         261
          263       4.621     3.243     0.677     0         0         0         0         0         0         0
          264       5.454     3.243     0.677     0         0         0         0         0         0         0
          265       6.287     3.243     0.677     0         0         0         0         0         0         0
          266       7.119     3.243     0.677     0         0         0         0         0         0         0
          267       7.952     3.243     0.677     0         0         0         0         0         0         0
          268       8.084     3.243     0.677     2         2         2         0         0         0         269
          269       8.189     3.243     0.677     1         1         1         1         1         1         0
          270       0.193     3.243     1.877     1         1         1         1         1         1         0
          271       0.298     3.243     1.877     2         2         2         0         0         0         270
          272       0.430     3.243     1.877     0         0         0         0         0         0         0
          273       1.263     3.243     1.877     0         0         0         0         0         0         0
          274       2.096     3.243     1.877     0         0         0         0         0         0         0
          275       2.928     3.243     1.877     0         0         0         0         0         0         0
          276       3.761     3.243     1.877     0         0         0         0         0         0         0
          277       3.893     3.243     1.877     2         2         2         0         0         0         278
          278       3.998     3.243     1.877     1         1         1         1         1         1         0
          279       4.384     3.243     1.877     1         1         1         1         1         1         0
          280       4.489     3.243     1.877     2         2         2         0         0         0         279
          281       4.621     3.243     1.877     0         0         0         0         0         0         0
          282       5.454     3.243     1.877     0         0         0         0         0         0         0
          283       6.287     3.243     1.877     0         0         0         0         0         0         0
          284       7.119     3.243     1.877     0         0         0         0         0         0         0
          285       7.952     3.243     1.877     0         0         0         0         0         0         0
          286       8.084     3.243     1.877     2         2         2         0         0         0         287
          287       8.189     3.243     1.877     1         1         1         1         1         1         0
          288       0.193     3.243     3.077     1         1         1         1         1         1         0
          289       0.298     3.243     3.077     2         2         2         0         0         0         288
          290       0.430     3.243     3.077     0         0         0         0         0         0         0
          291       1.263     3.243     3.077     0         0         0         0         0         0         0
          292       2.096     3.243     3.077     0         0         0         0         0         0         0
          293       2.928     3.243     3.077     0         0         0         0         0         0         0
          294       3.761     3.243     3.077     0         0         0         0         0         0         0
          295       3.893     3.243     3.077     2         2         2         0         0         0         296
          296       3.998     3.243     3.077     1         1         1         1         1         1         0
          297       4.384     3.243     3.077     1         1         1         1         1         1         0
          298       4.489     3.243     3.077     2         2         2         0         0         0         297
          299       4.621     3.243     3.077     0         0         0         0         0         0         0
          300       5.454     3.243     3.077     0         0         0         0         0         0         0
          301       6.287     3.243     3.077     0         0         0         0         0         0         0
          302       7.119     3.243     3.077     0         0         0         0         0         0         0
          303       7.952     3.243     3.077     0         0         0         0         0         0         0
          304       8.084     3.243     3.077     2         2         2         0         0         0         305
          305       8.189     3.243     3.077     1         1         1         1         1         1         0
          306       0.193     3.243     4.277     1         1         1         1         1         1         0
          307       0.298     3.243     4.277     2         2         2         0         0         0         306
          308       0.430     3.243     4.277     0         0         0         0         0         0         0
          309       1.263     3.243     4.277     0         0         0         0         0         0         0
          310       2.096     3.243     4.277     0         0         0         0         0         0         0
          311       2.928     3.243     4.277     0         0         0         0         0         0         0
          312       3.761     3.243     4.277     0         0         0         0         0         0         0
          313       3.893     3.243     4.277     2         2         2         0         0         0         314
          314       3.998     3.243     4.277     1         1         1         1         1         1         0
          315       4.384     3.243     4.277     1         1         1         1         1         1         0
          316       4.489     3.243     4.277     2         2         2         0         0         0         315
          317       4.621     3.243     4.277     0         0         0         0         0         0         0
          318       5.454     3.243     4.277     0         0         0         0         0         0         0
          319       6.287     3.243     4.277     0         0         0         0         0         0         0
          320       7.119     3.243     4.277     0         0         0         0         0         0         0
          321       7.952     3.243     4.277     0         0         0         0         0         0         0
          322       8.084     3.243     4.277     2         2         2         0         0         0         323
          323       8.189     3.243     4.277     1         1         1         1         1         1         0
          324       0.000     3.243     4.953     0         0         0         0         0         0         0
          325       0.430     3.243     4.953     1         1         1         1         1         1         0
          326       1.263     3.243     4.953     1         1         1         1         1         1         0
          327       2.096     3.243     4.953     1         1         1         1         1         1         0
          328       2.928     3.243     4.953     1         1         1         1         1         1         0
          329       3.761     3.243     4.953     1         1         1         1         1         1         0
          330       4.191     3.243     4.953     0         0         0         0         0         0         0
          331       4.621     3.243     4.953     1         1         1         1         1         1         0
          332       5.454     3.243     4.953     1         1         1         1         1         1         0
          333       6.287     3.243     4.953     1         1         1         1         1         1         0
          334       7.119     3.243     4.953     1         1         1         1         1         1         0
          335       7.952     3.243     4.953     1         1         1         1         1         1         0
          336       8.382     3.243     4.953     0         0         0         0         0         0         0
          337       0.000     3.726     0.000     -3        0         -4        0         0         0         0
          338       4.191     3.726     0.000     -3        0         -4        0         0         0         0
          339       8.382     3.726     0.000     -3        0         -4        0         0         0         0
          340       0.000     3.726     4.953     -3        0         -4        0         0         0         0
          341       4.191     3.726     4.953     -3        0         -4        0         0         0         0
          342       8.382     3.726     4.953     -3        0         -4        0         0         0         0

DRIFT   ANGLE
1     169     337

ELEMENT
!         N         MTYPE     I         J         K         L         M
          1         1         13        15        14        15        Z
          2         1         54        56        55        56        -Z
          3         2         21        19        20        19        Z
          4         2         21        23        22        23        Z
          5         2         29        27        28        27        Z
          6         2         62        60        61        60        -Z
          7         2         62        64        63        64        -Z
          8         2         70        68        69        68        -Z
          9         3         13        33        30        33        X
          10        30        21        37        31        37        X
          11        3         29        35        32        35        -X
          12        3         54        48        51        48        X
```

Table E-1: Input data for numerical model of SA1 (Continued).

13	30	62	49	52	49	X
14	3	70	50	53	50	-X
15	4	1	13	1	7	Z
16	4	2	21	2	8	Z
17	4	3	29	3	9	Z
18	4	4	54	4	10	Z
19	4	5	62	5	11	Z
20	4	6	70	6	12	Z
21	4	13	169	71	169	Z
22	4	21	170	77	170	Z
23	4	29	171	83	171	Z
24	4	54	172	156	172	Z
25	4	62	173	162	173	Z
26	4	70	174	168	174	Z
27	5	15	16	15	16	Z
28	5	16	17	16	17	Z
29	5	17	18	17	18	Z
30	5	18	19	18	19	Z
31	5	23	24	23	24	Z
32	5	24	25	24	25	Z
33	5	25	26	25	26	Z
34	5	26	27	26	27	Z
35	5	33	36	33	36	-X
36	5	34	37	34	37	-X
37	5	35	38	35	38	-X
38	5	36	39	36	39	-X
39	5	37	40	37	40	-X
40	5	38	41	38	41	-X
41	5	39	42	39	42	-X
42	5	40	43	40	43	-X
43	5	41	44	41	44	-X
44	5	42	45	42	45	-X
45	5	43	46	43	46	-X
46	5	44	47	44	47	-X
47	5	45	48	45	48	-X
48	5	46	49	46	49	-X
49	5	47	50	47	50	-X
50	5	56	57	56	57	Z
51	5	57	58	57	58	Z
52	5	58	59	58	59	Z
53	5	59	60	59	60	Z
54	5	64	65	64	65	Z
55	5	65	66	65	66	Z
56	5	66	67	66	67	Z
57	5	67	68	67	68	Z
58	6	36	85	84	85	Z
59	6	39	103	102	103	Z
60	6	42	121	120	121	Z
61	6	45	139	138	139	Z
62	6	37	91	92	91	-Z
63	6	40	109	110	109	-Z
64	6	43	127	128	127	-Z
65	6	46	145	146	145	-Z
66	6	37	94	93	94	Z
67	6	40	112	111	112	Z
68	6	43	130	129	130	Z
69	6	46	148	147	148	Z
70	6	38	100	101	100	-Z
71	6	41	118	119	118	-Z
72	6	44	136	137	136	-Z
73	6	47	154	155	154	-Z
74	7	85	86	85	86	Z
75	7	86	87	86	87	Z
76	7	87	88	87	88	Z
77	7	88	89	88	89	Z
78	7	89	90	89	90	Z
79	7	90	91	90	91	Z
80	7	94	95	94	95	Z
81	7	95	96	95	96	Z
82	7	96	97	96	97	Z
83	7	97	98	97	98	Z
84	7	98	99	98	99	Z
85	7	99	100	99	100	Z
86	7	103	104	103	104	Z
87	7	104	105	104	105	Z
88	7	105	106	105	106	Z
89	7	106	107	106	107	Z
90	7	107	108	107	108	Z
91	7	108	109	108	109	Z
92	7	112	113	112	113	Z
93	7	113	114	113	114	Z
94	7	114	115	114	115	Z
95	7	115	116	115	116	Z
96	7	116	117	116	117	Z
97	7	117	118	117	118	Z
98	7	121	122	121	122	Z
99	7	122	123	122	123	Z
100	7	123	124	123	124	Z
101	7	124	125	124	125	Z
102	7	125	126	125	126	Z
103	7	126	127	126	127	Z
104	7	130	131	130	131	Z
105	7	131	132	131	132	Z
106	7	132	133	132	133	Z
107	7	133	134	133	134	Z
108	7	134	135	134	135	Z
109	7	135	136	135	136	Z
110	7	139	140	139	140	Z
111	7	140	141	140	141	Z
112	7	141	142	141	142	Z
113	7	142	143	142	143	Z
114	7	143	144	143	144	Z
115	7	144	145	144	145	Z

Table E-1: Input data for numerical model of SA1 (Continued).

116	7	148	149	148	149	Z
117	7	149	150	149	150	Z
118	7	150	151	150	151	Z
119	7	151	152	151	152	Z
120	7	152	153	152	153	Z
121	7	153	154	153	154	Z
122	8	85	86	104	103	
123	8	86	87	105	104	
124	8	87	88	106	105	
125	8	88	89	107	106	
126	8	89	90	108	107	
127	8	90	91	109	108	
128	8	94	95	113	112	
129	8	95	96	114	113	
130	8	96	97	115	114	
131	8	97	98	116	115	
132	8	98	99	117	116	
133	8	99	100	118	117	
134	8	103	104	122	121	
135	8	104	105	123	122	
136	8	105	106	124	123	
137	8	106	107	125	124	
138	8	107	108	126	125	
139	8	108	109	127	126	
140	8	112	113	131	130	
141	8	113	114	132	131	
142	8	114	115	133	132	
143	8	115	116	134	133	
144	8	116	117	135	134	
145	8	117	118	136	135	
146	8	121	122	140	139	
147	8	122	123	141	140	
148	8	123	124	142	141	
149	8	124	125	143	142	
150	8	125	126	144	143	
151	8	126	127	145	144	
152	8	130	131	149	148	
153	8	131	132	150	149	
154	8	132	133	151	150	
155	8	133	134	152	151	
156	8	134	135	153	152	
157	8	135	136	154	153	
158	9	36	15	84	72	Z
159	10	13	86	71	86	Z
160	11	86	16	86	73	Z
161	12	15	87	72	87	Z
162	13	87	17	87	74	Z
163	14	16	88	73	88	Z
164	14	88	18	88	75	Z
165	13	17	89	74	89	Z
166	12	89	19	89	76	Z
167	11	18	90	75	90	Z
168	10	90	21	90	77	Z
169	9	19	92	76	92	Z
170	9	37	23	93	78	Z
171	10	21	95	77	95	Z
172	11	95	24	95	79	Z
173	12	23	96	78	96	Z
174	13	96	25	96	80	Z
175	14	24	97	79	97	Z
176	14	97	26	97	81	Z
177	13	25	98	80	98	Z
178	12	98	27	98	82	Z
179	11	26	99	81	99	Z
180	10	99	29	99	83	Z
181	9	27	38	82	101	Z
182	9	45	56	138	157	Z
183	10	54	140	156	140	Z
184	11	140	57	140	158	Z
185	12	56	141	157	141	Z
186	13	141	58	141	159	Z
187	14	57	142	158	142	Z
188	14	142	59	142	160	Z
189	13	58	143	159	143	Z
190	12	143	60	143	161	Z
191	11	59	144	160	144	Z
192	10	144	62	144	162	Z
193	9	60	46	161	146	Z
194	9	46	64	147	163	Z
195	10	62	149	162	149	Z
196	11	149	65	149	164	Z
197	12	64	150	163	150	Z
198	13	150	66	150	165	Z
199	14	65	151	164	151	Z
200	14	151	67	151	166	Z
201	13	66	152	165	152	Z
202	12	152	68	152	167	Z
203	11	67	153	166	153	Z
204	10	153	70	153	168	Z
205	9	68	47	167	155	Z
206	15	15	86	72	86	X
207	16	16	87	73	87	X
208	17	17	88	74	88	X
209	16	18	89	75	89	X
210	15	19	90	76	90	X
211	15	23	95	78	95	X
212	16	24	96	79	96	X
213	17	25	97	80	97	X
214	16	26	98	81	98	X
215	15	27	99	82	99	X
216	15	56	140	157	140	-X
217	16	57	141	158	141	-X
218	17	58	142	159	142	-X

Table E-1: Input data for numerical model of SA1 (Continued).

219	16	59	143	160	143	-X
220	15	60	144	161	144	-X
221	15	64	149	163	149	-X
222	16	65	150	164	150	-X
223	17	66	151	165	151	-X
224	16	67	152	166	152	-X
225	15	68	153	167	153	-X
226	1	181	183	182	183	Z
227	1	222	224	223	224	-Z
228	2	189	187	188	187	Z
229	2	189	191	190	191	Z
230	2	197	195	196	195	Z
231	2	230	228	229	228	-Z
232	2	230	232	231	232	-Z
233	2	238	236	237	236	-Z
234	3	181	201	198	201	X
235	3	189	202	199	202	X
236	3	197	203	200	203	-X
237	3	222	216	219	216	X
238	3	230	217	220	217	X
239	3	238	218	221	218	-X
240	4	169	181	169	175	Z
241	4	170	189	170	176	Z
242	4	171	197	171	177	Z
243	4	172	222	172	178	Z
244	4	173	230	173	179	Z
245	4	174	238	174	180	Z
246	4	181	337	239	337	Z
247	4	189	338	245	338	Z
248	4	197	339	251	339	Z
249	4	222	340	324	340	Z
250	4	230	341	330	341	Z
251	4	238	342	336	342	Z
252	5	183	184	183	184	Z
253	5	184	185	184	185	Z
254	5	185	186	185	186	Z
255	5	186	187	186	187	Z
256	5	191	192	191	192	Z
257	5	192	193	192	193	Z
258	5	193	194	193	194	Z
259	5	194	195	194	195	Z
260	5	201	204	201	204	-X
261	5	202	205	202	205	-X
262	5	203	206	203	206	-X
263	5	204	207	204	207	-X
264	5	205	208	205	208	-X
265	5	206	209	206	209	-X
266	5	207	210	207	210	-X
267	5	208	211	208	211	-X
268	5	209	212	209	212	-X
269	5	210	213	210	213	-X
270	5	211	214	211	214	-X
271	5	212	215	212	215	-X
272	5	213	216	213	216	-X
273	5	214	217	214	217	-X
274	5	215	218	215	218	-X
275	5	224	225	224	225	Z
276	5	225	226	225	226	Z
277	5	226	227	226	227	Z
278	5	227	228	227	228	Z
279	5	232	233	232	233	Z
280	5	233	234	233	234	Z
281	5	234	235	234	235	Z
282	5	235	236	235	236	Z
283	18	204	253	252	253	Z
284	18	207	271	270	271	Z
285	18	210	289	288	289	Z
286	18	213	307	306	307	Z
287	18	205	259	260	259	-Z
288	18	208	277	278	277	-Z
289	18	211	295	296	295	-Z
290	18	214	313	314	313	-Z
291	18	205	262	261	262	Z
292	18	208	280	279	280	Z
293	18	211	298	297	298	Z
294	18	214	316	315	316	Z
295	18	206	268	269	268	-Z
296	18	209	286	287	286	-Z
297	18	212	304	305	304	-Z
298	18	215	322	323	322	-Z
299	19	253	254	253	254	Z
300	19	254	255	254	255	Z
301	19	255	256	255	256	Z
302	19	256	257	256	257	Z
303	19	257	258	257	258	Z
304	19	258	259	258	259	Z
305	19	262	263	262	263	Z
306	19	263	264	263	264	Z
307	19	264	265	264	265	Z
308	19	265	266	265	266	Z
309	19	266	267	266	267	Z
310	19	267	268	267	268	Z
311	19	271	272	271	272	Z
312	19	272	273	272	273	Z
313	19	273	274	273	274	Z
314	19	274	275	274	275	Z
315	19	275	276	275	276	Z
316	19	276	277	276	277	Z
317	19	280	281	280	281	Z
318	19	281	282	281	282	Z
319	19	282	283	282	283	Z
320	19	283	284	283	284	Z
321	19	284	285	284	285	Z

Table E-1: Input data for numerical model of SA1 (Continued).

322	19	285	286	285	286	Z
323	19	289	290	289	290	Z
324	19	290	291	290	291	Z
325	19	291	292	291	292	Z
326	19	292	293	292	293	Z
327	19	293	294	293	294	Z
328	19	294	295	294	295	Z
329	19	298	299	298	299	Z
330	19	299	300	299	300	Z
331	19	300	301	300	301	Z
332	19	301	302	301	302	Z
333	19	302	303	302	303	Z
334	19	303	304	303	304	Z
335	19	307	308	307	308	Z
336	19	308	309	308	309	Z
337	19	309	310	309	310	Z
338	19	310	311	310	311	Z
339	19	311	312	311	312	Z
340	19	312	313	312	313	Z
341	19	316	317	316	317	Z
342	19	317	318	317	318	Z
343	19	318	319	318	319	Z
344	19	319	320	319	320	Z
345	19	320	321	320	321	Z
346	19	321	322	321	322	Z
347	20	253	254	272	271	
348	20	254	255	273	272	
349	20	255	256	274	273	
350	20	256	257	275	274	
351	20	257	258	276	275	
352	20	258	259	277	276	
353	20	262	263	281	280	
354	20	263	264	282	281	
355	20	264	265	283	282	
356	20	265	266	284	283	
357	20	266	267	285	284	
358	20	267	268	286	285	
359	20	271	272	290	289	
360	20	272	273	291	290	
361	20	273	274	292	291	
362	20	274	275	293	292	
363	20	275	276	294	293	
364	20	276	277	295	294	
365	20	280	281	299	298	
366	20	281	282	300	299	
367	20	282	283	301	300	
368	20	283	284	302	301	
369	20	284	285	303	302	
370	20	285	286	304	303	
371	20	289	290	308	307	
372	20	290	291	309	308	
373	20	291	292	310	309	
374	20	292	293	311	310	
375	20	293	294	312	311	
376	20	294	295	313	312	
377	20	298	299	317	316	
378	20	299	300	318	317	
379	20	300	301	319	318	
380	20	301	302	320	319	
381	20	302	303	321	320	
382	20	303	304	322	321	
383	21	204	183	252	240	Z
384	22	181	254	239	254	Z
385	23	254	184	254	241	Z
386	24	183	255	240	255	Z
387	25	255	185	255	242	Z
388	26	184	256	241	256	Z
389	26	256	186	256	243	Z
390	25	185	257	242	257	Z
391	24	257	187	257	244	Z
392	23	186	258	243	258	Z
393	22	258	189	258	245	Z
394	21	187	260	244	260	Z
395	21	205	191	261	246	Z
396	22	189	263	245	263	Z
397	23	263	192	263	247	Z
398	24	191	264	246	264	Z
399	25	264	193	264	248	Z
400	26	192	265	247	265	Z
401	26	265	194	265	249	Z
402	25	193	266	248	266	Z
403	24	266	195	266	250	Z
404	23	194	267	249	267	Z
405	22	267	197	267	251	Z
406	21	195	206	250	269	Z
407	21	213	224	306	325	Z
408	22	222	308	324	308	Z
409	23	308	225	308	326	Z
410	24	224	309	325	309	Z
411	25	309	226	309	327	Z
412	26	225	310	326	310	Z
413	26	310	227	310	328	Z
414	25	226	311	327	311	Z
415	24	311	228	311	329	Z
416	23	227	312	328	312	Z
417	22	312	230	312	330	Z
418	21	228	214	329	314	Z
419	21	214	232	315	331	Z
420	22	230	317	330	317	Z
421	23	317	233	317	332	Z
422	24	232	318	331	318	Z
423	25	318	234	318	333	Z
424	26	233	319	332	319	Z

Table E-1: Input data for numerical model of SA1 (Continued).

```
          425       26        319       235       319       334       Z
          426       25        234       320       333       320       Z
          427       24        320       236       320       335       Z
          428       23        235       321       334       321       Z
          429       22        321       238       321       336       Z
          430       21        236       215       335       323       Z
          431       27        183       254       240       254       X
          432       28        184       255       241       255       X
          433       29        185       256       242       256       X
          434       28        186       257       243       257       X
          435       27        187       258       244       258       X
          436       27        191       263       246       263       X
          437       28        192       264       247       264       X
          438       29        193       265       248       265       X
          439       28        194       266       249       266       X
          440       27        195       267       250       267       X
          441       27        224       308       325       308       -X
          442       28        225       309       326       309       -X
          443       29        226       310       327       310       -X
          444       28        227       311       328       311       -X
          445       27        228       312       329       312       -X
          446       27        232       317       331       317       -X
          447       28        233       318       332       318       -X
          448       29        234       319       333       319       -X
          449       28        235       320       334       320       -X
          450       27        236       321       335       321       -X

PROPS
!         N                   MTYPE             LABEL
          1                   SLOTTED           'EW Slotted Beam'
!         IPLAS   B       D       DB      SL      HL      WGT    JOP  IHS   IHB   IO   Y0   Z0 IPRNT
          1       0.444   0.174   0.654   0.0     0.3519  0.0    3    1     1     0     0    0
!         EC       FPC       FT
          27.8e+09 -40e+06 2.27e+06
!         ES       R     FSC       FST      L1      L2      D1      D2
          157e+09  0.1   -521e+06  521e+06  0.338  0.338  0.0315   0.09
!         ES       R     FSC       FST      L1      L2      D1      D2
          127e+09  0.1   -314e+06  314e+06  0.564  0.639  0.564   0.623
!         ES       R     FSC       FST      LENGTH  ANGLE
          157e+09  0.1   -521e+06  521e+06  0.588   45
!         G       FY      R     Alpha  Fcr   Fcc
          15e+06  40e+03  0.01  0.0    0.0   0.0
!         N1      A1       A2       A3       A4   A5   B1      B2     B3     B4   B5
          3       4.1e-4   4.1e-4   4.1e-4   0.0  0.0  -0.110  0.101  0.206  0.0  0.0
!         N1      A1       A2       A3   A4   A5   B1      B2     B3   B4   B5
          2       4.1e-4   4.1e-4   0.0  0.0  0.0  -0.110  0.206  0.0  0.0  0.0
!         N1      A1       A2       A3   A4   A5   B1      B2     B3   B4   B5
          2       1.13e-4  1.13e-4  0.0  0.0  0.0  -0.110  0.206  0.0  0.0  0.0
!         N1      A1       A2       A3       A4   A5   B1      B2     B3     B4   B5
          3       4.1e-4   4.1e-4   4.1e-4   0.0  0.0  -0.110  0.101  0.206  0.0  0.0
!         N1      A1       A2       A3       A4   A5   B1      B2     B3     B4   B5
          3       4.1e-4   4.1e-4   4.1e-4   0.0  0.0  -0.219  -0.154 0.179  0.0  0.0
!         TLIMT   CLIMIT  BETA          Fbo    L     TFACTOR   CFACTOR   eTT
          0.0025  0.005   1.0   0.2    1.0   1.0       1.0       1e-7
!         ESH         Esu         Fsu       OmegaF
          0.0226        0.1624      632e6     1.0
!         ESH         Esu         Fsu       OmegaF
          0.0336        0.2235      448e6     1.0
!         ESH         Esu         Fsu       OmegaF
          0.0226        0.1624      632e6     1.0

!         N         MTYPE             LABEL
          2         SLOTTED           'EW Slotted Beam'
!         IPLAS   B       D       DB      SL      HL      WGT    JOP  IHS   IHB   IO   Y0   Z0 IPRNT
          1       0.296   0.116   0.436   0.0     0.2346  0      3    1     1     0     0    0
!         EC       FPC       FT
          27.8e+09 -40e+06 2.27e+06
!         ES       R     FSC       FST      L1      L2      D1      D2
          157e+09  0.1   -521e+06  521e+06  0.225  0.225  0.062   0.101
!         ES       R     FSC       FST      L1      L2      D1      D2
          127e+09  0.1   -314e+06  314e+06  0.376  0.426  0.356   0.395
!         ES       R     FSC       FST      LENGTH  ANGLE
          157e+09  0.1   -521e+06  521e+06  0.392   45
!         G       FY      R     Alpha  Fcr   Fcc
          15e+06  40e+03  0.01  0.0    0.0   0.0
!         N1      A1       A2       A3       A4   A5   B1      B2     B3     B4   B5
          3       2.01e-4  2.01e-4  2.01e-4  0.0  0.0  -0.073  0.067  0.137  0.0  0.0
!         N1      A1       A2       A3   A4   A5   B1      B2     B3   B4   B5
          2       2.01e-4  2.01e-4  0.0  0.0  0.0  -0.073  0.137  0.0  0.0  0.0
!         N1      A1       A2       A3   A4   A5   B1      B2     B3   B4   B5
          0      0.0  0.0  0.0  0.0  0.0  0.0  0.0  0.0  0.0  0.0
!         N1      A1       A2       A3       A4   A5   B1      B2     B3     B4   B5
          2       2.01e-4  2.01e-4  0.0      0.0  0.0  -0.073  0.137  0.0  0.0 0.0
!         N1      A1       A2       A3       A4   A5   B1      B2     B3     B4   B5
          3       2.01e-4  2.01e-4  2.01e-4  0.0  0.0  -0.146  -0.103 0.119  0.0  0.0
!         TLIMT     CLIMIT    BETA      Fbo       L         TFACTOR   CFACTOR   eTT
          0.0025    0.005   1.0     0.2     1.0     1.0     1.0  1e-7
!         ESH         Esu         Fsu       OmegaF
          0.0226      0.1624      632e6     1.0
!         ESH         Esu         Fsu       OmegaF
          0.0336      0.2235      448e6     1.0
!         ESH         Esu         Fsu       OmegaF
          0.0226      0.1624      632e6     1.0

          3         SLOTTED           'NS Slotted Beam'
!         IPLAS   B       D       DB      SL      HL      WGT    JOP  IHS   IHB   IO   Y0   Z0 IPRNT
          1       0.296   0.116   0.436   0.0     0.2346  0      3    1     1     0     0    0
!         EC      FPC      FT
          27.8e+09 -40e+06 2.27e+06
!         ES       R     FSC       FST      L1      L2      D1      D2
          157e+09  0.1   -521e+06  521e+06  0.225  0.225   0.042   0.081
!         ES       R     FSC       FST      L1      L2      D1      D2
          127e+09  0.1   -314e+06  314e+06  0.376  0.426  0.336   0.375
```

Table E-1: Input data for numerical model of SA1 (Continued).

```
!         ES       R     FSC       FST      LENGTH  ANGLE
          157e+09  0.1   -521e+06  521e+06  0.392   45
!         G        FY      R     Alpha  Fcr   Fcc
          15e+06   40e+03  0.01  0.0    0.0   0.0
!         N1       A1       A2       A3       A4   A5   B1      B2     B3     B4   B5
          3        2.01e-4  2.01e-4  2.01e-4  0.0  0.0  -0.073  0.067  0.137  0.0  0.0
!         N1       A1       A2       A3   A4   A5   B1      B2     B3   B4   B5
          2        2.01e-4  2.01e-4  0.0  0.0  0.0  -0.073  0.137  0.0  0.0  0.0
!         N1       A1       A2       A3   A4   A5   B1      B2     B3   B4   B5
          2        1.13e-4  1.13e-4  0.0  0.0  0.0  -0.073  0.137  0.0  0.0  0.0
!         N1       A1       A2       A3       A4   A5   B1      B2     B3     B4   B5
          2        2.01e-4  2.01e-4  0.0      0.0  0.0  -0.073  0.137  0.0  0.0 0.0
!         N1       A1       A2       A3       A4   A5   B1      B2     B3     B4   B5
          3        2.01e-4  2.01e-4  2.01e-4  0.0  0.0  -0.146  -0.103 0.119  0.0  0.0
!         TLIMT     CLIMIT    BETA      Fbo       L         TFACTOR   CFACTOR   eTT
          0.0025    0.005     1.0       0.2       1.0       1.0       1.0       1e-7
!         ESH         Esu         Fsu       OmegaF
          0.0226      0.1624      632e6     1.0
!         ESH         Esu         Fsu       OmegaF
          0.0336      0.24        448e6     1.0
!         ESH         Esu         Fsu       OmegaF
          0.0226      0.1624      632e6     1.0

!         N         MTYPE     LABEL
          4         FRAME     Columns
!         ITYPE     IPINZ     IPINY     ICOND     IHYST     ILOS      IDAMG     IGA       IDUCT
          2         0         0         0         4         0         0         0         0
!         E         G           A       Jxx       Izz       Iyy       Asz       Asy       Sy        Sz        WGT
          24.9e9    11.6e9      0.81    0.11      0.033     0.033     0.81      0.81      0         0         0
!         END1z     END2z     END1y     END2y     FJ1z      FJ2z      FJ1y      FJ2y

          0         0         0         0         0         0         0         0
!         RA        RT        RFz       RFy
          0.1       0.1       0.1       0.1
!         H1        H2        H3        H4
          1.2       1.2       1.2       1.2
!         TY+       TY-       ALFA      BETA      IEND
          0         0         1.5       1         0
!         PC        PB        MBz       MBy       PT
          -24e5     -6e5      2.1e5     2.1e5     5.4e5
!         ALFA      BETA      NF        KKK
          0.25      0.45      1         2

!         N         MTYPE     LABEL
          5         FRAME     Beams
!         ITYPE     IPINZ     IPINY     ICOND     IHYST     ILOS      IDAMG     IGA       IDUCT
          2         0         0         0         0         0         0         0         0
!         E         G         A         Jxx       Izz       Iyy       Asz       Asy       Sy        Sz        WGT
          15e9      6e9       0.36      0.11      0.033     0.033     0.36      0.36      0         0         0
!         END1z     END2z     END1y     END2y     FJ1z      FJ2z      FJ1y      FJ2y
          0         0         0         0         0         0         0         0

!         N         MTYPE     LABEL
          6         SPRING    'Hollow-core continuity'
!         ITYPE     IHYST     ILOS      IDAMG   INCOND  ITRUSS  SL
          1         1         0         0       0.0     0.0     0.0
!         K1        K2        K3        K4      K5      K6      WGT      RF     RT
          11.8e4    11.8e4    11.8e4    11.8e2  11.8e2  11.8e5  0.0      0.0    0.0
!         FX+       FX-       FY+       FY-     Fz+     FZ-     ALPHA
          4.6e2     -4.6e2    4.6e2     -4.6e2  4.6e2   -4.6e2
!         MX+       Mx-       MY+       MY-     MZ+     MZ-     BETA
          4.6e1     -4.6e1    4.6e1     -4.6e1  2.3e4   -2.3e4

!         N         MTYPE     LABEL
          7         FRAME     Hollow-core
!         ITYPE     IPINZ     IPINY     ICOND     IHYST     ILOS      IDAMG     IGA       IDUCT
          2         0         0         0         0         0         0         0         0
!         E         G         A         Jxx       Izz       Iyy       Asz       Asy       Sy        Sz        WGT
          2.50E+5   1.04E+07  1         900       2.50E+5   2.50E+5   2.50E+5   2.50E+5   0         0         0
!         END1z     END2z     END1y     END2y     FJ1z      FJ2z      FJ1y      FJ2y
          0         0         0         0         0         0         0         0

!         N         MTYPE     LABEL
          8         Quadrilateral       'Hollow-core top'
!         ITYPE   ISHEAR   E      NU    THICK     WGT     IMEMB   IMATL    IHYST    ILOS
          0       0        30e+9  1.0   0.2       0       2       0        0        0

!         N         MTYPE     LABEL
          9         SPRING    'Concrete spring 1'
!         ITYPE     IHYST     ILOS      IDAMG   INCOND  ITRUSS  SL
          1         54        0         0       0.0     0.0     0.0
!         K1        K2        K3        K4      K5      K6      WGT      RF     RT
          191.8e5   0.0       0.0       0.0     0.0     0.0     0.0      0.0    0.0
!         FX+       FX-       FY+       FY-     Fz+     FZ-     ALPHA
          208.2e4   -1        0.0       0.0     0.0     0.0     0.0
!         MX+       Mx-       MY+       MY-     MZ+     MZ-     BETA
          0.0       0.0       0.0       0.0     0.0     0.0     0.0
!         TLIMT     CLIMIT    BETA      Fbo       L         TFACTOR CF   eTT
          0.0025    0.005     1.0       0.2       1.0       1.0     1.0  1e-7
          0         0         0         0         0         0       0    0
          0         0         0         0         0         0       0    0
          0         0         0         0         0         0       0    0
          0         0         0         0         0         0       0    0

!         N         MTYPE     LABEL
          10        SPRING    'Concrete spring 2'
!         ITYPE     IHYST     ILOS      IDAMG   INCOND  ITRUSS  SL
          1         54        0         0       0.0     0.0     0.0
!         K1        K2        K3        K4      K5      K6      WGT      RF     RT
          191.8e5   0.0       0.0       0.0     0.0     0.0     0.0      0.0    0.0
!         FX+       FX-       FY+       FY-     Fz+     FZ-     ALPHA
          208.2e4   -1        0.0       0.0     0.0     0.0     0.0
!         MX+       Mx-       MY+       MY-     MZ+     MZ-     BETA
          0.0       0.0       0.0       0.0     0.0     0.0     0.0
```

Table E-1: Input data for numerical model of SA1 (Continued).

```
!         TLIMT     CLIMIT  BETA     Fbo      L        TFACTOR CF   eTT
          0.0025    0.005   1.0      0.2      1.0      1.0     1.0  1e-7
          0         0       0        0        0        0       0    0
          0         0       0        0        0        0       0    0
          0         0       0        0        0        0       0    0
          0         0       0        0        0        0       0    0

!         N         MTYPE     LABEL
          11        SPRING    'Concrete spring 3'
!         ITYPE     IHYST     ILOS      IDAMG   INCOND  ITRUSS  SL
          1         54        0         0         0.0       0.0       0.0
!         K1       K2        K3       K4        K5        K6       WGT      RF     RT
          94.1e5 0.0       0.0      0.0       0.0       0.0      0.0      0.0    0.0
!         FX+      FX-       FY+      FY-      Fz+      FZ-      ALPHA
          134.6e4 -1     0.0      0.0      0.0      0.0     0.0
!         MX+      Mx-       MY+      MY-      MZ+      MZ-      BETA
          0.0      0.0       0.0      0.0      0.0      0.0      0.0
!         TLIMT     CLIMIT  BETA     Fbo      L        TFACTOR CF   eTT
          0.0025    0.005   1.0      0.2      1.0      1.0     1.0  1e-7
          0         0       0        0        0        0       0    0
          0         0       0        0        0        0       0    0
          0         0       0        0        0        0       0    0
          0         0       0        0        0        0       0    0

!         N         MTYPE     LABEL
          12        SPRING    'Concrete spring 4'
!         ITYPE     IHYST     ILOS      IDAMG   INCOND  ITRUSS  SL
          1         54        0         0         0.0       0.0       0.0
!         K1       K2        K3       K4        K5        K6       WGT      RF     RT
          94.1e5 0.0       0.0      0.0       0.0       0.0      0.0      0.0    0.0
!         FX+      FX-       FY+      FY-      Fz+      FZ-      ALPHA
          134.6e4 -1     0.0      0.0      0.0      0.0     0.0
!         MX+      Mx-       MY+      MY-      MZ+      MZ-      BETA
          0.0      0.0       0.0      0.0      0.0      0.0      0.0
!         TLIMT     CLIMIT  BETA     Fbo      L        TFACTOR CF   eTT
          0.0025    0.005   1.0      0.2      1.0      1.0     1.0  1e-7
          0         0       0        0        0        0       0    0
          0         0       0        0        0        0       0    0
          0         0       0        0        0        0       0    0
          0         0       0        0        0        0       0    0

!         N         MTYPE     LABEL
          13        SPRING    'Concrete spring 5'
!         ITYPE     IHYST     ILOS      IDAMG   INCOND  ITRUSS  SL
          1         54        0         0         0.0       0.0       0.0
!         K1       K2        K3       K4        K5        K6       WGT      RF     RT
          94.1e5 0.0       0.0      0.0       0.0       0.0      0.0      0.0    0.0
!         FX+      FX-       FY+      FY-      Fz+      FZ-      ALPHA
          134.6e4 -1     0.0      0.0      0.0      0.0     0.0
!         MX+      Mx-       MY+      MY-      MZ+      MZ-      BETA
          0.0      0.0       0.0      0.0      0.0      0.0      0.0
!         TLIMT     CLIMIT  BETA     Fbo      L        TFACTOR CF   eTT
          0.0025    0.005   1.0      0.2      1.0      1.0     1.0  1e-7
          0         0       0        0        0        0       0    0
          0         0       0        0        0        0       0    0
          0         0       0        0        0        0       0    0
          0         0       0        0        0        0       0    0

!         N         MTYPE     LABEL
          14        SPRING    'Concrete spring 6'
!         ITYPE     IHYST     ILOS      IDAMG   INCOND  ITRUSS  SL
          1         54        0         0         0.0       0.0       0.0
!         K1       K2        K3       K4        K5        K6       WGT      RF     RT
          94.1e5   0.0       0.0      0.0       0.0       0.0      0.0      0.0    0.0
!         FX+      FX-       FY+      FY-      Fz+      FZ-      ALPHA
          134.6e4 -1     0.0      0.0      0.0      0.0     0.0
!         MX+      Mx-       MY+      MY-      MZ+      MZ-      BETA
          0.0      0.0       0.0      0.0      0.0      0.0      0.0
!         TLIMT     CLIMIT  BETA     Fbo      L        TFACTOR CF   eTT
          0.0025    0.005   1.0      0.2      1.0      1.0     1.0  1e-7
          0         0       0        0        0        0       0    0
          0         0       0        0        0        0       0    0
          0         0       0        0        0        0       0    0
          0         0       0        0        0        0       0    0

!         N         MTYPE     LABEL
          15        SPRING    'Steel spring 1'
!         ITYPE     IHYST     ILOS      IDAMG   INCOND  ITRUSS  SL
          1         39        0         0         0.0       0.0       0.0
!         K1       K2        K3       K4        K5        K6       WGT      RF     RT
          37.2e7  0.0       0.0      0.0       0.0      11.8e2   0.0      0.0    0.0
!         FX+      FX-       FY+      FY-      Fz+      FZ-      ALPHA
          62.1e3   -62.1e3     0.0      0.0      0.0     0.0    0.0
!         MX+      Mx-       MY+      MY-      MZ+      MZ-      BETA
          0.0      0.0       0.0      0.0      4.6e1   -4.6e1  0.0
!         ESH       Esu       Fsu       OmegaF
          0.0227    0.1512    88.9e3    1.0

!         N         MTYPE     LABEL
          16        SPRING    'Steel spring 2'
!         ITYPE     IHYST     ILOS      IDAMG   INCOND  ITRUSS  SL
          1         39        0         0         0.0       0.0       0.0
!         K1      K2       K3      K4       K5       K6      WGT      RF     RT
          49.1e7 0.0      0.0      0.0      0.0      11.8e2  0.0      0.0    0.0
!         FX+      FX-       FY+      FY-      Fz+      FZ-      ALPHA
          81.9e3  -81.9e3  0.0      0.0      0.0      0.0     0.0
!         MX+      Mx-       MY+      MY-      MZ+      MZ-      BETA
          0.0      0.0       0.0      0.0      4.6e1   -4.6e1   0.0
!         ESH       Esu       Fsu       OmegaF
          0.0227    0.1512    117.2e3   1.0

!         N         MTYPE     LABEL
          17        SPRING    'Steel spring 3'
!         ITYPE     IHYST     ILOS      IDAMG   INCOND  ITRUSS  SL
```

Table E-1: Input data for numerical model of SA1 (Continued).

```
          1         39        0         0         0.0       0.0       0.0
!         K1        K2        K3        K4        K5        K6        WGT       RF      RT
          49.1e7    0.0       0.0       0.0       0.0       11.8e2    0.0       0.0     0.0
!         FX+       FX-       FY+       FY-       Fz+       FZ-       ALPHA
          81.9e3    -81.9e3   0.0       0.0       0.0       0.0       0.0
!         MX+       Mx-       MY+       MY-       MZ+       MZ-       BETA
          0.0       0.0       0.0       0.0       4.6e1     -4.6e1    0.0
!         ESH       Esu       Fsu       OmegaF
          0.0227    0.1512    117.2e3   1.0

!         N         MTYPE     LABEL
          18        SPRING    'Hollow-core continuity'
!         ITYPE     IHYST     ILOS      IDAMG     INCOND    ITRUSS    SL
          1         1         0         0         0.0       0.0       0.0
!         K1        K2        K3        K4        K5        K6        WGT       RF      RT
          11.8e4    11.8e4    11.8e4    11.8e2    11.8e2    11.8e5    0.0       0.0     0.0
!         FX+       FX-       FY+       FY-       Fz+       FZ-       ALPHA
          4.6e2     -4.6e2    4.6e2     -4.6e2    4.6e2     -4.6e2
!         MX+       Mx-       MY+       MY-       MZ+       MZ-       BETA
          4.6e1     -4.6e1    4.6e1     -4.6e1    2.3e4     -2.3e4

!         N         MTYPE     LABEL
          19        FRAME     Hollow-core
!         ITYPE     IPINZ     IPINY     ICOND     IHYST     ILOS      IDAMG     IGA       IDUCT
          2         0         0         0         0         0         0         0         0
!         E         G         A         Jxx       Izz       Iyy       Asz       Asy       Sy        Sz        WGT
          2.50E+5   1.04E+07  1         900       2.50E+5   2.50E+5   2.50E+5   2.50E+5   0         0         0
!         END1z     END2z     END1y     END2y     FJ1z      FJ2z      FJ1y      FJ2y
          0         0         0         0         0         0         0         0

!         N         MTYPE     LABEL
          20        Quadrilateral       'Hollow-core top'
!         ITYPE   ISHEAR   E      NU    THICK     WGT     IMEMB    IMATL     IHYST     ILOS
          0       0        30e+9  1.0   0.2       0       2        0         0         0

!         N         MTYPE     LABEL
          21        SPRING    'Concrete spring 1'
!         ITYPE     IHYST     ILOS      IDAMG     INCOND    ITRUSS    SL
          1         54        0         0         0.0       0.0       0.0
!         K1        K2        K3        K4        K5        K6        WGT       RF      RT
          191.8e5   0.0       0.0       0.0       0.0       0.0       0.0       0.0     0.0
!         FX+       FX-       FY+       FY-       Fz+       FZ-       ALPHA
          208.2e4   -1        0.0       0.0       0.0       0.0       0.0
!         MX+       Mx-       MY+       MY-       MZ+       MZ-       BETA
          0.0       0.0       0.0       0.0       0.0       0.0       0.0
!         TLIMT     CLIMIT    BETA      Fbo       L         TFACTOR   CF        eTT
          0.0025    0.005     1.0       0.2       1.0       1.0       1.0       1e-7
          0         0         0         0         0         0         0         0
          0         0         0         0         0         0         0         0
          0         0         0         0         0         0         0         0
          0         0         0         0         0         0         0         0

!         N         MTYPE     LABEL
          22        SPRING    'Concrete spring 2'
!         ITYPE     IHYST     ILOS      IDAMG     INCOND    ITRUSS    SL
          1         54        0         0         0.0       0.0       0.0
!         K1        K2        K3        K4        K5        K6        WGT       RF      RT
          191.8e5   0.0       0.0       0.0       0.0       0.0       0.0       0.0     0.0
!         FX+       FX-       FY+       FY-       Fz+       FZ-       ALPHA
          208.2e4   -1        0.0       0.0       0.0       0.0       0.0
!         MX+       Mx-       MY+       MY-       MZ+       MZ-       BETA
          0.0       0.0       0.0       0.0       0.0       0.0       0.0
!         TLIMT     CLIMIT    BETA      Fbo       L         TFACTOR   CF        eTT
          0.0025    0.005     1.0       0.2       1.0       1.0       1.0       1e-7
          0         0         0         0         0         0         0         0
          0         0         0         0         0         0         0         0
          0         0         0         0         0         0         0         0
          0         0         0         0         0         0         0         0

!         N         MTYPE     LABEL
          23        SPRING    'Concrete spring 3'
!         ITYPE     IHYST     ILOS      IDAMG     INCOND    ITRUSS    SL
          1         54        0         0         0.0       0.0       0.0
!         K1        K2        K3        K4        K5        K6        WGT       RF      RT
          94.1e5    0.0       0.0       0.0       0.0       0.0       0.0       0.0     0.0
!         FX+       FX-       FY+       FY-       Fz+       FZ-       ALPHA
          134.6e4   -1        0.0       0.0       0.0       0.0       0.0
!         MX+       Mx-       MY+       MY-       MZ+       MZ-       BETA
          0.0       0.0       0.0       0.0       0.0       0.0       0.0
!         TLIMT     CLIMIT    BETA      Fbo       L         TFACTOR   CF        eTT
          0.0025    0.005     1.0       0.2       1.0       1.0       1.0       1e-7
          0         0         0         0         0         0         0         0
          0         0         0         0         0         0         0         0
          0         0         0         0         0         0         0         0
          0         0         0         0         0         0         0         0

!         N         MTYPE     LABEL
          24        SPRING    'Concrete spring 4'
!         ITYPE     IHYST     ILOS      IDAMG     INCOND    ITRUSS    SL
          1         54        0         0         0.0       0.0       0.0
!         K1        K2        K3        K4        K5        K6        WGT       RF      RT
          94.1e5    0.0       0.0       0.0       0.0       0.0       0.0       0.0     0.0
!         FX+       FX-       FY+       FY-       Fz+       FZ-       ALPHA
          134.6e4   -1        0.0       0.0       0.0       0.0       0.0
!         MX+       Mx-       MY+       MY-       MZ+       MZ-       BETA
          0.0       0.0       0.0       0.0       0.0       0.0       0.0
!         TLIMT     CLIMIT    BETA      Fbo       L         TFACTOR   CF        eTT
          0.0025    0.005     1.0       0.2       1.0       1.0       1.0       1e-7
          0         0         0         0         0         0         0         0
          0         0         0         0         0         0         0         0
          0         0         0         0         0         0         0         0
          0         0         0         0         0         0         0         0
```

Table E-1: Input data for numerical model of SA1 (Continued).

```
!         N         MTYPE     LABEL
          25        SPRING    'Concrete spring 5'
!         ITYPE     IHYST     ILOS      IDAMG   INCOND  ITRUSS  SL
          1         54        0         0         0.0       0.0       0.0
!         K1        K2        K3      K4        K5        K6      WGT      RF     RT
          94.1e5 0.0      0.0     0.0      0.0       0.0     0.0      0.0    0.0
!         FX+     FX-       FY+     FY-     Fz+     FZ-     ALPHA
          134.6e4 -1    0.0     0.0      0.0     0.0    0.0
!         MX+     Mx-     MY+     MY-     MZ+     MZ-     BETA
          0.0     0.0     0.0     0.0     0.0     0.0     0.0
!         TLIMT     CLIMIT  BETA    Fbo     L       TFACTOR CF   eTT
          0.0025    0.005   1.0     0.2     1.0     1.0     1.0  1e-7
          0         0       0       0       0       0       0    0
          0         0       0       0       0       0       0    0
          0         0       0       0       0       0       0    0
          0         0       0       0       0       0       0    0

!         N         MTYPE     LABEL
          26        SPRING    'Concrete spring 6'
!         ITYPE     IHYST     ILOS      IDAMG   INCOND  ITRUSS  SL
          1         54        0         0         0.0       0.0       0.0
!         K1        K2        K3      K4        K5        K6      WGT      RF     RT
          94.1e5    0.0      0.0     0.0      0.0       0.0     0.0      0.0    0.0
!         FX+     FX-       FY+     FY-     Fz+     FZ-     ALPHA
          134.6e4 -1    0.0     0.0      0.0     0.0    0.0
!         MX+     Mx-     MY+     MY-     MZ+     MZ-     BETA
          0.0     0.0     0.0     0.0     0.0     0.0     0.0
!         TLIMT     CLIMIT  BETA    Fbo     L       TFACTOR CF   eTT
          0.0025    0.005   1.0     0.2     1.0     1.0     1.0  1e-7
          0         0       0       0       0       0       0    0
          0         0       0       0       0       0       0    0
          0         0       0       0       0       0       0    0
          0         0       0       0       0       0       0    0

!         N         MTYPE     LABEL
          27        SPRING    'Steel spring 1'
!         ITYPE     IHYST     ILOS      IDAMG   INCOND  ITRUSS  SL
          1         39        0         0         0.0       0.0       0.0
!         K1        K2        K3      K4        K5        K6      WGT      RF     RT
          37.2e7  0.0      0.0     0.0      0.0     11.8e2   0.0      0.0    0.0
!         FX+     FX-       FY+     FY-     Fz+     FZ-     ALPHA
          62.1e3   -62.1e3     0.0     0.0      0.0     0.0    0.0
!         MX+     Mx-     MY+     MY-     MZ+     MZ-     BETA
          0.0     0.0     0.0     0.0     4.6e1   -4.6e1  0.0
!         ESH       Esu       Fsu       OmegaF
          0.0227    0.1512    88.9e3    1.0

!         N         MTYPE     LABEL
          28        SPRING    'Steel spring 2'
!         ITYPE     IHYST     ILOS      IDAMG   INCOND  ITRUSS  SL
          1         39        0         0         0.0       0.0       0.0
!         K1      K2      K3      K4        K5        K6      WGT      RF     RT
          49.1e7 0.0      0.0     0.0      0.0      11.8e2  0.0      0.0    0.0
!         FX+     FX-       FY+     FY-     Fz+     FZ-     ALPHA
          81.9e3  -81.9e3  0.0     0.0      0.0     0.0    0.0
!         MX+     Mx-     MY+     MY-     MZ+     MZ-     BETA
          0.0     0.0     0.0     0.0     4.6e1   -4.6e1   0.0
!         ESH       Esu       Fsu       OmegaF
          0.0227    0.1512    117.2e3   1.0

!         N         MTYPE     LABEL
          29        SPRING    'Steel spring 3'
!         ITYPE     IHYST     ILOS      IDAMG   INCOND  ITRUSS  SL
          1         39        0         0         0.0       0.0       0.0
!         K1        K2        K3      K4        K5        K6      WGT      RF     RT
          49.1e7  0.0      0.0     0.0      0.0      11.8e2  0.0      0.0    0.0
!         FX+     FX-       FY+     FY-     Fz+     FZ-     ALPHA
          81.9e3  -81.9e3  0.0     0.0      0.0     0.0    0.0
!         MX+     Mx-     MY+     MY-     MZ+     MZ-     BETA
          0.0     0.0     0.0     0.0     4.6e1   -4.6e1  0.0
!         ESH       Esu       Fsu       OmegaF
          0.0227 0.1512  117.2e3       1.0
!         N         MTYPE             LABEL
          30        SLOTTED           'NS Slotted Beam'
!         IPLAS   B       D       DB      SL      HL      WGT    JOP  IHS   IHB   IO   Y0   Z0 IPRNT
          1       0.502   0.174   0.654   0.0     0.3519  0.0    3    1     1     0    0    0
!         EC       FPC       FT
          27.8e+09 -40e+06 2.27e+06
!         ES        R     FSC       FST      L1      L2      D1      D2
          157e+09  0.1   -521e+06  521e+06  0.338  0.338  0.0315   0.09
!         ES        R     FSC       FST      L1      L2      D1      D2
          127e+09  0.1   -314e+06  314e+06  0.564  0.639  0.564   0.623
!         ES        R     FSC       FST      LENGTH  ANGLE
          157e+09  0.1   -521e+06  521e+06  0.588   45
!         G       FY      R     Alpha  Fcr   Fcc
          15e+06  40e+03  0.01  0.0    0.0   0.0
!         N1      A1       A2       A3       A4   A5   B1      B2     B3     B4   B5
          3       4.1e-4  4.1e-4  4.1e-4  0.0  0.0  -0.110  0.101  0.206  0.0  0.0
!         N1      A1       A2       A3   A4   A5   B1      B2     B3   B4   B5
          2       4.1e-4  4.1e-4  0.0  0.0  0.0  -0.110  0.206  0.0  0.0  0.0
!         N1      A1       A2       A3   A4   A5   B1      B2     B3   B4   B5
          2       1.13e-4  1.13e-4  0.0  0.0  0.0  -0.110  0.206  0.0  0.0  0.0
!         N1      A1       A2       A3       A4   A5   B1      B2     B3     B4   B5
          3       4.1e-4  4.1e-4  4.1e-4  0.0  0.0  -0.110  0.101  0.206  0.0  0.0
!         N1      A1       A2       A3       A4       A5    B1      B2     B3     B4   B5
          4       4.1e-4  4.1e-4  4.1e-4  4.1e-4   0.0  -0.244  -0.159 0.159  0.244  0.0
!         TLIMT     CLIMIT    BETA      Fbo       L         TFACTOR   CFACTOR   eTT
          0.0025    0.005   1.0     0.2     1.0     1.0     1.0  1e-7
!         ESH         Esu         Fsu       OmegaF
          0.0226      0.1624      632e6     1.0
!         ESH         Esu         Fsu       OmegaF
          0.0336      0.2235      448e6     1.0
```

Table E-1: Input data for numerical model of SA1 (Continued).

```
!         ESH         Esu         Fsu       OmegaF
          0.0226      0.1624      632e6     1.0

WEIGHTS   0
!         N         WX        WY        WZ        Mx        My        Mz
          1
          342

LOADS 0
!         N         WX        WY        WZ        Mx        My        Mz
          1         0         0         0
          342       0         0         0

EQUAKE drift_sub_x_L1.txt
! IBERG   ISTART    DELTAT    ASCALE    END       VEL       DIS       TSCALE   IP
  3       1         0.01      -1.       -1        0         0         1        0

EQUAKE drift_sub_z_L1.txt
! IBERG   ISTART    DELTAT    ASCALE    END       VEL       DIS       TSCALE   IP
  3       1         0.01      -1.       -1        0         0         1        0

EQUAKE drift_sub_x_L2.txt
! IBERG   ISTART    DELTAT    ASCALE    END       VEL       DIS       TSCALE   IP
  3       1         0.01      -1.       -1        0         0         1        0

EQUAKE drift_sub_z_L2.txt
! IBERG   ISTART    DELTAT    ASCALE    END       VEL       DIS       TSCALE   IP
  3       1         0.01      -1.       -1        0         0         1        0
```